SP-383

ESA14

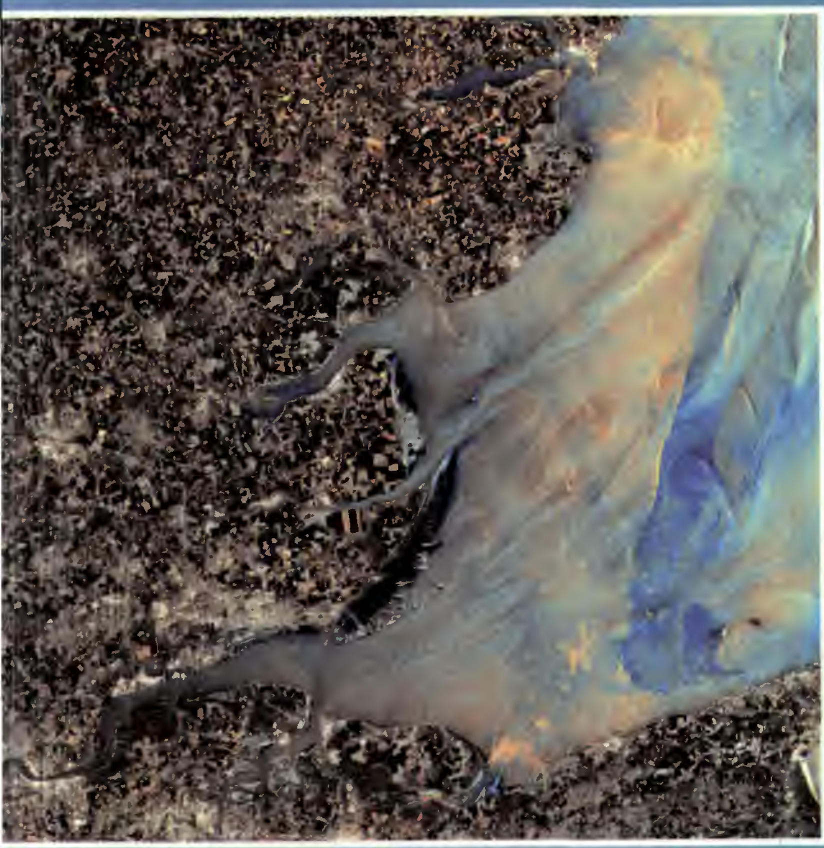

Second ERS Applications Workshop

London, UK
6-8 December 1995

esa
european space agency

esa SP-383
February 1996
ISBN 92-9092-215-X

Proceedings of
the Second International Workshop on

ERS Applications

London, 6-8 December 1995

european space agency / agence spatiale européenne

ESA SP-383
Second ERS Applications Workshop
London, UK, 6-8 December 1995

Published by:	ESA Publications Division ESTEC, Noordwijk, The Netherlands
Edited by:	T.-D. Guyenne
Price:	80 Dutch Guilders

ISBN 92-9092-215-X	Printed in The Netherlands

CONTENTS

FORESTRY

Chairman: F. De Grandi, JRC
Rapporteur: G. Calabresi, ESA/ESRIN

GEOID / GRAVITY / BATHYMETRY

Chairman: E.K. Biegert, GOSAP Project
Rapporteur: J. Benveniste, ESA/ESRIN

ENVIRONMENT / HAZARD / HYDROLOGY

Chairman: J. Achache, Institut de Physique du Globe
Rapporteur: M. Borgeaud, ESA/ESTEC

SEA-SURFACE FEATURES

Chairman: G.D. Strøm, Norwegian Space Centre
Rapporteur: J. Johannessen, ESA/ESTEC

SEA & ICE

Chairman: G.D. Strøm, Norwegian Space Centre
Rapporteur: J. Johannessen, ESA/ESTEC

FLOODING

Chairman: J. Achache, Institut de Physique du Globe

Rapporteur: G. Paci, ESA/ESRIN

GEOLOGY / DEM

Chairman: M. Doherty, ESA/ESRIN

Rapporteur: S. Coulson, ESA/ESRIN

SHIP ROUTING

Chairman: S. Sandven, Nansen Centre

Rapporteur: E. Attema, ESA/ESTEC

COASTAL ZONE MONITORING

Chairman: H. Wensink, ARGOSS

Rapporteur: S. Bruzzi, ESA, Paris

MAPPING

Chairman: E. Attema, ESA/ESTEC

Rapporteur: J. Lichtenegger, ESA/ESRIN

POSTER PAPERS

OVERVIEW OF ESA PROGRAMMES AND PLANS FOR DEVELOPMENT OF APPLICATIONS OF EARTH OBSERVATION SPACE DATA

L. EMILIANI
Director of Earth Observation and its Environment

G. DUCHOSSOIS
Head, Mission Management Office
Directorate of Earth Observation and its Environment

Over the past 25 years, space remote sensing techniques have enabled major advances in earth sciences, in particular for understanding the Earth's climate and environment. With the exception of meteorological satellite data which are now routinely fed into operational forecast models, for various reasons the development of other applications (e.g. land) has not progressed at the same pace (adequacy of data, data continuity, level of users' organisations and users' involvement, etc.). However, the situation is steadily improving (as has been demonstrated during this workshop) through various actions now underway.

Currently, the ESA Earth Observation programmes are following a strategy along two main directions:

- cooperation with EUMETSAT to provide continuity of the operational services to the meteorological community with :
  - METEOSAT second generation series, the first one scheduled for launch in 2000
  - METOP/EPS series, the first one scheduled for launch in 2001/2002
- development and exploitation of research and demonstration satellite systems:
  - ERS-1, launched on 17 July 1991
  - ERS-2, launched on 21 April 1995
  - ERS-1 and ERS-2 are currently being operated simultaneously ("tandem" mode)
  - ENVISAT-1 is scheduled for launch in mid-1999 thus ensuring ERS data continuity as well as opening new sectors of research and applications (e.g. marine biology, atmospheric chemistry)

After 4.5 years in orbit, all ERS-1 instruments are still in operation. Since the first ERS-1 Pilot Projects Workshop, the geodetic Phase (two interleaved 168-day repeat cycles April'94-March'95) has been completed. Using the data acquired during this period, global marine geoid and gravity fields have been determined with an unprecedented resolution/accuracy. Since 19 March 1995, ERS-1 is back to the 35-day orbit, a stable orbit configuration which enables consolidation of the results of the multidisciplinary phase.

The Commissioning of ERS-2 is well under way: the ERS-2 Radar Altimeter (and Microwave Radiometer) has been successfully commissioned (August 1995) by cross-calibration with ERS-1, while SAR (image and wave mode) commissioning (on-ground transponders, tropical rain forest overflights) was completed in September 1995. For the new instruments (ATSR, GOME, PRARE), the data acquisition required for GOME calibration has been successfully completed and geophysical validation has been on-going since end July 1995. Meanwhile, commissioning of PRARE and ATSR-2 is still on-going.

The first switch-on of the ERS-2 Wind Scatterometer in May 1995 was unsuccessful (triggering of the receiver overload protection). An extensive investigation campaign was then set-up, involving on-ground unit and engineering model testing, in-orbit tests, while the nominal Wind Scatterometer service continued to be provided by ERS-1. A work-around solution was eventually designed, validated and successfully tested, and commissioning of the ERS-2 Wind Scatterometer started on 15 January 1996.

The Tandem mission will be conducted until end May 1996. The main objectives are increased spatial and temporal sampling (in particular for Interferometry and monitoring of all surface changes), complementary use of instruments (e.g. SAR/WSC conflicts at coastline and use of different instruments covering the same area on ground). Both satellites are kept in a 35-day repeat cycle with a 30 minutes offset in the same orbital plane (i.e. 1-day offset in ground revisiting between ERS-1 and ERS-2). Different orbit maintenance scenarios are planned to ensure the availability of the most suitable baseline values (on global scale) for interferometric DEM (Digital Elevation Model) generation and in line with specific ground station acquisition campaigns.

During Commissioning Phase, interferograms using data from both satellites were succesfully generated within ESA. Products (not validated) over selected test sites were distributed to Fringe users participating in the validation who also confirm the feasibilibity of the methodology.

The Tandem operation of ERS-1 and ERS-2 offers a unique opportunity to achieve significant advances in both Earth sciences and applications for the next decade; in particular the use of SAR interferometry techniques should allow the generation of consistant and homogeneous medium resolution Digital Elevation Models over large portions of the Earth's land and ice masses; used in a differential interferometry mode, the SAR Tandem data sets will also offer the unique opportunity to detect and measure very small (of the order of a few centimetres) topographic changes such as those caused by earthquakes, landslides, volcanic activities, glacier motion.

It is ESA's intention to encourage both the scientific and application user community to take maximum advantage of this unique Tandem data set, thus opening new perspectives for science research and operational applications. To this end, ESA issued an Announcement of Opportunity on 17th January 1996, limited to purely scientific exploitation of the Tandem mission and focussing on the use of new techniques or methodologies in the validation, processing and interpretation of these data.

For all its missions, ESA is responsible for the promotion of scientific utilisation of data by the research community through various mechanisms (e.g. announcements of opportunity, research demonstration projects, etc.) and applications development by the operational/commercial community through other such mechanisms (e.g. call for applications pilot projects, application demonstration programmes, etc.), the ultimate objective being the transfer to pre-operational/operational stage. The development of applications by ESA also involves the coordination and/or cooperation with :

- ESA member states' national utilisation programmes
- the European Commission (EC), through programmes such as Trees, Mars and the CEO
- other programmes of international organisations (e.g. Africover with FAO ...)

For ERS-1 and ERS-2, 2 announcements of opportunity were issued in May 1986 (270 Principal Investigators) and December 1993 (340 proposals selected). The results of these scientific investigations were presented at the first two ERS-1 symposia in

- Cannes (November 1992): 450 participants, 150 presentations
- Hamburg (October 1993) : 700 participants, 270 presentations

The promotion of application demonstration and operational utilisation of ERS data led to the selection of 150 Pilot Projects worldwide in 1989 and 1993. Results of these projects were presented at the first ERS-1 Pilot Project Workshop in Toledo (June 1994): 220 participants, 100 presentations.

The Director General's proposal for Earth Observation at the ESA Council at Ministerial level held in Toulouse on 18-20 October 1995 includes a dual-mission strategy through the deployment of "Earth Explorer" (research-oriented) and "Earth Watch" (applications-oriented) satellite series.

The Earth Explorer missions will be research demonstration missions aimed at advancing the understanding of the different Earth systems processes, with each mission focussing on a particular field (e.g. atmospheric chemistry) or regrouping a limited number of research fields.

The Earth Watch missions will be thematic pre-operational or operational missions addressing the requirements of specific existing or emerging Earth Observation application areas, with the responsibility for such missions eventually being transferred to operational entities.

Candidate themes for an Earth Watch mission include

- coastal zone mission
- open oceans mission
- ice monitoring mission
- land surface mission
- atmospheric chemistry mission.

The selection of an Earth Watch mission will depend on economic justification and identification of potential partner(s). It is planned to use ERS-1, ERS-2 and later ENVISAT-1 as precursors and/or demonstrations for Earth Watch missions.

Earth Observations from space can provide useful and, in many cases, unique data/information for the monitoring of the Earth's environment and management of resources. The development of models assimilating space data is becoming increasingly important. ESA, with ERS and later ENVISAT-1, is paving the way to future Earth Watch missions developed from the outset with the full cooperation of users' entities who will ultimately take over the responsibility for these missions.

WELCOME ADDRESS

Derek Davis

Director General, BNSC, London, UK

I should like to welcome you on behalf of the Government and the British National Space Centre to this important ESA Applications Workshop at the Queen Elizabeth II Conference Centre. Mr Ian Taylor, the Minister for Space, had hoped to be with you this morning and would, I know, have given you strong encouragement in your work over the next couple of days – believing as he does that the use of space is such an important part of the picture. Guy Duchossois and others have indeed seen him in action at this very Centre, spreading the message about space data and products. He is, however, off today to India in connection with other responsibilities he has at the Department of Trade and Industry. He has asked me to pass on his best wishes to you for a very successful workshop.

The Earth-observation data markets are, in a way, a new challenge for space – a rather greater challenge than we normally spend time thinking about. In telecoms and broadcasting, the markets already existed. Space enhanced them, overcame barriers, enabled new players to enter and helped generate new products. In meteorology, similarly, there was an established activity where space data could be readily applied and where tangible improvements in performance were quickly achieved. With the benefit of hindsight one can exaggerate the ease with which these developments, that we all now take for granted, came about. But in much of remote sensing there is a real difference of kind. One has actually to establish the market, to search out the users and to identify the applications – some of which are wholly new territory and others of which are new and not immediately obvious ways of carrying on existing activities more effectively. This has been a major change of focus for the space community. In Earth observation many of us have had to reach beyond the collective past experience in space hardware and ground infrastructure for existing users and start thinking of ourselves as marketeers, as promoters, as pioneers of a new frontier – not a frontier in space but a new frontier among users on the ground.

We in the UK have been working at this for a number of years. I and my colleagues at BNSC welcome you here today and salute this workshop as warmly as we do precisely because it is our belief that applications development is vital to the future expansion of the remote-sensing market. The ERS missions, with Envisat to follow, provide an unrivalled opportunity for Europe to establish these uses and markets. Our objective is progressively to transfer responsibility for the management and investment required to exploit Earth-observation data from a Government R&D base to industry and other users. ESA's ERS applications programme is, therefore, not only welcome to us on merits. It is fully in line with UK objectives.

Applications development is an important element of the BNSC national Earth observation programme which seeks to exploit the UK investment in ESA programmes. There are three main activities:

1. Application Demonstration Projects
2. LINK Projects
3. Promotional Activities

Applications Demonstration Projects are supported under a BNSC programme started in 1992 to demonstrate the benefits of Earth observation data in civil applications. The programme objectives are:

- to demonstrate the applicability and value of space dervide data for formulating new solutions or enhancing existing solutions in selected applications areas;
- to promote EO science and technology transfer between academia and industry;
- to contribute to a climate which encourages investment in highly innovative EO applications by business and financial institutions and, in the medium and long term, helps industry succeed in attracting and developing European and international remote sensing business.

In the first round of the programme which is now nearing completion, seven projects have been supported with joint industry/BNSC funding. The results of these projects are extremely encouraging and some of them will be presented during the workshop. A key feature of the projects is the involvement of end-users from both the commercial sector (e.g. oil companies) and from Government Departments and Agencies (e.g. MAFF). In the second round of the programme, which has recently been started, eight projects are being supported with, on average, two thirds of the funding coming from industry and users and one third from BNSC.

The second main applications development activity is a new Earth-observation *LINK programme*, also jointly funded by Government and industry, to support innovative pre-competitive Earth-observation applications research. The LINK programme is targeted at end-user needs emerging from the recent UK technology foresight exercise. It is intended to bridge the gap between basic Earth-observation research under the Natural Environment Research Council (NERC) programme and the near-market applications under BNSC's applications development programme. In the first round of the LINK programme three projects are being supported on a 50/50 funding basis.

The third element of BNSC's approach involves activities aimed at expanding the customer base for Earth-observation data and services. The *promotional activities* include:

- dissemination of information on Earth-observation applications through existing Department of Trade and Industry mechanisms such as Business Links within the UK and Export Promotion Services outside the UK;

- liaison with other Government Departments such as Ministry of Agriculture, Fisheries & Food and Overseas Development Agency for whose programmes Earth-observation data can make a significant contribution;

- targeted promotional activities aimed at specific user sectors such as the educational community, the investment community and various sectors of commerce/industry; to be successful these activities really require a European rather than just a UK basis of approach;

I am sure that you will all have a great deal to tell one another and to learn from one another. Why are the results you will be presenting here in London so important? Because the investment in the ESA programmes can only be returned through the development of real operational services. Because the research paves the way for new applications and transforms the new data into information, information that can be used in the real world.

I wish you all a very successful workshop over the next couple of days. I look forward to hearing a little about progress when we meet up again at the reception this evening.

AGRICULTURE / LANDUSE

Chairman: **H. de Groof**
Rapporteur: **M. Rast**

THE USE OF ERS SAR DATA FOR AGRICULTURE AND LAND USE: AN OVERALL ASSESSMENT

Sylvie Rémondière*, Jürg Lichtenegger**
**Eurimage under contract to ESA - ESRIN Data Utilisation Section*
***ESA - ESRIN Data Utilisation Section, Frascati, Italy*
Tel. (39) 6 941801 Fax (39) 6 94180622

ABSTRACT

This paper focuses on the current status of the utilisation of ERS data for land use applications and in particular for agriculture. An overview of the projects' results as well as a detailed description of the more advanced utilisation of ERS data with respect to the operational status is presented. In view of successful demonstrations of crop type discrimination the EU will include ERS SAR data for a pre-operational demonstration. Issues regarding SAR post-processing to improve crop discrimination under specific conditions (hilly terrain, etc.) are also addressed.

INTRODUCTION

Since the ERS mission started, a number of projects have been performed to assess the capability of the SAR to image meaningful features on the land surfaces, also with the objective to replace or complement information extracted from optical satellite data. Recent results from the ESA Pilot Projects as well as other activities have encouraged the European Union, Value Added Companies and Institutes to test the use of ERS data for crop identification and natural resources management in pilot studies and also in some pre- operational programmes.

The Data Utilisation Section at ESRIN has conducted an evaluation of individual projects and provided an overall assessment by areas of application based on the Principal Investigators and Pilot Projects activity. In addition, projects under national programmes and commercial services developed by Value Added Companies have been analysed. The evaluation shows the level of performance for each application area and includes a number of conclusions regarding the potential for operationalisation.

OVERVIEW OF THE PROJECTS

The evaluation of ERS SAR data application for agriculture was performed over about 15 projects located either in European countries under temperate conditions or in tropical countries. The main objectives were:

- mapping of renewable resources,
- estimation of crop surfaces,
- crop conditions assessment,
- crop production forecasting,
- surveillance of crop declarations for fraud control,
- detection of damages and the assessment of their impact.

Basic information on renewable resources and crops is necessary for land use management and implementation of agricultural policy. Important results were obtained from projects performed within the framework of European programmes, linked to the requirements of the Common Agriculture Policy. Because of their importance for the ERS mission, we describe these programmes in more detail.

The MARS project, Monitoring Agriculture using Remote Sensing, aims at improving European production forecasts by the use of high resolution satellite data. Statistics are provided to the Directorate General for Agriculture of the EC (DG VI), and the European Statistical Office (EUROSTAT).

Within the MARS project, the MARS - STAT activity aim at timely estimate crop acreage and accuracy compared with the traditional pixel-based classification methods.

Integration of optical and radar data enhances the discrimination of land cover types. Some interesting results were obtained using the IHS (Intensity Hue Saturation) transformation as well as the Principal Component analysis. However, complementary optical/radar analyses are still at an experimental stage.

SAR interferometry also shows a potential for the discrimination of agricultural fields and forests. High interferometric coherence was found for low vegetation and bare soil surfaces and a loss in coherence for forest, making interferometric processing a potential tool for forest mapping. Furthermore, coherence measurements can be used to estimate field irrigation, to detect any performed field labour and also frost events.

OVERVIEW OF THE RESULTS

Out of the 15 projects, the main classification results confirm that ERS SAR data can be used for crop mapping, statistics and monitoring, in particular:

- to discriminate cereals from rape seed and high biomass crops such as sugar beet using multi-temporal ERS SAR data acquired between late May and July. The reliability of discrimination of field crops significantly improves as more SAR acquisitions are considered, i.e. as more temporal information is added. Classification performance also increases when optical satellite image is combined with multi-temporal ERS SAR data.
- for early crop identification, it has been successfully demonstrated that multi-temporal ERS SAR data acquired before end of June provide good discrimination of cereals, rape seed and grass fields. It has been also reported that ERS SAR data received during winter months improves early season crop classification by identifying tillage of particular crops. As a result, ERS SAR data has been included in the MARS-STAT project for pre-operational testing. This will contribute to fill the gap of missing optical data sets due to bad weather constraints.
- to separate grassland from other land cover types due to the very stable backscatter of grassland across the year. Even the distinction of different grassland classes is possible because degraded grassland has a slightly higher backscatter than managed grass-fields.
- to map rice fields and to monitor the crop growth using multi-temporal ERS SAR images due to the largest temporal dynamic range of rice compared to all other agricultural crops. Moreover there is a clear correlation between radar back-scattering signal and plant height. Also it looks promising to use temporal SAR information to retrieve yield-related parameters and to detect field management practices.

FUTURE PROSPECTS

Agricultural monitoring is probably the most important application for spaceborne surveillance systems in terms of quantity of data required. As a result of our evaluation of the available projects it has to be stated that ERS SAR has definitely a high potential to contribute significantly to such monitoring tasks, especially in the cloud-prone part of Europe and in the tropics. Recent reports of a pre-operational implementation of ERS SAR into an existing system supports these findings.

There is a high expectation for soil moisture estimation using SAR. Considerable efforts have been made in numerous projects. Regardless of the quality of the work, the results reported can not be considered matured for regular surveys. More investigations seems to be needed especially what concerns backscatter modelling.

However numerous issues of a technical and non-technical nature have still to be addressed in order for ERS SAR data to be used efficiently both for further demonstrations and for operational implementations.

The technical issues connected to the various problems scientists and application specialists are facing when working with SAR data. They include image filtering, segmentation and classification. Implementations of related tools tailored to ERS SAR products are still not available to the extend of an operational use.

potential yield. Since 1990, more than 50 test sites have been analysed throughout Europe. Acreage estimation is obtained by computer assisted photo-interpretation of up to 4 satellite images per year for each test site. ERS SAR data have been tested over several of these sites (Seville, Great-Driffield, Chartres, Bologna and Albacete). Procedures used in optical remote sensing applied to SAR were found not suitable. New methods using radar specific post-processing improved the results considerably. After a demonstration phase, ERS SAR data is now included in the project for pre-operational testing over 25 test sites, either to complement missing optical satellite data or to supplement information.

The MARS - PAC activity points at the verification and the control of area-based subsidies within the EU. Within each country approximately 5% of all farmers' declarations are checked using satellite remote sensing. Crop maps are obtained by computer assisted photo-interpretation and by automatic classification of high resolution satellite data, mainly SPOT and LANDSAT data. ERS SAR data have been successfully utilised over Northern test sites, in Ireland and the U.K., where optical satellite data were not available.

Another initiative by the EU in co-operation with ESA is pursued in Southeast Asia. There a total of eight ERS pilot projects are being fully supported by an ASEAN project. There are two pilot projects in each of the four participating countries, with a variety of different applications such as coastal zone mapping, crop rice mapping, land use mapping and hazards monitoring. The projects are clearly directed to the operational application of methodologies and results confirm that ERS SAR data are particularly useful for monitoring in tropical conditions. During the rainy season it might even be the only source of spaceborne information.

The results obtained within the MARS and the ASEAN projects were confirmed by other pilot project studies, e.g. the PASTA project in Germany dealing with SAR techniques to derive agricultural statistics and inspection of land use and the SARI rice growth monitoring project in Indonesia.

OVERVIEW OF THE METHODS APPLIED FOR DATA ANALYSIS

Different approaches are developed to extract information on renewable resources from ERS images:

- Analysis of temporal signatures,
- Pixel-based classification,
- Field-based classification,
- Integration of optical and radar data,
- SAR interferometry.

Temporal signatures of different crops are used as a tool for their discrimination. In several projects in UK, Germany and the Netherlands, changes in wheat backscatter in all development stages were studied and compared with temporal backscatter profiles of other crops. It was demonstrated that fields of winter wheat can be distinguished from other crops, especially during the very early season due to time-specific field preparation. In Thailand, Indonesia and Japan, changes in rice backscatter in different development stages were analysed. A characteristic and pronounced temporal signature during the growing season was discovered that enabled the discrimination of rice fields and their status with high reliability.

Pixel-based classification techniques normally used to classify optical imagery are hindered by image speckle. Application of speckle filters improves visual and digital land cover discrimination. In general filter performance was assessed in terms of reducing the variance for homogeneous land cover types. Significant improvement of statistics for both agricultural and non-agricultural land cover types was found, particularly when Lee or MAP filters were applied.

The field-based approach applied to SAR image classification overcomes the problem of speckle by the extraction of image statistics, such as the mean backscatter by field. An appropriate image segmentation is required. It can be performed using GIS information (land register) or field-boundaries extracted from high resolution optical satellite imagery or from averaged time-series of ERS SAR data. Several studies show a significant improvement of the classification

Practical solutions to geometric/radiometric corrections of SAR data when analysis from hilly terrain are required, have reached only the level of demonstrations. The integration of radar and optical data is an issue that needs to be further developed. In all these cases implementation strategies need to be found in order to streamline SAR post-processing, a prerequisite for any customised operational use. Moreover additional research is required for crop growth modelling versus backscatter and in interferometry especially with regard to information derived from coherence images.

Non-technical issues to be followed in the future consist mainly of enhancing promotion activities, including training addressed to decision-makers and not only to specialised technicians. There is a need to divulgate more effectively project result and this would require further geographically specific pilot and demonstration studies.

MONITORING AGRICULTURAL LAND PREPARATION ACTIVITIES WITH ERS-1 TO COMPLEMENT AND ADVANCE EARLY SEASON CROP ACREAGE ESTIMATES IN THE FRAMEWORK OF THE MARS PROJECT.

Guido Lemoine[1], Hugo de Groof[2] and H.J.C. van Leeuwen[1]

[1] *SYNOPTICS, Integrated Remote Sensing and GIS Applications BV, P.O. Box 117, 6700 AC Wageningen, the Netherlands.*
Tel: +31 317 426936 Fax: +31 317 425705 E-mail: main@synoptics.nl

[2] *Commission of the European Communities, Joint Research Centre, Institute for Remote Sensing Applications, Agriculture Unit, TP 440, 21020 Ispra (VA), Italy*
Tel: +39 332 785449 Fax: +39 332 789046 E-mail: hugo.de-groof@jrc.it

ABSTRACT

In this paper, the results of a pre-operational study on the use of ERS-1 backscattering signatures for early season agricultural crop class discrimination are discussed. The use of these data is based on the understanding that microwave backscattering signatures of bare field carry information on the surface structure of the field, which is a reflection of the field preparations carried out for specific cropping regimes in an area. Thus, we test our hypothesis that ERS-1 signatures can be used to identify crop specific tilths that precede the actual growth stage of the crop.

We show the use of this methodology for multi-temporal ERS-1 SAR imagery of the MARS Action B site at Great Driffield, United Kingdom. The data set encompasses 21 images between June 1994 and July 1995. The analysis of the ERS-1 data has been supported by numerous ancillary data sets, of which meteorological records, crop classification results of the previous season (1994) and a rapid ground survey in the spring of 1995 are the most important.

Our analysis shows that well-chosen early season imagery can significantly improve crop class separation with ERS-1 imagery. The study has also lead to various recommendations for the further development of a crop classification methodology based on the use of SAR signatures.

Keywords: ERS-1, agriculture, crop classification, early season.

1. INTRODUCTION

Since crop discrimination in optical remote sensing imagery is based on the reflectivity characteristics in the respective spectral bands, operational application of that technique is restricted to the vegetation cycle of the growing season. Reliable early crop acreage estimates can be obtained only after a significant crop coverage has developed, and only if cloud-free imagery is available.

Land preparation, or tillage, of agricultural fields is often directly related to the future crop type. For instance, winter crops, such as winter cereals and oil rape seed, are already sown in the fall. Significant crop coverage is only reached after the crop continues its growth in the spring. The difference in microwave backscattering from fields with varying roughness spectra (e.g. winter cereals seedbeds and ploughed fields) can be used to separate them in early season ERS-1 SAR imagery. Other field preparation activities in early spring, for instance, ridging or seedbed preparation, can also be monitored with well chosen multi-temporal ERS-1/2 data series. Thus, even before crops emerge, ERS backscattering signatures can be used to estimate crop acreage for various groups of crops.

This paper describes the results of an exhaustive study on multi-temporal ERS-1 signatures of the 94/95 fall, winter and spring period for identification of tilled fields in the UK Driffield area. The work has been carried out as a contract study #10653-94-12 F1ED ISP NL for the MARS Project of the Joint Research Centre of the European Commission.

2. METHODOLOGY

In this section, we shortly discuss the relevant theoretical background of microwave backscattering in order to be able to explain expected phenomena and trends in ERS-1 backscattering signatures of bare and vegetated agricultural fields, with an emphasis on bare soil and fields with partial vegetation covers. An advantage of this approach is that we can resort to rather simple models, which are easily implemented for forward simulation, and which allow conditioned inversion for quantitative analysis of signatures.

Microwave backscattering from an agricultural field depends on the physical and geometrical characteristics of the crop canopy and the underlying soil. A simplified model for the overall backscattering coefficient from vegetation can be given as (Attema & Ulaby, 1982):

$$\sigma^0_{\text{total}} = \sigma^0_{\text{canopy}} + \tau_1\sigma^0_{\text{soil}} + \tau_2\sigma^0_{\text{interaction}} \quad (1)$$

In (1), σ^0_{canopy}, σ^0_{soil} and $\sigma^0_{\text{interaction}}$ are the various contributions to the total backscattering coefficient of the canopy, soil and interaction components of the target. The transparency coefficients τ_1, τ_2 depend on the physical characteristics of the crop canopy and the frequency and polarization of the radar instrument. For the ERS-1 configuration we tend to neglect the term $\tau_2\sigma^0_{\text{interaction}}$ since most observations can be explained with the thus simplified model.

It follows from equation (1), that at the time in the growing season when all crops are fully closed, crop separation in backscattering intensity data should be based on their characteristic σ^0_{canopy}. In other studies using ERS-1 data (e.g. Schotten *et al*, 1995), it has been shown that crops can be separated in specific classes, such as grass, grains and broad leafed crops on the basis of their mid-season backscattering coefficients. Seasonal signature analysis for more than one year shows the potential to discriminate within these crop classes as well, in a repetitive, calibrated fashion (Borgeaud *et al*, 1995). However, discrimination between such crop classes as winter wheat and winter barley, and potato and sugar beet is only possible after the canopies have completely developed (beginning of July). In the period of crop emergence (April-June), there is considerable confusion between crop types. Referring to equation (1) again, it is obvious that this is related to a wide range of crop specific transparency coefficients τ_1, τ_2 (depending on variable vegetation emergence) and the characteristic seedbed structures in which the crop are planted (which influence σ^0_{soil} and $\sigma^0_{\text{interaction}}$).

Random bare soil

Backscattering from bare soil is governed by the geometry of the soil surface and the dielectric constant of the soil material at the surface (Ulaby *et al*, 1986). The surface geometry of agricultural fields reflects the applied soil tillage, which is related to crop specific land preparation activities, and subsequent surface erosion events.

Microwave backscattering from rough (soil) surfaces has been subject to extensive modelling research. We choose a simplified model of the type

$$\sigma^0_{\text{soil}} = f(\varepsilon)g(\sigma, \rho(\xi, \ell)) \quad (2)$$

In (2), $f(\varepsilon)$ is a function describing the dependency of σ^0_{soil} on the dielectric constant ε of the soil material (which, in turn, depends on soil physical characteristics and soil moisture content), and $g(\sigma, \rho(\xi, \ell))$ is a function describing the dependency of σ^0_{soil} on the geometric characteristics of the soil surface (with σ the rms-height and $\rho(\xi, \ell)$ the surface auto-correlation function). Recent examples of models which are in accordance with (2) are the semi-empirical models described by Oh *et al*, 1992 and the theoretical first order integral equation method (IEM model) by Fung *et al*, 1992.

Equation (2) implies that the backscattering sensitivities to varying geometric parameters and dielectric constant are separable as,

$$\frac{\partial\sigma^0_{\text{soil,dB}}}{\partial\varepsilon} = \frac{\partial f_{\text{dB}}(\varepsilon)}{\partial\varepsilon} \quad (3a)$$

and

$$\frac{\partial\sigma^0_{\text{soil, dB}}}{\partial(\sigma, \ell)} = \frac{\partial g_{\text{dB}}(\sigma, \rho(\xi, \ell))}{\partial(\sigma, \ell)} \quad (3b)$$

Thus, it is assumed that for all randomly rough surfaces, the sensitivity to the dielectric constant is equal. This roughly translates into equal sensitivity of all bare fields to soil moisture changes.

Row patterns

For agricultural surfaces which are tilled in a row-wise fashion, the surface roughness spectrum is no longer isotropical. It is well known that soil surfaces with a distinct row pattern have significantly different backscattering coefficients when viewed from different directions (Beaudoin, 1990). A theoretical model for regularly perturbed surfaces used in this study is described in Ulaby *et al*, 1986. In this model, local randomly rough surface backscattering intensities in the perturbed plane are integrated incoherently over the spatial period of the perturbation.

Vegetated surfaces

The overall backscattering coefficient for vegetated surfaces involves the terms σ^0_{canopy} and $\tau_1\sigma^0_{\text{soil}}$ (neglecting $\tau_2\sigma^0_{\text{interaction}}$). It is obvious that the variability in σ^0_{soil} is masked by the presence of the vegetation layer, but might still be discernible in the backscattering signal if τ_1 is sufficiently large. In principle, we should be able to use the reduced sensitivity to soil dielectric change for vegetated fields

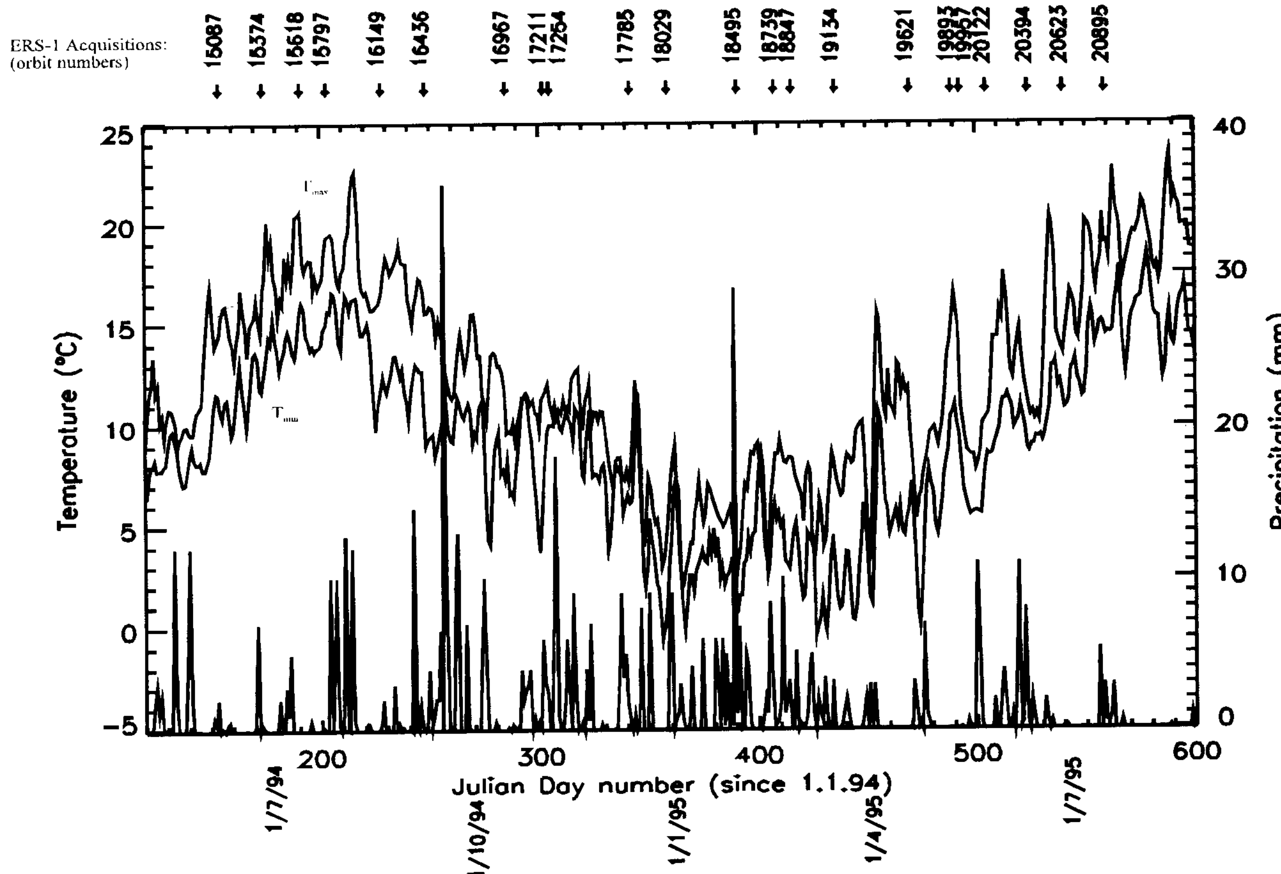

Figure 1. Percipitation and temperature profiles during ERS-1 acquisition period over the DRIF site.

in further crop delineation, especially in the spring season.

Trend simulation and model inversion

Backscattering models are of particular interest in so-called scenario simulation. With scenario simulation, the influence on the backscattered signal of expected cropping and tillage practices, crop development and surface processes and external conditions (for example, rain, frost) can be predicted. This type of forward simulation is of particular importance in the data selection procedure, e.g. to determine the expected dynamic range in the image (and compare this with quick look products), to check the influence of meteorological conditions on a data series, etc.

Model inversion can be used in support of class definition. For instance, a specific difference in backscattering coefficients between two (supposedly bare) fields can be used to estimate relative differences in rms-height, and if one of the fields is known, the absolute "roughness classes" and, hence, the tillage type.

3. MATERIAL

ERS-1 SAR data

For the study a set of 21 ERS-1 PRI images was used spanning the period between June 4, 1994 and July 14, 1995. During this period, ERS-1 was in three different orbital phases (the geophysical phases E and F and the "normal" multi-disciplinary phase G). The Great Driffield site (DRIF), which has is centre at 54°07' N and 0°31' W was covered by several adjacent tracks in the phases E and F and by two adjacent tracks in phase G. The analysis was concentrated in an area for which both ascending and descending node data could be acquired. Temporal resolution varied between 4 days (A/D node combination in May 1995) and 54 days. The latter, unfortunately, spanned the crucial spring period February 21 to April 16, 1995. This was due to the fact that 2 of the 3 ordered scenes for March were not acquired and the other one (of March 13) turned out to be unusable.

Ancillary data

The data analysis is supported by a range of ancillary data sets that are either part of the MARS' Agricultural Information System (AIS) or collected in the framework of the study. The first category consists of an extensive set of (daily) meteorological parameters for the DRIF site and crop acreage information of the period 1991-1994 (based on SPOT data and field surveys). In figure 1, temperature and precipitation records are plotted for the ERS-1 acquisition period. The acquisitions are indicated with their respective orbit number on top of the graph.

Additional activities under the study contract included the collection of a map data base (topographic maps at scale 1:25,000), the soil map, and the results of two dedicated field surveys in February and April 1995. Ground truth comprises crop type and tillage direction for more than 700 fields and detailed measurement of surface roughness and soil physical properties of a subset of these fields (20).

4. RESULTS & DISCUSSION

In figure 2 we have plotted signatures for all fields that evolve over time to the respective crop classes in the 1995 season. The line and error bars (one standard deviation) is for the group of fields that become wheat (WWH) fields. Error bars for the other crop classes are not shown, for reasons of clarity, but are, in general, somewhat smaller than that for the WWH class.

The number of fields that contribute to the average signatures in figure 2 ranges from 10 for 1995 sugar beet to 167 for 1995 winter wheat fields. Note that the averaged signatures still contain trends that are due to (1) cultivation direction effects, (2) local topography (3) local incidence variation and (4) unresolved misregistration errors. The analysis of the influence of those factors is not discussed in this paper, but we can state here that especially errors introduced by factors (2) and (4) affect the classification results in an adverse way.

A cluster analysis of the backscattering signatures in figure 2 and similar figures (for other crop sequences) has lead to several general conclusions:

- The dynamic range in single date summer imagery is much larger than during the fall and winter. The available spring data shows an increase in dynamic range again. Little information is gained from data between October and January.

- From December and onwards, there is a good separation between winter crops and future spring crops. This trend is consistent until February, with the exception of the January 27 data for which backscattering coefficient are affected by a snow cover. Apparently winter ploughing occurs only in the period late October to December.

- Signatures dramatically change in the period end of February to early June, reflecting both spring preparations for and emergence of the various spring crops and the development of the winter crops canopies. Already in mid-April, some winter rape (RAP) can be distinguished from winter cereals. Also potato (POT) can be separated from those spring crops that require smooth seedbeds (sugar beet (SBT), peas (PEA), spring cereals (SPC), spring rape seed (SPR)). This is because POT fields are prepared later and are planted in a ridged up seedbed. This distinction is less obvious in the May data. Later in the season, SPR and SPC are following the trends of their winter type counterparts, but obviously shifted in time.

- Both levels and spread in backscattering coefficients for winter cereals are similar in the 1994 and 1995 summer periods. Overall levels for the various other crops are also in the same order for the same period. This seems to suggest that signatures are indeed crop class specific, thus supporting claims to use backscattering signatures in a unsupervised classification approach.

- The spread in the WWH and winter barley (WBA) data increases after May, which is most likely related to crop phenological effects. We have not been able to separate WWH and WBA.

- Based on (late) summer signatures only, it is not possible to separate winter cereals from spring cereals.

- The total backscattering variation attributed to soil moisture is in the order of 6 dB (between a maximum October 30, 1994 and a minimum on April 16, 1995). This suggests a sensitivity of the ERS-1 instrument to soil moisture of 0.25 dB/vol%.

- The use of meteorological data allows us to predict signal variation quite accurately, except in the summer season. Soil wetness induced signal variation, however, is still obvious in the summer season even for fully developed crops.

Overall, figures of the type of figure 2 show interesting trends and various possibilities for separating a range of crop types. Based on these figures we have, for instance, developed a technique to combine four images in a single byte image that displays class separation based on backscattering signature variation.

With the ground truth on crop types, we have assessed the performance of a simple classification algorithm based on various image combinations. We find accuracies of up to 85% for the major crop types. However, our results are sometimes severely affected by misregistration, especially for smaller fields and when ascending/descending combinations are used.

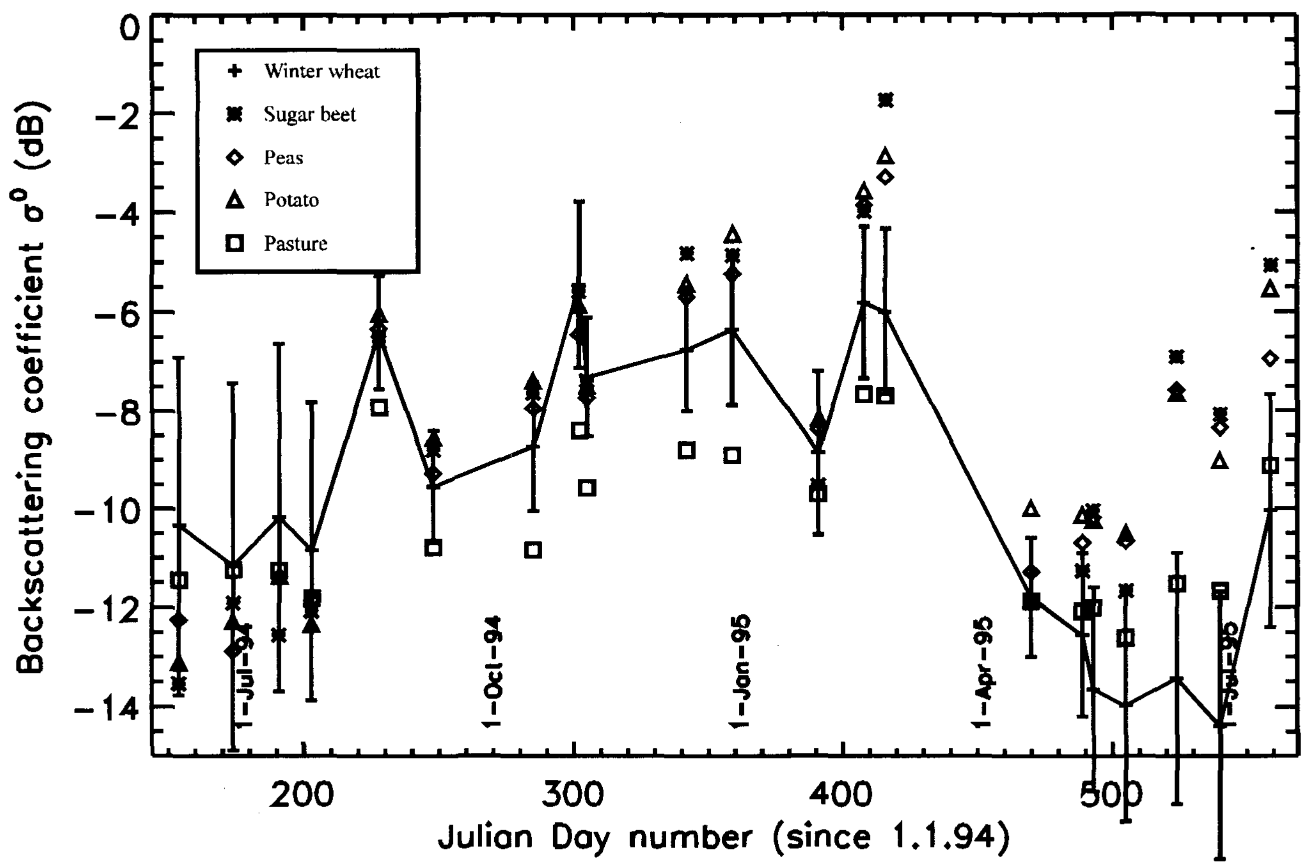

Figure 2. Averaged ERS-1 backscattering signatures for fields that were labeled as winter cereals (WIC) in the 1994 SPOT image and evolve to the crop classes in 1995 (indicated by the labels).

This is due to the fact that we have not applied proper geocoding with digital elevation models (only a tie-point warping was performed). We expect a significant improvement in classification accuracies when geocoding is applied. In comparison with classifications results based on SPOT data, we are optimistic about the possibility to obtain similar accuracies based on ERS-1 data alone, and probably better in areas for which SPOT data acquisition during the growing season is cumbersome.

5. CONCLUSIONS

We have presented a pre-operational technique to use ERS-1 SAR backscattering signatures in a crop discrimination exercise. We have shown that especially signatures from the period February-May enhance the possibility to separate classes due to the effects of crop specific tillage on the backscattering coefficient.

The methodology is rather straightforward. It's implementation as an operational technique sets some requirements for the SAR data delivery:

- SAR acquisition planning must be carried out well in advance. This implies a stable orbit scenario and a guarantee that pre-ordered data will also be acquired.
- For an increased site coverage, the possibility to acquire ascending/descending node combinations seems to be most appropriate (especially if geocoding is performed). A check of site coverage for the 60 MARS sites shows that, although the areas are only 40 by 40 kilometers in size, full A/D coverage (with only two images) is only the case for 21 of these (e.g. none in France or Spain!).
- Floating scene ordering would significantly improve A/D coverage (even if floating would be restricted to the node numbers used for ERS frame delineation). Optimum A/D coverage would also enable the selection of larger sized sampling areas (up to 60 by 60 km^2).
- Before actual ordering, the user should be able to screen quick-look data products. Quick look analysis would be supported by available meteorological data and model knowledge to estimate expected dynamic range. Quick look data might be usable for rough acreage estimates as well.

- In general, more than one ERS image is necessary to produce reliable estimates. Thus, the methodology should be highly automated. Also, pricing for basic SAR products should not be much above those of the current ERS products (i.e. RADARSAT's proposed prices are too high!).

Note that the possibility to use backscattering signatures in a calibrated repetitive fashion allows these to be used in an unsupervised classification procedure, which can be steered with model knowledge and environmental conditions. Furthermore, additional knowledge on backscattering behavior can be built into relevant classification algorithms. Also, new SAR instruments with additional system options (i.e. frequency, polarization, or incidence angle) can be easily integrated. Thus, the methodology is evolutionary, rather than static, as in the case of the current methodology based on optical data.

6. ACKNOWLEDGMENTS

This study has been carried out under contract #10653-94-12 F1ED ISP NL for the MARS-AIS Project of the Institute for Remote Sensing Applications, Joint Research Centre of the European Commission.

The authors would like to credit Dr. Edmond Nezry and Mr. Iwan Supit of the JRC for supportive actions and discussion. Field survey work was carried out in cooperation with Vissers Data Management (VDM) of Wageningen, the Netherlands.

7. REFERENCES

Attema E.P.W and F.T. Ulaby, 1978, Vegetation modelled as a water cloud, *Radio Sci.*, **13**, 119-124.

Beaudoin A., T. le Toan and Q.H.J. Gwyn, 1990, SAR Observations and Modeling of the C-band Backscatter Variability Due to Multiscale Geometry and Soil Moisture, *IEEE Trans. Geosci. Remote Sens.*, **GE-28**, 886-894.

Borgeaud M., J. Noll and A. Bellini, 1995. On the use of ERS-1 Multi-temporal SAR Data for Agricultural Applications, *Int. Geosci. Remote Sensing Symp. (IGARSS 1995) Digest*, 904-906, July 10-14, Florence, Italy.

Fung A.K., Z. Li and K.S. Chen, 1992. Backscattering from a Randomly Rough Dielectric Surface. *IEEE Trans. Geosci. Remote Sens.*, **GE-30**, 356-369.

Oh Y., K. Sarabandi and F.T. Ulaby, 1992, An Empirical Model and an Inversion Technique for Radar Scattering from Bare Soil Surfaces, *IEEE Trans. Geosci. Remote Sens.*, **GE-30**, 370-381.

Schotten, C.G.J., W.W.L. van Rooy and L.L.F. Janssen, 1993, Assessment of the Capabilities of Multi-temporal ERS-1 SAR Data to Discriminate between Agricultural Crops, *Int. J. Rem. Sens.* **16**, 14: 2619-2637.

Ulaby F.T., R.K. Moore and A.K. Fung. 1986, *Microwave Remote Sensing Active and Passive. Volume 3. From Theory to Applications*, Artech House, Norwood, Massachusetts.

ERS BASED EARLY ESTIMATION OF CROP AREAS IN EUROPE DURING THE WINTER 1994/1995

[1]Edmond Nezry, [1]Giampiero Genovese, [2]Gaute Aa. Solaas, [2]Sylvie Rémondière

[1] JRC/IRSA/AIS, TP440, 21020 Ispra (VA), Italy
Phone: +39-332-785449; e-mail: edmond.nezry@jrc.it
[2] ESA/ESRIN/Data Utilisation Section, Via Galileo Galilei, 00044 Frascati (Roma), Italy
Phone: +39-6-94180609; Fax: +39-6-94180632;
e-mail: gaute.solaas@mail.esrin.esa.it; sylvie.remondiere@mail.esrin.esa.it

ABSTRACT

This paper outlines the operational feasibility of very early ERS SAR based acreage estimation of non-cultivated terrain (set-aside, fallow, bare soils) and economically important crops, already during the winter season. This experiment has been carried out in a pre-operational real-time environment (rapid data order, acquisition, delivery, processing and exploitation). Its results have been used as a support to the Rapid Estimates of the European MARS (Monitoring of Agriculture with Remote Sensing) project in March 1995, before the first optical images could be acquired. They are confronted here with the first SPOT based estimates from the MARS project, obtained two months later.

I. INTRODUCTION: TOWARDS VERY EARLY CROP ACREAGE ESTIMATION

Crop areas estimation, as early as possible in the agricultural season, is a very important issue in the framework of remote sensing programs supporting agricultural policies. In particular, the MARS project includes a Rapid Estimates action fully dedicated to this task.
Nevertheless, as early as in the winter, the application of remote sensing to crop identification and crop areas estimates in Europe is a virtual reality problem, in the sense that no or very low agricultural vegetation cover is actually present on the ground. As a consequence, during most of the winter, agricultural targets are principally the soils on which crops will grow later on. Thus, it is generally not possible to identify directly crop species during winter, neither from field examination, nor from remote sensing image analysis.
For this reason, agricultural monitoring in the MARS project is carried out based on optical spaceborne imagery acquired during the growing season, when weather conditions become favourable and crops start developing their plant structure. As a result, the first MARS crop areas estimates are not available earlier than May.

II. AN APPROPRIATE METHODOLOGY BASED ON THE ANALYSIS OF ERS WINTER SERIES

In this context, it becomes useful to consider the specific sensitivity of the ERS SAR to important soil properties, such as surface roughness and moisture content. These properties of soils as well as their evolution over time are not casual, as far as agricultural surfaces are concerned. Therefore, a methodology has been designed, based on the experience acquired from previous research regarding: the physical modelling of C-band SAR backscatter [1], the influence of meteorological effects on the ERS radar cross-section over time [2], and the content of agricultural information [2-3] in ERS time series.
To discriminate between non-cultivated/cultivated surfaces and to identify the major crop types, this methodology exploits the causal relationships existing between soil properties and crop cultivation. It aims at an agriculture oriented understanding, interpretation and exploitation of the ERS time series, combining appropriately solid multi-disciplinary knowledge regarding the following topics:
- Agriculture and agronomy (crop calendars, tillage practices, and phenology of crops). General knowledge of agricultural practices and crop calendars at the site scale (40x40 km) provide the interpretation clues for the identification of the most important crop types [3].
- Radar remote sensing, with emphasis on the physics of interaction between the ERS incident C-band wave and natural media such as soils and vegetation. The sensitivity of the ERS SAR signal (radiometry, and to a lesser extent, texture) to soil roughness [2-5] at the beginning of the agricultural season is of particular importance to achieve complete detection of laboured land. From February on, volume diffusion effects observable on the first growing crops [4-7] are also exploited.
- Image processing, for both, the specific aspects of SAR image processing, and the statistical aspects of classification.
In addition, the methodology emphasises the use of application-relevant image information only, in order to ensure robustness to the disturbing effects of meteorological factors on the ERS radar cross-section over time.

III. PRACTICAL IMPLEMENTATION ASPECTS

In practice, the processing of the ERS time series is carried out in 5 steps:

1) Specific SAR data processing:
For all of the ERS PRI images, the following steps are performed:
- radiometric correction for ground range sampling (on top of the calibration procedure applied by the ERS Processing Facilities on PRI images [8]),
- adaptive speckle filtering [9],
- and accurate co-registration

2) Transformation of the time series (at least 3 acquisitions per-site, for topological correctness) into 3 synthetic channels, as uncorrelated as possible between each other, specifically designed to carry the information which is useful to our specific application.
Classical decomposition into uncorrelated synthetic channels using techniques based on Principal Components Analysis are discarded, mainly because these

techniques generally hinder further interpretation, either in terms of physical considerations on the origin of the image reflectivity, or of historical evolution in a time series.
Moreover, in order to extract selectively the physical and historical information relevant and meaningful to the actual application, we designed the following transformation, where we compute, for every pixel:
a) The mean backscattered amplitude during the period of observation ("backscatter" channel);
b) The range of radar cross-section variation during the period of observation ("variation" channel);
A previous study [2] showed that these first two channels provide a representation, in which urban, forest, grasslands/bare soils, and agricultural themes can already be separated using ERS time series. Another advantage of this representation is that it filters the disturbing effect of changes in meteorological conditions (temperature, soil moisture, etc.) on an ERS time series, which are responsible for a general ensemble modulation of about 2 to 4 dB (according to the site and in temperate European countries also to the season) of the temporal signatures [2] of all but the urban themes.
c) The date when the backscattered amplitude is maximum ("history" channel). For winter SAR observations, this third channel provides us with useful information regarding field preparation. Knowing from past experiments [2] that field labouring practices result in a very strong increase of ERS SAR signal (up to more than 10 dB), whose effect remains visible for a timeframe of about one month [2], this third channel provides an additional discriminator for crops identification, in relation to the knowledge of crop calendars provided that, as it is generally the case at the test-site scale, all fields dedicated to a given crop type are prepared at the same time. For some crops for which soil preparation took place a long time before the beginning of ERS observation (summer or early fall), crop phenology begins to play also a role which is registered by this channel as a maximum ERS SAR signal at the end of the observation period (February), when the dense agricultural vegetation cover exceeds 20-50 cm (cf. rape seed in the Chartres example), as observed and modelled in the literature [e.g. 5-7].
These synthetic channels have the main advantage to provide us with a understandable picture of the causes and of the history of the ERS radar cross-section of agricultural targets during the observation period.

3) Spatial segmentation is then carried out through isodata clustering [10] of these synthetic channels. This is a statistical method which can be regarded as one of the less bound to hypotheses, due to its statistical objectivity and impartiality.

4) The final crops (or group of crops) classes are identified through deductive interpretation of the synthetic channels using simultaneously general knowledge regarding agriculture (main crop types present on the site, crop calendars (e.g. Fig.2), tillage practices, crops phenology [e.g. 11,12]), physics (interaction wave/ medium), and statistics (examination of the structure of the clusters). In this way, a classification is obtained by recombination of the statistical clusters into well identified crops and land-use classes.

5) Detection and separate classification of the structural elements [9] (urban areas, main roads, rivers) improves consistently the spatial accuracy of the final result. Vector masks of forested/urban areas can also be used, either when statistical confusion remains between forested areas and some types of agricultural crops (cf. field peas in the Chartres example), or to exclude non-agricultural surfaces from the final classification.

IV. OPERATIONAL ASPECTS

Since operationality can not be demonstrated in controlled "laboratory" experiments (using old data of past, i.e. "perfectly known", situations), a real-time pre-operational ERS experiment was decided (ESA project PE-FRNE), to provide very early surface estimation of non-agriculture land (set-aside, fallow, bare soils) and economically important crops (winter cereals, etc.) over 3 very different test-sites of the MARS project during the winter of 1994/1995.

Although the SAR instrument had a very low priority within ERS-1 "Phase F" (Geodetic phase), from 15 Nov. 1994 to 18 Feb. 1995, ESA managed to acquire 19 frames (Fig.1) over the three test sites:
1) Albacete (Spain): 4 dates, 5 frames,
2) Bologna (Italy): 7 dates, 7 frames,
3) Chartres (France): 4 dates, 7 frames.

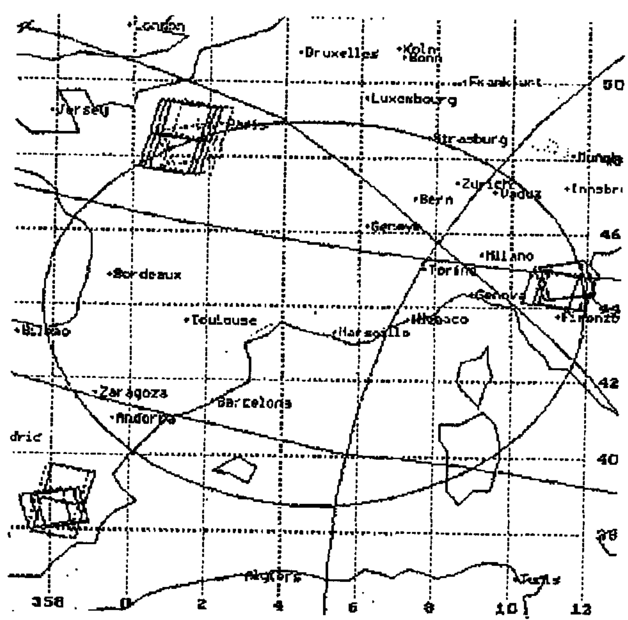

Figure 1: ERS-1 acquisitions (Phase F; 19 frames; 15 Nov. 1994 - 18 Feb. 1995) over the 3 test sites of Albacete (Spain), Bologna (Italy) and Chartres (France).

The ERS SAR PRI data were delivered within a delay of 4 to 20 days (average delay of 10 days), meeting the time constraints requirements for data delivery for the Rapid Estimates Activity of the MARS project.

The exploitation (post-processing, interpretation, and classification) of the ERS SAR data was conducted at the AIS, and concluded in March 1995. Classifications were send to ESA in April 1995 to take date.

Validation was carried out afterwards, confronting our acreage estimates of the sites, with the corresponding first MARS Rapid Estimates for 1995, produced in

May. These estimates arise from SPOT-based computer-aided classifications, using also ancillary information such as: last year classifications, ground survey, farmers declarations, statistical trends, etc.; estimated global accuracy was about 85% in 5 years of operation.

V. RESULTS

V.1) Chartres (France):

This site is located within one of the richest agricultural areas in Europe, and its monitoring is of particular importance for the estimation of cereals (mainly wheat) production in Europe. The site is shown in the multi-temporal colour composite image in Fig.3 (calibrated, filtered and co-registered ERS-1 images). Even if most of the local temporal variations in radiometry arise from the effects of agricultural activity, the signal level unbalance among the acquisitions giving an aesthetic colourful visual impression should be attributed to the effects of varying environmental conditions. It is visible that the site is hilly, with altitude variations up to about 400 m, but generally gentle slopes not exceeding 5º.
The synthetic channels carrying the selected information are produced on a per pixel basis, and shown in Fig.4. Together with the knowledge of local agricultural practices and calendars [12] (Fig.2), these synthetic channels provide the interpretation clues for the identification of ploughed field, bare soils and major crop types.

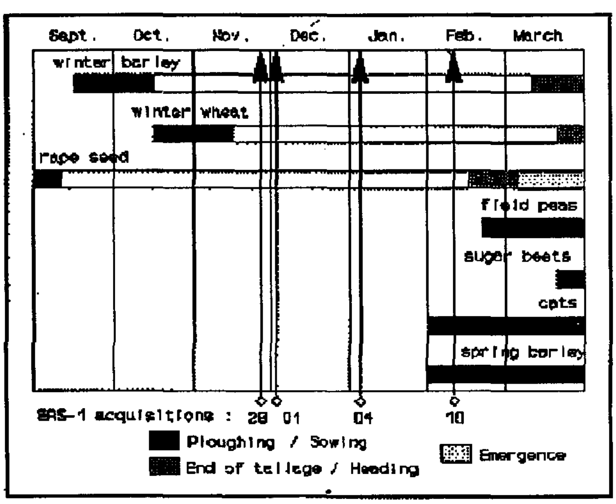

Figure 2: Chartres test-site: winter crops calendar and ERS acquisitions (winter 1994/1995).

The clustering is carried out using the three channels shown on Fig.4. Then, classes are gathered according to the conclusions of the analysis of both the synthetic channels and the structure of the clusters. Built-up areas, main roads and rivers are extracted and classified separately. Finally, a vector mask (urban/forest) is applied to the classification to discriminate other summer crops (i.e. field pees) from the forest.
The final 8-classes ERS classification is presented in Fig.5, where:
- non-cultivated soils/low natural vegetation are black;
- forest is green;
- wheat, on soils prepared before November, is red;
- wheat, on soils prepared early in November, is pink;
- other winter cereals are light grey;
- rape seed is yellow;
- soil prepared in February for summer crops, as well as field peas and fodder beets, are dark grey;
- urban areas, roads, and non arable land are light blue.

Examination of the classification shows a good robustness to the relief characteristics of this site.
The comparison between surface estimates retrieved from this ERS classification, and the SPOT based results is presented in Table 1. Since the classes identified using by the two classifications are slightly different, classes have been grouped into land-use families. Table 1 shows that good agreement, regarding the major land-use, is found between the two classifications.

Crops (areas in ha.)	ERS-1 4 dates from 28/11/94 to 10/2/95	SPOT 2-dates 4/3/95-5/5/95 derived classif.
Non-cultivated	14225	11499
Winter wheat	68178	70622
Other cereals	5357	10015
Rape seed	12834	11360
Summer crops	24368	25784
Non-agriculture	35038	30720

Table 1: Chartres test site. Comparison of early crop acreage estimates obtained using ERS (March 1995) and SPOT (May 1995) multi-temporal data.

V.2) Bologna (Italy):

This test site includes the major part of Emilia-Romagna, the richest Italian agricultural region. It is an almost flat plain, densely populated, located between the Po river in the north and the Apennine mountains in the south.
The colour composite shown in Fig.6 (calibrated, filtered and co-registered ERS-1 images), illustrates the complexity of landscape and land-use fragmentation (small agricultural fields, numerous rivers, important roads, cities and villages) of this site. On this site, the differences in soils (dejection from the Appenine, alluvial deposits, etc.), as well as the combined effects of winter rainfalls and agricultural activity, modify spatially and temporally the physical properties of terrain, resulting in a very colourful ERS multi-temporal image. In this case, information selection into the synthetic channels described above, simplifies image interpretation for crops identification, and improves the statistical result of a clustering whose purpose is the spatial segmentation of crop cultivations.
The final 9-classes ERS classification is presented in Fig.7, where:
- non-cultivated soils and fallow are brown;
- natural vegetation, orchards/vineyards are dark green;
- rice fields are black;
- winter cereals are red;
- sugar beet are pink;
- potatoes, and also corn fields, are light green;
- other summer crops are yellow;
- rivers and main roads are dark blue;
- built-up areas are light blue.

The comparison between surface estimates retrieved from this ERS classification, and the SPOT based results is presented in Table 2.

Crops (areas in ha.)	ERS-1 7 dates from 15/11/94 to 17/2/95	SPOT 2-dates 21/3/95-3/5/95 derived classif.
Non-cultivated	13029	13844
Rice	636	438
Orchards, etc.	23888	29280
Winter cereals	56139	43840
Sugar beets	23005	22295
Potato + maize	10463	10330
Spring crops	8729	7332
Non-agriculture	24109	32640

Table 2: Bologna test site. Comparison of early crop acreage estimates obtained using ERS (March 1995) and SPOT (May 1995) multi-temporal data.

Important differences regarding the two following themes can be observed:
- non-agricultural surfaces (over estimated in the MARS mask which includes part of the rice fields and spring cultivation, and has therefore been taken into account on a selective basis for the ERS classification),
- winter cereals due to overestimation of the MARS mask and to some confusion with perennial vegetation (orchards, vineyards, natural vegetation, etc.).

For all other crops, estimations show a good agreement.

V.3) Albacete (Spain):

This test site was chosen to evaluate our method on a site presenting some peculiar difficulties with regard to both geomorphology and agriculture. Most parts of the site are mountainous areas, with altitude variations from 200 to more than 1000 m. In addition, this site is poor in water resources and often affected by drought. More than one fourth of potentially arable land has been set aside in the last decade for low rentability. The major crops still cultivated in the area such as sunflower, maize and even barley require irrigation [11].
The colour composition shown in Fig.8 (calibrated, filtered and co-registered ERS-1 images), exhibits dominant grey tones, showing that meteorological conditions were almost constant (persistent drought) during the winter 94/95. The coloured areas are mainly due to the effects of tillage and irrigation. Mountain areas present important confusions due to the change in look angle and direction between ERS acquisitions.
The final 9-classes ERS classification obtained over this site is presented in Fig.9, where:
- non-imaged and masked areas are black;
- non-cultivated soils (set-aside/fallow land) are brown;
- forest (on mountain slopes) is dark green;
- vineyards and natural vegetation are light green;
- winter cereals (mainly barley) are orange;
- later cereals (e.g. spring barley) are red;
- sunflower (mainly irrigated) is light blue;
- corn fields (mainly irrigated) are yellow;
- urban areas are white;

Within mountain areas, the output of the clustering reflected the confusions due to the presence of strong relief, and it is clear that our classification procedure fails in these areas. Nevertheless, applying the mask used for the SPOT data on this site in the operational MARS activities, it is also clear that:
- the same classification problems are met in the same areas using optical remote sensing data;
- although the statistical definition of the clusters, performed at the scale of the whole site, is affected by the mountainous areas of the site, our classification procedure still performs successfully within areas which are flat or present limited relief.

VI. USER COST

The total user-cost of the project has been traced during the course of the experiment. This cost of about 16000 ECU (before taxes) can be split into three parts:
- Data cost: 9500 ECU for 19 ERS PRI frames,
- Manpower: 4600 ECU,
- Mortgage (equipment) and running costs: 1900 ECU.

It is worthwhile to note that now, in the operational ERS phase, for test sites chosen to coincide with ERS frames, data costs would be reduced by an average 35% per-site, and processing costs would be reduced by more than 50% per-site (much easier co-registration of frames on the repeat-pass orbit).

VII. CONCLUSION

This experiment shows that economically valuable ERS based estimation of non-cultivated areas and crop areas can be carried out operationally, very early in the agricultural season, using a methodology which is:
1) technically simple:
It requires only widely available state-of-the-art SAR data processing and data analysis methods. Moreover, good knowledge and understanding of SAR related physics, of SAR image processing, and of agriculture and agronomy, are required.
2) robust:
The selected ERS information relevant to our specific application is stored in the synthetic channels. This methodology proved robust to effects not directly related to the agricultural occupation of soils (environmental effects, soil types, etc.), to site-landscape complexity, and to geographical diversity.
3) direct:
The useful temporal characteristics of the agricultural targets are identified using only general SAR related physics and agricultural knowledge. They support an interpretation which is primarily based on a statistical analysis of the remote sensing data, and specifically oriented towards the identification of the agricultural themes of interest.
4) efficient:
As shown for Albacete, good performances are obtained for identification and area estimation of major crops and non-cultivated terrain, within a similar range of geomorphologic conditions, for which optical remote sensing is also successful. In addition, direct global comparison of the overall ERS signal level between acquisitions is already an indicator for important environmental conditions such as persistent drought.
5) competitive:
The total user-cost of such a project remains at a particularly competitive level, especially with the actual ERS-1/ERS-2 repeat-pass operational system.

ACKNOWLEDGEMENTS

The authors warmly thank Dr. G. Paci and Dr. J. Lichtenegger (ESA/ESRIN, Frascati, Italy), and Dr. G. Milillo (ASI/I-PAF, Matera, Italy), for their effective support during this project. Good methodological ideas are also due to Dr. G. Kattenborn (Univ. Freiburg, Germany). A debt of gratitude is extended to all the persons at ESA/ESRIN, ESA/ESOC, I-PAF, UK-PAF, JRC/IRSA (MTV, CEO units) who gave a hand, contributing to the success of this experiment. This work has been carried out under ESA project PE-FRNE.

BIBLIOGRAPHIC REFERENCES

[1] A.Beaudoin, T.LeToan, S.Goze, E.Nezry, A. Lopes, E.Mougin, C.C.Hsu, H.C.Han, J.A.Kong, R.T.Shin, 1994: "Retrieval of forest biomass from SAR data", Int. J. Rem. Sens., Vol.15, n°14, pp.2777-2796.

[2] G.Kattenborn, E.Nezry, G.DeGrandi, 1993: "High resolution detection and monitoring of changes using ERS-1 time series", Proc. of the 2nd ERS-1 Symp., 11-14 Oct. 1993, Hamburg (Germany), ESA SP-361, Vol.1, pp.635-642.

[3] H.G.Kohl, E.Nezry, M.Mróz, H.DeGroof, 1994: "Towards the integration of ERS SAR data in an operational system for rapid estimates of acreage at the level of the European Union", Proc. of the 1st Workshop on ERS-1 Pilot Projects, 22-24 June 1994, Toledo (Spain), ESA SP-365, pp.433-441.

[4] F.T.Ulaby, M.C.Dobson, 1989: "Handbook of radar scattering statistics for terrain", Artech House Inc., Norwood (MA), USA.

[5] U.Wegmüller, 1993: "Signature research for crop classification by active and passive microwaves", Int. J. Rem. Sens., Vol.14, n°5, pp.871-883.

[6] R.D.Martin, G.Asrar, E.T.Kanemasu, 1989: "C-band scatterometer measurements of a tallgrass prairie", Rem. Sens. of Environment, Vol.29, pp.281-292.

[7] H. Laur, 1989: "Analyse d'images radar en télédétection: Discriminateurs radiométriques et texturaux", Ph.D. dissertation, Univ. P. Sabatier, (France), 250 p.

[8] H.Laur, 1992: "ERS-1 SAR calibration: derivation of the backscattering coefficients in ERS-1 SAR PRI images", Technical Note, ESA/ESRIN, 17 p.

[9] A.Lopes, E.Nezry, R.Touzi, H.Laur, 1993: "Structure detection and statistical adaptive speckle filtering in SAR images", Int. J. Rem. Sens., Vol.14, n°9, pp.1735-1758.

[10] T.Lillesand, R.Kiefer, 1987: "Remote Sensing and Image Interpretation", Ch.10, John Wiley & Sons, Inc., New York, USA.

[11] G.Narciso, P.Ragni, A.Venturi, 1992: "Agrometeorological aspects of crops in Italy, Spain and Greece", EUR14124EN, Off. for Official Publ. of the EC, Luxembourg, 440 p.

[12] A.Falisse, 1992: "Aspects agrométéorologiques du dévelopement des cultures dans le Bénélux et les régions voisines", EUR13910FR, Off. for Official Publ. of the EC, Luxembourg, 212 p.

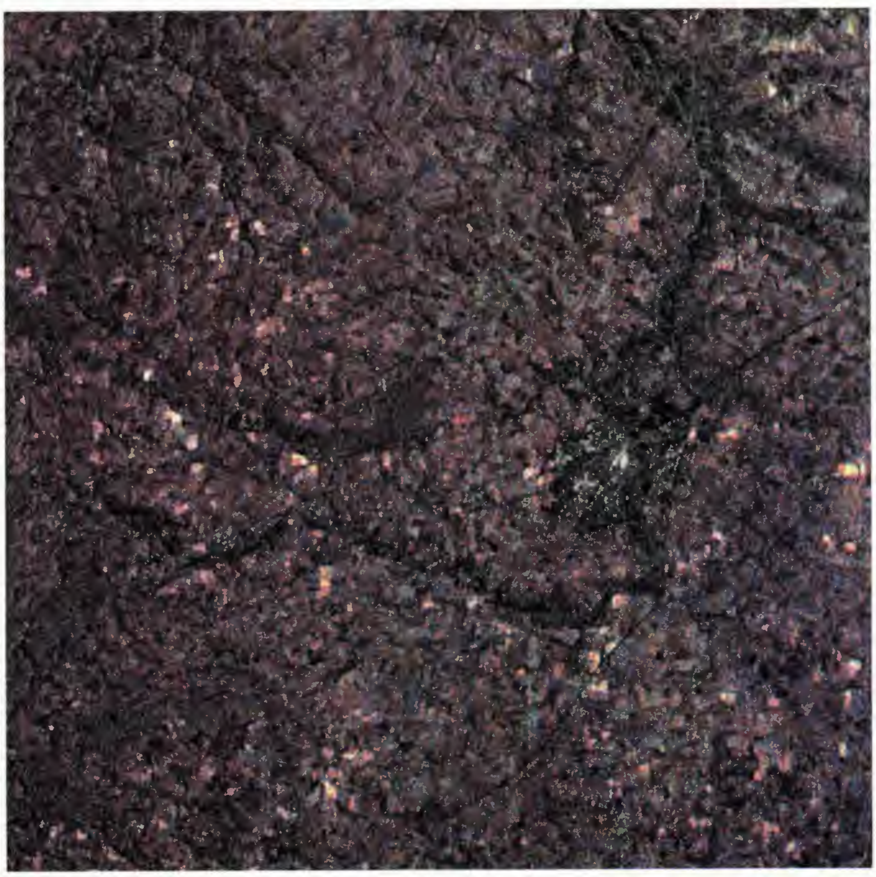

Figure 3: Multi-date ERS SAR imagery over the Chartres test site. Processed ERS-1 images: Nov.28 in red, Jan.4 in green and Feb.10 in blue.

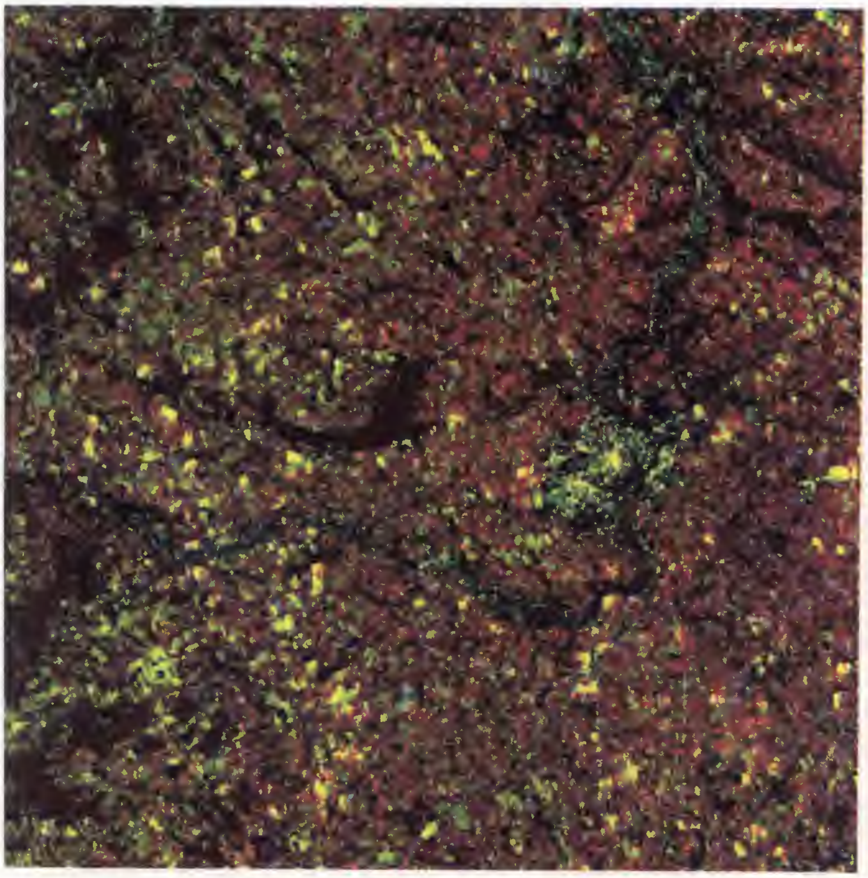

Figure 4: Chartres test-site. Synthetic channels, with the "backscatter" channel in red, the "variation" channel in green, and the "history" channel in blue.

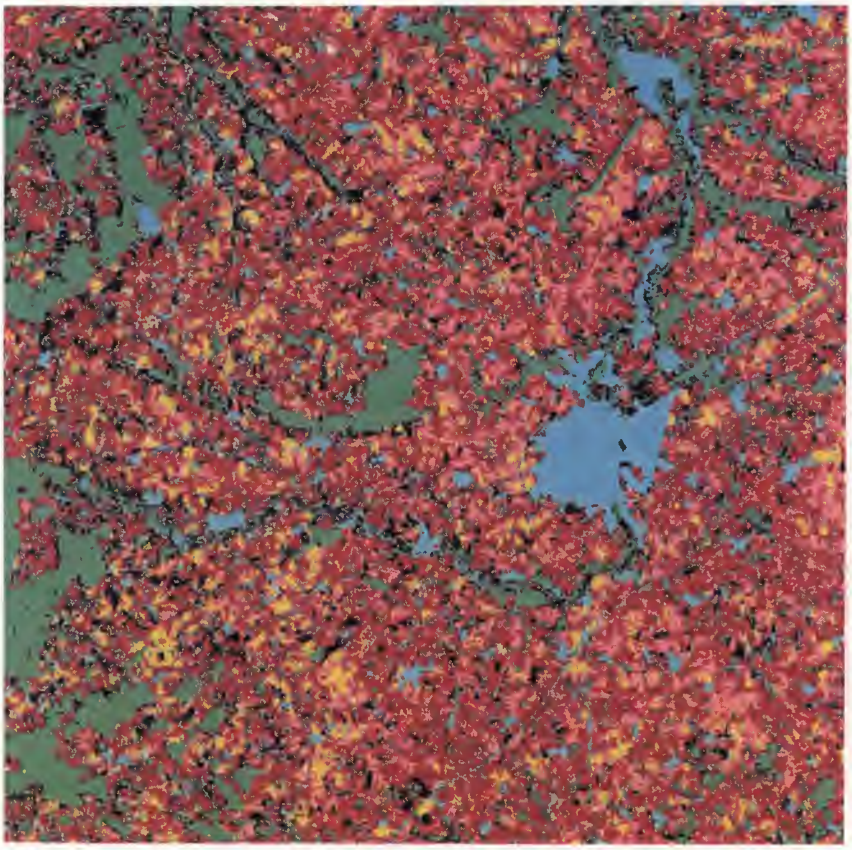

Figure 5: Final classification of the Chartres test-site (8-classes).

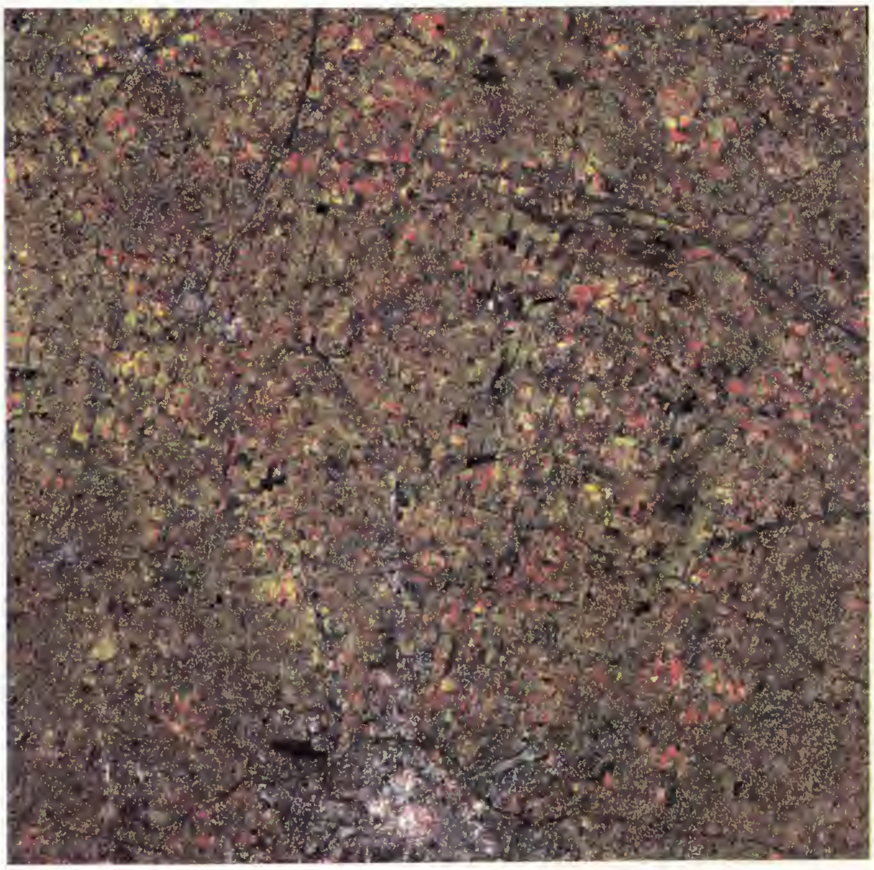

Figure 6: Multi-date ERS imagery over the Bologna test site. Processed ERS-1 images: Nov.15 in red, Dec.5 in green and Jan.11 in blue.

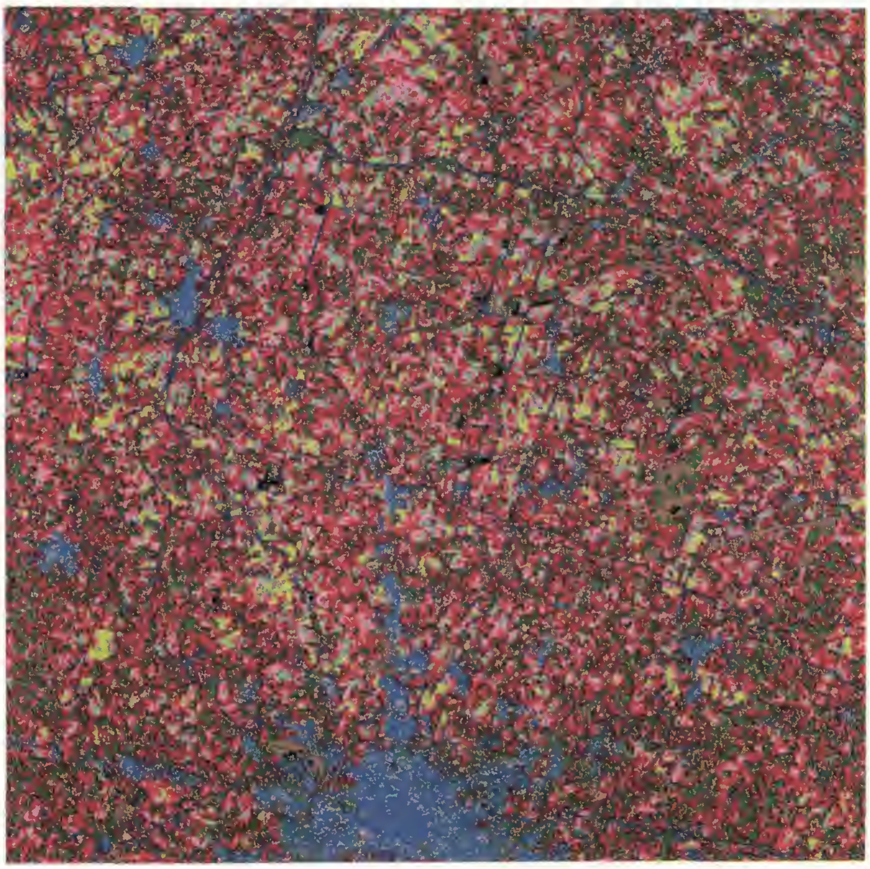

Figure 7: Final classification of the Bologna test-site (9-classes).

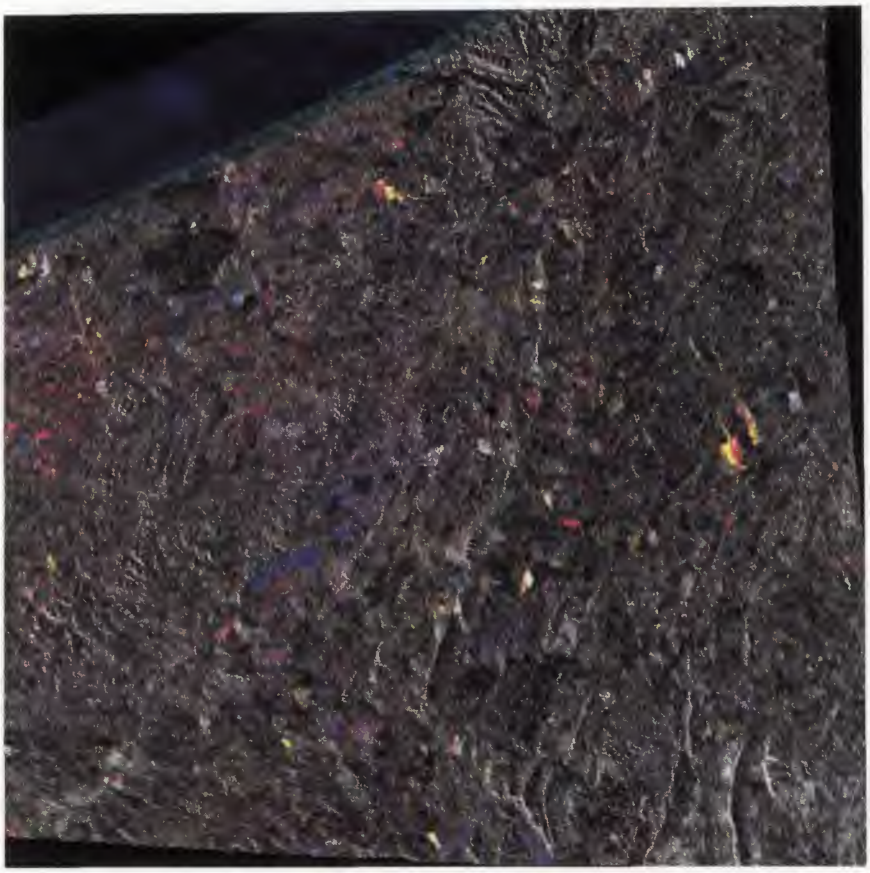

Figure 8: Multi-date ERS imagery over the Albacete test site. Processed ERS-1 images: Dec.6 in red, Jan.12 in green and Feb.18 in blue.

Figure 9: Final classification of the Albacete test-site (9-classes).

ERS SAR DATA FOR RICE CROP MAPPING AND MONITORING

J. Aschbacher[1*], A. Pongsrihadulchai[2], S. Karnchanasutham[2], C. Rodprom[3], D. R. Paudyal[4], T. Le Toan[5]

[1]European Commission-Joint Research Centre, TP441, I-21020 Ispra (VA), Italy
Tel: +39-332-78-5968, Fax: -78-5461, E-mail: josef.aschbacher@jrc.it
[2]OAE, Phaholyothin Road, KU Campus, Bangkok 10900, Thailand
[3]NRCT, 196 Phaholyothin Road, Bangkok 10900, Thailand
[4]DIP, SERD-RSL, GPO Box 2754, Bangkok 10501, Thailand
[5]CESBIO, Univ. Paul Sabatier, 31029 Toulouse, France

Abstract - The current study investigates the potential of ERS-1 SAR data for rice mapping and rice crop monitoring. The selected study area is located in Kanchanaburi province, West-Thailand. The rice growing area is irrigated, flat, homogeneously managed, and has large individual fields of at least one hectare size.

As regards rice mapping a digital classification based on multi-temporal, speckle-filtered ERS-1 SAR images was carried out to determine rice field acreage. The classification accuracy for rice fields is 89%. As regards rice crop monitoring the radar backscattering coefficient σ^o [dB] of rice fields was related to various phenological parameters on a field-by-field basis, such as plant height, plant moisture content, stalk diameter, leaf size, occurrence of standing water and crop yield. It was found that there is a good correlation between plant height and σ^o and between crop yield and σ^o, respectively.

The results are clearly pointing towards the operational application of the methodology and confirm that ERS-1 SAR data can be used for the purpose of rice crop mapping and monitoring. The use of radar data for rice monitoring is of particular interest because rice is mainly grown in tropical regions with quasi permanent cloud cover during the growing season.

INTRODUCTION

Rice is an important food crop. Two thirds of the world's population are living in Asia where rice is the prime source of daily food. Rice is also an essential source of income for many countries in the tropics, making it an important social, political and economic factor. Consequently, decision makers have placed the collection of information about the actual and predicted state of rice crops on the top of their political agendas. The two most interesting parameters to know are rice acreage and expected yield. Currently, the collection of this information is mostly based on interviews at the farmers or village level. The information gathering process is cumbersome, and sometimes unreliable information is given to Government authorities by the local people.

OBJECTIVES

The main objective of this study is to assess the usefulness of ERS-1 SAR data for the purpose of rice area mapping and crop monitoring, and to develop an optimum approach to achieve this objective. Recommendations shall be given towards the use of such data in an operational rice information & monitoring system.

STUDY AREA AND DATA BASIS

Study area

A study area of approximately 10x10 km size was selected in Kanchanaburi Province, West Thailand. The centre co-ordinates are 99.5 deg E and 14.0 deg N. The topography is generally flat, with a few single, steep limestone mountains. The rice growing area, however, is practically horizontal, with natural borders of only a few tens of centimetres height. Field management is similar over a large area, with field preparation, flooding, rice sowing and harvest taking place at almost the same time within the whole rice growing area. Individual fields are 1-2 hectares large. The fields are irrigated, and water supply is managed centrally. Therefore, the timing for field preparation and flooding is similar for all fields within the whole study area. The climate is humid tropical with seasonal monsoon rainfall from April to October [1].

* The work presented in this paper was carried out within the framework of the 'EC-ASEAN ERS-1 Radar Remote Sensing Project (ALA/ASN/91/28)". The project is funded by the European Commission (EC) with support from the European Space Agency (ESA) and the Association of South-East Asian Nations (ASEAN). In addition, the current project is supported by the Office of Agricultural Statistics & Economics (OAE) of the Thai Ministry of Agriculture and the National Research Council of Thailand (NRCT).

Data basis

Multi-temporal ERS-1 SAR data were available at eight acquisition dates, namely 22-Nov-91, 7-Oct-92, 24-Feb-93, 7-May-93, 11-Jun-93, 20-Aug-93, 29-Oct-93 and 3-Dec-93. Images were acquired by the Thai ERS-1 receiving station after April 1993 and processed to standard PRI format, whereas the earlier images were acquired and processed by the Indian receiving station. For the latter, image calibration was performed according to [2].

Within the whole area, ten sample areas of approximately ten hectares each were selected for detailed backscattering studies of rice fields. Extensive ground measurements were taken in parallel to ERS-1 data acquisitions during the main growth period of 1993 (August to December). Plant height, plant moisture content, plant density, number and size of leaves, stalk diameters, height of standing water were measured, together with more general observations regarding the state of the water/soil surface, state of plants, and weather at acquisition time [1]. The analysis of ERS-1 SAR data was further supported by aerial photographs and a high resolution optical satellite imagery taken by the Spot panchromatic sensor.

RICE PLANT GROWTH AND CROP CALENDAR

The current study deals with well irrigated rice fields. A typical rice growth cycle lasts between 120-180 days from planting to harvest, and varies with crop variety. There are three major growth phases, the *vegetative*, *reproductive* and *ripening phase*. After soil preparation rice fields are flooded. The *vegetative* phase starts either with direct sowing or transplanting in rows, and ends when plants have almost reached their maximum height of up to one metre. Plant height depends on variety. The *reproductive* phase starts when plants are flowering, and is followed by the *ripening* phase, when water is drained out, plants become drier and turn yellow, and the grains are ripening. The *reproductive* and *ripening* phase are constant for most varieties, and last about 35 and 30 days, respectively, while the length of the *vegetative* phase differs with variety. After harvest, a bare soil condition remains, sometimes with patches of standing water left [3].

In the current study area two harvests per year are common. The main growth period lasts from August to December, and a second crop grows from April to July. A typical value for crop yield in the study area is approximately 5-6 tons per hectare.

RADAR SIGNATURE OF RICE FIELDS

In ERS-1 SAR images, rice fields appear dark during the *vegetative phase* when the fields are flooded. During the *reproductive phase* radar backscattering increases and reaches a maximum in the *early ripening phase*. This maximum may plausibly be attributed to multiple radar reflections between vertical plant structures and the horizontal water surface at a growth stage when penetration to the surface is still possible. Later, during the *ripening phase*, the scattering from the volume of the canopy increases but penetration to the water or soil surface decreases leading to a slight darkening of the radar image [3,4].

DATA ANALYSIS AND RESULTS

According to the objectives of the study two issues were addressed, namely the use of ERS-1 SAR data for rice area mapping and crop monitoring, respectively.

Rice area mapping

Rice acreage can be retrieved from multi-temporal radar imagery making use of the unique backscattering signature of rice fields, which is significantly different from that of any other land-cover [1,3,5]. Fig. 1, as an example, shows an image taken on 6-Jun-93, where the rice growing area appears darker and can thus easily be discriminated from other land covers. A simple, pixel-based maximum likelihood classification was carried out, based on four Gamma MAP [6] speckle filtered radar images (6-Jun-93, 20-Aug-93, 29-Oct-93, 3-Dec-93). Ratio images (Jun/Dec and Oct/Dec) were included in the classification in order to compensate for mis-classifications of rice on the dark mountain back slopes due to topographic effects of imaging radars. The result of the classification is shown in Fig. 2. The classification accuracy for rice versus other land-use classes is 89%.

Figure 1: Multi-temporal ERS-1 SAR image of Kanchanaburi, W-Thailand. The ice fields are located in the centre of the image (dark).

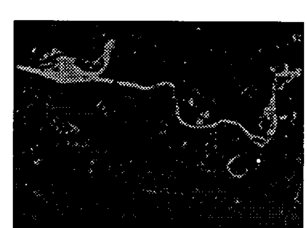

Figure 2: Rice area based on four ERS-1 SAR data acquisitions. Grey scale: rice (dark), water (bright), other land-use classes (black).

Rice Crop monitoring

Radar sensors have the potential to monitor rice plant growth regardless of cloud cover. An example of temporal radar signatures compared with rice plant height is shown in Fig. 3. The 'wind-disturbed' acquisition of 20-Aug-93 was substituted by two additional dates of the same growth cycle from earlier years (22-Nov-91, 7-Oct-92), where the growth pattern was similar to that of the 1993 cycle. Fig. 3 clearly shows a very similar trend between radar backscattering and plant height. A correlation between these two parameters is shown in Fig. 4. The correlation coefficient is r=0.77. Similar observations were obtained by [7], who reported correlation coefficients of r=0.98 between plant height and σ^o, however, based on 6 selected data pairs only.

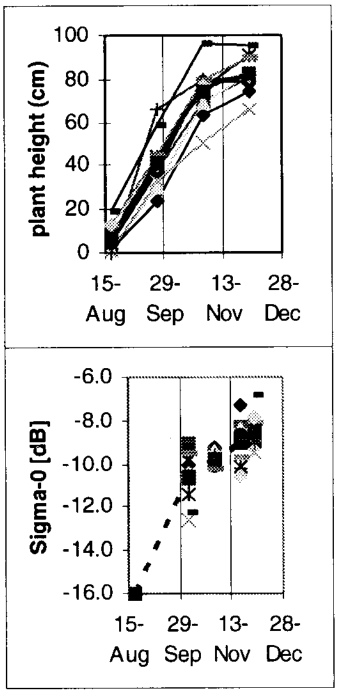

Figure 3: Rice plant height (top) and temporal radar signature (bottom) of ten rice fields in Kanchanaburi, Thailand (from [3]).

Further, a correlation between measured yield and σ^o values was carried out for the pre-harvest date 3-Dec-93. The fields were harvested 2-4 days later. The corresponding correlation is shown in Fig. 5. The correlation coefficient is r=0.87. This result, however, is, only preliminary because it was not verified with another data set due to lack of such data. Also, the sensitivity of radar backscattering is mainly related to the plant's total biomass, its moisture content and the plant's geometry, and grain yield may only be an indirect effect of these parameters.

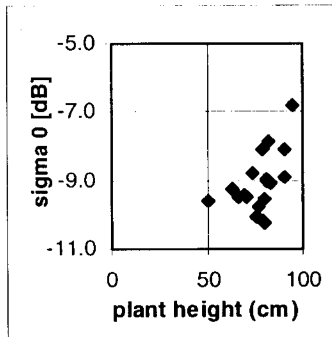

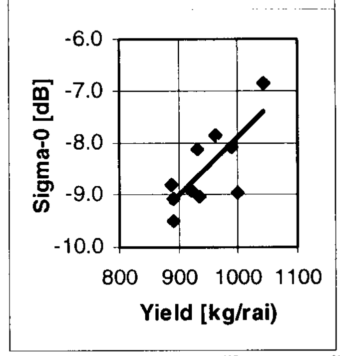

Figure 4 (top): Correlation between plant height and radar backscattering coefficient, including data from 29-Oct-93 & 3-Dec-93.

Figure 5 (bottom): Correlation between measured rice yield and radar backscattering coefficient, for the pre-harvest date 3-Dec-93.

CONCLUSIONS

Irrigated or flooded rice shows a very characteristic radar backscattering signature. In radar imagery, rice fields appear very dark during the flooded vegetative phase, and turn brighter during the reproductive and ripening phase. The dynamic range for σ^o is from -15 dB to -8 dB, and is thus larger than for any other agricultural crop. Radar imagery is therefore particularly suitable, also given the fact that rice crops can be monitored during the growth period which naturally coincides with high cloud cover.

In particular, the following conclusions can be drawn from the experience gained from this study and from related studies [1,3,4,5,7]:

<u>Rice area mapping:</u>

1. Multi-temporal ERS-1 SAR data is highly suitable for rice field mapping. The achieved mapping accuracy in the current study is 89% for rice fields against any other land cover.

2. At least three images should be available during the growth cycle. The optimum acquisition dates are during the flooded vegetative phase, at the end of the reproductive phase and shortly before harvest. An additional post-harvest image may be useful for better discrimination from other land cover classes in the surrounding.
3. The use of a pixel based standard maximum likelihood classifier is sufficient, although more sophisticated methods may yield slightly better results. Speckle filtering of the input data is mandatory.

Rice crop monitoring:

4. Multi-temporal ERS-1 SAR data is highly suitable for rice crop monitoring.
5. The radar backscattering coefficient is well correlated with rice plant height (r=0.77). Consequently, the use of radar data allows to determine the approximate stage of plant growth.
6. The radar signal shows a potential correlation with rice yield. However, this relation may be indirect, assuming that radar backscattering is more sensitive to parameters such as biomass, moisture and geometry of rice plants rather than grain yield itself.

The use of radar data for rice monitoring systems:

7. If an operational rice monitoring system is developed it is strongly recommended to include multi-temporal radar data as a prime data source.

REFERENCES

[1] J. Aschbacher and D. R. Paudyal, "Studies of rice fields in Thailand using ERS-1 SAR data", Proc. Natl. Conf. on ERS1/LANDSAT/SPOT Applications, Jakarta; 23-25 Nov. 1993, p. 9.3.1-9.3.9.

[2] D. R. Paudyal and J. Aschbacher, "ERS-1 SAR data calibration at the Indian National Remote Sensing Agency"; Asia-Pacific Remote Sensing Journal, Vol. 6, No. 2, Jan. 1994, pp. 117-120.

[3] J. Aschbacher, "Tropical Crops", chapter 6 in ESA-SP-1185 (Satellite radar in agriculture: Experience with ERS-1, Ed. M. Wooding et al.), ESA Publ. Div., ESTEC Noordwijk, November 1995, 71 pp.

[4] T. Le Toan, H. Laur and E. Mougin, "Multi-temporal and dual-polarisation observations of agricultural vegetation covers by X-band SAR images", IEEE Trans. Geosc. Rem. Sens., Vol. 27, No. 6, 1989, pp. 709-718.

[5] D. R. Paudyal, "An assessment of spaceborne radar remote sensing for monitoring of tropical agriculture", Doctoral thesis (unpublished), Asian Institute of Technology, Bangkok, Thailand, 1994.

[6] E. Nezry, A. Lopez and R. Touzi, "Detection of structural textural features for SAR image filtering", Proc. IGARSS 1991, pp. 2169-2172.

[7] T. Kurosu, T. Suitz, M. Fujita, K. Chiba and T. Moriya, "Rice crop monitoring with ERS-1 SAR: A first year result", Proc. 2nd ERS-1 Symp., Hamburg, 11-14 Oct. 1993, pp. 97-101.

ACKNOWLEDGEMENTS

The authors wish to warmly thank the researchers at the EC Joint Research Centre's Monitoring of Tropical Vegetation Unit, led by J-P. Malingreau, for their advise and support of the current work.

MONITORING OF AGRICULTURAL CROPS WITH ERS-1 AND JERS-1 MULTI-TEMPORAL SAR DATA AND CROP GROWTH MODELLING

Gerard J.A. Nieuwenhuis and Henk Kramer

DLO Winand Staring Centre for Integrated Land, Soil and Water Research (SC-DLO), P.O. Box 125, 6700 AC Wageningen, the Netherlands,
Tel +31 3174 74319, fax +31 3174 24812.

ABSTRACT

Temporal and spatial variation in radar backscatter have been examined using both ERS-1 and JERS-1 SAR images, to analyze crop growth conditions. Radar image interpretation was combined with radar backscatter simulation and crop growth modelling. Although theoretically the dynamic range in backscatter in time should be sufficient, results obtained were disappointing so far.
For 1992 different sets of multi-temporal ERS-1 SAR images were applied to map land cover. Applying a field-based classification method, results were obtained comparable with classifications using optical sensors like Landsat-TM and SPOT. Also pixel-based processing methods seem to be applicable using SAR images if preceding filtering techniques are used.
With a restricted data set of 1993 classification results obtained with ERS-1 and JERS-1 SAR data were compared with each other. Overall comparable results were obtained, although remarkable differences occurred. For example grassland was much better classified with ERS-1, while the results for fruit trees were much better using JERS-1 SAR data.

Key words: SAR time series, agricultural and environmental monitoring, crop growth, field-based classification

1. INTRODUCTION

Satellite remote sensing is used more frequently to obtain information on actual land cover and crop growth conditions. For regions with often cloudy conditions such as the Netherlands, regular data acquisition in the optical range of the electromagnetic spectrum is troublesome. Due to atmospheric conditions the applicability of satellite systems such as Landsat-TM and SPOT is seriously restricted for crop growth monitoring applications.
In the microwave range, however, data can be acquired independent of atmospheric conditions and time of the day. Therefore the data supplied by the imaging Synthetic Aperture Radar (SAR) on board of the European Remote sensing Satellite (ERS-1) and the Japanese Earth Resources Satellite (JERS-1) have a potential for environmental applications.

For the operational application of radar images in agricultural and environmental monitoring, knowledge dealing with the interaction mechanism of microwave radiation with soil and vegetation is required (Rijckenberg, 1994). If the interaction mechanism can be described, through inverse modelling measured radar backscatter can be related to relevant crop parameters and soil condition.
The applicability of ERS-1 SAR data to map land cover and to monitor crop growth was extensively investigated since the launch of ERS-1 (ESA Specialist Panel, 1995). In the Netherlands a project was initiated focused on the well-known Flevoland test-site (Nieuwenhuis and van Rooij, 1994). Because of the size and homogeneity of the agricultural fields in Flevoland, this area is well-suited for testing land cover classification methods and crop growth monitoring experiments. For the growing season of 1992, 1993 and 1994 ERS-1 SAR images were available with a frequency of about 10 till 15 days. For the growing season of 1993 also JERS-1 images were available, especially in the beginning and at the end of the growing season. Unfortunately images taken in the middle of the growing season were missing. To investigate the applicability of JERS-1 SAR images in relation to ERS-1, ERS-1 SAR images were selected close to the acquisition dates of the available JERS-1 images.
Based on the Flevoland experiments, the applicability of SAR images as supplied by ERS-1 and JERS-1 is discussed.

2. CROP GROWTH MONITORING

2.1 Crop modelling

For the crops sugar-beet and winter wheat Bouman (1992) developed an integrated model to simulate crop growth and radar backscatter depending on crop growth. The developed SUCROS (Simplified Universal Crop Growth Simulator) model is a mechanistic crop growth model describing the potential growth of a crop from irradiation, air temperature and crop characteristics. The radar backscatter was calculated using the Cloud model as developed by Attema and Ulaby (1978). For sugar-beet the original one-layer Cloud model was used and for winter wheat, the two-layer Cloud model as developed by Hoekman et al. (1982).

Figure 1 shows a typical result of the increase in radar backscatter with crop growth for sugar-beet as it may be expected from ERS-1 (CVV20) and JERS-1 (LHH40) measurements. In the presented simulations dry soil moisture conditions have been assumed. For such conditions the dynamic range in backscatter in time should be sufficient to obtain information on the initial crop growth conditions, i.e. sowing date of the crop. Performing crop growth monitoring this information is very important as the length of the growing season predominantly determines the final crop yield.

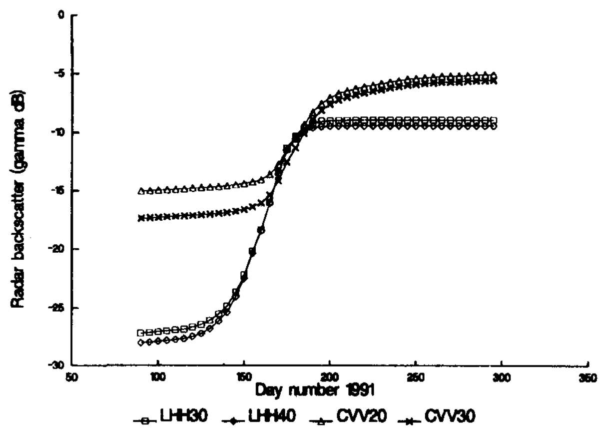

Figure 1. Simulated radar backscatter of sugar-beet for the 1991 growing season for two L-band (HH polarization, 30° and 40° angles of incidence) and two C-band (VV polarization, 20° and 30° angles of incidence) configurations.

2.2 ERS-1 time series

To assess crop growth, reference data were collected in the field. In 1992 soil moisture measurements were performed on 12 plots, where potatoes, sugar-beet, winter wheat and maize were grown. For 30 plots agronomic variables (e.g. sowing date, emergence date, harvest time and yield) were collected, while meteorological data were taken from standard meteorological weather stations in the surrounding.

For the main agricultural crops time series of radar backscatter were derived for the growing season of 1992 from the available ERS-1 SAR images (Figure 2).

In the beginning of the growing season large fluctuations in backscatter are found. These are most probably caused by different soil preparations and changes in soil moisture conditions. The profile of winter wheat (until harvesting beginning of August) and grass have in general a lower backscatter level than the other crop types. Potato and sugar-beet show similar profiles. The rather large increase in backscatter at the end of May is found for all crops except for winter

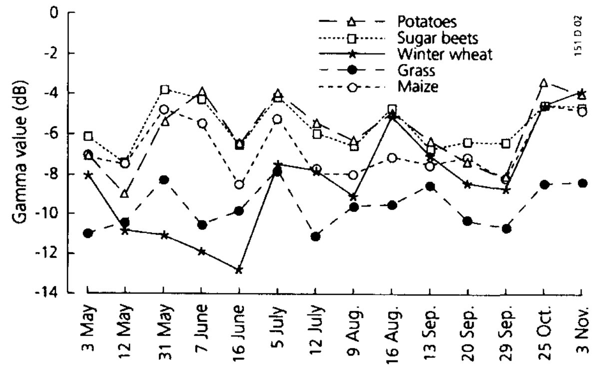

Figure 2. Multi-temporal plot of mean backscatter (Gamma, dB) for potatoes, sugar-beet, winter wheat, grass and maize as derived from ERS-1 SAR images acquired during the growing season of 1992.

wheat. This decline in C-band backscatter of winter wheat during the ear appearance in this period is often mentioned in literature (ESA Specialist Panel, 1995).

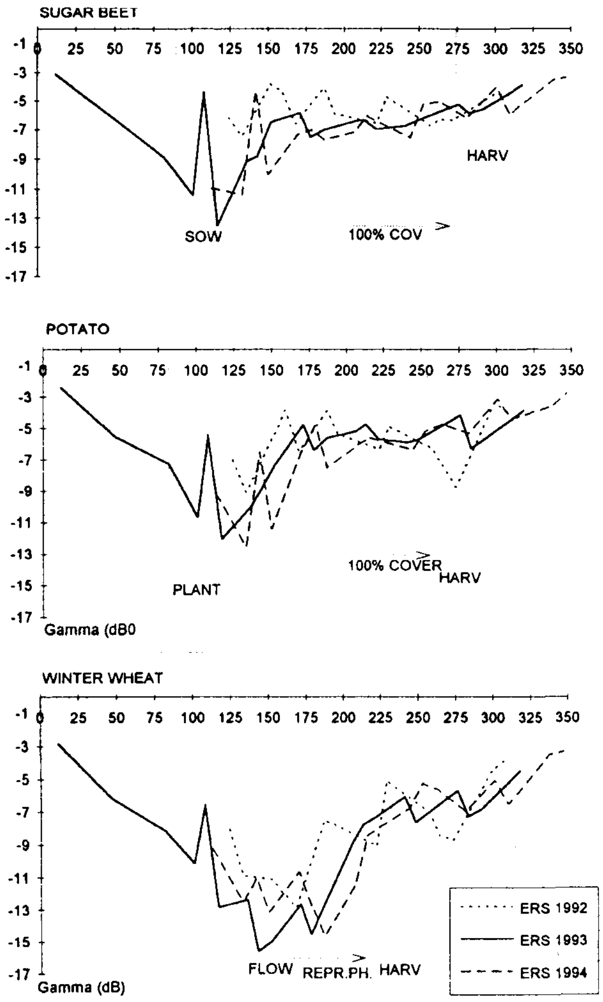

Figure 3. Multi-temporal plot of mean backscatter (Gamma, dB) for potatoes, sugar-beet and winter wheat as derived from ERS-1 SAR images for the growing season of 1992, 1993 and 1994.

object classification of JERS calibrated data (hectares)

reference

		potato	sugar beet	winter wheat	grass	maize	rapeseed	barley	fruit	horticulture	other	lucerne	bush	total	reliability
	potato	499	11	13	15	7	0	0	0	217	10	0	0	771	65%
	sugar beet	14	607	11	23	7	0	0	0	47	6	0	0	715	85%
	winter wheat	0	42	480	56	0	0	22	6	6	0	1	0	613	78%
	grass	41	0	26	91	0	0	0	0	26	0	28	3	215	42%
	maize	258	19	0	51	105	0	5	20	14	0	0	0	471	22%
classified	rapeseed	0	0	0	2	0	236	0	0	0	0	0	0	238	99%
	barley	20	12	97	178	0	0	263	2	47	41	0	0	661	40%
	fruit	0	20	0	0	0	0	0	177	5	0	0	30	232	76%
	horticulture	199	18	5	16	1	0	0	0	113	9	0	0	361	31%
	other	31	8	42	140	0	7	37	0	22	157	0	0	444	35%
	lucerne	0	0	153	45	0	12	0	0	0	0	296	0	506	58%
	bush	0	0	0	0	0	0	0	0	0	0	0	0	0	0%
	total	1061	736	828	617	120	255	327	205	498	223	325	34	5228	
	accuracy	47%	82%	58%	15%	88%	93%	80%	86%	23%	71%	91%	0%	58%	

object classification of JERS calibrated data (field count)

reference

		potato	sugar beet	winter wheat	grass	maize	rapeseed	barley	fruit	horticulture	other	lucerne	bush	total	reliability
	potato	40	1	3	2	1	0	0	0	15	1	0	0	63	63%
	sugar beet	2	50	1	3	1	0	0	0	8	1	0	0	66	76%
	winter wheat	0	3	29	12	0	0	2	1	1	0	1	0	49	59%
	grass	4	0	3	15	0	0	0	0	4	0	1	1	28	54%
	maize	19	2	0	2	12	0	1	1	3	0	0	0	40	30%
classified	rapeseed	0	0	0	0	0	4	0	0	0	0	0	0	4	100%
	barley	2	1	5	25	0	0	8	1	8	6	0	0	56	14%
	fruit	0	1	0	0	0	0	0	22	1	0	0	2	26	85%
	horticulture	17	2	2	2	1	0	0	0	19	2	0	0	45	42%
	other	2	2	6	21	0	2	2	0	5	5	0	0	45	11%
	lucerne	0	0	12	6	0	1	0	0	0	0	9	0	28	32%
	bush	0	0	0	0	0	0	0	0	0	0	0	0	0	0%
	total	86	62	61	88	15	7	13	25	64	15	11	3	450	
	accuracy	47%	81%	48%	17%	80%	57%	62%	88%	30%	33%	82%	0%	47%	

Table 1. Field-based classification results as obtained with 3 JERS-1 SAR images taken during the growing season of 1993.

The fluctuations in backscatter during the growing season can not be explained by the development of crop only. Probably weather conditions such as rainfall and wind influence radar backscatter.

For 1993 and 1994 comparable results were obtained. Figure 3 shows results for sugar-beet, potato and winter wheat. From the results it can be concluded that due to the fluctuations in backscatter in the beginning of the growing season it is hardly possible to derive information on the sowing date by comparing the measurements with simulated data such as shown in Figure 1. ERS-1 time series supply crop specific information. However, operational application of this information in a crop growth monitoring system is troublesome and should be further elaborated.

3. LAND COVER MAPPING

3.1 Application of ERS-1 multi-temporal data

The application of ERS-1 SAR data for mapping land cover was investigated extensively for the Flevoland test-site using images taken during the growing season of 1992 (Schotten et al., 1995).

Computer-based interpretation of SAR data for land cover mapping is complicated due to the presence of speckle. Among other things it hampers the application of pixel-based classification methods. A field-based approach involving the use of digital field boundaries to extract image statistics, such as the mean field backscatter, effectively overcomes the problem of speckle (Janssen, 1994).

Moreover the results which can be obtained with ERS-1 SAR data is strongly dependent on the available data set. Schotten et al. (1995) selected optional sets of ERS-1 images based on crop separability indexes (Dobson et al., 1992). Also the plotted time series (Figure 2) can be used to select suitable acquisition dates. It is quite clear that grassland can be distinguished from the other crops especially at the end of the growing season. To discriminate potato and sugar-beet could be troublesome, but probably an image taken at the end of September might solve this problem.

An eight-date set of ERS-1 SAR images, covering the period between 12 May and 3 November, yielded the best results with an overall accuracy of about 80 % applying a field-based classification method.

3.2 Comparison of JERS-1 and ERS-1

For the growing season of 1993 only 4 JERS-1 images were available. Unfortunately no images were acquired in the middle of the growing season. To be able to compare the applicability of JERS-1 and ERS-1 images, 4 ERS-1 images were selected close to the acquisition dates of the available JERS-1 images. The JERS-1 images of 28 March 1993 seemed to be of poor quality. Part of the image showed a clear distortion in radar object classification of ERS calibrated data (hectares)

reference

		potato	sugar beet	winter wheat	grass	maize	rapeseed	barley	fruit	horticulture	other	lucerne	bush	total	reliability
	potato	872	198	92	0	1	0	0	0	52	15	0	0	1230	71%
	sugar beet	40	297	35	42	18	0	65	33	26	14	0	0	570	52%
	winter wheat	7	77	388	43	5	0	0	0	54	6	0	0	580	67%
	grass	11	8	24	401	0	0	0	0	17	0	27	0	487	82%
	maize	6	11	48	8	79	0	30	0	20	0	0	0	201	39%
	rapeseed	5	22	2	0	0	249	56	0	0	0	2	0	336	74%
classified	barley	25	97	77	4	0	2	137	0	29	5	0	0	376	37%
	fruit	6	0	30	7	3	0	0	105	10	0	20	0	181	58%
	horticulture	49	12	59	5	14	0	12	11	137	8	0	0	307	45%
	other	40	14	67	12	0	4	0	26	42	163	0	0	367	44%
	lucerne	0	0	0	64	0	0	0	17	0	0	276	0	357	77%
	bush	0	0	8	31	0	0	26	12	112	13	0	34	236	14%
	total	1061	736	828	617	120	255	327	205	498	223	325	34	5229	
	accuracy	82%	40%	47%	65%	65%	98%	42%	51%	28%	73%	85%	100%	60%	

object classification of ERS calibrated data (field count)

reference

		potato	sugar beet	winter wheat	grass	maize	rapeseed	barley	fruit	horticulture	other	lucerne	bush	total	reliability
	potato	65	18	3	0	1	0	0	0	10	2	0	0	99	66%
	sugar beet	5	23	3	5	3	0	2	3	1	3	0	0	48	48%
	winter wheat	1	6	27	6	1	0	0	0	9	1	0	0	51	53%
	grass	1	1	2	61	0	0	0	0	2	0	1	0	68	90%
	maize	1	1	2	2	7	0	2	0	1	0	0	0	16	44%
	rapeseed	1	2	0	0	0	5	1	0	0	0	1	0	10	50%
classified	barley	2	8	7	1	0	1	6	0	5	1	0	0	31	19%
	fruit	1	0	3	1	1	0	0	11	2	0	1	0	20	55%
	horticulture	4	1	6	1	2	0	1	3	24	1	0	0	43	56%
	other	5	2	7	2	0	1	0	2	8	6	0	0	33	18%
	lucerne	0	0	0	8	0	0	0	5	0	0	8	0	21	38%
	bush	0	0	1	1	0	0	1	1	2	1	0	3	10	30%
	total	86	62	61	88	15	7	13	25	64	15	11	3	450	
	accuracy	76%	37%	44%	69%	47%	71%	46%	44%	38%	40%	73%	100%	55%	

Table 2. Field-based classification results as obtained with 3 ERS-1 SAR images taken during the growing season of 1993.

backscatter, making automatic classification methods nearly impossible.

For 1993 JERS-1 images were available acquired at 12 May, 7 August and 20 September. The corresponding ERS-1 images were respectively acquired at 16 May, 10 August and 5 September. A SPOT image of 2 July 1993 was used to establish the required field boundary data base.

The results of the field-based classification with the JERS-1 and ERS-1 data set are shown in Table 1 and 2 respectively.

Due to the restricted data set the overall accuracies are low (50-60 %) in relation to the results with an optimal data set (about 80 %). The difference in overall accuracy between JERS-1 and ERS-1 are negligible. However, per class remarkable differences occur. For example grassland could be classified with a reasonable accuracy with ERS-1, while with JERS-1 only poor results were obtained. Also for potato ERS-1 gave better results, while on the other hand sugar-beet was much better classified with JERS-1. Also clear differences are found for fruit trees. With JERS-1 accuracies of 86% (based on acreage, ha) and 88% (based on number of plots) are obtained, while with ERS-1 these accuracies are respectively 51% and 44 %.

4. CONCLUDING REMARKS

Within the framework of the Flevoland experiments, the applicability of ERS-1 and JERS-1 SAR imagery was investigated to set up an agricultural crop growth monitoring system.

Bouman (1991) showed the potential of radar backscatter time series to improve crop yield estimates. However, we found that with ERS-1 data it is hardly possible to improve crop growth modelling results in practice. As the obtained backscatter time series supply crop specific information, the integration of SAR backscatter data and crop growth modelling should be further elaborated

Land cover mapping with ERS-1 and JERS-1 data was very successful. For large areas regional agricultural statistics can be derived in an efficient way from the obtained classification results. Consequently regional data on crop yield can be obtained by combining the statistics with simulated crop yield values.

Based on experiments with an extensive data set of 1992, optimal ERS-1 acquisition dates have been determined. A few agricultural crops could already be distinguished early in the growing season. The early detection of crops with the help of ERS-1 SAR images can be an important information source to monitor land use, for instance to check field-based subsidies as supplied by the European Union.

ACKNOWLEDGEMENTS

This report describes a study that was carried out in the framework of NRSP-2 under responsibility of the Netherlands Remote Sensing Board (BCRS). Both ESA and NASDA are acknowledged for the deliverance of ERS-1 and JERS-1 SAR images.
Results were use of the project performed in the framework of the ESA-ESTEC study contract no. 1154/94/nl/nb(SC), which is managed by Synoptics.

REFERENCES

Attema, E.P.W. and F.T. Ulaby. 1978. Vegetation modelled as a water cloud. Radio Sci. 13 (2): 357-364.

Bouman, B.A.M. 1991. Linking X-band radar backscattering and optical reflectance with crop growth models. Ph. D. Thesis, Wageningen Agricultural University, the Netherlands. 169 pp.

Bouman, B.A.M. 1992. SBFLEVO and WWFLEVO; Growth models to simulate crop growth, optical reflectance and radar backscatter of sugar beet and winter wheat, calibrated for Flevoland. Report 163, AB-DLO, Wageningen, the Netherlands. 61 pp.

Dobson, M.C., L. Pierce, K. Sarabandi, F.T. Ulaby and T. Sharik. 1992. Preliminary analysis of ERS-1 SAR for forest ecosystem studies. IEEE transactions on Geoscience and Remote Sensing, Vol. 30, no 2; 203-211

ESA Specialist Panel. 1995. Satellite Radar in Agriculture: Experience with ERS-1. ESA Report SP-1185, Noordwijk, the Netherlands, 71 pp.

Hoekman, D.H.L., L. Krul and E.P.W. Attema. 1982. A multi-layer model for radar backscattering from vegetation canopies. In: Digest of the 2nd IEEE International Geoscience and Remote Sensing Symposium, Munich, West Germany, 1-4 June, pp 4.1-4.7.

Janssen L.L.F. 1994. Methodology for updating terrain object data from remote sensing data. PhD thesis, Wageningen Agricultural University, the Netherlands. 173 pp.

Nieuwenhuis, G.J.A. and W.W.L. van Rooij (eds). 1994. Application of ERS-1 SAR data in agriculture and forestry. Report 101, SC-DLO, Wageningen, the Netherlands. 182 pp.

Rijckenberg, G.J. 1994. Physical modelling in relation to the application of ERS-1 to agricultural studies. In: Application of ERS-1 SAR data in agriculture and forestry, Nieuwenhuis and van Rooij (eds), Report 101, SC-DLO, Wageningen, the Netherlands. 21-52.

Schotten, C.G.J., W.W.L. van Rooij and L.L.F. Janssen. 1995. Assessment of the capabilities of multi-temporal ERS-1 SAR data to discriminate between agricultural crops. Int. J. Remote Sensing, vol. 16, no. 14, 2619-2637.

COMPLEMENTARY USE OF ERS SAR AND OPTICAL DATA FOR LAND COVER MAPPING IN JOHOR, MALAYSIA

Brown, R.E. (1), Wooding, M.G. (1), Batts, A.J. (1), Loh Kok Fook(2); Ku Mohd. Noh (2); Laili Nordin (3)

1. Remote Sensing Applications Consultants (RSAC), Mansfield Park, Medstead, Alton, Hants GU34 5PZ, U.K.
Tel: (44) 1420 561377 Fax: (44) 1420 561388

2. Malaysian Centre for Remote Sensing (MACRES), PO Box 208, Lot CB100, 5th Floor, City Square Center, Jalan Tun Razak, 50400, Kuala Lumpur, Malaysia.
Tel: (60) 3 2645640 Fax: (60) 3 2645646

3. Department of Agriculture, Jalan Sultan Salahuddin Shah, 50632 Kuala Lumpur, Malaysia.
Tel: (60) 3 4403363 Fax: (60) 3 2947336

ABSTRACT

The objective of the project was to develop a methodology to improve land cover mapping and change detection, from a combination of multi-temporal ERS-1 SAR and optical data in a persistently cloudy area of Malaysia - Johor State.

Several dates of ERS-1 imagery for 1993 and 1994, and Landsat TM imagery for 1991-94, were acquired over Johor State. Existing land use maps of the area were used, both in paper and digital form. Field work was conducted in the area, which is largely a region of perennial vegetation, including large plantations of oil palm and rubber, and natural forest.

The study has concentrated on 2 methods of complementary use. Firstly the combination of ERS-1 and Landsat images, using simple band combination and IHS transformation. Secondly, multi-temporal ERS-1 images were used to update baseline maps produced from optical data, by overlaying vector maps to these images and digitising on-screen. Image-map products were produced for field survey and checking.

1. INTRODUCTION

This paper is concerned with a project in Johor State looking at the complementary use of ERS and optical images for land cover mapping. This pilot project forms part of a collaborative programme between the European Community, the European Space Agency and the countries of the Association of South-East Asian Nations (ASEAN). The EC-ASEAN ERS-1 Project aims to develop ASEAN capabilities to apply ERS-1 imagery to meet development and environmental needs through training and application demonstrations.

2. THE APPLICATION

The land cover of Johor is dominated by plantation crops such as oil palm, rubber, coconuts and pineapples; and natural forest. Most of the vegetation is therefore perennial with little seasonal change The Department of Agriculture is responsible for land cover mapping in Malaysia, and uses a combination of field survey, aerial photography and satellite imagery. Persistent cloud cover limits the availability of optical satellite data, for example the last complete TM coverage of Johor was in 1991. Some difficulties have been experienced in separating oil palm and rubber on TM images. The study area is shown in Figure 1.

Fig. 1 Study area

3. STUDY METHODS AND ANALYSIS

Eight multi-temporal ERS-1 images from the period July 1993 to March 1994 were used. These were geometrically corrected using 1:63,360 topographic maps, no terrain correction was performed. Lee, Frost and Gamma Map speckle filters were evaluated, a Lee 3x3 filter was found to be the most effective for visual analysis.

Land cover maps prepared by the Department of Agriculture from aerial photographs and Landsat TM images were used for reference, and specific field survey was undertaken. The topographic maps, dating from approximately 1970, also contained significant land cover annotation and highlighted long-term changes, particularly in plantation crops. Multi-temporal colour composites were produced, both to visually analyse in conjunction with the land cover maps and field survey data, and to identify changes against the baseline land cover maps. ERS image-maps were printed at 1:50,000 scale for field survey and checking.

4. VISUAL ANALYSIS

The multi-temporal ERS-1 images, and ERS-1/Landsat combinations, were visually analysed in comparison with land cover map and ground survey data. The following observations were made.

Oil Palm
Oil palm when mature is generally distinguishable by a high backscatter and therefore bright colours on multitemporal images. It also tends to be uniform in brightness with little variation between dates. Young oil palm up to 3 years from planting is more variable due to changes in ground cover and soil conditions, and is liable to be confused with rubber or forest.

There is a requirement to map broad age categories of oil palm plantation in Malaysia. Eighteen months to two years after initial planting oil palm plants are transplanted into their final position in bare ground or an herbaceous cover crop, and plantation ages are calculated from the time of transplanting. Land cover mapping from air photographs interpreted oil palm in three age categories:

Young: ≤ 3 years
Mature: > 3 years ≤ 25 years
Old: > 25 years

Recent updating of these maps has been carried out using Landsat imagery but these categories have not been used because they cannot be reliably identified visually, although McMorrow (1995) has looked at identifying age classes based on reflectance values, in Sabah.

Examples analysed using field survey data and plantation records, show that up to 3 years visual analysis of backscatter values could show replanting of young oil palm.

Rubber
Mature rubber generally appears darker than mature oil palm. However mature rubber can be confused with young oil palm, this is addressed in the following section on backscatter signatures.

Forest
Forest can be confused with mature oil palm. Most forest remnants now occur on hilly terrain where layover and shadow effects prevent any consistent interpretation.

Bananas
Bananas only occur in limited areas, however one field site was visited near Kampong Bukit Batu. This estate also includes small areas of oil palm and grassy areas without tree cover. The banana parcels are not very distinctive in comparison with oil palm and other perennial crops on TM. On the SAR images they appear very bright, and are much brighter than oil palm.

Coconuts and mangrove
The coastal area of mangrove, coconuts and mixed smallholder agriculture appears fairly uniform on the two dates of SAR available, and it is impossible to discriminate with these alone. Simple combination of two TM bands and one SAR date did not help in discrimination. Using IHS combination, detail from the TM does provides information and assists discrimination between coconuts and mangrove, and to a lesser extent between coconuts and oil palm.

If a TM image is available for the same date as the SAR there would be little advantage in combining the two. However a change in the coconut area could well be more obvious from an IHS combination of old TM and new SAR than on the SAR alone.

Pineapples
This is the only herbaceous crop looked at in the study, and the only non-tree crop to grow in large areas in Johor. Pineapple fields are very distinctive on TM - by virtue of their large size compared to the surrounding smallholder fields, the uniform texture, the colour of the growing crop, and the dark areas of bare peat soil within the fields. On the SAR image using two dates the colours are not clearly distinguished from those of oil palm, and are only visible by virtue of their shape and size. Pineapples are however distinctive on the IHS image, but all the information content comes from the TM.

Urban areas
Settlements show clearly as very bright areas. The new North-South highway, not marked on current maps, shows as a dark line.

5. BACKSCATTER SIGNATURES

In order to compare signatures between different dates, DN's were converted to backscatter values in decibels and calibrated using the constant for the Bangkok receiving station. Only a few samples were available for each land cover type, and for only 2-6 dates, so their analysis is indicative of backscatter characteristics rather than a definite characterisation.

Examples of the major land cover types identified on field survey, such as oil palm, rubber and pineapple, were analysed to extract mean backscatter signatures for several dates using customised software developed by RSAC. These were used to produce temporal profiles.

Oil palm

Oil palm shows a general tendency for backscatter to increase with age until the canopy has become complete and effects of surface conditions and variable leaf cover are no longer influential. The data analysed here is insufficient to determine the age at which backscatter no longer increases. Of the sites visited, none were in the mature class (3 to 25 years old). Due to the major expansion in oil palm plantations in Johor State, and Malaysia in general, occurred during the 1960's, most of the plantations are either in the old category or have just been replanted and are young (Polunin, 1988).

Young oil palm of 2 years old and under shows a much more variable profile, both between different examples, and between dates for the same sample, varying in the examples chosen from -9.5 to greater than -5 dB, see Figure 2. This is due to the effects of the ground layer before full canopy cover is reached, including cover crop or herbaceous weed layer, cultivations, soil and moisture effects. Large differences between 4 dates in January and February 1994 over a 6 week period suggest that ground conditions at this stage are more important than the oil palm canopy - and that changes in soil moisture or surface roughness are causing this variability.

By the time the trees are 3 years old, the profile has become much more stable, and matches the form of the old oil palm, but with a backscatter of approximately 1.5 dB lower, see Figure 3.

Fig. 2 Temporal backscatter profile of young oil palm

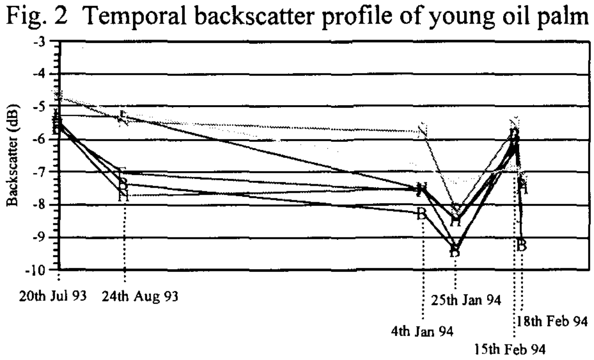

Fig. 3 Temporal backscatter profile of old/3 year palm

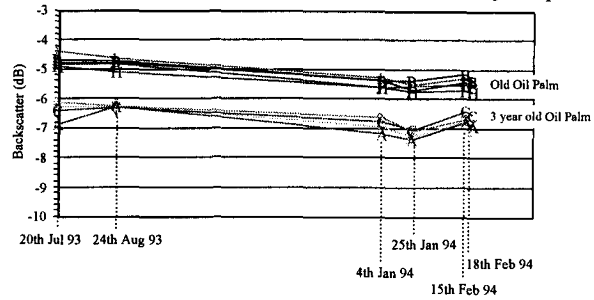

Rubber

Mature rubber has a lower backscatter than old oil palm, and presumably than mature oil palm, as observed in the visual analysis. There appears to be a risk of confusion between mature rubber and young oil palm with its lower backscatter.

Forest

The backscatter profile of three relatively flat forest sites falls between that of rubber and old oil palm, and overlaps 3 year old oil palm. It should be pointed out that much of the remaining forest in Johor is found on hilly terrain where shadow and layover effects on SAR imagery which has not been ortho-corrected will make backscatter values variable.

Bananas

Although only two dates are available for this area, the backscatter values are clearly higher than oil palm, -4 dB and higher, and indicate that the backscattering properties of the banana leaves make them easy to discriminate.

Pineapples and coconuts

The analysis of these two land covers is limited, with only two dates covering two sites. They do not suggest any clear discrimination is possible from the various stages of oil palm, with backscatter values of -6 to -7 dB.

6. CHANGE DETECTION

By combining different dates, ERS SAR can offer an advantage over optical data for change detection. Large areas of Johor do not change significantly either within the year or between years, because they are covered by non-seasonal and perennial tree crops or forest. Where there is significant change, such as felling and replanting of trees, this can be clearly and rapidly seen over large areas by bright colours, signifying varying backscatter between the composite dates. This is illustrated by the multitemporal composite of a large area of southern Johor State in January and February 1994 in Figure 4. Large areas of oil palm plantation appear uniformly bright, but there are more localised red areas where there has been some change.

Figure 4 Part of Johor State, Malaysia, near Johor Bahru

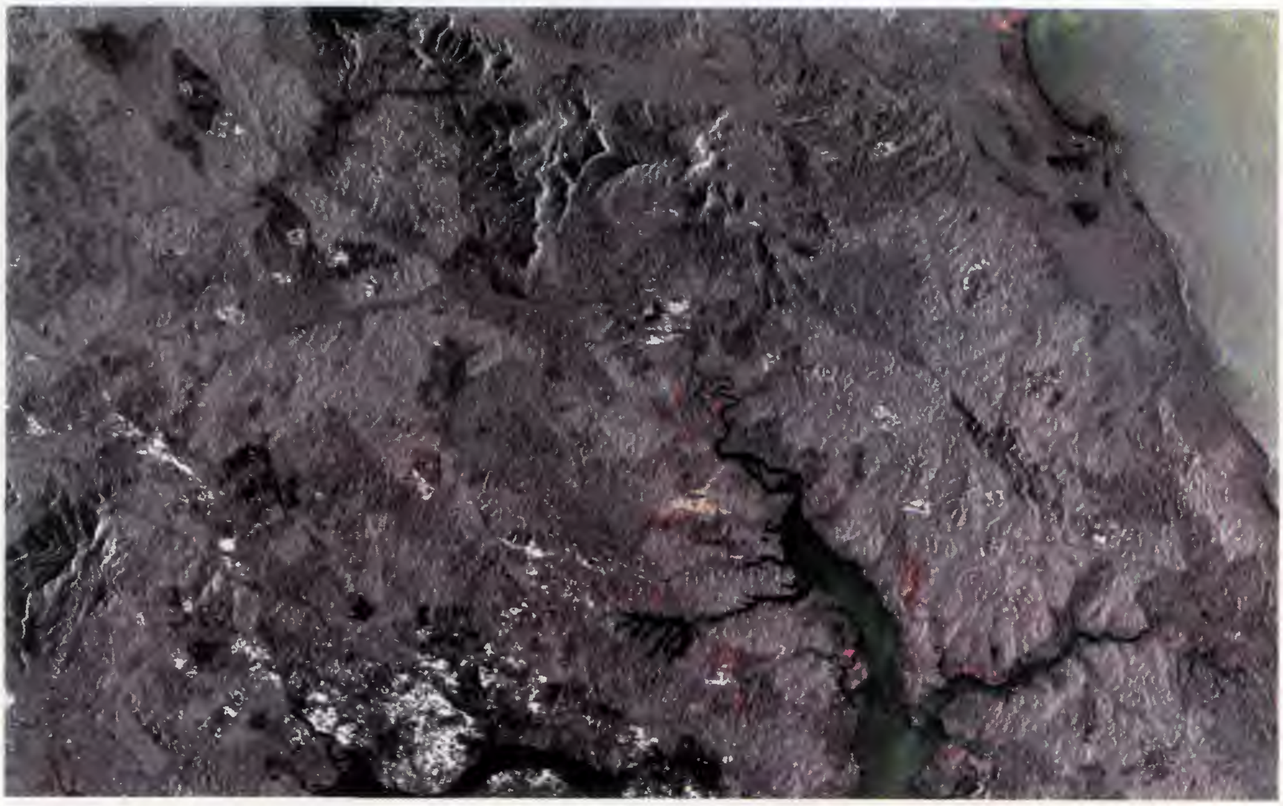

ERS-1 SAR Red: 4 January 1994 Green: 25 January 1994 Blue: 18 February 1994

Figure 5 Updating changes from forest to oil palm using ERS-1 SAR imagery

Landsat TM image, 11 March 1991
with 1990 land use map.
Red: Band 4, Green: Band 5, Blue: Band 3

Forest cleared to oil palm on TM image, but not yet updated on land cover map

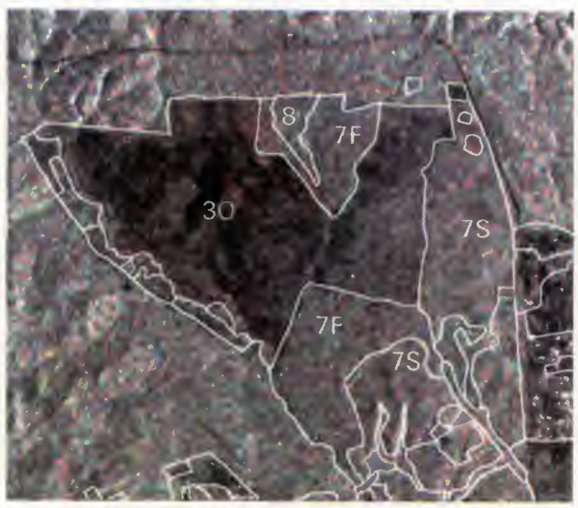

ERS-1 SAR image, Lee filtered 3x3,
with updated land use map
Red: 4 Jan, Green: 25 Jan, Blue: 18 Feb 1994

LAND USE CODES
30: Oil Palm 7F: Forest
7S: Scrub 8: Wetland Forest

The baseline land cover mapping requires optical imagery - satellite imagery such as Landsat TM or air photography, ERS SAR can then be used to update changes.

7. VISUAL MAP UPDATING

Change detection translates into updating land cover maps using visual interpretation. The raster satellite images are overlaid with vector land cover maps and changes made to the linework and coding as necessary. This can be achieved using hardcopy, or an integrated raster/vector system allowing on-screen digitising.

Figure 5 illustrates an area of forest near Bandar Tenggara which has been felled and replanted with oil palm since the 1990 land cover map. A 1991 TM image shows partial clearing which had been completed by the time of the ground survey. The 1994 SAR image now shows the clearance visible on the TM with 2-3 year old oil palm growing, and the rest of the cleared area planted more recently with oil palm. The land cover map can easily be updated over the SAR image to reflect the changes from forest to oil palm.

8. CONCLUSIONS

Multi-temporal ERS images by themselves are of limited value for land cover classification of tree plantation crops, because of small differences in the backscatter of different types and the temporal stability, or lack of seasonal change, of these crops.

ERS SAR is however capable of discriminating some major land cover types such as oil palm and rubber. With the exception of bananas the discrimination is no better than optical imagery. Bananas show very clearly on SAR due to the very high backscatter.

There is little advantage in combining ERS and Landsat images for land cover classification purposes: there may be only marginal improvement in cover discrimination and they are not generally available for dates close enough together to exclude the possibility of changes having occurred between the dates of the two sources.

There is however considerable potential in the use of multi-temporal ERS images for change detection and updating baseline maps prepared from optical images. The Malaysian Department of Agriculture is starting to use ERS image maps with land cover overlays for field checking of land cover change. Future work aims to exploit the potential of longer time series of images for change detection and map updating.

The best way for the two data types to complement each other would seem to be to use optical imagery when available for baseline mapping, and to use multitemporal ERS SAR for change detection and map updating. This seems particularly relevant for changes in large plantations and in forest cover.

An approach that has been used in the UK (Slater, Brown and Wooding, 1995) is to create a multitemporal composite with images from different years rather than from different months. With seasonal changes being of minor importance, a 3 year composite would effectively detect changes over a 3 year period covering large areas for relatively low cost.

REFERENCES

Slater, J., Brown, R.E., and Wooding, M.G. *The Use Of ERS-1 SAR For Monitoring Of Environmentally Sensitive Areas In England.* Proceedings of the Second ERS Publications Workshop, London, 6-8 December 1995. ESA Publications.

McMorrow, J. (1995). *The effect of oil palm age on Landsat TM spectral response.* Proceedings of the 21st Annual Conference of the Remote Sensing Society, 11-14 September 1995, University of Southampton, UK.

Polunin, I. (1988). *Plants and Flowers of Malaysia.* Times Editions, Singapore.

THE OPERATIONAL USE OF ERS-1 SAR DATA FOR THE CONTROL OF AREA BASED ARABLE AND FORAGE SUBSIDIES IN THE UK

Andrew Sowter, Gavin Brelstaff & Martin Davison*

National Remote Sensing Centre Ltd., Delta House, Southwood Crescent, Southwood, Farnborough, Hampshire, GU14 0NL, UK

Tel: +44 1252 541464, Fax: +44 1252 375016, Email: asowter@nrsc.co.uk

ABSTRACT

NRSC has developed an operational environment for the integration of ERS-1 SAR data into a process for the checking of farm applications for EU subsidies. This includes: ortho-rectification and referencing; full radiometric correction, including slope effects; and the preparation of data for photo-interpretation. This paper highlights the main requirements and capabilities of the system.

1. INTRODUCTION

Each year, the European Union (EU) undertakes a programme to control farmers' claims for subsidies under the Common Agricultural Policy (CAP). The programme, called "Control of Area Based Arable and Forage Subsidies using Remote Sensing" is undertaken throughout the EU under the direction of the individual member state.

The objective of the work is to use the available remotely sensed imagery to check what a farmer is growing during the current growing season against his claim for subsidies, identifying any mismatch. Data from spaceborne optical sensors, such as SPOT or Landsat, are most commonly used in the UK to provide this service to a high degree of accuracy. However, excessive cloud cover, common in Northern latitudes, often poses a threat to the acquisition of sufficient data to guarantee accuracy.

Synthetic Aperture Radar (SAR) offers a possible solution to this problem as its ability to penetrate cloud and its day-night capability ensures that, provided the instrument is in operation, an acquisition can be made. The availability of data from the ERS-1 mission made this a candidate source of data for the 1995 programme.

The main problems with SAR data are that:

- Many SAR images are required to separate even the most basic crop classes to a reasonable accuracy.

- SAR data are conceptually very different from optical data. Therefore it is not wholly obvious how they could be used to support photo-interpretation.

The National Remote Sensing Centre Limited (NRSC) has developed an approach to the use of SAR data in the framework of the EU programme that was used successfully on an operational basis during 1995. The following sections will highlight the approach to SAR data processing and photo-interpretation applied and highlight some of the problems and benefits encountered.

2. DATA PREPARATION

All SAR data used in 1995 were corrected for both geometric and radiometric effects.

The extent of geometric distortion in an ERS-1 SAR image is high. The extent of terrain height differences needed to produce a planimetric error of 50m is shown in Table 1 for ERS-1 and, as contrast, for RADARSAT. As is clearly shown, such levels of distortion are at least an order of magnitude higher than for optical data, even at grazing incidence angles. We conclude that, for accurate geo-referencing, terrain correction must be applied to all ERS-1 imagery to gain a reasonable level of accuracy.

Mission	Height Difference
ERS-1	17 - 24m
RADARSAT (Standard Mode)	18 - 60m
RADARSAT (Extended High Mode)	60 - 87m

Table 1. Terrain Height Differences Required to Produce a Geolocation Error of 50m

* Currently working with CRI at the Joint Research Centre, Italy.

All terrain correction was applied using NRSC's in-house TSAR software (Fern et al., Brelstaff et al.). TSAR performs a simulation of the imaging process, reducing the dependence on tiepointing, therefore supporting operational applications. The geolocation accuracy of TSAR in comparison with a polynomial stretch, both obtained using 11 tiepoints on a test agricultural site is shown in Table 2.

Method	Absolute RMSE
TSAR	21m
2nd Order Polynomial	327m

Table 2. Geolocation Accuracy of TSAR vs. a 2nd Order Polynomial Using 11 Tiepoints.

In addition to geometric correction, TSAR also performs radiometric correction of the following effects:

- ADC Saturation
- Replica Pulse Power
- Topographic Incidence Angle

All of these corrections are necessary to obtain accuracies of better than 0.5dB from ERS-1 data. Of these, the largest magnitude of correction was for the effect of incidence angle where it can be shown that, even for slopes deviating only 5 degrees from the horizontal, a 1dB correction of the radar cross section is necessary.

TSAR allows this correction to be applied through the calculation of the topographic incidence angle for each pixel located in an area of interest.

3. PHOTO-INTERPRETATION

As more than one SAR image is required to separate often the most basic of crop types, care must be taken to summarise the data for use in a Computer-Aided Photo-Interpretation (CAPI) environment. NRSC already has a tried and trusted approach to this task and the aim was to integrate the SAR data without interrupting the optical methodology.

This aim was satisfied through the use of:

- A combined optical and SAR automatic classification optimised on per-field signature characteristics.
- The inspection of SAR signatures which illustrate the temporal variation of the per-field radar cross section against time.
- The display of a colour composite image. This could be a multi-temporal image if three or less images are used; if higher then, perhaps, an image composed of the first three principal components could suffice.

The image characteristics used for the signature analysis and classification were extracted using field boundary information. This allowed all of the possible information about a field to be extracted and is therefore more optimal than, say, a pixel-based approach.

In 1995, the above information was displayed alongside any optical data for photo-interpretation.

4. SUMMARY

The above sections describe the basis for the use of SAR in the UK during the 1995 Control of Subsidies programme. SAR was used operationally with the following capabilities:

- Full correction of the geometric and radiometric effects of terrain.
- Field based information extraction.
- Full support of a CAPI methodology.

The results of the photo-interpretation using ERS-1 SAR in 1995 were excellent and the project was able to meet all its technical objectives.

5. PROBLEMS IN THE USE OF ERS-1 SAR DATA

1. ERS-1 was in a 35-day repeat cycle. This implies that there was very little choice of data that completely covered a moderately-sized site in this time.
2. Due to the 35-day cycle, it is impossible to plan for an acquisition on a specific date in the crop growing cycle - we are limited to the sampling implied by the repeat cycle.
3. Although we were assured that ERS-1 would acquire data over an area of interest

at every possible overpass, this was not, in fact, the case. Some images were missing from the expected dates and locations.

4. Currently, the data ordering system for ERS-1 does not allow the choice of a 'floating scene' - if an area of interest straddles two successive frame in an orbit, we must order both scenes for complete coverage - doubling the data cost.

5. The turnaround time between the acquisition of an image by the satellite and the delivery of a processed (PRI) scene is currently around 14 days at best. This restricts the potential sampling window for acquisitions over the site.

6. As of the Summer of 1995, there were still serious discrepancies between the PRI header formats of the various PAFs. For an automated operational process this is a significant problem.

6. CONCLUSIONS

Above, it has been demonstrated that an operational land-use monitoring scheme using ERS-1 SAR data was applied during the 1995 EU Programme "Control of Area Based Arable and Forage Subsidies Using Remote Sensing" in the UK. The operational implementation included full correction of the data for terrain effects and an optimal field-based approach to signature extraction. Furthermore, SAR was used to support a large scale computer-aided photo-interpretation scheme for the identification of agricultural land-use classes.

REFERENCES

Fern T. et al., 1995, "Topographical SAR - User Guide", NRSC Document TS-UG-NRL-SE-0001.

Brelstaff G., Sowter A. & Meadows, P., 1995, "Rectification, Calibration and georeferencing of SAR data for Land-Use Applications", Proceedings of the European Symposium on Satellite Remote Sensing II, Pons Sept. 1995, SPIE Vol. 2585 (in Press).

WINDS / WAVES / METOCEAN

Chairman: **D. Carter**
Rapporteur: **E. Oriol**

OPERATIONAL USE OF ERS-1 PRODUCTS IN MARINE APPLICATIONS

Guido Paci*, Gordon Campbell**

* Data Utilisation Section, ESA-ESRIN, Via Galileo Galilei, 00044 Frascati, ITALY

Tel: (39) 6 941870620, Fax (39) 6 94180622, email: Guido.Paci@mail.esrin.esa.it

** Serco Servizi Srl, under contract to Data Utilisation Section, ESA-ESRIN
Tel: (39 6 94180682), Fax (39) 6 94180622, email: Gordon.Campbell@mail.esrin.esa.it

ABSTRACT

One of the objectives of the ERS mission was to demonstrate the feasibility of commercial and operational utilisation of Earth Observation remote sensing data. A number of organisations are now making use of ERS data products, particularly in the marine applications area, at a number of different levels of development, ranging from technology demonstration to full operational use. These organisations fall into two broad categories:

- companies and institutes operating within the ESA and national development programmes
- value added companies obtaining data through commercial channels

This paper will focus on the current status of the utilisation of ERS data products within marine applications, citing particular examples of services provided from organisations within the ESA programmes and also from commercial service providers. Descriptions of the particular applications and an analysis of the market requirements will be given. In addition, future migration towards full operationalisation will be analysed and syntheses of the end user requirements and the performance levels required from an operational service provider will be presented. Actions required in order to meet the objectives implicit in the provision of an operational service will be discussed together with the role of ESA in facilitating development of a fully operational oceanographic use of ERS data.

1 INTRODUCTION

One of the activities undertaken by the ESA-ESRIN Data Utilisation Section was the analyses of application areas on a number of levels and from a number of perspectives. The scope of this analysis was primarily focused on projects within the PP and PI programmes but many national and commercial projects have also been subsequently included. This work has resulted in a comprehensive overview of each application area, a detailed knowledge of the status of individual projects within each application area, a detailed understanding of user requirements both from service provides and from data providers such as ESA and an awareness of the current status and future trends within the EO marketplace including the main issues at present as well as current developments and trends. In addition, actions aimed at developing the marketplace have been identified, based on problems and difficulties identified within each of the projects analysed. This paper presents some of the analyses and conclusions relating to marine applications of ERS data, with particular emphasis on marine forecasting and sea state climatology applications.

2 MARINE FORECASTING SERVICES

One of the key factors in the evolution of sea state forecasting services has been the development of the WAM model. The operation of the WAM model has been based on the assimilation of scatterometer corrected wind fields to generate the initial wind conditions for each time step. In addition, altimeter data have been utilised to correct the significant wave height forecasts at each time step before the model is propagated further forward. SAR wave mode data are now being used to provide corrections to the forecast wave direction and period parameters although the assimilation of these data is still at an early stage and some operators do not make use of this versatile data product.

A number of organisations are providing sea state forecasting services based on the assimilation of the LBR data products. These include:

- ECMWF
- UKMO
- METEO-FRANCE
- KNMI (Netherlands)

- DNMI (Norway)
- Delft Hydraulics/ARGOSS (Netherlands)
- MeteoMer (France)
- MUMM (Belgium)

In general, national meteorological offices provide a general wave forecast service to any user requesting information, whereas industrial service providers provide a product tailored to the requirements of individual customers. The end users include shipping operators and ship masters for route planning, offshore engineering companies in order to allow the efficient and safe execution of heavy engineering activities, coast guards and harbour management agencies, fishermen, coastal defence agencies and marine survey companies. Further applications include the integration of sea state forecast models with additional models such as slick evolution models in order to forecast the effects of an oil spill event. In addition, a similar, offline service providing sea state data for a particular location at a particular time is required by insurance companies and marine accident investigators in the settlement of accident and damage claims.

The figure below gives an overview of a generic processing chain for the incorporation of LBR data

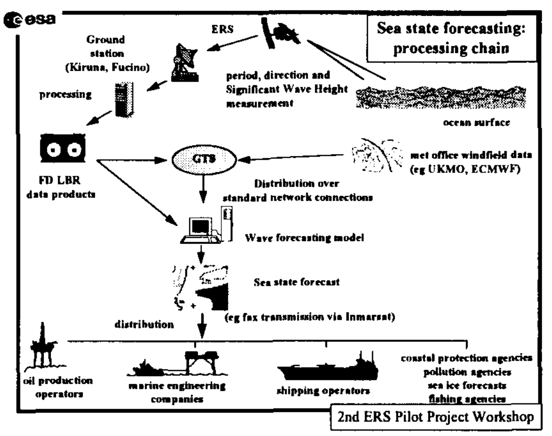

The key requirements in terms of data provision are reliable wind field data and a guarantee of delivery of the FD LBR data products in time for the assimilation into the forecasting models. Further requirements include the availability of computer hardware with sufficient processing power in order to implement the WAM model (or simplified versions) and reliable operational assimilation algorithms for incorporating the ERS data into the forecast models.

At present, many organisations have demonstrated positive impact from the assimilation of altimeter data and also of SAR Wave Mode data into the forecast models and are now routinely assimilating ERS data and distributing forecast products in a pre-operational scenario. Requirements for a migration towards a full operational service provision are discussed later.

3 SEA STATE CLIMATOLOGY SERVICES

Sea state climatology services are probably one of the best understood remote sensing applications in terms of the level of awareness and acceptance of the end users. End user application areas include marine warranty and underwriting services, coastal construction design and planning, naval architecture, ship routeing, offshore engineering site locations, survey planning, tourism development and management and naval strategy and operational analyses applications such as requirements definitions, sea trial planning and tactical decision making.

Organisations involved in the provision of sea state climatology services include:

- MeteoMer (France)
- Satellite Observing Systems (UK)
- Delft Hydraulics/ARGOSS (Netherlands)
- UKMO/BODC
- Oceanor (Norway)

The service is based on the incorporation of a number of datasets including altimeter derived significant wave height measurements, scatterometer based windfield measurements, SAR wave mode data, third party altimeter measurements (eg TOPEX Poseidon, Geosat, Seasat), wavebuoy measurements, weather station observations and ship master observations. The figure below illustrates the basic structure of a sea state climatology service.

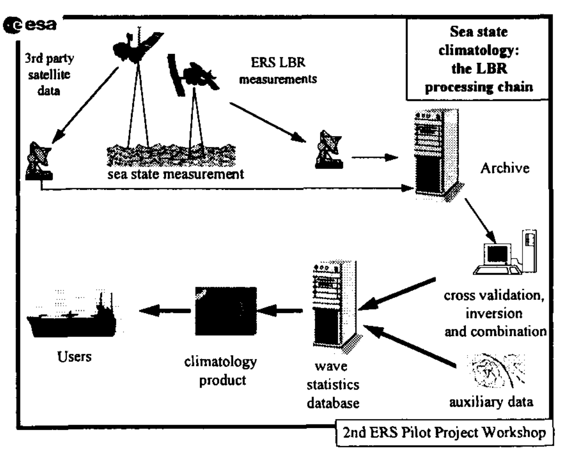

The capability to provide an adequate service is critically dependent of the ability to combine more than one data source in order to ensure a comprehensive data coverage with a suitable density of data points. This requires the availability of archive system calibration and instrument performance data in order to allow instrument cross calibration and validation between similar instruments on different platforms as well as cross validation between different instruments such as altimeter and wavebuoy comparisons. Considerable effort must be expended in order to build up a data base of wave climatology statistics which implicitly means considerable investment on the part of a service provider. As there are already wave atlas products available, end users can be difficult to convince of the added benefits of such climatolgy products that incorporate satellite data over conventional wave atlas data relying on in-situ data. Possible actions for stimulating this market are discussed in brief later in the paper.

4 END USER REQUIREMENTS

End user requirements in marine forecasting are primarily related to delivery time and accuracy both for short terms forecasts and also for medium to long term forecasts for the planning of offshore engineering activities. The format of the forecast product must be familiar and easy to use. Finally, end user confidence in the value of the product must be high. For applications such as ship routeing where a fixed low price route is available from a number of service providers, this is difficult. The costs when such a forecast is incorrect is immense however. On average, three ships with a displacement of over 500 tons are sunk every week and refit costs in dry dock for wave induced fatigue are considerable. For offshore operators, the tendency to try to cut operations costs as much as possible often leads to the temptation to attempt operations without a tailored forecast service. The task for service providers at present is to convince the end users that a quality product meeting all requirements can be delivered that is based on satellite data products and that this will make a positive impact to the normal operations of the end user.

In sea state climatology, end users are perhaps more aware of the cost benefit factors but there are still certain stagnation points preventing the exploitation of the full market potential. These include a low level of user confidence in the end product and a lack of a fully comprehensive demonstration of cost benefits arising from the utilisation of sea state climatology services.

5 SERVICE PROVIDER RESPONSIBILITIES AND REQUIREMENTS

Although many of the service providers are attempting to provide what is basically a commercial service which can be self financing and eventually profit making, there is still some way to go before fully commercial operations (in the sense that end users pay for the initial data provision) are realised. In part, this is due to the nature of the industry with small companies still relying on study, development, feasibility and proof of concept contracts in order to pay for the development of the operational services. End user investment is still lacking within Europe.

The service providers and "value added" institutions are in a difficult position however. On the one hand, there is a reliance on the availability of a data source that can provide suitable data of adequate quality to be delivered by a specified deadline. On the other hand, end users still require considerable further demonstrations in many areas (even within the more advanced marine application fields) of the benefits to be obtained from ERS data. Taking an extreme point of view, what the end users are currently being offered in some cases is a product or service that is guaranteed satisfactory for a restricted area under certain conditions with no firm delivery deadline. In order to further develop the service provided, further investment is required and some of this must come from the end users. The fact remains however, that some of the investment must come from the service providers themselves. This is difficult as the provision of such services does not guarantee immediate financial rewards. Such investment is, therefore, very difficult to justify. Nevertheless, some such investment must be forthcoming in order that the service provision industry can evolve from being continually reliant on 'space' and 'technology development' budgets of the European and national governmental institutions and instead start to involve finance from industry.

6 CONSEQUENCES FOR ESA

The principal responsibility for ESA as a data provider is to ensure a guaranteed data supply that meets the appropriate performance and quality criteria and to deliver each dataset by an agreed deadline. If these operational criteria cannot be met then applications such as sea state forecasting are impossible to implement in an operational scenario.

In addition to performance criteria, pricing policies are also important. If investment is to be forthcoming in a particular area of application development, investors require some estimate of the possible financial return. This in turn requires an estimate of how much the new service will cost and this depends on the pricing and distribution of both the data product provided by the data supplier and also that provided by the intermediate value added agencies. In particular, for services provided by meteorological agencies, WMO rulings on the exchange of meteorological data could have an effect on the level of service development. Some degree of stability in pricing and distribution strategy is required.

One further consequence for ESA is that there is a clear effort required to heighten awareness of the requirements of the end users and how these propagate back up the processing chain to the data providers. This generates a number of potential roles for ESA including that of stimulating further exploitation of the market by encouraging a greater degree of real end user involvement in future data exploitation and application development programmes.

7 FUTURE DEVELOPMENTS

The complex structure that currently characterises the remote sensing market within Europe inevitably means that any future progression will necessarily require some degree of cooperation between the data providers (ESA), the service providers and the end users. In particular, this means real financial investment in order to take service provision from what is basically a pre-operational phase to a fully operational utilisation of a commercially funded data source. This cooperation exists to a certain extent already. The various PP/PI and national data exploitation programmes have meant considerable cooperation between data suppliers and service providers. Obvious cooperation is already in place between a restricted subset of the end user community and the service providers. At present however, there is very little interaction between data suppliers and end users, for a variety of reasons. The figure below illustrates the interactions required in order to develop the market.

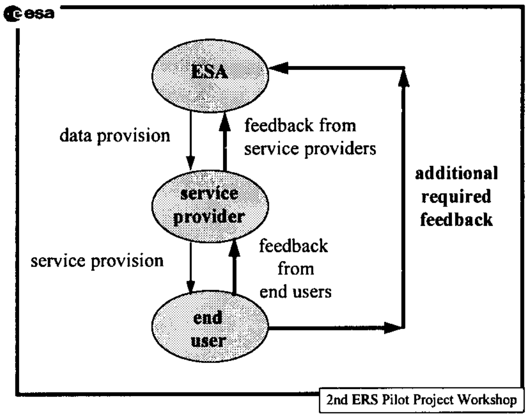

8 SUMMARY AND CONCLUSIONS

The present status of ERS data utilisation within marine application areas should be viewed in the context of the original mission objectives where it was stated that one of the aims of the ERS mission was to demonstrate the commercial feasibility of the utilisation of spaceborne microwave remote sensing data. The fact that a number of commercial companies are now beginning to provide commercial services which make use of ERS data means that this original mission objective has been met. However, the provision of operational services must evolve in order to provide better quality of end product tailored to the specific requirements of the end users.

Evolution of the market is definitely occurring but it is happening slowly. The correct trends are visible, in particular, with regard to an increased commercial utilisation of ERS data products. Many of the players involved in the service development are currently small companies however and are therefore more vulnerable to the financial climate than a larger player would be and less able to invest heavily in the development of an operational service.

REMOTE SENSING OF WIND AND WAVES OVER THE WESTERN MEDITERRANEAN SEA

P. Queffeulou, T. Elfouhaily and V. Kerbaol
IFREMER
BP 70, 29280 Plouzané, France
tel (33) 98 22 42 94 e-mail pierre.queffeulou@ifremer.fr
P. Le Borgne and J.M. Lefevre
METEO FRANCE

Abstract. The application of wind and wave remote sensing to the study of short spatial scale meterological events, in the western Mediterranean Sea is described. This is performed within the project PP2-F17A, "Etude du Mistral en mer à partir des données du satellite ERS-1". On one hand, ERS-1 altimeter and SAR data reveal off-shore increase of wind and wave during northerly wind regimes like Mistral. On the other hand electromagnetic modelling under development indicates that the real wind gradient might be a little less than that deduced from altimeter and SAR measurements due to the fetch effect on these measurements. Such applications will benefit to the improvement of the knowledge of meteorological forcing conditions in this area of the western Mediterranean Sea which plays a major role in deep water formation.
Keywords: mistral, western Mediterranean Sea, wind, waves, fetch, altimeter, SAR.

1. INTRODUCTION

Some application of wind and wave remote sensing to the study of local events of small spatial scales, such as Mistral and Tramontane, over the western Mediterranean Sea, is described. Though having large off-shore extension, due to the off-shore direction of the wind (Northerly to north-westerly) such events are often characterised by rapid changes in wind and wave in the near coastal waters, for instance over the Gulf of Lion, at scales ranging from a few tens of kilometers to one or two hundred kilometers. Small scale and near coastal effect are main constraints to remote sensing observations of such phenomena.

A short review of the available satellite-borne sensors usefull for this type of application is presented in section 2. Then, mean wind and wave field altimeter data are analysed (section 3). Examination of individual passes over Gulf of Lion, reveals some fetch effect on the altimeter backscatter coefficient and hence on the inferred wind altimeter wind speed (section 4). Some of the work presently performed in IFREMER department of Océanographie Spatiale in term of backscatter modelling for application in this domain is then shortly presented, first for the altimeter (section 5) and then for the SAR image mode (section 6).

2. WIND WAVE SENSOR REVIEW

The ERS-1 **scatterometer** allows to estimate the wind speed and direction over a 500 km swath, with a 50 km resolution, over a 25 km grid. Examples of such measurements during Mistral events [1] already revealed strong wind speed gradients over the north-western Mediterranean Sea. The use of such sensor might be of prime interest for the present subject but in practice its interest is strongly limited, for two main reasons. The first one is that the SAR image mode is often activated over the Mediterranean Sea, and when the SAR is on, the wind mode of the scatterometer can not be operated. The second reason is that accurate wind speed retrieval from the scatterometer is only possible if the 3 antennas of the instrument are operating together, and this is often not the case over the Mediterranean Sea because of many transitions between land and sea, and consequently switches off-on of antennas. Analysis of the scatterometer data over the Western Mediterranean shows that many measurements are not valid also because of land and island contamination of the signal. So, over the Mediterranean area of interest, statistical estimates based on ERS-1 scatterometer measurements are not significant.

The **SAR wave mode** produces short imagettes every 200 km in the along-track direction, allowing under certain conditions to get information on bidimensional wave spectra. Although the imagette resolution is high, the spatial sampling is not high enough for the present study.

The **SAR image mode** is often activated over the Mediterranean Sea, as previously indicated. The measurement resolution is high, allowing to get information on bidimensional wave spectrum. One limitation is the geophysical interpretation of the data, and particularly for short sea-state wavelength, as it is often the case for short fetch area. An other limitation of SAR image usefulness for our particular study is that Mistral is characterised by northerly to north-westerly wind, corresponding nearly to wave travelling in the azimuth direction of the radar, for which, at high wind, the wave pattern restitution is degraded. An other limitation is the narrow 100 km swath, which does not always permit to sample correctly events of interest. Nevertheless, SAR image processing developped in IFREMER department Océanographie Spatiale and application to the area, will be shortly described in section 6.

The **SSMI**, Special Sensor Microwave Imager, of the U.S. Defense Meteorological Satellite Program, estimates surface wind speed [2], using radiometer measurements in channels 19.35 GHz, 22.23 GHz and 37.0 GHz. Such measurements in Mistral events also reveal narrow areas of strong surface wind speed [1]. One interest of this sensor is its large swath (1400 km). The resolution is 50 km but the correlation between neighbouring pixels prevents from using the data inside the 100 km to 150 km limit off the coast.

The **altimeter** radar, though having a very narrow swath (about ten of km, along the nadir ground-track) offers the opportunity to get information on both wave height and surface wind speed (not direction), and at a high along-track sampling rate (about 7 km for ERS). Application of altimeter measurements is illustrated hereunder.

3. ALTIMETER WIND AND WAVE FIELDS

Altimeter radars on-board satellites allow the measurement of significant wave height (swh) and surface wind speed, along the ground-track with a resolution better than 10 km. Comparison of the altimeter coverages (Figure 1) of ERS-1, with a 35-day repeat cycle, and of TOPEX, with a 10-day repeat cycle, shows that the long cycle of ERS-1 associated with a better spatial sampling is more adapted than the TOPEX one to study spatial structure of local events such as Mistral and Tramontane.

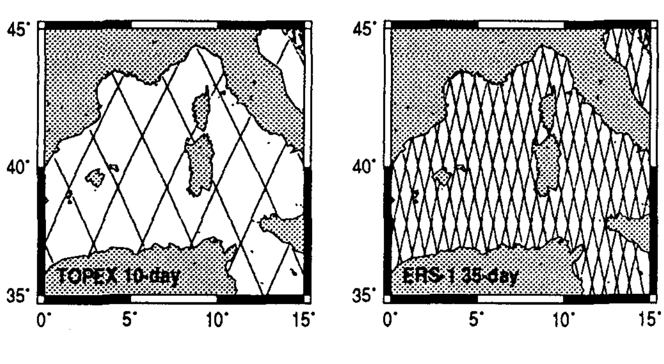

Figure 1: Altimeter coverage.

Mean values of ERS-1 altimeter measurement fields were computed over the time period from April 1992 to December 1993, corresponding to the 18 ERS-1 35-day repeat cycles (Figure 2). Original data are the OPR processed and provided on CD-ROM by French PAF CERSAT. Maximum for surface wind speed (7 ms^{-1}) and for significant wave height (1.8 m) are observed off the Gulf of Lion. Location of the maximum swh is shifted towards the South relatively to the location of the wind speed maximum. This can be explained by a fetch effect because the strongest wind speed are associated with northwesterly winds (for the present 18 cycle sampling). For the location of the maximum wind speed the fetch is not long enough to get fully developped sea and maximum swh, so that, further towards the South, though the wind speed is less, the swh is larger because the fetch is longer.

Seasonal mean wind speed fields (Figure 3) show a shift of the maximun towards the West between winter and summer months. The narrow maximum during summer certainly results from the impact of northerly to north-westerly winds over that time period.

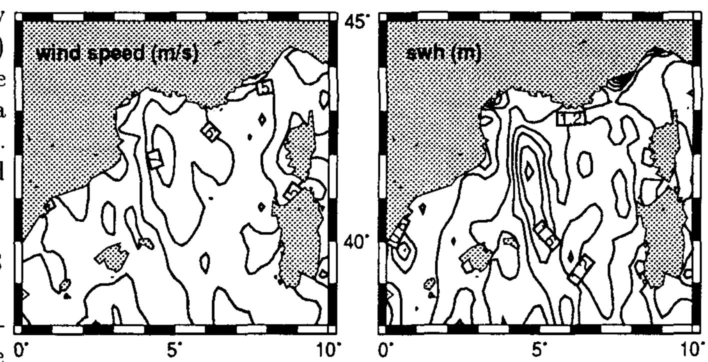

Figure 2: Mean ERS-1 altimeter wind speed and swh over the 18 35-day cycles.

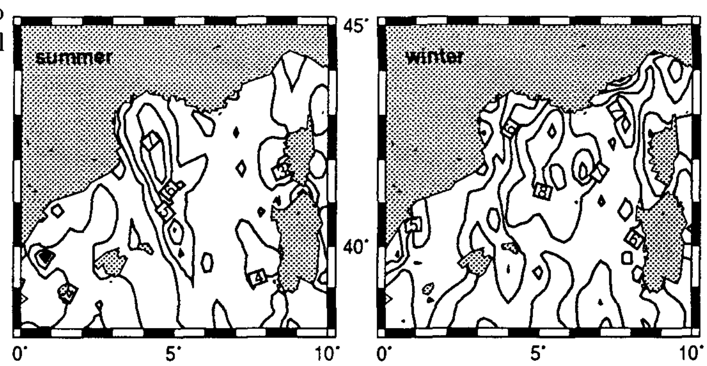

Figure 3: Seasonal ERS-1 altimeter wind fields.

4. INDIVIDUAL ALONG-TRACK MEASUREMENTS

The ascending passes along the particular ERS-1 ground track crossing Gulf of Lion (Figure 4) were examined. Among these, five particular passes were selected, corresponding to the strongest wind and wave conditions over the period, and to Mistral Tramontane events. Wind speed and swh measurements are shown as a function of the latitude on Figure 4. The most noticeable fact is the large increase of wind speed estimated from the altimeter measurement, when going off the coast. The corresponding swh increase is relatively lower, certainly because of combine effect of wind and fetch. This is clearly seen on the normalised representation of wind and swh as a function of distance to the coast (Figure 5). Wind speed and swh are normalised by the maximum value observed for each pass over the 400 km off-shore distance. These curves show significant gradient of wind speed and of swh, with comparable features among the passes. Nevertheless, one can wonder whether these strong off-shore gradients, particularly for wind speed, are realistic.

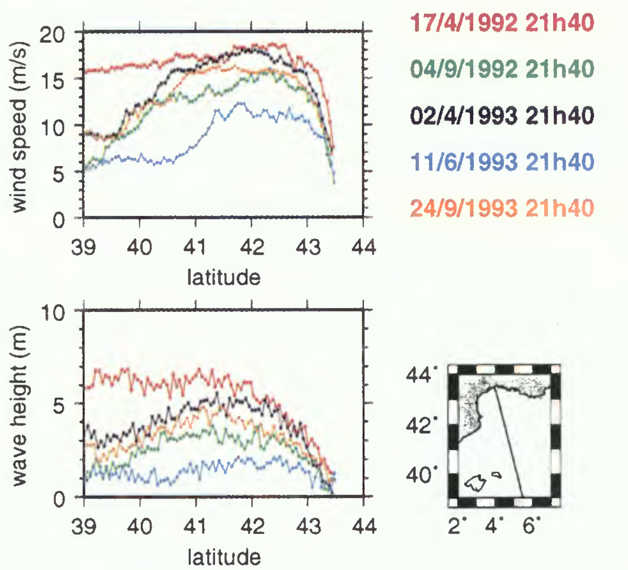

Figure 4: Wind and wave data along particular ERS-1 passes.

For off-shore winds like Mistral and Tramontane, it is known and it is currently observed by sailors that the sea surface wind speed strongly increases off-shore. Several factors contribute to this. A first one is the change in surface roughness when going from over the land to over the sea, resulting in a decrease of the surface friction. Secondly, the sea surface temperature being higher than the air temperature, an unstable atmospheric stratification is created. When the cold air spread ahead over the sea, the lower layers are warmed by the sea surface, which tends to decrease the stratification and consequently also to decrease the friction at the surface.

Some sea surface temperature (sst) gradient might also interact because of coastal upwelling, but on a minor sense. In fact, inspection of sst deduced from AVHRR data, at the french Centre de Météorologie Spatiale (Météo France), reveals a sst gradient about 3 degrees C over the Gulf of Lion, for one of the five cases selected above, but also homogeneous sst for an other case, for similar measured wind speed gradients in the two cases.

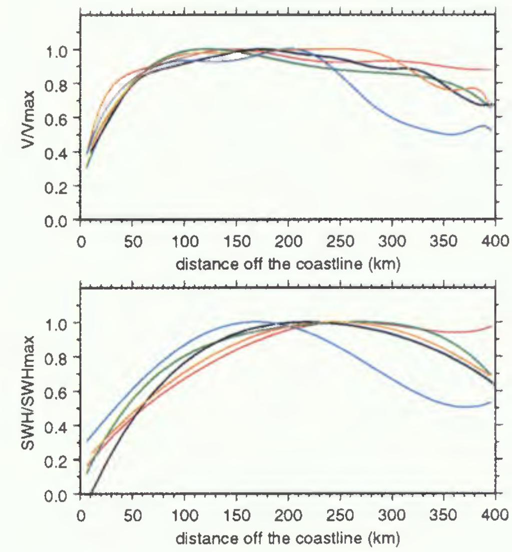

Figure 5: Maximum normalised wind and wave altimeter data.

Comparison of altimeter wind speed to the data of the 12 hour forecast wind fields from the french PERIDOT model of Météo France, shows that, near the coast, the altimeter wind speed is relatively low.

Indirect verification of the altimeter wind speed consistency can be performed as in [3]: from the altimeter swh measurement, the minimum wind speed needed for reaching the level of swh can be estimated, as a function of the fetch, using relationships such as given by [4], from JONSWAP experiment, or by [5], between wind speed, fetch and swh. Here the fetch is approximated as the along-track distance to the coast.

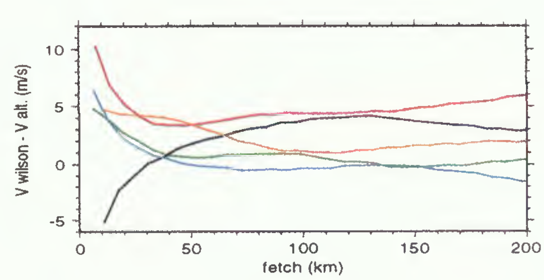

Figure 6: Difference between minimum wind speed from Wilson model and altimeter wind speed.

The curves of Figure 6 show the differences between the minimum wind speed needed to get the altimeter measured swh, using Wilson [5] relationship, and the altimeter measured wind speed. Largest differences are observed for shortest fetches. For four over the five selected cases the altimeter wind speed is greatly underestimated for fetch less than 50 km. Of course the uncertainty in applying the model [5] so as in the approximation for the fetch is large, but it seems that the altimeter wind speed might be underestimated for short fetches. The next step will be to quantify this underestimation in order to be able to estimate the right geophysical value for off-shore wind speed increase. Some work is presently in development for this, consisting in adding some information on the fetch, when needed, in the altimeter σ_0 to wind speed modelling.

5. ALTIMETER σ_0 AS A FUNCTION OF WIND SPEED AND FETCH

In practice, the surface wind speed is estimated from measurements of the radar backscatter, σ_0, by mean of an empirical model [6]. This empirical model was developed using SEASAT and GEOSAT altimeter data and buoy observations, not taking into account any fetch effect. One can however use an electromagnetic function based on the Kirchhoff approach to assess the effect of fetch on σ_0. A surface spectral representation is required to develop such theoretical model. We use in this study a JONSWAP type spectrum [4] for long waves and a Rodríguez [7] type spectrum for short waves. Hence, the omnidirectional spectrum can be written as:

$$S(k) = k^{-4}[B_l(k) + B_s(k)]$$

where $B_l(k)$ and $B_s(k)$ are the saturated spectra for long and short waves respectively, k being the wavenumber. The spectral level and shape were tuned to agree with observations from: [8] and [9] for the spectral peak; optical measurements of [10] for the mean square slope; [11] and [12] in the range of capillary-gravity waves around 2 cm wavelength.

The non-dimensional fetch parameter, X, is introduced by the wave age dependence of the spectral peak position and level. The wave age parameter Ω^{-1} is connected to the non-dimensional fetch by the relation: $\Omega = 11.6X^{-0.23}$, from [4]. The effect of the fetch on σ_0 is clearly shown on Figure 7. We observe that wind speed is under-estimated by the operational altimeter model [6] for short fetch cases. This result is in agreement with observations from the Mistral cases presented in previous section. However some inconsistency appears at low winds (about 5 ms^{-1}), where the spectral model was not fully tested.

6. SAR IMAGE PROCESSING OVER THE GULF OF LION

The dependence of SAR azimuth cutoff with fetch during Mistral events has been studied along the swath

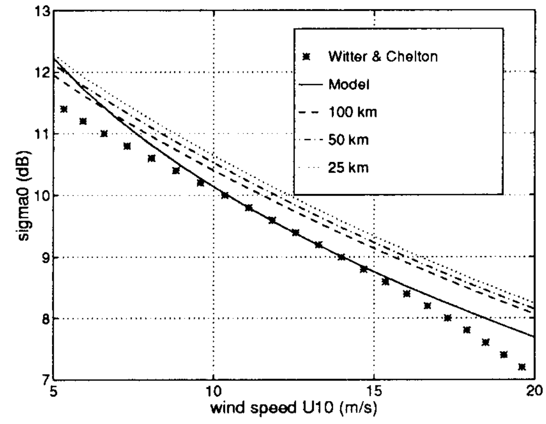

Figure 7: Altimeter σ_0 dependence on wind speed and fetch.

of both a SAR ERS-1 Precision image (PRI) and a Single Look Complex image (SLC), provided by ESRIN ERS Order Desk.

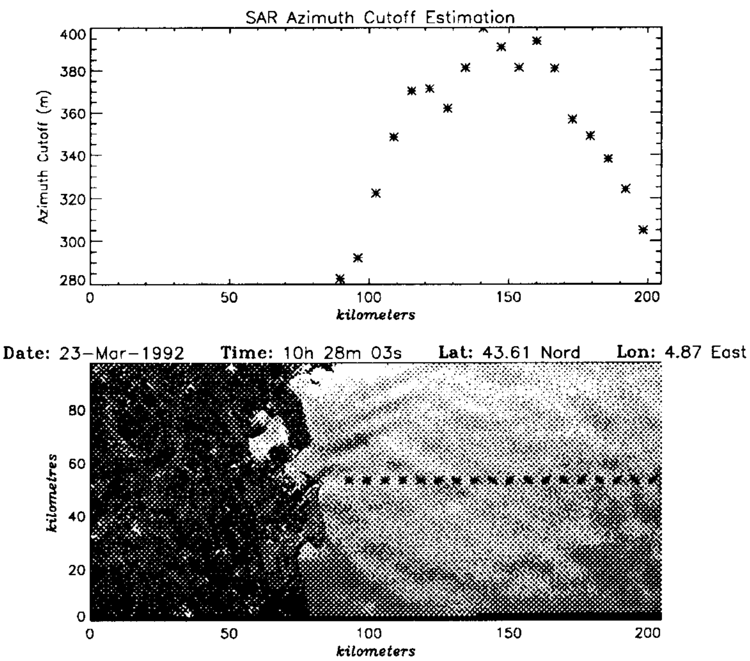

Figure 8: Estimated values of the azimuth cutoff along the radar swath for the PRI 3-looks image. Values are estimated in location indicated by stars on the image.

The motions occuring during the SAR integration time induce an azimuth smearing [13-14] that acts as a Gaussian low-pass filter on the azimuthal components of the SAR image spectrum. The cutoff wavelength that is typically of several hundred of meters prevents the SAR from imaging azimuthal wave systems shorter than about 200 meters. The SAR azimuth cutoff is directly bound to the standard deviation of total azimuthal displacement field during the SAR integration time and most of this quantity is related to the wind waves orbital velocities. It has then to be seen as a cinematic parameter. In particular, the estimated cutoff has revealed so far to be a good indicator for wind speed estimate, through a linear relation with the wind speed with a slope of 23.2 [15].

The azimuth cutoff has been estimated along the SAR swath (Figure 8). Geographical north corresponds to the left side of the image. The coastline is the north part of Gulf of Lion, just west of Marseille. The Rhône mouth can be seen in the middle of the coastline on the image. The observed off-shore increase of the cutoff is associated with increase of wind speed, through the above linear relation. However the estimated cutoff values have then been checked against theoretical values inferred from a fetch dependent sea spectral model (Figure 9) for wind speeds ranging from 2 to 15 ms^{-1}. It appears that the linear relationship underestimates the wind speed for fetch limited cases.

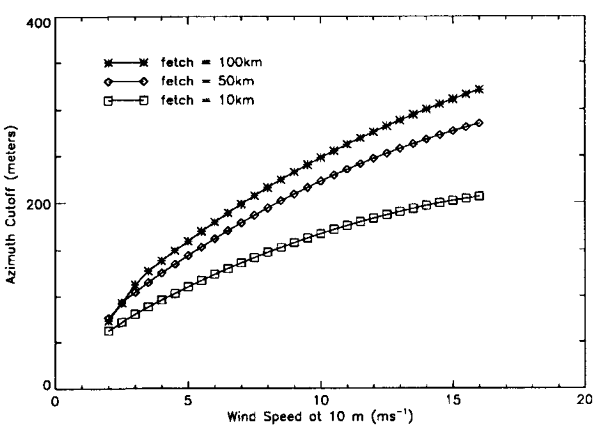

Figure 9: Estimate of the azimuth cutoff value for different wind speeds at 10 meters and different fetch values (10, 50 and 100 kilometers).

From this model, it becomes now possible to retrieve wind speed from the azimuth cutoff parameter estimation in taking into account the dependence of this parameter with both fetch and wind speed [16].

7. CONCLUSION

The ERS-1 altimeter has been shown usefull, on a 35-day repeat cycle orbit, to describe the wind speed and wave height fields in the western part of the Mediterranean Sea. Impact of high northerly to northwesterly winds, like Mistral and Tramontane, appears on global and seasonal wind fields.

The off-shore increase of wind speed for these types of meteotological regimes, is observed, but the real wind speed gradient might be a little less than that deduced from the altimeter measurements, because the altimeter backscatter coefficient is also fetch depending. An electromagnetic model is on development and already explains that for short fetches the altimeter wind speed might be underestimated when using the classical operational σ_0 wind model. The proposed elctromagnetic model has yet to be extended to low wind speed and tested relatively to accurate in-situ measurements.

Sar image processing development applied in such meteorological regimes, also showed the off-shore wind increase, together with some fetch impact on the radar measurement. This modelling has also to be quantitatively tested.

Application of such processings to remote sensed data will benefit to the improvement of the knowledge of meteorological forcing conditions in this area of the western Mediterranean Sea which plays a major role in deep water formation.

8. REFERENCES

[1] Queffeulou P. and A. Bentamy, Wind and wave field structures from satellite measurements during mistral events, Proceedings of the First ERS-1 Pilot Project Workshop, Toledo, Spain, 22-24 June, 1994, ESA SP-365, 15-19, October, 1994.

[2] Goodberlet, M. A., C. T. Swift and J. C. Wilkerson, Remote sensing of ocean surface winds with the special sensor microwave-imager, J. Geophys. Res., 94, 14547–14555, 1989.

[3] Ebuchi N., H. Kawamura and Y. Toba, Growth of wind waves with fetch observed by the GEOSAT altimeter in the Japan Sea under winter monsoon, J. Geophys. Res., 97, 809-819, 1992.

[4] Hasselmann, K., T.P. Barnett, E. Bouws, H. Carlson, D.E. Cartwright, K. Enke, J.A. Ewing, H. Gienapp, D.E. Hasselmann, P. Kruseman, A. Meerburg, P. Muller, D.J. Olbers, K. Richter, W. Sell and H. Walden, Measurements of wind-wave growth and swell decay during the Joint North Sea Wave Project (JONSWAP), Dtsch. Hydrogr. Z., Reihe A (8), 12, 95 p, 1973.

[5] Wilson B. W., Numerical prediction of ocean waves in the North Atlantic for December 1959, Dtsch. Hydrogr. Z., 18, 114-130, 1965.

[6] Witter D.L. and D.B. Chelton. A GEOSAT altimeter wind speed algorithm and a method for altimeter wind speed algorithm development, J. Geophys. Res., 96, 8853-8860, 1991.

[7] Rodríguez E., Y. Kim and J.M. Martin, The effect of small-wave modulation on the electromagnetic bias, J. Geophys. Res., Vol. 97, No. C2,2379-2389, February 15,1992.

[8] Kahma Kimmo K., A study of the growth of the wave spectrum with fetch. J. of Physical Oceanography, Vol. 11, No. 11, November, 1981.

[9] Dobson F., W. Perrie and B. Toulany, On the deep-water fetch laws for wind-generated surface gravity waves, Atmos. Ocean, 27 (1), pp. 210-236, 1989.

[10] Cox C.S. and W.H. Munk, Slopes of the sea surface deduced from photographs of sunglitter, Bullj. of Scripps Inst. Oncean., 6, 401-487, 1956.

[11] Jähne B. and K. S. Riemer, Two-dimensional wave number spectra of small-scale water surface waves, J. Geophys. Res., Vol. 95, No. C7, pages 11,531-11,546, July 15, 1990.

[12] Klinke, J. and B. Jähne, 2D wave number spectra of short wind waves - Results from wind wave facilities and extrapolation to the ocean, Optics of the Air-Sea Interface: Theory and Measurements, SPIE Proc. 1749, pp. 1-13, 1992.

[13] Hasselmann K. and S. Hasselmann, 1991, On the nonlinear mapping of an ocean wave spectrum into a SAR image spectrum and its inversion, J. Geophys. Res., 96, 10713-10729, June 1991.

[14] Brillinger D. R., Distributions of particle displacement via higher-order moment functions, IEE Proc.-F, Vol 140, No 6, December 1993.

[15] Chapron B., T. Elfouhaily, V. Kerbaol, A SAR Speckle Wind Algorithm, proc. of Second ERS-1 Workshop, IFREMER Brest, BP 70, 29280 Plouzané, France, 1994.

[16] Kerbaol V., T. Elfouhaily, B. Chapron and R. Garello, Fetch and wind speed dependence of SAR azimuth cutoff and higher order statistics in a Mistral wind case, IGARSS'96 (submitted).

USE OF ERS WIND AND WAVE DATA FOR NUMERICAL WAVE MODELLING AT METEO-FRANCE

Didier Le Meur, Hervé Roquet, Jean-Michel Lefèvre

Météo-France, 42, avenue Gustave Coriolis, 31057 Toulouse, France
Tel: (33) 61-07-82-95

ABSTRACT

ERS active microwave sensors offer clear advantages for the study of the sea-state. However their measurements have still been little exploited operationally. At the marine forecasting department of Météo-France, the application projects have been focused first on the use of the scatterometer wind data to improve the forcing of the sea-state model VAG by a re-analysis process. But in addition, an assimilation of the altimeter wind speed and significant wave height data has also been retained to improve directly the model fields.

Both methods have been tested concurrently with ERS-1's scatterometer and altimeter over the North Atlantic, evaluating their respective impacts mainly by comparison with the altimeter measurements from Topex/Poséïdon satellite. First results, obtained through two-month hindcast experiments, show an improvement in the description of the mean wave energy in each case, corresponding basically to better propagation directions with the scatterometer data and better significant wave heights with the altimeter data.

1. INTRODUCTION

The active microwave sensors on board of ERS satellites (altimeter, scatterometer, synthetic aperture radar or SAR) offer clear advantages for the study of the sea-state. They allow specially a global and continuous coverage, as well as a much better resolution than conventional observations from ships and buoys. Moreover, if the altimeter and the SAR describe directly the sea-state in terms of significant wave height (SWH) and energy spectrum respectively, the scatterometer, measuring the surface wind in speed and direction, is not less interesting for it : wave forecasting being rather a boundary condition than an initial value problem, numerical sea-state models benefit often more from a quality wind forcing than a good analysis.

In spite of their relevance, the data provided by those sensors have been little exploited yet. Indeed, the interpretation of radar measurements has needed long developments and remains relatively difficult, particularly in the case of the SAR. Moreover, the introduction of scatterometer data into atmospheric models has had little success with classical methods, so that in practice only altimeter data have been assimilated operationally.

The present paper describes the application studies carried out in that context at the marine forecasting department of Météo-France. The priority has been given to the use of the scatterometer data to improve the forcing of the operational second generation model VAG (Guillaume, 1987). Awaiting the avaibility of more suitable methods to assimilate that kind of data into atmospheric models, a simple re-analysis of the current forcing winds has been implemented. In addition to this re-analysis, a dedicated scheme has also been set up to assimilate the altimeter wind and wave data. Impact studies have then been carried out with both methods, performing parallel hindcast experiments over the North Atlantic with ERS-1 data and comparing the results mainly with the altimeter data from Topex/Poséïdon satellite.

2. WIND FORCING WITH SCATTEROMETER DATA

VAG is usually forced by the surface winds from the operational weather model ARPEGE (Courtier et al., 1991). This model uses a classical analysis scheme, in which its different 6-hour forecast fields (wind, temperature and geopotential) are updated by optimal interpolation with the available observations. To introduce ERS scatterometer data in the forcing of VAG, that analysis scheme has simply been restricted to the surface wind field, and re-operated leaving the successive 6-hour forecasts unchanged.

In a first approach, the isotropic and uncorrelated error model used for the optimal interpolation of conventional wind observations has been kept for the satellite data. An error of 2 m/s standard deviation in geographic components was thus allotted to ERS-1 scatterometer, against 3 m/s and 4 m/s for ships and buoys respectively. The existing methods have also been conserved for data selection and quality control, retaining only the closest observations to every analysis point, and comparing each of them in modulus and direction with the forecast and the analysis obtained without the considered observation.

Compared with a complete assimilation cycle, the re-analysis process defined in that way has the major defect not to integrate the data introduced in time. In return, it allows to give them a maximum instantaneous impact by reducing to a minimum the constraints imposed in the analysis scheme.

3. ASSIMILATION OF ALTIMETER DATA

Different methods have been applied to assimilate wind and wave altimeter data into sea-state models. The one developped at ECMWF for operational use in the third generation model WAM (Lionello et al., 1992) was chosen as a basis to implement a dedicated assimilation procedure in VAG.

Proceedings of the Second ERS Applications Workshop, London, UK, 6–8 December 1995 (ESA SP-383, February 1996)

That method is based on an optimal interpolation scheme in which the model significant wave height and wind speed fields are combined with the altimeter measurements according to a 6-hour cycle. The wave energy spectrum is then analysed through a scaling allowing to reproduce the total energy deduced from the interpolated SWH, and a stretching aiming at correcting the mean frequency. Two cases are distinguished to asses this stretching : when the windsea is predominant, the mean frequency is updated from a parametrization of the model growth, assuming that the wind duration is correct; when the swell prevails, the spectrum is stretched so as to ensure the conservation of the average steepness. The wind speed infered from the measurements is used only to control an analysed wind speed, derived from the significant wave height under the hypothesis of a correct ratio between the windsea and swell energies, and taken into account to rebuild the spectrum in the first case.

To fit the method, the original windsea and growth parametrizations established for WAM were replaced by those of the JONSWAP type inherent to VAG. Moreover, the optimal interpolation scheme was improved introducing a data selection and empirical correlation distances deduced from departure statistics between the altimeter and model data (250 km for the wind and 600 km for the waves).

4. PARALLEL FORCING AND ASSIMILATION HINDCAST EXPERIMENTS

VAG is usually operated over the North Atlantic, within a grid with a mesh size of about 150 km. For the present purpose, a fine-scale version of the model was implemented, using spherical coordinates with a 0.5-degree resolution and a spectrum of 22 frequencies by 18 directions (Fradon, 1994). Parallel forcing and assimilation hindcast experiments have then been carried out with ERS-1's sensors, driving the model successively with winds re-analysed at the same 0.5-degree resolution with and without the scatterometer data, and adding or not in the first case an assimilation of the altimeter data. Those experiments, called NODATA, SCAT and ALTI according to the data taken into account, were achieved in a first time over the months of October and November 1993, corresponding to the main observation periods of the sea-measurement campaign SEMAPHORE that took place in the Azores region (Eymard et al., 1994).

Off-line products from the french archiving and processing facility CERSAT (Quilfen, 1994) were used in the scatterometer case, retaining only one point out of two so as to match the analysis resolution. The fast delivery products from ESA were considered in the altimeter case, correcting the SWH calibration error detected during their validation (Queffeulou et al., 1992); an averaging to the analysis resolution, together with a quality control, was also performed in the beginning of the assimilation procedure according to the WAM method.

5. IMPACT OF THE SCATTEROMETER DATA

The impact of the scatterometer data was first assessed from departure statistics between the SCAT and NODATA wind and wave fields of October and November 1993. The means obtained exhibit a positive bias in the SWH at low latitudes, associated to an increase of the tradewinds in the SCAT case (figure 1). That bias, exceeding 50 cm over the Caribbean sea, suggests an under estimation of the tradewinds in the absence of scatterometer data, due to an already known shortcoming of weather model forecasts. The standard deviations show that apart from this systematic impact, most of the information is brought in terms of variability in mid-latitude perturbed regions, with maxima of 40 cm for the SWH (not shown).

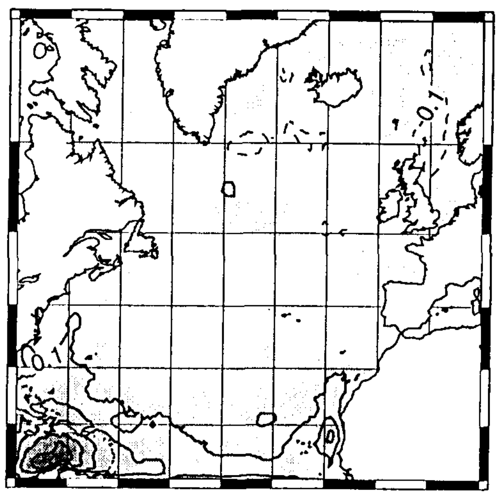

Figure 1 : Mean difference between the SCAT and NODATA SWH fields. Contour intervals are 0.1 m.

The results were then evaluated comparing the SCAT and NODATA fields with the wind speed and direction observations from the Marisonde drifting buoys deployed within SEMAPHORE (about 21000 data on a hourly basis), and with the altimeter SWH measurements from Topex/Poséïdon satellite (about 40000 data after quality control and averaging to the analysis resolution).

In order to make the study more conclusive, the comparisons were restricted to the situations having the largest departures between the SCAT and NODATA fields : minimum values were imposed in modulus respectively to the vector difference of the wind and to that of the mean sea-state defined by the SWH and the mean propagation direction. The agreement with the reference data was thus studied as a function of the impact of the scatterometer data.

The error curves obtained (figures 2a and 2b) denote a clear improvement in the presence of the scatterometer as the impact becomes relevant, both in terms of wind vector and SWH. That improvement is naturally more significant for the wind, which benefits directly from the data introduced. For the waves, the results are globally neutral and the agreement with the altimeter data is only enhanced at a 70 % confidence level beyond a threshold of about 2.5 m. Nevertheless the favourable cases amount to a proportion of 65 to 75 % above that threshold and, as shows a direct analysis, correspond basically to the perturbed situations of the highest importance.

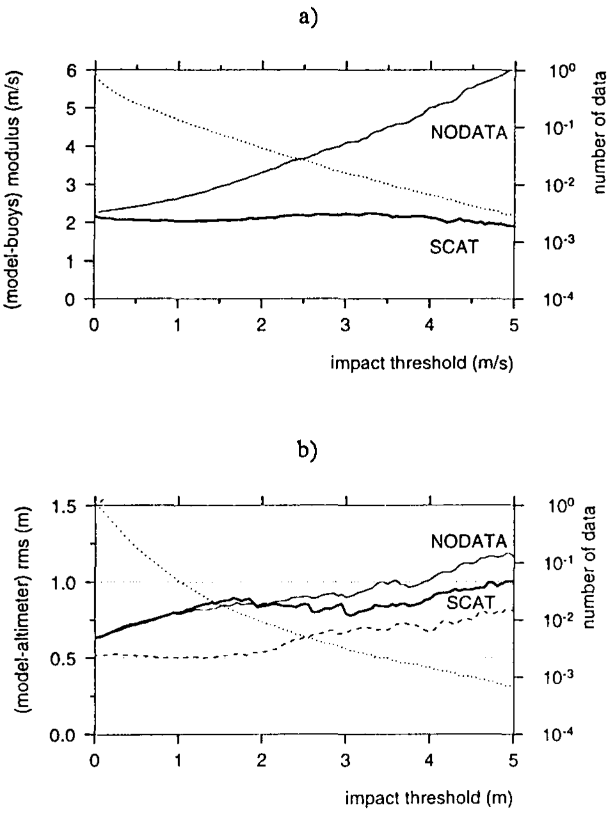

Figure 2 : Mean modulus error of the SCAT and NODATA wind fields with respect to the observations from Marisonde buoys as a function of the impact of the scatterometer data on the wind (a) and root mean square error of the corresponding SWH fields with respect to Topex/Poséïdon measurements as a function of the impact on the mean sea-state (b). The dotted lines represent the number of data exceeding a given impact threshold divided by the total number of data, and the dashed one for the waves indicates the proportion of favourable SCAT cases between 0 and 1 in the same scale as the error.

A new study, imposing a threshold on the wind and no longer the mean sea-state (figure 3), indicates that the information brought to the waves has paradoxically a negative impact as the wind corrections are being applied. Therefore the gain observed concerns mainly the swell and is limited by a certain degradation of the windsea. That degradation is probably due to the forcing scheme used, whose 6-hour constant window allows non-negligible time lags in the application of the scatterometer data.

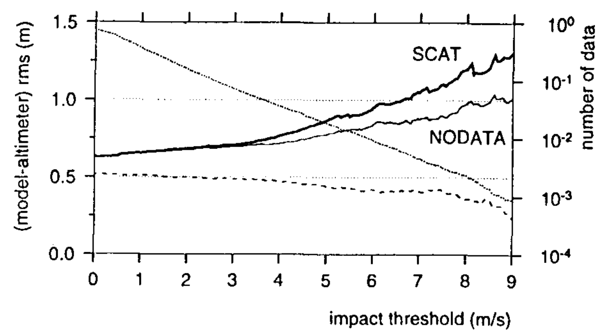

Figure 3 : Same as figure 2b, but with a threshold on the wind instead of the mean sea-state.

6. IMPACT OF THE ALTIMETER DATA

The impact of the altimeter data was assessed in mean and evaluated with respect to Topex/Poséïdon data from the ALTI and NODATA fields, alike for the scatterometer data. Morevoer its features were specified by comparing the results with the previous ones.

The mean difference between the ALTI and NODATA significant wave heights (figure 4) confirms the positive bias found at low latitudes with the scatterometer data. However, the maximum over the Caribbean Sea, with hardly more than 10 cm, is strongly reduced. In fact, the value obtained with the SCAT SWH (50 cm) can be found again comparing the altimeter data with the NODATA SWH. So, rather than an over estimation of the scatterometer measurements due to swell effects or boundary layer stability problems, the explanation is an insufficient integration of the altimeter data in the absence of a correction of the forcing wind. Alike for the scatterometer data, the (ALTI - NODATA) standard deviations still exhibit a main impact in terms of variability at mid latitudes, but with slightly higher maxima for the SWH (50 cm instead of 40 cm).

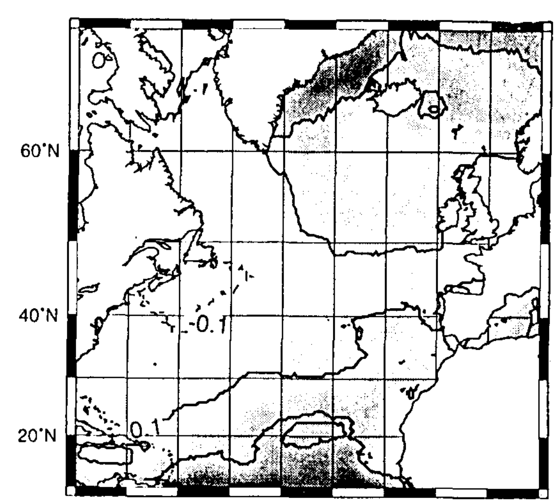

Figure 4 : Mean difference between the ALTI and NODATA SWH fields. Contour intervals are 0.1 m.

The error curves representing the agreement with Topex/Poséïdon data as a function of the impact on the mean sea-state (figure 5) also exhibit clearer results with the ALTI than the SCAT wave field : this time the gain is globally significant, with a reduction of the root mean square error by more than 10 % (64 cm to 57 cm), and stays significant at a 95 % confidence level to a threshold of 2.5 m. However the marginal impact is afterwards not more significant than in the case of the scatterometer, and on the contrary the ratio of favourable cases is somewhat reduced (55 to 60 %).

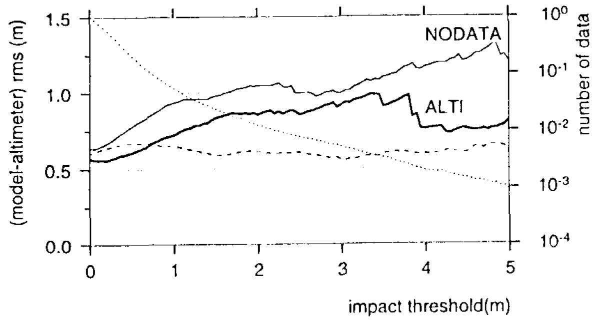

Figure 5 : Root mean square error of the ALTI and NODATA SWH fields with respect to Topex/Poséïdon measurements as a function of the impact of the altimeter data on the mean sea-state. The dotted line represents the number of data exceeding a givent impact threshold divided by the total numer of data, and the dashed one indicates the proportion of favourable ALTI cases between 0 and 1 in the same scale as the error in m.

Another evaluation, imposing a threshold on the significant wave height instead of the mean sea-state (not shown), allows to better distinguish the respective roles of the altimeter and scatterometer data : the former ones enhance directly the SWH, and as a consequence benefit to the modulus of the mean sea-state; the latter, on the other hand, affect little the SWH or even tend to deteriorate it because of the temporal shortcomings of the forcing scheme, and so provide necessarily a better description of the wave field's directions. Both kinds of data thus appear to be complementary, and likely to provide the largest benefit in case of joint use.

7. CONCLUSION

This work allowed to confirm the utility of ERS-1 scatterometer and altimeter data to feed numerical sea-state models, and to specify their respective impacts on the wave description : the altimeter data improve directly the significant wave height, and hence provide a perceptible gain on the mean energy field, whereas the scatterometer measurements, affecting mainly the propagation directions, have a more subtle but not less appreciable impact as the information brought becomes significant. Moreover the demonstration was made, together with Topex/Poséïdon altimeter, of the potential of those sensors to test wave models and, in return, of the relevance of the latter to produce cross-validations between satellite wind and wave measurements.

Further investigations are still needed, particularly to perfect the use of scatterometer data from a temporal point of view and better evaluate their influence on the representation of the wave spectrum, for example using ERS-1 SAR measurements. It is also necessary to check the relevance of a joint use of scatterometer and altimeter data, or again to widen the study period so as to account for seasonal effects. Nevertheless the results obtained are already encouraging enough to plan operational applications with the re-analysis and assimilation tools implemented in a near future, and to expect again more benefit from scatterometers with variational analysis schemes in a longer term.

8. REFERENCES

Courtier, P., C. Freydier, J. F. Geleyn, F. Rabier, M. Rochas, 1991 : The ARPEGE project at Météo-France. Workshop proceeedings, ECMWF.

Eymard, L. et al., 1994 : Experimental study of ocean-atmosphere exchanges. Preprints Second international conference on air-sea interactions and on meteorology and oceanography of the coastal zone, Lisbon, American Meteorological Society, pp 48-49.

Fradon, B., 1994 : Caractérisation des états de mer pendant la campagne SEMAPHORE. Note de travail de l'ENM, 459, Météo-France.

Guillaume, A., 1987 : VAG, modèle de prévision de l'état de la mer en eau profonde. Note de travail de l'EERM, 178, Météo-France.

Le Meur, D., H. Roquet, J. Tournadre, 1994 : Objective analysis of surface wind fields using ERS-1 scatterometer data. Proceedings of Second ERS-1 Workshop, IFREMER Centre de Brest, pp 76-81.

Queffeulou, P., J.M. Lefèvre, 1992 : Validation of ERS-1 altimeter wave and wind fast delivery products, Proceedings of ERS-1 Geophysical validation workshop, Penhors, European Space Agency.

Quilfen, Y., 1994 : ERS-1 off-line wind scatterometer products. Document de travail ERS-SCAT/IOA/DOS-01, IFREMER Centre de Brest.

APPLICATIONS OF WAVE STATISTICS ESTIMATED FROM ALTIMETER DATA

D J T Carter[1] & P D Cotton[2]

[1]*Satellite Observing Systems, Ltd., 15 Church Street, Godalming, Surrey, GU7 1EL, UK*
Tel: +44 (0) 1483 421213, Fax: +44 (0) 1483 428691, email djc@satobsys.co.uk

[2]*Southampton Oceanography Centre, European Way, Southampton, SO14 3ZH, UK*
Tel: +44 (0) 1703 596411, Fax: +44 (0) 1703 596400, email pdc@soc.soton.ac.uk

ABSTRACT

The need for wave climate statistics for a wide range of activities are briefly discussed. The impact of satellite data in providing the measurements from which these statistics may be derived is described, and examples of statistics obtained from altimeter data are presented. The need for continuing calibration and research activities, if the credibility of satellite-derived statistics are to become widely accepted, is stressed.

1. INTRODUCTION

We first describe the need for improved understanding of the global wave climate, the potential breakthrough offered by satellite measurements of wave height, and an example of a project attempting to utilise these data for commercial applications. We briefly describe how the radar altimeter measures waves, and the need for calibration of its estimates of significant wave height, then give some examples of wave climate statistics derived from these measurements.

2. THE PROBLEM

A knowledge of ocean waves is essential for any activity connected with the seas. The largest forces on ships, as well as on offshore rigs and coastal defences, generally come from surface waves, which can cause delay, damage and destruction. Ships - even 100 000 ton carriers - disappear in storms; offshore structures have been severely damaged by large waves and have to be regularly repaired against fatigue damage.

Estimates of wave climate, such as monthly average wave height or the 50-year wave height, are needed for planning operations and for design purposes. The better the estimates, the better the risks can be assessed and allowed for.

The difficulty of measuring ocean waves and the poor quality of individual visual estimates mean that we have a rather poor knowledge of wave climate, particularly in the southern hemisphere. Even in the NE Atlantic, a complete understanding of average conditions is lacking. The annual mean wave height here has shown an upward trend over the past thirty years, with very large variability from one year to the next - without a comparable increase in the local wind speed (Bacon & Carter, 1991). The reasons for this trend or for the inter-annual variability have not yet been fully explained.

The last few years also appear to have been unusually stormy in the West Atlantic. According to Cardone & Swail (1995), two widely reported events, the "Halloween Storm" of 26 October - 1 November 1991 and the "Storm of the Century" of 12 - 15 March 1993 gave significant wave height (H_S) values from Canadian buoys of over 15 m; these heights exceed current estimates of 100-year return values south of Nova Scotia by about 50%. More recently, H_S values exceeded 14 m at buoy 44141 (near 42°N 56°W) on the 6 April 1995, and reached 17.1 m on 11 September 1995 as Hurricane Luis passed by (suggesting a maximum individual wave height, crest to trough, of 30.8 m or 100 feet). The QE2 ran into Hurricane Luis, and the Captain reported that the ship was hit by one wave exceeding 90 feet; repairing the damage - although not serious - and the consequent delay must have cost Cunard many £10 000's. A bulk carrier which encountered this storm was in dock for repairs for a month.

Thus there is a serious need to improve our knowledge of wave climate, especially our knowledge of its variability and extremes. In only a few areas, such as off the East coast of Canada and the USA, are adequate buoy measurements available. Over vast areas of ocean the only source of data until recently have been visual observations, which are notoriously unreliable, and large numbers of them are required even to give a useful estimate of mean conditions.

3. THE SOLUTION

The introduction some twenty years ago of earth-observing satellites carrying radar altimeters and synthetic aperture radar (SAR) has provided, for the first time, routine measurements of ocean waves on a global scale; and has transformed our chances of understanding wave climate and its variability. During these twenty years, experience with the altimeter has confirmed its ability to measure significant wave height - after calibration, as accurately as any buoy. By comparison the translation of SAR returns into surface wave measurements has proved to be much more difficult; and this paper is confined to applications of altimeter data.

Proceedings of the Second ERS Applications Workshop, London, UK, 6–8 December 1995 (ESA SP-383, February 1996)

During these past twenty years, most of the work on satellite remote sensing of waves has concentrated on understanding and assessing the observations; and it is only since Geosat was launched in 1985 that global coverage has been obtained throughout the years - albeit with a gap of a couple of years between Geosat and ERS-1. Today we have three altimeters in orbit: ERS-1, ERS-2 and TOPEX/POSEIDON. These, operating at 1 Hz, together provide about 180 000 measurements of wave height each day! We now have sufficient years of data to begin providing operators with information for anywhere in the world, information comparable with that which had only been available previously at a few locations. We can also start to use the global coverage to investigate spatial scales and tele-connections, and hopefully to resolve the questions about inter-annual variability and increasing trends which are of such concern to operators; and possibly eventually to predict wave climate variability from year to year.

In 1992 the British National Space Centre launched a programme to develop the economic use of information derived from satellite remote sensing of the Earth, and in 1993 a consortium led by Satellite Observing Systems was awarded a project, which it called "WAVSAT", to demonstrate the commercial potential of wave data. It has established an on-line data base of altimeter data, currently of about 10 Gbytes, which is segmented by 2° latitude x 2° longitude to give speedy extraction of data for a specific area; and SOS is deriving estimates of wave climate from these data for a range of customers. Calibration and other scientific and statistical aspects of these derivations have been carried out in close co-operation with the James Rennell Division of the Southampton Oceanography Centre. This link to a research establishment is particularly valuable because it helps to reassure new customers of the accuracy of these novel data.

4. WAVE HEIGHTS FROM SATELLITE ALTIMETERS

4.1 Definition of significant wave height

Significant wave height, H_S, is a measure of the general sea state, an 'average' value of the prevailing conditions. It is defined as four times the statistical variance of the sea surface. The '4' was introduced to give values approximating to visual estimates of wave height. Either a spatial or a temporal estimate of variance can be used, so this definition of significant wave height can be applied equally to buoy data or to a stereographic photograph of the sea surface - or to a 'snap-shot' of the sea surface from a radar altimeter.

4.2 Estimating H_S from the radar altimeter

The higher the waves in the footprint of the radar pulse, the greater the interval between the arriva of the return pulse from the highest crests and from the deepest troughs. If the 'height' of the return pulse is kept constant by the application of automatic gain control (AGC), then the slope of the leading edge of the return provides an estimate of H_S

The footprint from which H_S is determined is around 5 - 10 km, depending on the height of the satellite and on H_S. See Chelton, Walsh and MacArthur (1989). To reduce the effect of noise, values of Hs from individual pulses are averaged to obtain 1 s values which are transmitted to ground stations, so estimates of significant wave height are obtained at 6 - 7 km intervals along the satellite track.

4.3 The accuracy of altimeter wave heights

The design accuracy of H_S specified to date for satellite radar altimeters has been 0.5 m rms or 10% of H_S, whichever is higher; and the 1 s values transmitted from satellites have generally achieved this accuracy. However, comparisons of these values against those from buoys in NOAA's National Data Buoy Center network have revealed persistent differences. A simple linear calibration has been found to lead to excellent agreement. For example, Carter et al (1992) found that Geosat under-estimated H_S by 13%; applying this correction gave a residual root mean square between Geosat and buoy data of 0.23 m. Cotton & Carter (1994) give calibrations for TOPEX and ERS-1 altimeters. Note that not only are the calibrations different for each altimeter, but that for ERS-1 OPR and for ERS-1 FD wave heights also differ. Preliminary investigations indicate that H_S values from ERS-1 FD and ERS-2 FD differ by 5 - 10%.

The estimates of H_S are also affected by sampling variability; two measures of H_S from a statistically stationary sea surface at different times or locations would not be identical. The size of this variability is determined by the wave spectrum and the area or duration over which the measurement is made. For an estimate of H_S from a 17 minute record, the standard error due to sampling variability is about 4% - 5%. Challenor (1983) shows that the sampling variability of estimates of H_S from the satellite altimeter 1 s value are of the same order of magnitude.

Careful validation of each 1 s value is necessary because the return pulse can be distorted if ice or land are in the footprint; very heavy rain and flat-calm seas can also cause problems, as can mispointing of the altimeter - Geosat was prone to this. Empirical checks have been determined over the years, see for example Toplis *et al*, (1993), but to date automatic procedures are not completely reliable.

5. WAVE CLIMATE STATISTICS

Given routine buoy measurements at a site then statistics, for example monthly averages, can readily be estimated. A probability distribution function can be fitted and estimates of percentiles such as the 100-year return value derived - but with increasing uncertainty as we go further into the tail of the distribution.

To calculate averages from satellite data, we have to select all data falling within some area about the position of interest. A compromise is required between using a large area providing many satellite transects and using a small area to ensure statistical homogeneity. See for example Carriez *et al* (1992). In general, a 2° latitude x 2° longitude bin seems a reasonable choice, but in the open ocean if estimating say monthly means then the result can be improved by including data from a larger area - or by smoothing over adjacent bins. In coastal waters an estimate of the spatial distribution of H_S within the bin has to be considered.

All the 1 s data falling within a bin might be analysed, but values from a single transect of the bin are highly correlated, so it would seem preferable to take an average from each transect, and in practice we generally use the median of the 1 s values, since it is more robust against outliers than the mean. The statistics are then calculated from the transect medians.

There is little physical or statistical justification for any particular probability distribution, but the Fisher-Tippett Type 1 distribution (FT-1) has proved to be a reasonable distribution for H_S at higher latitudes unaffected by tropical storms. It is given by:

$$\mathrm{Prob}(X<x)=\exp\left[-\exp\left(-\frac{x-\alpha}{\beta}\right)\right]$$

where α and β are the location and scale parameters respectively.

Carter et al. (1994) give examples of the use of this distribution, including a comparison of 50-year return values around the UK derived from Geosat data with those from buoy data.

Further research is needed into other possible analytical techniques, such as extreme value analysis and peaks-over-threshold, especially for areas affected by tropical storms. There is also a need to provide, jointly with H_S statistics, values of wave period and direction.

6. EXAMPLES

Fig.1 shows the cumulative probability distribution of median H_S values from Geosat, ERS-1 (OPR) and TOPEX data from the 2° bin centred on 45°N 131°W. Assuming data were obtained at 3-hourly intervals, then the 100 year return value is 14.2 m. Fig.2 shows a similar analysis for 43°N 55°W, but the FT-1 does not fit above about 5 m - probably because these high H_S values are often from extra-tropical hurricanes and not from the generally prevailing wave climate.

By analysing an array of bins, maps of statistics such as return values of wave height or of the most likely value, shown in Fig.3, can be derived.

The examples given so far are based upon the analysis of 2° bins, but the repeat tracks of the satellite can provide details of spatial variability, not obtainable in any other way. Fig.4 shows the considerable changes in mean H_S values over a few 100 km, because of sheltering by Patagonia from the prevailing Westerlies. Variations in wave height as the waves run into a current have also been seen in altimeter records (Gründlingh, 1994).

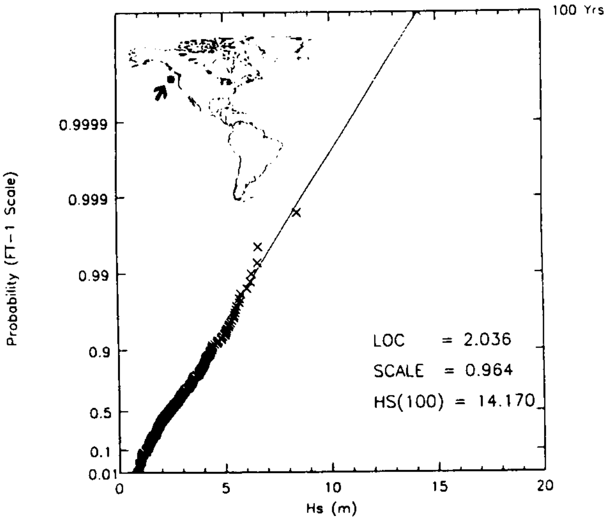

Fig.1 Cumulative probability distribution of H_S from 352 transects of 44°-46°N, 130°-132°W by Geosat, ERS-1 and TOPEX (1986-1994)

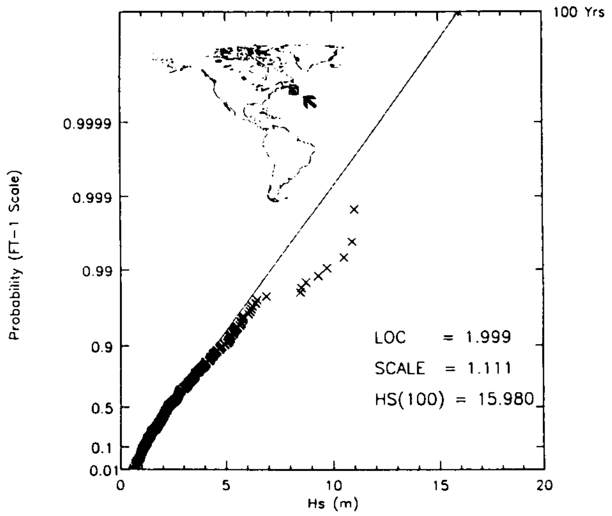

Fig.2 Cumulative probability distribution of H_S from 376 transects of 42°-44°N, 54°-56°W by Geosat, ERS-1 and TOPEX (1986-1994)

Estimates of extremes, such as the 100-year return value of H_S, from only a few years of satellite data, as from any data covering such a short period, have to be treated with caution. Confidence intervals can be placed upon the estimates, but these assume that the climate is not changing. 100-year return values in the NE Atlantic off Scotland derived from 1985 - 1989 are around 18-21 m, and derived from 1991 - 1994 are around 22-24 m (from Geosat data and ERS-1 plus TOPEX data respectively). This rather large increase, over roughly six years, is an indication of the variation on the time-scale of decades. Or could it be an harbinger of "global warming"?

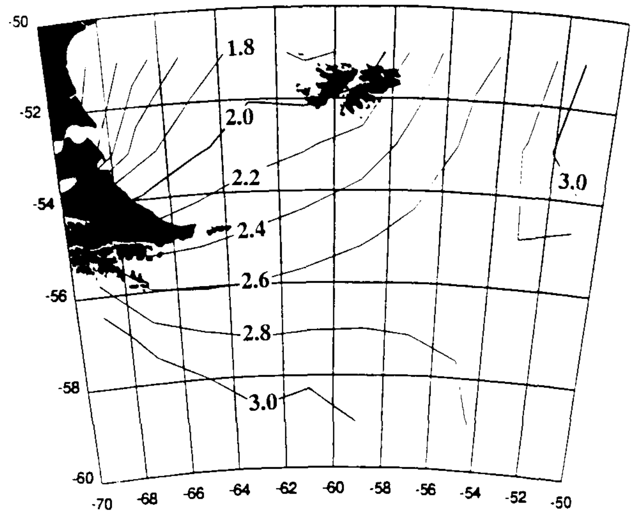

Fig.3 Most likely significant wave height (m) during May - July, estimated from Geosat, ERS-1 and TOPEX data, 1987-1994.

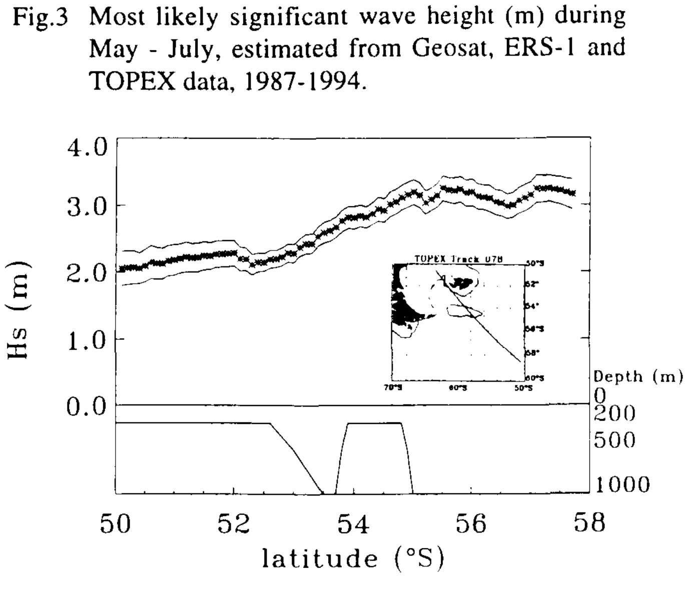

Fig.4 Mean Hs (m) from 33 passes along TOPEX track 078 from February 1994 to January 1995, with +/- standard error of the mean.

7. CONCLUDING REMARKS

Increasing concerns about the lack of knowledge of wave climate - highlighted by the development of the offshore oil and gas fields - have fortunately coincided with the deployment of satellite radar altimeters. These have been found to give remarkably accurate measurements of significant wave height - providing data are carefully validated and calibrated against buoy measurements; and will undoubtedly improve our understanding of the global wave climate, including its long-term variability.

Some examples have illustrated the derivation of wave climate statistics from these data. Research will further improve and extend the applications which can be addressed, but we already have an operational system, producing useful information for customers.

However, if wave climate statistics from satellite data are to become widely accepted amongst the offshore community, it is essential for all of us analysing these data to maintain good validation and calibration procedures, and not to claim too much from the data. Only if confidence in these data can be extended more widely into the offshore community, will commercial applications continue to expand.

REFERENCES

Bacon S. & Carter D. J. T. 1991, Wave climate changes in the North Atlantic and North Sea. Intern. J. Climatology 11, 545 558.

Cardone V. J. & Swail V. R. 1995, Uncertainty in prediction of extreme storm seas (ESS). Pp 1-20, Proc. 4th Intn. Workshop on Wave Hindcasting and Forecasting, Banff, Canada 16-20 Oct. 1995

Carter D. J. T., Challenor P. G. & Srokosz M. A. 1992, An assessment of Geosat wave height and wind speed measurements. J. Geophys. Res. 97, 11383-11392.

Carter D. J. T., Challenor P. G. & Cotton P D 1994, Estimating extreme values of significant wave heights from altimeter data. Pp 63-70, Proc. WMO/IOC Conf., Sept. 1993, Bergen, Norway.

Challenor P. G. 1983, Spatial variation of significant wave-height. Pp.451-460 in: Allan T. D. (Ed.) *Satellite microwave remote sensing*. Ellis Horwood Ltd.

Charriez P., Olagnon M & Tournadre J 1992, Confidence intervals associated with satellite measurements of wave and wind environment. Pp.313-320 Proc. 11th Intn. Conf on Offshore Mechanics and Arctic Engng.

Chelton D. B., Walsh E. J. & MacArthur J. L. 1989, Pulse compression and sea level tracking in satellite altimetry. J. of Atmos. &Oceanic Tech. 6, 407-438.

Cotton P. D. & Carter D. J. T. 1994, Cross calibration of TOPEX, ERS-1 and Geosat wave heights J. Geophys. Res. 99, 25025-25033.

Gründlingh M. L. 1994, Evidence of surface wave enhancement in the southwest Indian Ocean from satellite altimetry. J. Geophys. Res. 99, 7917-7927.

Topliss B. J., Challenor P., Tokmakion R. & Snaith H 1993, A Review of Geosat data over Canadian East coast waters. Canadian J. Remote Sensing, 19,117-130.

APPLICATION OF OCEAN SURFACE WIND AND WAVE INFORMATION FROM ERS IN ATMOSPHERE AND OCEAN MONITORING AND NUMERICAL FORECAST MODELS.

Lars Anders Breivik, Magnar Reistad, Harald Schyberg and Jens Sunde.

Norwegian Meteorological Institute (DNMI), P.O.Box 43 Blindern, 0313 Oslo, Norway.
Tel: (47) 22 96 30 00. Fax: (47) 22 96 30 50.

ABSTRACT.

Wind scatterometer data and altimeter wave heights are used by the on duty meteorologists in operational weather and wave monitoring. Both data types are assimilated in operational numerical models. The impact is small and limited to the first hours of the forecasts. To improve the impact in numerical forecasts the assimilation methods need to be renewed. This goes through development of coupled wind an wave analyses and new approaches to utilize the sea surface information.

Wave spectra retrieved from both SAR wave mode data and SAR image mode are operationally produced at DNMI. In the swell part of the inverted SAR ocean wave spectra there are information not present in the background wave model spectra. A method to assimilate SAR wave spectra in the operational wave model has been developed. The SAR wave assimilation is currently tested and evaluated in a parallel wave model routine.

1. INTRODUCTION

At the Norwegian Meteorological Institute (DNMI) ERS wind and wave data have been received operationally as LBR fast delivery data since the launch of ERS-1. DNMI participated in the calibration/validation activities of ERS-1 and is currently supporting ESA in evaluation of ERS-2. Both wind scatterometer data and radar altimeter data is in operational use for weather and wave analysis and forecasts. Methods to utilize SAR wave information is under development. The current status of data quality, availability and use of the data will be described.

2. SCATTEROMETER DATA IN NUMERICAL WEATHER PREDICTION.

In November, December and January 1992/93 the impact of the observations was tested on DNMI's operational limited area weather prediction model (Breivik et.al. 1993). The data were used in the analyses in a parallel routine and evaluated against the operational results. The assimilated scatterometer data were the ESA (European Space Agency) derived wind vectors received on GTS (Global Telecommunication System). These contained 5-10% of 180 degree wrong wind directions. To deal with this a special data control was introduced to check against first guess wind direction. Observations differing more than a certain angle were either rejected or simply turned 180 degrees. It was demonstrated that the data had little impact on the forecast except in some few cases. In these few cases the impact was mainly positive.

Experience indicated that by doing the wind retrieval locally the quality of the scatterometer wind observations could be increased. Operationally ESA is using 36-48 hours weather forecasts from ECMWF (European Centre for Medium Range Weather Forecast) as background to help in dealiasing. In an operational weather forecast centre a fresher, and hopefully better, background wind field is always available. Beside this, the routine for dealiasing could be improved upon. All information necessary for wind retrieval is received on GTS. Routines to operationally retrieve wind from the scatterometer measurements were implemented and tested at DNMI in 1993 (Breivik and Haugse, 1994). The routines build upon methods developed by ESA, ECMWF and UK Met.Office and were further developed and modified to give optimal results in our areas of interest and to minimize the dependence of the background. The resulting data quality is high. The standard deviation of differences in wind speed is approximately 2m/s. An example of scatterometer observations are given in Fig. 1. A low pressure centre south of Greenland is well observed by the scatterometer with wind speeds above 20 m/s.

The analysis of locally retrieved scatterometer data in the weather forecast model was tested in half a year in a parallel routine from August 1994 to January 1995. No extra data control on scatterometer data is performed after retrieval. The analysis is based on a Successive Correction method (Bratseth 1986) which, in an efficient way, converge to the results of Statistical Interpolation. The first guess for surface wind is the model 10 m wind interpolated within +/- 3 hours to the real observation time (Breivik et.al.1993). Prior to the analysis all observations are subject to a two step data quality control. In the 'gross control' the observations are checked against the background model fields. The deviation from the background is not allowed to exceed certain rather wide limits, and so obviously wrong data are rejected. This part of the control seldom affect the scatterometer winds. In second step a synoptic multivariate control

using the analysis method is performed. Since the analysis scheme is iterative we can check on the convergence related to each observation.
The results from the parallel run were verified against surface and upper air observations (Breivik, Haugse and Sunde 1995), and only very small differences in the quality of the results were found at all levels. The results in surface wind speed and mslp were however slightly improved.

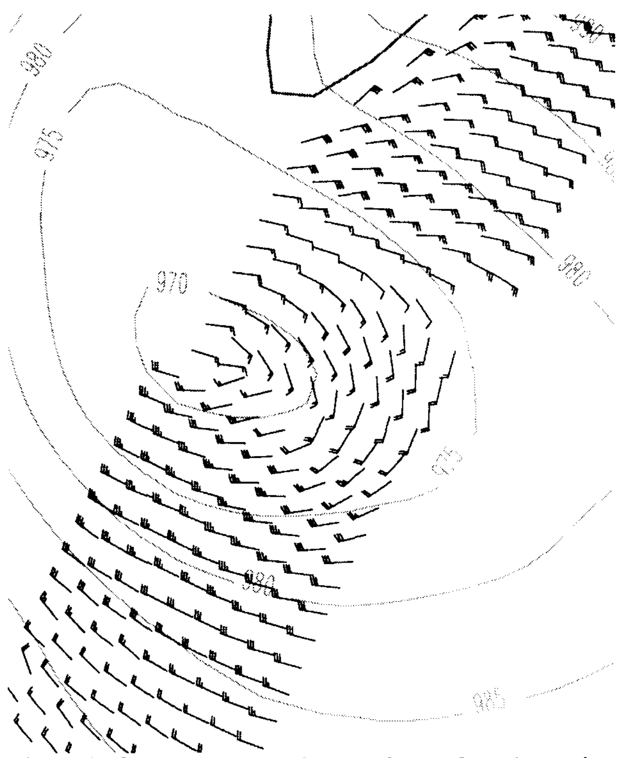

Figure1: Scatterometer observations of an intensive low pressure centre south of Greenland 1. December 1995.

It is generally accepted that observations from higher altitudes are far more important for the forecast quality than surface observations. On the northern hemisphere where the traditional vertical sounding network is dense enough to play the conclusive role, little impact are found by surface observations in general. One important reason is that the three dimensional analyses is not capable of correctly describing the error correlations between the surface and the upper air. The vertical co-variances, the relation between the analysis increments at the surface and in the free atmosphere, should be dependent on the synoptic situation. Under the development of a storm the degree of tilting of the system, and thereby the co-variances, will vary in time. In the most interesting cases, where rapid storms are developing, the analysis can introduce an erroneous correction in the upper air wind field on basis of correct increments at the surface. To fully utilize the information contained in a surface observation, it is therefore necessary to take the time development of the field into account in the analyses. This is referred to as four dimensional analysis including time as a fourth dimension. Four dimensional data analysis are under development at several centres.

The scatterometer data do give a positive impact on the sea surface wind analyses. This is important considering the use of the wind as input to oceanographic models of ocean waves and currents run at DNMI. Further work on use of scatterometer data is assigned development of improved analysis methods. This is also motivated by a need for consistent analysis of wind and waves, demonstrated in results from assimilation of ERS-1 altimeter data in DNMI's wave model.

3. ALTIMETER DATA IN NUMERICAL WAVE PREDICTION

Altimeter wave heights is used in operational wave monitoring at DNMI. An example of the data coverage is given in Fig. 2. Here both ERS-1 and -2 wave heights are plotted together with isolines of significant wave height, SWH, from the operational wave model WINCH.

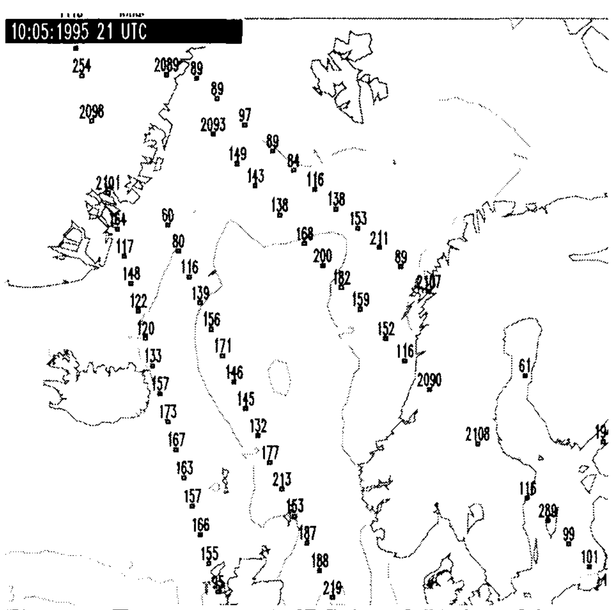

Figure2: Two passes of ERS-1 and ERS-2 altimeter wave height (cm) measurements 10 May. 1995.

The wave model WINCH is a regional wave model operationally run at DNMI for the Norwegian areas and the North Atlantic (Breivik and Reistad 1994). The model produces a full two dimensional wave spectrum at 15 frequency bands and 24 directional sectors on a 75 km grid. The wind at 10 m height is taken from DNMI's numerical weather prediction model to drive the wave model.

A method to assimilate SWH into the wave model has been implemented, and is now in operational use (Breivik and Reistad 1994). The method is based on a Successive

Correction analysis (Bratseth 1986) of observed and first guess wave model SWH. To correct the wave spectra on basis of the SWH analysis some pre-assumptions on the shape of the spectra are needed. We assume that the relation between wind sea and swell energy is correctly modelled by the wave model, and that the duration and direction of the wind used in the model is correct. The wave spectra is corrected, and so is the wind speed at the analysis time and the next advection time step.

Verification against independent buoy measurements from in the North Sea has demonstrated that the wave analysis has been improved by assimilation of altimeter data. There is positive impact also on the short forecasts. For forecasts longer than 18 hours the impact is limited. This is not unexpected since the wave prognoses are totally dependent on the prognostic wind fields. The input wind from the atmosphere forecast model is not corrected on basis of the wave analysis. The impact from the observations could probably be significantly improved if the wind field in the atmosphere forecast model was corrected consistent with the wave model.

4. SCATTEROMETER DATA AND ALTIMETER DATA IN COUPLED WIND-WAVE ANALYSES

As stated above, the impact of altimeter wave height assimilation in the wave model gradually decreases throughout the forecast as the prognostic winds from the weather forecast model decide the wave development. The impact can probably be improved if the wind in the weather forecast model were corrected consistently. The objective of DNMI's current ERS data utilization project is therefore to define and develop a coupled analysis system of wind and wave observations from the ERS scatterometer and altimeter. This is done within the two dimensional variational framework. The intension is not an independent analysis scheme for scatterometer data in the atmospheric forecast model and one for wave data in the wave model, but an analysis system for the sea surface taking all relevant data into account to produce consistent wind and wave analyses. The variational approach needs a specification of each part of a cost function to be minimized. For sea surface observations one need to specify the cost function in terms of the distance between the observed values and the analysis. The variational approach has several advantages when applied on a sea surface analysis. Observations can be used, only specifying the transformation from the field to be analysed to the measured quantity. Specification of the inverse relation, from measurement to analysed field, is not necessary. This means that for example when analysing the field of surface wind *vector*, altimeter wind *speeds*, for which no directional information exists, can be used directly. Also scatterometer winds, where there is a directional ambiguity, can be used directly in the analysis without any prior ambiguity removal. In addition the variational formulation makes it easy to impose additional physical constraints on the observations, e.g. a coupling between the ocean wave field and wind. One might also consider solving a two dimensional sea surface analysis as a contribution to developing a full four dimensional analysis system.

5. SAR OCEAN WAVE SPECTRA.

The ERS Wave Mode product is distributed daily on GTS. Wave Mode operation of the SAR measures the changes in radar reflectivity of the sea surface waves in 10x6 km 'imagettes' at intervals of 200 km along track. Unfortunately it has been realised that the ERS Wave Mode spectra suffer from a non-optimal processing which complicates its applicability. The received spectrum is a linear combination of the wanted wave modulation spectrum and the speckle spectrum. However, the relative weights of the two spectra have to be determined for each spectrum separately. The speckle spectrum has been determined by a special analysis of a set of imagettes and the scaling procedure is described in Samset and Krogstad, 1994. Due to the product's rather coarse resolution and limited frequency range, the inversion algorithm can been simplified compared to the algorithm needed for the full SAR images. The inversion algorithm is simple to implement, leads to a stable and robust iteration, and is computationally very fast.

The other type of SAR information operationally received at DNMI is ERS SAR Image Mode data delivered by Tromsø Satellite Station, TSS. In Image Mode, the SAR obtains strips of high-resolution imagery, 100 km in width, to the right of the satellite track. Each product from TSS consists of four spectra computed from sub-images within the 100x100 km SAR image. The sub-images cover each an area of approximately 18km x 18km. (Engen et.al. 1994)

The inversion of both Image Mode and Wave Mode applies a certain a priory wave information which is taken from a neighbouring grid point from the wave model, WINCH. Evaluation against WINCH shows that in the wind sea part of the spectra there is no information added by the SAR observations. All independent information is within the long wave part of the spectra (Breivik et. al. 1995). However, as described above, there is little to gain in assimilating wind sea information as long as not the wind input from the weather forecast model is affected. We therefore hope that the SAR swell information can be assimilated and give positive impact on the wave analysis and forecast results.

A method to assimilate SAR wave spectra in a numerical wave model is developed. In the analyses each frequency/direction bin is analysed independently, and the analysed spectra is interpolated in space by a version further developed from the analysis method derived for wave heights. The method is currently tested, using Wave

Mode data, on a parallel wave model run to study the impact. Figure 3 show an example of SAR and first guess WINCH spectra and the impact on the SWH field.

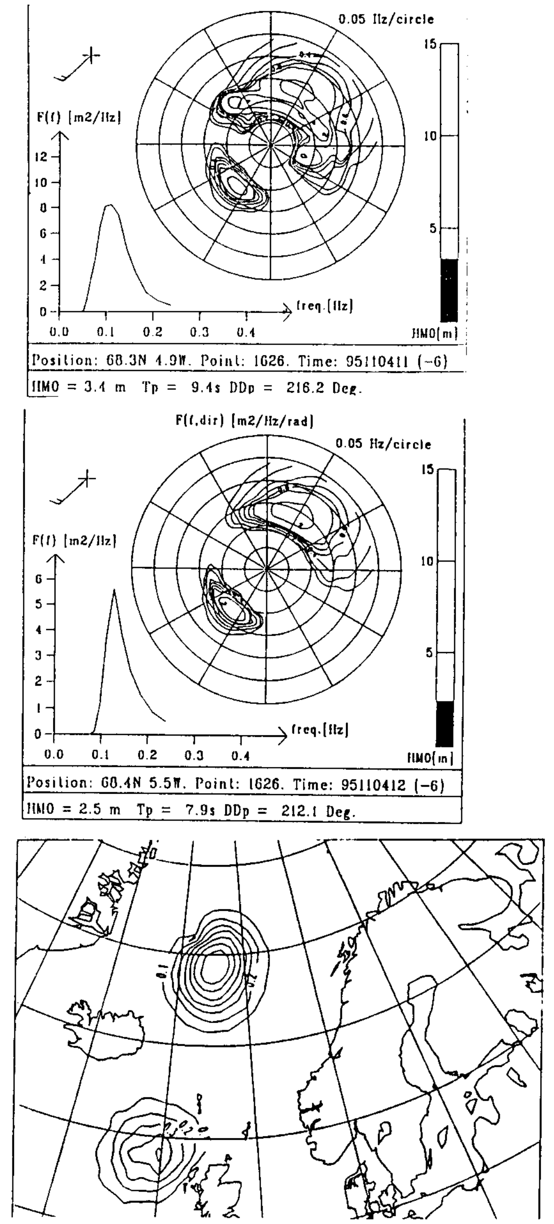

Figure3: SAR and firs guess wave spectra and assimilation impact on model SWH field.

Results so far indicate that the observations are too few to significantly improve the averaged results. Normally there are approximately 8 Wave Mode observations within our areas each assimilation cycle, and of these more than half is rejected by the quality control. There is also probably too little new information contained in the SAR observations compared to the wave model, however new processing methods for SAR data could probably improve the situation. Methods based upon ERS Single-Look Complex Product is developed (Engen and Johnsen, 1995).The new processed data will be tested in assimilation.

6. CONCLUSION

Wind scatterometer data and wave data from the altimeter are used by the meteorologists in daily weather and wave analyses and monitoring. Scatterometer wind and altimeter wave heights is assimilated in the operational weather and wave forecast models. The impact is mainly limited to the sea surface and the short forecasts. The limitations of the analyses seems to lay more in the traditional methods by which the observations are analysed than in the data quality, which is proven to be high. New methods for consistent analyses of wind and wave are under development.
SAR wave data is processed in near real time. The data contain independent information of the swell part of the spectra which can be utilized by assimilation in the wave model in some cases.

7. REFERENCES

Bratseth, A.M., 1986: Statistical interpolation by means of successive corrections, *Tellus*, 38A, 439-447.

Breivik, L.A., B. Haugse and M. Homleid, 1993, Results from Assimilation of ERS-1 Scatterometer Wind Information in an Operational Limited Area Weather Forecast Model. *Second ERS-1 Symposium - Space at the Service of our Environment*, Hamburg October 1993.

Breivik, Lars A., Baard Haugse, and Jens Sunde, 1995, Operational Use of Scatterometer wind information at the Norwegian Meteorological Institute. *DNMI Research Report* no. 1.

Breivik, L.A., B. Haugse, H. Krogstad, H. Johnsen and M. Reistad, 1995, Evaluation of SAR Wave Products. *DNMI Research Report* no. 2.

Breivik, L.A. and M. Reistad, 1994, Assimilation of ERS-1 Altimeter Wave Heights in an Operational Numerical Wave Model. *Weather and Forecasting*, Vol. 9 No. 3.

Breivik L. A., and B. Haugse 1994, Scatterometer Wind Retrieval at the Norwegian Meteorological Institute. *DNMI Technical Rep.* No. 124.

Samset, O. and H. E. Krogstad, 1994: Inversion of ERS-1 Wavemode Spectra, Documentation, SINTEF Rep. No. STF10 A94012. SINTEF, N-7034, Trondheim, Norway

Engen, G., H.Johnsen, H.E. Krogstad, S.F.Barstow, 1994, Directional Wave Spectra by Inversion of ERS-1 Synthetic Aperture Radar Ocean Imagery, *IEEE Trans. on Geosc. and Rem. Sens.*, Vol. 32, No. 2.

Engen, G. and H.Johnsen, 1995, SAR-ocean wave inversion using image cross spectra. *IEEE Transaction on Geosc. and Rem. Sens.*, 33(4): 1047-1056.

CONTRIBUTION OF ERS DATA TO CLIOSAT PROJECT, THE SATELLITE METOCEAN ATLAS

P. Lasnier, S. Loeul, H. Hajji, D. Bonicel, P. Charriez

MétéoMer, RN7, les Barestes, 83480 Puget sur Argens, FRANCE
Tel: (33) 94 45 66 11. Fax (33) 94 45 68 23

Abstract

The tremendous amount of all weather, world-wide and accurate measurements of wind and wave characteristics provided by satellite data enables time and cost-effective methods for the derivation of metocean parameters useful to marine and structure engineers. Within the CLIOSat project, MétéoMer, in a partnership with Ifremer, has developed an operational archiving and interrogation system of global wind and wave parameters in order to quickly answer engineers pre-project needs for metocean parameters. These wind and wave climates are presented either on coherent climate predefined areas on a PC atlas or on more specific customized areas through an on-line service.
This paper presents works that led to the elaboration of such products and some powerful examples of wind and waves climates obtained.

Keywords: metocean parameters, satellite data, wind and wave climate, directional spectral information.

I. Introduction

In the domain of assessing wind and wave climates for industrial needs, engineers often have to face problems linked to the availability of data. Among the different available sources of data, field measurements are the most accurate and reliable but they are generally sparse and bear time and cost constraints.
Ship observations offer opportunities to assess regional and global climates but are inaccurate specially, for long swells or in the case of sea-states composed of several swells. Moreover, they are gathered along the main maritime routes. Consequently, up to recently, atlases could only offer coarse grids and large uncertainties.
At last, hindcast models strongly depend on the quality of the input wind fields and require delays and costs which do not always fit operational needs.

Fortunately, satellite measurements have recently enabled new methods for the derivation of metocean parameters, due to their dense, global and all-weather coverage. ERS satellites as well as Geosat and Topex-Poseidon provide a tremendous amount of data which quality is similar to that of field measurement. Particularly, ERS satellites, with their Synthetic Aperture Radars (SAR) operating in wave mode offer, for the first time, global measurements of waves periods and directions, whereas their scatterometers measure wind speed and direction. Nowadays, for the first time, global and reliable measurements of metocean parameters can be provided to offshore engineers and ship or towed structures designers, even in remote and poorly documented areas.

CLIOSat atlas provides engineers with quick answers to their requests for characteristic sea state and wind parameters climatologies on pre-defined or on specific areas. These wind and wave climates (histograms, scatter diagrams, estimation of extreme values), are presented either on coherent climate predefined areas on a PC atlas or on more specific customized areas through an on-line service based on an archiving and interrogation system. Once the user has specified his area and period of interest, this service gives in less than 24h, information useful before decision-taking for pre-project orientation. Moreover, the user's choice is analysed by metocean experts in view of validating the climate coherency of the area and the statistic consistency of the results.

Several projects enabled the feasability studies and developments that led to the elaboration of CLIOSat, by MétéoMer and Ifremer. In particular, works have been carried out since 1991 in order to acquire methods on the management, the processing and the quality control of the data, within ESA's pilot projects.

Methods for the construction of climates have been elaborated in the frame of the ASPRO project (*Apport des données Satellitaires à la PRévision climatologique en Offshore* - Contribution of satellite data to offshore climate forecasting), within the CLAROM group (Club pour l'Action et la Recherche sur les Ouvrages en Mer).
Main results are briefly reminded hereafter firstly concerning the processing of data.

II. Elaboration of climates

The procedure is summarized in the organigram (figure 1) and includes the following steps :
- processing, qualification and quality control of all data,
- construction of climate consistent areas,
- statistics elaboration,
- analysis of climate data by a metocean expert

II.1 Data processing

Altimetric data: an altimeter is a radar sensor emitting pulses in the region of Ghz frequency which are reflected at the sea surface and analyzed on return. The shape of this echo is related to the significant wave height whereas wind speed can be derived from its intensity. At every second along the track of the satellite, altimeter Hs and wind speed are thus computed from averaged measurements. Altimeter raw data present good quality as one may see in figure 2, but need however to be calibrated and error checked before use, because erroneous high values can occur when the satellite flies over heavy rains (mainly in tropical areas) or flies from land to sea.
Within this scope, we have developed a specific processing method so that these wrong values are eliminated. In a first step, they are automatically detected and discarded, with the help of an algorithm. In a second step, each remaining high value is analysed by an operator for final validation. This method has now been applied to a dataset covering a 7 years duration including Geosat, ERS1 and Topex-Poseidon measurements.

Scatterometer data: the measurement principle of the scatterometer is based on the dependance of the normalised radar cross section on ocean roughness, which is dependent upon surface wind speed. In addition, the normalised radar cross section is anisotropic with respect to the angle between wind vector and incident radar beam. With the aid of several measurements of the same area, but from different directions, the actual wind vector in terms of speed and direction can then be determined. Relationship between normalised radar cross section, wind speed, wind direction, incidence angle of the scatterometer pulse and the signal polarisation enables the derivation of the wind parameters. At last, one can remove some remaining ambiguities of direction of the wind by comparing them against a meteorological analysis.
Then, the scatterometer offers one wind vector every 25 km within a 500 km swath. (see figure 3).

SAR measurements: SAR, Synthetic Aperture Radar, is an outstanding sensor, enabling the derivation of sea-state spectra. However, unlike altimeter and scatterometer, SAR raw data, which is an image spectrum, need a rather complicate processing to be used as sea-state spectrum. Unfortunately, relationship between the sea surface and its corresponding SAR image is not linear. In particular, the SAR image spectra offers the following features: information comprised between 7.5s and 25s, directional ambiguity 180° (these products are symetric), lack or loss of information for periods under 10s along the track of the satellite, eventual differences in localization of peak energies. Some of these aspects can be seen on figure 4.
Retrieval of the initial SAR wave spectrum from the raw data is carried out by the so-called SAR inversion. This method includes a first-guess spectrum, usually originated from a numerical wave model, using backtracing model for swell and scatterometer wind fields to compute wind sea, in order to remove the 180° ambiguity in direction.
This introduction of a local sea state model using scatterometer enables to derive wind sea from satellite data. Because of intrumental limitations of the SAR in wave mode, i.e. lack of information for periods below 7.5s and possible loss up to 10s along the track of the satellite, quite a great number of sea state conditions (wind sea, very short swell) could miss in statistics directly issued from SAR products, specially for closed seas (Mediterranean for example) and less often for open seas. Consequently, a special analysis step needs to be applied is illustrated in figure 5.

1/ For open seas

In the case of open seas, most of the sea-states show components of periods beyond 7.5s that can be easily provided by the SAR in wave mode whereas the missing information, below 7.5s, is restored through the wind sea component estimated from the sea state model implemented within the inversion procedure, using local scatterometer wind as input. Lastly, neighbouring altimetric Hs values are also used within this wind sea enhancement procedure, as a control of the likelihood of the total energy of the final estimated spectrum.

2/ Closed seas

Due to its instrumental limitation, SAR in wave mode cannot generally provide a good characterization of small periods sea states conditions mainly prevailing in closed seas (except for some storm conditions). As a consequence, the missing information is directly restored through the sea state local model, using the corresponding scatterometer winds as input. However, such information is not included into the statistics when SAR in wave mode measurements provide a reliable information, corresponding with an actual sea state condition with most individual component periods higher than 7.5s.

To conclude, information derived from SAR data can be processed as a classical sea-state spectrum. This leads SAR to be a fantastic source of data enabling to calculate moments of the spectral parameters characterizing the whole sea-state like significant wave height Hs, zero-crossing period $T_{0,2}$ and also determine the direction of the main spectral peak, or to go into the detail of each sea-state spectrum to derive the periods and directions of the spectral peaks both for the swell and the wind sea and also their individual heights (Tp, θp and Hs).

II.2 Accuracy of metocean parameters derived from satellite data

Hs measured from altimeter:
Extensive comparisons with field measurements have been achieved using the concept of local climate coherent area, carefully defined by a meteorologist, on which spatial altimeter data will be selected. Such a procedure thus yields to a statistical comparison of the altimeter and field measurements, on a great number of samples, still with climatology coherence. Figure 6 shows the comparisons between Geosat altimeter data and field Hs cumulative probabilities, on the Frigg area. Globally, a systematic underestimation of 25 cm is found for Geosat measurements, which is coherent with results of other authors except for high values; however, we think that our procedure enabled to acquire more data on these high values, giving more confidence in the result. Similar works have been undertaken for ERS1 and Topex-Poseidon that have enabled to determine corrections for Hs data. As a conclusion, once corrections and quality control procedures applied, Hs altimeter data offer accurate and reliable measurements.

Sea-state parameters originated from SAR measurements:
Comparisons of SAR spectral parameters against buoy measurements have been made in order to assess uncertainties on Hs, Tp, θp and T0,2, computed as recommended the IAHR (International Association for Hydraulic Research). They led respectively to the following figures: 50 cm, 1s, 15° and 1s. Figure 7 presents the result of comparisons of 58 couples of SAR and field measurements, for Tp and θp. Results of the validation of T0,2 calculated from SAR can be seen on figures 8a and 8b.

Wind parameters: Speed and directions
Extensive studies have been performed by several authors. Wind speeds issued from altimeters have been validated against field measurements. Main uncertainties results are 1.5 m/s for ERS1 and 2 m/s for Geosat and Topex-Poseidon.
An accuracy of 1.2 m/s for the wind speed and 15° for the direction was found for the scatterometer measurements.

II.3 Construction of climate coherent areas

The quality of the climate data originated from satellites depends not only on the accuracy of the raw data used, but also on the coherency of the whole dataset. To ensure this, metocean experts delimit climate coherent areas according to their knowledge of typical and extreme meteorological conditions. Figure 9 shows the cut out of the CLIOSat atlas on PC, which has been made in order to offer general climate information. For more specific requests, always at a pre-project level, on local sites, areas as shorter as 1x1° can be defined by experts, through the CLIOSat on-line service. Example is shown on figure 10.

III. CLIOSat products

The CLIOSat project is based upon the processing of all the existing altimeters, scatterometer and SAR data and their storage into an archiving and interrogation system. Suitable information concerning relevant metocean parameters can be extracted from this database for operational purposes of ship design, sizing of structures, planning of maritime works.
These climates of metocean parameters are presented either on coherent climate areas pre-defined by experts, on a PC atlas, or on areas defined according to the requirements of the customers, through an on line service.

III.1 Contents of CLIOSat

In order to suit the best industrial needs, an expertise committee, with members representing the main french industries concerned with the use of metocean parameters, controlled the relevance of the provided parameters with respect to their operational needs. This led to the following products available either in the CLIOSat altas on PC and on the on-line service.

- **CLIOSat atlas on PC:**

From world-wide wind and wave satellite measurements and on 169 areas, this atlas offers for quarterly and annual periods.

- **histograms**

1. *waves* :
   . significant height (total Hs) - (issued from the altimeter)
   . peak periods (cumulated wind sea and swell)
   . peak directions (cumulated wind sea and swell)

2. *wind* :
   . speed (issued from the altimeter)
   . direction (issued from the scatterometer)

- **scatter diagrams of spectral parameters of waves**
  1. Wind sea: (H_1, Tp_1, θp_1) and *swell* (H_2, Tp_2, θp_2) *components*

. peak periods (Tp_1 and Tp_2) / peak directions (θp_1 and θp_2) with percentage of multipeak seas
. peak periods (Tp_1 and Tp_2) / significant heights (H_1 and H_2) with percentage of multipeak seas
. peak directions (θp_1 and θp_2) / significant heights (H_1 and H_2) with percentage of multipeak seas

2. Global sea states:
. Hs, Tz, θpp (direction of the main peak)
. significant height / Tz period
. significant height (Total Hs) / direction of the main peak (θpp)

- **scatter diagrams - winds**

. wind speed/direction (issued from the scatterometer)

- **significant heights extrapolated to extreme conditions**

Considering the wideness of the CLIOSat pre-defined areas, 90 % confidence intervals on the estimated extreme Hs values are given, these ranges reflecting the disparities in the sea-state conditions.

This information is provided either under histograms and diagrams or under numerical files for they could be directly transfered and used with the own users' tools.
An example of the full dataset provided for a CLIOSat area is presented in annex.

- **CLIOSat on line-service:**

CLIOSat atlas provides information about general climates on coherent areas which have been pre-defined by metocean experts. Nonetheless, the user may wish the same basic statistics for pre-project purposes on a specified area within the previous pre-defined ones. In less than 24h, and for a specified area, CLIOSat on-line service provides the user with climate products useful in a pre-project phase. With this on line service, the user can specify his area *(localization, size)*, choose *his proper period: year, quarter and month.*

To define his own area, the user will benefit from metocean experts' advice who will analyse the chosen area in order to guarantee statistical consistency and climate coherence.

Products of this on line service are similar to those contained in the CLIOSat atlas, apart from extreme Hs values. Actually, due to satellite space and time repetitivities, some storm events can be missed on such small local specific areas, which considerably reduce the extrapolation reliability. As a consequence, for precise estimations of extreme Hs on local areas, the tail part of the initial satellite distribution has to be enhanced with results from storm hindcasts, which are first calibrated on satellite measurements in an extended location and then transfered towards the location of interest. This kind of elaborated products cannot be guaranteed within the prescribed time of this personalized on line service.

III.2 CLIOSat potentialities

To illustrate the powerful source of information provided by CLIOSat, some examples of wind and sea-state climates are presented hereafter.
For example, the CLIOSat area of Senegal, which is crossed by an area of low pressure, the intertropical convergence zone (ITCZ) also known as the 'doldrums' area, located between the trade wind regions of the two hemispheres, is of high interest. The seasonal displacements of the doldrums are evidenced by quarterly wind distributions off the Senegal coast.
On the first quarter period, (figure 11), the doldrums area, located in the south part of Senegal, disables south-eastern trade winds. During the third quarter of the year, the doldrums area going much further north enables passage of south-eastern trade winds, while occurencies of north-eastern trade winds decrease.
Quite badly known phenomena can be evidenced and quantified. Scatter diagram of periods and directions of spectral peaks for the Caribbean sea area of CLIOSat atlas shows very long swells (periods above 18s) coming from NNE, in the winter. These swells, which are generated off north-eastern United-States coast by lows, were not expected to easily cross the natural barrier of Caribbean islands (figure 12).

III.3 Application possibilities

CLIOSat offers climate information on winds and sea states, either on pre-defined climate consistent areas and periods within the Atlas, or for more specific areas and periods within the on line service. High quality information is thus available and is useful for any pre-project.
More elaborated parameters (sea state directional spectra in typical storm conditions, extreme conditions for an offshore or coastal area,...) are also available for a final design phase within provisions of services apart from CLIOSat.

Some among many other practical possibilities of CLIOSat are listed below:

- **Use for pre-projects**

- Climates for areas lacking in field measurements

- Quick outlook on basic climate products for any pre-project phase

- Preparation of specific studies and field measurements to obtain elaborated and refined parameters useful for the design or requalification of offshore and nearshore structures, the optimization of shipping routes,...

- Optimization of a field measurements campaign.
It is easy with CLIOSat to determine the periods of strong events so that it should limit field measurements campaigns.

- Estimating the reliability of field measurements
On a specific area representative of your measurement area, CLIOSat allows you to conclude about your field values representativity and consistency by a comparison with satellite climate products covering a longer period. This can be done also to assess the spatial and temporal variability of your measurements.

- **Naval architecture**

- Determination of typical and extreme conditions in order to optimize ship design according to given duties and routes requirements.

- **Marine operations**

- Optimization of the possible working periods
- Assessment of mean daily conditions

- **Maritime transports**

As the divisions in CLIOSat follow the main maritime routes, it is easy to determine the best periods for conducting sensitive routeing operations:

- Optimization of the shipping routes regarding each season,

- Refinement of previously known routes,

- Preparing routeing operations of ships or towed structures.

II.4 Prospects

The increasing number of satellites and daily flow of data impose a CLIOSat updating, either monthly for the on-line service or annually for the CLIOSat atlas. It is planned to add new data from the ongoing ERS1 and Topex-Poseidon missions and to take advantage of all ocean observation programs that will be operating for at least the next 10 years. In particular, ERS2 satellite which was launched in April 1995, will also provide waves periods and directions within sea states, whereas, at the end of the century, ENVISAT satellite, equipped with a SAR, together with sensors similar to those of ERS satellites, will provide directional data on a twice denser coverage.

IV. Getting more elaborated operational metocean parameters

CLIOSat aims at providing engineers with reliable and accurate metocean parameters. To ensure consistency of the statistics, measurements of each parameter are gathered on climate coherent areas pre-defined by metocean experts. Samewise, for the CLIOSat on-line service, statistics are provided on areas defined by experts. Because of instrumental limitations when satellites fly very close to the coasts, one cannot derive reliable metocean parameters nearshore, using satellite data only. Samewise, the coverage of the seas and oceans by satellites disable the elaboration of climates on very small areas (few km^2). CLIOSat atlas and on-line service thus offer wind and wave climates of offshore conditions that can be used, for instance, as 'first level information' to quickly assess a project feasibility but not at a design phase. (Parameters such as extreme local conditions, coastal values, offshore and coastal directional spectra of typical storm conditions are not given within CLIOSat).
However, procedures exist, that rely on the combination of satellite data, metocean, bathymetric and stochastic models, in order to derive local and near-shore metocean parameters. However, their setting is too long and complex to be performed in the frame of the CLIOSat on-line service.

V. Conclusion

For the first time, thanks to satellite data, reliable parameters originated from measurements can be offered to industrial users, even in remote areas. Detailed information issued from SAR measurements is now available, which can be as detailed as the characteristics of each individual components of a sea-state (spectral peak periods, direction and heights, percentage of crossed seas) or, related to the whole sea-state, significant wave height, zero-crossing period and direction of the main spectral peak.
Taking advantage of these recent achievements, an operational and cost-effective system, CLIOSat has been presented here for quick assessment of metocean parameters, on offshore conditions. CLIOSat provides engineers with wind and wave climates, for their pre-project needs, either on predefined coherent climates areas or on customized areas, through an on-line service, in less than 24 hours.

CLIOSat is meant to assist industrial users at a preproject phase. However, for more specific needs, for local areas and near shore locations, more elaborated procedures exist, that combine satellite data, metocean and stochastic models, in order to derive parameters available for the design of structures.

Acknowledgements

Since 1991, ESA granted MétéoMer several pilot projects, which enabled the feasability studies and developments that led to the elaboration of this atlas. Within the AVAL-SAR projects, the french Space Agency CNES has financially supported the ESA pilot projects, more particularly those relating to extracting operational parameters from the SAR in wave mode measurements.

Some of the methods for the construction of climates have been elaborated in the frame of our ASPRO project (*Apport des données Satellitaires à la PRévision climatologique en Offshore* - Contribution of satellite data to offshore climate forecasting), within the CLAROM group (Club pour l'Action et la Recherche sur les Ouvrages en Mer), with the FSH (Fond de Soutien aux Hydrocarbures) financial support.

An expertise and directing committee gave its constant and fruitful advice during the elaboration of CLIOSat. This group was directed by TOTAL and comprised the following french public organisms and private companies:
Bouygues Offshore, Bureau Véritas, Cesam, DCN, Elf Aquitaine Production, ETPM, IFP, IRCN, METEO-FRANCE, Océanide, Optimer, SHOM, STCPMVN and STNMTE.
The contributions of all these organisms are gratefully acknowledged here.

References

Carter, D.J.T., Challenor, P.G. & Srokosz, M.A. ' An assessment of GEOSAT wave height and wind speed measurements', *J. of Geophys. Res.*, Vol. 97 (1992, C7), pp. 11383-11392

Charriez, P., Olagnon, M., & Tournadre, J. 'Confidence intervals associated with satellite measurements of wave and wind environment', *Proc. Offshore Mechanics and Arctic Engineering*, OMAE Vol. 2 (1992) pp. 313-320.

Charriez, P., Olagnon, M. ' Relevance of satellite data for a reliability approach of design wave estimation', *Proc. Offshore Mechanics and Arctic Engineering*, OMAE Vol. 2 (1995) pp. 71-77.

De Sury, H., Charriez, P., Lasnier, P. & Olagnon, M. ' Contribution of satellite data to meteo-oceanic site characterization : A case study', *Proc. Int. Offshore and Polar Engineering Conf.*, ISOPE, 1994.

Gower J.F.R., 'Intercalibration of wave and wind data from Topex/Poséïdon and moored buoys off the west coast of Canada', Proc. of third thematic conference for marine and coastal environments, Seattle, Washington, September 1995, Vol I, pp 95-103.

Hasselmann, K. & Hasselmann, S. ' On the Nonlinear Mapping of an Ocean Wave Spectrum into a SAR image Spectrum and Its Inversion', *J. of Geophys. Res.*, Vol 96, C6(1991) pp. 10,713-10,729.

IAHR. Sea-state parameters, January 1986. Bulletin n°52.

Krogstad, H.E., Samset,O. & Vachon, P.W. 'Generalization of the nonlinear ocean-SAR transformation and a simplified SAR inversion algorithm', *Atmosphere and Ocean*, Vol. 32 (1994) pp. 61-82.

Labeyrie, J. 'ST.EX.OM : a statistical package for the prediction of extreme values', *Proc. 4th Int. Conf. on Engineering Software*, Springer Verlag, Berlin, ch.15 (1985) pp. 17-32.

Labeyrie, J. ' Stationary and transient states of random seas', *Marine Structures*, 3. 1 (1990) pp. 43-58.

Labeyrie, J. ' Time Scales and Statistical Uncertainties in the Prediction of Extreme Environmental Conditions', *Reliability Engineering and Safety*, 32 (1991) pp. 243-266.

Queffeulou, P. ' Altimeter wind and wave measurements', Proc. of second Ers-1workshop, March 1994, Ifremer, France.

Quilfen, Y., ' Scatterometer off-line precision products', Proc. of second Ers-1workshop, March 1994, Ifremer, France.

Tournadre, J. & Ezraty, R. 'Wind and sea state local Climatology by means of Satellite Radar Altimeter measurements', *Proc. Space and Sea Colloquium*, E.S.A SP132 (1990) Paris.

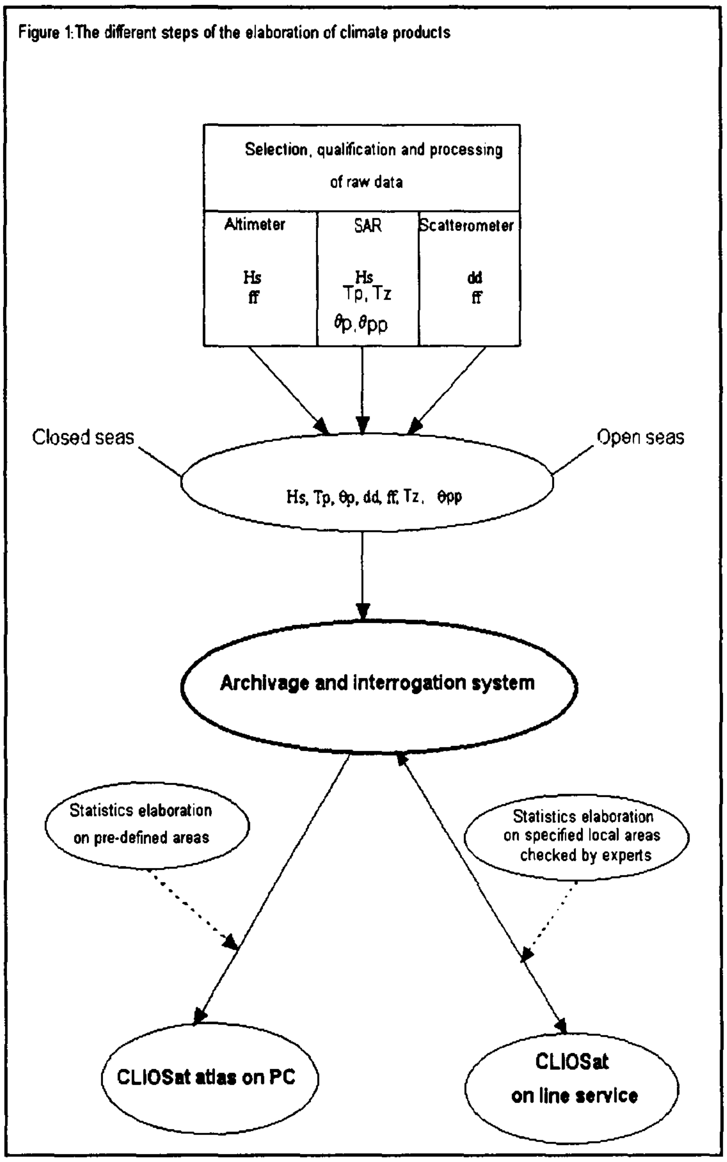

Figure 1:The different steps of the elaboration of climate products

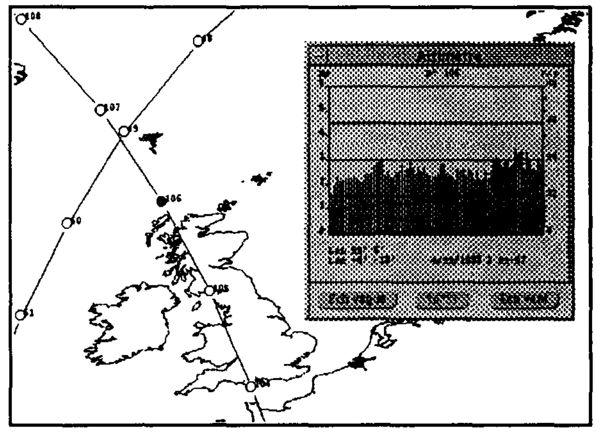

Figure 2: Altimetric measurements of Hs (vertical bars) and wind speed (line)

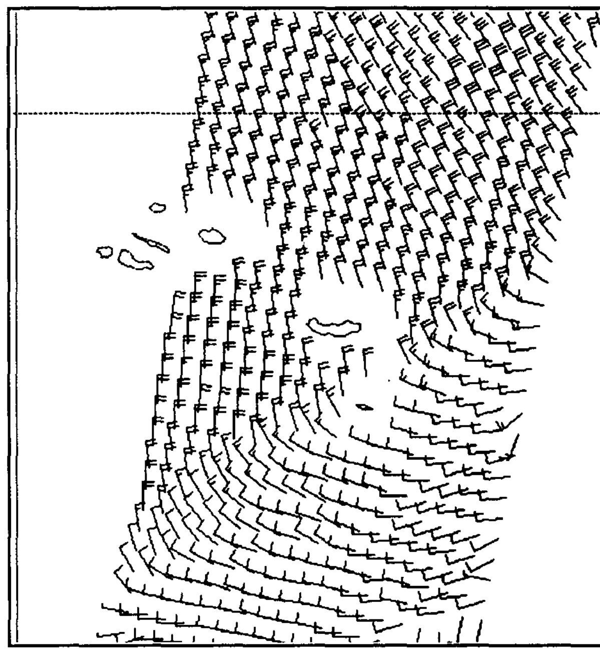

Figure 3: Scatterometer wind field

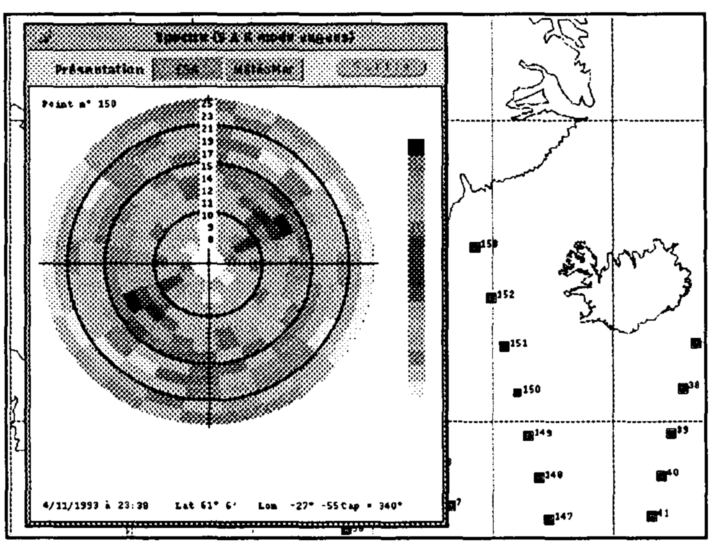

Figure 4: Example of SAR raw data showing 180° ambiguity

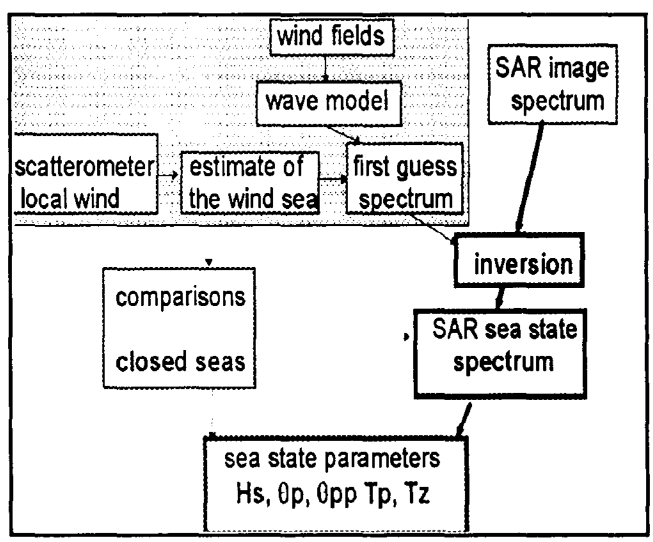

Figure 5: Flow chart for SAR data processing

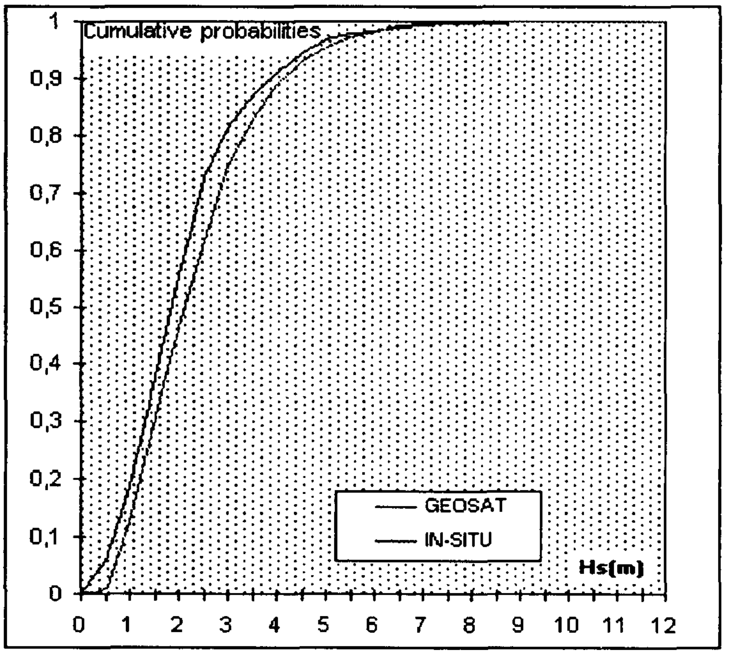

Figure 6: Comparison between Geosat altimeter data and field Hs measurements

Figure 7: Comparisons of SAR and buoy measurements for Tp and θp

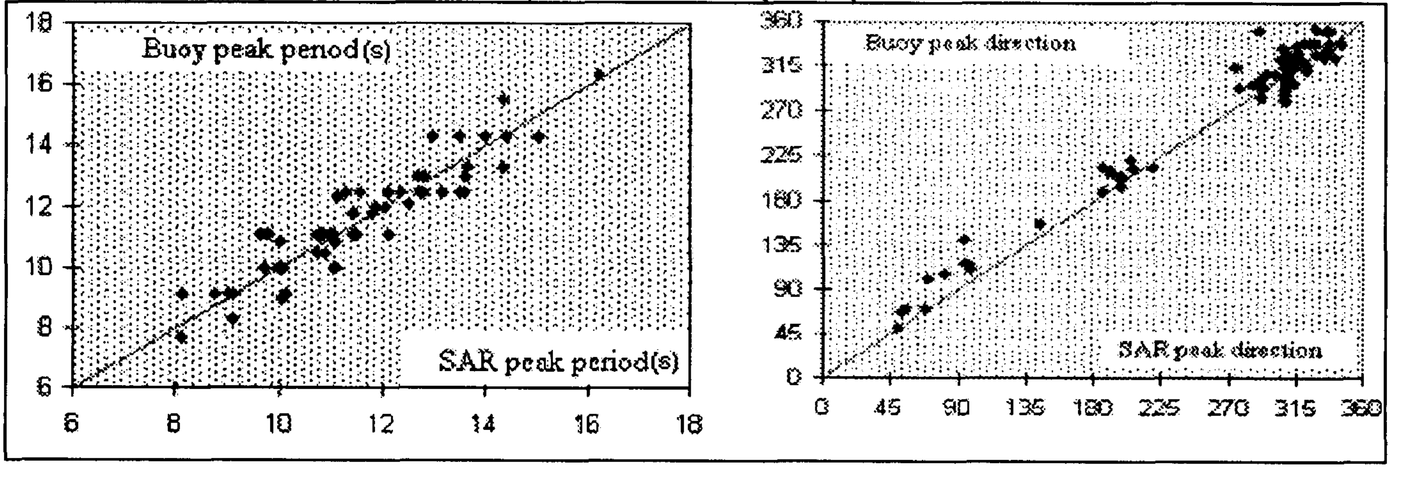

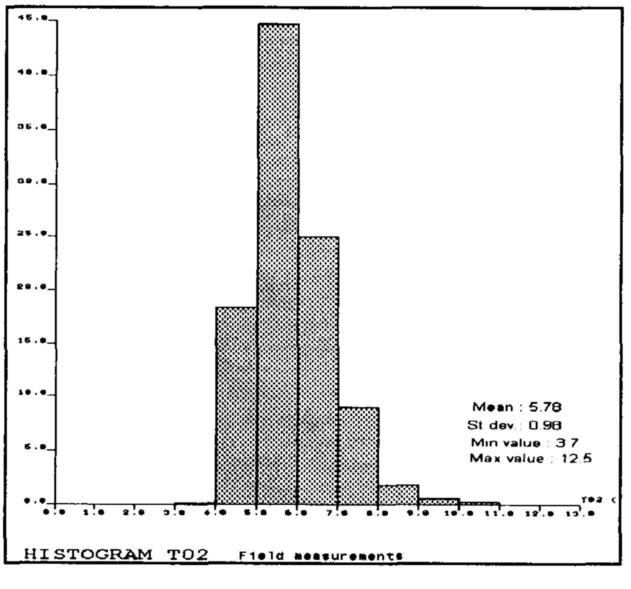

Figure 8a: Buoy T0,2 histogram (Carolina coast)

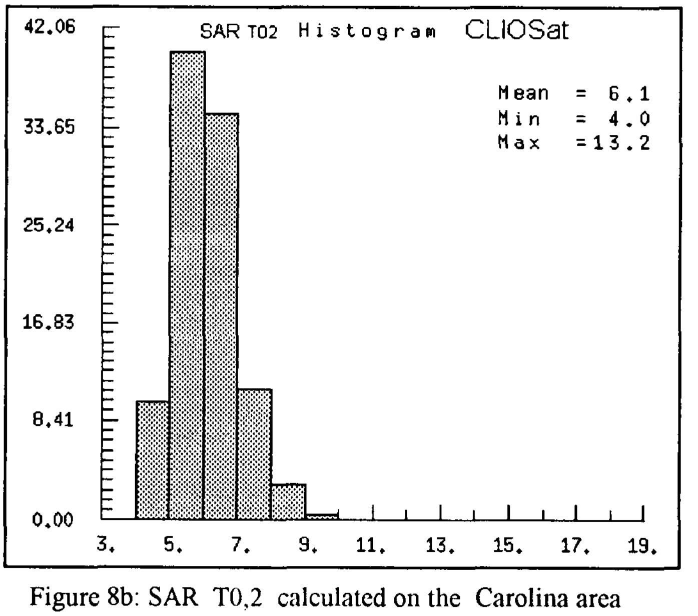

Figure 8b: SAR T0,2 calculated on the Carolina area

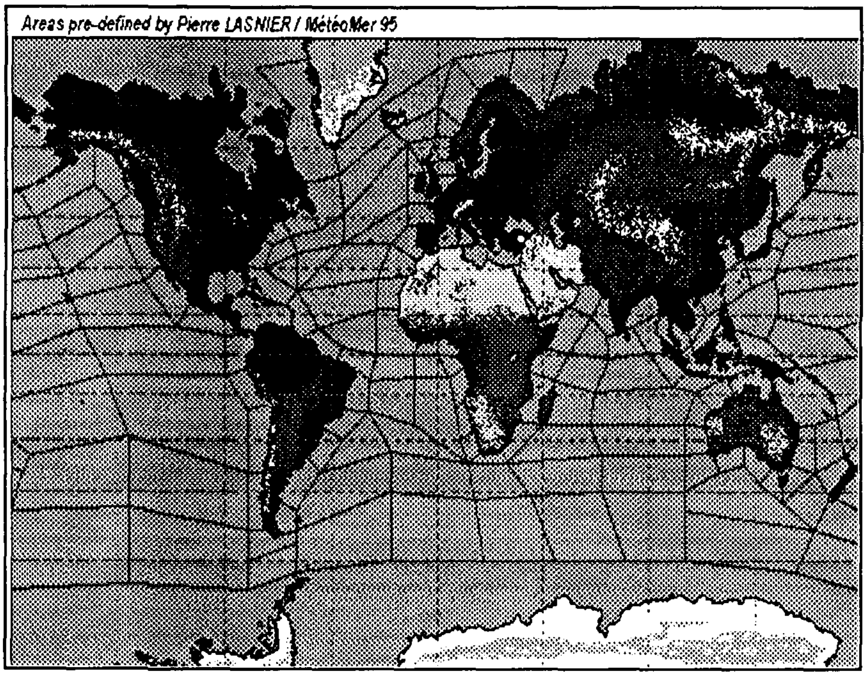

Figure 9: CLIOSat map

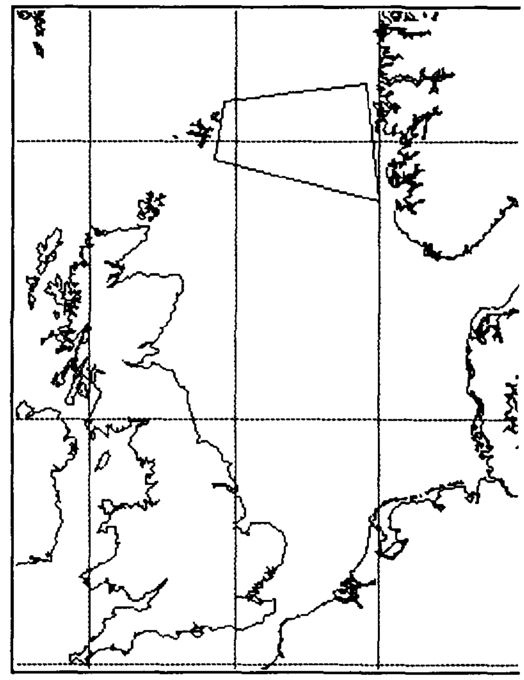

Figure 10: Example of a customized area of the CLIOSat on-line service

Figure 11

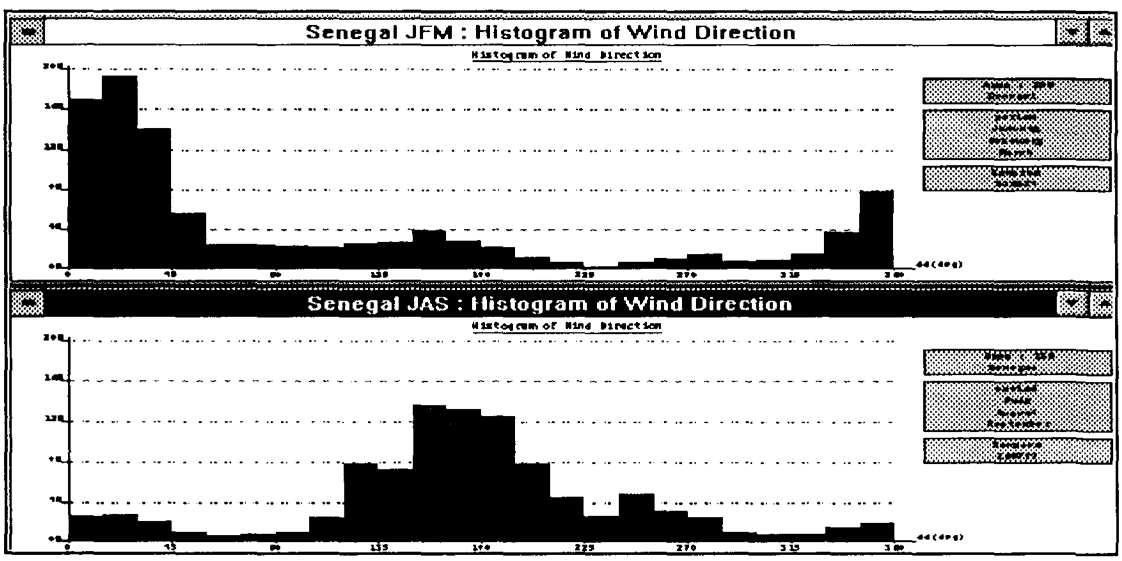

Figure 12

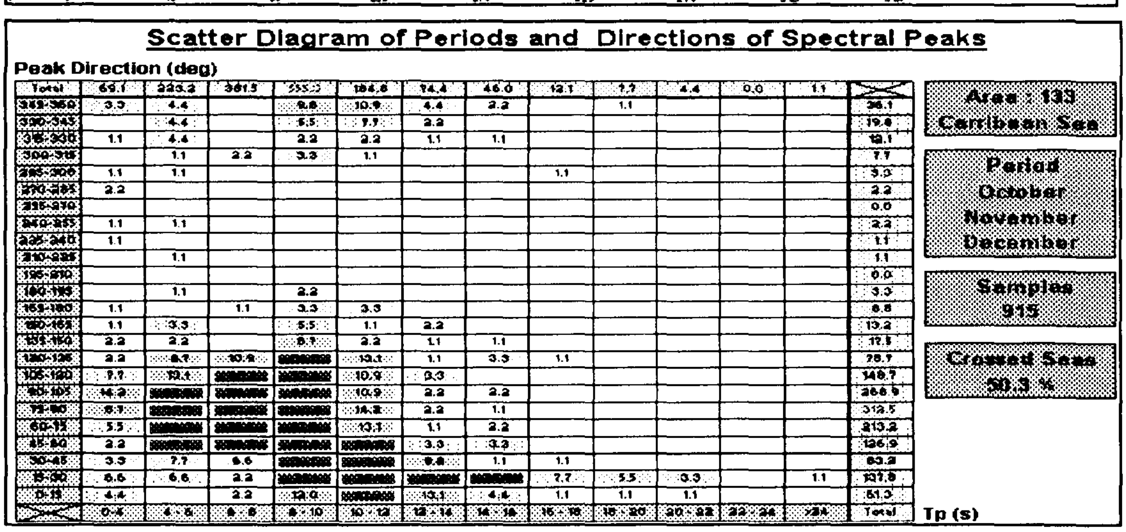

FORESTRY

Chairman: F. De Grandi
Rapporteur: G. Calabresi

TROPICAL RAINFOREST INVESTIGATION IN BRAZIL USING MULTITEMPORAL ERS-1 SAR DATA

Manfred Keil, Dominic Scales, Rudolf Winter*, Hermann Kux** & Joao Roberto dos Santos**

German Aerospace Research Establishment (DLR), Oberpfaffenhofen, Germany
Tel: (49) 8153-28-1377, Fax: (49) 8153-28-1445, e-mail: keil@dfd.dlr.de

** Joint Research Center Ispra (JRC), Varese, Italy*
*** National Brasilian Space Research Institute (INPE), S. Jose dos Campos, Brazil*

ABSTRACT

In a study site in the Southwestern Amazon (state of Acre/Brazil) multitemporal ERS-1 data have been investigated for monitoring of tropical forest, for landuse classification and change detection. The investigations within the ERS-1 pilot project PP2-D3 of ESA are integrated in a cooperation with the National Brazilian Institute of Space Research (INPE). The studies were incorporated in the TREES ERS-1 Study '94 (Malingreau et al, 1994).

Main objective of the project was to develop and test methods to use ERS-1 data for forest/ nonforest mapping and rainforest monitoring and, if possible, to differentiate landuse intensity. Several classification approaches of ERS-1 SAR data have been tested. The evidence based classifier EBIS (evidence based interpretation of satellite imagery, Lohmann 1991) proved as a suitable tool for forest/ nonforest classification and diversification of landuse, especially when using a new version including textural classification. The separation of forest / nonforest could be improved by multitemporal ERS-1 SAR data of the dry and wet seasons.The approach developed in an area of about 50 km by 60 km around the town Sena Madureira was successfully transfered to a region North of Rio Branco, the capital of Acre.

By the demonstration of the pilot project, the Techno-logical Foundation of Acre, FUNTAC, the regional center for remote sensing in Rio Branco, is to be assisted to apply radar data in satellite image interpretation for landuse change detection. FUNTAC as well as several regional Amazon remote sensing data centers have been instructed for radar imagery by radar interpretation courses performed by the cooperation partner INPE.

1. INTRODUCTION

In 1989, a cooperation between the German Aerospace Research Establishment (DLR) and the National Brazilian Institute of Space Research (INPE) was started to study remote sensing abilities for controlling the environmental impact of deforestation in the Amazon region and for mapping rainforest formations and anthropogenic land use. The study site was defined in the southwestern part of the Amazon basin near Rio Branco/Acre. Based on this cooperation and first studies of Landsat MSS and TM data recorded between 1975 and 1990 (Hoensch 1991), an ERS-1 pilot project (PP2-D3) started in June 1993, funded by the German Space Agency (DARA). In order to overcome the frequent cloud cover in the tropical regions, the ERS-1 C-band SAR data were to be tested for forest monitoring purposes.

Evaluation methods and classification schemes were to be developed for large area rainforest monitoring by ERS-1 data. Institutions like the technological center of Acre, FUNTAC, were to be assisted to apply radar data for landuse change detection. Main study objectives were the discrimination of forest / non-forest and registration of new deforested areas. The information content of ERS-1 SAR data was investigated also for the differentiation of forest types (dense and open rainforest) and different landuse classes, for the influence of seasonal changes and for the dependence on surface topography.

2. PROJECT SITE DESCRIPTION

The project site is located in the southwestern part of the Amazon Basin, 200 km from the Bolivian and Peruvian border. The area belongs both to the state of Acre and Amazonas, the capital of Acre, Rio Branco, is included as well as the town Sena Madureira northwest of Rio Branco, connected by one of the main transamazonian highways, the BR-364 (Fig. 1). The study area is covered by different tropical rainforest formations and, mainly along the BR-364, by human altered areas like pasture land and secondary forests. The rainforest formations and the geology are described in (Hönsch, 1993) and (Keil et al., 1995b).

The state of Acre has a long history of colonization, strongly pushed through commercial interests in rubber, in the last and the beginning of this century. Since the opening of the BR-364 in the early 70's as a main connection between the western part of Brazil with the Peruvian border, large deforestation activities took place mainly for 'governmental sponsored' cattle farming activities but also for colonization projects called 'PAD's. Along the BR-364, cattle farmers have pushed the deforestation, although in the last few years, since the suspension of the governmental supports, the speed of forest clearance decreased. The cultivation of pasture, the progress in burning and logging, as well as the actual regeneration process of deforested land into secondary forest or agroforest sites have a main influence on the equilibrium of the ecosystem. In the testsite, the dry period starts about end of May and continues up to mid–September. Within that period, annual burning of pasture land alters the seasonal vegetation cover. The most homogeneous aspect is shown during the end of the dry season.

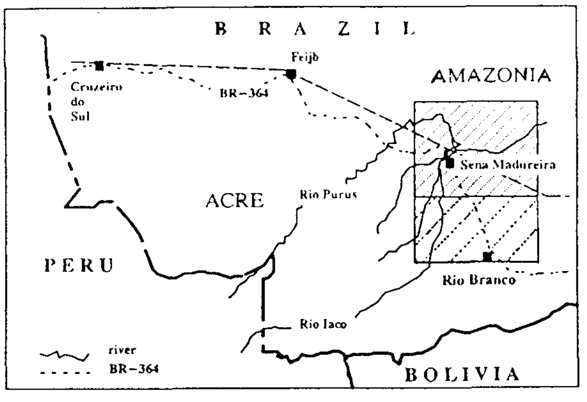

Fig. 1: Location of the testsite Sena Madureira / Rio Branco

3. DATA

ERS–1 SAR datasets were available of a period between April 1992 and August 1993; six descending scenes and data of four ascending orbits could be used as GEC (geocoded ellipsoid corrected) products. The main base of reference were Thematic Mapper scenes from September 1990 (for the Sena M. area), from August 1992 (covering Sena Madureira and Rio Branco) and from July 1994 (for the Southern part). ERS–1 datasets of 1994/95 were not available until now.

In June / July 1994 a field survey was performed in cooperation of DLR and INPE, with assistance of the Technological Foundation of Acre, FUNTAC, and the University of Acre. Besides field survey data concerning the landcover situation, mainly along roads around and between Sena Madureira and Rio Branco, a large number of handheld airphotos were taken during an overflight in a Cessna Skyline. During this survey, 12 profiles were registered in primary and secondary rainforest areas (Santos et al 1994).

4. METHODOLOGY

Within the study, the ERS–1 SAR datasets were evaluated by visual interpretation as well as by several approaches of supervised classification. In order to use the multiseasonal information content of ERS–1 SAR data, a co–registration of the data was essential, based on GEC products. This allowed also to compare ERS–1 analysis results with TM data analysis results. An overview of the data processing and evaluation is given by the flowchart in Fig. 2.

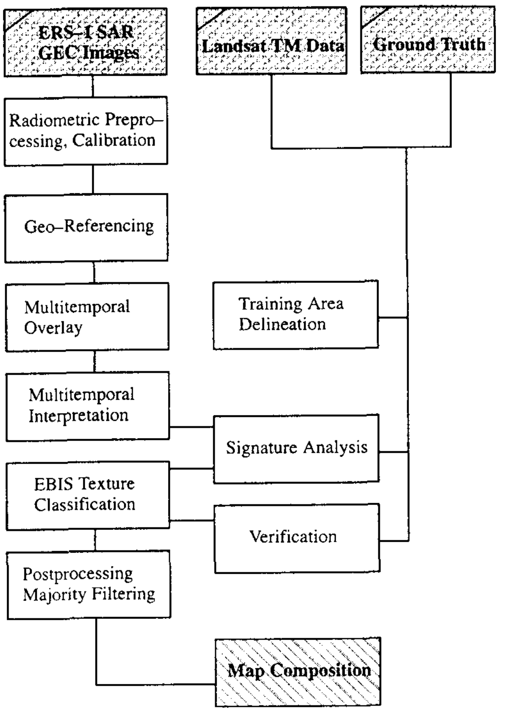

Fig. 2: Flowchart of data processing and analysis

A calibration into sigma–db values was performed. This allows the comparison of ERS data of different acquisition dates and also with other SAR data, e. g. from the SIR–C / X–SAR shuttle mission of 1994 (Keil et al, 1995a). For classification purposes, the transfer to db–values was not found to be essential.

Combination of Datasets

For data combination, co–registerded ERS–1 data and TM data have been resampled to 25 m pixel spacing. A TM based forest / nonforest classification was used to get the reference information on larger areas. This forest / nonforest mask was superimposed on monotemporal and multitemporal ERS–1 SAR datasets for visual interpretation and classification checks.

Classification

Several classification methods were tested for the ERS–1 datasets, including maximum likelihood classification of filtered data (e.g. using the Frost filter).

Especially investigated was the EBIS classifier by Lohmann, 1991. For the main study period, EBIS ("Evidence Based Interpretation of Satellite data") was available in a first version, in which local histograms in a certain window environment are evaluated for the class contribution, based on the assumption of multinomial distributions. In this version, the speckle and textural information in a pixel environment is taken into account by the distribution of the local histogram. Since the end of 1994, a new version of EBIS is usable for a broader community (integrated in the ERDAS IMAGINE software), also allowing texture classification. In the new version a new algorithm is used for classifying textures based on co–occurence feature vectors that are modelled as multinomial density functions (Lohmann 1994). For the ERS input data, nofiltering is necessary.

The classification studies have first been performed in two areas, one around Sena Madureira, 50 km by 60 km in size, the other (smaller) area 50 km Southeast of Sena Madureira along the BR–364. The method was then transfered to the study site Northwest of Rio Branco, 50 km by 50 km in size.

5. RESULTS

Visual Interpretation

A main advantage of visual interpretation of ERS SAR data is the possible delineation of topographic and geomorphological units, as the dominant ERS–1 SAR information within the rainforest areas is given by the relief. The drainage pattern are well to be distinguished (Kux et al 1994). By their geomorphological situation, several forest formations can be separated as described by Keil et al (1995b), shown for the Northern study area near Sena Madureira.

For monotemporal data, ERS data of the dry season delivers best contrast for visual delineation of forest / nonforest areas. The abilities of visual delineation are increased as textural and structural information can be integrated by an experienced interpreter, in addition to tone information. This is valuable in the hilly areas, affected by stronger relief influences, in comparison to automatic classification. Problems of delineation in regrowth areas can be reduced by combining ERS–1 datasets of the dry and wet season (Keil et al, 1995b).

The destruction and new clearing of rainforest areas cannot be detected as fast as by TM data. Even after a first burning a relatively high backscatter and texture remain, resulting from remaining stems and trees. Here the different features can be stated detected by Landsat TM, especially in the short wave infrared band with its sensitivity to vegetation damages and ground visibility, and the C–Band SAR, sensible to roughness parameter, to be noticed e.g. in Fig. 4. In this figure the third study area Northwest of Rio Branco is shown for mono–temporal and multiseasonal SAR data of 1992/93, in comparison to Landsat TM data of August 1992. The new cleared area at the upper left of TM scene (Southwest part of the "L" like facienda) can hardly be detected even in the multiseasonal ERS–1 scene. Additional texture filtering and combination of filtered products delivers more "suspicious areas" when applied according to (Kuntz & Siegert 1994), but the interpretation remains doubtful because of similar effects by microrelief.

Signature Analysis

In addition to visual interpretation of multitemporal combination products, the temporal behavior of different land use classes in the ERS–1 data was investigated, based on db–values. The rainforest areas proved to be quite stable along the seasons. Fresh pasture land shows a higher backscatter in the rainy season, e.g. in December, because of the increasing vegetation cover. Regeneration areas have a larger seasonal dependence than primary rainforest, too, which can assist multiseasonal classification. In the signature plots of Fig. 3, the original (non–filtered) data have been used, connected with high values for standard deviation of the training sites. This demonstrates the necessary use of preprocessing by adequate filtering or the application of textural analysis.

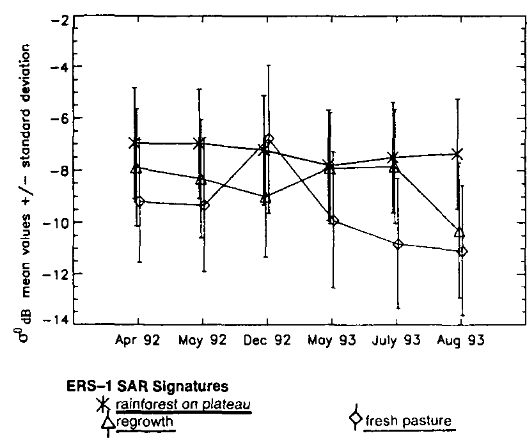

Fig. 3: ERS–1 signature plot for three training sites

Results of Classification

The best classification results were reached by the EBIS classifier. Using the local histogram approach, search windows of 7x7 or 9x9 were found to be adeqate. In the Sena Madureira site, the ERS–1 SAR scene from May 92 was used for monotemporal SAR classification. The forest / nonforest separation was successful in most of the areas. In the hilly terrain and along the boundaries of steep drainages, misclassification took place because of the relief influences. Misclassification within the forest areas can be reduced by post–classification filters (majority 7x7). Misclassification within deforested areas is due mainly to two reasons: 1. Changes in the relief and therefore in the radar illumination, 2. larger amounts of shrub vegetation or of remaining tree groups (e. g. palms), which lead to higher values of backscatter and also to texture variances.

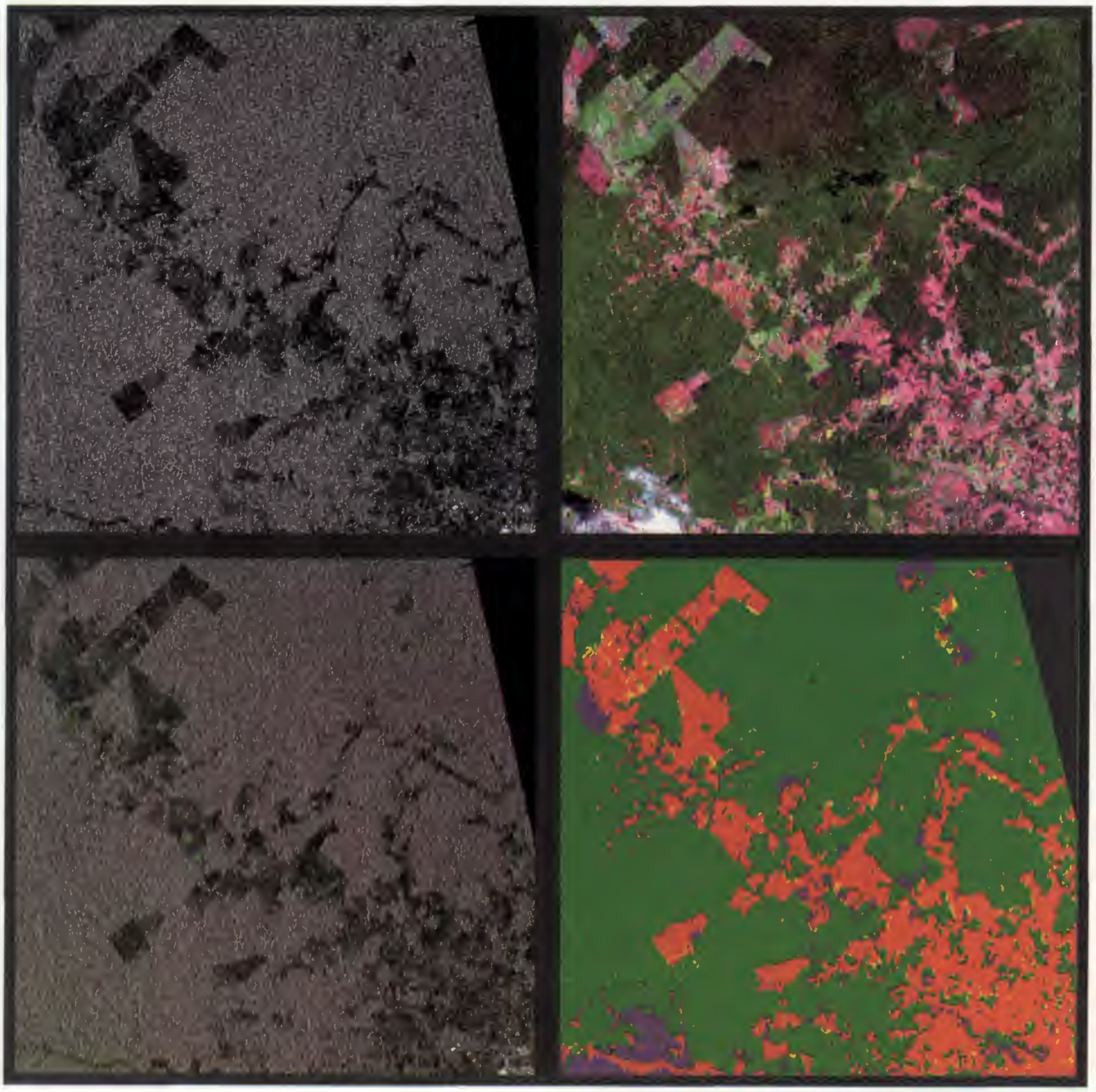

Figure 4: The third study site Northwest of Rio Branco, Acre, in different satellite image representations.
Upper left: Monotemporal ERS–1 SAR subscene of June 1992.
Upper right: Landsat TM subscene of August 1992, bands 5,4,3 (R,G,B).
Lower left: Multiseasonal ERS–1 SAR scene in the overlay of June 1992 (R,B) and Jan. 1993 (G).
Lower right: Comparison of the forest / nonforest classification result of multiseasonal ERS–1 classification and TM classification.
Green: Forest by ERS and TM, yellow: forest by TM, nonforest by ERS; orange: nonforest by TM and ERS, pink: nonforest by TM, forest by ERS.

By multitemporal/ multiseasonal classifications in the Sena Madureira site, an improvement in parts of the regeneration areas was reached. The datasets of April 92, May 92 and Dec 92 were used. The effort for multitemporal classification is higher, because the different states of vegetation in the scenes must be covered by a larger set of training areas. On the other hand, the separation between fresh pasture land and regeneration areas / plantations is improved because of the different vegetation development.

In the second study site along BR–364, both EBIS versions (local histograms and texture approach) could be applied. The use of horizontal and vertical co–occurence gave slightly better results for forest / nonforest classification (Keil et al, 1995b).

For assessment of classification accuracy regarding forest / nonforest separation, a forest / nonforest mask from TM data was used. In this mask, secondary forest older than about twelve years was included in the forest area. Comparing with the TM based mask, the ERS–1 classification delivered an agreement of 95 % to 98 % for forest areas. For nonforest areas, about 79 % were reached in the second site along BR–364, showing small influence of relief. In the Sena Madureira site, only 64 % agreement was gained by multiseasonal nonforest classification (Keil et al., 1995 b). This result is due to the strong influences of the hilly terrain and steep river intersections in this area.

The classification approach was transfered to the third subsite Northwest of Rio Branco in a further step. This subsite has been well covered by the SIR–C / X–SAR mission and allows comparisons with the shuttle data analysis (Keil, 1995a). For the multitemporal approach, datasets of ascending orbits of June 1992 and January 1993 have been used, partly also a scene of July 1993. By applying the textural EBIS classification, the forest / nonforest separation could slightly be improved in relation to the local histogram option. As to be expected from visual interpretation, the new cleared areas could hardly be detected in classification. This is shown by the overlay of TM and ERS–1 based forest / nonforest classification (lower right part of Fig. 4), where deforested areas are coded in pink when picked by TM, but not by ERS–1. These facts lead to an reduced agreement with TM for deforested areas which are still at 76 % (shown in red), not regarding the clouded areas. For the forest areas, there was an agreement of 97 % (areas in green). This demonstrates a successful transfer of the classification approach. The ERS–1 classification result Northwest of Rio Branco is shown in Fig. 5, representing three nonforest landcover classes.

6. DISCUSSION AND CONCLUSIONS

By the demonstration of the pilot project in the Western Amazon in the state of Acre, ERS–1data have proved to be successful for rainforest and deforestation monitoring in most of the areas. The main objective of the project was to develop and test a supervised classification approach which allows to perform forest / nonforest separation in large areas. For that purpose, the window based and textural classification approach of EBIS, available in a commercial image processing environment, was found to be a tool well adapted to the properties of radar data. The options of textural classification enlarges the abilities of automatic SAR data classification, especially when applied on multiseasonal radar data and followed by post–classification handling (e.g. by majority filtering).

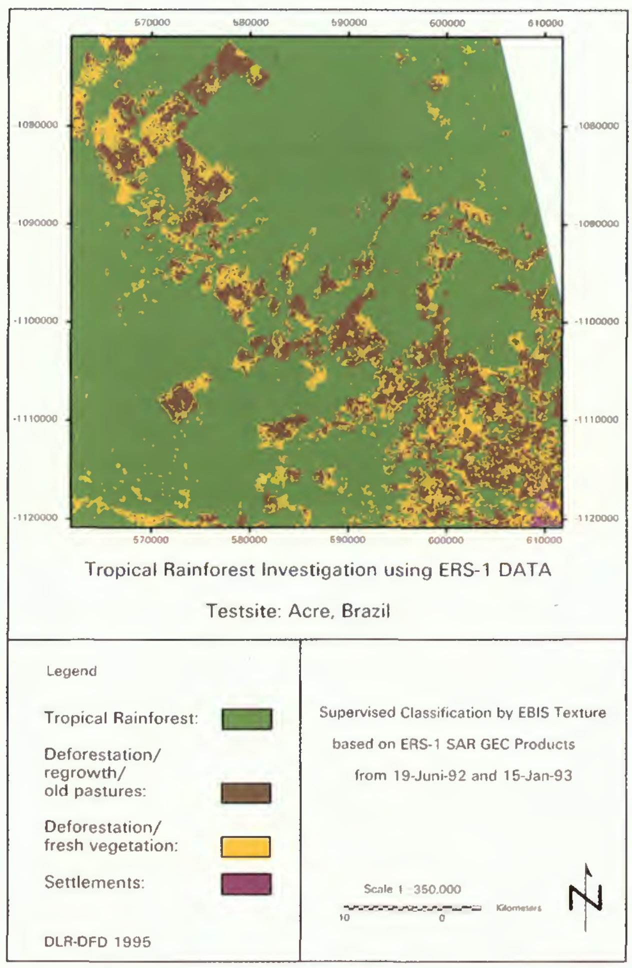

Figure 5: Classification result of the study site Northwest of Rio Branco

The large pasture areas for cattle farming are well to be detected. There remains a partial overlap of rainforest and regrowth areas and also of different types of plantations which deliver similar backscatter in the C–Band. In multiseasonal data additional information content can be used, responding on the different vegetation development of pastures, regrowth and primary / secondary rainforest. Misclassifications appear in hilly and intersected areas of strong topographic relief. Here visual post–interpretation can improve the results. Other problematic areas are newly destroyed and partly cleared rainforest areas which are hardly to be detected by automatic classification in the first year of deforestation. In order to cover also those newly destroyed rainforest areas, a subsequent visual interpretation of specially processed data (combinations of spatial and texture filtered products) seems to give success when used in a change detection mode.

The classification results are going to be prepared for map products 1 : 100 000. That is the scale used for map update and regional planning by the Technological Foundation of Acre, FUNTAC, and other Amazonian institutions, up to now based on Landsat TM data often available only once in two, three or four years. The mapping by ERS SAR can fill the gaps and enable a continuous rainforest monitoring. In order to transfer the abilities of radar remote sensing in the Amazon, radar analysis courses are performed by INPE several times a year in the Amazonian remote sensing centers.

7. REFERENCES

Hönsch, H. 1993, "Erfassung und Klassifizierung von tropischen Regenwaldformationen und anthropogenen Nutzungen anhand von multisensoralen Satellitenbilddaten am Beispiel Brasiliens", Dissertation Universität Trier, DLR–FB 93–15, Oberpfaffenhofen.

Keil, M., D. Scales, R. Winter, 1995 (a), "Investigation of Forest Areas in Germany and Brazil using SAR Data of the SIR–C / X–SAR and other Missions", IGARSS '95 Symposium, 10–14 July 1995, Firenze, Italy.

Keil, M., D. Scales, W. Semmt, R. Winter, H. Hönsch, G. Lohmann 1995 (b), "Tropical Rainforest Investigation with ERS–1 SAR Data in the Region of Sena Madureira, Acre/Brazil (TREES Study Area LAM–2)", Proceedings TREES ERS–1 Study '94 Workshop, 23–24 Febr. 1995, Ispra/Varese, Italy, in preparation.

Kuntz, S., F. Siegert, 1994, "Evaluation of ERS–1 SAR Data for Forest Monitoring in Indonesia", Proceedings of the First ERS–1 Pilot Project Workshop, Toledo/Spain, 22–24 June 1994 (ESA SP–365, October 1994).

Kux, H., F. A. Ahern, R. W. Pietsch, M. Keil, 1994, "Resource Management with Radar in Tropical Environments: A Case Study in Acre State, Brazil." Proceedings Eco Rio' 94, Symposium ISPRS Commission VII, 26–30 Sept. 1994, Rio de Janeiro.

Lohmann, G., 1991, "An Evidential Reasoning Approach to the Classification of Satellite Images", Doctoral thesis Technische Universität München, DLR–FB 91–29, Oberpfaffenhofen.

Lohmann, G., 1994, "Co–occurence–based Analysis and Synthesis of Textures", Intern. Conf. on Pattern Recognition, Oct. 94, Jerusalem, Israel.

Malingreau, J–P., J. Aschbacher, F. Achard, J. Conway, F. De Grandi, M. Leysen, 1994, "TREES ERS–1 Study '94: Assessment of the Usefulness and Relevance of ERS–1 for TREES." Proceedings of the First ERS–1 Pilot Project Workshop, Toledo/Spain, 22–24 June 1994 (ESA SP–365, October 1994).

Santos, J.R. dos, H. Kux, B. C. G. Pedreira, C. A. de Almeida, M. Keil, M. Silveira, 1994, "Mapping Areas of Regrowth in Tropical Rainforest using a Multisensoral Approach: A Case Study in Acre." Proceedings Eco Rio' 94, Symposium ISPRS Commission VII, 26–30 Sept. 1994, Rio de Janeiro.

Scales, D., M. Keil, R. Winter, 1994, "Tropical Rainforest Investigation in Brazil using ERS–1 SAR Data. " Proceedings of the First ERS–1 Pilot Project Workshop, Toledo/Spain, 22–24 June 1994 (ESA SP–365, October 1994).

MULTITEMPORAL EVALUATION OF ERS-SAR DATA FOR MONITORING DEFORESTATION TROPICAL RAINFOREST

Steffen Kuntz, Claudia Streck & Florian Siegert*
Kayser-Threde GmbH, Wolfratshauserstr. 48, 81379 München, Germany
Tel: (+49)-89-72495-119, Fax: (+49)-89-72495-291; e-mail: ku@kayser-threde.de

* *Zoologisches Institut, Ludwig-Maximilians-Universität, Luisenstr. 14, 80333 München, Germany*
Tel: (+49)-89-5902442, Fax: (+49)-89-5902450; e-mail: si@zi.biologie.uni-muenchen.de

ABSTRACT

The ESA pilot project "Tropical Rainforest and Use of Land Investigation" (TRULI, PP2-D11; funded by DARA) was aimed to investigate the capabilities of the ERS-1 satellite in a tropical rainforest environment. Using texture analysis and multitemporal approaches several land use classes and different forest types could be identified in a single ERS-1 SAR scene. Texture allowed to discriminate 1.) undisturbed forest of at least two different types 2.) shifting cultivation and agriculture, 3.) secondary forest, 4.) selectively logged forest 5.) clearings by fire and clear-cutting and 6.) settlements and major roads. Results of multitemporal data analysis showed that changes in area of classes No. 2., No. 4. and No. 5. can be readily detected in a sequence of four images covering one year. KFA1000 images from the Russian MIR space station, Landsat TM images and data acquired during two extensive field excursions served as a reference for SAR image interpretation. Based on our results, we believe, that the European radar satellite ERS-1 can be used operationally to monitor and analyse rainforest conversion and land use patterns in the Tropics at a scale 1 : 100 000. Because operationality and technology transfer towards Indonesia were of highest priority, all evaluation procedures and strategies were performed with standard computer equipment and commercial software packages. This equipment is already available in Indonesia and is currently used by Indonesian authorities. A 5 days workshop was held at BPN, the National Land Planning Agency, in Jakarta in September 1995 for training of local remote sensing experts in the use of ERS data.

1. INTRODUCTION

Tropical rain forests are highly endangered ecosystems. Fast economic as well as population growth result in increasing rainforest conversion rates all over the world. Only recently it is recognised that sustainable development and careful exploitation of natural resources is mandatory to assure future prosperity. With the launch of the European radar satellite ERS-1 in July 1991 a new powerful tool for land use planning and forest monitoring from space is available. The cloud penetrating capability of radar is especially suitable in tropical regions frequently obscured by clouds. The German ESA pilot project "Tropical Rainforest and Use of Land Investigation" (TRULI, PP2-D11) was established to investigate the capabilities of the ERS-1 satellite in a tropical rainforest environment. TRULI started in July 1993 and is funded by the German Space Agency (DARA). In Indonesia the project is supported by the German Society for Technical Co-operation (GTZ) and the National Land Planning and Mapping Board (Badan Pertanahan Nasional, BPN).

Main emphasis of the TRULI project was on the applicability of all evaluation methods to the possibilities and needs of the Indonesian partner organisation BPN. In the framework of the bilateral German-Indonesian LUPAM project (GTZ/BPN) officials were already trained in analysing optical satellite data using the ERDAS/IMAGINE© software package. Because we used this software for all processing steps, it will be easy to implement the developed methods for SAR image processing and interpretation in Indonesia.

The TRULI test area was located at the middle reaches of the Mahakam river in the province Kalimantan Timur. The vegetation is dominated by lowland Dipterocarp forests an all major land use types are found in the area. Russian KFA-1000 images from the manned space station MIR with 7m ground resolution and field data acquired during 2 extensive ground truth campaigns (October/November 1993 and September 1995) served as a reference for the SAR image interpretation and for verification of results.

2. ERS-DATA PROCESSING AND MAP PRODUCTION

The following flowchart (**Figure 1**) shows the workflow for the all image processing procedures applied in the TRULI project.

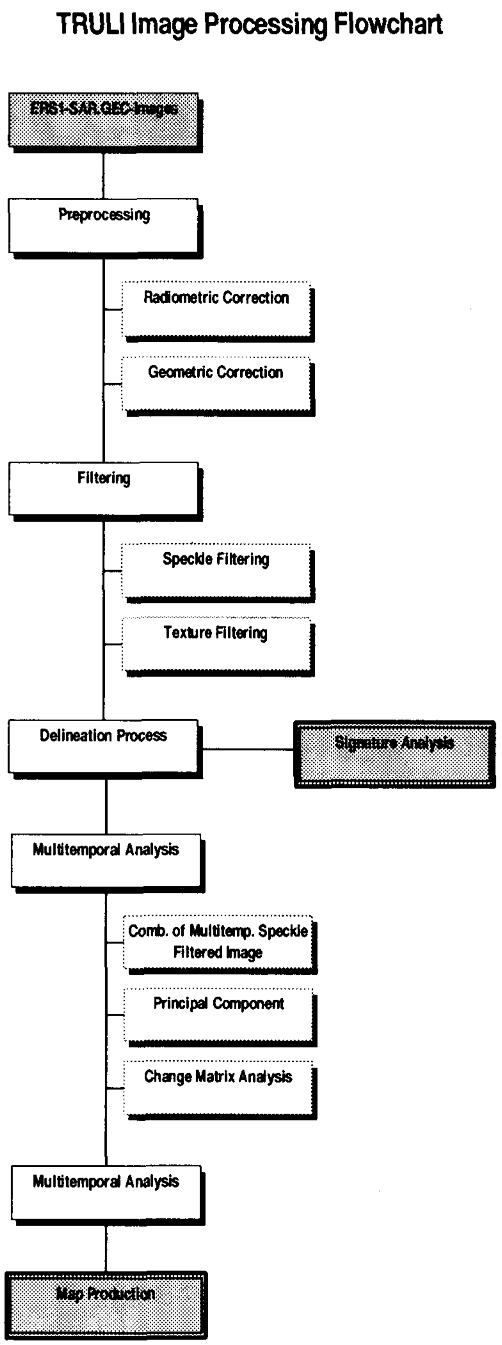

Figure 1: Overview: Flowchart of the image processing steps.

For all the processing steps shown in **Figure 1** we used public domain software provided by DLR Oberpfaffenhofen and an ERDAS Imagine ™ System on a SUN SPARC 10 Workstation equipped with a 5 GB Harddisk and 32 MB RAM. **Table 1** shows required processing times for the generation of a monotemporal RGB-Composite. In order to reduce the CPU time the SAR scenes have been resampled from 16 bit to 8 bit.

Table 1: Examples of CPU-Times for Image Processing **(from Siegert et al. 1995).**

Task (200 MB - 8 bit)	Time (hours.min)
Data-Import from Exabyte and Calibration	0.30
Import in IMAGINE (now 268 MB)	0,40
Histogram calculation	0.20
Data Reduction to 8 bit and Linear Stretching	0.45
Sigma and Median Filter - Kernel Size 7x7	4.50
Variance-Filter - Kernel Size 15 x15 (268 MB)	5.00
Variance - Filter- Kernel Size 31x31	15.00
Composite Generation (var15-sm-var31)	1.00
X - and Y Shift Calculation	0.30
Resampling (2 x 260 MB - 8 bit) nearest neighbour	1.50

All the applied image processing techniques and RGB image interpretation for rainforest monitoring have been discussed already in several papers (Kuntz & Siegert 1994a-1994d, Siegert et al., 1995). In brief the following tasks were employed:

- Enhanced monotemporal images were produced by applying different texture filters to one ERS-1 scene. The results of three different filter operations were then combined into a single RGB color image by assigning each texture feature to a different color channel. From these RGB images we produced land use maps in which each class is assigned a different color in the GIS overlay (see **Figure 5**).

- To investigate change detection we produced multitemporal RGB images by assigning the texture features of the 15x15 variance filter of the first image (7/1993) to the blue channel, the texture features of the 31x31 variance filter of the last image in the time series (9/94) to the red channel and the mean of three speckle filtered images (7/93+10/93+9/94) to the green channel. The mean-value-image of three ERS-1 data sets significantly improved the spatial resolution of the images for the visual interpretation, while the texture filters elucidate the changes which happened between the several acquisitions. From these composite images we produced change detection maps in which (among others) the conversion from primary to selectively logged forest is highlighted (see **Figure 5**).

- In a second approach we used a semi-automatic procedure to investigate changes in multitemporal image series. Using principal components of three data sets and their texture features, we found, that especially the 6th principle component contained most of the change detection information (here: forest conversion). Although it is not possible with this approach to explain why forest disappears, it allows to quantitate efficiently rainforest conversion as a whole using a simple semi-automatic density slicing method.

3. RESULTS

In short, the basic idea of the TRULI project for operational radar image evaluation was to produce enhanced ERS-1 images, which can be interpreted visually by Indonensian forestry officials and/or the land use planning board. Our aim was twofold: we investigated different processing techniques in order to obtain:

- a basic ecological and land use classification from monotemporal ERS-1 images,
- change detection information from multitemporal ERS-1 image series.

The RGB color images containing the texture features have a significantly improved information content for visual interpretation compared to simply speckle filtered radar images. They allowed to discriminate several land use classes which are important for rainforest monitoring:

1. **Undisturbed primary forest of two types:** Two natural forest types, *heath* forest and *Dipterocarp* forest, can be readily discriminated in processed ERS-1 images by their different shades of green and the absence of magenta-white spots in *heath* forest. The salt and pepper like appareance of these spots is an important feature of the enhanced ERS-1 images correlated to the roughness of the vegetation structure. In the case of *Dipterocarp* forests these spots are caused by corner reflection at the crowns of hugh emergent trees or gaps in the otherwise closed canopy, while in *heath* forests the trees are charcaterized by a closed smooth canopy with no emergents. **Figure 2** shows a direct comparison of the processed ERS-1 image (**A**) and the MIR KFA1000 image (**B**, the corresponding area is indicated by the white rectangle in **Fig. 2A**). While the *heath* forest is clearly detectable in the radar image as a dark green wedge it appears less clearly as a brownish colored wedge in the KFA1000 photograph. **Figure 2C +D** show the corresponding ground truth photographs acquired at the locations indicated by arrows in **Fig. 2A**. Due to extremely poor soils tree height and stem diameter are less than half in this *heath* forest compared to the neighbouring *Dipterocarp* forest. **Figure 2E** shows an aerial photograph acquired from a helicopter flying along the northern border region of the wedge (see arrow in **Fig. 2A**). As can be seen, there is a sharp boundary between the two forest types and the canopy appears much smoother in the *heath* forest (left) than in the *Dipterocarp* forest (right). The possibility to discriminate different forest types, which indicate soil quality, is an important tool for land use planning in tropical rainforests. Preliminary results obtained in another area in Kalimantan showed, that it is also possible to identify *peat swamp* and *mangrove forests* in processed ERS-1 images.
2. **Secondary forest:** The vegetation which grows immediately after burning of shifting cultivation fields or clearcutting consist mainly of a few light demanding plant species. Compared to primary forest the canopy of young secondary forest (0-20 years) is very smooth. Therefore secondary forests appear darker (low backscatter) in ERS-1 SAR images.
3. **Agriculture (shifting cultivation):** This landuse class appears as a belt of heterogenous patterns of small parcels with a mixture of high and low backscatter values and highly dynamic changes along the rivers.
4. **Selectively logged forest:** Selective logging (which frequently means over-exploitation) can be readily detected in RGB ERS-1 images. **Figure 3A+B** shows a comparison of two processed ERS-1 images 13 months apart. The arrow indicates a more or less undisturbed forest canopy in 7/93, which is broken by many magenta-white spots in 9/94 (right arrow). The appereance of these spots is directly correlated to gaps in the forest canopy. **Figure 3C+D** shows the effects of selective logging on forest canopy structure viewed from a helicopter. The closed canopy of the undisturbed lowland *Dipterocarp* forest (**C**) is severely damaged after logging (**D**). Ground survey showed that selective logging as practised in this area often destroys more than 50% of the canopy (Kuntz et al, 1994a). We believe that tree trunks act as corner reflectors since the magenta-white spots correspond to high backscatter values in all three filtered images. Furthermore the radar signal may be significantly influenced by the water content of the vegetation. Fast growing *macaranga* tree species fill the gaps a short time after the logging operation. The leaves of these species are much larger and have a higher water content than the leaves of the surrounding climax tree species leading to higher backscatter signals. The field survey showed that selective logging activities can be detected even if it was as much as 5 years ago. After

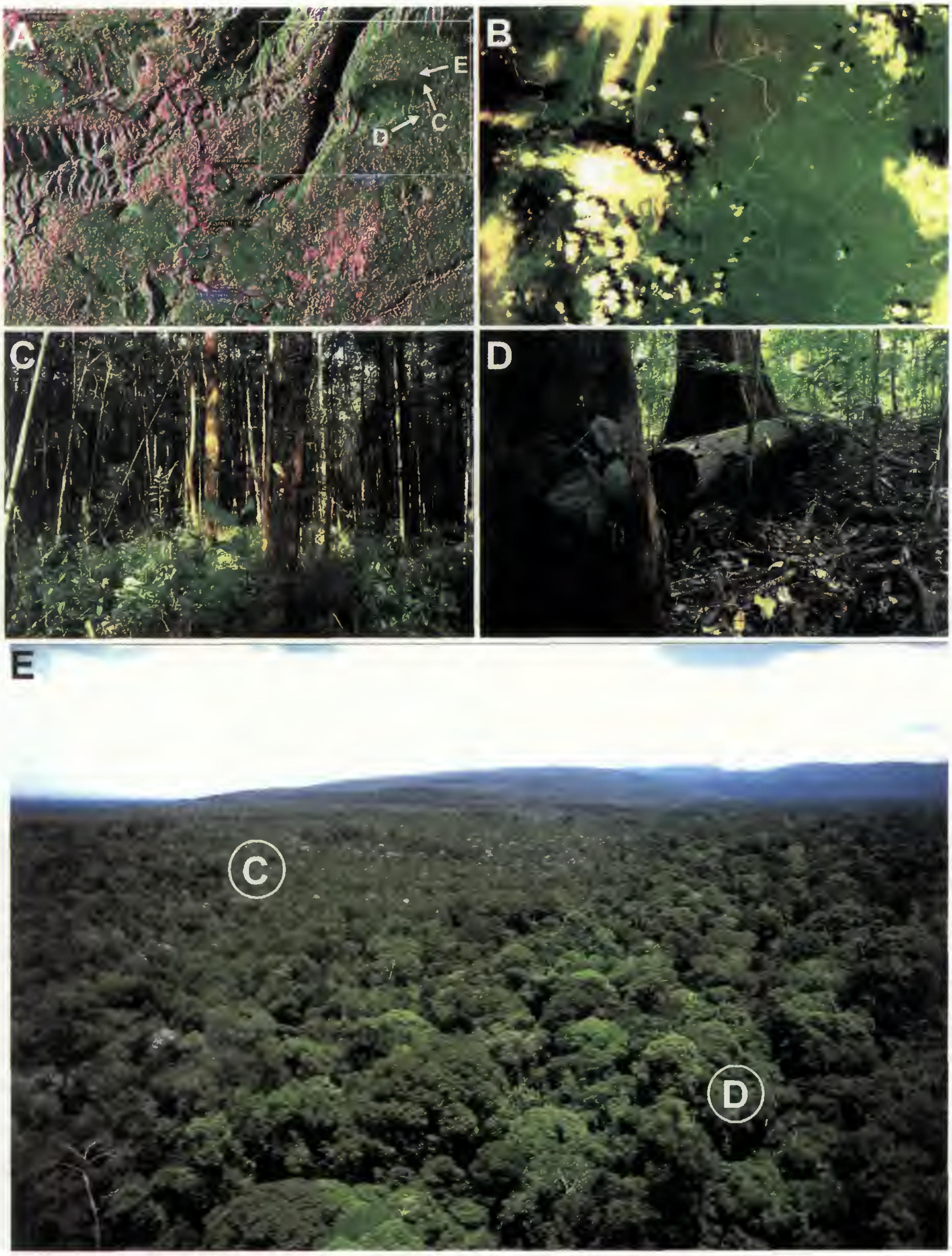

Figure 2

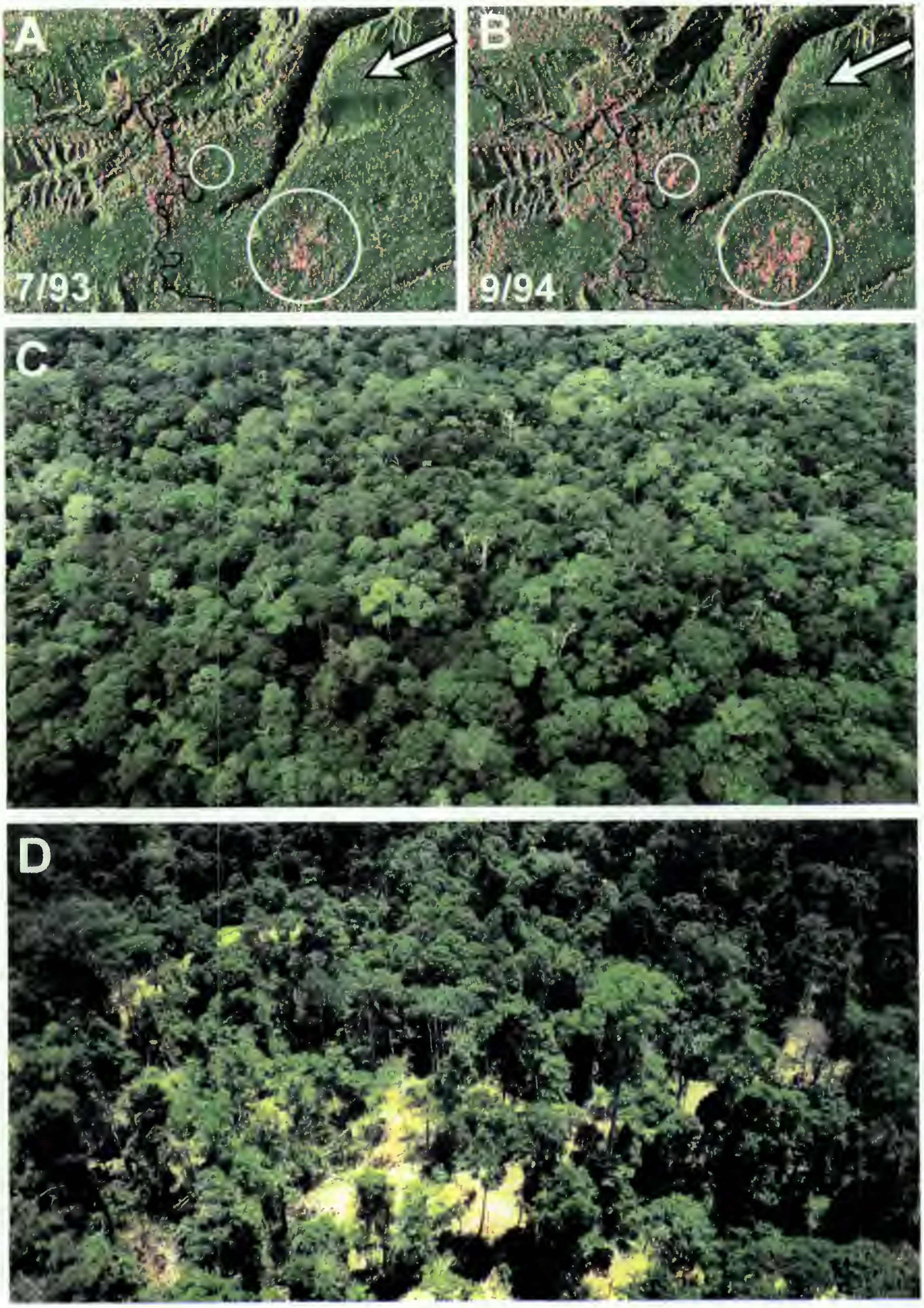

Figure 3

5-7 years the gaps are filled only halfway to the top and *macaranga* species still dominate the regrowing vegetation. Therefore we suppose, that the water content of the plant species as well as corner reflection is the reason why selective logging can be classified in the RGB radar images. The multitemporal analysis showed, that these properties are not correlated to short term differences in water content, since the signatures remain clearly distinguishable over time (see below).

5. **Settlements.** Even minor settlements can be detected based on corner reflection of metal roofed houses

6. **Clearcuts:** *Clearcuts due to logging operation* are most easily identified in the processed radar images as magenta-white areas. The two large circles in **Figure 3** show a large land clearing for plantations. The cleared area of 3600 ha nearly doubles within one year. The surface relief in these clearcutted areas is very rough in terms of radar backscatter. Usually the vegetation is burnt after felling, however many unburnt tree trunks remain scattered on the bare soil. After burning monocultures of several fast growing tree species are planted for pulp wood production. One year later the bare soil is completely covered by young trees and weeds. The radar backscatter of this class is high in all three filtered images and remains high in all 4 images of the time series. The high backscatter may occur due to a combination of the following properties: 1.) an undulating ground surface relief which is otherwise leveled out by the forest canopy, 2.) scattered tree trunks and 3.) young, fast growing trees with a high water content.
Clearcuts due to shifting cultivation are indicated by two small circles in **Figure 3**. Ground survey showed, that this large area (3000m x 800m) was cleared by local Dajak people for intensive rice production. This type of agriculture is aimed for export and not for subsistence. It is a relatively new action which is unwanted by local officials due to the increasing danger of land degradation. Scattered trees, which remain on the fields after burning, result in a high radar backscatter similar as described above. Secondary forests, a vegetation type which grows after shifting cultivation, is characterized by a smooth canopy structure resulting in low backscatter values and dark green color in the RGB radar images. After harvest immediately gras like weeds start growing. They are replaced by young trees in the following years.

We excluded mountainous areas from our analysis since here interpretation is much more difficult and not yet operational. Without sophisticated backscatter corrections the topography influences the signal in a way that ambiguities between various classes and shadow areas do hamper severely the analysis. Thus areas with a higher relief than approximately 100 meters were excluded from the analysis.

For the visual interpretation process we used three different images simultaneously:

- the multitemporal series of processed RGB radar images for basic classification,
- the result of the principal component transform and the change detection RGB image to identify clearcuts and shifting cultivation,
- and a black and white image of the mean-value-feature of three ERS-1 data sets.

Figure 4 shows a landuse map, scale 1:100.000, which was created by visual delineation of clearly detectable signatures according to the above described principles. Each class was identified visually according to an interpretation key, which was created during the first field field trip and by using KFA1000 images as a reference. Such maps can be readily used by officials of the land use planning board as well as foresters. In principle they can be produced every month.

In order to investigate the changes, which occure during one year in this area, we produced one map for July 1993 and another one for September 1994. By correlating the two GIS layers we obtained a change detection map, which indicates major land use changes. In **Figure 5** each color corresponds to a characteristic conversion process, e.g. red indicates the conversion of selectively logged forest into plantation or blue indicates the conversion of primary forest into selectively logged forest etc.

4. VERIFICATION OF IMAGE INTERPRETATION

The results of the RGB radar image interpretation were verified in several ways. In a first step we used MIR KFA1000 space photographs acquired in December 1991. From this data a digital landuse map of all cloudfree areas was produced. Secondly, we used the extensive ground truth data sampled during the first field trip. Here three logging concessions, showing different logging intensities, were visited together with regions of undisturbed *Heath* and *Dipterocarp* forest as well as areas of shifting cultivation. On many sample plots the basic vegetation types were listed and the logging intensity was quantified.

In September 1995 we conducted a second ground truth campaign, in order to finally verify the maps and the change detection results. Especially areas of highly dynamic changes, as identified in the ERS-1 images, were visited on ground and quantitative GPS measurements were performed to control the mapping accuracy. During an extensive helicopter survey we visited more than 80% of our test area and all ground

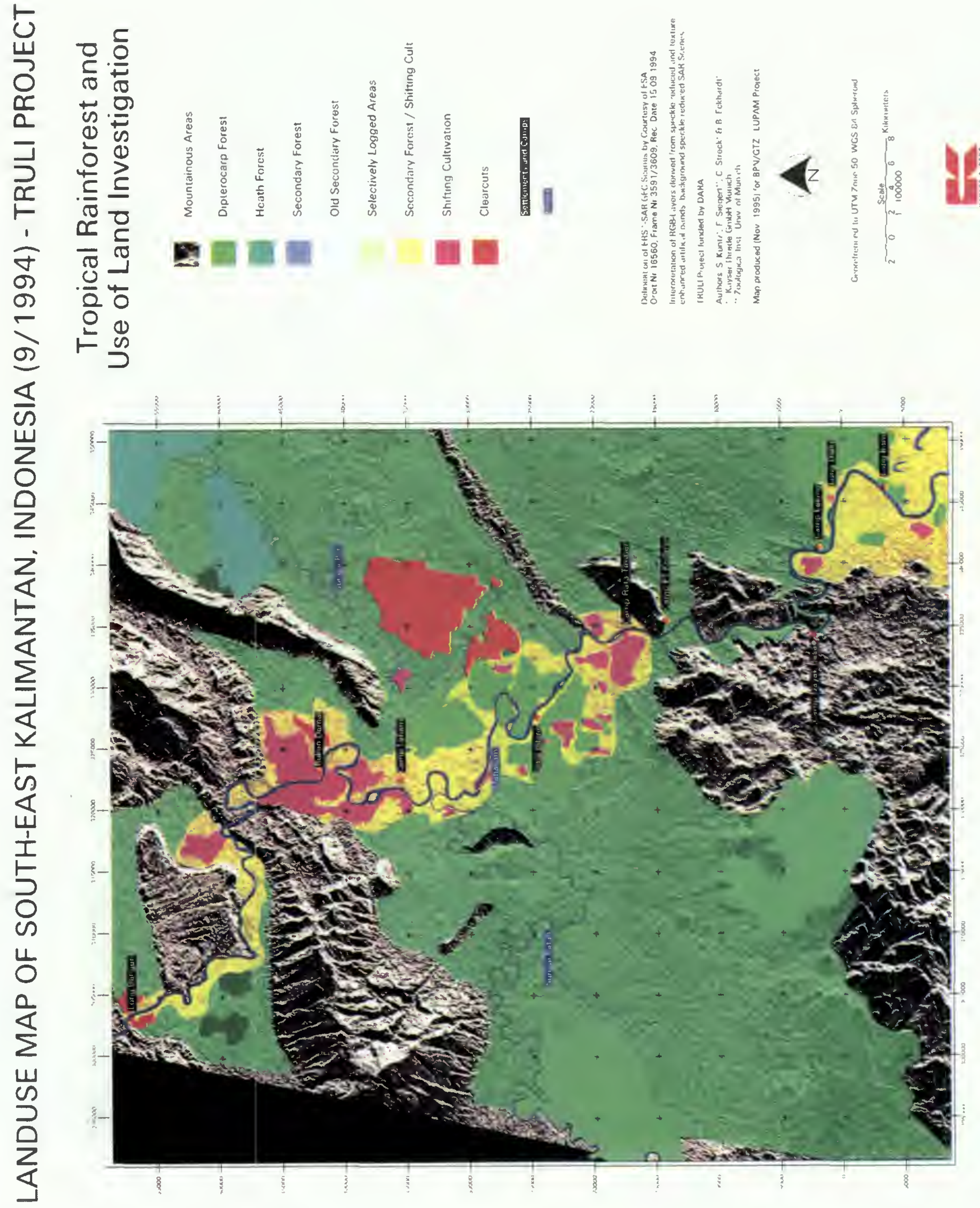
LANDUSE MAP OF SOUTH-EAST KALIMANTAN, INDONESIA (9/1994) - TRULI PROJECT
Tropical Rainforest and Use of Land Investigation
Mountainous Areas
Dipterocarp Forest
Heath Forest
Secondary Forest
Old Secondary Forest
Selectively Logged Areas
Secondary Forest / Shifting Cult
Shifting Cultivation
Clearcuts
Settlements and Camps
N
Scale
Kilometers

Figure 4

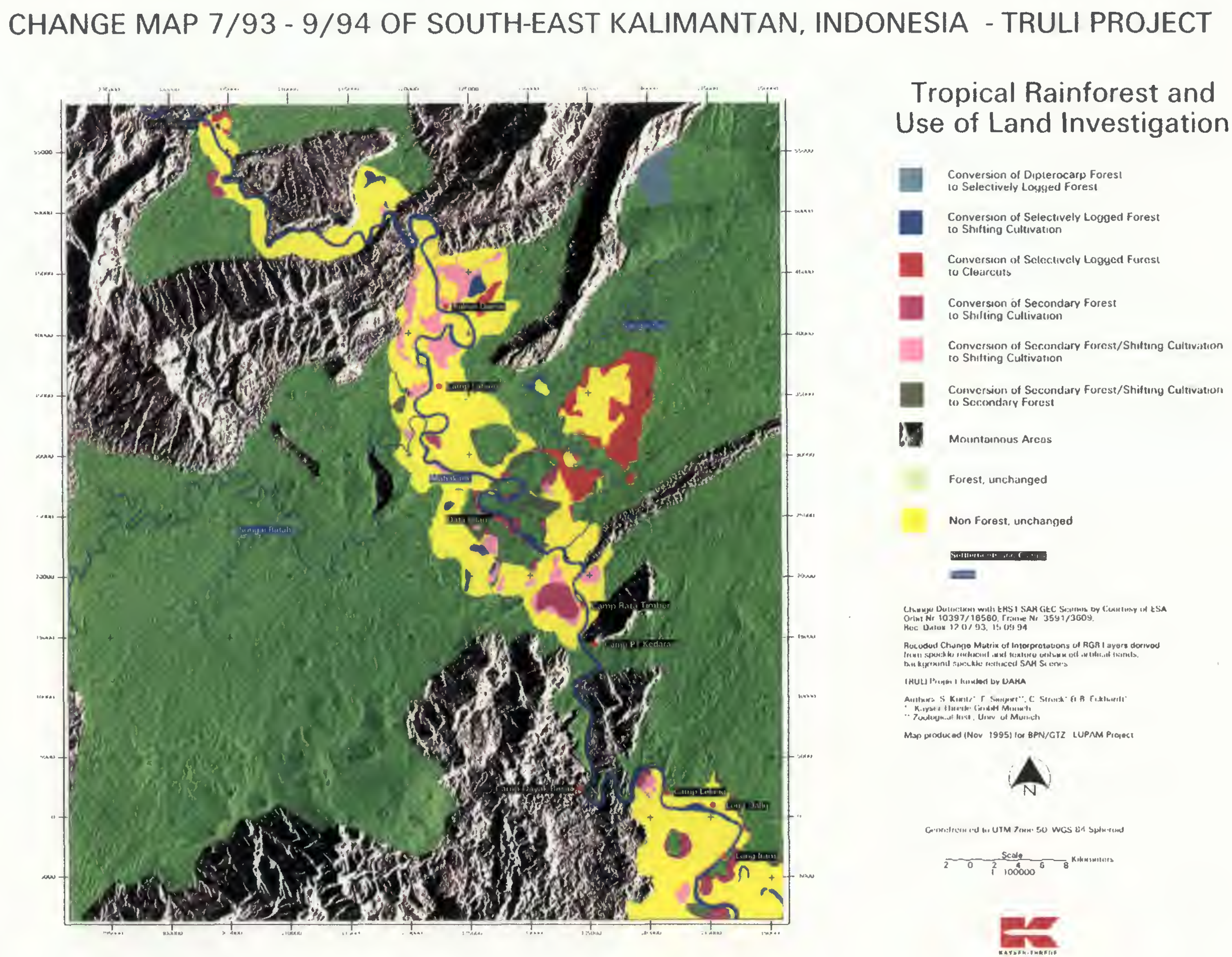
CHANGE MAP 7/93 - 9/94 OF SOUTH-EAST KALIMANTAN, INDONESIA - TRULI PROJECT
Tropical Rainforest and Use of Land Investigation
Conversion of Dipterocarp Forest to Selectively Logged Forest
Conversion of Selectively Logged Forest to Shifting Cultivation
Conversion of Selectively Logged Forest to Clearcuts
Conversion of Secondary Forest to Shifting Cultivation
Conversion of Secondary Forest/Shifting Cultivation to Shifting Cultivation
Conversion of Secondary Forest/Shifting Cultivation to Secondary Forest
Mountainous Areas
Forest, unchanged
Non Forest, unchanged
Change Detection with ERS1 SAR GEC Scenes by Courtesy of ESA
Orbit Nr 10397/16560, Frame Nr 3591/3609,
Rec. Dates 12 07 93, 15 09 94
Recoded Change Matrix of Interpretations of RGB Layers derived from speckle reduced and texture enhanced artifical bands, background speckle reduced SAR Scenes
TRULI Project funded by DARA
Map produced (Nov 1995) for BPN/GTZ LUPAM Project
N
Georeferenced to UTM Zone 50 WGS 84 Spheroid
Scale
2 0 2 4 6 8 Kilometers
1 100000

Figure 5

control points. Aerial photographs and videos from that flight served as a reference to control our classification results.

We found that all major land use classes and forest types were classified correctly in the multitemporal time series of processed ERS-1 images. Under the very difficult terrain conditions of the test site it was nearly impossible to quantitatively verify area estimates. However, we were able to compare the maps of a private timber concession (showing plans for the conversion of rainforest into plantation) with the results of our change detection analysis. Here, we found more than 90% accuracy. This is also true for selective logging. Shifting cultivation (with irregular patterns of different fields and succession phases) can only be detected using the principal components of the multitemporal texture features. Rice fields below a size of 3-5 ha cannot be detected reliably.

As a final test of our method we attempted a classification of an area which was unknown for us and from which no optical satellite data was available. During the second field trip this area - covering approximately 1,000 km^2 - was visited on ground and by helicopter. We found, that all landuse classes caracterised above were interpreted correctly with one exemption: A fifteen year old secondary forest was confused with primary forest. On ground it is very evident that this forest was overexploited by selective logging in the past (indicated by species composition). However, from space or even from the helicopter this discrimination is very difficult to accomplish, since the canopy roughness ressembles that of a primary forest.

5. SIGNATURE ANALYSIS

From many studies on various targets it was demonstrated that multitemporal ERS-data offer a much higher information content than single scenes. However, the „classical" approach, combining simply three speckle reduced images in a RGB-coded image, was not very satisfying for our investigation. We found, that the combination of various texture filters and the application of the principal component transform in combination with other computed bands resulted in much higher information content. The reliablility of our approach could also be verified by a detailed signature analysis of the texture features.

Calibrated 8 bit data (in grey values) served as input for the visual interpretation and delineation. Therefor mono- and multitemporal signatures for the 8 bit calibrated raw images and the variance filtered 15 x 15 and 31 x 31 images, respectively, have been evaluated. The monotemporal analysis comprised investigations for spatial stability of the targets and the suitability of the applied filters for the target discrimination.

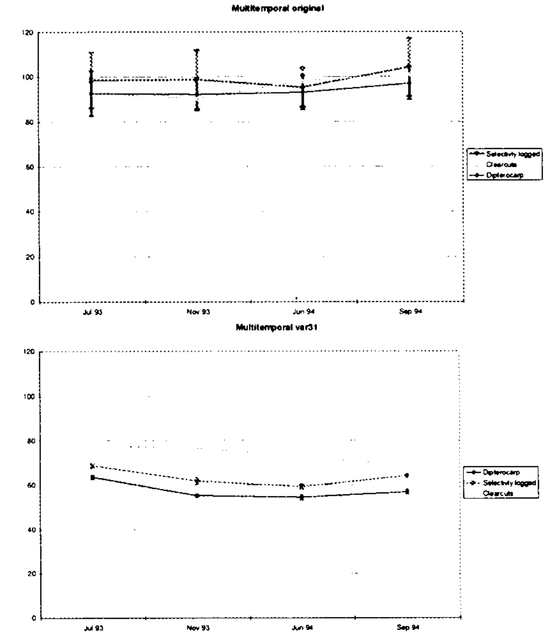

Figure 6: Comparison of signatures of speckle reduced ERS-1 data (mean and standard deviation of 3 different targets for 4 dates; resampled to 8-Bit) on the top, with the respective texture features derived from the variance filtered (31 x 31) image (bottom; from: Fuchs et al., 1995).

The upper diagram in **Figure 6** shows the mean intensities and standard deviations in greyvalues (8 bit) for three multitemporal signatures in the speckle filtered image. One can clearly recognize that the differences of the mean amplitude of the classes are overlayed by the standard deviations. Therefore it is not possible to distinguish these basic signatures in the unenhanced images either by visual or by simple computer aided classification means. The tonal differences (greyvalues) of the different classes are hidden by the high frequency spatial variation within the target area. However, the standard deviations themselves are different for the three classes. The lower diagram of **Figure 6** shows the multitemporal statistics derived from the variance 31x31 filtered multitemporal images. Here a clear discrimination of the three classes is possible (Fuchs et al., 1995). These results do also emphasize the applicability of our approach, demonstrating the importance of texture features to enhance the hidden information in ERS-1 data for interpretation and classification.

6. DISCUSSION

The results achieved so far were beyond our first expectations. In flat areas texture features allowed to discriminate 1) undisturbed forest of at least two different types, 2) shifting cultivation and agriculture, 3) secondary forest, 4) selectively logged forest, 5) clearings by fire and clearcutting and 6) settlements and major roads. Preliminary results of a multitemporal data analysis showed that changes in area of classes no. 2), 4), 5) respectively can readily be detected in image sequences only 6 months apart.

The interpretation of the processed ERS-1 images needs a skilled interpreter. Basic knowledge about the ecology, sociology and economic activities must be available in advance to obtain good interpretation results. In principle, this knowledge exists at different Indonesian authorities, like the forestry department or the land use planning board. The results of the interpretation process can be improved significantly using a multitemporal approach.

The monitoring system gets even more precise, if already existing official planning information (e.g. from maps showing active concession areas, transmigrasi settlements etc.) are available during the interpretation process (e.g. within a GIS). With such an approach we were able to identify even small areas of undisturbed rainforest in our ERS-data, which could not be identified by the spaceborne data alone. If it is known in advance, even from coarse maps (which normally are available to the institutions in charge of planning and control) where and when forest concessions are operating, it is even possible to monitor the intensity of the selective logging operation.

The technology transfer to Indonesia at the end of the TRULI project (September 1995) was very successful. A one week workshop for Indonesian key personnel at BPN, the National Land Planning Agency was held in Jakarta. 7 local remote sensing experts were trained intensively in the use of ERS image interpretation on their own equipment. Several planning authorities explained their definite interest in a further application of ERS-1 radar for rainforest monitoring and land use planning.

7. RECOMMENDATIONS

The field experience showed, that there is a significant lack of knowledge about the current situation in large parts of Borneo and that more precise and currant information is urgently needed by local officials. Due to the fast dynamics of economic development, the Indonesian rainforests are highly endangered by overexploitation and conversion to agricultural use. Many areas are developped without any rational planning or efficient control. Landsat images are not suitable for these purposes, since cloud free images are available only every 3-6 years for a certain area. In some regions there exist not even a single cloud-free Landsat image.

As the TRULI-project could demonstrate ERS-1 radar images can fill this gap. The most important advantage of ERS-1 and its successor ERS-2, compared to optical remote sensing systems, is their all weather capability. This opens up the possibility to receive a set of new images of e.g. the whole island of Kalimantan every month which allows to analyse series of 20 or more images acquired at successive time points over a certain area. This stabilises ERS-SAR signatures by averaging and furthermore allows detailed change detection analysis. Even with the lower resolution and the reduced information content (compared to high resolution optical data) ERS images can provide information about areas, where only little is known *on a regular basis*. This information is urgently needed by local experts and officials.

In the framework of a multistage monitoring system ERS-SAR data can be used for basic mapping and planning purposes. Areas of interest defined in SAR-images, can be examined in more detail using conventional survey methodology, like high resolution optical data from space, aerial photography, ground survey etc. Such a procedure would allow to reduce time and money for survey, looking only on regions where unwanted changes could be detected. Under these circumstances ERS-SAR images can provide essential information for forest monitoring and land use assessment in the most endangered and inaccessible regions of the world.

8. REFERENCES

De Beer J.H. & Mcdermot M.J., (1989). the economic value of non-timber forest products in south-east Asia. Netherlands Committee for IUCN, Amsterdam.

Fuchs, U., Streck, C., W. Bergbauer and S. Kuntz (1995): Investigations on Multitemporal Backscatter Characteristics and Applied Filters for Deforestation in Tropical Rainforests. Symposium Proceedings of the International Symposium on the Retrieval of Bio- and Geopyssical Parameters from SAR data for Land Applications, Toulouse, 10-13.10.1995.

Goldammer J.G. & Crutzen P.J. (1993). The ecological, atmospheric and climatic importance of vegetation fires. Dahlem Conference ES 13, john Wiley & Sons, Chichester.

Kattenborn, G., Nezry, E., De Grandi, G. & Sieber, A.J. (1993): High resolution Detection and Monitoring of changes using ERS-1 time series, Proc., 2nd ERS-1 Symp., 11-14 Oct. 1993, Hamburg, pp. 635-642.

Keil, M., Scales, D. & Winter, R. (1994): Tropical Rainforest Investigation in Brazil Using Multitemporal ERS-1 SAR Data, Paper pres. at the First ERS1-Pilot Project Workshop 22.-24. June 1994, Toledo, Spain.

Kuntz, S., Siegert, F. & Fritz, F. (1994a): Tropical Rainforest and Use of Land Investigation (TRULI), 1. Progress Report, Kayser-Threde GmbH, München.

Kuntz, S. & Siegert, F. (1994b): Evaluation of ERS-1 SAR Data for Forest Monitoring in Indonesia, Paper pres. at the First ERS1-Pilot Project Workshop 22.-24. June 1994, Toledo, Spain.

Kuntz, S. & Siegert, F. (1994c): Evaluation of ERS-1 SAR data for Tropical rainforest Monitoring, Earth Observation Quarterly, No. 45, Sept. 1994, ESA.

Kuntz, S. & Siegert, F. (1994d): Dipterocarp Forest Mapping and Monitoring by Satellite Data - A Case Study from East Kalimantan, in: Dipterocarp Forest Ecosystems - Ecology, Sustainable Management and Products, Indonesian-German Forestry Project, Faculty of Forestry / Mulawarman Univ., Samarinda, in press.

Leysen, M., Conway. J.A. & Sieber, A. (1993): Evaluating Multi-temporal ERS-1 data for Tropical Forest Mapping: Regional Mapping and Change Detection Applications. in: Proc., 2nd ERS-1 Symp., 11-14 Oct. 1993, Hamburg, pp.

Myers N. (1984). The primary source. Tropical forests and our future. W.W. Norton & Company, New York, London.

Peters C.M., Gentry A.H. & Mendelsohn R.O. (1989). Valuation of an Amazonian rainforest. Nature 339, 655-666.

Siegert, F., Kuntz, S. Claudia Streck, & Wolfgang Bergbauer: Land Use Planning and Monitoring in Indonesia using ERS-1 RADAR (SAR) Data. In: Proc. Int. Conf. on Remote Sensing and GIS for Environmental Resources Management- The Indonesian- European Experience, Jakarta, Indonesia, June 6-8, 1995.

Whitmore T.C., (1984). Tropical rain forests of the far east. Clarendon Press, Oxford.

CENTRAL AFRICA MOSAIC PROJECT: USING ERS-1 SAR DATA AT A CONTINENTAL SCALE

J.P. Malingreau, F. De Grandi, M. Leysen, E. Nezry
EC JRC Institute for Remote Sensing Applications
2120 ISPRA (VA) ITALY
Phone: 39 332 789823 Fax: 39 332 789073

ABSTRACT

The Central Africa Mosaic project is an attempt to bring spaceborne SAR data in an entirely new perspective, in the context of tropical forest monitoring. This objective represents a drastic change in the use of radar data, as it seeks to bring high resolution SAR data from the role of gap-filler and local hot spot analysis to the role of global mapping at a semi-continental scale. The project is carried out in the Monitoring of the Tropical Vegetation Unit of the Institute for Remote Sensing Applications at Ispra. It relies on SAR data acquired by the ESA ERS-1 satellite over the Central Africa basin, and processed by the German PAF in the Libreville station. This paper summarizes the major scientific and engineering issues of the project. Preliminary thematic results based on visual interpretation are reported.

At this stage of the project, it can be already concluded that the material provided by the ERS-1 Central Africa Mosaic constitutes a unique source of data on vegetation distribution at continental scale. The most celebrated "all weather" characteristic of active microwave sensing has taken its full meaning in the present case since a whole equatorial region has been covered on demand and in a minimum amount of time, and since a significant level of information on forest conditions has rapidly been extracted. This places the ERS-1 SAR approach firmly in a useful position in the set of instruments to be further exploited for tropical forest monitoring.

1. BACKGROUND and OBJECTIVES

The goal of this activity was to study the information content of a large set of SAR images systematically covering a whole biogeographical domain of Central Africa. This broad scope exploration was intended to concretely assess the possibility of extending to continental and, eventually, global scales the results of ERS-1 investigations which have so far been validated on smaller scales only. The investigation was thus carried out in full compliance with one of the joint JRC ESA TREES (Tropical Ecosystem Environment Observations by Satellites) Project objectives, which is to explore the role of new spaceborne earth observation instruments for global tropical forest monitoring [Mali, 94]. The extrapolation of single site studies to large area analysis is not straightforward and a series of specific issues was systematically explored during the course of the present work:

- large area coverage cannot be instantaneously obtained using an instrument with a narrow field of view and during an acquisition period (in the present case roughly 2 months) spatio-temporal variations inevitably occur across the area. Ways to identify them and take them into account in the mosaicking were developed.
- the SAR sensor is tailored to high resolution studies (30 meters); the passage to a continental and a fortiori global coverage requires a careful assessment of spatial sampling which takes into account signal to noise ratio, typical size of target features and data volume (important in view of an operational system). Given the lack of experience in this domain a mosaicking system tunable to various experimental resolutions was designed.
- multiple and blanket acquisitions over large geographical areas are not yet common; the possibility of using temporal variations in vegetation characteristics are thus limited and single-date image characteristics have to be more fully exploited (e.g. using filters working on second order statistics [Nezr 95]).
- the analysis of such a large number of images containing a broad variety of features and land cover conditions necessitates the development of an adequate methodology which can only be developed in phases. The first phase is per force one of exploration and identification of major image characteristics with respect to known ground vegetation characteristics. This first step is the one reported upon in the present paper.

2. THE MOSAIC ENVIRONMENT

The ERS-SAR mosaic of Central Africa contains 477 scenes from orbit 15674 to orbit 16306. Only the descending orbits have been processed. The data have been acquired during the period from July 15 to August 28, 1994. The data base contains 58 Gbyte of high resolution data and 1 Gbyte of low resolution data. All frames have been acquired by a mobile station installed at Libreville (Gabon) and processed by the German PAF.

Proceedings of the Second ERS Applications Workshop, London, UK, 6–8 December 1995 (ESA SP-383, February 1996)

The mosaic covers the whole tropical rain forest domain of Central Africa as well as the northern and southern transition zones (see Fig. 1). It contains parts of Cameroon, Nigeria, Gabon, Guinea Bissau, Republique Centr'Africaine, Congo Brazzaville, Zaire, Rwanda and Burundi. The territory covered by the mosaic is of more than 3,000,000 square km and, apart from Gabon and the eastern part of Zaire the terrain has little relief and is little dissected.

The ERS-1 data set constitutes the baseline of an information reservoir, around which a whole processing environment has been designed, in order to support the wall to wall thematic interpretation, which is at the moment linked, but not restricted, to the tropical forest mapping objectives of TREES.

FIGURE 1. Central Africa ERS-1 coverage

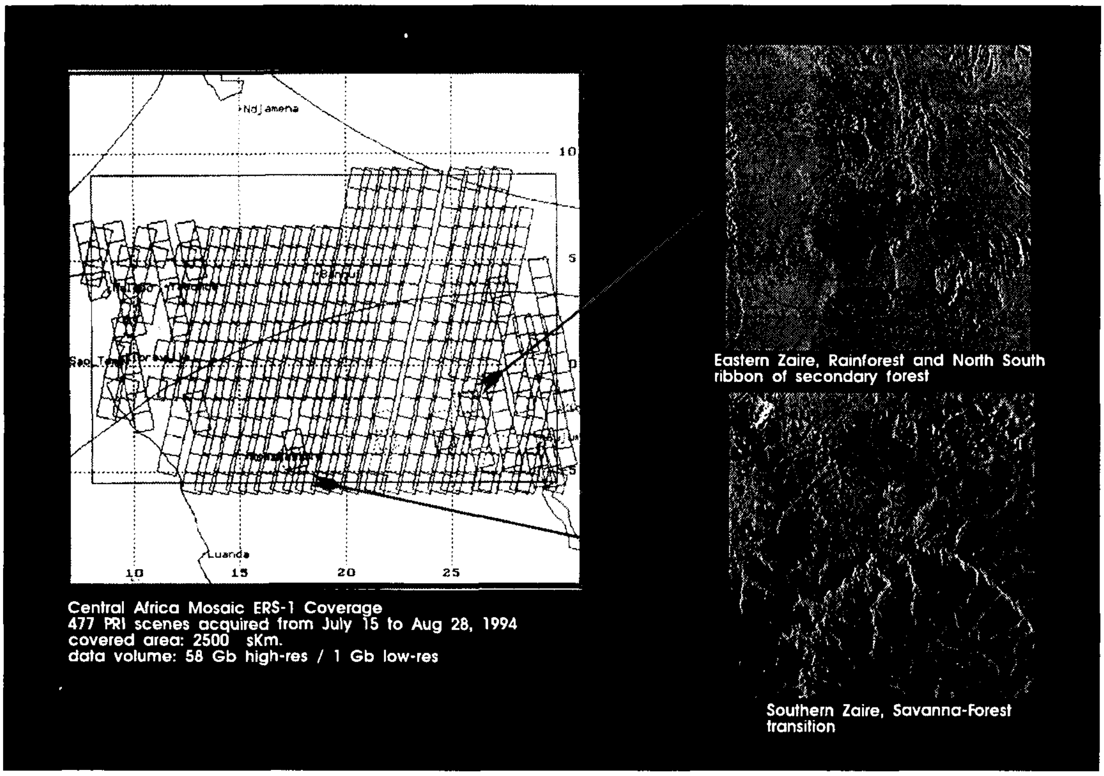

nal processing (such as speckle filtering) from the original PRI data. The whole information content of the original ERS data set is therefore conserved and also augmented as the mosaic machine evolves during the analysis and interpretation phase.

This concept can also be pushed one step further, and include other sensors' data among the information hierarchy. Indeed the IRSA MTV is preparing a software prototype where the ERS-1 mosaic baseline product, which is composed of the 100m compressed and cartographically projected ERS images, constitutes the reference to spatially query a database containing GIS data, AVHRR and TM products.

The mosaic environment is also an open environment, where new "engines" can be created to generate higher level data products, such as forest classification maps.

This processing environment rests on two fundamental principles: multi-resolution pyramidal information structure, and processing on demand.

Multiresolution information means that the whole collated coverage of the Central Africa basin is produced only at an optimal spatial resolution (100 m), with respect to visual interpretability and data volume. This baseline product can be considered as a reference gridding, where the user can navigate, zoom in at each point and access higher resolution products. These products are generated on request, and according to the specific needs of the thematic analysis. Typically they can be high resolution SAR data, which are generated after some sig-

Work is in progress in the IRSA MTV unit in this direction. In particular a signal processing technique which is under investigation is a multi-resolution decomposition based on wavelet theory. This technique seems to match very well with the intrinsic requirements of spatial multiresolution of the CAMP environment, but also extracts at the same time in the high spatial frequency domain information which is amenable to the implementation of texture classifiers.

A special purpose software machine has been implemented to support the CAMP processing, and is briefly described in the next section.

3. THE MOSAIC MACHINE

The mosaic software machine entails a number of data bases, that store data at various levels and keep threads among processing phases and house-keeping information.

The original PRI ERS data are processed in batches starting from the Exabyte media. They are calibrated for the effective scattering area according to the range incidence angle, and compressed to 100m pixel spacing using a FIR spatial filter.

FIGURE 2.The mosaic software machine

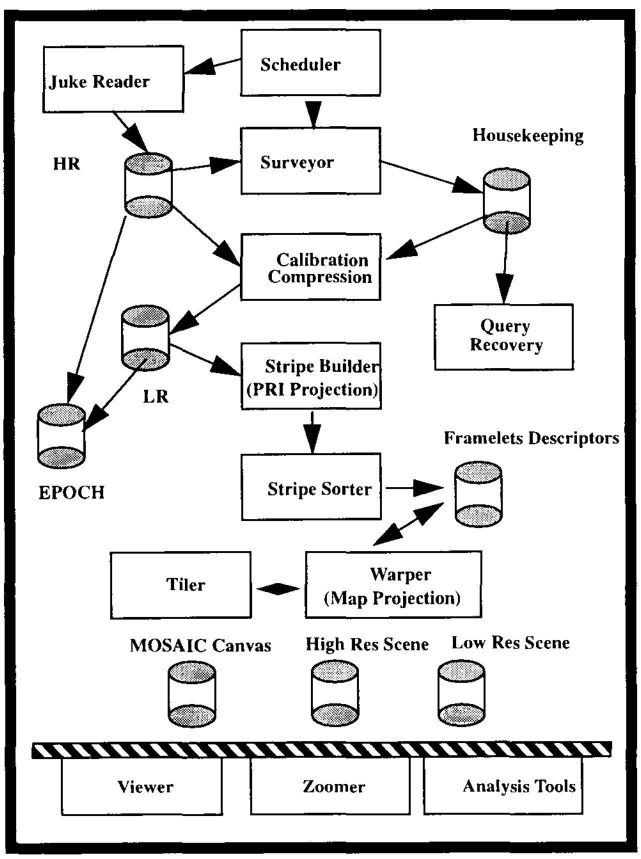

The PRI data are stored in the High Resolution (HR) database, which is physically allocated to a WORM disk archival system. In the same database other high resolution products, such as GMAP speckle filtered data sets, which are generated on demand, are stored. Also ancillary information is extracted at this stage form the ERS SAR leader file, such as the positions of the corner points of the image in cartographic coordinates.

It has to be noted in general that all the databases in the mosaic software environment are implemented using a simple but effective technique that consists of splitting the units of information (typically a SAR image) into a data item and a descriptor. Both are kept into standard Unix files. The coupling between the two is established by a file naming convention.

Synchronization of operations and databases is assured in this batch phase by the two modules Scheduler and Surveyor. At any moment exception handling is possible, with backtracking and restarting of the system in case of failures (network, or workstations).

The compressed SAR data, called framelets, are then stored in a second database, the LR (Low Resolution) database. This constitutes the foundation in terms of data sets, both for the thematic visual interpretation, and for the assembling of the mosaic canvas.

The framelets composition starts with the selection of all frames that belong to a stripe; a stripe is defined as a continuous set of frames, having overlaps in latitude, and corresponds to acquisitions done during one orbit of the satellite.

Each set belonging to a stripe is assembled using a coarse registration based on the image corner points and a fine registration using a cross correlation algorithm in the overlap area. Also radiometric balancing between framelets is performed when necessary. Actually due to the stability of the sensor the radiometry is quite stable over the period of acquisition of the whole mosaic. Nonetheless, in some exceptional circumstances, the down-linked signal is lost by the receiving station (DLR Libreville) and therefore the processing has to switch from acquired parameters to nominal parameters. This introduces anomalous "jumps" in the signal dynamic range between frames, which needs to be corrected.

The stripes are therefore generated in the SAR image reference frame (PRI ground range projected with no relief correction). Stripes are subsequently sorted in longitude, warped to a cartographic reference frame (GEM6) using a second degree polynomial fitting of all the corner point coordinates in the stripe, and pasted with a simple left right overlap algorithm into an incrementally growing canvas.

At several stages of the processing chain, graphical interactive tools allow the user to visualize the status of the processing, (such as synoptic maps of the processed stripes or framelets). Finally the "MosaicViewer", a visualization tool, can be used to roam spatially through the mosaic products at any level (HR, LR and final canvas) and to take advantage of the links between products to focus on special areas of interest.

The whole mosaic machine software was developed using a combination of C code and IDL programming environment.

4. PRELIMINARY THEMATIC RESULTS USING ERS DATA

The Africa Mosaic (CAMP) reveals a series of features which are of most relevance in the framework of the TREES project objectives. The preliminary results are also of high interest for global vegetation monitoring, a major objective of the International Global Change Research Program (IGPB). The mosaic represents, indeed, a unique and uniform cross section of important tropical biomes from the savannah and dry forest in the north, through the entire rain forest domain and again through seasonal formations south of the equator (savannah and edge of the Miombo Woodland). The design of this Central Africa mosaic is such that, since it crosses the equator it contains at the same time dry and rainy season acquisitions with a gradient of wetness in between.This allows a range of observations to be made with respect to the occurrence or to the lack of seasonal contrasts between various vegetation formations. The scale, resolution and bio-windows offered by the 1994 Central Africa Mosaic qualifies it as a truly global product, which satisfies a series of important conditions related to vegetation monitoring.

A few items of information derived from the visual analysis of the 100m pixel spacing products generated by the above described processing chain are presented here [Mali 95].

- the boundary between the rain forest - or in this case, more likely, a mix of evergreen/semi-deciduous mesophyllous forest formations - and the mixed seasonal - savannah formations to the south is extremely well marked (Fig. 3). This being a dry season acquisition in the south (July-August) the contrast between the evergreen cover and the more deciduous (trees) or senescent (grass) cover is well detected using the microwave approach.
- the boundary between the rain forest and the mixed savannah - gallery forest formations is also well marked in the northern parts of the Congo basin examined so far (Fig. 4); this is rather surprising since acquisitions have been obtained in the middle of the northern rainy season (July-August).
- deforestation fronts, a major focus of interest in the TREES approach, are not frequent in the Central Congo Basin. Yet one example in Southern Zaire (Fig. 5) shows features associated with the dynamics of those fronts in an unmistakable manner.
- unexpectedly, the ribbon of secondary formations following the older road network of Zaire is visible in the SAR microwave return signal by contrast with the surrounding primary forest (Fig. 6). These forest "galleries", correspond to the pattern of land management which since colonial time has essentially followed the road communication system.
- in the rain forest domain itself the range of visible features is somewhat limited. This maybe due to compounded reasons. Lack of recent deforestation activities, diffuse patterns of agricultural expansion or the inability to separate primary forest and older secondary regrowth with no clear geometrical patterns, are possible explanations. Texture analysis could lead to a better discrimination of deforestation features in the forest canopy.
- data over selected areas taken at one month interval are available for a few overlapping stripes. They reveal change patterns related to the impact of fires on the herbaceous vegetation cover. Burn scares are readily visible in the southern and eastern savanna at the fringe of the Central Congo Basin [Mali 1995].

The results of this preliminary and still partial investigation are encouraging on several grounds:

- at first they indicate that, contrary to what is commonly expected, the ERS-1 SAR coverage may represent a unique source of data on vegetation at continental and global scales. The assemblage of more than 400 images foreseen in the Central Africa Mosaic tells us a lot about this very new perspective on SAR coverage.
- second, the mosaic is helping to formulate a more relevant research agenda in view of operational tropical forest monitoring.
- third, while the processing of such a large amount of data and their assembling into a mosaic needs major investments in terms of expertise and equipments, it appears possible to establish operational processing chains which can feed the analysts with highly usable products. The global coverage aspects of the exercise is therefore further reinforced by the advances made in the streamlining of all the necessary operations.

5. CONCLUSIONS

Processing of the Central Africa Mosaic has been completed, and the mosaic canvas containing the ensemble of the ERS images at 100m resolution and in cartographic projection will now be composed together with annotations and vector GIS information retrieved from the IRSA MTV databases on Central Africa into a photographic quality hard copy product.

Meanwhile the visual interpretation and analysis of the data set is proceeding exhaustively, and other promising research avenues are explored. For instance simple change detection algorithms over the overlay areas have already revealed very important features. On another

FIGURE 3.

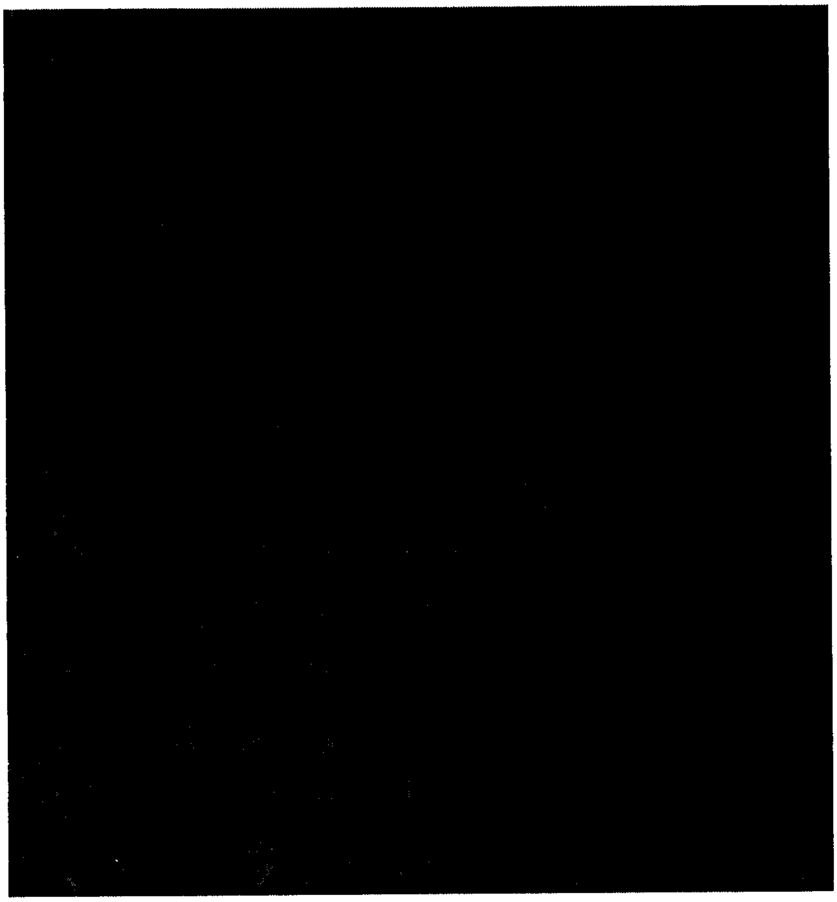

FIGURE 4.

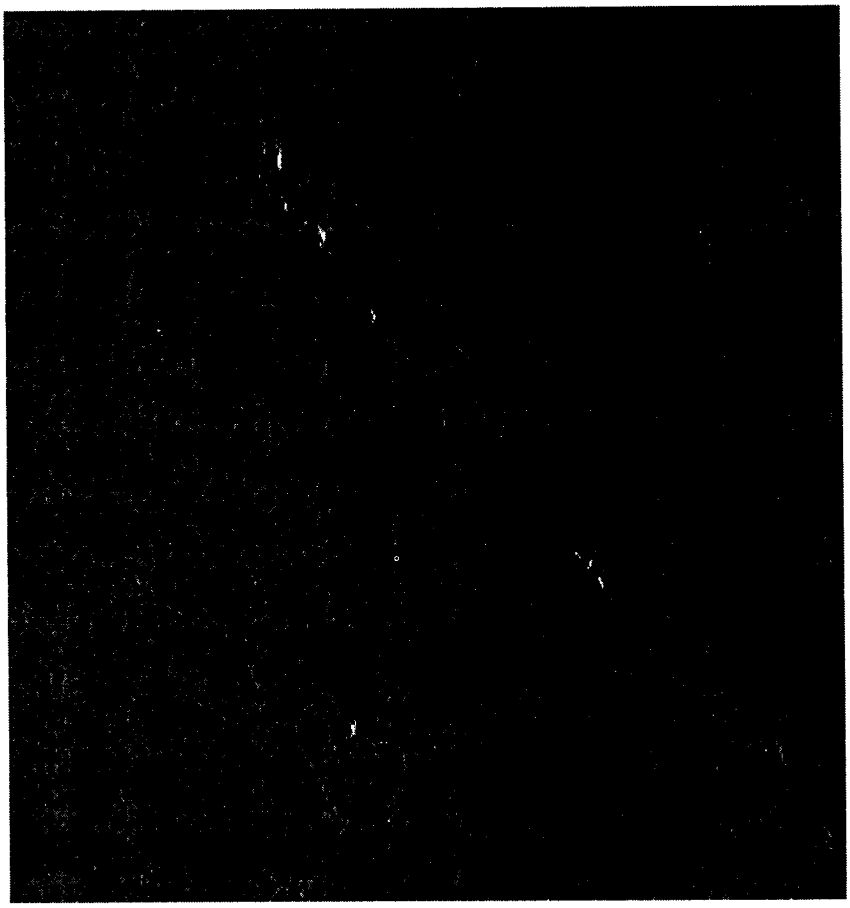

FIGURE 5.

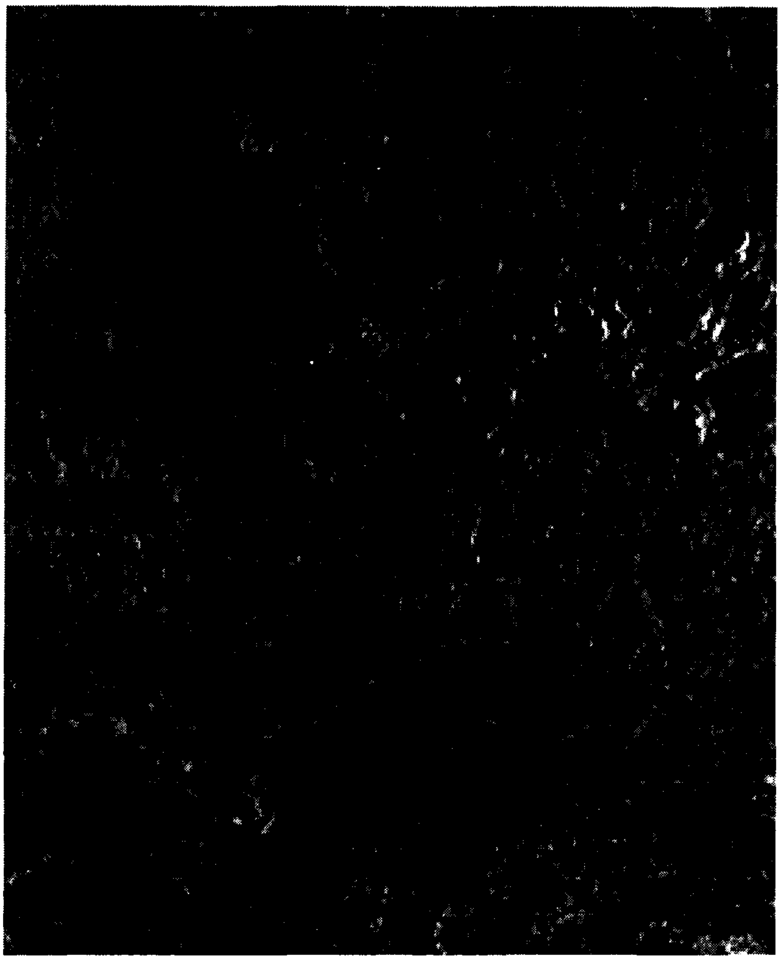

FIGURE 6.

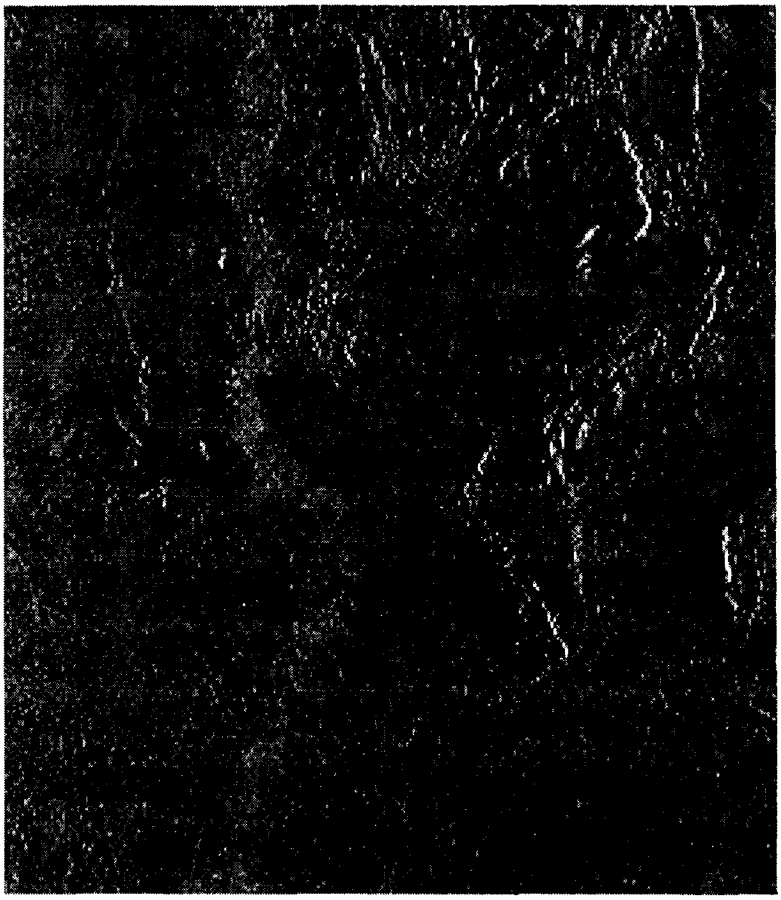

side, the investigation of automatic analysis and thematic information retrieval algorithms has started in cooperation with other R/D Institutions.

At this stage of the project, we can already conclude that the material provided by this ERS-1 Central Africa Mosaic constitutes a unique source of data on vegetation distribution at continental scale. The most celebrated "all weather" characteristic of active microwave sensing has taken its full meaning in the present case since a whole equatorial region has been covered on demand and in a minimum amount of time, and since a significant level of information on forest conditions has rapidly been extracted. This places the ERS-1 SAR approach firmly in a useful position in the set of instruments to be further exploited for tropical forest monitoring. As already indicated the same material also provides a precious starting point for the elaboration of an application oriented research agenda which will further improve our capability to monitor the earth's environment.

6. ACKNOWLEDGEMENTS

H. De Groof of the IRSA AIS unit is thanked for his contribution in the preliminary design phase of the Central Africa Mosaic project (CAMP). We would also like to acknowledge the highly professional work of the CAMP software development team, G. Perna, (AIS Studio Associato, Milan Italy) and E. Franchino (CISI, Milan, Italy); all the IRSA MTV technical staff members, who contributed directly or indirectly to the CAMP project. P. Mayaux (DaVinci, Belgium) who prepared the GIS overlays and annotations. The impressive technical contribution of the DLR (Germany) and ESA for the SAR raw data acquisition and processing, which are the foundation over which the CAMP project could be built, is acknowledged.

7. REFERENCES

[Degr 95] G. De Grandi, M. Leysen, E. Nezry, A. Bresesti, F. Amar, A. Fung, "Wave Scattering Modeling of a Natural Target under Time Evolution: a Test Case", *Proc. IEEE IGARSS '95 Florence Italy.*

[Lebr 54] J. Lebrun, G. Gilbert, "Une classification ecologique des forets du Congo", *Publications de l'INEAC, Serie scientifique,* no. 63, 1954.

[Mali 94] J.P. Malingreau, J. Aschbacher, F. Achard, J. Conway, F. De Grandi, M. Leysen, "TREES ERS-1 Study 94: Assessment of the usefulness and relevance of ERS-1 for TREES", *Proc. of the First ERS-1 Pilot Project Workshop,* Toledo, Spain, June 1994.

[Mali 95] J.P. Malingreau, M. Leysen, G. De Grandi, 'Burn Scars in Tropical Vegetation Identified by ERS-1 SAR Data', *IGBP-DIS 2nd Workshop on Global Fire Monitoring,* Ispra Italy Oct 17-19, 1995.

[Nezr 95] E. Nezry, M. Leysen, G. De Grandi, 'SAR Speckle and Scene Spatial Statistics Estimators for Image Filtering and Classification', *Proc. IEEE IGARSS '95,* Florence Italy.

APPLICATION OF ERS-1 SAR -DATA IN LARGE AREA FOREST INVENTORY

Erkki Tomppo, Petri Mikkelä, Ari Veijanen, Kai Mäkisara, Helena Henttonen, Matti Katila[1], Jouni Pulliainen, Martti Hallikainen, Juha Hyyppä[2]

[1] *Finnish Forest Research Institute, Helsinki, Finland*
Tel: +358-0-85705340. Fax: +358-0-625308
[2] *Helsinki University of Technology, Laboratory of Space Technology Espoo, Finland.*
Tel: +358-0-4512378. Fax: +358-0-460224

ABSTRACT

The main objectives of the study are to test the applicability of ERS-1 SAR images in estimating forest resources of large areas (e.g., at sub-national, national, or larger level), and to develop an operative forest inventory system which utilises SAR data. The SAR data is used together with other information sources. Six test areas, three in Finland and one in Canada, one in China and one in Russia have been selected for the study. So far, only images from Finnish test sites have been analysed.

The results from this study show that the backscattering properties of boreal forests are affected heavily by seasonal changes as well as weather conditions before and during image acquisition (moisture in needles and soil). This phenomenon can be utilised by using multi-temporal images. A new promising inversion method for estimating volume of growing stock has been developed. It uses a semi-empirical backscattering model, multi-temporal images, and estimated soil and needle moisture.

The field plots with regeneration cuttings (clear-cuttings) can be identified reasonably well with a regression model. This can be utilised in updating of field data by means of growth models and cutting statistics.

1. INTRODUCTION

The total land area of Finland is 30.5 million hectares and the forestry land area is 26.4 million hectares, of which 20.1 million hectares is classified as productive forest land (the mean annual increment is at least 1 m^3/ha). The total growing stock is 1 900 million m^3 and the annual increment is 80 million m^3. Private persons own 63 % of the forest area, the state 24 %, and companies 9 %, the rest belonging to municipalities, parishes etc. The turnover of the Finnish forest industry is 10 500 million ECU (1994) and the value of export 9 000 million ECU, corresponding to 50 % of the net income from foreign trade.

The National Forest Inventory of Finland (NFI) has produced large-area forest resource information for over 70 years for management planning of Finnish forestry and forest industries. In addition to ground measurements, the current operational system uses satellite image data (Landsat TM) and digital map data (e.g., arable land, built areas, roads, digital elevation model when applicable). The most serious problem in the current method is that clouds often prevent obtaining satellite images from the same growing season when the ground measurements have been made.

The Laboratory of Space Technology at the Helsinki University of Technology has developed a helicopter-borne scatterometer (HUTSCAT) (Hallikainen et al. 1993). It is a dual-frequency (5.4 and 9.8 GHz) FM-CW, internally and externally calibrated radar designed for co- and cross-polarised backscattering measurements of natural targets, such as forests. Due to the ranging capability, the HUTSCAT can probe the canopy from the top to the bottom with a range resolution of 65 cm (Hyyppä 1993).

The feasibility of the HUTSCAT in estimation of the stand characteristics of sample plots was evaluated in an earlier study (Hyyppä 1993). It was shown that the mean square error of radar-derived mean and dominant tree heights estimates compared to field-measured ones was 1.3 metres and the error of the volume estimates at stand level correspondingly 31.3 m^3/ha (20 %). HUTSCAT measurements have also been used in deriving a semi-empirical forest backscattering model (Pulliainen et al. 1994).

2. OBJECTIVES OF THE STUDY

The objective of the study is to develop methods for utilising ERS-1 SAR images in large area forest inventories, such as national forest inventories. The emphasis is thus in *large scale estimates of forest parameters*. Use of the HUTSCAT -instrument in practical forest inventory is also studied. A cost-benefit analysis of the method will be an essential part of the project.

3. MATERIAL

3.1.Test sites

Six different test areas (listed in Table 1) representing mainly boreal or sub-boreal forests have been chosen for the study. The size of each site is 100 km × 100 km.

There have been difficulties in collecting all the necessary data sets, e.g. DEM, for some of test sites. Therefore, research has been carried out mainly at the Porvoo site. In addition, a Sodankylä test site in Northern Finland from

Proceedings of the Second ERS Applications Workshop, London, UK, 6–8 December 1995 (ESA SP-383, February 1996)

another project has been utilised. Other sites will be analysed later.

Table 1. The six test sites of the study.

Name	Country	Latitude	Longitude
Porvoo	Finland	60° 45"	25° 30"
Teijo	Finland	60° 10"	23° 00"
Inari	Finland	69° 40"	27° 30"
Sortavala	Russia	61° 50"	31° 00"
Hebei	China	48° 50"	130° 10"
Whitecourt	Canada	54° 25"	244° 20"

3.2 Field measurements

The NFI sample plots are used as ground truth data and, to some extent, as reference data, too. The plots used in this study were established and measured in 1986. The plots are located in L-shaped clusters, the distance between clusters being 8 km in the north-south direction and 7 km in the east-west direction. One cluster consists of 21 Bitterlich-type sample plots (relascope factor 2) with an interval of 200 m.

The sample plots located at least 30 m from the nearest stand boundary were re-measured for the study in summer and autumn 1993. The total number of these plots was 444. The plots were geolocated with GPS. Tree species, breast height diameter, crown storey, and tree quality class were measured from tally trees. Each 7th tally tree was measured as sample tree, measurements involving increments, bucking, damages, etc. The usual stand characteristics were measured from the surrounding forest stands.

Stand level inventory data measured for operative forest management planning were utilised in reliability assessments. These data are based on visual ground estimation with relascope measurements and information from false colour aerial photographs.

Stand level data were collected for three different blocks, 119 and 393 ha of spruce dominated forest and 142 ha pine dominated forest. The mean stem volumes were 121, 153, and 126 m^3/ha, respectively, and the total number of stands was 358 in eight forest holdings. Field checks of stand data were carried out in 1992 and 1993.

For justifying the results at a medium size area level, summary results of stand level inventories were available from 8 areas of sizes 560 to 6300 hectares. The mean volume of growing stock varies by areas from 123 to 160 m^3/ha.

3.3. Radar data

ERS-1 SAR.PRI -images from the summer and autumn 1993 and winter and autumn 1994 have been received, rectified and processed. The total number of images used in the study was 25.

A program called VIP (made by VTT Automation in Finland) was used for geometrical rectification of the ERS-1 images. It uses as input a digital elevation model (DEM) (pixel size 25 m, resolution 0.1 m), an ERS-1 SAR.PRI image, and optionally a digital map for ground control point collection. The output consists of three image channels: the rectified image data, the ground area per pixel, and the the local incidence angle. The output pixel size used in this study was 25 metres.

HUTSCAT measurement have been conducted along NFI sample plot lines in late summer 1994. The predefined survey lines have be flown using a GPS receiver for navigation.

3.4. Ancillary data

Digital map data are applied to separate forestry land from other land use classes. The applied themes are arable land, roads, and other built areas. Water areas are extracted from Landsat TM images.

The ground reference data also includes the meteorological statistics including the daily precipitation information. These data were acquired from several meteorological stations at different locations on the test site for the five month period from 1st of May to 1st of October. Data values include the sum of daily precipitation for every day in that time span. The precipitation values for the entire test site were calculated using interpolation methods.

Thorough soil type measurements, and, simultaneously with the ERS-1 measurements, soil moisture measurements, have been conducted for selected test areas in the Porvoo test site.

4. METHODS

4.1 Speckle Removal

Several image filtering methods for speckle removal have been tested. The tested methods are 1) principal component analysis (PCA) for multi-temporal images, 2) EPOS filtering (Hagg 1994), 3) Iterated Conditional Modes method (ICM) based on Gibbsian random field assumption and introduced by Besag (1986), 4) Sigma filter (Lee 1983) and 5) simulated annealing method. For more details, see Tomppo et al. (1994).

4.2 Image segmentation

Speckle of SAR images can also be removed by averaging the backscattering coefficients within the segments in a segmented image. Several segmentation algorithms have been tested. The method giving best results was based on ideas presented by Pappas (1992) and modified in this study for SAR images.

In segmentation, an image is divided into homogeneous regions in which the observations are similar to each other. Ideally, a segment corresponds to a forest stand homogeneous with respect to forest characteristics. When the individual pixels yield poor estimates of the stem volume, the mean of observations within a segment may provide more accurate estimates for small areas. We have experimented with segmentation methods incorporating initial classification of pixels. A path-connected set of pixels classified into the same class is regarded as a segment.

Our segmentations were based on six SAR images. A logarithmic transformation of observations was performed before segmentation. To use the NFI sample plots as a training set, we grouped the plots into classes by the development class and the dominant tree species. Each class was characterised by the mean of observations in the SAR images. The pixels of a test area were classified into the classes by the ICM algorithm (Besag 1986). This yields satisfactory segmentations, but the results can be improved by more time-consuming methods.

After initialisation by ICM, segmentation was continued by adaptive clustering (Pappas 1992). In this method, the class means depend on the location of a pixel, and the means are updated iteratively. At each pixel, a class mean is estimated over a small window from the average of observations currently classified into the class. The estimation and classification alternate until convergence. Finally, it was worth eliminating the smallest segments by a merging algorithm. A randomly chosen segment was merged with a neighbouring segment selected to minimise the difference between the means of observations in the segments. If the difference was statistically significant, the two segments remained separate.

4.3 Parameter estimation

Three methods have been tested in estimating the interesting forest characteristics, a variation of K-nearest neighbour classification method, regression analysis, and an inversion method.

The basic *K-nearest neighbour* (K-nn) classification algorithm is as follows. The Euclidean distance in the feature space, $d_{i,p}$, is computed from the pixel p to be classified to each pixel i whose ground truth is known (sample plots). Take $d_{(1),p}, ..., d_{(n),p}, (d_{(1),p} \leq .... \leq d_{(n),p}), n \sim 5-10$ define

$$w_{(i),p} = \frac{1}{d^2_{(i),p}} / \sum_{i=1}^{n} \frac{1}{d^2_{(i),p}} \tag{1}$$

Define the estimate $\hat{m}_p$ of the variable M for the pixel p

$$\hat{m}_p = \sum_{j=1}^{n} w_{(j),p} \cdot m_{(j),p} \ , \tag{2}$$

where $m_{(j),p}$, $j = 1, ..., n$, are the values of the variable M in the n closest pixels to the pixel p in the spectral space (Tomppo 1991).

Linear regression estimation has been applied with the NFI sample plots and segmentation based average smoothing of the backscattering coefficients. The models have been derived by tree species.

The most promising results so far has given the *inversion method* developed by Pulliainen (1994). It utilises a semi-empirical forest backscattering coefficient model, multi-temporal ERS-1 SAR images, and the estimated soil and canopy moisture of the images. The semi-empirical model needs field measurements of forest parameters (growing stock volume) on a subset of the area being examined, e.g., on the sample plots. The model has been derived by means of the helicopter-borne HUTSCAT scatterometer, (Pulliainen et al. 1994).

It the first inversion stage, the forest backscattering model is fitted to sample plot data. The soil and canopy moisture are assumed constant but unknown within each image. The growing stock volume is obtained from the NFI data. The results of the this inversion are the soil and canopy moisture estimates for each ERS-1 SAR image used in the analysis. The average behaviour of the backscattering coefficient as a function of tree stem volume is also obtained from this inversion.

In the second stage, the images are split into sub-areas and stem volume estimates for all sub-areas are obtained by fitting the backscattering model into a multi-temporal set of ERS-1-based backscattering coefficients (average σ^0 values for each sub-area). The values of soil and vegetation moisture are those determined in the first stage. Hence, the conditional distribution of sub-area-wise σ^0 and the stem volume estimate for this sub-area is:

$$p\Big(\overline{\sigma}^0 | (V, \overline{m}_{v,v}, \overline{m}_{v,s}, \overline{c})\Big) =$$

$$B \cdot exp\Big(- \sum_{j=1}^{K} \frac{1}{2\sigma^2} \{c_j \cdot [\sigma^0_V(V, m_{j,v,v}) + t^2(V, m_{j,v,v}) \cdot \sigma^0_g(m_{j,v,s})] - \sigma^0_j\}^2 \Big), \tag{3}$$

where

$\overline{\sigma}^0$	=	$((\sigma^0)_1, (\sigma^0)_2, \ldots, (\sigma^0)_K)$, a vector containing average backscattering coefficients of a sub-area for K ERS-1 SAR images,
V	=	forest stem volume of sub-area,
$\overline{m}_{v,v}$	=	estimated volumetric canopy moisture (vector) for each SAR image,
$\overline{m}_{v,s}$	=	estimated volumetric soil moisture (vector) for each SAR image,
$\overline{c}$	=	calibration constant due to the systematic and random difference between the model and the ERS-1 data,
B	=	norming constant,
σ	=	standard deviation of σ^0 (same for each image),

and the iteration problem to estimate the stem volume V (which is now the only unknown parameter) for a certain sub-area is

$$\textit{Minimise} \sum_{i=1}^{K} \{c_j \cdot [\sigma_V^0(V, m_{j,v,v}) +$$

$$t^2(V, m_{j,v,v}) \cdot \sigma_g^0(m_{j,v,s})] - \sigma_j^0\}^2. \tag{4}$$

4.4 Identification of clear-cut areas

The forest resource information of an area can be updated either by re-measuring the field-plots or by updating the field data using other information. The other information can be, e.g., growth models and total removals. In Finnish forestry, the removals are known by regions, i.e, the exact locations of the removals are not known. These models and data have been used in NFI earlier to update the forest resource information by assigning the cuttings to the plots, which most probably have been cut. If the removals could be assigned to the really harvested field plots, the accuracy of the model-based updating could be increased.

In order to find the clear-cut areas using ERS-1 SAR images, the images are divided into two groups by their acquisition date. If a forest stand has been clear-cut, it is assumed to be mature in the images of the first group and the observations from the stand should resemble observations from a mature forest. In the second image group, the mean backscattering coefficient over the stand should exhibit different behaviour in the clear-cut areas.

The mean backscattering coefficient over a stand is compared with the average backscattering coefficient in the NFI sample plots. The mean difference

$$D_i(r) = \frac{1}{N} \sum_k \frac{(y_{ik}(r) - m_k)^2}{var_k}, \tag{5}$$

is calculated, in which $y_{ik}(r)$ denotes the mean of observations over the ith stand in the kth image in the rth group of images, m_k denotes the mean of observations in the NFI sample plots (mature forest), and var_k is the variance of observations in the NFI sample plots.

In a logistic regression model, a stand has been clear-cut with a probability

$$p_i = \frac{\exp\{\beta^t x_i\}}{1 + \exp\{\beta^t x_i\}}, \tag{6}$$

in which β is the vector of parameters and x_i is the vector of explanatory variables. The mean backscattering coefficient is compared with mean coefficients m_k from mature forests in a model with

$$\beta^t x_i = \beta_0 + \beta_1 D_i(1) + \beta_2 D_i(2) + \beta_3 D_i(1) D_i(2) +$$

$$\beta_4 D_i^2(1) + \beta_5 D_i^2(1). \tag{7}$$

5. RESULTS

The reliabilities of the estimates have been assessed at stand level, forest holding level, and forest region level comparing SAR -based estimates with independent field measurement based estimates. Different estimation methods have been applied.

5.1 Reliability of results at stand level

The performance of the K-nearest neighbour classification method has been reported in Tomppo et al. (1994).

Combined use of segmentation and linear regression was tested by estimating the stem volume in the stands of the Mäntsälä test area. Due to the noise in the SAR images, the segment boundaries did not match very well real the stand boundaries. Nevertheless, segmentation may facilitate the detection of clear-cuttings and other small-scale, but distinct, changes in stem volume. The regression models were fitted to data from NFI plots within a distance of 30 km from the test area. One estimate was calculated for each segment using the average backscattering coefficients in the segment, and the estimate was assigned to each pixel within the segment. The estimates were compared with known stem volumes in the forest stands. The total area of the stands was 620 hectares. The correlation coefficients between observed and estimated volumes were rather low: 0.29 for total and spruce volumes and even as low as 0.08 and 0.04 for volumes of pine and deciduous species. The corresponding root mean errors were 96 and 37 m^3/ha and bias from -2.6 to 8.2 m^3/ha. The moisture estimates have not yet been utilised as additional information in these experiments.

The inversion method was applied to tree stem volume estimation in two of the test sites. The estimates were computed at the forest stand level from a multi-temporal ERS-1 SAR data set. The 100 nearest sample plots were used for estimating the soil and canopy moistures.

Tree stem volumes were estimated using of formula (4). The correlation coefficients between the estimated and the field measurement based volume estimates are given in Table 2. For the two test sites, they are 0.64 and 0.63. The rms errors are 90 - 98 m^3/ha, respectively. The correlation coefficients are calculated by weighting the stands with the stand area. Known stand boundaries have been used.

Table 2: ERS-1 SAR-based tree stem volume estimates.

Test site	Number of stands	r	RMS error m^3/ha	SAR vol. est.	Field vol. est.	Mean volu. of NFI plots
Mäntsälä	198	0.64	90	161	154	144
Ohkola	91	0.63	98	126	126	131

Table 3: Region level comparisons of tree stem volume estimates.

Region	Area (ha)	Vol (m^3/ha)	Vol est	Pine	Pine est.	Spruce	Spruce est.	Non-con.	Non-con. est.
hapu	1678	143	151	51	31	73	97	18	21
hirv	2659	128	148	24	29	89	95	14	21
kyta	3061	138	146	33	30	89	94	15	20
lauk	1842	136	146	34	30	84	91	16	22
mapo	6151	160	150	22	26	119	98	17	20
ohko	3695	158	147	31	29	106	99	20	21
oitt	2781	149	152	29	29	105	100	14	20
torp	551	123	148	17	28	87	96	19	22
Total	22418	147	148	29	29	100	97	16	21

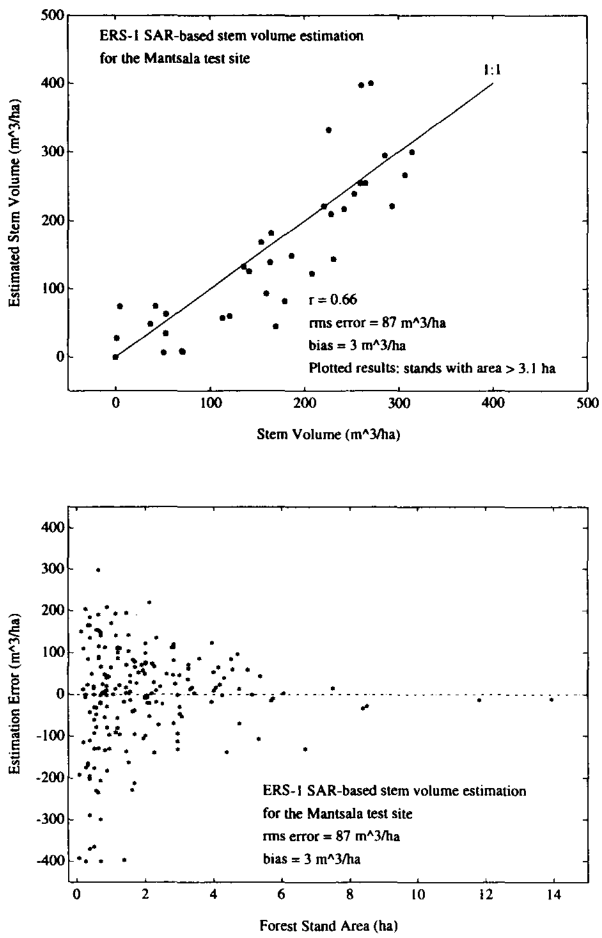

Figure 1: Above: Inversion method based stem volume estimate against the true stem volume. Below: Residuals against stand size(ha).

The estimates from the inversion method have also been justified by comparing the overall stem volume estimates of the two sites with field measurement based ones and with mean volumes of training sample plots. The results show that the inversion method significantly improves the estimates based on the overall mean of training areas (NFI plots). Figure 1 shows the estimated stand volume on one test site against the true stem volume and the estimation error against the area of the stand. The error is reasonably low if the area is 3 hectares or more.

5.2 Reliability at forest region level

The total volumes from the stand level inventories were used as comparison data in assessing the reliability of the estimates at forest region level. The field measurements of regional inventories have been carried out in the years 1990-1993. The estimates are based on visual assessment and only a small number of measurements. Eight forest regions were used. The total areas vary from 559 to 6256 hectares, total forest land area being 22 418 hectares.

Only K-nn based estimates have been tested so far. The estimated and measured mean volumes by tree species are given in Table 3. The K-nn method together with ERS-1 SAR images seems not explain well the deviations from the grand means of species volumes of the training data set (NFI plots).

Table 4 shows the deviations of the total mean volumes for the forest regions from the grand mean of stand level inventories. The areas of the regions as well as their mean volumes, v, are given. The deviations of v from the grand mean V (= 147.35 m^3/ha), v - V, are compared with the deviations of the estimates from the grand mean of estimates, v_e - V_E. It can be seen that the deviations of the estimates from their mean are much smaller than the real deviations of mean volumes of the grand mean volume. This means that only a small part of real variation can be explained by K-nn method. However, moisture estimation and the inversion method may improve the results. It has not yet been tested at region level.

Table 4: Deviation of means and their estimates from grand means.

Test site	Area ha	v m^3/ha	v - V m^3/ha	v_e - V_E m^3/ha
hapu	1678	143	-4.35	2.33
hirv	2659	128	-19.35	-0.67
kyta	3061	138	-9.35	-2.67
lauk	1842	136	-11.35	-2.67
mapo	6151	160	12.65	1.33
ohko	3695	158	10.65	-1.67
oitt	2781	149	1.65	3.33
torp	551	123	-24.35	-0.67
Total	22418	147.35	0.00	0.00

5.3 Identification of clear-cut areas

The model (6) is fitted using one Landsat TM image (r=1) acquired before 23 ERS-1 SAR images (r=2). In a data set of 83 mature stands in the Landsat image, the estimates for the parameters are $\beta_0 = -2.59$, $\beta_1 = 0.02$, $\beta_2 = 1.27$, $\beta_3 = 0.00$, $\beta_4 = 0.00$ and $\beta_5 = -0.06$. A large difference $D_i(2)$ implies that a stand has been clear-cut. The logistic regression model provides classification: a stand with probability p_i larger than 0.5 is probably a clear-cut area. With this classification rule, 20 % of the stands were wrongly classified. If the threshold 0.5 is substituted by 0.38, the misclassification rate will decrease to 12 %. These results are obtained only when we know that the stands have been mature in the first images. If there is no ancillary information about the maturity, higher classification errors arise. For a heterogeneous data set of 276 stands with varying maturity, the misclassification rate was 20 % which looks promising, too.

5.4 Effect of the soil moisture

In order to justify the reliability of the inversion method in assessing soil and needle moisture, weather condition measurements have been carried out on a part of the mineral soil NFI sample.

The volumetric soil moisture typically ranges from 5 to 15 % on moraine lands (the most usual soil type in Finland). For spruce and pine mires (peat soils), and for clay soil, higher soil moisture values are seen. The results show that the effect of soil moisture on the backscattering is higher than on the stem volume, see Tomppo et al. (1994).

6. CONCLUSIONS

The methods for utilising ERS-1 SAR images in large area forest inventory are under development. The behaviour of backscattering properties of boreal forests are investigated. The following conclusions were drawn so far.

The correlation of the backscattering coefficient to forest biomass can change from positive to negative depending on weather and seasonal conditions. The highest positive correlations can be observed in cases where the ground is either very dry or covered by wet snow. The highest negative correlations are evident after heavy rain when the soil is still wet, but the forest canopy is back to its normal moisture value.

The estimation of stem volume using ERS-1 SAR data requires data representing at least two cases: the other with a positive and the other with a negative correlation of the backscattering coefficient to stem volume. When multitemporal data are employed, the radar speckle evident in a single image can be reduced using principal component analysis or filtering methods.

The most promising results in estimating forest parameters have been given so far by multi-temporal images, estimation of soil, and canopy moisture between images and the inversion estimation method. Modelling of the moisture variation within an image may still improve the results. Methodology development for these applications will continue.

Detecting of clear-cut areas by means of multi-temporal images works reasonably well. This can be utilised in model-based updating of forest resource information.

The new inversion method and detecting of clear-cut plots may provide some operational use for ERS-1 SAR data in large area inventories.

7. REFERENCES

Besag, J.E. 1986. On the statistical analysis of dirty pictures (with Discussion). *J.R.Statist.Soc. B*, 48, 259-302.

Hagg, W. & Sties, M. 1994. Efficient speckle filtering of SAR images. *Proceedings of IGARSS'94*, vol IV, 2140-2142.

Hallikainen, M., Hyyppä, J., Haapanen, J., Tares, T., Ahola, P., Pulliainen, J. & Toikka, M., 1993. A helicopter-borne 8-channel ranging scatterometer for remote sensing, Part I: system description. *IEEE Transactions on Geoscience and Remote Sensing*, 31, 161-169.

Hyyppä, J. 1993. Development and feasibility of airborne ranging radar for forest assessment. Helsinki University of Technology, Laboratory of Space Technology.

Lee, J.S. 1983. Digital Image Smoothing and the Sigma Filter. *Computer Vision, Graphics and Image Processing*, 24, 255-269.

Pappas, T. N. 1992, An adaptive clustering algorithm for image segmentation. *IEEE Trans. Acoustics, Speech, and Signal Processing*, 40, 901 - 913.

Pulliainen, J. 1994. Investigation in the backscattering properties of Finnish boreal forests at C- and X-band: a semi-empirical modeling approach. Laboratory of Space Technology, Helsinki University of Technology. Report 19, 121 p.

Pulliainen, J., Heiska, K., Hyyppä, J. & Hallikainen, M. 1994. Backscattering properties of Boreal Forest at C- and X-bands. *IEEE Trans. Geoscience and Remote sensing*, vol 32, pp. 1041-1050.

Tomppo, E. 1991. Satellite Image-Based National Forest Inventory of Finland. *International Archives of Photogrammetry and Remote Sensing*, 28, 419-424.

Tomppo, E., Hallikainen, M., Mikkelä, P., Henttonen, H., Katila, M., Pulliainen, J., Heiska, K., Hyyppä, J. & Tares, T. 1994. Application of ERS-1 SAR -data in large area Forest Inventory. Project PP-SF1, *Proceedings of the First ERS-1 Pilot Project Workshop*, Toledo, Spain, ESA SP-365, pp. 235-240.

GEOID / GRAVITY / BATHYMETRY

Chairman: **E. Biegert**
Rapporteur: **J. Benveniste**

Mapping the sedimentary basins of the Barents and Kara Seas using ERS-1 gravimetry

Louis Géli[1], Frédérique Blanc[2], Emmanuel Auger[3] & Jean-François Girard[2]

[1]IFREMER, Marine Geosciences Department, B.P. 70, 29280 Plouzané-Cédex
[2]C. L. S., Space Oceanography Group, 18 Avenue Edouard Belin, 31055 Toulouse Cédex
[3]Université de Nice, Sophia-Antipolis, 06108 Nice Cédex 02

ABSTRACT

ERS-1 derived gravimetry reveals interesting features of the basement of the Kara and Barents Seas which have not been chartered in recent, previous compilation maps of sedimentary thicknesses in the Arctic Ocean (Gramberg and Puscharovski [1989], and Jackson and Oakey, [1990]). The data also indicate the presence of a north-south trending gravity high associated with the maximum depth of both the Near Base Cretaceous and the Intra Early Permian reflectors within the South Barents Sea and the North Barents Sea Basins. This suggests that the formation of these basins is probably related with crustal thinning and upwelling of dense mantle material. Further geological studies are needed to interpret our gravimetric data, which directly addresses the problem of understanding the gravity signature of deep, old, sedimentary basins.

I. Introduction

The continental shelf in the Arctic north of Russia consists in a series of epicontinental seas, which are the offshore continuation of potentially oil and gas rich basins on land (Figure 1). The Barents Sea, where the oilfields of Kolgyev, Pomov, and Gulyayev have been discovered, lies north of the Timan-Pechora-Basin, a major oil and gas reservoir of the present day Russia. The Kara Sea, with the recently discovered Russanov and Leningrad oilfields, appears as the northern extension of the oil and gas rich West Siberia Basin, which includes the Urengoy and Ob oil and gas giant fields (in the early 80's, the West Siberian Basin was providing 58% of the oil and 32% of the gas of the USSR). The Laptev Sea is considered to be part of the poorly explored Lena-Tungunska and Vilnuy Basin petroleum provinces, between the Ienisseï and Lena rivers. East of the Verkhoyansk suture Range, the East Siberia Sea and the Chukchi Sea are -geologically speaking- part of the Pacific Mobile Belt. The geology of all these epicontinental seas is poorly known, due to the remoteness, the inhuman climatic conditions and the huge costs associated with seismic exploration.

The European Remote Sensing satellite (ERS-1) is the first satellite to provide non-classified altimetric data north of 72°N. Launched in July 1991, it has been on its 168-days repeat orbit since april 10th 1994, offering the densest gravimetric coverage ever obtained at a global scale at these latitudes, with an along track resolution of about 7 km, and an across track resolution ranging from 7 km at 60°N to 2.6 km at 80°N. Thus, it may represent an unique geophysical tool for studying the geological structures off the arctic coast of Russia.

The PEGASE project was designed to study the feasability of using the ERS-1 inferred gravity field to map and study the sedimentary basins of the russian arctic continental margin. This project results from an active collaboration between three french groups : the CLS Space Oceanography Group (Toulouse), the Marine Geosciences Department of IFREMER (Brest), and the "Groupe de Recherche en Géodésie Spatiale" (GRGS, Toulouse). CNES selected the project for funding in october 1992 (ref. 92/CNES/0382 - AVAL SAR). ESA approved it in march 1993 (ref. PP2-F14).

II. The data

The results presented hereafter are based on the 168 days repeat orbit data spanning the period between apil 10th 1994 and march 21st 1995. As most of the existing validation processes have never been tested at such high latitudes, special attention was given to data processing (data reduction, filtering and processing are described in detail in former progress reports of the PEGASE project (e.g. Géli and Blanc, 1994); what is new here is that we corrected tide and orbit errors using the most accurate and simultaneous TOPEX/POSEIDON data).

III. The free-air gravity anomaly field

III.1 Method

Due to the density contrast between basement rocks and sedimentary rocks, changes in depth of sedimentary basins induce local variations of the gravity field. These variations induce perturbations, that can be detected in altimeter measurements. However, for wavelength less than 100 km, these perturbations are more readily detectable in the gravity anomaly field (if r is the distance from the measurement point to the source of anomalous density, the gravity signal decreases with r^{-2}, while the geoid signal decreases with r^{-1}). Because we are interested in geological structures of dimensions as small as 100 km, the gravity field is used hereafter.

To derive the gravity anomaly field from the geoid height measurements, we used the method described by Sandwell (1991), and Mc Adoo and Marks (1992). This

Proceedings of the Second ERS Applications Workshop, London, UK, 6–8 December 1995 (ESA SP-383, February 1996)

method consists in 1) computing the along-track derivative on each geoid profile (prior to this, the geoid is referred to the JGM-2 low order geoid model cosine tapered between degrees 25 and 35; at the end of the whole process, the low-order geoid model will be added back to the residual gravity anomaly grid); 2) interpolating the along track derivatives to two uniform grids of ascending and descending slopes, respectively; 3) converting these grids into two comparable grids of east and north vertical deflection grids, which, in turn, are used to calculate the grid of gravity anomaly. The key point of this method is that no correction for radial orbit error is made on the altimeter data in the process for producing a grid of gravity anomalies.

III.2 Results and implications for the study of the structural geology of the Barents Seas

In order to remove the long wavelengths components of the gravity field that may be related with sources within the lower mantle, as well as those related with some kind of regional compensation, we removed the orders < 35 of the development in spherical harmonics (we used the JGM-2 model, although more recent models exist, including the data described by Kogan & McNutt, 1993). In the following, we only deal with the high pass filtered gravity field.

The seafloor of the Siberian Arctic platform is relatively flat, with depths shallower than 500 m. At first approximation, the shorter wavelengths (< 100 km) of the free-air gravity field are correlated with basement topography and/or with heterogeneities within the basement. To check this, the high-pass gravity field for the Barents and Kara Seas was compared with available contoured maps of sedimentary thickness. The problem with this type of maps is that, in areas formerly controlled by the Soviet Union, the source of the data is generally unknown, and the contours are generally not consistent from one map to the other.

The first example (Figure 2, bottom) is a comparison with the map compiled by Jackson and Oakey [1990]. In this compilation, three soviet maps (Anonymous [1978], Anonymous [1983], and Pogrebitskii et al [1984]) that showed sedimentary contours were used as a basis for contouring vast regions, because they were supported by independent information. The isocontours of the map were digitized, and superimposed on the free-air gravity map (Figure 2). The gravity data exhibits a major depression in the south-westernmost part of the Barents sea, which corresponds to a prominent geoid low, -3 m deep. Because the area is a zone of dense seismic coverage located under norwegian control, the ERS-1 derived gravity contours are well correlated with the sedimentary thickness contours. The shape of the Nordkapp and the Hammerfest basins can be recovered from the gravity data (the isopachs are consistent with the isogals).The consistency does not hold in areas of poor seimic coverage, or in areas that were under soviet control. For instance, an outstanding observation is in the south Barents Sea basin (near 40°E, 72°N) : the gravity data reveals that this structure is actually divided in two sub-basins which are associated with gravity lows of less than -15 mgals, and separated by a ridge of positive gravity signature. In the Kara Sea, an important basin with a gravity low of -20 mGals is also revealed near 62°E, 72°N : this basin does not show up in the sedimentary contour map. In most areas of poor coverage, the ERS-1 derived gravity field would definetely modify the isocontours of Jackson and Oakey [1990]. The comparison with the synthetic map of the main structural elements of the Barents Sea of Johansen et al. [1993] yield the same conclusions as in the previous case, the major feature being the existence of two sub-basins dividing the south-Barents Sea Basin .

The second example (Figure 2, top) is a comparison with the map of Gramberg and Puscahrowski [1989]. This map is published by JEBCO Seismic Ltd, a russian company installed in London. It is a compilation of 8 russian tectonic or structural maps, including the satellite imagery geological map of the USSR (scale 1:2500000; Ministry of Geology of USSR, editor E. A. Kozlovski). The source of the data in these maps is generally unknown or not available to foreign scientists. The first observation is that major differences exist between this map and the one of Jackson and Oakey [1990]. The Barents Sea, most particularly, appears to be divided in two parts by a south-north trend paralleling the 42nd meridian in the russian map. This trend does not appear in Jackson and Oakey [1990], but it shows up in the ERS-1 derived gravity map. We think that this S-N trend probably exists, since it is the continuation of an indentation in the Arctic margin, which is associated with an offset of the Nansen spreading center. More generally, it seems that the russian map is more consistent with the ERS-1 gravity contours than the map of Jackson and Oakey [1990] : the satellite data can be used to compare the validity of different sedimentary thickness maps.

On the gravity map, we also superimposed the contours of the maximum depth of the Near Base Cretaceous reflector (Figure 3, top) and the contours of the Early Permian reflector (Figure 3, bottom). The database used by Johansen et al (1993) for deriving these contour maps includes most commercial and published scientific seismic data in Norwegian waers, al seismic data in former Soviet waters, and all data from exploration drilling in the region. Data from adjacent outcrops and shallow offshore wels have also been used. In the east, reports and results were made by Arcticmorneftegasravedka, Soyuzmorgeo, Sevmorneftegeofizika, Niimorgeofizika and Vniimorgeo. A north-south trending gravity high is associated with the maximum depth of both the Near Base Cretaceous and the Intra Early Permian reflectors within the South Barents Sea and the North Barents Sea Basins. This is an important observation suggesting that the formation of these basins is probably related with crustal thinning and upwelling of dense mantle material.

IV. Variation of sediment thickness, based

on the inversion of the high-pass filtered gravity field

IV.1 The inverse problem

Sedimentary basins are commonly associated with negative gravity anomalies due to the low density of the basin fill compared with the density of the surrounding rocks. Our purpose here is to determine the geometry of the depth and shape of the sedimentary basins of the Siberian Epicontinental Seas, given the free-air gravity anomaly field derived from ERS-1 altimetry. Provided correct density estimations and regional gravity field are available, the unknown parameter is the topographical relief of the sediment-basement interface. Hence, the calculation of the basin configuration is a gravimetric single interface inversion problem.

IV.2 Estimating the density versus depth relationship

The inversion of gravimetric data requires the assumption of a density-depth function.

The first problem at these high latitudes is to estimate the effect of sub-sea permafrost on the depth/density relationship. Eigtheen thousands years ago, there was an all-time low in sea-level, which was 130 m lower than today (Shackelton and Bennet, 1975). Accordingly, some permafrost must have developed in the zones where current sea bottom was exposed to atmospheric cold. Nevertheless, the peak in cold temperature 18000 years ago was sharp, not letting much time for the ice to form. Lachenbruch (1982), in his study of the Prudhoe Bay area, gives a rate of 15m per year for the melting consequent on ocean re-invasion. This means that over 18000 years, some 250 m of ice might have molten (from an initial 650 m in Prudhoe Bay). Thus, if any permafrost is present, it must be confined to depths of a few hundred meters. This result is confirmed by direct resistivity measurements (Palacky and Stephens, 1992). For this reason, and because the densities of ice and free-water are only slightly different, it is unlikely that the effect of permafrost might be noticeable in our results.

When considering sediments, composed of water and a matrix of heavy, incompressible particles, one has to consider their compaction under the effect of the pressure applied by the overlying matter. At low depth, the increasing pressure drives the water away from the solid particles, which results in a high gain of density. At greater depth, the drainage of water diminishes the interstitial space, and solid particles come into contact with each other.When no more movement is possible, the density reaches a maximum. Following Granser (1987), we thus propose to use hereafter an exponential function $\rho r(z)=\rho 0.\exp(-\lambda.z)$ to model the density contrast at a given depth and the maximum ($\rho 0$ is the density contrast at the sea bottom).

To find the best suited $\rho 0$ and λ for the Barents Sea, we use the results of Johannsen et al. (1990), giving the ages of the sedimentary layers according to their depth in the Barents sea, and the results of Holliger & Klemperer (1987) -hereafter referred to as H & K- giving the density of the sedimentary layers according to their age in the North Sea (Figure 4). In the process, we assume that rocks in the Barents Sea have the same density as rocks of the same age in the North Sea, although rocks in the North Sea are deep seated, (and thus undergo a great compaction pressure),while they tend to outcrop in the Barents Sea where erosion has washed-away the younger layers. The depth/density curve that we finally get is shown in figure 5.

IV.3 Theory

In the following development, we use notations and hypothesis of Parker (1972).The gravitational potential U , as measured in the point r_0 , can be writen , according to its definition :

$$U(r_0)=\gamma\int_V dv.\rho_0.\frac{e^{-\lambda z}}{|r-r_0|}$$

Where γ stands for the gravitational constant, $\rho=\rho_0\exp(-\lambda z)$ is the density-depth relation, and **r**, **z** span the volume V of the anomaly. Let us now consider the Fourier transform of the potential :

$$F(U(r_0))=\int_X ds_0.U(r_0)\rho_0.e^{ikr_0}$$

Following Parker (1972) step by step, the volume V is considered as the itersection between the domain D(x,y) where the function h is not uniformly equal to zero, and the domain for z varying between o and h.

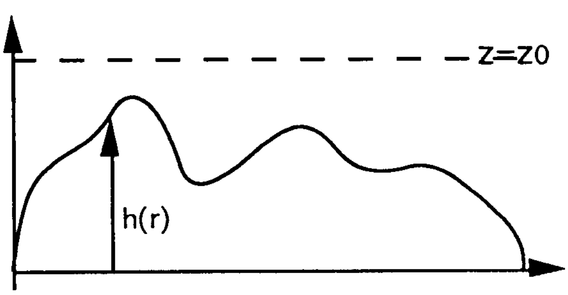

Using the above notations, we write :

$$F(U(r_0))=$$

$$\gamma\rho_0\int_X ds_0\int_D ds\int_0^h dz.\frac{e^{-\lambda z}}{|r-r_0|}.e^{ikr_0}$$

Interchanging the order of integration and solving the integral over ds_0, one obtains :

$$F(U(r_0)) =$$

$$2\pi\gamma\rho_0 \int_D ds \int_0^h dz.e^{-\lambda z} e^{ikr} \frac{e^{-k(z-z_0)}}{|k|}$$

The integral over z between o and h is easily computed :

$$\int_0^h dz.e^{(|k|-\lambda)z} = -\frac{1-e^{(|k|-\lambda)h}}{(|k|-\lambda)}$$

Provided that :

$(|k|-\lambda)h<<1$

we can expand the exponential into a Taylor series :

$$F(U(r_0)) =$$

$$2\pi\gamma\rho_0 e^{-kz_0} \int_D ds.e^{ikr} \frac{1}{|k|} \sum_{n=1}^{\infty} \frac{(|k|-\lambda)^{n-1}}{n!} h^n(r)$$

Which is written as a sum of Fourier transforms :

$$F(U(r_0)) =$$

$$2\pi\gamma\rho_0 e^{-kz_0} \frac{1}{|k|} \sum_{n=1}^{\infty} \frac{(|k|-\lambda)^{n-1}}{n!} F(h^n(r))$$

In the Fourier domain, the gravity field is expressed by :

$$F(\Delta g) = |k| F(U)$$

which gives the following "adapted Parker formula" :

$$F(\Delta g) = 2\pi\gamma\rho_0 e^{-kz_0} \sum_{n=1}^{\infty} \frac{(|k|-\lambda)^{n-1}}{n!} F(h^n(r))$$

This last equation can be used to determine h in a iterative process (Oldenburg 1974) by extracting the term n=1 in the ininite sum and using an expression of the type h=Q(h) as follows :

$$\frac{F(\Delta g)}{2\pi\gamma\rho_0} e^{kz_0} = F(h(r)) + \sum_{n=2}^{\infty} \frac{(|k|-\lambda)^{n-1}}{n!} F(h^n(r))$$

The expression h=Q(h) can thus be writtens as :

$$h(r) = F^{-1}\left\{ \frac{F(\Delta g)}{2\pi\gamma\rho_0} e^{kz_0} - \sum_{n=2}^{\infty} \frac{(|k|-\lambda)^{n-1}}{n!} F(h^n(r)) \right\}$$

At each step , the latest value h of the topography is inserted into the right-hand term of the above expression, a new correction to h is computed, and the process repeated until satisfactory convergence is met.

IV.4 Practical procedure and final results :

In practice, the computing procedure can be summarized as follows :

1) Compute the best geoid using all available corrections

2) Compute the deflections of the vertical and the free-air gravity anomalies using the method of Sandwell (1991)

3) Filter out the long wavelengths of the gravity field in order to remove the effect of heterogenities deeply seated in the mantle. In this work, the orders > 35 of the JGM-2 gravity model were removed.

4) Remove the effect of sea-bottom topography, using Parker's method (1972) and downward continue the corrected gravity field to the sea-bottom level.

5) Compute sediment thickness assuming that the density of sediments increases exponentially with depth using the method described here above.

Let E be the base of the layer in which the density of the sediment varies exponentially with depth. The final results that we get are depth variations of interface E relatively to an arbitrary $z=z_0$ reference level. These results are summarized in Figure 5. The depth variations of E and the gravity anomaly field across the Barents Sea are compared to the variations of the sediment thickness inferred from seismic data. The abrupt variations in the gravity data appear to be relatively well correlated with deep seated faulting at the base of the sedimentary basin. However, in the South Barents Sea Basin, the greatest sediment thickness is correlated with a gravity high.

IV.5 Preminiminary geological interpretation :

Several tectonic events have had major influences on the evolution of the Barents Sea area. The caledonian orogeny culminating in Late Silurian-Early Devonian set up a structural framework that has been important for the subsequent evolution of the western areas. Paleozoic subduction and the subsequent collision between the eastern plates and the easternmost shelf areas resulted in the Uralian Orogeny in Permian and early Triassic times.

In the Greater South Barents Sea area, Early to Middle Devonian extension formed graben and half graben systems. Late Permian was a period of tectonic activity with crustal extension and rapid subsidence and sedimentation. In Late Permian times, the sedimentation increased as a response to the Uralian collision and uplift. Tectonically, the Early Triassic was the most active period in the East Barents Megbasin, with extension and rapide subsidence. Lat Permian extension and subsidence contiuned into the Triassic and the subsidence rates accelerated n the Eary Triassic. Extreme subsidence and associated fault systems were also reported by Verba (1985). The collapse of the greater Uralian foreland system created space for large volumes of sediments to be deposited in Mesozoic times.

Figure 5 indicates a good correlation between deep faulting within the sediments and abrupt variations in the gravity field. Thus, the syn-sedimentary deep seated faulting associated with Early to Middle Devonian extension that can be recognized in the seismic data seems to be also recognizable in our gravity data (figure 5). In the cental part of the basin, the pre-Upper Devonian strata are deeply buried, and the possibility of metamorphism or complete absence of these strata was first suggested by Gramberg (1988). The presence of a proeminent gravity high that is associated with the contours of the maximum depth of the early Permian reflector (Figure 3) supports strongly this hypothesis. The gravity data thus suggest that the formation of the North and South Barents Sea basins is probably related with crustal thinning and upwelling of dense mantle material.

V. Conclusions

The ERS-1 derived gravity data is an unique tool for studying the geometry of sedimentary basins in remote areas, such as the Barents and the Kara Seas. Due to our inability to determine one single, realistic relationship between sediment density and depth for the whole area of the Barents and Kara Seas, gravity data alone cannot be used to determine the thickness of the sedimentary basins. However, the data provide a new insight of deep structure of the Barents Sea Basins. Most particularly, the comparison of the ERS-1 derived gravity map with existing isopach maps inferred from seismic data indicate a negative correlation between the gravity amplitude and the thickness of the sediment layer in the South and North Barents Sea Basins.

The analysis of the ERS-1 derived gravity data addresses unexpectedly fascinating geological problems, such as the understanding of the gravity signature of deep, sediment filled basins.

REFERENCES

Géli, L., Blanc, F., 1994, *Mean Sea Surface Height, Geoid and Free-Air Gravity Anomalies in the Siberian Epicontinental Seas derived from ERS-1 Radar Altimetry : Preliminary Results*, Progress Report, PEGASE Project, (CNES ref. 92/CNES/0382).

Gramberg I. S., 1988, *Barents Shelf Platform*, PGO, Sevmorgeofizika, Nedra, Leningrad, 263 pages.

Gramberg I. S., J. M. Puscharovski, 1989, *Map of the relief of the heterogeneous basement of the Arctic region and adjacent areas*, 1:10 000 000, compiled and translated by JEBCO Seismic Limited, JEBCO House, 22 Armoury way, London SW18 1EZ.

Granser, H., 1986, *Convergence of iterative gravity inversion*, Geophysics, 51, 1146-1147.

Granser, H., 1987, *Three-dimensional interpretation of gravity data from sedimentary basins using an exponential density-depth function*, Geophysical Prospecting, 35, 1030-1041.

Holliger, K. & Klempere, S., 1987, *A comparison of the Moho interpreted from gravity data and from deep seismic reflection data inthe northern North Sea*, Geophysical Journal, 97, 247-258.

Jackson H. R., G. N. Oakey, 1990, *Sedimentary thickness map of the Arctic ocean*, in : vol L, the Decade of North American geology, Geological Soc. Am.

Johannsen S. E., B. K. Ostisty, O. Birkeland, Y. F. Fedorovsky,V. N. Marirosjan, O. B. Christensen, S. I. Cheredeev, A. Ignatenko, L. S. Margulis, 1993, *Hydrocarbon potential in the Barents sea : play distribution and potential*, in : Arctic geology and petroleum potential, T. O. Vorren et al., Editors, Elsevier Publisher.

Kogan, M. G., & McNutt, M., 1993, *Gravity field over Northern Eurasia and Variations in the Strength of the Upper Mantle*, Science, 259, 473-479.

Lachenbruch, H. 1982, *Permafrost, heat flow and the geothermal regime at Prudhoe Bay, Alaska*, J. Geophys. Res., vol. 87, NO B11, p. 9301-9316.

Mc Adoo D. C., K. M. Marks, 1992, *Gravity fields of the southern ocean from Geosat data*, Journal of Geophysical Research, 97, 3247-3260.

Oldenburg, D.W., 1974, *The inversion and interpretation of gravity anomalies*, Geophysics, 39, 526-536.

Palacky, G. J., & Stephens, L. E., 1992, *Detection of subbtoom ice-bonded permafrost on the Canadian Beaufort Shelf by ground electromagnetic measurements*, 57, 1419-1427.

Parker, R. L., 1972, *The rapid calculation of potential anomalies*, Geophys. J. R. Astron. Soc., 31, 447-455.

Rovenskaya A. S., Nemchenko N. N., 1992, *Predictions of hydrocarbons in the West Siberian Basin*, Bull. Centres Rech. Explor.-Prod. Elf-Aquitaine, 16, 285-318

Sandwell D. T., 1992, *Antarctic marine gravity field from high density satellite altimetry*, Geophys. J. Int, 109, 437-448.

Smith W. H. F., P. Wessel, 1990, *Gridding with continuous curvature splines in tension*, Geophysics, 55, 293-305.

Shackelton N.J and Bennet, J.P, 1975, *Paleotemperature history of the cenozoic and the initiation of Antartic glaciation : Oxygen and carbon isotope analysis in DSDP sites 277, 279 and 281*. Initial reports DSDP, v. 29, p 743-755.

Verba, L. M., 1985, *The Barents-Kara mega downwarp and its role in the evolution of the West Arctic Shelf*, In : The geologic structure of the Barents shelf, Collection of papers, PGO, Sevmorgeologia, Leningrad (in russian).

FIGURE CAPTIONS

Figure 1 : Oil and gas regions of the former USSR, after Rovenskaya & Nemchenko. [1992].

Figure 2 : Color map of the ERS-1 derived free-air gravity anomaly field of the Barents Sea (the color scale is in mGals). **Top :** sedimentary thickness contours after Jackson and Oakey [1990] are superimposed on the gravity map. **Bottom :** sedimentary thickness contours after Gramberg and Puscharovski [1989] are superimposed on the gravity map.

Figure 3 : Color map of the ERS-1 derived free-air gravity anomaly field of the Barents Sea (the color scale is in mGals). The east-west straight black line crossing the Barents Sea indicates the seismic line shown in figure 6. **Top :** contours of the maximum depth of the Near Base Cretaceous reflector after Johannsen [1993] are superimposed on the gravity map. **Bottom** : contours of the maximum depth of the Early Permian reflector after Johannsen [1993] are superimposed on the gravity map.

Figure 4 : This figure explains how we derived the density vs depth relationship in the Barents Sea. Due to the lak of direct data, we used an average of the density of rocks vs depth on the Northern North Sea (after Holliger and Klemperer, 1989), and considered that rocks in the Barents Sea could be given the same density as rocks of the same age in the North Sea.

Figure 5 : Density vs. depth relationship used in our calculations. Below about 5 km, the density of the sediments is constant about equal to 2600 kg/m^3. About the 5 km level, the density varies as $\rho=\rho_0 e^{-\lambda z}$. Here : ρ_0=2250 kg/m^3, and λ = 0.5 km^{-1}.

Figure 6 : **Top :** Depth variations of interface E relatively to an arbitrary $z=z_0$ reference level along a line crossing the Barents Sea from east to west (E is the base of the layer in which the density of the sediment varies exponentially with depth; the location of the line is shown in figure 3). **Bottom :** Variations of sediment thickness along the same line, inferred from seismic data (after Johansen et al [1993]).

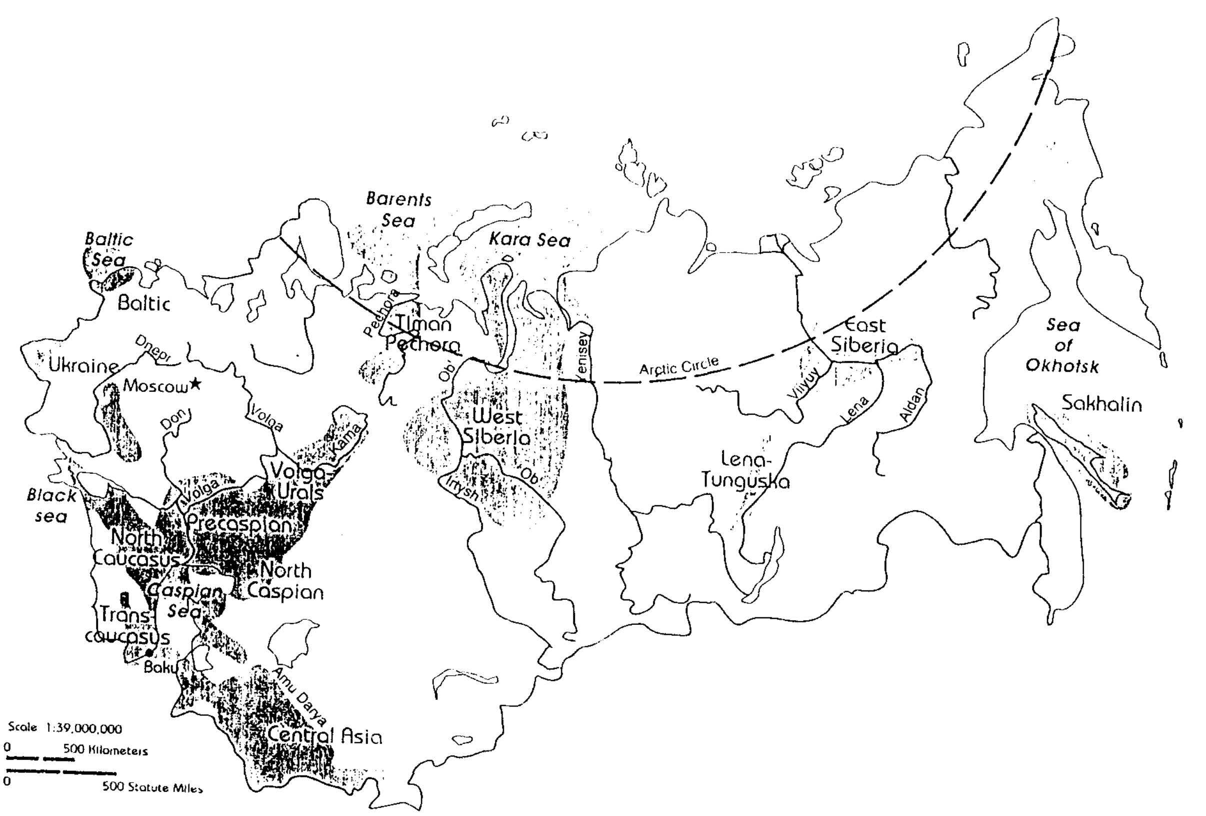

Figure 1 : Oil and gas regions of the former USSR, after Rovenskaya & Nemchenko. [1992].

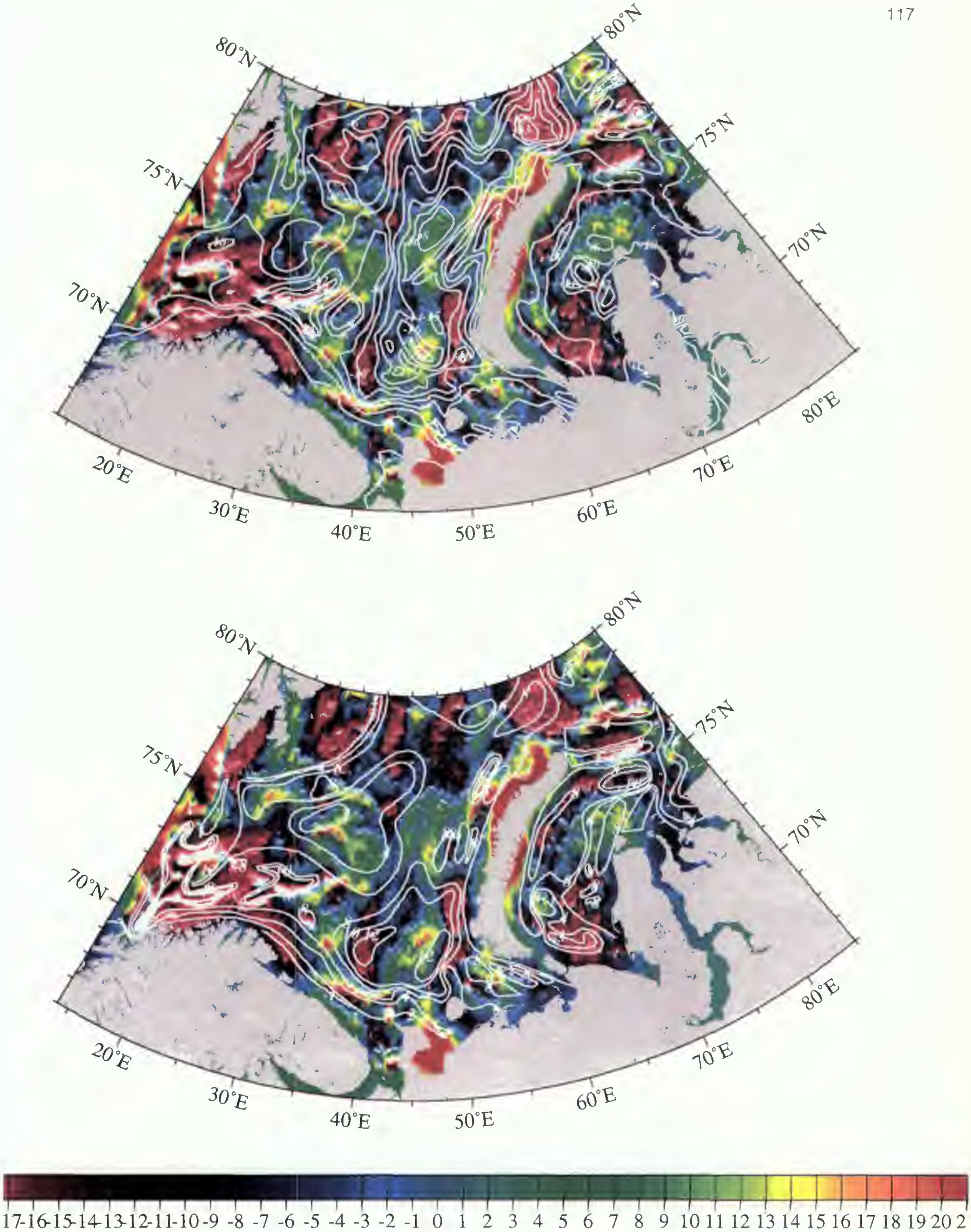

Figure 2 : Color map of the ERS-1 derived free-air gravity anomaly field of the Barents Sea (the color scale is in mGals). **Top :** sedimentary thickness contours after Jackson and Oakey [1990] are superimposed on the gravity map. **Bottom :** sedimentary thickness contours after Gramberg and Puscharovski [1989] are superimposed on the gravity map.

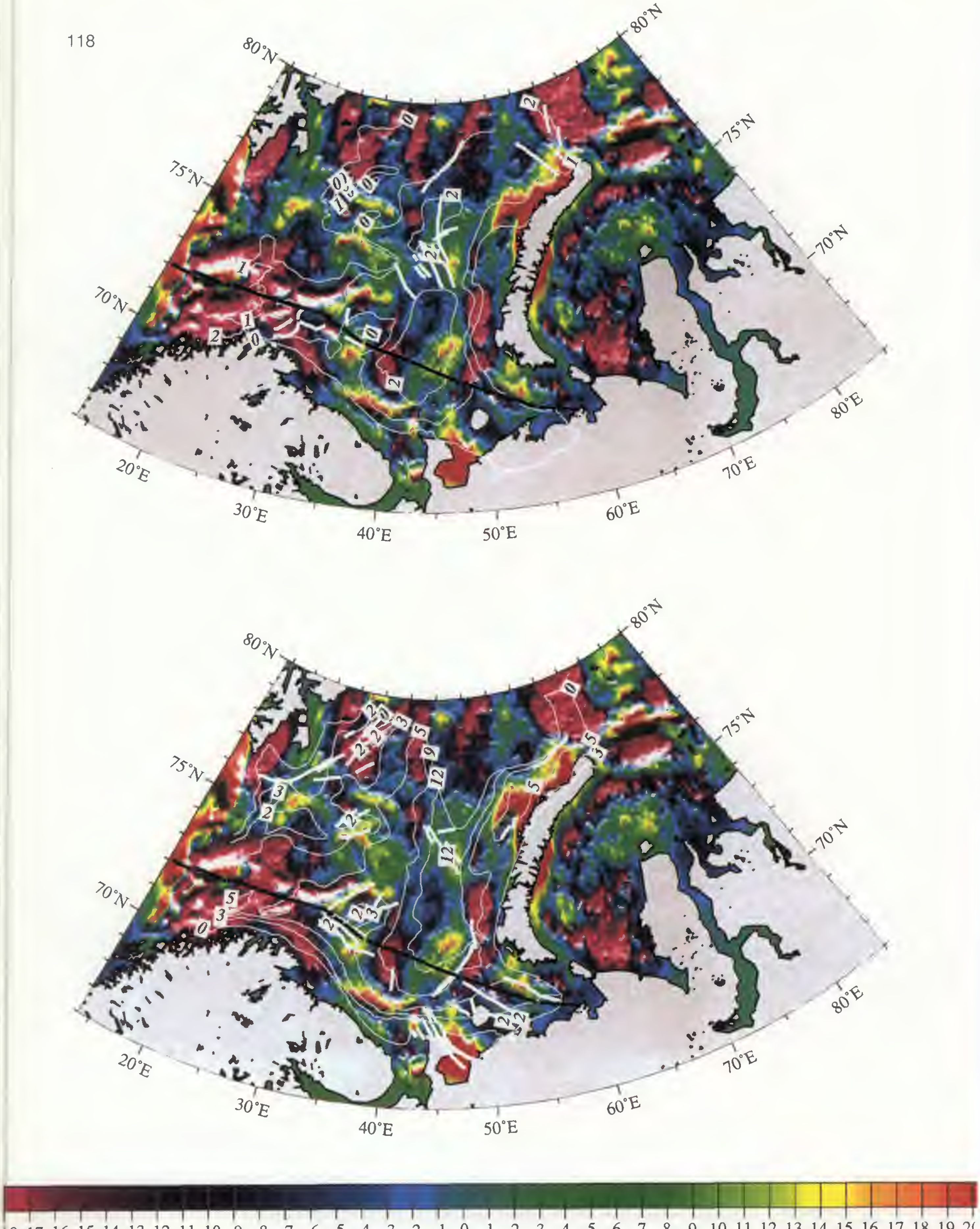

Figure 3 : Color map of the ERS-1 derived free-air gravity anomaly field of the Barents Sea (the color scale is in mGals). The east-west straight black line crossing the Barents Sea indicates the seismic line shown in figure 6. **Top :** contours of the maximum depth of the Near Base Cretaceous reflector after Johannsen [1993] are superimposed on the gravity map. **Bottom :** contours of the maximum depth of the Early Permian reflector after Johannsen [1993] are superimposed on the gravity map.

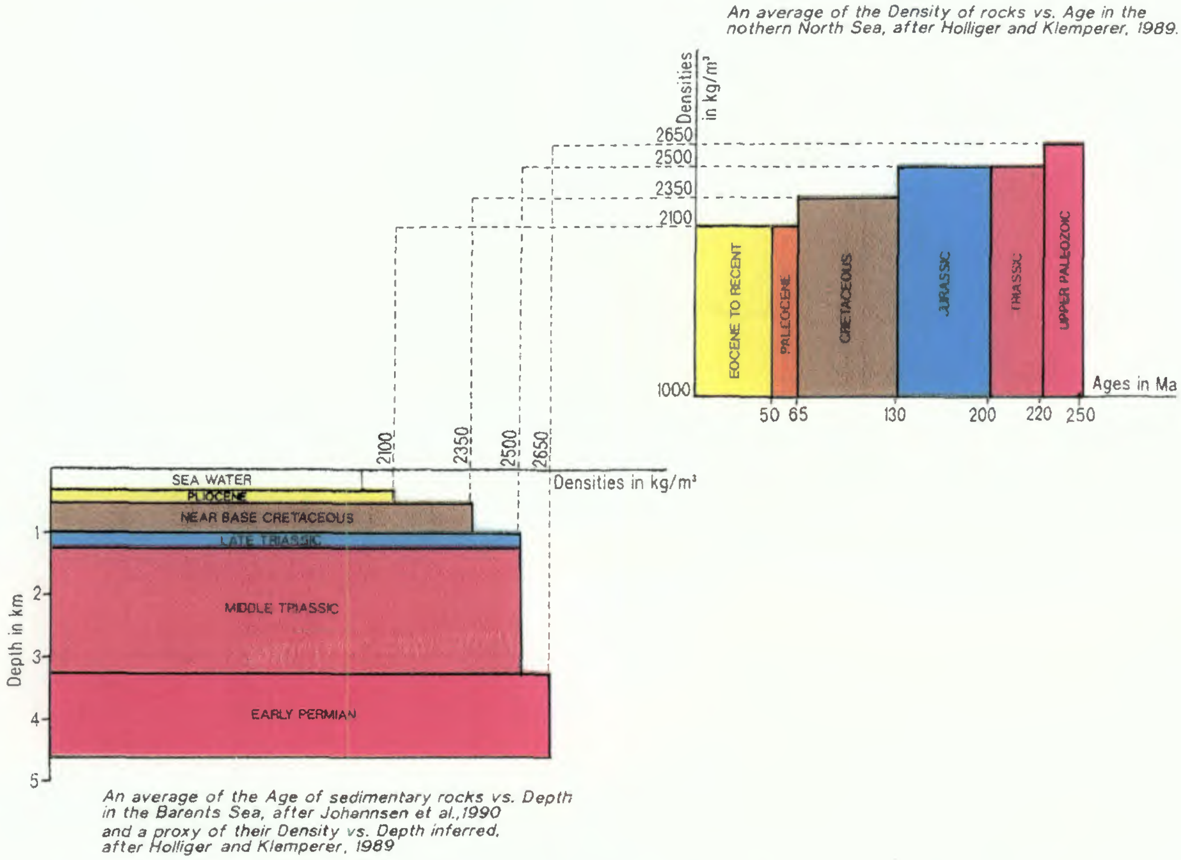

Figure 4 : This figure explains how we derived the density vs depth relationship in the Barents Sea. Due to the lack of direct data, we used an average of the density of rocks vs depth on the Northern North Sea (after Holliger and Klemperer, 1989), and considered that rocks in the Barents Sea could be given the same density as rocks of the same age in the North Sea.

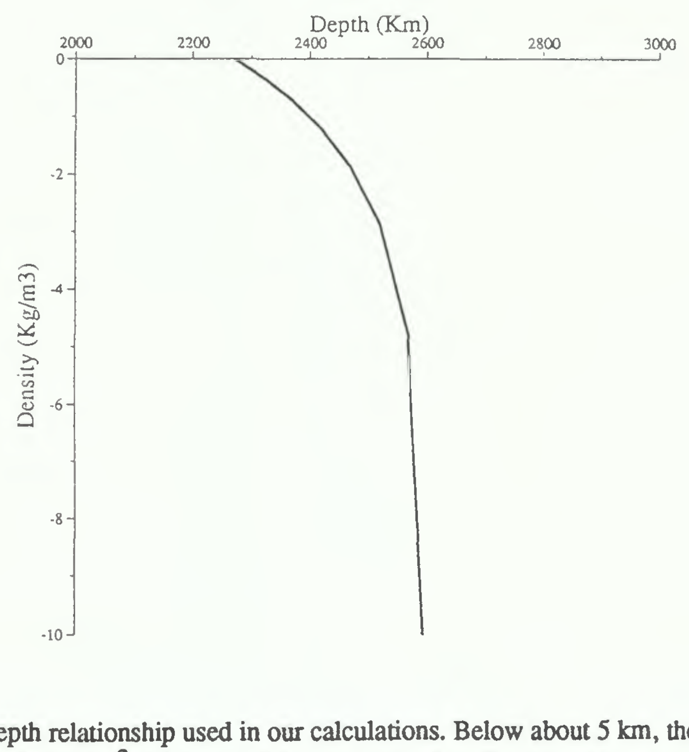

Figure 5 : Density vs. depth relationship used in our calculations. Below about 5 km, the density of the sediments is constant about equal to 2600 kg/m^3. About the 5 km level, the density varies as $\rho=\rho_0 e^{-\lambda z}$. Here : ρ_0=2250 kg/m^3, and λ = 0.5 km^{-1}.

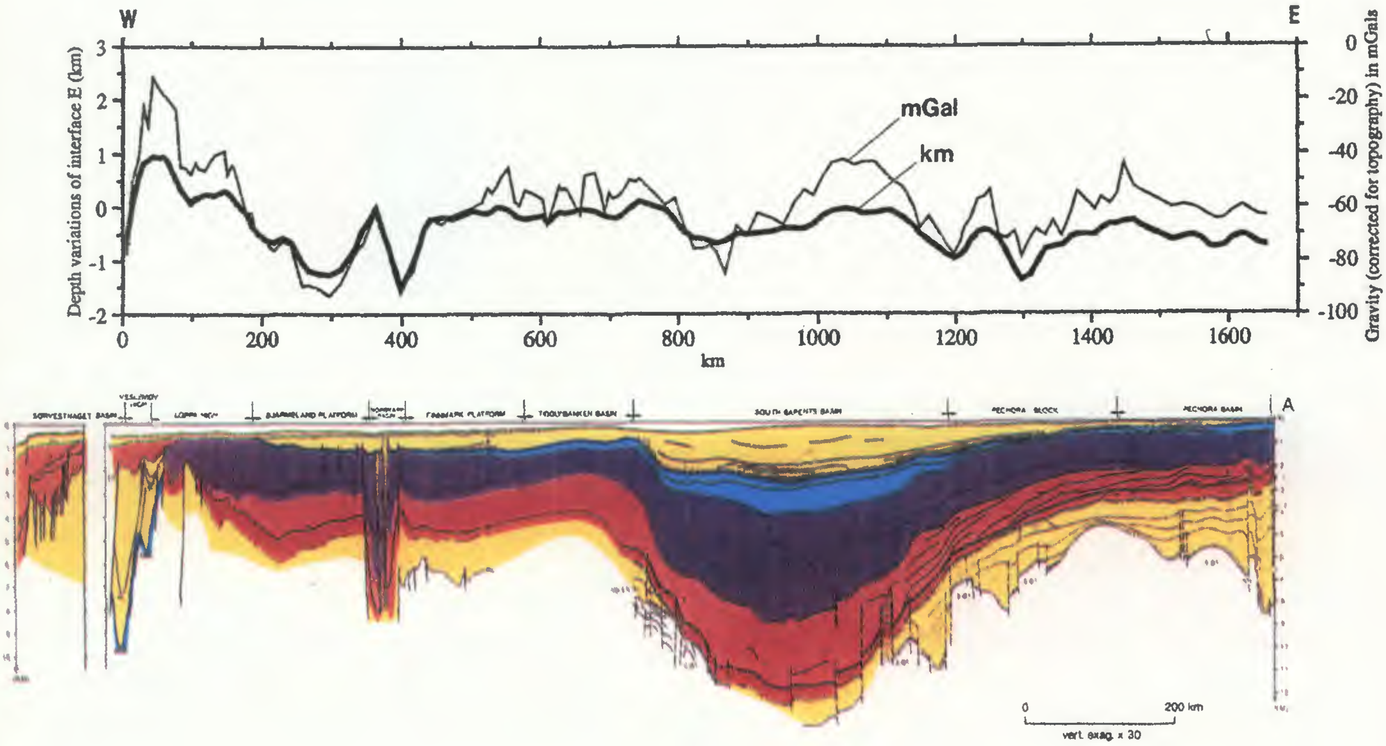

Figure 6 : **Top :** Depth variations of interface E relatively to an arbitrary $z=z_0$ reference level along a line crossing the Barents Sea from east to west (E is the base of the layer in which the density of the sediment varies exponentially with depth; the location of the line is shown in figure 3). **Bottom :** Variations of sediment thickness along the same line, inferred from seismic data (after Johansen et al [1993]).

MARINE GRAVITY FOR OFFSHORE OIL EXPLORATION (GRAVSAT)

Gordon W Jolly and Anna Joffe

Satellite Observing Systems, Ltd., 15 Church Street, Godalming, Surrey, GU7 1EL, UK
Tel: +44 (0) 1483 421213, Fax: +44 (0) 1483 428691, email: info@satobsys.co.uk

ABSTRACT

In April 1994, the first European Remote Sensing satellite, ERS-1, was manoeuvred into the first of two 168-day repeat orbits which were completed in March 1995. This Geodetic Phase produced a ground track sampling pattern with an equatorial spacing of around 8 km. Radar altimeter data from this phase as well as the recently declassified Geosat Geodetic Mission have been used with the GRAVSAT processing software to generate high resolution marine gravity maps over the United Kingdom Continental Shelf. Results are presented from a validation exercise undertaken with in-situ ship measured gravity anomalies which has demonstrated excellent agreement both in the identification and location of features.

1. INTRODUCTION

Geophysical exploration has traditionally depended on surface or low altitude remote sensing for its survey information in new offshore regions. With the advent of publicly available, high density satellite altimetry, frontier exploration can now be made more cost effective though the generation of accurate altimetric gravity anomaly maps. GRAVSAT was developed under the British National Space Centre's Applications Development Programme to satisfy this. To be of practical use to the offshore exploration community, any satellite gravity survey must be able to demonstrate a resolution of better than 20km, *Sailor* [1994]. At this point, it becomes possible to identify important geophysical features at a worthwhile scale including the distribution of sedimentary basins and basement highs, boundary and subsidiary faults and the depocentres of basins.

2. SATELLITE RADAR ALTIMETRY

A radar altimeter operates by measuring the delay between emission of a short microwave pulse and the subsequent detection of the returned echo, recording the arrival time and distortion of the returned signal. The shape of the leading edge of the returning pulse provides information on significant wave height within the instrument footprint as well as an estimate of the time-of-flight of the radar pulse. Both of these factors have an influence on the accuracy and resolution of high resolution gravity field determined from these data.

In high sea states, the time-of-flight for the leading edge of the pulse reflected by the wave troughs is significantly greater than that for the crests which may be several metres closer to the satellite. This not only increases the uncertainty of the instantaneous sea surface height above a theoretical reference, but also allows the pulse footprint to grow to a greater radius on the sea surface, hence returning a signal from a larger area. High wave heights in the footprint therefore result in a reduction in the theoretical spatial resolution of each altimetric height measurement as well as reducing the reliability of the raw height measurements.

Once a range measurement has been extracted from the returned radar echo, it may be subtracted from the estimated radial height of the satellite to provide an estimate of the instantaneous sea surface height immediately below the satellite. Environmental corrections to remove the effects of atmospheric refraction as well as ocean-atmosphere interaction allow an ocean height signal to be derived which contains static geoid and sea surface topography components as well as dynamic tidal and ocean geostrophic current signatures. To varying accuracies, each of the remaining oceanographic signals may be subtracted to leave residual sea surface height estimates which contain only the gravity field component plus oceanographic and instrument noise. The largest residual error for both ERS-1 and Geosat is that caused by uncertainty in the precise radial height of the satellite at the time of the observation. The effect of this can be reduced in a number of ways, for example by using the more accurately determined TOPEX/Poseidon orbits to correct those of ERS-1. Dual-crossover correction of this kind removes two of the three dominant orbit error components between latitudes 66°N and 66°S (constrained by the orbital pattern of TOPEX/Poseidon) but can also lead to amplification of some geographically and temporally correlated components, *Jolly & Moore* [1995] To remove remaining long wavelength errors, the first along track derivative is used to extract the signal of greatest importance for offshore exploration, i.e. that below a few hundred kilometres in wavelength.

3. THE MARINE GEOID

The largest factor that distorts the geoid from a perfect sphere is the oblate shape of the Earth. In addition, significant long wavelength regional variations exist which may be attributed to geological conditions deep below the surface. Heat generated by the core is transmitted to the surface slowly by immense convection currents of molten rock which help to drive the motion of the continental plates. From the point of view of the gravity field, convection currents produce volumes of hot rising fluid as well as cooler, sinking columns. From the laws of thermodynamics there is a difference in the densities of hot and cool currents which result in large scale differences in the local density of the mantle and hence the gravity field experienced at the surface above.

Floating on the mantle are the continental plates, consisting of two distinct kinds of crust known as the lithosphere: continental crust is 50-100 km in depth and constitutes the bulk of the land area; oceanic crust on the other hand is much thinner, of the order 5-10km in depth. In places such as the Mid-Atlantic Ridge, this crustal layer is being continuously added to as the European and North-American plates slowly drift further apart, widening the Atlantic.

Due in part to its greater thickness, the continental crust often contains different rock types, not only within geographical areas but at different depths, for example through sedimentary deposition. Both of these are associated with density variations which in turn cause distortions to the geoid, although at shorter wavelengths than mantle effects. The topography of the solid crustal layers also produce density fluctuations which influence the geoid, due principally to the difference in density between the fluid of the ocean or atmosphere and that of the underlying rock.

Mapping the short wavelength distortions to the Earth's gravity field is performed using the GRAVSAT suite of programs as an operational service to the offshore oil and gas exploration industry.

4. GRAVSAT GRAVITY ANOMALY DETERMINATION

The mean sea surface closely conforms to the Earth's geoid, the first vertical derivative of which is known as the gravity anomaly, defined by,

$$\Delta g(\mathbf{x}) = -\frac{\partial V(\mathbf{x},0)}{\partial z}$$

where V in the gravitational potential at the point $\boldsymbol{x}$ on the reference ellipsoid. Due to the problems associated with orbit error contamination of the altimeter range measurement, direct calculation of the mean sea surface is inappropriate for the mapping of short wavelength features, *Jolly* [1995]. GRAVSAT analyses are therefore based on a derivative of the methods described by *Sandwell* [1992]. This approach exploits the long wavelength nature of the orbit error and other contaminating signals by evaluating the sea surface slope as measured along track. From the along-track gradients, orthogonal east and north vertical deflection can be derived, denoted by $\eta(\boldsymbol{x})$ and $\xi(\boldsymbol{x})$ respectively. These two quantities are related through Laplace's equation, from which the gravity anomaly can be expressed in terms of east and north vertical deflections, i.e.,

$$\frac{\partial \Delta g}{\partial z} = -g_{\circ}\left[\frac{\partial \eta}{\partial x} + \frac{\partial \xi}{\partial y}\right]$$

By taking the Fourier transform of each of the gridded east and north deflections, the Fourier transform of the gravity anomaly can be expressed as

$$\Delta g(k,0) = \frac{i g_{\circ}}{|\mathbf{k}|}\left[k_x \eta(\mathbf{k}) + k_y \xi(\mathbf{k})\right] \tag{1}$$

To compute gravity anomalies from along-track satellite altimetry, therefore, a regular grid of east and north deflections are constructed. These grids are then fast Fourier transformed into the frequency domain whereupon the result of equation (1) can be evaluated and then inverse Fourier transformed back into the spatial domain. As this method makes use of fast Fourier transforms, it is at risk from aliasing, edge effects and other harmonic contamination, therefore great care must be taking in the choice of filters, windows and sampling strategies which may vary from region to region.

5. SEA-TRUTH VALIDATION OF RESULTS

The validity and usefulness of remotely sensed information can only be assessed by application to real problems and through comparison with in-situ ground truth data. Validation of GRAVSAT processing to produce gravity anomalies has been undertaken using ship survey data supplied by the British Geological Survey over parts of the United Kingdom Continental Shelf. An area of current interest to the offshore exploration industry can be found in the North Western Approaches, illustrated for the West of Shetland area in figure 1.

A small test area to the west of the Outer Hebrides was selected for the ship validation and 16 sections 140km long were taken at 0.1° intervals running North-South through both the gridded ship and satellite data close to the original ship tracks. In addition, a second area running parallel to the continental shelf was selected and a total of ninety-nine parallel sections, each 130km long and 1200m apart were taken running North-South through both the gridded ship survey and the satellite survey data. Figure 2 illustrates one pair of profiles from the Hebridean test area. In all of the sections obtained, the satellite gravity fields were smoother than the ship fields but in all cases there was good general agreement in the magnitude, location and extent of gravity anomaly features. By comparing the mean power spectra of the ship data with the residual sections obtained by subtracting ship and satellite gravity profiles, an indication of the comparative resolution of these datasets may be obtained. These spectra are plotted in figure 3 for the Shetland test area, and figure 4 for the Hebridean test area.

Figure 3 clearly shows good agreement at wavelengths above 22km. Between 14.6km and 22km there is also a significant correlation between the two gravity signals. Below 14.6 km, the data show no correlation. Ship survey data in this area are comprised of tracks which are approximately 10km apart, running North-east to south-west and north-west to south-east, i.e. at 45° to the direction of the gravity sections. The theoretical resolution of the gridded ship 'truth' data is therefore between 14.1km and 20km, depending of the correlation of errors within the survey.

Figure 4 illustrates the resolution of the gridded satellite data when the comparison is made close to the ship survey tracks and along the same direction. From this plot, it is again evident that signal recovery is good above 20km and that there is significant correlation of signal down to around 12km. Between 9 and 12 km, there is some ambiguity regarding the correlation of signals. Below 9km there is no apparent correlation in the ship and satellite measured gravity fields.

These results compare well with the expected limiting resolution imposed by the altimeter footprint which for 5m significant wave height corresponds to a spot size of around 7km. With careful optimisation, such as in this case, the shortest wavelengths a satellite gravity field survey can resolve are defined by the instrument noise, the physical characteristics of the altimeter pulse and the quality of environmental corrections used .

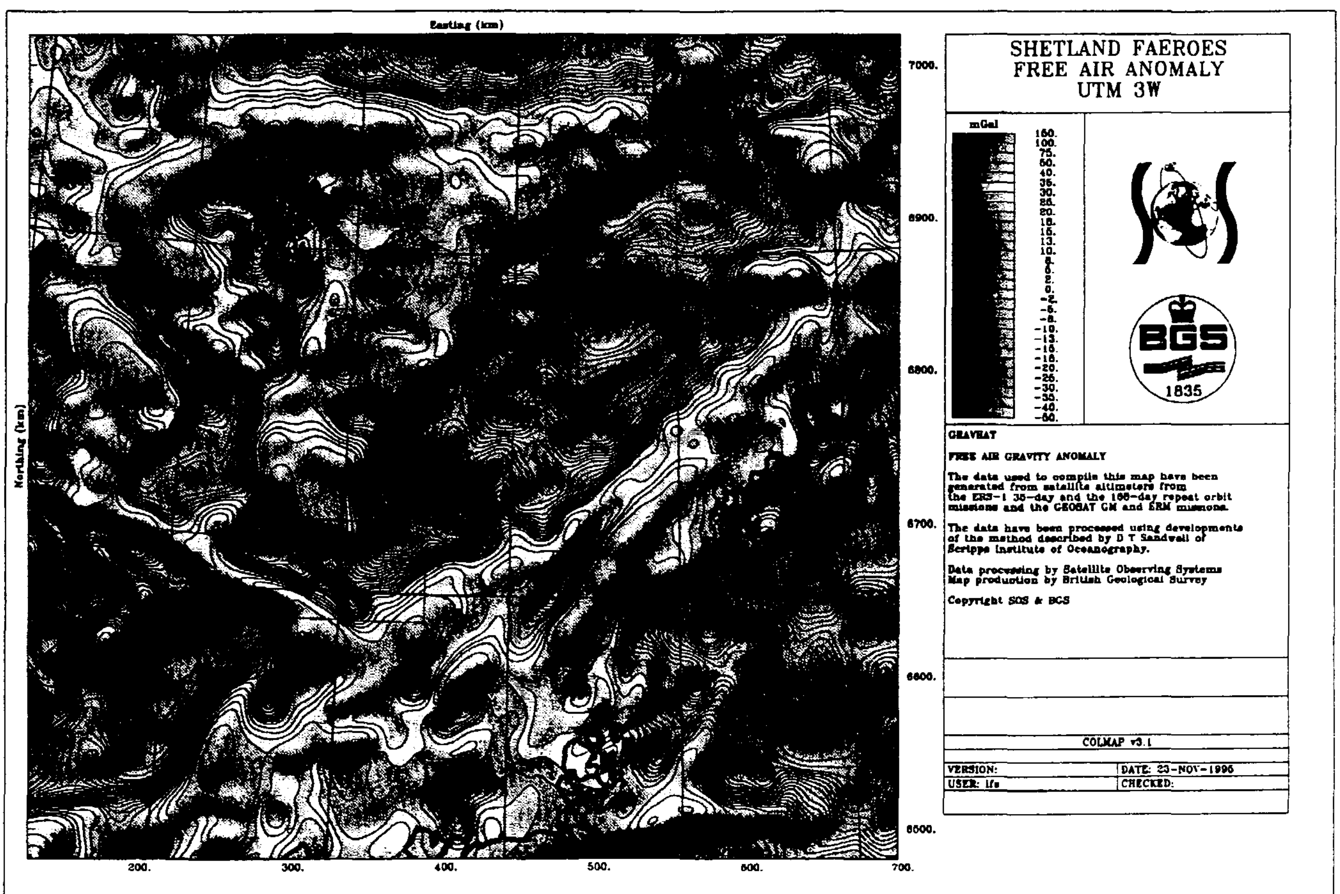

Figure 1. Contour shaded relief map of GRAVSAT Gravity anomalies west of the Shetland Islands.

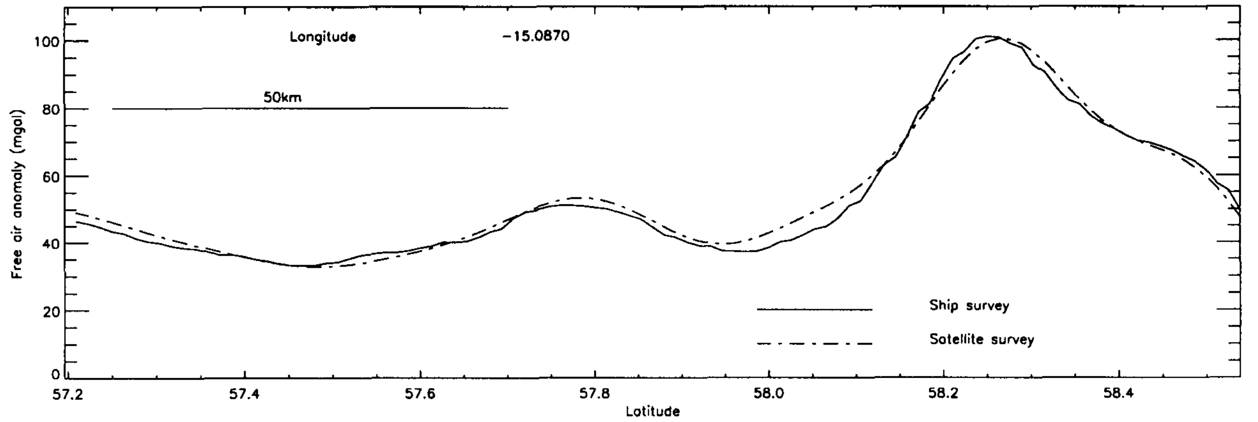

Figure 2. Section through ship and satellite derived free air gravity anomaly data to the North-west of Scotland.

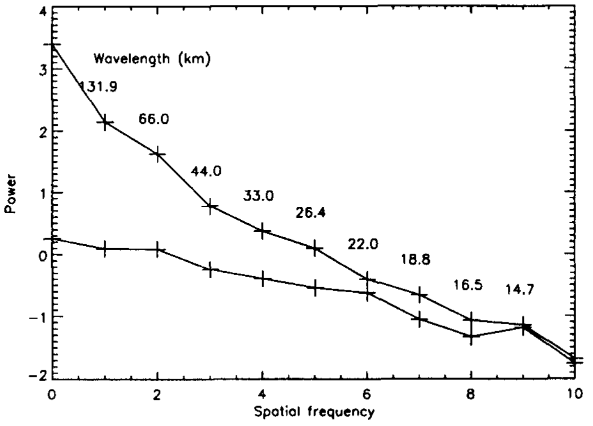

Figure 3. Power spectrum of Ship derived free air gravity anomalies (upper line) and the residual field (lower line) following subtraction of GRAVSAT derived satellite gravity anomalies west of the Shetland Islands (99 slice mean power spectra).

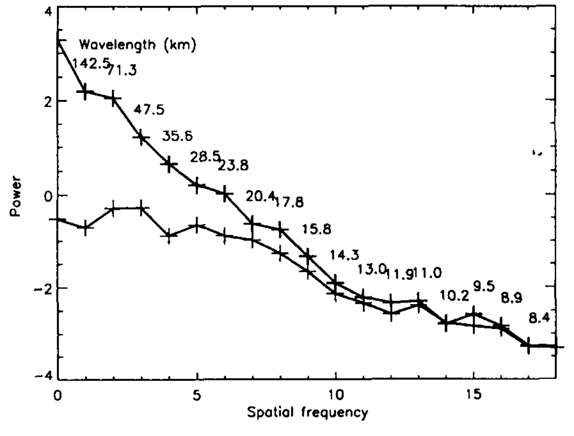

Figure 4. As for figure 3, west of the Hebrides from 16 sections taken close to ship tracks.

6. CONCLUSION

Satellite altimeter data from the ERS-1 and Geosat long repeat missions have finally allowed the derivation of noise limited two dimensional gravity surveys for any offshore area of the world. Previous limitations introduced by the wide separation of ground tracks are no longer the limiting factors. Instead it has been demonstrated that noise in the raw altimetric measurement and its subsequent environmental correction now define the resolution of detailed satellite gravity fields

The requirements of the offshore exploration community for a potential field survey such as that supplied by GRAVSAT are that it provides better than 20km resolution. This paper has described the verification that satellite gravity maps produce a result that is consistent with conventional ship surveyed data, resolving a similar signal down to wavelengths of around 12km.

7. REFERENCES

Jolly, G.W, *Satellite borne radar altimetry - empirical orbit error refinement and Ocean Signal recovery techniques*, PhD Thesis, Aston University, 1995.

Jolly, G.W., and P. Moore, Accuracy assessment of TOPEX/Poseidon dual crossover correction of ERS-1 altimetry, *Adv. Space Res.*, 1995.

Sailor, R. V., *Personal communication*, 1994.

Sandwell, D.T., (1992), Antarctic marine gravity field from high-density satellite altimetry, *Geophys. J. Int.*, **109**, 437-448.

PROJECT GOSAP (PP-USA.1)
GULF OFFSHORE SATELLITE APPLICATIONS PROJECT

E.K. Biegert

The Geosat Committee, Inc. and Shell Exploration and Technology Company
Bellaire Technology Center, 3737 Bellaire Blvd., Houston, Texas 77025 U.S.A.
Tel: (1) 713-245-7140 Fax:(1) 713-245-7850 Internet: biegert@shellUS.com

R.N. Baker
AMOCO Production Company

R.V. Sailor
TASC

K.E. Schaudt
Marathon

I.R. MacDonald
Texas A&M University

B. Tapley and C.K. Shum
The University of Texas

J. Amos
Earth Satellite Corporation

J.L. Berry
Shell Exploration and Technology Company

J. Hess
University of Aberdeen

ABSTRACT

The Gulf Offshore Satellite Applications Project (GOSAP) is being undertaken by members of the petroleum, marine, and environmental industries representing several companies, government agencies, and universities under the auspices of the Geosat Committee with the support of the European Space Agency to determine how best to use remote sensing technology to address offshore problems and operations faced by exploration and marine engineering organizations. The GOSAP team is evaluating the potential for satellite-based offshore exploration, ocean engineering, and environmental applications using combined satellite and airborne measurements constrained by real-time "sea truth."

Our experiments and comparison of observations of natural slicks and related phenomena from ERS-1 SAR data and other satellite imagery to water-column, sea-surface, and sea-floor measurements collected from fixed and mobile platforms in the Gulf of Mexico confirm that ERS-1 SAR imagery is a valuable slick detection tool. GOSAP took this technology from a research status and demonstrates that this technology has definitely moved to a commercial footing.Our experiments in the Gulf of Mexico confirm the utility of ERS-1 altimeter data for observing the gravity field, eddies, and ocean currents. Our regular use of the data in making business decisions demonstrates that it is also in a commercial status. The availability of ERS-1 altimetry was largely responsible for prompting the U.S. government to release classified satellite altimetry data.

GOSAP participants are determining if ERS-1 satellite imagery and altimetry can be used to properly define eddy current regimes in a real-time cost-effective basis and are developing a method to disseminate data products. The Gulf of Mexico has unique current regimes: the Loop Current and the eddies that are shed as vortices from it. Precise definition of spatial extent and magnitudes of eddy currents is lacking, but satellites have the potential to resolve these issues. ERS-1 SAR and Landsat TM imagery are combined with infra-red satellite data (limited by cloud cover and seasonal water surface temperature differences), deployment of current measurement devices, shipboard Acoustic Doppler Current Profiler, and underwater cables,

This pilot project has seen the successful transfer of technology and applications from a pure research stage to commercial viability. Within GOSAP, we are fortunate to have participants encompassing research organizations, sophisticated users of ERS-1 data, and value-adding companies who have worked together to define problems, implement solutions, and develop commercial products.

COMMERCIALIZATION

GOSAP is a highly successful project that has taken its applications from concept and turned them into commercial ventures. Its participants form a productive mix of industry, government, and academic organizations involving researchers, developers, and end-users in a synergistic consortium. We involve the end-user directly in basic research and in product development, shortening the application commercialization cycle.

GOSAP was crucial in demonstrating to the exploration industry the utility of ERS-1 SAR data. It allowed them to evaluate the data and technology in a cooperative research environment within which value-adding companies developed and provided commercial products tailored for the users' needs.

Participants joined GOSAP for various reasons, but all participated directly in the work and contributed data, staff time, and other resources, such as instrumented rigs, buoys, ships, submarines, helicopters, and aircraft for sea truthing activities. Listen to what some of our participants said were the reasons they joined GOSAP:

" a perfect partnership,"
"to leverage our research budget,"
"65:1 rate of return,"
"to participate in a technical exchange,"
"provided important information for in-field verification,"
"to monitor the competition,"
"to obtain SAR data,"
"to get access to ERS-1 data,"
"unique opportunity for a small company to gain exposure."

Over the four years GOSAP has been active, we estimate that **members** have invested over **$13 million** in direct project costs (staff and purchase of imagery) and in the applications resulting from GOSAP. These estimates do not include grants and in-kind contributions such as surface vessels, aircraft, helicopters, buoys, and other sea-truthing efforts.

GOSAP Business Impact		
Applications		*4-year Total*
Satellite Gravity		**$1.5 MM**
Slick Detection	**Imagery**	**$6 MM**
	Staff	**$5.6 MM**

In addition, the project has enabled several graduate students to become involved with research and has led to the awarding of graduate degrees from three universities. Before the project is complete, we expect to have several additional degree candidates complete their work.

GOSAP Academic Impact		
Degree	*Awarded*	*Additional Expected*
Master	3	2
PhD	2	2

GOSAP participants have actively published their results, including graduate student dissertations, peer-reviewed scientific publications, internal corporate reports, reviews in "trade journals," and presentations at meetings of professional societies.

Business Implications

GOSAP participants are using the technologies developed and demonstrated in our project, are purchasing ERS-1 data for their own use, and are purchasing value-added services and products developed by members.

Within the exploration community, satellite gravity and slick detection technology are used in risk-reducing roles that translate directly into economic benefits. GOSAP members actively employ both technologies in their exploration ventures, each of which is usually a multi-million dollar venture:

GOSAP Exploration Impact	
Technology	*Plays / Year*
Satellite Gravity	**20**
Slick Detection	**30**

Satellite gravity still lacks the resolution (4-5 mGals at 20-30 km) to replace marine gravity (0.1 mGal at 500 m), but in many frontier areas it is the only gravity available with adequate areal coverage. Consequently, it is increasingly being used in regional studies. GOSAP member company EDCON offers a commercial service producing customized gravity maps incorporating satellite gravity.

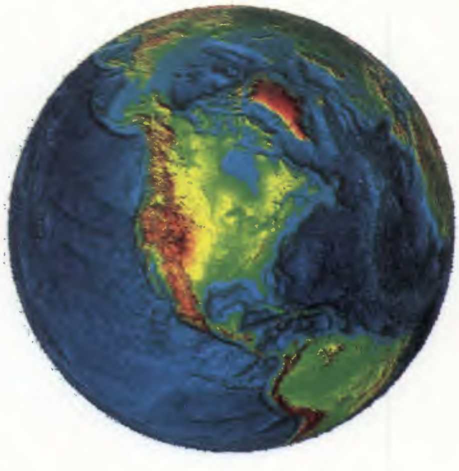

Satellite Gravity Map of the Earth courtesy Dave Sandwell

As an exploration tool, the remote identification of hydrocarbon seeps is particularly useful to geologists responsible for large or frontier regions. General models describing seepage from source to surface must consider mechanisms for migration, geometry and density of migration channels (faults, fractures, and preferential directions of permeability and porosity), barriers to migration, either physical or chemical, and ultimate expulsion at the sea floor or land surface, followed by degradation and dispersion. GOSAP member company

Earth Satellite Corporation offers a commercial slick detection service.

PROJECT SUMMARY

The Gulf Offshore Satellite Applications Project (GOSAP) was initiated in 1991 by a cooperative agreement between the Geosat Committee, Inc. and the European Space Agency (ESA). The project is a multi-organizational cooperative research effort to determine how best to use remote sensing technology to address offshore problems faced by the exploration and marine engineering industries.

Remotely sensed data integrated with "sea truth" are used to quantify meteorologic and oceanographic events, to detect and track ocean currents and gyres, to image the seafloor, to map subsurface geology, or to detect oil seeps and slicks from orbital altitudes.

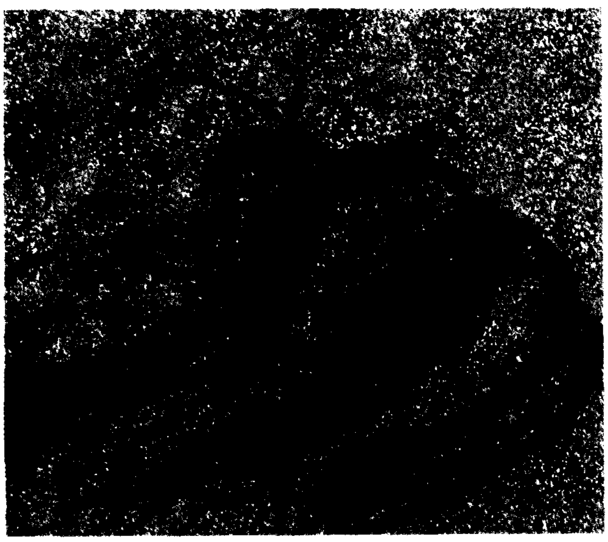

SCIENTIFIC ACHIEVEMENTS

Beginning in the Fall of 1992 the European Space Agency acquired ERS-1 SAR imagery for GOSAP over the Santa Barbara and Gulf of Mexico test sites. In coordination with the Gulf of Mexico overflights, a very comprehensive program of sea truth was conducted by various agencies, ranging from sea bottom submarine observations, sea surface sampling from ships and platforms, aircraft overflights, and imagery from several satellites.

Processing of SAR, Landsat, and SPOT data by GOSAP members resulted in excellent images of oil slicks at both test sites. Sea, air, and spaceborne measurements were correlated to determine optimum procedures for detecting and monitoring oil in marine environments.

A notable achievement for GOSAP was the first "top down" seep detection. GOSAP participants worked closely with ESA officials, the ERS-1 Order Desk, the Canadian Center for Remote Sensing, and Radarsat International to obtain a quick release of ERS-1 images shortly after they were acquired. Earthsat analyzed the SAR images, located the slick sources, and directed the waiting surface vessel to the observed slick. Once on station, the crew collected surface samples and launched a special deep diving submarine to visit the most active seep sites and pinpoint seepage locations on the seafloor. Benthic communities were observed, geochemical samples were acquired, oceanographic measurements were made, and seep rates were determined by placing special collecting devices over the active seep.

In the summer of 1995 a repeat of this exercise was attempted. A surface vessel and submarine revisited the seep location seep location and collected samples in coordination with an ERS-1 overflight. Unfortunately, the Canadian receiving station was unable to acquire the SAR image due to power loss in a thunderstorm.

RADARSAT APPLICATIONS

GOSAP members continue to be interested in working together to advance our understanding of seeps, slicks, and their detection by spaceborne radar instruments. Our follow-on project to evaluate RADARSAT SAR data was 1 of 60 selected from a field of 133 proposals. In this new undertaking, we will expand our areas of interest to include cold water sites and will focus on increasing our ability to predict and use the shapes (morphology) of slicks and their interaction with winds and currents.

Geosat®

THE GEOSAT COMMITTEE

The Geosat Committee provides a unique forum and network contacts within the commercial sector of the remote sensing user industry. It conducts special cooperative research projects among members and with government and academic institutions when advantageous to the membership.

The Geosat committee facilitates access and availability of aerospace and airborne earth observation data for members worldwide.

The Geosat Committee provides a collective voice on members' developing needs to suppliers of satellites, aerospace and airborne earth observation data, and related technologies so that suppliers may provide data and services appropriate to members' requirements.

ACKNOWLEDGMENTS

We give special thanks to Lisa McArthur, Geosat Administrator, and also to F.B. Henderson III, former President of Geosat who initiated GOSAP. The European Space Agency provided ERS-1 data and published several brochures containing our material. Use of the submarine Johnson *Sea-Link* was partially funded by the University of North Carolina at Wilmington National Undersea Research Center. Some of the slick commercialization efforts and research was funded by NASA EOCAP Program contract number NAS3-444 to Earth Satellite Corporation.

Oil Slick Detection

Ralph N. Baker (Amoco)

John Amos	**Earthsat**
John Berry	**Shell**
Ed Biegert	**Shell**
Jim Brooks	**Texas A&M**
Dave Buthman	**Unocal**
Scott Hill	**Chevron**
Ian MacDonald	**Texas A&M**
John McKeon	**Arco**
Roger Mitchell	**Earthsat**
Thomas Parr	**Tasc**
Jonathan Pershouse	**Mobil**
Peter Price	**Marathon**
Jim Reilly	**Enserch (Astronaut)**
D. Smith	**ONR**

Satellite Oceanography

Develop methods for eddy detection

Ken Schaudt (Marathon)
George Forristall (Shell)

Doug Biggs	**Texas A&M**
Jared Black	**Unocal**
Mavis Driscoll	**TASC**
Ian MacDonald	**Texas A&M**
Thomas Mitchell	**Texaco**
Joseph Sandlin	**CWI Airways**
David Sheres	**U. S. Mississippi**
C.K. Shum	**U. Texas-CSR**
Byron Tapley	**U. Texas-CSR**
Jim White	**TASC**

Satellite Gravity

Develop and compare satellite gravity maps

Richard Sailor (TASC)
C.K. Shum (UT-CSR)

Ed Biegert	**Shell**
Bob Borger	**Mobil**
Alan Herring	**EDCON**
Ron Phair	**Texaco**
Byron Tapley	**Univ. of Texas - CSR**

wth contributions from:

David Sandwell	**ScrippsInstitute**
Bill Haxby	**LaMont-Doherty**
Dick Rapp	**Ohio State University**

OFFSHORE BASIN SCREENING™ FROM ERS SATELLITE

Nigel Press and Geoff Lawrence*

Nigel Press Associates Limited, Edenbridge, Kent, TN8 6HS, UK and *TREIC° Limited, Knebworth, Hertfordshire, SG3 6DB, UK

Tel: +44 1732 865023. Fax: +44 1732 866521 Email: info@npa.co.uk

Abstract

This is a brief description of a new, low-cost, remote sensing technique that helps offshore oil explorers focus activity and prioritise expenditure. The technique is based on systematic analysis of satellite radar and integrating the results with gravity data derived from satellite altimetry, and with other geological information.

Introduction

Oil explorers use seismic surveying to map sub-surface structures that might have oil; it is expensive, the average cost of a conventional seismic survey is US$3500 per km^2. Now, ERS products can be integrated with geological information to provide new information to oil explorers offshore that saves time and money by prioritising seismic expenditure and focuses on the most prospective basins. This Offshore Basin Screening™ service provides gravity maps, derived from satellite-based altimeter measurements, that represent the sub-surface geological structure beneath the sea, combined with a map of sea-surface slicks, resulting from natural oil seepage, analysed from satellite radar pictures.

The major risk in exploration is whether a particular sedimentary basin will have a source of hydrocarbon. Onshore, oil explorers map surface seepage of oil or gas as clues to the presence of buried hydrocarbon source. Offshore, there was no generally available low-cost method to identify these seepage clues until our team, led by NPA Limited, developed the Offshore Basin Screening™ method. The ERS radar can, at times of low to moderate wind speed, systematically detect slicks over vast swaths of ocean, whatever the cloud or light conditions. During a two-year demonstration programme at NPA Limited, supported by the UK Government's British National Space Centre and the oil industry (who provided the validating data vital to our ability to develop the integrated methodology) we established rules to categorise the diverse slicks observed on radar pictures. As a result, we are able to characterise slicks originating from sea-floor natural oil seepage. Concurrently, we processed altimetry from ERS and other satellites to produce the most detailed satellite marine gravity maps yet available and developed modelling techniques to analyse these data.

Radar data for slick mapping

We analyse several satellite radar images per scene footprint, because the sea is dynamic and varies with even slight changes of wind, tide and current, and to test the repetition of slicks, Because of the overlap of satellite tracks, two scenes from the same footprint can result in 6-times repeat cover in parts.

Slicks form only within a narrow wind-speed envelope. The SAR images are acquired only for dates that have low wind speeds within this envelope. The precise wind envelope has been established through controlled tests during the central Mediterranean Demonstration Project and confirmed in other areas. For radar images acquired on dates for which the wind is appropriate (we select these by comparing radar data archives and a wide range of hindcast weather data and models) we are confident that all slicks above 150 m long are being detected on ERS and simulated-Radarsat SAR images.

Discriminating seepage-slicks

Slicks are distinct regions of low or no backscatter on the radar image and therefore appear black or dark on radar images. These result from a reduced or null return of the incident satellite radar signal (which views the ocean through cloud and night) because the radar is reflected away from the sensor by a flat part of the ocean. The flatness originates partly by damping of surface capillary waves by oil and oil-like material but radar does not detect oil directly. The radar detects the decrease in backscatter resulting from the damping of waves and the amount of damping varies with the slick's physical properties, particularly the visco-elastic properties.

Up to November 1995, we have analysed 1000 satellite SAR images acquired on dates with appropriate wind-speed, covering several million km^2 of ocean from the UK and Irish Continental Shelves, mainland Europe Continental Shelves, Caribbean, Gulf of Mexico, Adriatic, Mediterranean, Falklands Shelf and several areas offshore Southeast Asia and South America. Slicks from 100 m to tens of km long are mapped in all regions tested, ranging from water depths of 20 m to 1000 m, sea surface temperatures from 7° to 29°, varying salinity and on seas with strong persistent currents to no currents. We are confident that our demonstration programme has established for the oil industry that slicks can be mapped routinely and reliably on satellite radar for an acceptably low cost (<50¢ per km^2) and that the slicks originating in natural oil seepage can be discriminated from other slicks. However, our demonstrations show that **only a very few slicks have a seepage origin and** that seep-slicks are discriminated only by applying, systematically and objectively, empirical rules derived from an extensive knowledge database. These rules were established during our demonstrations and by observing slick behaviour around the globe.

Slicks vary in size, shape, orientation in relation to waves, currents and wind and in thickness. Most seep-slicks are sub-micron thickness: typically sheens and iridescent films around 0.05µm. These thin slicks are observed to respond to wind and current differently than the thicker oil-containing slicks resulting from pollution or the ultra-thin natural film slicks that occur extensively world-wide. We have developed special processing algorithms to handle the full-resolution SAR data and analyse the slick behaviour and context.

Slick types

Seven categories of slick were identified in the original controlled demonstrations and five categories are used in operational surveys by applying the empirical rules.

Seep-slicks are not confused with freshly dumped pollution slicks. Pollution slicks resulting from the illegal dumping of oil from ships are thicker than seep-slicks, and therefore respond to wind, which often blows the edge of a slick, downwind, into "feather-edge" streaking. Freshly polluted oil follows the wake of the ship and therefore the oil slick retains a characteristic linear shape for the 7 to 10 days they exist on the surface before breaking up and sinking.

The bulk of the slicks mapped on radar images acquired at the appropriate wind-speed envelope are formed from a natural film that has nothing to do with oil. This natural film, composed of organic molecules originating in the decay of plankton and algae, is extensive, forming a molecule (a few ångstroms thick) or so thick boundary to the sea. It slicks in response to differential wind shear, compression by waves, especially internal waves and by differential current movement and boundaries. The natural film often forms up to 90% and more of the total slicks on wind-compliant radar scenes.

Pattern of slick distribution

Our experience and that from the oil industry for onshore seeps, is that individual seeps are only infrequently attributable to individual hydrocarbon accumulations. The position of slicks on ERS images is known to within 300 m and can be visited by boat and sampled in order to type the source if required. This has been done successfully by companies participating in our demonstrations. Sampling only the top micron of the surface and analysing the strongly hydrolysed sample requires special techniques. Observations show that the horizontal displacement of seep-slicks from their sea-floor vent is probably no more than twice the depth of water, and is unlikely, therefore to be more than 2 km from their submarine source.

The significance of the seep-slick distribution is established only by correlation with sub-surface geological features or seismic data. In the shallow Mediterranean we demonstrated a close relationship of the pattern of seep-slicks and the principal hydrocarbon source kitchens, those sub-surface regions in which sediments with source rock have been buried deep enough to generate oil or gas. 78% of seep-slicks in the Mediterranean demonstration are vertically above source-kitchens. Although one-for-one relationship of seep and oil accumulation is unlikely, explorers expect to see a coincidence of accumulations and seeps, even though the experience of onshore demonstrates that seeps are rarely traced to accumulations. In the Mediterranean demonstration a third of the seep-slicks are within one or two km from a position vertically above one of ten hydrocarbon accumulations containing oil, condensate and gas and oil with a range of API values.

Most seep-slicks are close to the pathway for the seepage, normally faults, especially those bounding sedimentary basins. The Porcupine Basin off western Ireland is a good example of this. Seep-slicks are concentrated along the bounding faults of the Porcupine Basin, which is clearly defined by the satellite gravity. Some of the seep-slicks of Porcupine correspond closely to sea-floor seep features (carbonate knolls resulting from the oxidation of seeping hydrocarbon) that represent the sites of the submarine hydrocarbon seepage source of the seep-slicks.

Satellite gravity

We have also developed methods to compute gravity from satellite radar altimeters. In order to achieve the best across-track resolution, we have merged the multiple-repeat tracks of ERS-1 35-day cycle plus the dense single tracks of the 168-day cycle with altimetry from two previous satellites (Seasat and Geosat) and the current TOPEX/Poseidon satellite as control. Excellent understanding of regional geological structure results from the interpretation of this gravity data, which has been used to infill and link ship-borne gravity surveys.

We have found that ERS-1 can resolve along track features of about 15 km wide. Across track resolution depends on the separation of the altimeter tracks. The 35-day phase ERS-1 tracks are separated by about 80 km at the equator, only marginally better than previous satellites, but the track separation for the 168-day phase data is about 16 km and 8 km when the second 168-day geodetic phase is incorporated. This has resulted in across-track separation as little as 2 km at UK latitudes. Processing altimetry from five satellite missions imposes a huge burden on computer resources but has proved to be a significant step in producing results comparable to ship-borne gravity at a fraction of the cost. In several areas off north-west Britain and offshore South East Asia we have been able to show that regional patterns found in these new satellite data are exactly the same as those produced at much greater expense and effort by ship-borne surveys.

The main benefit of the satellite gravity is its comprehensive and systematic global coverage. We have developed methods to merge the satellite data with ship-borne and land gravity, both public domain and proprietary oil company data, which has better resolution of smaller local geological features, and can be used to control and enhance the satellite data.

Acknowledgements

The Offshore Basin Screening™ product and service resulted from a development programme supported by funds from the UK Government's British National Space Centre. The development was undertaken by Richard Chiles, Mark Holliday, Paul Karwinskii, Nigel Press and Ross Smail of Nigel Press Associates Limited, Edenbridge, Kent, UK, Geoff Lawrence of TREIC^{O}L, Knebworth, Herts., UK, Trevor Macklin and Tony Rye of GEC-Marconi Research Centre, Great Baddow, Essex, UK and John Milsom and Robert Holt of the Department of Geological Sciences of the University College London, UK.

Second ERS Applications Workshop (London, 6 - 8 December 1995)

Detection of sea bottom topography with ERS SAR PRI images on the Belgian continental platform by analysing the sea surface characteristics caused by the meteo-marine conditions on the sea bottom morphology on the moment of satellite passage.

Vande Velde Linde, Jaspar Annick. & Vernemmen Carlos.
Research Unit Marine and Coastal Geomorphology, Department Geography,
University of Gent, Belgium
Tel: (31)9-2644636 Fax: (31)9-2644970

ABSTRACT

Until now bathymetrical maps are created by means of digital depth measurements from echosounders or multibeam equipment. The invested energy and money are enormous.
A new methodology to perform actual bathymetrical maps using ERS-1 SAR images is evaluated. This method is based on the relationship between the sea surface characteristics (roughness differences and patterns) derived from the ERS-1 images and the seafloor morphology (sandbanks and gullies). An analysis of the influence of the combinated action of parameters such as currents, tides, morphology of the seabottom and the effect of meteo-marine conditions on the sea surface is the basis of this research.
The relations (expressed in distances) between the sea surface characteristics (rough and smooth sea surfaces and their boundary lines), detected on the ERS-1 SAR images recorded during different meteo-marine conditions, and the underlying crestlines of the sandbanks are tabulated.

DESCRIPTION OF THE RESEARCH AREA

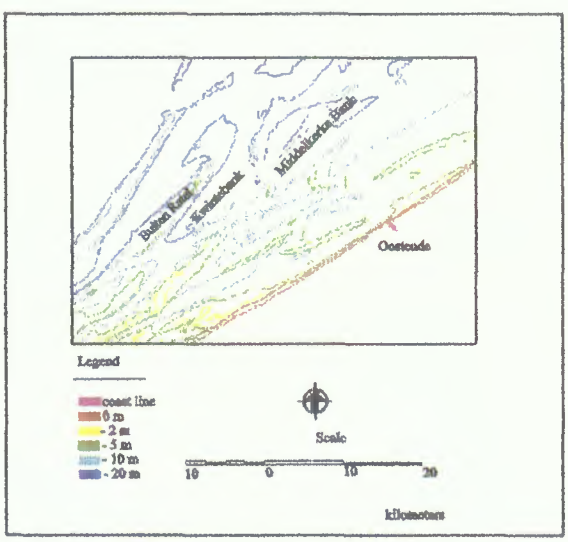

Figure 1: Location research area

The research area covers the Flemish banks offshore the Belgian coast. These are a group of parallel sand banks with a SW-NE direction and slightly oblique to the sandy macrotidal coast (figure 1). The banks are separated by swales dipping to the NE and are generally not deeper than 30 m below mean spring low water level. The banks are about 20-30 km in length, 1 - 2 km in width and 10 - 20 m high. In some parts of the banks, the crest zone rises to less than 4 m below spring low water level. The cross sections of the banks are asymmetric (Figure 2:. track rG19, rG21, rG23), the NW slope is over the whole bank steeper than the SE slope. The slope angles vary between 1.7° and 1.9° for the NNW slope and 0.5° on the SE slope. Two sandbanks are used in this investigation, the Middelkerke Bank and the Kwintebank.

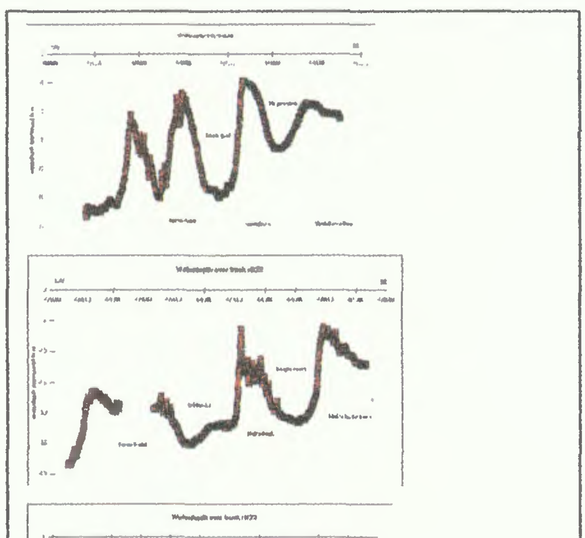

Figure 2: Cross sections of the Flemish Banks

MARINE DATA

In order to analyse as accurately as possible the ERS-1 SAR.PRI images in relation to the underlying bottom topography, ten field campaigns on board of the vessel "Belgica" were carried out on dates, as close as possible to the registration date of the ERS-1 images in order to monitor the bathymetric and meteo-marine characteristics.
During these campaigns, following data are recorded every time over the same reference tracks, perpendicular to the length axis of the banks and the gullies: waterdepth in m below the water level (frequency: 2/sec), sea water temperature, sea water salinity, chlorophyll-a (6 seconds), as well as the meteo-marine conditions (10 minutes).
The water depth recordings are corrected first for the movements of the ships caused by waves and secondly for the tidal influences by using tidal curves. Interpolation between the corrected data over the sailed tracks forms the basis for isobaths and surface maps.

We also considered whether optical images could provide indirect or direct information about the bathymetry. The direct visual detection of the sandbanks in the North Sea on the optical images is impossible because of the high sediment load of the sea water. On the other hand, seawater temperature, salinity and chlorophyll-a changes are detectable on optical images and could serve as valuable proxy data. This is why the relation between these parameters and the bathymetry was studied. Eventual correlation between these oceanographical data and the bathymetry, derived from in situ measurements, would provide indirect bathymetrical information from optical images. However , no satisfactory correlations were found.

The current data used for the interpretation of the characteristics observed on the ERS-1 images are provided by the current atlas.
Meteo data, e.g. wind speed and direction, were obtained from the KMI for images recorded but not covered by a Belgica campaign.
In order to create maps of the observed sea surface phenomena in relation to the underlying bottom topography during the different meteo marine conditions, additional to the digital data recordings, visual observations of the sea surface, were carried out. Special attention was paid to the sea surface roughness differences and boundary lines. An inventory of their characteristics was made. Positions were recorded digitally and analogously.

ERS-1 DATA

The ten ERS-1 SAR.PRI images used, were processed during very different meteo-marine conditions. The raw data were calibrated into σ_0-values with an original program (Vande Velde L. et all, 1995). After calibration, a rectification was applied by means of ground control points situated on the Belgian coastline. Speckle was reduced by means of a median 7 by 7 filter.
Following 3 remarkable structures could be distinguished over the sea surface after application of three classification methods: rough sea surface areas (white), smooth sea surface areas (black) and intermediate roughness areas.

COMPARISON OF THE MEASURED DATA IN SITU AND THE ERS-1 IMAGES

A first step consists in the superimposition of the visually observed boundary lines between the smooth and the rough sea surface detected on the ERS-1 images, marking the crestlines on two cross-sections through the banks and the gullies (figure 3), one for the northern part of the bank and one for the southern part.
The 3 general structures and the boundary lines observed on the images are orientated in the same direction as the crestlines of the banks (SW-NE). But their location related to the underlying crestlines, is different on most of the images.

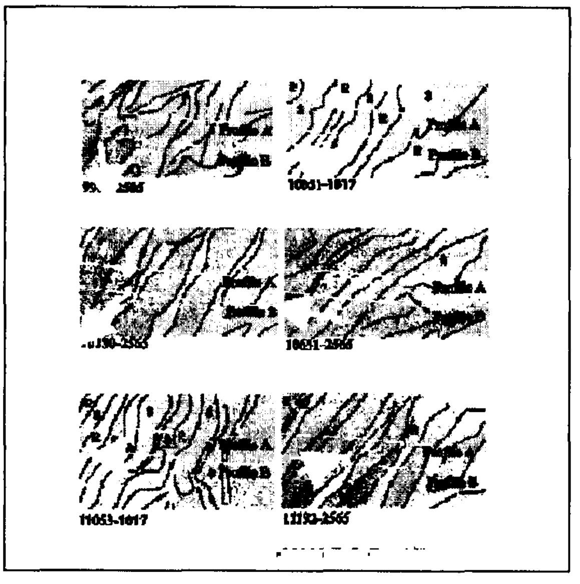

Figure 3: Visually observed boundary lines on the ERS-1 images.

QUALITATIVE ANALYSIS AND HYPOTHETICAL HYDRODYNAMIC PROCESSES.

Three hypothetical hydrodynamic processes are proposed based on a first visual evaluation. They are function of the meteo-marine parameters (especially the current direction) and are conditioned by the sea bottom morphology.

Hydrodynamic process 1 (figure 4). The currents move from the range NNW-SSW at high speed, while the watermass is flowing towards the steep tilted flanks of the banks. Due to the high speed and the steepness of the flank (1.7° - 1.9°), a part of the watermass is flowing back westwards of the crestline. This reflux generates a foamline west of the crestline. The sea surface between the crestline and the superficial breakline is rough.

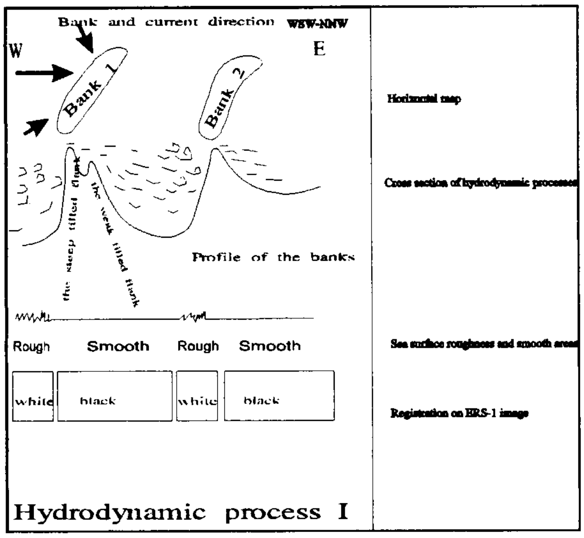

Figure 4: Hypothetical hydrodynamic process 1

Hydrodynamical process 2 (figure 5). The watermass comes from the NNW-NE sector or the SSW-WSW sector. The currents flow parallel to the longitudinal axis of the sandbanks and the current speed is low. The process can be divided in two parts depending on which side of the flanks the watermass is flowing.

In the first case, the current flows parallel to the crestline of the bank but with an inclination towards the most inclined slope. The watermass flows to the most inclined slope and because of this obstacle, a foamline occurs west of the bank. Another part of the watermass flows over the crestline and due to the volumetric changes (from a low volume into a large volume), the high current speed changes into a low current speed. This causes at the boundary just between both areas a foamline east of the crestline. The sea surface is rough west of this boundary line and smooth to the east.

In the second case, the current is parallel to the longitudinal axis but with an inclination towards the weakly inclined slope of the bank. The currents flow from the NNE-ENE sector and the SSE-SSW sector towards the weakly inclined slope. Due to the volumetric changes between the areas east and west of the crestline a foamline occurs west of the crestline.

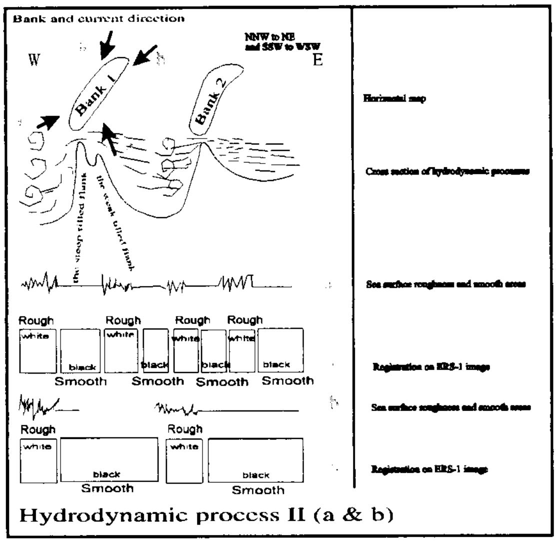

Figure 5: Hypothetical hydrodynamic process 2

Hydrodynamic process 3 (figure 6). The watermass flows from the ENE-SSE sector which is perpendicular to the weakly inclined slope of the bank. The watermass can flow over this slope and a foamline occurs west of the bank, due to the volumetric changes.

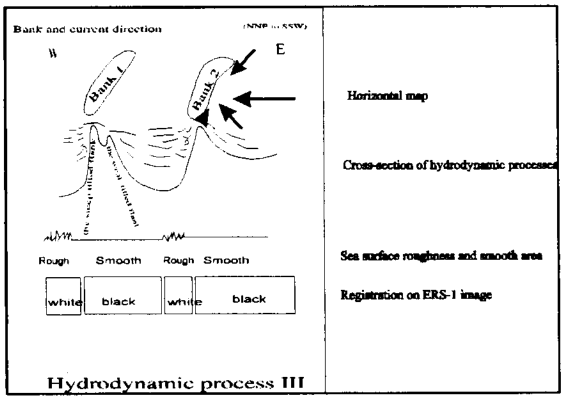

Figure 6: Hypothetical hydrodynamic process 3

QUANTITATIVE ANALYSIS

The hypothesis is tested by means of a qualitative analysis.

The waterdepth values and the corresponding σ_0 values are plotted in a cross-section for each track sailed and for all the ERS-1 images (figure 7). The waterdepth values are taken from the campaigns as close as possible to the satellite images recording dates.

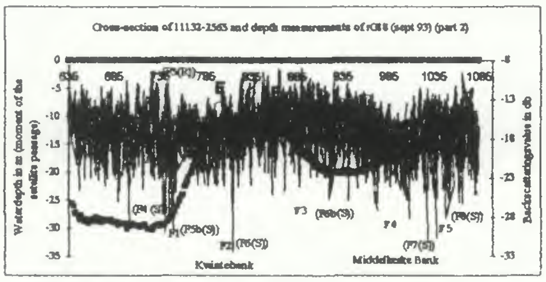

Figure 7: Cross section of the sigma-naught and the waterdepth values

The σ_0 values oscillate between - 8 db and -23 db. Extreme maximum and minimum values can be observed (figure 7). The positions of these extreme values and their interpolation lead to the appearance of lines located parallel to the crestlines of the banks (figure 8).

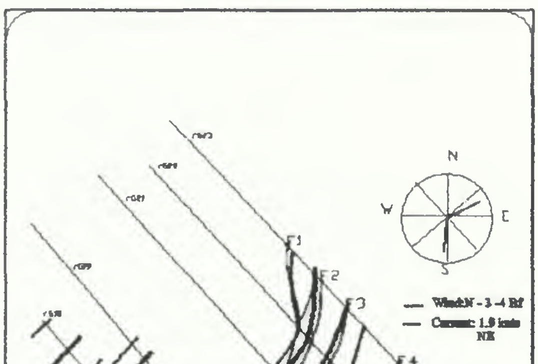

Figure 8: Positions of the extreme backscatteringvalues

By application of a median filter 7 by 7 on the σ_0 -values, it is clear that the extreme points correspond to the boundary line between the rough and the smooth sea surfaces. Depending on the positions of extreme values, rough and smooth boundary lines can be distinguished. By superimposing the boundary lines obtained for each image over the crest and base lines of the banks, it is obvious that the position of these lines changes from image to image depending on the meteo-marine conditions during the recordings.

The processing of the cross sections into maps with extreme backscattering values results also into relational tables where the distances of each extreme backscattering value against the most westwards crestline of a bank is given, for each track and that is elaborated for each image. A mean value of the extreme points of one boundary line is calculated in order to obtain a mean distance of each boundary line according to the highest crestline of the bank. These distance values are summarised in figure 9 which gives all the mean distances of the detected boundary lines for each image. The meteo-marine conditions during the moment of the recording of the image are also added.

	9901-256 (07/06/93) 2h05 before HW (FT)	10051-1017 (17/06/93) 1h17 before HW (FT)	10130-2565 (23/06/93) 3 h before HW (FT)
Winddirection, Current direction, Kwintebank, Middelkerke Bank, Route	2-3 Bf, 0.9 knt	2-3 Bf, 1.1 knts	0.[illegible] knt, 3-4 Bf
F1	180.6 m A=13.7	409.6 m A=14.1	294 m A=11.4
F2	41.6 m A=12.9	300.6 m A=15.4	82.2 m A=12.6
F3	273.6 m A=14.05	806.6 m A=14.7	819.4 m A=11.8
F4	470.9 m A=13.4	1235.3 m A=13.5	1789.1 m A=14.6
F5	929 m A=14.9	795.2 m A=10.6	404.4 m A=12.8
F6	727.1 m A=14.3	217 m A=11.6	99.4 m A=14.6
F7	146.7 m A=13.4	1010.7 m A=15.1	257.3 m A=14.3
F8	703.5 m A=13.6		707.2 m A=15.2

Figure 9: Part of the "distance - superficial boundary line - underlying crestline - table"

VERIFICATION OF THE HYPOTHESES BY MEANS OF CLASSIFYING THE ERS-1 IMAGES

The 14 ERS-1 images are grouped into 4 classes (and subclasses) depending on the meteo-marine conditions (especially current direction) during the image recording (figure 10).

Class 1 consists of all images where the current direction is perpendicular to the steep tilted flank of the bank and comes from the WSW-NNW

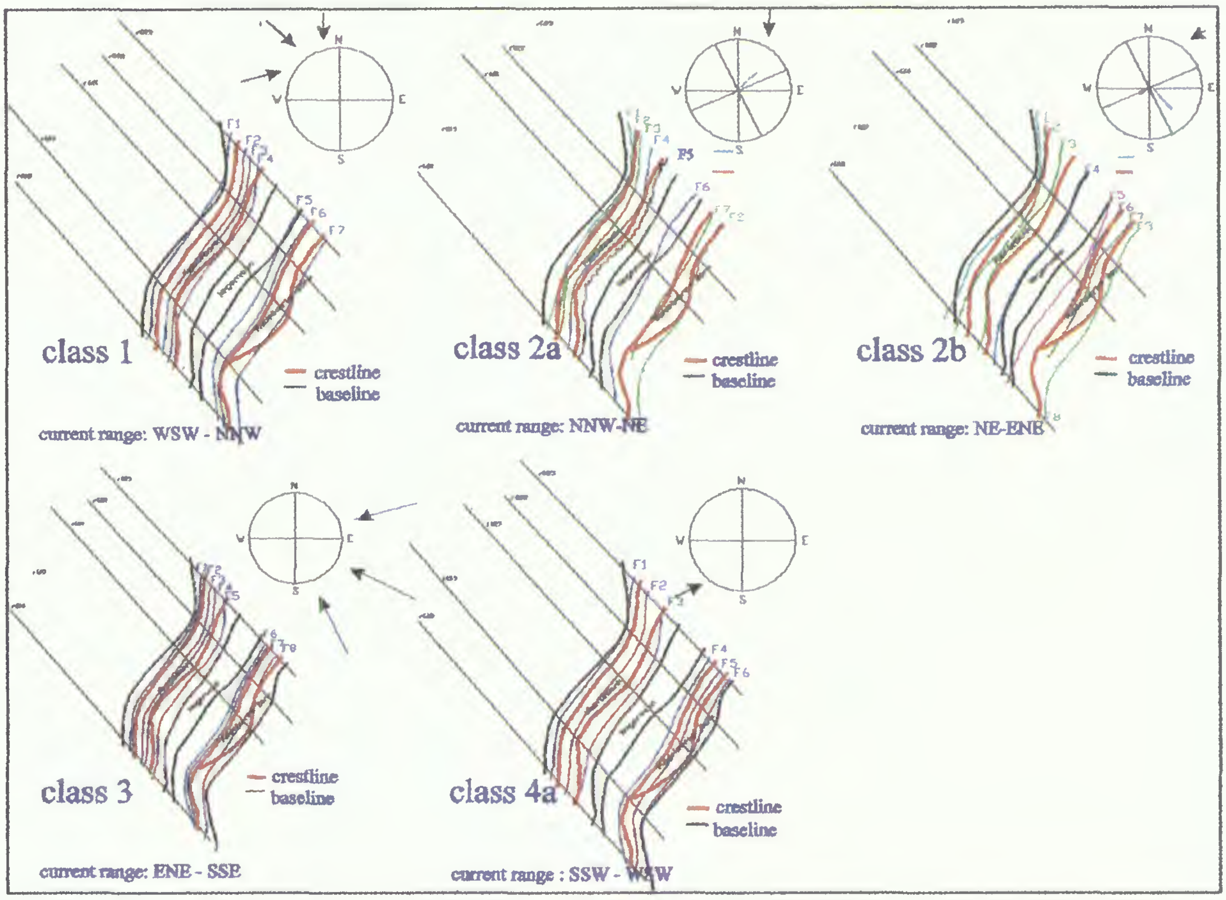

Figure 10: The 4 classes of the ERS-1 images , depending on the current direction on the moment of the image registration

sector. Class 2a includes all images where the current is coming from the NNW-NE sector while class 2b groups all images where the current is coming from the NE-ENE. Class 3 includes all images were the current range is coming from the ENE-SSE sector. Class 4a groups all images with a current from the SE-WSW sector almost parallel to the axis of the sandbank but with an inclination towards the less gentle inclined slope.

The mean positions of the extreme σ_0 and the deduced boundary lines will be compared with the hypothetical hydrodynamic processes: class 1 will be compared with hypothetical hydrodynamic process 1; class 2a with process 2a; class 2b with process 2b; class 3 with process 3 and class 4a with process 2a. An image recorded during class 4b conditions is not available yet.

Figure 11 summarises the mean distances of the observed boundary lines, according to the crestline located most westwards relative to the bank, on the different images for the proposed classes.

The distance of the boundary lines are expressed against the first (most westwards) crestline of the bank. The number of boundary lines (7) does not correspond with the number of boundary lines as advanced by the hydrodynamical hypotheses.
This is due to the fact that the bank morphology is more complex than the morphology suggested by the hypothesis. It is shown in figure 1 that small linear ridges, also known as sandwaves, are present on top of the sandbank and especially near its north-east edge. These sandwaves with a height of 1 to 3 m, also occur on the sandbank slopes. The top of large dunes have a minimum depth of 6 m. The crestlines of the large dunes can often be traced over several hundreds of meters. The watermass flowing above the sandwaves undergoes the same hydrodynamical process as above the crestline of the bank.

The (a) or (?) in the table means acceptance of or doubt about the correspondence of the location of the boundary lines observed on the images and those proposed by the hydrodynamical processes.

	current range	F1	F2	F3	F4	F5	F6	F7
class 1	WSW-NNW	594 m W of KB (a)	299 m E of KB (a)	702 m E of KB (a)	1213 m E of KB (?)	720 m W of MB (a)	183 m W of MB (a)	951 m E of MB (?)
class 2a	NNW-NE	180 m W of KB (a)	41 m W of KB (a)	273 m E of KB (a)	470 m E of KB (a)	727 m W of MB (a)	147 m E of MB (?)	703 m E of MB (a)
class 2b	NE-ENE	294 m W of KB (a)	82 m W of KB (a)	813 m E of KB (a)	1789 m E of KB (?)	99 m W of MB (a)	201 m E of MB (a)	707 m E of MB (a)
class 3	ENE-SSE	307 m W of KB (a)	84 m W of KB (a)	361 m E of KB (a)	581 m E of KB (a)	1343 m E of KB (?)	379 m W of MB (a)	F7: 207 m W of MB (a) F8: 559 m E of MB (a)
class 4a	SE-WSW	461 m W of KB (a)	511 m E of KB (a)	1427 E of KB (a)	284 W of MB (a)	304 m E of MB (a)	1004 m E of MB (a)	

Figure 11: Mean distances - position boundary lines - position underlying lines for the different classes

INTERPRETATION OF THE OBSERVED SUPERFICIAL LINES DURING THE BELGICA CAMPAIGNS

The observation of superficial lines during the Belgica campaigns lead to the creation of maps where the positions of the lines may be compared with positions of the lines proposed by the hypothetical hydrodynamic processes. During the September 1994 campaign, the 5 observed lines correspond with their proposed hydrodynamical process. For February 1995, 3 of the 5 lines correspond with the proposed locations. Only for June 1995, no strong relationships between the locations of the observed superficial lines and the location of the boundary lines proposed by the hypothetical hydrodynamic processes could be found. These anomalies are to be explained by algae bloom. This causes superficial lines similar to those generated by the hydrodynamical processes.

CONCLUSIONS

Based on the comparison of the results of the qualitative analysis, namely the location of the detectable boundary lines between rough and smooth sea surfaces derived from the ERS-1 images, and the quantitative analysis, we can assert that the limitations of interpretation, caused by the meteo-marine conditions during registrations for the detection of the boundary lines, and which are related to the position of the crestlines, are no longer a restriction for the qualitative analysis. All the radar images, independent of the meteo-marine conditions during the image registration, contain submarine morphological information to be deduced. The location of extreme backscattering values are related to the location of the underlying crestlines of the banks, and this distance relationship depends on the direction of the current present at the moment of the image registration.

It is important to draw the attention on the fact that until now no bathymetric information, absolute waterdepth, can be deduced, but the position of the crestlines can be determined from radar image interpretation. Further analysis should monitor sediment transport paths running over the seabottom in order to provide also decisionmakers with more critical information about sand exploitation, ship routings and dredging operations.

REFERENCES

DE MOOR, G., LANCKNEUS, J., 1993. Sediment mobility and morphodynamics of the Middelkerke Bank. Final Report Mast Project - 0025-C.

VANDE VELDE, L., VERNEMMEN, C., DE MOOR, G., Jaspar , A., 1994. Detection of sea-bottom topography with ERS-1.SAR.PRI images on the Belgian Continental Platform. First workshop on ERS-1Pilot Projects, Toledo, Spain, 22-24 June 1994.

VANDE VELDE , L., JASPAR, A., VERNEMMEN C., 1995. Derivation of the backscattering coefficient σ_0 (this volume).

ACKNOWLEDGEMENTS

The technical assistance during the project by S. Louwye is greatly acknowledged.

Derivation of the backscatteringcoefficient σ_0 in ERS-1 SAR.PRI products with Erdas IMAGINE 8.1 ModelMaker.

Linde Vande Velde , Prof. Dr. C. Vernemmen
Laboratory Physical Geography, Unit for Coastal and Marine Geomorphology, University of Gent, Krijgslaan 281/S8 9000 Gent, Belgium
tel: 31/9/264.46.36 - fax: 31/9/264.49.70 - E-mail:linde@selifa.rug.ac.be
UNIVERSITEIT GENT

The data in SAR.PRI images, as distributed by the different PAF's is expressed in intensity values per pixel. At symposia and in papers, however, there is an increasing demand to express the relationships between the backscatteringvalue σ_0 and the studied phenomena.
In order to cope with this requirement, we have developed a sigma naught program using the IMAGINE ModelMaker Module, to transform the intensity values to decibel values.

I. Theory of the σ_0

The entire program is based on the formulas as developed by Laur (1992). In his work Laur describes the equation to determine the backscatteringcoefficient σ_0, of an area located at incidence angle α (figure 1).

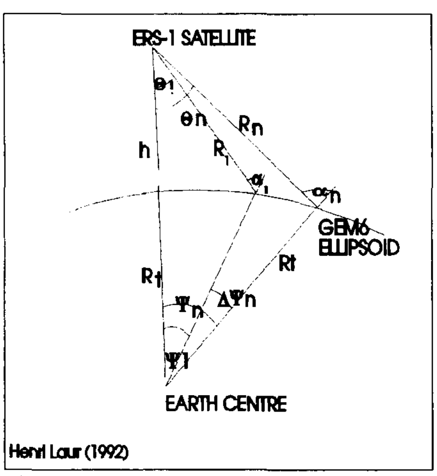

Figure 1

This paper presents the program for the derivation of the backscatteringcoefficient which may applied to the products of the different PAF's (D-PAF, UK-PAF, EECF), but can only be applied on images registrated after the 1st of September 1992; these products are corrected for the antenna pattern and are compensated for the range spreading loss.

$$\sigma_0 = \frac{\langle I \rangle}{K(\alpha)} = \frac{\langle I \rangle \times \sin \alpha_n}{K \times \sin \alpha_{ref.}}$$ where

$$\langle I \rangle = \frac{1}{N} \times \sum_{i=1}^{N} DN_i^2 \text{, with}$$

DN_i is the digital number of a pixel i, proportional to the square root of the intensity I_i received from the ground resolution cell corresponding to pixel i.

α_n : is the local incidence angle, this angle varies for each column of the image,
K : the calibration constant.
To express the backscatteringcoefficient in decibels (Laur, 1992):

$$\sigma_{0(decibel)} = 10 \times \log_{10} \sigma_0$$

To obtain the incidence angle α_n (the local incidence angle), at a pixel n, the user need to retrieve the following information from the product header:

- the zero Doppler range t_1 of the first range pixel: these values are ranging between 5500×10^{-6} and 5550×10^{-6} seconds.
- the incidence angle α_1 of the first range pixel: this value is situated between 19.2 and 19.8 °
- the geodetic latitude λ of the centre of the image
- calibration constant K
- equatorial earth radius a (in km)
- polar earth radius b (in km)

Values for 5 and 6 are based on the ERS-1 reference ellipsoid: GEM6 (Goddard Earth Model 6, the oblateness coefficient= 1/298.257).

II. To read the tapes: the header files and the ERS-1.SAR.PRI image

For users who are not very familiar with the ERS-1 SAR.PRI data, it is useful to explain how to read the raw ERS-1 data, and where the data, K, $\alpha_1, t_1, a, b, \lambda, \alpha_{ref.}$ needed as input for the program in the Model Maker Module, can be found. The raw ERS-1 SAR.PRI data can be delivered by the UK-PAF, D-PAF or the Italian-PAF. The overall structure is almost the same for each of the different PAF's, but some minor differences in the structure should be mentioned.

The band structure has been created in the PAF's as follows:
file1.img:4 360 bytes records header files
file2.img:7; 1: 720 bytes records header files, 1: 4096 bytes records header file, 1: 1620 bytes records header file, 1: 1838 bytes records header file, 1: 8600 bytes records header file, 1: 212 bytes records header file, 1:724 bytes records header file
file3.img :2; 1: 720 bytes records header file, :8192: 161925 bytes records for the image
file4.img: 1: 360 bytes records for the image info.

The UNIX commands[1] to read the tape structure and the different files is as follows:
To read the tape enter following commands
dd if=/dev/rmt/(name of the exabyte tape expl. 4mn) of=file1.img count=4 bs=360
dd if=/dev/rmt/(name of the exabyte tape expl. 4mn) of=file2.img count=7 bs=8600
dd if=/dev/rmt/(name of the exabyte tape expl. 4mn) of=file3.img count=8192 bs=16192
dd if=/dev/rmt/(name of the exabyte tape expl. 4mn) of=file4.img count=1 bs=360
file1.img, file2.img are the header files where all the image info is available, these files are ASCII files, file3.img is the image and is Generic Binary Data, file4.img consists also some image info and is an ASCII file. To read the header files, it is sufficient to open them in a text editor. To read the image use the **IMPORT/EXPORT** module from Imagine 8.1., 'Generic Binary Data', 'Input file': file3.img 'output file': give a name e.g.: rawers1.img

	UK-PAF	ITALIAN-PAF
the data description		
Data Format	BSQ	BSQ
Data type	unsigned-16 bit	unsigned-16 bit
Tape/File options		
File Header Bytes	16192	16012
Image dimensions		
Image record length	16192	16012
Line header bytes	0	0
Rows	8000	8201
Columns	8096	8000
Bands	1	1
BSQ-options		
Band header bytes	0	0
Band trailer bytes	0	0

[1] All UNIX commands are written in italic

III. The model

The first part of the model consists of the calculations of some numerical constants, different for each ERS-1 image. The calculations of these parameters can be performed by means of a simple spreadsheet program. In this case we used the spreadsheet program EXCEL. The constant values are (Laur, 1992):

1. the earth radius:

$$R_t = a \times \sqrt{\frac{\cos^2\lambda + \left(\frac{b}{a}\right)^4 \times \sin^2\lambda}{\cos^2\lambda + \left(\frac{b}{a}\right)^2 \times \sin^2\lambda}}$$

2. $R_t + h = \sqrt{R_t^2 + R_1^2 + 2 \times R_t^2 \times R_1^2 \times \cos\alpha_1}$ where

$R_1 = c \times \frac{t_1}{2}$,

h= ERS-1 altitude,

c= $3 \times 10^8 m/s$,

t_1 = the zero Doppler range time

3 ψ_1 = the earth angle (angle between the vertical of the satellite and the vertical of the pixel measured at the earth centre), of the first range pixel is given by:

$\psi_1 = \alpha_1 - \theta_1$

with θ_1 = Arccos$=\frac{R_1 + R_t \times \cos\alpha_1}{R_t + h}$

The calculations for these values in EXCEL are created as follows:

	A	B	Example	C		A	B	Example
1	equatorial earth radius	a = ?	**6378144**		15	$(R_t)^2$	=PRODUCT(B14;B14)	4.05139E+13
2	polar earth radius	b = ?	**6356759**		16	c	3.10^8	300000000
3	b/a	= B2 / B1	0.99664714		17	R_1	=B16*(B13/2)	834660
4	$(b/a)^2$	= PRODUCT(B3;B3)	0.99330552		18	$(R_1)^2$	=PRODUCT(B17;B17)	6.96657E+11
5	$(b/a)^4$	= PRODUCT(B4;B4)	0.98665587		19	$\alpha_{(ref.)}$	$\alpha_{(ref.)}$ = ?0	**23.052**
6	geodetic latitude	λ = ?	**51.59**	3.14	20	$\alpha_{(ref.)}(rad.)$	= B19 * C6/180	*0.4023333*
7	$\lambda_{(rad)}$	= B6 *C6 /180	0.90041536		21	α_1	α_1 =?	**19.414**
8	λ^2	=PRODUCT(B7;B7)	0.81074782		22	$\alpha_1(rad.)$	= B21 * C6/180	0.338838221
9	$\cos\lambda$	=cos(B7)	0.62128455		23	$\cos\ \alpha_1(rad.)$	= cos(B22)	0.943141468
10	$\cos^2\lambda$	=PRODUCT(B9;B9)	0.38599449		24	Rt + h	= SQRT(B15 + B18 + (2* B14 * B17 * B23))	*7157637.3*
11	$\sin\lambda$	=sin(B7)	0.78358503		25	$\cos\ \theta_1$	=(B17 + (B14 *B23))/B24	0.955316404
12	$\sin^2\lambda$	=PRODUCT(B11;B11)	0.61400550		26	θ_1	= Acos(B25)	0.300067958
13	zero Doppler range t_1	t_1 =?	**0.0055644**		27	ψ_1	= B22 - B26	*0.0387703*
14	the earth radius R_t	=B1*SQRT((B10+(B5*B12))/(B10+(B4*B12)))	*6365056.1*		28	K		***666110***

The data in bold are taken from the header files. The data in boxes are needed as input data in the model created in the Model Maker Module (Imagine 8.1.).

Following formulas, (Laur H., 1992) will be repeated to understand the model:

1. to obtain the value of the earth angle at a pixel n: $\psi_n = \psi_1 + \Delta\psi_n = \psi_1 + \frac{(n-1) \times \Delta r}{R_t}$ where Δr = PRI. ground range = 12.5 m.

2. to obtain the slant range R_n at pixel n: $R_n = \sqrt{R_t^2 + (R_t + h)^2 - 2 \times R_t \times (R_t + h) \times \cos\psi_n}$

3. to obtain the incidence angle α_n: $\cos\alpha_n = \frac{(R_t + h)^2 - R_n^2 - R_t^2}{2 \times R_n \times R_t}$

Once the incidence angle for each pixel n is calculated, the basic formula: $\frac{\langle DN_i \rangle^2 \times \sin(\alpha_n)}{K \times \sin(\alpha_{ref.})}$ can be calculated. This result (19, flowchart 1) is an image where the values express the backscattering value for each pixel. The values are expressed in 'floating data' and are positive. To obtain the backscatteringcoefficient σ_0 in decibel, the $\log_{10}$ of the σ_0 image has to be measured and multiplied by 10: $\sigma_0(decibel) = 10 \times \log_{10}\sigma_0$. This image has negative values and is also expressed in floating data.

IV. Explanation to create the model with the Model Maker Module (Imagine 8.1.)

1. Draw the model as in flowchart 1.
2. Click two times on both , **(1) and (2)** in flowchart 1, and fill in the **name of the raw ERS-1 data** : rawers1.img. Be sure the image is not rectified, or filtered and verify that *the raw image has no rows nor columns consisting only of zeroes*. You can verify this by means of the 'utility function', 'image info', 'vue', 'pixels'. If there exists columns and/of rows of only zeroes, a subset of the raw data has to be created, without these columns and rows containing only zeroes: (rawers1withoutzeroes.img).
3. For the **scalars (3), (4), (5), (6) and (7)**, you have to click two times and fill in the **values K,** R_t, $\alpha_{(ref.)}$, **Rt + h and** ψ_1 calculated earlier in EXCEL. Be sure all data of angles are expressed in radians !
4. Click two times on function **(8),** in the definition circle you have to fill in **FLOAT <arg 1>**. By clicking two times on <arg 1> , you have to put the mouse on the input image, <arg 1> will then be replaced automatically by **the input image (rawers1withoutzeroes.img)**. By clicking two times on **(10)**, give name **image1** and click on 'temporary file only', don't forget to sign 'floating data'.
5. Function (9), **PIXELX**, creates an image where each column receives the number of this column: so if an image consists of 8000 columns, all the pixels of the first column receive value 1 and the pixels of the last column receive value 8000.

6. Output file **(11)** is the result of function (9); give name e.g. **image2** and click on 'only temporary file' and 'floating data'.

7. Fill in following formula in function **(12): $n11_Float + (($n6_image2 - 1) * 12.5 / $n8_Float)**. This function relates to original formula of Laur (1992):

$$\psi_n = \psi_1 + \Delta\psi_n = \psi_1 + \frac{(n-1)\times\Delta r}{R_t}$$

8. Output file **(13)** is the result of function (12); give name e.g. **image3** and mark 'only temporary file' and 'floating data'.

9. Fill in following equation for function **(14)**: **sqrt (($n8_Float * * 2 + $n10_Float * * 2) - (2 * $n10_Float * $n8_Float * cos($n18_image3)))**.
This function relates to the following formula:

$$R_n = \sqrt{R_t^2 + (R_t + h)^2 - 2 \times R_t \times (R_t + h) \times \cos\psi_n}$$

10. The output file **(15)** is the result of function (14); give name e.g. **image4** and mark 'only temporary file' and 'floating data'.

11. Fill in following equation for function **(16)**: **Acos (($n10_Float * * 2 - $n21_image4 * * 2 - $n8_Float * * 2) /(2 * $n21_image4 * $n8_float))**. This function relates to following formula:

$$\alpha_n = Arc\cos\frac{(R_t + h)^2 - R_n^2 - R_t^2}{2 \times R_n \times R_t}$$

12. The output file **(17)** is the result of the application of function (16): give name e.g. **image5** and mark 'only temporary file' and 'floating data'.

13. Write following definition in function **(18): $n5_image1 * * 2 * sin ($n24_image5) / $n7_Float * sin ($n9_Float)**, This definition relates to the following formula: $\sigma_0 = \dfrac{\langle I \rangle \times \sin\alpha_n}{K \times \sin\alpha_{ref.}}$

14. The output file **(19)**, is an image showing the positive backscattering values (floating data); give name: e.g. **sigmanaughtpos.img**

15. For function **(20)**, following formula has to be introduced: **10 * $\log_{10}$ ($n27_sigmanaughtpos)**. This relates to the following formula: $\sigma_0(decibel) = 10 \times \log_{10}\sigma_0$

16. The output file **(21)** receives a name: e.g. **sigmanaughtdb.img**, mark 'floating data' and 'continuous', this is the image for the negative backscatteringvalues in decibels.

Once all the input data are introduced in the flowchart and the output data are described, the program must be saved, and can run by clicking on 'run'

VI. The script

The script function of ModelMaker Module of ERDAS allows to get the text file of the program where changes may be introduced.

\# K
\# Rt
\# $\alpha_{ref.}$
\# Rt + h
\# ψ_1
\# ψ_n
\# R_n
\# α_n

```
# set cell size for the model#
SET CELLSIZE MIN;
# set window for the model
SET WINDOW UNION;
# set area of interest for the model
SET AOI NONE;
# declarations
INTEGER RASTER n1_ rawimage ILE OLD NEAREST NEIGHBOR AOINONE"rawimage.img";
INTEGER RASTER n2_rawimage FILE OLD NEAREST NEIGHBOR AOI NONE"rawimage.img";
FLOAT RASTER n5_image1 FILE DELETE_IF_EXISTING IGNORE 0.000000 ATHEMATIC FLOAT
SINGLE"image1.img";
FLOAT RASTER n6_image2 FILE DELETE_IF_EXISTING IGNORE 0.000000 ATHEMATIC FLOAT
SINGLE"image2.img";
FLOAT SCALAR n7_Float;
FLOAT SCALAR n8_Float;
FLOAT SCALAR n9_Float;
FLOAT SCALAR n10_Float;
FLOAT SCALAR n11_Float;
FLOAT RASTER n18_image3 FILE DELETE_IF_EXISTING IGNORE 0.000000 ATHEMATIC
FLOATSINGLE"image3.img";
FLOAT RASTER n21_image4 FILE DELETE_IF_EXISTING IGNORE 0.000000 ATHEMATIC
FLOATSINGLE"image4.img";
FLOAT RASTER n24_beeld5 FILE DELETE_IF_'EXISTING IGNORE 0.000000 ATHEMATIC
FLOATSINGLE"image5.img";
FLOAT RASTER n27_sigmanaughtpos FILE DELETE_IF_EXISTING IGNORE 0.000000
ATHEMATIC FLOAT SINGLE "sigmanaughtpos.img";
FLOAT RASTER n30_sigmanaughtdb FILE DELETE_IF_EXISTING IGNORE 0.000000 ATHEMATIC
FLOAT SINGLE "sigmanaughtdb.img";
{#
# load scalar n7_Float#
n7_Float = 751399.000000;
# load scalar n8_Float
n8_Float = 6365061.700000;
# load scalar n9_Float
n9_Float = 0.400746;
# load scalar n10_Float
n10_Float = 7145092.800000;
# load scalar n11_Float
n11_Float = 0.037920;#
# load scalar n11_Float
n11_Float = 0.037920;
# function definitions
n6_image2 = PIXELX ;
n18_image3 = $n11_Float + (($n6_image2 -1) * 12.5 / $n8_Float );
n21_image4 = SQRT ( $n8_Float ** 2 + $n10_Float ** 2 - (2 * $n8_Float * $n10_Float * COS(
$n18_image3 ) ) );
n24_image5 = ACOS ( ($n10_Float ** 2 - $n21_image4 ** 2 - $n8_Float ** 2)/(2 * $n21_image4 *
$n8_Float));
n5_image1 = FLOAT ( $n1_rawdata ) ;
n27_sigmanaughtpos = $n5_image1 ** 2 * SIN ( $n24_image5 ) / $n7_Float *SIN ( $n9_Float ) ;
n30_sigmanaughtdb = 10 * LOG10 ( $n27_sigmanaughtpos ) ;
}
QUIT;
```

V. The flow chart of the model

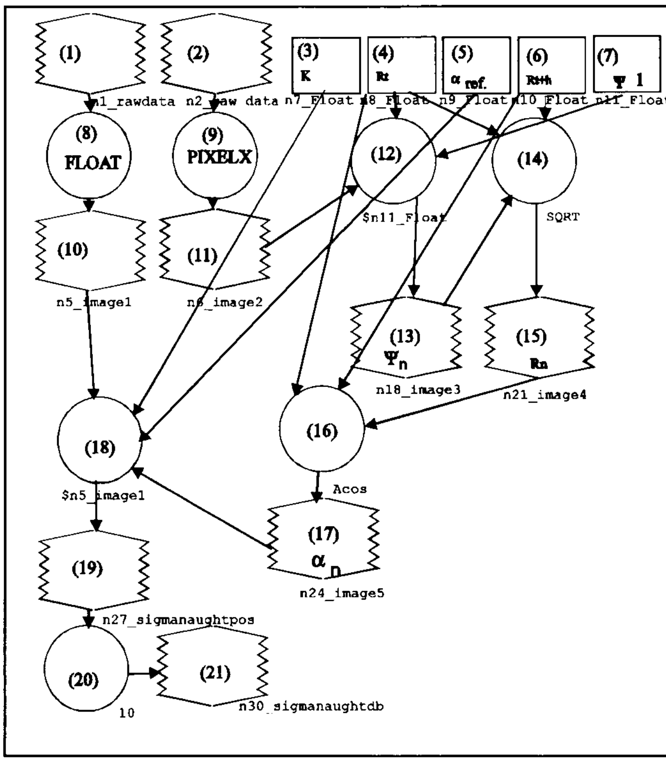

VII. Bibliography:

Laur H., 1992, Derivation of Backscattering coefficient σ_0 in ERS-1 SAR.PRI PRODUCTS.

THE INTERESTS AND LIMITS OF ERS1 SAR DATA FOR THE BATHYMETRIC AND TOPOGRAPHIC CARTOGRAPHY OF SHALLOW WATERS SEA BOTTOM AND TIDAL FLATS

Yves Cornet

Département de Géographie physique et Quaternaire, Université de Liège, Bât. B11, 2, Allée du 6 Août, B-4000 Liège

Tel: + 32 41 665335. Fax: +32 41 665722

ABSTRACT

The use of SAR data to realise a cartography of sea bottom in shallow water area (less then 15 to 20 m) and inter-tidal area is based on the relationship between sea surface characteristics and backscattering of radar electromagnetic waves.

In shallow waters the sea surface topography and roughness are influenced by the global and local meteorological conditions and tides characteristics of the sensing moment.

Global meteorological conditions of the hours before this acquisition influence the swell. Local meteorological conditions which determine the local wind direction and velocity. Its short time variability influences the sea surface roughness resulting from the field of capillary waves.

The interaction between tidal currents' velocity and direction and morphological features of the sea bottom is responsible of sea surface roughness modifications due to turbulence.

Various structures are visible on different SAR images in function of the variability of the environmental conditions presented above. The multitemporal analysis of ascending and descending frames is primordial to realise a satisfying cartography. This involves some methodological precautions for the pre-processing of the frames: speckle reduction, radiometric calibration and georeferencing.

After this pre-processing phase, we performed qualitative and quantitative comparisons of the georeferenced frames with a DEM of the Belgian shelf, the studied area. These comparisons has given us the possibility to define the ideal environmental conditions for ERS1.SAR bathymetric cartography. A statistical model relating the depth of the DEM and σ° has also been adjusted and tested on the basis of random samplings. No univocal relationship between depth and σ° with spatial signification could be established.

Moreover, along the Scheldt estuary (tidal flats area of Saaftingen and islands) the effects of roughness, moisture, water level and soil cover have allowed us to distinguish and realise a cartography of tidal channels and evaluate the mobility of islands.

1. INTRODUCTION, AIMS AND METHODOLOGICAL FLOW CHART OF THE RESEARCH

This research[1] has been realised on the North Sea continental shelf between Zeebrugge and Walkeren and in the Scheldt estuary (Fig. 1). The aims of this research can be synthesised by the 3 next questions:

1. Bathymetrical cartography in troubled water using visible remote sensing is impossible. SAR remote sensing is an alternative to observe sea bottom bathymetry in shallow water. Is this alternative applicable? Which is the ideal methodological approach to apply this technics? If it is, what is the precision of the detection of sea bottom morphology using SAR images?

2. In function of this precision, is it possible to assess the modifications of the morphology and of the bathymetry in shallow water area?

3. If it is possible, which are the meteo-marine and hydrodynamic conditions that can favour the application of SAR remote sensing to morphological and bathymetrical mapping?

4. Is the exploitation of SAR images applicable to the intertidal area of the Scheldt estuary?

It is well known that the factors that influences SAR imaging of sea surface are numerous and our former expertise (Ozer *et al.*, 1992, Ozer *et al.*, 1993a and 1993b, Comhaire *et al.*, 1994) incited us to perform an interpretation of a great number of SAR images which are more representative of the diversity of these factors' combinations. In fact, the sea surface backscattering is mainly influenced by « topography » and « microtopography » of this surface. The topography is

[1] Pilot Project PP2-B2. The research has been subsidised by the Federal Office for Scientific, Technical and Cultural Affairs (Belgium) (project TELSAT/III/12/009). It is the continuation of two other studies also subsidised by this office: the TELSAT/II/16 project (Ozer *et al.*, 1992; Ozer *et al.*, 1993; Cornet *et al.*, 1993) and the TELSAT/II/XX/609 feasibility study performed in collaboration with HAECON S.A. (Ozer *et al.*, 1993; Comhaire *el al.*, 1994)).

correlated with sea swell (Ulaby *et al.*, 1982; Cornet *et al.*, 1993) and structures of the same spatio-temporal scale. The swell is determined by global meteorological conditions and its propagation in shallow water is influenced by the bottom morphology.

« Microtopography » of sea surface is determined by shorter spatio-temporal scale phenomena like capillary waves and other structures resulting from turbulence. The first one are dependent on the local wind variability, on hydrologic characteristics of sea water and on structure of lower atmosphere correlated with variability of sea water and air temperature difference (Sasaki *et al.*, 1988; Francis, 1992; Askari *et al.*, 1993; Johannessen *et al.*, 1993). The second one are influenced by hydrodynamic conditions: tide state and velocity and direction of tidal currents that interact with the sea bottom bathymetry (Lodge, 1982; Kasichke *et al.*, 1983; Schuchman *et al.*, 1984; Vogelzang, 1989; Vogelzang *et al.*, 1989 and 1990; Wensink & Vogelzang, 1990; Boer & Vogelzang, 1992; Vogelzang *et al.*, 1992, Calkoen *et al.*, ND; Hesselmans *et al.*, ND).

The influences on SAR imaging of other larger spatio-temporal scale phenomena like internal waves (La Violette, 1987; Dawson & Hugues, 1991) and eddies (Johannessen *et al.*, 1993) are also described in the literature but are not typically of our test area.

In function of these information's, an appropriate methodology (Fig. 2) of definition of environmental conditions, that can influence SAR imaging, of ERS1.SAR.PRI image processing and of qualitative / quantitative multitemporal interpretation of SAR images is suggested in this paper to reach the aims presented above.

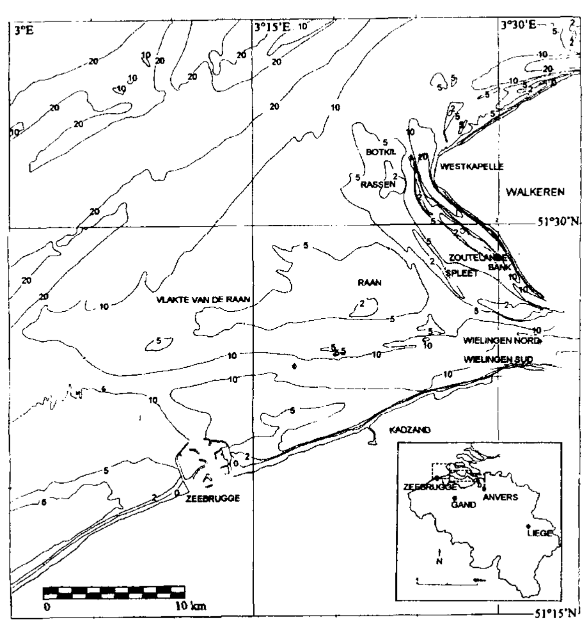

Fig. 1: Location of test areas: the Belgian continental shelf between Zeebrugge and Walkeren and the Scheldt estuary.

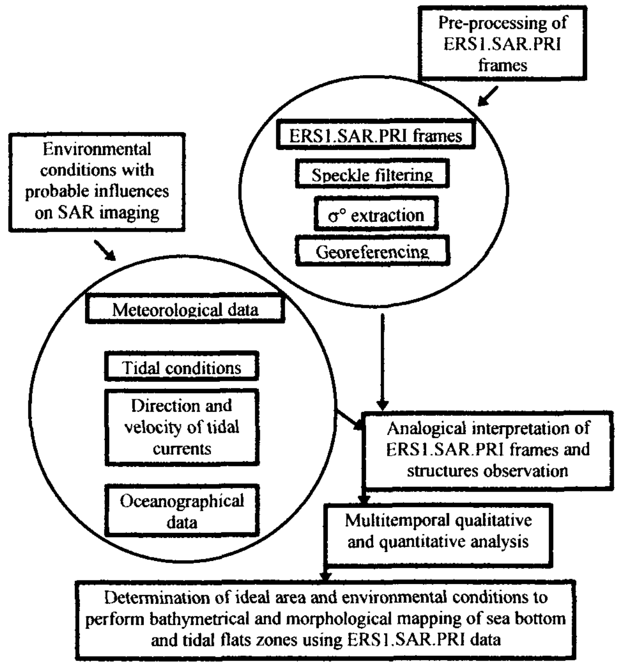

Fig. 2: Methodological flow chart

2. DEFINITION OF THE ENVIRONMENTAL CONDITIONS AT THE SENSING TIME OF ERS1.SAR DATA

The environmental conditions at the sensing time of each used ERS1.SAR.PRI image are presented in the table 1.

The tidal conditions in Zeebrugge have been computed using the « Annuaire des marées » edited by the Services Hydrographiques et Océanographiques de la Marine (Paris).

Tidal currents have been estimated for 4 points located in the test area using the map « Noordzee Vlaamse Banken van Gravelines tot Ooostkapelle (scale: 1/100000) » edited by the « Dient der Kusthavens - Hydrografie » in 1992. The figure 4 shows the tidal currents distribution in the test area for each analysed frame.

The only homogenous meteorological data for all the SAR frames is the daily synoptic bulletin of the « Institut Royal Météorologique » of Belgium. Unfortunately, this bulletin gives wind direction and velocity for only two stations located on the coast. The Middelkerke station is the nearest of our area. Moreover the bulletin gives for each day two values: one at 6.00 (UT), in the morning, and one at 18.00 (UT), in the evening. These two values are only indicative. In effect, the moment, the time resolution and the location of synoptic wind data are not ideal for SAR remote sensing marine study: during the oceanographic campaigns we registered wind velocity very higher than the values registered in Middelkerke (Tab. 1) and its high time variability could be observed. This is not possible when we use synoptic observation from I.R.M. bulletin.

Three oceanographic missions have been done during 3 periods containing the SAR image sensing moments. This period is quite long to have an instantaneous sketch of collected data on the entire area in comparison with time variability mainly induced by tide cycle. But no alternative is possible because of the relatively large dimension of the studied area. During 2 campaigns concerning our test area (in simultaneousness with the sensing of the images 11361/2565 and 12134/2565), we acquired each ½ second the position of the vessel in UTM co-ordinates (m), the depth (m), the swell height (unfortunately, during the second mission, the swell height has not been measured because of technical defection) (cm), sea water temperature (°C), sea water salinity (g/l) and concentration in A-chlorophyll (μg/l). Each 5 minutes, the next meteorological parameters have been measured: wind velocity (m/sec), atmospheric pressure (HPa), air temperature (°C) and air moisture (%).

Moreover, HAECON S.A. has supplied us with a DEM of the sea bottom (Fig. 5). Its resolution is 100 m and the height have been extrapolated and computed after tidal and swell reduction applied to the measured depths with a nominal precision of 1 cm.

1	2	3	4	5	6	7	8	9	10	11	12	13	14
3996	1035	ASC	20/04/92	21:48:21	D	VE	BM	0.85	-	0.7-2.1	E	7	TTB
4848	2565	DSC	19/06/92	10:40:49	D	VE	BM	1.40	+	0.7-2.4	NNW	44***	TB
5499	1035	ASC	03/08/92	21:49:22	D	I	BM	0.25	-	0.8-2.0	S	11	0
6351	2565	DSC	02/10/92	10:29:52	D	ME	MM	2.95	?	0.8-1.8	S	4	TTB
6852	2565	DSC	06/11/92	10:29:48	M	VE	MM	3.10	?	0.8-2.4	SSW	11	M
7002	1035	ASC	16/11/92	21:48:26	I	ME	PM	4.00	-	1.2-1.6	WSW	33	M
7854	2565	DSC	15/01/93	10:29:44	D	ME	BM	4.00	-	1.1-1.9	S	39	0
11361*	2565*	DSC	17/09/93	10:40:54	M	VE	PM	3.00	?	0.8-2.4	S	26(46)	0-M
12134*	2565*	DSC	10/11/93	10:43:46	D	ME	PM	3.35	?**	0.6-1.8	S	24(46)	0-M
16565*	2565*	DSC	15/09/94	10:44:28	M	ME	PM	3.45	?	0.6-1.8	S	11	0

Legend
* Oceanographic campaign realised in simultaneousness with SAR data acquisition.
** Mean swell height registered during the oceanographic campaign: 1 m.
*** This value seems to be excessive in comparison with values registered at the other synoptic stations
1 Orbit; **2** Fame; **3** Sensing mode: ASCending or DeSCending; **4** Sensing date; **5** Sensing time; **6** Tide: M = coming up, D = going down and I = intermediate situation; **7** VE = spring tide, ME = death water tide and I = intermediate tide; **8** BM = low water, MM = mean water and PM = high water; **9** Water height in Zeebrugge expressed in m above mean height of low spring tide water; **10** Perception of swell structures on the SAR image: visible (+), invisible (-) or uncertain perception (?); **11** Maximal and minimal tidal currents velocity for the 4 points where we computed the value of tidal current vector (in kn.); **12** and **13** Wind direction (coming from) and velocity (in km/h) in Middelkerke or registered during the oceanographic campaigns (between parenthesis); **14** Contrast perception on SAR image: TTB = excellent, TB = very good, M = moderate, 0-M = moderate / null, 0 = null.

Tab. 1: Analysed frames, tidal conditions, swell conditions, tidal currents, wind velocity and direction and contrasted area on the SAR images.

3. PROCESSING OF ERS1.SAR.PRI FRAMES

Speckle reduction

The first step of the ERS1.SAR.PRI image processing is the speckle reduction. 3 filters have been tested: the median filtering, the n sigma filtering and the statistical filtering (Matteini, 1992; Cornet *et al.*, 1993). The 2 sigma filtering with a 5x5 kernel dimension has been used because of the best analogical quality of the results.

σ^o extraction

The second step of the processing is the σ^o extraction using the results of the calibration phase (Laur, 1992). This step is necessary because of the multitemporal aspect of the research and to allow the qualitative and quantitative comparison of different frames sensed with different geometrical characteristics.

Nevertheless, a methodological remark must be done about the succession of the 2 first steps of the processing. A standardisation of processing should be proposed. In effect, no statistical argumentation has been found in the literature about the succession of this 2 steps: does the speckle filtering must be performed before or after the σ^o extraction? Moreover, our aim is to preserve the perception of microscalar structures. This aspect avoids the exploitation of 25x25 (number of pixels must be at least 500) kernels imposed by Laur (1992) to insure the statistical validity of the σ^o extraction. We then chose a compromise between the different exigencies of this research. In our methodological procedure, the speckle filtering before the σ° extraction is justified because of the necessity to perform a low pass filtering before σ° extraction (Fig 6).

Georeferencing

The last step is the georeferencing of the frames. The reference for georeferencing is the DEM. The quantitative comparison between the SAR frames and the DEM is one of the last aims of the research. We then realised a cubic convolution resampling for all the frames to reach a 100 m resolution. A first order polynomial model has been used to perform the geometrical correction. This order allows us to minimise the location error in open sea where no ground control point is available. The RMS error computed on the ground control points chosen along the coast is always lower than 100 m.

All the frames resulting from this processing procedure are presented on the figure 4. All these frames have then been submitted to the qualitative and the quantitative interpretation.

4. ANALOGIC INTERPRETATION OF THE MULTITEMPORAL SAR IMAGES SERIES

The comparison of the 10 situations presented on the figures 3 and 4 allows us to do the next observations.

1. The wind velocity determines the visibility of structures probably influenced by sea bottom morphology. When synoptic wind velocity in Middelkerke is lower than or equal to 7 km/h, structures are perceptible. When synoptic wind velocity in Middelkerke is higher than 11 km/h, they are no more perceptible.

2. The zones where the structures are well contrasted, are corresponding to the zones where the current velocity is higher. When the current velocity is high the perception of structures probably influenced by the sea bottom morphology is independent of the tidal current direction regarding the sea bottom slope (Botkil, Rassen, Spleet and Zoutelande zones). Nevertheless, when the current velocity is low, in the Scheur area on the frames 4848/2565 and 6351/2565 for instance, the tidal currents direction that allows the visibility of structures is parallel to steepest sea bottom slope. Generally, slope oriented in the same sense than the current is characterised by low backscattering and the slope oriented in the other direction is characterised by high backscattering. But the structure is not located at the vertical of the sea bottom morphological feature that induces the sea surface structure (the eastern border of the Spleet bank is a very good example of this effect). This induces a location error which can be very higher than the resolution of the DEM and than the RMS error of the georeferencing of the SAR frames.

3. The confrontation of the frames 3996/1035, 4848/2565 and 6351/2565, characterised by a different tide height, shows that depth variations influence sea surface state when the depth is lower than 9 - 10 m (in the Spleet zone), it means 6 or 7 m under the height reference of the bathymetrical map for these cases.

4. Some structures correlated with wind effect and hydrologic influences are also perceptible and independent of bathymetry. For instance, on the frame 4848/2565 an edge between a bright area and a dark area is visible on the north east side of the Zeebrugge. Oceanographic campaigns never show well marked fronts. The probable explanation of this edge is a obstacle effect on a rapid south-west coming wind. On the frame 3996-1035, some dark linear structures are visible. They are probably correlated with the propagation of coastal water in the open sea direction in relation with tidal currents direction.

5. Very often, contradictory situations are observed. A same area can appear on different frames with different backscattering characteristics and 2 area with different depth can have the same backscattering. For instance, the high sea bottom area of the Zoutelande on the frame 6852/2565 and its southern extremity on the frame 7002/1035 are very bright. The very deep northern anchorage area of the Wielingen is also very bright on the frame 7002/1035. As a set off, on the frame 6852/2565, the top of the Zoutelande is dark....

5. QUANTITATIVE RELATIONSHIP BETWEEN DEPTH AND BACKSCATTERING OF SEA SURFACE

In spite of this conclusion we performed 2 random sampling in a multiband file containig a mask determining the positive depth area, the DEM and the 10 processed frames. As proposed in the past (Ozer *et al.*, 1993b), the first sampling is destinated to adjust a statistical model correlating the depth and the σ°. The second one is destinated to test the validity of the model. For each sampling 25 % of the total number of pixels has been selected. No univocal relationship with spatial signification has been found between depth and backscattering for the 10 considered situations.

6. TOPOGRAPHICAL MAPPING OF TIDAL FLATS

The only area where multitemporal exploitation of SAR frames is applicable to perform topography is the tidal flats zone of Saaftingen. In effect, Comhaire (Comhaire *et al.*, 1994) showed two examples of multitemporal composition of SAR images on the Scheldt Estuary. She realised on the basis of this compositions a cartography of the tidal channel of the tidal flats of Saaftingen and registered the mobility of the islands of the same estuary (Fig. 7). Surface roughness influenced by regular field of ripple marks producing Bragg resonance and moisture saturation of the sand in the tidal channel and on the emerged part of islands can explain the visibility of these features on multitemporal compositions of SAR frames sensed at different moment of the tidal cycle.

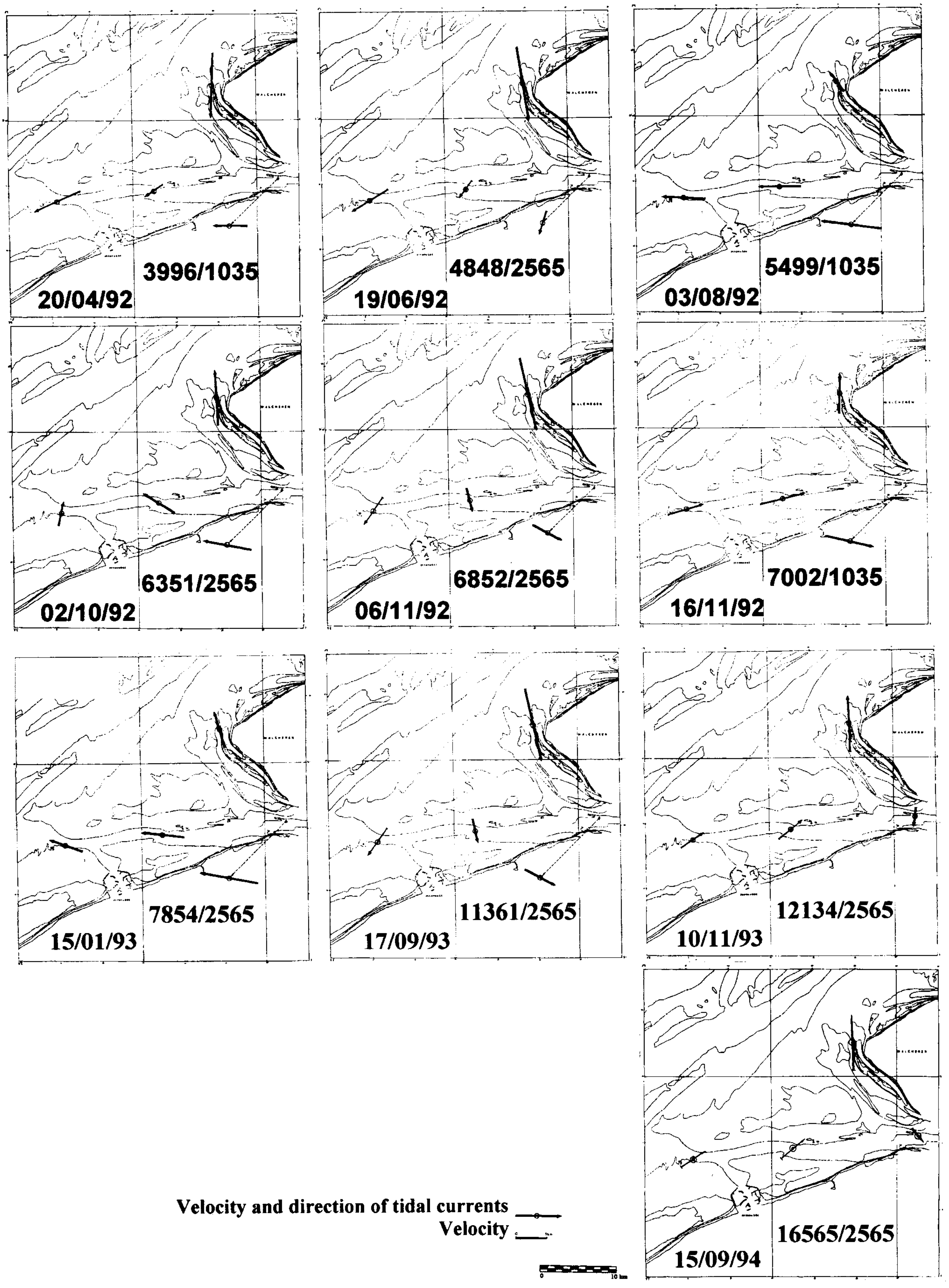

Fig. 3: Tidal currents of the studied area at the sensing time of the analysed frames (Fig. 4).

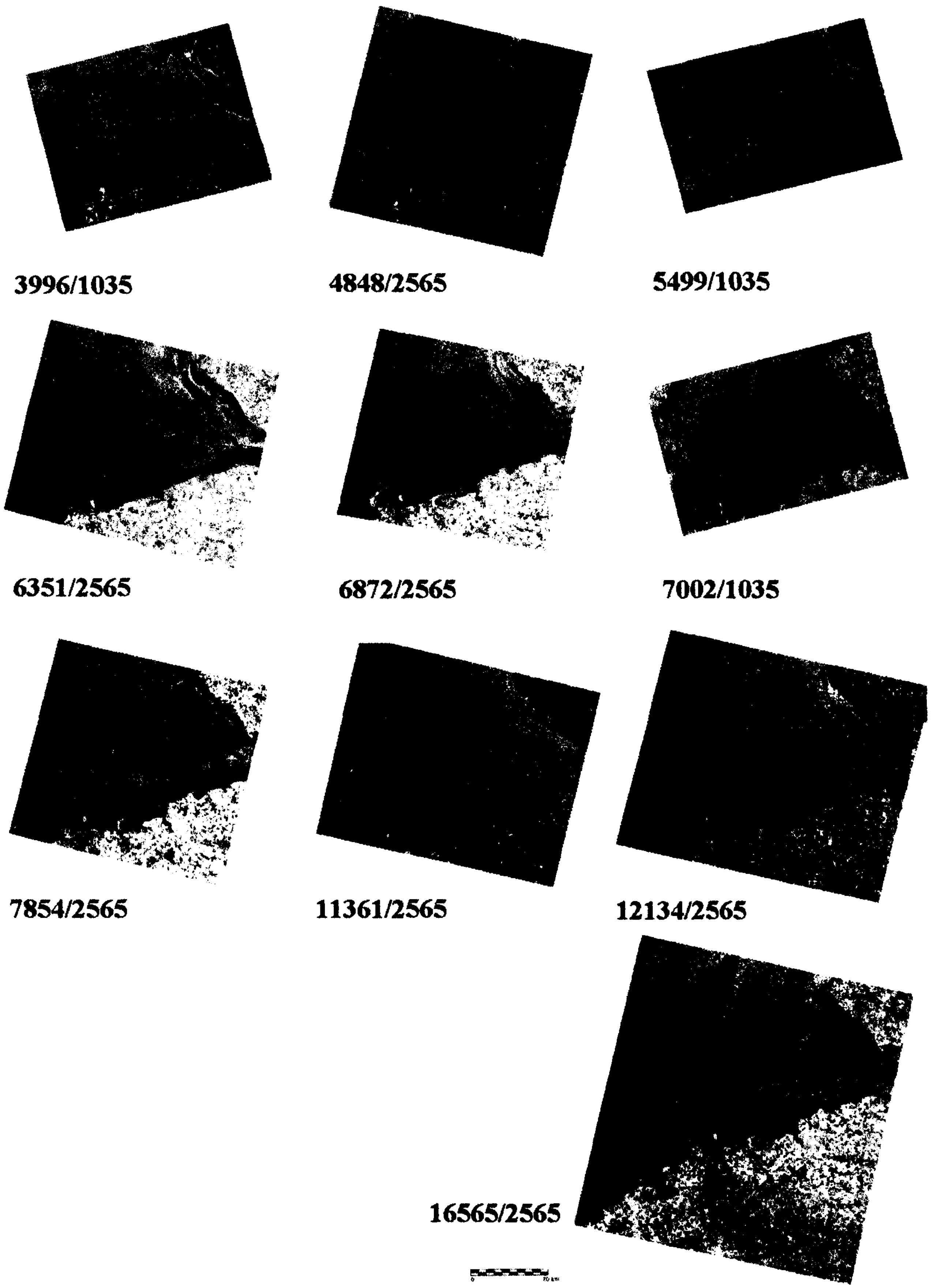

Fig. 4: Analysed subsets after processing (speckle filtering, σ° extraction and geometric correction).

Fig. 5: DEM of the studied area (from HAECON S.A.): depth going up from blue to red.

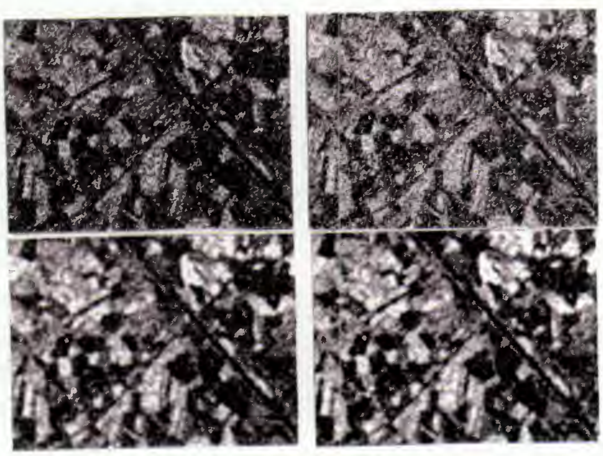

Fig. 6: An example of 4 kinds of pre-processing. The last one has been chosen and justified (see text).

Legend:

Original data	Subset after $\sigma°$ extraction
Subset after sigma filtering (5x5, 2σ)	Subset after sigma filtering (5x5, 2σ) and $\sigma°$ extraction

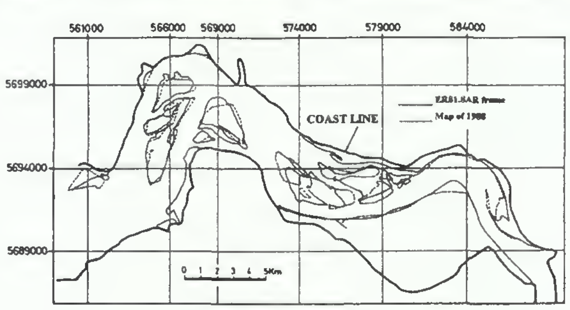

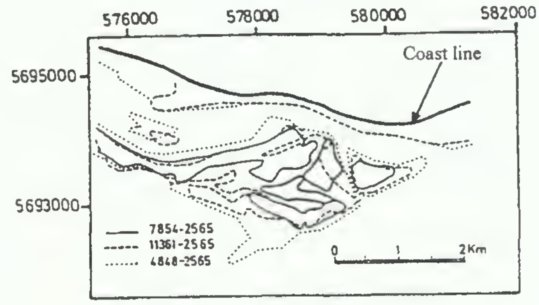

Fig. 7: 2 Illustrations of the detection on SAR images of the mobility of different islands in the Scheldt estuary (Comhaire *et al.*, 1994).

7. CONCLUSIONS

ERS1.SAR.PRI data can be exploited to realise the cartography of islands and tidal channel in intertidal area of estuaries. A multitemporal analogic interpretation is necessary to perform this cartography. An appropriate processing methodology must then be applied to the data to perform the multitemporal composition.

In shallow water area, wind velocity, tidal currents direction and velocity influence the visibility of structures on SAR images that can be correlated with bathymetry but this relationship between sea bottom morphology and sea surface backscattering has no spatial validity. SAR data must be used to optimise the ship echo sounding survey and interpolation process to compute the depth. Moreover, because of the limited depth at which depth variations can influence SAR imagery of sea surface, diachronic interpretation is also useful in this case. So, the same kind of processing must be applied to the SAR data.

REFERENCES

Askari F., Geenaert G., Keller W.C. & Raman S., 1993, Radar imaging of Thermal fronts. *Int. Journ. Remote Sensing*, 14, 2, pp. 275-295.

Boer S. & Vogelzang J., 1992, Mapping of sea bottom topography with spaceborne SAR. *BCRS report n° 91-14*, 89 p.

Calkoen C.J., Wensing G. & Hesselmans G.H.F.M., ND, Mapping of sea bottom topography. *Delft Hydraulics*, pp. 29-31.

Comhaire A. L., Ozer A. & Jaspar A., 1994, The contribution of ERS1 and SPOT data in the morphologic and bathymetric study of the North Sea and the Scheldt Estuary. *Proc. of the First ERS-1 Pilot Project Workshop*, 22-24 June, Toledo, Spain, pp. 297-302.

Cornet Y., Comhaire A.L. & Ozer A., 1993, Significativity of wave length computation using spatial autocorrelation theory on SAR image of ERS1. *Proc. of the Second ERS-1 Symposium « Space at the Service of* *our Environment »*, Hamburg, Germany, 11-14 October, pp. 941-944.

Dawson T.W. & Hugues B.A., 1991, Comparisons between measured and theorical results for C and Ku bands backscatter from natural occurring internal wave current patterns. *IEEE Transactions on Geoscience and Remote Sensing*, 29, 1, pp. 157-166.

Francis J., 1992, Remote sensing of oil spills in the marine environment. *Earth Space Review*, 1, 3, pp. 16-22.

Hesselmans G.H.F.M., Calkoen C.J. & Wensink G., ND, Retrieval of sea bottom topography from radar imagery. *Delft Hydraulics*, 52 p.

Johannessen J.A., Schuchman R.A., Johannessen O.M., Davidson K.L. & Lyzenga D.R., 1991, Synthetic aperture radar imaging of upper ocean circulation features and wind fronts. *Journ. Geophysical Research*, 96, C26, pp. 411-422.

Johannessen J.A., Roed L. & Wahl T., 1993, Eddies detected in ERS1 SAR images and simulated in reduced gravity models. *Int. Journ. Remote Sensing*, 14, 11, pp. 2203-2213.

Kasichke E.S., Schuchman R.A. & Lyzenga D.R., 1983, Detection of bottom features on Seasat synthetic aperture radar imagery. *Photogrammetric Engineering and Remote Sensing*, 49, 9, pp. 1341-1353.

La Violette P.E., 1987, Satellite image analysis techniques applied to oceanography. *Naval Ocean Research and Development Activity*, NSTL, Bay of St Louis, Missisipi 39529-5004, USA.

Laur H., 1992, ERS-1 SAR calibration. Derivation of backscattering coefficient $\sigma°$ in ERS-1.SAR.PRI products. *E.S.A.*, ESRIN, Frascati, Italy, 16 p.

Lodge D.W.S., 1982, Surface expressions of bathymetry on Seasat synthetic aperture radar images. *Space and New Concept Department*, Royal Aircraft Establishment, Farnborough, Hampshire GU 14 6TD, England.

Matteini, 1992, Study on structure detection and new speckle filtering techniques for ERS1 images. *E.S.A.*, ESTEC, The Netherlands, 60 p.

Ozer A., Cornet Y. & Comhaire A.L., 1992, Morphodynamique des côtes et caractéristiques énergétique de la houle étudiée grâce au SARde ERS-1. *Proc. of the First ERS-1 Symposium « Space at the Service of our Environment »*, Cannes, France, 4-6 November, pp. 851-855.

Ozer A., Cornet Y. & Comhaire A.L., 1993a, Corrélation entre les données météo-marines et la dynamique des plages: contribution de la télédétection (ERS1). *Rapport final, projet TELSAT/II/16, SPPS*, 31 mars, 169 p. + annexes.

Ozer A., Jaspar A., Cremer J.F. & Cornet Y., 1993b, Etude de faisabilité pour la cartographie des fonds sous-marins de la plate-forme continentale belge par télédétection. *Rapport final, projet TELSAT/II/XX/609, SPPS*, 7 octobre, 35 p. + annexes.

Reutov E.A.& Shutko, 1992, Estimation of the depth to a shallow water table using microwave radiometry. *Int. Journ. Remote Sensing*, 13, 12, pp. 2223-2232.

Sasaki Y., Asanuma I., Muneyama K., Naito G. & Susuki T., 1988, Microwave emission and reflection from the wind-roughened sea surface at 6.7 and 18.6 GHz. *IEEE Transactions on Geoscience and Remote Sensing*, 26, 6, pp. 157-166.

Schuchman R.A., Lyzenga D.R. & Meadows G.A., 1984, Synthetic aperture radar imaging of ocean bottom topography via tidal current interactions: theory and observations. *Ed. Ann Arbor*, Michigan, USA.

Ulaby F.T., Moore R.K. & Fung A.K., 1982, Microwave remote sensing. Active and passive. Volume 2: Radar remote sensing and surface scattering and emission theory. *Artech House, inc.*

Vogelzang J., 1989, The mapping of bottom topography with imaging radar. A comparison of the hydrodynamic modulation in some existing models. *Int. Journ. Remote Sensing*, 10, 9, 16 p.

Vogelzang J., Wensink G.J., de Loor G.P., Peeters H.C., Pauwels H. & van Gein W.A., 1989, Sea bottom topography with X band SLAR. *BCRS-89-25, Netherlands Remote Sensing Board, final report, project TO-3.10.*, 84 p.

Vogelzang J., Wensink G.J., de Loor G.P., Peeters H.C. & Pauwels H., 1990, Sea bottom topography with X-band SLAR evaluation of existing models. *Proceedings of IGARSS '88 Symposium*, Edinburgh, Scotland, pp. 1303-1307.

Vogelzang J., Wensink G.J., de Loor G.P., Peeters H.C., Pauwels H., 1992, Sea bottom topography with X-band SLAR: the relation between radar imagery and bathymetry. *Int. Journ. Remote Sensing*, 13, 10, pp. 1943-1958.

Wensink G.J. & Vogelzang J., 1990, Remote sensing provides vital information. Mapping the sea bed. *Land and Water International, Remote Sensing Special*, pp. 13-15.

ENVIRONMENT / HAZARD / HYDROLOGY

Chairman: **J. Achache**
Rapporteur: **M. Borgeaud**

SOIL MOISTURE AND HYDROLOGICAL MODELLING USING RADAR AND OPTICAL REMOTE SENSING : A CASE STUDY IN BRITTANY (France)

Anne-Laure Cognard, Cécile Loumagne, Michel Normand
CEMAGREF, Hydrologie, BP 121, 92185 Antony, Cedex France,
Phone : (33).1.40.96.60.54 - Fax : (33).1.40.96.61.99

Catherine Ottlé, Daniel Vidal-Madjar
CETP/CNRS, 10/12, Av. de l'Europe, 78140 Vélizy, France
Phone : (33).1.39.25.49.12 - Fax : (33).1.39.25.49.22

Alain Vidal
LCT, Cemagref-Engref, Maison de la Télédétection,
500, Rue Jean-François Breton, 34093 Montpellier Cedex 5, France
Phone : (33).67.54.87.19 - Fax : (33).67.54.87.00

ABSTRACT

The present paper reports on an investigation on the possibility of using radar and optical remotely sensed data in hydrology. A former paper had described the methodology and the first results of this research conducted in the frame of a ERS.1 pilot-project. The first aim of the project is soil moisture monitoring in order to improve outflow forecasting methods on agricultural river basins. New results are presented from the data acquired during the 1992-1994 period in central Brittany (France). Ground-truth data from the Naizin research watershed have been compared with ERS.1 SAR data at the basin scale. The results of the winter periods (phases B and D) are in good agreement. This confirms the possibility of monitoring surface soil moisture at the basin scale during the periods of low vegetation density with the spaceborne ERS.1 SAR. The calibration relationship was tried on a large number of basins during the phase B (1992 winter). The paper presents maps showing the space-time variations of surface soil moisture at the basin scale over the Brittany region. The second aspect of the project is the development of a hydrological model, taking into account the mean characteristics of the surface (soil and vegetation cover), and able to simulate soil moisture and catchment runoff. This model was calibrated over the Naizin watershed using terrain and remote sensing data. Then, it was applied on the other Breton river basins where a large dataset of NOAA/AVHRR has been constituted. The results of the simulation are generaly in good agreement with the measurements. At the present stage, the assimilation of combinated remote sensed data (ERS.1/SAR and NOAA/AVHRR) in the model is in progress in order to validate the methodology. Finally, the possibility of application of this methodology in operational hydrology is discussed.

1. INTRODUCTION

Remote sensing may be used in different domains of hydrological modelling. The assessment of surface characteristics are already used in hydrological models. A new domain is the use of remote sensing data to assess the variations of time variable parameters, like soil moisture or evapotranspiration. These parameters may be used to control the model simulations, and they may be also assimilated in the models as input data.

In this paper, we present the results of a work still in progress, consisting in the synergistic use of radar, optical and thermal infrared data for hydrological modelling of small agricultural watersheds in Brittany (France). This study is prepared within the framework of an ESA pilot-project (PP2.F10) entitled "Estimation of the mean soil hydric state of small agricultural basins using remotely sensed data : Application to the calibration and the validation of a hydrological model". A former paper (Normand et al, 1994) has presented the methodology and the first results of this project. New results were obtained with the spaceborne ERS.1 Synthetic Aperture Radar on a test watershed. We have compared these results with the former ones in order to evaluate the ability of ERS.1 to derive an index representative of the moisture state of river basins. Then, we present an application of the calibration relationship to the cartography of the soil water state variations of a large number of Breton watersheds using a SIG. In the second part of the paper, the results of the hydrological model able to simulate runoff and soil moisture are presented. Then, the possibility of assimilating remote sensing data in the model and the applicability of the methodology in operational hydrology are discussed.

Proceedings of the Second ERS Applications Workshop, London, UK, 6–8 December 1995 (ESA SP-383, February 1996)

2. STUDY AREA

Brittany is one of the two regions of France, with Alsace covered by ERS.1 SAR imagery every 3 days during the so-called ice-phase B and D ranging from January to March, in 1992 and 1994 respectively. The figure 1 shows a map of Brittany with about thirty watersheds selected for the project and the tracks of ERS.1 for the 3 day cycle (figure 1a) and the 35 day cycle (phase C, from April 1992 to December 1993) (figure 1b).
One of these basins, the Naizin research watershed, has been chosen to conduct the ground-truth operations scheduled to calibrate the SAR data and the hydrological model. The test site was previously described (Mérot et al, 1994, Normand et al, 1994). Brittany has a wet temperate climate. The precipitations occur principaly in automn and winter. The relief of this region is not greatly marked. Generaly, land use on the river basins is characterized by intensive agriculture with cereals, corn, vegetables, pasture for milk productions, and indoor stockfarming. The area of the basins ranges from 12 km² (Naizin watershed) to 471 km².

3. DATA BASE

Ground data

- Hydrological and Meteorological data :

The hydrological and meteorological network of Brittany provides long series of outflow and rainfall data for the river basins selected in the scope of the project : HYDRO data base (Ministère de l'Environnement) for the outflows, and METEO FRANCE data base for rainfall and other meteorological data : air temperature, air humidity, wind speed, solar radiation.
The test site, Naizin research watershed has its own hydrological and meteorological data base.

- Soil moisture :

Ground truth measurements were carried out on the test site (Naizin watershed) to assess the capacity of the ERS.1 SAR in evaluating the soil surface water content (Cognard et al, 1995) : First, a one-point automatic permanent measurements site with capacitive soil moisture sensors was installed in the north of the basin. Secondely, 12 test fields were selected throughout the basin. 20 extensive ground truth campaigns were conducted from January 1992 to March 1994, to estimate soil moisture (of these fields) in the upper layer (0-5 cm) using the gravimetric method.

Remote sensing data

- SAR images

Ascending and descending ERS1 orbits cover Brittany during the phase B, C and D. The Naizin watershed is seen at least once every 3 days during the phases B and D in the ascending orbit, and two times every 35 days during the phase C. The number of images for the other selected basins depends on their respective geographic situation (Figure 1). The images provided by ESA are SAR Precision Image Products (PRI). The basins have been first located on one SAR image. Then, the backscattering coefficients have been derived according to the documents given by ESA (Laur, 1992), for almost all the available images in the case of the Naizin watershed. For the other river basins only a part of the SAR data has been interpretated.

- AVHRR/NOAA images

Almost all the cloudless AVHRR/NOAA11 images available on Brittany over the duration of the project have been acquired in order to obtain reflectance values in the visible and near infrared domains, and to obtain radiance values in the thermal infrared. Reflectances are good indicators of the vegetation cover and radiances are in relation with surface temperatures.

4. RESULTS AND DISCUSSION

4.1. Soil moisture

- ERS/SAR calibration on surface soil moisture.

The comparison between radar data and ground truth at different spatial scales has been partly presented by Cognard et al, (1995), and Normand et al, (1994). The comparison on the basin scale is interesting for hydrological application of the mean radar signal over the basin. On this scale, it has been shown that during the fall, winter and early spring periods there is a clear linear correlation with the automatic measurements. On the other hand, the correlation is poor during the periods of denser vegetation canopies.
It is now interesting to examine the results on the entire period including the new results of the phase D (figure 2).
The comparison of phases B and D, shows variations of the radar signal occuring at a high level of soil moisture depending on precipitation events. The correlation between the radar data and the soil moisture measurements gives very similar results for the two phases, with a high sensitivity to the soil moisture variations (Figure 3). These results confirm the ability of the ERS1/SAR to follow up the variations of the surface soil water state on the basin scale during the period of low vegetation density and for a high level of soil moisture.

- Soil moisture state variations at the region level.
The radar signal evolution has been studied for the other selected river basins, showing variations linked to the rainfall events. Assuming that the radar signal behaviour is invariant beside the surface soil moisture of all the studied zone, the radar calibration found on the test site during the winter period was extented to the whole central Brittany. Using a SIG, figure 4a is a representation of the mean soil moisture state of the selected river basins at three characteristic dates during phase B, after an important rainfall event. Signifiant space-time variations of this parameter can be observed during the 1992 winter. In order to attennate the influence of the respective physical characteristics of the river basins, figure 4b presents the relative variation of soil moisture in comparison with a date of reference (January 31). These results confirm the possibility of monitoring surface soil moisture at a regional scale during the periods of low vegetation density with ERS.1/SAR.

4.2 Hydrological modelling

- The hydrological model.
The GRHUM model used in this study (Loumagne et al, 1995) (figure 5) is based on a daily rainfall-runoff model (Edijatno and Michel, 1989). The soil is modeled as a two-layer system : a surface superficial layer and the bulk layer representing the root zone. The exchanges between the two layers depend on the soil moisture conditions. The NDVI index computed from AVHRR data is used to estimate the rate of vegetation cover which partitions soil evaporation from evapotranspiration. Rainfall efficiency depends on the moisture in the soil bulk level. The accuracy of the model in reproducing discharges observed at the outlet of the catchment and its ability to simulate soil moisture have been checked.

- Results from the Naizin research watershed.
The GRHUM model was calibrated over the Naizin research watershed. Figure 6 compares the NDVI computed with NOAA/AVHRR images to the rate of vegetation coverage computed on the basis of ground vegetation survey for the whole year 1992. The calibration of the model over the 1989-1991 period gives very good results in simulating streamflow at the outlet (the Nash criterion is equal to 90,6%). The model remains performant over the control period (1992-1993) with a Nash criterion equal to 79% (figure 7a). Figure 7b represents the evolution of the relative surface soil moisture simulated by the model over the control period. The comparison of the simulation with the radar data (mean radar signal over the basin) gives results in good agreement during the periods of low vegetation density.

- Results over watersheds selected in Brittany.
A model validation was also performed on the 30 basins selected in Brittany. These basins were chosen because rainfall-runoff data were available for more than 6 years. The mean Nash criterion has a high level (89.4%) over the calibration period and decreases normally during the control period (78.9%). An example of these results is given on figure 8a showing simulated and measured streamflows of the Evel river for the control period (Nash = 86.5%). Figure 8b shows the comparison of the surface soil moisture simulated by the model with the mean radar signal during the same period (1992-1993).
These results confirm the ability of the GRHUM model to simulate soil moisture and catchment runoff and open the possibility to use radar data in hydrological modelling at the regional scale.

5. CONCLUSIONS

A new methodology for using remote sensing data in soil moisture and hydrological modelling was presented in a former paper (Normand et al, 1994). The reported work confirms that ERS.1/SAR is able to give quantitative informations concerning the surface soil moisture evolution at the basin scale during the periods of low vegetation density and for a high level of soil moisture. The possibility of mapping these variations on a regional level was tried over Brittany during phase B. The comparison between the mean radar signal evolution over the selected watersheds and the soil moisture simulated by the hydrological model shows that the both evolutions are similar over winter 3 day cycles. This offers the possibility of using radar data in the hydrological model in order to improve streamflow forecasting during the wet winter period. The usefulness of the radar data acquired during the period of high vegetation density could not be demonstrated because, in that case, the ERS.1/SAR signal is highly dependent on the vegetation cover evolution.
The hydrological model elaborated in the framework of the pilot-project was calibrated upon the Naizin test-site and successfully tested upon the central Brittany watersheds. Using the same approach as Ottlé et al, 1994, it is now possible to assimilate optical and thermal infrared remote sensing data from NOAA/AVHRR in the hydrological model to infer land uses, annual cycles of vegetation and evapotranspiration. This work is still in progress and consists in the synergistic use of radar, optical and thermal infrared data for improving watershed runoff forecasting with an adapted hydrological model.
The present step is the assimilation of soil moisture information integrated over the whole watershed. The development of operational methodology for hydrological applications is nevertheless subject to several conditions. First, the frequency of the radar data acquisition : The ERS.1 three day orbiting phase seems to be adequate. Secondly, the rapidity of the processing of the radar data in order to reach the compatibility with the other hydrological data. Thirdly, the possibility of taking into account the influence of the

vegetation cover on the radar signal to obtain soil moisture data throughout the year.
The results already obtained in the framework of this project make us confident that it will be possible to improve hydrological modelling of gauged and ungauged basins with remote sensing data.

ACKNOWLEDGEMENTS

The authors would like to thank ESA for the support of this study through the provision of ERS.1 images in the frame of the PP2.F10 pilot-project. The images were partly processed by GEOSYS Company in Toulouse. This project was supported by the French National Space Agency (CNES) and the French National Remote Sensing Program (PNTS).
The authors wish also to thank Ch. Cann from CEMAGREF (Rennes), who manage the Naizin research watershed, and all their colleagues from CEMAGREF (Antony) who participated in the ground-truth campaigns, specially P. Ansart, M. Ferry and J.L. Rosique.

REFERENCES

- Cognard A.L., Loumagne C., Normand M., Olivier Ph., Ottlé C., Vidal-Madjar D., Louahala S., Vidal A., 1995. Evaluation of the ERS.1/Synthetic aperture radar capacity to estimate surface soil moisture : Two-year results over the Naizin watershed. Water Resources Research, 31, 4, 975-982.

- Edijatno, Michel C., 1989. Un modèle pluie/débit journalier à 3 paramètres. La Houille Blanche, 2, 113-121.

- Laur H., 1992. Derivation of backscattering coefficient σ° in ERS.1/SAR. Doc. ESA, PRI Products, ESA/ESRIN, Rapport ESA n°1, 16p.

- Loumagne C., Chkir N., Normand M., Ottlé C., Vidal-Madjar D., 1995. Introduction of the soil-vegetation-atmosphere continuum in a rainfall-runoff model for remote sensing data assimilation. Submitted to IAHS review.

- Mérot P., Crave A., Gascuel-Odoux C., Louahala S., 1994. Effect of saturated area on backscattering coefficient of the ERS.1 synthetic aperture radar : first results. Water Rsources Research, 30, 2, 175-179.

- Normand M., Chkir N., Cognard A.L., Imberti M.C., Loumagne C., Ottlé C., Vidal A., Vidal-Madjar D., 1994. Estimation of surface soil moisture from ERS.1/SAR data for hydrological modelling purposes. Proceedings of the first ERS.1 Pilot Project Workshop, Toledo, Spain, June 1994, ESA SP-365, 97-102.

- Ottlé C., Vidal-Madjar D., 1994. Assimilation of soil moisture inferred from infrared remote sensing in a hydrological model over the HAPEX-MOBILHY region. J. of Hydrology, 158, 241-264.

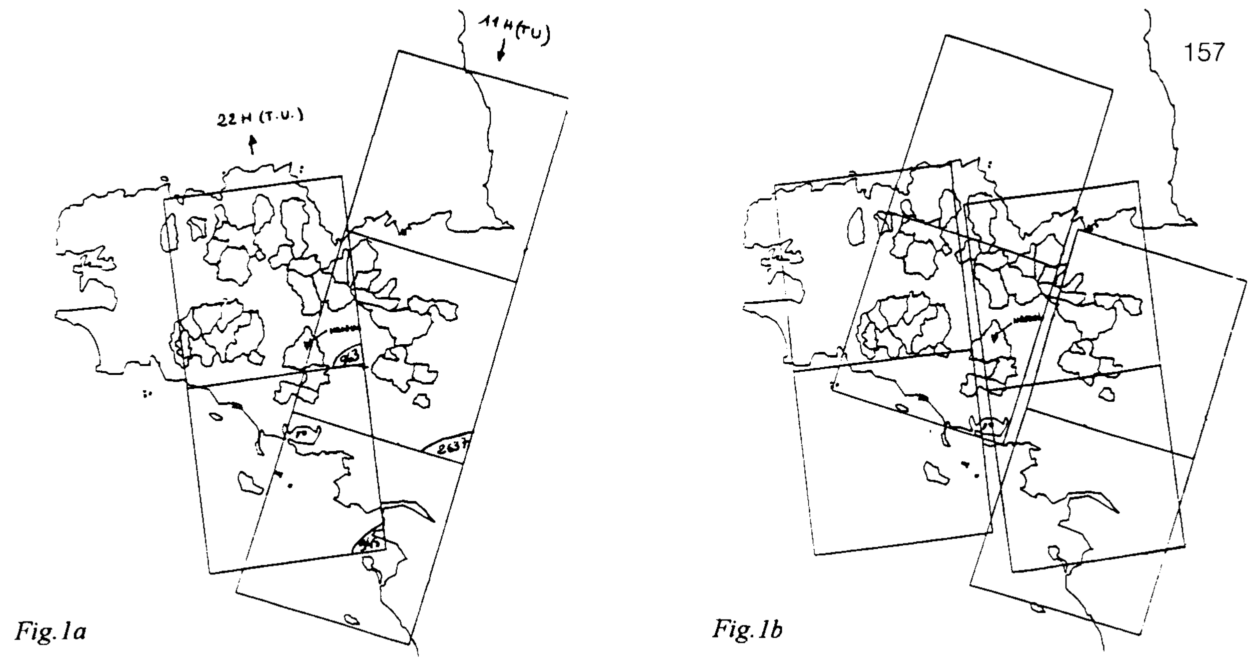

Fig. 1 - Map of Brittany showing coverage of ERS-1 SAR images during the phases B and D (Fig. 1a), and during the phase C (Fig. 1b).

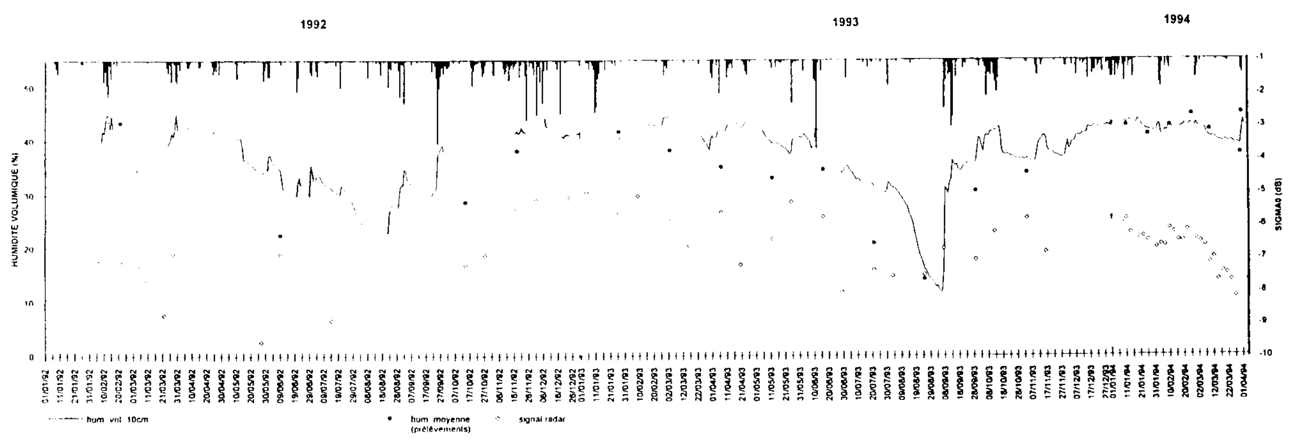

Fig. 2 - Evolution of the mean radar signal over the Naizin research watershed and results of soil moisture measurements (years 1992-1993-1994).

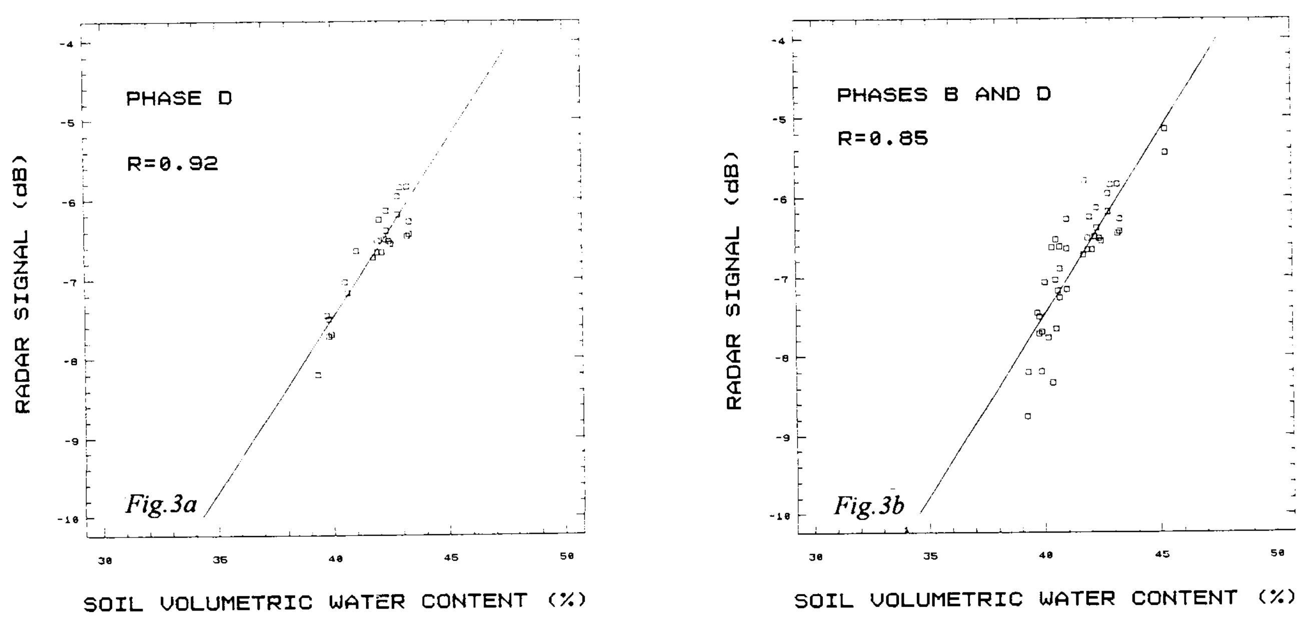

Fig. 3 - Correlation between the mean radar signal over the Naizin watershed and the point automatic soil moisture measurements separately for phase D (Fig. 3a) and for phases B and D (Fig. 3b).

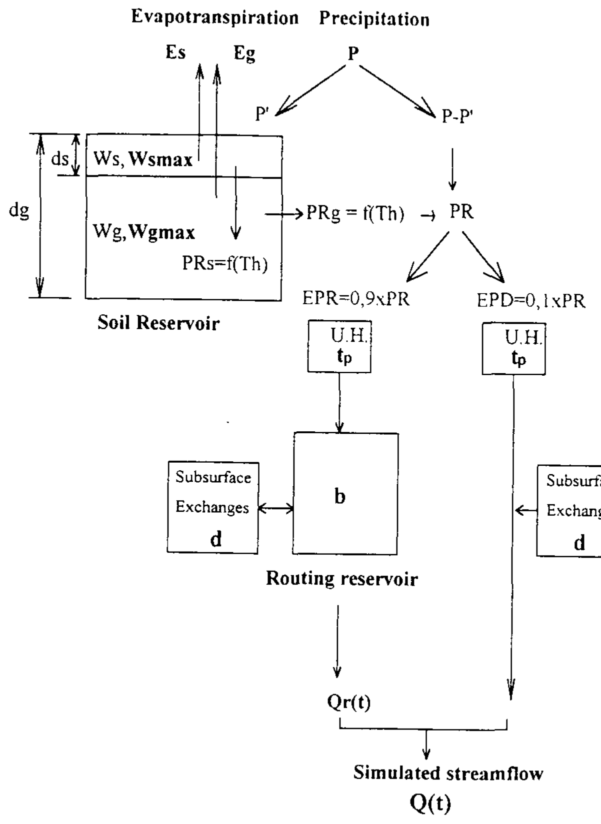

Fig.5 - GRHUM model structure

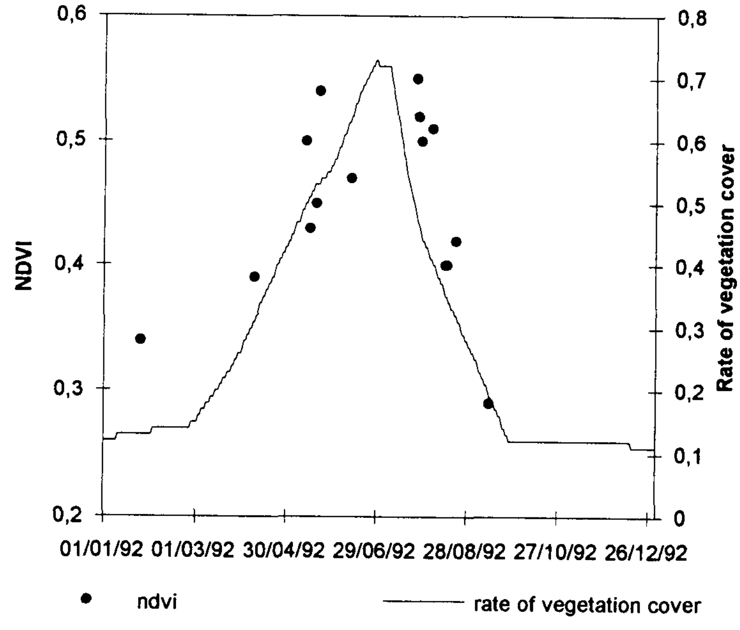

Fig.6 - Comparison between the rate of vegetation cover and the NDVI over the Naizin watershed

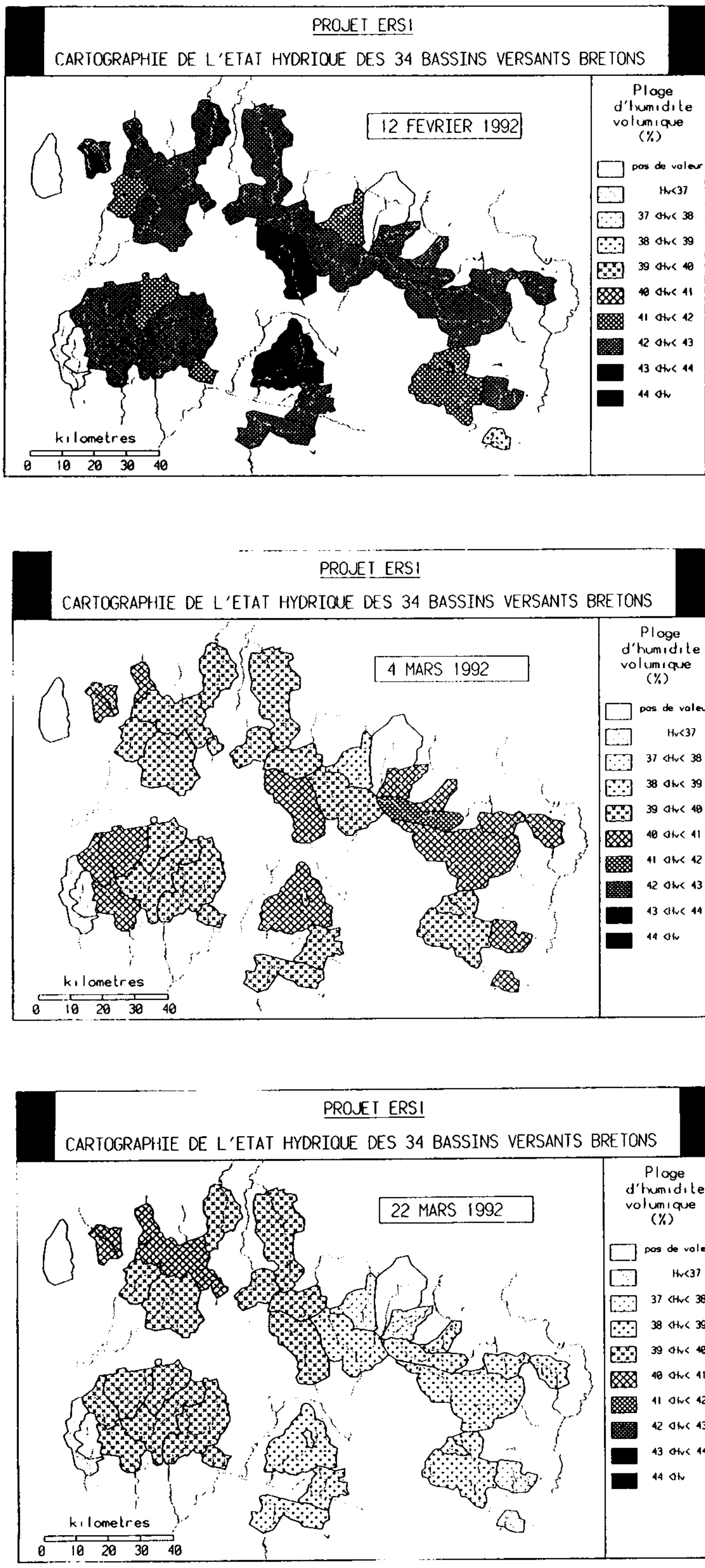

Fig.4a - Map of mean surface soil water state over Brittany watersheds at three different dates (Phase B)

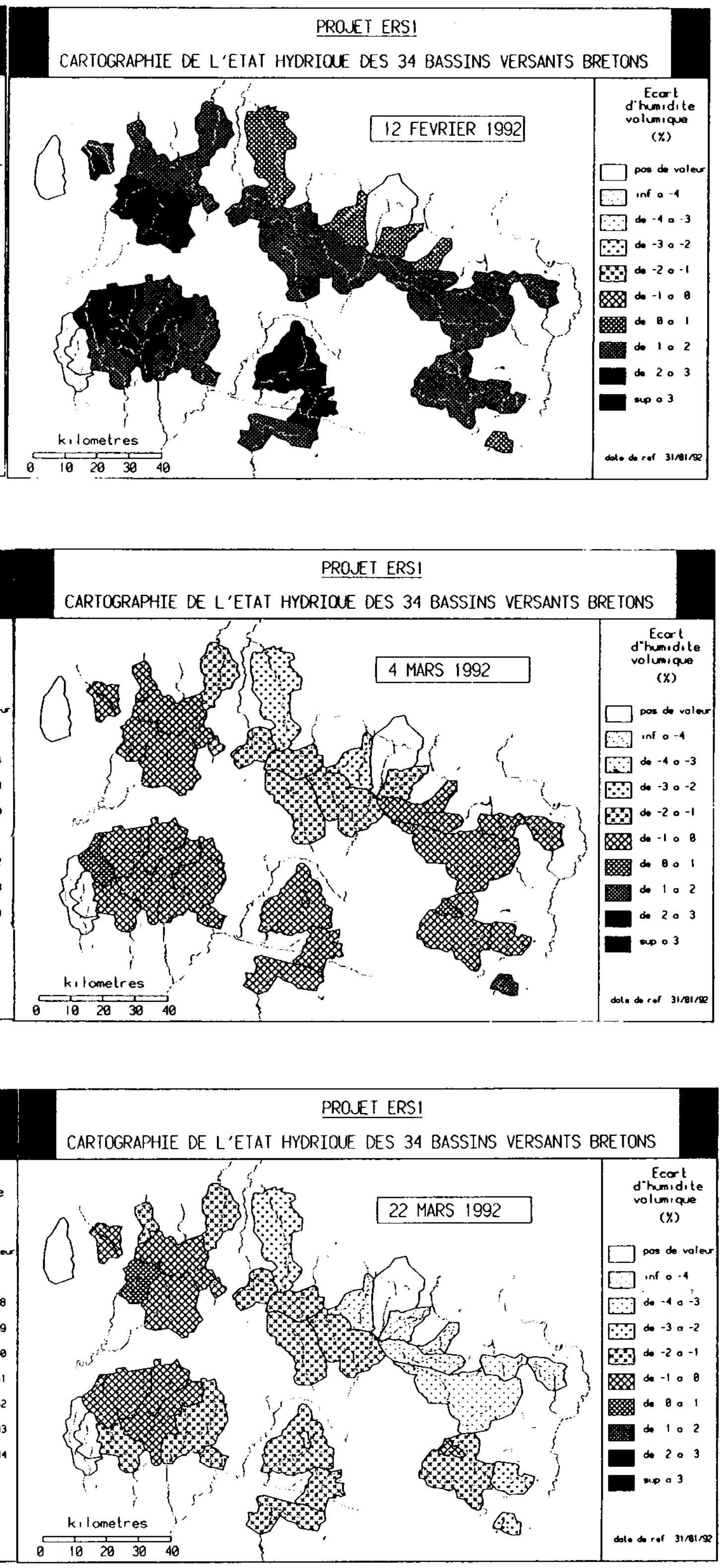

Fig.4b - Map of relative variations of surface soil water state over Brittany watersheds in comparison with a date of reference (January 31, 1992)

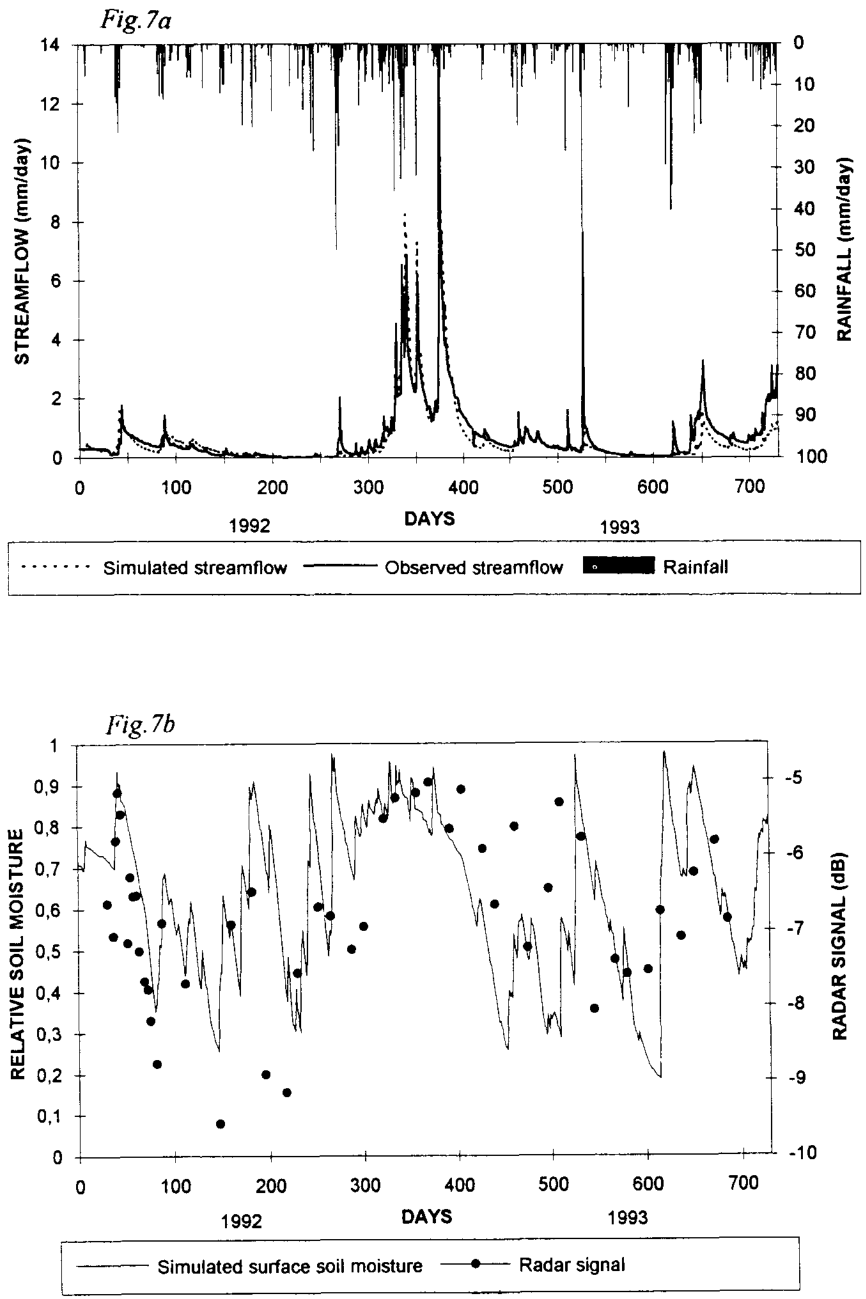

Fig.7 - Comparison between observed and computed streamflow (Fig.7a) and between mean radar signal and simulated soil moisture (Fig. 7b), over the Naizin basin for the years 1992-1993 (GRHUM model).

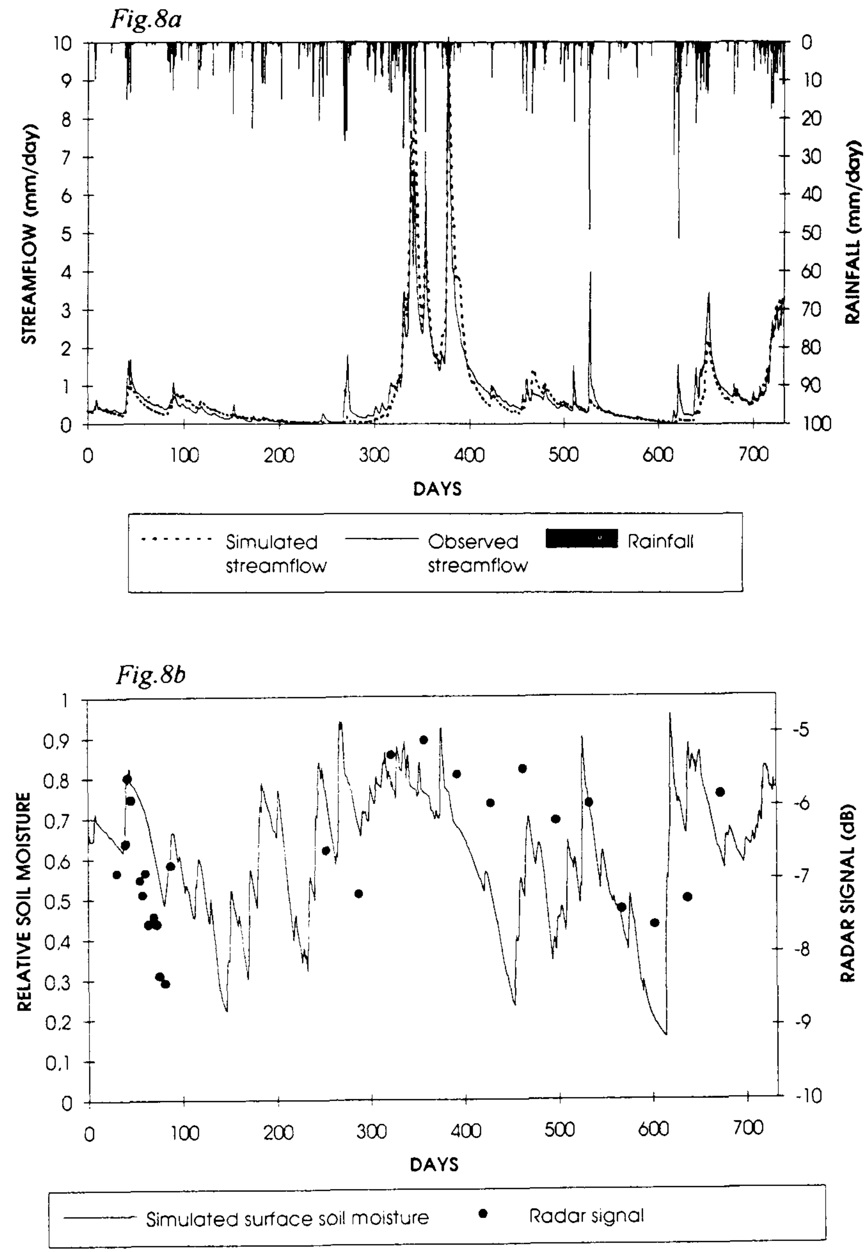

Fig.8 - Comparison between observed and computed streamflow (Fig.8a) and between mean radar signal and simulated soil moisture (Fig.8b), over the Evel basin for the years 1992-1993

MULTI-TEMPORAL ERS SAR DATA IN HYDROLOGICAL AND AGRO-ENVIRONMENTAL APPLICATIONS

CASE STUDY : THE ALSACE PLAIN

FELLAH K.*, BESNUS Y.**, CLANDILLON S.*, MEYER C.*, THOLEY N.*, and DE FRAIPONT P.*

* SERTIT, Boulevard Sébastien Brant, 67400 Illkirch, Tel : (33). 88.65.52.00, Fax : (33).88.65.51.99.
** LSIIT/GSTS, Boulevard Sébastien Brant, 67400 Illkirch, Tel : (33).88.65.50.44, Fax :(33).88.65.51.53.

ABSTRACT

Using a regional database, containing optical and ERS-1 SAR satellite imagery, plus data layers treating different aspects of the natural environment, this work involves evaluation studies of the potential of SAR data in hydrological and agro-environmental applications. This paper summarizes the work performed within this framework and attempts to identify present operational applications. Two approaches were utilized in this research. The first, a photo-interpretation approach, is applied to flood zone detection during an exceptional hydrological event, while the second a signal processing approach is aimed at performing quantitative bio-geophysical parameter measurement. In the latter, soil moisture is the parameter under investigation, while others such as the effect of vegetal cover were studied. The results show that there exists, at a regional scale, a strong correlation between the backscattering coefficient as calculated using ERS-1 imagery and a soil moiture parameter. Furthermore, this study points out that, due to statistical properties of speckle in SAR data, the level of accuracy of the soil moiture estimate depends on the scale at which the backscattering coefficient is measured. There exists therefore, a minimum spatial scale at which the quantification of a bio-geophysical parameter can be determined at a sufficient confidence level.

Remerciements,

Ce programme a été mis en oeuvre et enrichi grâce au Conseil Régional d'Alsace, et au Centre National d'Etude Spatiale, qui contribuent à son financement, à l'Agence Spatiale Européenne qui procure toutes les facilités pour la fourniture des données SAR, à l'ESTEC-Earth Science Division pour leur coopération technique, et grâce à la contribution de Météo France, du Service des eaux et des milieux aquatiques d'Alsace et de l'Institut National de la Recherche Agronomique de Colmar, pour la fourniture de diverses informations nécessaires à la constitution de la base de données relative aux milieux naturels de la région étudiée.

1. INTRODUCTION

The study area, the Ried Centre Alsace, is situated between Strasbourg and Colmar on the Alsace plain. It is a very flat area, strongly influenced by water, being the flood zone of the Ill, a Rhine tributary. Beneath it is the largest drinking water quality aquifer in Europe. After canalization of the Rhine, an intensification of agricultural practices has occurred that has led to environmental changes, changes that the authorities wish to evaluate and control (sensitive biotope protection measures, CAP, land set-aside).

This work lies within this context and the objectives are to evaluate hydrological information that can be obtained from ERS satellite data and to define its applications in agricultural and environmental fields. Two approaches were used, a photo-interpretation approach for flood event detection during an exceptional hydrological event and a quantitative approach for measurement of bio-geophysical parameters. In the quantitative approach, soil moisture is the parameter under investigation, while others such as the effect of vegetal cover were studied. This work is performed within a geographical information system using an extensive multi-source regional data base.

2. DATA BASE

The programme's first stage involved the building of a large data base aimed at isolating information relating to soil moisture by dissociating and evaluating the importance of the parameters that affect radar signal return. The data base contains calibrated ERS-1 SAR and optical satellite data, plus exogenous data, all the data are georeferenced and therefore superimposable.

ERS-1 data

More than twenty essentially springtime or autumnal ERS-1 images were selected between 1991 and 1995. These periods reflect contrasting hydrological regimes. Meteorological data were used in choosing ERS-1 scenes enabling the differentiation between moisture due to rainfall and that caused by other factors (soil moisture retention, water table, etc..).

Optical satellite data

ERS-1 synchronous, SPOT XS data, between 1991 and 1993, allowed the realization of a precise landuse classification. Thematic masks were defined per class (water, forestry, grassland, crops, urban) permitting the segmentation of the radar data. These were analyzed theme by theme in the double aim of measuring between theme radar signal variations and of detecting the intra theme variations.

Exogenous data

These are comprised of a DTM, scanned cartographic data (piezometric, pedological and substrate deposits data), providing information on the natural environment, administrative cadastral coverage, and, aiding ERS-1 selection, meteorological data, particularly rainfall data that were spatially mapped. These are completed by synchronous airphoto and field data, the observations consisted of taking ground and air photographs plus the noting of diverse characteristics (landuse practices, surface rugosity, vegetal growth stage, qualitative estimation of soil moisture and composition).

3. FLOOD EVENT DETECTION

Remote sensing technique potentialities in flood event detection are of great interest in the flood zone of the Ried Centre Alsace. This potentialities have been tested over the Camargue region, while envisaging an eventual application of the methodology in Alsace. A poster demonstrating the extent of the October 1993 Camargue flood was edited in 1993 on behalf of the CNES and SPOT Image. This contract was carried out via an ERS/SPOT integration using a 26/03/93 SPOT XS image and two ERS-1 scenes from the 16/10/93 and the 01/11/93 (Tholey et al., 1995).

This study shows that ERS-1 multitemporal analysis combined with SPOT XS data affords flood monitoring and therefore furnishes information relative to flood extent, flood persistence, flood impact and therefore flood damage.

At present, the use of SAR data in the detection and monitoring of floods can be considered as operational. The fields of application can be identified as follows: natural hazard risks; regional planning and environmental monitoring. The potential users and actors are: state services and local/regional planning authorities; civil protection authorities; insurance companies and building industries.

4. QUANTITATIVE MEASUREMENT OF BIO-GEOPHYSICAL PARAMETERS

The aim of this approach is to attempt to determine a quantitative measurement of a bio-geophysical parameters from ERS-1 data. Soil moisture is a particularly interesting example of these geophysical parameters. With its system configuration parameters (C-band, VV polarization) and an incidence angle of 23°, the ERS-1 SAR should provide near optimal sensitivity to soil moisture in combination with a minimal sensitivity to soil surface and vegetation roughness (Ulaby, 1974). For these reasons, a study of soil moisture was performed using a GIS type information system over the Alsace plain.

4.1 Researching a quantitative approach for soil moisture retrieval

The work realized to date is at a regional scale. Before studying the sensitivity of SAR to soil moisture, tests on signal temporal stability and on the effects of land cover were realized. This work has given rise to publications (Fellah et al., 1994) that are summarized below.

ERS-1 SAR signal temporal stability

In order to enable the comparison of backscattering coefficients obtained for all scenes, it is important firstly to ascertain the stability of the signal and the influence of the incidence angle per theme considered. A test was therefore performed for several land cover types taken from a multitemporal SPOT XS classification on two ERS-1 scenes acquired 12 hours apart with no rain being recorded within the time interval. The backscattering coefficient calculated for the grassland, cropland and forest themes on both ERS-1 images is very stable (less then 0,15 dB variation). An excellent backscattering stability is noted. It is therefore possible to define a thematic signature for each theme taken into account.

Effect of landcover on the signal

An analysis of backscattering coefficient temporal variations vis-à-vis the following landcover themes, forestry, grasslands and croplands, was carried out between Spring 1992 and Autumn 1993. The forestry's backscattering coefficient is practically stable at -7.7dB +/-0.2dB. Between Spring and Autumn, the backscattering coefficients for both grassland and cropland augment by 2dB and 3dB, respectively. These variations are, in particular, explained by the evolution of the vegetal cover between Spring and Autumn. Equally, a backscattering coefficient variation for the grassland and cropland themes is observed in the case of temporally close acquisitions for which landuse would have no changed. The reason for these variations must be directly linked to soil moisture variations.

Sensibility of ERS-1 SAR to soil moisture variation

The aim of this analysis is to pinpoint the sensibility of ERS-1 SAR image backscattering coefficients to the volumetric soil water content. To accomplish this, a rainfall event preceding the 17/04/92 ERS-1 acquisition was mapped with respect to the backscattering coefficient retaining the two themes grassland and cropland. As detailed in Fellah et al. (1994) and shown in Fig. 1, there is a strong correlation between the ERS-1 SAR backscattering coefficients calculated over large surfaces and volumetric soil moisture content linked to recent rainfall events.

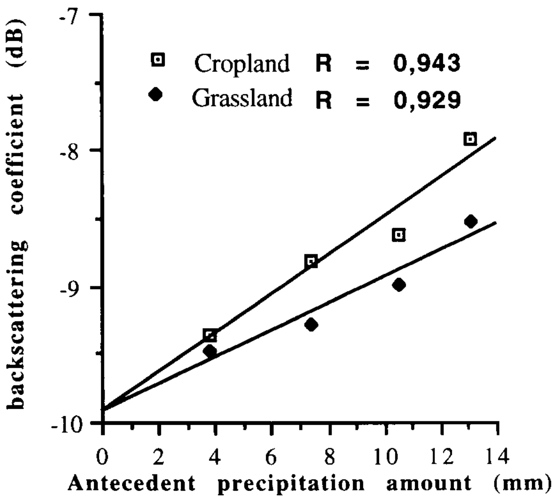

Fig. 1. Correlation between backscattering coefficient and antecedent precipitation amount.

With the potential for measuring soil moisture having been demonstrated, it is important to identify the types of applications in which routine measurements of soil moisture could be useful. In the case of hydrological applications, studies are performed aimed at estimating the spatial and temporal distribution of soil moisture content for different types of applications at various spatial scales of observation: from local scales for agriculture to global scales for climate models. The results as obtained at a regional scale, open interesting fields of applications in the meteorological and environmental fields and inversion algorithms are therefore being investigated. Furthermore, this study points out that, due to the statistical properties of speckle in SAR imagery, the accuracy level of of the soil moisture estimate depends on the scale at which the backscattering coefficient is determined.

4.2 Impact of observation scale on the level of accuracy of the soil moiture estimate.

In order to test the potential and limitations of ERS-1 SAR in local to global scale hydrological applications, the impact of observation scale on SAR radiometric resolution and therefore on the level of accuracy of the soil moisture estimate has to be investigated.

Impact of observation scale on SAR radiometric resolution.

Using the well-known intensity averaging technique, variations in the backscatter measurement due to radiometric resolution errors are a function of the number of pixels used for the derivation of the backscattering coefficient as illustrated in Fig. 2.

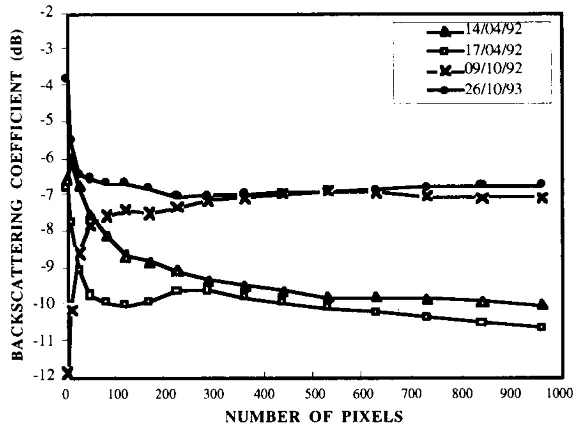

Fig. 2. Backscattering coefficient versus the number of pixels from data extracted from ERS-1 SAR GEC products for a cropland area on four different dates.

Backscatter measurements were performed over a test site consisting of cropland using four different acquisition dates with georeferenced ERS-1 SAR GEC images. With a low number of pixels N, a high variability of the measured backscattering coefficient is noted. For higher values of N, the measured backscattering coefficient converges to one value. If the instrument noise is assumed to be negligible and if the area of investigation is perfectly homogeneous and flat, this value would be the expected backscattering coefficient for the area.

Interpreting a time series of these measurements at different scales of observation could lead to different or even contradictory results. Therefore, a prerequisite in the temporal and spatial analysis of the backscattering coefficient's behavior is the determination of the amount of pixels for which the backscattering coefficient measurement is statistically valid in order to relate this measurement to bio-geophysical information with a sufficient confidence level.

Relationship between SAR radiometric resolution and observation scale.

Depending on the statistical uncertainties in the SAR signal due to speckle, the radiometric resolution varies as a function of the product's Effective Number of Looks and the spatial integration of pixel values within a certain area of interest corresponding to a specific observation scale. A study based on a statistical modelling of the SAR signal over natural surfaces has been investigated in collaboration with ESTEC, Earth Science Division. A relationship between SAR radiometric resolution and observation scale has been established and validated in the case of ERS-1 SAR product. The methodology and the validation of the SAR radiometric accuracy assessment are described in detail by Bally and Fellah (1995). Table 1 illustrates the impact of the spatial integration of pixels values on the radiometric resolution. Confidence levels are presented versus the number of pixels within an area of interest.

Table 1: Confidence levels versus area of interest extent in pixels for radiometric resolution ranging from 0.5 dB to +/- 5 dB.

Radiometric resolution: bounds around mean intensity (+/-) (dB)										Number of ERS-1 pixels		
0.5	1.0	1.5	2.0	2.5	3.0	3.5	4.0	4.5	5.0			
Confidence level, (%)										near range	mid swath	far range
15	30	43	55	66	74	81	86	89	92	1	1	1
17	34	49	62	73	81	87	91	93	95	5	5	4
19	38	54	68	78	86	90	94	96	97	7	6	5
28	53	71	84	92	96	98	99	99	99	12	11	10
34	62	81	92	97	99	99	99	99	99	18	16	14
39	69	87	96	99	99	99	99	99	99	24	21	19
59	89	98	99	99	99	99	99	99	99	61	54	48
75	97	99	99	99	99	99	99	99	99	121	107	95
84	99	99	99	99	99	99	99	99	99	182	161	143
89	99	99	99	99	99	99	99	99	99	242	214	190
93	99	99	99	99	99	99	99	99	99	303	268	238

The following example illustrates the use of the relationship between radiometric resolution and observation scale. In this example, the following requirements are established:

- Required measurement accuracy is 5% for soil moisture retrieval between a range of 10 to 40% (Evans, 1995).
- Using ERS-1 PRI product and the experimental results over the Flevoland test site (Borgeaud et al., 1993), the above requirement corresponds to a backscattering coefficient measurement accuracy of 0.5 dB.

At pixel scale, the confidence level for +/-0.5dB accuracy bounds is very low (15%). A +/-0.5dB measurement accuracy cannot be achived with suitable confidence level unless intensity averaging is applied with a consequent sacrificing of spatial resolution. If the number of pixels is larger than 214 pixels in the mid swath region the required accuracy bounds are obtained for the measurement with a confidence level of 90%. This corresponds to an area of interest of at least 3 hectares which represents the minimum spatial scale of observation to meet user requirements.

The outcome of study's evaluation of the accuracy of the backscattering coefficient briefly presented here, permits the definition of the statistical validity of the backscattering coefficient measurement as a function of observation scale. This relationship permits the determination of a minimum spatial scale compatible with a certain confidence level to estimate a bio-geophysical parameter, (Fellah et al., 1995).

5. CONCLUSION

It has been shown in this paper, that the photo-interpretative approach, as applied to flood zone detection, whilst involving ERS-1 multitemporal analysis combined with SPOT XS data, enables the monitoring of floods. Hence, it furnishes information relative to flood extent, flood persistence, flood impact and therefore to flood damage. Flood event detection can be considered therefore as an operational application in several fields (natural hazard risk assessment, environmental monitoring and regional planning).

Furthermore, in the quantitative approach for soil moisture retrieval, a strong correlation between the ERS-1 backscattering coefficient and a soil moisture parameter was found at a regional scale. This study also points out that this correlation is not valid for local observation scales. Due to this, a relationship between SAR radiometric resolution and observational scales has been investigated, established and validated in the case of ERS-1 SAR products. This permits the determination of a minimum spatial scale at which the backscattering coefficient measurement can be achieved with a given level of confidence in order to derive quantitative bio-geophysical information. Moreover, it confirms that interesting perspectives exist for large scale applications (meteorological / environmental) and presently, with this in mind, inversion algorithms are being investigated under an ESA pilot project AO2-F112.

6. REFERENCES

Bally P. and Fellah K., 1995, Evaluation of the accuracy of the Backscattering Coefficient Measurement in SAR data products. ESA - *Earth Sciences Division, technical note, July 1995*, 36pp.

Borgeaud M., Noll J., Bellini A., 1993, Use of ERS-1 SAR data for land applications. *Proceedings of the Second ERS-1 Symposium : Space at the Service of our Environment, Hambourg, 11-14 Oct. 1993*, ESA SP-361, pp 845-847.

Evans D.L., 1995, Spaceborne Synthetic Aperture Radar: Current Status and future Directions. A Report to the Committee on Earth Sciences. *NASA Technical Memorandum 4679, Washington, D.C.*, 171 pp.

Fellah K., Besnus Y., Clandillon S., Ettajani A., Meyer C and de Fraipont P., 1994, Multi-temporal ERS-1 SAR data in environmental studies: researching a quantitative approach for soil moisture retrieval. *Proceedings of the First ERS-1 Pilot Project Workshop, Toledo, 22-24 june 1994*, ESA SP, 85-92.

Fellah K., Bally P., Besnus Y., Meyer C., Rast M. and de Fraipont P., 1995, Impact of SAR radiometric resolution in hydrological and agro-environmental applications. *Proceedings of the International Symposium on the Retrieval of Bio and Geophysical parameters from SAR data for Land Applications, Toulouse, 17-20 october 1995.*

Tholey N, de Fraipont P, Clandillon S., Fellah K, Yescu H, 1995, Examples of the use of Remote Sensing at SERTIT in the Field of Water Management. *Satellites Systems for Environment Crisis Management EUCOSAT Workshop on Water Management, 6th July 1995, Dijon, France.*

Ulaby F.T., 1974, Radar Measurements of Soil Moisture Content. *IEEE Trans. on Antennas and Propagation*, Vol. AP-22, N°2, 1974, pp 257-265.

APPLICABILITY OF SAR INTERFEROMETRY FOR OPERATIONAL MONITORING OF LANDSLIDES

J. Achache*,B. Fruneau and C. Delacourt

Département Etudes Spatiales, Institut de Physique du Globe de Paris
4 place Jussieu, 75252 Paris Cedex 05 France
Tel : 33.1.44.27.24.05 - Fax : 33.1.44.27.33.73

ABSTRACT

The technique of SAR interferometry has been shown to lead to accurate large-scale surface displacements mapping. Here, we demonstrate the capability of SAR interferometry to monitor small displacements on the scale of landslide with the same accuracy as ground measurements. Six different interferograms of the Saint-Etienne-de-Tinée landslide in southern France are derived from ERS-1 SAR images during the summer of 1991. Deformation fringes are clearly evidenced on these interferograms and show a steady-state deformation which can be modelled. This model is characterised by a gradient of displacements from the top to the bottom, and some lateral variations. Displacements obtained from SAR are shown to be very consistent with ground measurements and to provide a much more detailed description of the surface displacements. A similar description could only be obtained from the ground by significantly increasing the number of targets, thus increasing the cost of the ground monitoring.

1. INTRODUCTION

Landslides can be a major threat to populations in mountainous areas. Even when they occur away from inhabited areas, landslides can be a significant hazard and have a serious economic impact by blocking roads and rivers. The "La Clapière" landslide is a good example. It is located near Nice, in Southern France, on the left bank of the Tinée river.

This landslide, which extends over a few km^2 between 1100 m and 1700 m, is bounded at the top by a high lobate scarp (fig.1). It is also characterized by an active scree slope on the NW part. A competent layer, known as the barre d'Iglière, produces a sub-horizontal mechanical discontinuity at mid-level in the landslide

It threatens to obstruct the valley, and then may lead to an overflow of the upstream village of Saint-Etienne-de-Tinée. This hazard has been mitigated with significant road and tunnel construction. It has also been monitored by laser-ranging since 1982. Such a permanent monitoring requires the deployment and servicing of several tens of laser reflectors as well as daily measurement operations. We propose in this paper to apply the technique of SAR interferometry (Zebker et Goldstein, 1986 ; Gabriel *et al.*, 1988) to this landslide, in order to demonstrate its capability for studying small scale deformations. In particular, we compare the characteristics of SAR monitoring derived from this analysis to those of ground measurements.

Figure 1: The "La Clapière" landslide

2. INTERFEROMETRY

We constructed six interferograms with images acquired by ERS-1 with a 3-days repeat cycle, on descending orbits, on August 20, 23, 26, 29 and September 4, 1991.The interferograms are generated on a massively parallel computer (Connection Machine 5) (Delacourt *et al.*, 1996). The effect of topography in each interferogram is removed using a 5 m x 5 m DEM of the site provided by Institut Géographique National of France (Massonnet *et al.*, 1993 and 1995). The resulting differential interferograms are then projected from SAR geometry to DEM geometry. They correspond to a contour map of the component of the surface displacement field in the direction of the line of sight of the satellite. Significant phase variations associated with the landslide can be detected on these interferograms.

Figure 2 shows examples of 3-days and 9-days interferograms. The 3-days interferogram (fig.2a) provides the clearest picture of the landslide, due to its small baseline and a very short time interval. Its boundaries are well described, especially the

* *now at BRGM, Direction de la Recherche*
3 av. C. Guillemin, BP6009, 45060 Orléans Cedex 2.

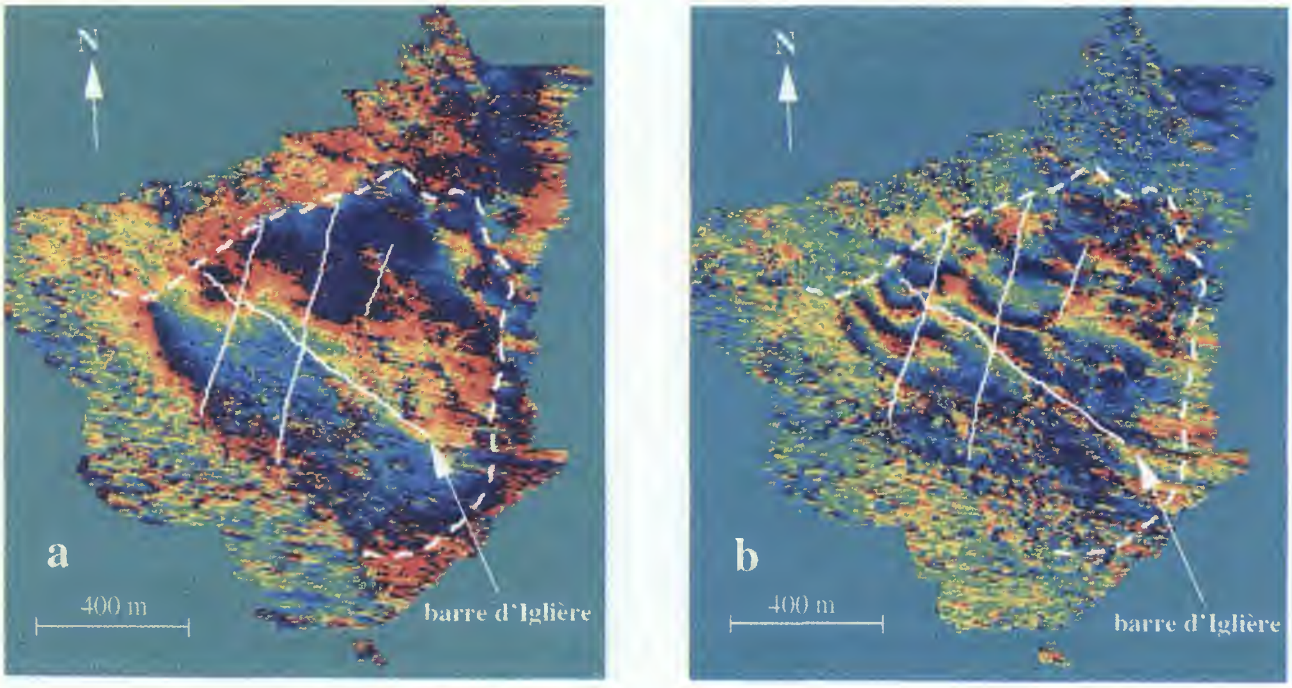

Figure 2: **a**. Differential interferogram of the 23-26 pair projected on the Digital Elevation Model. Dashed lines represent the limits of the landslide. Continuous lines correspond to the barre d'Iglière and N20° subverticl faults. **b**. Same as fig.2a for the 20-29 pair.

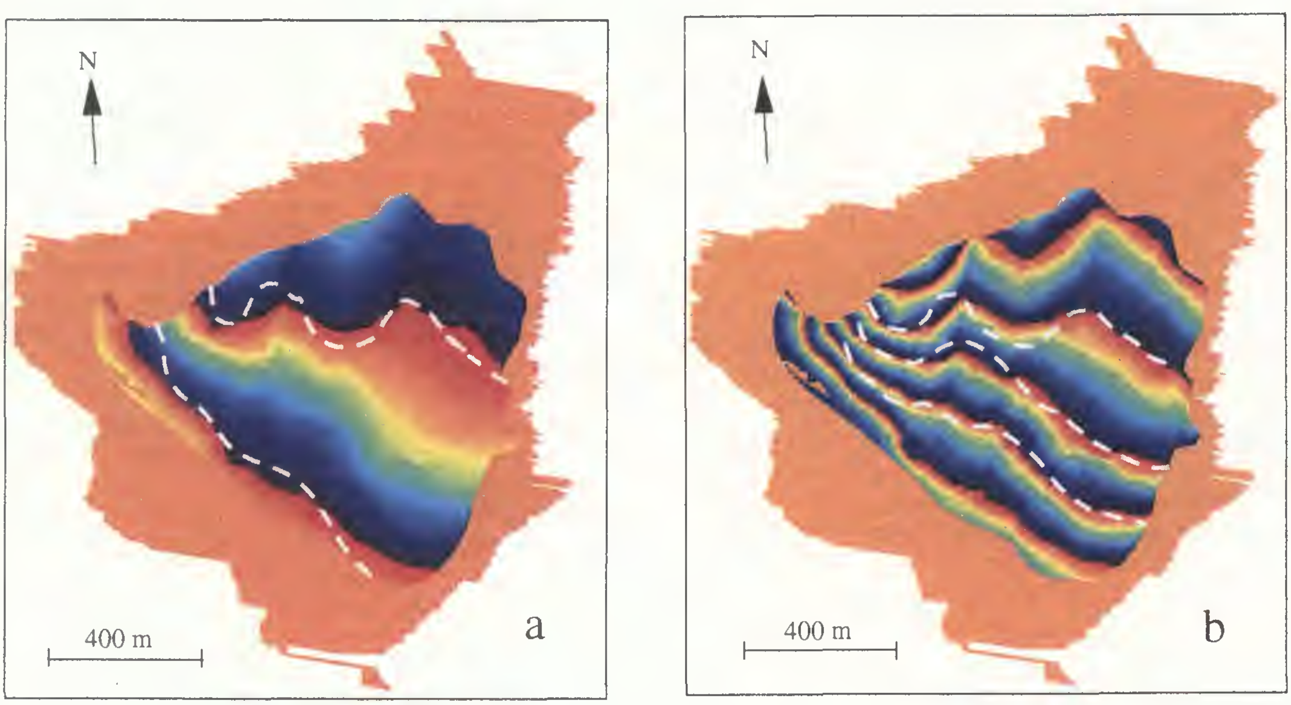

Figure 3: **a**. Synthetic interferogram based on a translational kinematic model. A top-to-bottom gradient of displacement which gradually decreases across the landslide from 1.5 cm/100 m in the NW to 0.5 cm/100 m in the SE. This interferogram should be compared with the 3 days interferogram of fig. 2a.Dashed lines correspond to the phase discontinuities observed on the real interferogram of fig.2a. **b**-The displacement field is increased be a factor 3 with respect to fig. 3a. To be compared with the 9 days interferogram of fig. 2b.

northwestern part and the 2 lobes at the top. The others present fringes with a lower SNR, because of larger baselines and larger time intervals. All computed interferograms are shown to be similar. The number of fringes increases linearly with the elapsed time between the various image acquisitions, while their overall geometry remains the same. This suggests that the observed landslide motion is stationary over the period surveyed. On all six interferograms, NW-SE trending fringes attest of a downhill movement characterised by a gradient of displacement from the top to the bottom of the landslide, the motion decreasing towards the bottom. A full phase rotation is equivalent to a displacement gradient of 3.9 cm along the landslide average steepest slope. The fringe intervals are not constant over the landslide, suggesting both downhill and lateral variations of the displacement gradient. This gradient changes from top-to-bottom, especially in the SE part: the gradient is very low between the intermediate scarp and the "barre d'Iglière" and seems to increase below this layer. This is consistent with the hypothesis that this layer behaves as a competent layer that blocks the movement and maintains some coherence in the upper part of the massif. From the active scree slope towards the SE, i.e. towards the right side, one observes a progressive increase of the fringe separation, indicating a decrease of the displacement gradient. This variation occurs near the N20° faults that cut the landslide.

The landslide (Fruneau *et al.*, 1995b; Fruneau, 1995) can be shown to be consistent with a simple model of translational slide with a variable gradient of displacement (fig.3). Furthermore, this modelling confirms the stationarity of the displacements.

Figure 4 displays the difference between modelled and observed fringes of the 23-26 pair. We observe a nearly uniform phase value over the area of the landslide, indicating a good agreement between the two interferograms over most of the sliding zone. At the eastern top of the slide, figure 4 displays significant phase variations over a small area. This evidences a small unit in the landslide which movement is rapid, and which has not been taken into account by the uniform translational model.

3. COMPARISON BETWEEN SAR AND GROUND MEASUREMENTS

The interferometric analysis provides accurate estimates of the displacement gradients in close agreement with existing ground measurements. Figure 5 shows displacement vectors monitored on ground superimposed on displacement vectors derived from our model (which gives a smoother representation that the noisy real interferograms). Some discrepancies are observed on fig. 5b near the bottom of the slide. This can be explained by the fact that interferometry provides only the gradients of displacement. Then only relative displacements can be evaluated because of the discontinuity of the movements between the landslide and the steady massif and ground reference points are necessary to determine absolute displacements. A constant displacement corresponding to the bottom displacement should be added to our model. This shows the complementarity of ground and SAR measurements. Absolute displacements vary from an average value of 5 mm/day at the bottom of the landslide, to 1.5 cm/day in the middle, and about 4 cm/day at the top.

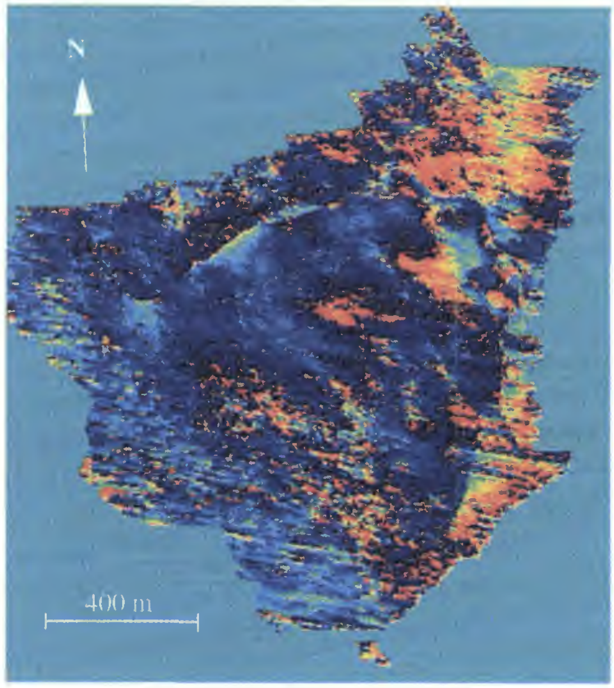

Figure 4: Difference between the real and the modelled interferograms of the 23-26 pair.

4. LIMITATIONS

The major limitation of SAR interferometry is the loss of coherence between the 2 images due either to changes in the orbital geometry of the two acquisitions or to ground surface changes. The two orbital tracks have to be within a few hundred meters to preserve the coherence. This limits the number of interferograms which can be produced from satellite images (among the 10 potential interferograms which could be generated with the 5 ERS-1 images, only 6 have good coherence). Ground-surface changes also affect directly the contribution of individual ground targets to the phase. Coherence loss then occurs often in the presence of vegetation or surface water. This is the case for interferograms of the landslide (see the upper part of the interferograms). We note that the active scree slope where there is little vegetation remains the most coherent part.

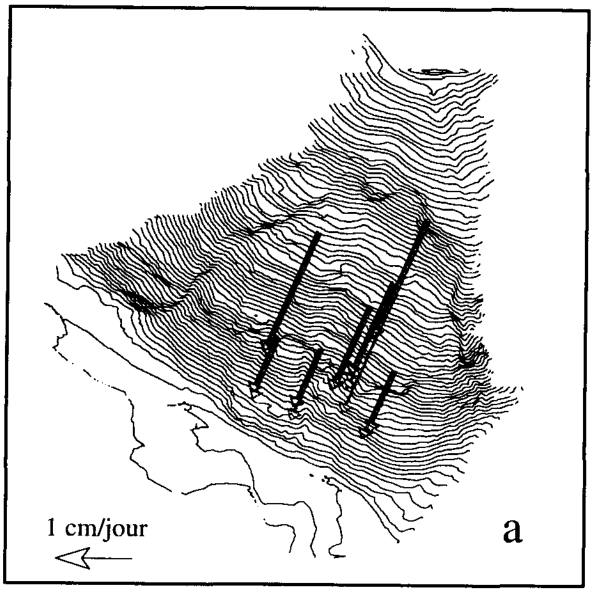

Figure 5: **a**. Displacement vector measured on ground by laser telemetry (grey arrows) and computed from the model (black arrows) for the 20-29 period. **b**. Same as fig.5a for the 26-04 period.

5. SAR VERSUS GROUND MONITORING

The accuracy of the two techniques is comparable. But the resolution is much better in the case of SAR interferometry, as a higher density of measurements can be achieved at no extra cost. SAR monitoring provides continuous displacement fields in comparison with discrete ground measurements. It also allows to detect local instabilities (in this study we detect a small block at the upper east part) which may not be disclosed by ground measurements if it has not been anticipated and laser targets have not been installed in this particular area.

The costs of SAR images and processing are considerably lower than the cost of network deployment and maintenance (measurements, calibrations, repairs). Furthermore, SAR interferometry is an all time - all weather method. It requires however the existence of a DEM, and of 1 or 2 reference points to achieve absolute displacements.

6. CONCLUSION

This investigation demonstrates the capability of SAR interferometry to monitor surface displacements at the scale required for this application. If this technique can be applied to all landslides where SAR images are available, it will represent a significant cost reduction with respect to ground surveying techniques. This technique is dependant on the loss of coherence due to vegetation.

The development of a similar technique of survey with ground radar is under investigation, and could be also promising for landslide monitoring.

7. REFERENCES

Delacourt, C., Duviols, J.L., Fruneau, B., et Achache, J., 1996, SAR interferometry processing using massively parallel computers, submitted to *Computers and Geosciences.*

Fruneau, B., 1995, Interférométrie différentielle d'images SAR. Application au glissement de terrain de la Clapière, Thèse d'université, Paris 7, 200p.

Fruneau, B., et Achache, J., 1995, Détection du glissement de terrain de Saint-Etienne-de-Tinée par interférométrie SAR et modélisation, *C.R. Acad. Sci. Paris*, t.320, Série IIa, p. 809-816.

Fruneau, B., Achache, J., et Delacourt, C., 1995, Observation and modelling of the Saint-Etienne-de-Tinée landslide using SAR interferometry, submitted to *Tectonophysics.*

Gabriel, A.K., Goldstein, R.M., et Zebker, H.A., 1988, Mapping small elevation changes over large areas: differential radar interferometry, *J. Geophys. Res.*, **94**, p. 9183-9191.

Massonnet, D., Rossi, M., Carmona, C., Adragna, F., Peltzer, G., Feigl, K., et Rabaute, T., 1993, The displacement field of the Landers earthquake mapped by radar interferometry, *Nature*, **364**, p. 138-142.

Massonnet, D., Briole, and Arnaud, A., 1995, Deflation of Mount Etna monitored by spaceborne radar interferometry, *Nature*, **375**, p. 567-570.

Zebker, H.A., et Goldstein, R.M., 1986, Topographic mapping from interferometric Synthetic Aperture Radar observations, *J. Geophys. Res.*, **91**, p. 4993-4999.

THE USE OF ERS-1 SAR FOR MONITORING OF ENVIRONMENTALLY SENSITIVE AREAS IN ENGLAND

Slater, J. (1), Brown, R.E. (2), and Wooding, M.G. (2)

1. ADAS, Brooklands Avenue, Cambridge, CB2 2BL
Tel: (44) 1223 462762 Fax: 1223 455911

2. Remote Sensing Applications Consultants, Mansfield Park, Medstead, Alton, Hants GU34 5PZ
Tel: (44) 1420 561377 Fax: (44) 1420 561388

ABSTRACT

This work was carried out as part of a project investigating the suitability and accuracy of satellite imagery for monitoring Environmentally Sensitive Areas (ESAs) in England. ESAs are designated areas of the countryside where farmers are encouraged to conserve and enhance characteristic landscapes and wildlife habitats.

In the Broads ESA monitoring concentrates on detecting the reversion of arable land to the traditional grazing marshes. The possibility of grass crops within an arable rotation makes the interpretation of single-date optical data uncertain, but the cost and cloud problems of optical imagery make the acquisition of several years of imagery impractical. It was found that using 3 years of single date ERS-1 imagery combined as a multi-temporal composite, allowed a rapid and cost-effective visual evaluation of whether arable farmland had permanently changed to grassland. This is an example of a simple but operational use of ERS imagery.

1. INTRODUCTION

The Broads ESA is one of 22 in England designated by the Ministry of Agriculture, Fisheries and Food (MAFF). The scheme encourages, through the voluntary participation of farmers, traditional forms of agriculture in order to maintain and enhance the characteristic landscapes and wildlife habitats of the areas designated. The Broads ESA covers some 30,000 hectares of river valley, marsh and fen in Norfolk and north Suffolk. A principal aim of this scheme is to stop and reverse the trend of conversion of traditional grazing marshes to arable production.

All ESAs are subject to an environmental monitoring programme to determine the impact of each scheme (Hooper, 1992) which is carried out by ADAS, an executive agency of MAFF. The accurate and cost effective detection of land cover changes between arable and grassland is a significant requirement of the monitoring programme. In 1993, a project was initiated to assess the feasibility of using satellite imagery within the programme. A key requirement was that any map updating system could be used by existing monitoring personnel with limited experience of image analysis. For operational monitoring, visual interpretation was used for change detection.

2. DATA

As part of the environmental monitoring programme for the Broads ESA (MAFF, 1991) a baseline land cover map was produced from 1:10,000 scale infra-red aerial photography flown in April/May 1987. This map shows the extent and distribution of the major land cover classes, such as grassland, arable, fen, reedbed and woodland at the outset of the scheme. The ESA was reflown in 1990, and a map of land cover changes produced using the new photography. These maps were digitised to produce change data and consist of polygons depicting areas of uniform land cover with associated land cover codes. Individual field boundaries are not shown.

Landsat TM images for 14 October 1987 and 6 April 1990, and ERS-1 SAR images for 20 November 1991, 12 November 1992 and 28 October 1993 were used.

3. ANALYSIS

Analysis was carried out using ERDAS IMAGINE software with the Vector Module and a customised map updating module. A display masking technique was used to check systematically for land cover changes (Brown, Slater and Askew, 1994). A viewer was opened in which the 1990 Landsat image was overlaid with the 1987 land cover vectors. A mask was used to hide all land outside the ESA boundary. Using the highlighting facility in IMAGINE, which is associated with the vector attribute table, areas of a particular land cover type from the 1987 map, for example arable, were viewed by 'painting out' all non-arable land. Looking between the 'painted out' areas to the 1990 image, any changes from arable to another land cover class could be more easily identified visually. A copy of the vector dataset in a separate viewer was updated where changes were identified.

Figure 1 Using ERS-1 SAR for change detection in The Broads ESA

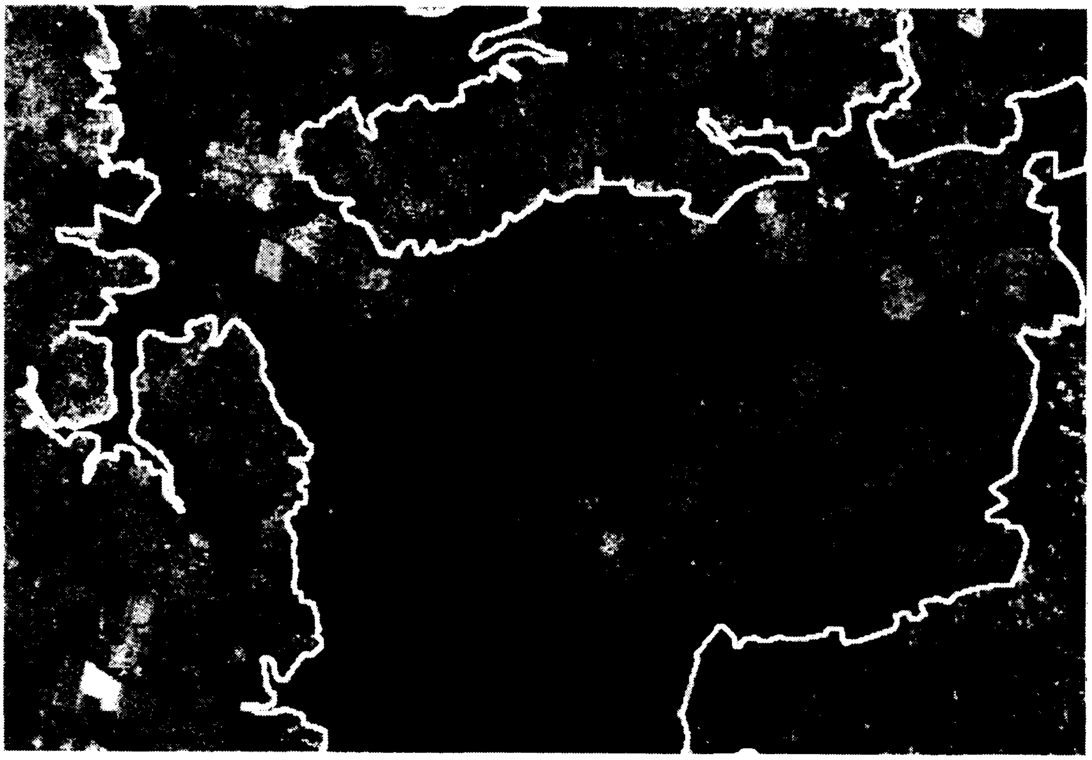

© ESA 1991, 1992, 1993

Multiyear ERS-1 SAR image of part of The Broads ESA, delimited by the white line. Arable areas are bright, grassland is dark.

Band 1 (Red) : 20 November 1991
Band 2 (Green) : 12 November 1992
Band 3 (Blue) : 28 October 1993

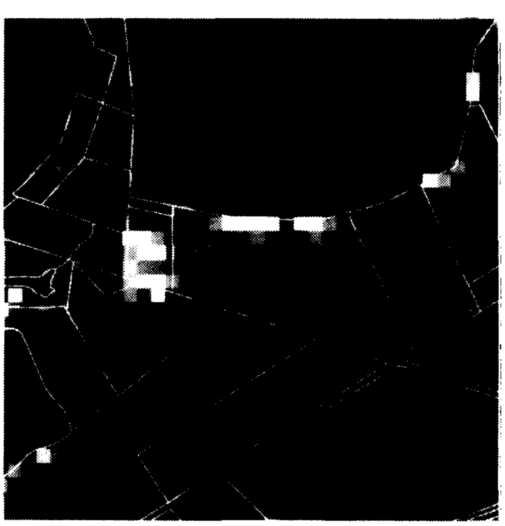

1991

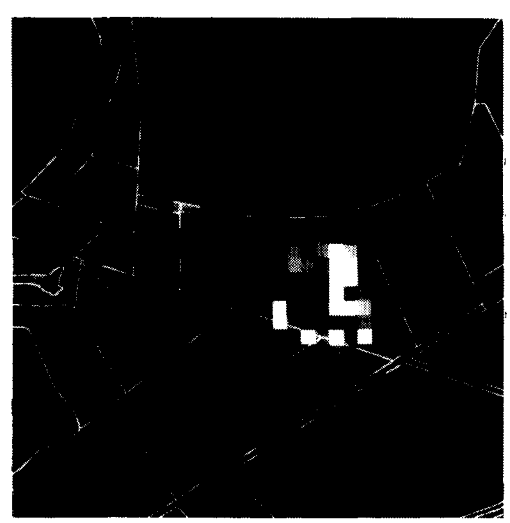

1992

Extract of the ESA with single-year images and land cover vectors.
The bright fields are arable, dark areas are grass.
Note that both arable areas are grass in the other year, suggesting that the grass cover is part of an arable rotation.

4. EVALUATION

An updated change map based on the 1990 Landsat image was produced for a subset of the Broads ESA covering 9366 hectares, in the valleys around the lower reaches of the rivers Ant and Thurne, the Hickling Broad area and the Halvergate Marshes. This was compared to the map previously produced from aerial photography (Slater and Askew, 1992). In all, about 10% of all arable land in the subset area has reverted to grassland use, principally as a result of the ESA scheme. Very little of the total area changed to arable and most of this was missed by visual interpretation from satellite imagery. A larger area of grassland interpreted from imagery for land not in the ESA agreement, 95 hectares instead of 65, is due largely to the ambiguity of deciding whether a grass cover implies permanent grassland or grass ley in arable rotation. Grass leys in arable rotation (temporary grassland) are part of an arable management regime and treated as arable land in the operation of the ESA scheme. The estimate of new grassland on land in the ESA agreement was very close, 227 instead of 228 hectares, due to the assumption that changes to grass cover would be permanent as a result of the ESA scheme.

Visual interpretation of imagery tended to overestimate change from arable to permanent grassland, due to confusion with temporary grass leys. It should be remembered that data derived from aerial photography is also subject to interpretation errors and is not equivalent to 'ground truth' data.

5. ERS-1 SAR IMAGERY FOR CHANGE DETECTION

Preparation of radar imagery
For visual interpretation purposes, the original 16 bit images were converted to 8 bit imagery. In order to preserve the required range of values, the images were divided by a constant before this conversion. Two multi-date composite images were created for The Broads ESA: a multitemporal image of 3 dates in 1992, and a multi-year image of 1991, 1992 and 1993.

Spatial Filtering for speckle suppression
A Lee filter was found to improve the ease of interpretation, however this initial work was carried out on unfiltered imagery due to the unavailability of the specialised software at the time.

Assessment of within-year multitemporal ERS-1 imagery
Using the 1992 image (30 July, 8 October, 12 November) grass and arable separated reasonably well, although no reference data for this year was available for rigorous comparison. Grass appears dark, and the rough surface of cultivated bare soil appears light, which is what would be expected from previous research on crop discrimination in East Anglia (Wooding, Zmuda and Griffiths 1993). Large arable fields are clearly discriminated from the surrounding grassland in the Halvergate Marshes, but the smaller fields in the valleys are less clear and are not always large enough to overcome the effect of speckle. Drainage ditches show changes and can be confusing. Summer grass management, i.e. cutting for hay or silage, may suggest changes which are not relevant; and grass areas appear darker in the multi-year image. The November band gave the best single-band discrimination between the 2 cover types.

Assessment of multi-year multitemporal imagery
This used a colour composite of autumn images from 1991 (20 November) in red, 1992 (12 November) in green and 1993 (28 October) in blue. A part of this image is shown in Figure 1. Arable can generally be discriminated from grass based on the grey tone of a single radar image acquired in autumn, the later dates in November being most effective for discrimination. Grass appears dark and the rough surface of bare soil appears light. There are fields where tones are ambiguous and as with other imagery used in the project, this increases for smaller fields which comprise only a few pixels. Where a dark tone appeared in the composite image the field had been under grass cover for three consecutive years. A red, green or blue tone indicated bare soil on one image within the period. Mixed bright tones and near white tones indicated continuous arable production.

6. USING A TIME SERIES FOR DISCRIMINATION OF PERMANENT AND LEY GRASSLAND

The particular issue addressed with the radar imagery was the accurate assessment of whether new grass land cover is permanent or part of an arable rotation. A run of data can be used to track fields to make a more definite decision on the likelihood of new non-agreement grassland being permanent. Aerial photographic cover over a run of years is too costly an option for the added benefit gained in increasing map accuracy and the likelihood of obtaining easily comparable cloud free Landsat imagery over a number of years is low. ERS SAR offers a source of seamless data covering large areas at a relatively low cost without the problems caused by cloud cover.

The 1991-1993 composite radar image for the study area, was used together with 1990 and 1994 TM imagery, to track 21 fields of new non-agreement grassland. These fields were identified from visual updating using 1990 satellite imagery and/or aerial photographs and include fields where there were discrepancies in change detection results using the two methods. Although no reference data on cropping was available for the sample of fields clear spectral signatures indicating arable or grass cover over the 3 years were seen on the composite radar image for 12 of the sample fields. A further 4 fields had clear signatures for 2 out of 3 years. No clear assessment of land cover over the three years could be made for 7 fields. The results suggest that the method may be suitable for operational use particularly if late autumn imagery can be obtained in all years.

An advantage of using a multi-year image is that 3 years of data can be quickly assessed in a single viewer. Areas where possible change is identified can then be analysed as single bands, i.e. single years, to verify changes. A disadvantage compared to the Landsat imagery is that small fields are less distinct and would be very difficult to locate without the vector maps on top.

The results confirmed that farmers on non-agreement land are converting arable to long term grassland use; with new grassland clearly evident each year on composite 1991-93 SAR imagery and still present on 1994 TM imagery, confirming that much of the overestimation of grassland based on a single year Landsat interpretation was in fact correct, and not just part of an arable rotation.

Fields were misinterpreted using both Landsat and aerial photo data sources, and in some cases fields which had appeared to revert to grassland have become arable again. In some cases the availability of 5 consecutive years of imagery clarified whether apparent changes to grass were permanent. Visual interpretation of a time series of satellite images is proving more accurate in resolving this issue than a single date of air photography or satellite imagery.

These results confirm the difficulties of identifying new permanent grassland no matter what the data source. However, the addition of multiple years of ERS SAR imagery to track the history of arable and grassland cover should help increase the accuracy of change detection.

7. POTENTIAL USES OF ERS IMAGERY IN ESA MONITORING

The technique described above was used operationally in the 1995 resurvey of The Broads ESA as a complement to aerial photos. The use of SAR imagery is also being actively considered for arable/grassland discrimination in other ESAs. The ability of ERS imagery to define the extent and distribution of winter flooding in the Somerset Levels and Moors ESA is currently being investigated.

8. CONCLUSIONS

This assessment of a simple use of ERS-1 imagery for a specific purpose proved an unexpected success, and has been partially adopted for an operational environmental monitoring requirement, to complement both aerial photography and optical satellite imagery. This study has shown that, subject to limitations of scale, this imagery can be used to discriminate arable farming from grassland in a lowland area of England. It has the advantage of being both a reliable and relatively cheap source of remote sensing data. It is feasible to buy several years of data which then can be visually assessed in a single pass as a multi-year composite image.

ACKNOWLEDGEMENTS

BNSC and MAFF funding of the Environmental Monitoring of Protected Landscapes project, are gratefully acknowledged.

REFERENCES

Brown, R., Slater, J. and Askew, D. 1994. Environmental Monitoring of Protected Landscapes - Monitoring Environmentally Sensitive Areas using satellite imagery, within GIS. AGI '94 Conference Proceedings, Association for Geographic Information, London.

Hooper, A.J. 1992. Field monitoring of environmental change in the Environmentally Sensitive Areas, in Whitby M.C. (ed.) ITE Symposium No. 27 Land Use Change: the causes and consequences, pp 52-59 HMSO London.

MAFF 1991. The Broads. Environmentally Sensitive Area Report of Monitoring 1991.

Slater, J. and Askew, D. 1995. Mapping Arable/Grassland Land Cover Changes by Satellite. Presented at EN&IN Conference, Budapest.

Wooding, M.G., Zmuda, A.D. and Griffiths, G.H. 1993. Crop discrimination using multi-temporal ERS-1 SAR data, Proceedings 2nd. ERS-1 Symposium - Space at the service of our environment, Hamburg, ESA SP-361.

URBAN CLIMATOLOGICAL PARAMETERS DERIVED FROM MULTISENSOR SATELLITE DATA OF ERS-1 AND LANDSAT-TM

Eberhard Parlow[1], Dieter Scherer[1], Horst-Dieter Beha[1], Hermann Goßmann[2] & Hans-Martin Braun[3]

[1]*MCR Lab, University of Basel, Spalenring 145, CH-4055 Basel*
Tel.: (+41) 61 2726480 Fax.: (+41) 61 2726923 email: parlow@ubaclu.unibas.ch

[2]*Institute of Physical Geography, University of Freiburg, Werderring 4, D-79098 Freiburg*
Tel.: (+49) 761 2033527 Fax.: (+49) 761 2033527

[3]*Raumfahrt und Systemtechnik GmbH, Abt-Vitus-Str. 4, D-88682 Salem*
Tel./Fax: (+49) 7553 6404

ABSTRACT

The urban climate is a locally limited man-made climate modification, which becomes more and more important since urban population is increasing and urban agglomerations are growing. A more striking fact is that this climate modification directly influences people's living and working sphere. In Germany 32 % of the total population is living in 73 cities with more than 100.000 inhabitants. Including the huge amount of smaller cities of 10.000 to 50.000 inhabitants one can expects that 60 to 75 % of the Central European population lives in urbanised areas. In many European countries there is a growing awareness on urban climate which leads to legal controls and the implementation of aspects of urban climate into planning strategies. By means of high resolution satellite data of ERS-1 and LANDSAT-TM many climatologically relevant parameters can be elaborated and can be used as input or validation data for mesoscale models of wind fields, ventilation and human bioclimate like cold stress in winter respectively heat stress in summer. Examples are presented from two testsites in the Upper Rhine Valley for the computation of aerodynamic roughness from ERS-1 data, a very detailed landuse classification with special emphasis to urban classes by using a multi-sensor approach with ERS-1 and LANDSAT-TM as well as meteorological informations of surface broadband albedo, surface temperature and net radiation from LANDSAT-TM.

1. INTRODUCTION

Planning our environment - be it urban or rural - means an anthropogenic impact on natural or semi-natural conditions. In urban agglomerations man's activities result in a complete and not invertible change of various environmental factors like climate, hydrology, vegetation, biodiversity, air chemistry etc. These changes directly influence the living and working spheres of mankind. Up to now there is an increasing pressure on the urbanized regions not only in industrial nations but also in developing countries. Keywords to be mentioned are urbanization, rural exodus, industrialization and urban heat island. Depending on the relevant environmental laws, which differ among the countries, urban planning demands for improved and more detailed analysis of the urban climate in scales which can only be carried out by using sophisticated numerical models and simulations. Besides many basic research needs to understand the complexity of the climate system, to an increasing extend climate models need a lot of spatially distributed data with the best spatial resolution available. This is both the challenge and the potential for remote sensing to make these data available to solve the important questions and to elaborate expertise of practical applications. Data extracted from remotely sensed data are characterized by their

- high spatial resolution,
- spatial availability over large areas,
- physical nature,
- temporal homogeneity even across national boundaries and
- potential easily to be updated.

2. MULTISENSOR APPROACH

Within the ERS-1 Pilot Study ERSCLiP (ERS based Climate Project) satellite data from ERS-1 and Landsat-TM are used to extract climatological parameters relevant for urban climate studies. The study was carried out at two testsites in the Southern Upper Rhine Valley at Freiburg/FRG and Basel/Switzerland. ERSCLiP was closely connected to the running climate project REKLIP, an international cross-border regional climate project (Parlow 1992, 1995; Fiedler 1992; IGBP 1993).

The conceptional framework of the multisensor analysis was to compute primary data sets of

Primary dataset	Sensor used
Aerodynamic roughness length	ERS-1
Landuse	ERS-1, Landsat-TM
Surface albedo	Landsat-TM
Surface temperature	Landsat-TM

Proceedings of the Second ERS Applications Workshop, London, UK, 6–8 December 1995 (ESA SP-383, February 1996)

In a further step a second set of derived data is extracted

- All wave net radiation which is the key factor of energy budget,
- Storage heat flux and
- Available energy.

The various resulting data can be integrated in numerical models like

- windfield models or
- bioclimatic models to compute heat stress conditions during summer.

An example of ERS-1 and Landsat-TM composites of the Basel testsites, which were used as input data for further analysis, are presented in figures 1 and 2. For the multitemporal ERS-1 composite data from 7th June 1992, 5th May 1992 and 4th September 1991 are used. The Landsat-TM composite is from 11th July 1991. So a temporal correspondence of multisensor data is guaranteed.

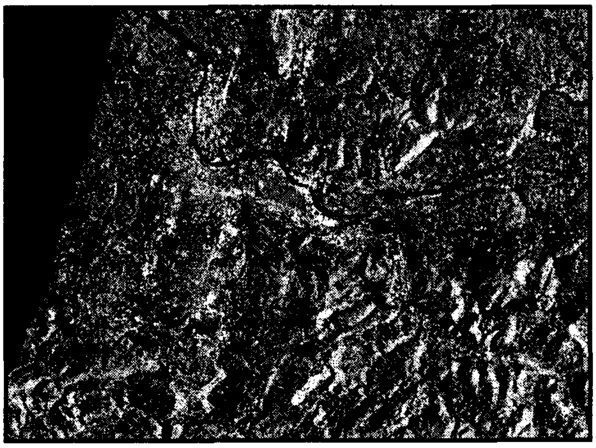

Fig. 1 : Multitemporal ERS-1 Composite Basel

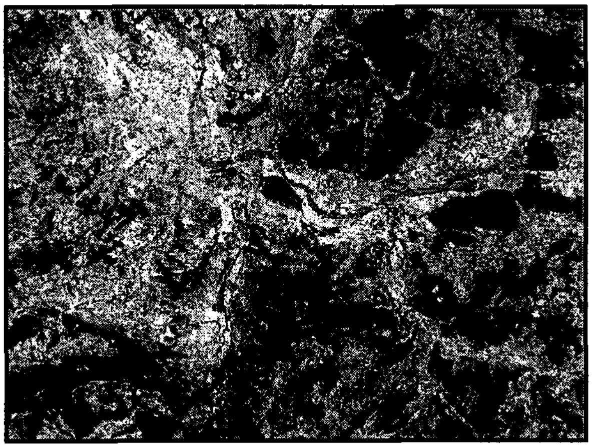

Fig. 2 : Multispectral Landsat-TM Composite Basel

For classification purposes a principal component analysis (PCA) was carried out with ERS-1 data from 22nd of May 1991 and Landsat-TM data from 11th July 1991. So a temporal correspondence of satellite data was guaranteed. No data were available in the top right corner of ERS-1 due to frame limitation. Therefore this area is only represented by Landsat-TM data and the information growth can easily be detected. Information of ERS-1 is nearly completely stored in the 3rd PC which increases the variance by 10 %. PCs 1-3 have a total variance of 98 %. Fig. 3 shows the RGB-composite of ERS-1 and Landsat-TM.

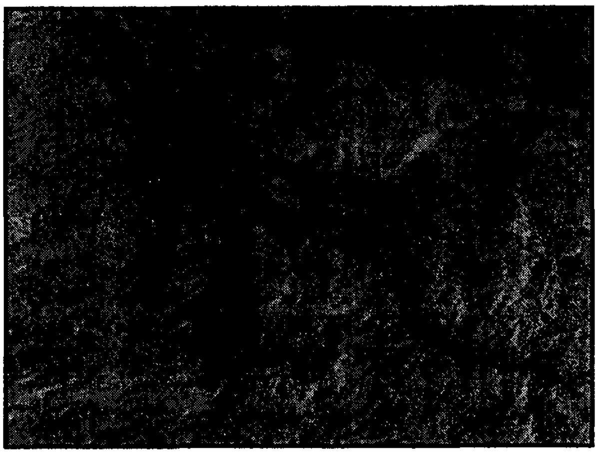

Fig. 3: Principle component RGB-composite of ERS-1 and Landsat-TM data fusion. Red colours correspond to ERS-1 information.

3. URBAN LANDUSE CLASSIFICATION

A detailed landuse classification of the testsite Basel was carried out by combining data from multitemporal ERS-1 and Landsat-TM. A total of 35 classes could be separated with 17 urban/industrial classes. The accuracy of the classification was 90.5 % and the improvement of the multisensor classification versus a pure Landsat-TM approach was +5 % in general and up to +7 % for some urban classes. Landsat-TM data was corrected from terrain induced illumination effects (Parlow 1996a). Fig. 4 shows the result of the landuse classification of the urban agglomeration of Basel/Switzerland. The accuracy and spatial resolution is appropriate enough to be applied for several planning purposes and climate analysis studies of the local authorities. Class definition was made according to the urban climatological relevance and the needs and definitions of the planning authorities (Scherer et al. 1996b, Beha et al. 1996). The integration of ERS-1 data helped especially to separate the various settlement types and industrial areas, because their structural physiognomy was better detected from ERS-1 as compared to Landsat-TM. Urban classes are presented in red and orange colours, forests in green, water in blue and arable land in brown colours.

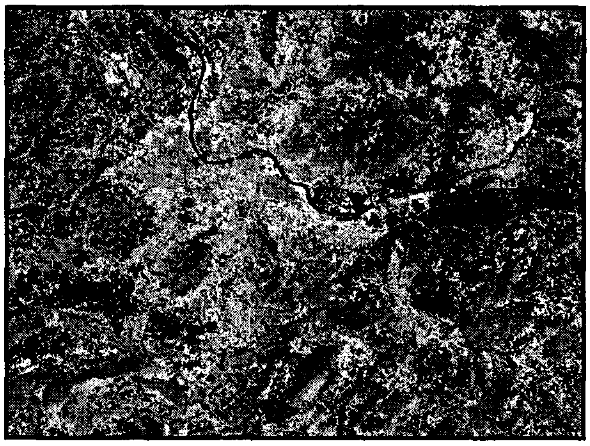

Fig. 4: Multisensor landuse classification of the urban agglomeration of Basel

4. METEOROLOGICAL DATA LAYERS DERIVED FROM LANDSAT-TM

Landsat-TM data was used in combination with numerical radiation models to compute various meteorological radiation fields which are relevant to urban climate. The methodological steps are summarized briefly. For more detailed information it is referred to Parlow (1996b). From illumination corrected optical data surface solar albedo was calculated. A digital terrain model gave the input parameters to compute solar irradiance with respect to inclined surfaces in mountainous areas. An arithmetic combination of albedo times solar irradiance results in the shortwave net radiation. After correction of atmospheric influences channel 6 of Landsat-TM corresponds to surface temperature and terrestrial longwave emission. By using vertical temperature and humidity profiles from weather station the atmospheric counter radiation can be parametrized quiet easily. Finally spatially distributed shortwave and longwave radiation fluxes are existing and the net radiation can be calculated. Fig. 5 and 6 give an information of albedo, shortwave radiation balance, surface temperature and all wave net radiation.

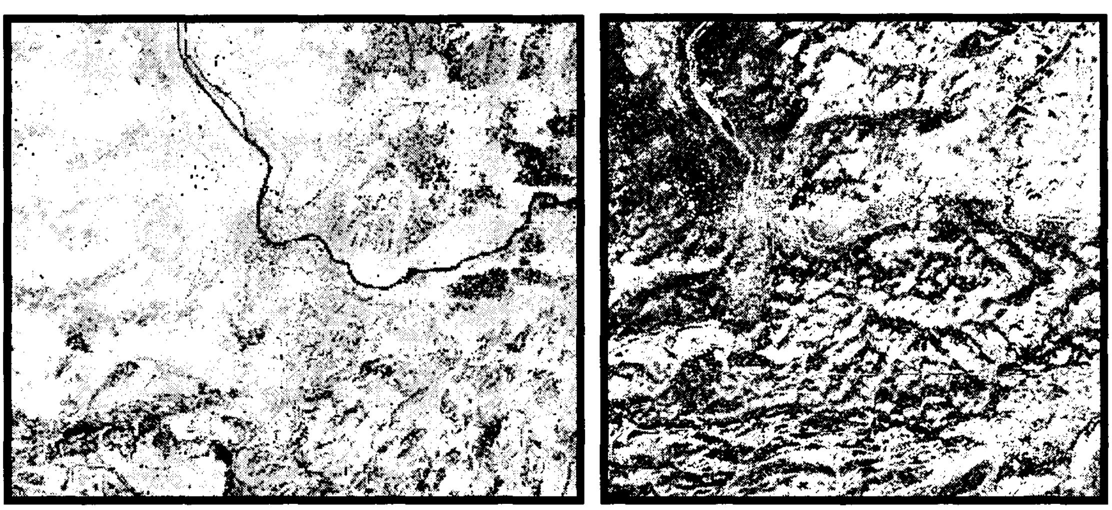

Fig. 5 : Surface albedo (left) and shortwave net radiation (right) of the agglomeration of Basel/Switzerland computed from Landsat-TM data and numerical radiation models for the time of Landsat-TM overflight.

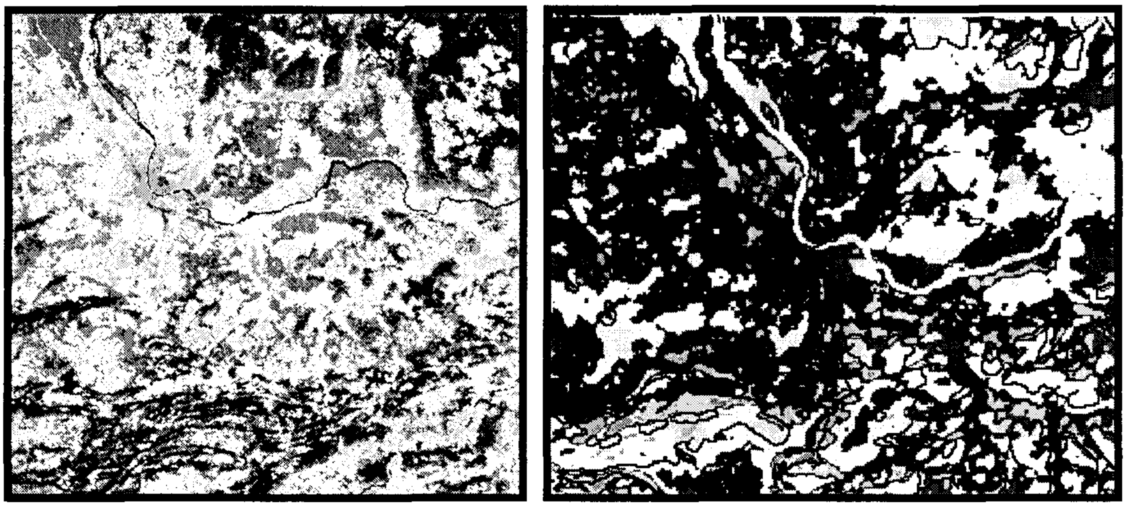

Fig. 6 : Surface temperature (left) and net radiation (right) of the agglomeration of Basel/Switzerland computed from Landsat-TM data and numerical radiation models for the time of Landsat-TM overflight.

5. AERODYNAMIC ROUGHNESS LENGTH FROM ERS-1 DATA

Modeling of wind fields is a standard application of urban climatology. The flow pattern of wind is an important information for the propagation of air pollutants, for temperature distribution and bioclimatic parameters like heat stress. Wind speed and turbulence structure is influenced directly by aerodynamic surface roughness. In micrometeorology this parameter is called aerodynamic roughness length (z_0). It determines the vertical wind profile. Aerodynamic roughness length was derived from ERS-1 data for non-forested areas in the Basel testsite. Roughness lengths of forests could not be calculated form SAR data because normally they have a high roughness length but low digital counts in SAR imagery. So forests had to be treated separately. Fig. 7 shows aerodynamic roughness length. For further methodological informations it is referred to Scherer et al. 1996a.

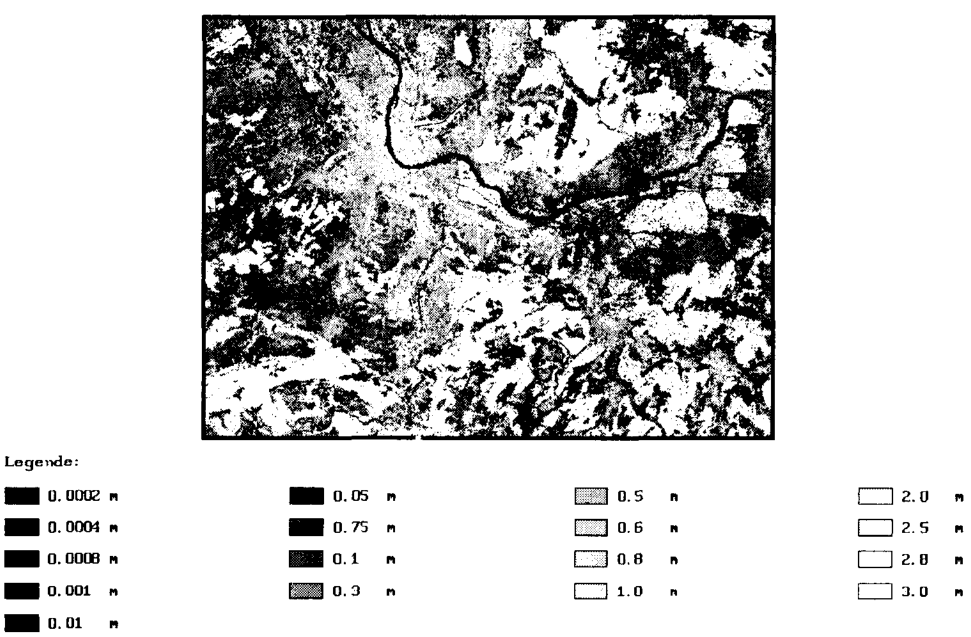

Fig. 7 : Aerodynamic roughness length z_0 of the city of Basel derived from ERS-1 data

The vertical wind profile can be written as:

$$\bar{u}(z) = \frac{u_*}{k} \ln \frac{(z-d)}{z_0}$$

with $u(z)$ = windspeed at height z
u_* = friction velocity
k = von Karman's constant (0.4)
z = height
d = zero plane displacement
z_0 = aerodynamic roughness length

The application of a windfield model for planning purposes is shown in fig. 8. Using the model FITNAH the local wind field was computed for the ERSCLiP testsite Freiburg/FRG. Results of windfield models can be improved if better input data of aerodynamic roughness, landuse and radiation fluxes are made available. Satellite data have the potential to fill this gap.

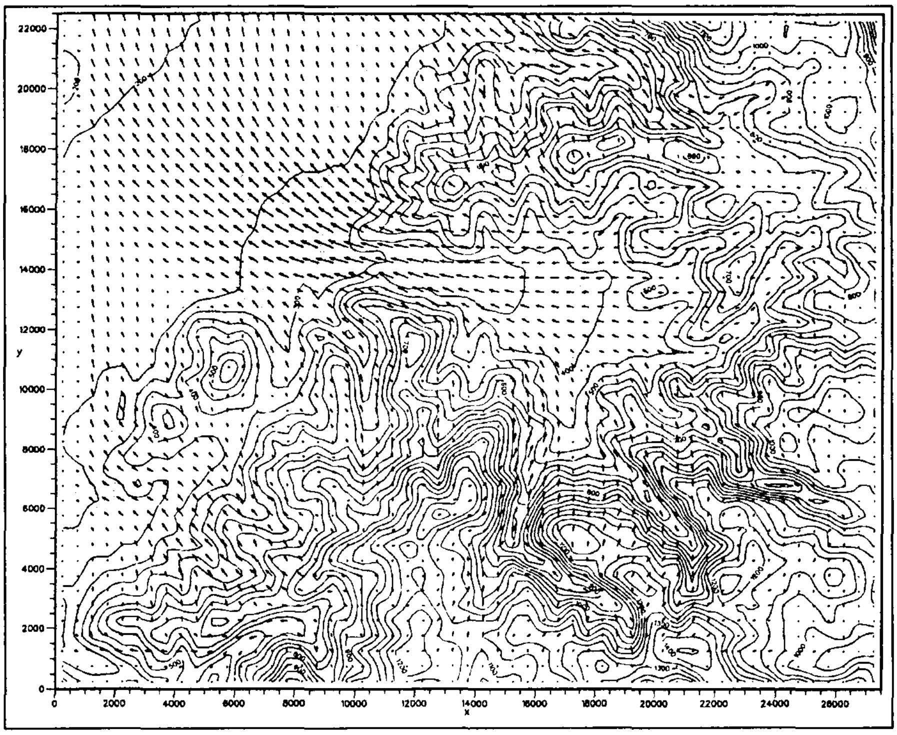

Fig. 8 : Result of a windfield modeling of ERSCLiP testsite Freiburg/FRG during nighttime. A local mountain-valley wind system is blowing from the Black Forest to the Upper Rhine Lowland (top left). .

6. MODELING OF URBAN HEAT STRESS

In many European countries bioclimate maps are an important tool for planning. The thermal influence on man which results e.g. in summer heat stress is an extremely complex meteorological process. Heat stress is an important parameter in medicine especially during rehabilitation of people with coronar deseases. During days with heat stress the mortality rate increases significantly.

Heat stress is impossible to be measured because in addition to air temperature there are a lot of other variables like air humidity, wind speed, net radiation and the human metabolism rate which have to be considered. The only possibility to compute and map heat stress conditions is by using bioclimate models. The model used computes the total energy budget of man including heat production as a result of his acticity, his heat release due to transpiration etc. and the insulation effects of the cloths. The model again needs a variety of spatially distributed input data like landuse with its vertical structure, aerodynamic roughness, terrain conditions etc. The German Weather Service created a sophisticated bioclimate model to compute summer heat stress and winter cold stress, taking the variables mentioned into account (Jendritzky 1991; 1992). This model was used to compute the number of days with heat stress conditions during summer for the city of Basel (Jendritzky 1995). Fig. 9 shows the result of modeling of the days with heat stress during summer for the study area of Basel. Comparing the image with fig. 4 the influence of urban landuse can be seen. In the city of Basel several urban heat islands can be identified and correlated to densely built-up areas.

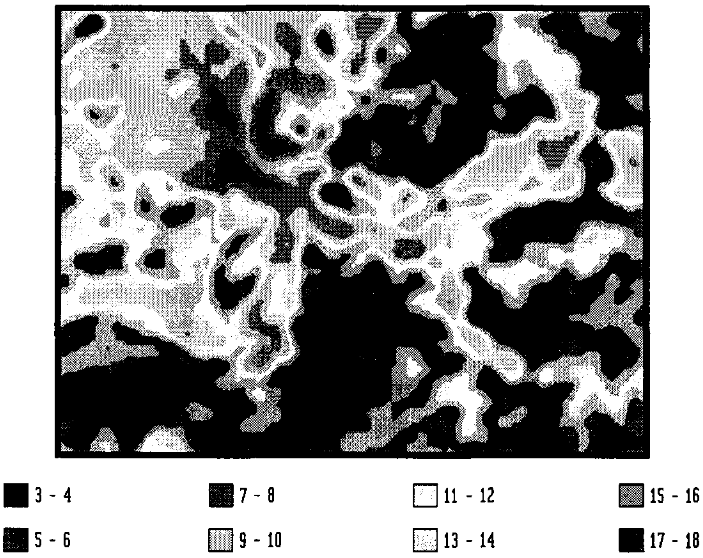

Fig. 9 : Number of days with heat stress during summer for Basel/Switzerland

7. CONCLUSIONS

Data from high resolution satellites like ERS-1 have a enormous potential to be used in urban climatological studies. The fusion of microwave data of ERS-1 data with optical data from Landsat-TM offers a lot of possibilities to elaborate spatially distributed data sets which directly contribute to urban climate or can be used as input variables of mesoscale models. The spatial resolution is appropriate enough that both data and results can be integrated in planning activities of the official authorities and other applications. The pilot study ERSCLiP successfully showed the potentials of ERS-1 and Landsat-TM data in the study areas of Basel/Switzerland and Freiburg/FRG.

8. REFERENCES

Beha, H.D., E. Parlow & D. Scherer. 1996. Land-use classification of the agglomeration of Basel/Switzerland combining multisensorial satellite data from Landsat-TM and ERS-1. In: Parlow, E. (ed.): Progress in Environmental Research and Applications. Balkema-Publishers Rotterdam (in press).

Fiedler, F. 1992. Das Regio-Klima-Projekt. Wie regeln die natürlichen Energieumsetzungen das Klima in einer Region? *KfK-Nachrichten, Kernforschungszentrum Karlsruhe*, 24, 3, p. 125-131.

IGBP, 1993: Biospheric Aspects of the Hydrological Cycle. The Operation Plan. IGBP, Report No. 27, Stockholm.

Jendritzky, G. 1991. Zur räumlichen Darstellung der thermischen Umgebungsbedingungen des Menschen in der Stadt. *Freiburger Geographische Hefte*, 32, 1-18.

Jendritzky, G. 1992. Bioklimakarten in unterschiedlichen Maßstäben. *Ann. d. Meteorologie* 28, 86-89.

Jendritzky, G. & A. Grätz. 1995. Bioklima. In: Fiedler, F.: Klimaatlas Oberrhein Mitte-Süd. Offenbach a.M.

Parlow, E. 1991. Einstrahlungskorrekturen - eine Anwendung für digitale Geländemodelle in der Satellitenfernerkundung. *Freiburger Geographische Hefte*, 34, 1991, p. 111- 118.

Parlow, E. 1992. REKLIP - Klimaforschung statt Meinungsmache am Oberrhein. *Regio Basiliensis* **33,** 2, p. 71-80

Parlow, E. 1995. REKLIP - an overview. *Theoretical and Applied Climatology.* In press.

Parlow, E. 1996a. Correction of terrain controlled illumination effects in satellite data. In: Parlow, E. (ed.): Progress in Environmental Research and Applications. Balkema-Publishers Rotterdam (in press).

Parlow, E. 1996b. Net Radiation in the REKLIP-Area - A Spatial Approach Using Satellite Data. In: Parlow, E. (ed.): Progress in Environmental Research and Applications. Balkema-Publishers Rotterdam (in press).

Scherer, D., U. Fehrenbach, E. Parlow & H.D. Beha. 1996b. Determination of aggregated areal types from a Landsat-TM and ERS-1 based land-use classification for the agglomeration of Basel/Switzerland. In: Parlow, E. (ed.): Progress in Environmental Research and Applications. Balkema-Publishers Rotterdam (in press).

Scherer, D., E. Parlow & H.D. Beha. 1996a. Roughness parameter derivation from ERS-1 and Landsat-TM satellite data for the agglomeration of Basel/Switzerland. In: Parlow, E. (ed.): Progress in Environmental Research and Applications. Balkema-Publishers Rotterdam (in press).

SEA-SURFACE FEATURES

Chairman: **G. D. Strøm**
Rapporteur: **J. Johannessen**

OIL SPILL DETECTION BY USE OF ERS SAR DATA
- From R&D towards pre-operational early warning detection service -

J.P. Pedersen[1], L.G. Seljelv[1], G. D. Strøm[2], O.A. Follum[3], J.H. Andersen[3], T. Wahl[4], Å. Skøelv[4]

[1] Tromsø Satellite Station, N-9005 Tromsø, Norway, Tel: (47) 77 68 48 17, Fax: (47) 77 65 78 68
[2] Norwegian Space Centre, P.o. Box 85 Smestad, N-0309 Oslo, Norway, Tel: (47) 22 52 38 00, Fax: (47) 22 52 23 97
[3] Norwegian Pollution Control Authority, P.o. Box 125, N-3191 Horten, Norway, Tel: (47) 33 04 41 61, Fax: (47) 33 04 42 57
[4] Norwegian Defense Research Establishment, P.o.Box 25, N-2007 Kjeller, Norway, Tel: (47) 63 80 70 00, Fax: (47) 63 80 72 12

Abstracts

A project for utilisation of ERS-1 SAR data for detection of oil spill at sea was started in 1991 as part of the Norwegian Space Centre's (NSC) national ERS-1 program. A pre-operational service utilising infrastructure for near real-time processing, analysing and distribution has been developed. Tromsø Satellite Station (TSS) took over the responsibility for operation of the pilot service in 1994.
The service covers two different operational aspects, i.e. near real-time detection and early warning of possible oil spills at sea in close co-operation with national pollution control authorities, and offshore oil exploration activities for oil companies. A phased service development model has been applied, from R&D until the current pre-operational use of ERS-1 SAR images. The developments include both service infrastructure and an operational concept. A number of important results regarding the detection capabilities of the ERS-1 SAR have been derived. Finally, activities towards utilisation of data from the future radar satellites have also been initiated.

Introduction

Since the mid 80's development of the use of satellite radar data for marine applications has been a high priority strategy within the national Norwegian space policy. Norway has become a member of ESA, and participates the ERS programme. Tromsø Satellite Station (TSS) has been developed as a national facility for

ERS data acquisition, processing and distribution. The national strategy has been to focus on near real-time data handling, meaning that the required information or data shall be at the users' site within one hour after the satellite overpass.

The core elements of the infrastructure at TSS is the CESAR processor and the broad band satellite distribution system IDUN. Both infrastructure elements have been developed by Norwegian industry in close co-operation with the R&D institutions.

The Norwegian oil spill detection project was originally proposed in response to ESA's Announcement of Opportunity for ERS-1 in 1986. This project has later achieved the status of an ESA Pilot project. The project has been funded by international sources, it has been performed under the responsibility of a steering committee chaired by NSC. It is important to recognise that the end user represented by the Norwegian Pollution Control Authority (SFT) has participated in the project even from the beginning. The phased development model and the results from the project have been widely published, and have found large interests outside the project [1, 2, 4, 5, 6, 7].

Service Development Phases

The project development from the start in 1990 has consisted the following phases:

Phase 0: 1990-91.
Responsible institution: OCEANOR a.s.
Activities: Literature survey, ERS-1 prelaunch preparations, planning of field experiment.

Phase 1: 1991
Responsible institution: OCEANOR a.s.
Participating institutions: SFT, NDRE, Esso, Statoil
Activities: A dedicated oil spill experiment at Haltenbanken in August 1991, where 3x20 tons of oil was released within the ERS-1 coverage, and studied under various meteorological conditions and sea states.
Result: The detection capabilities of the ERS-1 SAR, and its dependence upon the wind conditions were demonstrated.

Phase 1B: 1992-93
Responsible institution: NDRE
Participating institutions: SFT, OCEANOR a.s, Spacetec a.s, Norwegian Computing Centre
Activities: Transmission of ERS-1 SAR low-resolution images via datalink from TSS to NDRE for further analysis immediately after data reception in order to demonstrate the near real-time capabilities.
Images containing suspicious oil spill like features were sought verified by SFT by use of the surveillance aircraft. Experiment on automatic image analysis and feature extraction were performed. The operationalisation aspects were also studied.
Result: More than 150 ERS-1 SAR images were analysed, and the feasibility of near real-time operations were demonstrated. The detection capability dependence upon the wind conditions and the sea state (calm days) were demonstrated.
SFT formally requests offshore oil rig operators for explanation of satellite observations.

Pilot Demonstration Phase: 1993
Responsible institution: NDRE
Participating institutions: SFT, OCEANOR a.s., NERSC, TSS
Activities: A larger scale activity of the preceding phase was performed in close co-operation with SFT. The problems of distinguishing real oil spills from natural slicks were addressed in details. Training of the operators at TSS in SAR image interpretation was initiated. A fruitful co-operation with the Dutch Rijkswaterstaat was initiated.
Result: 260 ERS-1 SAR images were analysed in near real-time, and clearly demonstrated the capabilities of detecting various types of pollutants. Practical criteria for discriminating between real oil spills and natural slicks were established by NERSC.

(Pre-)Operational Phase: 1994-
Responsible institution: TSS
Participating institutions: SFT, NDRE, NERSC.
Activities: From Summer 1994 TSS took over the responsibility for the operations of the pre-operational service. ERS-1 and ERS-2 SAR images are analysed on a routine basis at TSS, and observed possible oil spills are notified about to the national pollution control authorities.
Additional service activities include analysis of SAR images in terms of identification of natural oil seepage from the seafloor. A more detailed description of the service is given in this paper.
Emphasis have also been made to establish cooperation with users outside Norway.

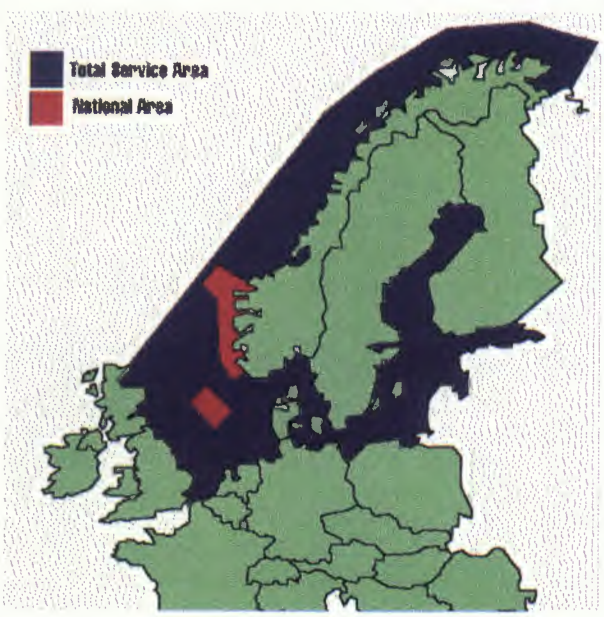

Figure 1: Pre-operational service area.

Detection capabilities

The extensive use of ERS-1 and ERS-2 SAR low resolution (i.e. 100 meter resolution) images during the project has demonstrated the ERS satellites capability to detect even very thin pollutants in low wind speed of 3-4 m/s and thick emulsions at higher speeds of 10 m/s [2, 7].

Other pollutant examples detected during the project include: crude oil forming emulsions, run-off water from acid-pitch depository on land, drilling fluid from off-shore oil rigs, waste from fish production plants, and fish fat remaining at the sea surface after fishing trawler catches.

Two main problems concerning the detection capabilities have been demonstrated [7]:
- At low wind speeds, ocean slicks of natural origin are frequently observed and may cause false alarms unless experienced operators or very advanced pattern recognition methods are used.
- At high wind speeds the pollutant may be mixed with the sea water and no surface effect is detected by the SAR (e.g. the "Braer" disaster January 1993).

Pre-operational service

The main service infrastructure elements are the ERS SAR data handling facilities at TSS. These consist the fast SAR processor (CESAR) capable to generate a 100x100 km SAR image within 6-8 minutes, and respectively the 2 Mbits/sec satellite (IDUN) and the 64 kbits/sec image data distribution links. The capacity of the data distribution facilities allows near real-time image data transfer from TSS to the end users, i.e. the SAR images can be at the users´ site less than one hour after acquisition.

Automatic detection of potential oil spills was at an early phase considered to be mandatory for the service. Algorithm for this purpose has been developed and verified during the project [7, 8]. Experiences have, however, shown otherwise. Whereas the automatic slick detection is done within a few minutes, a trained operator can analyse a SAR scene within a much shorter time. The pre-operational service is therefore mainly based upon human, computer supported analysis and interpretation.

When entering the pre-operational phase in Summer 1994, the knowledge developed at NDRE was physically transferred to TSS. The operators at TSS has been through an extensive training period, and they are now responsible for the service operations. On the average the service now analyse more than 300 ERS SAR scenes per month, which significantly exceeds the number from the previous phases.

Important service improvements in 1995 include implementation of a new service information distribution tool, SARA. SARA is based on PC and e-mail technology, and has been developed by Telenor R&D in Norway. The SARA tool has now been installed at more than 10 users sites in Europe. In addition, a dedicated service workstation has been described and is under development.

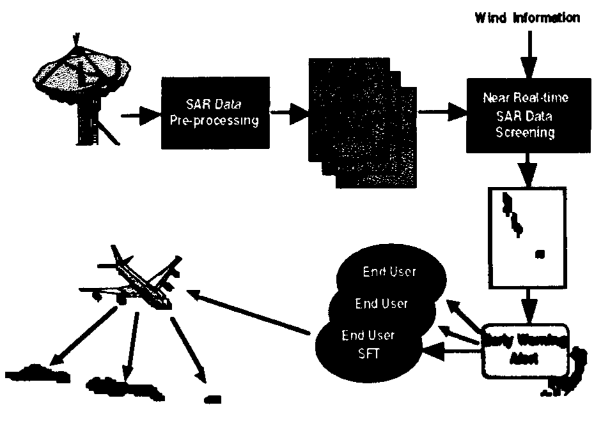

Figure 2: National Oil Spill Detection Service Infrastructure Concept.

The main goal of the pre-operational service is to serve the end users with reliable information on possible oil spills within two hours after satellite overpasses. The primary analysis areas cover Norwegian waters, and have been defined by the Norwegian Pollution Control Authorities (SFT). However, as a result of co-operation with other countries, the total monitoring areas have been largely extended. The current service therefore includes a near real-time analysis of ERS-1 SAR data both from the Norwegian coastal waters, and from more central European coastal waters (Figure 1). Information about possible oil spills are routed either directly, or via SFT, to the responsible national authorities. This service represents a first step towards establishing a fully operational service covering Norwegian and adjacent waters. The objective is within 3 years to establish a fully operational oil spill detection service utilising satellite and additional information.

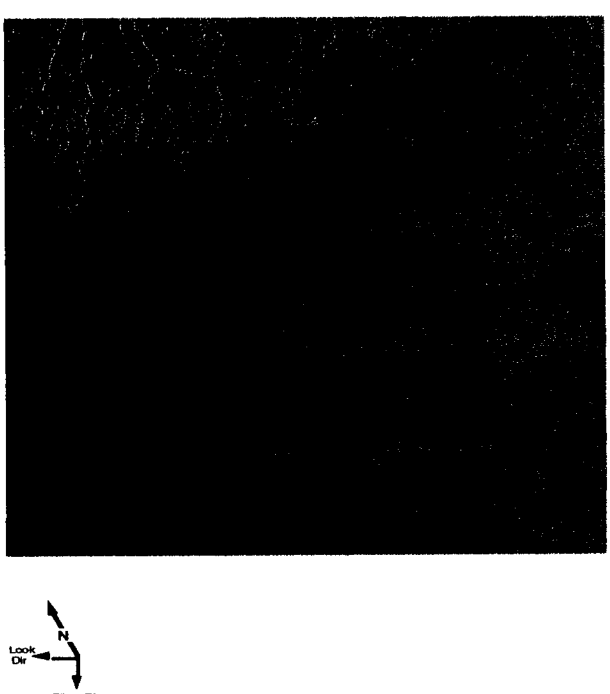

Figure 3: ERS-1 SAR image of a confirmed oil spill off the southern cost of Norway (upper right). Image size approx. 70 x 50 km.

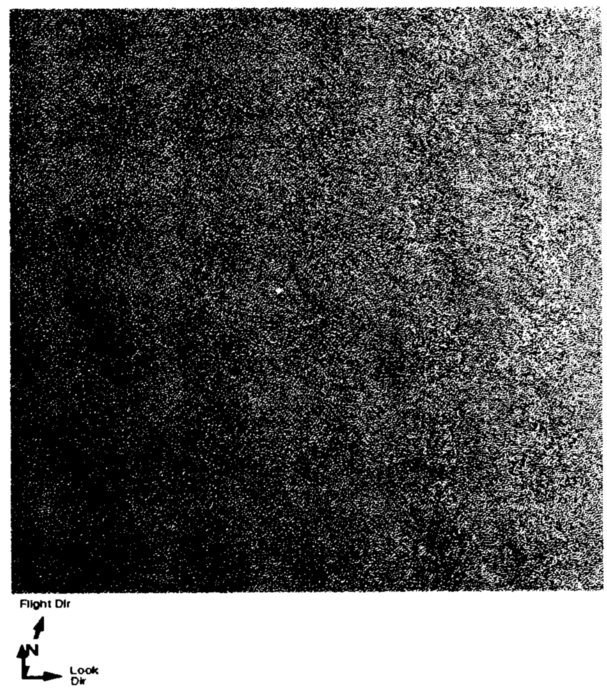

Figure 4: ERS-1 SAR image dated 94-11-25 of a confirmed oil spill from an off-shore oil rig in the North Sea. Image size approx. 70 x 50 km.

Near real-time ERS SAR data read out at TSS is the current primary source of satellite input information for identification of possible oil spills/slicks. Since the availability of ERS-2 SAR data last summer, data from both satellites have been applied extensively. The one day off-set between ERS-1 and ERS-2 coverages has clearly demonstrated a strongly improved temporal coverage of the service areas. The service has hence clearly demonstrated the benefits from the Tandem Mission Period for operational, near real-time applications.

Assessment of ERS data has already been implemented in the national system for oil and chemical pollution reporting in Norway (Figure 2). The SFT surveillance aircraft operations are also co-ordinated according to the ERS-1 overpasses. In addition, SFT has an agreement with DNMI regarding use of their oil drift model and other meteorological assistance whenever an oil spill is identified. This part of the service is operated outside TSS. Figure 3 and 4 show two examples of ERS-1 SAR images containing confirmed oil spills off the coast of Norway.

In mid-1995 a proposal based on this project was selected by the EU/Centre for Earth Observation (CEO) as one of the cases for the Application Proof-of-Concept studies, where the objective is to assess and document user requirements.

Natural Seepage Studies

Another service application has focused on application of ERS-1 SAR data for detection of natural oil seepage from the seafloor off the coast of Norway. From the analysis of a total of 150 ERS-1 SAR images, 10 seepage candidates have been identified. None of these candidates have, however, been confirmed by any in-situ observations. 8 of the candidates were detected at very favourable wind conditions (i.e. wind speed less than approx. 5 m/s). Comparison of the observed candidates with wind speed and direction estimates shows a reasonable good match between observed slick direction and wind speed direction.

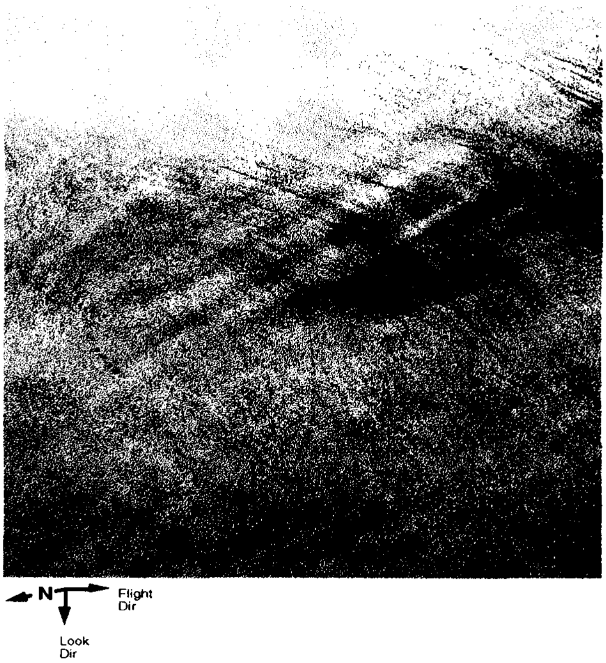

Figure 5: ERS-1 SAR image showing a dark droplet formed seepage candidate (centre left position). Image size is approx. 60 x 60 km.

A new signature pattern appearing as small (approx. 0.3 x 0.3 km) patches stretching out in the wind/current direction was also discovered. This signature is associated with seepage droplets which reach the sea surface at different times. The 'droplet signature' has been detected 4 times during the study [1]. Figure 5 shows an example of the droplet signature pattern observed during this work.

Main Users

The service now available is the result of a co-operation between Norwegian Space Centre (NSC), the Norwegian Pollution Control Authority (SFT), Norwegian Defence Research Establishment (NDRE), ESA, Marine Spill Response Corporation (MSRC), the oil companies Statoil and ESSO and Tromsø Satellite Station. The primary objective of the first phase is to establish a pre-operational service for national users. However, in parallel with the nationally focused activities the early phase will also include international marketing activities. The coverage area in combination with the near real-time capabilities of Tromsø Satellite Station represent advantages that are important for the international marketing. Co-operation with pollution control authorities in other European countries (Sweden, Finland, The Netherlands, Germany and UK) has also been developed during the recent project phases [3].

Future Development

The results obtained from the project have demonstrated that there is still a need for continuous service improvements. Both shorter term activities dealing with improvements of existing algorithms, products and systems, and longer term activities dealing with new developments and improvements are undertaken.

During the first half of 1996 RADARSAT data will become avialable, and will be used by the service. This satellite will have the capability to cover a larger area than the ERS satellite, and the SAR can also operate in additional modes compared to ERS. The capability of RADARSAT to detect oil is not yet fully understood, especially the limitations towards the outer parts of the swaths have to be considered. Assessment of the capabilities of RADARSAT for detection of oil at sea has therefore been given high priority for the coming years.

Later on, ENVISAT will be launched by ESA. The ASAR onboard ENVISAT will also operate in additional modes compared to ERS. The ENVISAT detection capabilities will therefore also be addressed during the coming years.

From a technical point of view, a largely improved temporal and spatial coverage is expected towards the new century. Improvements in terms of temporal coverage has also been demonstrated during the ERS-1 and ERS-2 Tandem Mission period. It is, however, most likely that service cost aspects will be the most critical factors in terms of operational service establishments.

Conclusions

The new radar satellites such as ERS, RADARSAT and ENVISAT represents a new tool for establishing operational oil spill detection services. Large, repetitive coverage of remote areas under practically all weather conditions are the main advantages from these satellites. The costs per unit covered is also comparable, end even cheaper than the costs obtained from traditional operational systems [7].

It is, however, important to notice that satellite data cannot fully replace other monitoring platforms such as aircrafts. Aircraft operations can, however, be more efficient and costs effective by using the satellite and the aircraft data jointly for operational monitoring.

Norway has since early 80´s been heavily engaged in the development of the use of satellite SAR data for marine applications. A pre-operational satellite based oil spill detection service developed in close co-operation with the national end user SFT, and now offered by the service provider TSS is a result of this engagement.

The focus has been to develop the near real-time capability to provide information about possible oil spills at sea to end users both in Norway and in other European countries. Today TSS is capable to inform an end user in Northern Europe about possible oil spills within their territorial waters within less than two hours after ERS SAR data acquisition.

The activities within the oil spill detection development project have clearly demonstrated the ERS SAR capabilities of detecting oil spills at sea even under rougher sea states than initially was expected. It is therefore expected that SAR data from the new radar satellites will become more and more important sources of information for operational pollution monitoring at sea. TSS covers large parts of the Northern European waters, and already has a data handling infrastructure specially developed for near real-time provision of data and information to the users. TSS could therefore play a central role as the satellite data handling facility within an operational European oil spill detection service.

The improved temporal covergae obtained during the ERS Tandem Mission Period has been important for the users dealt with by the service. The Tandem Mission has hence been of benefits for operational users in addition to the off-line interferometric community. These benefits could hence represent a positive contribution towards increasing the users capabilities and willingness to increase their financial contributions to a further development of a commercial EO business. It is therefore recommended that the satellite operator ESA make maximum efforts to provide ocean data from both satellites for operational applications during the remaining Tandem MIssion Period, and that a discussion of a possible extension of this period for more operational purposesa is raised soon.

Acknowledgements

The Norwegian oil spill development project has been co-ordinated by the Norwegian Space Centre on behalf of a steering committee with representatives from ESA, Marine Spill Response Corporation (MSRC), the oil companies Statoil and ESSO. These have all made substantial contributions to the project. The valuable information obtained from Rijkswaterstaat in the Netherlands is also gratefully acknowledged.

References

1. Anderssen, T., J.P. Pedersen, L.G. Seljelv, 1994, *Oil Spill Detection Using Satellite based SAR, Detection of natural Seepage*, TSS Final report.

2. Bern, T-I., S Moen, T Wahl, T Anderssen, R Olsen, J A Johannessen, 1993: *Oil spill detection using satellite based SAR, Completion report for Phase 0 and 1*, Photogrammetric Eng. & Remote Sensing, Vol 59, pp 423-428.

3. Pellemans, A.H.J.M., W.G. Bos, H. Konings, R.W. van Swol, 1994, *Oil Spill Detection on the North Sea Using ERS-1 SAR Data*, Report, Directorate-General for Public Works and Water Management, the Netherlands.

4. Skøelv, Å., T Wahl, 1993: *Oil spill detection using satellite based SAR*, Phase 1B Completion report.

5. Wahl, T., T Anderssen, Å Skøelv, 1994.a: *Oil spill detection using satellite based SAR,* Pilot Operation Phase, Final Report, NDRE.

6. Wahl, T., Å Skøelv, J.H. Andersen, 1994.b: *Practical Use of ERS-1 SAR Images in Pollution Monitoring*, In: Proceedings IGARSS'94 Pasadena, IEEE 0-7803-1497-2/94.

7. Wahl, T., Å. Skøelv, T Anderssen, J.P.Pedersen, J.H. Andersen, O.A. Follum, G.D. Strøm, T-I. Bern, H. Hamnes, R. Solberg, 1994.c: *Radar Satellites: A new tool for pollution monitoring in coastal waters,* Paper submitted for publication in international journal.

8. Weisteen, K., A.H.S. Solberg, R. Solberg, *Detection of oil spill in SAR images using a statistical classification scheme*, In: Proceedings IGARSS'93 Tokyo August 1993.

SAR SURVEILLANCE OF OCEAN SURFACE SLICKS

Ola M. Johannessen, Heidi A. Espedal, Alastair D. Jenkins, Johan Knulst*, Torill Hamre, Stein Sandven & Paul Samuel

Nansen Environmental and Remote Sensing Center (NERSC)
Edvard Griegs vei 3a, N-5037 Solheimsviken, Bergen, Norway
Tel: (47) 55 29 72 88. Fax: (47) 55 20 00 50

**Swedish Environmental Research Institute, Aneboda, S-36030 Lammhult, Sweden*

ABSTRACT

ERS-1 SAR data have demonstrated their capability to detect ocean surface slicks, including natural films as well as man-made pollutants such as oil spills. Surface slick patterns also depict a number of ocean phenomena, such as eddies, fronts, and internal waves.

The possibility of observing and classifying surface slicks in SAR images has been tested in demonstration projects, where SAR data have been used in combination with meteorological and oceanographic data to monitor surface winds, fronts, and current patterns (Espedal & al., 1995a; Samuel & al., 1995ab). We foresee that the synergy of SAR data and data from infra-red and optical satellite sensors will play an important role in operational oceanography.

The main problem in using SAR for ocean monitoring is how to classify surface slicks according to characteristic image expressions, backscatter profiles and gradients, geographical occurrence, and weather limitations. A conceptual model for distinguishing various types of surface slick is proposed, based on a number of case studies (Hamre & al., 1995). The model provides the first version of a SAR classification scheme for surface slicks, to be used in operational ocean monitoring.

1. INTRODUCTION

Synthetic Aperture Radar (SAR) data from the ERS-1 satellite provide detailed images of sea surface processes and phenomena independent of light and cloud conditions. Such images have been available for more than three years, and expertise in interpreting and extracting geophysical and other parameters from the images has been gradually established (Johannessen & al., 1991, 1993, 1994, 1995ab). Although SAR imaging of the sea surface still remains an area requiring further research, there are several features and processes which can be routinely monitored by SAR at the present stage. The most important of these are wind fronts, current fronts, eddies, current meanders, internal waves and surface slicks

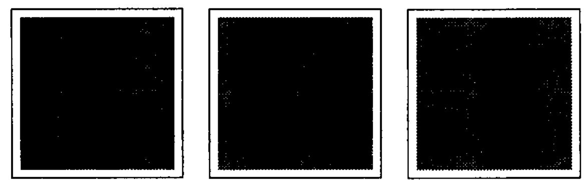

(a) Nat. film (b)Grease ice (c) Oil

Fig. 1. Slicks in ERS-1 SAR images
((a) and (b) 25 × 25 km, (c) 12.5 × 12.5 km)

such as oil spill. Ship detection is also an important application of SAR data. Norway has developed an efficient processing and distribution system which enables near real-time use of such data from the ERS satellites. These facilities are very important in the operational scenario, now that additional SAR coverage is afforded with RADARSAT.

However, in preparation for operational slick detection it is necessary to streamline the procedures for selecting, ordering and transferring SAR data from the downloading facility at Tromsø Satellite Station (TSS), carrying out the necessary processing of the data, creating a database to facilitate storing, categorization and selection of the SAR data, and to provide easy access to relevant data from other satellite sensors, numerical models and field measurements.

2. RESULTS OF CASE STUDIES

The main problem in SAR surveillance of slicks is to classify the various ocean phenomena or surface materials which cause the low backscatter in the SAR images. These phenomena can be oil spills, natural films, grease ice, low-wind areas, rain cells, current shear zones, internal waves, and upwelling. Examples of slicks in SAR images are shown in Fig. 1.

Natural film is a microlayer of organic substances secreted by fish and several planctonic species. Under relatively calm conditions such microlayers can form uniformly across extensive ocean areas. Accumulation may take place in regions of high biological ac-

Proceedings of the Second ERS Applications Workshop, London, UK, 6–8 December 1995 (ESA SP-383, February 1996)

Table 1. Summary of the different oil slick look-alikes, and their expressions and limitations in ERS-1 SAR imagery (Hovland-Espedal & al., 1994).

Geophysical Phenomenon	SAR image expression	Geographical occurence	Weather limitations	Backscatter values [dB]	Radar contrast [dB]	Gradient [dB/100m]
Natural film	reconfigures easily when interacting with currents	coastal regions and regions of upwelling	dissolves at wind speeds above 7m/s	-24 to -15	2.5 - 3 - 4.2	1.5 - 5
Grease ice	large black areas	mainly along ice edge, but also found in open water	winter season, or cold nights close to ice edge	-24 to -14	13	1-2
Threshold wind speed	large dark areas	everywhere	wind speed less than 3m/s	-24 to -18	9.7	0.3-0.5
Wind sheltering by land	dark regions near land	in vicinity of land boundaries and in fjords	even at high wind speeds (15m/s)	-24 to -12	6 - 8	1.5-3.0
Rain cells	bright cells with dark centres	sub-tropical regions	heavy rain and strong winds	-24 to -8	3.5 - 15	0.1-0.3 1.4-5.0
Internal waves	series of parallel bright-dark lines	in shallow waters	wind speed less than 8m/s	-24 to -8	0.8	0.4-1.0
Wave current interaction along shears	narrow, bright or dark curving signatures	areas of strong currents	wind speed less than 10-12m/s	-24 to -8	2-6.3	0.2-0.4
Upwelling	dark areas	divergence zones of surface currents, mainly near coasts	wind speed assumed less than 6-8m/s	assumed: -24 to -15		
Oil spill	dark areas	everywhere	wind speed less than 10-12m/s	-25 to -10	0.6 - 9.8	8 - 5

Original Data © ESA/TSS 1993. Image analysis NERSC

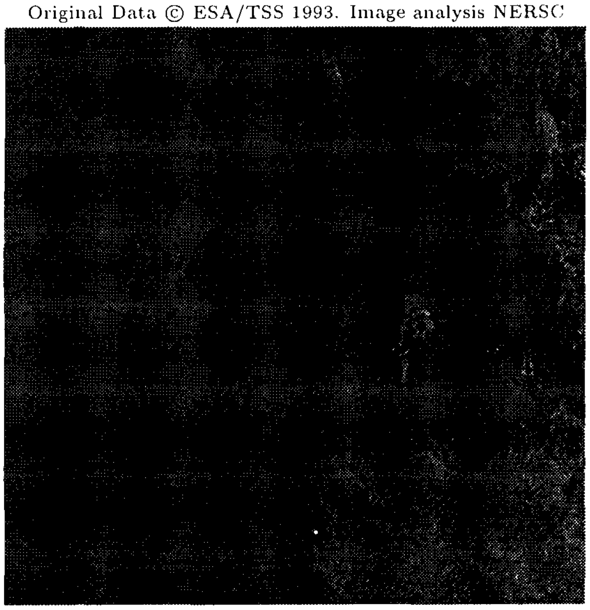

Fig. 2. SAR image of natural film outside Haugesund, Norway, 1993 June 26. (Image width 62.5 km.)

tivity, i.e. in coastal regions, in regions of upwelling, (Alpers & al., 1991; Ochadlick & al, 1992), and along current boundaries (Johannessen & al., 1995b).

A large number of SAR scenes have been examined with regard to surface slick observations. A summary of this study is provided in Table 1 after Hovland-Espedal & al. (1994).

Different cases of natural film have given backscatter values in the region between -24 dB and -15 dB. They usually dissolve at wind velocities above 7 m/s (Scott, 1986). Because they are fragile to interaction with currents, including both shear and convergence, such slicks easily configure into spatial variations that are related to the surface current circulation pattern (Johannessen & al., 1993). This will in turn allow us to recognize some cases of natural film, i.e. slicks which are aligned according to general circulation patterns. In Fig. 2 the film has interacted with the surface current and therefore reveals the circulation pattern of the imaged region. Rain cells, grease ice and wind sheltering by land are also seen to provide sharp gradients with large damping.

The oil slicks in this investigation have been found to give radar backscattering values in the region between -25 dB and -10 dB. Oil spills tend to remain much more concentrated than natural films, probably because they contain larger amounts of viscous fluid and so have more resistance to current shear and down-mixing. Thus they provide greater wave damping, from surfactant materials contained in the oil as well as their bulk viscosity (Jenkins, 1995), and tolerate stronger ambient winds. The oil spill configuration can then sometimes be used to distinguish oil from natural film.

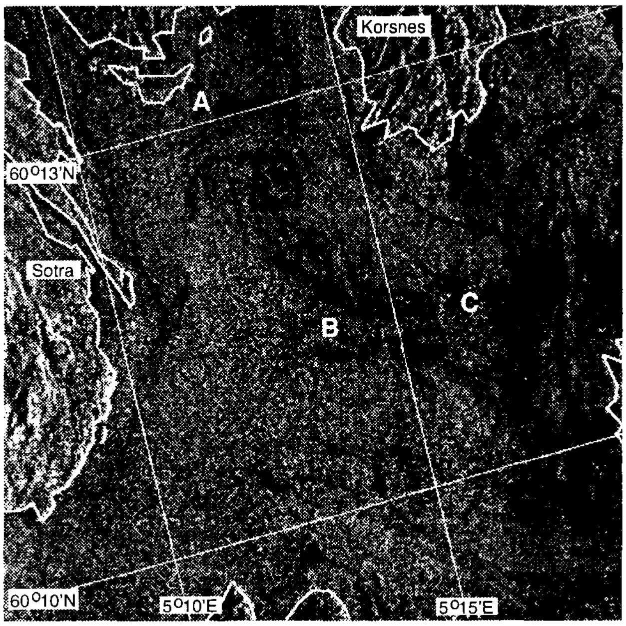

Original data ©ESA/TSS 1994. Image analysis NERSC

Fig. 3. Part of the high resolution ERS-1 SAR image from Korsfjorden, south of Bergen, 1994 September 29, 1150 UTC, showing the experiment area. A low-resolution version of the image was sent by Internet from Tromsø Satellite Station (TSS) to NERSC for analysis, and the field team then navigated to the nearest slicks (A–C), using the Global Positioning System (GPS).

Experiment in Korsfjorden

Natural film has earlier been shown to represent the largest problem when using SAR to detect oil spills (Hovland-Espedal & al., 1994). As an attempt to learn more about how to distinguish these in SAR imagery, an experiment was carried out on 1994 September 29 in the fjord outside Bergen (Espedal & al., 1995b). Samples of the sea surface were taken simultaneously with ERS-1 SAR coverage (Fig. 3) of the area. A teflon drum attached to a remotely controlled model boat was used to obtain the samples. Both slick and non-slick areas (surface and bulk water samples) were included in the experiment. Weather and current information was obtained from a buoy near the experiment area. The wind was also measured both inside and outside slick areas to exclude wind gusting as a possible explanation for the areas with damped backscatter. The samples were analyzed for differences in several chemical parameters to verify whether the dark patches in the SAR image could be related to increased biological activity, i.e. to natural film or to some kind of oil spills (alkane trace analysis).

The result of the experiment showed that there was a significant difference in chemical composition, both in the water column and in the surface microlayer, between the areas with slick coverage and the areas outside the slicks. The concentration of fatty acids in the presence of slicks was generally an order of magnitude greater than for slick-free areas. The radar backscatter decreased by between 6 dB and 17 dB in slick-covered regions.

A further program of slick sampling was performed in September 1995 during the NORCSEX'95 field experiment in conjunction with the tandem phase of ERS-1/ERS-2. The remotely-controlled sampler was deployed from the R/V *Håkon Mosby*. Simultaneous atmospheric boundary layer, surface wave, current and hydrographic data were collected, using ship-borne and buoy instrumentation, and satellite observations included SAR and AVHRR/ATSR infrared imagery.

Original Data © ESA/TSS 1993/1994. Image analysis NERSC

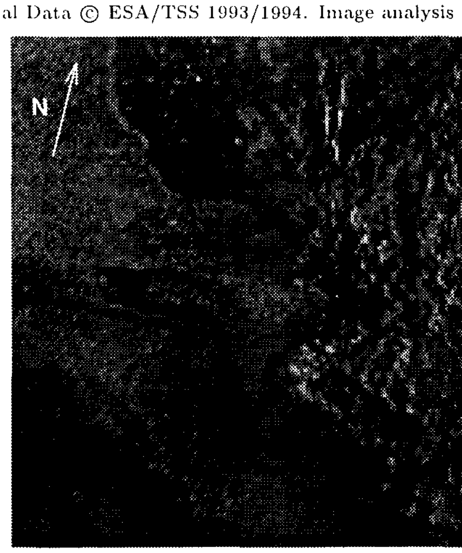

Fig. 4. SAR image of fish oil from processing plant, 1993 November 8. (Image width 14 km.)

Fish oil from a fish processing plant

A slick can be seen extending out from the coast and curving southwards out into the sea in Fig. 4. The synoptic meteorological analysis showed northeasterly winds of about 10 m/s in the imaged area, but local observations indicate somewhat lower speeds of about 5 m/s, also from the northeast. This low wind speed is ideal for slick detection and the oil drift is also seen to be in accordance with the observed wind direction.

The slick is believed to be fish oil from a fish processing plant located at Sirevåg near Egersund. Slicks have been detected earlier in SAR images over this area. In one particular case, on 1994 September 15 (image not shown) this was confirmed by State Pollution Control Authority (SFT) aircraft surveillance, who estimated that the slick contained 10 litres of oil, with an estimated thickness of $0.01 \mu m$.

East of Shetland: Low wind and ship spills

Fig. 5 shows two SAR images to the east and north of Shetland. In the upper image, four dark winding signatures (A–D) are found behind bright points indicating ships. The dark slicks are believed to be diesel oil or fish oil spilled out to the sea by the ships.

In the lower image we see a marked boundary between dark and bright areas (E). The low radar backscatter is believed to be due to extremely low winds. In the bright strip (F) between the two darker areas, a number of dark spirals and curves signifying eddy activity are observed.

Statfjord platforms

The image in Fig. 6 is from the oil-producing area in the northern North Sea, west of the Norwegian Trench.

Original Data © ESA/TSS 1994. Image analysis NERSC

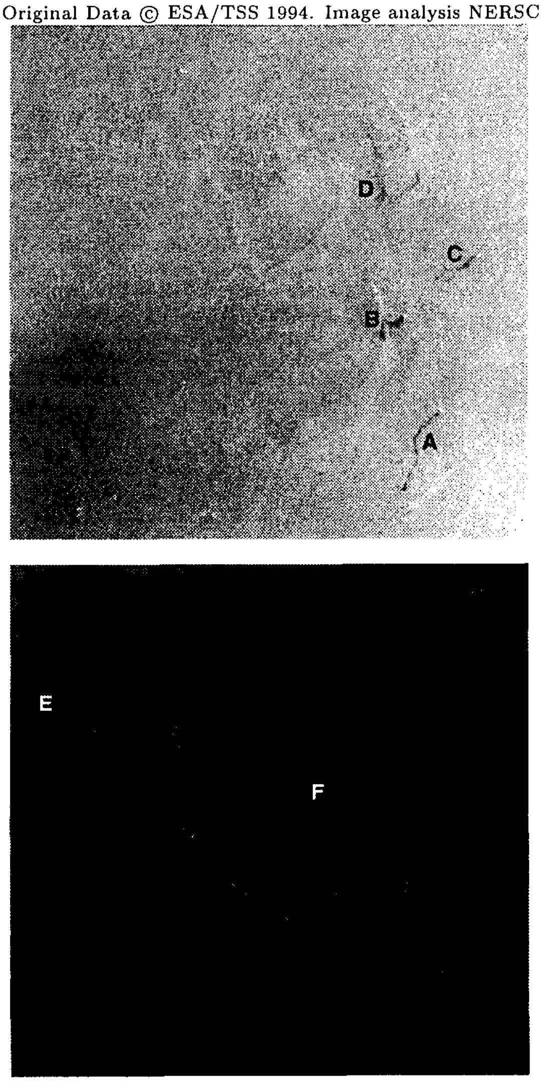

Fig. 5. SAR images east of Shetland on 1994 October 27. (Upper image width 50 km; lower image width 33 km.)

Original Data © ESA/TSS 1994. Image analysis NERSC

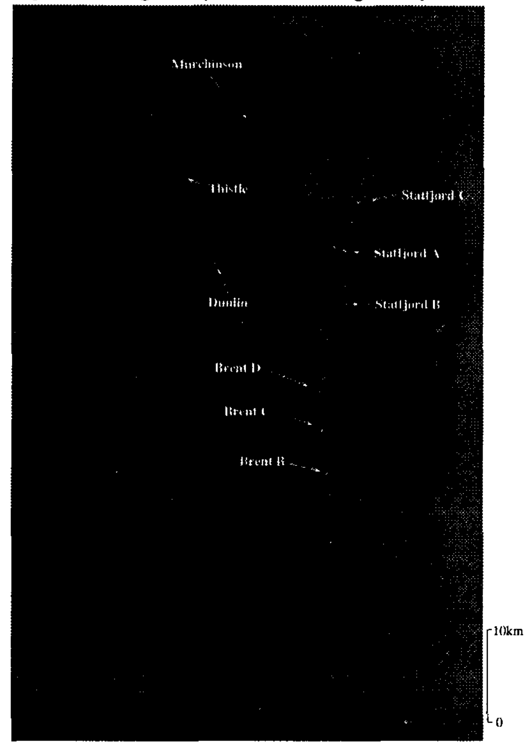

Fig. 6. SAR image, Statfjord area, 1994 October 30. The dark area to the right of the image may be due to low windspeed. The dark, curved features emanating from some of the bright points (oil platforms) are believed to be oil slicks or drilling fluid residue. (Image width 51 km.)

To the right of the image, a large dark patch, probably caused by low windspeed, can be seen. The Statfjord A, B and C platforms are to the left of this dark area. Dark slick-like features can be seen to emanate from some of the oil platforms. The time of year, shape and form of the slicks make it unlikely that they are of natural origin. The slicks are also seen to be connected to the bright spots which are boats or plattforms. They are therefore believed to be some sort of spill, such as oil or drilling fluid.

3. CLASSIFICATION MODEL

A concept for detection and discrimination of oil spills in SAR imagery is illustrated in Fig. 7. The main steps in the method are as follows. In the first step (A) we analyse the backscatter values and the texture of the image in order to detect dark features which may contain oil contamination. In this step, automatic routines can be used as an aid to detect slicks. But as many natural phenomena, such as low wind, can produce dark features in a SAR image, additional analysis must be carried out to eliminate them. Some of these features, such as those caused by internal waves, wind rolls, atmospheric gravity waves and rain cells, can be excluded immediately

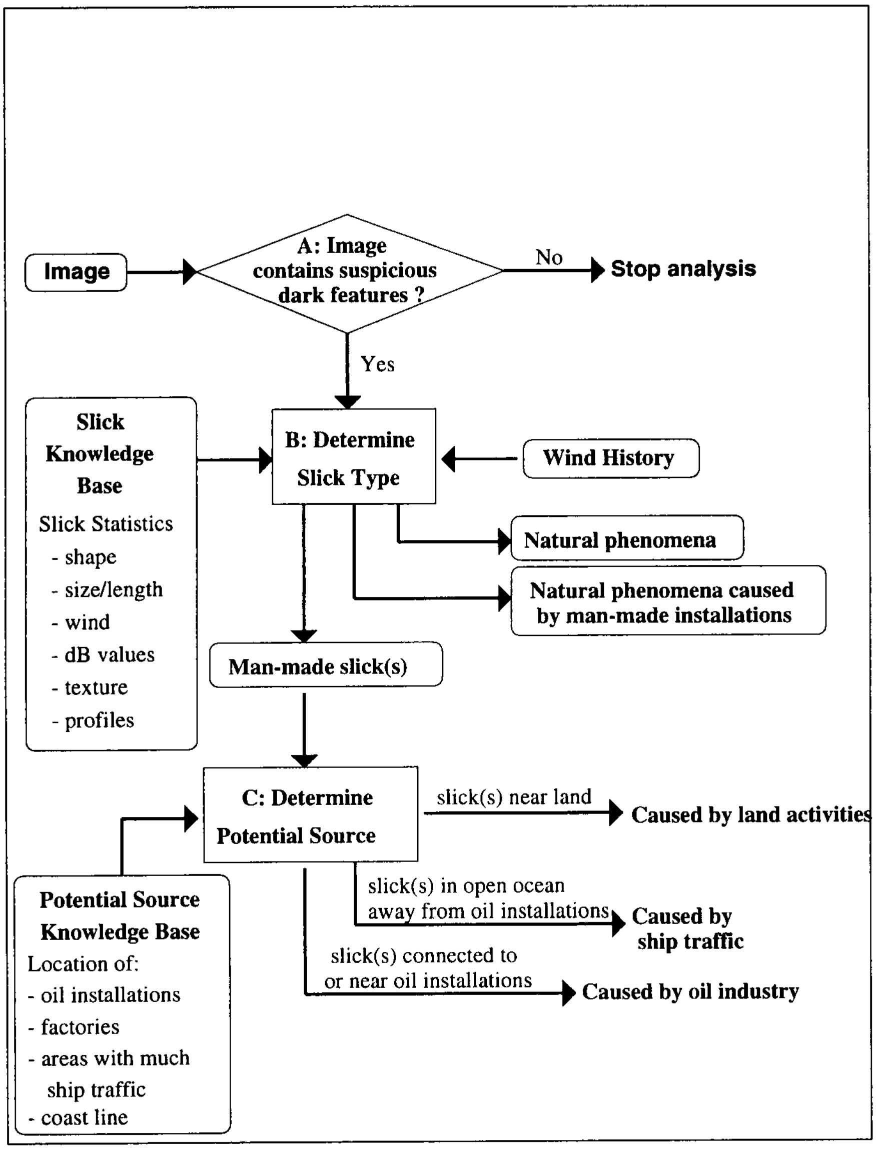

Fig. 7. A concept for detection and discrimination of oil spill in SAR imagery.

due to their characteristic shapes and configurations. The remaining slicks, which could not be classified using these simple means, must be further analysed in the second step (B). Here, additional information such as knowledge of previous slicks and wind (both instantaneous and historical), is applied to discriminate man-man slicks from those caused by natural phenomena. Wind speed is an important parameter for deciding whether a slick is man-made, as natural film will quickly disperse for winds stronger than 7–8 m/s (Espedal & al., 1995a). However, it may not always be possible to distinguish a man-made slick from one caused by some natural phenomenon. Finally, potential emission sources are sought (C). If a slick has been classified likely to be as man-made, additional information about the location of potential emission sources, is used to establish the origin of the spill. In open ocean, platforms and ships can be seen as bright spots, and if the slick is connected to such a spot it is most likely to have been emitted from there.

4. CONCLUSION AND RECOMMENDATIONS

Dark features visible on SAR images are caused by natural film and a number of other phenomena ('look-alikes'), in addition to oil spills, and it is important to discriminate between these in operational oil spill monitoring. Natural film is important for the Earth's climate system as it influences air-sea mass, momentum, and heat fluxes, and active microwave remote sensing should prove very useful in its global quantification.

Our studies have shown that the different types of ocean surface slick damp out centimetre-scale waves, causing low-backscatter (dark) areas in SAR imagery. We have now taken samples of the surface microlayer simultaneously with ERS-1 SAR coverage of an area, to investigate the composition of natural film and its effect on radar return. Chemical analysis indicates some correlation with increased biological activity, in that fatty acid concentration was enhanced in slick-covered areas.

A classification scheme has been developed to distinguish man-made oil spill from other look-alikes in SAR images. This scheme requires the use of a substantial knowledge base, including ambient meteorological history, the location of potential pollution sources, and a comprehensive database of ocean phenomena, their geographical and seasonal occurrence, and their representation in SAR imagery. Without such substantial background information it will be impossible to identify uniquely any particular slick-like feature.

Acknowledgements.

This work was supported by the Norwegian Research Council, the European Space Agency, and the Norwegian Space Centre.

5. REFERENCES

Ochadlick, A. R., Cho, P., & Evans-Morgis, J. (1992) Synthetic Aperture Radar observations of currents colocated with slicks. *J. Geophys. Res.*, 97(C4): 5325–5330.

Alpers, W., Wismann, V., Theis, R., Hühnerfuss, H., Bartsch, N., Moreira, J., & Lyden, J. (1991) The damping of ocean surface waves by monomolecular sea slicks measured by airborne multi-frequency radars during the SAXON-FPN experiment. In *Proceedings, IGARSS'91, Finland*, volume 4 pp. 1987–1990.

Espedal, H. A., Hamre, T., Wahl, T., & Sandven, S. (1995a) Oil spill detection using satellite based SAR, Pre-operational phase (A). NERSC, Bergen, Technical Report No. 102. [T. Wahl is with the Norwegian Defense Research Establishment].

Espedal, H. A., Johannessen, O. M., & Knulst, J. C. (1995b) Natural films in coastal waters. In *Proceedings, IGARSS'95, Florence, Italy, July 10–14, 1995*, pp. 2106–2108. IEEE, Pisacataway, New Jersey.

Hamre, T., Espedal, H., Samuel, P., & Sandven, S. (1995) Operator's manual for slick analysis. NERSC, Bergen, Special Report No. 37.

Hovland-Espedal, H., Johannessen, J. A., & Digranes, G. (1994) Slick detection in SAR images. In *Proceedings, IGARSS'94, Pasadena, California*, volume 4 pp. 2038–2040. IEEE, Pisacataway, New Jersey.

Jenkins, A. D. (1995) Wave damping by a thin layer of viscous fluid. Submitted to *Phys. Fluids.*

Johannessen, J. A., Digranes, G., Espedal, H., Johannessen, O. M., Samuel, P., Browne, D., & Vachon, P. (1994) SAR ocean feature catalogue. ESA Publication esa-SP-1174, ISBN 92-9092-133-1, ESA Publications Division, ESTEC, Noordwijk, The Netherlands.

Johannessen, J. A., Røed, L. P., Johannessen, O. M., Evensen, G., Hackett, B., Pettersson, L. H., Haugan, P. M., Sandven, S., & Shuchman, R. (1993) Monitoring and modeling of the marine environment. *Photogramm. Engng & Rem. Sens.*, 59: 351–361.

Johannessen, J. A., Shuchman, R. A., Digranes, G., Lyzenga, D. R., Wackerman, C., Johannessen, O. M., & Vachon, P. W. (1995a) Coastal ocean fronts and eddies imaged with ERS-1 SAR. Accepted by *J. Geophys. Res. Oceans.*

Johannessen, J. A., Shuchman, R. A., & Johannessen, O. M. (1995b) Synthetic aperture radar on ERS-1. In *Oceanographic Applications of Remote Sensing* (eds. F. Dobson and M. Ikeda). CRC Press, Boca Raton, Florida, USA, pp. 27-44.

Johannessen, J. A., Shuchman, R. A., Johannessen, O. M., Davidson, K. L., & Lyzenga, D. R. (1991) Synthetic aperture radar imaging of upper ocean circulation features and wind fronts. *J. Geophys. Res.*, 96(C6): 10411–10422.

Samuel, P., Grong, E., Espedal, H. A., Søiland, H., Hamre, T., Martinussen, I., & Sandven, S. (1995a) Integrated operational use of SAR images in marine forecasting: A feasibility and demonstration project for detection of oil spill and other phenomena at the sea surface. NERSC & the Programme for Ocean Monitoring and Forecasting, Bergen, Special Report No. 33.

Samuel, P., Jenkins, A. D., Espedal, H. A., & Sandven, S. (1995b) Ocean Monitoring Using SAR. Final project report prepared under Contract No. 1037/94/NL/US with the Norwegian Space Centre and the ESA Prodex Programme. Technical Report No. 101, NERSC, Bergen.

Scott, J. (1986) Surface Films in Oceanography. ONRL Workshop Report C-11-86 p.19.

ERS DETECTION OF SOFT AND HARD TARGETS AT SEA: WHAT CAN BE OPERATIONALIZED?

Åge Skøelv & Terje Wahl

Forsvarets forskningsinstitutt (Norwegian Defence Research Establishment, FFI),
P O Box 25, N-2007 Kjeller, Norway
Tel: + 47 63 80 70 00. Fax: + 47 63 80 72 12

ABSTRACT

In Norway the potential of using the ERS SAR for different ocean surveillance applications, in near real time, has been investigated. Three different applications, namely detection of ships and ship wakes, icebergs, and oil slicks, are discussed. It is concluded that the steep incidence angle makes ERS far from optimal for ship and iceberg detection, while oil slick detection using ERS SAR has been developed into a pre-operational stage in Norway.

1. INTRODUCTION

The all-weather capacity and independence of daylight, together with the large areas covered, make spaceborne synthetic aperture radar a promising instrument for ocean monitoring, especially at high latitudes.

In Norway the emphasis has been on near real-time use of SAR images and therefore a complete ERS-1 SAR processing, distribution and analysis chain was established. This includes a receiving station, Tromsø Satellite Station (TSS) with fast processing capacity and high-bandwidth distribution systems. Typically, SAR images would arrive at the user site 1–2 hours after the satellite had passed.

For the whole period of ERS-1 operation, FFI has been involved in investigating the potential of the SAR instrument for different maritime applications. In this paper, the potential of detecting different types of targets at sea will be discussed, and also the degree to which this can be operationalized.

We will describe the possibilities of using ERS SAR for detection of "hard" targets like ships and icebergs and "soft" targets like oil slicks. The latter application will only be briefly described since there are already several reports dealing with the development of that application (e g, Wahl, Skøelv *et al* 1994, Pedersen *et al* 1995).

2. SHIP DETECTION

Ships are usually seen as bright targets against a darker background in SAR images. The backscatter from the sea varies with the wind speed and with incidence angle (or range position in the image). Due to the rather steep incidence angle of ERS (approx. 23°), there may be considerable backscatter from the surrounding sea, especially at some wind speed. Thus small ship targets can sometimes be invisible in an ERS SAR image.

During the more than four years of ERS-1 operation, a large number of ships have been seen in ERS SAR images analysed at FFI. A total number of more than 800 ship targets have been stored in a database. The identity of most of these ships is unknown. In some cases, especially in connection with campaigns, external sources like coastal radars, coast guard vessels and naval stations have supplied information about position and identity of ships in a given area at the time of ERS-1 overflight. Although the number of identified ships in our database is relatively small, we have several scenes from the same area, showing the same ships (e g, ferryboats), under different weather conditions.

The radar cross-section of a ship depends on several parameters, notably ship dimensions, hull and superstructure shape, type of materials, incidence and aspect angle Quantitative estimates of detection capability, includin superstructure and aspect angle dependence, would re quire a larger number of identified ships than has bee available. As a very rough summary of ERS-1 results, w may say that:

- On a calm sea surface (0–2 m/s wind speed) most ship will be visible as bright point targets.
- At a wind speed of 5 m/s, ships with a length below 5 m may be lost.
- At a wind speed of 10 m/s, ships with a length belo 100 m may be lost.

Based on these results, one could not recommend pre-o erational use of ERS-1 for fisheries enforcement.

Several types of wakes can be seen behind ships in SA images. In an analysis of ship wakes found in Seasat SA images, the so-called dark turbulent wake was the mc frequent feature observed (Wahl *et al* 1986).

Some basic wake statistics obtained from ERS-1 imag are shown in Tables 1 and 2, for full and low resolution i ages, respectively. A few laid-in ships registered in the database are not included, but there may still be ships that were not actually moving at the time of data acquisition.

Wake type	Number of observations	Average length [km]	Max length [km]	Frequency, relative to [%]	
				All ships	Ships with wakes
Dark turbulent wake	269	2.4	20.2	68.1	99.6
– of these, with bright edge	44			11.1	16.3
Kelvin arms	39	1.9	6.7	9.9	14.4
– of these, dark	2				
– of these, bright	37				
Narrow-V	1	1.1	1.1	0.3	0.4
Internal wave	1	50	50	0.3	0.4
Stern waves	1	n. a	n. a	0.3	0.4
Number of ships, total	*395*				
Number of ships, with wake(s)	*270*				
Number of images	*30*				

Table 1 Ship wake statistics, ERS-1 full resolution images.

Wake type	Number of observations	Average length [km]	Max length [km]	Frequency, relative to [%]	
				All ships	Ships with wakes
Dark turbulent wake	224	2.8	10.8	57.1	97.8
– of these, with bright edge	36			9.2	15.7
Kelvin arms	22	2.5	5.2	5.6	9.6
– of these, dark	1				
– of these, bright	21				
Narrow-V	0			0.0	0.0
Internal wave	0			0.0	0.0
Stern waves	0			0.0	0.0
Number of ships, total	*392*				
Number of ships, with wake(s)	*229*				
Number of images	*42*				

Table 2 Ship wake statistics, ERS-1 low resolution images.

The images analysed in the two tables do not necessarily cover the same scene. Therefore, the frequencies of occurrence can not be directly compared. If we, however, only consider scenes where both full and low resolution images exist, we obtain the results in Table 3. We find that both the number of ships and the number of wake lines decrease considerably when going from the full resolution image to the low resolution product. The low resolution product has several advantages, e g, smaller data size and less speckle, which makes it a tempting choice for ship detection purposes. The loss of data is however more than can be accepted. We have therefore investigated the potential of products made by averaging less pixels than the low resolution product. A large number of ships are lost in the averaging process, and the frequency of occurrence of the various wake types decreases. However, there are only minor differences between the numbers obtained from the 2 x 2 and 3 x 3 averaged images.

Wake type	Frequency, relative to total number of ships [%]		Frequency, relative to number of ships with wake(s) [%]	
	Full res	*Low res*	*Full res*	*Low res*
Dark turbulent wake	75.7	56.7	100.0	100.0
– of these, with bright edge	10.7	6.2	14.2	10.9
Kelvin arms	13.6	4.1	17.9	7.3
Narrow-V	0.0	0.0	0.0	0.0
Internal wave	0.0	0.0	0.0	0.0
Stern waves	0.0	0.0	0.0	0.0
Number of ships, total	*140*	*97*		
Number of ships, with wake(s)			*106*	*55*
Number of images	*4*	*4*		

Table 3 Ship wake statistics, comparing full and low resolution versions of the same scenes.

The orientation of all turbulent wakes and Kelvin arms relative to the satellite flight direction has also been investigated. Most turbulent wake lines seem to have an angle of 60° or less with the azimuth direction. There is no obvious explanation for this. The process behind the formation and imaging of turbulent wakes are not well understood, and different explanations might give rise to different predictions about angular dependence.

Concerning the Kelvin arms, the angular dependence is even more clear. There are almost no Kelvin arms with an angle above 60° relative to the flight direction. This fact supports one of the hypotheses concerning the imaging of Kelvin arms, namely that is is due to specular reflection from the wave fronts.

3. ICEBERG DETECTION

In September 1992 a campaign, organized by several oil companies, was carried out in the Barents Sea to study icebergs born from the glaciers at Franz Joseph Land. Ships, helicopter, aircraft, and satellites were used. During this campaign full and low resolution ERS-1 SAR images were analysed at FFI (Anderssen *et al* 1993).

The major contributions to the SAR signature of an iceberg in open water comes from specular reflection from the front facing the radar, multiple reflection from the iceberg/water corner, backscatter from the top surface, melting water suppressing capillary waves, radar shadow, and wind shadow. The relative strength of these sources may depend on aspect angle and wind speed.

The main impression from the analysis was that a large number of icebergs were visible in the SAR images. The typical iceberg signature was a bright point and a darker area surrounding the iceberg (probably due to melting water). Low wind conditions were very favourable for iceberg detection. Comparison between full and low resolution images showed that all iceberg candidates were visible in both, as can be expected for large objects.

Comparison between low resolution SAR images and in-situ observations revealed that the majority of the grounded icebergs that were studied in-situ could be detected in the SAR image. However, there were examples of rather large icebergs (> 200 m) which turned out to be very hard to detect even at favourable wind conditions. We assume that unfavourable aspect angles resulted in a very low backscatter in these cases. Since there were no strong correlations between iceberg size and radar backscatter, it seems that aspect angle is equally important as iceberg size. Thus, small icebergs could be as easily detected as larger ones. Therefore, it will be difficult to estimate iceberg dimensions from ERS-1 images.

Stronger winds will increase the backscatter from the sea surface, making iceberg detection harder. A combination of strong winds and unfavourable aspect angles may cause even large icebergs (≈ 1 km) to remain undetected.

4. OIL SLICK DETECTION

In Norway a radar satellite oil spill detection project has been running since 1991, with several phases:

An ERS-1 oil spill field experiment took place on Haltenbanken outside Central Norway in July–August 1991. In this experiment three releases of 20 tons of oil each, were performed (Bern *et al* 1993).

This field experiment was followed by two periods, June 1992–January 1993 and April 1993–December 1993, with near real-time analysis (performed at FFI) of low resolution ERS-1 SAR images delivered by Tromsø Satellite Station (TSS) from Norwegian waters. In case of a possible oil spill the Norwegian Pollution Control Authority (SFT) was alarmed, and they would, if possible, try to verify the observation using their surveillance aircraft (Skøelv & Wahl 1993, Wahl, Anderssen *et al* 1994). Several events demonstrated the capacity of the ERS-1 SAR in detecting even thin organic layers under favourable weather conditions (Wahl, Skøelv *et al* 1994).

Based on the experience from the preceding phases, a pre-operational phase started in June 1994 and is still running (Pedersen *et al* 1995). SAR image analysis, based on manual inspection, is now being done at TSS as a matter of routine. There is a close cooperation between TSS and SFT, and the flight pattern of the SFT surveillance aircraft is adjusted not to cover the same areas as the satellite, unless an alarm is sounded from TSS.

5. CONCLUSIONS

The ocean surface is the background against which ships, ship wakes, icebergs, and oil slicks are to be detected. The steep incidence angle of ERS (varying between 20° and 26°) gives a strong backscatter from the sea. The radar is also very sensitive to wind speed, such that much of the dynamic variation occur between 0 m/s and 4 m/s wind speed.

The rather steep incidence angle makes the ERS SAR far from optimal for ship detection, especially for detection of typical fishing vessels, even at rather low wind speed. On the other hand, larger ships (length > 120 m) are easily detected. Bases on these conclusions, operational use of ERS SAR for fishery enforcement purposes does not seem feasible.

Similar size considerations apply to icebergs, where wind strength and aspect angle seem important for the detection capability.

On the other hand, the large dynamic variation that occurs for low wind speeds, in combination with the favourably low noise-equivalent σ_0, makes the ERS SAR an excellent instrument for oil slick detection.

Thus, oil slick detection is the only ERS application discussed here that has been developed into a pre-operational level, and with a large potential for future operational use (from a technical point of view). It should be stressed, however, that the conclusions as to ship detection are based on the Norwegian need to detect smaller ships (e g, typical fishing vessels).

6. REFERENCES

Anderssen T, Skøelv Å, Wahl T, 1993, ERS-1 SAR Iceberg Detection Experiment, Final Report (delivered to Mobil Exploration Norway). Forsvarets forskningsinstitutt.

Bern T I, Wahl T, Anderssen T, Olsen R, 1993, Oil Spill Detection Using Satellite Based SAR; Experience from a Field Experiment. *Photogrammetric Engineering & Remote Sensing,* 59, 423–428.

Pedersen J-P, Seljelv L-G, Wahl T, Skøelv Å, 1995, The Norwegian oil spill detection project – from R&D to pre-operational early warning detection service. *Proceedings, Remote Sensing for Oil Exploration and Environment, Space Congress,* Bremen, 23–24 May 1995 (ISBN 3-929663-11-2), 126–138.

Skøelv Å, Wahl T, 1993, Oil Spill Detection Using Satellite Based SAR. Phase 1B, Completion Report. Forsvarets forskningsinstitutt.

Wahl T, Anderssen T, Skøelv Å, 1994, Oil Spill Detection Using Satellite Based SAR. Pilot Operation Phase, Final Report. Forsvarets forskningsinstitutt.

Wahl T, Eldhuset K, Aksnes K, 1986, SAR Detection of Ships and Ship Wakes, *Proceedings, SAR Applications Workshop,* Frascati, 16–18 September 1986 (ESA SP-264).

Wahl T, Skøelv Å, Andersen J H S, Strøm G D, Anderssen T, 1994, Pollution monitoring using ERS-1 SAR images, *Proceedings, First Workshop on ERS-1 Pilot Projects,* Toledo, 22–24 June 1994, 389–393.

SEA & ICE

Chairman: G. D. Strøm
Rapporteur: J. Johannessen

EVALUATION OF THE ERS.SAR HIGH RESOLUTION PRECISION IMAGES IN THE OPERATIONAL MAPPING OF SEA ICE IN THE KAP FARVEL WATERS.

Rashpal S. Gill, Poul Nielsen & Hans H. Valeur,

Danish Meteorological Institute, Lyngbyvej 100, DK 2100 Copenhagen Ø, Denmark.
Tel. (45) 39 157342, Fax. (45) 39 157300

ABSTRACT

The full resolution precision images (PRI) off Cape Farewell were evaluated by comparing them with near simultaneous underflights data which consisted of manual observations, photographs and video recordings. Furthermore a comparison was made between the relative ice information in these images and with their low resolution counterparts. The results of the evaluation showed that, in areas which had a low backscatter from capillary waves, many of the ice floes or icebergs not visible in the low resolution images could be identified in the PRI´s. However, image contrast of the PRI's was found to be very poor especially in wind infested waters. Because of this, identification of the most important ice parameter from a navigational point of view; the position of the ice edge, was much worse in these images than in the low resolution images.

To distinguish between regions of ice from water simple filters were developed. Filtering based on the power-to-mean ratio was found to be fairly successful.

1. INTRODUCTION

The Danish Meteorological Institute (DMI) is responsible for the operational mapping of sea ice in the Greenland waters for the safety of navigation. The mapping is based on observations with specially equiped aircraft (de Havilland Twin Otter) and a helicopter (Ecureuil AS 350 B2) based in Narssarssuaq, and on satellite data received at the DMI ground stations in Greenland and near Copenhagen. To an increasing extent the mapping is based on AVHRR images from NOAA satellites in near real time.

However, cloud cover often limits the use of AVHRR imagery for ice mapping. This is especially true in the Cape Farewell area which is characterised by frequent storms and clouds. In these waters ice mapping is mainly based on aircraft reconnaissance which are made two to three times per week in the ice season and on request. To minimize the need for air observations, imagery from cloud independent systems, such as the ERS.SAR, are being evaluated.

2. ICE CONDITIONS

From the Arctic Basin and through the Fram Straits sea ice of several metre thickness drifts into the Greenland sea. For greater part of the year, this multi-year ice together with the first year ice, formed locally, reaches the Cape Farewell area, continues around the southern tip of Greenland and often it even drifts several hundred kilometres up along the west coast. The width of the ice belt is about 200-400 km in the Fram strait, reducing to about 100-200 km off Scoresby Sound (71 °N) and even narrower from there to Cape Farewell. The average speed of the ice drift in the East Greenland Current is 10-20 km per day, fastest along the ice edge. The ice floes in the Fram Strait are often up to 50 km across or more. During the drift along the coast, the floes break into smaller pieces and are mixed with first-year sea ice formed locally, particularly at the ice edge. South of Scoresby Sound the floe sizes seldom exceeds 5 km. Eventually in the Cape Farewell area the floe sizes are usually less than 100m. However, these are mostly multi-year floes of thickness greater than 2m and are danger to shipping.

Along the west coast of Greenland, apart from the ice drifting around Cape Farewell from the east coast, all the sea ice is mainly first-year ice, formed locally. In the Baffin Bay/Davis Strait between Canada and Greenland an ice cover builds up during the winter, reaching a thickness of about 1m. The variability of the sea ice off west and north-west coast is far smaller than off the east coast. Pressure ridges along the west coast are also smaller than their eastern counterparts and, more importantly, they are poorly consolidated first-year features. Thus Baffin Bay is largely navigable all the year round with large ice breakers.

Proceedings of the Second ERS Applications Workshop, London, UK, 6–8 December 1995 (ESA SP-383, February 1996)

3. DATA SET

This consists of several underflights made along the west coast of Greenland and in the waters off Cape Farewell (the southern most tip of Greenland). During the flights photographs were taken every few minutes, video recordings were made, and further the ice was mapped by visual observations and by a 360 ° mapping radar. Underflights in the Baffin Bay were made on 26th, 27th April and 2nd May 1994 and off Cape Farewell on the 30th May, 1st, 6th, 10th and 13th June 1994.

ERS.SAR low resolution images have been received from the telemetric stations in Kiruna, Tromsø, West Freugh (courtesy of The Defence Research Agency (DRA) and Matra Marconi Space, UK), in near real time, and via D.PAF (DLR, Oberpfaffenhofen, Germany) from Gatineau. The full resolution PRI images were obtained via the normal ESA channels.

Furthermore, AVHRR images from the NOAA satellites and the ice charts produced by the ice patrol for the above dates were also used in the comparison.

4. EVALUATION METHOD

Only a qualitative evaluation of the ERS.SAR images is presented here. The evaluation method thus simply consists of comparing the ERS.SAR images with the underflight data, and with the AVHRR imagery and the ice charts produced by the ice patrol for the above dates. The results of the evaluation of the low resolution images for Baffin Bay and Cape Farewell have already been presented (Nielsen et al., 1994 and Gill et al., 1995, respectively). The question of image avaliability, areal coverage, frequency of coverage, have also been addressed (Nielsen et al., 1994). The present paper, concerns only with the evaluation of the full resolution precision images off Cape Farewell.

To distinguish between regions of ice and water simple filters based on amplitude and power pixel averaging, including pixel skipping to improve the image contrast (Thomsen et al., 1995), were developed. In particular, filter based on the power-to-mean ratio (PMR)

$$PMR = E\{I^2\} / E\{I\}^2$$

where E{I} is the expectation value and I in the pixel intensity was tested following Skriver (1994) who found that this texture parameter could be used to discriminate between water and ice. The evaluation was carried out by computing the PMR values from the full resolution PRI's for a 32*32 pixels size window and comparing them with the original image. Furthermore an *image composite* was also found to be helpful which was produced by displaying the PMR grey values on one colour board and a similarly reduced original image on another board. The *image composites* presented in this article were produced by displaying the PMR image on the green board and the SAR image on the red and blue boards of a high resolution Imagraph colour screen monitor.

5. RESULTS

The areas off Cape Farewell that were investigated, together with the flight paths (sketched between the letter pairs A´s and B´s) and the ERS frames, are shown in figure 1.

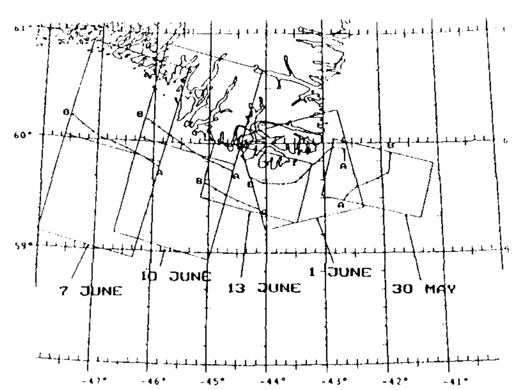

Figure 1. Map of the ERS frames, with dates, that were investigated off Cape Farewell.

Below results are presented for the 1st, 10th and 13th June. However, the evaluation of the low resolution images for the *these* dates, and others, have already been presented (Gill et al. 1995 which also contain additional aerial photographs).

5.1 1st. June 1994

The observational area lies about 20km off the southern most tip off Cape Farewell (see figure 1). The low resolution SAR image is shown in figure 2a. The imaging time was 0:45 UTC and the time of the air reconnaissance was 15.10-15:40 UTC. The ice chart indicated the floes to be less than 100m. The wind was about 5m/s from the north west along the west coast, and a wind of similar strength, from the north east, along the east coast. The air temperature was about 0 °C.

Sample of the aerial photographs are produced in figures 2b and 2c and the corresponding PRI images of the ice regions in the field of view of the camera are shown in figures 2d and 2e respectively. The photograph in figure 2b, taken from position A at an altitude of 1400 feet, indicates ice concentration of 7/10 - 9/10 in the foreground, further photographs indicates that the area marked p1, to the left of A also consists of ice but with slightly smaller concentration (about 7/10), while this part of the low resolution image is relatively all white. After careful examination the PRI image of this part (figure 2d) does indicate some presence of ice but apart from the grey regions of the image it is not certain whether the rest of the white regions are all ice or capillary waves infested waters. The photograph in figure 2c (altitude 2000ft.), taken at position B, indicates, on the otherhand, practically no ice, all the way to the coast, which is split by a stratified layer of cloud. Furthermore, the area to the left of this photograph, marked p2 on the image, is also all open water. It is difficult to conclude from the low resolution image and the PRI image (figure 2e), of this region, whether the grey values (almost white appearance) are due to a high concentration of ice or are due to capillary waves.

Figure 2f shows the PMR filter image composite (not geocoded). For display reasons this image has been magnified by 4. This image clearly shows 2 distinct regions. Comparing the photographs with this filter it can be generally concluded, after allowing for the ice movement between the time of satellite pass and the aerial observations, that the magenta parts (low PMR values) are the water regions and the green parts are ice and surprisingly, the brightest green parts are nilas covered waters with some small floes (highest PMR values). Thus, filter image appears to be helpful in the interpretation of the SAR image.

5.2 10th June 1994

The observational area lies about 20km off the south west coast off Cape Farewell (indicated in figure 1). The low resolution SAR image is shown in figure 3a. The imaging time was 14:09 UTC and the time of the air reconnaissance was 16.50-17:15 UTC. The synop data indicated that there was a light wind of about 5m/s wind from the south west and the air temperature was about 2 - 5 °C.

Figure 3b shows the aerial photograph at position A (altitude 7000 ft.), along the flight path. Comparing this photograph with the low resolution image, it is clear that the ice edge can be easily stated. Other aerial photographs indicates that the region marked p1 on the image is mainly water. However, the grey values in this area appear almost white and are nearly indistinguishable from the ice region to the north. Figure 3c is part of the PRI for this region. As can be seen from the figure the ice edge is less distinct than the low resolution image. This is due to the fact that the PRI is only a 3-look product (thus the low contrast) while the low resolution image is 96-look (it is produced by averaging 2*2 pixels of the 24-look image and therefore the number of looks are in fact < 96). The contrast of the ice edge in the PRI also improves significantly, after averaging 2*2 (or more) pixels. This is in fact a one great advantage of the PRI product, namely, because of the large number of pixels avaliable, it provides an opportunity to experiment with different number of pixel averaging (including skipping) and with filters.

Figure 3d, shows the part of the PRI (after 2*2 pixel averaging) of the circular region seen in the low resolution image. Comparing the aerial photograph with this image many of the icebergs seen in the photograph can be identified. However, this was not always the case, on the contrary many of the icebergs seen in other photographs (Gill et. al.,1995) could not be identified in the images.

5.3 13th June 1994

The observational area lies off the southern most tip off Cape Farewell. The low resolution SAR image is shown in figure 4a. The imaging time was 14:04 UTC and the time of the air reconnaissance was 13.10-13:50 UTC. The synop data indicated that, at the time of the satellite pass, there was a light wind of about 5m/s wind from the south west and the air temperature was between 6 - 10 °C.

Figures 4b shows an aerial photograph taken from A along the flight path from an altitude of 7000 ft. In figure 4b the ice edge and the 2 ice belts behind it, seen in the middle of the photograph, stretching horizontally, are clearly visible on the low resolution image as dark bands and are marked with p1.

Figure 4c is part of the PRI of the three ice belts seen in figures 4a and 4b. Clearly, because of the low contrast, the ice belts are almost lost in the background sea clutter. On the otherhand, the ice belts can be clearly identified after averaging the PRI with the window size of 2*2. The contrast improves as the window size is increased.

Figure 4d shows the PMR filter image. In this figure the water regions, again appears magenta and the ice regions green and the very bright green areas are essentially nilas covered waters. Furthermore, what is most interesting in this filter image is that it clearly show the continuation, south westwards, of the ice belt nearest to the camera in figure 4b. This is confirmed by aerial photographs (Gill et. al., 1995). On the otherhand, in the low resolution image, this part of the ice belt (marked with p2), is essentially lost in the background clutter.

6. DISCUSSION AND CONCLUSIONS

A number of full resolution PRI ERS.SAR images off Cape Farewell, from 30th May - 13th June 1994, were evaluated by comparing them with the air reconnaissance data. The main conclusions that can be drawn are that the PRI are helpful in resolving many of the ice features such as ice floes and icebergs in nilas covered waters or in low wind conditions. However, because of the low contrast in the PRI's, they were found to be less useful in the identification of the ice edges or ice belts especially in wind infested waters. These ice features can be better identified by averaging groups of PRI pixels. Thus all the ice information that is in the low resolution images, and more, is also in the PRI's. It can be obtained by a suitable pixel averaging. In this respect, given the large number of pixels of the PRI's (~ 8000*8000 pixels) these can be used to determine the optimal ERS.SAR image product for these waters and to experiment with filters. Image product with pixel size of 25m * 25m or 50m * 50m, appears to be most useful in these waters.

Filtering based on the PMR was found to be helpful as illustrated for the 1st and the 13th June data. For these dates the PMR values from the water areas were found to be lower than those from the ice regions. However, this was not always case; for the 10th June (not included because of lack of space) the opposite was found to be true. This in fact should not be surprising as PMR is essentially a measure of *heteromogeneity* and the pack ice in fig. 3a "appears" more homogeneous than the water regions. The most important result for the 10th June was that the PMR values from the water region p1 (fig. 3a) were *different* from the ice regions to the north, which is not suggested by the low resolution and the PRI images, figures 3a and 3c, respectively. PMR values were useful in distinguishing between regions of water, ice *and* regions that were essentially nilas covered with perhaps low concentration (~ 1/10) of small (< 50m) ice floes (highest PMR values). Clearly, further tuning of this filter in different wind and ice conditions is required.

Finally to answer the most important question, namely are the ERS.SAR images used at the DMI on a operational basis? The answer is no! This is simply because the ERS data do not meet the basic operational requirements, in terms of areal and frequency of coverage, to monitor the ice conditions in the Greenland waters. The ice informations in these waters are required at least 2-3 times per week. Nevertheless, the images are still very useful when combined with and as a support to the interpretation from other (primary) source of data and for the acquirement of the necessary SAR image interpretation skills which will be useful for the forthcoming missions.

7. ACKNOWLEDGEMENTS

The authors wishes to thank K.Q. Hansen with the processing of the images.

8. REFERENCES

Gill R.S., Valeur H.H. & P. Nielsen, "Evaluation of the ERS.SAR images in the operational mapping of sea ice in the Greenland waters", European symposium on satellite remote sensing II, Paris, 2586-16, 1995.

Nielsen P., Pedersen F.B. and Valeur H.H., "ERS-1 SAR images and operational mapping of sea ice in the Greenland waters, preliminary results of a pilot project", Proceedings of the First ERS-1Pilot Project Workshop, Toledo, Spain, pp 175- 182, 1994.

Skriver H.,"On the accuracy of estimation of ice type concentration from ERS-1 SAR images", Proceedings 14th EARSeL Symposium, Gothenborg 1994.

Thomsen B.B., Skriver H. & Pedersen L.T.,"Seasonal variations in active microwave signatures of sea ice in the Greenland Sea during 1992 and 1993", IGARRS' 95, pp 644-646, 1995.

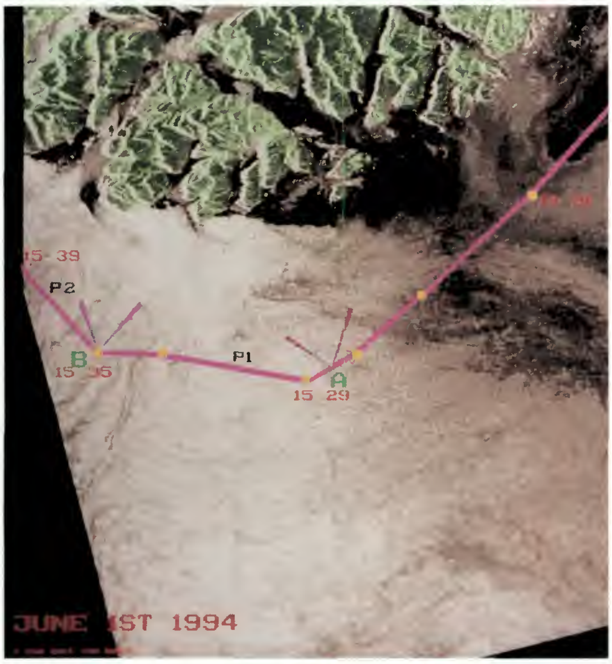

Fig. 2a. ERS.SAR low resolution image from 1st June 0:45 UTC.

Fig. 2f. Filter based on the PMR (not geocoded) for 1st June. Water appears magenta and ice green and very bright green is nilas covered waters.

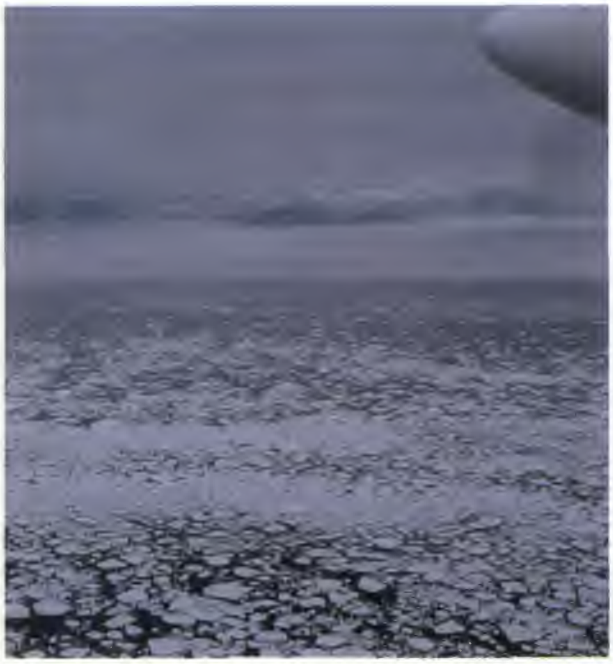

Fig. 2b Photograph taken at 15.28 UTC from position A marked in fig. 2a.

Fig. 2c Photograph taken at 15.35 UTC from position B marked in fig. 2a.

Fig. 2d. Part of the PRI image of the ice seen from position A in fig. 2a.

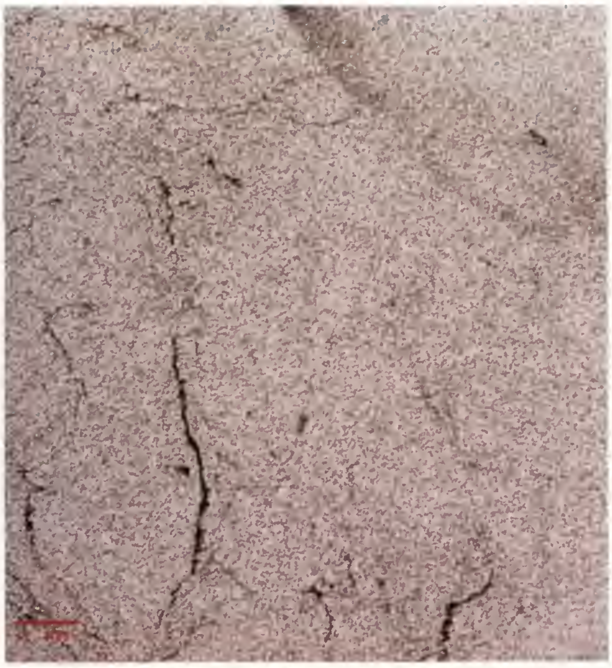

Fig. 2e. Part of the PRI image of the ice seen from position B in fig. 2a.

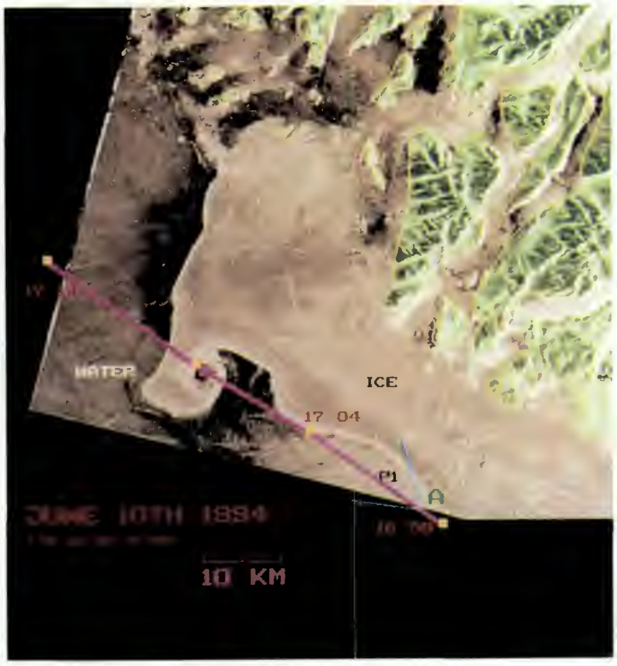

Fig. 3a Low resolution SAR image from 14.09 UTC, 10th June.

Fig. 3b Photograph taken at 17.00 UTC from position A.

Fig. 3c. Part of the PRI image of the ice seen from position A in fig. 3a.

Fig. 3d. Part of the PRI image (after 2*2 pixel averaging) of the circular ice feature seen in fig. 3a.

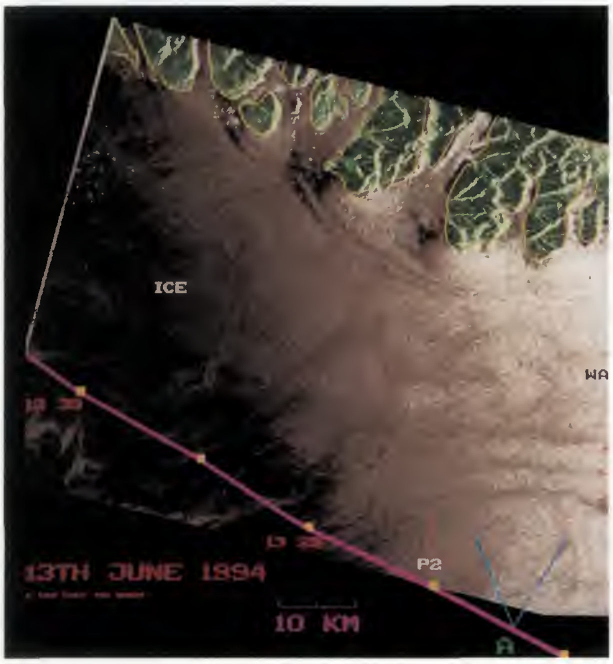

Fig. 4a Low resolution SAR image from 14.04 UTC, 13th June.

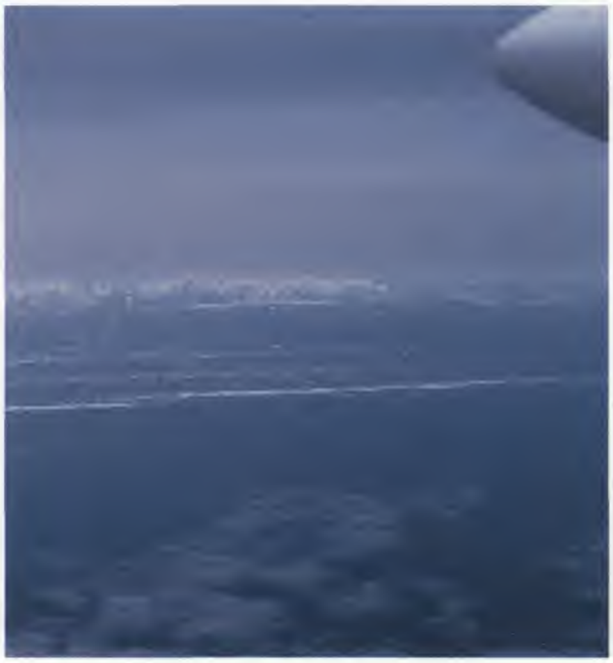

Fig. 4b Photograph taken at 13.21 UTC from position A.

Fig. 4c. Full resolution PRI image of the 3 ice belts seen from position A in fig. 4a.

Fig. 4d. Filter image based on the PMR (not geoceded) for 13th June .

EXPERIENCES AND CONCLUSIONS OF OPERATIONAL ICE MONITORING WITH ERS-1 SAR

Einar-Arne Herland
Space Technology
Technical Research Centre of Finland
Metallimiehenkuja 10, P.O.Box 13031
FIN-02044 VTT, Finland
Tel. +358 0 4561, Telefax +358 0 456 4496
E-mail: Einar-Arne.Herland@vtt.fi

ABSTRACT

Finnish foreign trade is strongly dependent on an efficient merchant fleet, since 85 % of the foreign trade is transported by sea. 25 % of the transport is done during the time of traffic restrictions due to ice in the Baltic Sea. The sea trade is expected to rise 30-40 % during the coming 10 years. During the winter about 4000 vessels visit Finnish harbours, and the total cost of the transport in ice infested waters is about US$ 200 million.

The Finnish Board of Navigation maintains a fleet of eight icebreakers in order to keep harbours open through the winter. 23 harbours are kept open throughout the year. The total cost for the icebreaker service is US$ 30 million, 35 % of which depends upon the severity of the winter.

Since the launch of ERS-1 in 1991, SAR FD-images have been received in Finland, processed and transmitted onwards to the icebreakers and the Ice Service. The paper describes the system that has been built up, the experiences that have been gathered during these winters, and the requirements for an operational system to be established.

INTRODUCTION

The northernmost part of the Baltic Sea is covered by ice for more than 6 months during normal winters and the maximum icecover extent, which on the average occurs in the beginning of March, exceeds 400 000 square kilometers. Finland has no icefree harbours while 85 % of foreign trade is done by sea transport. 25 % of this occurs during the period with traffic constraints due to ice. During the ice season approximately 4000 ships visit Finnish harbours, and with an average of four days in ice infested areas, the total cost of this traffic amounts to 200 million US$ per year. Additional costs to harbour operations and industry are incurred by delays in the sea traffic.

The Finnish Board of Navigation maintains a fleet of 8 icebreakers by means of which it keeps open 23 harbours throughout the year. The cost of the icebreakers is about 30 million US$ (1994) per year, 35 % of which depends on the severity of the winter.

The Ice Service, which belongs to the Finnish Institute of marine Research, collects information on the ice situation, analyses it and produces forecasts. Ice charts are made daily. Including all the ice areas, ice information is usually given from the end of November until the end of May. The Ice Service operates in close cooperation with the Traffic Bureau of the Finnish Board ofNavigation.

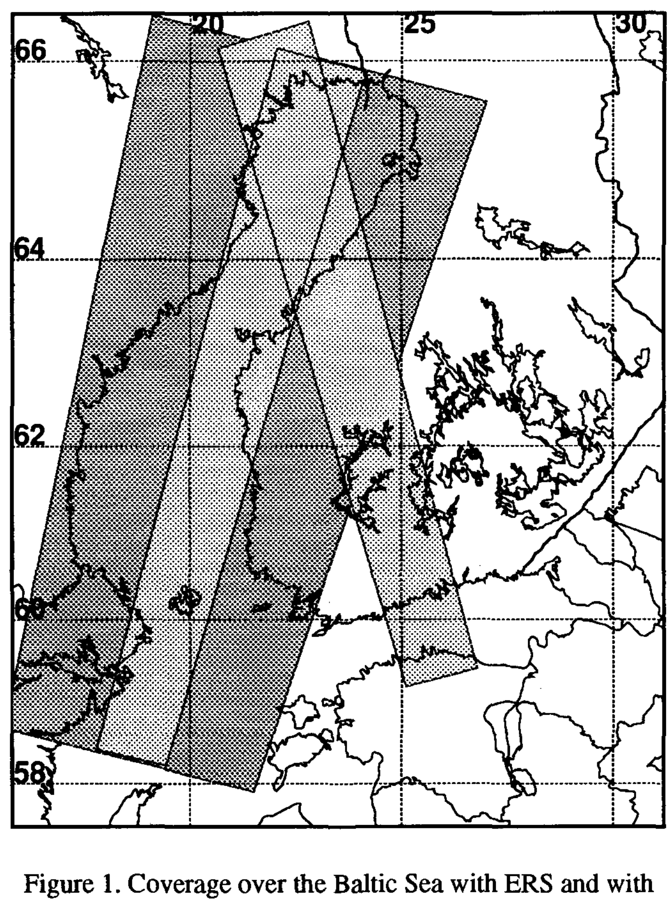

Figure 1. Coverage over the Baltic Sea with ERS and with RADARSAT/ENVISAT.

The collection of ice information utilizes several sources: NOAA satellite images, reports from icebreakers and from ice observation stations along the cost, most of them close to the winter harbours, and also ice reconnaissance aircraft are used, although to a much lesser extent than before the extensive use of satellite images. NOAA images have been

Proceedings of the Second ERS Applications Workshop, London, UK, 6–8 December 1995 (ESA SP-383, February 1996)

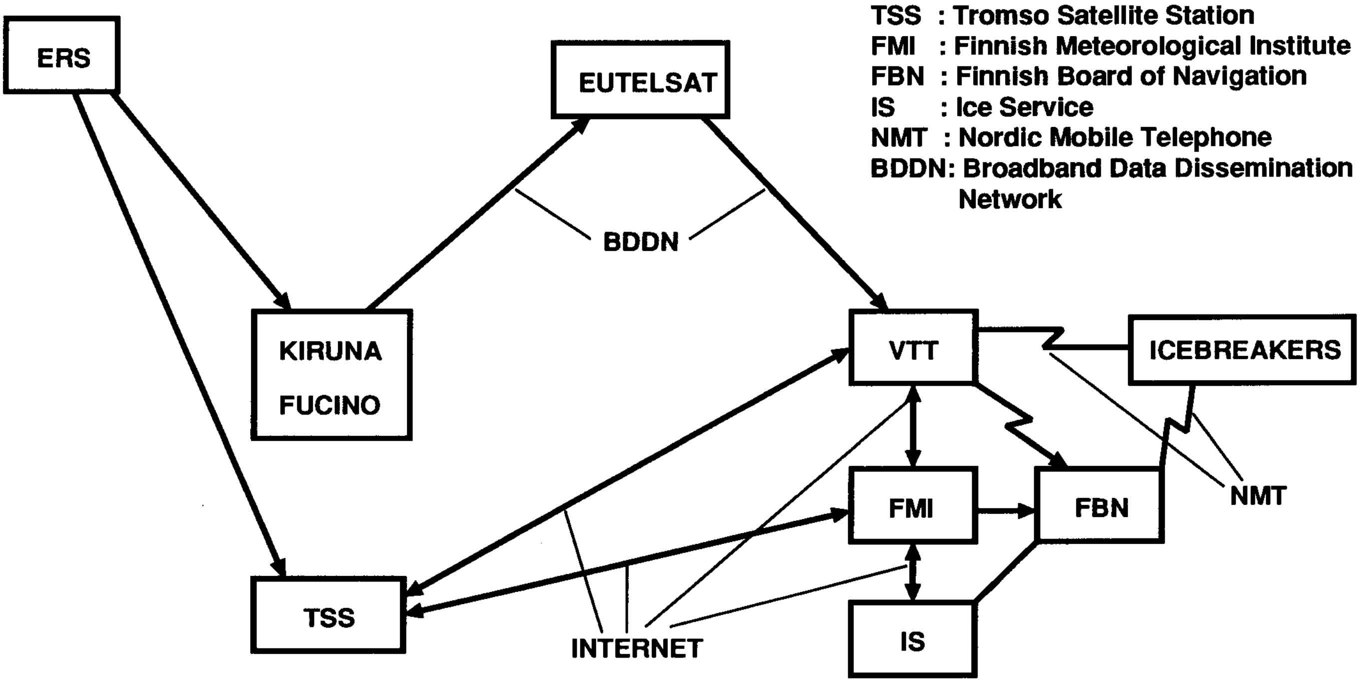

Figure 2. Image handling system supplying ERS-1 SAR images to the icebreakers and the Ice Service.

used for almost 30 years, and real-time images since 1981. Since the launch of ERS-1 in 1991, the Ice Service has received ERS-1 SAR images on an experimental basis.

The total yearly budget of the Ice Service is approximately 600 000 US$. Collection of ice information represents about 25 % of the total costs.

EXPERIMENTS 1992-95

During the last four winters ERS-1 SAR images have been used for monitoring the ice conditions in the Baltic Sea. These images have been supplied free of charge by ESA as part of an AO-project (Announcement of Opportunity) and a pilot project. During the last two winters, the Tromsö Satellite Station in Norway has provided the ESA images free of charge.

Figure 1. shows the coverage of an ERS-1 swath over the Baltic Sea. Figure 2. shows the system used for image acquisition, processing and distribution. Because of the continuous development work throughout the period, the system has undergone major changes since 1992. During the first two winters, the BDDN (Broadband Data Dissemination Network) developed by ESA was used for reception of SAR FD-images with full resolution (30 m). During the last two winters, however, only 100 m resolution images from the Tromsö Satellite Station have been used. During 1992 a telephone link was used for image distribution from VTT to the Finnish Board of Navigation and to the Ice Service. This was later replaced by a data network, and during 1994 and 1995 the Ice Service has received the images on the Internet. Distribution of images to the icebreakers is done on the icebreakers' real-time information exchange system IRIS.

The processing of the images is based on automatic rectification of the images by using the given image corner coordinates. During the early phases both the ESA and the TSS processors contained errors affecting the image geolocation. These errors introduced positioning errors of up to several kilometers, but they have later on been corrected.

During the first three winters all the image processing was done at VTT, and the image products were then distributed to the icebreakers and the Ice Service. At the end of 1994, however, the whole image reception and processing system was moved to the Ice Service, where it was operated as part of the operational routines in 1995.

More details on the technical aspects of the experiments can be found in the references.

CONCLUSION

SAR images have been found to be very useful for monitoring of the ice conditions. Compared with NOAA images, the most important property, in addition to the higher spatial resolution, is the ability to aquire images during periods of rapidly changing weather conditions, when also the ice conditions undergo rapid changes and optical images are of no use because of the cloud cover.

The narrowband transmission channel to the icebreakers limits the amount of imagery, and the resolution, that can be sent to the icebreakers. One possibility would be to follow the icebreaker reports on the IRIS system in order to track the icebreaker movements and optimize the location and resolution of the transmitted images. This was not done during the projects because there was no real-time access to the IRIS data for the project team.

ERS-1 is not an operational satellite and the provision of images did not satisfy operational requirements. The narrow swath width of ERS-1 (see figure 1) was not a very serious constraint for the icebreaker use of the images, except that it had an impact on the repeat cycle for a given area. For the Ice Service, however, regular coverage of the whole area is of crucial importance. This problem will be alleviated with the RADARSAT and ENVISAT SARs.

Spatial resolution of 100 m is sufficient for ice charting, but icebreakers could benefit from even higher resolution. This would require optimized selection of the area to be covered. With 100 m resolution, images can be distributed on the Internet, even for the large swath widths of RADARSAT and ENVISAT. Combined with fast processing of the SAR raw data, this allows the images to arrive at the user within 2-3 hours after the satellite overpass. The processing constraints in terms of maximum number of consecutive images from a single pass are unacceptable from an operational point of view, and were indeed removed when data were obtained from TSS. The BDDN system, which was designed for near real-time users, seems to have been overtaken by the Internet as a distribution channel for SAR images for operational purposes. This is both a result of the rapid development of the Internet, and also the acceptance of 100 m resolution as sufficient for ice monitoring. The timing of ERS-1, with its descending pass at noon, local time, in Finland, is also unsuitable for the Ice Service, since the ice charts are prepared in the morning, and the SAR images do not arrive until 2-3 pm. RADARSAT will be an improvement also in this respect.

A particularly intriguing question is the effect of image price on the utilization. All the SAR images used for ice monitoring in Finland have been provided free of charge, so this point is still quite unclear. It can be argued that no operational entity is yet willing to pay for the data because the current satellites do not yet provide an operational service, and that the current price per image is unreasonably high considering the large amounts of data needed by operational ice monitoring, and the low utilization of a single image. Willingness to pay for the data must, however, be based on either an improved product that justifies the price, or corresponding savings elsewhere. The former possibility is somewhat limited since ships entering ice infested waters pay a fixed price depending only on the ice classification of the ship, and not according to time spent in the ice. Savings resulting from improved ice monitoring and forecasting will therefore not cause any direct increase in income for marine traffic authorities. The possibility of achieving reduced expenses elsewhere depends strongly on the type of expenses. It is typically difficult to achieve savings where labour costs are high, while reductions in services bought from outside the organization are much easier to achieve. Reconnaissance flights are an example of the latter.

Automatic ice chart generation is currently a heavily researched topic. Ultimately success in this area would replace the people currently making ice charts with a computer. Evaluation of new algorithms is naturally done by people with long experience in making ice charts. It seems plausible to assume a certain conservatism regarding accepting a totally automatic approach. A reasonable prediction seems to be ice charts that are still produced manually, but with advanced graphic utilities and ice classification algorithms as an aid in the process.

ACKNOWLEDGMENT

The projects have been partially funded by the Technology Development Centre of Finland (TEKES). Additional funding was obtained from ESA through a series of three projects in connection with the International Space Year.

REFERENCES

Herland, E-A., and Berglund, R. 1995. Demonstration of operational sea ice monitoring in the Baltic Sea with ERS-1 SAR, Int. Journal of remote Sensing, 1995, in press, 13 p.

Herland, E-A. 1994. Operational ice monitoring with ERS-1 SAR. Proc. of the First ERS-1 Pilot Project Workshop, Toledo, Spain, 22-24 June, 1994, ESA SP-365, pp. 135-138.

Herland, E.-A., Seinä A., Leppäranta, M., 1994, "ISY Real Time Ice Monitoring Demonstration in the Baltic Sea", Contract report, ESA, May 1994.

Herland, E.-A., 1993, "Real time ice monitoring demonstration in the Baltic Sea", Proceedings Second ERS-1 Symposium, Hamburg, Germany, 11-14 October, 1993, ESA SP-361, pp.681-685.

Herland, E.-A., Berglund, R., 1992, "Demonstration of ERS-1 SAR sea ice mapping in the Baltic Sea", Proceedings of the Central Symposium of the International Space Year Conference, Munich, Germany, 30 March - 4 April, 1992, ESA SP-341, pp. 1009-1013.

SAR IMAGE CLASSIFICATION ACCORDING TO THE ICE DEFORMATION

Markku Similä

Finnish Institute of Marine Research
P.O. Box 33, FIN-00931 Helsinki, Finland
Tel. +358 0 613941, Fax + 358 0 61394494, E-mail: simila@fimr.fi

THE ABSTRACT

An automated sea ice classification algorithm has been developed and tested in the Finnish Institute of Marine Research. The algorithm derives from ERS-1 SAR an ice chart with four categories: open water, smooth ice, deformed ice and highly deformed ice. The algorithm has been tested in the seasonal ice zone in the Baltic Sea with promising results.

Keywords: Baltic Sea, sea ice, ERS-1, SAR, classification

1. THE OPERATIONAL ICE CHARTING IN FINLAND

The Baltic Sea belongs to the seasonal ice zone. The ice conditions in the Baltic Sea have a large variation. The maximum annual ice extent ranges from 12 % to 100 % being on average about 50 % (Ref. 1). The ice season starts in November in the northern Bothnian Bay and reaches its annual ice extent maximum in the beginning of March. At this point the Bothnian Bay, The Gulf of Finland and the northern part of the Baltic Sea Proper have usually freezed (see Fig. 1). After that the ice covered area gradually begins to decrease and in April there appears ice in most winters only in the Bothnian Bay. Hence in a normal winter all Finnish harbors are surrounded by ice and some harbors need an icebreaker to assist the winter shipping for even as long as five months.

The Baltic Sea ice conditions are monitored and reported by the Finnish Ice Service which is a part of the Finnish Institute of Marine Research (FIMR). The most important product of the Ice Service is a daily ice chart. which describes the ice situation in the whole Baltic Sea.

FIMR has participated in the ERS-1 SAR Application Oriented Pilot projects of ESA. The current AO project is called Operational Sea Ice Charting (OSIC). The main aim of this project have been to construct a classifier which could separate open water from ice and produce an ice map according to the deformation of the ice field. The navigational considerations have been of primary interest when this classifier have been designed. Radiometrically uncalibrated, geometrically rectified Fast Delivery Low Resolution ERS-1 SAR images with a resolution of 100 m by 100 m have been used as source data. The land is masked away from the image. In this paper the classifier is described and its performance is evaluated.

2. CLASSIFICATION ALGORITHM

The goal of the classification algorithm is to produce an ice map with the following four qualitative categories: open water, new ice or smooth ice, deformed or rafted ice, and strongly deformed ice. The distinction between the third and fourth classes is somewhat vague because the quantitative description of the ice field deformation is so incomplete. This distinction would be difficult to make even if validation data would be available. The interpretation for the category of the highly deformed ice field is that this category consists of those areas where the shipping is most troublesome.

The first version of this algorithm without the open water class is described in some length in Ref. 2. The algorithm is based mainly on three hypothesis. In the following the problems associated to each hypotheses are also indicated.

a) There appear three different ice deformation classes in the image area.

Problem: The number of classes varies. It may happen that e.g. only thin ice occurs in addition

to open water. However, the classifier is unable to determine the correct number of ice classes.
b) There exists a clear dependency between the degree of the ice deformation and the local intensity value fluctuation.
Problem: The magnitude of the local fluctuation in the image does not depend uniquely on the degree of ice deformation, e.g. a move from one ice type category to another may cause a big jump in the intensity level. However, the magnitude of the local fluctuation and the degree of ice deformation correlates strongly.
c) The blockwise mean autocorrelation separates open water and ice.
Problem: In the used classification approach the size of this pixel block is 8 by 8 pixels and hence it is insufficient to reliably discriminate between these classes.
First, it should be remarked that the feature c) is not speculated but it has been empirically verified by the author using many images. It is discussed more in Ref. 3. What comes to the hypotheses b) the wavelet coefficient is chosen to represent the local irregularity and fluctuation in two dimensions.
Utilizing the hypothesis the following classifier is constructed.
Phase 1:
Mallat's decomposition (Ref. 4) is applied to the SAR image three consecutive times. The detail images in each scale are added together. Then these three scale dependent sum detail images are added together. As a result we get a sum detail image which describes the local variation in three different scales. The value of the pixel in the final sum detail image is a wavelet coefficient which indicates the local roughness of the original image in the corresponding 8 by 8 pixels block.
Phase 2:
The final sum detail image is classified by the magnitude of the wavelet coefficient. To this end it is assumed that the wavelet coefficients of each class are generated according to a different normal distribution. Hence the whole distribution of the sum detail image can be modeled as a mixture density with three components. The nine parameters of the mixture density are estimated using the likelihood principle and SEM algorithm (Ref. 5).
Phase 3:
The blockwise (8 by 8 pixels) mean autocorrelation is calculated. If this mean correlation is less than the selected threshold value 0.2 and the pixel block belongs to the smooth ice category according to the classification, the pixel block is interpreted to represent open water. In all other cases the pixel block represents ice.
The result of this three stages classification algorithm is the desired ice chart with the four qualitative categories.

3. PERFORMANCE OF THE ALGORITHM

Scatterometer measurements have given support for some assumptions concerning the presented algorithm (Mäkynen, 1995, private communication). According to those results the wavelet coefficient is small for both open water and smooth ice as it is assumed in the classification algorithm. However, the correlation coefficient has not been observed to be essentially smaller for open water than for ice which is an essential assumption in the phase 3 of the algorithm. This can be due to the one-dimensional character of the scatterometer data.
The performance of the algorithm will be illustrated by two examples. The image 1 (Fig. 2) tests in the first place the ability of the algorithm to detect large open water areas. As can be seen from the classification result the large open water area is correctly identified. The small new ice area is wrongly classified to represent either deformed ice or open water. The strong backscatter from the new ice area is probably due to the relatively high salinity. It is known, however, that no open water situated in the new ice area although the human interpreter could perhaps assume it to be so also. The classification of the old ice field corresponds coarsely with the visual interpretation.
The image 2 (Fig. 3) consists of ice fields and small land areas. The recently frozen lead can be easily detected in the classification result. Also the difference between smooth and deformed ice is discernible. Part of the smooth ice is classified as open water. This is an error which occurs regularly with the algorithm but misclassified open water areas are seldom larger than just a few pixels.
Usually the classification results are in harmony with the outlined goals. Low ice concentration areas and narrow leads are, however, problematic for the classification algorithm.

4. CONCLUSIONS

A sea ice classification algorithm with four classes for the seasonal ice zone has been presented. The classes are defined with paying a special attention to the winter navigation problems. An intensity based classification is deliberately avoided (compare Ref. 6). Two feature images, a correlation image and a wavelet based roughness image, are derived from an ERS-1 SAR image. The classification algorithm utilizes these images from which follows that the resulting ice map has a resolution of 800 m by 800 m. The behavior of the algorithm has turned out to relatively stable in temperatures below 0° C. Although an exact geophysical interpretation for the ice classes is impossible to give, the algorithm separates the smooth ice from the deformed ice relatively reliably as well as the ice covered area from open water. Also the classes in the resulting ice map have usually a correct order according to the degree of ice deformation. The algorithm has been tested in the Baltic Sea using the SAR images from the winter periods 1993-94 and 1994-95.

5. REFERENCES

1. Seinä, A. and Palosuo, E., 1993, Itämeren suurimpien vuotuisten jääpeitteen laajuuksien luokittelu 1720-1992 (Abstract: The classification of the maximum annual extent of ice cover in the Baltic Sea 1720.1992), *Meri*, 20, 5-20.
2. Similä, M. and Helminen, J., 1995, "The identification of the deformed sea ice fields from ERS-1 SAR image by wavelets", in *Proc. IEEE Geoscience and Remote Sensing Conf.* (IGARSS'95), Firenze, pp. 868-870.
3. Similä, M., 1994, "SAR image segmentation by a two scale contextual classifier" - in *Image and Signal Processing for Remote Sensing*, Jacky Desachy, Editor, SPIE 2315, pp. 434-443, 1994.
4. S. Mallat, "A theory for multiresolution signal decomposition: the wavelet representation", *IEEE Trans. Pattern Anal. and Machine Intell.*, vol. PAMI-11, pp. 674-693, July 1989.
5. G. Celeux ja J. Diebolt, 1992, "A stochastic approximation type EM algorithm for the mixture problem", *Stochastics and Stochastics Reports*, Vol. 41, 119-134.
6. Fletterer, F. M., Gineris, D., and Kwok, R., 1994, "Sea ice type maps from Alaska Synthetic Aperture Radar Facility imagery: An assessment", *J. Geophys. Res.*, vol. 99, No. C11, pp. 22,443-22,458.

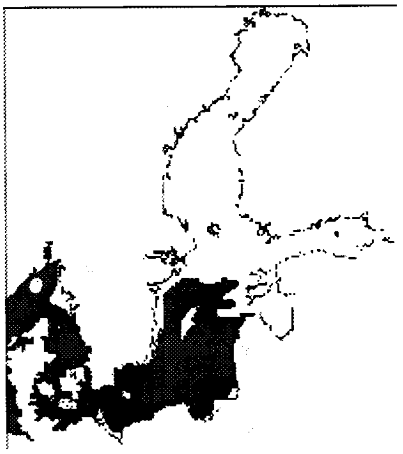

Fig. 1 The maximum extent of ice cover in an average winter.

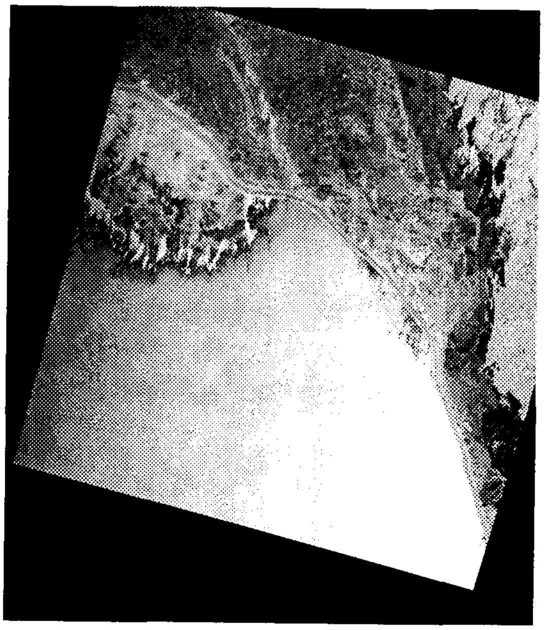

Fig. 2a ERS-1 SAR image 23. 03. 1994. Processed by Tromsö satellite station, © ESA.

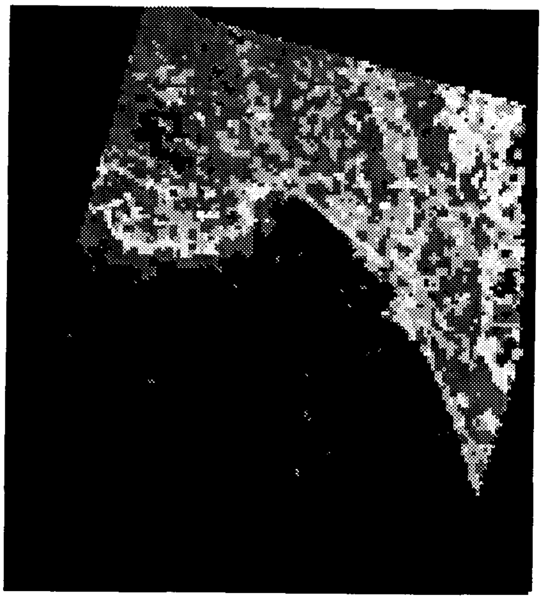

Fig. 2b The classification result for the image 2a. Black indicates open water. Otherwise, the brighter the pixel the more deformed ice it represents.

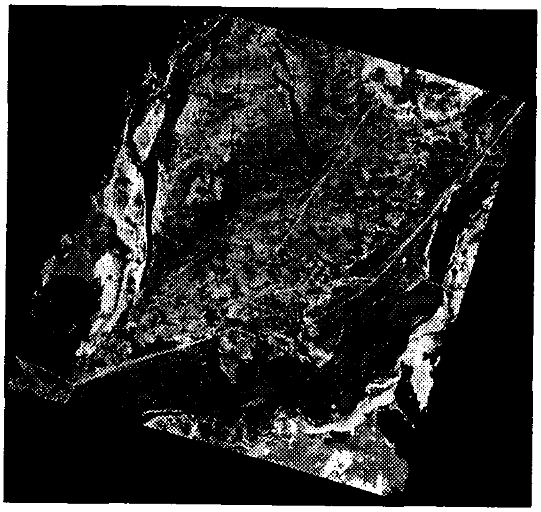

Fig. 3a ERS-1 SAR image 12. 02. 1994. Processed by Tromsö satellite station, © ESA.

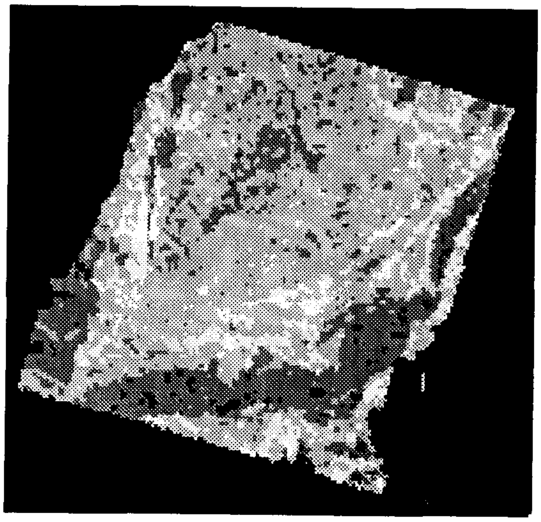

Fig. 3b The classification result for the image 3a. Black indicates open water. Otherwise, the brighter the pixel the more deformed ice it represents.

DETERMINATION OF SEA ICE EXTENT AND ICE TYPES USING THE AMI-WIND, ANTARCTICA, 1992 - 1995

Robert Ezraty, Francis Gohin, Philippe Bryère, Christophe Maroni & Alain Cavanié

Dépt. d'Océanographie Spatiale, IFREMER/Centre de Brest, B.P. 70, 29280 Plouzané, France
Tel : (33) 98224299. Fax : (33) 98224533. Email : ezraty@ifremer.fr

ABSTRACT

Sea ice can be distinguished from open water using the AMI-Wind. Because of its resolution, the AMI-Wind cannot compete with the SAR which is much more suited for ship navigation in sea ice covered areas. There is no doubt that in the vicinity of a receiving station and taking into account the financial costs of a systematic survey of the ship route, SAR is a well suited sensor for this purpose as it has been demonstrated in the Arctic. The situation is rather different in the Antarctic where permanent receiving stations do not exits. At the same resolution as that of the AMI-Wind, passive microwave radiometers (SSM/I) do provide valuable information about sea ice extent in the Antarctic, although some difficulties still remain in the discrimination of sea ice types and in the estimation of their respective concentration. Because of its stable signature, its continuous operation (when SAR is not switched on), and the systematic data processing by CERSAT, the scatterometer can provide valuable inputs to the monitoring of sea ice on a regional scale. To illustrate this potential, a video film was elaborated ; it shows the weekly evolution of ice backscatter and ice extent over the whole Antarctic ocean from 1992 until 1995.

1. INTRODUCTION

Passive microwave radiometers as the SSMR and the SMM/I have been used since two decades to monitor sea ice over both polar caps (Zwally *et al.* 1983, Gloersen *et al.*, 1992). The ground resolution of the SSM/I and that of the AMI-Wind are very similar (50 x 50 km), although the swath of SSM/I is 3 times wider than that of the AMI-Wind, there is no doubt on the valuable inputs of SMMR and now of the SSM/I data in monitoring sea ice for scientific and operational purposes.

The ability of the AMI-Wind to detect sea ice has already been proven ; it is out of the scope of the present paper to present the detail of sea ice discrimination using the C-band scatterometer of ERS-1. The reader may refer, for example, to Cavanié and Gohin (1992 and 1995), Cavanié *et al.* (1994), Gohin and Cavanié (1994), for detailed description of the method and validation of the geophysical results. Some of these validations were performed by comparisons with analysis of concomitant passive microwave data from the ATSR/M on board ERS-1 (Ezraty *et al.* 1994) and the SSM/I (Gohin, 1995a).

Of course, because of its resolution and its all weather imaging capability, SAR is now the favored tool for precise ship routing in sea ice areas. Taking into account the costs of systematic SAR data processing, most of these operational applications are performed in the Arctic Ocean not only because of the economic importance of this area but because permanent receiving stations exist at high latitudes in the Northern hemisphere. The situation is somehow different in the Antarctic where only temporary SAR receiving stations have been installed for scientific expeditions.

This presentation intends to show that because AMI-Wind data is routinely available, it can be used operationally either alone or as a complement to passive microwave data to ease identification and monitoring of sea ice extent, ice types and ice drift on a regional scale. These capabilities are illustrated by a video film presenting the weekly evolution of the backscatter of the AMI-Wind over the Antarctic Ocean from May 1992 until April 1995.

2. THE REQUIREMENTS FOR OPERATIONAL USE OF THE AMI-WIND OVER SEA ICE

2.1 Scientific background

The behavior of the AMI-Wind backscatter as a function of the incidence is presented in figure 1 which is extracted from Gohin, 1995a. The curve representing the "over sea water" backscatter is an average value which includes the wind vector effect ; its detailed analysis is the basis of the wind vector retrieval algorithm (Cf. for example Quilfen and Cavanié, 1991). Over sea ice, the behavior of the backscatter is essentially related to the ice type, including marginal ice (mixture of small broken floes and water), smooth first-year ice of the consolidated pack or multi-year ice. For instance, the NRCS at high incidence angle attains its highest values for the marginal ice which is broken and rafted. As high values of σ° are also reached for multi-year ice, another characteristic of the backscatter is needed for pertinent discrimination. For that purpose, the derivative of the backscatter as a function of the incidence angle at low incidence angle has proven to be representative as it is related to the open water concentration. However, an accurate sea ice concentration cannot be estimated because of σ° sensitivity to wind conditions. The absolute value of the derivative is high over open water and marginal ice while the contrary is observed over the old ice.

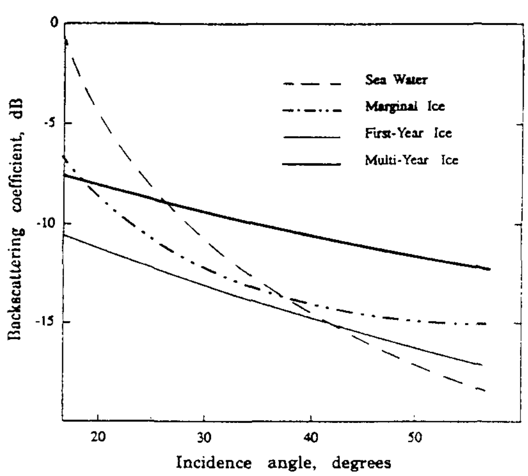

Figure 1. Schematic behavior of σ° as a function of incidence angle (from Gohin, 1995)

In practice, over the Antarctic ocean, the key parameters used jointly to discriminate the various target types are the backscatter coefficient at 50° incidence angle (σ°_{50}) and the derivative of the backscatter coefficient as a function of incidence angle at 28° incidence angle, $(d\sigma^\circ/d\theta)_{28}$.

2.2 Sea Ice products

Given the experience gained at IFREMER on sea ice monitoring using the AMI-Wind and the operational capability of CERSAT, a systematic processing of the backscatter data over both polar oceans has been performed for the existing data set. This effort will continue for the forthcoming data.

The data products are mapped on the National Snow and Ice Data Center grid in order to ease the joint use of SSM/I data. Aside the two main parameters, namely : σ°_{50} and $(d\sigma^\circ/d\theta)_{28}$, three others parameters are also mapped : The sea ice mask deduced from the maximum likelihood distance of the wind vector algorithm, and σ° at 24 and 40° incidence angle. A full description of these products can be found in Gohin, 1995b.

In order to present these operational products, a color video animation over the Southern Ocean has been produced, from 1992 until 1995. Each image corresponds to a one week time period. Since the backscatter signature of sea ice is not influenced by atmospheric perturbations (which is not the case for SSM/I, especially in the Southern Ocean), typical patterns can be accurately followed as a function of time providing new insights into the dynamics of sea ice, either at global or at regional scale. Typical phenomena like the Weddell sea ice gyre or the opening and closing of the Ross sea polynya can be observed.

2.3. Data availability

Operational use doesn't mean necessarily real time access to the data. Although σ° scatterometer data are distributed on the GTS to dedicated meteorological agencies for wind application purposes, a privileged user, having ESA agreement, may access scatterometer data 24 hours after measurement through the Fast Delivery Product data files received at CERSAT. For applications which do not require real time data access, CERSAT produces off-line reprocessed wind (Quilfen, 1995) for which special attention is given to the sea ice extent. This data is now distributed on CD-ROMs by IFREMER/CERSAT. Presently, routine processing of sea ice products are also performed on a weekly basis ; it is also planned to distribute these products in the near future.

Since almost 25 % of the total scatterometer data set is located over the two polar oceans, there is a high probability that any high latitude location, say above 60°, be sampled by the scatterometer swath at least once every three days. There are however, two limitations. The first one is that the AMI-Wind cannot be operated when the SAR is switched on ; this occurs quite often over the North polar cap, specially in Canadian areas. The second is related to the orbit inclination of ERS-1 and the geometric configuration of the scatterometer (the nearest available incidence angle is located at 250 km on the right of the ground track, and the swath is 500 km wide.). It follows that for the North polar ocean, latitudes up to 88°N can be analyzed, while in the South polar ocean, some areas as the innermost part of the Ross sea, cannot be sampled at low incidence angles, and thus $(d\sigma^\circ/d\theta)_{28}$ cannot be estimated there.

3. CONCLUSIONS and PERSPECTIVES

Because the AMI-Wind offers a spatial resolution quite similar to that of the SSM/I, its possible contribution to sea ice monitoring must be judged in comparison with this instrument. For Europeans interested in applications, the SSM/I data has become available in 1995, trough the World Wide Web, with a few hours of delay, while AMI-Wind data is put on line within a few hours through the Global Transmission System of the World Meteorological Organization. This may appear presently of little importance to end users, since SSM/I data is introduced in the ice charts produced in the USA and internationally broadcast, but is certainly important for meteorological services already using such data for several different purposes. The question of convenient and rapid access to the data will gain importance with METOP, whose two-swath, operational scatterometer will offer practically as good geographical coverage of sea ice regions as the SSM/I, with higher resolution (25 km). Before METOP, scheduled for 2002, NSCAT which is planned to be launched in 1996, on ADEOS, will provide other backscatter parameters (Ku-band, VV and HH polarization) with a double swath and 25 km resolution which will permit further research concerning sea ice monitoring.

Because sea ice is a complex medium, evolving with age and regional conditions, we do not claim that scatterometers are "stand alone, do it all" sensors, but we are convinced that the AMI-Wind provides valuable information on ice types, ice extent and ice motion at ocean basin scale.

4. REFERENCES.

Cavanié, A., Gohin, F., Quilfen, Y., and Lecomte, P., Identification of sea ice zones using the AMI-WIND : Physical bases and applications to the FDP and CERSAT processing chains, in *Procs. Second ERS-1 Symposium*, Space at the Service of our Environment, Hamburg, Germany, 11-14 October 1993. ESA. SP 361, Vol. II, pp.1009-1012, Jan. 1994.

Cavanié A. and Gohin, F., Interpretation of ERS-1 Scatterometer Data over Sea Ice, in *ERS-1 Geophysical Validation Workshop Proceedings*, 27-30 April 1992, Penhors, Bretagne, France. ESA wpp-36, pp. 199-201, August 1992.

Cavanié A. and Gohin, F., Sea Ice Studies with Scatterometers, in *Oceanographic Applications of Remote Sensing*, M. Ikeda and F.W. Dobson Editors, CRC Press, pp. 359- 366,1995

Ezraty R., Gohin, F. and Cavanié, A., Arctic sea ice during the winter to summer transition as seen by the AMI-Wind and ATSR/M of ERS-1, Microwave Remote Sensing of Sea Ice, *EARSel Advances in Remote Sensing*, **3**, 100-111, 1994a.

Gohin F. and Cavanié, A., A first try at identification of sea ice using the three beam scatterometer of ERS-1, *Int. J. Remote Sensing*, **15**, 1221-1228, 1994.

Gohin F., Some active and passive microwave signatures of Antarctica sea ice from mid- winter to spring 1991, *Int. J. Remote Sensing*, **16**, 2031-2054, 1995a.

Gohin F., ERS-1 AMI-Wind backscatter grids for the polar regions, *Tech. Rep.* DRO/OS, IFREMER, 1995b.

Gloersen P., W. J. Campbell, D. J. Cavalieri, J. Comiso, C. L. Parkinson and Zwally, H. J., Arctic and Antarctic Sea-Ice, 1978-1987: Satellite Passive-Microwave Observations and Analysis, NASA Scientific and Technical Information Branch, *NASA SP-511*, 290pp., 1992.

Quilfen Y., ERS-1 Off-line Wind Scatterometer Products, *Ref. C1-EX-MUT-CD0000-03-IF*, Version 1.1, 58pp., CERSAT, IFREMER, France, 1995.

Quilfen Y., A. Cavanié, A high precision wind algorithm for the ERS-1 scatterometer and its validation. *Procs. IGARSS* 1991, Espoo, Finland, 873-876, 1991

Zwally H. J., J. C. Comiso, C. L. Parkinson, W. J. Campbell, F. D. Carsey and Gloersen, P., Antarctic Sea Ice, 1973-1976: Satellite Passive Microwave observations, NASA Scientific and Technical Information Branch, *NASA SP-459*, 206pp., 1983.

MONITORING THE ICE MOVEMENTS WITH ERS SAR INTERFEROMETRY IN THE ANTARCTIC REGION

Karl-Heinz Thiel, Philipp Hartl, Xiaoqing Wu

Institute of Navigation, University Stuttgart, Keplerstraße 11, 70174 Stuttgart, Germany, Fax: (49) 711 121 2755

ABSTRACT

Monitoring the changes of the ice cover and the movement of the ice in the Antarctic region continuously, is quit difficult in this remote area. ERS SAR Interferometry provides a tool to perform this task. For the region around Hemmen Ice Rise it is demonstrated, that topography , tidal variations and horizontal displacements can be estimated.

INTRODUCTION

The Institute of Navigation (INS) is involved in the development of interferometric SAR (INSAR) since 1989 and has shown in the Bonn experiment in cooperation with POLIMI/ Mailand and ESRIN/Frascati the potential of INSAR and differential INSAR (D-INSAR). In the interdisciplinary working group OEA (ocean - ice - atmosphere), funded by the German Ministry of Research and Technology the INS applied the methods to the Antarctica. With respect to this co-operation special test areas were chosen on the Ronne Ice Shelf.

TEST FIELD ON THE SHELF ICE

This area was chosen due to the fact that some other experiments were carried out during the Antarctic summer 1992 while the ERS 1 Ice Phase. During the Ice Phase every three days a SAR image could be acquired from the same place.

In cooperation with the IFAG/Frankfurt Corner Reflectors were deployed and surveyed with GPS. The main question was, whether the interferometric method would work on ice and snow. Applying the developed algorithm, which were already tested in the Bonn area, we found clear fringes for some pairs and no fringes for other combinations. There was also a clear degradation for the fringes with larger time difference between acquisition dates. Correlating the INSAR results with the daily weather reports (recorded by the IFAG scientist) it could be seen, that a snow storm has changed the surface such, that no interferometric calculation could be performed - the coherence between the images was very low.

Further analysis of this data revealed some more problems. In this wide and almost featureless shelf ice area we had no fixed reference points, thus the flow of the shelf ice could not be estimated. The shelf ice movement was eliminated by the coregistration of the SAR images. Thus the interferogramme only allowed for determining the topography of the shelf ice, which was very flat. Searching through the available data for a better test area we found the region around Hemmen Ice Rise (HIR) beside Berkner Island (BI).

COARSE DISPLACEMENT ESTIMATION

The topography of HIR, an elongated hump, allowed for the assumption that there is almost no movement on the top. Also the glacier on BI will show a much lesser movement than the shelf ice. Thus HIR and BI could provide reference points for the coregistration of the two SAR images. With respect to these fixed points the displacement of the pixels on the shelf ice from the first to the second acquisition can be estimated in slant range and azimuth direction. Using phase correlation techniques the adjustment of small areas can be done with 1/10 to 1/20 of one pixel. Performing this coregistration across the complete scene the relative displacement vectors result from the combination of azimuth displacement, slant range displacement and a correction value for the tidal height variation of the shelf ice between the two images acquisition times. The tidal correction is done by a constant value for the shelf ice area, assuming a almost parallel uplift/subside of the ice sheet. The shearing zones around HIR and along BI will produce

Proceedings of the Second ERS Applications Workshop, London, UK, 6–8 December 1995 (ESA SP-383, February 1996)

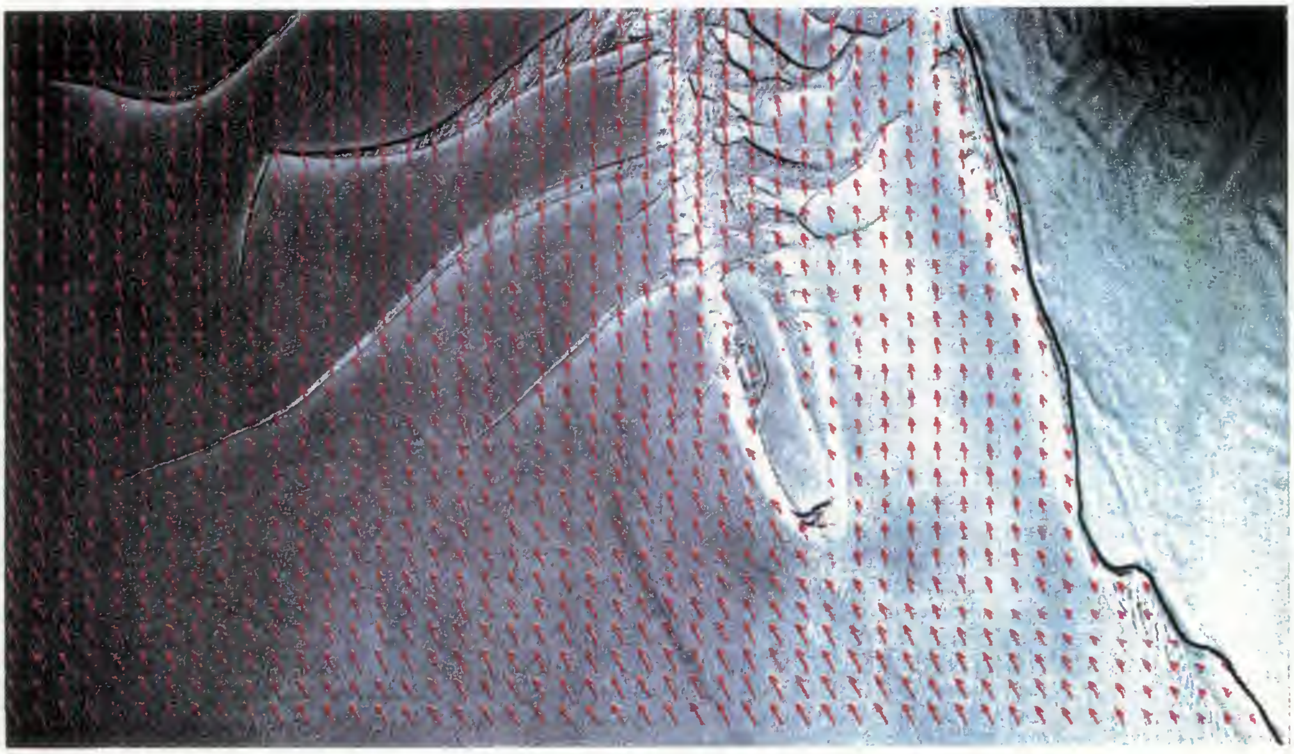

Figure 1: Pixel displacement from coregistration with grounding line (‒ represents 6 meter within 3 days)

an error caused by the variable tidal height changes.

With a pixel size of 4x20 m the accuracy of estimating the displacement is about 40 cm in azimuth direction and 1 m in slant range (Figure 1). With respect to a fixed reference point this estimated displacement vector is an absolute value, allowing to calculate the velocity field of the area with help of the time difference between the two SAR acquisitions. This can be improved by taking the mean value for small areas or applying a two dimensional filter function. Further improvement results from the usable time interval between the acquisition dates - longer intervals reduce the velocity error. But this is quite critical in the Antarctic region due to a weather changeable ice and snow surface.

This method gives a coarse information for absolute displacements provided that there are fixed reference points. It is also helpful that only two SAR images are necessary and it still works in areas where no features are available and optical methods fail.

Further interferometric processing revealed an interesting result: a fringe pattern (Figure 2) produced by different effects

- topography
- topography variation
  - * horizontal movement
  - * vertical movement.

The main task results in separating the different effects in order to estimate

- the digital elevation model
- the tidal variation
- the hor. velocity field of the surface

Figure 2: Example of an interferogramme (17th Jan. 1992 and 20th Jan. 1992)

TOPOGRAPHY

The estimation of the topography will only produce correct values when no surface changes occur or an accurate knowledge of the variation is available to calibrate for these effects. Using differential INSAR constant movement terms of the ice surface can be eliminated. The remaining fringes mainly show the tidal variation on the shelf ice and the topography on HIR and BI. The estimated DEM (Figure 3) showed a good correspondence with the height values given in a map. Nevertheless further analysis will be necessary to reduce the influence of error producing effects.

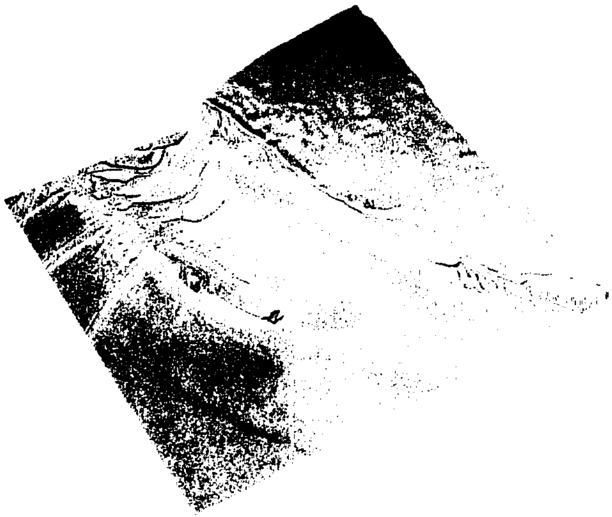

Figure 3: Topography of Hemmen Ice Rise and Berkner Island

TIDAL VARIATION

The differential fringe images show high frequent fringe pattern around HIR and along BI. The outcome of the analysis and discussion with experts (Ch. Doake, British Antarctic Survey) was that tidal height movement caused a bending of the ice sheet along the waterfront. Counting the fringes we were able to estimate the height differences between the two interferogrammes. The tidal values given by Ch. Doake result in a difference of about 85 cm. The fringe count is 32 at the southern top of HIR. This corresponds to 96 cm. This is quite good an agreement, because the uncertainty of the tidal model is about 10 cm. Counting the fringes from HIR to BI we have only a difference of one fringe, probably caused by a height difference and some uncertainties in the fringe pattern in the shearing zones.

GROUNDING LINES

This high frequent fringes are also an indicator for the grounding lines. The grounding lines give the position where the glacier is moving from the dry land in the sea. Taking the transition from high frequent to lower frequent fringes in the shearing zones, we can define the grounding line in this area. This line is plotted in figure 1 and shows that from an intensity image it will be quite difficult to extract this line without good experience.

PRECISE MOVEMENT ESTIMATION

We know that the precision in estimating the slant range changes is the order of or less than one centimeter but the precision of azimuth changes is only in the order of 0.5 m. Therefore, when the azimuth changes are used to describe the surface movement, the precision is poor and a detailed movement can not be detected. Anyhow it is possible to describe the detailed surface movement by using only the slant range changes, if another interferogramme of the same area at the same observation times but with different orbit directions is available. The ascending orbits of ERS-1 over the Antarctic have a crossing angle of about 48° with the descending orbits. And the observation from the ascending orbits was made about 3 hours earlier, although the time interval for two successive observations is the same for both the ascending and the descending orbits. Generally, very small slant range changes result from 3 hour time shift if the climate in the 3 hours remains stable.

Under this condition, we have analysed the relative motion of a shelf ice rift and the relative motion of the shelf ice between HIR and BI by using the ERS-1 SAR images collected on 26 and 29 Jan, 1992 from the descending orbit 5301 and the ascending orbit 5499. figure 4a and figure 4b are the interferogrammes around a glacier shift near HIR obtained from the descending and the ascending orbits, respectively, where the interferogramme in figure 4b is rotated clockwise 48°. Because the area in figure 4 is very flat, the phases of the interferogrammes contain mainly the information about the slant range changes within 3 days. And the slant range changes can be decomposed into the elevation and the horizontal changes. Because shelf ice in figure 4 is on the see water, the elevation changes caused by tides can be taken as constant in such a small area (about $24x20 \ km^2$). Except for the tidal changes, the elevation changes caused by other factors are very small and can be neglected for the flat ice sheet on the see water.

Figure 4a: Unwrapped relative phase of shelf ice (descending orbit)

Figure 4b: Unwrapped relative phase of shelf ice (ascending orbit)

Let us take point A as the reference point in figure 4. The phases relative to the reference point A in figure 4 are the result only from horizontal movements, because the elevation changes of the ice sheet is the same. From figure 4a and figure 4b, the ground range changes in two directions with 48° crossing angle can be measured and used to obtain the horizontal motion vector of every point relative to the reference point A. figure 5 is the relative movement map calculated from the two interferogrammes. In figure 5 each contour line represents 0.5m/3 days displacement. From figure 5, we see that the ice around the rift in the center of the image rotates clockwise around the reference point and increases the width proportional to the distance between the reference point and the margin point. As an example the width change between the two points B and in figure 5 is estimated. The relative motion vectors of point B and C are (1.12m/3 days, 7.7°/3 days) and (1.78m/3 days, 28°/3 days), respectively, where the first component is the amplitude and the second is the direction of the motion. The difference of the two relative motion vectors is 0.82m/3 days. Such a relative motion will double the width between B and C within 20 years.

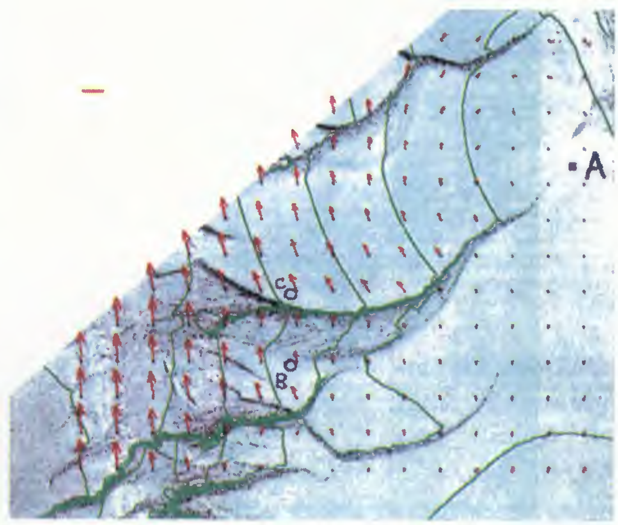

Figure 5: relative movementsof shelf ice (-- 2m/3days, contourlines 0.5/3days)

Figure 6a: Unwrapped phase around HIR (descending orbit)

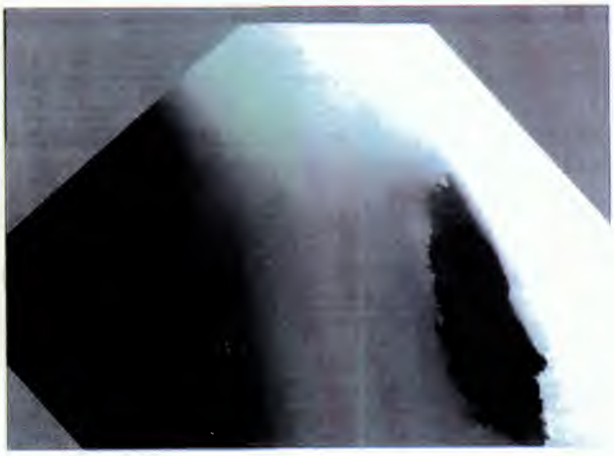

Figure 6a: Unwrapped phase around HIR (ascending orbit)

Another example is the measurement of the relative horizontal movement of the shelf ice between HIR and BI. figure 6a and figure 6b are the phase unwrapped interferogrammes obtained from the descending and the ascending orbits. Point A is selected as the reference point. And figure 7 is the relative horizontal movement calculated from figure 6. Each contour line represents 0.5m/3 days. The absolute horizontal movement can be obtained from figure 7, if the absolute movement of the reference point A is available. According to figure 1, the horizontal movement of Point A is about (0.76m/3 days in ground range, -2.8m/3 days in azimuth). The sum of the relative movement in figure 7 and the movement of the reference point give the absolute horizontal movement of the shelf ice and is shown in figure 8. The horizontal movement between HIR and BI, which is shown in figure 8, agrees very good with the theoretic movement of shelf ice between two banks.

CONCLUSIONS

A lot of information could be extracted from the ERS SAR images with help of interferometric and differential interferometric methods. The quality and the extensive results provide a new class of information. This methods will allow to estimate the velocity of glaciers in other areas and monitor changes in remote areas like Antarctica, Greenland and other distant places. With help of the TANDEM mission we expect a further improvement in the interferometric products.

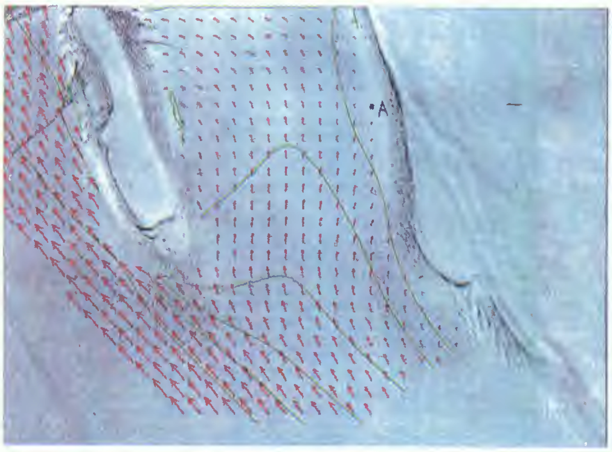

Figure 7: Relative movements of the shelf ice around HIR (-- 2m/3days, contourlines 0.5m/3days)

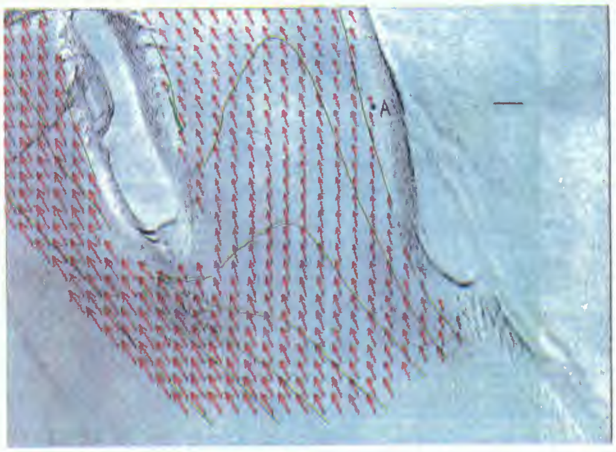

Figure 8: Absolute movements of the shelf ice around HIR (-- 6m/3days, difference between contourlines 0.5m/3days)

REFERENCES

R.M. Goldstein and H.A. Zebker. Interferometric radar measurment of ocean surface currents. Nature, 328:707-709, 1987

MASSONNET, D.; CARMONA, C; ROSSI, M., "An Earthquake Test Site Studied by Differential Interferometry" International Symposium - From Optics to Radar, SPOT and ERS-1-Applications, Paris, 10-13th May, 1993.

HARTL, P.; THIEL, K.-H., "Fields of Experiments in ERS-1 SAR Interferometry in Bonn and Napex", International Symposium - From Optics to Radar, SPOT and ERS-1 Applications, Paris 10th-13th May, 1993.

USE OF ATSR DATA FOR MONITORING THE ANTARCTIC CONVERGENCE ZONE

P. Lasnier, H. Hajji, P. Michon
MétéoMer, RN7, 83480 Puget sur Argens, FRANCE

Tel: (33) 94 45 66 11. Fax: (33) 94 45 68 23

Abstract

The Sea Surface Temperature measurements retrieved from the ERS-1 Along-Track Radiometer often give an excellent opportunity for monitoring the Antarctic Convergence Zone. A comparison between the theoritical and the satellite observed zones has demonstrated the feasibility of estimating its position and thus, enables to supply more real time information for sailing boat records.

Keywords:

ATSR, Sea Surface Temperature, Antarctic Convergence Zone, Ship routeing

Introduction

The excellent Sea Surface Temperature (SST) measurements coming from the ERS-1 Along-Track Scanning Radiometer (ATSR) is opening up new possibilities for the study of atmospheric boundary layer and dynamical oceanography. In the second symposium held by the European Spatial Agence, in Hamburg (1993), some results of the ATSR products were presented, showing the usefulness of the SST for studying the air/sea interaction, the filaments and fine structure in turbulent mixing, the global change. The accuracy of the ATSR algorithm in the presence of aerosol contamination was also shown. In these studies, the authors highlighted the high resolution achieved by the ATSR, thus enabling the possibility of detecting fine structures such as mesoscale eddies.

Moreover, the knowledge of the Antarctic Convergence Zone position is very useful for ships and sail routeing. Indeed, this area is characterized by a fast west-east sea drift current and great probabilities of sea ice concentration southward (bergs in particular).
The main purpose of this pilot project is the feasability study of the determination of the Antarctic Convergence Zone position by using the SST from the ERS-1 ATSR. This experiment was held by MétéoMer before O. de Kersauson's (french skipper) ship passes the area. It tried to give the sailor more information and thus to warn about ice risks, to avoid passing in the low centres, and to allow the boat going faster by using the maximum western drift sea currents and astern winds, and to take the far south polar route which is the shortest one in the world tour competition.

In section 1, the characteristics of the Antarctic Convergence Zone will be briefly introduced, section 2 reminds the ATSR instruments, section 3 presents the data processing method used in this study while section 4 shows some results.

1) Characteristics of the Antarctic Convergence Zone

From the equator to the poles, the SST varies from a maxima of 30°C to a minima of -1.9°C, corresponding to the freezing sea temperature. The west-east distribution can be modified by winds, sea currents, and continents. In some areas called convergence zones, the isotherms present strong gradients. Dense water is sinking under lighter water.

Different reasons are linked to the existence of the Antarctic Convergence Zone (*Paul Tchernia*, 1978):
- hydrological phenomena in deep and surface waters;
- meridional density distributions;
- topography and basin configurations;
- wind vectors repartitions.

The Antarctic Convergence Zone takes place mainly in the West-East regime between 35° and 65° South and partly in the East-Antarctic area regime. From the meteorological point of vue, these regimes correspond to the south part of the anticylonic circulation formed by the subtropical anticylones of St Hélène in the Atlantic Ocean, Mascareignes in the Indian Ocean, Kermadec in the South-West Pacific Ocean, and Pâques in the South-East Pacific Ocean. These regimes correspond also to the north part of the polar cyclonic depressions.

Figure 1 presents the principal regimes in the south hemisphere including the mean position of the Antarctic Zone. This position varies from a season to another.

2) Along Track-Scanning Radiometer (ATSR)

The ATSR consists in two instruments, an Infra-Red Radiometer (IRR) with 4 channels (1.6, 3.7, 10.8, and 12um) and a Microwave Sounder (MWS) with 2 channels (23.8 and 36.5 GHz). The ATSR was designed to provide the following types of data observations (ERS-1 Along Track-Scanning Radiometer Products User guide, 1995):

- sea surface temperature with an absolute accuracy of better than 0.5 K and a spatial resolution of 50 km, in conditions of up to 80% cloud cover
- images of surface temperature with 1 km resolution, 500 km swath and relative accuracy around 0.1K
- measurement of the atmospheric integrated water content (vapour and liquid) in order to compute the most problematic path delay in the signal of the Radar Altimeter.

The ERS-1 IRR views the surface at two angles, one close to the nadir (0°) and the other at 47°. The two channels forming the MWS collect data forward and behind the nadir point with a separation of 60 km. This technique enables to have more sea surface temperature measurements in case of little cloudy atmosphere.

3) The ATSR images and the operational uses

In this study, the ATSR images only are used. These products are distributed in real time to MétéoMer via Aérospatiale Cannes by the Norvegian Space Center, Tromso satellite station. Data are transfered by Internet service.
The processing system developed in MétéoMer checks all the pixels data and controls the quality and validity of the measurement. When an image pixel is cloudy, both in the vertical and inclined paths, the sea surface temperature is not used.
Bearing in mind the Convergence Zone which is characterized by a very cloudy weather and the repetitivity of ERS-1, we divided the zone into 6 areas. In each area we collected the SST images during a 10-15 days period preceeding the boat passage (Table 1). The data volume used should ensure a best coverage of the area of study. The choice for this long period is expected to be in accordance with the temperature stationarity.

According to the atmospheric conditions mentioned above, the SST field measurements issued from the SST data images processing system are discontinuous, making impossible an automatic drawing of the isotherms: only pixels which are free of clouds are used. Thus, the output of the processing system is an irregular SST field and consequently all the isotherms are drawn by hand.

4) Results

4.1. SST images

Figure 2 shows the full swath of the ATSR. The SST patterns demonstrate the high resolution achieved by this instrument. The image shows fine structures which are physically coherent. The dominant features of this image are the presence of warm water to the north latitudes and cold surface to the south. A nice warm-centred eddy can be observed on the top of the image.

4.2. Detection of the Antarctic Convergenge Zone position

Since the Convergence Zone is located between 2°C and 12°C isotherms (*Paul Tchernia*, 1978) and the high resolution of the SST images (see above), we tried to draw all the isotherms (2,3,4,5,6,8,10 and 12).
The analysis of the isotherms retrieved from the ATSR images are coherent with the atmospheric conditions based on the ECMWF wind fields and the scatterometer wind vectors. As expected, it has revealed strong gradients around the antarctic convergence zone.
In area 4, the convergence position was missed since the images processed in this area presented too high sea surface temperatures. So this position should be more south

Figure 3 shows a best agreement between the theoritical Convergence Zone and the one retrieved from ERS1 measurements. Some differences exist which are mainly due to the variability of its position to the mean one.

4.3. Temporal variability of the Antarctic Convergence Zone:

One interesting further result is presented in figure 4. It shows the season variability of the Convergence Zone. During the south hemisphere summer, the convergence moves southward outcome of increasing temperature and in winter, it reaches areas northward consequently to the temperature decrease.

Conclusion

The main objective of this pilot project is achieved. Thus, SST measurements from the ERS-1 ATSR can be used in real-time for monitoring the Antarctic Convergence Zone position. The meteorological analysis is in accordance with the results issued from these measurements and the comparison shows a good agreement.
Another result demonstrated the possibility of observing the seasonal displacement of this

phenomenon. Processing all the ERS-1 ATSR images can lead to providing the seasonal position of the Antarctic convergence zone, thus giving a more climate information on its position.

Nevertheless, some areas where we need to know the position of the Convergence Zone are very cloudy and the retrievement of SST is hasardeous. Moreover, the SST may vary substantially in 10-15 days periods so that it leads to a possible error in the temporal variability and position detection of the Antarctic Convergence Zone.
The detection of the Convergence Zone is crucial for sailing in terms of security and performance.
For operational uses, these spectacular results encourage us to resume the same experiment for further races around the Antarctica. To overcome the problems of clouds, we will use both the Altimeter and the Scatterometer for ice detection

Acknowledgements

The ATSR products are used by courtesy of the European Space Agence. The SST images were processed and provided via the Aérospatiale Cannes by the Norvegian Space Center, Tromso satellite station.

References

P. Tchernia, 1978: Océanographie Régionale, Description physique des océans et des mers. Ecole Nationale Supérieure de Techniques avancées.

ERS-1 Along Track-Scanning radiometer Products user guide, issue 1.0, 7 july 1995. Pf-UG-NRL-OP-002. UK PAF by NRSCL.

Proceedings of the Second ERS-1 Symposium. 11-14 October 1993, Hamburg, Germany. ESA publication.

Table 1

ZONES	LIMITE GAUCHE	LIMITE DROITE	DATE DEBUT	DATE FIN
1	20 W	40 E	29/01/95	10/03/95
2	40 E	95 E	11/03/95	24/03/95
3	90 E	140 E	25/03/95	06/04/95
4	140 E	160 W	07/04/95	27/04/95
5	160 W	80 W	27/04/95	05/05/95
6	80 W	20 E	06/05/94	24/05/95

Figure 1 : Main regimes in the south hemisphere

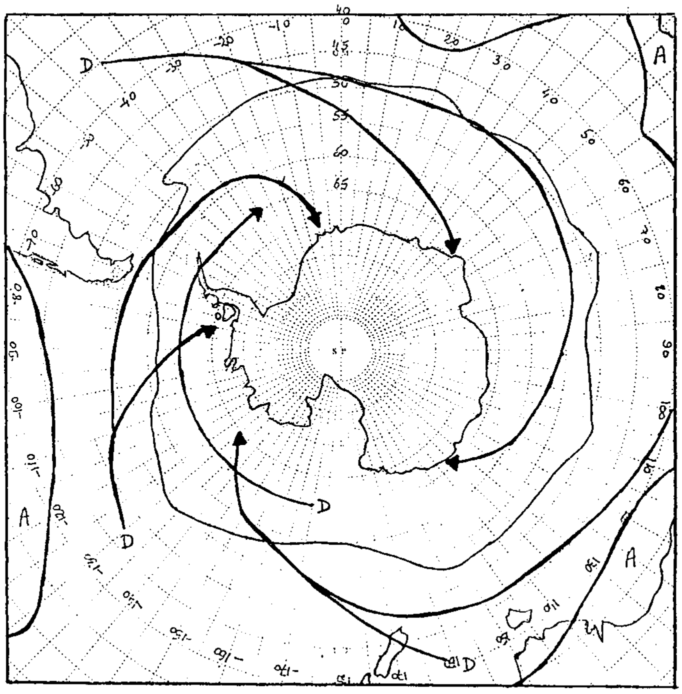

Figure 3 :
______ theoritical convergence
.... observed convergence

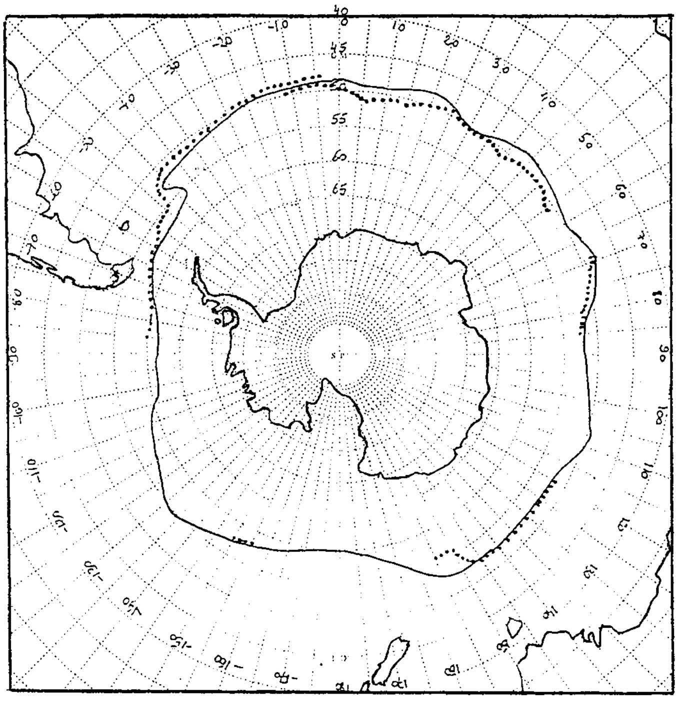

Figure 2

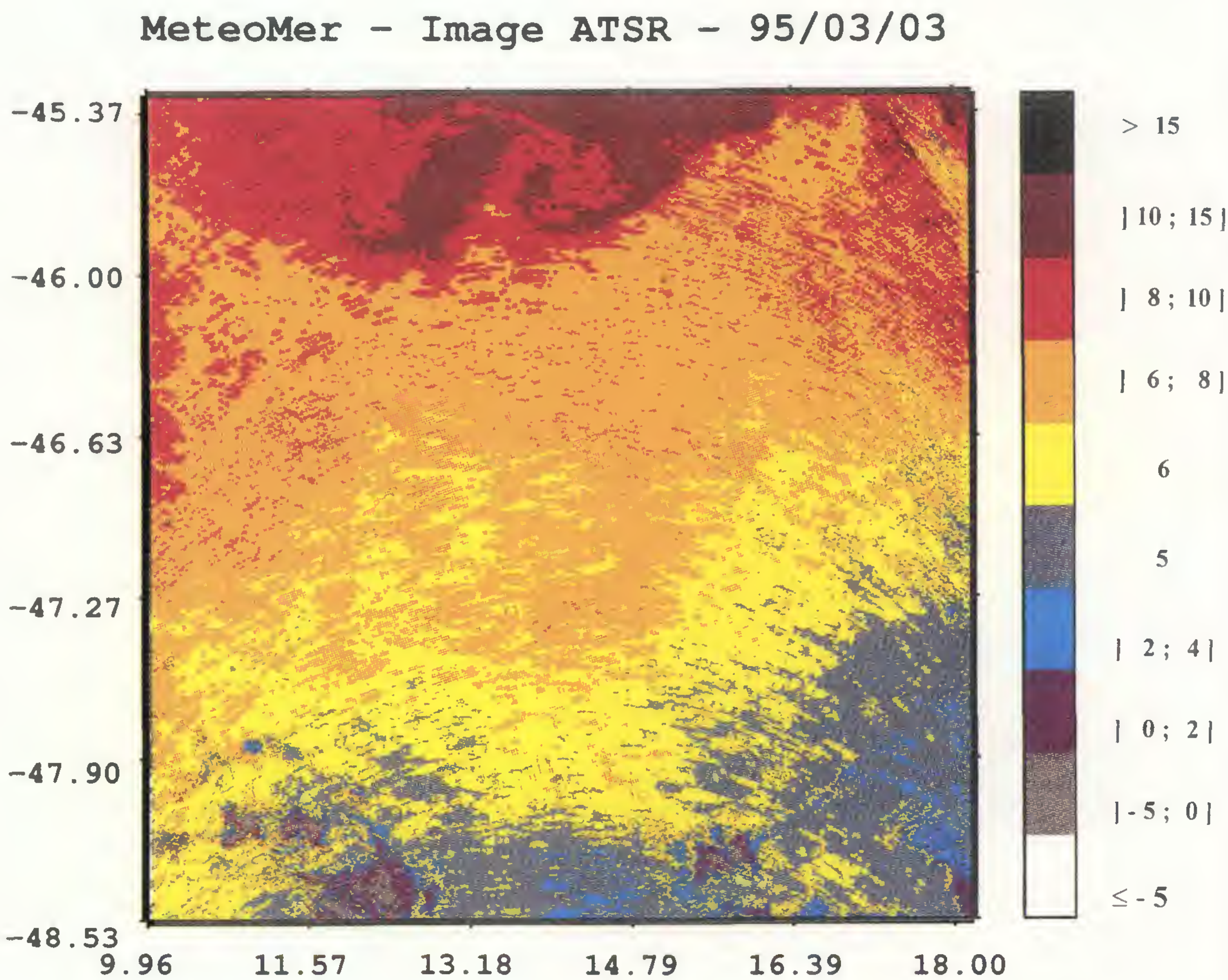

Figure 4

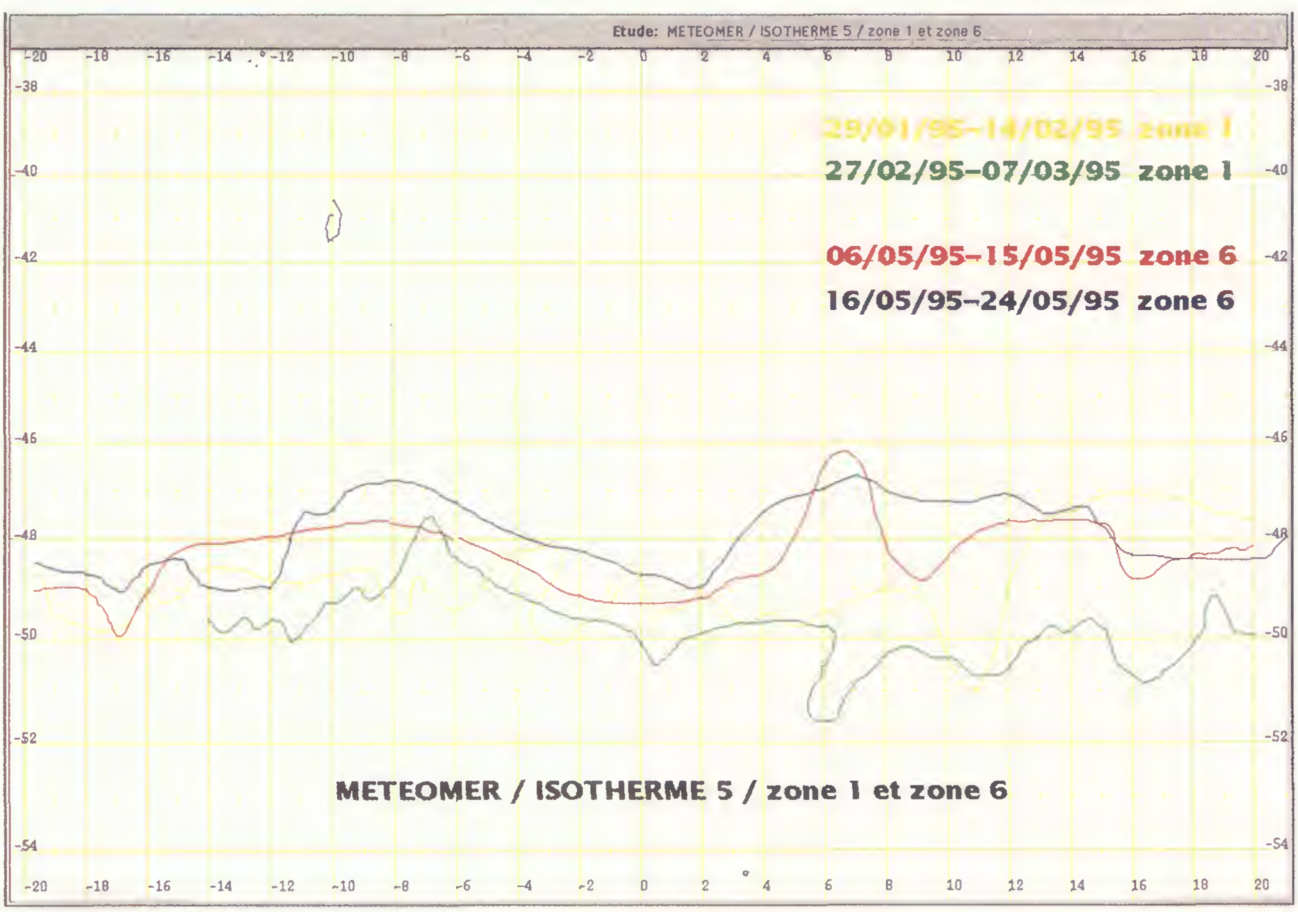

MONITORING OF LEAD FORMATION AND ENERGY EXCHANGE IN THE WEDDELL SEA

Marcus Thomas and Rainer Roth*

* Pilot Project Leader
Institut für Meteorologie und Klimatologie
Universität Hannover
Herrenhäuser Straße 2, D-30419 Hannover, Germany
phone: (+49) 511 762 4413, fax: (+49) 511 762 4418

ABSTRACT

During winter, the opening and closing of leads or polynyas in sea ice covered regions govern the heat exchange between the ocean and the atmosphere. One of the most important questions in modeling dynamic and thermodynamic processes within sea ice is the temporal and spatial variability of open water/thin ice areas. Since in the central Weddell Sea the ice drift is to the most extent driven by the atmospheric forcing, the developement of leads and polynyas can, especially during the austral winter when melting is unlikely, be related to the synoptic situation. An ice classification approach based on radiometric and geometric properties and an estimation of sensible heat fluxes using additional meteorological data (synoptical analysis, ECMWF model) is shown. In most of the analyzed cases, the spatial distribution of leads and their size is correlated to their position relative to the prevailing low pressure systems.

Keywords: ice classification, ice production, leads, polynyas, heat exchange, Weddell Sea.

1. INTRODUCTION

As parameterization of heat exchange in the polar regions is difficult, climatological values are often used for an estimation. Due to investigations on dynamic and thermodynamic processes of the sea ice it is a well-known fact that the opening and closing of leads or polynyas govern the heat exchange between the ocean and the atmosphere in ice covered regions. In the sea ice, the formation of new ice is controlled by the energy balance at the surface, and especially by the heat fluxes which are far more effective then radiation processes. While the ice cover acts as a heat resistance for the freezing beneath the ice, ice formation is most effective in open water areas. Leads (linear shaped) or polynyas (larger open water areas) arise from divergent ice motion driven by the wind.

Therefore, a detailed analysis of the temporal and spatial variability of open water/thin ice areas is necessary. The problem is the rapid change of the open water net area which is caused by the changing of the wind fields in relation to the prevailing weather situation. In addition, high resolution ice motion trajectories are needed to calculate the divergence of the ice motion from an ice velocity field which cannot been derived from the trajectories of drifting buoys. The buoy investigations rather show trajectories of the mean ice motion in the Weddell Gyre.

In-situ measurements in the Weddell Sea like the *Winter Weddell Sea Project 1986 (WWSP '86)*, the *Winter Weddell Gyre Studies 1989 and 1992 (WWGS '89, WWGS '92)* could not give large-scale spatial informations on dynamics and thermodynamics of sea ice and leads whereas the ice modeling include these processes without spatial or temporal limits (see for instance Hibler and Ackley (1983), Lemke et al. (1990) or Wefelmeier (1992)). To prove the modeling results, remote sensing is useful for spatial and temporal observations. However, for optical and thermal infrared sensors, there are limitations due to the insufficient ground resolution and to cloud cover restrictions. Only the SAR allows a detailed observation and a study of the spatial distribution of leads in areas which are influenced by complex synoptical pressure systems which are mostly accompanied by compact cloud covers.

2. THE WEDDELL GYRE

The Weddell Sea is a region of high variability of the sea ice extent. The ice covered area varies between approximately $1.1 \cdot 10^6$ km² and $4.4 \cdot 10^6$ km². This large amplitude is mainly attributed to dynamic rather than to thermodynamic effects (Hibler and Ackley, 1983). The nearly permanent wind forcing by low pressure systems migrating from west to east causes the sea ice cover to rotate slowly in an clockwise direction, forming the Weddell Gyre. This mean motion can reasonably be measured by drifting buoys set out on the ice (Fig. 1). These measurements are also suitable for calculating the mean divergence of the ice motion in larger spatial scales. The net divergence of the Weddell Sea ice motion is positive (see Kottmeier et al., 1991) and the ice motion can in most cases be considered as free drift. This is due to the fact that the ice drift towards lower latitudes is not influenced by continental boundaries. Furthermore, new ice which is being formed in the northeastern part of the Weddell Sea is transported through the southern and western regions while growing thicker and becoming older and rougher, so that the eastern part of the Weddell Sea is during winter dominated by first year ice whereas the western regions are mainly covered with thicker, rougher multiyear ice, although all age groups are present (Lange and Eicken, 1991).

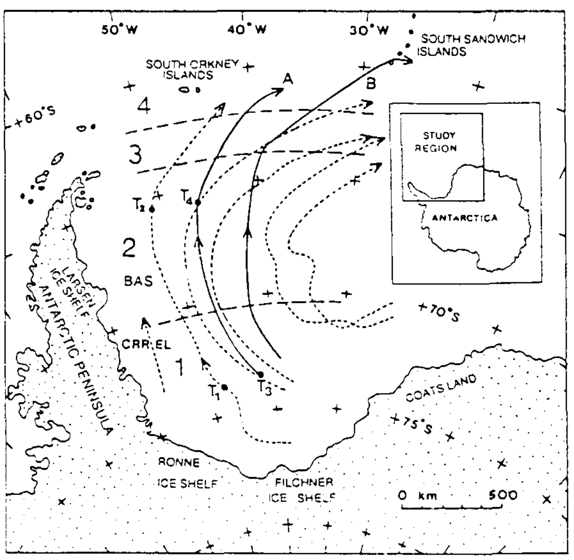

Fig. 1. The clockwise ice drift in the Weddell Sea, visualized by the track of drifting buoys (Ackley and Holt, 1984).

3. LEAD FORMATION PROCESSES

The dynamics of sea ice is mainly linked to the atmospheric wind field. Therefore, the formation of offshore leads and polynyas is due to positive divergences in the momentum transfer from the atmosphere into the sea ice. This can be due to a divergence in the wind field, to lateral inhomogeneities of the ice surface roughness, or both. Moreover, the passing of a low pressure system in the vicinity a given point in the pack ice can cause lead formation as a result of the locally changing wind field, the inertia of the ice pack, and the direction of the ice drift. As a result, the lead formation in the easstern Weddell Sea mostly occurs in the west of a loe pressure systems, i.e. after the lows have passed a particular point considered because there the averaged wind direction points to the north, i.e. towards the ice edge where the ice drift is not influenced by coastal boundaries. To illustrate this effect, an example from July, 1992 is shown.

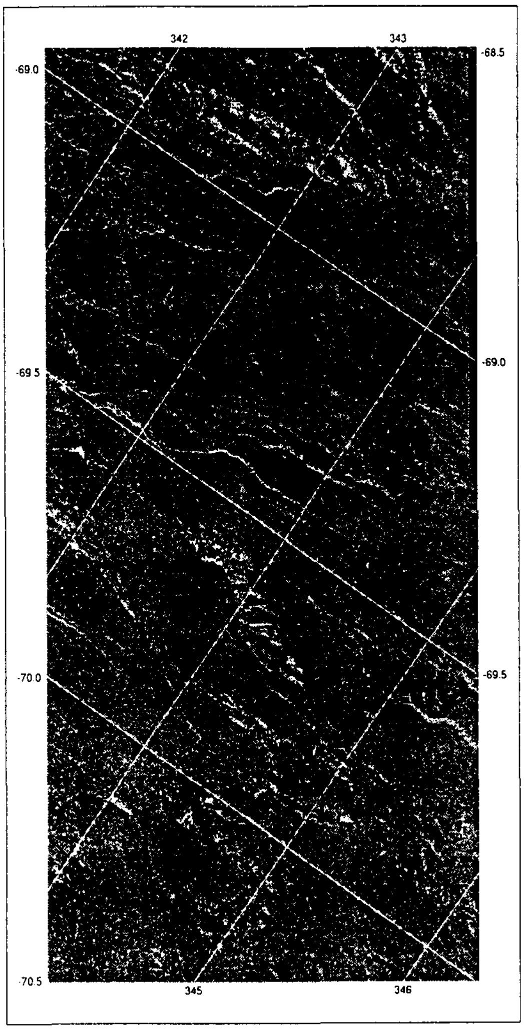

Fig. 2. SAR image, 01-JUL-92, 01:44 UTC. Image size 100 x 200 km².

Fig. 2 shows a SAR-PRI image from July 1st, 1992 acquired in the central Weddell Sea at 01:44 UTC. The area shown is 100 x 200 km². The dominating linear features (leads) are aligned in zonal direction. The ECMWF analysis from 00 UTC shows that the Weddell Sea is dominated by a large low pressure system with its center at 62° S, 20° E. During the following 36 h, this low moves slowly southward until its center reached 66° S, 20° E on July 2nd, 12 UTC (Fig. 3). The core pressure decreases from 959 hPa to 950 hPa on July 2nd, 06 UTC. The pressure gradient in the image area increases until July 1st, 12 UTC, leading to a maximum wind speed of 24.4 m/s from the west. Consequently, the open water areas have increased on the next image taken on July 2nd, 09:26 UTC, when the ERS-1 revisited the area during a descending track.

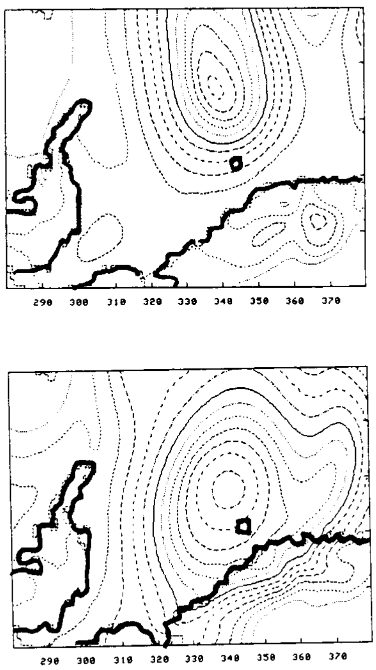

Fig. 3. ECMWF mean sea level pressure fields. Upper: 01.07.92, 00 UTC. Lower: 02.07.92, 12 UTC.

Fig. 4 shows 50 x 50 km² sections of the images. The sections are chosen to include common features, not the same geographical area. In the 32 hours between the two overflights, the ice pack has drifted 46.8 km in WSW direction resulting in an average drift speed of 40 cm/s which is a very high value but corresponds well to the rule-of -thumb that the ice drifts with approximately 2% of the geostrophic wind speed (Thorndike and Colony, 1983).

For our investigations, the differential ice drift is more important. In Fig. 4 it is evident that the zonal orientated lead has broadened considerably; the maximum lead width in Fig. 4a is 500 m whereas in Fig. 4b the dominating lead is up to 3000 m wide. A detailed analysis of the backscatter distribution of the sections shows the presence of 3 main surface classes: Smooth 1st year ice (FYS), rough 1st year ice (FYR), and open water (OW). Using a straigthforward classification method (median filtering, threshold values) described in Roth et al. (1994), the area distribution can be calculated:

Sf. class	1st image	2nd image
FYS	32.5%	31.4%
FYR	63.6%	58.4%
OW	5.9%	9.2%

Hence, the portion of open water areas has nearly been doubled during the 32-h-period. Using linear temporal

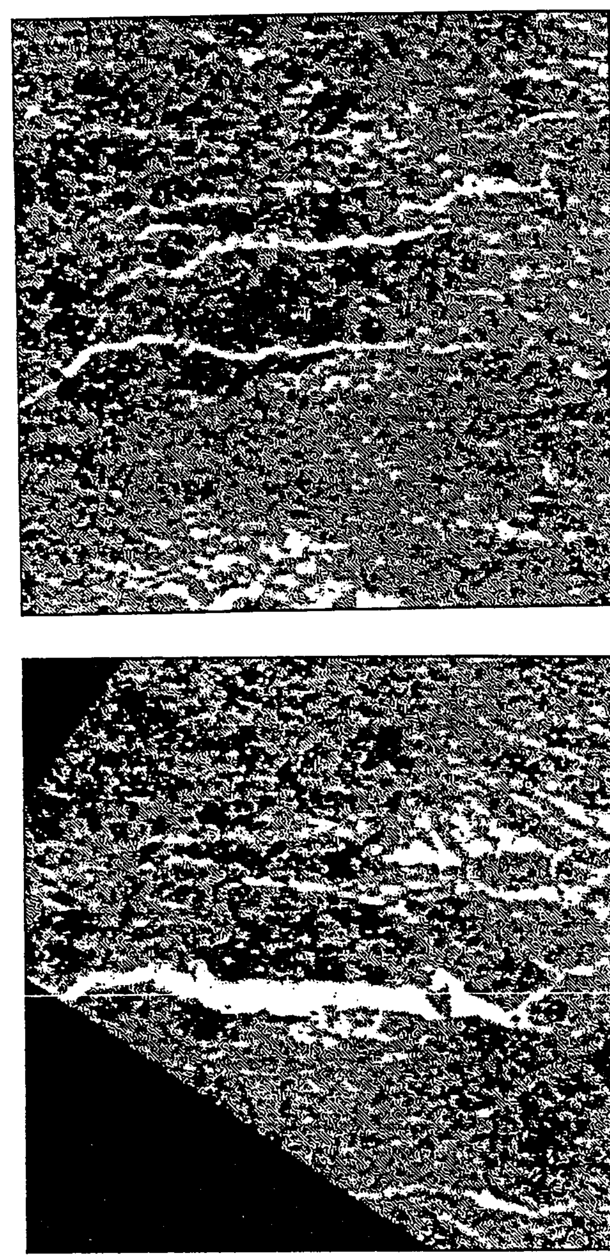

Fig. 4. Sections of SAR scenes from 1st/2nd July, 1992. Image size 50x50 km². Similar surface features are shown, rather than same geographical areas.

interpolation between the 6-hourly ECMWF analysis data, the 10-m-wind speed related to the two sections is 14.3 m/s and 9.6 m/s, respectively; the ECMWF air temperature field yields $T_{2m}=-21°C$ for both scenes. We now use this values in an bulk approach to calculate the sensible heat flux H from the leads into the atmosphere:

$$H = \rho \, c_p \, c_H \, u_z \, (T_0 - T_z)$$

where ρ is air density, c_p the specific heat of air for constant pressure, c_H the bulk transfer coefficient for sensible heat which is taken as $c_H=1.5\cdot10^{-3}$, T_0 the surface temperature which is set to the freezing point of seawater (-1.8°C), and u_z and T_z wind speed and temperature in the height z, respectively. With this notation, a heat flux into the atmosphere is counted positive. Assuming an ice surface roughness length that is given in the ECMWF data set ($z_0=1\cdot10^{-3}$ m) the resulting 2-m-wind speeds from the logarithmic wind profile law are 11.4 m/s and 7.7 m/s, respectively. This yields sensible heat fluxes of $H_1=427$ W/m² and $H_2=288$ W/m², respectively.

For an estimation of the overall ice production connected with the images shown, we assume an average heat flux into the atmosphere being $H_0=358$ W/m². This flux is equivalent to a heat loss of $W=4.9\cdot10^8$ J/m² within the 32 h considered, producing 146 kg of sea ice per square meter, or an ice sheet with a thickness of 62 cm (using $\rho_{ice}=900$ kg/m³). Instead of closing the leads, however, the new-formed frazil ice is being drifted to the downwind edges of the leads and there accumulated to form a grease ice "wedge" (Bauer and Martin, 1983). This result eludicates the important role of the leads in the thermodynamics of the winter pack ice: ice formation by congelation at the bottom of the pack ice is slower by about an order of magnitude.

In the next example, the area considered is situated on the west side of the center of a low pressure system. The wind direction, therefore, is from the south. Although there is no large pressure gradient, the SAR image (100·100 km²) shows large areas of open water which are mainly aligned in zonal direction. Here, as opposite to the example above, the wind direction is normal to the main lead direction (Fig. 6). The width of the leads is larger than in the first case study. An analysis of the weather history shows a fairly stable synoptic situation with a nearly stationary lowpressure system centered at 64°S, 10°E resulting in southerly winds in the image area. This weather situation in the eastern Weddell Sea didn't change since 60 h before image acquisition (Fig. 5).

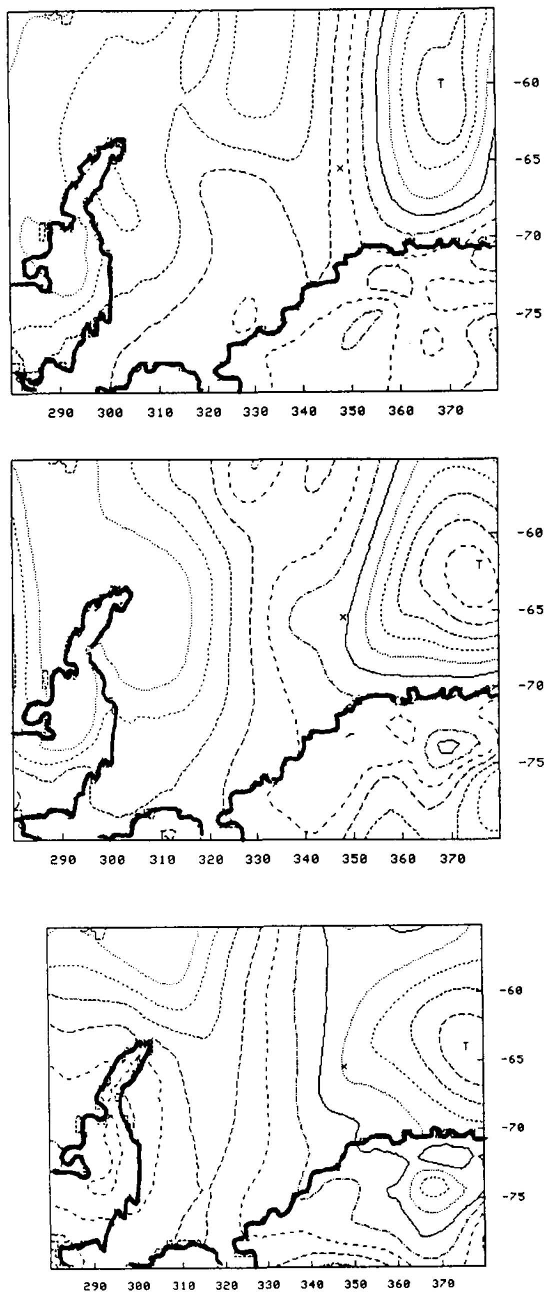

Fig. 5. MSL pressure field (ECMWF data) from 12-Jul-1992 12 UTC (upper), 13-Jul-1992 12 UTC (center) and 15-Jul-1992 00 UTC (lower).

In case of this lead formation process, the long-time forcing of the ice pack in north direction is probably the cause for the developement of the large leads rather than a short-time occurence of high wind speed. The fraction of the image area covered by leads amounts to 5.2%. Using again the temporal interpolated wind speed and temperature data from ECMWF ($u_{10}=8.6$ m/s, $u_2=6.9$ m/s, $T=-22°C$), the sensible heat flux from the leads into the atmosphere is $H=269$ W/m².

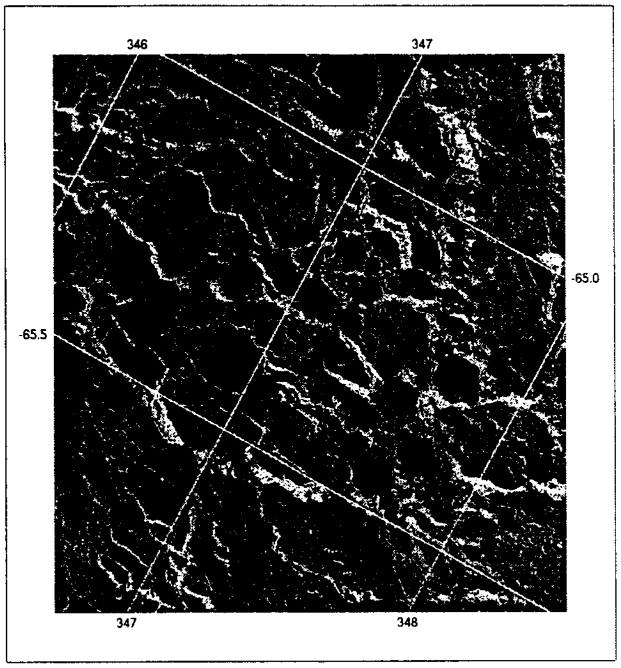

Fig. 6. SAR image form 15-Jul-92, 01:05 UTC sho wing wide leads which are aligned mainly zonally.

Leads can occur dark (very low backscatter) in the SAR images if the wind speed is very low and/or if the lead is covered with thin, very smooth ice (nila). The thin ice cover dramatically decreases the heat transfer from the ocean to the atmosphere, but is still up to one order of magnitude larger than in the surrounding first year/multiyear pack ice (Maykut, 1978). A to some extent more detailed image of such a type of lead is presented in Fig. 7. The location is near the coast of the Antarctic Peninsula in the western Weddell Sea.

For analyzing the backscatter behaviour of the surface structures, we show a section of the σ_0-values derived from the pixel values along the depicted diagonal line. The pack ice shows the usual backscatter of second-year ice (-9 to -8 dB) which is very likely to be found in that region of the Weddell Sea. The leads have very low backscatter (<-20 dB) which makes is hard to distinguish their surface between open water and thin ice because of the low wind speed (u_2=2 m/s). If we look into the ECMWF wind field data (Fig. 8), it becomes more likely that the leads are frozen because the wind speed had been low (< 6 m/s) since 30 h before, so the new formed ice couldn't be transported to the down wind edges of the leads.

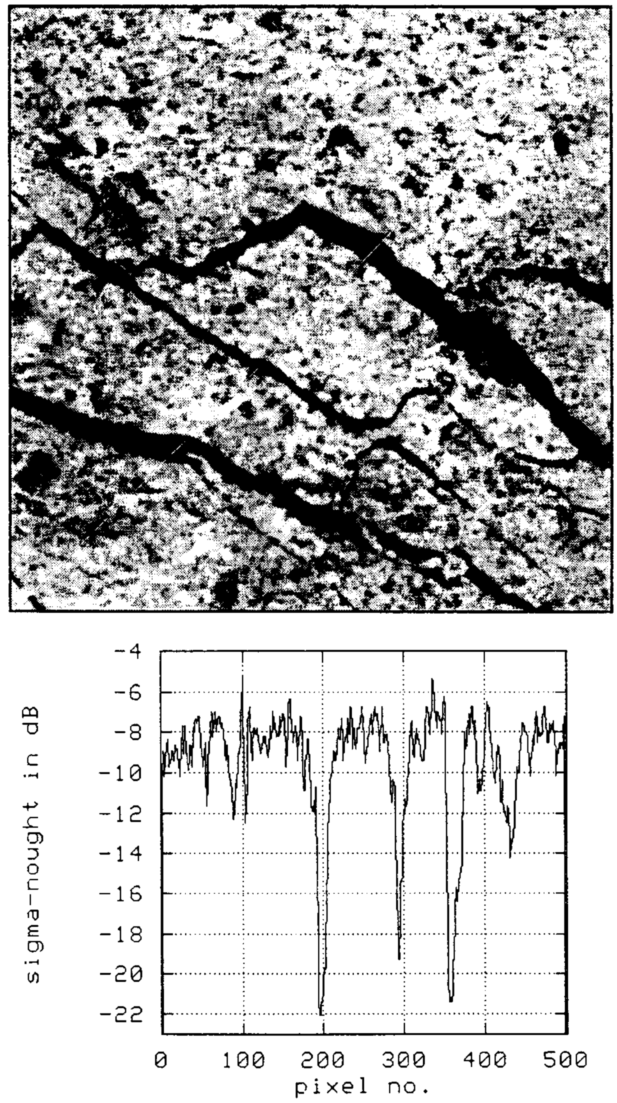

Fig. 7. Upper: Section of a SAR scene acquired July 25th, 1992, 12:24 UTC. The image size is 12.5 x 12.5 km². Image center coordinates: 66.7°S, 56.5°W.
Lower: Profile of backscatter values along the line shown in the SAR image.

The coast of the Antarctic Peninsula formes a natural boundary for the ice drift in a way that only wind directions a with components to the east and/or north are suitable for causing divergent ice motion. The weather history of this example provides evidence of how the leads were formed: For at least 30 h (between July 23rd, 00 UTC and July 24th, 06 UTC) there were strong winds with up to 13 m/s coming from westerly directions. These are suitable for causing the leads to open. At northern edges of the leads, the backscatter coefficient is slightly increasing before transition to the values of the multi-year ice pack. This can be due to the fact that during the formation of the leads, the frazil ice had been swept in dowmwind direction.

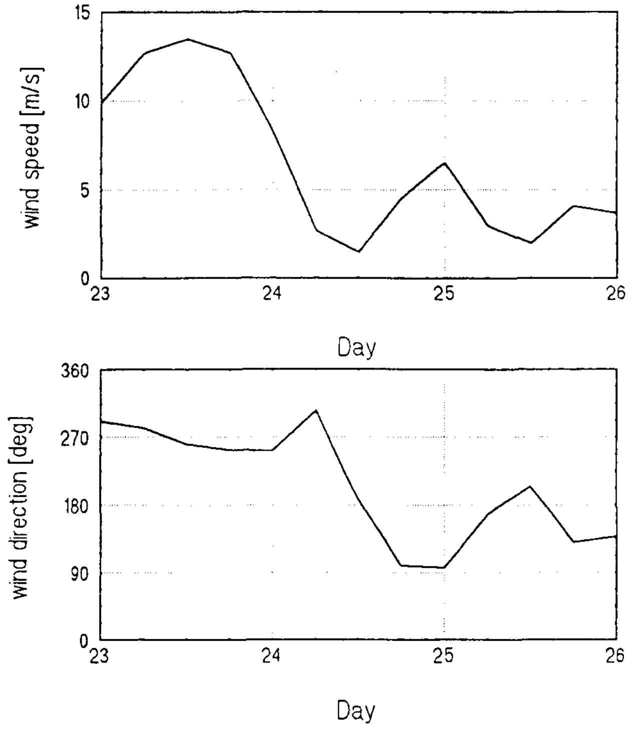

Fig. 8. Temporal variation of the wind from ECMWF data for the SAR image in Fig. 7. The cross depicts the SAR acquisition time. Time given in fraction of day in July, 1992.

4. CONCLUSIONS

Due to its high spatial resolution and the independence of cloud cover and daylight, the ERS SAR instrument is the most suitable spaceborne tool for detecting leads in ice-covered regions. When taking into consideration the actual synoptic situation as well as the weather history, the difficulties in discriminating between open water and frozen leads can often be overcome, and the "history" of the lead formation itself can be described. This is an important result, because due to the ERS orbit configuration and the rather narrow swath with of the SAR, multiple observations during the lead formation occur mainly by chance. However, by closer investigation of the formation processes using more case studies, the mechanism of the opening and closing of leads will be described in more detail, taking into account parameters like surface roughness, ice strength, ice floe distribution, atmospheric stratification and others, which in this study have not been included yet. In the future, this parameters will be derived and be used as additional input data for sea ice/ocean models such as described in Lemke et al. (1990). Finally, we are expecting to use these kind of sea ice models as a tool for lead forecast based on standard weather forecast data like from the ECMWF model.

5. ACKNOWLEDGEMENTS

Our research work has been carried out in the framework of the ESA Pilot Project PP2-D8 which was supported by the German Ministry for Research and Technology under contract 03PL504D. The authors would like to thank ESA and the D-PAF for supplying the ERS SAR data and the Alfred-Wegener-Institute for Polar and Marine Research for supplying additional meteorological and remote sensing data.

6. REFERENCES

Hibler, W.D., & S.F. Ackley 1983, Numerical simulations of the Weddell Sea pack ice. J. Geophys. Res., 88, 2873-2887.

Lange, M.A., & H. Eicken 1991, The sea ice distribution in the northwestern Weddell Sea, J. Geophys. Res., 96, No C3, 4821-4837.

Lemke, P., W.B. Owens, & W.D. Hibler 1990, A coupled sea ice-mixed layer-pycnocline model for the Weddell Sea, J. Geophys. Res. 95, No C6, 9513-9525.

Maykut, G.A. 1978, Energy exchange over young sea ice in the central Arctic, J. Geophys. Res., 83, No C7, 3646-3658.

Roth, R., O. Schulze, M. Thomas, T. Rothe, & R. Brandt 1994, Sea-ice and climate-an approach usimg SAR data, Proc. 2nd ERS-1 Symposium Hamburg, ESA SP-361, 323-327.

Thorndike, A.S., & R Colony 1982, Sea ice motion in response to geostrophic winds, J. Geophys. Res., 87, No C8, 5845-5852.

Wefelmeier, C. 1992, Numerische Simulation mesoskaliger, dynamischer Wechselwirkungen zwischen Atmosphäre, Eis und Ozean, Ber. d. Inst. f. Meteorol. u. Klimatol. d. Univ. Hannover, 42, 141pp.

FLOODING

Chairman: **J. Achache**
Rapporteur: **G. Paci**

THE USE OF ERS DATA FOR FLOOD MONITORING: AN OVERALL ASSESSMENT

Gianna Calabresi

ESA/ESRIN, Earth Remote Sensing Exploitation Department, Frascati, Italy

National and regional authorities in charge of prevention, monitoring and relief actions – before, during and after floods – need to rely on as many sources of information as possible, in order to better manage the event and its consequences. Among the various sources of information, remote sensing in general and the SAR technology in particular, are recognised as valuable tools.

In fact, ERS SAR data, used alone or in conjunction with other types of sensor data, have proved to be suitable in most issues related to flood events.

In the 1992-95 period, in coincidence with significant flood events occurred in Europe, several projects and studies aimed at demonstrating the usefulness of ERS SAR data were conducted with encouraging results. The experience gained by scientists, research institutes, value-adding companies, and users is summarised in this paper, which is meant to provide an overall assessment of advantages as well as disadvantages in using this type of data. Critical areas, such as the dialogue between producers of information and users, the correspondence of remote sensing product offer to the demand by users, the need of services more specifically tailored to user needs are also examined.

1. INTRODUCTION

The application of SAR information to floods is supported by two main factors.

Flood extent delineation maps derived from SAR data acquisition performed soon after floods, are often the unique available, operational tool in the hands of authorities in charge of a first evaluation and assessment of the catastrophe.

Furthermore, SAR, because of its weather independence, is a unique source of information, if one considers that sunshine can hardly be expected during a flood.

SAR can give a contribution in the various phases of:

- prevention, i.e. modelling of river basin dynamics for future planning;
- monitoring, i.e. mapping of flood events in order to contribute in quick emergency aid management;
- relief, i.e. timely damage assessment and identification of risk areas.

2. FLOOD EVENTS IN RECENT YEARS

Several floods occurred in Europe from 1992 to 1995. The most significant ones are listed in Table 1 with their relevant geographic location.

All events were carefully studied by experts belonging to various scientific research teams and value-adding companies.

The most common project output were maps with flood extent delineation, obtained using ERS/SAR, SPOT, airborne SAR, Landsat-TM, SIR-C datasets alone or in combination. GIS information was essential in almost all projects.

3. FLOOD IN THE PIEDMONT REGION, ITALY

The end-1994 flood in the Piedmont Region, Northern Italy was the most studied natural event in recent years and the worst disaster ever in the area during this century.

The map generated using ERS SAR information allowed the competent authorities to derive a first assessment of order of magnitude and damages. The map is now integrated into the regional GIS for manifold re-use, such as agricultural damage evaluation, comparison of today's situation with town expansion in flooded areas during the past century, land-use planning and monitoring activities in general.

Figure 1 shows the Tanaro River, near Alessandria, during the flood of 4, 5 and 6 November 1994. The map section contains GIS information (raster-based) combined with SPOT panchromatic and ERS-1 SAR data interpretation. It is a good example of multisensor data use. The SPOT image interpretation, made from the panchromatic data collected only 17 days after the event, allowed to map the entire damaged area by means of the sensor response to the fine material sedimented during the flood. The availability of ERS-1 SAR data in near real-time (9 November) allowed, instead, to monitor the event soon after its occurrence. The inundated areas (in green) correspond to paleo-meanders of the Tanaro River.

Proceedings of the Second ERS Applications Workshop, London, UK, 6–8 December 1995 (ESA SP-383, February 1996)

Table 1

Important Flood Events in Europe (Time Period: 1992-1995)

River/s	Region/Country	Time Period
Ouveze	Vaison-la-Romaine, France	Sept 1992
Arno, Nievole	Tuscany, Italy	Oct/Nov 1992
Lesse	Famenne-Ardenne, Belgium	Beginning 1993
Rhone	Camargue, France	Oct/Nov 1993
Lesse	Famenne-Ardenne, Belgium	End 1993
Rhine, Main, Sieg	Cologne, Bonn, Germany	Dec 1993
Rhine	Neuwieder Becken, Germany	End 1993 Beg. 1994
Rhone	Camargue, France	Jan 1994
Werra, Weser	Thuringia, Germany	April 1994
Var	Var, France	Nov 1994
Tanaro, Belbo, Bormida, Po (in part)	Piedmont, Italy	Nov 1994
Rhine, Main, Sieg	Cologne, Bonn, Germany	Jan 1995
Rhine, Waal, Maas	Nijmegen, The Netherlands	Jan 1995
Gudbrandsdalslågen, Glomma	South of Oslo, Norway	June 1995

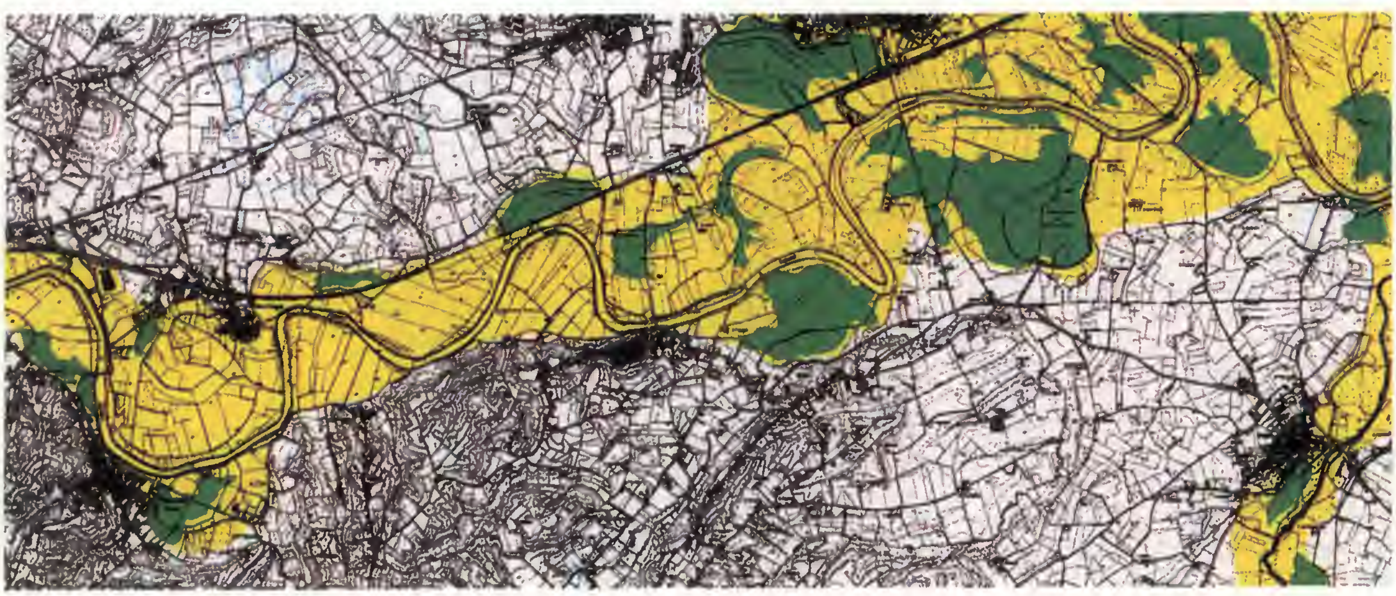

Figure 1 *(Courtesy of CSI – Consorzio Sistema Informativo, Italy)*

4. FLOODED AREAS IN SOUTHERN FRANCE

Torrential floods have affected southern France from 1992 onwards. Among them, the floods in the Rhone Valley (October 1993 and January 1994) and in the Var Valley (5 November 1994) showed the characteristics of real oceanic floods. ERS SAR information was available for all these dates. The possibility to derive flood extent delineation maps, allowed a quick understanding of the phenomenon.

Figure 2 shows flooded areas around Avignon, Rhône Valley, southern France. The multitemporal map is derived from the combination of Landsat-TM data (July 1993) used for vegetation and cartography, and of 10-m SPOT panchromatic images (February 1994) used to

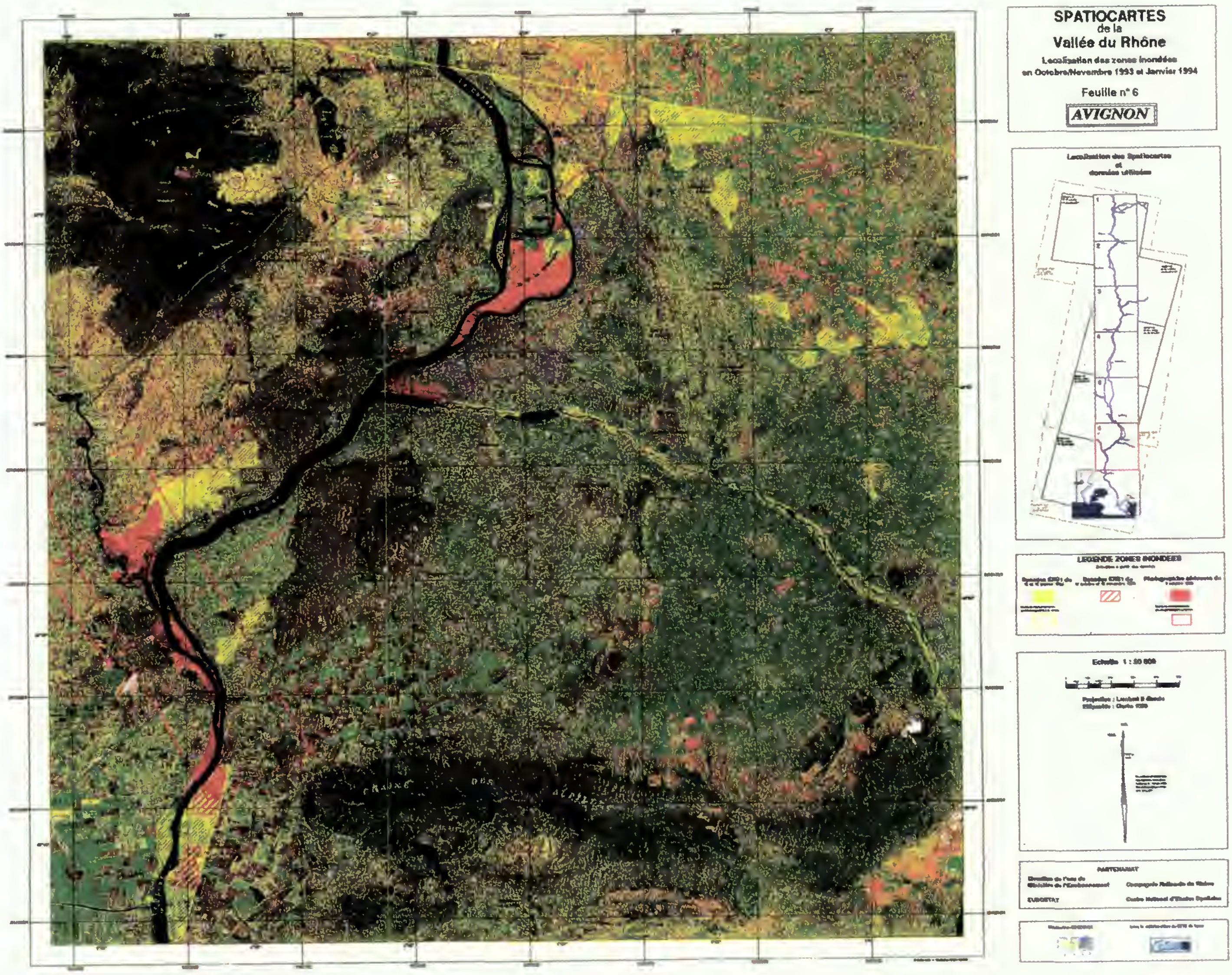

Figure 2

(Courtesy of Geoimage, France)

determine built-up areas and infrastructures. The areas inundated on 12 and 15 January 1994 (in yellow) and on 16 October 1993 (in red) were superimposed to this map. The data were taken from two colour compositions produced from ERS-1 SAR images.

Once the multitemporal approach is followed, one of the selected dates must fall during or close after the flood maximum. By combining the characteristic response of the zones under water appearing in the SAR images with one or two images acquired before or after the event, it is possible to map the land under water at the time of acquisition of the image showing the rise of water.

To further complement the ERS-1 data, the flooded areas were digitised with a good result on aerial photographs taken on 9 and 10 October 1993.

5. RIVER FLOOD ANALYSIS IN BELGIUM

Following periods of heavy rainfall in early and late 1993 along the Lesse river, in the ecological region of Famenne-Ardenne in southern Belgium, ERS-1 SAR imagery was used to study the flooding development. As cloudy conditions prevail in this region throughout the winter, the availability of SAR was essential.

River flood extent assessment and mapping were carried out and a better insight of dynamics of flood development was obtained, by means of an analysis based on SAR geocoded image pairs. Among the benefits deriving from such an analysis for land-use planning, the possibility to update river flood inundation maps is certainly a very significant one.

Figure 3 is an example of inundation map along the river Sambre (principal tributary, with Lesse, of the Meuse

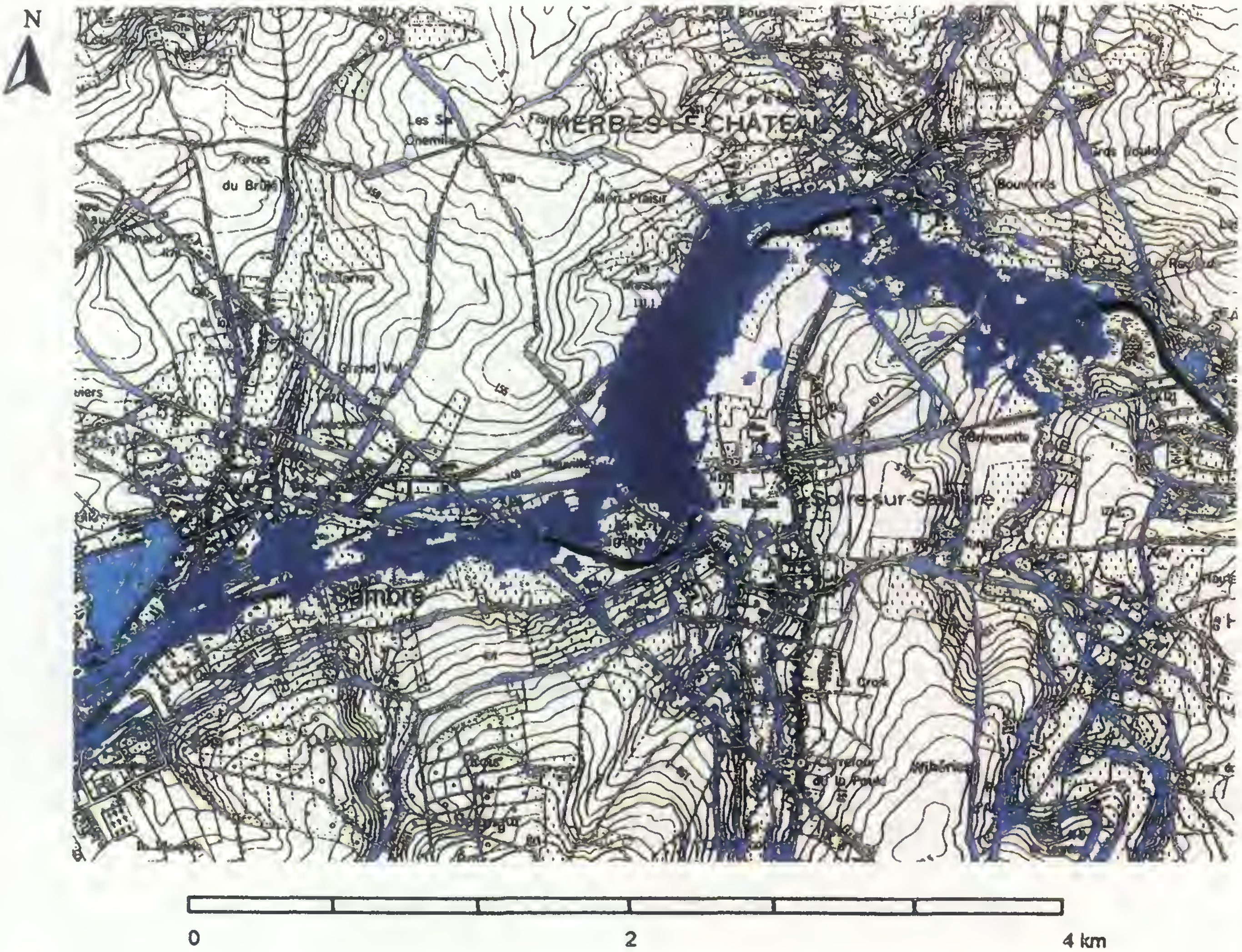

Figure 3 *(Courtesy of the University of Gembloux, Belgium)*

river), near Merbes-Le Chateau, Walloon Region. The inundated areas (in blue) are assessed through the application of a normalised difference index on ERS-1 SAR multitemporal data acquired during Phase D 3-day cycle.

6. THE 'SARFLOOD' FORUM: AN INTERESTING EXPERIENCE OF ESRIN

In December 1995, a meeting of flood experts was held at ESRIN, Frascati, Italy. The purpose of the meeting was to compare the existing expertise of both satellite information providers and users, in compliance with ESA's Earth Observation Programme which aimed at pursuing not only scientific but also application and operational/commercial domain objectives.

Among other, the following elements of interest emerged from the contributions:

a) From the satellite information providers' side

- Flood extent delineation maps were a relatively easy output to obtain from all project/study activities carried out in Europe in connection with the 1992–95 flood events (see Table 1).
- The 'presence' of ERS SAR, common to all those events, was extremely useful.
- GIS is recognised as essential to locate inundations precisely.
- For detailed mapping, the complementary role of aircraft data and DEMs is ascertained.
- ERS-1 SAR is satisfactorily employed in high-resolution model validation for flood forecasting.
- In typical cases, such as whenever a better understanding of remote hydrological areas of hard access is required, SAR contribution reveals to be particularly useful.

b) From the user side

- Flood extent maps are often used as input to the cartography of flooded areas, thus forming a database at government's disposal for formal declaration of 'disaster area'.

- Maps are in many cases used as 'technical documents' in decisions concerning land-use planning. It has happened in France, where the Ministry of Environment used the SAR-derived map to oppose the National Railway Company's planning of train routes in inundable areas.

- A good SAR information-based inventory of flooded areas can lead to operational flood monitoring and relief activities. It was the case of the Pisa Province Authority in Italy, now near to sign a convention following the successful results obtained by a Project in the River Arno Basin's area. (See Profeti & McIntosh's paper in this volume).

- Insurance, re-insurance companies are a new category of users of SAR data applied to flood risk management. Although still at a pre-operational level, their awareness of SAR data techniques together with a knowledgeable experience in using SAR with integrated tools (GIS and similar) is demonstrated in flood and storms models developed to produce loss estimates.

7. THE ROLE OF INTERNATIONAL ORGANISATIONS

In the context of Council of Europe's activities related to risk management, the contribution of space technology in general, and of SAR in particular, is fundamental and is acknowledged through several demonstration projects.

Natural risk issues are also part of the 5th Framework Programme of Research and Technological Development undertaken by the European Union.

In flood related issues, Eurimage's Earth Watching Project proves to be able to ensure a good link with the media through their 'Within 24 hours' ERS SAR image release via electronic data network, based on low-resolution satellite data acquisition.

8. RESULTS TRANSFER – CONCLUSIONS

The transfer of results from scientific/research world to end-users is critical.

Constraints of various kind have to be considered, such as, among other, a certain lack of confidence in the SAR instrumentation, still looked at as 'hard to handle and process'. Proper involvement of users, better understanding of their needs, availability of more information seem to be the weak points in such a complex process.

More precise and detailed cost-benefit analyses are needed to promote a wider use of SAR for floods.

In addition, the following actions seem to be required:

- Selection of the most appropriate approach towards the end-user, in order to analyse his real needs.

- Inclusion of decision makers as participants to Workshops, Conferences and similar.

- Availability of 'ready-to-use' information for quick integration into GIS.

- Increase of on-line data dissemination service opportunities, to facilitate real-time operations.

- Encouragement of operational/commercial actions by value-adding companies or similar by means of more specific and 'aggressive' dossiers of information.

9. REFERENCES

ERS Data Utilisation – ESRIN: *Proc. of the First ERS Thematic Working Group Meeting on Flood Monitoring*, 26-27 June 1995.

G. Calabresi, Flood Monitoring Workshop Report, in: *Earth Observ. Quart. no.49*, Sept. 1995.

E. Bonansea (CSI–Consorzio Sistema Informativo): Mapping of 1994 flood in Piemonte Region – An example of remote sensing and GIS application, *Proc. 1st ERS Thematic WG Mtg. on Flood Monitoring*, June 1995.

S. Delmeire & L. Marinelli (Geoimage), Identification of flooded areas in the Rhone and Var river valleys, France, using ERS-1 data, *Proc. 1st ERS Thematic WG Mtg. on Flood Monitoring*, June 1995.

M. Badji (Univ. of Gembloux, Belgium), Characterisation of flood-inundated areas and delineation of poor drainage soil using ERS-1 SAR imagery, *Proc. 1st ERS Thematic WG Mtg. on Flood Monitoring*, June 1995.

THE USE OF ERS SAR DATA TO MANAGE FLOOD EMERGENCIES AT THE SMALLER SCALE

Heather MacIntosh, Giuliana Profeti

Università degli Studi di Firenze, sede di Prato, Piazza Ciardi, 25 - 50047 Prato, Italy
Tel: (39) 574-602520. Fax: (39) 574-602515

ABSTRACT

This paper deals with the experimentation activity carried out by the Civil Engineering Department of Florence University (Italy) in co-operation with Eurimage (Rome, Italy) and the Pistoia Province (Italy). The aim of the study is to research into the possibilities of ERS SAR data utilisation to aid local government in the management of flood emergencies.
The area selected for the study is the Fucecchio Marsh (Tuscany, Italy), in which flooding events are very frequent. Based upon the specific requirements of local government, the applicability of ERS SAR data to map flooded areas in the Marsh has been assessed. The advantages of using the maps obtained from ERS SAR images in the post-flood relief activity have been outlined as well. This article describes the results of the study, with particular reference to the users' requirements and the cost/benefit analysis.

1. INTRODUCTION

ERS SAR data are a powerful tool to monitor flooded areas, as it has been showed recently in the First Flood Monitoring Workshop, held at ESRIN (Frascati, Italy).
With the exception of an experimental work performed after the Alessandria Flood in 1994 (Bonansea, 1995), in Italy flood mapping is still performed with traditional methods. The purpose of the present work, which has been carried out by the Civil Department of Florence University in co-operation with Eurimage (Rome, Italy) was to demonstrate the utility and convenience of the use of SAR data in flood mapping, even when a limited territory is affected. To this purpose, the co-operation of a potential user of the product was needed. An agreement was reached with Pistoia Province (Tuscany, Italy), whose territory is frequently affected by flooding events.
The Environmental Office of Pistoia Province helped in the compilation of a requirements' list that a SAR-derived map has to fulfil. To obtain a complete list, experts of the neighbouring provinces have been interviewed too. Then the costs of traditional ground surveys have been estimated, to be compared with the costs of satellite-based mapping.
This paper describes the feasibility study on the use of satellite data for flood survey and relief at the local scale, emphasising the user's requirements, the results obtained in the SAR data processing, and the cost/benefit analysis of this kind of service.

2. THE STUDY AREA

The area selected for the feasibility study is the Fucecchio Marsh (*Padule di Fucecchio*) located at the boundary of the administrative districts of Pistoia, Pisa and Florence (Tuscany, Italy). The Fucecchio Marsh is one of the most important wetlands in Italy. When Italy subscribed the International Convention of Ramsar (1973), it was chosen as one of the 24 European wetlands to be studied and preserved. Among the various problems related to the preservation of the Marsh, there is the protection from flash-flood events, that are quit common (nine were registered in the years 1990-1993). To save this unique environment, hydraulic interventions in the area are required. In 1994, the Pistoia Province and the Land Reclamation Board installed a network of gauges in the Marsh area. They also committed a feasibility study to Florence University, on the hydrological modelling of the area, which included a feasibility study on a flood monitoring service based on the use of ERS SAR data, carried out in co-operation with Eurimage.

3. USER'S REQUIREMENTS

In order to study the feasibility of using ERS SAR images to map flooded areas at the local scale, it is fundamental to examine the needs of the potential users of the maps. The list of requirements, compiled in co-operation with the experts of Pistoia Province and other provinces of the Tuscany Region is:

1. *map scale*: 1:10.000 (preferred), 1:25.000 (tolerated);
2. *errors*:
   2.1. error on boundary positioning: 2 mm on the map, equivalent to 20 meters at the 1:10.000 scale and 50 meters at the 1:25.000 scale;
   2.2. tolerance on the estimation of the flooded area's surface: not specified;
3. *processing time*: better than 0.5 day/Km^2;
4. *output format*: boundary of the flooded areas in a vector format compatible with the user's GIS.

Only the map scale and the error on the boundary position are strict requirements, as it is logical when a local event is being mapped. Regarding processing time, an improvement on the performing of a complete ground survey is requested, but its entity is not specified. Finally, the specifics of the furniture (media, support, etc.) have not been listed above, with the exception of the output format. All the local administrative authorities in Italy are now equipped with a geographical information system, and therefore a vectorial output format is a standard requirement.

4. DATA PROCESSING

The time of study was during a period of heavy rainfall and consequent flooding in October/November 1992. Two SAR images were obtained for this period, one before the flooding occurred (16/10/92), the other 4 days after the flood (04/11/92) (see fig. 1).

Visually, the images showed a distinct temporal difference in the region of study, the post flooding image having a much darker tonality with greater coverage area. This feature of SAR imagery may be easily used by a photointerpreter to extract the areas covered by water. However, computer-aided image processing techniques may be used to obtain the prediction of the extent of flooding in shorter times by the analysis of the signal variations.

The research has therefore involved the development of a variety of methods to extract the cells that represent the flooded areas of an image. The purpose of this part of the research was to provide the final users with a guide for deciding the best kind of processing of SAR image, depending on the required product accuracy, processing time and experience of image processing. This guide will not be described in this paper, that deals with the feasibility of flood mapping with SAR data. For this purpose, a medium-level data processing was assumed (MacIntosh and Profeti, 1995), classifying the two SAR images. This method has proven to be effective in producing a flood extent map (see fig. 2).

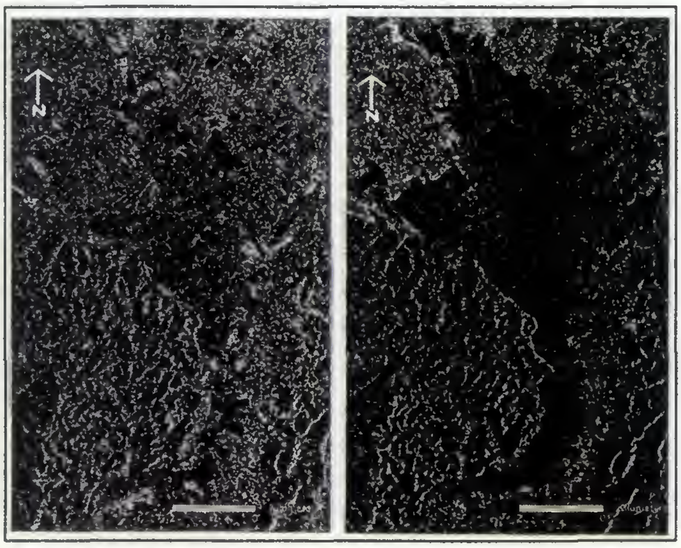

Fig. 1: These SAR images show the Fucecchio Marsh on 16/10/1992 (left) and 4/11/1992 (right), before and after the flooding event of October 31st, 1992. Rivers and swamped areas are dark.

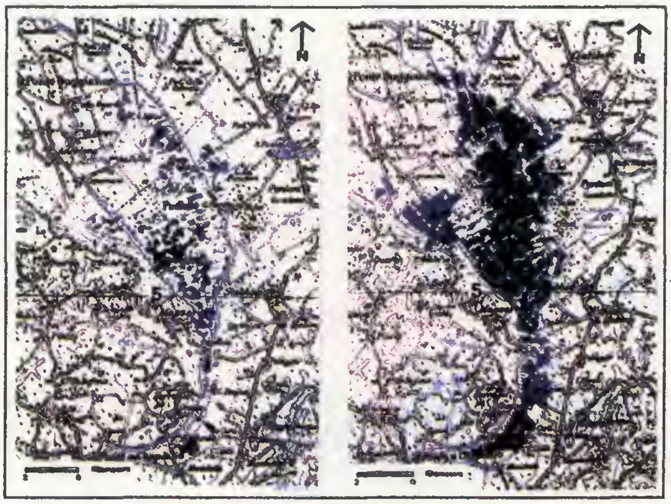

Fig. 2: Flood extent map of the Fucecchio Marsh. Areas in blue represent water. Left: 16/10/1992, 4.94 Km^2. Right: 4/11/1992, 16.94 Km^2.

5. ANALYSIS OF THE RESULTS

The map of flooded areas obtained by processing ERS SAR data had been analysed on the base of the user's specifics regarding map scale and error on boundary positioning. The results of the analysis are summarised below:

Map scale. The 1:10.000 scale is a standard format for thematic mapping at the provincial level, while 1:25.000 is used at the regional level. The common restitution scale of SAR images and derived products is 1:25.000. For general purposes, the 1:25.000 scale has been declared acceptable by the users. This scale has therefore been considered in the subsequent analysis.

1. *Error in the identification/positioning of the boundaries*: at the 1:25.000 scale, the required error limit is 2 mm on the map, equivalent to 50 meters, or 8 pixels. The estimated *a priori* error on the Padule event was 1.5 pixels for the georeferencing process, plus 1 pixel in the identification of edges by classification. A mapping survey had not been carried out in correspondence of the event under examination, but a great part of the boundaries corresponded to geomorphologic and urban features (alluvial terraces, roads, etc.) that are easily identified on a topographic map. The *a posteriori* error has therefore been calculated comparing the boundary of the flooded areas identified in the image with the position of the geomorphologic features identified in the topographic map. The average error obtained with this procedure was 32 meters (2.56 pixels) with a maximum error of 43 (3.44 pixels). This requisite has therefore been fulfilled.

The tolerance on the estimation of the flooded area's surface has not been specified as one of the main objectives in flood mapping is the correct positioning of the boundary between flooded and non-flooded areas. In fact, these maps are also used as the base for the distribution of refunds among the inhabitants of the area.

To conclude this paragraph, it is necessary to make an important observation. The post-flood SAR image was acquired on the study area when the flooded terrain was still covered by water. In this case, the use of SAR data allows to identify easily the flooded surfaces. If the SAR image is acquired when part of the flooded surfaces are not still covered by water, it is necessary to identify them looking for wet surfaces instead, on the base of an increase in radar backscatter. This kind of processing requires an higher knowledge of the characteristics of the study area, and the accuracy of the results may not be anticipated. At present, this problem is avoided by the high acquisition frequency (an average of 3 images/month) of SAR data by ERS-1 and ERS-2. However, the main concern of the potential users of this service regards the availability of images in the future, when ERS-1 will stop acquiring images.

6. RELIEF

To complete this study, it is important to put into evidence the advantages of using the maps obtained from ERS SAR images in the post-flood relief activity. Relief is perhaps one of the most important aspects of flood monitoring. The need to know the flood affected area, the amount and type of damage sustained, and what is needed to relieve the immediate consequences, is uppermost at the smaller scale too. The maps obtained from SAR imagery can be immediately combined with other thematic data to provide such information, while the traditional maps must be digitised first. Therefore, the use of SAR data allows to save time and money in the relief activity too. A few examples have been produced to complete the feasibility study, and are described below.

The flood extent map can be used in combination with the pedological map (fig.3a), the land use map (fig.3b), the digital terrain model (DTM) (fig.3c), and the channel network vector layer, and any consequent combination of these, to provide more detailed information on the flood statistics. Information such as average flood height and volume for each individual soil type and land use class can be provided and prove useful for the estimation of crop or structure damage. An example of information which can be provided is given below in the form of flood risk and damage assessment maps. The flood extent map was firstly combined with a digitised pedological map of the area. Statistics on the damages are immediately obtained. The flood risk map (see fig. 4a) contains, in order, the areas of soils which show a greater increase in water coverage at the time of the flood. A vector layer of the channel network has been overlaid onto this map to demonstrate that the areas most at risk are also near a denser assembly of channels. The same processes were carried out with a digitised land use map. With these results an assessment of the damages to crops and structures involved was determined and a map of the damages produced (see fig. 4b).

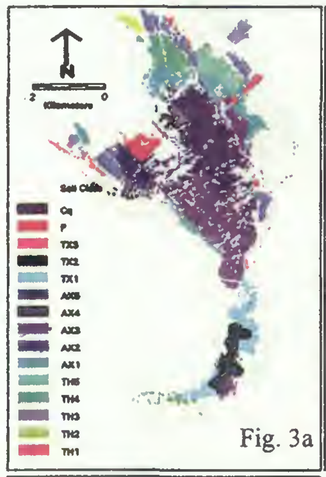

Fig. 3a

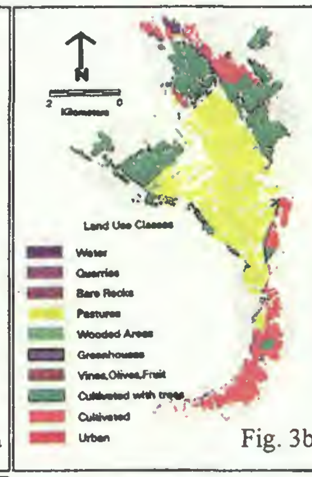

Fig. 3b

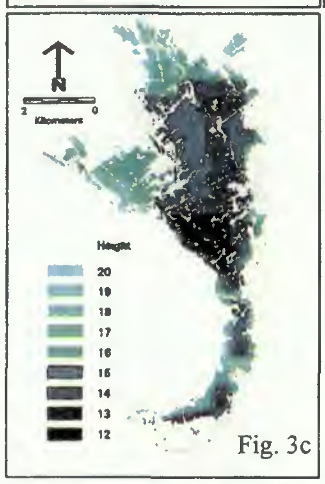

Fig. 3c

Fig. 3. Flood extent map of the Marsh in combination with:
3a. the pedological map, (USDA classification);
3b. the land use map;
3c. the digital terrain model, (height in meters above the sea level).

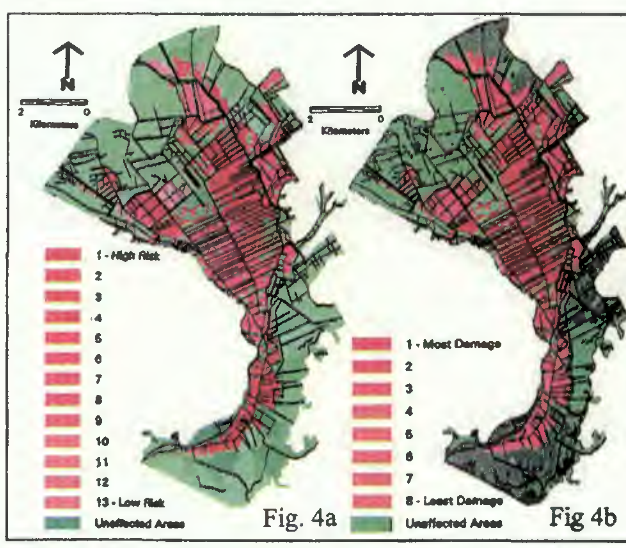

Fig. 4a Fig 4b

Fig. 4. Flood risk and damage assessment maps, as at 4/11/92, overlain with the river channel network. In fig. 4a, green areas (unaffected) represent different soil types; in fig. 4b, different soil uses.

All these data can be obtained in a very short time using maps derived from SAR data and a geographical information system. If traditional surveys are carried on, the time necessary to produce and digitise the maps is too long to use the results in the relief activity. This represents a waste of opportunities, as every administrative authority is now equipped with a GIS. Hence, the use of SAR data allows also a better exploit of the existent resources.

7. COST/BENEFIT ANALYSIS

The Italian legislation does not oblige the local administrative authorities to map the extension of flooded surfaces after an event. Some municipalities always carry out a complete study of the event, including a mapping survey, while others only compile a list of places where the event occurred.

Based upon this premise, it is evident that the use of SAR data may be interesting for local authorities only if it leads to an effective decrease in costs.

To compare the costs of satellite and ground survey, only the delimitation of the flooded areas has been taken into account. In fact, the production of maps from ERS SAR data does not eliminate the necessity of ground surveys, in which data on flood dynamic and structural damages is sought. Such investigations must be carried out anyway, and therefore their costs must be calculated separately.

1. *Mapping through ERS SAR data*:
   - 1.1. Flood extent: one day/man for georeferenced data, two for PRI data (including georeferencing), for one or more SAR images.
   - 1.2. Risk and damage assessment: if the necessary thematic data are already available in raster/vector format, risk/damage assessment maps such as the ones described above may be produced in 1 day/man.
2. *Mapping by ground survey*:
   - 2.1. Flood extent: ground surveys of this kind cover an average of 3 - 4 Km^2/day, employing two operators. Restitution is then performed at an average of 20 Km^2/day at the 1:25.000 scale.
   - 2.2. Risk and damage assessment: the time of digitising (20 Km^2/day at the 1:25.000 scale) must be added to 1.2.
3. *Comparison between the two cases*: To carry out the comparison, it has been first assumed that a SAR image contains the whole affected area. Regarding the choice of data, working on flatlands the less expensive solution is to acquire PRI data and then correct them with the GCP method. Thus, converting the present cost of a SAR PRI image in the equivalent number of day/man, it is easy to see that at present, the use of SAR data is less expensive than a ground survey when the extension of the flooded area is greater than 20 Km^2.

   Regarding the production of thematic maps, the use of SAR-derived products is convenient anyway. The convenience increases with increasing areas

To conclude this analysis, it must be underlined that flooding events generally interest more than one locality; therefore, it is still convenient to use SAR data for flood inventory. For example, in the case of study the Fucecchio Marsh was flooded for an extent of 16 Km^2. Other two neighbouring zones were flooded in the same event, for a total flooded surface of 53 Km^2.

It must also be noticed that these zones belong to distinct administrative authorities; therefore, the use of SAR data is economical if a single study of the event is conducted. This reason, in addition to the cost of an image processing facility shows that the best solution for the local administrative authorities is to obtain maps of flooded areas from an external provider that uses SAR images.

8. CONCLUSIONS

ERS SAR data has been proven to be successful in flood mapping and post-flood activity in a study carried out on the Fucecchio Marsh (Tuscany, Italy). Even at the smaller scale, ERS SAR data can provide quick and detailed information that fulfil the final user's requirements. This study has encountered the interest of the local authorities, and it is believed that its dissemination will contribute to the diffusion of the use of ERS SAR data for flood monitoring.

REFERENCES

BONANSEA E., (1995) - Mapping of 1994 flood in Piemonte region: an example of remote sensing and GIS application. First ERS Thematic Working Group Meeting on Flood Monitoring, Frascati (Roma, Italy), June 26-27, 1995.

MACINTOSH H., PROFETI G. (1995) - ERS SAR and Landsat Thematic Mapper data application to flood prevention and damage assessment in Italy. First ERS Thematic Working Group Meeting on Flood Monitoring, Frascati (Roma, Italy), June 26-27, 1995.

PROCEED. of the "First ERS Thematic Working Group Meeting on Flood Monitoring", (Frascati, Italy), June 26-27, 1995. ERS Data Utilisation Section, ESRIN.

ACKNOWLEDGEMENTS

The authors thank Dr. Aldo Argentieri (Eurimage) and Dr. Francesca del Tredici for their help.

ASSESSMENT OF THE MAPPING CAPABILITIES OF ERS-1 SAR DATA FOR FLOOD MAPPING: A CASE STUDY IN GERMANY

Regine Oberstadler, Helmut Hönsch, Dagmar Huth

Company for Applied Remote Sensing (GAF), Leonrodstr. 68, 80636 Munich, Germany
Tel: (49) 89-121528-0. Fax: (49) 89-1233-148

ABSTRACT

The applicability of ERS-1 SAR data for flood mapping under operational conditions was examined by the company GAF under contract of the German space agency DARA. Investigated was the flood event along the Rhine valley in winter 1993/94.

In order to carry out an examination adapted to the needs of the end-user, the specific user requirements concerning information about flood events were identified in an initial phase. Items of major interest were the achievable mapping accuracy of the flood extent and the flood level, the production of corresponding maps and the run-off. The information thus obtained was integrated into the definition of the project objectives. It was further used to define the applicability as well as the inadequacy of ERS-1 data with regard to their operational use for flood mapping.

First a detailed analysis of the temporal aspects of traditional mapping methods and an investigation based on the satellite data was executed. These steps were followed by a visual interpretation of the imagery in combination with an automatic classification. A post-classification processing was then carried out, which included the application of various filters to determine the flood boundary.
When comparing the performance of the methods employed, the visual interpretation proved to be the more accurate method. For both methods of classifying images, problematic features identified were settlements, forest and bushes, and regions with layover and fore-shortening effects.
A comparison between the flood level derived from satellite data and the one registered by the water authorities revealed a height difference in the range of 0.5 to 2.0 m. The relatively coarse resolution of the sensor and problems with the accurate delineation of the flood line proved to be the main causes for the discrepancy.

The conclusion of the study is a clear indication that flood monitoring with ERS-1 data can provide satisfactory results for some user needs. However, for more accurate data a survey taking field measurements remains indispensable.

1. INTRODUCTION

In recent years, the Rhine valley was afflicted by severe floods, which inundated large areas and causesd considerable damage to buildings and the infrastructure. To deliminit the detriment effect of future floods, exact measurements of the amount of water and the corresponding spatial extent of the inundation are needed. Such information will assist in the dimensioning of dikes and embankment constructions, support the identification of retention areas and allow the delineation of flood endangered areas.

In Germany, the supervision of the main waterways is under the responsibility of the Water Authority Boards, which are also in charge of the recording of floods. This task includes the registration and mapping of flood events and the instigation of operations to control floods.
The method used by the water authorities to acquire flood data is to send a team of experts into the field for taking direct measurements. For this purpose plugs are placed at 500 m intervals, marking the highest water-level within the river profile. Afterwards the plugs are measured. However, an exact geographic reference of each plug is not provided.This method is very precise and produces data with a high degree of accuracy, which ranges from 5 to 20 cm. The data satisfies the requirements of hydrological calculations, for which an accuracy of a few decimetres is essential.

Despite the high accuracy of the ranging, the Water Authority Boards are thinking about new possibilities to derive the flood level. The reason for this is that the method is expensive because it is time-consuming, staff-intensive and because data processing takes a relatively long time.
Another problem is, that pedestrians often vandalize the plugs so that gaps in the data base appear. Finally, the highest water-level is only marked in the main river course; areas where the water has flown behind the dike are neglected.

Water gauge	Acquisition date of the traditional measurement		Acquisition of ERS-1 SAR data		water height (cm) measured by the water authority boards	water height at ERS-1 pass	Height difference
	Date	Time	Date	Time			
Koblenz	23.12.93	9:30	25.12.93	10:25	949	840	109
Bonn	23.12.93	18-22:00	25.12.93	10:25	1013	950	63
Cologne	24.12.93	0-6:00	25.12.93	10:25	1063	1017	46

Table 1: Acquisition date of the water-level measurements and the corresponding water height.

ERS-1 SAR data cannot provide datasets with decimeter accuracy. Nevertheless they are appropriate to overcome some of the difficulties the navigation staff has to cope with: they can be obtained relatively quickly enabling an immediate view of the actual flood situation. The geographical reference is available and the data is easy to combine with digital information such as digital maps.
Moreover, the great advantage of ERS-1 SAR is the ability to acquire data without restrictions from weather conditions.

The objective of this study therefore, is to examine the mapping accuracy of ERS-1 SAR data in comparison with the results of the Water Authority Boards. The satellite data was investigated in view of an operational use for flood mapping taking into account the restrictions of data acquisition, satellite parameters, time aspects of data processing and analysis, as well as thefinancial components.

2. DATA BASE AND SITES

The inundation of the Rhine valley in December/January 1993/94 was recorded on three multi-temporal ERS-1 SAR images. Fortunately, just on the end of December the 3-day orbit of the ERS-1 mission started, therefore th following subsequent images could be collected:
25.12.1993, 31.12.1993 and 03.01.1994. The acquisition time was 10:25 a.m. As reference for a normal water-level one scene of June from 10.06.1992 was used.
SAR.GTC products were chosen because geometric distortions were corrected and therefore the combination with auxiliary data sets (i.e topographic maps, landuse data, etc.) is possible.

Each scene maps an area of about 100 x 100 km between Duisburg (Nordrhein-Westfalen) and Koblenz (Rheinland-Pfalz)

As project testsites, three river sections were chosen, each of them covering an area representing the size of one mapsheet 1:25.000. In accordance with the water authority boards, the testsites had to meet special requirements: they include river shores which are not protected by dikes or have steep river banks. They also cover regions where the water had flown behind the dike.
The river sections between Porz and Bonn as well as around Koblenz seemed to be suitable for the investigation. The location of the testsites is shown in Figure 1.

As additional data sets the corresponding mapsheets, digital and analog, as well as aerial photography data, Koblenz, proved to be helpful for data interpretation. which unfortunately only exist for parts of the testsite
The flood-level measured, the river profiles, the foreland profiles as well as registrations of the water-level per hour for the gauges Koblenz, Bonn and Cologne were made available by the water authority boards.

Time Aspect of ERS-1 SAR Data Acquisition

Because floods constitute temporal occurrences with wave characteristics, different advances of the wave front and flood levels are recorded across a satellite image. Therefore, the time and place of the data collection is of fundamental importance for an investigation using satellite data.
The temporal difference between the highest flood level at a site and the level recorded by ERS-1 at the date of the image acquisition is thus variable. For Koblenz, for example, the image was acquired about two days after the flood peak, while the wave front passed Bonn about 1.5 days earlier. At Cologne, the peak event occurred only 3 hours before the time when the image was taken, because the wave remained steady for some hours. The acquisition dates of the field measurements and the ERS-1 as well as the resulting decrease of the flood levels are presented in Table 1.

Figure 2 indicates the wave propagation during the time of data collection and demonstrates at what flood situation the ERS-1 scenes map the flooding.

In general, the timely collection of data and the processing of ERS-1 images forms an important factor in operational projects. Under normal conditions requests for the acquisition of ERS-1 data should be made at least four weeks before the date indicated. Processing the data requires an additional two weeks. This amounts to a total of six weeks for the data acquisition and processing.
In urgent cases, ESA and the affiliated PAF's try to manage the ERS-1 acquisition requests and the data processing in less time. If the satellite station is aware to the request, low resolution quicklooks are available 4 hours after the acquisition. These images were used successfully for the Christmas flooding of 1993 in the Cologne/Bonn area, giving an overview in just a view hours.
Full resolution products can be delivered within 10 Minutes from the satellite station to the archiving and processing centres. The constraint is however, that the transmission is planned once a day for each station near midday. Requests for data made in the early afternoon will only be transmitted the following day. Only for very exceptional purposes it is possible to plan another transmission.

3. METHODOLOGY

3.1 Identification of Data Users

Of particular importance to the project was a close contact with the data users. User requirements had been obtained by questionnaires, which concentrated on a comparison of user needs and the data provided by ERS-1 data. Overall, the users of flood data can be devided into two groups:
- data users interested in information concerning the water volume (i.e. national and federal institutes)
- data users interested in the flood-level and the extent of the inundation (i.e. the Water Authority Boards, the federal institute for hydrology, emergency organisations, headquarter for flood defence, insurance and re-insurance companies as well as planning authorities).

Various products are required by the users, which can be established by ERS-1 SAR data:
- a quick view of the flooding;
- maps which delineate the extent of the inundation;
- an indication of the run off;
- a measurement of the flood level ;
- proof for surfaces which are inundated due to a rise of the ground water-table.

Because insurance companies index their customers on the basis of postal code districts, it seems to be appropriate to express the extent of the flood for equivalent regions.

The flooded ares for individual classes of landuse can be derived from classified Landsat TM data. The water volume can be determined using a digital elevation model. This data can be used for model validation.

3.2 Data Analysis

The software packages used during the study were ERDAS IMAGINE and ARC/INFO. The ERS-1 SAR data was scaled from 16 bit to 8 bit data by a linear histogram stretch to allow for easier data handling without affecting the informational content of the data.

3.3 Visual Interpretation

First step taken during the examination phase was a visual interpretation of the aerial photographs of Koblenz. These photographs allow a clear identification of the satellite images and were used to verify the results.

The satellite images were interpreted directly on-screen, producing different flood lines which document the variations in the water-level. The interpretation was carried out on a color composite because inundated areas are displayed as clearly visible colours. By comparison, the interpretation of a single ERS-1 scene is rather arduous, because the human eye is only capable to distinguish a very limited number of grey values. Additionally, some backscatter values of inundated areas are not very characteristic at all and can only be detected by using images acquired at different dates.

The interpretation used a combination consisting of one scene (i.e. GTC of 25.12.93), a difference image derived from the scene under investigation and the image dating from 03.01.1994, and a reference image from June 1992. This data combination proved to be the most suitable for the visual interpretation.

A reference scene is not strictly essential for the interpretation. However, in case of uncertainities with the interpretation it was found to be benefical to be able to compare the grey values of the presumed inundated areas with those representing the non-flood state.

3.4 Automatic Classification and Filtering

Besides applying a visual interpretation to the images an automatic classification was carried out. The objective was to find a rapid and operational method for mapping floods, whereby an automatic classification seemed to be at the most suitable approach.
The classifier used was a new evidence-based classification algorithm called EBIS (**E**vidence **B**ased **I**nterpretation of **S**atellite Images)(Lohmann, 1991). The EBIS- classification, was recently implemented in the ERDAS Imagine software package. It is based on the mathematical concept of "evidentional reasoning"

according to the "Dempster-Shafer-Theory". This structural and pixel-based algorithm employs co-occurrence matrices and local histograms as feature spaces. These matrices describe, at which frequency specific neighbourhood-relations occur for a group of pixels. All feature spaces display an individual polynomial distribution. From these the program simulates its own classes, which are structured but randomly distributed. Different distribution functions can be applied like the Gaussian distribution and the multinomial, window-based distribution. No additional pre-processing, such as enhancement or filtering, is necessary. Moreover, such operations could have a negative effect on the classification accuracy.

The best classification results were achieved by classifying two images, the GTC of the 25.12.1993 and the GTC of the 03.01.1994. Tests of the classification with only one acquisition date or with all three dates in combination produced inferior results.
Only classes of water were separated from those of non-water, using about 10 different training classes. As parameters, the local histogram and multinomial distribution were applied.

Following the classification, the class „water“ was homogenized by using various spatial filters. This procedure allowed to avoid gaps inside the class and, where required, to extend the outer boundary of the water class. This step is necessary, because the class boundaries are poorely represented with the EBIS classifier.

3.5 Measurement of the Flood Level

In the case of a flood event, the mapping teams of the Water Authority Boards always try to seize the peak wave. Because the wave normally remains steady for some hours, it can be assumed that the data sets of the water authority boards accurately represent the highest flood level.
As for satellite data, the temporal difference between the highest water-level and the time of data acquisition date has to be considered.

To derive flood-levels from ERS-1 images, the visually delineated flood-boundar ,which was more accurate than the classification result, was plotted onto transparencies in combination with the foreland profiles (as line). This plot was then superimposed over the corresponding mapsheets of 1:5000. At the intersection of the flood-line and the foreland, the relief information of the map was registered.
This information was established only for the Porz test site, which means a distance of 19 Km along the river course.

4. RESULTS AND DISCUSSION

The visual interpretation of ERS-1 SAR images produced good results. Nevertheles, the identification of the virtual flood line was problematic in some areas.
Uncertainities arose, for example, where steep slopes produced radar shadows and fore-shortening effects which obscured or concealed the landuse information.
Furthermore, the backscatter reponse of many forested areas is very similar to that of inundated land. As a consequence, the flooded areas were found to be difficult to separate from forests. In those instances, the information provided by the corresponding map sheet proved to be a valuable source of auxiliary data for the correct identification of the two classes.

An accurate separation of flooded from non-flooded settlements was also found to be difficult. In many cases the high backscatter produced by buildings overlaid the backscatter of inundated areas. Besides, flooded roads were quite often too small to be distinguished.

Another critical point was the number of trees in built-up areas, in particular in one-family housing estates. There the density of trees is comparatively high so that flooded surfaces are hidden by the trees and cannot be detected.

Inaccurate delineation also occurred in cases, where embankment constructions or port installations produced high backscatter values,which dominated the reponse of the surrounding areas. In some cases, the reflection was so strong that the interpreted flood-line run inside the normal river bed.

A test of the reliability of the visual interpretation effectuated by comparing the flood lines with those derived from aerial photographs. The results are graphically depicted in Figure 3.
In general, the flood lines produced by the two methods were found to coincide properly, despite the presence of problematic sections mentioned above.

Overall, the visual interpretation of ERS-1 SAR data seems to be an appropriate method to provide a ready account of the flood situation. It is furthermore a suitable means to derive the boundary of flooded open or arable land and, with some restrictions, of built-up areas. Yet, in terms of accuracy the interpretation of aerial photographs was found to yield superior results.

With regard to the classification, the results obtained were encouraging and demonstrate the usefulness of the EBIS algorithm for the classification of radar data (Figure 4). The program is easy to use and produces relatively rapid acceptable results. However, various mis-classifications of water occured in the arable land class, which had to be addressed by either filtering the image or editing the data manually. The mis-classification arose, because forested areas and wet arable land shows similar backscatter signatures to inundated land. On the whole,

the flooded area is relatively heterogenious, enclosing a variety of grey values.
Incorrectly classified were also layover zones due to their low backscatter, which resembles the one of open water.
Moreover, a correct delineation of the flood line was troublesome in those areas, which had already been problematic in the visual interpretation, such as settlements.

A considerable improvement over the classified image was the application of filter steps (Figure 5). A notable portion of flooded surfaces, which were classified as arable land, could be adjoined to the class „water". As it had been expected, this procedure also increased the amount of pixels incorrectly classified as „water" within arable land. These pixels were eliminated manually according to the topographic map sheets. A comparison of the results obtained from the visual interpretation with those from the filtered classification revealed that most of the obviously inundated areas were correctly classified by the algorithm (Figure 6). Forests and one-family housing estates, however, as well as steep slopes had also been classified as water.

Unfortunately, there were no estimations available on the flood extent from the Water Authority Boards to verify the findings. Even in the absence of such data it was very apparent that the visual interpretation produced better results than the image classification.

To demonstrate the receding flood level, the flood boundary of all dates were combined and are shown in Figure 7. Clearly visible are those areas, which were affected the longest by the flood as well as „flooded islands", which are probably originated from the rise of the ground water table.

4.1 Measurement of the Water Height

The results obtained from the measurements of the water level with ERS-1 SAR data is presented in Figure 8. Severe irregularities are visible, which can be attributed to the following effects:
- Extremely low values refer to sections of the river, where corner reflectors near the bank (produced by embankment constructions or port installations) dominate the reflection. In those instances, the flood line was placed even inside the river bed. Another point is that if the water is held back by dikes, than there is no possibility to define the water-level.
- Very high water-levels can normally be related to measurements taken in built-up areas. As mentioned above, it is difficult to exactly define flooded areas inside settlements. This situation is aggrevated by the circumstance that on maps contour lines are often absent inside settlements. The correct definition of the water height is, therefore, a complex task and is often the result of an approximation.

The comparison of the measurements of the water height exhibit a variation of 0.5 to 2.0 m. The results have to be interpreted in consideration of the delay in the acquisition of the two measurements, which resulted in a height difference of about 54 cm at the testsite Porz. When taking this shift into account the discrepancy between the two methods was reduced to about 10 to 50 cm (see Figure 9).

5. CONCLUSION

Comparing the results obtained during the study with the demands expressed by the end users, the following conclusions can be drawn:

- The acquisition capabilities of ERS-1 cannot ensure the exact recording of the maximum flood event. Therefore, an operational use is not conceivable for this purpose at present.

- The mapping of the flood extent for arable land is possible with high degree of accuracy. Yet, in built-up areas, forested land or steep slopes, no definitive delineation of the flood line is feasible.

- To allow the estimation of the highest water-level with ERS-1 SAR data, the interval between the acquisition of the scenes has to be reduced. The coverage of the ERS-1 SAR image records different water-levels in different parts of the image.

- ERS-1 SAR data are too coarse to map the flood level with satisfactory accuracy in Germany. However, in regions where SAR data represent the only available source of information, the results are potentially very useful.

- Flood maps were found to be of use for emergency organisations and planning authorities and allow the generation of a flood database. Moreover, they indicate those areas, which are flooded as a consequence of a rise in the ground water-table.

6. REFERENCES

CORVES C. 1994. Assessment of multi-temporal ERS-1 SAR and Landsat TM data for mapping the Amazon river floodplain, Proc. of the Second Euro-Latin American Space Days, Buenos Aires, Argentina, ESA SP-363.

ESA, 1993. ERS User Handbook, esa Sp-1148, 2nd edn, ESA Publications Division, Noordwijk.

LECONTE, R., PULTZ, T.J. 1991. Evaluation of the potential of Radarsat for flood Mapping and using simulated satellite SAR imagery, *Canadian Journal of Remote Sensing*, 17, 241-249.

LOHMANN, G. 1991. An Evidentional Reasoning Approach to the Classification of Satellite Images, DLR Forschungsbericht FB 91-29.

PULTZ, T,J., LECONTE, R., ST-LAURENT, L., PETERS, L. 1991. Flood mapping with airborne SAR imagery: Case of the 1987 Saint-John River Flood, *Canadian Water Resources Journal*, 16, 173-189.

MATTHEWS, J., GAFFNEY, S. 1994. A study of flooding on Lough Corrib, Ireland during early 1994 using ERS-1 SAR data, Proceedings of the First ERS-1 Pilot Project Workshop, Toledo, Spain, ESA SP-365.

SCHREIER, G. 1993. SAR Geocoding: Data and Systems, Herbert Wichmann Verlag GmbH, Karlsruhe.

ULABY, F.T., MOORE, R.K., FUNG, A.K. 1981. Microwave Remote Sensing. Active and Passive, Vol. 1, London.

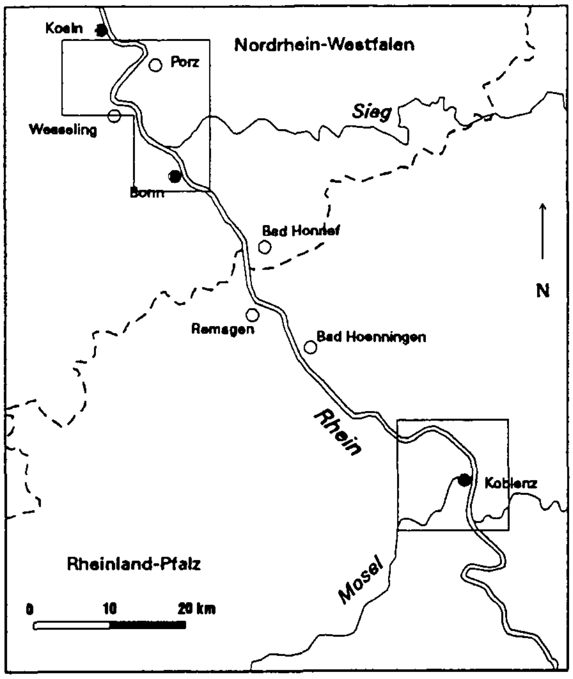

Figure 1: Location of the project testsites

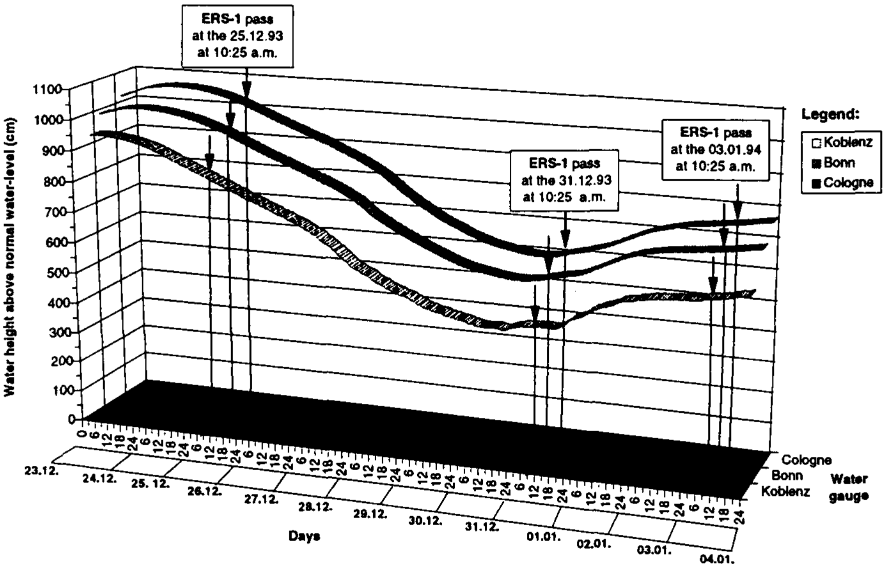

Figure 2: Water-level measurement per hour for the water gauges Koblenz, Bonn and Cologne from 23.12.93 to 04.01.94. The date and time of the ERS-1 pass is indicated to show what flood situation is mapped on the satellite images.

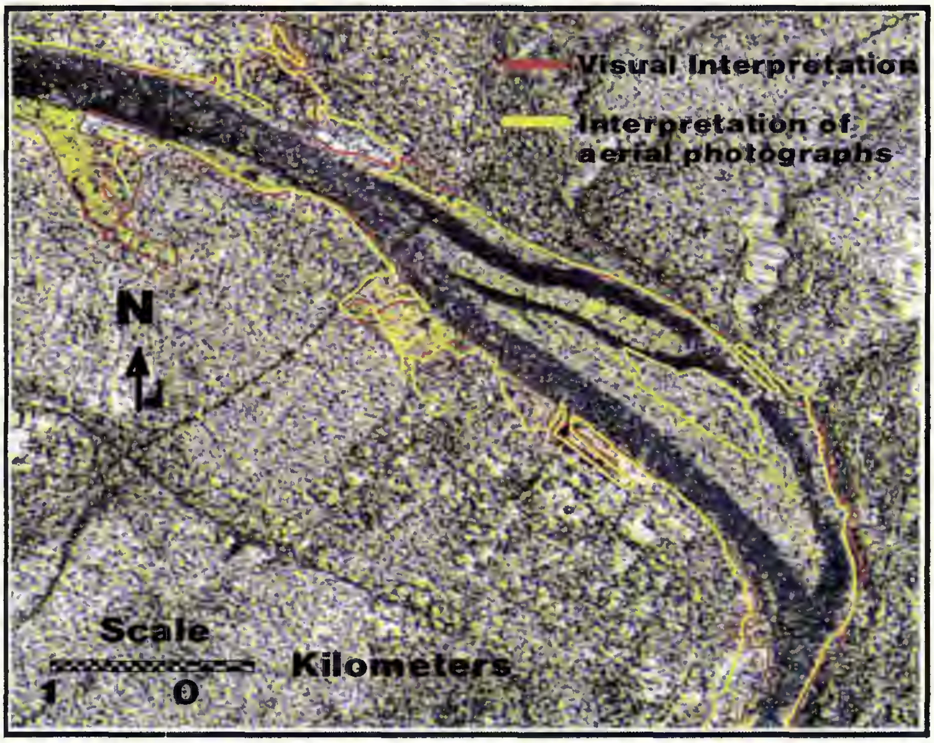

Figure 3: Visual interpretation of the aerial photography data and the satellite data for parts of the testsite Koblenz (the section is located north of Koblenz)

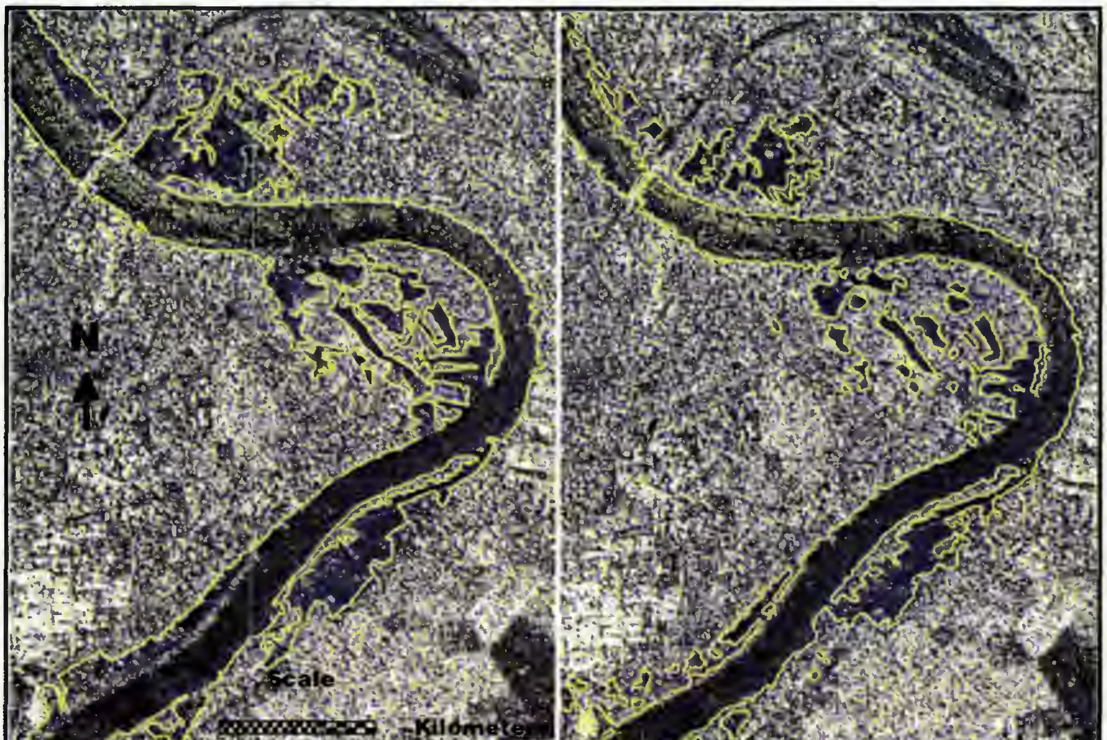

Figure 6: Comparison of the visual interpretation of the ERS-1 SAR data with the EBIS classification result for parts of the testsite Porz (river section near Porz)

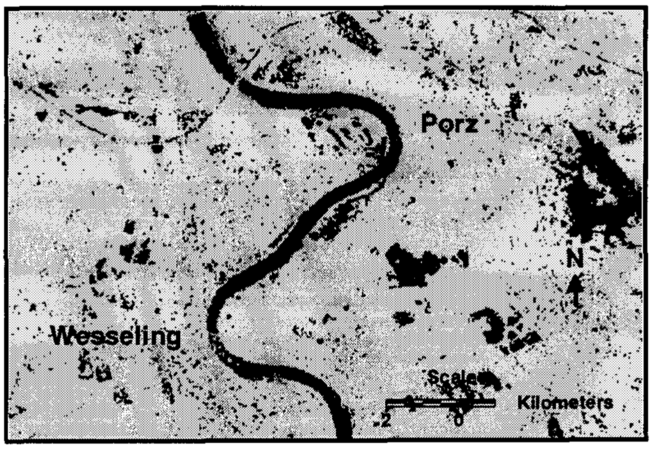

Figure 4: EBIS classification for the testsite Porz

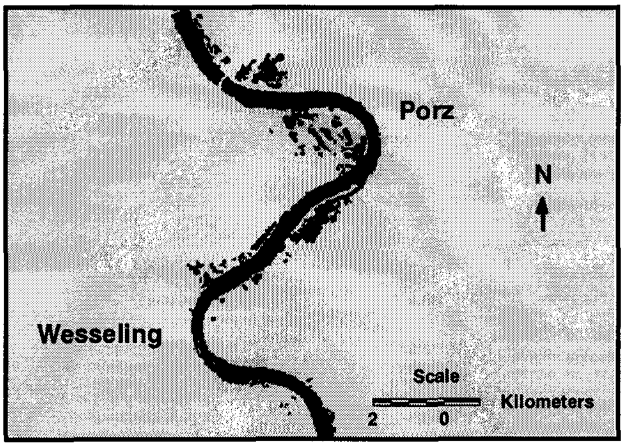

Figure 5: Filter result for the testsite Porz

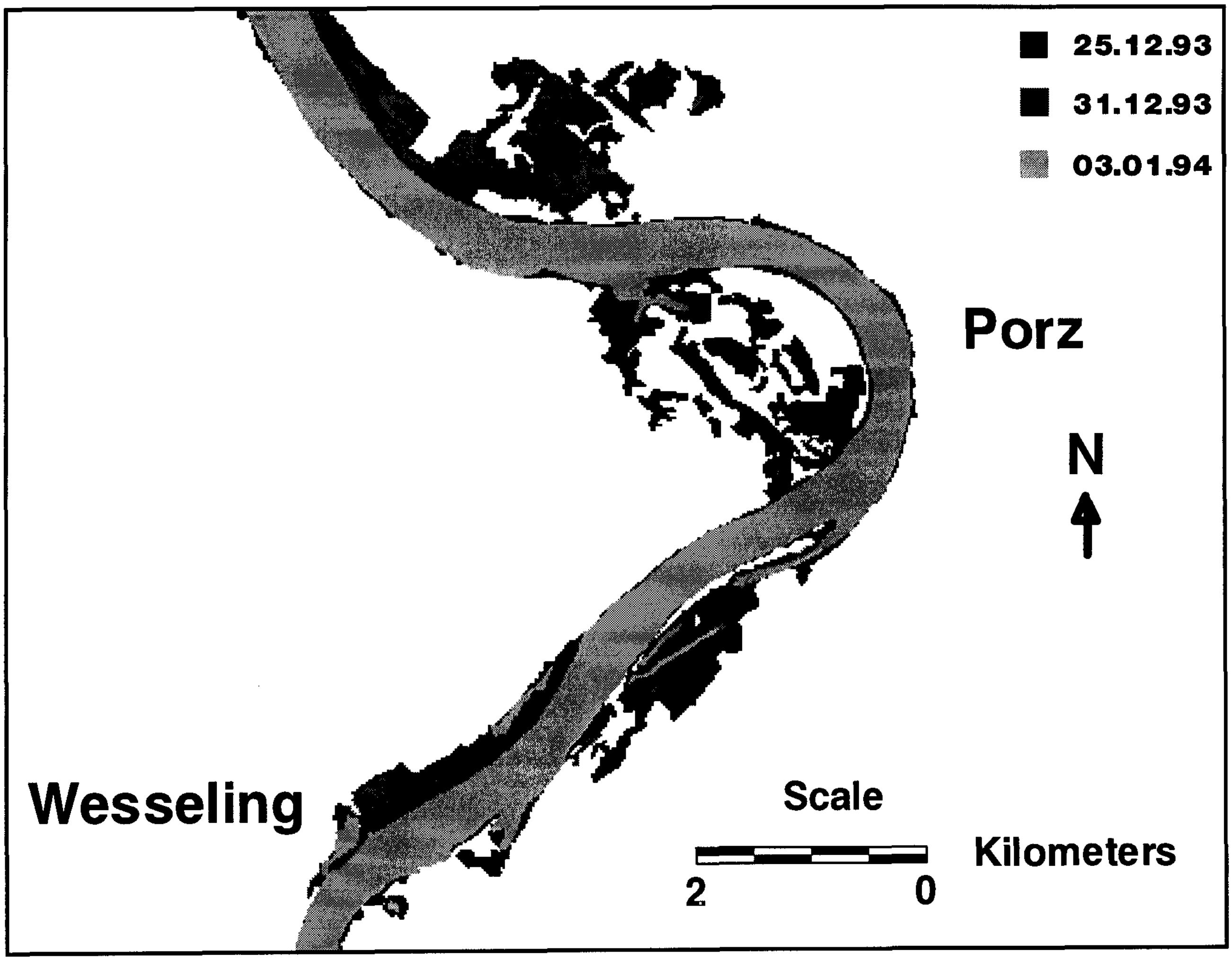

Figure 7: Demonstration of the flood decrease for the testsite Porz

Figure 8: Measurement of the flood-level with ERS-1 SAR data for the left river bank in comparison to the traditional measurement results.

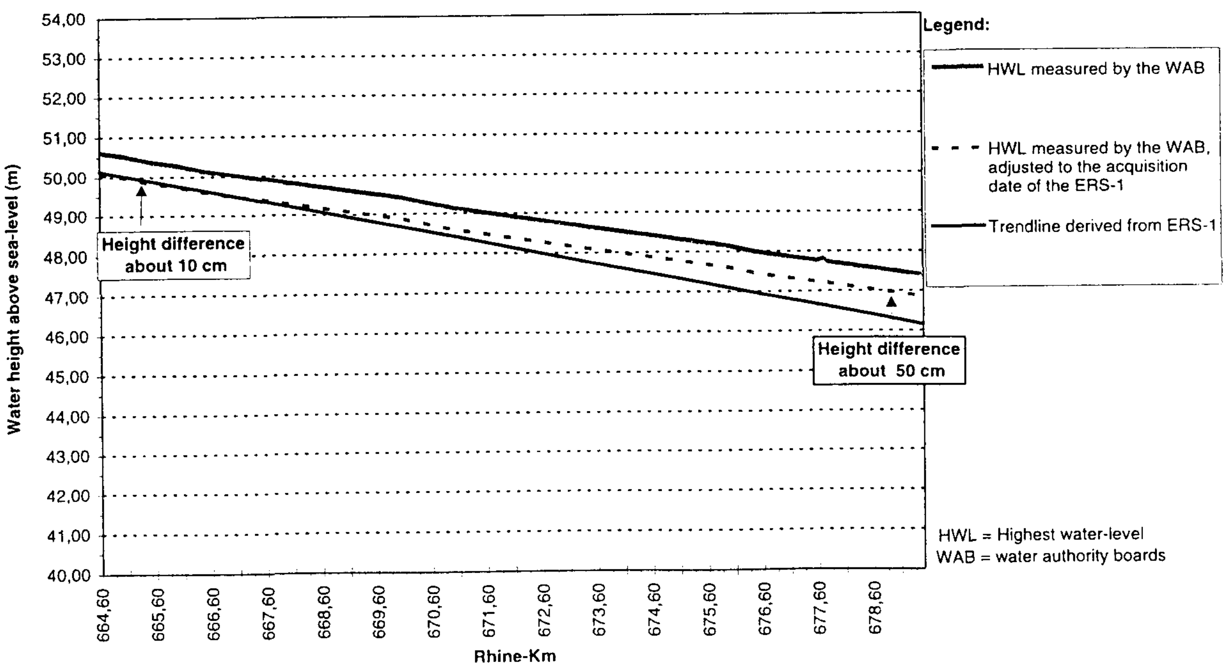

Figure 9: Comparison of the flood-level measurement using ERS-1 SAR data with the traditional measurements for the left river bank. The ranging of the water authority boards has been adjusted to the water decrease due to the time delay of the ERS-1 acquisition date.

GEOLOGY / DEM

Chairman: **M. Doherty**
Rapporteur: **S. Coulson**

A NEW APPROACH TO MAP ACTIVE FAULTS RELATED TO SEISMIC HAZARDS.

EXAMPLES OF THE ATACAMA (CHILE) AND DEAD SEA (MIDDLE EAST) FAULT ZONES

Jean Chorowicz, Cherif Chalah, Pierre Chotin, Catherine Mering, Jean-Paul Rudant & Jean-Claude Vicente

LGGST, Case 129, Paris 6 University, 4 place Jussieu, 75252 Paris cedex 05, France
Tel: (33) 1 44 27 50 89. Fax: (33) 1 44 27 50 85

Yaakov Arkin

Geological Survey of Israel, 30 Malkhe Israel St., Jerusalem 95501, Israel
Tel: (972) 2 31 42 11. Fax: (972) 2 38 06 88

Charles Ichoku & Arnon Karnieli

Ben Gurion University of the Negev, J. Blaustein Inst. for Desert Research, Sede Boker Campus, 84990 Israel
Tel: (972) 7 56 58 74. Fax: (972 7 55 50 58

ABSTRACT

On the example of the Atacama Fault Zone, in Northern Chile, SAR ERS imagery has proved to be operational and particularly convenient for neotectonic studies because it mainly expresses topographic features. In addition, geometry of acquisition is sufficiently controlled to allow estimate of the scarps' heights. SAR ERS data cover large regions and consequently permit extensive observations at regional scale. Active faults are underlined by small steep slopes along discrete scarps. The slope angle can be estimated from intensity values on the radar image. Using this approach, mapping of active faults can be routinely accomplished and is necessary for mitigation of seismic hazards.

1. INTRODUCTION

Large fault zones are the locus of high magnitude earthquakes at shallow or intermediate depth. A fault zone comprises several faults, trending in different directions, along which earthquakes may occur. A given fault or fault segment is sometimes aseismic but nonetheless has to be considered as active because earthquakes occur with long time recurrence (seismic gap), and in this case may be strong. Precise mapping of all the active faults related to a fault zone is essential for mitigation of seismic hazards.

In this paper, we first give the general structural setting of the Atacama Fault Zone (AFZ). We then present visual image analysis of the active fault pattern and describe an approach to estimate scarp heights from radar image. We finally suggest relationships between active faults and steep topographic slope angles.

2. GENERAL STRUCTURAL SETTING OF THE ATACAMA FAULT ZONE

Lying parallel to the coast in Northern Chile (Fig.1), the Atacama Fault Zone (AFZ) is more than 1,100 km long and 30 to 50 km large. In the studied area, there is a seismic gap, and a big earthquake is expected (recurrence one century), but the detailed mapping of active faults is not done.

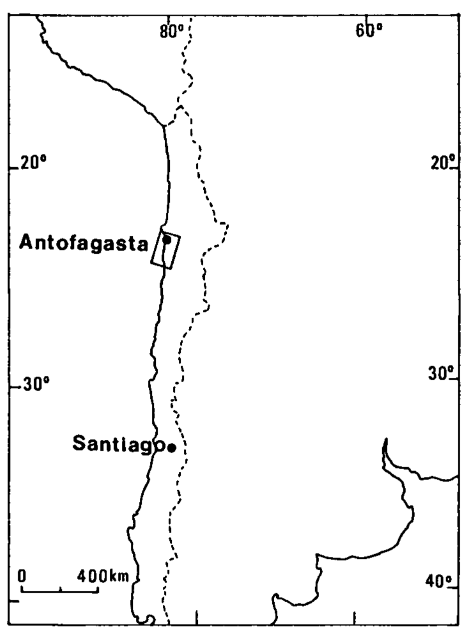

Fig.1. Location of the studied area in Northern Chile.

The Northern Chilean Coastal Cordillera has suffered several tectonic events since the beginning of the Andean cycle in late Triassic time (Turner et al., 1984; Scheuber and Andriessen, 1990; Scheuber and Reutter, 1992; Scheuber et al., 1994; Scheuber, 1994). Since late Miocene, the AFZ has suffered major brittle

Proceedings of the Second ERS Applications Workshop, London, UK, 6–8 December 1995 (ESA SP-383, February 1996)

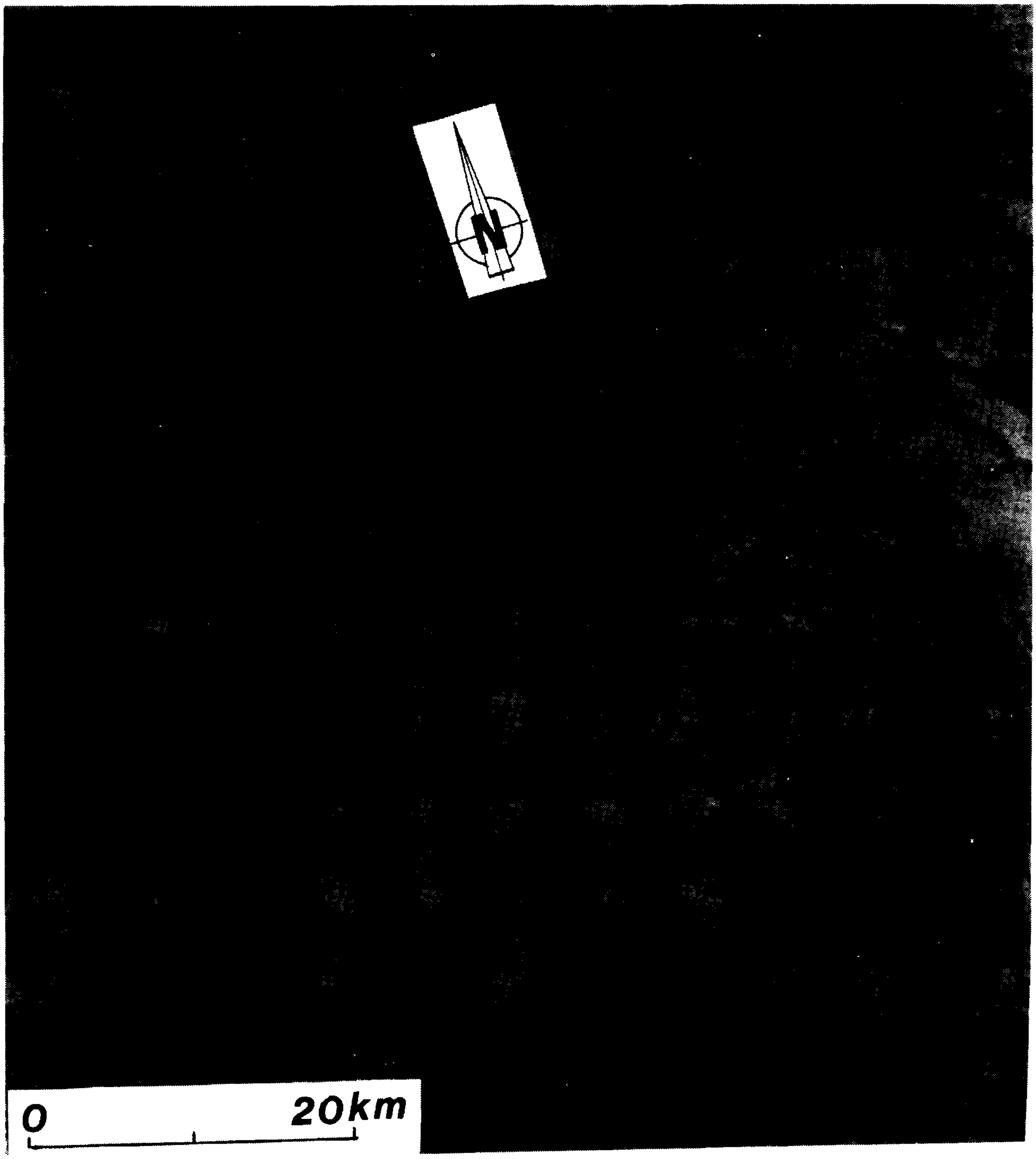

Figure 2. Negative print of ERS-1 SAR scene, acquired in descending orbit, illumination from ESE, displayed at 25 m ground resolution.

reactivations continuing until Present. Since 15 Ma (Alpers and Brinhall, 1988), the climate is hyper-arid and, as a consequence, active tectonic geomorphic features are poorly eroded.

3. MAPPING OF ACTIVE FAULTS BY VISUAL ANALYSIS OF SAR ERS-1 IMAGES

Methodology

We have principally used a set of ERS-1 SAR scenes, in descending orbits, illumination from ESE. We have generated images yielding 25 m ground resolution. Images were produced at 1/200,000 scale, in negative (Fig.2). This type of presentation of the image has the advantage to display in dark the bright slopes facing the radar and affected by shortening and layover effects, giving the impression of shadow. Slopes backing the radar are then clear and give the impression to be illuminated. They are rich in information because generally stretched.

SAR ERS-1 data have synoptic views permitting to describe structures which cover large surfaces. The data provided concern objects of large dimensions and can be considered as complementary to detailed microtectonic field analysis.

Observations

The fault zone (Fig.3) is easterly bounded by the N-striking Remiendo fault, facing east (Okada, 1971). In the east of the region, the fault scarps are ancient because they are eroded and partly buried under recent deposits.

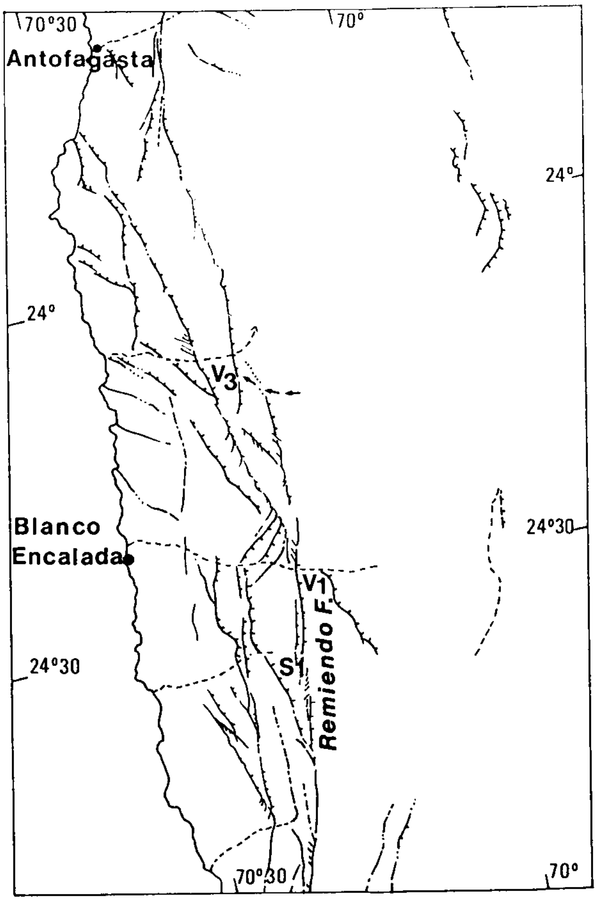

Figure 3. The central part of Atacama Fault Zone, analysed from SAR ERS imagery.

The Remiendo fault cuts a large valley (V1) in which runs a distinct thalweg. Hervé (1987) has examined ignimbrites on the floor of the paleovalley and ash deposits in the detritus fan at the scarp foot. Age determination (K-Ar) yields respectively 19 Ma and 5,5 Ma.

Between locations V1 and S1, the Remiendo scarp is divided into several parallel scarps shaping a ramp system, which generally are associated with normal faulting. To the west, the V3 thalweg seems to be left-laterally offset for 1,3 km.

In the study area active faults can be identified by continuous scarps. Some have been first described by Okada (1971). Active faults are characterised by scarps changing in height along the strike. Many of the faults we have observed on the radar images had been previously partly mapped, whatever their age. However, radar imagery has significantly enhanced the mapping of the active fault system more specifically. There is a number of ancient (lower Cretaceous to early Cenozoic) faults, previously mapped, which are not portrayed on the images (Fig.4). Some relatively recent faults are underlined by distinct scarps, but they also are partly overlain by recent deposits. We classify these faults as 'recent but inactive'.

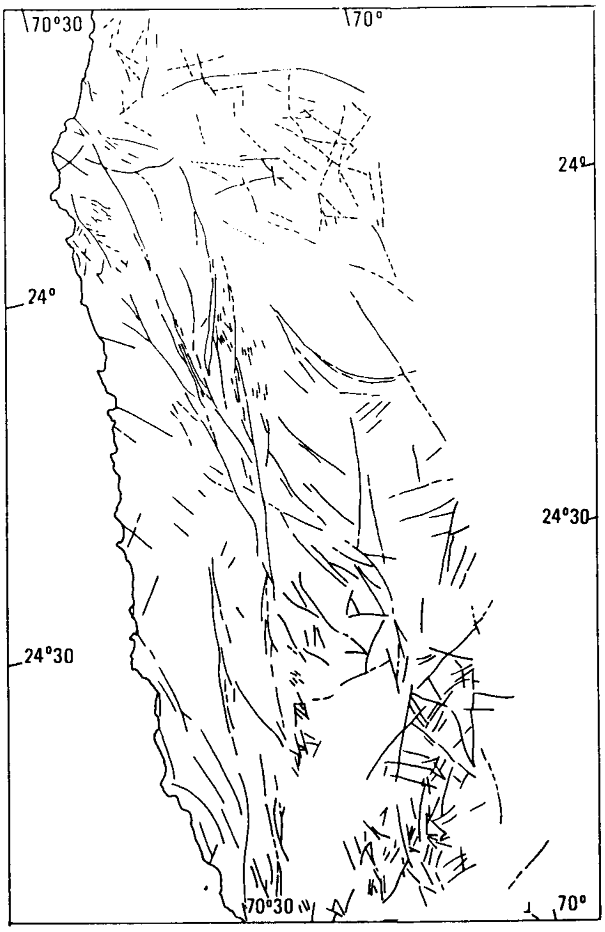

Figure 4. Fault mapping compiled from litterature, including ancient (lower Cretaceous to early Cenozoic) faults which are not portrayed on the SAR ERS-1 images.

The radar system principally displays changes in the relief due to recent (post-Miocene) deformation. It makes the difference between ancient, recent but inactive and active faults. The radar images also show regular back-slopes of large dimensions (10 km in the east-west direction.) which all dip westwards. The back-slopes are principally regular planes of tilted blocks, typical of an extensional regime and we consequently consider that the faults are normal.

4. MEASUREMENT OF THE HEIGHT OF FAULT SCARPS

Original SAR ERS-1 scenes have a pixel size yielding 12.5 m X 12.5 m on the ground. It is well established that changes in intensity of the SAR signal is mainly correlated to variations of the relief. ERS-1 SAR data consequently represent a potentially valuable tool to detect small variations in the topography and to measure the height of fault scarps. In the special case of the north-trending Atacama fault zone, radar illumination is quite at right angle to fault lines, and faces scarps (illumination is from ESE for the descending node images we use). This configuration has allowed us to develop a methodology based on extraction from the image of strongly illuminated slopes, corresponding to fault scarps, forming lines which thickness is related to height.

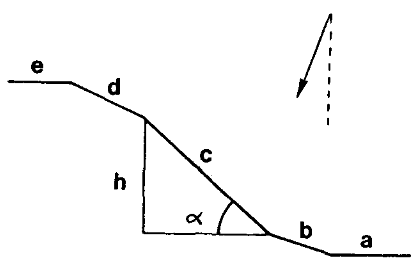

Figure 5. Schematic cross-section of a fault scarp, line segments representing sections of pixels. (a): the footwall; (b): the foot of the scarp where occurs accumulation of detrital deposits; (c): the main fault scarp, almost the fault plane; (d) and (e): the eroded scarp top.

A fault scarp in cross-section can be schematised as in Fig.5, line segments representing sections of pixels. Pixels of the (a) type represent the footwall and are more or less horizontal. Pixels of the (b) type represent the foot of the scarp and have a relatively gentle slope due to accumulation of detrital deposits. Pixels of the (c) type correspond to the main fault scarp, which is almost the fault plane when recent tectonic reactivation has occurred. The dip of fault planes in the studied area is approximately 60°, yielding a mean 50° for the slightly eroded fault scarps. Pixels of the (d) and (e) types have more gentle slopes because they form the eroded scarp top.

Slopes facing the radar are responsible for strong echoes with the greatest amount of retrodiffusion occurring when slope is perpendicular to the radar beam (Ulaby et al., 1982), which corresponds to a 67° angle in the case of SAR ERS-1 scenes (Fig.2). Foreshortening due to distortion accompanies strong echoes. Along segment (c), the foreshortening effect will be then constant, supposing there are not other effects due to roughness and soil moisture variations. Scarps develop generally in a unique terrain, rending roughness constant. Atacama region is very dry and soil moisture can be considered to be very little. The slopes of lower and upper parts of the scarp yield lower radiometry than part (c). Extracting from the image the high values corresponding to part (c), will form long lines. In the case of the Atacama fault zone, we suppose in first approximation that (c) fault scarps have everywhere the same dip and that only the scarp height varies. (a) + (b) and (d) + (e) surface can be considered as invariant, only (c) changes if height varies. In this case, thickness of lines is proportional to height.

Extraction of the fault line from the SAR image (Fig.6a) was obtained from a high threshold of the grey tones. We choose a filtering method which reduces the speckle while restoring the connectivity of thin features. The Connected Centre Filter (Mering and Parrot, 1994). Some white components still remained on the resulting images (Fig.6b). The small ones were eliminated by Geodesic Reconstruction (Serra, 1982), (Fig.6c).

The fault lines were then computed automatically, using a distance function. On a binary image, a distance function is an image transformation which provides for each pixel belonging to connected components, a distance value which corresponds to a distance between the pixel and the edge of the component. Computed distance values form grey levels in a Distance Image, which was calculated by the algorithm of Daniellson (1980). Thickness has been computed using the Distance Image. The maximal thickness (Fig.6d) is the greatest value of the distance function within a connected component. This values is unique and affects all the pixels of the component by means of a Geodesic Dilatation of the Distance Image into the original Binary Image.

A mean value of 650 m seems a reasonable result since scarp dips are generally close to 55°.

5. MEASUREMENT OF SLOPES : EXAMPLE OF THE DEAD SEA FAULT

The above example on the AFZ computes fault height assuming the slope angle (α) of scarp surface is known. However, scarps face radar illumination and are consequently subjected to foreshortening, rending difficult estimate of the slope angle. To compute the slope angle, it would be better to use radar illumination backing the scarp face.

We have observed in positive print a SAR ERS-1 image viewing the Dead Sea Fault Zone (DSFZ) with illumination from ESE, backing active faults scarps located east of the Jordan Valley (Fig.7). There is no foreshortening in this case, and all the slopes are well exposed. Active faults are bordered with dark surfaces which underline steep dipping slopes. As these slopes are located along the fault line, they are interpreted to be poorly eroded and related to recent activity. From the intensity of the dark pixels, and by comparison with

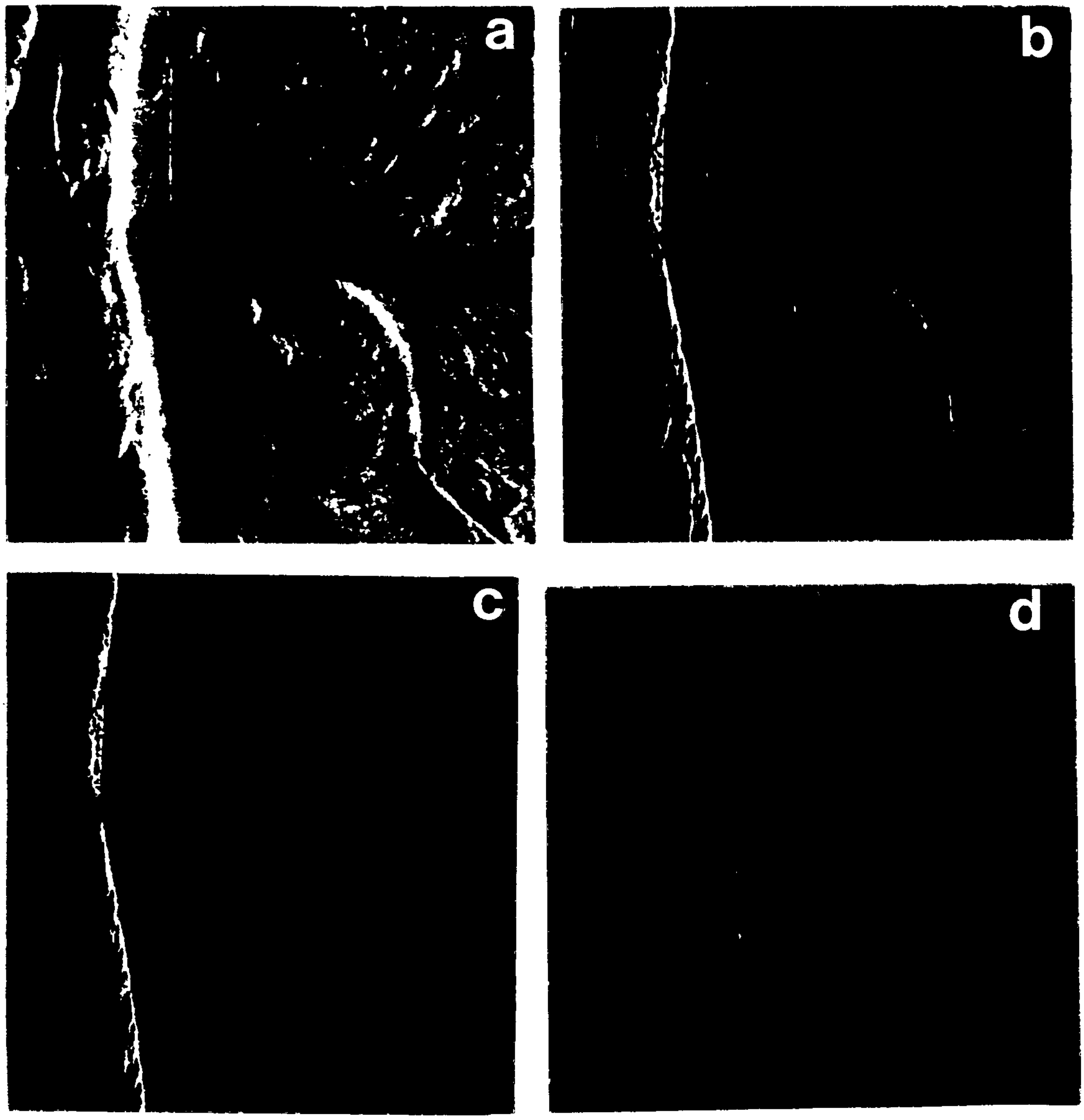

Figure 6. Succession of processes to estimate the height of fault scarp. (a): original SAR image; (b): extraction of the fault line from the SAR image from a high threshold of the grey tones; (c): filtering which reduces the speckle while restoring the connectivity of thin features (Mering and Parrot, 1994), followed by Geodesic Reconstruction (Serra, 1982); (d): Computed distance values forming grey levels in a Distance Image, which was calculated by the algorithm of Daniellson (1980).

surfaces which slope angle is already known, it is theoretically possible to estimate the slope angle. The scarp height can be subsequently computed.

6. CONCLUSIONS

This work is not yet achieved but it gives trends to develop operational mapping of active faults from SAR images. This approach is complementary to the survey of seismic activity.

Radar imagery is particularly convenient because it accentuates topographic features, specially scarps which mainly express neotectonic structures (Franceschetti et al., 1994). In addition, geometry of acquisition is sufficiently controlled to allow estimate of the scarps' height. Cross-orbits images (descending and ascending) are required.

Visual interpretation of SAR images allows mapping of recent faults and their distinction from already mapped ancient faults. Estimate of relief slope angles is the criteria showing active faults. Not yet eroded steep scarp faces may be small, and their size fall under the ground resolution of current Digital Elevation Models (50m). Ground resolution of SAR ERS images, yielding 12,5 m is better and would permit to map a number of these active faults. Mapping can be done extensively because the imagery has a synoptic view.

Identification of active faults using this approach has to be made with precaution for local topographic effects of lithologic contrast may occur. This methodology

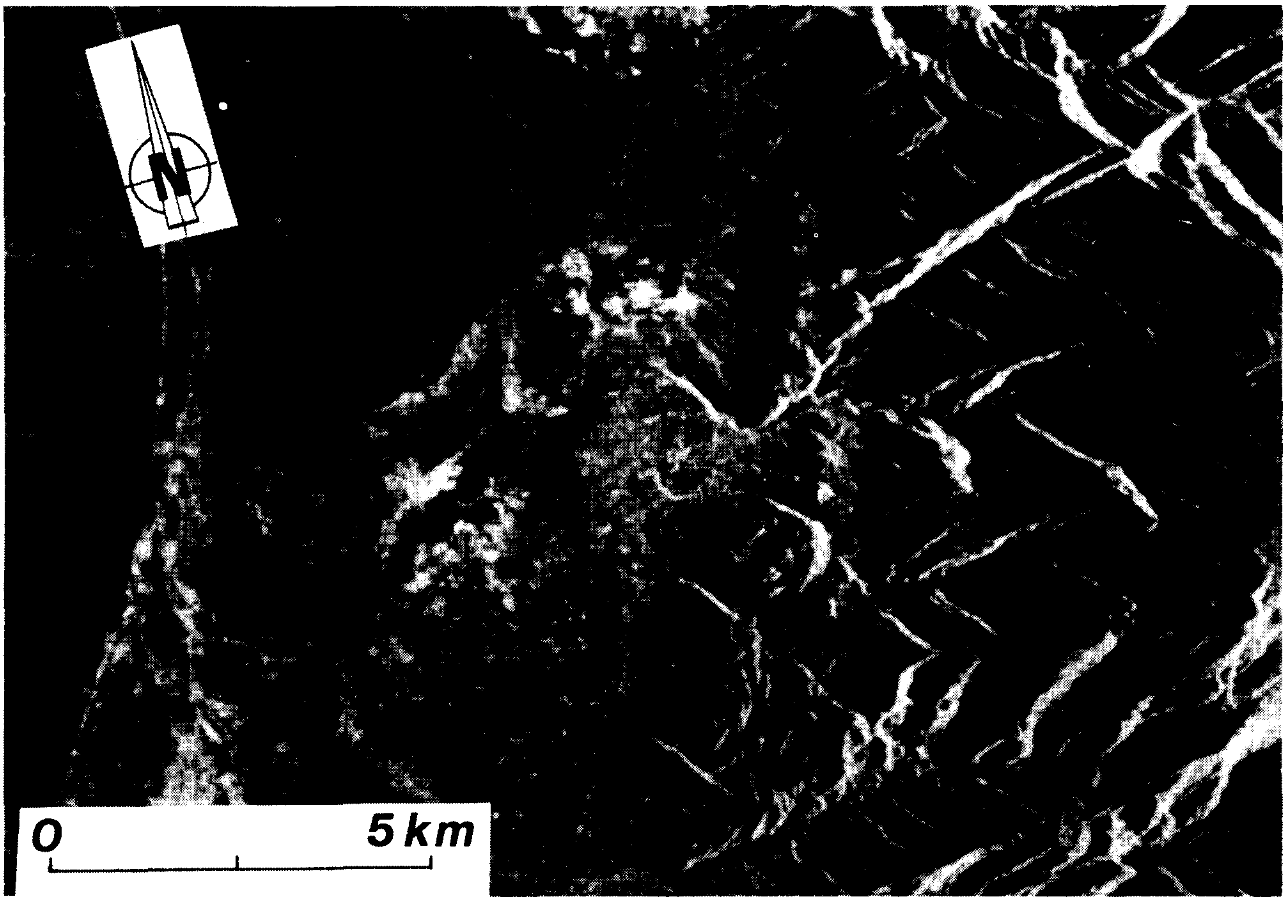

Fig.7. Positive print of a SAR ERS-1 image over the Dead Sea Fault Zone (DSFZ), illumination from ESE, showing dark strips related to active faults scarps located east of the Jordan Valley.

deserves a first research period of testing and evaluation before being routinely applied in highly populated regions, in Europe for instance.

Acknowledgements

This work is being accomplished under projects AOF7 and AO2.F112 of the European Space Agency (Principal Investigator, Jean Chorowicz), and with supports from the Centre National d'Etudes Spatiales and the Israeli Space Agency.

7. REFERENCES

Alpers C.N. & G.H. Brinhal, 1988, Middle Miocene climatic change in the Atacama desert, northern Chile : evidence from supergene mineralization at La Escandita. *Geol. Soc. America Bull.*, 100(10), 1640-1656.

Daniellson P.E., 1980, Euclidian Distance Mapping. *Computer Graphics and Image Processing*, 14, 227-248.

Franceschetti G., R. Marino, M. Migliaccio & D. Riccio, 1994, On SAR simulation on three-dimensional scenes. *SPIE, 2316, SAR data Processing for Remote Sensing*, 192-198.

Hervé, A., 1987, Movimiento normal de la falla Paposo, Zone de Falla Atacama, en el Mioceno. Chile. *Rev. Geol. Chile*, 31, 31-36.

Mering, C. & J.F. Parrot, 1994, Radar image analysis using morphological filters. Mathematical Morphology and Its Applications to Signal Processing, J. Serra and P. Soille (eds), *Kluwer Akademic Publisher*, 353-360.

Okada A., 1971, On the neotectonics of the Atacama fault zone region. Preliminary notes on Late Cenozoic faulting and geomorphic development of the Coast Range of northern Chile. *Bull. Dep. Geography, Univ. of Tokyo*, 3, 47-65.

Turner P., H. Clemmey & S. Flint, 1984, Paleomagnetic studies of a Cretaceous molasse sequence in the Central Andes. Coloso Formation, northern Chile. *J. Geol. Soc. London*, 141, 869-876.

Scheuber E. & P.A.M. Andriessen, 1990, The kinematic and geodynamic significance of the Atacama fault zone, norhtern Chile. *J. Struct. Geol.*, 12(2), 243-257.

Scheuber E. & K.J. Reutter, 1992, Relation between tectonics and magmatism in the Andes of Northern Chile and adjacent areas between 21° and 25°S. *Tectonophysics*, 205, 127-140.

Scheuber E., T. Bogdanic, A. Jensen & K.J. Reutter, 1994, Tectonic development of the North Chilean Andes in relation to plate convergence and magmatism since the Jurassic. In: *Reutter K.J., E. Scheuber & P. Wiggereds*, Tectonics of the Southern Central Andes, Springer, 121-139.

Scheuber E., 1994. Tektonische enwicklung des nordchilenischen aktiven kontinentalandes : der einflub von plattenkonvergenz und · rheologie. *Geotektonische Forschungen*, 81, E. Schweizerbart'sche Verlaysbuch, Stuttgart, 131p.

Serra J., 1982. Image Analysis and Mathematical Morphology. *Academic Press*, London, 411p.

Ulaby F.T., R.K. Moore & A.K. Fung, 1982, Microwave Remote Sensing: Active and Passive. Volume II, *Addison-Wesley*, 607 p.

THE CONTRIBUTION OF ERS1 SAR DATA IN NEOTECTONICS

Yves Cornet & Pierre Ozer

Département de Géographie physique et Quaternaire, Université de Liège, Bât. B11, 2, Allée du 6 Août, B-4000 Liège
Tel: + 32 41 665335. Fax: +32 41 665722

ABSTRACT

In structural geology and geomorphology, the determination of the relationships between various scales of analysis is primordial to insure a coherent interpretation of observed structures. Therefore, it is important to use observation's and interpretation's methodologies that are compatible with the scale of analysis: satellite imagery for the regional scale, aerial photography for local scale and *in situ* meso and micro structural measurements for the meso and micro scales of observation.

On the one hand SAR imagery is a useful tool for the regional recognition of lineations. In the Ecuadorian Andes, where this study has been performed, SAR imagery is nearly only influenced by the geomorphology. Moreover in this country, where cloud cover is quasi permanent, SAR imagery insure the visibility of the earth surface.

On the other hand in such a geomorphological context the typical geometric distortions of SAR images enhance preferentially certain morphostructural features which are also put out of shape. It is then very difficult to stack the layers of information's about structures and particulary lineations localised on SAR images in a GIS.

Nevertheless, regional scale lineations can be recognised on SAR images and can be compared with other kind of analysis, for instance, with local scale lineations. Traditionally these lineations are interpreted in function of their horizontal dimensions. We propose a 3D analysis of these lineations. We discuss the possibility to use SAR remote sensing as input for this kinds of analysis. The main problem of the 3D interpretation is their relative vertical and horizontal dimensions.

The results of regional scale SAR observation and 3D analysis of lineations can easily be confronted with the results obtained at the local or meso scales of observation and with other sets of data like seismic and geodetic data to assess the neotectonical risk.

1. INTRODUCTION

This paper presents a methodological exploitation of ERS1.SAR images and the first results obtained in the Andes (Ecuador)[1]. This research in neotectonics and natural hazards assessment have been realised on an area where 3 hydroelectric dams have been planned or still constructed.

2. THE TEST AREA

The 3 sites are located in the « Cordillera Real » or Eastern Cordillera of the Ecuadorian Andes. This zone crosses the country from north to south (Fig. 1) and is mainly characterised by a magmatic and metamorphic bed-rock (Baldock, 1982). On the western side and eastward, the different morphostructural entities located in the neighbourhood of the Cordillera Real are the Coastal plain, the Western Cordillera, the Interandean Valley. On the eastern side of the Eastern Cordillera, the Sub Andean Zone is located (Tibaldi & Ferrari, 1991).

The morphostructural context of the different zones is presented on the figure 2 and 3. The Ecuadorian Andes are constituting a limnair collision chain (Debelmas & Mascle, 1993) between an insular arc, actually represented by the Western Cordillera and the continental margin of the Amazonian plate actually represented by the Eastern Cordillera and the Sub Andean Zone. The Interandean Valley is a suture zone between the two Cordilleras. This area and its margins are considered as zones with major seismic risks due to superficial earthquakes (D.C. & E.P.E., 1991). This Interandean Valley is a graben covered by a thick layer of undifferentiated basalt and filled by Pliocene and Quaternary pyroclastic deposits (Aspden & Litherland, 1992) resulting from the activity of different volcanoes of the active continental margin or of the suture zone. Some of these volcanoes, the Igualata for instance, were active during the Tertiary. The Chimborazo and the Altar, were active during the Quaternary and the Cotopaxi and the Tungurahua are still active now. The Tungurahua is located on the right side of the Pastaza river near the town of Baños where 2 dams have been planned. Since 1537, 25 eruptions have been registered and the last one was in 1918 (Barberi *et al.*, 1988). The

[1] Pilot Project PP2.B7. The research has been subsidised by the Federal Office for Scientific, Technical and Cultural Affairs (Belgium) and realised in collaboration with the Instituto Equatoriano de Electrificación (INECEL)

slope of this volcano is 37°. The risks of « lahrs » and ashes fall deposits mobilisation or mud flows are very important.

The stress distribution in the area has evolved since the end of the Hercynian cycle. From this moment till the Middle Cretaceous (Albian), the context was extensive. Between the Albian and the Pliocene extensive and compressive periods alternated; the 3 main compressive periods of Upper Cretaceous, Upper Eocene and Upper Miocene - Lower Pliocene have been observed (Debelmas & Mascle, 1993).

Concerning the recent motion of soil and the correlated structural features, Winter and Lavenu (1989) have recognised 4 entities: the Southern Ecuador, Central Ecuador (our test area), Northern Ecuador and Sub Andean Zone.

The Southern Ecuador have been characterised by a Neogene rotation of $\sigma 1$ from N20E till N110E. At the end of the Pliocene and during the Pleistocene, $\sigma 1$ was probably vertical; $\sigma 2$ and $\sigma 3$ were respectively south-north and N140E oriented. During the Pleistocene in an extensive context, Winter and Lavenu (1989) have described a mean vertical motion of 12±6 mm/year.

The Central Ecuador is now characterised by an east-west oriented $\sigma 1$, a vertical $\sigma 2$ and a north-south $\sigma 3$. The result of this orientation of stress axes is an extensive horizontal thrust context reactivating former fracture system. Along the Pallatanga fault, Winter and Lavenu (1989) have shown by geomorphometrical analysis the evidence of a mean horizontal dextral thrust motion of 4.5 mm/year during the 2 last millions of years and 4.4±1.6 mm/year during the last 10000 years.

In northern Ecuador, the compressive context with inverse or horizontal thrust motions has been pointed out (Winter & Lavenu, 1989) since Upper Pliocene.

At least inverse motions are generally observed in the Sub Andean Zone (Winter & Lavenu, 1989).

In this morphostructural context, Hall and Wood (1985) have performed a remote sensing study using one of the rare LANDSAT images with a poor cloud cover. They showed the evidence of 7 north-west/south-east and 1 south-west/north-east oriented lineations. The intersection of last one, the Guayaquil-Pallatanga lineation, and another one, the Pastaza-Esmeraldas lineations, seems to be very important because it could be at the origin of the noumerous earthquakes of Riobamba (Tab. 1)

Date	City	Intensity	Destructions
15/3/1645	Riobamba Baños	IX VIII	Partial destruction Partial destruction
22/11/1687	Ambato, Latacunga, Pelileo et Pillaro	VIII	No information
20/6/1698	Ambato Riobamba et Latacunga	X XI	Total destruction Partial destruction
6/7/1736	Saquisili et Pujili Latacunga	VIII VII	Partial destruction Partial destruction
22/2/1757	Latacunga Ambato, Saquisili et Pujili	IX VIII	Total destruction Partial destruction
10/5/1786	Riobamba	VIII	Partial destruction
4/2/1797	Riobamba	XI	Total destruction (6300 deaths)
15/9/1944	Latacunga et Saquisili	VII	Partial destruction
5/7/1949	Ambato, Baños, Guano, Pillaro et Pelileo	XII	Total destruction of Pelileo (landslide) and important destruction in other areas

Tab. 1: Historical sismicity of the test area.

3. AIMS OF THE STUDY AND METHODOLOGICAL FLOW CHART

We have used and compared 4 observation tools for regional and local geomorphologic analysis: ERS1.SAR.GEC images, SPOT PAN images, 1/50000 topographical maps and 1/60000 aerial photographs. The observations and interpretations realised by these means have been controlled by 2 prospecting campaigns. During these one we performed qualitative geomorphologic controls and mesostructural measurements. In this kind of study, ERS1.SAR data are just a source of data among many other one. The advantages and limits of SAR data have been evaluated in comparison with the other kinds of observation's means in function of the scale of analysis, of the possibility of integration in GIS and of the possibility to submit the collected information's at a computer processing developed in our laboratory and briefly presented in this paper.

The different steps of one methodology are presented on the figure 4.

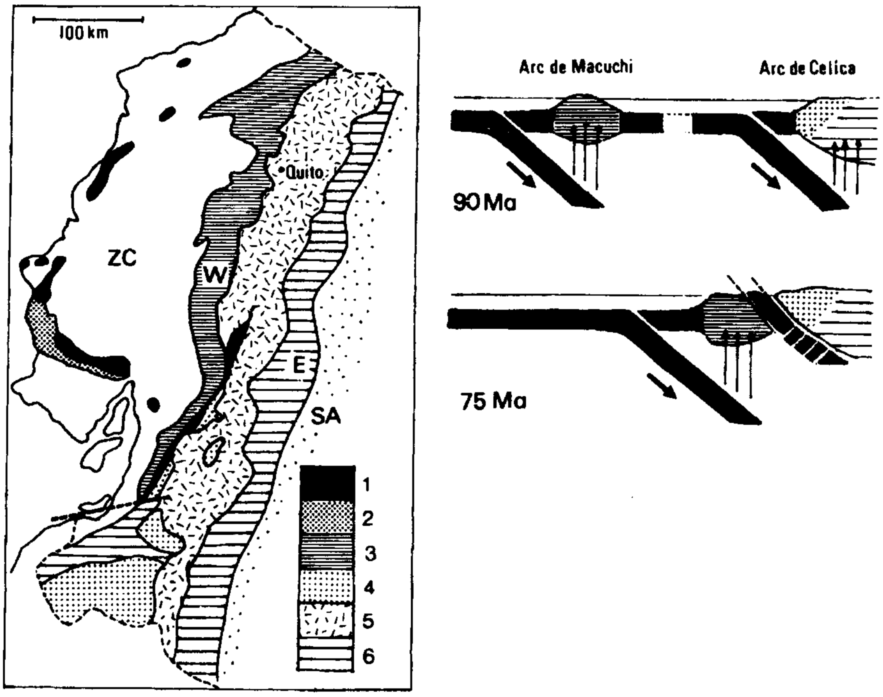

Fig. 2: Morphostructural entities of Ecuadorian Andes and interpretation of the Upper Cretaceous evolution (from Debelmas & Mascle, 1993).

Legend: 1. Ophiolites; 2. Sediment associated with ophiolites; 3. Volcano-detritic formation of Macuchi (insular arc); 4. Volcano-detritic formation of Celica (activ margin of South American plate); 5. Tertiary and Quaternary volcanism; 6. South American Mesozoic and Paleozoic substrate; W. Western Cordillera; E. Eastern Cordillera; SA. Sub Andean Zone; ZC. Coastal zone.

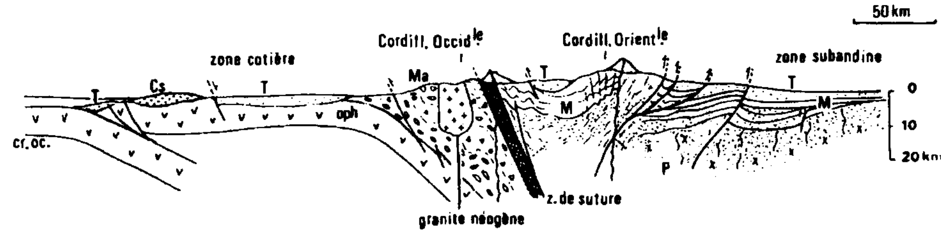

Fig. 3: Geological transect in the Ecuadorian Andes (from Delbelmas & Mascles, 1993).

Legend: P. Precambrian and Paleozoic; M. Undifferenciated Mesozoic; Ma. Macuchi formation (Cretaceous volcano-detritic complex); Cs. Upper Cretaceous; T. Tertiary; oph. Ophiolites; cr.oc. Oceanical crust.

4. DETECTION OF LINEATIONS ON ERS1.SAR IMAGES

The first step of the research is the detection of lineations. This detection have been performed on a mosaic of 2 ERS1.SAR.GEC frames (7413/3627 and 7413/3645). The geocoding of these frames have been done by the D-PAF. The projection of the image in a ground range reference system using 2 different mean heights of projection ellipsoid for the 2 different frames (2384 m for the southern frame and 1879 for the northern one). This height difference have produced deformations and problems during the stitching. The image have then been sigma filtered using a 5x5 window and a 2 σ tolerance. The lineations' detection have been performed analogically and digitised on screen at different scales of observation.

The figure 5 shows an example of full resolution interpretation and the figure 6 shows 2 examples of interpretations at a regional scale.

At the end of the first step of the research we can conclude that:

1. In this area with very frequent cloud cover, 85 % of LANDSAT MSS and TM images sensed between 23/10/72 and 3/5/89 are not exploitable because of cloud cover higher than 40 %. SAR images present than

a great interest in comparison with visible satellite imagery.

2. In area where relief is very accentuated, SAR is mainly influenced by the component of the slope in the range direction. The other bio-geophysical and human influences are negligible. So, SAR images are mainly influenced by geomorphology which is very interesting in comparison with visible satellite imagery and aerial photographs.

3. The SAR images are not exploitable at a local scale of observation because of the distortions induced by the relief. Orientation, location and dimension of the detected lineations in relation are not correct. The observed lineations can not be introduced in GIS. The detection of lineations on SAR images and its integration must be realised by analogical transposition on the map which is most of the time impossible. The necessity of SAR interferometry to realise terrain geocoding of SAR images is then very important to avoid this kind of disadvantage. In effect, the financial cost of the realisation of accurate DEM using other traditional technics on extended area or the absence of topographical maps avoids other alternatives. Moreover, in this kind of study, the realization of a DEM reduces the interests of SAR images.

4. At the regional scale of observation, geometrical distortions induced by the relief become negligible in confrontation with the great extension of observed lineations. The SAR can then be useful to detect regional scale structures but traditional technics used for visible imagery (directional filtering for instance) can not be used. The contextual interpretation must be realised because of the influence of the orientation of the structure in comparison with the look direction (Fig. 7): V shape converging in the antenna direction for the crest lines oriented in the range direction and V shape converging in the opposite direction for the also valley oriented in the range direction. We observed for instance the prolongation of the Guano fault (Fig. 6) on the right side of the Rio Chambo along the Rio Blanco. This area have been prospected during the terrain campaigns. Broken pebbles and fine sediments filling fractures in Pleistocene fluvioglacial deposits have been observed. The hypothesis of a probable recent motion is then demonstrated in the Rio Blanco area (Ozer *et al.*, 1994).

5. 3D ANALYSIS OF LINEATIONS: COPLANARITY TEST

Traditionally the interpretation of lineations is performed in function of their 2D distribution. In 1992, Eliason has proposed a geometrical and statistical technics which allows the exploitation of the vertical dimension to realise an interpretation of the structural signification of lineations. The computational technics we suggest in this paper is based on the publication of Eliason (1992)[2]. It allows the elimination of the 2π ambiguity and the comparison of regional and local scale observations with observations realised *in situ*, for instance with mesostructural measurements collected at the scale of the outcrop.

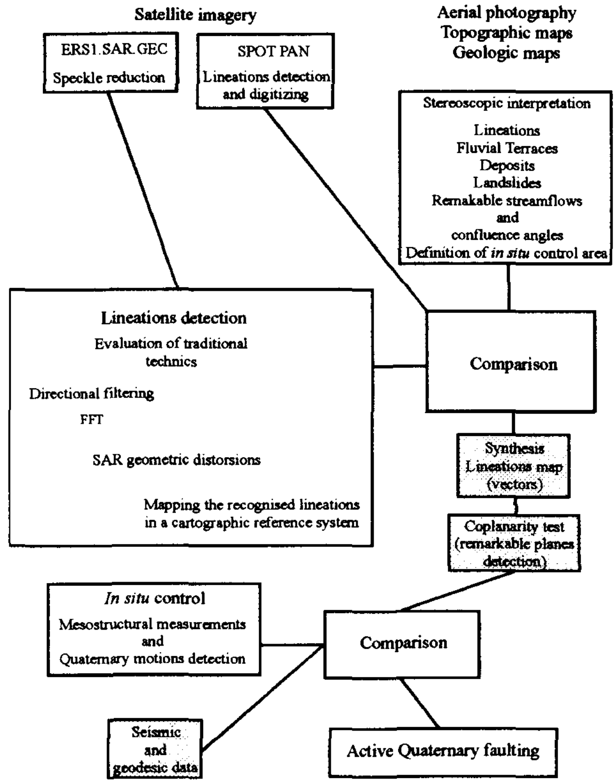

Fig. 4: Methodological flow chart.

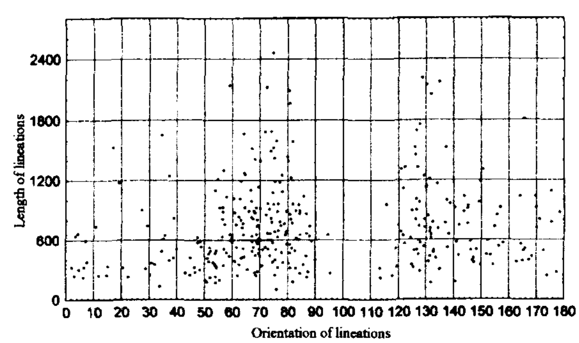

Fig. 7: Diagram showing the characteristics (length and orientation) of the lineations digitised on the subset of the figure 5. The perception of some lineations is enhanced on SAR images in function of their direction regarding the range.

[2] We thank Dr. A. Demoulin of our laboratory for the noumerous advices he gave to us to insure a correct integration of structural and geomorphological concepts in the analysis and the development of the algorithm presented in this paper. We also thank Dr. W. Mees of the Royal Military Academy for the control of geometrical and statistical analysis realized for the development of the coplanarity test algorithm.

Data set description

The data on which the coplanarity test is applied is a set of N lineations represented by N vectors defined by their extremities $[(X_1,Y_1,Z_1)\ ;\ (X_2,Y_2,Z_2)]$ and determined by satellite images, aerial photographs and topographical maps interpretation. All co-ordinates are given in a cartographic reference system (UTM for this study) (Fig. 8).

Principles of the coplanarity test algorithm

The coplanarity test algorithm is based on 4 successive subroutines (Fig. 9):

1. PLANSTA computes the equations of the 4 planes that can be find combining 2 vectors or 4 points (defining 2 vectors) 3 by 3.

2. COPLANA2 (simple coplanarity or 2 by 2 coplanarity test algorithm) computes the angle between each vector of which only one point has been used to define the corresponding plane and the normal vector of this plane. For each combination of 2 lineations, 4 angles can be computed. If at least one of these angles is higher then $90°-\alpha$ and lower than $90°+\alpha$, the coplanarity of the 2 lineations is accepted. α is a given tolerance. This routine determine a coplanarity of 2 lineations (Fig. 10).

3. PLANMOY1 computes the equation of the mean plane corresponding to each case of simple coplanarity.

4. COPMULTI (multiple coplanarity or coplanarity test applied to more than 2 lineations) computes the angle between the normal vector of each plane determined by PLANMOY1 and all the lineations that have not been used to define this plane. If the angle is higher then $90°-\beta$ and lower than $90°+\beta$, the coplanarity of the considered lineation and plane is accepted. β is a given tolerance.

After this step, a mean plane is defined by PLANMOY1 on the basis of the different lineations which are considered as coplanar after the execution of COPMULTI.

For instance, the results of this coplanarity test can be presented in a Schmidt canvas after a Lambert projection of the inferior hemisphere poles (Wallbrecher, 1986) of each plane obtained after the last execution of the PLANMOY1. The figure 11 shows such a representation for the 104 lineations of the figure 8 after the application of the coplanarity test using 2° for both α and β.

Interpretation of the results of the coplanarity test

Firstly we observe that the mean plane trends to become more horizontal when the number of coplanar lineations increases. This is due to the fact that the higher the number of lineations the higher is the horizontal dispersion in comparison with vertical variation. This observation suggests that the coplanarity analysis must be performed in area where the relief is accentuated and at a local scale of observation: the lineations that induce the detection of near vertical planes have a little horizontal component in comparison with their vertical component. These two facts of observations are in disagreement with the conditions for SAR images exploitation's to detect lineations to be submitted to our test.

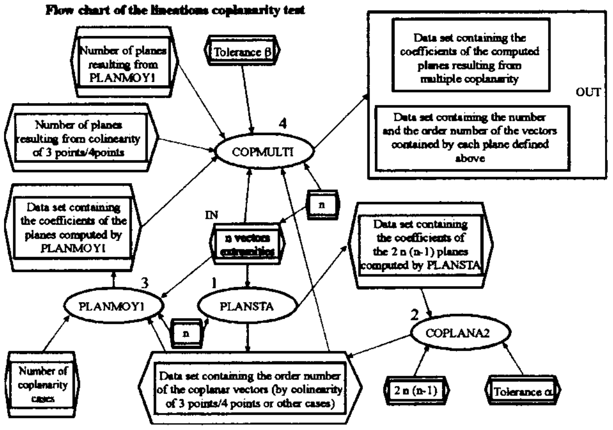

Fig. 9: Flow chart showing the structure of the coplanarity test.

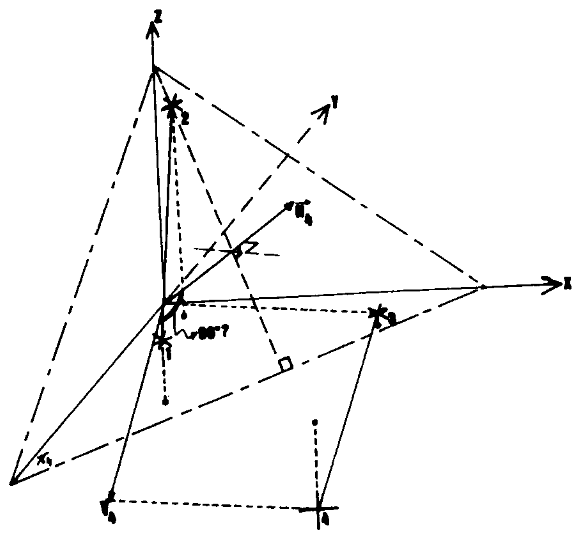

Fig. 10: Principles of the coplanarity test.

Secondly, regarding the geomorphological point of view, independently of the number of lineations belonging to each plane, we observe that the number of planes with southward dip direction are more numerous and characterised by lower dip value than the plane with a northward dip direction. This is the result of the choice of a test area which is located asymmetrically in confrontation with the direction of the main river, the Pastaza; the second possible explanation is the more frequent case D of the figure 12. The interpretation of such a chart is than not only based on structural influences like those described on the figure 12 but also by geometry of the catchment which can be influenced by several hydrological and other factors.

The discrimination between the different influences and the comparison with *in situ* mesostructural measurements is now being performed in our laboratory.

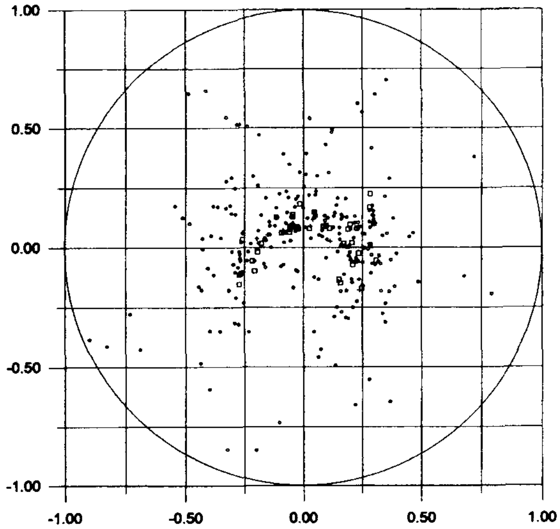

Fig. 11: Stereogram representing the poles of planes in a Schmidt inferior hemisphere canvas after Lambert projection. O: less than 4 lineations in the plane; □: 4 lineations; +: 5 lineations; Δ more than 5 lineations.

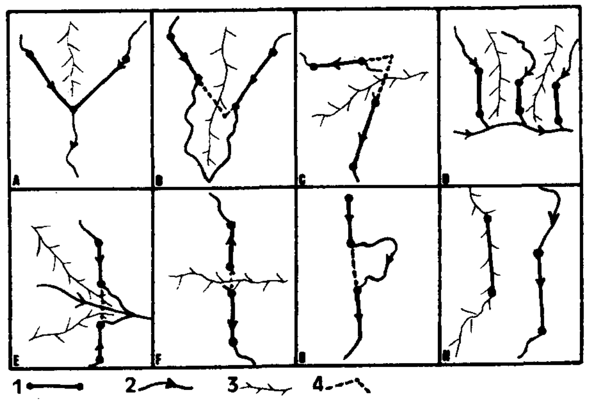

Fig. 12: Geomorphological signification of different kinds of lineations' coplanarity. 1. Lineations; 2. Rivers; 3. Crest lines; 4. Prolongation and 3D intersection of lineations.

6. CONCLUSION

The conditions of exploitation, advantages and disadvantages of ERS1.SAR are evaluated in this conclusion regarding the other kinds of observation's means in function of the scale of analysis, of the possibility of integration in GIS and of the possibility to submit the collected information's at a computer processing developed in our laboratory, the lineations' coplanarity test.

Advantages

1. The influence of the morphology is predominant on SAR images of area where relief is very accentuated.

2. SAR images are favourable for the little scale (regional scale of observation) detection of structural features.

3. In the meteorological context of Ecuador, SAR images are not weather dependent.

Disadvantages

1. Geometrical distortions avoid the exploitation of SAR images to realise local scale interpretation and lineations detection. The terrain geocoding is necessary but the realisation of accurate DEM is economically and technically impossible at a regional scale and should destroy any interest of SAR data. SAR interferometry is the only way to get accurate data that can be introduced in GIS and compared with other kinds of information's or submitted at the coplanarity test. In effect, this test induces a non linear propagation of errors and can only be applied in area characterised by very accentuated relief. The accurate precision of lineations' location is then very important.

Conditions of exploitation

1. The image processing technics used to realise the interpretation of visible images are not applicable on SAR images.

REFERENCES

Aspden J.A. & Litherland M., 1992, The geology and Mesozoic collisional history of the Cordillera Real, Ecuador. *Techtonophysics*, 205, pp. 187-204.

Baldock J.W., 1982, Geologia del Ecuador. Boletin de la explicacion del Mapa Geologico de la Republica del Ecuador, escala 1:1000000. Quito, DGGM.

Barberi F. , Coltelli M., Innocenti F., Navarro J.M. & Santacroce R., 1988, Plio-Quaternary volcanism in Ecuador. *Geol. Mag.*, Great Britania, 124, pp. 1-14.

D.C. & E.P.E., 1991, Mapa sismotectonico del Ecuador. Escala: 1:1000000 & Memoria explicativa. Quito, 47 p.

Debelmas J. & Mascle G., 1993, Les grandes structures géologiques. Ed. *Masson*, 299 p.

Eliason J.R., 1992, Mapping fractures remotly for earthquake hazard assessment by the use of topographic and seisms hypocenter data. *Episodes,* 15, 1.

Hall M.L. & Wood C.A., 1985, Volcano-tectonic segmentation of Northern Andes. *Geology*, 13, pp; 203-207.

Observatorio Astronomico de Quito, 1959, Breve historia de los principales terremotos en la Republica del Ecuador. Ed. *Observatorio Astronomico de Quito*, 37 p.

Ocola L.(Organizacion de Estados Americanos & Centro Regional de Sismologia para America del Sur), 1984, Proyecto de sismicidad andina SISAN. Voluman III: Catalogos sismicos: Republica del Ecuador, *Instituto Geofisico del Peru*, Lima, 152 p.

Ozer P., Cornet Y., Moreno A. & Ozer A., 1994, Natural risks evaluation by remote sensing: lineaments research in the Pastaza bassin (Ecuador). *Proc. of the First ERS1 Pilot Project Workshop*, 22-24 June, Toledo, Spain, pp. 205-209.

Tibaldi A. & Ferrari L., 1991, Multisource remotely sensed data, field checks and seismicity for the definition of active tectonics in Ecuadorian Ande. *Int. J. remote sens.*, 12 (11), pp.2343 -2358.

Wallbrecher E., 1986, Tektonische und analitische Arbeitsweisen. Ed. F. *Enke Verlag*, Stuttgart, 244 p.

Winter T. & Lavenu A. ,1989, Tectonique active en Equateur: Ebauche d'une nouvelle interprétation géodynamique », *Bull. Inst. Fr. Et. And.*, 18 (1), pp 95 - 115.

Winter T., 1990, Mécanisme des déformations récentes dans les Andes équatoriennes. *Thèse de doctorat, Université de Paris-Sud, Centre d'Orsay*, 167 p.

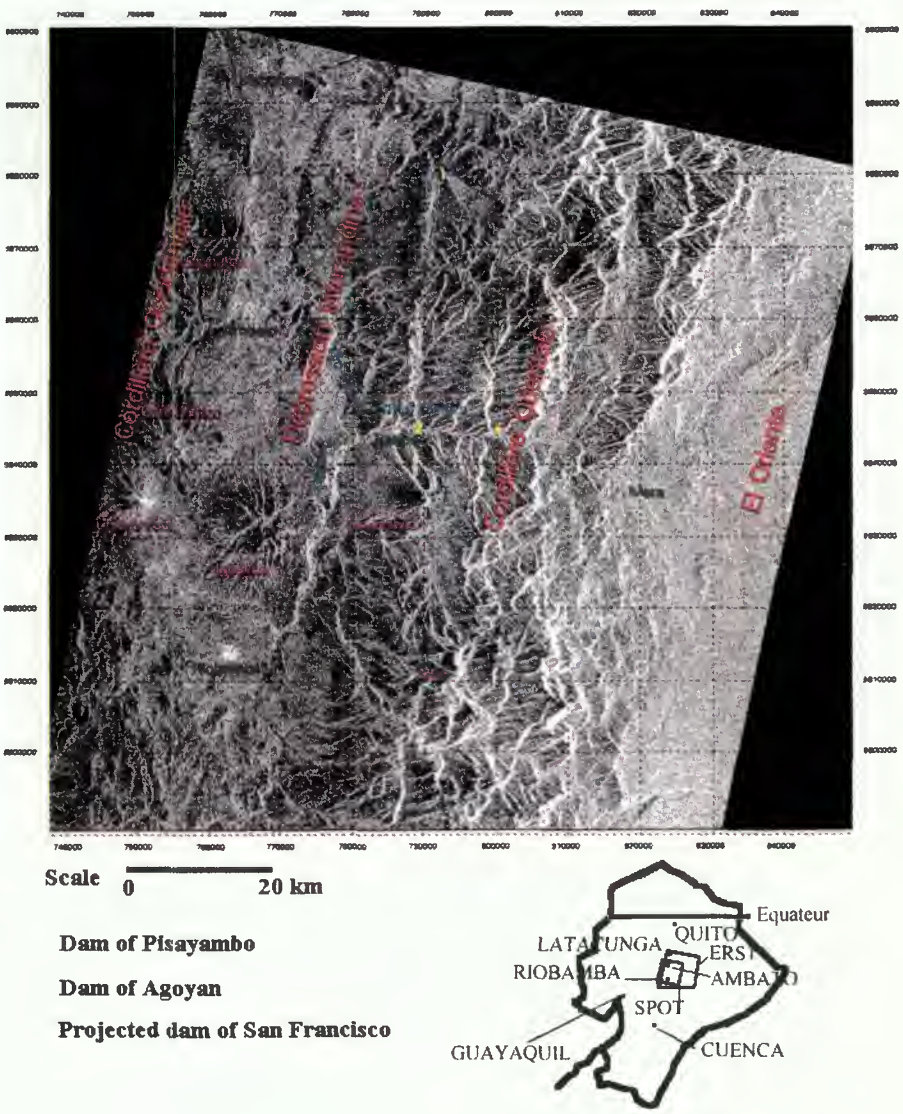

Fig. 1: ERS1.SAR.GEC mosaic of the test area.

Fig. 5: Full resolution interpretation of a 1024x1024 pixels subset of the SAR mosaic (Baños area). In white: the digitised lineations. In the central part of the subset we can observe the Rio Pastaza flowing eastward. The contextual V shape rule (see text) is well illustrated by the apparent disposition of the affluents of the Pastaza (mainly by the high gradient of the first order affluents).

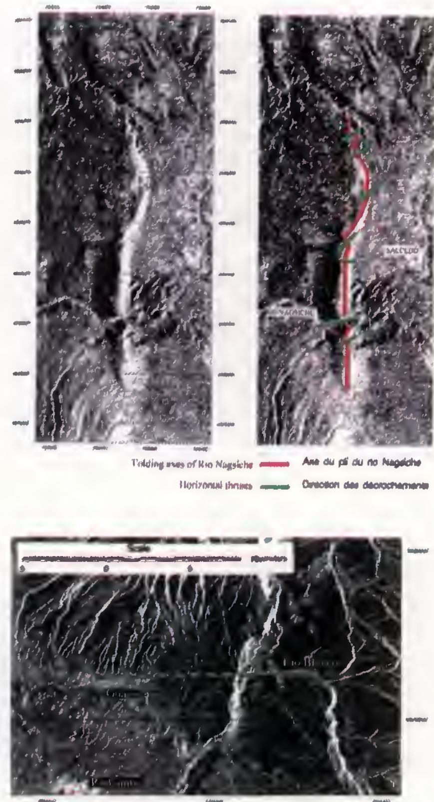

A.

B.

Fig. 6: Two examples of analogic interpretation of SAR frames. A. Western border of the Interandean Valley: Red line: folding axe of Rio Nagsiche; Green line: probable horizontal thrust. B. Red line: the well known Guano Fault and its prolongation along the Rio Blanco observed on the SAR image and, as shown by *in situ* observations, probably active during the Quaternary.

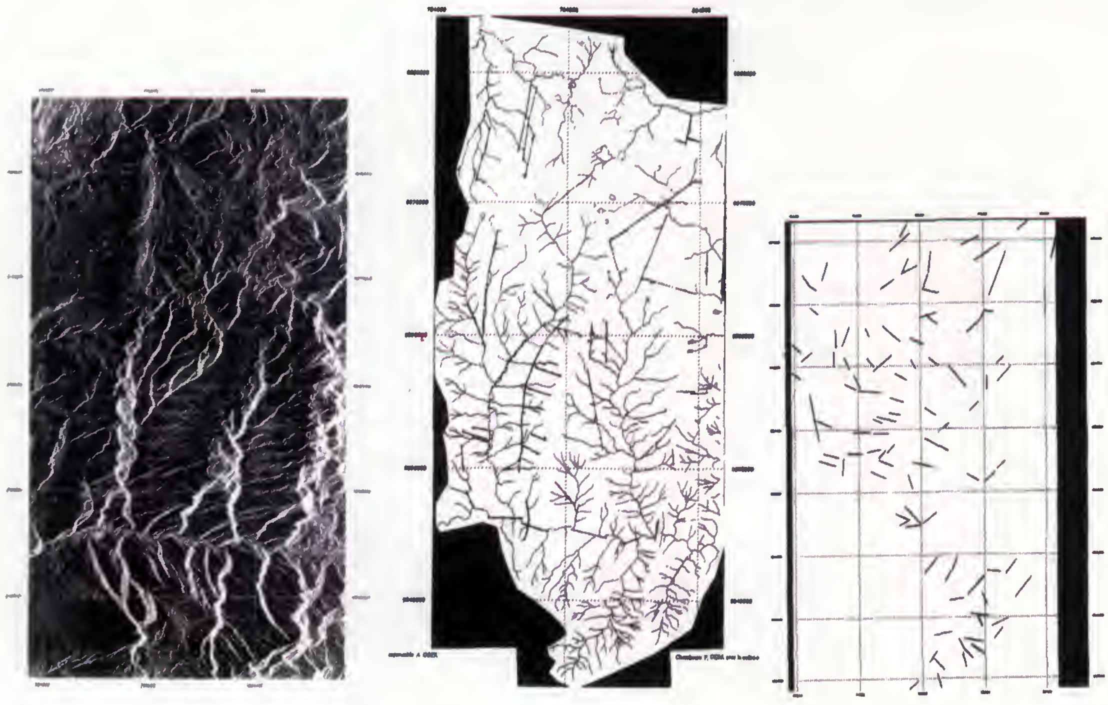

A. B. C.

Fig. 8: Coplanarity test area. A. SAR image; B: Hydrographical network and particularities; C. Data set of lineations.

ERS-1 GEOLOGICAL APPLICATIONS

M. Antoninetti (*), R. Loizzo (§), M.Pappalepore (#), P.Pieri (#), G. Sylos Labini (§)

* IRRS-CNR, Via Ampere 56, 20131 Milano, Italy
(Tel.+39.2.70643662, Fax +39.2.70643660)
§ ASI/CGS Loc.Terlecchia P.O. Box 11, 75100 Matera, Italy
(Tel.+39.835.377201-222-215-211, Fax +39.835.339005)
Dep.Geology and Geophysic, Via Orabona 4, 70100 Bari, Italy
(Tel.+39.80.5442571-5442633, Fax+39.80.5442625)

ABSTRACT

This work is part of a larger Pilot Project presented during the first ESA Workshop on ERS-1 Applications held in Toledo on June '94 [1].
Results obtained by the analysis of ERS-1 data in geological investigations, compared with the ones from optical LANDSAT TM data are reported. Multitemporal ERS-1 images acquired in ascending and descending orbit have been selected on the test site known as "Fossa Bradanica" (Southern of Italy). Since this area is a mountainous region ERS-1 Geocoded Terrain Corrected data provided by the Italian Processing and Archiving Facility (Matera, Italy) has been required.
A large analysis on the data set has been carried out, either by photointerpretation or by automatic image processing techniques.
In a first step a visual tectonic lineaments detection has been performed on the SAR images. Lineaments obtained have been represented as rose diagrams and then compared to the ones obtained from Landsat TM data acquired on the same test-site and in the same season.
In the second step the data set has been used in a lithological classification. At this purpose LANDSAT TM data alone and multisensor integrated data set has been analyzed with a Maximum Likelihood Classifier.
Either in lineament detection or in lithological classification the results obtained shown a very interesting complementarity between ERS-1 and LANDSAT TM data for geological applications.

1. INTRODUCTION

The main objective of this work is to evaluate the possibility to use different remotely sensed data in geological investigations. We intend particularly to evaluate the contribute of ERS-1 data in geomorphological inspections, lithological mapping and lineaments mapping.
In fact whereas the optical data analysis in geological investigations are well consolidated, the use of SAR images in this field has to be more investigated, improving the techniques for SAR image analysis and interpretation.

2. TEST AREA

The study area is the southern part of the foredeep of the Apennine chain that is a deep elongated in NW-SE direction. The eastern margin of the Bradanic trough is represented by the Apulian foreland and the western zone is formed by the thrust sheets of the Apennine chain. This chain is a Neogene orogenic belt.
Holocenic alluvial deposits are present in the coastal zone of the region and along the river bed. They are prevalently formed by clay and sandy clay. Forward the hinterlands a series of marine terraces, mostly cut into the sedimentary fill of the Bradanic through, are present. They are considered as a record of the interference between tectonic uplift and successive late Pleistocene transgressions-regressions of glacio-eustatic origin. These terraces, developed in interfluvial areas, are formed by sand and conglomerates. There is also the marly and silty clay of the Bradanic sequence [2].
Vegetation cover is typical of the Mediterranean regions. The coastal zone is characterized by the presence of conifer forest along the dune's belt. Cropland, orchards, vineyards, olives, vegetables are well distributed either on the alluvial sediments or on the marine terraces. The hinterland presents clays partially covered by Mediterranean scrubs.

3. DATA SET AND ANALYSIS

The available data set on the test area consists of optical LANDSAT TM and ERS-1 images acquired in different seasons. Since the SAR images present distortion of the real structures due to the side looking radar, the use of Geocoded Terrain Corrected data (GTC) is necessary to compare the ERS-1 information with the ones from the different sources (optical data, cartography, ground truth). In this work ERS-1.GTC products, provided by the Italian Processing and Archiving Facility (I-PAF), have been considered and registered with the georeferenced optical data.

The LANDSAT TM data set is the following:

2 January '92
28 May '93
21 July '93.

The ERS-1 data set that includes images acquired both in ascending and descending orbit is the following:

24 November '92	Descending Orbit
18 May '93	"
27 July '93	"
14 November '92	Ascending Orbit
12 June '93	"
21 August '93	"

The data analysis has been carried out in two steps:

- LINEAMENTS DETECTION
- LITHOLOGICAL CLASSIFICATION.

In these two phases not all the data set has been considered, but the best images have been selected depending on the kind of application considered.
Because of the higher topographic enhancement of the winter LANDSAT TM image, the lineaments detection has been performed only on the data acquired in this season for the ERS-1 data too. The lineaments are detected by visual interpretation considering all the structural alignment, purged of others linear structures corresponding to natural vegetation or lithological linear boundaries, anthropic structures etc... .
On LANDSAT TM data the detection has been accomplished on different band combination, but the band 7 alone resulted the more significant thanks to its brightness. On ERS-1 images several filters, aimed to eliminate the speckle effect, have been applied to check their usefulness in tectonic studies, but the results have shown a contrast decrease and, consequently, a worse visual identification of lineaments. So for lineaments detection on ERS-1 images no filter has been applied
The lineaments observed on optical and SAR data have been analyzed and compared, considering their statistical distribution. The interest is focused on the statistical significance of the lineaments' pattern as a whole rather than an interpretation of individual lineaments. This method statistically minimizes errors and incongruities arising from subjective manipulation.
The frequencies of the identified elements are graphically represented as rose diagrams in which the azimuthal field has been divided into eighteen angular sectors 10° each (Fig. 1-3). Moreover the lineaments' length has been taken in account grouping them in three classes: the first for lineaments less than 3 Km long, the second for lineaments having length between 3 Km and 6 Km, the last for the ones longer than 6 Km.

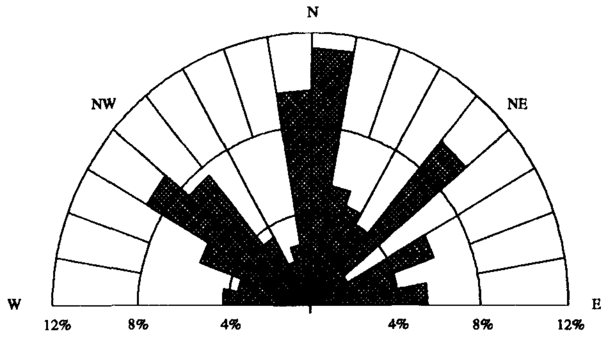

Fig. 1. Rose diagram representation of Landsat TM lineaments detected by visual interpretation.

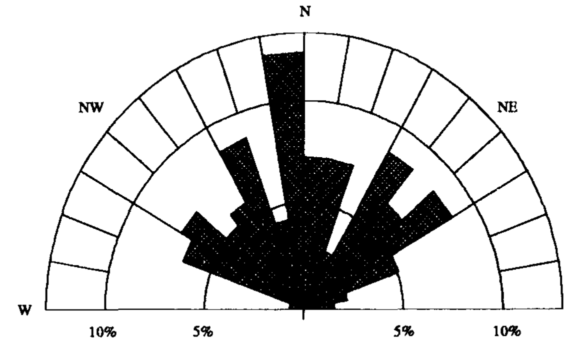

Fig. 2. Rose diagram representation of ERS-1 descending orbit lineaments detected by visual interpretation.

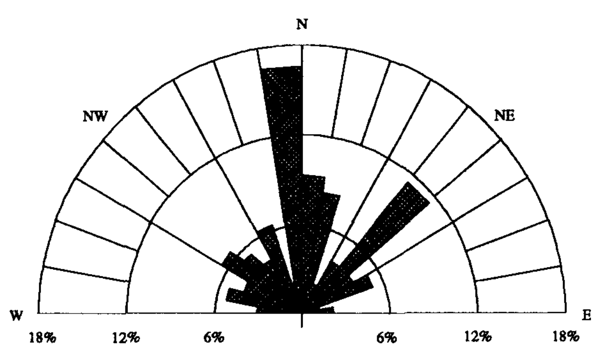

Fig. 3. Rose diagram representation of ERS-1 ascending orbit lineaments detected by visual interpretation.

In the second phase of the image analysis the feasibility of a statistical approach in automatic classification of lithological units using ERS-1 and LANDSAT TM data has been evaluated.
To select the best date for this kind of application the vegetation cover and the sunlight elevation have been taken in account. In fact the vegetation cover represents an obstacle to the correct classification of the

lithological units. Moreover the shadowing effects make confused the signatures.
On the LANDSAT TM images the NDVI (Normalized Differential Vegetation Index) has been calculated and used to mask the vegetated area. The most indicated image for the lithological classification resulted that acquired in the summer. In fact on this image the signatures were very homogeneous and the percentage of non masked pixels, corresponding to bare soils, was about the 55%. The summer LANDSAT TM image has been considered alone and integrated with the ERS-1 images acquired in the same period both in ascending and descending orbit. Before the integration ERS-1 images have been resampled at the same resolution of Landsat TM (30m) and filtered for speckle suppression with a local region filter on 5x5 windows [3]. The signatures corresponding to various lithological units have been extracted on the two data set and evaluated considering the confusion matrix calculated by a Maximum Likelihood Classifier (Tab. I, Tab. II).

4.RESULTS

The total number of lineaments observed is 147 on the LANDSAT TM image and 139 and 97 on the ERS-1 in ascending and descending orbit respectively.
The LANDSAT TM rose diagram show three principal statistical trends. The dominant trend is in the N-S direction (350°-10°) with lineaments prevalently having intermediate length, while the other two peaks are in the NW-SE direction (300°-320°) with lineaments longer than 6 km and in NE-SW direction (50°-60°) with very short lineaments.
The ERS-1 descending orbit lineaments show principal trends quite similar to the LANDSAT TM ones even though there are two peaks in NW and NE directions.
Also in the ERS-1 ascending orbit rose diagram there is a predominant trend in N-S direction (350°-10°), representing lineaments prevalently having length among 3 and 6 Km, and a trend in NE-SW direction (50°-60°) with lineaments longer than 6 Km. A lack of lineaments is present in the others directions.
Between ERS-1 and LANDSAT TM rose diagrams a significant difference is evident in E-W direction. In fact the LANDSAT TM presents the 10% of lineaments respect to the 2% of the ERS-1 in descending orbit and the 5% in ascending orbit.
Between the overall ERS-1 (ascending and descending orbit) and Landsat-TM lineaments there is an overlap of about 37%. In this calculation the overlap between ERS-1 in ascending and descending orbit has been taken in account.
By a geodynamic point of view NW-SE (Apennines direction) and NE-SW (anti-Apennines direction) are dominant structural directions in the study area, as reported in literature [4].
The first one represents long tectonic structures, corresponding to Apennines thrust faults (late Miocene - middle Pliocene faulting), as well as normal faults (formed from late Miocene to Holocene). The second one represents shorter structures, mainly normal faults (formed from late Miocene to Holocene), creating a trellis arrangement in agreement with the neotectonic extensional evolution of the area.
The N-S statistical trend, showed in all three rose diagrams, does not correspond to structures recognized in the study area, as reported in literature; however they may be related to N-S trending regional structures affecting neighboring areas.

The results obtained in the signatures evaluation for lithological classification are reported in Tab. I and Tab. II in the form of a Maximum Likelihood Classifier confusion matrix. These results report a percentage of correct classification of about 89% for the LANDSAT TM data alone. The most confused classes are urban areas, alluvial deposits and clays.
More interesting results have been obtained when Landsat TM and ERS-1 images have been integrated in a single data set. As reported in Tab. II, for the multisensor data set the overall percentage of correct classification is very high (94%). Particularly the classes of clay, urban and alluvial deposits are more distinct.

			Reference Data				
Classif.	Clay	Beach	Water	Rec. alluv.	Alluvial Dep	Marine Dep	Urban
Clay	92.26	0	0	1.22	8.44	4.43	3.94
Beach	0.03	96.02	0	1.3	0.05	0	0.36
Water	0	0	96.74	0	0	0	0
Rec. alluv.	0.86	1.2	0	97.1	0.74	0	1.97
Alluvial Dep	5.18	0.4	1.09	0.15	83.97	1.16	15.05
Marine Dep.	0.17	0	0	0	0.05	92.62	0
Urban	1.49	2.39	2.17	0.23	6.75	1.8	78.67
Column Tot	2894	251	92	1311	2015	1558	558

Tab. I.: Confusion Matrix of LANDSAT TM data

			Reference Data				
Classif.	Clay	Beach	Water	Rec. alluv.	All. Dep.	Mar. Dep.	Urban
Clay	96.32	0	0	0.66	7.39	4.08	0.74
Beach	0.03	95.53	0	0.37	0.1	0	0
Water	0	0.41	97.98	0	0	0	0
Rec. alluv.	0.14	2.44	0	98.31	0.8	0	1.66
Alluvial Dep	3.27	1.22	1.01	0.66	88.72	1.66	5.71
Marine Dep.	0.07	0	0	0	0.15	93.37	0
Urban	0.17	0.41	1.01	0	2.84	0.89	91.9
Column Tot	2878	246	99	1359	2004	1569	543

Tab. II: Confusion Matrix of LANDSAT TM and ERS-1 data

5. CONCLUSIONS

The use of remote sensed data, allowing a regional synoptic recognition, could enable to have a complete geological characterization of regions of interest. Particularly in geomorphological inspections remote sensing allows to reveal structures that usually are difficult to be identified as a unique lineament during field surveys, due to the environmental conditions: vegetation cover, anthropic infrastructures, slopes, rivers and other morphological constraints.

Moreover the results presented in this work show that in the analysis of ERS-1 and LANDSAT TM data the integrated use of different sensors in geological application may improve the possibility to study the geological properties.

6. REFERENCES

- [1] G. Sylos Labini & al., "Coastal and rivers dynamics studies by means of space techniques", ERS-1 Pilot Project Proceedings, ESA SP-365 ISBN 92-9092-302-4, pp.191-194.

- [2] Ciaranfi N., Maggiore M., Pieri P., Rapisardi L., Ricchetti G., Walsh N. "Considerazioni sulla Neotettonica della Fossa Bradanica", CNR Pubbl. N.251 del Prog. Fin. Geodinamica, 1979; pp.73-95.

[3] Nagao, Makoto, Takashi Matsuyama, "Edge preserving smoothing", Computer Graphics and Image Processing, Vol.9, pp. 394-407, 1978.

[4] AA. VV., "Italian Geological Map of Southern Apennines", 1988.

Relief Restitution by Radargrammetry

Laurent MARINELLI, Lionel LAURORE
GEOIMAGE
80, route des Lucioles
06560 Valbonne - FRANCE
Tel : (33) 93 00 40 00 - Fax : (33) 93 00 40 01

Abstract **- This article presents a method of automatic restitution of the relief from ERS SAR stereoscopic images. This technique which inspires itself from methods which are used in optical stereoscopy is called Radargrammetry. For commercial purposes we developed the software package originating from the whole of the radargrammetric sequence. This software package enables us from a SAR stereoscopic pair to obtain a DEM in a cartographic projection selected by the user and the creation of ortho-images.**

I. INTRODUCTION

Radargrammetry is used to find from two images of SAR amplitude the altimetric features of each points common to both images. The planimetry features, which depend on the altitude, can then be deduced.

Several researchers have studied this method and have succeeded in extracting the altitude data by adapting their digital stereoplotter developed for SPOT data [1] to the data originating from SAR sensors [2] [3]. As far as we are concerned, our objective is to develop an automatic version of the processings of the SAR stereoscopic images.

The GEOIMAGE Company is commercializing a digital cartography software. One of the modules of this software package is used for determining DEMs from optical stereoscopic pairs provided both by satellite images -SPOT, Landsat, .. - and aerial images. In order to take advantage of the SAR satellite images and of the availability of an increasing number of data - ERS-1&2, JERS-1, RADARSAT,...- we integrated in our software package the possibility of processing this type of images. Until now we have taken into account only the ERS model but the great similarity between the SAR satellite sensors let us consider an easy and fast integration of other sensors.

The developed software enables us to get a DEM in cartographic projection automatically and to determine the altitude of each point of the two images. This last point thus facilitating the creation of the two ortho-images corresponding to the pair.

II. THE RADARGRAMMERY

Radargrammetry is based on the correlation of amplitude images of a pair of SAR images. Its application mainly requires the determining of the matching of the points between the two images in order to measure the parallax ; then the knowledge of the geometry of the sensor which acquires the images.

In actual fact, it is easy to notice that the parallax generated between two images varies with the altitude of the ground points and in this way to show the existence of an effect of stereovision in the case of SAR images acquired from different angles.

In a ground range representing of the radar images (Fig.1) we have the following data relationships [4] :

$$p_1 = h * \cot(\alpha_1)$$
$$p_2 = h * \cot(\alpha_2)$$

where p_1 (resp. p_2) is the relief displacement in ground range, when the incidence angle of the wave is α_1 (resp. α_2).

We can then deduced the relationship between the parallax difference $dp = p_2 - p_1$ and the height h of the point in the case of the same side stereo :

$$h = \frac{dp}{\cot(\alpha_2) - \cot(\alpha_1)}$$

Operating radargrammetry requires the complete modelization of the geometry of the viewing. That is to say it is necessary to integrate in a single model the characteristics of the radar

Proceedings of the Second ERS Applications Workshop, London, UK, 6–8 December 1995 (ESA SP-383, February 1996)

sensor, the attitudes of the platform which carries it, the modelization of the Earth surface and the parameters of the projection in which we wish to reference the displayed points. This modelization enables us then to determine the locating function. This function links the pixel coordinates in the image -slant range, time- of a point with its ground coordinates in the cartographic projection included in the previously described model.

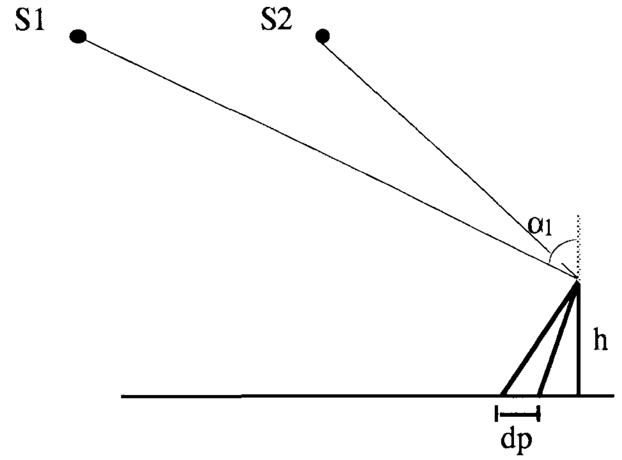

Fig. 1 : SAR strereo geometry

The geometric modelization enables us to have a function of passage image-ground as well as an reverse function such as :

$$(X,Y) = F(p,q,h)$$
$$(p,q) = G(X,Y,h)$$

where (p,q) are the line column coordinates of the point in the image and (X,Y) its coordinates in the cartographic reference. We can notice that the position of the point in the image and in the cartographic reference always depends on its height. And as the visual aspect of the SAR images suggests, the relief induces a strong distortion in the position of the points in the image. So, this effect is all the more emphasized in the ERS cases that the incidence angle is low -in the range of 23° in the centre of the scene-. Then we find for ERS that a variation Δh of the altitude implies a variation $\Delta p = \Delta h * \cot(23) \; = 2.4 * \Delta h$ in the point position.

Knowing both functions of passage enables us to determine the height of the points according to their disparities, that is to say according to the size of their parallax difference and to locate their position on Earth.

III. THE RADARGRAMMETRIC MODULE

Now, we are going to describe the successives stages of our radargrammetric sequence.

Preparation of the data :

First, we are going to select in the overlapping part of the images, the area in which we wish to determine the DEM. Then, in order to adjust the geometric model of each image, we take a ground control point between the two images in the previously selected area. This ground control point enabling us to rectify a translation error which might be made in the computation of the geometric model and which can be due to the unreliability of the parameters included in the modelization.

Calibration :

This processing will allow us to limit the area of search for the homologous points. It consists in projecting both images in an epipolar reference. The search area is no longer the whole image but is limited to a curve for each point -see plate 2- in each image [5]. Then, in order to still reduce the search time we rectify both images so as to make the epipolar curves straight and horizontal. At that point, the research is only monodimensional. Determining the epipolar curves requires the geometrical modelization of the viewing.

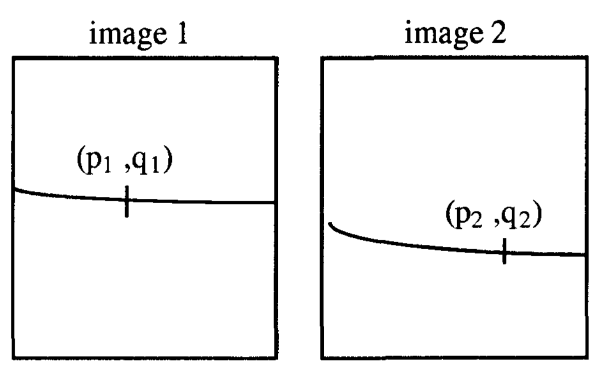

Fig. 2 : Epipolar curves

Radiometric improvements :

This phase aims at contrasting the images in order to improve the visual accuracy between the various structures contained in them. It includes among other things a global spreading of the dynamic followed by local enhancement of the contrasts and a radiometric equalization of the images between each other.

The matching :

By means of this phase we will be able to determine the matching between all the pixels in order to create a disparity map.

The algorythm which is developed is not based on a simple method of correlation of the grey levels which is too sensitive to the differences in radiometry and too heavy to operate ; it is based on a principle of hierarchical correspondence of the characteristic structures of the image.

Then we proceed to multi-scale matching. That is to say we extract the main structures of the image in a shaded resolution - by a sub-sampling of the images -then we determine their matching. Afterwards we recommence the extraction of the visible structures in a less shaded resolution but still taking into account the matching which was acquired in the previous phase. We then reiterate the same process with less and less shaded images until we match the images in full scale and therefore the smallest objects which make them up.

The radiometric content of the SAR images are strongly linked to the ground morphology, a pair of SAR images will therefore clearly show the same charateristical structures. The use of our correlator -which is based on a correlation of the image structures- with SAR images appears to be particularly well adapted. All the more so that the principle of multi-scale correlation according to which it functions enables us during the various sub-samplings to reduce the speckle noise and therefore to increase the accuracy of the matching. During each resolution it is possible to carry out manual corrections.

Altitude :

By using the geometrical model we can determine from the value of the parallax difference the altitude at each point of the image.

Projection :

This last phase enables us not only to project the DEM in the cartogaphic reference which we require. But also to create an ortho-image from either of the two images of the pair.

IV. STUDY SITE

The parallel orbits of ERS-1 during the 35 day cycle allow the setereoscopic effect on the overlapping area of the tracks. In actual fact, there is an incidence angle variation in this area of 5°.

The selected study site is located in the Alpes-Maritimes "département" in France since to validate our results we have at our disposal a DEM from a SPOT pair on this area as well as topographic surveys. Moreover, this "département" shows marked contrasts in term of relief, the altitude varying from 0 to 3,000 metres.

We selected two ERS images (Fig. 3), the first is dated October 20th, 1994 -Orbit : 17067, Frame : 2727-, the second one was acquired on November 6th 1994 -Orbit : 17311, Frame : 2727-.

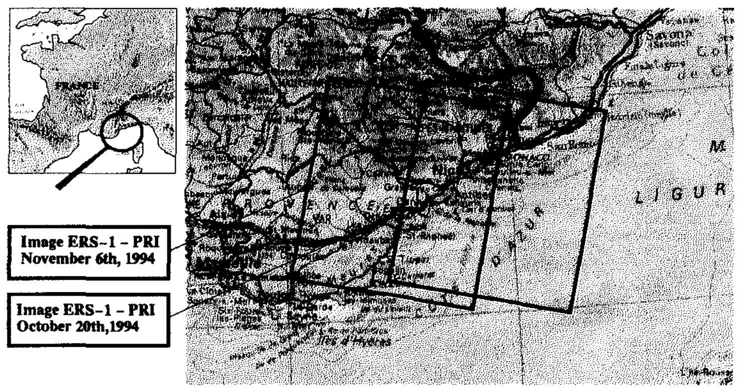

Fig. 3 : Localization of the study site

The small difference in incidence between the two images of a pair guarantees a close radiometry and therefore an a priori easy correlation of both images. The zone which is common to the two images has a width at the latitude of our study site - that is to say of nearly 45°- of 40 kilometres for full scene images 100 kimometres wide.

We have then followed all our radargrammetrical sequence as was previously described. The results show a very coherent DEM (Fig. 5) set apart on a very limited area. This incoherence in the relief originates from the matching phase. Actually, the zone in question (Fig. 4) is located at the edge of the Var valley and the existence of very nearby high relief -1,400 metres- generates a very marked effect of layover and foreshortening. It appears totally impossible to find the right matching even with the naked eye.

The two images were selected as well as to do a cartography of flood [6], wich happened in the Rhone Valley on November 5th 1994. So we have one image acquired 17 days before the flood, which enables us to locate the areas permanently under water. The other image acquired during the flood shows the rise of the waters. Using the DEM generated from these two images , we can perfectly overlap these images and make a coloured composition (Fig. 6) showing in red the fooded areas. The date-channel associations are the following : -November 6th : red channel, October 20 th : green and blue channel.

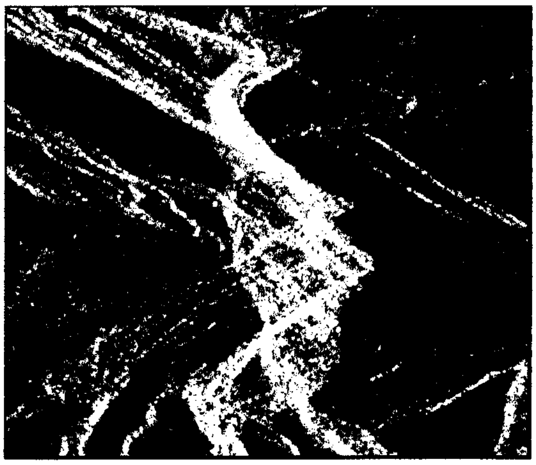

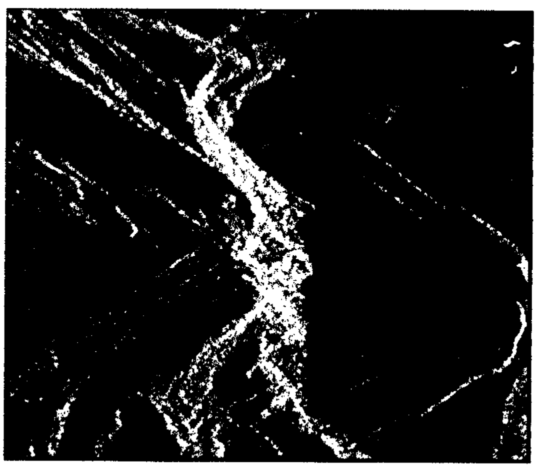

Fig. 4 : Zone of difficult matching

V. CONCLUSION

In this article whe have presented our sequence of automatic production of DEMs by radargrammetry. Nearly all of the overlapping zone of the images of the stereoscopic pair could be processed efficiently and enabled us to produce a DEM. In this way we were able to verify the right correlation of the ERS-1 images -during the 35 day cycle- between adjacent tracks. However, concerning some very limited zones where there is a too important effect of layover and foreshortening -zone of high gradient in altitude-, radargrammetry, as well as other methods of relief restitution using radar images with low incidence -of the ERS type- cannot be used to determine a relevant altimetric datum.

Finally, because of its generaical conception at the level of the geometric model, our sequence can very quickly accept data from other sensors -JERS-1, RADARSAT,...-. This will enable us to increase the cover in number of stereoscopic pairs and will thus increase the operative capacity of this method of relief restitution. In this way we will be able to create DEMs from mixed pairs - for instance ERS-1/JERS-1, which will enable us to obtain a more sizeable overlapping zone and a possibility of more important thematical applications, through the use of different wave lengths.

REFERENCES

[1] T.Toutin and M. Beaudoin, "Real-time extraction of planimetric and altimetric features from digital stereo Spot data using a Digital Video Plotter", in Photogrammetric Engineering and Remote Sensing, vol. 61, no. 1, pp. 63-68, January 1995.

[2] T.Toutin, "Airborne SAR stereo restitution in a mountainous area of Cost Rica : first results", in IEEE Transactions on Geoscience qnd Remote Sensing, vol. 33, no. 2, March 1995.

[3] F.W. Leberl, M. Millot, R.S. Wilson, M. Karspeck, B. Mercer, and S. Thornton, "Radargrammetric image processing with a softcopy strereo workstation", in Proc. 8th Thematic Conference Geologic Remeote Sensing, Denver 1991.

[4] F.W. Leberl, "Radargrammetric image processing", Artech House, 1990.

[5] H.Guichard, G.Ruckbush, E.Sueur, S.Wormser, "Stréréovision numérique SPOT : une approche originale de formation des images épipolaires et de mise en correspondance", in Colloque SPOT1 Utilisation des images, Bilan , Résultats, pp. 1371-1392, Paris 1987.

[6] J.Noyelle, S.Delmeire, L.Marinelli, "Identificaton of flooded areas in the Rhone and Var river, France, using ERS-1 data" in First ERS Thematic Working Group Meeting on Flood Monitoring, Frascati-Italy 1995.

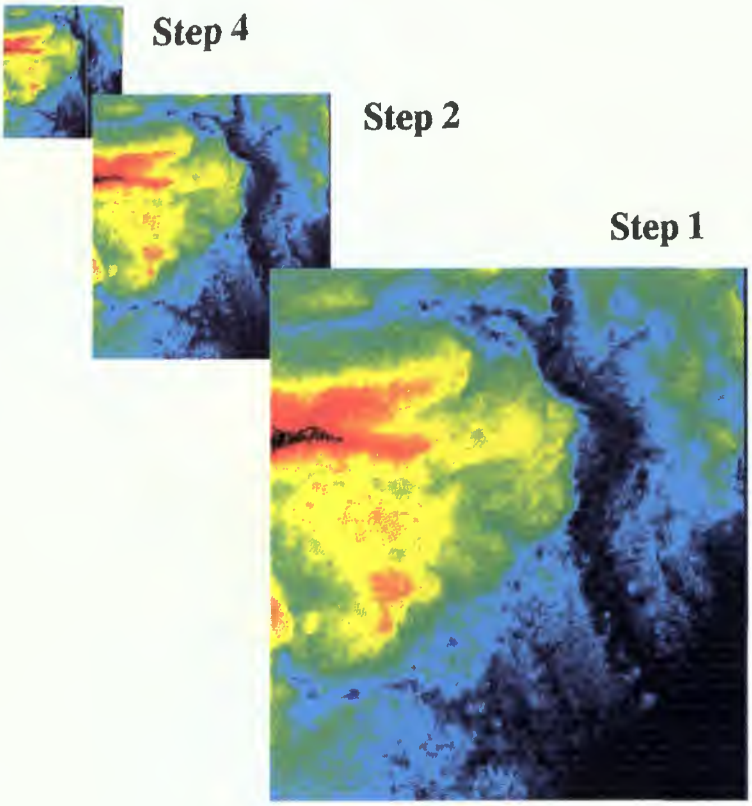

Fig. 5 : DEM in a multi-scale approach

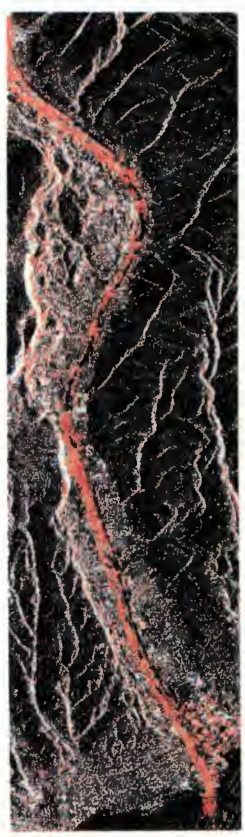

Fig. 6 : Coloured composition on the Var valley

GIVING AN OPERATIONNAL STATUS TO ERS INTERFEROMETRIC APPLICATIONS

Marc Rossi

CNES, the Frensh Space Agency, 18 av. E. Belin, 31055 Toulouse cedex, France
Tel: (33) 61-27-42-62. Fax: (33) 61-27-31-67

ABSTRACT

CNES has been working on the SAR interferometric techniques for years and with ERS data since the launch of ERS1 in 1991. Some very interesting results were obtained (Landers earthquake, deflation of Mount Etna volcano, DEM generation...). CNES is now giving an operational status to those applications :

• A completely automatic interferometric chain has been developed.

• A special effort on education is made by inviting scientists and distributing CNES interferometric software to the scientific community.

• A systematic survey of a large tectonic site has been started at CNES.

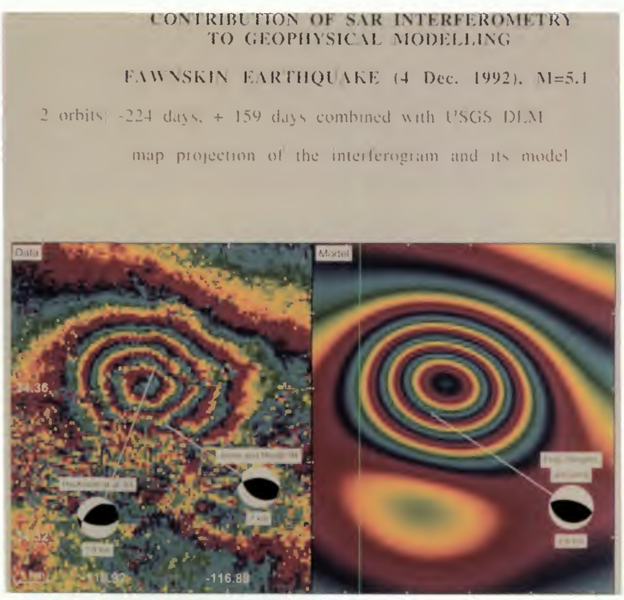

Fig. 1. Earthquake deformation field mapped by radar interferometry (on the left, CNES processing, ERS1 data) and associated model (on the right, by GRGS [K. L. Feigl at al., 1995]).

1. INTRODUCTION

CNES has started in 1985 [D. Massonnet, 1985] a research program on detection of small tectonic displacements with interferometry [A. K. Gabriel et al., 1989]. SAR interferometry (INSAR) has first been proposed in 1974 [L. C. Graham, 1974] and allows also digital elevation model (DEM) elaboration [H. A. Zebker and R. M. Goldstein, 1986].

The studies at CNES have mostly been theoretical before 1991 but since the launch of ERS1, we have processed hundreds of ERS scenes. SAR interferometry has now reached an operational status at CNES, with a commercial distribution of INSAR products through SPOT IMAGE and of interferometric DEMs through ISTAR.

2. MAIN RESULTS OBTAINED AT CNES WITH ERS1 INTERFEROMETRY

2.1. Mapping of earthquake deformation fields

We applied SAR interferometry to about ten earthquake sites. The average results quality was good with an average RMS misfit of about 1 to 2 centimetres and led to accurate modelling of the phenomena using elastic half space models [K. L. Feigl at al., 1995].

The displacement field of the Landers earthquakes have been the first published results [D. Massonnet et al, 1993-a][D. Massonnet et al, 1994]. Results on other earthquake sites have later been published in the geophysical literature [D. Massonnet and K. Feigl, 1995].

2.2. Monitoring of volcano deformations

Four volcanoes or caldera were part of CNES investigation program (Etna, Pinatubo, Merapi, Long Valley).

Even interferograms of poor quality contribute significantly to the success of the modelling as we observed in our study on Mount Etna [D.Massonnet et al, 1995].

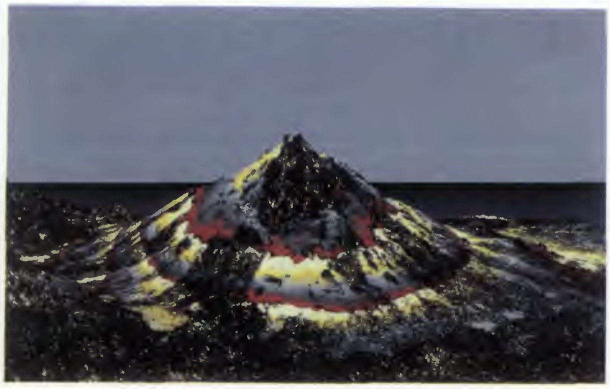

Fig. 2. Perspective view of the volcano deflation following eruption of Mount Etna (CNES processing, ERS1 data) published in NATURE.

2.3. Generation of Digital Elevation Models

Most of the interferometric DEMs we elaborated, in cooperation with ISTAR, have an accuracy comparable to the several metres of the stereoscopic DEMs obtained with optical data [L.Renouard and F.Perlant, 1994]. A study on a site of Ukraine with an orbital separation of 1100m close to the theoretical limit where the interferometric effect would disappear [D.Massonnet and Th.Rabaute, 1993] however tend to show that ERS interferometry can reach an ultimate accuracy of about one metre when used in relatively flat areas, such as the ones subject to flooding.

The assessment of flooding is a traditional use of SAR data for two reasons; first, flooded areas are generally covered by clouds and the all-weather capability of SAR is critical. Second, relatively still waters are relatively easy to recognise on a radar image since they are very dark. The prospect of the availability of DEMs of metric or sub-metric accuracy could enhance dramatically the use of SAR data. It could allow an easy mapping of the areas to be flooded and the amount of water required to do so.

At CNES, we have several test sites under investigation. These studies are aimed at quantifying precisely the ultimate accuracy of DEM computation using ERS-1 data.

Figure 3 shows the fringe pattern associated with a pair of ERS-1 images taken on the South West of France with a time interval of 6 days. The orbital separation was over 600 metres. This large separation amplifies the stereoscopic effect and therefore the sensitivity to topography. Here every fringe represents an altitude of 20 metres (the altitude of ambiguity). To perform ground truth with this site we will use a very precise data base of over 700 reference points with a position known to half a metre. Once we have assessed the accuracy, we will have to check the feasibility of such a precise topography assessment with countries subjected to frequent flooding, especially in equatorial or tropical environment.

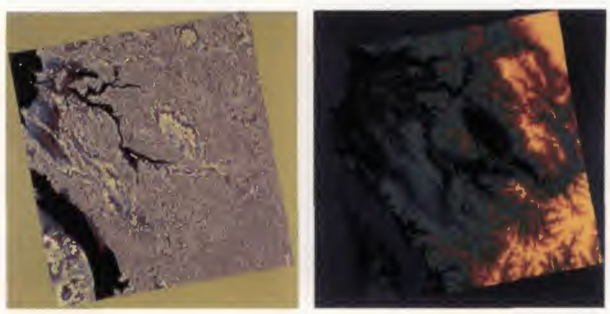

Fig. 3. Interferogram with a 20m altitude of ambiguity (on the left, CNES processing, ERS1 data) and the accurate Digital Elevation Model generated from it (on the right, ISTAR processing).

2.4. Data selection strategy

The accuracy of the results of interferometric studies is mainly limited by the contribution of atmospheric propagation heterogeneity [D. Massonnet et al., 1993-b]. The limitation is especially important in the study of very small displacements such as the centimetre-sized rift we observed in Iceland over one year. This contribution can be detected using a pair-wise logic which requires many observations.

In analysing a large data set, we learnt to select data acquired by night whenever possible. However, daytime acquisition is required when an observation along different angles of view is needed. An alternate solution is to observe the site combining satellites with different geometry, as we have done on the Northridge (California) earthquake.

3. CNES AUTOMATIC INTERFEROMETRIC CHAIN

We developed an automatic differential interferometry software tool, which is used for the production of topographic models as well as for new scientific developments in cooperation with field specialists. The tool produced results with ERS-1 as well as JERS-1 [M. Rossi et al, 1995], X-SAR or SIR-C and uses the DEM elimination method to produce displacement maps. This method has been choosen to avoid the difficult unwrapping process [R. M. Goldstein et al., 1988] required by standard differential interferometry [R. M. Goldstein et al., 1993].

This software tool, called DIAPASON[1], works from a pair of radar raw data or single look complex images and a digital elevation model (DEM). If the DEM is not available we substitute the geoid or the ellipsoid to it. Otherwise, the topographic contribution is automatically retrieved from the interferogram, which can be placed into any map coordinates or kept in slant range geometry. The tool, based on the application of the digital elevation model elimination method, produces a result which can be used to increase the accuracy of an existing DEM through the analysis of residual fringes or to give information on possible displacements.

The DEM is used at four critical steps of the processing :

- it predicts the deformation between the images using preliminary orbits, including the small deformation due to topography. This predicted deformation is compared to the actual deformation obtained from local correlation. Two constant offsets (range and azimuth)

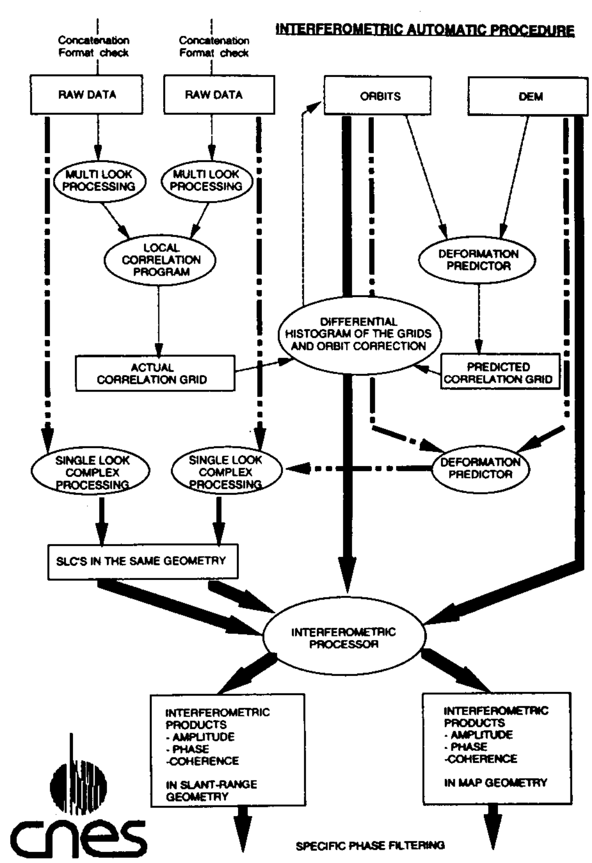

Fig. 4. Synopsis of the interferometric chain.

---

1 Differential Interferometric Automated Process Applied to Survey Of Nature.

generally suffice to characterise the differential comparison. This method is equivalent to comparing the whole images by correlation to obtain only two constant offsets. The quality of the result reflects this huge signal to noise ratio; the accuracy on the offsets is on the order of 3% to 5% of a pixel size in both directions.

- it allows the production of a fake amplitude image, which is then compared to one of the radar images and gives, by correlation, the absolute position of the images with an accuracy of a fraction of the DEM cell size.

- it selects, during data fusion, the optimal slope dependant finite (at most five range pixels) impulse response filter which maximises the coherence, thus contributing to the quality of the fringes.

- it allows the prediction of the topographic and orbital fringe pattern of the pair, which we subtract from the interferogram, creating the differential product.

The output products are map corrected most of the time to the DEM (with the same cell size) and are made of three channels : a combined serial multi-look image of the amplitude, an interferogram made of the phases from the complex averaging on the cell size and a coherence computed on the cell size.

The multi-look image of the amplitude is useful for the user to locate targets of interest.

The coherence image gives a confidence level for each pixel of the interferogram. It also shows where the ground surface has been modified from one data take to the other.

The interferogram measures the ground displacement at the wavelength scale (a few centimetres) and the topographic contribution if no DEM has been used.

We introduced the notion of altitude of ambiguity which is convenient to quantify the orbital configuration of a given interferometric pair [D. Massonnet and Th. Rabaute, 1993]. It is equal to the change of elevation which produces a change of one topographic fringe in the interferogram.

The best orbital configurations for INSAR correspond to very close orbits, where the stereoscopic difference of path produced by the topography is minimal. This situation leads to very high altitudes of ambiguity and is optimal for ground displacement measurements.

The worse orbital configurations give altitudes of ambiguity of slightly less than ten metres in the case of ERS-1. We obtained usable results with 8.5 metres on very flat areas.

4. SOFTWARE AND KNOW-HOW DISTRIBUTION EFFORTS

4.1. Distribution of the interferometric chain DIAPASON

To extend the use of ERS interferometry, CNES has decided to make its automated interferometric chain widely available.

The software will be distributed in its existent VMS version from the beginning of 1996. A UNIX version is under development and will be distributed by summer 1996.

Two different licenses will be offered : a scientific one and a commercial one.

The first one is intended for scientific teams who want to process themselves interferometric products, possibly after adaptation of the software to their particular needs, but without commercial distribution of the products. The scientific license will be given freely.

The second one should be contracted by firms interested in CNES interferometric chain to commercially produce interferometric products, or to include it in a (possibly larger) software package to be sold. This license will have to be purchased and will imply royalties on future product sales.

The VMS version presently runs at CNES on Dec-Alpha workstations with 64 Megabytes of RAM and 1 Gigabyte of disk storage.

4.2. Cooperation with thematic scientists

Since the beginning of its interferometic activities, CNES initiated cooperation with specialised scientists for the geophysical interpretation of interferometric results in order to validate those results and to transfer the know-how acquired at CNES to the scientific community. To improve this transfer, CNES has also decided to invite volunteer scientists to work for a while in its premises.

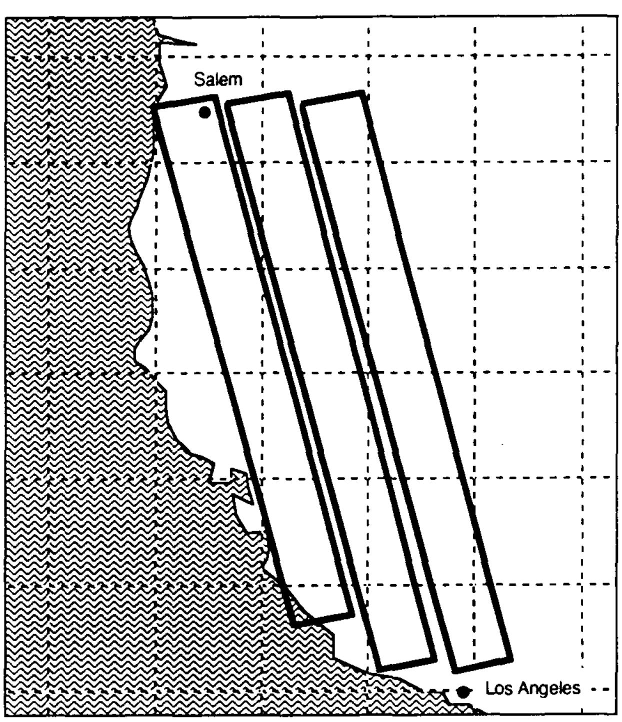

Fig. 5. Location map of the three ERS tracks (120, 163 and 206) involved in the large scale tectonic survey currently carried on at CNES. Each track is about ten frames long.

5. LARGE SCALE TECTONIC SURVEY EXPERIMENT

CNES is undertaking a large scale tectonic survey which provides a prototype for data analysis centres dedicated to tectonics. A 400,000 square kilometres area in California and Oregon (fig. 5) started to be imaged ten times by ERS-1 and ERS-2 under an investigation program accepted by the European Space Agency.

The data are routinely processed and archived after reception at CNES. This experiment will generate an unique interferometric data set for long term stability assessment, for earthquake detection and tectonic activity measurements.

6. CONCLUSIONS

CNES has turned interferometry into operational applications, such as earthquake and volcano deformation mapping or digital elevation model elaboration. The automatic interferometric software tool developed at CNES, called DIAPASON, is available to the scientific community and a large scale survey has been initiated as a prototype for data analysis centres dedicated to tectonics.

7. REFERENCES

K. L. Feigl at al., 1995, Estimation of an earthquake focal mechanism from a satellite radar interferogram : Application to the December 4, 1992 Landers aftershok, Geophysical Research Letters, vol 22, n° 9, pp 1037-1040, 1 May 1995

L. C. Graham, 1974, Synthetic interferometer radar for topographic mapping, Proc. IEEE vol 62 n° 6 - June 1974

A. K. Gabriel et al., 1989, Mapping small elevation changes over large areas : differential radar interferometry, Journal of Geophysical Research, vol. 94, pp 9183-9191

R. M. Goldstein et al., 1988, Satellite radar interferometry : Two-dimensional phase unwrapping, Radio Science, vol 23 n° 4, pp713-720

R. M. Goldstein et al., 1993, Satellite radar interferometry for monitoring ice sheet motion : Application to an antartic ice stream, Science, vol 262 n° 23, pp1525-1530, December 1993

D. Massonnet, 1985, Etude de principe d'une détection de mouvements tectoniques par radar, CT/PF/TI/AS n° 326 (internal memo) - 16 nov 85

D. Massonnet and Th. Rabaute, 1993, Radar Interferometry : Limits and Potential, IEEE (TGARS) vol 31 n°2, Marsh 1993

D. Massonnet et al., 1993-a, The displacement field of the Landers earthquake mapped by radar interferometry, Nature vol 364 n° 6433 - 8 July 1993

D. Massonnet et al., 1993-b, Accuracy and Artefacts level in Interferometric DEM, Colloque Spot ERS PARIS 10-14 mai 1993

D. Massonnet et al., 1994, Radar interferometric mapping of deformation in the year after the Landers earthquake, Nature vol 369, 19 May 1994

D. Massonnet and K. Feigl, 1995, Satellite radar interferometric map of the coseismic deformation field of the M=6.1 Eureka Valley, California earthquake of May 17, 1993, Geophysical Research Letters, vol. 22, n°12, 1541-1544, 15 June 1995

D. Massonnet et al., 1995, Deflation of Mount Etna monitored by spaceborne radar interferometry, Nature vol 375, 15 June 1995

L. Renouard and F. Perlant, 1994, Comparison of the SPOT DEM and the ERS interferometric DEM, 14th Symposium Topography from Space, Goteborg - 8-10 june 1994

M. Rossi et al., 1995, JERS-1 SAR image quality and interferometric potential, submitted to IEEE (TGARS)

H. A. Zebker and R. M. Goldstein, 1986, Topographic mapping from interferometric SAR observations, Journal of Geophysical Research, vol. 91, n° B5, 10 April 1986

SHIP ROUTING

Chairman: **S. Sandven**
Rapporteur: **E. Attema**

ICEWATCH - ICE SAR MONITORING OF THE NORTHERN SEA ROUTE

Ola M. Johannessen*, Stein Sandven* and Vladimir V. Melentyev**

*Nansen Environmental and Remote Sensing Center
Edvard Griegsvei 3a, N-5037 Solheimsvik, Norway
Tel: + 47 55 29 72 88, fax: + 47 55 20 00 50

**Nansen International Environmental and Remote Sensing Center
Korpusnaya Str. 18, 197042 St. Petersburg, Russia
Tel: + 7 812 230 78 37, fax: + 7 812 230 79 94

ABSTRACT

Use of Synthetic Aperture Radar (SAR) images from satellites is a technology which is playing an increasingly important role in operational sea ice monitoring. SAR images, with a resolution of 100 m, can distinguish different ice types and map leads, polynyas, shear zones, landfast ice, drifting ice and location of the ice edge. The SAR is the only instrument which provide high resolution images under different cloud and light conditions.

In several demonstration projects the Nansen Center in Bergen and St. Petersburg have used ERS-1 SAR images to monitor sea ice conditions in the Northern Sea Route from 1991 to 1995. The projects have been performed in close cooperation with icebreakers belonging to Murmansk Shipping Company. From 1995 SAR ice monitoring is established as the first joint project in earth observation between the European Space Agency and the Russian Space. The objective of the joint project is to make SAR data from ERS and ENVISAT available for Russian users of ice data on an operational basis. The project also includes a plan for a SAR receiving station in Siberia.

1. INTRODUCTION

The Northern Sea Route is the sailing route along the coast north of Russia from the Barents Sea in west to the Bering Strait in east (Fig. 1). The ice conditions restrict sea transportation which requires ice class vessels as well as icebreaker assistance throughout the year. In summer there is traffic in the whole sailing route, whereas in winter it is mainly the western part which is used serving the ports on the Yenisei River.

An extensive ice monitoring and forecasting service has been built up in Russia over the last 50 years with a main objective to serve the icebreaker service in the Northern Sea Route. Use of spaceborne SAR has not been a part of this service.

NERSC first demonstrated use of ERS-1 SAR data for near real-time ice mapping in the Northern Sea Route in August 1991, only a few weeks after the launch of the ERS-1 satellite. SAR derived sea ice maps were then sent by telefax to the French polar vessel *L'Astrolabe* during her voyage through the Northeast Passage from Norway to Japan [Johannessen *et al.*, 1992 a,b]. This demonstration was evaluated

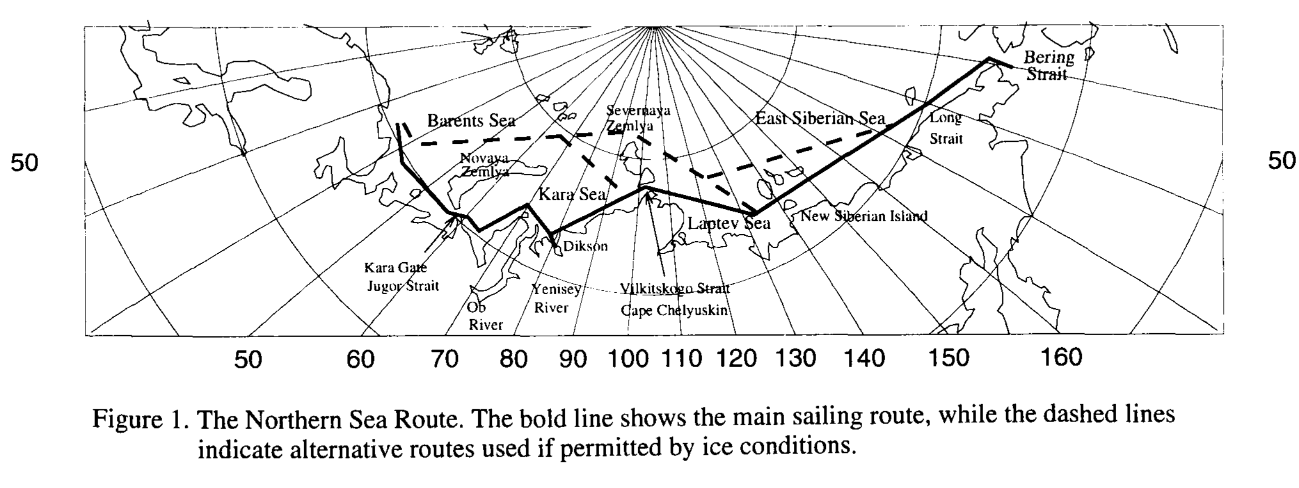

Figure 1. The Northern Sea Route. The bold line shows the main sailing route, while the dashed lines indicate alternative routes used if permitted by ice conditions.

Proceedings of the Second ERS Applications Workshop, London, UK, 6–8 December 1995 (ESA SP-383, February 1996)

as very interesting by the captains and sea ice experts onboard the Russian icebreakers which escorted *L'Astrolabe* through the ice-covered parts of the route. Since 1993 SAR ice monitoring demonstrations have been carried out on several Russian icebreakers [Johannessen *et al.*, 1994, 1995]. In all these demonstration experiments, a scientist from the Nansen Center in St. Petersburg stayed onboard the icebreakers and analyzed the SAR images in cooperation with the captain and ice pilots. In addition to the ice navigation these experiments also had scientific objectives to study sea ice phenomena and their SAR signature along the Northern Sea Route at different times of the year.

2. SEA ICE PARAMETERS DERIVED FROM SAR DATA IN THE NORTHERN SEA ROUTE

Sea ice parameters observable by SAR can be categorized in one of the following three classes:

Ice boundaries and features. The most important boundaries which can be detected in SAR images are ice edges, ice floe identification and boundaries between areas of different ice types. The most common observable ice features are leads, shear zones, ridge areas and ice edge phenomena such as ice eddies, ice tongues and wave propagation in ice. The detection of boundaries and features requires some backscatter gradients which can be enhanced by image processing techniques such as histogram equalization, filtering, line detection and other methods.

Motion of ice features. With repeated SAR coverage over the same ice area it is possible to observe the displacement of features which can be recognised in images obtained at time intervals of a few days. The ice motion can be calculated by several algorithms which can automatically recognise features such as ice floes and leads. The ice motion vectors shown in Fig. 2 are calculated by a spatial correlation technique (Kloster et al., 1992) using images taken at three day interval in Ob river estuary in February 1994. The image shows the boundaries between moving and stationary ice, such as "stamukha" which is ice stuck to the sea bottom in areas (area A), and landfast ice stuck to the shores of islands (area B) and coasts (area C). The image shows an example of coastal polynya formation when southerly winds drives the pack ice northwards, leaving areas of open water which refreezes due to the low air temperatures. The refrozen polynya is clearly identified by the dark signature in the SAR image.

Classification of ice types. SAR backscatter statistics for various ice types and surface characterisitcs are important input data for ice classification (Fig. 3). This statistics is based on a number a validation experiments and takes into account SAR parameters such as frequency, polarisation and incidence angle. In addition to a pixel-by-pixel classification it is also

Figure 2. ERS-1 SAR image of the ice-covered Ob river estuary in February 1994. The image is composed of three scenes and covers 300 by 100 km. The arrows denote the ice displacement vectors between 24 and 27 February. The mean ice velicoty is 15 cm/s. Original data © ESA/TSS 1994.

important to include use of various texture analysis techniques in order to extract pattern information in the images. To obtain an optimal classification of the ice types it is necessary to use other available data such as in situ observations, meteorological data and other satellite data.

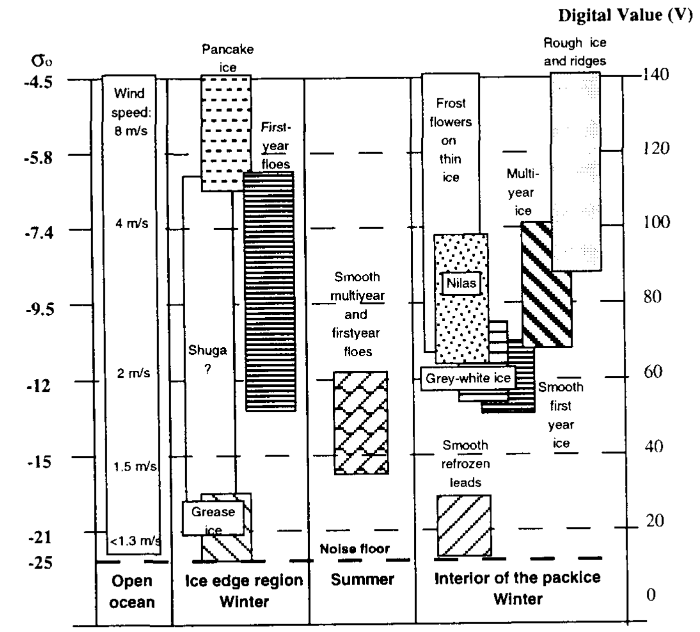

Figure 3. ERS SAR backscatter values for different ice types. (Sandven et al., 1994)

3. ANALYSIS OF ERS SAR DATA REQUIREMENTS

In the Northern Sea Route, Tromsø Satellite Station can read down and process SAR images as far east as 107° E which includes the Vilkitskogo Strait. In the East Siberian Sea and the Chuckhi Sea Alaska SAR Facility can read down and process SAR data. No receiving station can obtain SAR data in the Laptev Sea. It is therefore necessary to have a receiving station in central Siberia which can cover the whole Northern Sea Route.

An example of a 3-day SAR coverage of the Kara Sea region is shown in Fig. 4 where approximately 25 scenes were needed to cover the sailing route between the Pechora Sea and the Yenesei River. The gaps in the 3-day coverage is about 200 km along the route. A one-month coverage of this area, which is the most important part of the sailing route in the winter, would require 250 scenes. If the coverage should include the whole sailing route west of Cape Chelyuskin it would require about 500 scenes per month. In the summer season, when there is ship traffic along the whole Northern Sea Route the data requirements will be variable, depending on the total amount of sea ice. In order to provide year round ice information from ERS

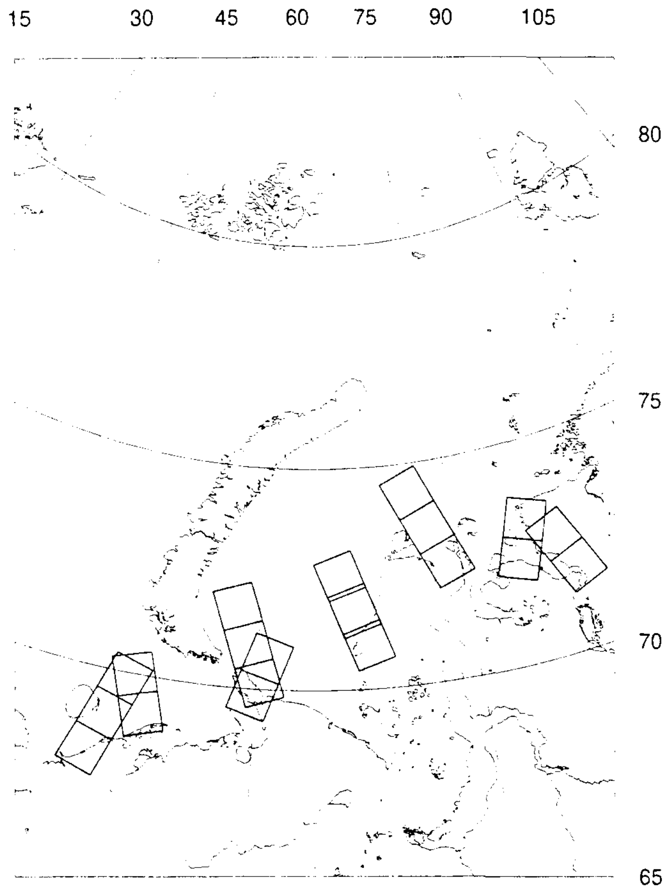

Figure 4. ERS SAR coverage of the area between the Pechore Sea in west and Yenisei river in east during a three day period.

the number of SAR scenes needed to cover the major parts of the Northern Sea Route would be of order 5000 per year.

The ERS SAR data requirements for an operational system can be summarized as follows:

1. The 14 daily ERS orbits, the 100 km SAR swath width and the lack of a receiving stations covering the Laptev Sea are limiting factors in an operational service. Optimal use of SAR data in the most important parts of the sailing route is necessary to improve the monitoring capability.

2. The ESA data ordering system is acceptable, but the advance time needed to order SAR scenes should be reduced. The processing and distribution procedures used at Tromsø Satellite Station satisfies the needs of an operational ice monitoring system.

3. It is difficult to coordinate geographic and temporal coverage of SAR scenes with the icebreakers' sailing route. Time - distance diagrams for the SAR coverage, combined with the ship's sailing schedule (Fig. 5) can be used to receive optimal SAR data for ice navigation.

4. The transmission of ERS-1 SAR images to users at sea in near real-time is problematic, mostly because the Inmarsat services are limited at high latitudes. Operational transmission of data to MOH in Dikson and other land-based users can be established.

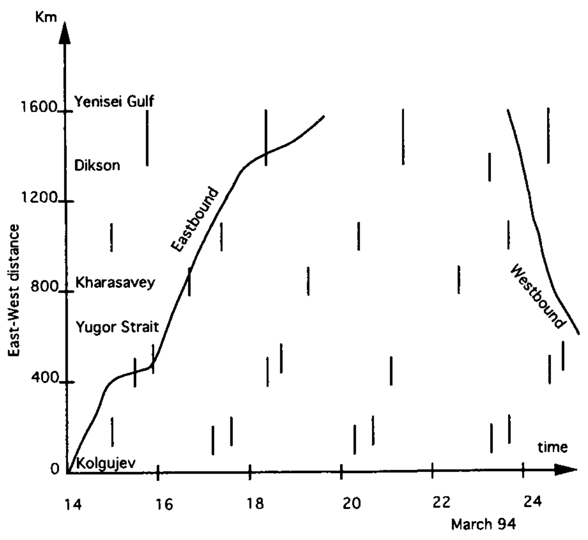

Figure 5. Time - distance diagram for planning of SAR data acquisition along the sailing route. The vertical bars indicate time and location of ERS SAR scenes obtained in March 1994 when ERS-1 was in a 3-day repeat cycle.

4. AN OPERATIONAL ICE MONITORING SYSTEM FOR THE NORTHERN SEA ROUTE USING ERS SAR DATA

The ice monitoring and forecasting is organised under the Russian Hydro-Meteorological Committee and the Ministry of Transport. The key institutions operating the ice monitoring service are the Marine Operational Headquarters (MOH) located in Dikson (for the western part) and Pevek (for the eastern part). The MOHs operate the ice services in cooperation with Murmansk Shipping Company and the Arctic and Antarctic Research Institute. The ice service uses a wide range of observations from satellites, aircraft, icebreakers, helicopters, coastal stations and drifting ice stations. Ice forecasting, both short-term and long-term, is also included in the service.

In order to establish use of ERS SAR data in the operational Russian ice service the following elements must be included:

1. Selection of SAR coverage in strategic areas
Since ERS cannot provide SAR coverage for the whole sailing route it is important to focus the data acquisition to critical areas such as the Kara Gate, Jugor Strait, Vilkitskogo Strait, the New Siberian Islands and Long Strait which can all be covered by eisting receiving stations.

2. Real-time access to SAR data
The acquisition of SAR scenes in near realtime is an essential part of an operational system. Near real-time is considered to be within 6 - 12 hours after the satellite overpass. A time delay of 2 - 3 hours is currently performed in production and distribution of SAR images from Tromsø Satellite Station. Similar access to SAR data is needed for the whole Northern Sea Route.

3. Data ordering procedure
Ordering of SAR data is currently a two -step operation. First, request for SAR acquisition over a given area is submitted to ESA ESRIN about a month in advance. A data production order is then submitted to the receiving station 1 - 7 days in advance. This data ordering procedure should be streamlined in an operational system.

4. Interpretation of SAR images
The validation experiments have provided good insight into many of the ice characteristics of the Northern Sea Route and how they are reflected in the SAR images. In situ obervations of ice and meteorological parameters have been useful in the interpretation of the SAR images (Johannessen et al., 1992a ,b, c, 1995). An interpretation catalogue for SAR ice signatures for ice observers in the Northern Sea Route needs to be produced.

5. Quantitative ice parameters from SAR
Classification of multi-year ice, first-year ice, thin ice and open water can usually be derived from the SAR images. In the summer, when the ice and snow is melting, it can be difficult to identify the ice edge and classify ice types. Ice motion and ice concentration can be calculated. Ice edge, leads and polynyas can be accuaretly mapped. Ice thickness cannot be estimated from SAR images, and methods for localization of ridges are not well developed. It is also difficult to distinguish different stages of young ice because the backscatter changes rapidly as the ice is deformed. More validation studies are needed for better quantification of ice types and ice phenomena in SAR images.

6. Linking ERS data to the Russian ice monitoring services

Routines are currently established to transmit SAR data to the users in Russia. Near real time data are obtained from Tromsø Satellite Station whereas off-line data are ordered from ESRIN. The receivers in Russia are NPO Planeta which forward the data to Arctic and Antarctic Research Institute, MOH in Dikson, Murmansk Shipping Company and selected icebreakers (Fig. 6). Direct links to the icebreakers are necessary to provide real-time data which are coordinated with the ship's sailing schedule. The ice observations on the icebreakers are also important for validation and assessment of the SAR-derived ice information (Fig. 7).

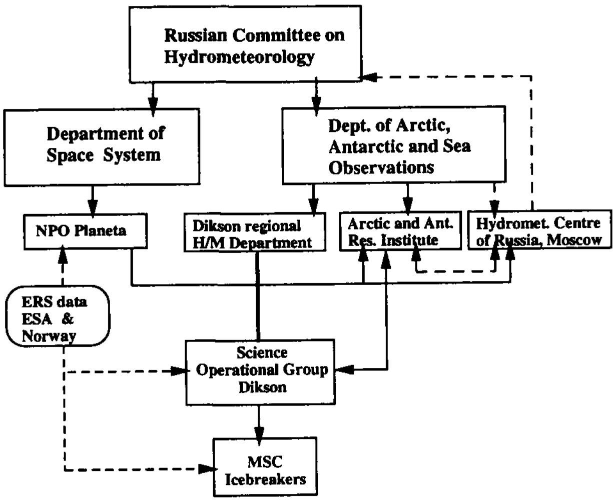

Figure 6. The structure of the Russian hydro-meteorological services and the linking of ERS SAR data to th e various institutions. The arrows indicate the flow of ice data and information.

5. USE OF SIDE-LOOKING RADAR (SLR) ON THE OKEAN SATELLITES

Another useful spaceborne sensor for ice monitoring in addition to SAR is side-looking radars (SLR) offered by the polar orbiting Okean satellites. These data are available on daily basis in 500 km wide swaths at 1.5 km resolution. An example of a SLR stripe covering the eastern Barents Sea and some of the Kara Sea is shown in Fig. 7. The firstyear ice is seen as gray signature around Novaya Zemlya and in the northeastern Barents Sea. The multiyear ice is seen as bright signature north of Franz Josef Land. Open water in Pechora Sea has the darkest signature in the image. In addition to radar data Okean also provide passive microwave and optical data in the SLR swath.

The data from the Okean satellites, which have been in operation since 1983, are processed and interpretated in Research and Production Association NPO Planeta which has an archive of radar images of different regions of the Arctic.

ERS-1 SAR 21. Sep. 13:40 GMT. © ESA/TSS

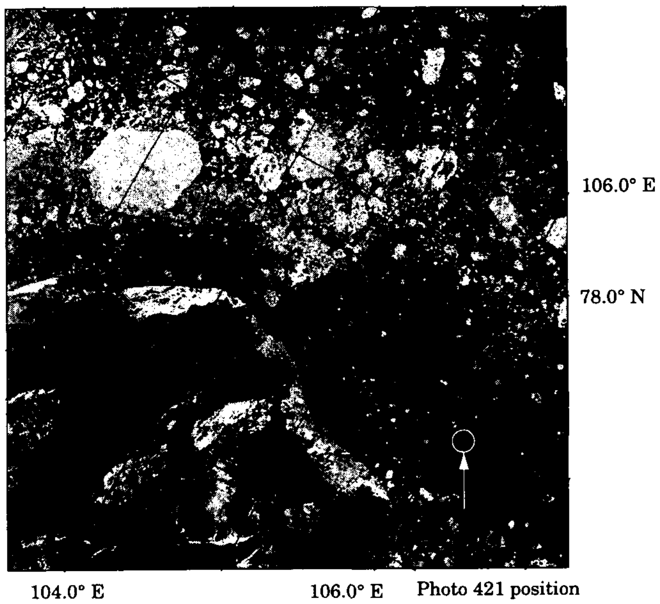

Figure 7. Photograph of an icebreaker convoy documenting the ice conditions in the area east of Cape Chelyuskin on 24 September 1994 (upper figure). The SAR image from 21 September (lower figure) covers the same area. The circle indicates the location of the icebreaker.

6. CONCLUSION

ERS-1 SAR images have been used in ice monitoring of the Northern Sea Route in several demonstration campaigns since 1991. The experience from use of SAR data onboard Russian icebreakers to assist in ice navigation is very positive although ERS-1 can only provide data in selected parts of the Northern Sea Route. In this project a concept for integrating ERS SAR data in the Russian ice monitoring service is demonstrated. The system is currently tested in pilot demonstration phase. In addition to data acquisition and interpretation the project will also address data integration and classification, data transmission techniques and assessment of user requirements.

7. ACKNOWLEDGEMENT

The project has been supported by the Norwegian Research Council, European Space Agency, Russian Space Agency and Murmansk Shipping Company.

8. REFERENCES

Johannessen, O.M. *et al.*. ERS-1 SAR ice routing of *L'Astrolabe* through the Northeast Passage. *Arctic News-Record*, Polar Bulletin 8 (2), 1992a, 26-31.

Johannessen, O.M. and S. Sandven,. ERS-1 SAR ice routing of "L'Astrolabe" through the Northeast Passage. *NERSC technical report no. 56*, February 1992b.

Johannessen, O. M., L. H. Pettersson, S. Sandven, V. V. Melentyev, M. Miles, K. Kloster, L. P. Bobylev, M. Stette, Å. Drottning and K. Ya. Kondratyev. Real-time sea ice monitoring of the Northern Sea Route using ERS-1 satellite radar images. Terra Orbit Technical Report no.1/94, Bergen, July 1994, 33 pp.

Johannessen, O. M., S. Sandven, K. Kloster, M. Miles, V. V. Melentyev and L. Bobylev. A Sea Ice Monitoring system for the Northern Sea Route using ERS SAR data. NERSC Technical Report no. 103, September 1995, 50 pp.

Kloster, K., H. Flesche and O.M. Johannessen. Ice motion from airborne SAR and satellite imagery. *Adv. Space. Res.* 12 (7), 149-153, 1992.

Sandven, S., O. M. Johannessen, K. Kloster and M. Miles. SIZEX'92 ERS-1 SAR validation experiment. EARSeL Advances in Remote Sensing Vol. 3, no. 2 - XII, pp. 50 - 56, 1994.

Figure 8. Okean SLR image of the Novaya Zemlya area on 28 December 1994 (Courtesy NPO Planeta).

TEST OF A NEW ONBOARD SHIPROUTEING SYSTEM

Susanne Lehner[1], Thomas Bruns[2], Klaus Hasselmann[3]

[1] Deutsche Forschungsanstalt für Luft– und Raumfahrt
D – 82230 Weßling

[2] DWD, Seewetteramt
D–20304 – Hamburg

[3] Max–Planck Institut für Meteorologie
D – 20145 Hamburg

ABSTRACT

ERS–1 SAR wave mode spectra are assimilated into the third generation wave model WAM and the improved wave forecasts are then used for a new onboard shiprouteing system.
The forecast wave spectra are partitioned into their dominant windsea and swell components (significant wave heights, directions and periods). These parameters together with the wind fields are transmitted every twentyfour hours to the ship. A route optimization is performed onboard using a Bellmann algorithm
The shiprouteing system was succesfully tested onboard the Hapag Lloyd container ship BONN EXPRESS during a north Atlantic and Pacific crossing. Optimal routes of fuel consumption, for a ten day ECMWF weather forecast and, as reference, the analyzed fields are shown and compared to recommendations of the German Seewetteramt and the actual route of the ship.
Optimal routes in respect to fuel saving, speed and safety are intercompared.
Further application as well as transfer to routine operation is discussed.

1. INTRODUCTION

Important progress in wave analysis and forecasting was achieved by the development of the third generation wave model WAM (WAMDI, 1989). However, results are still limited by the errors in the wind fields, due partly to insufficient sea surface wind data for assimilation in atmospheric models.
Since the launch of ocean observing satellites global coverage of sea surface winds has improved and in addition wave data, like the significant wave height from the Altimeter and 2d wave spectra measured by the Synthetic Aperture Radar (SAR), have become available in real time. Therefore, wave modellers have become interested in wave data assimilation to improve model results and also correct the wind fields from wave field corrections. In a combined wind and wave data assimilation scheme these analysed winds can then be used as input into atmospheric models. Improved wave forecasting is of great value for coastal warning and shiprouteing systems as well as for off shore operations, while improved wave analysis yields improved wave statistics, needed for example to determine the wave forces in the design of ocean and coastal structures.

The two–dimensional instantaneous ocean–wave images of the SAR clearly contain valuable information on the full two–dimensional wave spectrum, the basic function completely characterizing the local sea state. However, because of nonlinear imaging effects due to motions of the sea surface the SAR spectra are distorted, and in addition the propagation direction of the waves can only be determined with standard imaging techniques within 180 degree ambiguity (Hasselmann et al 1990) .
The derivation of a closed nonlinear integral expression describing the mapping of an ocean wave spectrum into a SAR spectrum has enabled the operational implementation of an iterative inversion technique for retrieving ocean wave spectra from SAR spectra (Hasselmann and Hasselmann 1991). The algorithm is based on the minimization of a cost function, using a WAM wave model spectrum as a first guess. It has since been extended to yield smooth, calibrated SAR retrieved spectra by Brüning et al. (1993) and Hasselmann and Brüning (1994).
In recent years several simple schemes have been developed to assimilate significant wave height data from the altimeter into wave models (Thomas et al, 1988, Janssen et al, 1989, Lionello et al, 1990 , Lionello et al 1994,

Günther, 1992).
To correct the 2d wave spectrum from wave height information only, these schemes used either second generation wave models, which prescribe the shape of a wind–sea spectrum, or had to introduce additional assumptions regarding the spectral shape in adjusting the energy level of the spectrum.
These difficulties are due to inadequate information in the assimilation of the full wave spectrum retrieved from the SAR spectra.
The inversion of SAR wave mode spectra and an assimilation scheme for 2D wave spectra for the WAModel including wind corrections, is described in Heimbach, (this issue). An alternative wind correction method based on a Greens function approach is presented in Bauer, (this issue).

2. OPTIMAL SHIP ROUTES

Interest in optimizing ship routes by minimizing fuel consumption received a strong impetus during the oil crisis of 1972, a detailed discussion can be found in Soeding (1989).
In general, the shiprouteing problem is the task of determining an optimal ship route which, for given weather conditions, minimizes some cost function J, dependent on fuel consumption, ship safety, time of arrival and other factors. Thus:

$$J(\mathbf{x}, \mathbf{v}, t_a) = \int_{t_s}^{t_a} F_c(\mathbf{x}, \mathbf{v}, \mathbf{par})\, dt + \alpha_{arr}\, F_{arr}(T, t_a)$$

$\mathbf{v}(t) = \dfrac{d\mathbf{x}}{dt}$ ship velocity

$\mathbf{x}(t_s) = \mathbf{x}_s$, $\mathbf{x}(t_a) = \mathbf{x}_a$ coordinates of start , arrival

$F_c(\mathbf{x}, \mathbf{v})$ cost function for fuel, engine damage and hazards

$F_{arr}(T, t_a)$ cost function for untimely arrival
T planned time of arrival

The fuel component of the cost function is evaluated for a given ship by a Holtrop–Mennen algorithm (1982), using tables of resistance depending on ship speed at given weather conditions from the Hamburger Schiffbau Versuchsanstalt (HSVA, Boese et al. 1974). To the fuel cost function penalty terms for possible engine damage and hazard areas are added with appropriate weights.
The optimization problem is solved using a Bellman type optimization algorithm (Bellman 1967).
The algorithm was implemented on a PC onboard the Hapag Lloyd Container ship BONN EXPRESS and tested during four voyages across the Atlantic and Pacific. Further information on the system and the test conditions are given in Frembgen, (this issue).
The procedure for route optimization was as follows:
The ten day ECMWF wind and wave forecast was formatted by the German Marine Weather Service (SWA) and daily transmitted to the ship via INMARSAT. In the North Atlantic, an ice warning boundary was also transmitted. The optimization was calculated onboard, with the aid of a graphical user interface.
Simultaniously, the German Marine Weather Service provided independent recommendations via telex, fax or phone.

3. TEST VOYAGES

The system was successfully tested onboard the Hapag Lloyd container ship BONN EXPRESS during the following four voyage transects:

1) Thamesport – Halifax, sailing 10.05.95, 6 UTC;
weather conditions:
mainly easterly winds Beaufort force 5 to 6, highest sea states 3 to 4 meters
The most southward occurrence of icebergs was 40N 50W.

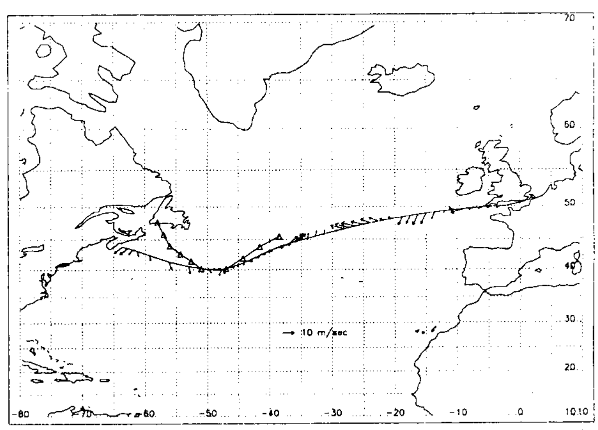

2) Oakland – Yokohama, sailing 4.06.95, 22 UTC;
weather conditions:
in the beginning southerly winds around Beaufort force 7, later turning east , then north; highest sea states 4 meters

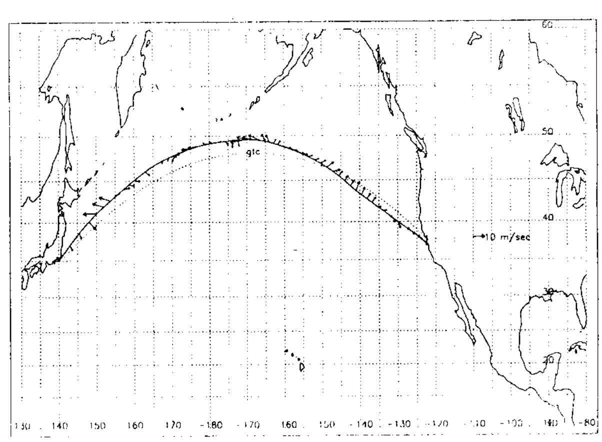

3) Yokohama – Seattle, sailing 29.6.95, 18 UTC; weather conditions:
winds turning from southwest, south to northwest during the voyage, up to Beaufort force 5; highest sea states 3 meters

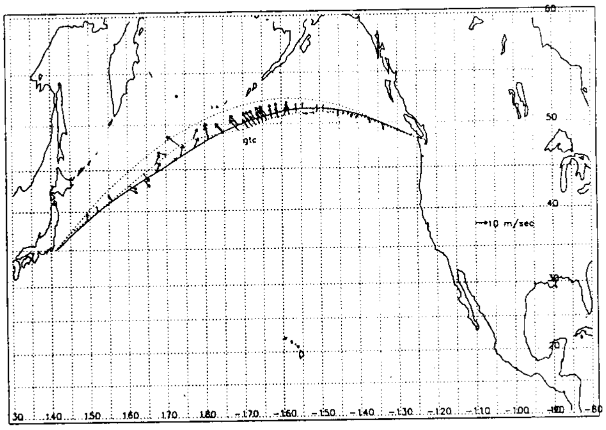

4) Halifax – Antwerpen, sailing 28.6.95 6 UTC; weather conditions:
winds initially north to east force 4, later west to southwest up to Beaufort force 6, highest sea states 3m ;
The most southward occurrence of icebergs was 45N 50W

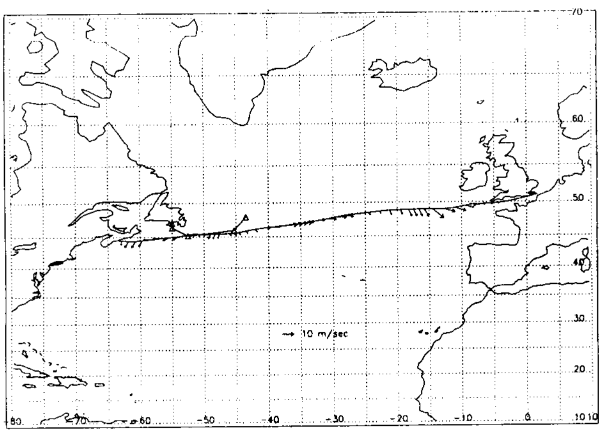

The figures show the four journeys, the optimal route calculated by the optimization system and the wind and ice conditions encountered during the passage.
Due to the relatively weak wind conditions and low sea states, the potential fuel savings on the optimal routes did not exceed 1%, if compared with the shortest navigable routes.
However, the optimization system proved to be useful even under summertime weather conditions:
The system automatically evaluates shortest navigable routes in presence of icebergs.

On the passage to Yokohama the master did not follow the calculated optimal route sligtly north of the great circle, but spent an additional 6% of fuel by going via the Aleutes.
Additional information on the performance of the route optimization system is given in Frembgen, (this issue).

4. ROUTE COMPARISONS

Most benefit from a route optimization can be expected in heavy weather conditions, of course.
As the weather conditions were very calm during the test voyages, comparisons of the route optimization system with the recommendations of the German Marine Weather Service (SWA) and between fore- and hindcasts are given on virtual passages for different weather situations in November and December 94.
Fig. 2 shows an ensemble of daily optimal westbound hindcast routes calculated by SWA for November 94. Two classes of optimal routes can be distinguished, depending on the variability of storm tracks. The high frequency of southern routes reflects a nothward shift of the Aleutian low, not allowing to cruise along routes close to, or north of the great circle.

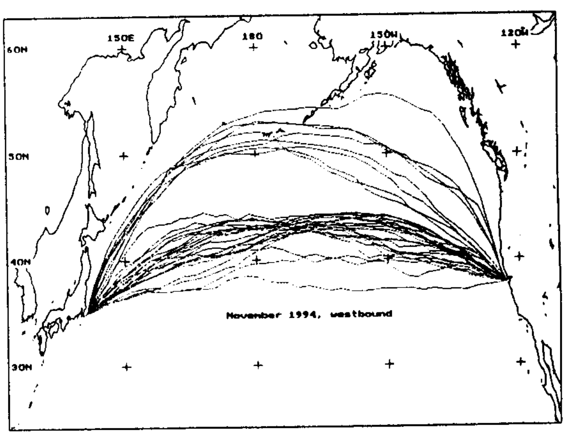

Figure 2 Statistic of optimal routes for November 1994

When comparing the SWA recommended routes with the optimized routes of the present system, in all cases routes of the same classes were recommended by both systems, although routes may differ in detail. Figure 3 shows for example a comparison for a Pacific passage starting on the 20.11.95.
Figure 4 compares fore- and hindcast fuel optimized routes for the same period of time.
After 4 days the fore – and hindcast weather differ substantially, with the result that the optimal forecast route is situated further northward.

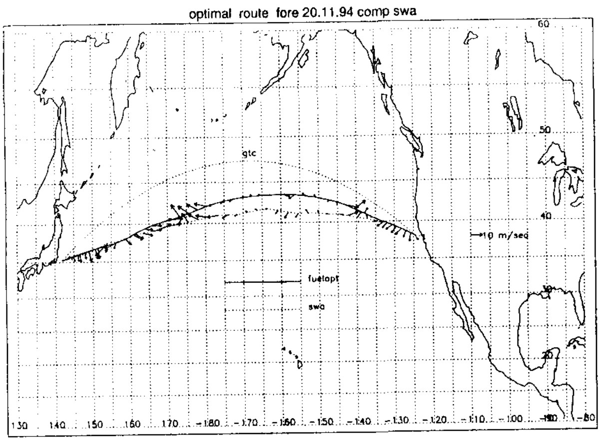

Figure 3 Comparison of SWA recommended route and route of the present system

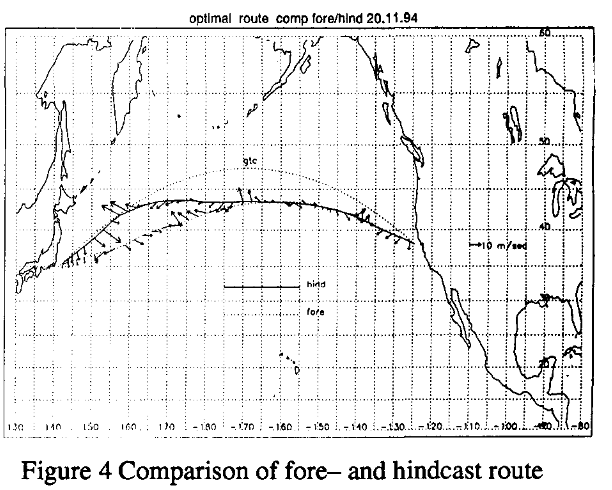

Figure 4 Comparison of fore– and hindcast route

Figure 5 shows a crossing of the Pacific starting on the 5.12.95 during very severe weather conditions. The colors show sea state in one meter contour spacing. In the gulf of Alaska waves higher than 15m are encountered. The yellow line shows the great circle route. Loss of ship or severe damage is possible on this course. The red route is the fuel optimized route, avoiding the severe storm to the south, later turning north, avoiding storms on the great circle. The green route is a second minimum of the optimization, much longer than the red route but safer.
In this case it would seem to be too high a risk to choose the fuel optimal route, since the weather forecast could turn out to be incorrect, the severe storm in the Gulf of Alaska moving southward faster or even intensifying.

5. CONCLUSIONS

The succesful test of an onboard optimization system has provided a bundle of experience and new ideas. Developers are therefore encouraged to integrate onboard shiprouteing into operational shore–based weather information systems. For ship operators an onboard system will soon turn out to be a profitable tool, not only avoiding hazards, but also reducing fuel consumption by an average of 5%.
The value of the system should improve with improved medium range weather and wave forecasts resulting from ERS–1/2 wind and wave data assimilation in operational forecast models.

6. REFERENCES

1. Bellman, R., 1967, Introduction to the Mathematical Theory of Control Processes Vol 1. Academic Press New York–London

2. Boese, P., P. Schenzle and P. Blume, 1974,Programmsystem zur Berechnung der Schiffsgeschwindigkeit unter Dienstbedingungen, Inst für Schiffbau, Bericht Nr. 303.

3. Brüning, C., S. Hasselmann, K. Hasselmann, S. Lehner and T. Gerling, 1993, First evaluation of ERS–1 synthetic aperture radar wave mode data, TAOS 1,

4. Günther, H., Lionello, P. and P.A.E.M. Janssen, 1992, Assimilation of altimeter data in a global third generation wave model, J. Geophys Res., 97, C9, 14453–14474.

5. Hasselmann, K., R. K. Raney, W.J. Plant, W. Alpers, R.A. Shuchman, D.R. Lyzenga, C.L.Rufenach, and M.J.Tucker, 1985, Theory of synthetic aperture radar ocean imaging: A MARSEN view, J. Geophys Res., 90, 4659–4686.

6. Hasselmann, K. and S. Hasselmann, 1991, On the nonlinear mapping of an ocean wave spectrum into a SAR image spectrum and its inversion, J. Geophys Res., C96, 10713–10729.

7. Holtrop, J, et G.G.J. Mennen, 1982, An Approximate power prediction method, International Shipbuilding Progress Nr. 7, 166–170

8. Janssen, P.A.E.M., P. Lionello, M. Reistad and A. Hollingsworth, 1989, Hindcasts and data assimilation studies with the WAModel during the Seasat period, J. Geophys Res., C94, 973–993.

9. Lionello, P., H. Günther and P.A.E.M. Janssen, 1990, Assimilation of altimeter data in a global ocean wave model, in: Proc. of the second conference oceans from space, Venice.

10. Lionello, P., H. Günther and P.A.E.M. Janssen, 1994,A sequential assimilation scheme applied to global wave analysis and prediction. Accepted for publication in Journal of Marine Systems.

11. Thomas, J., 1988, Retrieval of energy spectra from measured data for assimilation into a wave model, Q.J. Royal Meteorol. Soc. 114, 781–800.

12. Soeding, H., 1989, Schiff im Seegang, in: Sicherheit und Wirtschaftlichkeit großer und schneller Handelsschiffe, edit. O. Geisler and H. Keil, VCH.

13. WAMDI group, Hasselmann, S et al., 1988, The WAM model – a third generation ocean wave prediction model, J. Phys. Oceanogr. 18, 1775–1810.

Figure 5 Oakland – Yokohama, sailing 5.12.95
colors show waveheight in 1m contour spacing

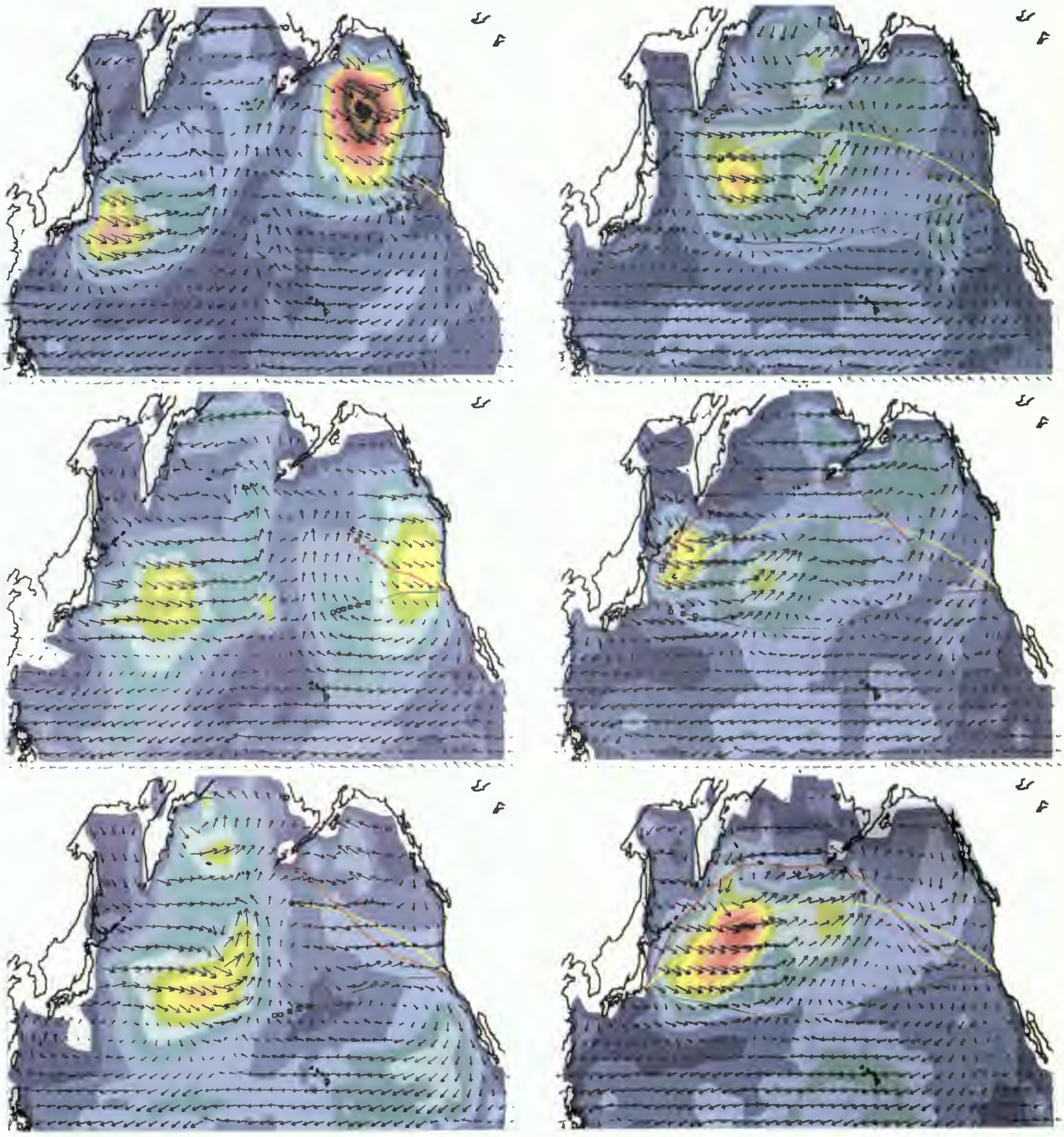

APPLICATION OF WAVE SPECTRAL RETRIEVALS FROM ERS-1 SAR WAVE MODE DATA FOR IMPROVED WIND AND WAVE FIELD ANALYSES

P. Heimbach, S. Hasselmann, C. Brüning and K. Hasselmann

Max-Planck-Institut für Meteorologie, Bundesstr. 55, D-20146 Hamburg, Germany
Tel. (+ 49) - 40 - 41 17 33 77, Facs.: (+ 49) - 40 - 41 17 32 98, e-mail: heimbach@dkrz.de

Abstract

This paper focusses on the operational applications of two-dimensional wave spectra retrieved from ERS-1 SAR Wave Mode data. An improved algorithm for retrieving ocean wave spectra from SAR Wave Mode imagette spectra is described and used to assimilate wave data into the WAModel. The assimilation is based on an optimal interpolation method applied to a spectral partitioning representation of the wave spectrum. Information on the wave field is used to correct both the wave and wind field. Finally, first results are presented of a statistical intercomparison between ocean wave spectra derived from ERS-1 SAR Wave Mode spectra and from the WAModel for a 2 1/2 year data set.

1 INTRODUCTION

With the development of the third generation wave model WAM ([15]), which explicitly solves the energy balance equation for the two-dimensional wave variance spectrum, a powerful tool has become available for research and forecasting applications (see also Komen *et al.* [7]). The WAModel has been extensively validated through implementation at operational forecasting centres such as the European Centre for Medium Range Weather Forecasting (ECMWF) and at many research institutions.

However, prior to ERS-1 no data has been available which provided both continuous global coverage and information on the full two-dimensional spectral structure of the wave field. Thus, validation against observations has been restricted to individual field experiments and relatively sparse operational buoy measurements (for an overview see [7]).

Operational assimilation of wave data has so far been implemented only for significant wave height data retrieved from the ERS-1 altimeter (Lionello *et al.* [8]). A single wave parameter, however, is necessarily of limited value in updating the full two-dimensional wave spectrum. Knowledge of the detailed structure of the wave spectrum, on the other hand, is essential not only for reliable wave predicition, but also for many applications, such as shiprouteing and offshore activities, involving the computation of the response of various structures exposed to complex wave forces. A separation of the wave field into windsea and swell components is furthermore required for the development of an advanced wind and wave data assimilation scheme, as outlined below, which attempts to combine wind and wave data in a dynamically consistent simultaneous update of both wind and wave fields.

The operation of the ERS-1 Synthetic Aperture Radar (SAR) in the so-called SAR Wave Mode (SWM) provided for the first time global two-dimensional wave spectral data in near real time. In contrast to the SAR 100 km full-swath mode, which can be operated only during maximally 10 % of the orbit and while in line-of-sight of a ground station, during SWM operation 10 × 6 km snap shot imagettes are collected globally every 200 km along the satellite track. The data are stored on board and transmitted to the ERS ground stations, where they are processed to power spectra, the so called ERS.SWM.UWA Fast Delivery Product (FDP), on a reduced 12 × 12 polar wavenumber grid (for a description see [4]).

The retrieval of ocean wave spectra from the Wave Mode imagette spectra is not straightforward, since the SAR imaging mechanism is strongly nonlinear due to the distortions induced by the wave orbital motions (the velocity bunching mechanism). This leads, among other effects, to a loss of information beyond the so-called azimuthal cut-off, corresponding to wavelengths in the satellite flight direction shorter than typically 100m. In addition, ocean wave spectra from satellite SAR images (as presently processed) suffer from a basic 180° frozen-image ambiguity.

Nevertheless, the relation between ocean wave spectra and SAR imagette spectra is basically well understood (see [10] and references therein), and through the derivation of a closed nonlinear integral describing the mapping of an ocean wave spectra into SAR spectrum, Hasselmann and Hasselmann ([11]) were able to develop an efficient inversion algorithm enabling a reliable retrieval of ocean wave spectra from SAR imagette spectra within the computational constraints of real-time operational applications.

The original inversion algorithm has been validated (see [3]) and has recently been improved ([13] and [14]), as shortly summarized in the following section. Section 3 describes the assimilation of ocean wave spectra retrieved from SWM imagette spectra in the WAModel. It is shown that measurements of the wave field yield also corrections of the wind field which drives the waves. To reduce the computational requirements in accordance with the restrictions of operational applications, the detailed two-dimensional spectral information is projected onto a smaller set of spectral parameters by partitioning the wave spectrum into a number of individual wave systems. Each wave system, obtained through a modified form of Gerling's partitioning technique ([5]), is characterized by a mean energy, frequency and propagation direction . Finally, in section 4 first results from a statistical intercomparison between ocean wave spectra retrieved from SWM spectra and from the WAModel over a 2 1/2 year period are presented. Despite good overall agreement, small but systematic discrepancies are revealed when the spectra are partitioned into windsea and swell systems. The seasonal and regional stratification of the data provides a useful climatological sea state data base.

2 The retrieval of ocean wave spectra from SAR imagette spectra

The inversion of the closed nonlinear spectral transform relation defining the mapping of an ocean wave spectrum into a SAR image spectrum is carried out iteratively (Hasselmann and Hasselmann ([11]). A SAR spectrum is first computed, using the forwards transformation relation, from a first guess spectrum obtained from a model. The input spectrum is then iteratively modified until a cost function representing the error between the simulated and observed SAR spectra is minimized. The cost function penalises not only the error between observed and simulated SAR spectrum, but also the deviation of the modified wave spectrum from the first-guess spectrum. This has the effect of inserting information from the first guess wave spectrum where information from the SAR spectrum is lacking, namely in resolving the 180° ambiguity and at high wavenumbers beyond the azimuthal cut-off. An important feature of the retrieval algorithm is that the retrieved wave spectra can be calibrated internally, independent of the instrument calibration, using the observed level of the clutter-noise spectrum in the high wavenumber domain beyond the wave spectral signal (see [1]).

Although the original method of Hasselmann and Hasselmann yielded generally reliable retrievals, occasional deficiencies were observed:

(i) The azimuthal cut-off wavelengths were sometimes too high, the inverion algorithm being unable to adjust the input spectra to reproduce the observed cut-off.

(ii) The spectra occasionally exhibited discontinuities in the transitional region connecting the low wavenumber part of the spectrum, which had been modified by the SAR data, and the high wavenumber region beyond the cut-off, in which the original first-guess spectral form was retained.

(iii) In a few cases in which the retrieved spectrum differed significantly from the first-guess spectrum, the simulated and observed SAR spectra also showed larger discrepancies. This was due to the fact that the retrieved spectrum was not allowed to adjust completely freely, but was partially constrained by the first-guess spectrum.

(iv) Finally, the simulated SAR spectra tended to have sharper azimuthal cut-offs than the observed SAR spectra. This was attributed to the smoothing incurred in the SAR spectra of the ESA Fast Delivery Product, which were represented on a 12 × 12 polar (log) wavenumber grid. This last effect was corrected by introducing a similar smoothing filter in computing the simulated SAR image spectra at each iteration step of the cost function minimisation.

To resolve the first three shortcomings, two modifications where introduced into the retrieval algorithm ([13]).

1. A third term was added to the cost function explicitly penalizing errors in the cut-off wavenumber. To accomodate this term, the overall energy level of the wave spectrum was adjusted,

in addition to the energy distribution itself. This affects the wave spectrum also in the high wavenumber region of the spectrum beyond the azimuthal cut-off, where no direct SAR information is available. However, the approach is justified by the fact that the high-wavenumber part of the spectrum contributes significantly to the rms orbital velocity, which determines the cut-off.

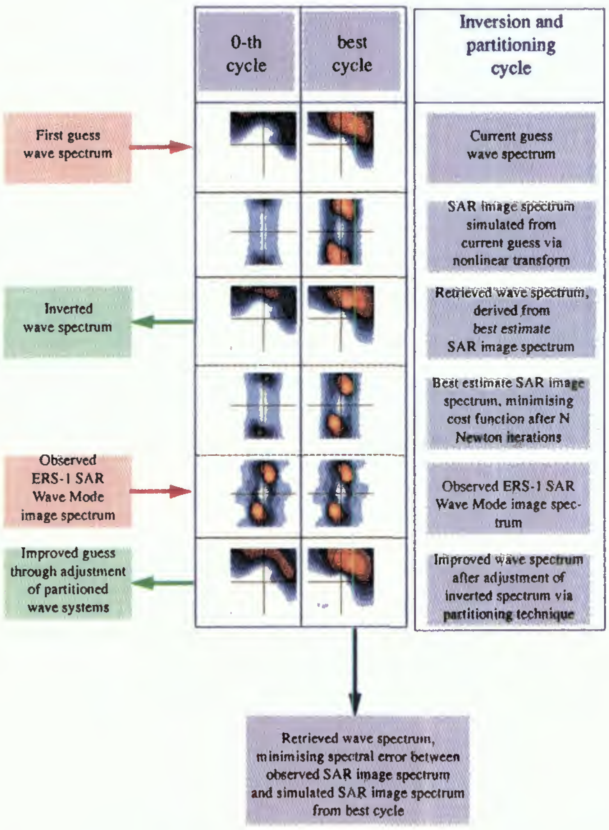

Figure 1: Different steps in the retrieval algorithm, illustrating the iterative improvement of the simulated SAR image spectrum

2. To achieve a smooth transition across the cut-off region, the wave spectrum was decomposed into a number of wave systems, using a modified version of Gerling's partitioning scheme (described briefly in section 3). After cross-assigning the individual first guess and inverted wave systems, the first guess wave systems were adjusted to the systems inferred from the inverted spectrum by modifiying the characteristic mean wave-system parameters (significant wave height, mean frequency and mean propagation direction) by a suitable rotation and rescaling in frequency and energy. A modified input (second guess) spectrum was then reconstructed by superimposing the adjusted wave systems of the original first guess spectrum. Occasionally, a low-wavenumber wave system was found in the SAR-inverted wave spectrum which had no counter-part in the first guess. Such wave systems, indicating swell which the model failed to predict, were simply superimposed onto the modified input spectrum. The modified spectrum now served as an improved input spectrum in a subsequent inversion cycle, the whole procedure being repeated several times if necessary.

   The additional iteration loop on the input spectrum allowed the final retrieval to decouple from the original first guess spectrum, thus leading to a closer agreement between observed and final simulated SAR image spectrum.

   However, it was found that repeated application of the inversion cycle using the iteratively improved input spectrum ultimately leads – in combination with the spectral partitioning scheme – to a gradual broadening of the spectrum and a divergence of the simulated and observed SAR spectra. Thus the iteration on the input spectrum was terminated at the iteration cycle yielding the smallest error between the simulated and observed SAR spectra.

The different steps of the modified retrieval algorithm are illustrated in Figure 1. The figure demonstrates also, for the example chosen, the improvement in the agreement between the best estimate and observed SAR image spectra which can be achieved by iterating the input spectrum.

3 Assimilation of SAR wave data using an optimal interpolation scheme

Existing wave data assimilation schemes have been developed so far only for significant wave heights H_s derived from the ERS-1 altimeter (altimeter wave heights have been or are available also from other satellites such as SEASAT, GEOSAT or TOPEX/POSEIDON, but not in real time, as required for operational applications). In the scheme of Lionello *et al.* ([8]), which has been implemented operationally for global wave forecasts at ECMWF, a set of H_s-values obtained within a given observational time interval is optimally interpolated to all model grid points which lie within a correlation length from the observed data points. The updated model wave field is then obtained by adjusting the total energies of the model wave spectra to agree with the analysed H_s field. At the same time, the frequency scales of the spectra are adjusted, using either fetch and duration laws, in the case of windseas, or the condition that the mean wave slopes remain unchanged, in the case of swell.

The optimal interpolation method of Lionello *et al.* ([8]) can be readily generalized to wave spectral data derived from ERS-1 SWM spectra using the retrieval algorithm described in the previous section. For this purpose, both the WAMmodel and SAR-retrieved wave spectra are partitioned into their individual wave systems ([12], [13]), each of which is characterized by three mean parameters: significant wave height H_s, mean frequency $\bar{f}$ and mean propagation direction $\bar{\theta}$. This represents a significant reduction of the full two-dimensional spectral information to a manageable data set amenable to operational data assimilation. Conveniently, the wave system parameters at the locations of the SAR observations are already computed in the process of the retrieval. However, the partitioning is also carried out at all other model gridpoints within a correlation length scale of the observation points.

To establish a correspondence between observed and modelled wave systems, and between modelled or observed wave systems at different locations, a suitable cross-assignment criterion must be introduced. This is based on a dimensionless distance between the wave systems, defined in the three-dimensional phase space of the model parameters. Observed wave systems which cannot be assigned to a modelled system are introduced as additional wave systems into the updated wave field. However, model wave systems for which no counterpart is found in the SAR retrievals are not deleted from the updated wave field. In this case it is assumed that the SAR was unable to observe the wave system because of low signal-to-noise levels, azimuthal cut-off limitations or other instrumental contamination problems.

Having cross-assigned the observed and model wave systems, updated fields of wave system parameters can now be constructed by standard optimal interpolation. The updated full wave spectrum at each model grid point is recovered by superimposing the corrected wave systems. Gaps are filled by parabolic interpolation.

Corrections in the wave field can be used to infer errors in the driving wind field. For this purpose, the wave systems can be separated into windsea and swell. In practice, it is found useful to introduce also a third wave system class representing mixed windsea and swell. This occurs mainly in turning wind situations in which the usual criterion for a pure windsea is not satisfied, but the wave system is nevertheless still being influenced by the wind. Wave systems are regarded as pure windsea if the component of the wind velocity in the mean propagation direction of the wave system is greater than 1.3 times the phase velocity of the wave system (defined in terms of the mean wave system frequency). The remaining components are then either pure swell or mixed windsea/swell systems. The wind field can now be corrected using the corrected mean wave parameters of the windsea systems. Applying empirical power law relationships for the dependency of the windsea spectral scale parameters on duration or fetch (see [9] and [8]), the duration or fetch dependency can be eliminated to express the local wind speed directly as a function of the total energy (or significant wave height) and mean frequency of the windsea. Since these parameters are updated by the wave data assimilation scheme, one obtains also a corrected wind field. Figure 2 shows as example wind field corrections for the Atlantic inferred from SAR data obtained during a six-hour observation window on November 3, 1992. In a final step the corrected and first guess wind field can be subjected to a further optimal interpolation analysis to yield a best estimate wind field.

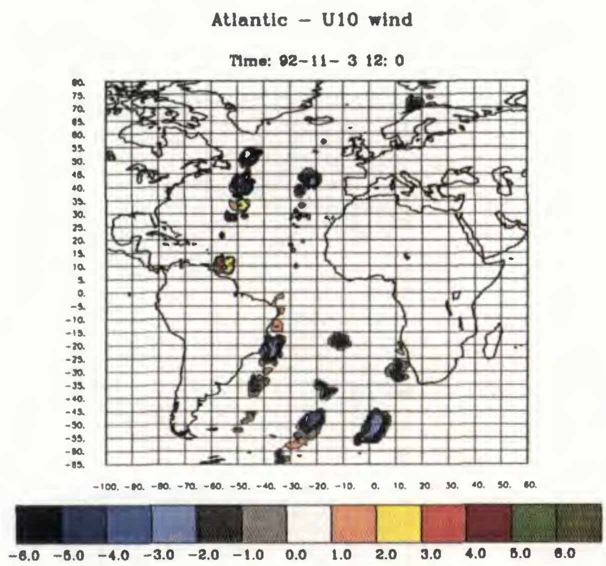

Figure 2: Wind field corrections for a 6 hour assimilation window

4 Statistical intercomparison between SWM-derived and WAModel spectra

The improved retrieval algorithm described in Section 2 has been applied to derive spectral wave parameters from the ERS-1 SWM data for the 2 1/2 year period July 1992 - December 1994 (additional data after this period are currently being processed). Continual long term time series of spectral wave parameters with global coverage are valuable both for research and for the establishment of a global wave climatology. Approximately 1 000 spectra per day were processed, of which about 5 % had to be rejected due to poor signal-to-noise ratio. For another roughly 15 % a reliable inversion failed. The remaining spectra were subjected to various intercomparisons with model spectra computed operationally with the WAModel on a global 3° × 3° grid at ECMWF. In addition to standard integral parameters such as the total significant wave height and wave period, the characteristic parameters of individual wave systems were intercompared both globally and on a regional and seasonal basis. While the spectrally averaged parameters showed good general agreement, the intercomparison of individual wave systems indicated small but systematic discrepancies.

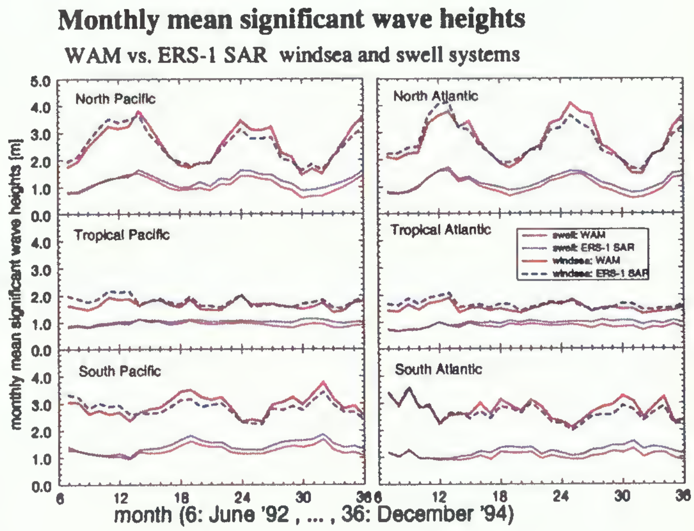

Figure 4: Time series of monthly mean H_s of windsea and swell systems for different ocean basins. Curves for WAM and for ERS-1 SAR retrievals are depicted.

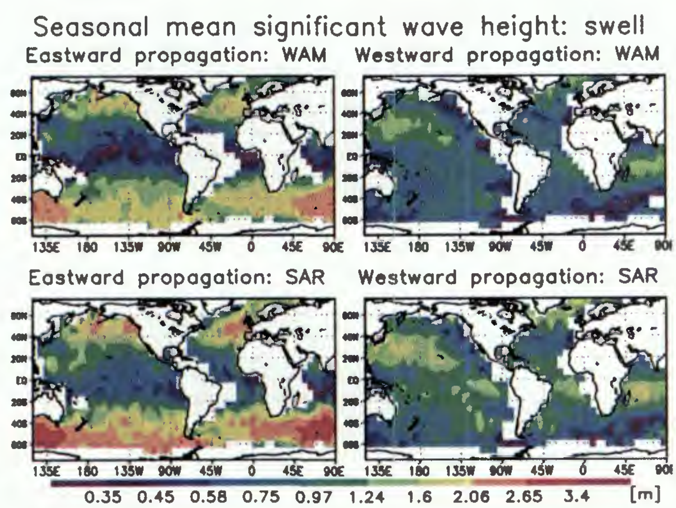

Figure 3: Seasonal mean significant wave heights of swell systems travelling to the East (left panel) or West (right panel) for the period Sept. to Nov. 1994.

Figure 3 depicts as example the average significant wave height of swell systems travelling to the East (left panel) or West (right panel) for (northern-hemisphere) Autumn 1994. The influence of the trade winds is clearly seen in the tropical wave systems travelling to the West, Note also the large swell systems emerging from the regions of high wave activity in the Southern Ocean. Figure 4 shows the corresponding time series of windsea and swell for the North, Tropical and South Pacific and Atlantic in the two propagation directions for the full 2 1/2 year period. The systematic deviations between model and observed wave heights cannot be attributed to erroneous input wind fields alone: the WAModel tends to overpredict the wave height for windsea systems, whereas swell is underpredicted. The data indicate a slightly too strong dissipation source term in the WAModel at low frequencies and a somewhat too strong wind input source function. However, more detailed investigations, including analyses of individual events, are needed to clearly identify the causes of the discrepancies.

5 Conclusions

Detailed knowledge of the two-dimensional wave spectrum is necessary for many applications, including wave prediction, wave research, ship routeing, offshore activities, the construction of reliable wave climatologies and, ultimately, an improved understanding of air-sea interaction processes and the development of coupled atmosphere-wave-ocean models. The synthetic aperture radar is at present the only instrument capable of providing such data continuously and with global coverage.

However, to reliably retrieve ocean wave spectra from observed SAR image spectra, the nonlinear image distortion due orbital motion effects must be taken into account. This problem has been successfully solved by an improved retrieval algorithm based on an efficient inversion of a closed nonlinear forwards transformation relation. The application of the algorithm in an optimal interpolation assimilation scheme yields not only an update of the global two-dimensional wave spectral field, but provides also corrections of the driving wind field.

The statistical analysis of 2 1/2 years of ERS-1 data yields good overall agreement of the ERS-1 retrievals with the WAModel computations with respect to net significant wave height. However, small but systematic discrepancies between the modelled and retrieved wave heights for windsea and swell systems suggest that the WAModel physics can still be improved. The information contained in the ERS-1 spectral retrievals needs to be investigated in greater detail to identify the origins of the deviations found in this first exploratory statistical analysis.

Acknowledgements

This work is a contribution to the ESA pilot project PP2-D1 "Derivation and assimilation of ERS-1 wind and wave data" which is coordinated by Werner Alpers, Institut für Meereskunde, Universität Hamburg. Björn Hansen from ECMWF kindly provided the collocated WAModel spectra. We are also gratefull to R. Brokopf and C. Bennefeld for their assistance.

References

[1] Alpers, W. and K. Hasselmann, 1982: Spectral signal-to-clutter and thermal noise properties of ocean wave imaging synthetic aperture radars. *Int. J. Remote Sensing* **3**, 423-446.

[2] Bauer, E., S. Hasselmann, K. Hasselmann and H. C. Graber, 1992: Validation and assimilation of Seasat altimeter wave heights using the WAM wave model. *J. Geophys. Res.* **C97**, 12671- 1268

[3] Brüning, C., S. Hasselmann, K. Hasselmann, S. Lehner, T. Gerling, 1994: First evaluation of ERS-1 synthetic aperture radar wave mode data. *GAOS* Vol 2, pp. 61-98.

[4] ERS USER HANDBOOK, esa SP-1148, 1993

[5] Gerling, T.W., 1992: Partitioning sequences and arrays of directional wave spectra into component wave systems. *J. Atmos. Ocean. Techn.* **9**, 444-458.

[6] Hansen,B., C. Brüning and C. Staabs, 1994: Global comparison of significant wave heights derived from ERS-1 SAR wave mode, ERS-1 altimeter and TOPEX altimeter data. in: *Space at the Service of our Environment, Proceedings of the Second ERS-1 Symposium, Hamburg, Germany, 11-14 October 1993.* ESA SP - 361, 1994

[7] G.J. Komen, L. Cavaleri, M. Donelan, K. Hasselmann, S. Hasselmann und P.A.E.M. Janssen: Dynamics and modelling of ocean waves, Cambridge University Press, Cambridge, UK, 1994, 560 pp.

[8] Lionello, P., H. Günther and P.A.E.M. Janssen, 1992: Assimilation of altimeter data in a global third generation wave model. *J. Geophys. Res.* **C97**, 14453-14474.

[9] Hasselmann, K., D.B.Ross, P. Müller and W. Sell, 1976: A Parametric Wave Prediction Model. *J. Phys. Ocean.* **6**, 199-228.

[10] Hasselmann, K., R.K. Raney, W.J. Plant, W. Alpers, R.A. Shuchman, D.R. Lyzenga, C.L. Rufenach and M.J. Tucker, 1985: Theory of synthetic aperture radar ocean imaging. A MARSEN view. *J. Geophys. Res.* **C90**, 4659-4686.

[11] Hasselmann, K., S.Hasselmann, 1991: On the nonlinear mapping of an ocean wave spectrum into a synthetic aperture radar image spectrum and its inversion. *J. Geoph. Res.* **96** 10713- 10729

[12] Hasselmann, S., C. Brüning and P. Lionello, 1994: Towards a generalized optimal interpolation method for the assimilation of ERS-1 SAR retrieved wave spectra in a wave model. *Space at the Service of our Environment, Proceedings of the Second ERS-1 Symposium, Hamburg, Germany, October 1993.* ESA SP - 361.

[13] Hasselmann, S., C. Brüning, K. Hasselmann and P. Heimbach, An improved algorithm for the retrieval of ocean wave spectra from SAR image spectra, submitted to *J. Geoph. Res.*

[14] Hasselmann, S., C. Bennefeld and P. Heimbach, 1996: Algorithm for retrieving ocean wave spectra from SAR image spectra, Technical Report of the *German Climate Computer Centre, DKRZ,* in preparation

[15] WAMDI group, 1988: The WAM model - a third generation ocean wave prediction model. *J. Phys. Oceanogr.* **18**, 1775-1810.

AN OPERATIONAL WAVE FORECAST SYSTEM USING WIND AND WAVE DATA

Eva Bauer,[1] Susanne Hasselmann[2] and Klaus Hasselmann[2]

[1] Institut für Meereskunde, Universität Hamburg, Troplowitzstrasse 7, D–22529 Hamburg, Germany; Tel: +49-40-4123-6518; Fax: +49-40-4123-5713; e-mail: eva.bauer@dkrz.de

[2] Max-Planck-Institut für Meteorologie, Bundesstr. 55, D–20146 Hamburg, Germany;

ABSTRACT

The development of a comprehensive wind and wave data forecast and assimilation system is an ongoing task. At ECMWF a wave forecast system using the wave model WAM has been implemented. The wave data from the ERS-1 altimeter are assimilated operationally. This existing scheme is further developed towards a scheme in which waves and winds are updated simultaneously in a dynamic consistent way. The results obtained from different wave data assimilation schemes so far are encouraging.

1. INTRODUCTION

Ocean wave forecasts have many valuable applications, including ship routeing and off-shore activities. The value of these applications will grow with increasing reliability of wave forecasts and extensions in the period with useful forecast skill.

Wave forecasts at the European Centre for Medium Range Weather Forecasts (ECMWF) and many other wave forecasting centres are made using the state of the art third generation wave model WAM (WAMDI Group, 1988; Komen et al., 1994). The model is driven by winds from the ECMWF weather forecast. An important input for reliable wave forecasts is the knowledge of the initial sea state from which the wave model starts the forecast simulation.

The model sea state can be measured globally and continuously with observations of the sea state by the altimeter (wave height) and the synthetic aperture radar (SAR, 2d wave spectrum) onboard the ERS-1/2 satellites. The satellite observations are incorporated in the wave model using wave data assimilation schemes. The initial wave data assimilation methods were relatively simple (Bauer et al., 1992; Lionello et al., 1992). But from these methods useful experience was gained on the application of remote-sensed wave parameters for the validation of wave models.

Significant wave heights of the ERS-1 altimeter are now assimilated operationally at ECMWF. An extended assimilation scheme using integral spectral wave data from the ERS-1 SAR has recently been developed (Bauer et al., 1995a; Hasselmann et al., 1995b).

Since ocean waves are continuously driven by the wind field, the assimilation of wave data yields satisfying results only if the wind fields are continuously updated consistently with the corrections of the wave data. Therefore, the goal is to develop a coupled wind and wave data assimilation system.

In the following results are presented from two wave data assimilation schemes. Firstly, the positive impact of the wave data assimilation scheme currently used at ECMWF based on an optimal interpolation method is demonstrated. Secondly, an application study with the Green's function assimilation method is presented. The Green's function assimilation scheme is designed to detect errors in both the local and in the past wind fields. This method uses two-dimensional wave spectra retrieved from the ERS-1 SAR wave mode image spectra (Hasselmann and Hasselmann, 1991; Brüning et al., 1994; Hasselmann et al., 1995a). It will be shown that wind corrections are often derived from swell, which has to be updated at its location of origin in the past.

2. ASSIMILATION OF SIGNIFICANT WAVE HEIGHTS

The assimilation of significant wave heights through optimal interpolation at ECMWF corrects the sea state of the model in the vicinity of the observations (Lionello et al., 1995). Off-line observations from the TOPEX altimeter provide an independent data set for quality assessment of the significant wave heights from the wave model WAM. An improvement on wave prediction through the data assimilation method is obvious from scatter diagrams which compare the significant wave heights from the wave model with spatially and temporally collocated significant wave heights from both the ERS-1 and the TOPEX altimeter before (fig. 1) and after assimilation (fig. 2).

The significant wave height data sets can be described more precisely by the major and minor axes of their elliptic distribution. The major axis of the ellipse represents the rms variability of significant wave heights and the minor axis the degree of agreement between the data pairs. A close agreement is expressed by a narrow elliptic shape characterized by a small second principal component of the data covariance matrix. The minor axes are clearly reduced

Proceedings of the Second ERS Applications Workshop, London, UK, 6–8 December 1995 (ESA SP-383, February 1996)

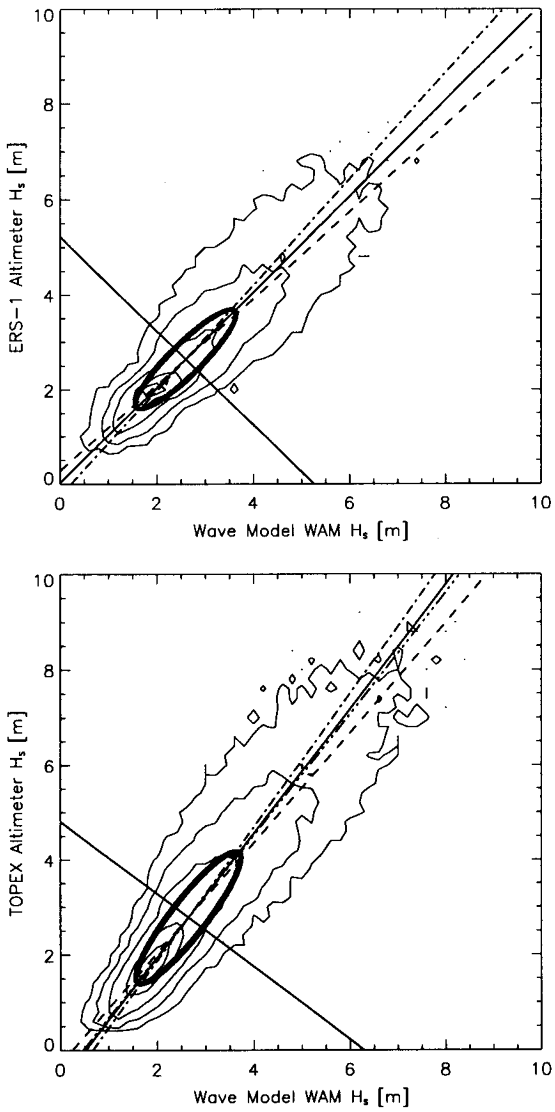

Figure 1: Scatter diagram of global significant wave heights from the wave model WAM before assimilation of ERS-1 altimeter data (May 1993) compared to altimeter data from ERS-1 (top) and TOPEX (bottom). Also shown are the ellipse indicating the principal components, and regression lines.

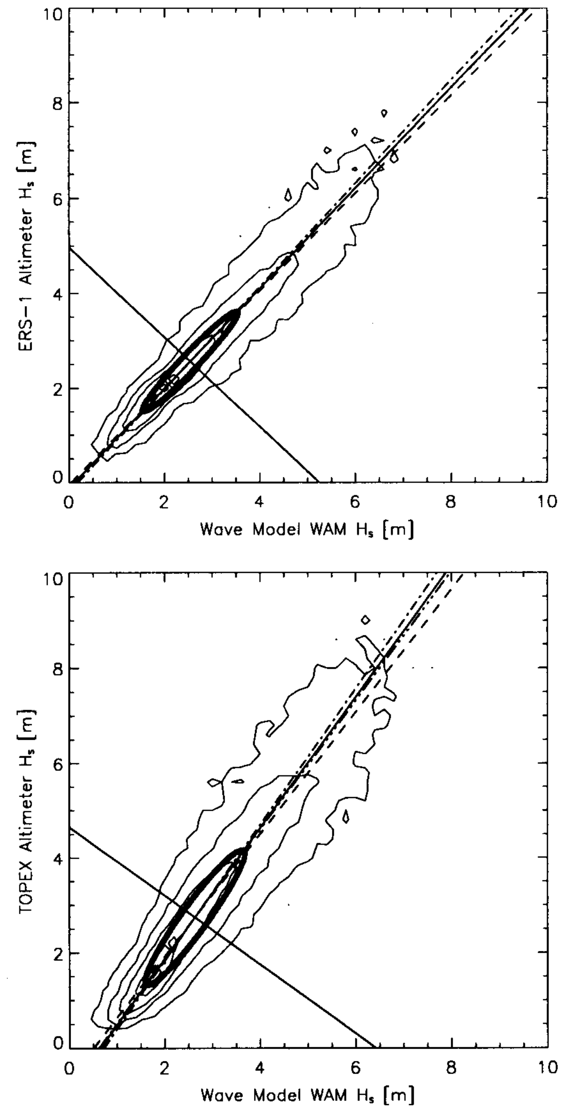

Figure 2: Same as Figure 1 for September 1993 after data assimilation.

after August 1993, when the assimilation procedure at ECMWF was implemented operationally (fig. 3).

3. ASSIMILATION OF OCEAN WAVE SPECTRA

The Green's function assimilation method makes use of the frequency-direction spectra of ocean waves which are retrieved from the SAR wave mode image spectra. Assimilating those data into the wave model WAM yields wind corrections with respect to the driving wind fields (Bauer, 1994; Bauer et al., 1995b). The strength and direction of the wind corrections are retrieved from a linearised relation between the perturbations of the wave energy and the wind derived from the wave model. To solve this relation the Green's function of the perturbed system has to be determined. Introducing a δ-function approximation of the Green's function, the most efficient location in space and time for the wind correction can be derived uniquely.

An investigation using the Green's function method in a study in the Atlantic revealed systematic errors in the driving wind fields. Deficiencies in the wind fields produce locally incorrect windsea which is later transformed into incorrect swell. The incorrect swell continuous traveling along its great circle path until it reaches a coast, yielding repeated identifications of the same wind correction at the same location from different observed spectra at different times and places.

For November 1992 the model predicted significant wave heights in the Atlantic tend to be slightly larger than from the ERS-1 SAR wave mode data, as seen from the slope of the regression line (fig. 4). In the beginning of November 1992 a severe storm occurred in the North Atlantic. The wind speed of the storm in the ECMWF model field is overestimated

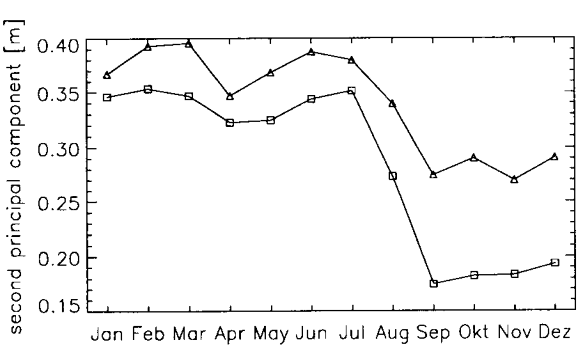

Figure 3: Second principal components (minor elliptic axis) determined from monthly data of the WAM model collocated with ERS-1 data (squares) and TOPEX data (triangles) for 1993. In August 1993 the assimilation of significant wave heights from the ERS-1 altimeter into WAM was started operationally.

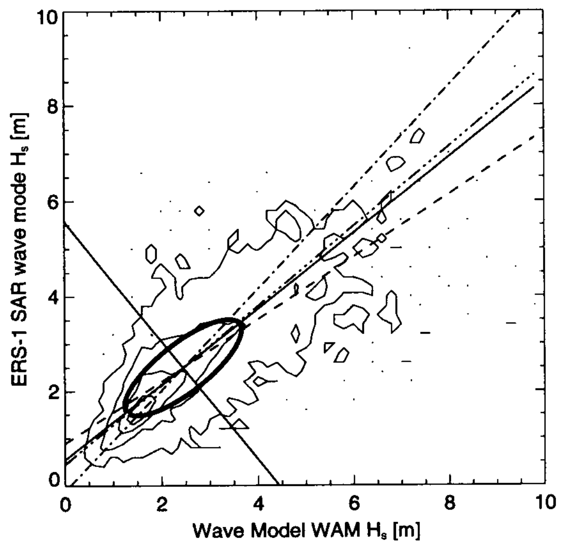

Figure 4: Scatter diagram of significant wave heights from the wave model WAM collocated to ERS-1 SAR wave mode data in the Atlantic for November 1992. Also shown are the ellipse with the principal components, and regression lines.

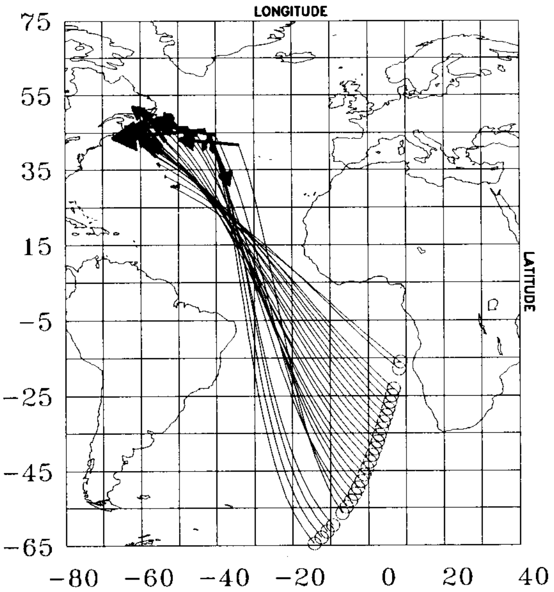

Figure 5: Wind corrections in the NW Atlantic retrieved from Green's function assimilation using ocean wave spectra derived from SAR wave mode spectra measured between 0936 and 0950 on November 15, 1992 in the SE Atlantic. Observations and wind corrections are connected through great circle paths.

in comparison to other data. The storm produced an overprediction of significant wave heights which is still visible ten days after the waves were first generated (fig. 5). The overestimated significant wave heights of the swell observed in the South Atlantic can still be used to infer the wind field error of the transient storm in the North Atlantic.

4. CONCLUSIONS

The benefit on ocean wave prediction from satellite observations has been demonstrated by two different assimilation methods. The method of optimal interpolation implemented at ECMWF clearly improves the determination of the model sea state used to initialize the wave forecast.

The method of optimal interpolation corrects the local sea state. However, to maintain the wave field correction, the driving winds must also be corrected. Since ocean waves consist to a high percentage of swell this implies that nonlocal wind corrections need also be determined.

The detailed analysis of windsea and swell has become possible through the two-dimensional ocean spectra retrieved from the SAR measurements. The information contained in these spectra can be used to extract wind corrections using the Green's function method. The method was shown to be able to detect local and nonlocal errors in the wind fields which are found to be consistent along the path of the waves.

The applications of wave data assimilation has been shown to have a positive impact. The resulting improvements in the ocean wave predictions and forecasts will contribute to the efficiency and security of open ocean and off-shore activities.

Acknowledgements

The work constitutes a contribution to the ESA Pilot-Project PP2-D1 "Derivation and assimilation of ERS-1 wind and wave data" coordinated by PI Werner Alpers, Institut für Meereskunde, Universität Hamburg. The work was funded by the research program "Klimarelevante Prozesse im System Ozean-Atmosphäre-Kryosphäre " (SFB318) by the Deutsche Forschungsgemeinschaft, and by the German Space Agency (DARA) under contract 50 EE 9413.

5. REFERENCES

Bauer, E., 1994, Assimilation of ocean wave spectra retrieved from ERS-1 SAR into the wave model WAM. *Proc. of the Second ERS-1 Symposium*, Oct. 11-14, 1993, Hamburg, Germany, ESA SP-361, 27–32.

Bauer, E., S. Hasselmann, K. Hasselmann & H.C. Graber, 1992, Validation and Assimilation of SEASAT Altimeter Wave Heights Using the WAM Wave Model. *J. Geophys. Res.*, 97, 12671–12682.

Bauer, E., S. Hasselmann & C. Brüning, 1995a, Application of wave spectra retrieved from ERS-1 SAR wave mode spectra in a wind- and wave-data system. *Proc. of IGARSS'95, Firenze Italy*, 1643-1645.

Bauer, E., K. Hasselmann, I.R. Young & S. Hasselmann, 1995b, Assimilation of wave data into the wave model WAM using an impulse response function. accepted by *J. Geophys. Res.*.

Brüning, C., S. Hasselmann, K. Hasselmann, S. Lehner & T. Gerling, 1994, A first evaluation of ERS-1 synthetic aperture radar wave mode data. *The Global Atmosphere and Ocean System (GAOS)*, 2, 61-98.

Hasselmann, K. & S. Hasselmann, 1991, On the nonlinear mapping of an ocean wave spectrum into a synthetic aperture radar image spectrum and its inversion. *J. Geophys. Res.*, 96, 10713–10729.

Hasselmann, S., C. Brüning & K. Hasselmann, 1995a, An improved algorithm for the retrieval of ocean wave spectra from SAR image spectra. (in preparation)

Hasselmann, S., P. Lionello & K. Hasselmann, 1995b, Assimilation of 2d-wave spectra retrieved from ERS-1 SAR wave mode image spectra into the WAM model. (in preparation)

G.J. Komen, L. Cavaleri, M. Donelan, K. Hasselmann, S. Hasselmann & P.A.E.M. Janssen, 1994, Dynamics and modelling of ocean waves. *Cambridge University Press*, Cambridge, UK, 560 pp.

Lionello, P., H. Günther & P.A.E.M. Janssen, 1992, Assimilation of altimeter data in a global third generation wave-model. *J. Geophys. Res.*, 97, 14453–14474.

Lionello, P., H. Günther & B. Hansen, 1995, A sequential assimilation scheme applied to global wave analysis and prediction. *J. Marine Systems*, 6, 87–107.

WAMDI Group (S. Hasselmann, K. Hasselmann, E. Bauer, P.A.E.M. Janssen, G.J. Komen, L. Bertotti, P. Lionello, A. Guillaume, V.C. Cardone, J.A. Greenwood, M. Reistad, L. Zambresky & J.A. Ewing), 1988, The WAM model - A third generation ocean wave prediction model, *J. Phys. Oceanogr.*, 14, 1775–1810.

A DEMONSTRATION OF SHIP ROUTING WITH NEAR REAL TIME ERS-1 DERIVED ICE CHARTS

Kim Partington[1], Bill Hodson[2], Kristian Teleki[3], Gareth Rees[3], Morten Larsen[4] and Anthony Graves[5]

[1]*GEC-Marconi Research Centre, West Hanningfield Rd., Gt. Baddow, Chelmsford, Essex CM2 8HN, UK*
Tel: (44) 1245 473331. Fax (44) 1245 475244

[2]*SAIC Ltd., Poseidon House, Castle Park, Cambridge CB3 0RD, UK*
Tel: (44) 1223 460747. Fax (44) 1223 60245

[3]*University of Cambridge, Scott Polar Research Institute, Lensfield Rd., Cambridge CB2 1ER, UK*
Tel: (44) 1223 336559. Fax (44) 1223 336549

[4]*Nunaoil A/S, Pilestrade 40C, 1112 Copenhagen K, Denmark*
Tel. (45) 3332 2932. Fax (45) 3332 3165

[5]*Matra-Marconi Space (UK) Ltd., Anchorage Rd., Portsmouth, PO3 5PU, UK*
Tel: (44) 1705 664966 Fax (44) 1705 674642

ABSTRACT

The polar regions are particularly difficult to monitor using conventional observing methods and so represent an important market sector for information derived from synthetic aperture radar. A wide range of operators make use of sea ice information including resource survey groups, transportation companies and weather forecasting agencies.

An ERS-1 Pilot Project was established in 1992 to promote the operational use of ice information from SAR. This culminated in a near real time demonstration of the provision of high level ice charts to a seismic survey vessel off Greenland. This made use of a West Freugh-based facility for rapid dissemination of SAR image products, known as RAIDS, and an ice workstation which is able to produce a range of high level sea ice products from SAR data. This paper describes the elements of the prototype operational ice monitoring facility and reviews the developments needed to fully address user requirements.

1. INTRODUCTION

The ERS-1 Pilot Application Project for Polar Operations was initiated in 1992. In addition to receiving a quantity of ERS-1 SAR data to support development of the application, the project received financial support from the British National Space Centre, as part of its mandate to promote the commercialisation of remotely sensed data. The project is aimed at stimulating the market for SAR data in areas of sea ice, where there is no viable alternative to satellite data for regular, large coverage views of the surface.

The market is best stimulated by users being involved in demonstrations which are as realistic as possible. Off-line demonstrations of products do not have anything like the impact of near real time demonstrations where the users obtain products in the context of actual operations, albeit for a limited period. It is only through these on-line demonstrations that potential customers can be convinced of the utility of the products being offered.

A near real time demonstration was therefore set as a goal for the project. To achieve this, the various elements of a prototype operational facility were established and brought together. Figure 1 shows the facility and its various elements.

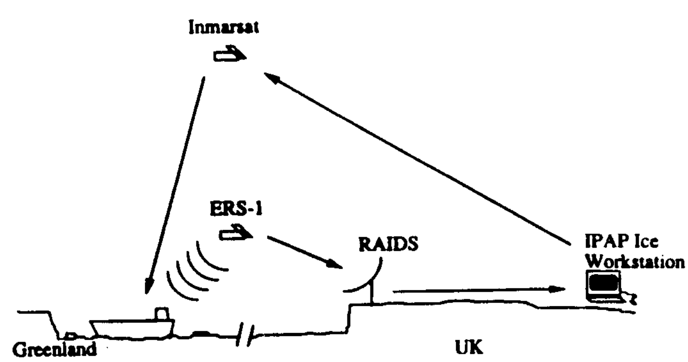

Figure 1. Prototype operational ice monitoring facility using the ERS-1 SAR, the Rapid Information Dissemination System (RAIDS), the Ice Workstation and links to user via Inmarsat.

The following sections review the elements of the demonstration facility.

2. RAIDS

The Rapid Information Dissemination System (RAIDS) is a facility for the provision of electronic on-line access to ERS 1&2 data direct from West Freugh ground station. West Freugh has coverage extending along the eastern coast of Greenland as well as Arctic areas north of Europe.

Access to RAIDS imagery on-line requires a PC or UNIX workstation, the User Access Terminal software and a modem link. The products are downloaded by dialling through to RAIDS, logging on via password access and selecting images of interest. The baseline product is a 100 m pixel product which has 24 looks and which corresponds to the same coordinate frame as the ESA precision image product. Browse images with 400 m pixels and precision sub-scenes with 12.5 m pixels are also available, the latter covering an area of 25 x 25 km. For sea ice monitoring, the 100 m pixel images were used. The use of RAIDS does not preclude the requirement to schedule the SAR for acquisitions over the area of interest.

The downloaded image file is accompanied by a text (header) file which gives information on image coordinates, acquisition date and time. This information is used further along in the processing chain to enable the image data to be translated into appropriate map projection.

RAIDS has been accessed with no major problems encountered. However, improvements are planned through the introduction of direct data capture to provide automatic end-to-end processing. In addition, image access via wider bandwidth media such as the Internet are being explored. When these improvements are implemented, lag times in provision of SAR-derived products will be reduced to levels which are even more attractive for operational use.

3. ICE WORKSTATION

The Ice Workstation is designed to produce sea ice charts using SAR data. To achieve this, it carries out several basic functions, as illustrated in Figure 2.

The image data are pre-processed before any ice information is extracted. Pre-processing includes registration to selected map projection, sampling to an appropriate pixel size (normally 100 m by 100 m), land-masking to avoid processing of land data and radiometric calibration (if required).

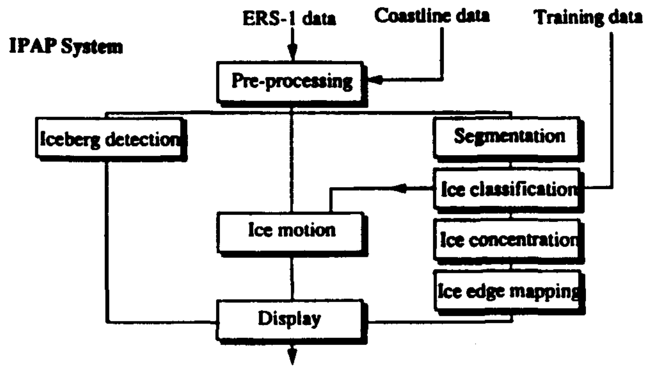

Figure 2. An illustration of the Ice Workstation, showing the main components of the system.

Different processing schemes are then used depending on the product required. If iceberg detections are to be provided, then the image data are processed in raster and morphological and thresholding operations are used to pick out the characteristic neighbouring bright and dark signatures associated with icebergs in open water. If ice motion is required, then a pair of pre-processed images are passed into the ice motion sub-system and a hierarchical cross-correlation scheme is used to find ice motion vectors, with the cross correlation coefficient used to filter out poor matches.

If an ice edge or ice type concentration product is required, then the data are converted into a vector format through segmentation, with homogeneous regions in the image given backscatter, texture and shape attributes which can be used in the classification. A pre-selected training dataset can then be used to classify the image data, using a supervised classifier, before ice type concentration or an ice edge product is output in raster format. The classification outputs confidence information to assist the user in assessing the product. In practice, variations in wind speed, surface temperature and other factors make the classification procedure a computer-assisted manual classification, as a training dataset derived for one set of circumstances is rarely applicable to other circumstances. Nevertheless, the algorithm is very efficient at classifying regions from a relatively small training dataset.

Finally, the products are provided with header information and suitable annotation in a Display module.

Examples of products are shown in Figures 3 to 6.

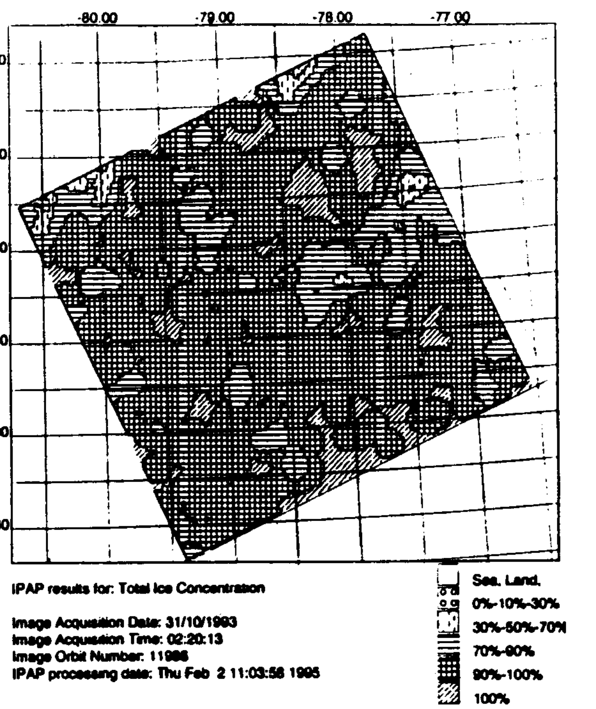

Figure 3. Example of ERS-1 derived total ice concentration product from the ice workstation.

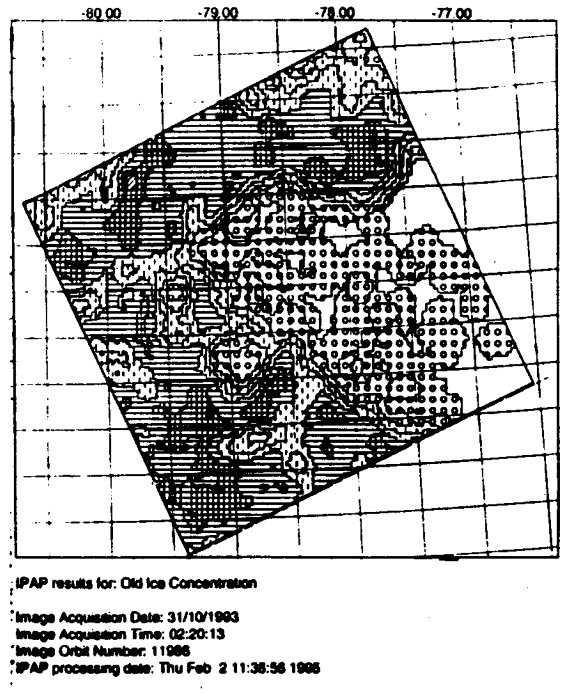

Figure 4. Example of ERS-1 derived old ice concentration product from the ice workstation.

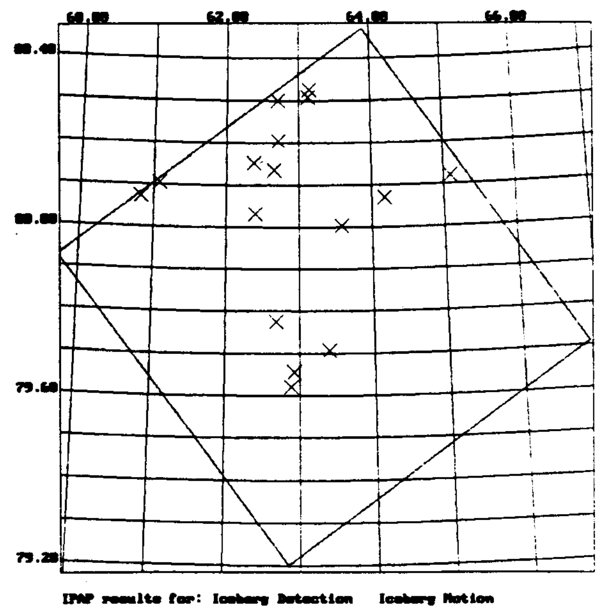

Figure 5. Example of ERS-1 derived iceberg detection product from the ice workstation.

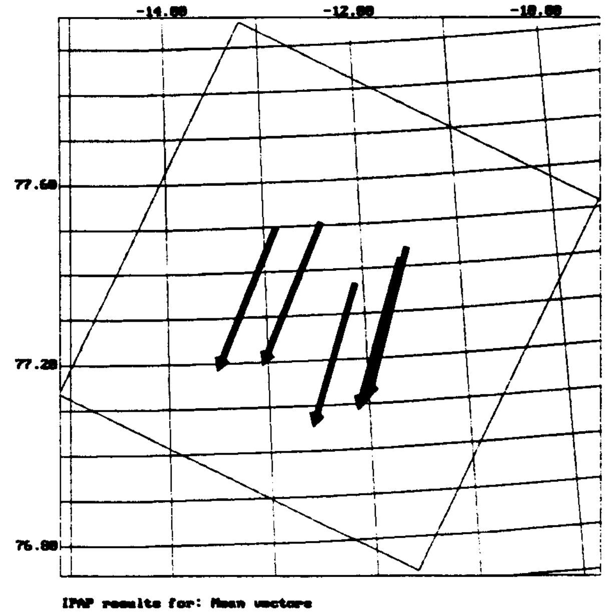

Figure 6. Example of ERS-1 derived ice motion product from the ice workstation.

4. NEAR REAL TIME DEMONSTRATION

A near real time demonstration was carried out in August 1994, over a 12 day period with the cooperation of Nunaoil, who operate a seismic survey vessel the "Thetis" off Greenland, where they are undertaking a programme of geophysical surveys. The region of activity can be covered by high ice concentrations even during August. The area of interest was defined in advance and acquisitions planned via ESRIN. For each day during the trial, a single frame was identified as being high priority and was processed rapidly to appear on the RAIDS bulletin board an hour or less after data acquisition. On each day of the trial, facsimile correspondance via Inmarsat provided information on the following day location of interest, based on ice conditions and other factors. This information also identified any problems with transmission of previous products and identified requirements on product type for the following day.

Once the data appeared on the RAIDS Bulletin Board, the frame was downloaded via standard telephone lines via a modem, together with a header. The data were then processed to generate an ice chart and this was then transmitted as a hardcopy print via facsimile on Inmarsat.

5. ASSESSMENTS

The trial, and other off-line analyses of products, provided the basis for an assessment of the products. The opportunity to compare AVHRR-derived ice charts (which is the more conventional product) with helicopter video observations and observations by eye was invaluable and provided a rapid learning opportunity for the end-user.

The achievements of the trial were in providing products between 2 and 4 hours of data acquisition. Towards the end of the trial, the SAR-derived ice charts were received more quickly than the AVHRR-derived ice charts. Post-trial analysis indicated that there was a clear correspondance between ice concentrations derived from AVHRR data and those obtained from SAR, although at middle concentrations, there was a discrepancy. It is not clear whether this is a problem with the AVHRR or SAR-derived ice concentrations, or both.

The sampling of ERS-1, combined with uncertainties in the position of the ship, were such that it was not possible to generate an ice motion product in the vicinity of the ship. However, off-line analysis of the product indicated that this was robust for three day repeat data in areas of pack ice.

The iceberg product was not generated as the ship was operating in areas of sea ice, where the iceberg detection algorithm does not work. Off-line assessments of the performance of this algorithm, with data from Franz Josef Land and from the Canadian Bergsearch '95 Programme indicate good detection probabilities in open water, with about 40% of bergs in the size range 15-60 m. diameter being detected with 100 m pixel data and all bergs over 120 m in diameter being detected. Analysis of this product continues.

A number of improvements were recommended following from the trial, including:

- ♦ Digital transmission of products;
- ♦ Ship-borne facility for ingestion, display and co-registration of ice chart products from different sensors (including marine radar);
- ♦ A Bulletin Board service which provides easy selection of data based on location and time and which includes high level ice charts in addition to basic image products;
- ♦ Access to meteorological information on temperature and wind speed and direction to assist in generation of training datasets for classification;
- ♦ Pricing of data as part of a service rather than solely on an image-by-image basis. This would make sense where access to data is important but the total demand is unknown in advance.

6. CONCLUSIONS

The experience of the project indicates that an ice monitoring facility would best be operated as a single node for ice and meteorological products, with some requirement on the end-users to have on-board facilities for the reception and limited manipulation of these products. The prototype ice monitoring facility used in this project was invaluable in providing the end-user with a feel for the value of the products. Further assessment work is planned with end-users and with Radarsat data. Upgrades to RAIDS and improved sampling of Radarsat should provide opportunities to further stimulate the market for SAR-derived ice products.

7. ACKNOWLEDGEMENTS

ERS-1 data was provided by the European Space Agency. The project was sponsored by the British National Space Centre, and managed by the UK DRA.

POTENTIALS OF SAR FOR SEA ICE SHIP ROUTING BASED ON EXPERIENCES OBTAINED WITH ERS-1 SAR IN THE BALTIC SEA

Bertil Håkansson and Mats Moberg

Swedish Meteorological and Hydrological Institute, S-601 76 Norrköping, Sweden

Tel: (46) 11 158385 Fax: (46) 11 170207 e-mail: bhakansson@smhi.se

ABSTRACT

Seasonal ice cover occurs every winter in the Baltic Sea. Depending on the severity of the ice season, shipping is more or less obstructed. Substantial resources are allocated in Sweden to facilitate winter navigation in the form of a huge icebreaker fleet. In optimizing icebreaker operations a thorough knowledge of present and future ice conditions as well as weather forecasts is required. To meet this demand the Ice Service at SMHI uses all possible sources of information on ice conditions such as observers on the coast and on ships as well as remote sensing information from air and satellite.

As a part of ESA AO-1 and Pilot Project programme, application experiments were carried out during two winter seasons using ERS-1 SAR imagery. The results obtained were encouraging, especially regarding the operational use onboard the icebreakers in matters of optimizing the route in the icefields when convoying and conveying route information to merchant ships going by there own. A considerable gain in optimization of icebreaker operations can be achieved with the additional information provided by the SAR imagery. Considering that the total cost for the icebreaker service during the winter 1993/94, which engaged up to six icebreakers simultaneously, was approx. 140 MSEK of which just bunker expenditures amounted to 20 MSEK, it is obvious that even minor improvements in icebreaker tactics will give a substantial cost reduction. In times with more dynamic ice conditions, access to SAR data can surely contribute even more in reducing costs.

With the launch of Radarsat, SAR information can be accessible on an operational basis. Time and coverage are the crucial issues whether the usefulness of SAR information can be fully utilized for operational use. SAR sea ice data should cover all the area of interest once a day and the data should be available whitin 2 to 3 hours at the Ice Service Center. Experiences show that segmentation and/or classification of the imagery is not crucial for the interpretation onboard the icebreakers since this is done by highly skilled officers, but of course such derived SAR image products could be valuable complements in the future. Of great importance is, however, that the SAR imagery can be distributed whithin a reasonable transmission time and presented in a way onboard the icebreakers that suits navigational needs of the users.

1. INTRODUCTION

Sea ice occurs every winter in the Baltic Sea with an extensively varying areal coverage (Fig. 1 and 2). The icebreaking and navigation activities in the area are intensive and depend on daily sea ice and weather information to keep the traffic safe and efficient. The compiled daily information on sea ice conditions and forecasts are distributed among shipping interest, ships, icebreakers, fishermen and many others, and are requested for both planning and operational activities. The information is in the form of ice and sea surface temperature charts, ice and weather bulletins, ice forecasts and routing advices.

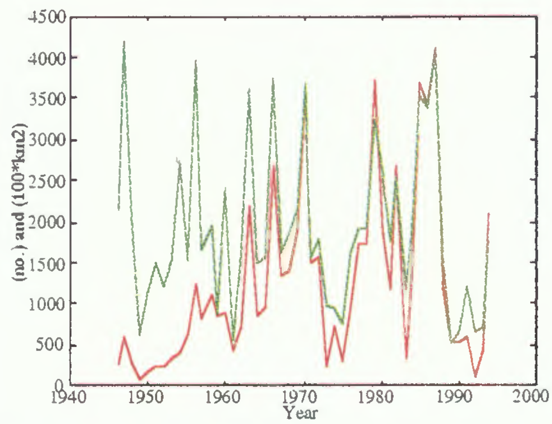

Fig. 1: Annual maximal ice extent (green/grey) in the Baltic Sea (from Seinä and Palosuo, 1993) and annual number of icebreaker assists (red/black), including towing numbers.

Remote sensing imagery has been in use for some decades as a basic information source for the winter navigation in the Baltic. Most important is NOAA AVHRR imagery for mapping sea surface temperature, which is a basic variable for cooling and new ice formation forecasts. During winter the imagery is often a major observation data set for real-time ice mapping of ice edges, leads, thin and thick ice. However, the extensive cloud coverage and the bad sun illumination during mid winter, limiting the usefulness of infrared and visual satellite remote sensing for winter navigation, are the reasons for the search of new sensors less sensitive to atmospheric disturbances.

Proceedings of the Second ERS Applications Workshop, London, UK, 6–8 December 1995 (ESA SP-383, February 1996)

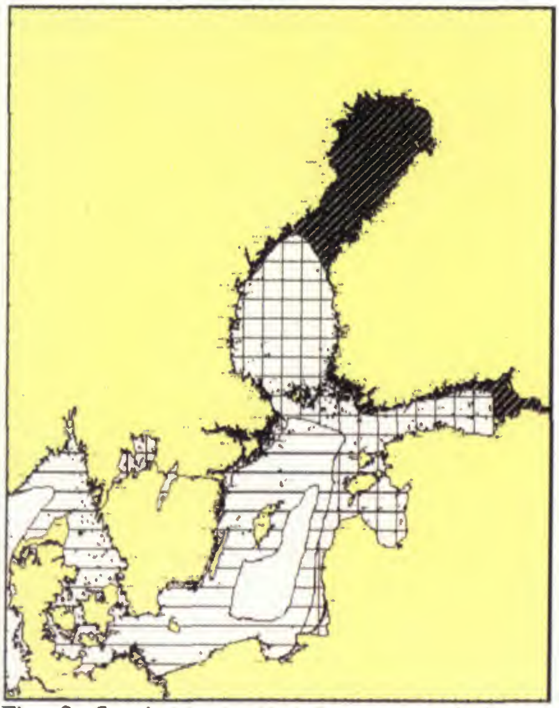

Fig. 2: Sea ice coverage, on average, during a mild (black), normal (cross marked) and severe (line marked) winter in the Baltic Sea area. Note that also the eastern part of the North Sea (i.e. Kattegat and Skagerrak) is ice covered during a severe winter.

Today the most promising sensor is the Synthetic Aperture Radar. At our institute we have built up experiences handling satellite-borne SAR data for ice mapping and icebreaker operations in the Baltic. We have during the last 4 years conducted research projects together with microwave groups at Chalmers University in Göteborg and the National Defence Research Establishment in Linköping. Airborne SAR was used in calibration and validation experiments in the Baltic during the winters of 1987 and 1988. A pilot project demonstrating the possibilities with ERS-1 SAR imagery for winter navigation was carried out in 1992 and in 1994 with good results and with a large response from icebreaker officers (Håkansson et. al., 1995). All the work so far has been performed with funding from the National Space Board and from the National Maritime Administration, whereas ESA has put forward ERS-1 SAR data in real- and delayed time. In many of the projects we have cooperated with Finnish research groups at the Finnish Institute of Marine Research and the Helsinki University.

2. BASIC INFRASTRUCTURE FOR WINTER NAVIGATION

2.1 ICE MAPPING

The daily ice and sea surface temperature chart is produced at the Ice Service digitally with the IceMap software. This UNIX-based system is an application for computer aided design of charts, where raster based satellite image processing display is combined with interactive, object oriented drawing.

When drawing, geocoded satellite images from AVHRR or SAR can be displayed as a background when creating the ice/temperature chart. The chart consists of normal drawing symbols (ovals, lines, text) and different hatched areas of ice as well as special symbols for ice edges, cracks, rafted ice and ice ridges and other ice chart symbols. As IceMap is object oriented, editing an old ice chart is easy. This reduces the amount of work needed to produce a new chart as the changes usually are rather small in a day-to-day perspective. The drawing on the display is faciliated by a Bezier-curve-tool.

Sea surface temperatures can be assimilated from as well point measurements as from AVHRR IR-images. There is support for an automatic generation of isotherms.

As already mentioned, one of the most valuable sources of information hitherto on the ice conditions is, when available, NOAA AVHRR. Regurlarly information from ice breakers and coastal stations forms the base level of ice data. Occasionally, air observations from the air force and the icebreaker based helicopters are accessible.

Of course, every new ice chart is based on the previous one and in situations with great ice dynamics and perhaps no information from sea areas subject to this, the marine meteorologists have to rely partly on forecasts from weather models and the sea ice forecasting model in order to analyze the current ice situation.

2.2 FORECASTING

The Ice Service also has the obligation for issueing forecasts for the weather and the ice conditions in order to facilitate planning of the icebreaker operations at both the tactical and the strategic scale.

For weather forecasts HIRLAM (High Resolution Limited Area Model) is used, and for ice prediction the new ice-ocean model BOBA.

BOBA, which in its first version was introduced during the winter of 1992/93, is a coupled ice-ocean model system simulating both dynamic and thermodynamic processes. The dynamical part is based upon a two-dimensional coupled ice-ocean model that resolves the horizontal space and time and the thermodynamic part of the system is based upon a one-dimensional coupled ice-ocean model that resolves the vertical space and time for different regions in the Baltic Sea. The model is forced using meteorological fields from HIRLAM.

The forecasted parameters are: water cooling, ice formation, ice growth and decay, ice drift and ridging, vertical mean currents, sea levels and water warming.

2.3 COMMUNICATIONS

Two types of SAR images are received at SMHI and are converted to 8-bit format and transformed into a Mercator projection based on the control points given in the image header file. A Mercator image with 200 meters pixelsize is created for each scene.

The images are then analysed and classified manually by the ice service staff as a support for the daily production of ice charts.

Images aimed for use onboard the icebreakers are distributed digitally from SMHI, utilizing the Nordic Mobile Telephone system and an image compression technique. To keep an acceptable dissemination time to the ice-breakers, the image size is fixed to 512 by 512 pixels. This restriction requires a selection of a narrow area with full resolution or an appropriate resampling of a larger area.

For distribution and graphical presentation on-board icebreakers of maritime information, satellite images as well as weather and ice forecasts the Iceplott software is used. This is an application developed jointly for the Swedish and Finnish National Maritime Agencies.

The information is presented on Macintosh computers with large screens, situated on the icebreaker bridges. Positions of icebreakers, merchant ships as well as harbours are plotted on a graphic coordinate system showing the contour map of the Baltic Sea. Text information as harbour status and latest icebreaker reports can be accessed.

When available, satellite images as AVHRR or SAR are placed over the contour map, giving information on ice conditions. Satellite images are correctly placed in this coordinate system, regardless of image scale.

3. PRE-OPERATIONAL TOOLS

3.1 SAR USEFUL FOR SEA ICE MAPPING

The geometric resolution of satelliteborne SAR (30 -150 meters) is a kind of optimized value for interpretation needs and spatial coverage. Too detailed geographic information obtained from SAR imagery for operational products such as the ice chart is not efficient, taking into account the scheduled time for chart deliveries and the time available for production. One should also have in mind that, presently, the Icemap system needs a human driver and decisionmaker, since the system depends on subjective interpretation, of the imagery and other observation datasets, by the ice meteorologist. Today this is a prerequisite since the sea ice variables, and hence the ice code system, is difficult to translate into a numerical language. More important, the imagery used for ice chart drawing is not free from ambiguity, since wind waves in open water areas can have similar backscatter characteristics as ridged ice. In addition, the microwave backscatter respons during warm air conditions is damped, lowering the image contrast. The human interpreter can take these problems into account, since he has additional information with which to compare (model forecast, past ice and weather development, contacts with icebreakers, for example). Hence, presently we are not ready to entirely rely on objective analysis of SAR imagery as an operational tool.

Nevertheless, SAR imagery is greatly appreciated, since it provides reliable information on ice roughness regular in time during cold weather conditions when ice navigation can be very hazardous (Håkansson et.al., 1995). It is, thus, an important observational data set to improve the resolution and the accuracy of the ice chart. This product is now also used to initialize the ice forecasting model of the Baltic Sea (Omstedt and Nyberg, 1995). Evidently, it is necessary to make the ice chart as accurate as possible, since it will have strong influence on the accuracy of the forecast.

3.2 NOWCASTING OF SHIP ROUTING

Ship routing in ice infested seas is mostly realized from the icebreakers. Hence, it is necessary to provide the breakers with dedicated SAR imagery in real time, of course, together with other relevant information. The imagery can improve the routing of the icebreaker itself. To find the most efficient route, taking into account time of arrival and costs, both for the icebreaker and for the assisted or towed vessel(s). However, during stable weather conditions the route is more or less determined in advance, since it is most efficient to use previous icebreaker leads between main ports in the area of action. When winds and temperatures change the imagery will be of great concern, either to find the old breaker lead or to keep away from heavily ridged areas and search for open leads.

Another aspect of routing vessels in sea ice, is concerned with remote routing, in which case the transport hours of the icebreaker can be reduced. Using imagery it is possible to suggest a route suitable for the ice class of the merchant vessel. In this case it is possible to save fuel, since the icebreaker can stay in port or just continue with the operation at hand. Of course, this activity is not new, but SAR imagery can increase the reliability of the routing. An example, was given to us (cf. Håkansson et.al. 1995) by the master of icebreaker Ymer. In this case a merchant vessel was taken out of port by a local tug. No imformation of the actual ice situation outside the port was known to the tug master. So he left the vessel in a ridged area, which had to wait for further assistance from Ymer. A few hours later Ymer was provided with an FD ERS-1 SAR imagery, showing that the area not far offshore the merchant vessel was covered with level ice, in which the merchant vessel could manage on her own. Hence, with a daily image coverage the Ymer master easily could have informed the local tug master about the ice conditions and advised him to tow the vessel further offshore into the level ice area.

3.3 BENEFITS

We believe that safety can be increased by increasing the quality and quantity of sea ice information, which, for example, can be provided using SAR imagery. However, it is very difficult to evaluate it or even estimate the safety in quantitative terms. It is easier to estimate the potential in more efficient navigation. We present below a crude example of how to quantify saving costs.

During the winter 1993/94 the total costs for the Swedish icebreaker operations were approximately 140 MSEK (≈ 16 MECU). During this ice season, which can be described as typical, 6 icebreakers were engaged. Their activitities can be divided into transportation (7800 hours), assists (4700 hours) and tows (660 hours). Variable costs are not easily identified, but bunker and lubricant costs amounted to 20 MSEK with a mean-per-hour cost of 1500 SEK.

In the northern Baltic, ice ridges on average cover 50 % of the area during the mid winter period (Climatological Ice Atlas). We estimate that about half of this area is occupied by heavily ridged areas. Hence, it can be argued that icebreakers spend 25 % of their assisting and towing time penetrating heavily ridged ice areas. Suppose these can be avoided in 50 % of the time, using SAR imagery. Then about 600 hours can be saved or the costs can be brought down approximately 0.9 MSEK, crudely. In this case we do not take into account that bulk costs per hour may be larger when passing through ridged ice than going in level ice.

The second case, using remote routing, should bring down the amount of both icebreaker transport and assist hours. It is however notoriously difficult to estimate the increased efficiency. Nevertheless, perhaps these hours can be lowered with 5 %; corresponding to 0.9 MSEK based on the averaged numbers above.

4. DEVELOPMENT OF NEW TOOLS AND DATA

4.1 ICE RESISTANCE CONCEPT

In ship routing wave forecasting is a prerequisite for keeping transport time as close as possible to scheduled time. For the same reason forecasts of sea ice conditions has to be available for routing winter navigation. Ship performance tests has been carried out in the Baltic (Thompson and Liljeström, 1994). An ice resistance index (Ri), based on propulsion power (P) and speed (S) was defined:

$$Ri = a * (P/S) \qquad (1)$$

where a is ship dependent constant. By logging the propulsion power, the speed, the ice type and typical ice thickness, the performance index can be estimated for various ice types. The next step is to use the backscatter from SAR imagery to characterize the ice type, and by inverting eq. (1) the speed can be found. This concept can be of value for ship routing in ice infested seas, but further tests and evaluation studies are needed.

4.2 OBJECTIVE ANALYSIS OF SAR

Ice type discrimination-algorithms of SAR imagery is under development worldwide in the research community. In Sweden we have found that ice roughness is the most important variable, determining the backscatter signal from ERS-1 SAR imagery (Carlström and Ulander, 1995) during cold weather conditions. Their results may constitute an important step towards the development of algorithms for retrieving different types of ridges. For the winter navigation and ship routing in the Baltic the knowledge of ridged areas and type of ridges are prerequisite, especially for the development of the performance index.

4.3 RADARSAT

We are planning to use Radarsat ScanSar data for icebreaking activities in the Baltic together with Finnish Institute of Marine Research and BSH in Germany. Radarsat offers data which appears to be more adapted to large-scale ice mapping than ERS imagery, since we will have almost a daily coverage of areas of the size of the Gulf of Bothnia (500*500 km^2). Also the polarization and incidence angles are chosen to give a good sea ice characterization, although the wide incidence angle itself can produce some false backscatter information, depending on where in the swath range the ice type may occure. It is expected that HH polarization will damp open water surface waves compared to VV polarization, as well as give better contrast between ridges and level ice.

Table 1: Technical outlooks

Feature	ERS SAR	RADARSAT
Frequency	C-band	C-band
Polarisation	VV	HH
Resolution	30 m	50 (100) m
Swath width	100 km	300 (510) km
Incidence angle	20° - 26°	20° - 40° (49°)

The imagery will hopefully be tested during a three year period for its capability as an operational tool in sea ice navigation activities.

REFERENCES

Carlström, A. and L. Ulander 1995: Validation of backscatter models for level and deformed sea ice in ERS-1 SAR images. Int. J. Remote Sensing, in press.

Climatological Ice Atlas for the Baltic Sea, Kattegat, Skagerrak and lake Vänern. SMHI, Norrköping, Sweden and FIMR, Helsinki, Finland, 1982. Distr. National Maritime Administration, S-601 78 Norrköping, Sweden. ISBN 91-86502-00-X.

Håkansson, B., Moberg, M. and T. Thompson (1995): Real-time use of ERS-1 SAR imagery for ice service and icebreaking operations in the Baltic Sea. Int. J. Remote Sensing, in press.

Omstedt, A. and L. Nyberg 1995: A coupled ice-ocean model supporting winter navigation in the Baltic Sea. Part 2. Thermodynamics and meteorological coupling. SMHI RO, No. 21, pp 30.

Seinä, A. and E. Palosuo 1993: The classificationof the maximum annual extent of ice cover in the Baltic Sea 1720 - 1992. Meri, 20, 5-29.

Thompson, T. and G. Liljeström 1994: Ship performance and ice resistance index. In Baltic Experiment for ERS-1 (BEERS), Winter Navigation Research Board, Research Report No. 51, 1994, Ed. Lars Ulander, pp 113-122.

COAST

Chairman: **H. Wensink**
Rapporteur: **S. Bruzzi**

ERS DATA TO SUPPORT COASTAL AND OFFSHORE APPLICATIONS

G.H.F.M. Hesselmans, G.J. Wensink, C.J. Calkoen, and C.F. de Valk

ARGOSS, P.O. Box 61, 8325 ZH Vollenhove, the Netherlands
Tel: (31) 527-242299, Fax: (31) 527-242016, Email: info@argoss.nl

ABSTRACT

Remote sensing imagery can be used complimentary to bathymetric surveys in shallow coastal waters. At ARGOSS a new technique has been developed and operationalized to assess bathymetry of coastal zones from microwave remote sensing information. An examples of the technique is presented. ERS-1 SAR data have been used to assess the depth in the coastal zone of the Netherlands. These bathymetric maps can be used to optimize survey activity, and provide data about areas inaccessible to the survey vessel. The example shows that survey effort can be reduced considerably.

1. INTRODUCTION

Knowledge of the sea bottom topography is important for purposes like shipping, fishery and all kinds of offshore activities, such as dredging, building of offshore constructions and pipeline laying. Measuring the sea bottom topography with the present state of the art technique is expensive. In this paper it is demonstrated that a combination of traditional and remote sensing (RS) techniques can greatly reduce the costs.

Traditionally, bathymetric information is obtained by means of ship based (multi-beam) echo sounders. This technique can be very time consuming and expensive, especially in remote areas. Therefore, a new method to obtain bathymetric information from RS imagery has been developed and operationalized at ARGOSS. Research projects were financially supported by the Netherlands Remote Sensing Board (BCRS) and the European Community (EC).

The satellites currently used to obtain microwave data are the first European remote sensing satellites (ERS-1 and ERS-2). They provide images of nominal dimensions of 100 km x 100 km. Based on these images bathymetric maps have been made at ARGOSS. The spatial resolution of these maps is 12.5 m x 12.5 m. This spatial resolution is sufficient to locate small objects such as rock pinnacles, coral heads and sea mounts. An example using ERS-1 SAR data is presented in this paper.

2. THEORETICAL BACKGROUND

The extraction of bathymetric information from microwave data is based on wave current interaction. Under favourable meteorological and hydrodynamic conditions (moderate winds and strong tidal currents), air- and spaceborne Synthetic Aperture Radar (SAR) imagery show features of the bottom topography of shallow seas (Alpers and Hennings 1984, Calkoen et al 1993). Microwave radiation can penetrate at most a few centimetres in the water. Therefore, SAR data can reflect properties of the sea surface only. The bottom topography can be observed due to the interaction between, bottom, current, and sea surface roughness. Here, a brief description of this process will be presented. A more detailed mathematical formulation is given in Calkoen et all [1993].

It is generally accepted that the imaging mechanism consists of three steps.

(1) Interaction between (tidal) current and bottom topography results in modulations in the surface current velocity. The flow velocity is reduced in deep areas and increased over shallower areas such as the top of a sand wave. This relation can be described by several models with an increasing level of complexity: continuity equation, shallow water equations, and the Navier Stokes equations. Note that the continuity equation provides only the depth averaged current which has be translated to the surface.

(2) Modulations in surface current velocity cause variations in the wave spectrum. As the surface current velocity decreases (increases), waves propagating in the water are being compressed (expanded) and their wavelength decreases (increases). Thereby redistributing wave energy over the spectrum.

(3) Variations in the wave spectrum cause modulations in the radar backscatter. The intensity of the radar signal reflected by the water surface depends on both the wavelength of the radar signal and the wavelength of the surface waves. The highest reflection values are

Proceedings of the Second ERS Applications Workshop, London, UK, 6–8 December 1995 (ESA SP-383, February 1996)

obtained near the Bragg wavelength. The reflection being proportional with the wave height. The Bragg model takes only radar backscatter at the Bragg wavelength into account, whereas more sophisticated models, such as the Holliday model consider the contributions at other wavelengths as well.

On this basis, computer models describing the currents, waves and electromagnetic scattering can be used to interpret the radar images. At ARGOSS, such models with different levels of complexity and physical detail are available for each step. Suitable models for most applications encountered until now are the continuity equation for (1), a relaxation model for (2) and Bragg radar backscattering for (3). From these models, a model suite was constructed which predicts the radar backscatter from bottom topography, depth-averaged current and wind. This model suite has been inverted and used to estimate the bottom topography in shallow seas from radar imagery with the help of data assimilation: a first guess of the topography is corrected iteratively, until the difference between predicted and measured radar backscatter is minimal.

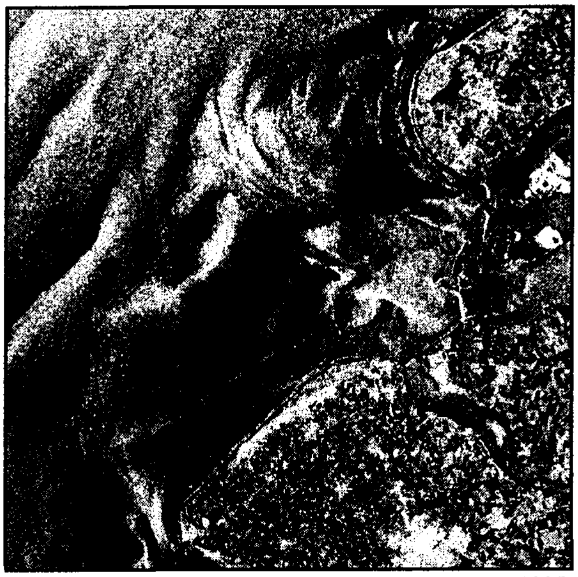

Figure 1 ERS-1 SAR image recorded June 1995.

3. APPLICATION OF MICROWAVE DATA IN THE DUTCH COASTAL ZONE

The delta area in the South of the Netherlands is of great public interest. An ERS-1 image of the area is shown in Figure 1. After a large flood in 1953, a number of coastal defence constructions, called the "Delta Works" have been build. These works include stronger dikes, and the closure of tidal inlets by semi-permeable dams. Due to these human interventions, current conditions have changed dramatically. As a consequence sedimentation

Figure 2 Bathymetric map obtained by linear interpolation between sounding data. Depth ranges from 0 m (white) to 25.5 m (black).

transport has changed and bottom topography is likely to change further in the next decades. Since a large part of the Netherlands is located below mean sea level, any change in bottomtopography may change safety levels of the coastal defence works. Therefore, surveys are executed on a regular basis along the whole of the Dutch coast by governmental agencies.

A depth map based on linear interpolation of sounding data collected along the Southern shores of the Netherlands is shown in Figure 2.

Figure 3 Bathymetric map based on ERS-1 SAR imagery. Depth ranges from 0 m (white) to 25.5 m (black).

In a demonstration project the potential of remote sensing has been shown. For this project ERS-1 SAR data were used. Optical remote sensing data are almost useless due to the high turbidity levels of the North Sea. Selection was based on favourable hydro-meteorological conditions (large tidal currents, and windspeed between 2 and 5 Beaufort). The results of the analysis are shown in Figure 3. Note that some sounding data have been used to calibrate the model and to determine the large scale trends.

The differences between both maps are quite small. A histogram showing the error distribution is given in Figure 4.

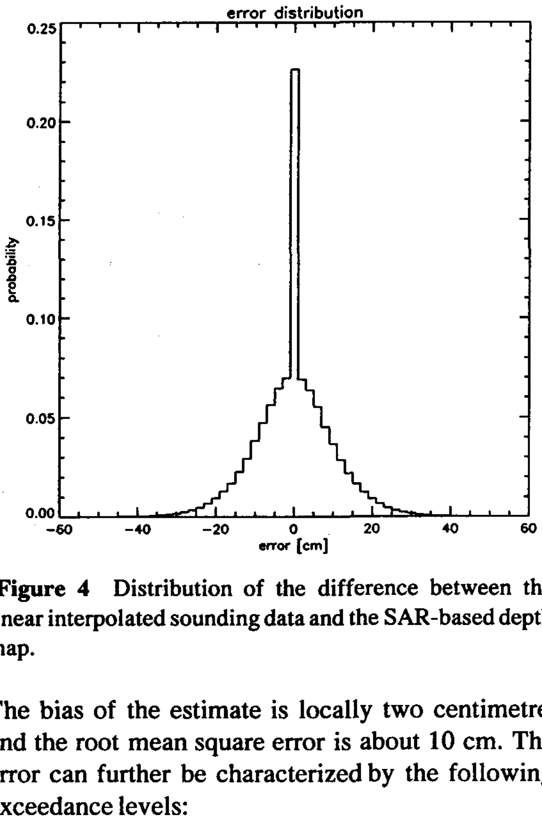

Figure 4 Distribution of the difference between the linear interpolated sounding data and the SAR-based depth map.

The bias of the estimate is locally two centimetre, and the root mean square error is about 10 cm. The error can further be characterized by the following exceedance levels:

10 %	16 cm
5 %	20 cm
1 %	30 cm
0.1 %	54 cm

The maximum error found is 1.82 m. These errors are comparable with the natural variability in depth found within a single grid cell (25 x 25 m^2). The SAR data reveal sand waves on the North-West shore of the peninsula Walcheren. These sand waves perpendicular to the shore have a wavelength of about 250 m. These sand waves could not be detected from the sounding data, because the section lines are about 200 m apart. The presence of these sandwaves has been confirmed by local authorities.

4. DISCUSSION AND CONCLUSIONS

Accurate depth estimates can be obtained by microwave remote sensing techniques. Microwave techniques require favourable wind and current conditions. However it is independent of cloud cover, which is a serious problem for optical remote sensing techniques. The accuracy of the estimated depth may be close to that obtained with traditional shipbased echo sounding. Furthermore, it has been shown that bathymetry based on remote sensing may yield information supplementary to survey data:

- depth in areas inaccessible to the survey vessel
- detection of small hydrographic features (sand waves in the example)

Other advantages of remote sensing are the ability to monitor large areas in a short time. The imagery covers areas of about 100 x 100 km^2. Using remote sensing the distance between section lines can be increased considerably. The resulting reduction in survey costs will most surely outweigh the additional costs needed to acquire and process the remote sensing data.

5. REFERENCES

Alpers, W., and Hennings, I., A Theory of the Imaging of Underwater Bottom Topography by Real and Synthetic Aperture Radar, *Journal of Geophysical Research*, Vol. 89, No. C6, pp 10,529-10,546, November 20, 1984.

Calkoen, C.C., Kooi, M.W.A. van der, Hesselmans, G.H.F.M., and Wensink, G.J., The imaging of sea bottom topography with polarimetric P-, L-, and C-band SAR. Report BCRS project 2.1/AO-02. Netherlands Remote Sensing Board. Delft 1993.

Hesselmans, G.H.F.M., *Bathymetry from landsat-TM images*, DELFT HYDRAULICS report H831, May 1989.

Spitzer, D., and Dirks, R.W., Bottom influence on the reflectance of the sea, *Int. J. Remote Sensing*, Vol. 8, No. 3, 279-290, 1987.

POTENTIAL USES OF ERS-1 SAR DATA FOR THE MALAYSIAN COASTAL ZONE

Mohd Ibrahim Seeni Mohd & Samsudin Ahmad
Centre for Remote Sensing, Faculty of Surveying and Real Estate
Universiti Teknologi Malaysia, Locked Bag 791, 80990 Johor Bahru, Malaysia
Phone: +(6 07) 550 2969 Fax: +(6 07) 556 6163 Internet: sam@fu.utm.my

D.H. Hoekman
Department of Water Resources, Wageningen Agriculture University
Nieuwe Kanaal 11, 6709 PA Wageningen, The Netherlands

H. Greidanus
TNO Physics and Electronic Laboratory, P.O. Box 96864, 2509 JG The Hague, The Netherlands

ABSTRACT

Satellite remote sensing using visible and infrared wavelengths is not very suitable in the tropics because of the cloud cover problem. Radar remote sensing can overcome this problem although it may not possess some of the advantages of sensing in the optical wavelengths.

This paper reports on the results of a study that has been carried out under the EC-ASEAN ERS-1 project, subproject MAL-2, to derive coastal zone information from the synthetic aperture radar (SAR) data of the ERS-1 satellite over the coastal areas of Terengganu and Sarawak (Malaysia). The PCI EASI/PACE and ErgoVista digital image processing software were used to analyse SAR PRI images. The digital image processing carried out include geo-referencing, filtering and calibration.

The University of Texas at Arlington Radiative Transfer Canopy Model (UTA) was used to derive backscatter values expected from different types of dominant vegetation which were then compared with the backscatter values obtained from the ERS-1 SAR data.

In the study, the radar bathymetry model implemented at TNO was used to assess a number of maritime features in the images potentially caused by topography of the sea bottom. The contrast profiles produced by the model were compared to profiles extracted from the ERS-1 images.

The ERS-1 data were also processed to obtain ocean wave spectra in order to derive information about ocean wavelength and direction using 2-dimensional Fourier Transform. The study also included visual interpretation of oil slicks, ships, ship wakes and some coastal features such as river outflows and fronts.

1. INTRODUCTION

Satellite remote sensing using the visible and the infrared wavelengths have been used very successfully in various applications related to earth resources studies and monitoring of the environment. This is also the case for applications related to the marine environment. For instance, useful results have been obtained in sea surface temperature, suspended sediment concentration, ocean colour and bathymetry studies. However, in some applications, there are limitations in the use of the optical wavelengths such as in studies related to sea bottom topography in turbid waters, ocean waves and oil slicks.

The use of radar remote sensing has many advantages in comparison with optical remote sensing techniques. By far the most important factor is the virtual insensitivity of radar to atmospheric conditions. This allows the regular collection of site observations independent of cloud cover or time of overpass. On the other hand, the interpretation of radar imagery over land and ocean are not as straightforward as that of the more commonly used visible and infrared remote sensors. Usually, special image processing techniques must be applied on the radar imagery to make it more readily interpretable. Furthermore, the interpretation of the backscattering process that underlies the radar image formation must be well understood with respect to the physical characteristics of the targets under observation and the specifics of the radar instrument.

The objective of this study is to develop a suitable methodology for mapping coastal features and land cover using multi-temporal ERS-1 SAR satellite data. The study includes shallow water bathymetry, wave spectra analysis, detection of oil slicks and mapping of natural and artificial features. Some modelling work for vegetation backscattering and bathymetry was also

Proceedings of the Second ERS Applications Workshop, London, UK, 6–8 December 1995 (ESA SP-383, February 1996)

carried out in order for some comparisons to be made to the ERS-1 data. Through this study, local scientists were able to acquire knowledge and experience in the analysis of ERS-1 SAR digital data.

2. DATA PROCESSING & ANALYSIS

For this study, two test areas were selected. One area stretches from Kuala Terengganu to Dungun on the north-east coast of Peninsular Malaysia, and one near Kuala Baram on the north-west coast of Sarawak (Figure 1). Both areas are characterized by large outflowing rivers and are affected by coastal erosion and accretion during the monsoon season.

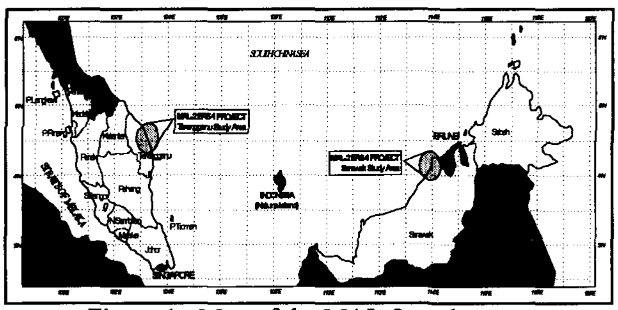

Figure 1 : Map of the MAL-2 study area.

During the duration of the study, several scenes of ERS-1 SAR PRI data were acquired and used. These data were received by the Bangkok receiving station and made available by ESRIN and Bangkok.

The data processing and analysis involved in this study include geo-referencing, filtering, calibration, vegetation backscattering, bathymetric signatures, ocean wave spectra and visual interpretation for oil slicks, ship and ship wakes.

Digital Image Processing

Since ERS-1 PRI images has already undergone slant-to-ground range correction at the Processing and Archiving Facility, SAR multi-temporal images were registered to each other by applying a shift in the x and y direction. The geo-referenced images were co-registered with existing maps of the area for comparisons.

Various filters including Lee, Frost and Gamma MAP filter were used to reduce speckle noise from the images in order to compare the results visually for land areas.

In order to obtain absolute backscatter values from the ERS-1 SAR data, calibration was done by using the constant provided by ESRIN and Bangkok station.

Vegetation Backscattering Model

In order to understand radar backscatter from vegetation, the University of Texas at Arlington (UTA) Radiative Transfer Canopy Model (Karam et al., 1992) was used to derive backscatter values expected from different types of dominant vegetation in the study area, viz. rubber, oil palm and paddy. The parameters used in the model were obtained from ground observations which included tree height, soil roughness, soil moisture, leaf radius, leaf density, leaf orientation, branch radius, branch density, trunk radius, trunk density, etc.

Backscatter values were also extracted from the ERS-1 SAR data in order to make comparisons. The results are shown in figures 2(a), 2(b), 2(c) and 2(d).

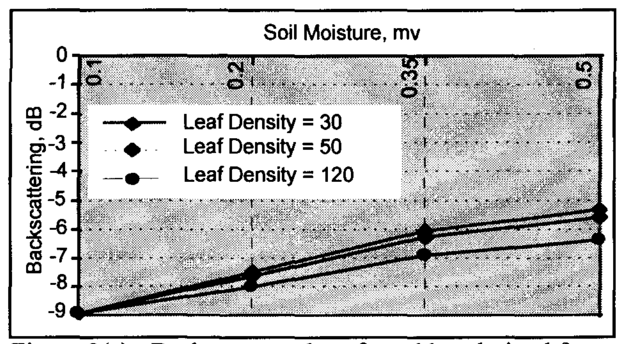

Figure 2(a) : Backscatter values for rubber derived from the UTA model

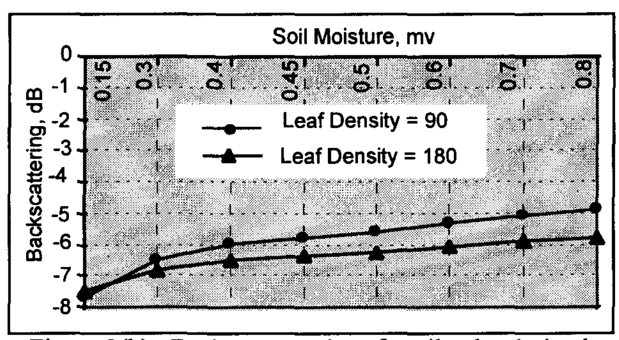

Figure 2(b) : Backscatter values for oil palm derived from the UTA model.

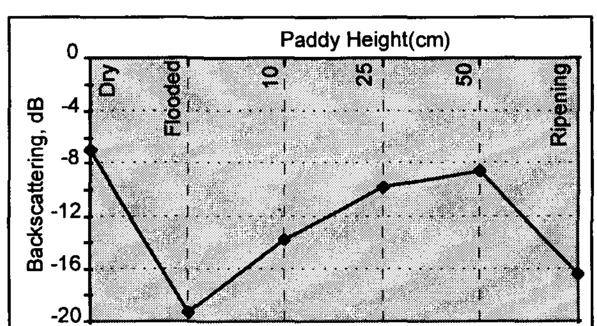

Figure 2(c) : Backscatter values for paddy derived from the UTA model.

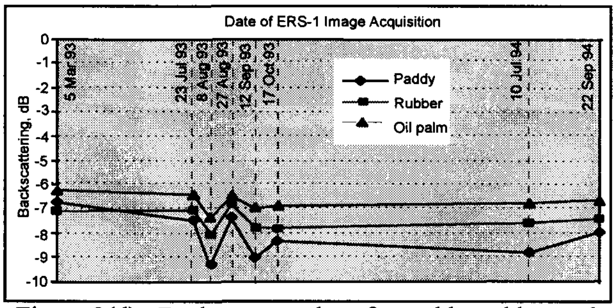

Figure 2(d) : Backscatter values for paddy, rubber and oil palm extracted from the multi-date ERS-1 data.

Bathymetry Signature Model

In the study, the radar bathymetry model implemented at TNO was used to assess a number of maritime features in the images potentially caused by topography of the sea bottom. This model is based on the action balance equation, weak hydrodynamic interaction theory and Bragg scattering (Vogelzang, 1989). The model which is suitable for shallow waters was run using estimated bathymetric profiles based on available hydrographic charts, and wind and current velocities and directions at the time of ERS-1 imaging. The contrast profiles produced by the model were compared to profiles extracted from the ERS-1 images. The results are shown in figures 3(a), 3(b) and 3(c).

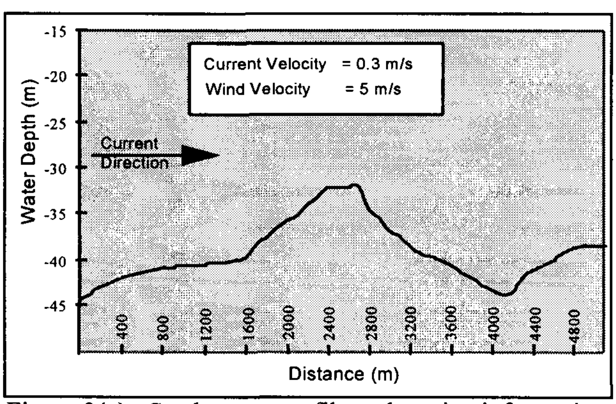

Figure 3(a) : Sea bottom profile and marine information in the study area.

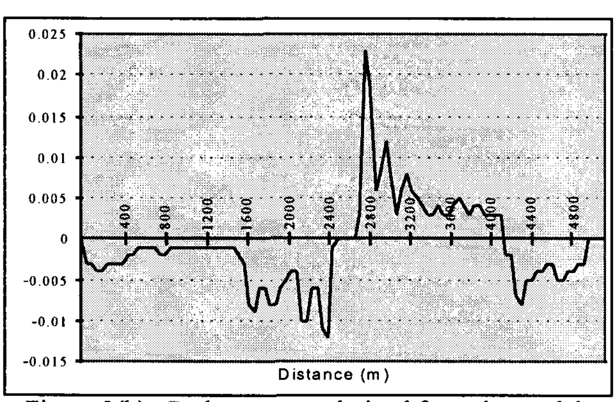

Figure 3(b) : Radar contrast derived from the model.

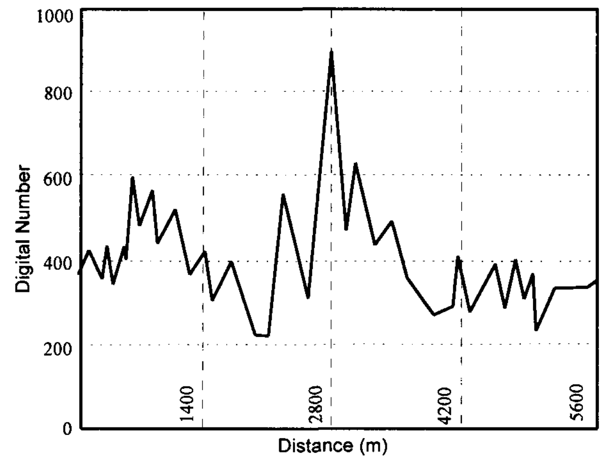

Figure 3(c) : Profile from ERS-1 data.

Ocean Wave Spectra

ERS-1 data has been demonstrated to provide ocean wave information in terms of wavelengths and directions. ErgoVista software was used to calculate wave spectra from PRI images. Single SAR image frames comprising of 512 x 512 image pixels was extracted. Since each pixel represents a 12.5 m x 12.5 m area, the entire image frame corresponds to a 6.4 km x 6.4 km patch on the ocean surface. The frame size provides a sufficiently large area that at least 10 cycles of very long surface waves, up to 640 m in length, can be included in a single image frame. They are also small enough that the ocean can be reasonably assumed homogeneous within a frame (Monaldo, 1991).

The wave spectra were calculated based on a 2-dimensional Fast Fourier Transform, with smoothing in the spectral domain and spatially averaging for noise reduction, and a correction for the stationary instrumental response function. The results are shown in figure 4. This process was repeated for other frames in the image.

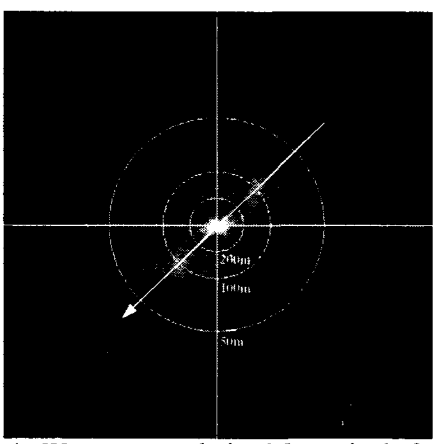

Figure 4 : Wave spectra derived from single frame on ERS-1 data acquired on 5 Mar 93. Circle and arrow represent ocean wavelength and direction respectively.

Visual Image Interpretation

For visual interpretation, both single and geo-referenced multi-temporal images were used to recognise different types of vegetation and their changes especially in the coastal land areas using unfiltered and filtered images.

ERS-1 images were also used to detect oil slicks, ship and ship wakes and water fronts.

From the visual interpretation of the processed images, it was possible to locate oil slick areas which appear as dark patches because of the damping of the ocean wave due to the oil layer which reduce radar backscatter. Ship and ship wakes have also been identified on the image with the wakes trailing for several kilometers behind the ship. Water fronts where water from the rivers meet with the sea water is also clearly visible in the images.

3. RESULTS & DISCUSSIONS

From the single ERS-1 SAR image, it was difficult to delineate different types of vegetation. However, by using multi-temporal images, it was possible to detect temporal changes in the paddy crop due to different stages of growth.

Among the filters used, the Gamma MAP filter using 11x11 window produced the best visual results where point targets are clearly visible and land use boundaries are more distinct.

The vegetation backscatter simulation results show that rubber plantations have a fairly stable backscatter level of -7.0 dB (Figure 2(a)). The backscatter values obtained from ERS-1 data also show a fairly stable signal around -7.5 dB (Figure 2(d)). For oil palm plantations, the results from the model and the ERS-1 data show the same trends as for rubber with a fairly stable signal in the range of -6.0 to -7.0 dB (Figures 2(b) and 2(d)). As for paddy fields, the simulations show that the backscatter can be very low for flooded bare fields, but can be considerably higher as a result of wind or when the area is dry. When the plant grows the backscatter continously increases up to -8.0 dB and drops again when the plants ripen or turn yellow. The results obtained from the ERS-1 data range from -6.7 to -9.0 dB (Figures 2(c) and 2(d)). These results are acceptable considering the fact that the ERS-1 data used in the study were acquired during mid to end of the paddy season.

The radar contrast derived from the bathymetric signature model was quite consistent with the shape of the sea bottom profile obtained from hydrographic charts. The results obtained from ERS-1 data also compares well with the above results (Figures 3(a), 3(b) and 3(c)).

From the ocean wave spectra analysis, the wavelength and direction of the ocean waves have been determined from the images (Figure 4). The dominant wavelength is about 200 m. The spectra show 180° ambiguity as the wave propagation direction is not resolved.

4. CONCLUSIONS

From the work that has been carried out in the study, the ERS-1 SAR data has shown great potential in deriving information on land and sea areas. Although the results of the study are encouraging, further studies need to be done to improve the results in order to operationalise the use of ERS-1 data. However, in order to achieve this, suitable mechanisms should be made available in order to obtain timely data especially in sea areas which are dynamic in nature.

5. ACKNOWLEDGEMENTS

The authors wish to thank the EC/ESA for funding and supplying of ERS-1 SAR data. Thanks are also due to the University of Texas at Arlington for the use of the Radiative Transfer Canopy Model and to TNO for the use of the bathymetry model. The contributions from the co-investigators, Dr. Mohamed Said Mat Lela, Mr. Henry Litong Among as well as post-graduate students in Universiti Teknologi Malaysia, Mr. Lau Yok King and Mr. Khor Soong Wei are duely acknowledged.

6. REFERENCES

Karam, M.A., A.K. Fung, R.H. Lang and N.S. Chauhan, 1992, A microwave scattering model for layered vegetation, IEEE Transactions on Geoscience and Remote Sensing, Vol.GE-30, pp.767-784.

Monaldo, F.M., 1991, The consequences of sampling variability on the estimation of wave number and propagation direction from spaceborne SAR image spectra, IEEE Transactions on Geoscience and Remote Sensing, Vol.29, No.1, pp. 113-119.

Vogelzang, J., 1989, The mapping of bottom topography with imaging radar : A comparison of the hydrodynamic modulation in some existing models, Int. J. Remote Sensing, Vol.10, No.9, pp. 1503-1518.

Algae Monitoring of the Wadden Sea Using ERS/SAR Data in an Operational Environment

Oliver KRÄMER; Peter LOHMANN

GEOSCAN Deutsche Gesellschaft für Fernerkundung und Umweltanalytik mbH
Gelber Stern 1; 31134 Hildesheim
Tel.: 05121-76900 Fax: 05121-769015

Abstract

This paper presents the final results of a coastal monitoring system (WAMOS) along the Wadden Sea coast of the North Sea. By detailed photo and multispectral survey flights the interactions between the C-band microwaves and the tidal flat surface could be described. Based on these results the operational modules for Algae Monitoring (AMO) and hydrography (STROM) could be developed.
However, for transferring the third module for sediment classification (WORK) into an operational environment some basic research still has to be done.

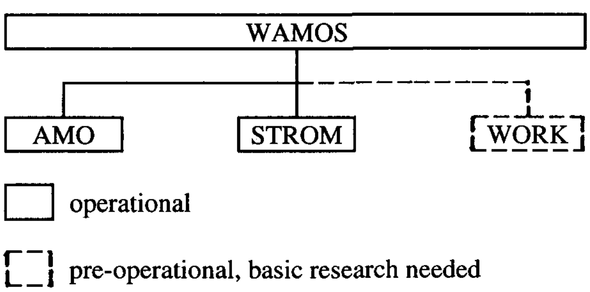

Fig. 1: Schematic survey of the WAMOS system

1. Geographical Description of the Investigated Area

The investigated area of Spiekeroog belongs to the backbarrier tidal areas of the German Wadden Sea and is part of an old barrier island chain. The whole Wadden Sea covers nearly 10.000 km² (FLEMMING & DAVIS 1992). The German Bight can be divided into three characteristic tidal types (REINECK 1982):

- open tidal areas
- bight or estuary tidal areas
- backbarrier tidal areas

The investigated area can be divided into a western part and into an eastern part by the tidal flat watershed leading from Harlesiel to the island of Spiekeroog. The mean tidal range in the wastern part is about 2.6 m, in the estern part 2.8 m (ERCHINGER 1993).
Since 1000 A.D. the seaward moving dyke line causes changes in the energy level of the backbarrier deposition system. The result is a continuous shifting to coarser grain sizes (sand fractions) especially along the dyke line. The remaining mud fractions can be led back to the existance of organic layers during almost the whole year long.
The existance of the large organic layers find the explanation in the high fertilizer input of the intensive agriculture along the Harlinger Land in the southern region. The fertilizer input runs to 120 kg/ha+a (HERR 1992).

2. Ground Truth Sampling and Basic Maps

In order to validate and to interpret the remote sensing data sets, an extensive ground truth sampling had to be carried out. This was done by the Senckenberg Research Institute in Wilhelmshaven. Tidal flats are highly dynamic surfaces in an almost constant environment (compared to terrestrial surfaces). The tidal dynamics cause changes in the surface roughness from tide to tide. The different field teams have only four hours time to get to their sampling locations and to take samples. During the three campaigns the following parameters were investigated:

- sediment grain size (in phi)
- sediment temperature (in the upper cm's)
- sediment moisture content (in weight %)
- sediment surface roughness (only some specific locations)

From the beginning of the project in 1993 until the end in 1994 we had to increase the number of samples from 41 to 200 and we also had to change the sample sites to more homogeneous locations.
The maps available (mainly from the National Park authorities) were obsolete and had to be replaced by up-to-date remote sensing related maps. This was, on the one hand, done by cartographic descriptions of the investigations of the Senckenberg Research Institute, on the other hand by the validation of the multispectral data acquired during the campaigns. These maps included:

- morhological features
- benthos communities
- sediment distribution
- organic layers

Proceedings of the Second ERS Applications Workshop, London, UK, 6–8 December 1995 (ESA SP-383, February 1996)

3. Optical Remote Sensing

In addition to the microwave data we used two Landsat TM miniscenes and three Daedalus AMS images parallel to aerial photos acquired with our own equipment.

The optical data sets should have no time shift in comparison with the ERS-1 SAR data. However, we could fulfil this condition only in winter 1994 and summer 1994.

Field campaigns					
1993 summer		1994 spring		1994 summer	
Date	Data Set	Date	Data Set	Date	Data Set
11.05.1993	Landsat TM				
14.06.1993	ERS-1 SAR	21.01.1994	ERS-1 SAR		
10.07.1993	ERS-1 SAR	20.02.1994	ERS-1 SAR	29.07.1994	ERS-1
19.08.1993	Daedalus AMS (TIR) Colour Infrared photos	04.03.1994	Daedalus AMS Landsat TM ERS-1 SAR b/w IR photos	10.08.1994	Daedalus AMS ERS-1 SAR Colour photos
19.08.1993	Daedalus + CIR	22.03.1994	ERS-1	30.08.1994	ERS-1
23.08.1993	ERS-1 SAR				

Fig. 2: Field campaigns

The aerial photographs served as highly geometric accurate reference (orthophotomap, DEM), first of all to geocode the multispectral Daedalus data. Furthermore, a low-level flight in 1994 was to deliver decisive information about ripple fields (ripple marks and orientation) to interpret the ERS-1 SAR data.

The work flow for the processing of optical data included the following steps:

1. radiometric correction (destriping, light correction)
2. atmospheric correction (ATCOR)
3. geocoding
4. interpretation: image fusion, classification, visual interpretation

Furthermore, we chose two steps in the interpretation to optimize the results according to DOERFFER & MURPHY (1988):

1. extracting the terrestrial surfaces by delineating with polygons
2. unsupervised classification with five classes to remove water bodies and organic layers

As a result of these steps only uncovered sediment surfaces remained in the image. So we could minimize misclassification between terrestrial surfaces and sediment surfaces. Especially the removing of organic layers was necessary, because organic layers mask the information about sediment grain size in multispectral scanner data. In a visual comparision of the maps of the Senckenberg Research Institute and our classification results we could find a close correlation with the sediments of the sand fraction. At least the sediment classification was carried out by a supervised MLH classification, using the channels of Red and NIR (COLEMAN & MONTGOMERY 1987, CONDIT 1970, DAVIS et. Al. 1979, GERBERMANN & NEHER 1979). In contrast to the work of DOERFFER & MURPHY (1988) a PCA brought no optimization of our work. The results of a linear regression between surface reflectance values (Red, NIR) and grain sizes of the sand fraction were too inaccurate ($r = 0.6$).

Because of the high dynamics of the tidal area image fusion techniques (PCA, IHS transformation) could only be applied to the data set of 04.03.1994 (YESOU et. Al. 1993). In other cases the different water levels prevented an application. To reduce the speckle effects we filtered the SAR data with statistical filters. However, there was no information gain for visual interpretation or automatic classification. Even the classification with neuronal networks (carried out by the Technical University of Munich) showed no valuabel results. The main error source for misinterpretations is the similarity of the backscattering characteristics of tidal flats and water surfaces. Object boundaries change from acquisition date to acquisition date in multitemporal images (in strong contrast to terrestrial surfaces).

4. Backscattering Characteristics of Tidal Flat Surfaces in the Wadden Sea

The backscattering characteristics of tidal flat surfaces like tipple fields or algae covers differ significantly from those characteristics of terrestrial surfaces in ERS-1 SAR data.

With high sediment moisture (20 - 45 % weight) the penetration is lower than 1 cm in the upper layer and is similar to the penetration in the sea surfaces. Only in sandy dune areas with a moisture content lower than 15 weight % the penetration of several cm's causes a reduction of backscattering to the sensor. On tidal flats backscattering is dominated by the surface roughness (orientation and form of small ripple marks). Therefore, we can observe BRAGG backscattering on tidal surfaces which is normally more typical of water surfaces (ROBINSON 1985). Applying the simplified BRAGG criteria:

$$\lambda_S = \frac{\lambda_R}{2 \cdot \sin\theta_0}$$

λ_R = wavelenght of SAR (5.3 cm)
λ_S = wavelenght of the surface structure
θ_0 =SAR incidence angel (23°),

BRAGG scattering occurs over small ripples between 4 - 10 cm wavelenght and angles up to ∅ = 40°.

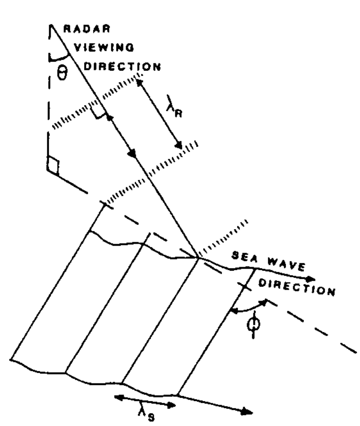

Fig. 3: Bragg scattering geometry: surface-wave direction at angle ∅ to plane of radar waves

On mud flats and flats with bulky organic layers there is specular reflection with low backscattering coefficients.

5. Monitoring Modules

The final results showed clearly that two of the three proposed modules are really operational. The third module of Sediment Monitoring (WORK) contains still too much pre-operational steps. The interactive delineation of object boundaries is practicable for an area of 5 x 5 km² area, but not for a whole coastal zone (KRÄMER el al. 1994). Correlations between backscattering and sediment moisture content or sediment grain size are too low.

5.1 Hydrography (STROM)

The focal point of a monitoring of tidal currents is the mapping of the current vectors in wide channel system areas in relation to their changes in time. In the backbarrier tidal flat area the so-called tidal currents are the main factors of morphological surface design. On the one hand, currents are steered by tidal inlets and channel systems, on the other hand, the tidal currents cause large-scale erosion and sedimentation. The interpretation of tidal currents is done by using ERS-1 median-filtered images at low tide. The images contain quasi-periodic "current vectors" within the large channels in the ERS-1 SAR data.

The calculation of the median image using ERS-1 multitemporal data sets has the following effects:

1. aperiodic phenomena are suppressed such as speckle effects, phenomena with a certain regularity such as tidal currents are enhanced and can be detected more easily
2. multitemporal data sets guarantee that current phenomena are recorded in sufficient numbers, monotemporal images represent only a short period of time in surface dynamics

The current vectors in the main channels represent the shipping routes with deeps down to 15 m with current velocities of 90 m/sec. By means of time series the movement of those current vectors which are indicators for changes on the channel bottom can be detected and topographical surveys can be directed to those areas.

Morphological changes, mainly big channel displacements after storms, can be mapped on the basis of simple overlays in the RGB spectrum, formed by multitemporal data sets.

1 x,y= 3412334,5958118	9 x,y= 3414873,5955706
2 x,y= 3412613,5957966	10 x,y= 3414748,5955401
3 x,y= 3412740,5958144	11 x,y= 3415508,5955604
4 x,y= 3412969,5957991	12 x,y= 3416930,5955300
5 x,y= 3413273,5957763	13 x,y= 3417514,5955731
6 x,y= 3413553,5957991	14 x,y= 3417641,5956290
7 x,y= 3413807,5957991	15 x,y= 3418631,5956722
8 x,y= 3414238,5957509	

Fig. 4: Current vectors from 1993 with their geographic location (Gauß-Krüger) in the backbarrier area of Spiekeroog

5.2 Algae Monitoring (AMO)

In the course of the year backscattering characteristics of tidal flats are influenced by changing ripple marks and even more by the appearance of organic layers. In certain tidal areas (along the watershed in still-water areas) the layers occur frequently from spring until autumn. With growing layer thickness backscattering changes from a diffuse one to a specular one, which can be clearly delineated. The bulky organic areas appear in ascending and descending path data on dark objects in the images.

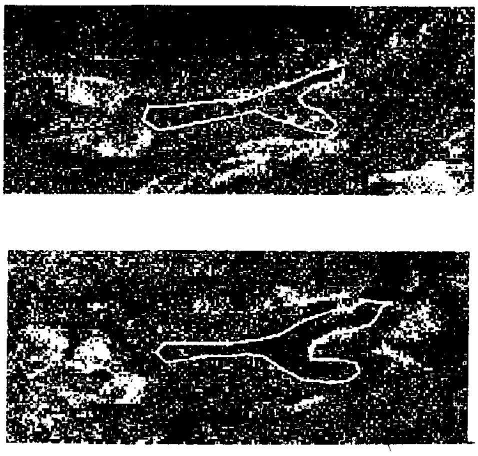

Fig. 5: This figure shows a part of the Martensplate with growing organic layers (which appear darker)

Algae classification is a more visual process applying the knowledge of an interpreter. However, for the first interpretation a multispectral image must define a starting situation (a kind of calibration of the SAR data). By interpreting the continuous time series of ERS-1 SAR data an algae cover map of one year is obtained, considering the different water levels and possible morphological changes.

During this pilot project ERS-1 SAR data have proven their applicability in an operational Wadden Sea Monitoring of ecologically sensitive areas.
The results are available in ARC/INFO format and can be easily integrated in the existing Wadden Sea Database (WADABA).

Here, GEOSCAN would like to thank the Senckenberg Reseach Institute in Wilhelmshaven for the intensive and sometimes dangerous ground survey, the Wadden Sea National Park Authority of Lower Saxony for the coopration, ESA for the ERS-1 data and last but not least DARA GmbH for sponsoring the pilot project.

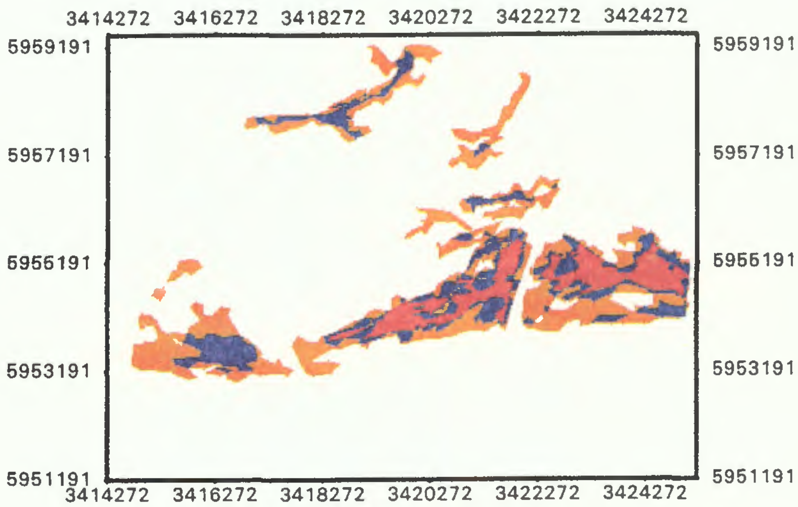

Fig. 6: Algae cover map from 1994 obtained by interactive interpretation of ERS-1 SAR data.
Red: Algae cover from March - October
Blue: Algae cover from July - October
Brown: Algae cover from July - September

Literature

COLEMAN, T.L.; MONTGOMERY, O.C. (1987): Soil Moisture, Organic Matter and Iron Content Effect on the Spectral Characteristics of Selected Vertisols and Alfisols in Alabama.- Photogrammetric Engineering & Remote Sensing, Vol.53,No.12, 1659-1663

CONDIT, H.R. (1972): Application of Characteristic Vector Analysis of the Spectral Energy Distribution of Day Light and the Spectral Reflectance of American Soils.- Applied Optics 11, 74-86

DAVIS, C.F. et al.: The Use of Remote Sensing in the Determination of Beach Sand Parameters

DOERFFER, R.; MURPHY, D. (1988): Factor Analysis and Classification of Remotely Sensed Data for Monitoring Tidal Flats.- Helgoländer Meeresuntersuchungen 43 (1989), 275-293

FLEMMING, B.W.; DAVIS, R.A.(1992): Holocene Evolution, Morphodynamics and Sedimentology of the Spiekeroog Barrier Island System (Southern North Sea).- Senkenberg am Meer, Bericht 92/2

ERCHINGER, H. F. (1993): Küsteningenieurwesen - In: BRETSCHNEIDER, H.; LECHER, K.; SCHMIDT, M.: Taschenbuch der Wasserwirtschaft, Hamburg und Berlin, 7. Aufl.

GERBERMANN, A.H.; NEHER, D.D. (1979): Reflectance of Varying Mixtures of a Clay Soil and Sand.- Photogrammetric Engineering & Remote Sensing, Vol.45, No.8, 1145-1151

HERR, E.W. (1992): Die Bedeutung der Marschgewässer für den Naturschutz.- Mitt. aus der Norddeutschen Naturschutzakademie, 3.Jhg., Heft 2, 9-12

KRÄMER, O.; LOHMANN, P.; SASSE, V. (1994): Application/Utilization of Data Sets Obtained by the Combination of ERS-1 and MS Satellite Data for Monitoring of the Wadden sea - Proc. of First ERS-1 Pilot Project Workshop held in Toledo, Spain, 347-351

REINECK, H.E. (1982): Das Watt, Frankfurt/Main

ROBINSON, C.S. (1985): Satellite Oceanography, Chichester, Sussex, England

YESOU, H. et al. (1993): Merging Seasat and Spot imagery for the study of geological structure in a temperate agricultural region - Remote Sensing of environment, 43, 265-279

COASTWATCH: SAR MONITORING OF COASTAL CIRCULATION AND WIND FIELD FEATURES

Paul Samuel, Stein Sandven & Ola M. Johannessen[1]

Nansen Environmental and Remote Sensing Center, Edvard Griegsvei 3A, N-5037 Solheimsviken, Norway.
Tel: (47) 55-297288. Fax: (47) 55-200050

[1] Also at *Geophysical Institute, University of Bergen, Bergen, Norway.*

ABSTRACT

This paper presents selected examples of ERS-1 SAR images around the Norwegian coast to demonstrate their usefulness in monitoring coastal circulation and wind field features. The data were analysed in conjunction with surface wind and current fields obtained from numerical models run at the Norwegian Meteorological Institute (DNMI), and NOAA AVHRR imagery, when available. Similar frontal structures are observed in both a SAR image and a nearly-coincident AVHRR image. The modelled current fields, while not displaying all the finer detail of the SAR imagery due to the low resolution, are useful in explaining the features seen. Wind field computed from a SAR image using the CMOD4 algorithm are compared with the analysed winds from DNMI. There is good agreement at some points, but the winds derived from the SAR show spatial variability that the low-resolution field from the DNMI does not capture.

1 INTRODUCTION

There is increasing need for better and regular monitoring of coastal ocean and atmospheric phenomena. With SAR technology, new methods have become available for the detection and monitoring of such features. At the Nansen Center, several ongoing and completed projects (Johannessen *et al.*, 1994; Johannessen *et al.*, 1995a; Johannessen *et al.*, 1995b; Samuel *et al.*, 1995a; Samuel *et al.*, 1995b) involve the use of SAR to monitor ocean and wind features off the Norwegian coast. A large number of SAR images are analysed and the observed features discussed in terms of the current and wind fields obtained from the Norwegian Meteorological Institue (DNMI). Commonly occurring features in the SAR images relate to ocean current fronts, eddies, current meanders, internal waves, surface slicks, wind fronts, wind rolls, atmospheric gravity waves and rain cells. To aid in the interpretation, nearly-coincident infrared images, and surface wind and current fields obtained from the Norwegian meteorological service are also examined.

2 CIRCULATION FEATURES

A number of SAR images with signatures typical of upper ocean features such as current meanders and eddies were examined. These features are manifested in SAR images through four mechanisms, 1) damping of short gravity waves by the presence of natural slicks aligned along the frontal boundary and spiralling around eddies; 2) short gravity wave - current interaction along shear and/or convergence zones within the front; 3) changes in wind stress induced by strong gradients in the sea surface temperature; and 4) long gravity wave refraction by currents (Johannessen *et al.*, 1995b). The relative importance of these mechanisms depends, among other things, on the time of year. For instance, the first mechanism is expected to dominate during spring and summer when relatively calm weather permits natural slicks to accumulate. During autumn and winter on the other hand, generally high wind conditions cause such slicks to disperse and the other three mechanisms account for most of the signatures in the images.

The ERS-1 SAR image shown in Figure 1 was acquired off the southern tip of Norway on September 18th, 1994. The DNMI predicted surface current vectors overlaid on the image show a current following the coastline towards the west with speeds increasing from about 0.05 ms^{-1} near the coast to about 0.2 ms^{-1} at the outer edge of the SAR image. The SAR image shows a clearly defined frontal boundary in the east and some branching frontal structures in the west. These features are absent in the modelled current field, due to the comparatively low resolution of 20 km. However, a NOAA infra-red image acquired on the same day (Figure 2) shows a frontal boundary whose location and shape are in good agreement with that seen in the SAR image.

Two ERS-1 SAR images obtained over the continental shelf to the southeast of the Shetland islands show a number of meandering structures and small vortices with diameters of 10 – 20 km (Figure 3). Similar features are observed in a number of SAR images over this area and they might be generated by the interaction of the shallow bathymetry with the relatively strong current (see the DNMI surface current vectors overlaid on the images). The DNMI current field shows a highly variable current field with current speeds over 0.15 ms^{-1} in the upper part of

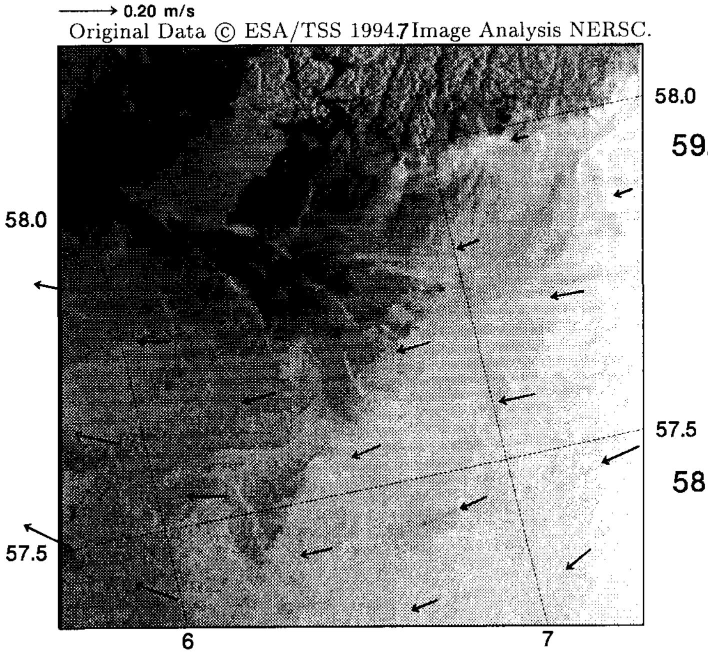

Figure 1: SAR image off the south coast of Norway on September 18, 1994, with the surface current vectors from the DNMI prediction.

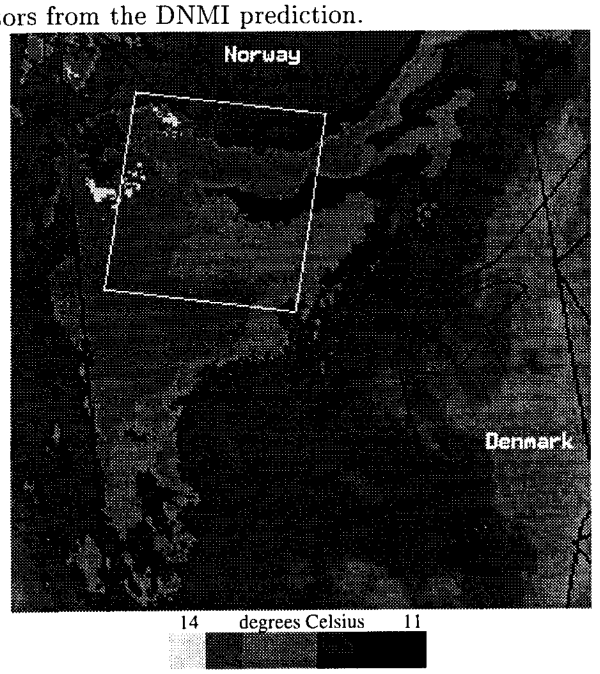

Figure 2: NOAA infra-red image on 18.09.94, with the location of the SAR image outlined in white.

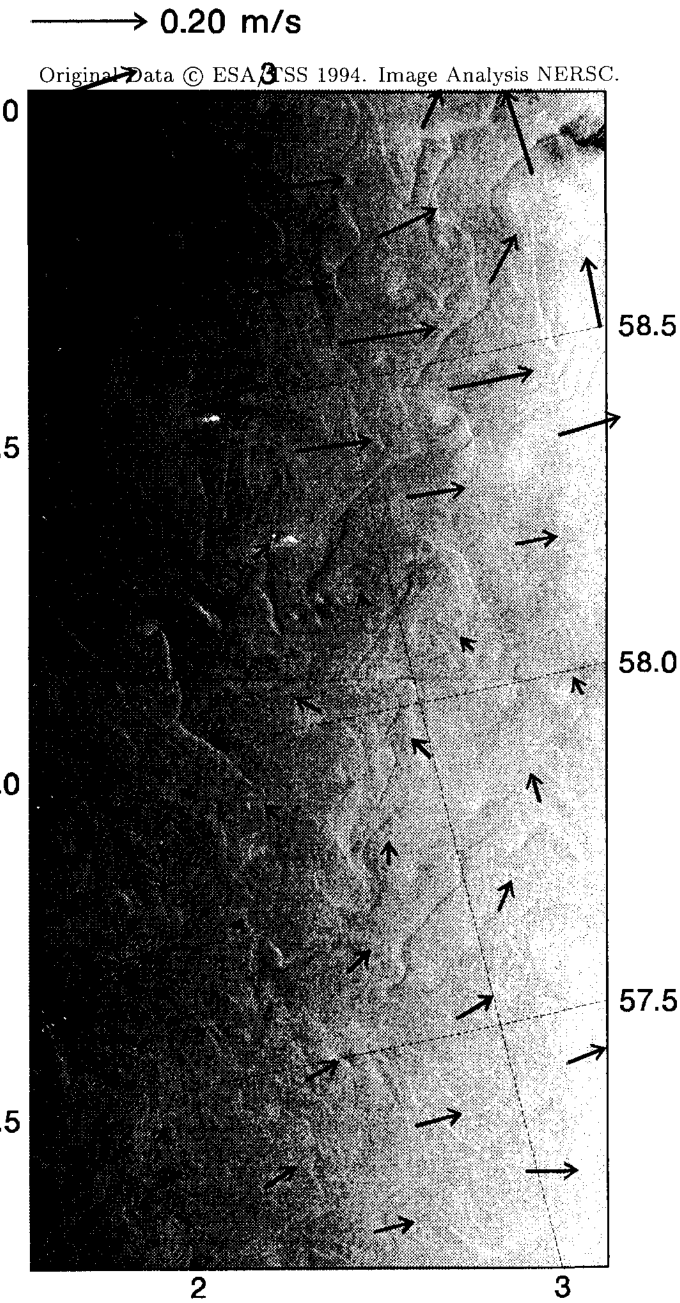

Figure 3: ERS-1 SAR images off south-west Norway on 02.11.94, with the surface current vectors from the DNMI prediction.

the SAR images. However, again due to the low resolution, it is unable to capture the short-scale features.

3 WIND FIELD FEATURES

Many of the SAR images reveal features which can be related to the atmospheric boundary layer. Features that are relatively easy to identify are 1) rain cells with accompanying wind squalls, which have a characteristic cloud-like form with a dark area where rain damps the Bragg waves, either surrounded by or adjacent to a bright area where the wind squalls increase surface roughness (Figure 4); 2) atmospheric gravity waves, which are manifested as relatively broad dark parallel lines with a spacing between 1 and 20 km (Figure 5); 3) wind rolls, which give rise to a characteristic streak-like pattern (Figure 6) which can extend over entire image frames.

The streaks due to wind rolls are usually observed only under moderately high wind speeds and are oriented parallel to the wind direction. The image of the 5th November (Figure 6) presents a case for application of the CMOD4 algorithm (Stoffelan and Anderson, 1993) to compute wind speeds, since the wind streaks extend over almost the entire image and indicate the wind direction, which is necessary as input to the algorithm. The algorithm actually computes radar backscatter cross-section given the wind speed and direction relative to the radar look direction. Here, we have inverted the algorithm by computing a lookup table of backscatter cross-sections at the input wind direction for a range of wind speeds and subsequently selecting the wind speed which gives the closest backscatter cross-section to that observed in the image. Prior to the computation the backscatter cross-section was averaged over 64 pixels (6.4 km) in the range and azimuth directions.

The result of the computation is presented in Figure 7, where the 4 wind vectors from the DNMI analysis is also shown. It is seen that the computed winds agree with the DNMI analysis in the left side of the SAR image, where the wind speeds are of the order of 10 ms^{-1}. However, the CMOD4 wind speeds decrease towards the right to less than 5 ms^{-1}, while the DNMI winds are largely constant. There is no independent validation of either of the wind fields, but this example illustrates the value of SAR imagery as a means for obtaining high resolution wind fields in selected areas.

4 CONCLUSIONS

This paper presents some examples of the use of SAR imagery together with AVHRR images and modelled surface current and wind fields in order to monitor coastal circulation and wind field features.

The DNMI current surface field available for this study only had a resolution of 20 km, compared to the 100 m resolution of the low resolution SAR images used. Hence, it was not possible to verify all the details of the current features seen in the SAR imagery alone. However, in general, the images analysed showed features broadly aligned with the direction of the current vectors. AVHRR imagery, where available, also shows frontal features similar to those seen in the SAR images.

During the ERS-1/2 tandem NORCSEX 95 experiment (with O.M. Johannessen as chief scientist) conducted off the south and west coasts of Norway, *in situ* measurements of the current field in selected SAR swaths were obtained using Acoustic Doppler Current Profiler (ADCP), Conductivity-Temperature-Density (CTD) sections and SEA-SOAR sections. These data are being analysed and are expected to yield validation data sets for the ERS-1/2 SAR current feature detection capability. During the experiment, SAR images were analysed at NERSC and transferred to the ship which was then directed towards areas with interesting features.

The operational ocean models run by DNMI is seen to be inadequate for the purpose of SAR validation and interpretation. At NERSC, we have plans of implementing coastal area numerical models with resolutions down to 1 km in order to aid in the interpretation of SAR images for operational applications.

The SAR images examined also contain a number of wind field features. The CMOD4 algorithm appears to be able to yield high-resolution wind fields and this will be useful both for research studies and for engineering applications related to offshore installations. Further study is required for examining methods to extract wind directions automatically from SAR images also in cases where streaks are not present.

Acknowledgements:
This study was funded by the Norwegian Space Centre and the European Space Agency through the PRODEX programme.

REFERENCES

Johannessen, J., Digranes, G., Espedal, H., Johannessen, O., Samuel, P., Browne, D., and Vachon, P. (1994), *SAR Ocean Feature Catalogue*, Number ESA SP-1174, ESA Publications Division, ESTEC, Noordwijk, The Netherlands.

Johannessen, J. A., Shuchman, R. A., Digranes, G., Wackerman, C., Johannessen, O. M., and Lyzenga, D. (1995a), Costal ocean fronts and eddies imaged with ERS-1 SAR, *J. Geophys. Res.*, In Press.

Johannessen, J. A., Shuchman, R. A., and Johannessen, O. M. (1995b), Mesoscale variability studies with SAR on ERS-1, in *Oceanographic Application of Remote*

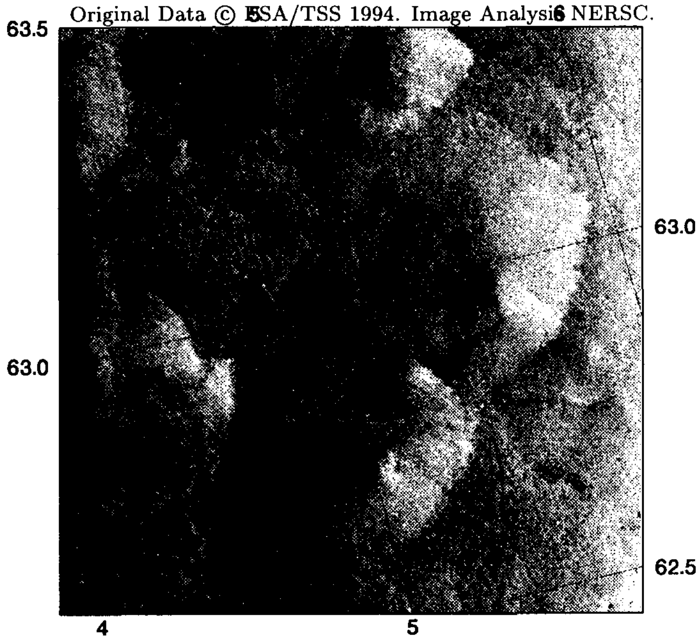

Figure 4: Rain cells in an ERS-1 SAR image off the west coast of Norway on 16.10.94

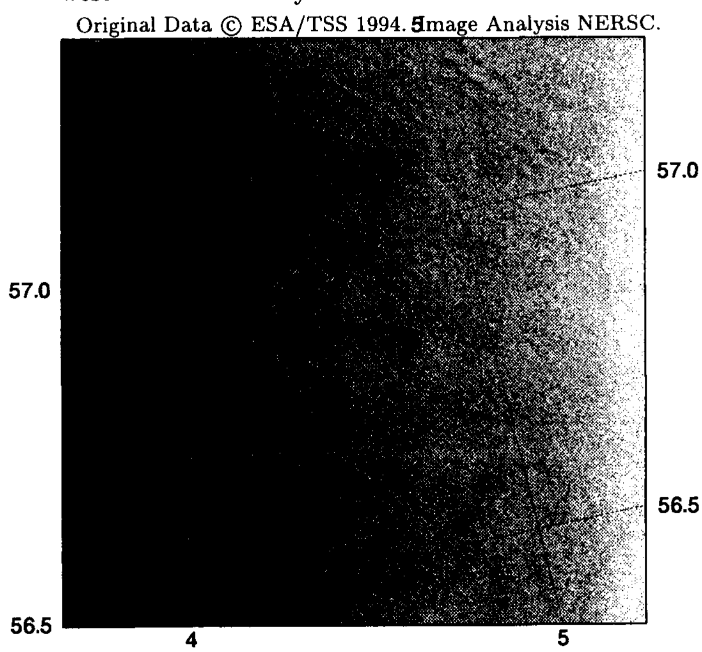

Figure 5: Atmospheric gravity waves in an ERS-1 SAR image off the south-west coast of Norway on 22.10.94

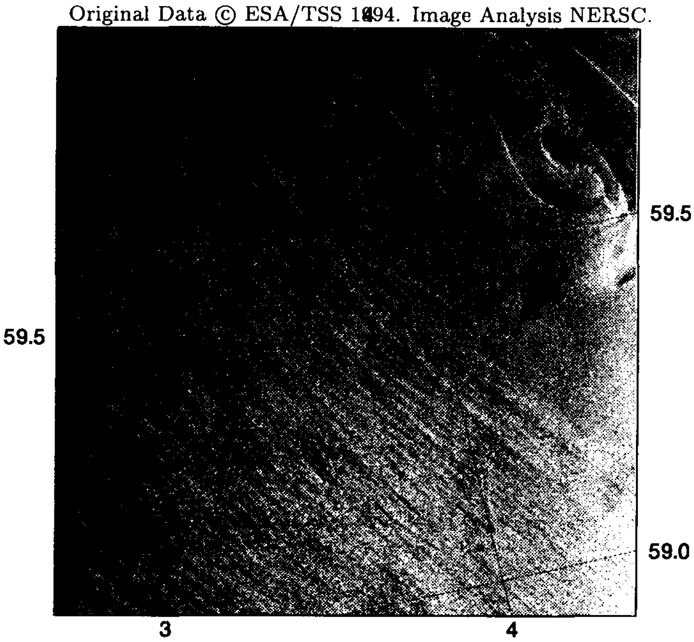

Figure 6: Streaks due to wind rolls in an ERS-1 SAR image off the west coast of Norway on 05.11.94

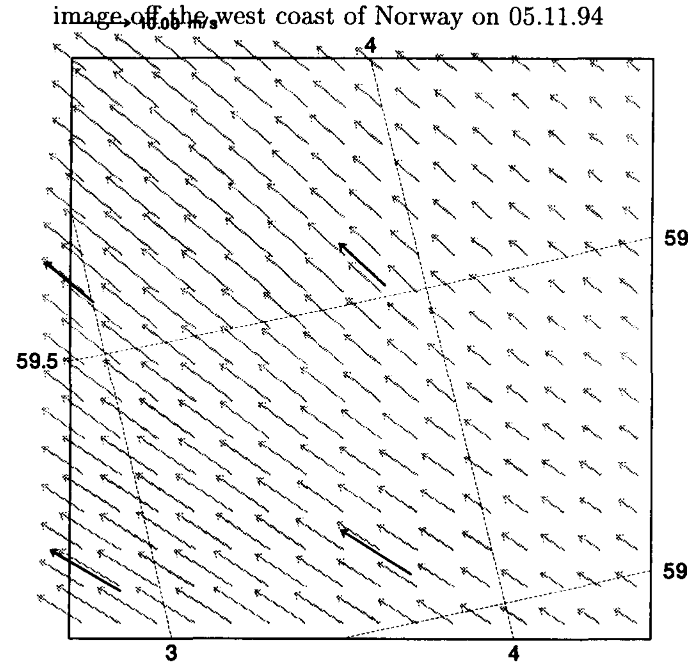

Figure 7: Wind vectors computed using the CMOD4 algorithm (in grey) and from the DNMI analysis (in black) for the image shown in Figure 6

Sensing, edited by Ikeda, M. and Dobson, F., CRC Press Inc., Boca Raton, USA.

Samuel, P., Grong, E., Espedal, H., Søiland, H., Hamre, T., Martinussen, I., and Sandven, S. (1995a), Integrated operational use of SAR images in marine forecasting, Technical Report 33, Nansen Environmental and Remote Sensing Center, Bergen, Norway, Special Report.

Samuel, P., Jenkins, A., Espedal, H., and Sandven, S. (1995b), Ocean monitoring using SAR, Technical Report 101, Nansen Environmental and Remote Sensing Center, Bergen, Norway.

Stoffelan, A. and Anderson, D. L. T. (1993), ERS-1 scatterometer data characteristics and wind retrieval skill, in *Proc. 1st ERS-1 Symp., Space at the Service of our Environment, 4–6 Nov. 1992, Cannes, France, ESA SP–359 Vol. 1*, pp. 41–47.

MAPPING AND MONITORING THE TIDAL FLATS OF COASTAL AREAS ON BASIS OF SEQUENTIAL ERS SAR

Yiman Wang and B.N. Koopmans

International Institute for Aerospace Survey and Earth Sciences (ITC),
P.O.Box 6, 350 Boulevard 1945, 7500 AA, Enschede, The Netherlands
Tel: (31) 53-4874444, Fax: (31) 53 4874336

ABSTRACT

The ERS-1 radar satellite provided an opportunity for testing the use of sequential radar data for mapping of the tidal flats in an area of the Wadden Sea, The Netherlands. SAR images acquired during periods with wind velocities higher than 5 ms^{-1} are good for water line delineation. Bathymetric channel delineation is best with current velocities of 1-2 ms^{-1} during outgoing low tide.

Water lines delineated from 9 SAR images acquired during 1993 were used for a construction of a digital elevation model (WALDEM). For each image acquisition time a water surface model was constructed which was correlated with the respective water line resulting in height values for the points along the water line. The heights were TIN interpolated for the area above low water. The resulting WALDEM was combined with the information for the channel pattern below the low water line, indicating the stream channels but not quantitative depth information.

For validation the WALDEM was compared with the DEM obtained by bathymetry. The height differences between the WALDEM and the DEM (bathymetry) on basis of pixel-by-pixel comparison gives an average of -5 cm and a standard deviation of 28 cm.

The resulting WALDEM may lead to operational use of the water line method from radar images for topographic mapping of the inter tidal zone. Over longer periods it makes change monitoring possible and determination of zones of erosion and sedimentation in the inter tidal zone.

1. INTRODUCTION

The Wadden Sea, including a string of barrier islands, is a tidal flat area of 8000 square kilometres along the north coast of the Netherlands, northwest Germany and southwest Denmark. The study area was selected in the western part of the Dutch Wadden Sea (figure 1).

The Wadden Sea is one of the most important and highly sensitive coastal tidal areas in the world. This large tidal area has an important nursery function for many commercial fish, shrimp and shell fish species.

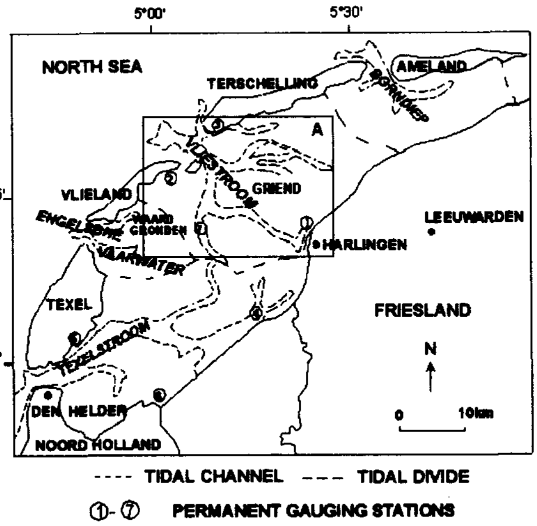

Figure 1. Study area (A) in the western Dutch Wadden Sea

Under the semi-diurnal tides, the water exchange between the North Sea and the Wadden Sea continuously remodels the coastal configuration and the bottom topography of the channel systems and related ebb and flood deltas.

The ecological balance should be carefully maintained. Disturbance of this fragile ecosystem looms from many sites. Excessive shell fishing threatens to destroy the mussel banks. Drilling for oil and gas exploration carries the danger of environmental pollution. Excessive tourists and recreational activities disturb the tranquillity of the region and so do the military bombing and shooting exercises of the air force. Toxic discharge carried by Rhine and Meuse into the North Sea enters the Wadden Sea through the inlet channels and gets concentrated here.

For monitoring such a sensitive area, constant updating of topographic and bathymetric maps is required.

Conventional mapping methods consist of terrestrial geodetic levelling over the tidal flats and echo sounding over the channels and offshore areas. These methods are costly and time consuming. The ship-borne echo sounding is carried out during the period of high tide, under the assumption that the water surface in that

Proceedings of the Second ERS Applications Workshop, London, UK, 6–8 December 1995 (ESA SP-383, February 1996)

period is horizontal. The reference plane of the sea level height is made on the basis of water level measurements from nearby gauging stations. The original echo-sounding data were recorded along the survey line in 2-5 metres interval, while the spacing between the survey lines is about 200 metres. Height approximation between the lines are obtained by interpolation.

2. OBJECTIVES OF THE ERSWAD PROJECT

The objectives of the ERSWAD project are:

1) To use multiple ERS-1 images acquired during different stages in the tidal cycle for mapping of tidal flats and low coastal areas.
2) To monitor changes in coastal configuration over longer periods and to map areas of sedimentation and erosion and dynamic changes in the stream and gully pattern of the Wadden Sea.

Satellite imagery are providing a synoptic image over a large area, acquired during a short moment, representing a certain stage in the tidal cycle. By obtaining a number of satellite images of which acquisition time represents different stages of the tidal cycle, water lines at different water levels may be mapped. The water lines represent the water-land boundaries at time of image acquisition. The water lines will represent contour lines in the hypothetical case that the water surface is horizontal. However, with incoming and outgoing tide from several inlets, the water surface is irregular but may be modelled. Using the water level model at time of image acquisition, height values can be calculated for the different points along the mapped water line. If this procedure is repeated for a number of different tidal stages, an interpolated elevation map can be produced for the tidal flat area between high and low tide.

3. DATA SET USED FOR ERS RADAR WATER LINE PROCEDURE

The twenty radar images reviewed in the study (Koopmans et al, 1995) do show strong differences in signal response over the different areas. Shuchman et al (1985) and Vogelzang et al (1989) discussed the relation between radar backscatter and bottom topography. Moderate to high current velocities are required to make bottom features visible on radar images.

The following generalizations can be made:

- For land-water boundary mapping, more than 60% of the images acquired can be used for the planned water line mapping program.
- Images acquired during a period with a wind velocity higher than 5 ms^{-1} are good for water line delineation. The dry flats contrast strongly with the light grey tone which is often uniform for the water surfaces.
- Wind velocities lower than 5 ms^{-1} allow for poor differentiation between land and water. The water surfaces vary very much in tone. The influence of surfactants is very large which gives irregular patterns and tones.
- The discernibility of the channel and gullies is not clearly wind related. Wind velocities between 3.4 and 10 ms^{-1} seem to be more favourable.
- The stream pattern is masked by high sea clutter with wind velocities larger than 10 ms^{-1}. This is in accordance with what was reported by Moens and Ruddick (1994).
- Low and outgoing tides seem to form the best tidal conditions for channel pattern delineation when stream velocities are in the order of 1-2 ms^{-1}.
- For visibility of the ebb tidal delta, no straight forward relationship with tidal situation or wind force have been found. Only three images are very good for information on the ebb tidal delta. They represent 2 outgoing high tide images and 1 incoming low tide image.

The nine selected ERS-1 SAR images over 1993 were subsequently geocoded to the Dutch Rijksdriehoeksmeting (RD) coordinate system. By registering a few ground control points from the surrounding permanent land area on the basis of the topographic maps (1:50,000), an affine transformation with nearest neighbour resampling method was performed.

An adaptive filter Improved Lee Filter with 7 x 7 convolution kernel (in software EASI/PACE, PCI) was applied for the speckle reduction and edge preservation before the land-water classification. The final water line map was derived from the vectorizing of the boundary of the land-water classification map. With the prior knowledge of the area, a screen digitization of the water lines by human interpretation was also done where necessary. This provided a water line map shown in figure 2.

4. WATER SURFACE MODEL: THE CORRECTED WADDEN MODEL (CWM)

Use has been made of the "Wadden" model provided by the National Institute for Coastal and Marine Management (RIKZ) (Robaczewska et. al.,1991). This model provides the simulation of the tidal water levels and the tidal current velocities in the Wadden Sea. It is based on calculations involving 26 harmonic components as tidal and rest currents at the North Sea, climatic conditions, water stowage as result of only strong wind and wave action, sea floor bathymetry and sea floor roughness, the expected current drag and the interaction in time between the different channel systems. The model yields the data in a grid system of 500 m with a temporal resolution of 2.5 minutes and simulates the tidal conditions quite well.

To evaluate the model, the time series data of the Wadden model were compared with the tidal gauging records over the same period. The differences , which are not constant, are principally a result of local change of wind velocity and wind direction. The model takes the wind information into account only when the wind velocity exceeds 8 ms^{-1}.

To overcome these differences between real measurements and the Wadden model, it was decided to improve the model by including data from the gauging stations in the area for the time of data acquisition. By adding correction values derived from the differences between measured and modelled values for the gauging stations and their interpolated values in a 500 m grid, a first step in correcting the Wadden model was made (table 1).

Table 1.The correction of the Wadden Model based on gauging records (example 16-05-1993, in cm)

Stations	Measured	Modelled	Correction
Vlieland	-79	-35	-44
W.Terschelling	-88	-43	-45
Harlingen	-100	-40	-60
Kornwerderzand	-108	-53	-55
Oude Schild	-29	+5	-34
Den Oever	-63	-32	-31

A second correction was applied to improve the model with respect to bottom drag causing a water surface curvature over the flats. The knowledge about the water surface curvature was obtained through a measurement campaign carried out during 7-21 April 1994. During this campaign with 14 pressure loggers spaced along a transect of 7 km over the Waardgronden the water levels were measured during a 14 days period with time interval of 1 minute. This experiment gave us insight into the curvature of the water surface during incoming and outgoing tide over the flats. A full description is given in the special ERSWAD report on this experiment (Wang et al. 1995).

The "channel domain" (areas deeper than -110 cm, the average low tide line in this area) can be clearly separated from the "flat domain" (areas between low water line: -110 cm and high water line) on the basis of the bathymetric DEM. For the flat domain the bottom drag causes a water gradient of 1:10.000 during incoming tide. During outgoing tide the water surface slopes gently towards Inschot channel. The water surface curvature is less expressed as in incoming tide. The slope gradient towards the channel is in the order of 12 cm over 3000 m.

The actual correction of this surface curvature is further adjusted according to the time in the tidal cycle and the distance towards the low tide line along the channel edges.

The corrections have been applied in zones of 500 m from the channel edges (low tide line: -110 cm) towards the central part of the flats. The DEM of the corrected water surface model (CWM= Corrected Wadden Model) was then densified to a 12.5 m grid size equal to the SAR pixel size.

5. EVALUATION OF THE WATER LINE DIGITAL ELEVATION MODEL (WALDEM)

The merging of the water line data derived from the SAR images (fig.2) with the Corrected Wadden Models (CWM) at time of each image acquisition gave the height values for each water line from different images. Of course no values are available within the channel domain. Over the flat domain a higher density of height points are found at places where the topographic changes are higher than over the parts of the flats where height differences are minimal. This distribution of height points can be trusted more and will be more useful than a ground survey with a grid distribution where minor depressions and channels may be easily missed in between the 200 m line spacings.

An interpolation programme was run on the basis of TIN (Triangulated Irregular Network) module in Arc/Info, the same procedure used for the DEM creation on basis of the bathymetric echo sounding survey of 1992/93. The resulting Water Line Digital Elevation Model (WALDEM) on basis of the water line method is given in figure 4.

It should be stressed that with the water line procedure the height information is only obtained between the high and low water lines. In the channel domain the stream patterns are indicated in figure 4 in shades of blue not indicating depth information but only backscatter variations of the radar image of 20-8-1991. These backscatter variations are influenced indirectly by the bottom topography representing differences in small scale wave fields as the result of differences in current velocities and current vectors (Koopmans et al, 1995). The presence of surfactants and foam along the steep channel gradients often strongly influences the radar response values. Calkoen and Wensink (1993) have been using the grey value differences for bathymetric optimalisation of ship-based surveys.

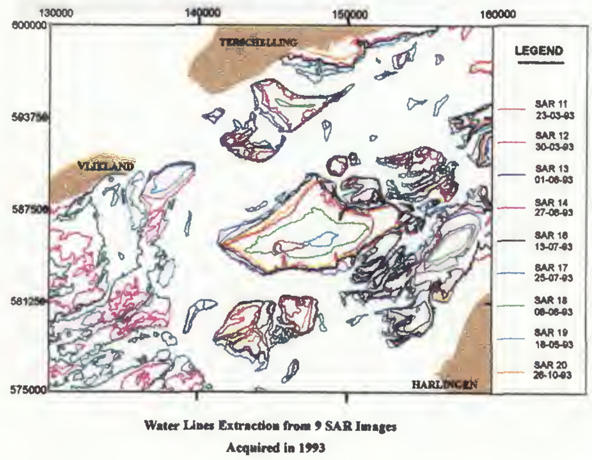

Figure 2. Water Line Extraction from 9 SAR Images Acquired in 1993

A comparison of the DEM (fig. 3) obtained through the bathymetric survey of Rijkswaterstaat in 1992/93 (Vakloding programme) with the WALDEM (fig. 4) demonstrates the large similarity.

The height differences between WALDEM and DEM give a mean difference of -5 cm (WALDEM lower than DEM) and a standard deviation of 28 cm.

93% of the pixels along the water lines are within the ± 50 cm difference range, 73% within ± 30 cm.

The difference contribution may be due to:

A. Water line procedure
   1) Georeferencing errors
      - not larger than 1 pixel (12.5 m in horizontal)
   2) Water line delineation
      - several pixels in transitional zones but not along channel edges
   3) Water surface modelling
      - smaller than 20 cm vertically
   4) Interpolation method selection

B. Verification DEM (Bathymetry)
   1) Bathymetric measurements
      - approximately 30 cm rms error for simple one dimensional bathymetric assessment system
   2) Interpolation between bathymetric survey lines.

6. CONCLUSIONS AND RECOMMENDATIONS

The water line procedure based on satellite radar imagery appears to be a reliable method for precision topographic mapping in the tidal range.
More than 60% of the radar images acquired may be used for water line delineation. Wind velocities lower than 5 ms^{-1} often preclude a reliable discrimination between water and dry shoal surfaces, and images acquired under these conditions cannot be used.

With a 35 day cycle (17 day sub-cycle) sufficient imagery will become available during the year for applying this method. The procedure may be developed as a semi-operational system.

The WALDEM produced in the study is a raster map in 12.5 metres pixel size similar to the pixel size of the ERS-1 data. From this data file a contour line map may be derived.

Differences between WALDEM and DEM are for 93% within ± 50 cm, and for about 73% within ± 30 cm vertical precision.

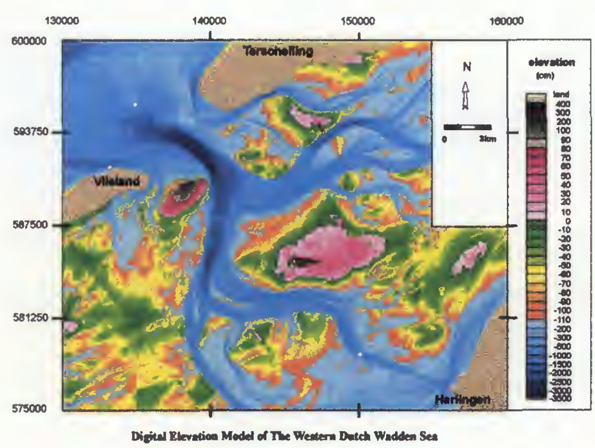

Figure 3.Digital Elevation Model of the Western Dutch Wadden Sea Using Sounding Data by Rijkswaterstaat, 1992.

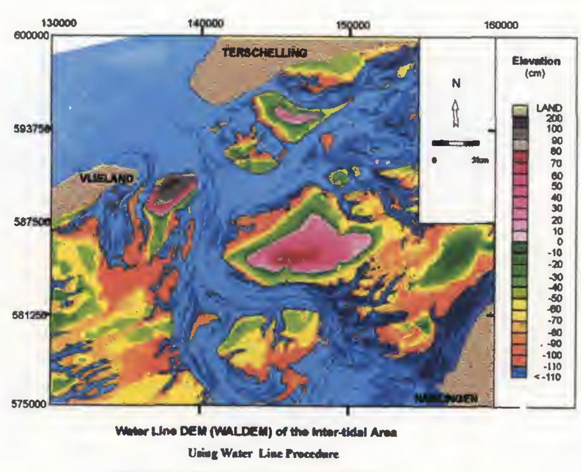

Figure 4. Water Line DEM (WALDEM) of the Inter-tidal Area Using Water Line Procedure with Multiple ERS-1 SAR Images (1993.3-1993.10)

As stated before, present mapping of the tidal areas is carried out by Rijkswaterstaat on a basis of bathymetric measurements over the channels and tidal flats. Each year a sector about 1/6 of the tidal area of the Dutch Wadden Sea is surveyed in detail along transects about 200 metres apart. The digital data along the transects are interpolated and a digital elevation model is constructed.

In the water line method, a selection of optimal SAR images with respect to the tidal situation and with respect to wind velocities is made. Digital data handling requires geocoding of the imagery and water line extraction. The water surface model (Wadden Model of RIKZ) for the acquisition time of the images is required and should be corrected on basis of existing gauging records and water surface curvature. The interpolation programme for construction of a WALDEM is similar to the DEM construction with the bathymetric method.

The water line method is restricted to quantitative height measurements over the flats between high and low tide lines. In combining the two methods - bathymetry over the channels and water line method over the flats - a considerable saving can be made on bathymetric surveying. This will reduce the field surveying by boat by more than 50 percent.

Moreover the SAR area coverage allows for a monitoring on a more regular basis (once every or second year) to determine zones of erosion and sedimentation and the changes in the channel pattern.

The present results are very encouraging and may lead to an operationalization of the method for topographic mapping in the inter tidal zone.

ACKNOWLEDGEMENT

The ERSWAD project was formulated under the Announcement of Opportunity for the utilisation of ERS-1 and J.ERS-1 data, issued by the European Space Agency (ESA) and the Japanese Space Agency (NASDA) respectively.

The research project was carried out at ITC in cooperation with the North Netherlands Division of Rijkswaterstaat who provided echo sounding data for DEM and support in the water level measurement campaign. Thanks are due to the National Institute for Coastal and Marine Management (RIKZ), Rijkswaterstaat for providing the Wadden Model and the gauging records needed for the water surface modelling. The assistance of A. Prakken, K.B. Robaczewska and R. van Dijk are kindly acknowledged. Funding for the project has been provided by the Netherlands Remote Sensing Board (BCRS).

REFERENCES

Calkoen C.J. and G.J. Wensink 1993, "Use of ERS-1 SAR to optimize ship-based bathymetric surveys in the Waddenzee, *Report Delft Hydraulics* pp. 21.

Koopmans B.N. and Y. Wang, 1995, "ERSWAD project- Measurement of land-sea transition from ERS-1 SAR at different phases of tidal water." Netherlands Remote Sensing Board, *BCRS report 95-20* pp 64.

Moens J.B. and K. Ruddick, 1994, "ERS-1 SAR Imagery of the Rhine-Meuse discharge front". Preliminary result in *Proceedings First Workshop on ERS-1 Pilot Projects,* Toledo, Spain. ESA SP 365, pp. 385-389.

Robaczewska K.B., R.P. van Dijk, R. Plieger and M. Soerdjbali, 1991, "Een Model van de Nederlandse Waddenzee voor Berekening van Waterbewegingen Water Kwaliteit", *GWAO-91.010*, p. 11 pl. 15.

Shuchman R.A., D.R. Lyzenga and G.A. Meadows, 1985, "Synthetic aperture radar imaging of ocean-bottom topography via tidal-current interactions: Theory and observations, *Int. J. Remote Sensing Vol. 6 (7)*, pp. 1179-1200.

Vogelzang J., G.J. Wensink, G.P. de Loor, H.C. Peters, H. Pouwels and W.A. van Gein, 1989, "Sea bottom topography with X-band SLAR", *BCRS report 89*, 25, final report project TO-3.10, pp. 84.

Wang Y., B.N. Koopmans and D. de Hoop, 1995, ERSWAD project -Operation Logger, *ITC report*, (in press).

IMPROVED COASTAL ZONE MANAGEMENT AND FLOOD FORECASTING USING SAR-DERIVED INTER-TIDAL DIGITAL ELEVATION MODELS

David Mason[1], Ian Davenport[1] & Roger Flather[2].

1. *Natural Environment Research Council Environmental Systems Science Centre (ESSC), The University of Reading, Whiteknights, PO Box 227, Reading RG6 6AB, U.K.*
Tel: (44)-1734-318743. Fax: (44)-1734-755865.

2. *Proudman Oceanographic Laboratory (POL), Natural Environment Research Council (NERC), Bidston Observatory, Birkenhead, Merseyside L43 7RA, U.K.*
Tel: (44)-151-653-8633. Fax:(44)-151-653-6269.

ABSTRACT

The potential for improved coastal zone management and flood forecasting using the 'water-line' method for constructing and monitoring digital elevation models of inter-tidal zones is considered. The current status of the technique is described. Plans for further development towards an operational system for commercial end-users are discussed.

1. INTRODUCTION

This paper considers the potential for using ERS SAR data for constructing and monitoring digital elevation models (DEMs) of inter-tidal zones for use in coastal zone management and flood forecasting.

The inter-tidal DEM construction technique concerned is known as the 'water-line' method (Koopmans and Wang 1994, 1995) and involves the use of remote sensing and hydrodynamic modelling. From a remotely sensed image the position of the shoreline (the land-sea boundary) is determined using image processing techniques, and this vector boundary is registered to map coordinates. Heights relative to mean sea level are superimposed on the boundary using the total tide plus surge water elevations given by a hydrodynamic tide-surge model run for this area for the time of image acquisition with the meteorological conditions pertaining at that time. From multiple images obtained over a range of tide and surge elevations it is possible to build up a set of heighted shorelines within the inter-tidal zone, and from this a raster DEM may be interpolated. The method allows the construction of an inter-tidal DEM over a large area relatively rapidly, as well as frequent subsequent monitoring of the DEM to detect changes.

This technique is currently being developed for scientific end-users within a project funded under the U.K. Land-Ocean Interaction Study (LOIS) Community Research Programme. However, it also has clear potential for non-scientific applications.

Changes in beach profiles can indicate potential threats to environmentally protected sites and can provide invaluable information for establishing requirements for coastal defences and monitoring their effects. Therefore, within the U.K., inter-tidal DEMs are currently used by bodies such as maritime local authorities and the National Rivers Authority (NRA) concerned with the monitoring of coastal defence systems and with the protection of environmentally sensitive inter-tidal areas such as salt marshes. Recent European legislation on habitat monitoring and U.K. legislation relating to the introduction of statutory Shoreline Management Plans have imposed formal monitoring requirements.

At present the organisations concerned either produce their own DEMs or rely on data supplied by the NRA. For example, NRA Anglian measures beach heights along transects up to 2.5km long from the sea wall perpendicular to the sea edge over most of its coastline from the south bank of the Humber to the Thames Estuary. Transects are generally spaced at 1km intervals and are sampled at 20m intervals twice-yearly. Conventional survey techniques are used in the inter-tidal zone, whilst transects extending below the low water mark are surveyed by bathymetric sounding. This type of survey is labour intensive and costly and large areas can be sampled only sparsely and relatively infrequently. The sparse sampling means that only poor height estimates can be obtained between adjacent transects. For areas such as Morecambe Bay there are large logistical difficulties and very real dangers in obtaining ground based data over the extensive beach area where the tide comes in faster than walking pace.

The water-line method may be able to complement the land-based surveying and reduce the amount of this necessary. Whilst it cannot achieve the centimetre accuracy of conventional surveying, it is able to 'fill in

Proceedings of the Second ERS Applications Workshop, London, UK, 6–8 December 1995 (ESA SP-383, February 1996)

the gaps' between transects in considerable detail. Still more important given the dynamic nature of the inter-tidal zone, it can increase the temporal sampling frequency significantly. As it is likely to be cheaper than conventional surveying, it could be a boon to the many organisations who currently find it difficult to fund regular monitoring of beach levels.

The improved inter-tidal topography generated by the method should also lead to improved prediction of flooding in coastal regions. Flood prediction is made using tide-surge models, and these require an accurate knowledge of bathymetry for correct modelling of the tide and surge, particularly in shallow water. In the U.K., the resulting water level predictions are used by the Storm Tide Warning Service to issue flood warnings for sections of the U.K. coast to local authorities (Flather et al. 1991).

2. THE WATER-LINE TECHNIQUE

Before describing plans for moving towards an operational system, the existing technique is briefly reviewed. The method is described in detail in (Davenport et al. 1995) and only a summary is given here, with additional discussion of recent developments.

The method is particularly suited to the use of SAR imagery, as the all-weather day-night capability of SAR allows a much higher image acquisition rate than that achievable using visible-band remote sensors. A semi-automatic method of delineating the shoreline has been developed to reduce the substantial effort and subjectivity that would be involved in manual delineation within each ERS-1 SAR image. A coarse-fine resolution processing strategy is employed, in which sea regions are first detected as regions of low edge density in a low resolution version of a complete SAR scene, then image areas near the shoreline are subjected to more elaborate processing at high resolution using an active contour model (Mason and Davenport 1995). Figure 1 shows a subimage of the Wrangle Flats area of the Western Wash with detected shoreline segments overlain. About 50 subimages have been processed using the method for a variety of regions within the LOIS Humber/Wash study area, and for many different tidal states. Over 90% of the shoreline determined appears visually correct. The remainder may be corrected using a sophisticated manual editing facility. A complete ERS-1 SAR scene can be processed in 1-2 hours on a SUN-10/50 using C-coded algorithms. Because each SAR scene provides only one shoreline, a very large amount of data must be handled, and it has been necessary to develop what is virtually an operational system to cope with the shoreline extraction process. This could readily be taken over to a full operational scenario.

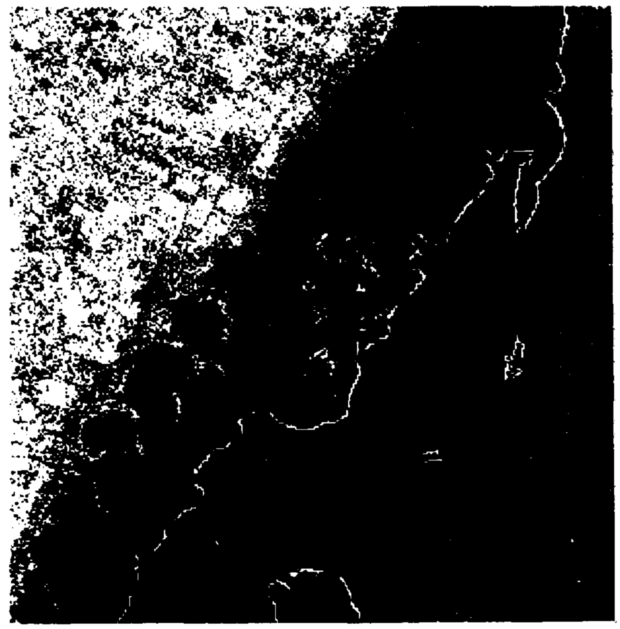

Figure 1. ERS-1 SAR subimage of Wrangle Flats, Western Wash (1024x1024 pixels) (c. ESA) with shoreline segments overlain.

The hydrodynamic model used is based on depth-averaged hydrodynamics, including tides and the effects of meteorological forcing (Flather 1994). A finite difference method is used to solve the equations on a 1.2km grid covering the east coast of England between Whitby and Cromer. The model formulation is essentially the same as employed in storm surge forecast models used operationally in the U.K. to provide coastal flood warnings. These models provide open sea boundary conditions of tide and surge for the present model. In a similar manner to the method used by Koopmans and Wang (1995), increased accuracy is obtained by correcting the model heights using local tide gauge information.

Recent work has concentrated on the development of the interpolation process, which constructs a spatio-temporal DEM from a set of shorelines. This must interpolate in the two spatial dimensions and in time. In order for changes in the DEM with time to be detected, it is necessary for each interpolated value to have an uncertainty associated with it so that the degree of confidence in a change can be established. The interpolator must also be capable of taking into account any drifts which are present, in particular the height

Figure 2. Composite shoreline coverage of Wrangle Flats.

trend perpendicular to the sea edge. To satisfy these requirements, we employ universal block kriging.

Figure 2 shows 33 shorelines of the Wrangle Flats region derived from images acquired over the three-year period 1992-4. In order to perform kriging, variograms in the space directions and time direction have been constructed from these shorelines. The variogram encapsulates the degree and form of spatio-temporal dependence of a variable over a region, and must be modelled for use in the kriging process. The data used in the spatial variograms has been detrended for a linear trend in the x (E) and y (N) directions, as the beach slope at Wrangle runs roughly northwest to southeast. Analysis and modelling of the variograms is still proceeding, but a preliminary assessment is that the variation in space can be modelled by an isotropic linear variogram of slope 0.0006 m^2/m up to 2500m, and the variation in time by a linear variogram of slope 0.0001 m^2/day up to 1100 days. The nugget variance of 0.05 m^2 present in both space and time variograms is largely due to the error in shoreline heighting.

Kriging is carried out in 3-D space-time, with a linear drift allowed in x and y. In the kriging process, the interpolated value of a block is a weighted average of the observed sample values in the block neighbourhood, with the largest weights being assigned to the samples nearest the block centre. A minimum of 4 and a maximum of 16 shoreline samples are selected for each block's interpolation. In order to ensure a reasonably uniform distribution of sample points, the 3-D space around each block centre is divided into eight segments along x, y and t axes passing through the block centre, and not more than three samples may be selected from each octant. In addition, only a single sample is allowed from any one shoreline per octant. This reflects the fact that two nearby points on the same shoreline will be very highly correlated, so that selection of both points rather than just one of them will introduce little new information into the kriging process.

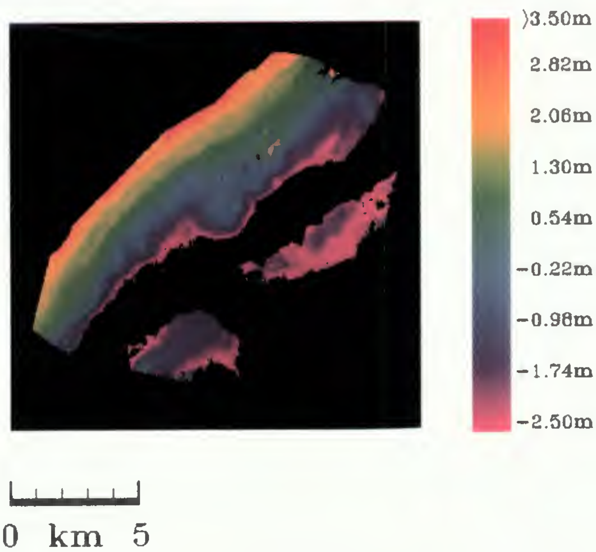

(a)

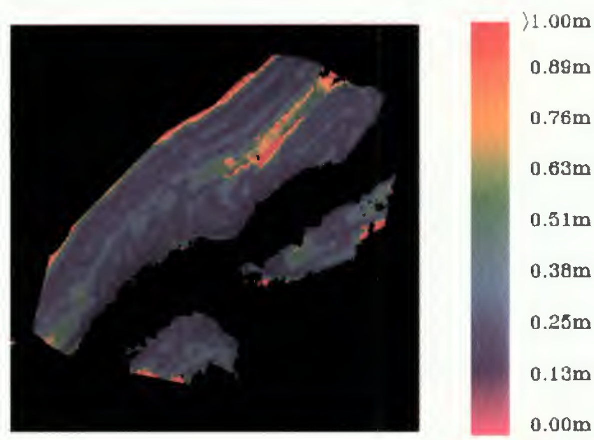

(b)

Figure 3. (a) DEM for Wrangle Flats (b) error map for (a).

Figure 3a shows the interpolated DEM for the 12km x 12km area of Wrangle Flats for the three-year period 1992-4, using a 50m x 50m kriging block size. Figure 3b shows the corresponding error map. Note that errors are larger at mid-tide because of the greater density of shorelines at high and low tide than at mid-tide due to the harmonic nature of the tides. For this particular combination of beach, remote sensor, model, data set and kriging parameters the average of the standard deviations on the interpolated values is about 25cm. A smaller error can be obtained at a cost of reduced spatio-temporal resolution by increasing the kriging block size.

In the above, all the shorelines have been grouped into a single time interval to create a spatial DEM. Kriging in 3-D also makes it possible to search for changes occurring over this period by comparing DEMs from different time intervals (e.g. 1992 and 1994). We are currently investigating the resolving power of the system for change detection using this facility.

3. THE INDUS PROJECT

We have recently been funded for a 2-year LINK project (Inter-tidal DEMs using satellite data (INDUS)) under the British National Space Centre Earth Observation LINK programme. The aim of this project is to carry out further precompetitive research in order to reach a position from which an operational system can be developed for a commercial end-user. The LINK partnership involves both the organisations able to undertake the technical development (ESSC and POL) and a commercial company able to provide and exploit the links to end users, namely National Remote Sensing Centre Ltd (NRSCL). The objectives and structure of the project are described below.

(1) Elicitation of user requirements.
A user requirement study will be undertaken in order to obtain the views of a substantial set of end users, including the NRA, English Nature and the New Forest District Council. The particular issues to be addressed are the height accuracy, spatial resolution and temporal sampling frequency required. The costs of this and other alternative methods of DEM production will also be compared. Alternative methods include conventional surveying, bathymetric sounding, airborne scanning laser altimetry, and SAR interferometry and stereophotogrammetry from both aircraft and satellite platforms. The requirements elicited from the users will form the basis against which the DEM products will eventually be assessed.

(2) Improvement of the technique.
There are two areas in which the current technique is known to require improvement, namely the accuracy of the hydrodynamic modelling and the precision of shoreline delineation. Substantial improvements should be possible in both areas.

It is important to reduce model errors because, rather than being random, they may take the form of systematic height errors along large sections of an individual shoreline. Model errors arise from several sources, including uncertain bathymetry affecting tide and surge propagation; limited resolution not fine enough to resolve complex channels and intertidal areas; errors in wind forcing giving inaccurate surge components; errors in the externally generated surge and tide introduced on open boundaries; and the use of simplified physics. For example the Humber - Wash model presently used in the LOIS project does not account for river flows, causing errors in the upper part of the Humber estuary, and also neglects effects of wind waves (set-up and set-down). In order to minimise these last errors and avoid the additional need to run wind wave models, only images acquired during periods of low wave activity are currently used to construct the DEM.

Our requirement of the model is that it should provide the most accurate measure of shoreline elevation possible at time of overpass. The current tide-surge model is a forecasting tool which estimates water elevations at time of satellite overpass by spinning the model up using meteorological data from the previous few days. Our feeling is that the best way of improving model accuracy in this case is to assimilate into the model run observations taken near the overpass time, and both after as well as before this. Observations could include local tide gauge data and satellite altimetry. In essence the tide-surge model would supply the spatial variations in water elevation whilst the tide gauge and altimeter data would supply the overall geodetic datum. We intend to examine both simple computationally-undemanding assimilation methods (which are often very effective though not formally optimal) and formally optimal computationally-demanding methods such as Kalman filtering and 'model fitting'.

Errors in the position of the shoreline arise due to the finite resolution of the SAR, and in the process of image registration. Both these errors appear to be no more than a single pixel. We intend to consider a number of options in this area. For example, the signal-to-noise ratio of edges and hence their detection efficiency and positional accuracy might be improved by using more sophisticated processing (such as simulated annealing) in the neighbourhood of the shoreline. The priority is probably improving the registration process, not simply to reduce the registration error but also to make the method easier to implement, as it involves a substantial amount of data handling. The registration process is an integral part of the process but is labour-intensive and tedious. It is difficult to find the same control point in two SAR images because of speckle. Also, whilst the SAR resolution error is probably fairly random, errors due to misregistration affect large sections of an individual shoreline in a systematic fashion. Possibly automatic registration software matching edge images derived from two SAR scenes (one of which had previously been registered to a map) could be developed.

(3) DEM generation for different test sites.
The system limitations will be tested by applying the technique to several geographic areas with varying characteristics. Three test areas have been selected with contrasting conditions of beach slope, beach material, tidal regime and wave climate, namely the LOIS Humber/Wash region, the New Forest coastline and Morecambe Bay.

(4) Assessment.
Finally the results of the study will be assessed by the end users in relation to their requirements. NRSCL will also assess the commercial potential of the product in relation to the U.K., European and World markets, taking into account the levels of interest shown, the requirements of users and the degree to which the product can meet these requirements.

4. CONCLUSION

The potential of the method for constructing and monitoring an inter-tidal DEM over a large area relatively rapidly and frequently has been demonstrated. It is also apparent that there is potential for applying the technique in the areas of coastal zone management and flood forecasting. The forthcoming INDUS project provides us with an ideal vehicle for moving the technique forward towards an operational system for commercial end-users.

5. ACKNOWLEDGEMENTS

We are grateful to ESA for supplying SAR data under the ERS Pilot Programme. This is LOIS publication number 55 of the LOIS Community Research Programme, carried out under a Special Topic Award from the Natural Environment Research Council, NERC contract F60/G6/12 and GST/02/777. Thanks are due to Clinton Blight for assistance in the preparation of the figures.

6. REFERENCES

Davenport, I., D.C. Mason, R.A. Flather & G.J. Robinson, 1995, Towards a digital elevation model of the Humber coast inter-tidal zone using remote sensing. *Proc. Third Thematic Conf. on Remote Sensing for Marine and Coastal Environments*, Seattle, 18-20 Sept. 1995, I.245-I.255.

Flather R.A., 1994, A storm surge prediction model for the northern Bay of Bengal with application to the cyclone disaster in April 1991. J. *Physical Oceanography* 24(1), 172-190.

Flather R.A., R. Proctor & J. Wolf, 1991, Oceanographic forecast models, in *Computer Modelling in the Environmental Sciences* (Eds. Farmer D. G. and Rycroft M. J.). Oxford University Press. 15-30.

Koopmans B.N. & Y. Wang, 1994, Satellite radar data for topographic mapping of the tidal flats in the Wadden Sea, The Netherlands. *Proc. Second Thematic Conf. on Remote Sensing for Marine and Coastal Environments*, New Orleans, 31 Jan - 2 Feb, 1994.

Koopmans B.N. & Y. Wang, 1995, Measurement of land-sea transition from ERS-1 SAR at different phases of tidal water. *Netherlands Remote Sensing Board Report 95-20*, pp64.

Mason D.C., I. Davenport, R.A. Flather, B.S. McCartney & G.J. Robinson, 1995, Construction of an inter-tidal digital elevation model by the 'water-line' method. *Geophysical Research Letters* (in press).

Mason D.C. & I. Davenport, 1995, Accurate and efficient determination of the shoreline in ERS-1 SAR images. *IEEE Trans. Geoscience and Remote Sensing (submitted).*

WIND MEASUREMENTS USING ERS–1 SAR

Wolfgang Rosenthal[1], Susanne Lehner[2], Jochen Horstmann[1], Wolfgang Koch[1]

[1] GKSS
D – 201502 Geesthacht

[2] Deutsche Forschungsanstalt für Luft– und Raumfahrt
D – 82230 Weßling

ABSTRACT

The ERS SAR is used to derive mesoscale wind fields as input for numerical models of dynamical processes in shallow water and coastal areas.
Since the SAR is working with the same wavelength as the scatterometer, the signal can be evaluated by the same algorithm as the scatterometer signal (C–MOD 4 Algorithm from ESA after adaptation of some instrument specific parameters as for instance the inclination angle), and local wind speed can be derived pixel by pixel. The wind direction is determined by a method that uses the average direction of wind rows visible on SAR images.The dependence of the backscattering coefficient of the sea surface on range is discussed and compared to theorie.
At low windspeeds SAR textures appear, which are caused by water contents or hydrodynamical parameters. The influence of these textures on wind measurements is investigated.
The SAR is capable to fill the gap in measurements of high resolution wind fields. The knowledge of these wind fields is essential to a better numerical modelling of coastal transport processes and therefore to an improved coastal management.

1. INTRODUCTION

Since 1991 the first radar satellite ERS–1 from ESA has been working succesfully. The altimeter as well as scatterometer data have been transmitted to the weather services routinely and they are used for the reconstruction of marine–meteorological weather events.
However despite its great capabilities, the 100x100km full resolution SAR scenes have not been used very frequently for routine purposes, except for the efforts of some groups detecting oil contamination in the oceans (Alpers, 1994) , Bathymetrie (Hennings,1988) or wind fields (Johannessen, 1994)
One of the reasons is that many phenomena which are visible in a ERS–SAR images are not yet clarified compleltly.
Among other parameters also water depth, current edges, wind velocity and wind direction influence the backscatter in SAR images.
Figure 1 shows an ERS–1 SAR image of the Rügen area from the 12.08.91. Wind direction and relative changes in the wind speed due to shadowing effects especially behind the famous white cliffs of Rügen are clearly visible.

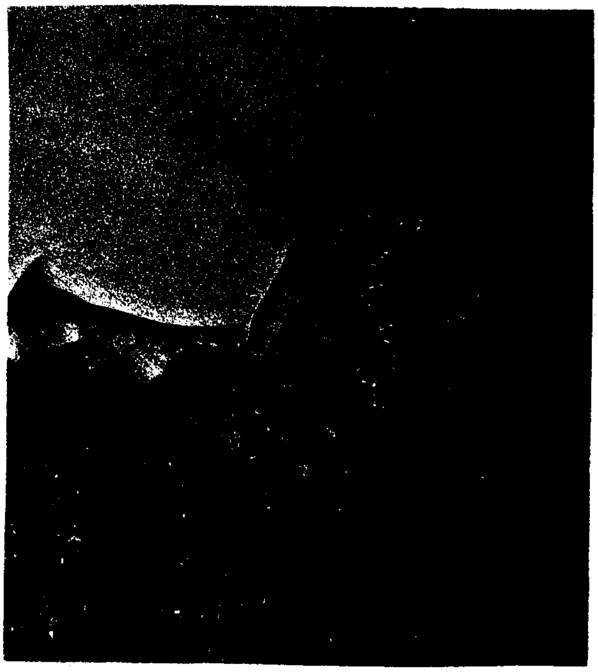

Figure 1 Rügen, 12.8.91

Proceedings of the Second ERS Applications Workshop, London, UK, 6–8 December 1995 (ESA SP-383, February 1996)

2. WIND MEASUREMENTS WITH ERS–SAR

Onboard ERS–1/2 is a tool for wind measurement, the wind scatterometer. This instrument uses a wave length of about 5 cm (C–Band) – the same radar wavelength as the SAR. The backscattered energy from the sea surface is averaged over an area of 12.5x12.5 km^2. This is a measure of the wind speed which causes the roughness of the sea surface. The backscatterded energy is also dependent on the viewing angle relative to the wind direction. This feature is exploited to determine the wind direction.

Comparisons of the scatterometer winds with in situ data (Stoffelen et al., 1993, Behrens et al., 1993) show that the scatterometer is a very useful instrument to improve wind field measurements in special areas which are not covered by conventional stations.

However the scatterometer is not an ideal instrument due to its coarse resolution in coastal zones. Data are falsified without warning to the user by backscattering mechanisms which are not caused by the influence of wind. Islands, shoals, surface–active matters or current edges may be such disturbing backscatter sources in the covering area of the scatterometer.

Since the ERS–SAR is working with the same wave length as the scatterometer, the signal can be evaluated by the same algorithm as the scatterometer signal, for instance the ESA CMOD 4 algorithm (Stoffelen, 1993). Several authors have studied the relation between σ_0 values of the global ERS scene and surface winds (Johannessen et al. 1994, Shuchmann et al 1993). Shuchman et al. determine for NORSCEX'91 data the regression line:

$$(1) \qquad [\,\sigma_0\,]_{dB} = -12.7 + 0.7\,[\,U_{10}\,]_{dB}$$

without correction for wind direction.

They do not look into the effect of changing incidence angle in range of the SAR scene which may cause a difference in σ_0 of up to 6 dB.

3. CALIBRATION OF ERS – SAR BACKSCATTER ON THE SEA SURFACE

The grey values of the ERS SAR PRI images are converted to σ_0 values using the ESA algorithm (Laur, 92).

$$(2) \qquad \sigma_0 = \frac{< I^2 >}{K} \; \frac{\sin\theta}{\sin\theta_{ref}}$$

We acknowledge the information from H. Laur on a saturation problem for the onboard analog to digital converter of ERS–1 (Meadows 1995, Scoon et al. 1995), which means that ERS–1 images have to be radiometrically recalibrated. This recalibration has not been applied yet to the subsequent data.

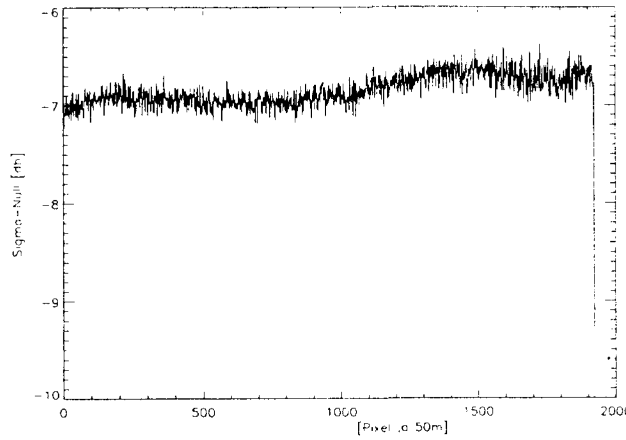

Figure 3a Range dependence of rainforest backscatter

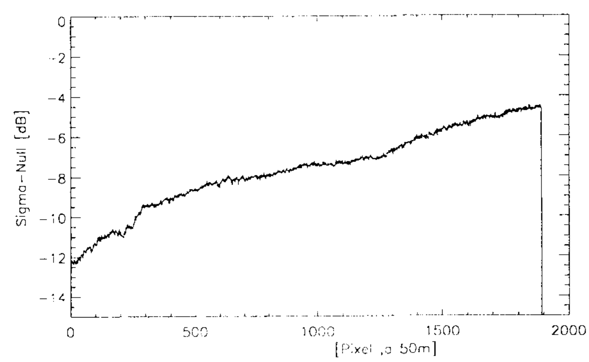

Figure 3b Range dependence of ocean backscatter

Figure 3 shows the mean of up to a 1000 rows of $[\,\sigma_0\,]_{dB}$ of a SAR image a) of Amazonian rainforest and b) of an ocean surface in the Baltic sea.

While the backscatter of the rainforest scene is fairly independent of incidence angle, it shows a strong dependency for the ocean surface. Because of the anisotropie of ocean waves the backscatter σ_0 is further dependent on incidence angle θ, the difference of direction of windspeed ϕ und azimuth look angle δ, and wind speed U_{10}. After Wright 1968:

$$(3) \qquad \sigma_{ij}(\theta) = 8\,\pi\,k^4\,\cos^4\theta\,\mid g_{ij}(\theta)\mid^2\,F(\,K_x, K_y)$$

where F is the two dimensional ocean wave spectrum, k radar wavenumber, K= 2 k sin θ wavenumber of the ocean waves at Bragg resonance condition and g Fresnel coefficient for VV polarisation.

For perfectly conducting materials g_{vv} is :

$$(4) \qquad g_{VV}(\theta) = (\,1 + \sin^2\theta) \,/\, \cos^2\theta$$

and the ocean wavespectrum F

$$(5) \quad F \sim K^{-4} \sim k^{-4} \ \sin^{-4}\theta \ \cos^2(\phi - \delta)$$

therefore the range dependency of σ_0, that is the dependency of backscatter on the incidence angle is proportional to

$$(6) \qquad \sigma(\theta) \sim (\ 1 + \sin^2\theta)^{\ 2} \ \sin^{-4}\theta \ \cos^2(\phi - \delta)$$

The algorithm CMOD4 uses relationship (3) and some Legendre polynomial fitting to determine windspeed and direction from σ_0 of the three different scatterometer antennas.

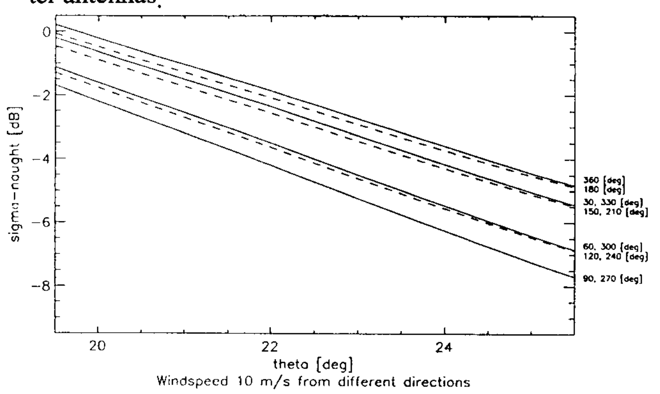

Figure 4 Dependence of σ_0 on incidence angle at U_{10} 10 m/sec

Figure 4 shows the incidence angle against expected σ_0 for ERS SAR at a winspeed of 10 m/sec for different windirections, figure 5 the incidence angle against expected σ_0 for different windspeeds, winddirection against line of sight of the antenna.
Properly calibrated ERS SAR images can therefore obviously give detailed information on the mesoscale wind field and as well help to discriminate on additional structures like slicks and ice.

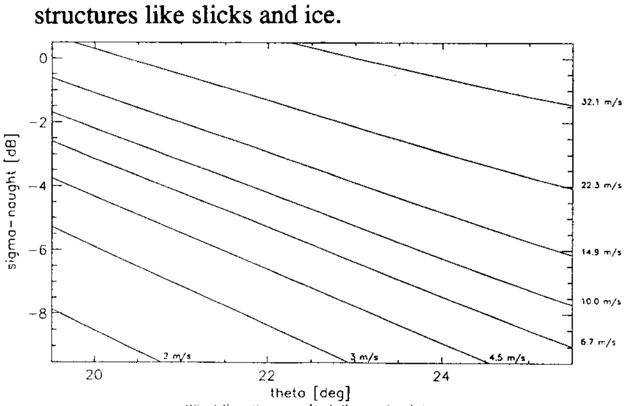

Figure 5 Dependence of σ_0 on incidence angle for different values of U_{10}

4. MODEL COMPARISON

σ_0 values of ERS–1 SAR scenes of the Baltic island of Rügen were averaged to one kilometer grid size and compared to the respective case of a model output of the mesoscale wind model GESIMA, that was developed at GKSS (Kapitza et al. 1993). Figure 6 shows the wind speed U_{10} computed by the mesoscale atmospheric model GESIMA for the satellite flight of figure1.

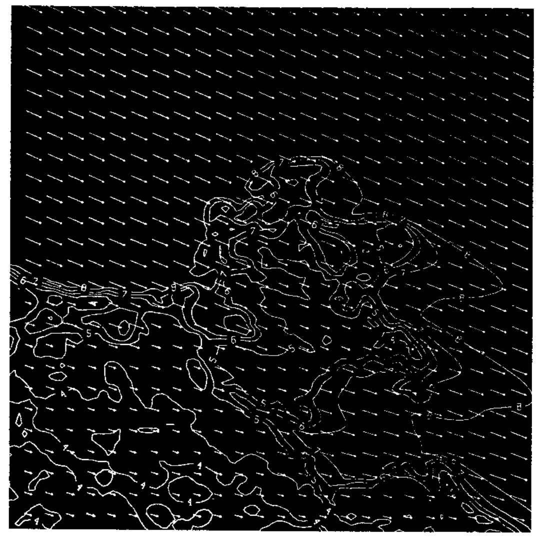

Figure 6 Wind speeds computed by the mesoscale atmospheric model GESIMA for the satellite flight of figure1

In a more detailed study the mesoscale wind field at the south east side of the Baltic island of Rügen, the Greifswalder Bodden is compared

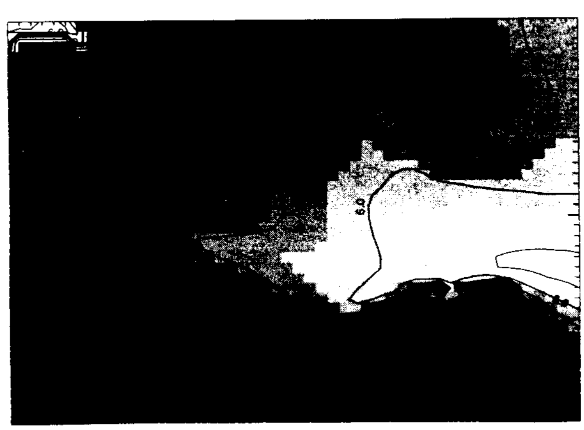

Figure 7a GESIMA model U_{10} over Greifswalder Bodden for satellite flight figure 1

Figure 7 a) shows isolines of the result of GESIMA in m/sec and 7b) the grey values of the ERS SAR image.The SAR image clearly shows a much finer detail in wind structure and a higher variability in wind direction. Information of this kind should be very valueable for model improvement.

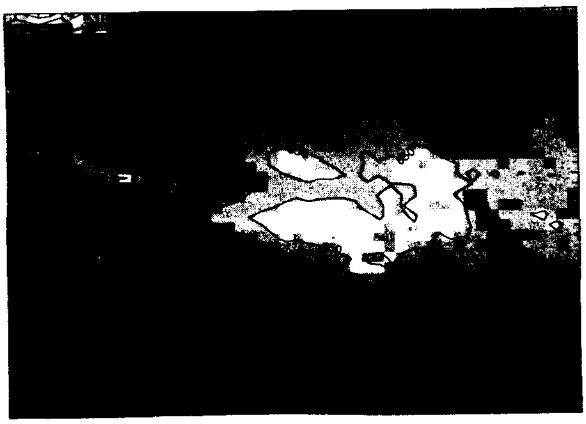

Figure 7b Greylevels of the respective ERS SAR image

Figure 8 shows a logarithmic regression between the U_{10} model of GESIMA and the σ_0 values of the SAR image of the 12.8.91. The NORSCEX regression line is included.

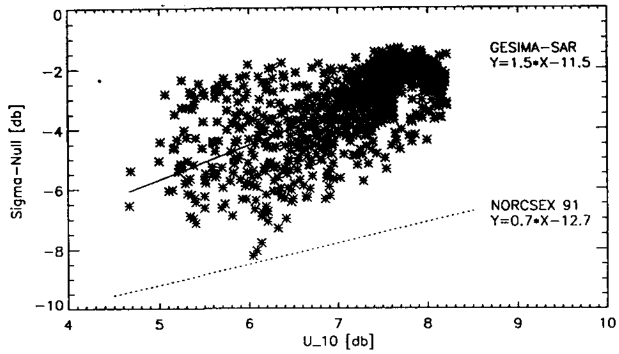

Figure 8 Regression GESIMA – SAR

The scatter of the plot shows the difference between the snapshot of the ERS–1 SAR of a highly turbulent windfield and the mesoscale model simulation assuming a stationary situation. There seem to be difficulties for the model to reproduce the situation of wind shadowing behind the cliffs.

5. CONCLUSIONS

It is obvious that ERS SAR is a very valuable tool for the improvement and tuning of mesoscale windfield models like GESIMA

There is quite a strong incidence angle dependency for SAR images, which for exact evaluation of a windfield algorithm has to be studied using a statistic over a lot of different ERS SAR scenes.

Prior to this obviously an absolute calibration procedure of the SAR images has to be achieved.

From this further insight into the CMOD 4 algorithm is to be gained. Especially reasons for the failure of CMOD 4 due to other influences like fronts and slicks will become obvious.

6. REFERENCES

1. Alpers,W., 1994, X–SAR/SIR–C Shuttle–Unterfliegung, Operationsplan, Uni Hamburg, Inst. f. Meereskunde

2. A. Behrens and D.Schrader, 1993, ERS 1 measurements in comparison with wind and wave forecast results, Proc of the 2nd ERS–1 Symp., Hamburg

3. Hasselmann, K., R. K. Raney, W.J. Plant, W. Alpers, R.A. Shuchman, D.R. Lyzenga, C.L.Rufenach, and M.J.Tucker, 1985, Theory of synthetic aperture radar ocean imaging: A MARSEN view, J. Geophys Res., 90, 4659–4686.

4. Hennings I., 1988, Bodentopographie auf Luft– und Satellitenbildern im Mikrowellenbereich und im sichtbaren Bereich des elektromagnetischen Spektrums, GKSS 88/e/41, GKSS, Geesthacht

5. Johannessen J. A.Vachon, O. Johannessen, 1994, ERS–1 SAR imaging of marine boundary layer processes, Earth Observation Quarterly , nr.46 (ESA publication)

6. Kapitza H. and D.Eppel, 1992, The non–hydrostatic mesoscale model GESIMA, Beitr. Phys. Atmosph., 65, 129 – 146

7. Laur H., ERS–1 SAR calibration derivation of backscattering coefficient σ_0 in ERS–1.SAR.PRI Products, ESA/ESRIN Technical Note, in preparation

8. Meadows P. and P.Wright, 1994, ERS–1 SAR Analog to Digital Convertor Saturation, Proc. of the CEOS SAR Calibration Workshop, Ann Arbor Michigan

9. Shuchman R., J.Johannessen, C.Rufenach, K.Davidson and Ch.Wackerman, 1993, Determination of wind speed and direction using ERS–1 SAR data during NORCSEX'91, Proc of the 2nd ERS–1 Symp., Hamburg

10. Scoon A. and I. Robinson, to appear, Demonstration of an improved calibration scheme for ERS–1 SAR imagery using a wind retrieval model

11. Stoffelen E. and D. Anderson, 1993, Wind retrieval and ERS–1 scatterometer radar backscatter measurements, Advanced Space Research, 13, 5, 53–60

12. Wright J., 1968 , A new model for sea clutter, IEEE Trans. Antennas and Propag., AP–16, 217–223

MAPPING

Chairman: E. Attema
Rapporteur: J. Lichtenegger

CARTOGRAPHIE GÉNÉRALE ET THÉMATIQUE EN CONTEXTE TROPICAL HUMIDE A PARTIR DES IMAGES ERS1: EXEMPLES EN GUYANE FRANÇAISE.

Rudant J.P (1), Baltzer F (2), Deroin J.P (3), Fromard F (4), Hoff M (5), Lointier M (6), Maître H (7), Marinelli L.(8), Mougin E (9), Pénicand C.(10), Prost T.(11)

1 -Université Pierre et Marie Curie,LGGST,Boite 129,4 place Jussieu, 75252 Paris Cedex 05
Tél : 33 (1) 44 27 50 87, Fax : 33 (1) 44 27 50 85, Émail : jpr@osiris.lgs.jussieu.fr
2 - Université Paris XI, Laboratoire de Pétrologie Sédimentaire, Bât.504, 91000 Orsay
3 - BRGM, Direction de la Recherche, 45060 Orléans
4- ICIV, 13 av. du Colonel Roche, 31000 Toulouse
5 - ORSTOM et UPMC, Laboratoire de Botanique Tropicale, 12 rue Cuvier 75005 Paris
6 - ORSTOM, Laboratoire d'Hydrologie, 911, av. Agropolis, BP 5045, 34032 Montpellier
7 - Télécom-Paris, Laboratoire Image, 43 rue Barrault, 75014 Paris
8- Société Géoimage, Les Espaces de Sophia, Sophia Antipolis
9 - CESBIO, 9, av. du Colonel-Roche, 31000 Toulouse
10 - DGA / CEGN, 16 bis, av. Prieur de la Côte-d'Or, 94114 Arcueil
11 - Musée Goeldi, Département Écologie, CP 399 Bélem, 66040 Parà, Brésil

Résumé

L'exploitation des images ERS1 en Guyane Française a donné lieu à des développements dans les domaines de la cartographie (générale et thématique). Dans le domaine de la cartographie générale, ont été réalisées une mosaique regroupant 18 scènes et des spatio-cartes géocodées au 1/100000 sur les régions de Cayenne et Kourou à partir de séquences multitemporelles. Dans celui de la cartographie thématique, nous avons pu montrer l'intérêt des images ERS1 pour les disciplines suivantes: dynamique littorale, hydrologie, géologie-géomorphologie , topographie et écologie forestière.

Une couverture de spatiocartes ERS1 au 1 / 200000 est actuellement en cours de réalisation sur l'ensemble du territoire (voir l'article de Tonon et al. dans ce volume)

Nous avons pu l'utiliser pour effectuer la présentation d'un "évènement nouveau" en insérant dans la mosaique l'image JERS1 de la retenue du barrage de Petit Saut acquise en mars 1994.

1- INTRODUCTION

Nous présentons ci dessous une synthèse des résultats que nous avons pu obtenir dans le domaine cartographique sur la Guyane Française, grâce aux images ERS1. Les possibilités offertes par la synergie ERS1-JERS1 sont également mentionnées. Le texte qui suit emprunte beaucoup aux articles cités en référence où l'on pourra trouver de nombreuses illustrations complémentaires.

Une présentation du contexte géographique du site d'étude (climat tropical humide) en rapport avec l'utilisation des images ERS1 et JERS1 pour les applications thématiques traitées peuvent être trouvées dans plusieurs des publications citées en bibliographie. (Balt 93,Dero 93, Loin 92, Ruda 94 et 95).

2- CARTOGRAPHIE GÉNÉRALE (Voir Ruda 94, Workshop ESA de Tolède)

2-1 Réalisation d'une mosaïque de 18 scènes

Une mosaïque regroupant 18 images RSO-ERS1 (Rosaz et al.1993) a été établie à partir d'une couverture totale du territoire obtenue entre avril et décembre 1992. Le traitement a consisté en des corrections géométriques (translation et rotation) et radiométriques visant à annuler sur la forêt les effets de la variation d'incidence (19° à 26°) à l'intérieur d'une trace. Le coefficient de rétrodiffusion variant plus rapidement avec l'incidence en mer que sur la forêt, des discontinuités radiométriques persistent donc entre traces sur l'océan, au nord de la scène. Des contrastes de radiométrie sont également visibles à terre entre images acquises à des dates différentes ; ces contrastes correspondent alors aux évolutions naturelles des milieux rétrodiffusants au cours du temps.

2-2 Iconocartes au 1/100 000 sur les régions de Cayenne et de Kourou

La combinaison d'images acquises à des dates différentes sur une même zone permet de réduire la part aléatoire du signal due au chatoiement (*speckle*) , sans pour autant augmenter la taille du pixel. Mise à profit sur les régions de Cayenne et de Kourou (Pénicand et al.), cette technique nous a permis d'établir des iconocartes au 1/100 000 en superposant 3 images. La **figure 1** permet une comparaison entre la carte IGN actuelle au 100000 et la spatiocarte ERS1.

2-3 En cours actuellement (Hors projet Piole): réalisation de spatiocartes au 1 / 200000 sur l'ensemble du territoire, par spatiotriangulation d'un grand nombre de scènes.(voir l'article de Tonon et al., ce volume).

Destinée à faciliter leur usage, une notice explicative accompagnera ces spatiocartes. Elle comprendra une introduction décrivant les spécificités de l'imagerie radar en contexte tropical humide et des éléments d' interprétation sur des sites test.

2-4 Conclusion relative aux échelles de restitution des documents sur support papier:

Les échelles pratiques de restitution dépendent des traitements subis par les images:

-le 1 / 200000 pour une scène PRI seule , sans traitement géométrique;

-le 1 / 300000 pour une mosaique obtenue à partir d'une seule couverture, avec rééchantillonnage et rotation

-le 1 / 200000 pour une spatiocarte obtenue à partir de deux couvertures, avec rééchantillonnage et rotation

- le 1 / 150000 ou le 1 / 100000 pour une spatiocarte

Figure 1 -La haute résolution multidates, comparaison avec une carte IGN au 1 / 100000

L'image ERS1 permet des différenciations texturales très fines grâce à l'excellent rendu de la morphologie (en particulier les bas fonds sont rendus avec une texture très lisse). Le relief est plus lisible que sur la carte IGN. Les informations présentées sur les deux documents sont complémentaires. La faible incidence de 23°, permet ici cette sensibilité aux faibles reliefs alors qu'elle est handicapante dans les régions de relief plus tourmentés.

L'avenir en zone tropicale est certainement aux spatiocartes radar.

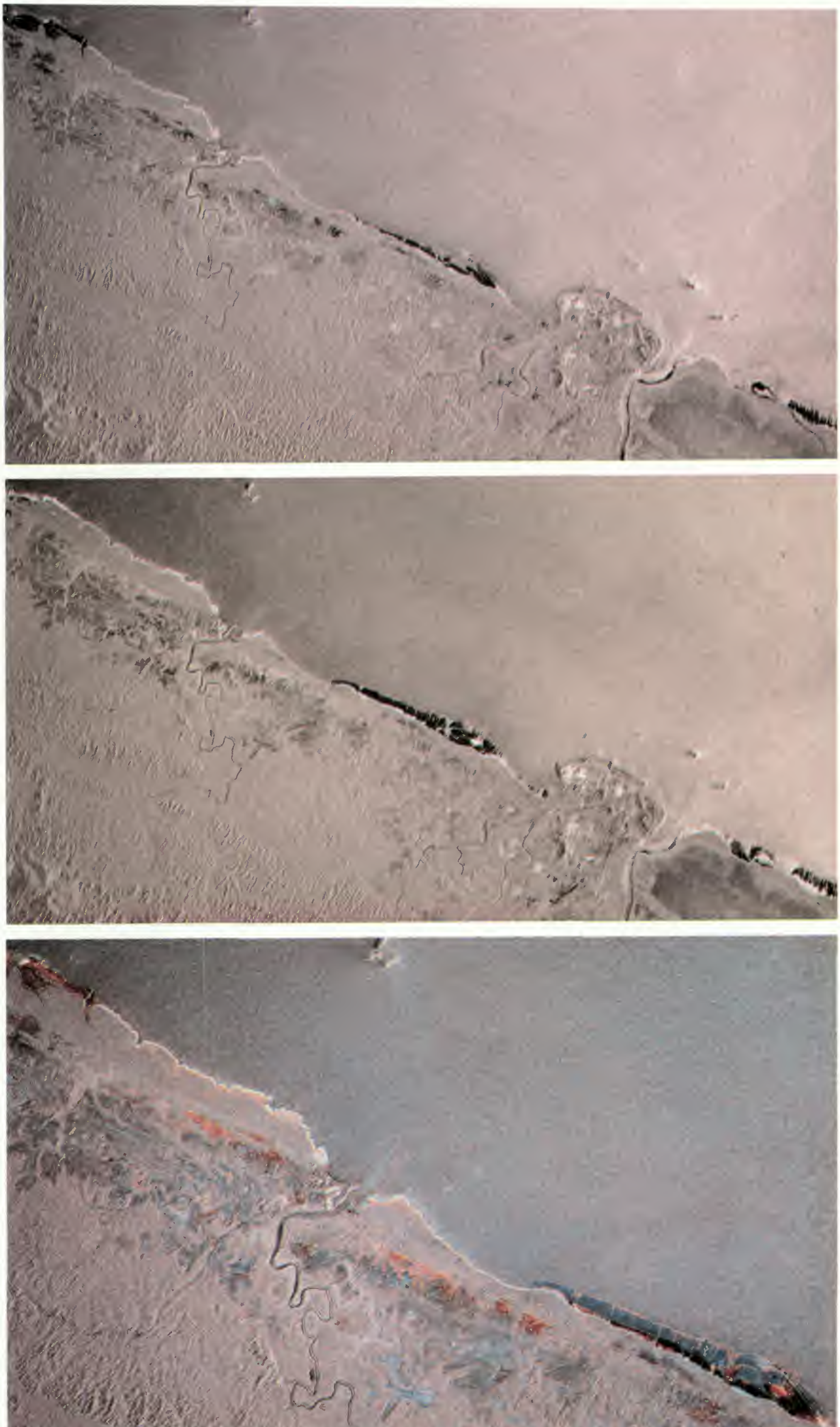

Fig 2 -Evolutions côtières: mise en évidence des aires de sédimentation et de l'érosion par composition multidates: Une simple composition colorée des images des 3 mai 1992 (en haut en bleu) et 14 novembre 1993 (au milieu en rouge) prises toutes deux à marée basse met en évidence une évolution significative du trait de côte à l'Est et à l'Ouest de Kourou, extension vers l'Ouest et vers le large du banc de Tonate (en noir) et érosion d'une bande littorale de mangroves décadentes (trait de côte très clair sur les images) obtenue à partir de 3 couvertures, avec rééchantillonnage et rotation:

- le 1 / 50000 est accessible lorsqu'on superpose plus de 6 scènes de la même zone

3 CARTOGRAPHIE THÉMATIQUE (Voir aussi Ruda95)

3-1 Dynamique littorale

L'apport des images concerne principalement:

-Le suivi des aires de sédimentation récentes (vase molle et lisse) à marée basse (fig1)

Les aires correspondantes apparaissent en noir sur les deux types d'images utilisées (ERS1, JERS1) car la rugosité des surfaces considérées est extrèmement faible.

Dans le cas de ERS1, les rétrodiffusions de l'océan et de la plaine littorale sont en général nettement plus élevées que celle de la vase lisse et une segmentation des zones correspondantes est possible sur un simple critère radiométrique. Dans certains cas exceptionnels, par mer calme, la différenciation vase-océan devient plus difficile à l'extrémité de la trace (incidence 26°).

-Les limites bathymétriques vues par ERS1

La répétition des acquisitions permet d'obtenir les limites bathymétriques vase lisse-océan correspondant aux différents niveaux de marée existant les jours d'acquisition (**Ruda 94**). L'instabilité des bancs de vase limite la généralité des conclusions lorsque les dates de prise de vue sont trop distantes. L'apport de ce type de relevé serait encore plus interessant si une scène avait pu être acquise à chaque passage du satellite; la variabilité des niveaux de marée aurait alors permis une étude continue de l'évolution des bancs et l'estimation plus précise de certains paramètres quantitatifs associés à la sédimentation (volumes de sédiments déposés, pente des bancs ..).

Deux images acquises à marée basse à 18 mois d'intervalle montrent des évolutions significatives; érosion au voisinage de Kourou et accrétion vaseuse au voisinage de Tonate (**Ruda 95**).(**Fig 2**)

Détection du trait de côte sur les images ERS1

Les techniques de segmentation markovienne hiérarchique permettent de relever automatiquement la limite existant entre palétuviers adultes et arbres tombés au sol (**Desc 95**). La précision du tracé est suffisante pour envisager de pouvoir suivre quantitativement le phénomène d'érosion qui affecte la mangrove sur certains secteurs. Le trait détecté est peu sensible au niveau de la marée car il s'agit d'une bande d'arbres morts couchés au sol qui se trouve à la limite d'un rideau d'arbres verticaux.

-La spatialisation de l'évolution géochimique de la sédimentation littorale (Balt 93)

Les images ERS1 peuvent être utilisées pour spatialiser les aires de développement homogène de végétation dans les zones de vasières intertidales et subtidales ainsi que dans les marais saumâtres d'arrière mangrove. Des mesures in situ (Ph, Salinité, teneur en eau, Potentiel Redox) sur les sédiments sont effectuées entre la surface et 2 m de profondeur grâce à des carottages effectués sur des transects perpendiculaires à la côte. Ces mesures permettent de corréler les types de végétation rencontrés et les propriétés physico-chimiques des sédiments sous jacents .

3-2 Hydrologie:

Elaboration de diagrammes fonctionnels de petits bassins versants côtiers (ERS1)

L'exemple traité concerne la zone de la crique Karouabo (à 20 km à l'ouest de la ville de Kourou).

Les images ERS1 acquises en mai et juin 1992, c'est à dire en plein coeur de la saison des pluies, présentent un intérêt exceptionnel car elles constituent les premières données images spatiales de haute résolution exploitables en une telle saison.

Une synthèse diachronique de trois scènes ERS1 acquises à trois semaines d'intervalle grâce aux chevauchement d'orbites parallèles a permis une spatialisation des informations, relativement au rôle que chaque milieu peut jouer vis à vis du stockage de l'eau et de sa circulation (**Loin 93, 94**).

3-3 Géomorphologie quantitative et geologie

L'excellente perception des reliefs sur les images ERS1 de la Guyane résulte de plusieurs facteurs :

- la faible incidence moyenne du faisceau (23° au centre de la scène) est supérieure aux pentes que l'on rencontre couramment sur les reliefs de la région, ce qui évite les rabattements,
- l'existence d'un couvert forestier dense et très homogène, rend en première approximation le coefficient de rétrodiffusion indépendant de l'incidence locale,
- la longueur d'onde utilisée pour ERS1 est faible (6 cm) et la pénétration des ondes dans les feuillages limitée à quelques mètres; l'image restituée est alors celle du toit de la canopée

Radaclinométrie, radargrammétrie (Tono 93)

La technique de radarclinométrie, qui se fonde sur l'analyse des variations radiométriques en fonction de l'incidence locale (donc de la pente et de l'azimut des flancs de relief considérés) fournit, appliquée sur les données ERS1 en Guyane, des estimations de dénivelées avec une précision de l'ordre de 10 %.

La technique radargrammétrique met à profit les différences d'angles de visée pour les zones de recouvrement obtenues à partir d'orbites adjacentes et déduit les altitudes des parallaxes observées. Des tests effectués grâce à cette technique montrent que le couvert forestier n'est pas un obstacle à son application pour un couple d'images ERS1 correspondant à une zone de recouvrement orbital.

Des tests sont actuellement en cours pour évaluer les possibilités offertes par des couples mixtes ERS1-JERS1. La différence de longueur d'onde ne devrait pas être un obstacle majeur à l'application de la méthode car en zone de relief couvert de forêt dense, les images sont principalement modulées par la morphologie.

Les tests prévus par la technique interférométrique, quant à eux, n'ont pu être effectués car les répétitions d'orbites disponibles présentaient des distances inter-traces trop importantes pour donner des conditions expérimentales satisfaisantes.

Repérage des zones basses le long des fleuves

Les zones basses du lit majeur des fleuves et de leurs principaux affluents sont caractérisées sur les images ERS1 par une texture fine due au fait que le couvert forestier présente, (dès que l'on s'écarte quelque peu du cours d'eau proprement dit) , un état homogène d'épaisseur très lentement variable . Cette texture lisse en l'absence de signature géomorphologique permet au photointerprète d'isoler aisément le lit majeur

La partie isolée correspond soit à des forêts marécageuses, constamment inondées, soit à des forêts sur flat, inondées seulement en saison humide. Globalement, il s'agit d'aires de dispersion des crues. **(Hoff 96)** fournit une cartographie des forêts inondables entre le barrage de Petit saut et Saut Bérard en aval. Cette capacité de l'imagerie micro-ondes à permettre la cartographie des zones de bas fonds représentent une qualité originale dans des contextes climatiques où l'imagerie optique est souvent inopérante.

Cartographie morphostructurale

L'aptitude de l'imagerie ERS1 à restituer, malgré les distorsions géométriques, une information géomorphologique extrèmement détaillée permet dans de nombreux cas de différencier les lithologies sur des critères texturaux. La comparaison entre des extraits d'images et la carte géologique correspondante est en général significative à cet égard.(Voir Dero 93, Ruda 95) Les divers faciès d'érosion rencontrés dans la région dépendent de la lithologie des formations sous jacentes et induisent des signatures radar spécifiques.

4- SYNERGIE ERS1-JERS1

La synergie ERS1 - JERS1 est particulièrement nette lorsqu'on s'interesse aux formations de la plaine littorale. Les longueurs d'onde en bande C et L ont en effet des comportements nettement différents pour les paysages de savanes et marais rencontrés. Il s'ensuit qu'une simple composition colorée restitue une information directement corrélable aux formations végétales présentes sur le terrain. La **figure 3** met en parallèle la carte de végétation établie sur la région de Kourou à l'aide de moyens traditionnels (analyse de photographies aériennes et campagne de réalité terrain) avec une combinaison trichrome obtenue à partir de deux images ERS1 et d'une image JERS1.

Cette synergie s'exprime également d'une manière particulièrement spectaculaire lorsque l'on fusionne une image récente JERS1 de la retenue du barrage de Petit Saut avec la mosaïque disponible sur l'ensemble de la Guyane.**(Fig 4)** L'image JERS1 de mars 1994, acquise 3 mois après le début de la mise en eau du barrage de Petit Saut, a subi deux transformations géométriques: la première destinée à assurer la coincidence des points les plus bas par transformation polynomiale, la seconde par corrélation (technique radargrammétrique) de manière à mettre les reliefs en correspondance.

5 CONCLUSION

Dans le contexte tropical humide de la Guyane Française, l'imagerie radar ERS1 a montré dans les domaines thématiques envisagés dans cette note, dynamique littorale, hydrologie, géomorphologie, ainsi que dans le domaine de la cartographie opérationnelle une aptitude générale à répondre aux questions posées par l'utilisateur d'images de télédétection. L'échelle de travail est bien entendu limité par la résolution des images mais nous avons vu sur les exemples traités que la disponibilité de séquences multitemporelles permettait d'améliorer l'échelle usuelle du 200000 pour se rapprocher du 100000 voire du 50000 è si le nombre de scènes superposables est supérieur à 6.

L'importance des possibilités offertes fait que le nombre des utilisateurs actuels et / ou potentiels est élevé: citons :Armée de Terre, BRGM, CNRS (en particulier le programme Environnement), EDF, Office du Tourisme, Ministère de l' Environnement, ORSTOM, Groupement de laboratoires ECOLAB, SYLVOLAB, Sociétés de service en cartographie et de développement logiciel, Universités.

Références:

Les Proceedings évoqués pour les Symposiums de Cannes et Hamburg ainsi que pour le Workshop SAREX sont des éditions ESA;

Proceedings Symposium ERS1 Cannes,France Nov 1992, ESA SP 354 (Ci après "Cannes")

Proceedings Symposium ERS1 Hamburg,Allemagne, Oct 1993, ESA SP 361(Ci après "Hamburg")

Final Results Workshop SAREX 92, Paris, Déc 1993, ESA WPP 76 (Ci après "Paris")

Proceedings Workshop ESA Tolède, Juin 1994, ESA-SP365, .(Ci après "Tolède").

(Balt 93) Baltzer F., Plaziat JC., Prost MT., Rudant JP., Dechambre M. (1993) Use of SAREX, ERS and Erasme data for a comparison between geochemical measurements oninterstitial waters and vegetation distribution in equatorial littoral swamp sediments: an example from Marais Leblond, French Guiana.Workshop"Paris" pp 215 - 222.

(Dero 93) Deroin JP., Braux C., Cautru JP., Rudant JP., Toux L. (1993) ERS1 SAR: an aid for geological mapping and mineral exploration in rain forest areas. Symp. " Hamburg" pp 897-902.

(Desc 96) Descombes X., Moctezuma M., Maître H., Rudant J.P., Coastline detection by a Markovian segmentation on SAR images, Signal Processing

(Disa 95) Disalvo Magali, Comparaison des images ERS1 et JERS1 sur le plan géométrique et radiométrique, Rapport de fin d'études d'ingénieur IGN, Stage à l' Université Pierre et Marie Curie, Juin 1995

(Hoff 96) Hoff M., Rudant J.P., Apport des images radar à l'étude des berges des fleuves tropicaux: cas du Sinnamary lors de la mise en eau du barrage de Petit Saut (Guyane Francaise), CRAS, soumis

(Loin 93) Lointier M.,Rudant JP., Sabatier D., Prost MT., Nezry E, Degrandi G, Conway J, Sieber AJ. (1993) Contribution of ERS1 SAR data to hydrologic approach in tropical area: example in French Guyana. Symposium " Hamburg" pp 1267-1272.

(Loin 94) Lointier M. , Rudant J.P., (1994) - Contribution du SAR de ERS1 à l'analyse hydrologique en milieu tropical humide : résultats du programme ppF12 en Guyane. Journées Hydrologiques de l'Orstom. Montpellier. Orstom éd, sous presse.

(Pinc 95) Pinciroli M., Caractérisation fractale du réseau hydrographique en imagerie radar ERS1, projet de fin d'études, Laboratoire Images, Télécom Paris, Juin 95

(Ruda 94) Rudant J.P.,Baltzer F.,Deroin J.P.,Lointier M., Maitre H., Penicand C., Prost M.T., Sabatier D (1994).;Possibilités cartographiques offertes par ERS1 en contexte tropical humide,Exemples en Guyane Française, Apports spécifiques des séquences multitemporelles.Workshop "Tolède", pp 371- 376.

(Ruda 95) Rudant J.P., Baltzer F. , Deroin J.P. , Lointier M., Maître H., Mougin E. , Pénicand C. , Prost M.T. , Apport des images satellitaires ERS1 et JERS1 dans le domaine de la cartographie générale et thématique en contexte tropical humide.Exemples en Guyane française et régions limitrophes, Journées de cartographie

radar, Cannes Nov 94, Cahiers de la Société Française de Photogrammétrie et de Télédétection, sous presse
(**Ruda 95**) Rudant J.P. , Baltzer F. , Hoff M. , Lointier M.,.Maitre H., Bilan des Informations quantitatives et semiquantitatives extraites de l'analyse desimages ROS satellitaires ERS1 ET JERS1 et utilisées pour la cartographie thématique en contexte tropical humide., Colloque Télédétection micro-onde, extraction de paramètres bio et géophysiques, Toulouse 10-13 octobre 1995, sous presse
(**Tono 93**) Tonon M., Rudant J.P., Sabatier D., Nezry E., Degrandi G., Sieber A.(1993) Relief Estimation in Tropical context (French Guiana) with SAR-ERS1 imagery. Symposium "Hamburg" pp 1261-1268.

Remerciements: Ce projet a eu le support des organismes participants, du CNES et du Ministère de l'Environnement.

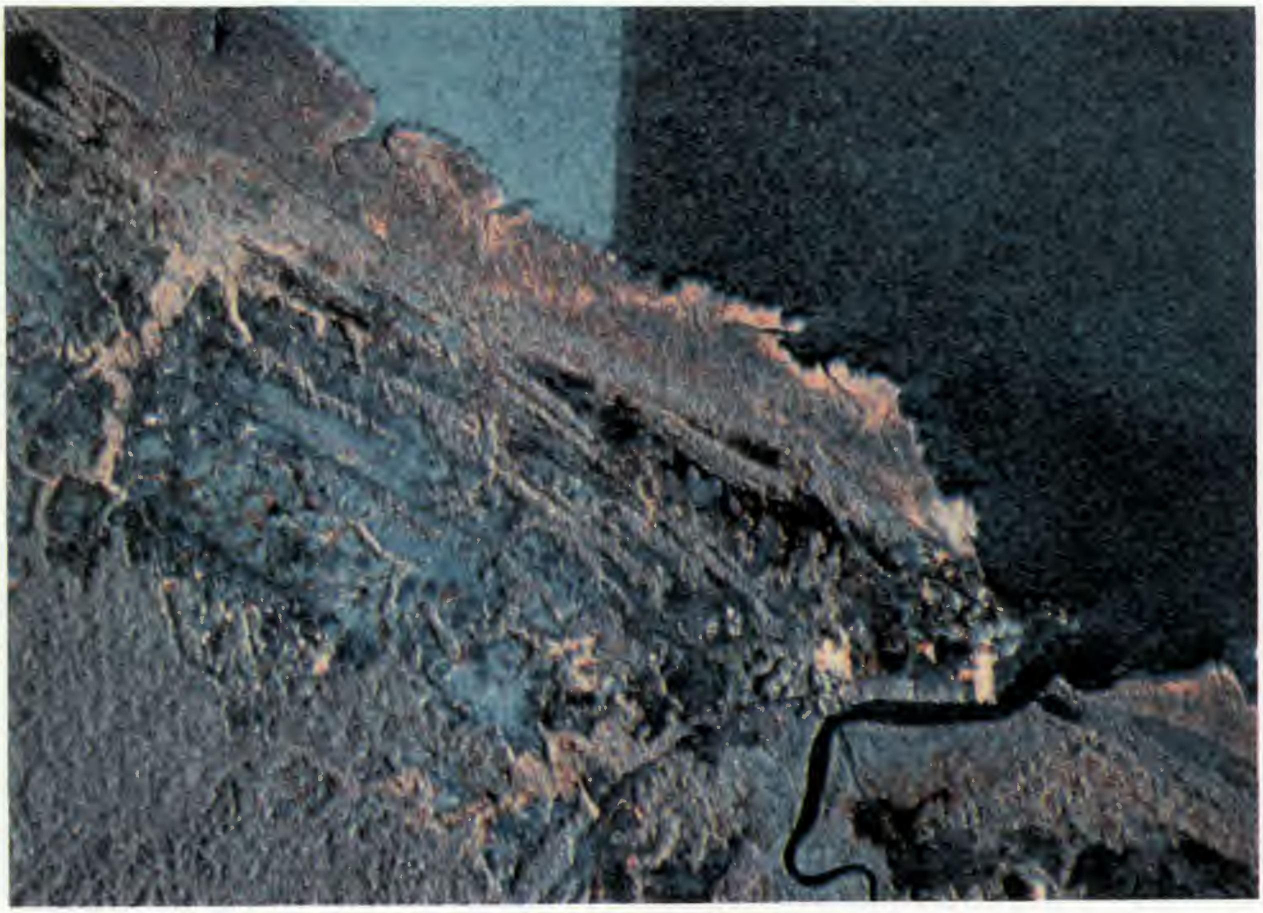

Fig 3a- Fusion ERS1-JERS1 dans la région de Kourou confrontation avec la carte de végétation au 1 / 50000 établie sur le site par F. Fromard et H.Puig (Contrat CNES-Kourou)

Les compositions trichromes sur Kourou et Sinnamary ont été obtenues en composant 2 images ERS1 du printemps 1992 (bleu-vert) avec une image JERS1 de février 1993 (rouge).

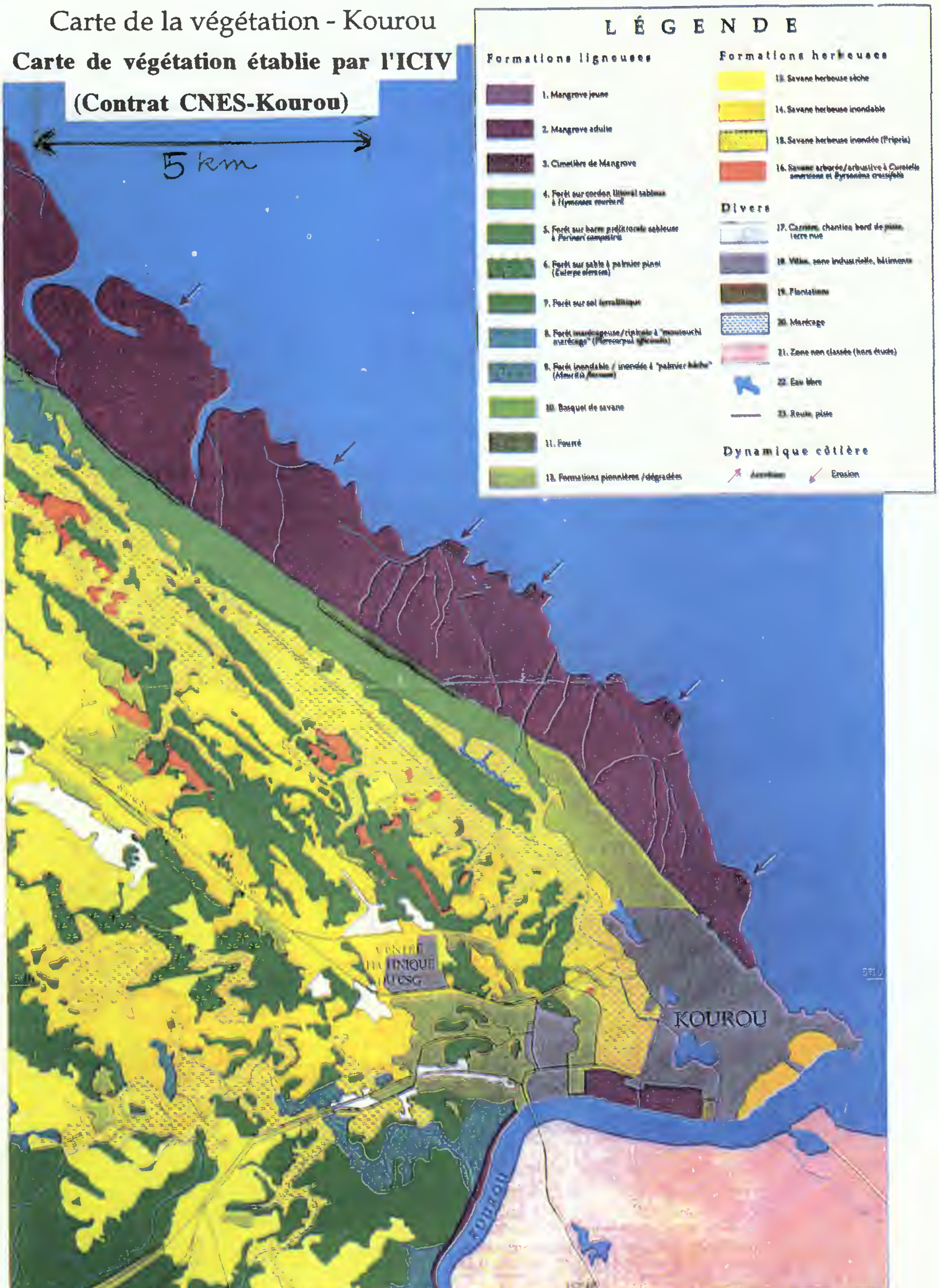

© LET/ICIV - CNRS. UPS. 1995

Réalisation technique : M. Aizpuru

Fig 3 b- Comparaison d'une fusion ERS-JERS (Voir Fig 4b) avec cette carte de végétation établie par l'ICIV sur la région de Kourou. La synergie ERS1 - JERS1 est particulièrement nette lorsqu'on s'interesse aux formations de la plaine littorale. Les longueurs d'onde en bande C et L ont en effet des comportements nettement différents pour les paysages de savanes et marais rencontrés. Il s'ensuit qu'une simple composition colorée restitue une information directement corrélable aux formations végétales présentes sur le terrain. Nous mettons ici en parallèle la carte de végétation établie à l'aide de moyens traditionnels (analyse de photographies aériennes et campagne de réalité terrain) avec une combinaison trichrome obtenue à partir de deux images ERS1 et d'une image JERS1.

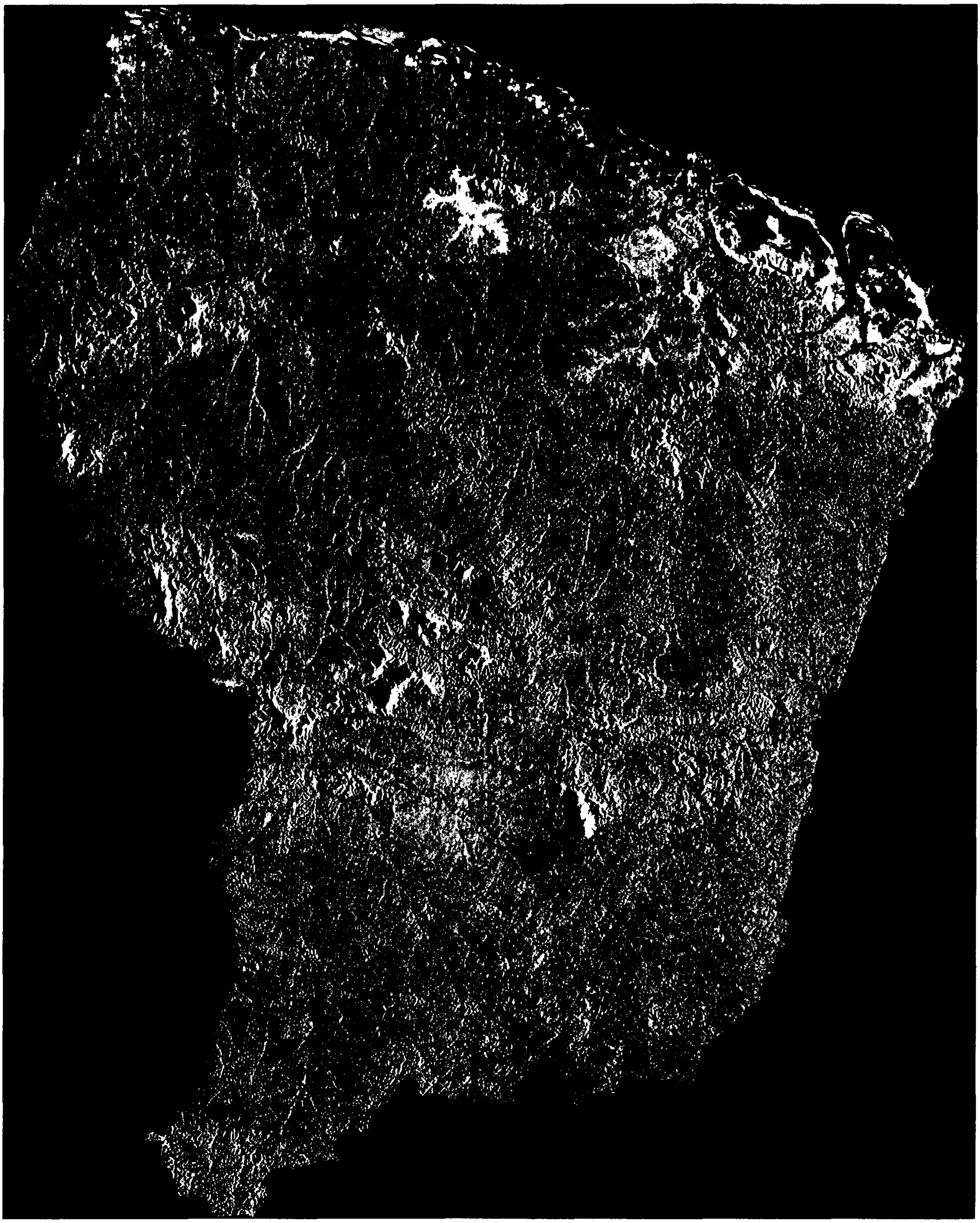

Fig 4 -Image ERS1 avec le barrage de Petit Saut vu par JERS1 : Incrustation de la retenue du barrage de Petit Saut vue par JERS1 (mars 1994) dans l'image ERS1(antérieure à la mise en eau). La radiométrie plus claire de la surface inondée sous couvert est probablement due à des rétrodiffusions importantes sur les dièdres existants à l'angle des troncs et de l'eau libre. La densité affaiblie de la végétation permet à l'onde radar (en bande L) une pénétration accrue du couvert forestier. Cette perception n'est néanmoins possible qu'à condition que l'eau atteigne un niveau suffisant au pied des arbres. Il s'ensuit que la surface apparente n'est pas la surface réelle. (le barrage est dans l'axe de l'image, en haut à 3 cm du trait de côte)

MAP COVERAGE OF FRENCH GUYANA BY SPACE TRIANGULATION OF ERS IMAGES

Michaël Tonon, Jean-Philippe Cantou, Patrick Gigord, Sylvia Sylvander, A. C. de Gaujac

IGN-Espace, parc technologique du canal, 24 rue Hermès, 31527 Ramonville Saint Agne, FRANCE
Tel : (33) 62 19 18 18. Fax : (33) 61 75 03 17

ABSTRACT

The central and southern parts of French Guyana are poorly mapped regions mainly covered by rain forest. Due to cloudy weather conditions, it is impossible to improve these maps using optical imagery. The french Ministry of Defence and the National Geographic Institute have decided to map the whole territory using ERS images. The achievement of this product will be performed by IGN-Espace, the service of the French National Geographic Institute specialized in the production of space-derived cartography, in cooperation with the CEGN ("Cellule d'Etudes en Cartographie Numérique" of the French Ministry of Defence) and the Pierre et Marie Curie University (UPMC, Paris). The project consists in producing ERS spacemaps at the scale 1:200000 by space triangulation of a multidate coverage (2 * 18 ERS PRI images). A DTM produced by IGN-Espace will be used for the geocoding. The GCPs will be picked up from existing maps over the northern part of the territory. This project will help to validate on a large set of images the ERS space triangulation method of IGN-Espace.

1- CONTEXT

1-1 THE TROPICAL CONTEXT

French Guyana is a french department in South America, localized between latitudes 2° and 6° north (see fig. n°1). It has a tropical climate with two rain seasons a year and a cloudy weather throughout the year.
The territory is mainly covered with a tropical rain forest. The coastal plain is the most inhabited region : the rest, very underpopulated, counts few indian villages and gold washer camps. Rivers constitute the only communication links to penetrate the inland of French Guyana territory.

1-2 THE EXISTING CARTOGRAPHY

In the central and southern parts of Guyana, the existing cartography is unprecise, old and uncomplete. The reasons are the impenetrability of the rain forest and the continuous cloudy sky : surveying on the ground or with optical sensors is virtually impossible.
Over the coastal plain only, there is a regular IGN map sheet coverage at the scale of 1:25000. Every one of them contains contour

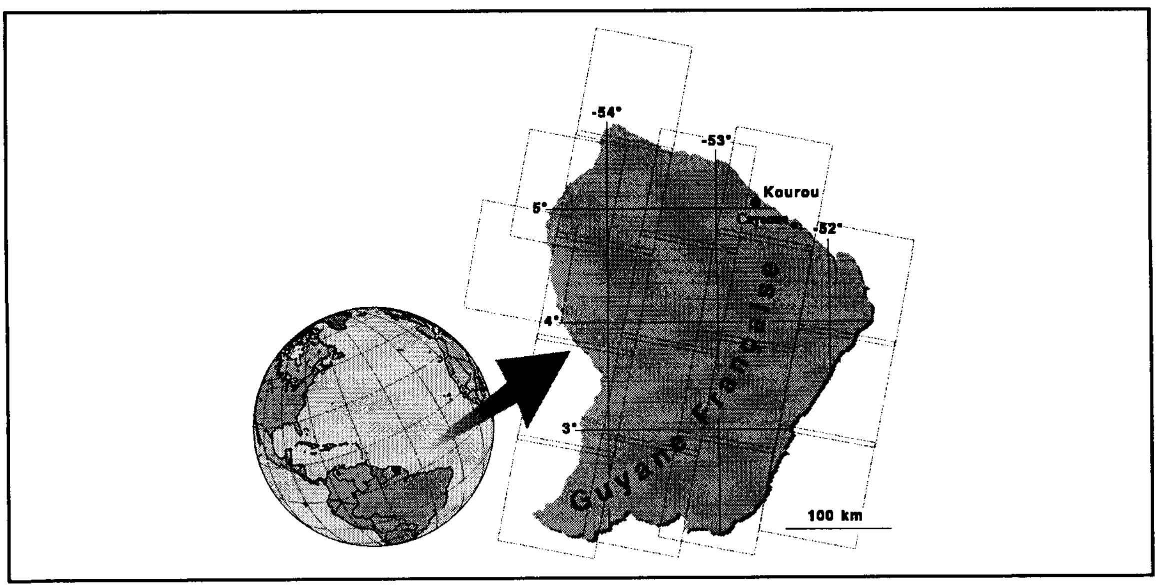

Fig. 1 French Guyana localization.

lines with a good geometrical accuracy.
A satisfactory 1:50000 map sheet series, derived, for the frontcoast only, from the 1:25000 sheets, covers the north third of the country. All of them contain good contour lines and dense spot heights sprinkling.
A general cartographic coverage exists at the scale of 1:100000 and 1:200000 in the form of sketches. Indeed, only the hydrographic network is present, without any altimetric information (except some very rare spot heights). Moreover, the geometrical accuracy of such sheets is bad (100-200 m., perhaps poorer), on one hand because of the lack of knowledge one has about their geodetic system (astronomic surveys) and, on the other hand, because of an internal distortion due to the bad reliability of the ground surveys.
Finally, there is a general map at the 1:500000 scale made for tourist purposes, with few elevation information. The geometrical accuracy of such a map is uncertain, above all in the south.

1-3 THE CHOICE OF RADAR IMAGERY FOR MAPPING

The choice of radar imagery comes, of course, from the continuously cloudy weather but also from the high rigidity of the radar internal and orbital geometry. A few GCPs are needed, eventually with no large spatial distribution. Moreover, due to the homogeneity of the block of radar images when using space triangulation, it is possible to determine the internal quality of the existing mapping. Then, we are able to rectify the geometry of the bad southern maps thanks to the good radar images modelization performed with the northern maps.

1-4 THE ORIGIN OF THE RADAR MAPPING PROJECT

Up to now, there was no study of the ability of ERS to cover large areas with good geometry. Therefore the CEGN and IGN-Espace, in partnership with UPMC, has decided to establish a radar multidate mosaïc at the 1:200000 scale on the whole territory. IGN-Espace, the department of the french national geographic institute specialized in space-mapping, is responsible for producing the mosaïc and the ten guyanese spacemaps. The French Army organized a mission on the ground in Guyana to make GPS observation for the mapping project.

2- METHODOLOGY

The methodology has been defined by IGN-Espace. It is illustrated by the figure n°2. The multitemporal mosaïcs will be obtained by the merging of two ERS coverages, acquired at two different time periods :

- a coverage of 18 PRI images acquired in 1992 (descending mode);

- a coverage of 18 PRI images acquired in 1993-94 (descending mode);

- a datastrip of 5 images (ascending mode).

All images of both radar coverages are rectified with a DTM in the local geodetic and projection systems.

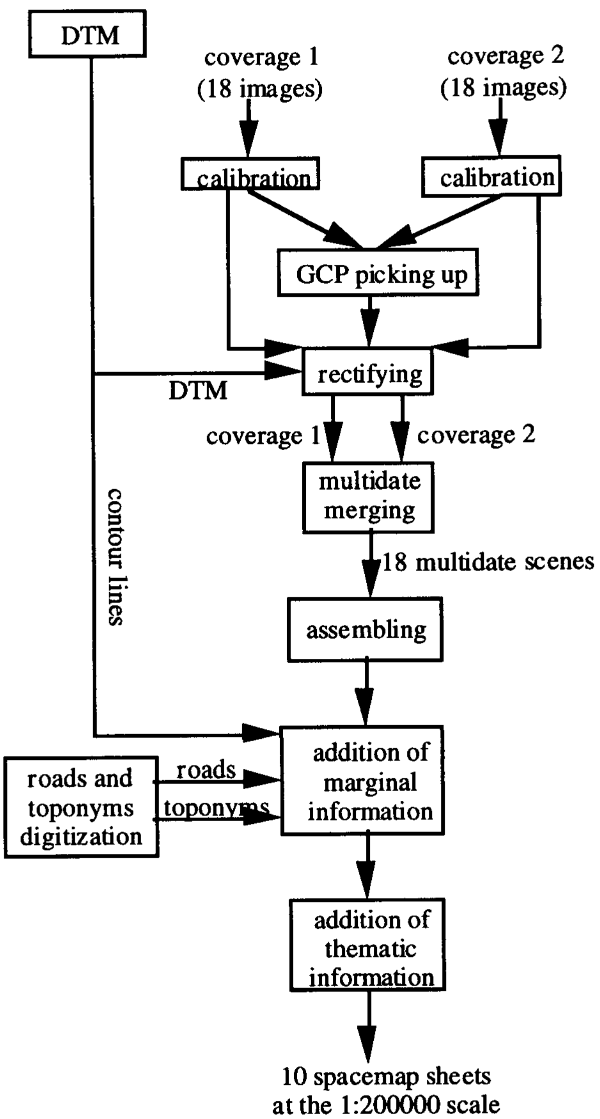

Fig.2 Methodology developed by IGN-Espace to achieve the spacemap coverage of French Guyana.

2-1 SPACE TRIANGULATION

All radar scenes are geocoded through space triangulation techniques (see references n°1 and 2). The space triangulation is performed only on the 1:50000 map series : the quality of the northern 1:50000 allows to come up a good modelization on all the coverage and to use the model to correct the 1:200000 maps. First, some GCPs are picked up both on the 1:50000 maps and the image. Theoretically, our space triangulation software only needs a single GCP to register an ERS data strip. Because of, on one hand, the difficulty to identify details in the guyanese radar imagery (with speckle and rain forest), and on the other hand the doubtfull maps geometrical accuracy, we decided to take about ten points for each data strip. These GCPs are picked up near the coast, where the cartography is the best. Moreover, ground surveys achieved specially by french troops in august 95 provided some GPS observation both in the frontcoast and along the east and west boarders (along Oyapock and Maroni rivers). It is possible to use some of these GPS observation as GCPs. Inside a data strip, we took two tie points per adjoining scenes. Between two data strips, we took 5-6 tie points.
All tie and ground control points chosen for the first coverage were used again for the second one. Then, all images were rectified with the DTM at the 1:200000 scale.

2-2 THE DTM REALIZATION

There was no global guyanese DTM before our work. We used some pieces of existing DTM and created the remainder. The only altimetric data bases available were :
- an IGN DTM over the coastal plain derived from the 1:25000 coverage ;
- the world DTM "Digital Chart of the World" (DCW) : it is very deficient on French Guyana with a lack of data on the most part of the territory, except in a small region near the surinamian boarder.

So, we tried to use the existing cartography to generate the missing DTM.

In the north, where 1:50000 series has contour lines, we used the following process (see fig. n°3) :
- an operator made a selection of principal contour lines which describe the relief as fairly as possible, on a tracing paper with pencils ;
- all tracing papers (40 sheets) were scanned, vectorized, geocoded ;
- all vector curves were identified by assigning them their height ;
- all 1:50000 maps spot heights were digitized.

In the south of the country, we decided to use radar images to rectify spot heights coordinates picked up on the geometrically bad 1:200000 maps.

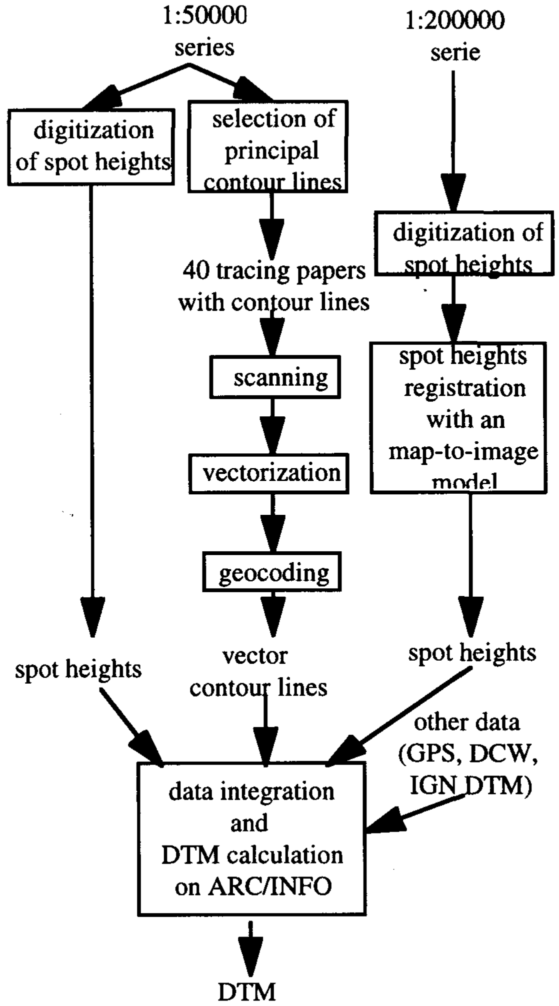

Fig. 3 DTM realization

The idea is to use radar images as the geometrical reference and to rectify the maps as being the most distorted objects. Indeed, the good knowledge we have of ERS flight parameters permitted us to calculate an approximate image-to-1:200000 map model. Then, we used this model to rectify digitized spot heights coordinates. Now, we are able to modelize map distortions and to apply this model to correct the digitized spot heights coordinates. Such a procedure is very interesting and original, because it is the radar imagery itself, thanks to its excellent geometrical quality, which is able to correct the geometry of an old and bad cartography.

We will use also the GPS observation to complete the DTM and as check points to evaluate the absolute planimetric accuracy of the spacemaps.

Finally, five scenes in the ascending mode of the same datastrip across the Guyana will give us five stereopairs with the descending coverages, and allow to calculate locally some elevations. The accuracy of such elevations is almost 5 m. (see reference n°2). These elevations will be used to densify the DTM locally.

All elevation data will be collected in Arc/Info which will generate the global DTM.

2-3 DIGITAL DATA PROCESSING AND ASSEMBLING

Each scene is recalibrated in order to correct the fading effect of radar imagery. Indeed, a geometrical factor depending from the local incidence angle makes the image darker as it is farther from the satellite track. This effect is all the more visible as you assemble two next radar scenes, that's why it must be corrected. Then, the two multidate coverages are merged, in order to reduce speckle effects.The mosaïc is made two by two images, and datastrip by datastrip. Finally, we will cut ten mosaïcs corresponding to the ten 1:200000 space maps of the map sheet index.

2-4 ADDITION OF MARGINAL INFORMATION

Each mosaïc is framed with cartographic coordinates around the image in order to become a real cartographic document. On the image itself, we overlay :

- some contour lines from the DTM ;

- some toponyms selected on the 1:200000 map series ;

- principal roads from the 1:50000 map series.

No digitized hydrographic network will be overlaid, because the more important rivers will be directly visible on the images. Moreover, UPMC will coordinate the achievement of a notice, which will give some information about the interpretation of radar imagery in a tropical context.

3- CONCLUSION

This project is under process. Started in August 95, it shall be finished on spring 96. IGN-Espace will produce the only global, homogeneous, complete and geometrically-good cartography in French Guyana, through ERS radar imagery and space triangulation technics. Such a product gives interesting prospects in space cartography of tropical and equatorial zones. The excellent geometrical quality of ERS radar imagery allows to obtain a satisfying modelization in spite of an uncomplete and uncertain cartography, which is the case of many equatorial areas.

4- REFERENCES

1- Sylvander S. & Gigord P. 1995, Apport de l'imagerie ERS a la localisation de détails terrestres, Rapport interne IGN-Espace.

2- Sylvander S. & Gigord P. 1995, Exploitation tridimentionnelle d'images ERS1, Bulletin S. F. P. T. n°138.

3- LAUR H. 1992, Derivation of Backscattering coefficient sigma0 in ERS1 SAR PRI products.

4- Rudant J. P. & al. sous presse, Apport des images satellitaires ERS1 et JERS1 dans le domaine de la cartographie générale et thématique en contexte tropicale humide, bulletin S.F.P.T.

POTENTIAL OF ERS-1 IMAGES FOR CHARACTERIZATION AND DETECTION OF MAN-MADE STRUCTURES: ROAD NETWORK AND URBAN AREAS

Florence Tupin, Christophe Gouinaud, Henri Maître, Jean-Marie Nicolas
Département Images
Ecole Nationale Supérieure des Télécommunications
46 rue Barrault, F - 75013 Paris
e-mail:tupin@ima.enst.fr
tel: (33-1) 45 81 76 42 fax: (33-1) 45 81 37 94

Abstract

The resolution of ERS-1 images should let us detect man-made structures like roads and urban areas. After a brief survey of the captor response to these objects, we propose two methods to detect them: one to extract the main axes of the road network, and the other one to extract urban areas. We illustrate the results obtained for the road detection on 3 typical landscapes: flat and agricultural landscapes, hilly ones, and tropical ones, and we show how difficulties increase with the presence of relief. Some urban detections are presented both on European towns and Guyana ones.

Résumé

La résolution des images ERS-1 devrait permettre la détection des constructions humaines comme le réseau routier et les zones industrielles. Après de rapides études des réponses du capteur, nous proposons ici 2 méthodes : une pour extraire les principaux axes routiers, l'autre pour détecter les zones urbaines. Nous présentons les résultats de la détection du réseau sur 3 sortes de paysages typiques : paysage plat et agricole, paysage accidenté, et paysage tropical. Les difficultés rencontrées augmentent avec le relief. Des résultats de détection urbaine sont également présentés, sur des villes européennes et guyanaises.

1 Introduction

The aim of this paper is to underline the capabilities of automatic or semi-automatic detection of man-made structures on ERS-1 images (PRI product), which have a resolution of 12,5 m. The methods proposed, still in research stage, should permit further applications. The road network detected (even partial) could be used for automatic registration with a map or an other image (SPOT for instance). Urban areas delimitation should permit estimation of residential expansion, and could be very useful specially for developing country towns.

2 Road network detection

2.1 Short study of the captor response to the road

ERS-1 images result of the backscattering of a coherent electromagnetic wave, therefore they present a noisy appearence because of the speckle phenomenon. The ERS-1 wavelength being 5.6 cm, roads can be considered as smooth. The electromagnetic wave is usually totally reflected, and because the normal of the ground does not coincide with the emission-reception axe of the satellite, roads appear very dark (radiometric minima). But the wave is sometimes reflected by road borders (like crash barriers, ramps, tree borders...), and in some particular cases of orientation may appear very bright (radiometric maxima). So roads can be detected in an ERS-1 image as dark structures as well as bright ones.

2.2 Method

The proposed method works in 2 steps. We first apply local (or low level) detectors, and then link the road (or structure) segments obtained. We present two techniques to connect the segments: a deterministic one, and a stochastic one, the latter allowing better results specially in mountainous regions. Actually, we apply the whole method twice, first on a reduced image, and then on the full resolution one.

2.2.1 2 local detectors

The traditional techniques developed on optical images ([1], [2]) fail when applied on SAR data. Their main drawback is a different behaviour on bright or dark regions (the false alarm rate increases with the

Proceedings of the Second ERS Applications Workshop, London, UK, 6–8 December 1995 (ESA SP-383, February 1996)

brightness of the region). This is due to the particular properties of speckle: on homogenous areas, mean and standard deviation are proportional. So we developed specific tools, dedicated to SAR images, and taking into account the presence of speckle. We present here 2 line detectors developed for road detection, and working on the 16 bit PRI-images.

- A detector based on the ratio between pixel values:

  The first detector is based on the Touzi edge detector [3], which uses the ratio between the average values of 2 regions [4] (figure 1a). The new detector has been adapted to the detection of line structures by coupling edge detections on both sides of the road (figure 1b), and is defined as:

$$r_s^* = min(r_{c_2}^*, r_{c_3}^*)$$

$$r_{c_i}^* = 1 - min(\frac{\overline{x_i}}{\overline{x_1}}, \frac{\overline{x_1}}{\overline{x_i}})$$

  where $\overline{x_i}$ is the average value of the pixels belonging to region i. An extensive statistical study of this detector has been made [5], where the detection probabilities and false alarm rates have been derived (figure 2b). From this study, the ratio line detector exhibited a good behaviour, and permit us to define theoretical thresholds, from the knowledge of the minimum contrast we want to detect, and the false alarm rate we tolerate.

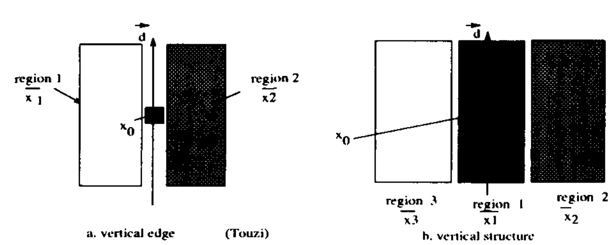

Figure 1: Edge and structure models

- A detector based on the cross-correlation :

  We propose a second new edge detector, resulting in a more localized response than the ratio line detector. The idea is similar to Hueckel's one [6]. For each pixel x_0 of the image, we define the step-edge corresponding to a neighborhood V_{x_0} of x_0 and a chosen direction $\vec{d_k}$, and minimizing the quadratic mean error. This edge is composed by two constant regions of values $\overline{x_1}$ and $\overline{x_2}$ separated by $\vec{d_k}$. Once this ideal edge defined, the validity of the hypothesis "*there exists an edge in x_0 with the direction $\vec{d_k}$*" is tested. In order to do this, we compute the normalized centered cross-correlation between the pixels values of V_{x_0}, and the ideal edge corresponding to V_{x_0}.

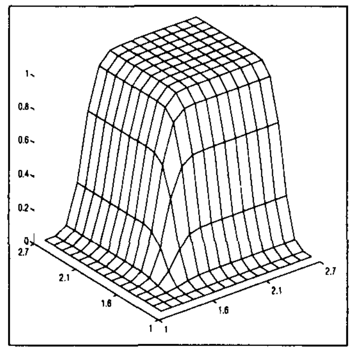

a. Detection probability fonction of the contrasts between regions 1 and 2, and 1 and 3, with a threshold of 0,3.

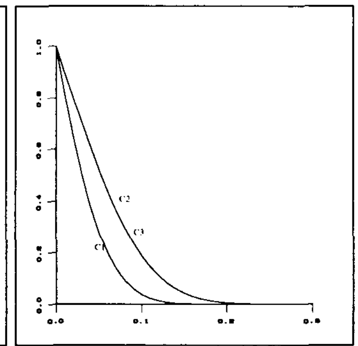

b. False alarm probability fonction of the threshold, for different contrasts between region 1 and 2 k_2, and between 1 and 3 k_3:
$C_1 : k_2 = 2, k_3 = 1,5;$
$C_2 : k_2 = k_3 = 2;$
$C_3 : k_2 = 2, k_3 = 4;$
$C_4 : k_2 = 4, k_3 = 6.$

Figure 2: Satistic study of the ratio line detector

  The cross-correlation coefficient ρ_c is :

$$\rho_c^2 = \frac{1}{1 + (n_1 + n_2)\frac{n_1\gamma_1^2\overline{c}^2 + n_2\gamma_2^2}{n_1 n_2(\overline{c}-1)^2}}$$

  where n_i is the number of pixels of region i, $\overline{c} = \frac{\overline{x_1}}{\overline{x_2}}$, and γ_i the variation coefficient (ratio of standard deviation and mean), which measures homogeneity in radar imagery scene. As for the ratio line detector, the structure detector is defined by $min(\rho_{c_2}, \rho_{c_3})$, where ρ_{c_i} is the edge response between region i and 1.

  The same study as for the ratio line detector has been made, but because of the complexity of the expression, we compute simulations to obtain the results. In case of homogeneous areas both detectors provide very similar results.

The first detector is less precise (it can give for instance a good response in presence of a specular reflector, and it gives multiple responses for one structure), but is less sensitive to the hypothesis (3 homogeneous areas are required). So we keep both detectors.

Actually we use for each local detector a 7 times 11 pixels mask, and we compute the response in 8 directions, and for 3 widthes of the central line (see figure 1). The choice of the mask sizes is a compromise between 2 constraints. On the one hand, the neighborhood must be as large as possible to reduce the false alarm rates, on the other hand the number of directions must be small enough to limit the computation time. We combine the 2 responses corresponding to one direction with the operator $\sigma(x, y)$

[7]:

$$\sigma(x,y) = \frac{xy}{1-x-y+2xy}$$

and we keep the best of the 8 responses, and its direction. Then we do some local processing to improve the detection (suppression of isolated pixels, a first linking between pixels with close directions...).

2.2.2 Segment connection

In order to connect the segments detected at the previous stage, we propose two methods, a deterministic one, and a stochastic one specially adapted in case of difficult detection (this is the case for slight mountainous regions). They both work on the segments obtained after the first step followed by a thining and a polygonal approximation.

- The deterministic method has been originally developed for SPOT images in [8] and adapted. Segments are grouped under closeness and angular criteria. Well adapted for SPOT images and high quality ERS-1 images, the results are poor when the obtained segments are too short or insufficient.
- The stochastic method was first developed to deal with these difficulties. It is built to cope with partial detection and with false alarms. Markovian fields permitting to take into account contextual or a priori information are well adapted for this kind of problems.

  A Markovian field is defined on a segment graph. The set of segments corresponds to the segments detected by the first step, and all the possible connections between them. Two energies are defined: one which represents the link to the data (the ERS-1 image) E_1, and one which corresponds to our "a priori" knowledge on the structure of an "ideal" road network E_2. E_1 is defined through the response of the 2 local detectors of part 1. E_2 is defined on a set of segments which share an extremity (composing a clique) and include the following knowledges about roads:

  1. roads are long (out of context they should never stop),
  2. they have a low curvature,
  3. intersections are rare.

  This modelisation of roads is powerful, and makes us able to suppress almost all the "false" segments, and connect the "good" ones, even if large gaps separate two segments.

2.2.3 Some practical aspects

The whole method is applied twice. First on a reduced image (obtained by a 2x2 pixels grouping), then on the full resolution one. We obtain 2 networks, one for the roads appearing large in the ERS-1 image, and the other one for the thin roads. The presented results are the superposition of these 2 networks on the ERS-1 images.

2.3 Results and analysis

We want to emphasize the fact that all the results proposed below are obtained with the same set of parameters. The local detector thresholds are those given by theoretical studies. The parameters included in the Markovian field have been empirically chosen, but fixed once and for all. Results are presented with the original image, and can be compared to a registered map (when available). The detected roads correspond to dark structures only. We note that every linear structure whose response is close to the road one, is detected (it is the case for channels, thin rivers, or tracks).

In actual state, the first part of the method (low level detections) takes 10 minutes on a SPARC 2000 for a 1024x1024 image, and the second part 15 minutes (depending on the choice of the energy minimization algorithm).

2.3.1 Flat and agricultural landscape

ERS-1 images of this kind of landscape are usually easy to interpret. Fields and roads structure the landscape, and both are often well delimited. The chosen image is a part of the North-Holland scene. Since the network is thin, we have only used the full resolution image.

The results obtained are very satisfying: few wrong detections, and almost all the visible roads (or linear structures) are detected (figure 6).

2.3.2 Hilly landscape

The landscapes usually found in Europe are generally less structured as above. Besides they may be slighty mountainous, damaging the local detector results. We have chosen an image of Aix-en-Provence (South of France).

Results illustrate the difficulties encountered in relief regions. The right part of the Aix image presents false detections caused by the presence of very bright structures located near the crest lines. But the main roads visible in the ERS-1 image are well localized (figure 6).

2.3.3 Tropical landscape

It is probably the most difficult landscape to analyse, since roads are often hardly visible. We have chosen

a. Original image of North Holland ©ESA.

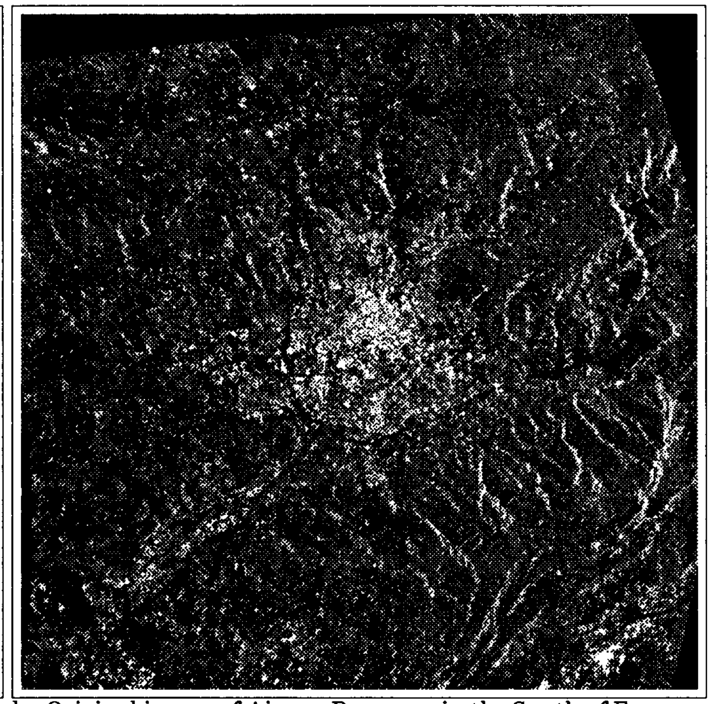

b. Original image of Aix-en-Provence in the South of France ©ESA.

a. Final result of road detection superimposed on the ERS-1 image of North Holland.

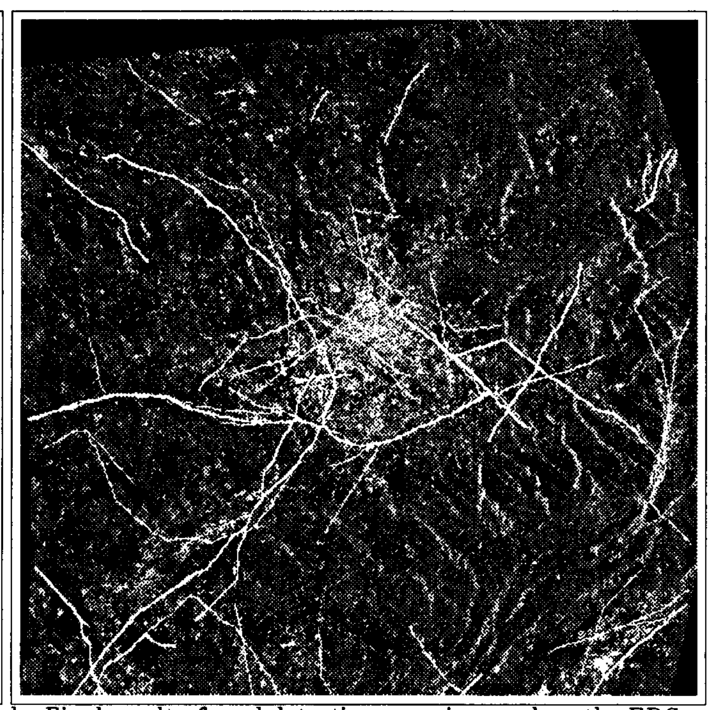

b. Final result of road detection superimposed on the ERS-1 image of Aix-en-Provence.

Figure 6: Road detection on a flat and agricultural landscape (left column), and on a hilly one (right column).

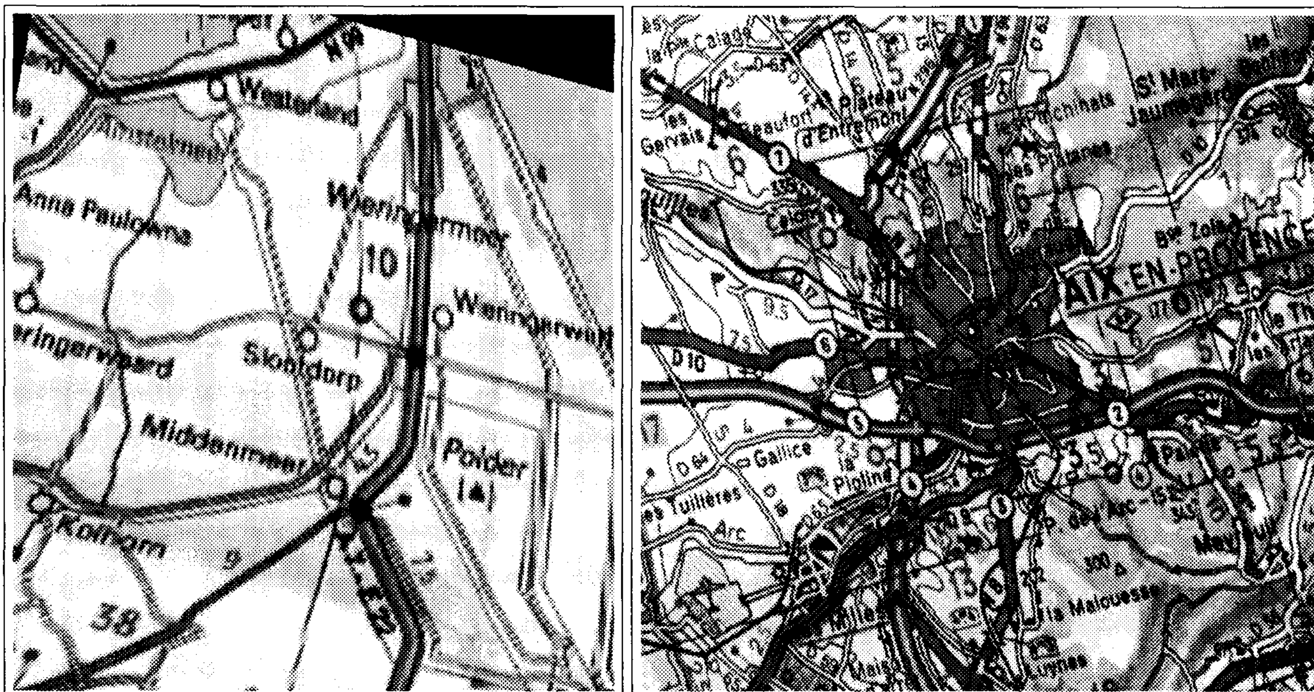

a. Map corresponding to the image of North Holland ©Michelin.
b. Map corresponding to the image of Aix-en-Provence ©Michelin.

Figure 7: Maps of North Holland and Aix-en-Provence (France).

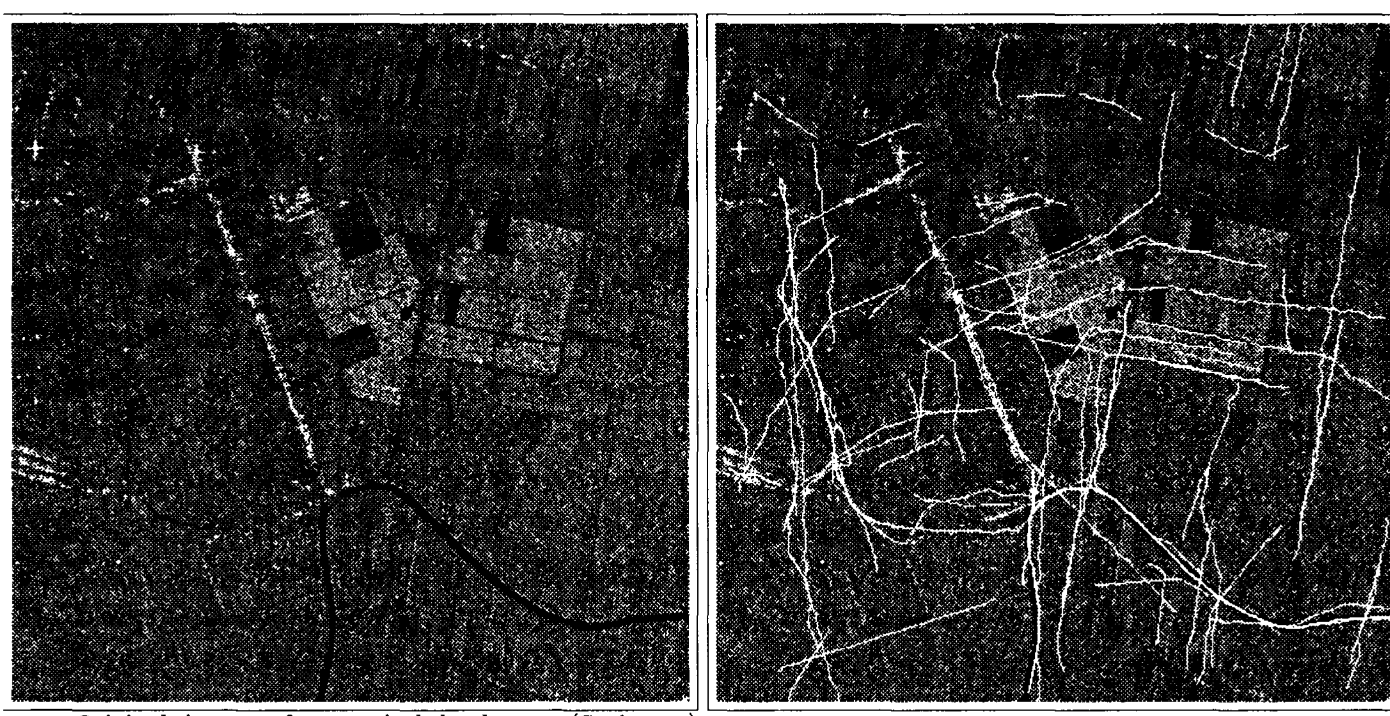

a. Original image of a tropical landscape (Suriname) ©ESA.
b. Final result of road detection.

Figure 8: Road detection on a tropical landscape (Suriname).

a part of Suriname.

2.3.4 Conclusion

These results show the potential of ERS-1 images to detect the main axes of the road network. They are satisfying on flat landscapes, but degraded on hilly ones.

3 Urban area detection

In this section we present the main lines of our method to detect urban areas (detailed in [9]), which consists in 2 parts: the first one deals with the detection of bright points characterizing industrial areas, and the second one with more homogeneous regions like large towns, where the concentration of strong reflections becomes very important.

3.1 Study of urban region response to the captor

We propose first a urban object classification in 3 sets, depending on their geometry and their roughness, and yielding a model of backscattering law.

3.1.1 Smooth surfaces

Following the usual rule of Rayleigh, a surface is considered as smooth when $\Delta h << \frac{\lambda}{8cos(i)}$, with Δh the quadratic mean deviation of height, λ the wavelength of ERS-1, and i its incidence angle. For this type of surface, retrodiffusion laws are Snell-Descartes' ones, and so the object geometry determines the captor response. Depending on the incidence direction i, objects may have either a strong response or no response at all (taking into account the multiple reflections caused by dihedral and trihedral objects).

3.1.2 Rough surfaces

It is the case of objects with irregularities on the scale of the wavelength, like vegetation for instance. These objects can be described by the Goodman model [10], assuming some properties for the phase and amplitude of elementary reflectors inside a resolution cell. We get an explicit backscattering law (which will be called here "χ"), linking A, the amplitude of the received signal, with L the number of looks (3 for Precision Images), and α the parameter of the law [11]:

$$P(A) = \frac{2L^L}{(2\alpha^2)^L\Gamma(L)}A^{2L-1}e^{-\frac{LA^2}{2\alpha^2}} \qquad (1)$$

Γ represents the Gamma fonction. There exists also a relation linking α with the mean value $\overline{A}$ of the region (assumed to be homogeneous).

3.1.3 Conductor surfaces

This is for instance the case of metallic surfaces, used as rooftops in tropical lands and in industrial areas. They are never plane, and act as periodic lattices. For some particular surface shapes (corrugated iron for instance) we can approximate a model and find an explicit law.

3.1.4 Characteristics of the global backscattering law

The global backscattering law of urban areas is the result of the composition of the 3 previous laws, with proportions depending on the areas. This provides some particular characteristics compared to the "χ" law of rough surfaces:

- There are more dark pixels, because of the Snell-Descartes responses in an unfavorable configuration (no response to the captor).
- There are more bright pixels, because of the Snell-Descartes responses in a favorable configuration, and constructive interferences.
- The intermediate values around the mean caused by speckle are not so much modified.

Using these remarks we aim at estimating the probability that a pixel belongs to a town.

3.2 Fail of classical approaches

One classical method to detect urban areas consists in calculating first or second order statistics to obtain some discriminant information. We want to emphasize 2 problems which limit the use of such a method.

First it can be shown that the sizes needed to estimate statistics of speckle samples are very large. For instance the variation coefficient estimation with a confidence of 5% around the theoretical value, and with a probability of 99%, needs a 42x42 window size. This corresponds to a 525x525m sample on the ground. So large areas will hardly be homogeneous in many towns. Estimation of skewness will also need similar very large windows.

Secondly it can be shown that the statistics of some non-urban areas (forests for instance) are sometimes very close from the statistics of urban areas. It is the case of the radiometric mean.

It is why we propose new detection methods.

3.3 Detection criteria proposed

3.3.1 Urban bright points detection

Having a region described by a "χ" law with known parameter, we know the probability of an intensity value A, and the probability for A to exceed a given value. We may compare for any region the measured probability with the theoretical one under hypothesis of fully developed speckle. In order to estimate the parameter of the law in the window, the local histogram is built on a 30x30 window, then it is smoothed, and we deduce α from it, using the last remark of §3.2.4.

A pixel which amplitude value has a probability lower than a fixed threshold is temporary classified as bright. We then calculate the proportion of bright points in a 15 pixel radius disk around any temporary bright pixel. If it is more than 1% (at least 2 temporary bright pixels), the pixel is definitively kept as bright in the final classification.

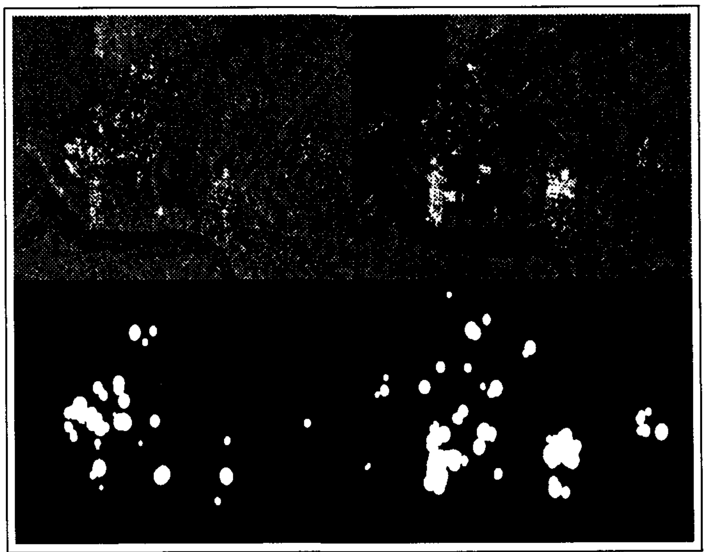

a. Bright point detection on the region of Kourou: above the original ERS-1 image, below the detection result.

b. Bright point detection on the region of Kourou: above the original JERS-1 image, below the detection result.

Figure 3: Bright point detection on ERS-1 (left column) and JERS-1 images (right column).

3.3.2 Urban areas detection

The previous method is well adapted to industrial areas characterized by isolated bright points. But, for instance in towns, they may form a very compact region, and are not "isolated" at all. To detect these regions, we propose to cut the local histogram (calculated on a 60x60 window) in 2 parts, with a threshold s. In the higher part, $\Sigma = P(A > s)$ is computed and compared to the highest frequency f_{max} of the low part. When $\Sigma > f_{max}$ the central pixel receives s as value, and the threshold is decreased. The process is iterated until all the pixels are classified. The thresholds have the form $\mu + k\sigma$ (μ is the mean, and σ the standard deviation of an area of totally developed speckle). Then the result is thresholded to obtain urban areas. A blind classification establishes the threshold value k by testing the regions of radii 15 pixels around the detected bright points.

3.4 Results and analysis

The results are illustrated on an image of Kourou (French Guyana) for the bright points detection method, figure 3b, and on an image of Aix en Provence for both methods, figures 4 and 5.

The urban areas detection method is developed to be used with other captors, like the radar satellite JERS-1 (figure 3b), or SPOT for instance. The table below shows the ratio of good detection (urban pixels actually detected by the method), and false detection (detection of pixels which are not in urban areas), in a supervised learning case or an automatic one.

Regions	Captors used	Learning	Detection rates	False alarms rates
Lelystad	ERS-1 JERS-1	supervised	90 %	10 %
Lelystad	ERS-1 JERS-1	automatic	75 %	9 %
Aix en Provence	SPOT ERS-1	supervised	79 %	3 %
Aix en Provence	SPOT ERS-1	automatic	78 %	5 %
Kourou	ERS-1 JERS-1	automatic	70 %	20 %

To conclude, the proposed method gives good results on any sort of landscapes, and is robust enough to work on hilly regions. The results are improved when used with other captors, radar or optic.

4 Conclusion

Radar images are particularly difficult to interpret. Nethertheless dedicated detectors (adapted to the particular statistics of speckle images) give useful results, allowing a first interpretation of the landscape (main road network, and urban repartition).

Acknowledgements

We want to thank J.P. Rudant for some of the im-

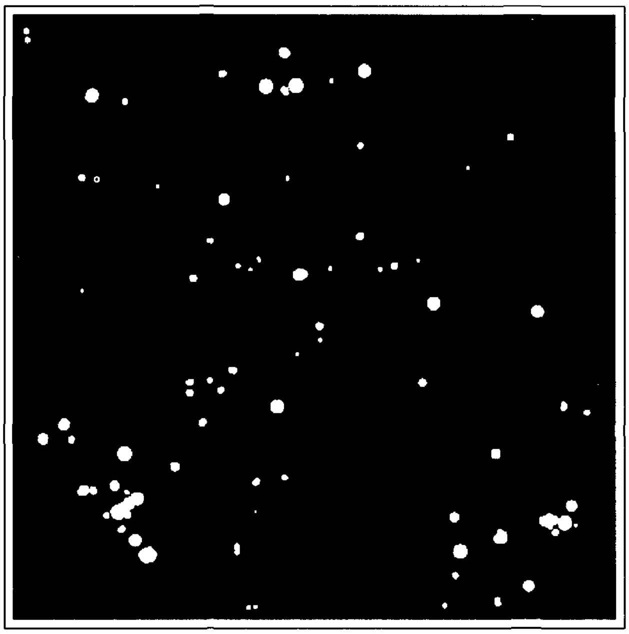

Figure 4: Bright point detection on the region of Aix-en-Provence, a first stage towards town detection.

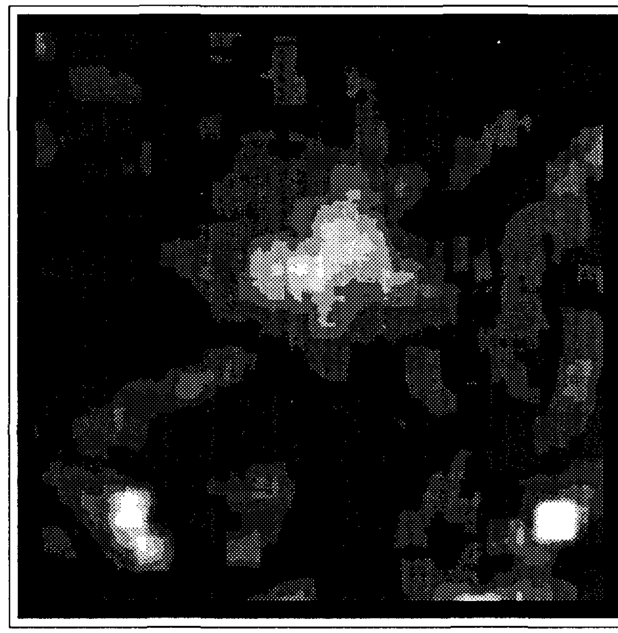

Figure 5: Map of the k-values on the region of Aix-en-Provence. This map will be thresholded to select the urban areas.

ages illustrating this work.

References

[1] R. Nevatia and R. Babu. Linear feature extraction and description. *Computer Graphics and Image Processing*, 13(3):257–269, 1980.

[2] G. J. VanderBrug. Experiments in iterative enhancement of linear features. *Computer Graphics and Image Processing*, 6(1):25–42, January 1977.

[3] R. Touzi, A. Lopes, and P. Bousquet. A statistical and geometrical edge detector for SAR images. *IEEE Transactions on Geoscience and Remote Sensing*, 26(6):764 - 773, November 1988.

[4] A. C. Bovik. On detecting edges in speckle imagery. *IEEE Transactions on Acoustics, Speech and Signal Processing*, 36(10):1618–1627, October 1988.

[5] F. Tupin, C. Gouinaud, H. Maître, and J.P. Crettez. Détection du réseau routier sur des images radar ERS1. *RFIA AFCET 96 (Rennes)*, January 1996.

[6] M. H. Hueckel. An operator which locates edges in digitized pictures. *Journal of the Association for Computing Machinery*, 18(1):191–203, January 1971.

[7] I. Bloch. Information combination operators for data fusion: A comparative review with classification. *IEEE Trans. SMC (to appear)*, 26(1), January 1996.

[8] M. Roux, J. Lopez-Krahe, and H. Maître. Recalage image spot / carte routière. *XVIIe Congrès ISPRS, Washington*, pages 384–391, 1992.

[9] C. Gouinaud and H. Maître. Classification criteria for radar images of urban areas. *Colloque CNES-IEEE, Toulouse (France)*, October 1995.

[10] J.W. Goodman. Some fundamentals properties of speckle. *Journal Optical Society of America*, 66(11):1145–1150, 1976.

[11] H. Laur. *Analyse d'images radar en télédétection, discriminateurs radiométriques et texturaux.* PhD thesis, Université Paul Sabatier de Toulouse, 1989.

POSTER PAPERS

RAPID INFORMATION DISSEMINATION SYSTEM (RAIDS)

Mr Anthony Graves
Matra Marconi Space UK, Anchorage Road, Portsmouth, Hampshire, PO3 5PU, United Kingdom.
Tel: +44 (0) 1705 674468, Fax: +44 (0) 1705 674642, E-mail: tonyg@nobbler.demon.co.uk

Introduction

The Rapid Information Dissemination System (RAIDS) is a facility to generate and provide electronic on-line access to ERS SAR data direct from the ground station. Fully operational since June 1994, RAIDS has been processing and distributing data from the West Freugh ground station in South West Scotland, supplying a range of SAR image products.

The baseline RAIDS system provides the customer with access to Quick Look image products for all ERS SAR image observations of the UK. The advantages of real-time access to SAR data is evident in the increasing number of applications developing within the group of RAIDS users.

RAIDS SAR Image Applications

The range of images currently supplied by RAIDS is varied in location and content. Images from Greenland, Scandinavia, and the Baltic, to Europe, the Mediterranean, and North Africa, are regularly available through RAIDS.

Current uses of this data cover both land and sea applications, and are often concerned with the dynamic or real-time monitoring of environmental phenomena and events. More developed applications include, oil slick detection, flood monitoring, and ice berg detection and mapping. These applications are now evolving into complete environmental services. Take ice berg monitoring for example; It is now possible to provide accurate ice maps to ships in arctic waters in near real-time conditions, and so provide a significant navigational aid to improve the safety and efficiency of arctic shipping.

RAIDS Data Coverage

The RAIDS facility routinely generates Quick Look SAR image products for all ERS SAR image observations of the British Isles. Within the UK coverage box, shown below, all acquired ERS SAR data is processed and made available to RAIDS users.

The ERS SAR is typically operated during descending orbit passes over the UK, imaging a strip of the earth in a 100km wide swath. Such passes occur over the UK coverage box approximately every other day. With ERS-1 in a 35 day repeat orbit, these passes progressively migrate across the UK box, providing full coverage every 17.5 days.

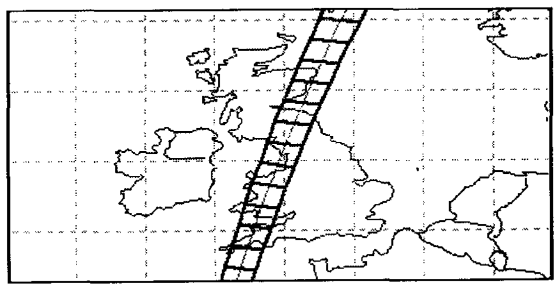

RAIDS UK Coverage Box

To acquire processed RAIDS images of any area within the West Freugh Ground Station Reception Footprint, shown below, but outside of the UK coverage box, it is necessary to order the data in advance. Once acquired this data is available through RAIDS to all users. Orders can range from single one-off images to long term data acquisition of a large area.

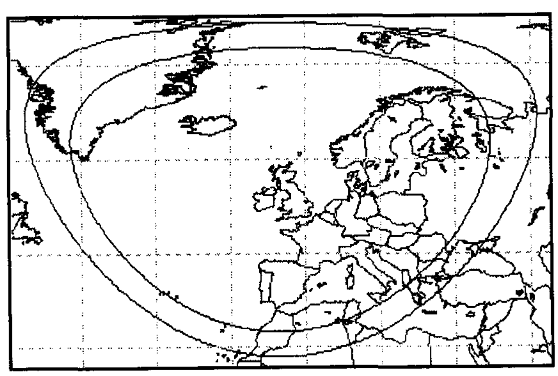

West Freugh Ground Station Reception Footprint

RAIDS Image Data Access

RAIDS image products can be electronically accessed on-line or requested off-line from the image archive.

To access RAIDS imagery on-line, customers require a PC or UNIX workstation, User Access Terminal Software, and a modem link. Once registered as a user, the customer can dial up the West Freugh Ground Station and login to the RAIDS system via password access. The RAIDS image products are stored in the image library by frame and date of acquisition. The user can select the desired scene which is automatically

Proceedings of the Second ERS Applications Workshop, London, UK, 6–8 December 1995 (ESA SP-383, February 1996)

transferred to the users host computer. The transferred image can then be viewed using the access terminal software. A text file is transferred with each image giving details of scene co-ordinates and image acquisition date and time.

Image products are held on-line in the RAIDS image library for between 21 and 28 days. At the end of each week, all image products are transferred to the RAIDS image archive. Customers wishing to obtain off-line image products should order these through the image archive service.

Operation of the ERS-1 SAR instrument is controlled by ESA. To gain information on the ERS-1 orbital parameters and acquisition schedule, the RAIDS (UNIX version) user access terminal includes 'Bernard' an ERS-1 world coverage tool. This allows the user to view the ERS-1 orbit, and determine which areas will be imaged and processed to RAIDS. It can also be used as a RAIDS image archive tool allowing the user an easy-view, catalogue, and administration system. For an alternative information source on the ERS-1 schedule, RAIDS users can obtain a copy of the DESC 'Display Earth Station Coverage' software. This is available free of charge from the ESA ESRIN ERS-1 help desk.

RAIDS Image Products

The baseline product generated by the RAIDS facility is a reduced resolution product (Quick Look Image). This image has a spatial resolution of 100m and constant pixel size. Twenty four looks are used to remove most of the radar speckle. The image product scene location will correspond to standard ESA frames and will be located in the same co-ordinate frame as the ESA precision image product. The Subsidiary and Browse images are produced by averaging groups of pixels, and provide easier data selection and handling, and reduce the users telephone access time.

Precision Subscene images (25km x 25km) can also be produced by the RAIDS facility. These image products are to the full ESA precision image specification ie 25m resolution. Such images should ideally be requested in advance of ERS SAR image acquisition, although under special circumstances it may be possible to produce a precision subscene from data in the on-line library, if a specific feature or area of interest has been highlighted on the QL1 or QL5 image products and requires more detailed investigation.

Table of RAIDS product specification

	Browse Image "BRO"	Subsidiary Quick Look"QL1"	Baseline Quick Look"QL5"	Precision Subscene "PSn"(n=0..9)
Image Size @	251 x 257 pixels	1004 x 1030	2008 x 2060	By Request 2008 x 2080
Pixel Dimensions	400m x 400m	100m x 100m	50m x 50m	12.5m x 12.5m
Spatial Resolution	< 800m x 800m	< 200m x 200m	< 100m x 100m	25m x 25m
File Size @	64KB (8 bits log compressed)	1MB (......"......)	4MB (......"......)	4MB (......"......)
Number of Looks	>100	96	24	6
Swath Extent @	100km x 100km	100km x 100km	100km x 100km	25km x 25km
Projection	Ground range zero doppler	←.....".....→	←.....".....→	←.....".....→
Look Bandwidth	----	----	75 Hz azimuth 4 MHz range	300 Hz
Radiometric Res.	----	<0.77 dB	<1.5 dB	2.5 dB
Format	Cross Track Raster	←.....".....→	←.....".....→	←.....".....→
File Transfer @ **Time (14.4 kbaud)**	30 seconds	10 minutes	40 minutes	40 minutes

RAIDS User Group

RAIDS has been set up to actively promote the use of SAR imagery, and to encourage the development of SAR applications. It is therefore appropriate that a user group be set up to form links between members, and for the exchange of knowledge to further the application of satellite imagery. It will also allow RAIDS to be customer lead in its future development. The User Group will be started during 1995, alongside the various developments outlined below, and the release of the UNIX User Access Terminal.

RAIDS is a significant opportunity for any organisation wishing to use SAR data as an introduction to remote sensing, or for the development of specific SAR applications, in both commercial and academic organisations.

RAIDS Architecture Overview

The RAIDS facility is a turnkey system designed to give routine production access to satellite SAR image products. Such a system provides the data user with a flexible information service, allowing image data supply to be matched to image data application. A schematic architecture for the initial West Freugh configuration, subsequent data dissemination and archive, is shown in the diagram below.
Scenes that lie within the RAIDS coverage box, and pre-ordered scenes from within the whole Ground Station footprint, are transcribed using the existing West Freugh transcription facilities. The output raw data tape is then loaded into the RAIDS SAR processor. Once initiated, processing is automatic for the entire image strip. Output image products are written to the on-line image library, and may be accessed remotely from a User Access Terminal.

Future developments to the RAIDS service will provide:

- Direct data capture to remove data flow bottlenecks at the reception and transcription facilities. This will extend coverage to the full Ground Station reception zone and allow fully automatic end to end processing.

- Electronic image access via wider bandwidth distribution media e.g. Internet. This will reduce customer image access and transfer time.

- Introduction of ERS-2 data as it becomes available, with the possibility of other satellite data in the future.

The RAIDS system may be integrated with any ERS SAR Ground Station facility.

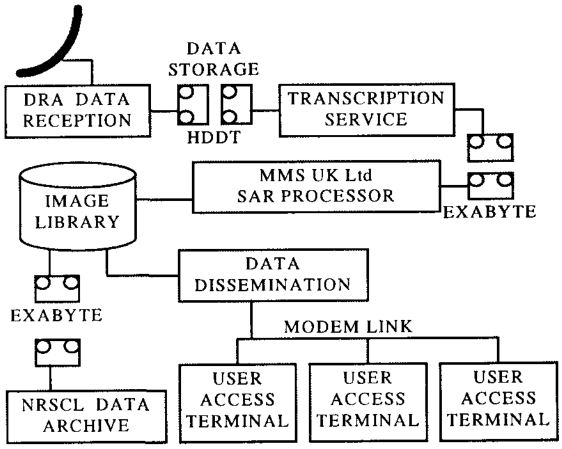

RAIDS data acquisition and distribution network

The RAIDS Programme is being developed by a consortium lead by Matra Marconi Space UK Ltd, and includes the DRA Farnborough, and the NRSC Ltd.

USE OF ERS DATA FOR CROP MONITORING

A. CARROU(*) ; T. RABAUTE(**)

(*) CISI, Direction Observation de la Terre - 13 rue Villet, BP 4042, 31029 TOULOUSE CEDEX - FRANCE
Tél. : (33) 61.17.66.66 - Fax : (33) 61.34.84.15

(**) SCOT CONSEIL - 1 rue Hermès, Parc Technologique du Canal, 31526 Ramonville St Agne - FRANCE
Tél. : (33) 61.39.46.00 - Fax : (33) 61.39.46.10

ABSTRACT

During a first study, a methodology based on radar imagery was defined to monitor agriculture resources. The approach consists in considering the speckle as an information and involves the concept of texture on ERS data. Several classifying parameters, chosen because they are relevant to radar imagery or because they are suitable for texture characterization, have been validated through a statistical analysis aimed at selecting the most discriminant informations.

The former study, carried out on four european sites, showed convincing results of classification obtained on multitemporal data. These results are confirmed on four new areas. The exploited data are representative of the diverse agricultural conditions in Europe and correspond to the years 1992 and 1993 with a mean of four ERS data per site and per year. This great number of data reinforces the robustness of the approach, showing the usefulness of texture in radar images for crop assessment. The different steps of the processing will be presented, as well as a synthetis of the results provided by the analysis of each site and the interest of multitemporal acquisitions will also be discussed.

1. INTRODUCTION

The general aim of this study is to assess the feasibility of using SAR Data in an operational system of crop monitoring. During a first phase, methodology axes were considered in order to define how radar data can be used to separate different crop types. These axes included the use of statistics and texture informations to characterize land covers, and the combination of multitemporal data. This approach is validated in the second phase, by applying the associated techniques to a wide number of study sites.

2. STUDY SITES

Eight agricultural areas were chosen for this work : Arles and Bourges in France, Albacete and Seville in Spain, Great Driffield in the UK, Mainz and Essen in Germany and Foggia in Italy.

These areas are already being studied within the Mars Action B European Project, which notably simplifies the validation aspect of our study. For each site, we had a history of field enquiries (for 1992 and 1993), and we were able to use the previous interpretation work which had been done with visible imagery.

These sites were also chosen, because they showed zones with small relief variations, in order to eliminate geometric and radiometric rectification problems that would have arisen on non flat areas.

As a consequence, we were able to reproject Spot images and classification results on ERS data with a simple technique of polynomial deformation computed from a set of corresponding points.

3. METHODOLOGY

Our vision of an operational system of crop monitoring using SAR images supposes, first a all, that we are able to segment the images into parcels, then to classify them with relevant discriminant parameters. This procedure must be reliable for all kinds of observed zones with various culture covers.

- Data processing Organization -

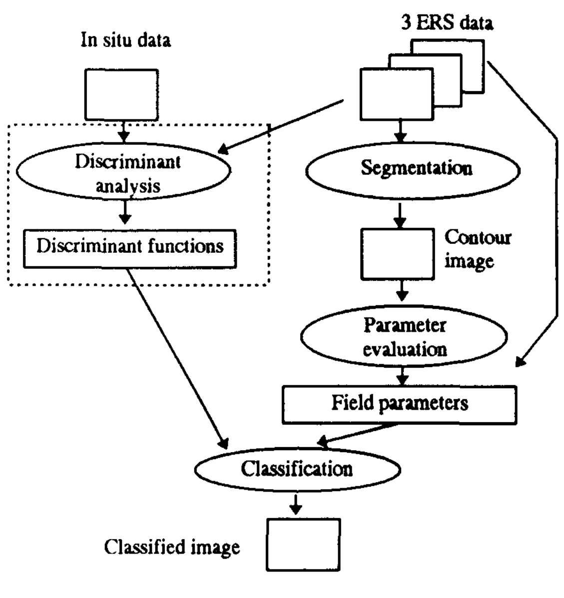

Proceedings of the Second ERS Applications Workshop, London, UK, 6–8 December 1995 (ESA SP-383, February 1996)

Concerning the segmentation step, different algorithms have been considered, such as watershed line or region growing methods. Classification should also be performed with a well known method, such as "dynamic grouping".

The cover discrimination is, in our opinion, the most critical step. For that reason, our work concentrated on the determination of relevant discriminant parameters, in order to adapt the classification step to the crop set corresponding to the considered site. This determination is performed through a discriminant analysis, based on samples corresponding to the main crop types : in our case, these samples were taken with the help of the results of image interpretation for the years 1992 and 1993 made within the MARS Action B Project using Spot and Landsat images, and validated by in situ surveys.

The sampling of one class of culture cover includes several observations on a single site. An average of 50 observations at least, for each crop type of interest and on each site are necessary to obtain significant results, which means that about 250 samples have been selected on each of the eight zones.

These samples are used to compute two kinds of parameters :

- statistical parameters : such as mean, mean deviation, standard deviation...
- textural parameters : the auto-correlation function calculated in different directions and at different distances.

The whole set of parameters includes 30 values for a given sample. Whithin the first phase of the study, this number was reduced to a subset of 12 values which represented a good compromise for the different sites on monotemporal data.

To achieve this, statistical tests were applied on each of the discriminant parameters using Fisher's ratio within an analysis of variance (one way anova). The hypothesis tested is the equality of the mean of each class observation related to the specific parameter.

In order to introduce multitemporal concept, we worked with three dates. The corresponding values were combined to give the mean for the three dates, and the differences for each consecutive data pair.

The combination results then allow to define discriminant functions.

– Example of Canonical Discriminant Functions on the site of Bourges –

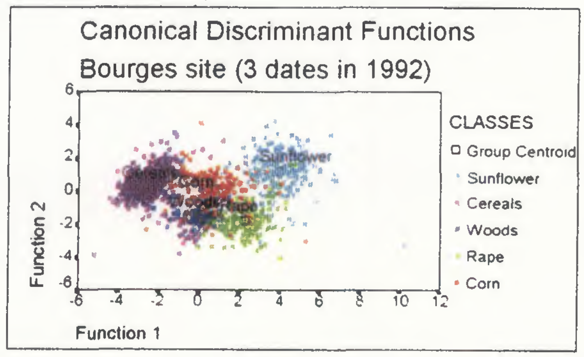

The combined parameters and the associated functions are validated on the sample set of each site. The results are evaluated through a confusion matrix showing the rate of well reassigned samples for each class.

Classes	1	2	3	4	5	
1	**70,7**	8,4	12,6	4,2	4,2	1- Corn
2	3,4	**86,6**	4	0	6	2 – Rape
3	3,3	0	**90**	6,7	0	3 – Woods
4	2	0,2	5,1	**92,7**	0	4 – Cereals
5	1,9	3,3	1,9	0,5	**92,4**	5 – Sunflower

Global classification : **88,5 %**

Confusion matrix (% Initial vs reassigned classes of observation)

4. RESULTS ANALYSIS

The methodology described above was applied to the different sites, and led to the following results :

Sites	Year	Months of acquisitions	Results (rate of well reassigned samples)
Great–Driffield	92	april, may, july	70,60 %
	93	march, june, july	71,84 %
Essen	92	may, august, september	92,08 %
	93	may, june, july	80,21 %
Foggia	92	may, june, july	74,30 %
	93	may, july, august	75,41 %
Mainz	92	april, may, september	75,24 %
	93	may, june, august	77,55 %
Séville	92	may, july, september	70,52 %
	93	april, june, july	55,21 %
Albacete	92	–	–
	93	may, june, july	60,13 %
Arles	92	march, march, april	54,42 %
	93	may, june, september	66,16 %
Bourges	92	may, june, july	88,47 %
	93	march, april, july	54,53 %

The rate of identified samples is generally good, more particullary for the sites including large fields with regular shapes. Some sites show results of less good quality : this can be explained by the temporal distribution of radar images which is not optimal for crop discrimination (this is the case for Seville in 1993 and for Arles in 1992), or by the predifined land cover classes which might for instance mix crop types corresponding to very different radar backscattering (this is the case for Arles in 1992 where Winter Wheat and Rapeseed are associated in a same class).

Some land covers can also have similar characteristics from texture point of view, such as forests and heaths or wastes. Results can reach more than 90 % of well identified parcels for specitic classes such as forests (100 % on the site of Essen in 1992) or cereals (92,7 % on the site of Bourges in 1992).

5. CONCLUSIONS

This study, based on factorial discriminant analysis using texture and tone parameters on the SAR ERS images, shows that crop discrimination is quite feasible with these images and that radar data contain the needed information. ERS PRI images may therefore be considered in operational systems for crop monitoring.

Use of multi temporal data (three dates) allows to obtain reliable separation in most cases.

However these data must be carefully chosen and the acquisition period must fit the growing season for the main crops of a given site.

The definition of a segmentation technique relevant for SAR imagery, which is currently under study, will allow to make our approach complete before the implementation of our methodology.

6. BIBLIOGRAPHY

[BEAUPERE-92] A. BEAUPERE
"Classification d'images de radar par mesures de texture"
Thèse de Doctorat, Université Paris VI, Juin 1992

[LAUR-89] H. LAUR
"Analyse d'images radar en télédétection : discriminateurs radiométriques et texturaux"
Thèse de Doctorat, Université P. Sabatier, Mar. 1989

[SAFA-89] F. SAFA
"Le speckle en imagerie cohérente : propriétés statistiques, relation entre l'image cohérente et l'image incohérente ; essai de filtrage morphologique"
Thèse de Doctorat, Université P. Sabatier, Mai 1989

[DEMAILLY-94] C. DEMAILLY, T. RABAUTE
"Etude de l'apport spécifique des données radar ERS-1 à l'établissement de statistiques agricoles"
Rapport d'étude final, Janvier 1989

BACKSCATTERING AND SURFACE ROUGHNESS: THEIR POTENTIAL USE FOR GEOLOGICAL MAPPING OF ARID AREAS WITH THE ERS 1 RADAR, ATAR SITE, MAURITANIA (PP2-F6)

Jean-Paul Deroin*, André Simonin** & Dominique Legendre***

**BRGM Research Division, BP 6009 45060 Orléans cedex 2 France*
Tel: (33) 38 64 38 34. Fax: (33) 38 64 33 61

*** IMAGEO CNRS, 191 rue Saint-Jacques 75005 Paris France*

**** BRGM French Geological Survey, BP 6009 45060 Orléans cedex 2 France*

ABSTRACT

The experiments carried out as part of pilot project PP2-F6 of the European Space Agency, concerned lithological and structural discrimination in an arid environment. Data were obtained from test sites selected in the *Baten* area, near Atar (northern Mauritania). This is a flat and arid area, where only surface roughness can be considered as a variable criterion, slope angle and soil humidity being zero. The ERS 1 data were geo-coded according to procedures developed at BRGM.

From a thematic viewpoint, the main results concern roughness, lithology, and structure.

From a methodological viewpoint, we can make two main remarks: The influence of the geocoding on the readability of the data, is negligible for the flat areas that were studied and, the risk was confirmed of using non-geocoded data for structural studies

1. INTRODUCTION

Geological mapping of arid regions where exposures commonly are good, is possible with data obtained in the visible realm of the electromagnetic spectrum because favourable climatic conditions allow systematic data acquisition and detailed morphological studies [e.g. Maxwell and Haynes, 1989]. Supervised terrain classification as well as all of the common techniques for improving dynamic range, can be used to produce a map that is both similar and complementary to direct field observations (Alwash & Zilger, 1994).

However, outcrops in arid regions are commonly covered by a sandy veneer, or even a cover of thick superficial, often mobile, formations. Furthermore, the arid climate is propitious to modification of the original rock surface by desert varnish, by spalling of the rock and through the alteration of certain minerals. Such physico-chemical weathering changes the nature of the surface, and thus the surface roughness and dielectric constant of the geological formations.

Work carried out during the Shuttle Imaging Radar projects SIR-A (1981) and SIR-B (1984) on sites in Egypt and Sudan led to the development of radar studies in desert regions. The L band (24 cm) was used to reveal a palaeo-drainage network in the Egyptian Western Desert that is invisible both on Landsat images and in the field (Breed *et al.*, 1983; Elachi *et al.*, 1984; Davis *et al.*, 1993), but which is shown as dark areas beneath the surficial formations. In most of these studies, radar data were combined with optical data (Schaber and Breed, 1993; McCauley and Breed, 1993).

2. OBJECTIVES OF THE STUDY IN MAURITANIA

As part of the pilot project of the European Space Agency dealing with geological mapping of arid regions using radar imagery (PP2-F6), the work carried out in Mauritania primarily dealt with the effects of partial or total masking of bedrock by surficial formations. The specific analysis of ERS 1 radar images thus aims at:

- identifying the geomorphological and geological phenomena for which radar provides information that is complementary to that of optical techniques (here, SPOT XS);
- testing the ability of radar signals to detect structures or rock types under windblown sand (erg zone);
- identifying the characteristic surface nature of the main morphological structures in desert regions (reg, erg, glacis, hammada, etc.);
- comparing the purely structural information in the radar image with data gathered using optical techniques, all of which is then compared to field data;
- analysing the effects of geocoding on the legibility of the images.

3. SUBJECT AND METHODS

3.1. Test site

The Atar region is located in the centre-north of Mauritania, near the border with the former Spanish Sahara (Rio de Oro), in the Saharan climate zone. Its approximate co-ordinates are N. 20°30', W. 13°00', and it is located in the Adrar massif, a region of arid plateaux progressively invaded towards the east by sand from the Ouarane Erg near Guelb er Richat. The Adrar is located in the heart of the West African craton, an extensive peneplain with an average altitude of 400 m.

To the west, the Amsaga peneplain has an average altitude of just over 100 m. Its flat topography is marked by several inselbergs (*guelbs*). The transition zone with Adrar's main cliff is called the *baten*. This area with an average elevation of more than 200 m to the north is gradually buried by the Arouaba Erg. The plateaux or *dhar* (hammada) that make up the Adrar *sensu stricto* dominate this western unit by a straight NE-SW escarpment that is 300 to 500 m high.

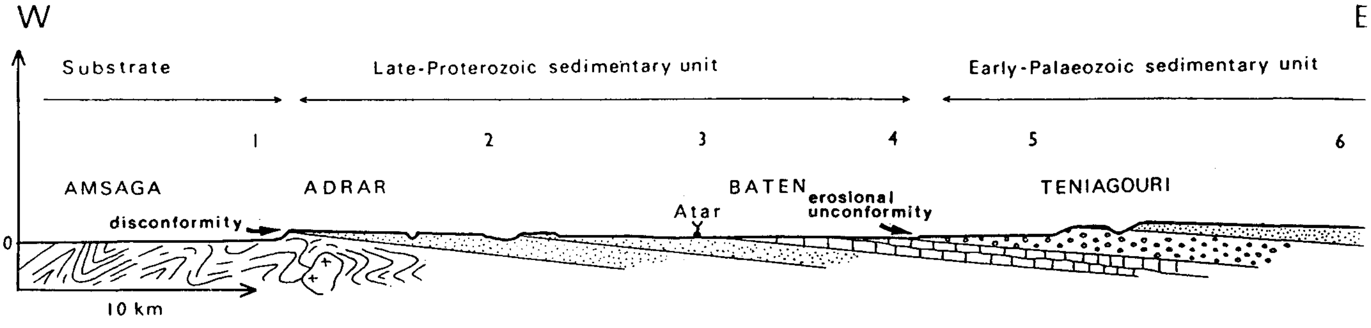

Fig. 1. Typical cross-section of the Atar area (see also text for explanations)

3.2. Geology

The geological setting of the site is simple, being made up of a monoclinal pile of sedimentary rock overlying a migmatite basement (high-grade metamorphism). This basement (Fig. 1, no.1) is formed by the eastern limit of the Amsaga, which in the region of Guelb el Grâra, 32 km SW of Atar, consists of leptynite containing several quartzose levels with copper showings. It forms part of the Reguibat ridge of Early Proterozoic age that strikes NE all the way to the Tindouf Basin (Algeria).

The first sedimentary unit, which unconformably overlies the metamorphic basement and is 370 m thick, consists of a succession of Late Proterozoic rocks comprising sandstone, dolomite and argillite. At the base, the succession (Fig. 1, no.2) is dominated by sandstone (Agueni and Foum Chor formations) that forms two cuestas separated by a soft clayey slope (Azougui formation) (Fig. 1, no.3). At the top of the succession, the rocks are mainly dolomite and contain stromatolites (Fig. 1, no. 4). Above a channelling disconformity, a Cambrian-Ordovician succession is characterized at the base by tillite (deposits of glacial origin) that that have a "soft" topographic expression (Fig. 1, no. 5). The overlying jasper and especially quartzite form prominent ledges (Fig. 1, no. 6). Regionally, Silurian graptolite-bearing schist and Devonian calcareous sandstone are found as well, but such rocks are not exposed in the study area.

The rocks in this area have undergone only slight deformation, the overall dip being at the most a few degrees to the east or southeast. The, partially mobile, dunes are rarely more than 50 m high and cover a large part of the study site. We can distinguish the Ogolian and the ancient ergs, the latter containing more fluviatile deposits and being located below deposits of the Inchirian transgression that took place during the last Interglacial period around 100,000 years B.P.

3.3. ERS 1 data

ERS 1 data were used in the PRI form for interpretating. Single-look complex data were also used for the methodological study of geocoding of radar images (Deroin and Simonin, 1995 ; Legendre, 1994).

3.4. Optical data

The cartographic reference data is the mosaic of SPOT scenes from 22/01/91 and 12/02/91. The wavelength field lies in the visible (green and red) and near-infrared spectra: λ_1= 0.50-0.59 µm, λ_2= 0.61-0.69 µm, λ_3= 0.79-0.90 µm. This mosaic was used in a previous study (Deroin and Motti, 1994), and can be used as a reference for photo-geological interpretation. A DEM was made by the ISTAR company through crosscorrelation of SPOT images. The quality of this model makes it an essential auxiliary tool for geocoding.

4. EVALUATION OF LITHOLOGICAL AND STRUCTURAL INFORMATION PROVIDED BY ERS RADAR DATA

The litho-structural content of the radar data was systematically compared to the reference established with SPOT XS imagery (Fig. 2, more details in Deroin *et al.*, in prep., and in Deroin and Simonin, 1995):

- Substratum rocks, such as sandstone, claystone and carbonate, or metamorphic rocks in the case of the relative basement, as well as the lightly covered glacis and the pediments (erosion glacis in softer rock) that develop at the foot of the escarpment, are covered by regs and are associated with the monoclinal back slopes.
- Superficial unconsolidated formations: sandy-silty cover in low areas, or alluvial sheets along the main drainage axes, and aeolian material that accumulated as dunes downwind of the escarpments, or as veneer of variable thickness covering the substratum.

It must be remembered that this study is primarily based on the surficial nature of the rocks, and that, except for the monoclinal backslope, bare rock is not actually exposed.

4.1. Case of rock formations

Based on the lithology of regional formations, we can distinguish two main levels of observation whose significance is only revealed through multispectral data:

- Lithological units: Certain boundaries, clearly visible in the morphology and almost perpendicular to the incident beam, can also be seen on the ERS data.
- Traces of marker beds too small (several metres to up to 20-30 m) to be visible on radar data (nominal pixel size 12.5 m, but with a spatial resolution of around 25-30 m, depending on the backscattering of objects).

4.2. Case of superficial formations

The surficial aeolian-sand accumulations or sandy-silty deposits in dry river beds, which cover bedrock, are distinguishable on the SPOT image by their generally light to very light colour, often saturated in the case of mobile dunes. Rocky surfaces (reg, pediment sheets) are mainly blue, commonly covered by a light component due to sandy veils.

On the ERS image, in the case of flat superficial formation surfaces (dry river beds, for example), there is little backscattering because of the smoothness of the surface (specular effect). Only microrelief can cause strong backscattering, and only if it is turned towards the receiver. Where the sandy veneer is irregular and thin it does not show on radar data. In some cases (see below), the radar signature of surficial aeolian formations is "transparent", whereby the structure and texture of the bedrock below the sand veneer are visible, the thinness of this veneer apparently being the main cause of the transparency.

4.3. Structural information

In general, fewer fractures are detected by ERS than by SPOT. This is all the more true where fractures are small and poorly expressed in the field. The extreme case is that of joints, which are almost never seen on the radar image. Qualitatively, it is evident that fractures parallel to the incident beam are poorly detected or absent from radar data.

Radar imagery is nevertheless of interest in the areas with numerous sandy bands in the northeast. From the optical image, it is not always easy to recognize the purely structural features of lineaments, outlined by the linear dune rows formed behind escarpments by downwind sand accumulation.

4.4. Objects for which the optical image is preferable

Although the major fractures of the unit are clearly visible on the two types of data, there are disparities; their perception on the ERS data is systematically better for directions perpendicular to the incident beam (about N110°E). Some directions with an azimuth between N090°E and N120°E disappear. The most marked occultation is that of the N120°E fault, which is invisible on the radar image due to the fact that it is parallel to the incident beam, despite its being clearly marked by the drainage as a canyon 120 m deep.

Some geomorphological objects are also very difficult to see on ERS 1 data. The drainage network that comes from unit b and rapidly disappears in the east under the dune cover is an example. On radar data, only a smoother texture characterizes an area where dunes are absent. The network of stable dunes is differently recognized on the two types of images. On optical data it is primarily the shadow to the west of the dunes that enables the differentiation between dunes and the sandy environment, but on radar data it is mainly the side facing the signal (the east side of dunes) that helps in identifying the summit-like structure of dunes, standing out in relief against the sandy deposits. While the perception of dune structures is mostly similar on the two types of data, it is better on the optical data because of the higher resolution, which detects the small dunes that do not seem to be high enough to modulate the radar signal.

The quality of the exposures (and the simple tectonic structure) enables detailed observation of lithological formations such as object. Such data can also be used to define, on the SPOT image, the dip of the beds (here systematically oriented towards the east or the southeast). This information is not given by radar.

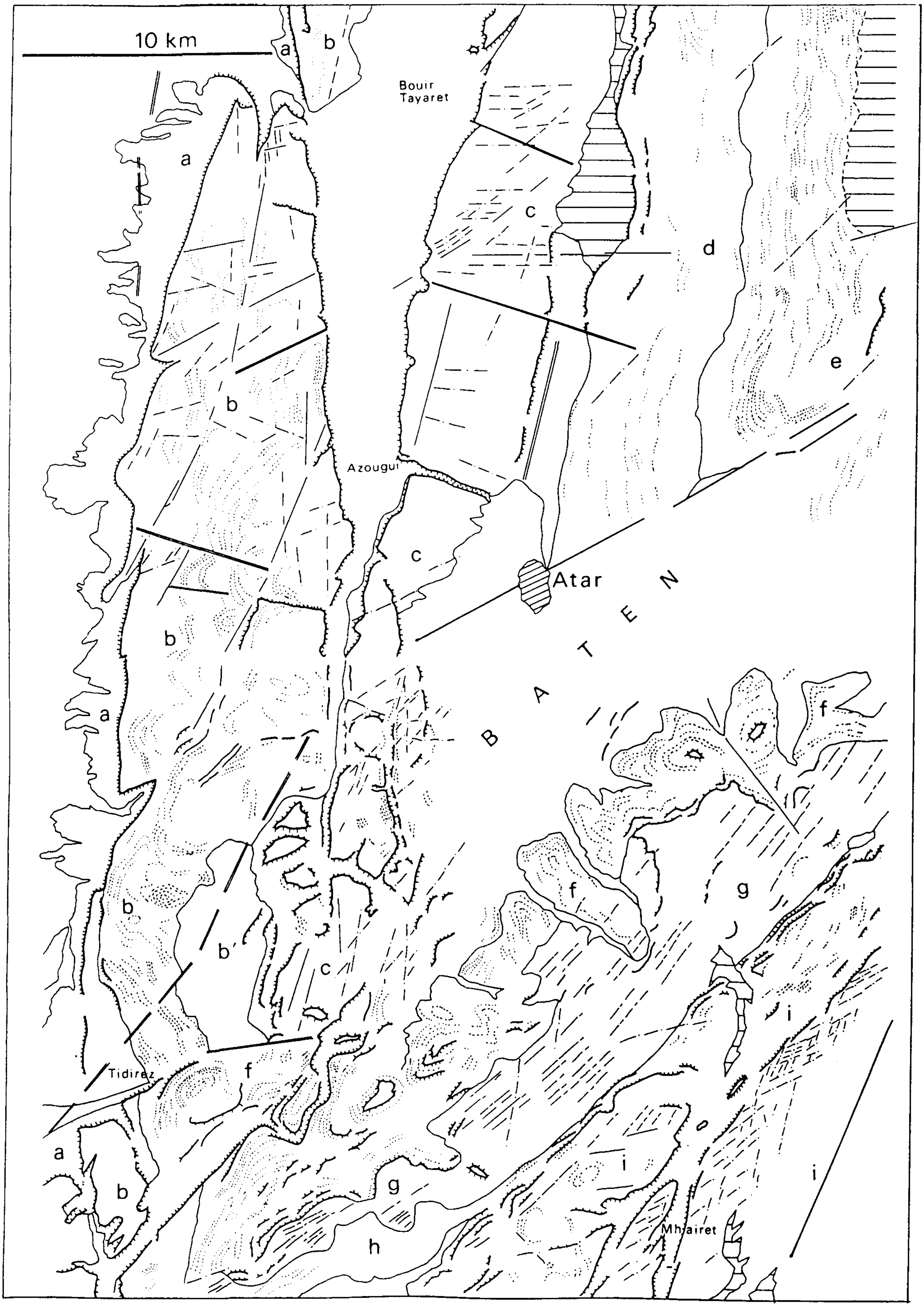

Fig. 2. Interpretation of radar (ERS 1) and optical data (Spot XS)

4.4. Themes for which the radar image is preferable

Using radar data, we can recognize rock structures under sand cover because of "transparency". This phenomenon is well known to photo-interpreters and can be defined as the ability to visualize the limits and/or texture of a geological object (fault, lithology, vein, etc.) in an area where it is not directly recognizable in the field. This is the case in optical imagery for the tracing of fractures in areas of thick surficial cover.

With radar imagery, transparency can be magnified through greater penetration, because the active signal can theoretically penetrate certain media, notably dry and loose sand. We also know that penetration depth depends on the wavelength of the signal and that it is greatest for long wavelengths. The C band (5.6 cm) is therefore theoretically not optimal for the study of this phenomenon.

Transparency was observed in units H and I. In H, the sand cover is very thin (0 to 5 cm). Elsewhere there are vast dune fields (ergs) such as those trapped in the longitudinal Azougui depression, the height and width of which reach about 20 m, but which could not be measured precisely. Their characteristic response on the ERS 1 image is that of large sand accumulations, well known from the SIR-A data.

4.5. Difficulties in interpretation due to geocoding

The geocoding of ERS images does not seem to cause any major difficulties in interpretation. However, some points for which the geometric rectification of the radar data may increase the uncertainty or decrease the analytical precision, may have to be studied in detail.

In general, textures and structures are altered by geocoding. It is as if we were superimposing a filter on the original speckle in the image, smoothing out certain contrasts and blurring some linear features. The large flat areas caused by the "transparency" phenomenon as well as the dykes in the southeast of the image are a good illustration of this. This alteration effect is nevertheless slight and generally does not modify the analysis.

Isolated objects are most affected by geocoding. This is the case with the outlier in the west of unit C. Its characteristic form, clearly visible on the original image, is blurred on the geocoded image. In this specific case, it seems that we loose the geometric relationship between the shaded area to the west and the illuminated hillock facing east. This type of difficulty could also be due to a slight imprecision in the DEM.

The phenomenon of dip inversion seen on the non-geocoded image is locally observed in the Early Paleozoic tillite. This is due to the fact that the higher points seem to be drawn towards the sensor and that the slopes on either side simulate the shape of a bed dipping west because of the radar orbit. Such effects have been also described from the Ethiopian Afar by Chorowicz *et al.* (1995).

Geocoding thus seems to influence the precision of the contour/location, but certainly less so than other parameters such as the observation scale. Indeed, passing from 1:100,000 to 1:200,000 scale causes modifications of the same nature as those characterized by the smoothing of areas of homogeneous texture, i.e. an apparent decrease in speckle when passing to a smaller scale.

For flat zones, any geometric distortion effects are extremely weak.

5. CONCLUSION

From a thematic viewpoint, the main conclusions concern:

- Roughness. A relationship was developed for the empirical quantification of backscattering in a stony-desert environment, which is purely mineral, arid and flat, and where the maximum elevation of blocks seems to be the dominating influence on σ_0. Such landscapes, known as reg, glacis, etc., have sufficiently clear-cut characteristics to minimize the risk of confusion, even though this risk increases with decreasing surface roughness. An example is the confusion between fine sandy-silty deposits from streams and a superficial sand cover, a relationship that is described by the function $\sigma_0 = -15.2 + 4.56.\ln h_{max}$ with the remarkable correlation of 94% (Fig. 3).
- Lithology. Compared with optical frequencies, hyperfrequencies are of reduced interest for the direct recognition of rock types. However, an understanding of surface conditions enables a fairly fine lithological distinction into reg, glacis, structural dip-slope, etc.
- Structure. The test showed the aptitude of the radar in the C channel for detecting structures by means of the 'transparency' phenomenon. This involves the tracing of boundaries between lithological units below a thin sand cover. Lacking systematic measurements of sand thickness, it is difficult to define the limits to perception. Moreover, the study also showed that the detection of structural features not only depends upon the ratio between incidence angle and azimuth of the structure.

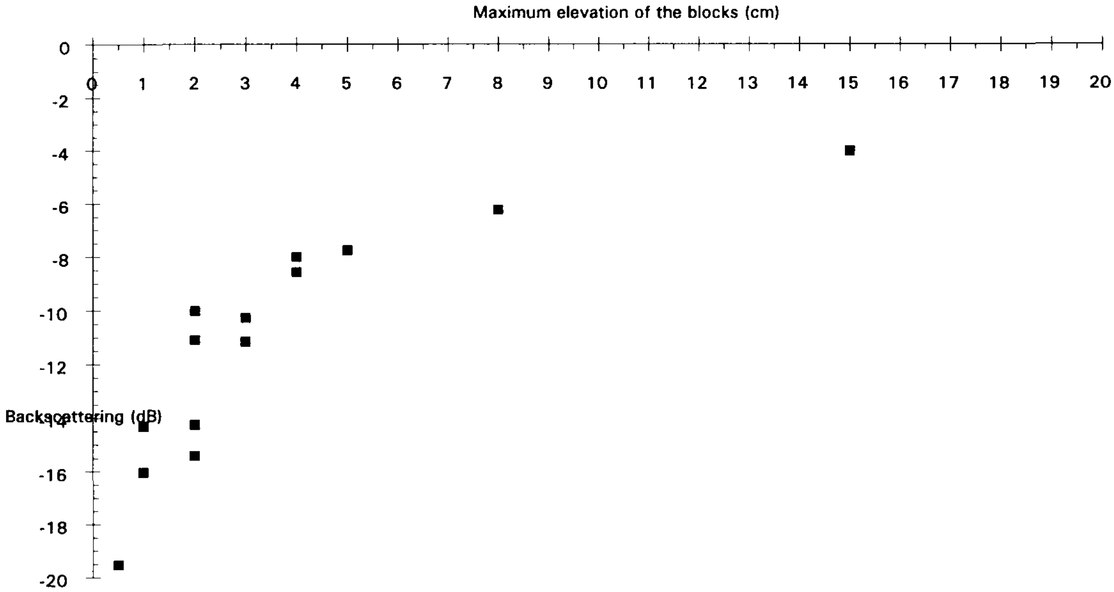

Fig 3. Relationship between backscattering and maximum elevation of blocks (after Deroin et al., 1995)

From a methodological viewpoint, we can make two main remarks:

1) The influence of the geocoding on the readability of the data, is negligible for the flat areas that were studied. In areas with a stronger relief, geocoding can lead to difficulties in geomorphological recognition, such as in the case of inselbergs, and thus decrease the discriminating power for textures and structures.

2) The risk was confirmed of using non-geocoded data for structural studies, if no account is taken of the effects of slope-inversion and directional anisotropy. We do know, however, that the latter can be partially obviated by the use of pseudo-stereoscopic image couples.

The work presented here was carried out as part of the European Space Agency project PP2-F6 "Radar and geology in arid regions", supported by the Centre National d'Études Spatiales (CNES) within the AVAL SAR programme. Logistic support for field operations was provided by the Détachement Militaire d'Assistance Technique (DMAT) in Atar and facilities were provided by the Mauritanian Office of Geological Research (OMRG) in Nouakchott. This study is part of the BRGM Research Division project P01 "Perspectives for the Use of New Sensors in the Earth Sciences". This becomes BRGM publication n°95,049.

REFERENCES

Alwash, M.A., and Zilger, J., 1994, Remote sensing-based geological mapping of the area west of Al Madinah, Saudi Arabia. *International Journal of Remote Sensing*, 15, 1, 163-172.

Breed, C.S., Schaber G.G., and McCauley, J.F., 1983, Subsurface geology of the Western Desert in Egypt and Sudan revealed by Shuttle Imaging Radar (SIR-A). Spaceborne Imaging Radar Symposium. *Jet Propulsion Laboratory Publication*, 83-11, 10-12.

Chorowicz, J., Koffi, B., Chalah, Ch., Chotin, P., Collet, B., Poli, J.-Th., Rudant, J.-P., Sykioti, O., and Vargas, G., 1995, Possibilités et limites de l'interprétation géologique des images (SAR) ERS1. *Bull. Soc. franç. Photogramm. Télédétection*, 138, 82-95.

Davis, P.A., Breed, C.S., McCauley, J.F., and Schaber, G.G., 1993, Surficial geology of the Safsaf region, South-Central Egypt, derived from remote-sensing and field data. *Remote Sensing of Environment*, 46, 183-203.

Deroin, J.-P., Legendre D., and Simonin, A., 1995, An empirical model for interpreting the relationship between backscattering and arid land surface roughness as seen with the SAR. *Proceedings of CNES/IEEE Symposium*, Toulouse, October 1995, (in the press).

Deroin, J.-P., and Motti, É., 1994, Geological interpretation of the image facies of a Spot satellite image map. *Revue de Photo-Interprétation*, 6, 5, 139-141 and 155-166.

Deroin, J.-P., Motti E., Simonin, A. and Legendre, D., in prep., Comparison of potential for using optical data and synthetic aperture radar for geological mapping in arid regions (Atar, Western Sahara, Mauritania).

Deroin, J.-P., and Simonin, A., 1995, Apport des données ERS 1 en cartographie des milieux arides : site de démonstration d'Atar (Mauritanie). BRGM Report, R 38 238, 53 pp.

Elachi, C., Roth, L.E., and Schaber, G.G., 1984, Spaceborne radar subsurface imaging in hyperarid regions. *IEEE Transactions on Geoscience and Remote Sensing*, GE-22, 4, 383-388.

Legendre, D., 1994, Géocodage d'images radar. Réalisations et perspectives. BRGM report, R 38173, 42 pp.

Maxwell, T.A., and Haynes, V., 1989, Large-scale, low-amplitude bedforms (chevrons) in the Selima Sand Sheet, Egypt. *Science*, 243, 1179-1182.

McCauley, J.F., and Breed, C.S., 1993, Comparisons between the Nile river, Egypt and the Colorado river, USA. In: *Geoscientific research in Northeast Africa*, edited by U.Thorweihe and H.Schandelmeier (A.A.Balkema, Rotterdam), 723-727.

Schaber, G.G., and Breed, C.S., 1993, Subsurface mapping with imaging radar in deserts of Africa and Arizona. In *Geoscientific research in Northeast Africa*, edited by U.Thorweihe and H.Schandelmeier (A.A.Balkema, Rotterdam), 761-765.

SAR image processing techniques evaluation and tuning to different applications.

M. Melis[1], L. Piazzo[1], G. Solaas[2], G. Pacheco[2], P. Bally[2] and H. Laur[2].

(1) SPACE ENGINEERING S. p. A., via dei Berio 91, I-00155, Rome (Italy).
(2) ESRIN, via. G. Galilei, I-00044, Frascati (Italy).

The activities reported were performed within the framework of ESRIN contract No. 11396/95/I_HGE.

Abstract

In this paper a methodology for the evaluation of SAR images processing techniques is proposed, which allows to compare different algorithms and to tune their parameters to different applications. The methodology has been applied to three general purpose SAR images processing algorithms used in a selected set of applications: crop classification, oil slicks enhancement and ship detection. In the paper the methodology is outlined and the results obtained for the three applications are reported.

Introduction

A great number of applications exploiting spaceborne SAR imagery appeared in the last years, due to the interesting characteristics of this type of data. Both computer processing and human intervention are requested in any application, as it is very difficult to develop completely automatic techniques. Of course an interest exists in delivering the largest possible part of the application burden to the computer; to this end every day new techniques are proposed, which use more and more complex algorithms. However new techniques must be validated, and their processing parameters must be tuned on each application; thus a need exists for robust and formalized testing and tuning methodologies. Within this framework, the authors have been concerned with the evaluation of a set of general purpose SAR image processing algorithms, and with the tuning of their parameters for use in a selected set of applications including, but not limited to, crop classification, oil spill monitoring and ship detection.

Methodology

For a particular algorithm, the evaluation methodology is based on the identification of a set of **success criteria**, i.e. a set of goals which the algorithm is required to reach. For any success criterion a set of **quality measurements** is then established, i.e. a set of measurements which allow to quantitatively evaluate how well the success criterion is met. The introduction of success criteria and quality measurements clarifies the separation between the goals of the algorithm (which are normally stated informally, in natural language and are relative to one or a few applications) and the measurements which can be performed in order to assess the quality of the algorithm (which are formal procedures involving the measurement of numerical values and are relative to a particular success criterion). The clear definition of the success criteria and of the quality measurements allows different algorithms to be compared on the basis of a particular success criterion and to identify competing success criteria (i.e. trade-offs); it also provides a framework for the tuning of the algorithm parameters with respect to specific applications: an application usually identifies a subset of crucial success criteria; the related quality measurements can be used as a guideline to set the algorithm parameters, and the insight gained in the evaluation phase can be fully exploited in the application phase.

Algorithms and success criteria

The set of algorithms involved in the study is composed of a Despeckle module (based on a non linear, structure retaining filter (similar to that proposed in [1,2])), a Feature Extraction module (based on wavelet (Gabor) transform [3,4,5]) and a Classification module (based on an unsupervised Kohonen neural net approach [3,6]). The three algorithms are the core of a SAR Image Processing library developed at Space Engineering, which comprises several other processing tools.

Algorithm	Success Criterion
Speckle filtering	Radiometric accuracy
	Noise suppression
	Texture preservation
	Edge preservation
	Strong scatterers preservation
	Linear features preservation
Features Extraction	Uniform areas enhancement
	Textured areas enhancement
	Linear structures enhancement
	Edges detection
Classification	Classification accuracy

Table 1: the success criteria.

In the study, success criteria have been established for each algorithm, and quality measurements defined for each success criterion. The measurements have been performed on a comprehensive set of ERS-1 SAR images, varying values of the algorithm parameters, in order to analyze the interaction between the parameters and algorithm performance. In Table 1 we report the list of the success criteria identified for the three algorithms: the results of the whole study, including the identified quality measurements, the measurements results and the analysis of the effect of processing parameters on the results can be found in [9].

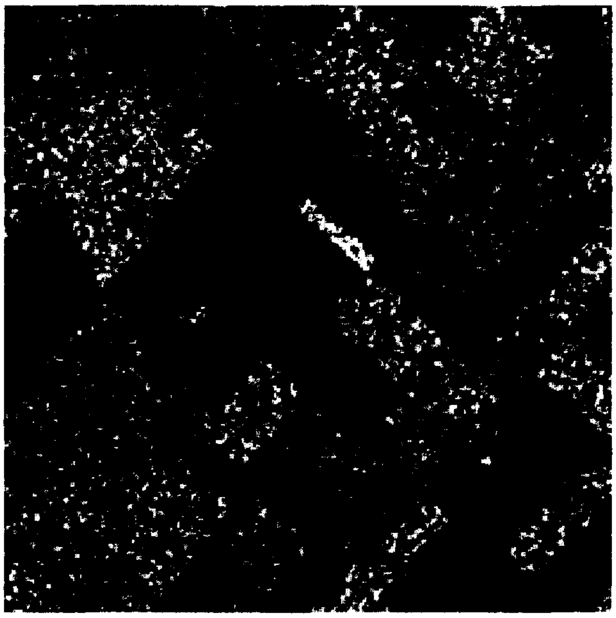

Figure 1: the Flevoland test site. ERS-1 PRI, Orbit 10316, Frame 2547.

Applications

In this section we present examples of the results obtained using the three general purpose algorithms in a selected set of applications: these examples are taken from the application phase of the study, where the insight gained on the behaviour of the algorithms in the evaluation phase is exploited in order to tune the algorithm to different applications. A very brief description of the processing chains will be given, together with examples of the obtainable results: a deeper description of the application phase results and methods can be found in [10].

Crop classification

The classification of an agricultural area should supply a thematic map in false colours where each different color corresponds to a different type of crop.

It is well known that multi-spectral data improve the correct classification rate with respect to the case in which monochromatic data are used, because different crops exhibit different multi-spectral signatures.

In order to obtain good classification accuracy using single frequency (C-Band, VV-polarization) ERS-1 SAR images it is necessary to use multi-temporal data, i.e. a set of images taken at different dates: in this way crops can be identified based on the different multi-temporal signature that they exhibit.

The classification can be supervised or unsupervised. In the first case an a-priori multi-temporal signature (identifying a class) is required for each type of crop and the classification process attributes each pixel to the most likely class: these a-priori signatures should be provided by the user. In the unsupervised case, the classification algorithm itself estimates these signatures; to perform this task, a representative subset of the input data is first analyzed, in order to determine the classes, and then the whole input data set is classified as in the supervised classification: in this case the user task will be that of assigning each class to a particular crop. The classification algorithm used in this work is unsupervised.

A problem encountered when using 3-looks ERS-1 PRI images for classification is the speckle noise that they exhibit, which implies a great variability (i.e. a very low reliability) for the value of the single pixel; to overcome this problem it is necessary, during the classification of a particular pixel, to take into account the pixel context, i.e. the values of the surrounding pixels.

In the tested classification method, the classification is performed on a pixel by pixel basis, using the unsupervised neural net classifier module; a preprocessing of the images is needed; it is based on the Despeckle module plus a gaussian lowpass filter, and allows to take into account the context of each single pixel. The processing chain is thus composed of three steps: the multi-temporal images are (1) speckle filtered, (2) lowpass filtered and (3) fed to the neural network classifier which produces the thematic map.

The speckle reduction step is a good example of how the evaluation phase can help the parameter tuning in the application phase: for this particular application the two relevant success criteria among those listed in Table 1 are the "Radiometric Accuracy" and "Noise Suppression" success criteria. The "Radiometric Accuracy" success criteria indicates as one of the goal of the Despeckle module that of perfectly preserving the mean backscattering coefficient of an homogeneous area (as a field is): it is clear that the goal is mandatory for this application because the pixels will be later classified based on their measured backscattering coefficient. The "Noise Suppression" success criteria states that one of the goal of the Despeckle module is that of removing as much as possible speckle: clearly this goal is very important in order to enhance the accuracy of the backscattering coefficient measurement thus facilitating the successive steps. The quality measurement results (see [9]) obtained indicate that the Despeckle algorithm is quite successful with respect to the "Radiometric Accuracy" success criteria, almost irrespective of the parameters controlling the Despeckle module, while the parameter values have a great impact on the noise removal capabilities of the module: thus, for this application, the parameter of the Despeckle algorithm can be tuned using the measurement results relative to the "Noise Suppression" success criteria as a guideline.

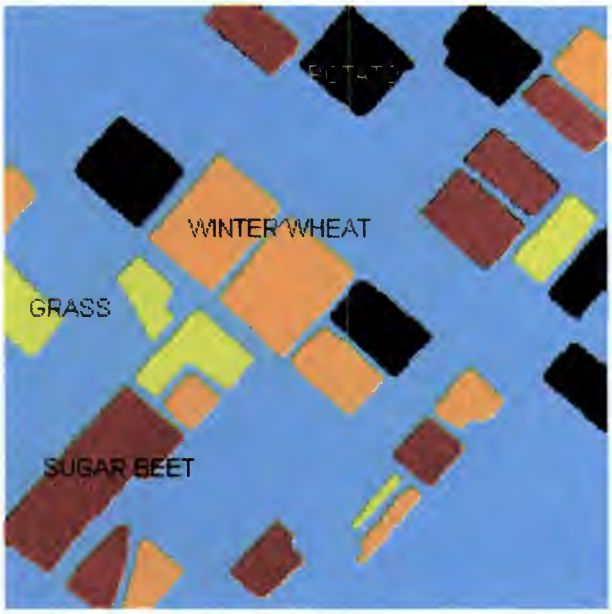

Figure 2: thematic map obtained from the ground truth.

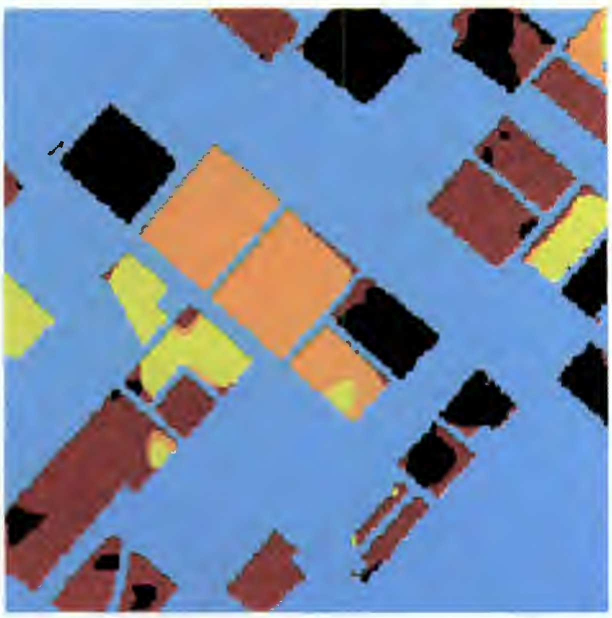

Figure 3: thematic map produced by the neural net classifier.

The test site is the Flevoland Polder, in the Netherlands, for which a ground data collection exists ([7]). Four ERS-1 PRI of this test site were allowable (frame 2547, orbits 8312, 9314, 10316 and 11819) taken in February, April, July and October 1993 respectively: in Figure 1 we plot the July original image. Four crops were selected: winter wheat, potato, sugar beet and grass. In Figure 3 the thematic map produced by the neural classifier is plotted; comparing it with the thematic map obtained (manually) from the ground truth (plotted in Figure 2) it can be seen that a good agreement exists between the two. In Table 2 the confusion matrix is reported: the overall correct classification rate is about 67%. It should be noted that some errors may be present in the ground truth data: this is strongly indicated in Figure 4, which displays the despeckled SAR image of the test site in false colors with superimposed field boundaries. The two crops which are more difficult to separate are potato and sugar beet: this results is in perfect agreement with the results reported in [8], were it is shown that these two crops display very similar multi-temporal signature.

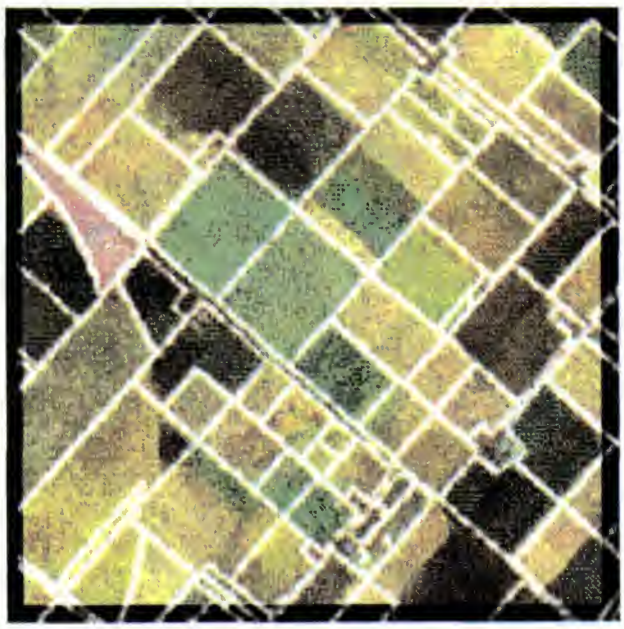

Figure 4: false colour image of the test site with ground truth superimposed

crops	potato	sugar	wheat	grass	others
potato	63.2	26.4	2.2	1	5
sugar	26.8	59.8	5.6	2.4	3.2
wheat	7	8	67	5	10.6
grass	0.2	3.6	3.4	80	10.2

Table 2: confusion matrix for the Flevoland test site.

Oil slicks detection

Oil slicks detection is usually performed by visual inspection of a processed SAR image. The goal of the processing is to facilitate the visual inspection of the image; a typical processing can be a speckle filtering.

In the study, the Feature Extraction module has been used to process the image in order to enhance the oil slicks thus allowing easier and safer visual inspection.

Two forms of preprocessing have been implemented: oil slick edge detection and oil slick contrast enhancement.

Figure 5: oil slick. ERS-1 FDC, orbit 15488, frame 2835.

Oil slick edge detection is obtained using the Feature Extraction module with parameter tuning based on the "Edge Detection" success criterion. Edge detection is performed by means of a bank of Gabor filters with different orientation and by a non linear combination of the resulting filtered images. The method is particularly well suited for edge detection on SAR images as it is capable to reject speckle noise to a great extent.

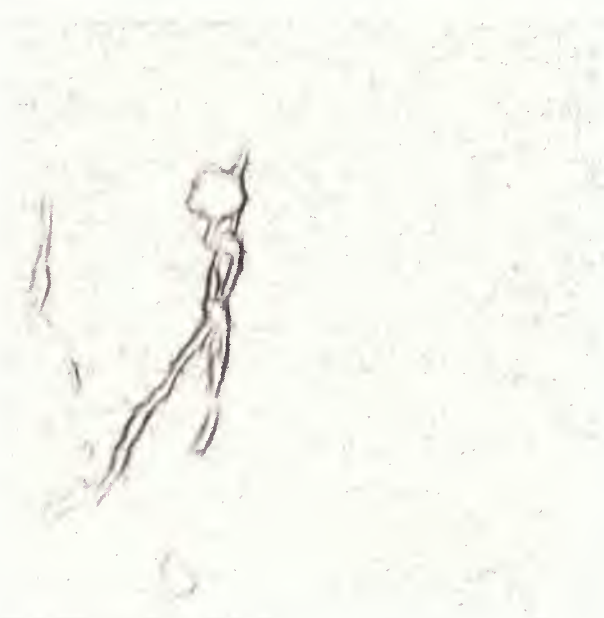

Figure 6: oil slick edge detection.

Oil slick contrast enhancement aims at increasing the separation between the slick and the background. Contrast enhancement is performed by means of a bank of multi-scale filters with different bandwidth and by a non linear combination of the resulting filtered images. The contrast enhanced image is well suited for further processing aiming at the perfect separation between the slick and the background and at the automatic identification of slicks.

Figure 7: oil slick after contrast enhancement and region growing.

Figure 8: ERS-1 FDC, orbit 15488, frame 2835: a ship is clearly visible.

In Figure 5 the image of an oil slick is plotted: the figure is obtained from an ERS-1 FDC taken in 1993 (orbit 15488, frame 2835) over the Eolian Island. In Figure 6 the edge detected image is plotted. In Figure 7 we plot the result of applying a standard region growing algorithm to the contrast enhanced image: the contrast enhancement allows the algorithm to perfectly separate the slick from the background.

Figure 9: the linear features enhanced image.

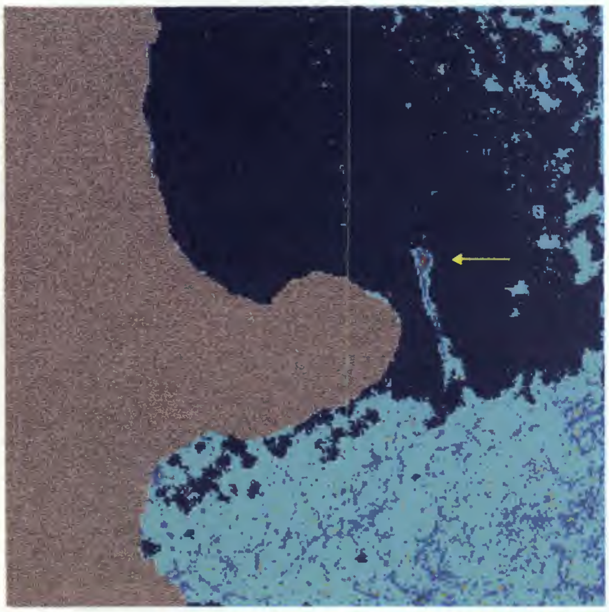

Figure 10: example of ship detection; ships belong to the "red" class.

Ships detection

The ships detection application aims at the automatic identification of ships in a SAR image.

Several steps are required to perform ships detection. The first task is the separation between land and see on the image, in order to reduce number of false alarms. The sea part of the image is further processed by the Feature Extraction module. A ship can be characterized as a bright point (strong scatterer) with a wake, embedded in a noisy background. According to this observation three images are obtained from the original one using the Feature Extraction module: (1) a strong scatterer detected image, (2) a linear features enhanced image, used to capture the wake, and (3) a Gaussian low-passed image, where speckle noise is substantially weakened. These three images are then fed to the neural classifier, which produces a classified image: if the number of classes and the parameters of the network are properly chosen one of the resulting class shall contain only pixels belonging to ships. Depending on the ship speed, to take into account the Doppler effect, the linear features enhancement algorithm will use oriented filters with a shift that is a function of the angle between the ship direction and the satellite flight direction.

As an example in Figure 8 an image where a ship is present is plotted (the image is again obtained from the ERS-1 FDC, orbit 15488, frame 2835, over the Eolian Island); in Figure 9 the linear features enhanced image is plotted; Figure 10 is the classified image: all and only the pixels relative to the ship belong to the same class (the one displayed in red).

References

[1] A. Lopes, E. Nezry, R. Touzi and H. Laur: "Structure detection and statistical adaptive speckle filtering in SAR images", Int. J. Remote Sensing, vol. 14, no. 9, pp. 1735-1758 - 1993

[2] A. Lopes, R. Touzi and E. Nezry: "Adaptive speckle filters and scene heterogeneity", IEEE Trans. on Geosci. and Remote Sensing, vol. 28, no. 6, pp. 992-1000 - Nov. 1990

[3] M. Melis, A. Lazzari, 'Multitemporal and Single Image Features Extraction, from ERS-1 SAR Image Data, with Wavelet Transforms and Unsupervised Neural Networks', Proceedings of the First ERS-1 Pilot Project Workshop, Toledo, Spain, 22-24 June 1994.

[4] A.C. Bovik, M. Clark, W.L. Geisler : "Multichannel texture analysis using localized spatial filters" , IEEE Transaction on pattern analysis and machine intelligence, vol. 12, no. 1, January 1990.

[5] M.R. Turner : "Texture discrimination by Gabor functions" , Biological Cybernetics, vol. 55, pp. 71-82, 1986.

[6] T.K. Kohonen : "The self-organizing map" , Proceedings of the IEEE, vol. 78, no. 9, September 1990.

[7] M. Vissers, J. Noll: "Ground data collection for the JERS-1 and ERS-1 campaign in Flevoland (NL) 1993", ESTEC, 1993.

[8] M. Borgeaud, J. Noll, A. Bellini: "On the use of ERS-1 multitemporal SAR data for agricultural application", proceeding of the 1995 International Geoscience and Remote Sensing Symposium, IGARSS, 1995.

[9] ESRIN contract No. 11396/95/I_HGE: "Methodology validation document", 1995.

[10] ESRIN contract No. 11396/95/I_HGE: "Application Demonstration document", 1995.

ERS-1 SAR DATA FOR SUGAR BEET YIELD PREDICTION

S.P.Vyas, M.D.Steven and H. Xu
Department of Geography, Uni. of Nottingham, Nottingham, NG7 2RD, UK
Tel : +44 115 951 5442. Fax : +44 115 9515249

M. Milnes
Logica UK Ltd., 74 Portsmouth Road, Cobham, Surrey, KT11 1HY, UK
Tel : +44 171 637 9111 Fax : +44 1932 869103

K.W. Jaggard
IACR-Broom's Barn, Higham, Bury St Edmunds, Suffolk, IP28 6NP, UK
Tel : +44 1284 810 363 Fax : +44 1284 811191

ABSTRACT

The Sugar Beet Prediction and Management Project is a three year project to develop a system for regional yield prediction of sugar beet, initially in the UK. The system primarily uses Earth Observation data from the SPOT and Landsat satellite systems but the availability of these data is limited by cloud cover. Radar remote sensing systems such as ERS-1 SAR can penetrate cloud and provide regular data covering persistently cloudy periods. ERS-1 SAR has been found in our work to be well correlated with leaf area index, allowing estimates of crop cover and productivity compatible with those made from SPOT. This indicates that ERS-1 SAR data are a viable subsitute for optical data in an operational yield forecasting system.

OBJECTIVES

1. To estimate the relationship of radar backscatter, measured by ERS-1 SAR, with Leaf Area Index (LAI) and soil moisture.

2. To validate this calibration on an independent data set

3. To apply crop canopy cover indices derived from ERS-1 SAR in the yield prediction model

PROJECT OVERVIEW

Forecasts of potential sugar yield are provided through the sugar beet growing season, based on satellite observations of crop canopy cover at various stages of development. These observations are used in conjunction with corresponding regional weather information, crop sowing dates and soil types to provide successively refined yield forecasts as harvest time approaches.

1994 FIELD EXPERIMENT

On June 27-28 1994, a ground-truth experiment was conducted to measure the relationship between Radar Backscatter σ^0 and Leaf Area Index (LAI) L in nine fields of Sugar Beet. The values were fitted to a modified version of a model by Leeuwen and Clevers (1994):

$$L=(\mathrm{Cos}\theta/2B).\ln(\sigma^0.A.\mathrm{Cos}\theta)/(C'(1+D'.m_s)-A.\mathrm{Cos}\theta)$$

Where θ is the local viewing angle, m_s is volumetric soil moisture (%), σ^0 is measured in power units and D' was pre-determined from earlier studies as 0.0603. The fitted coefficients are -

A=0.3259, B=0.167, C'=0.0452.

The canopy cover fraction is estimated using following formula:

$$f = 1 - \exp(-K.L)$$

Where f is the fraction of incident solar photosynthetic irradiance intercepted or absorbed by leaves and L is the leaf area index. K is normally a constant for a given crop type, (K=0.71 for sugar beet).

FIELD CAMPAIGN 1995

The radar model was tested on independent data in 1995 by comparing LAI values predicted by the model with leaf area and soil moisture values collected for two fields on seven overpass dates.

DATA USED

ERS-1 SAR data from the following 7 dates were used for the 1995 study.

Date	Pass	Time
03.6.95	Descending	Day
22.6.95	Descending	Day
29.6.95	Ascending	Night
08.7.95	Descending	Day
18.7.95	Ascending	Night
27.7.95	Descending	Day
03.8.95	Ascending	Night

RADAR IMAGE PROCESSING

Backscatter values were extracted from the study fields using ERDAS IMAGINE software and calibrated. Leaf area was then estimated from the calibrated backscatter coefficients using the measured soil moisture as a supplementary input to the model.

YIELD MODEL

The yield model, which provides a forecast of sugar produced per hectare of sugar beet crop, is represented by the equation:

$$Y=k*\int_{t_{sowing}}^{t_{harvest}}(S.f.e.p)dt$$

Where:
k = a correction factor to account for losses
S = solar radiation
f = fraction of radiation intercepted by crop
e = conversion coefficient (to dry matter)
p = partitioning coefficient

The way in which crop cover (f) varies with time for sugar beet, is modelled using a parameterised profile of crop cover which is initially defined in terms of default parameters. The crop cover values obtained from a sequence of satellite observations taken through the growing season are utilised by fitting the f-profile to these values. The profile is then used as input to the sugar beet yield model, along with weekly meteorological data (used up to the current date), climate data (used to cover future crop growth up until harvest) and regional sowing dates. The growth model is further refined with a water stress model.

RESULTS

The 1995 results are consistent with those of 1994 except for data collected on June 3rd, when the backscatter values were outside the normal range of the model. When the 1994 model is used to predict LAI and cover, there is generally good agreement. One of the experimental fields (A) shows a strong relationship. Excluding June 3rd, the RMS error in crop canopy cover estimates is 12% including a slight negative bias of the prediction of 8 %.

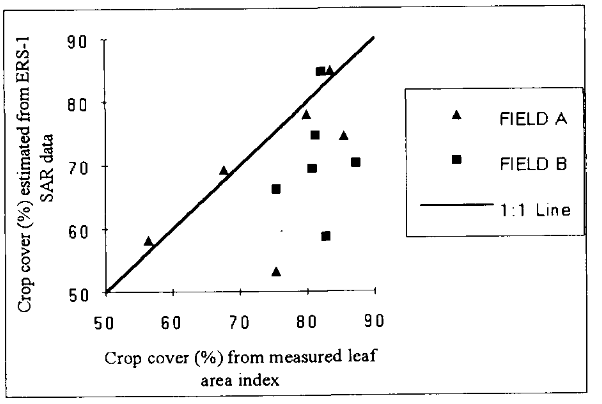

Figure 1 : Comparison of crop cover (%) estimates using measured leaf area index and ERS-1 SAR data

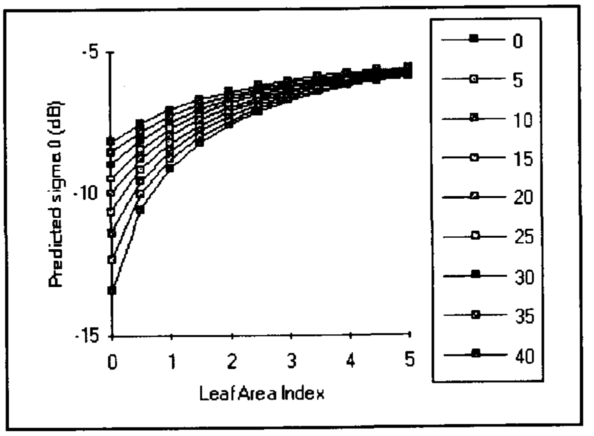

Figure 2 : Fitted model vs. leaf area index for different soil moisture content (%)

CONCLUSIONS

The modified version of Leeuwen and Clevers' model is physically realistic, provides a good fit and has an extended sensitivity to LAI and soil moisture content. It can also be inverted analytically. The ERS-1 SAR data have been shown to be sensitive to leaf area during the early growing season of Sugar Beet, which is a critical period for input to the crop growth model. Thus, ERS SAR data are expected to be a realistic viable alternative to existing optical data in an operational sugar beet yield forecasting system.

ACKNOWLEDGEMENTS

This work was undertaken as part of the Applications Development Programme sponsored by the British National Space Centre (BNSC).

REFERENCES

Leeuwen, H.J.C. van and J.G.P.W. Clevers (1994) Synergy between optical and microwave remote sensing for crop growth monitoring, in Proceedings of the Sixth International Symposium of Physical Measurements and Signatures in Remote Sensing, 17-21 January 1994, Val d'Isère, France, pp1175-1182.

Xu, H., M.D. Steven, and S.P. Vyas (1995) Logistics of data combination in the crop profile model. Technical Note submitted to Logica, UK, SBP-UN-TN-009, Issue 1. 12 May 1995, 7pp.

Xu, H. and M.D. Steven (1994) Radar modelling of sugar beet using ERS-1 SAR data. Interim report submitted to Logica, Technical Note: SBP-UN-TN-006, issue 2, 20 October 1994, 39pp.

Données ERS/SPOT pour inventorier l'occupation du sol -District Fédéral de Brasília

Iuli **NASCIMENTO** - Institut d'Aménagement et d'Urbanisme de la Région d'Ile-de-France - IAURIF

avec la collaboration de :
Jean **BERTHIER** - IAURIF
Bernard **KIENTZ** - Matra Cap Systèmes - MCS
Jean-Paul **RUDANT**- Université Pierre et Marie Curie -PMC

Abstract

L'IAURIF (Institut d'Aménagement et d'Urbanisme de la Région d'Ile-de-France), bureau d'études du Conseil Régional d'Ile-de-France, utilise la télédétection spatiale dans les domaines de l'environnement et de l'aménagement, en France et à l'étranger depuis près de 20 ans. Cette expérience a permis de dégager quelques principes de portée générale permettant la reproductibilité des travaux et la garantie de résultat.

L'IAURIF pour les aspects thématiques, MCS (Matra Cap Systèmes) pour le traitement d'images et l'Université Pierre et Marie Curie pour l'assimilation des données radar, se sont associés pour développer une application pilote sur l'aménagement régional à partir de l'imagerie ERS. Le financement de l'expérimentation a été fait sans aucun apport extérieur.

Introduction

Une cartographie généralisée ou thématique de l'occupation du sol est la base des applications en urbanisme (planification, monitoring, études multicritères d'environnement, croisements de données socio-

économiques, etc.). La principale difficulté est d'obtenir une description de l'espace qui satisfasse les urbanistes. La télédétection offre une vision de la ville dans son environnement et contribue à la prise de conscience écologique planétaire.

Les applications de la télédétection en urbanisme et en aménagement sont encore peu nombreuses par rapport aux projets environnementaux, agricoles ou géologiques. Après des débuts prometteurs et un regain d'intérêt avec l'avènement des satellites de seconde génération dits "à haute résolution spatiale" (SPOT et Landsat) ainsi que la mise en orbite du satellite européen (ERS) apportant des données radar, on attend toujours une véritable percée et la fin des problèmes posés par les couvertures nuageuses de certaines régions du Globe. La télédétection spatiale n'est pas la panacée, mais ses qualités intrinsèques de vue synoptique, de répétitivité et d'accessibilité des données de toute la surface terrestre, apportent une réponse aux énormes besoins en information pour des coûts et délais raisonnables, permettant de "connaître à temps" pour mieux maîtriser l'organisation de l'espace.

Le District Fédéral de Brasilia a été retenu car en plus du site de plateau présentant de nombreuses vallées encaissées, il existe un grand nombre d'informations (images SPOT et Landsat, occupation du sol, géologie, géomorphologie, relief, etc.) et une très bonne connaissance du terrain. Il s'agit de la réalisation d'une cartographie simplifiée de l'ensemble du District Fédéral à partir des données ERS et vérification de la pertinence du résultat obtenu d'après les données du SICAD (Système Cartographique du District Fédéral). Ce type de document est fort apprécié pour l'élaboration de schémas directeurs d'aménagements régionaux. Les données ERS s'avèrent très performantes dans la restitution des informations géomorphologiques et hydrologiques.

Traitements effectués

Image SPOT
image du 20/07/87 (KJ 710/382):

- modélisation physique à l'aide de points d'appui saisis sur la carte de la DSG (armée brésilienne) à l'échelle du 1/25000 de Brasília ;
- rectification (interpolation bicubique) sur la scène au pas de 20 mètres (projection UTM fuseau 23) ;
- amélioration des contrastes ;
- transformation au format .lan (Arc-info).

Image ERS 1
Image utilisée en mode PRI (precision product), orbite 4649 du 05/06/92 - 13h20 TU - segment 3933 , centre de la scène sud : -16,194°, nord : +48,022°.

ERS 1 fonctionne en bande C, à une fréquence de 5,3 GHz, soit à une longueur d'onde de 5,66 cm. Une image comporte environ 8200 lignes de 8000 pixels et chaque pixel (12,5 mètres) est codé sur 2 octets, une image couvre donc 100 km x 100 km.

Proceedings of the Second ERS Applications Workshop, London, UK, 6–8 December 1995 (ESA SP-383, February 1996)

Une réduction de dynamique permettant le passage d'un codage 16 bits à un codage 8 bits a été réalisée, selon la transformation suivante :
- valeur sur 8 bits = 16 bits/3, ce qui entraîne une saturation des radiométries initiales supérieures à 765.

Ce passage de 16 bits de codage à 8 bits est une procédure simple qui donne des résultats moyens sur des zones urbaines. Dans ce cas, les bâtiments risquent d'être saturés et une partie de l'information perdue. Pour le cas de Brasília, l'apport de l'image ERS a été un plus pour accentuer le contraste entre l'urbain et la végétation.

Le croisement des différentes informations

Une modélisation polynomiale (degré 1) a été faite à l'aide de points d'appui, saisis sur l'image SPOT rectifiée ensuite comme cette image. Il en résulte une composition colorée avec l'image ERS dans le canal bleu (XS-1), le canal vert (XS-2) et le canal rouge (XS-3). Cette fusion d'images a apporté une considérable amélioration des contours en milieu urbain.

Ensuite, a été superposé sur l'image ERS le réseau hydrographique existant pour mesurer l'importance de l'apport de l'imagerie radar dans le domaine de l'hydrographie. Ces données se sont avérées très performantes pour cartographier le réseau hydrographique des régions à fortes couvertures nuageuses.

Sur le croisement (ERS + SPOT) ont été superposées les données sur l'occupation du sol pour vérifier la possibilité de réaliser des cartographies multidates et calculer ainsi la consommation de l'espace naturel et/ou agricole pour l'urbanisation (cf. illustrations ci-après).

Conclusion

Conçue en tant qu'expérimentation, l'imagerie radar est un apport indéniable surtout pour l'hydrographie et la géomorphologie. Cet outil peut pallier le manque d'information pour les régions où la couverture nuageuse est importante. Outre les applications citées ci-avant, les images ERS peuvent être utilisées pour élaborer des schémas régionaux d'organisation de l'espace. Fusionnée aux données optiques (SPOT ou Landsat), cette source d'information peut s'avérer très performante pour élaborer des inventaires d'occupation du sol, informations clés pour la réalisation de schémas directeurs d'aménagement et d'urbanisme. Ces premiers resultats nous permettent d'espérer le développement futur d'autres applications dans ce domaine.


Image ERS1 + Réseau hydrographique - BRASILIA


Image SPOT - BRASILIA
20 Juillet 1987

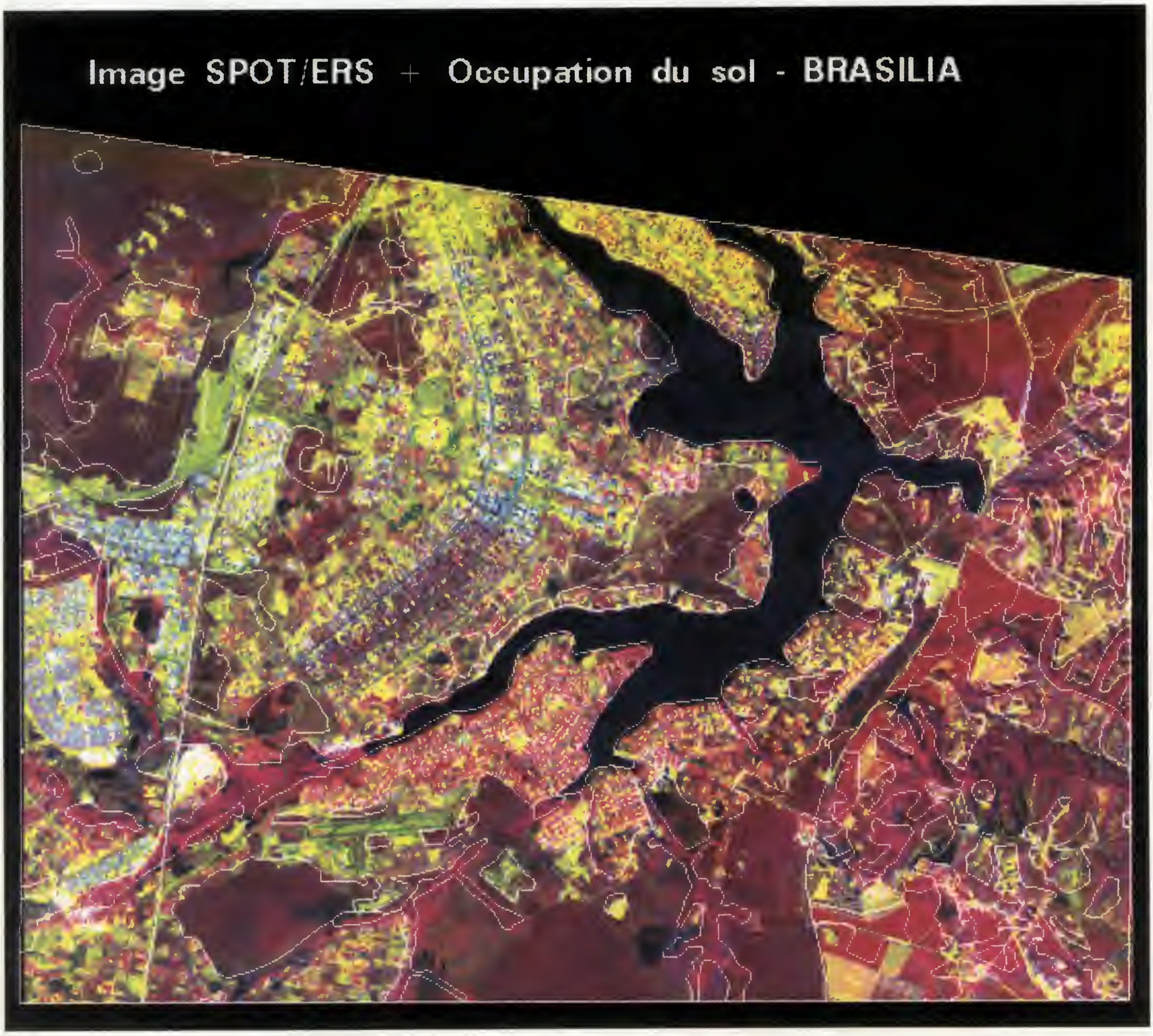

en rouge : agriculture
en rose vif : forêt galérie
en rose clair : végétation naturelle
en jaune : végétation herbacée
en vert : sol latéritique
en bleu clair : urbain
en bleu foncé : eau
en blanc : sol nu

Pour l'image SPOT :
© CNES. 1987
Distribution SPOT Image

Image ERS 1
05 juin 1992

Occupation du sol simplifiée - Brasilia

IAURIF - CODEPLAN

1990

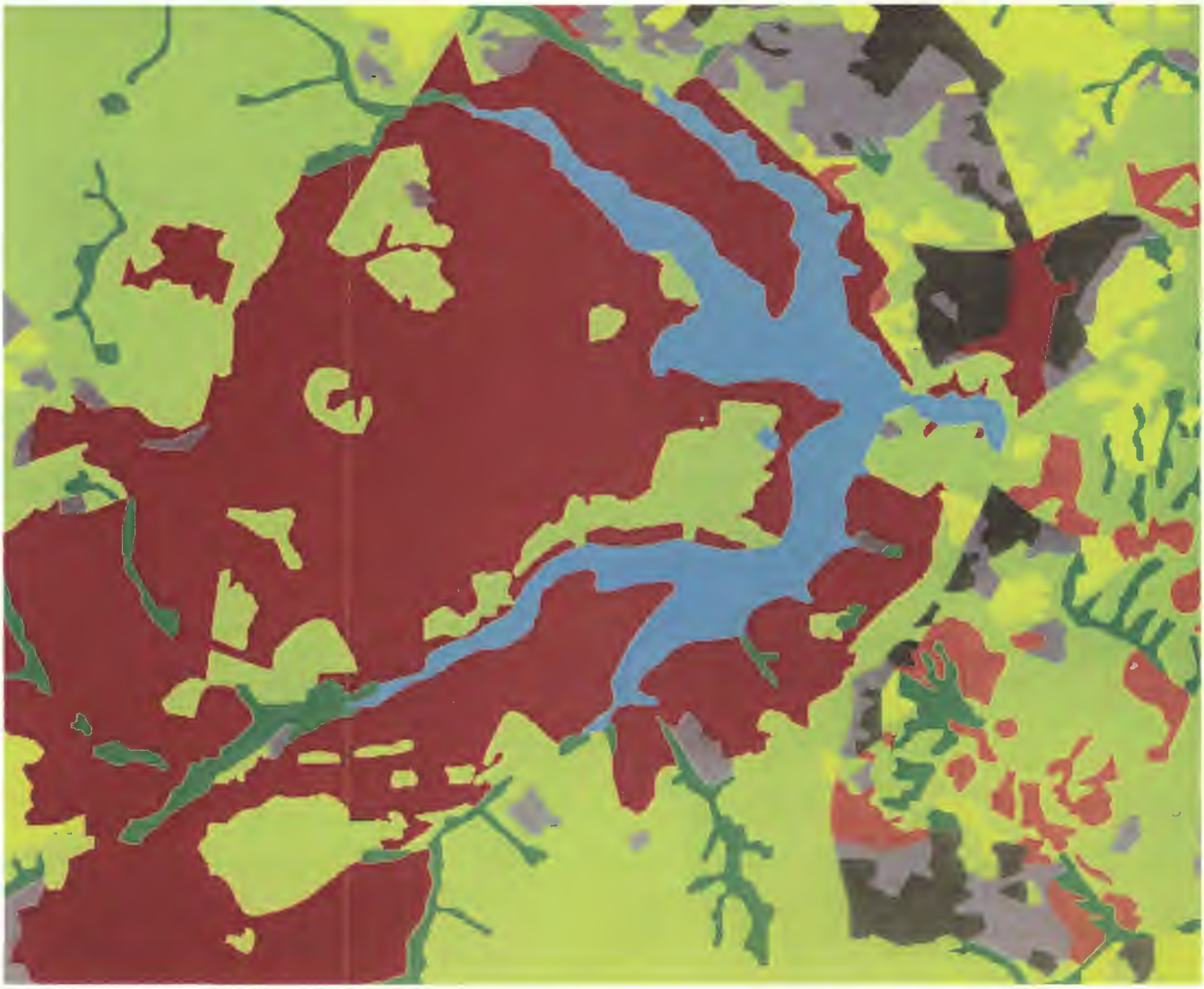

en rouge : espace urbain consolidé

en orange : espace urbain non consolidé

en jaune : zone rurale

en vert foncé : bois et zone humide

en vert pâle : savane arbustive et herbacée

en gris : déboisement, sol nu, brûlis

en bleu : lac, plan d'eau

Second ERS Applications Workshop
London 6-8 December 1995
ESA - Queen Elizabeth II Conference Centre

Project code:
PE.FAO.R01

COMPLEX USE OF RADAR AND OPTICAL & IR REMOTE SENSING DATA FOR SPECIFIC APPLICATIONS ON THE DANUBE DELTA, THE CONTINENTAL PLATFORM OF THE BLACK SEA AND THE SEISMIC ZONE VRANCEA.

Nicolaie OPRESCU

Technical Univ. of Civil Engineering, Remote Sensing Lab,B-dul Lacul Tei 123,Sect.2,code 72302,Bucharest Romania,T./ F: +40 1312 7780.

Cora BRĂESCU,Adrian PETRICA,Anca POP,Florin ŞERBAN

Institute of Optoelectronics,Remote Sensing Department,T./F. +40 1312 4545

Manuel VAIS

Romanian Oil Corporation PETROM, Computing Centre,T./F. + 40 1659 7140

Bucharest - ROMANIA

ABSTRACT

In the ***introduction - background - aims*** are presented: the situation in the transition - reform period, throungh which our country is now passing, the structural changes, some difficulties; it describes also some leading ideas and aims. After a brief presentation of the characteristics of the chosen *test zone,* the present *available means* are described:

a) graphic station - supercomputer TITAN and EASI/PACE software;

b) remote sensing terrain laboratory, situated in the Danuble Delta;

c) aero - satellite recordings.

Data processing and other actions carried out: acquiring and homogenising-compatibilisation of data, rectifying and registration of the recordings, segmentation of the SAR - ERS images, filters for attenuating the speckle type noise, other processings: RGB and IHS color composites, including RGB - IHS - RGB transforms, supervised and unsupervised classifications, different types of contrast streching methods, principal components, comparaisons between the results, using also the comfusion matrix.

Obtained results:

a) monitoring of the "red blossoming"-biological pollution and the oil slicks type pollution, in the coastal zone;

b) monitoring of the morphological coastal modifications;

c) monitoring of the sediment discharge and depositing regime in the sea;

d) seasonal vegetation indices, together with reducing the number of the needed satellite recordings for some of the thematics.

In the final part of the paper some *proposals for further developments* are made.

1. INTRODUCTION - BACKGROUND - AIMS.

In Romania, as well as in the other Central / Eastern European countries crossing this period of transition and reforms, we can see some characteristics focused, in this case, on remote sensing specific:

- The remote sensing problem applied in various branches of national economy is facing the major hindrance: the lack of satellite recordings, or the lack of money to provide them. We have to use at a maximum level the few satellite recordings we have, which we have got from international cooperations, so we cannot conceive and run programs that need some types of recordings, from adequate and precise dates:

- Practical, satellite recordings we receive in programs and projects of international cooperation, are "historic" by the time they come to us so they can't be used for fast and medium time variable objects and phenomena.

- Ground determinations necessary in remote sensing process are not done at the satellite passing dates, but by the calendar of specialised organisations, and not beeing adapted to the specific needs of remote sensing.

- The lack of specific and clear rules for satellite recordings circulation between institutions and organisations in our country makes the adequate use of this recordings even more difficult.

- The lack of standardisation, and the incompatibility between existing hard & soft systems of remote sensing (some of them quite sophisticated and performant) hinder the experience exchange and technology transfer between users, and the "team spirit" efectively working in multi & interdisciplinary system - so needed în this domain cannot be achieved.

- However, the remote sesing, beeing in some cases the only way to solve some of the modern life problems, at a national level (the whole country), but mainly uncentralised, must be promoted even in our hard economic - financial conditions.

So, our reentrance in Europe and in the World takes real sacrifices from us; but we like to express our wish and intentions not to lose touch with the advanced and top technologies.

The issue of mapping and thematic determinations for our country in this transition and reforms, as well as the inherent difficulties we face must be directly connected with structural changes in principles, technique and methodology of this very dynamic domain, including the imminent appearance and disponibility of high power satellite recordings of geometric and radiometric resolutions; this last aspect makes us to reconsider the technological process of remote sensing, in hybrid and analogical processing methods, digital respectively, on other bases, reviewing the possibility of adequate use of analogical photogrammetry - classic systems, analytic and digital.

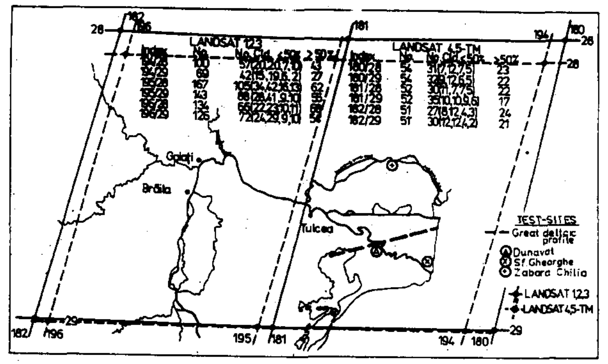

Figure 1.
LANDSAT coverage over the area : no.57(20-Sp,20-Sm,7-A,10_W) Sp-Spring;Sm-Summer;A-Autumn;W-Winter

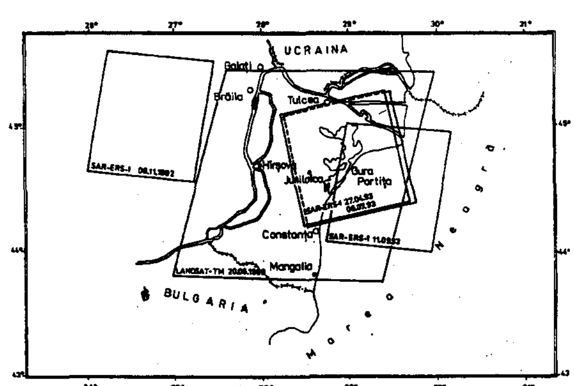

Figure 2.
Evidence of SAR - ERS - 1 PRI and LANDSAT TM recordings over the area which are already have at our disposal, with the positioning of the "in-situ "data determinations.

Basic and guiding ideas for treating and solving complex problems by remote sensing refere to:

(a) establishing the specific strict necessary needs of users at territorial, regional and local level, by priorities, hierarchy, by importance and urgence reasons;

(b) the focusing of interest and efforts on the terrestrial segment of the chain of remote sensing processing and generally of the available systems we have, as well as to reduce to a minimum point (strictly necessary) of the number of satellite recordings for the purposed thematic;

(c) hierarchaly use of the ways of data processing methods and analysis, analogical, hybrid and digital strictly necessary, with effective integration of endo and exogene parameters sources after their relative or absolute compatibilisation (reference system, calibration- , registration-synergism, etc.);

(d) the technology transfer ways serie directly to the users is closely and continuously watched, as step by step this verified and tested technology can be properly launched.

(e) usually, we achieve the ground sampling with pancromatic and sometimes with color IR aerophotograms due to the very dificult field condition .

2. TEST - SITE

The Danuble Delta is one of Europe's most extensive wetlands in a natural state; it forms a unique series of interrelated ecosystems, with its large reed beds, maze of with their mosaic of ferests and semi-arid grasslands; the Delta ecosystems cover about 564.000 ha; of this 442.000 ha lie within Romania.

The Danube Delta and the coastal zone of the Black Sea represent areas of high scientific interest; the Danube Delta represents the world's largest surface compactly covered with rush (reed); this interest grew because the Danube Delta was declared in 1990 a natural reservation of the Biosphere.

The macro characteristics of the choicen test - site are more significantly, because this test - site includes the continental platforme of the Black Sea, the Danube Delta, the last part of the Danube lower basin and a hill - mountain zone with a great seismic interest the Vrancea Zone in turning Carpatians.

The means and available possibilities and the ones beeing in elaboration process are also mentioned.

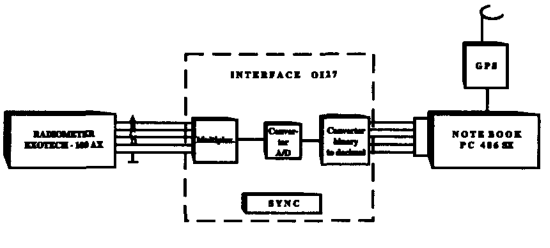

Figure 4.
The system configuration for recording and processing of the radiometric values - digital one, using a professional interface 0127 and PC note-book 486SX.(in the future connected with GPS and videography).

(1) Graphical Station for processing Aero-Satellite recordings (hardware: super computer TITAN 3000 with graphic terminals and peripherals; software:

X Windows System - V.11R5, EASI/PACE (V. 5.3), DORE (V. 5.2), AVS (V. 5.0));

(2) Equipment for acquisition and management "in situ" data gathering: Exotech 100 AX Radiometer (with filters for LANDSAT MSS & TM) linked with a notebook 486 DX2(see fig 4); a terrain remote sensing laboratory in the Danube Delta with geometric and radiometric targeting (see fig 3):

(3) we have 3 available recordings ERS-1 PRI taken on the 30.04; 09.07 and 13.08.1993 and also some SPOT and LANDSAT MSS & TM, and also repetitive aerial photos.

3. PRELIMINARY ACTIONS AND PRE-PROCESSINGS:

3.1. Acquisitionig and homogenising-compatibilising of endogene and exogene parameters;

- the 3 multitemporal recordings SAR-ERS-1 PRI;
- repetitive recordings LANDSAT MSS & TM and SPOT;
- aerial repetitive panchromatic photos, IR and color IR;
- topographic maps with contour lines at 0.25m, pedological maps,
- piezometric profiles, hydrological data, metheo data, quantitative and qualitative profiles, coastal evolution determinations; a.s.o.

3.1.1. The three ERS recordings rectifying, taking into account of the first one;

3.1.2. The registration of the LANDSAT MSS & TM and SPOT recordings;

3.1.3. The synergism between MSS & TM and SPOT recordings with SAR - ERS taken as reference (principaly it's been taken the best resolution recording as base);

3.1.4. Marine drilling profiles and their afferent classical determinations positioning on the aerial satellite recordings;

3.1.5. Radiometric seasonal profiles built on characteristic and suggestive directions, basicaly on the "Great Deltaic Profile"; and on different ecosystems (see fig 5);

3.2. Preliminary processings of SAR - ERS recordings, taken as relative reference level;

3.2.1. ERS recordings segmentation:

(a) on ecosystems bases;

(b) on hydrographic basins and microbasins bases;

(c) visual, with succesive adjustments using pdf (Probability Density Function);

3.2.2. Speckle attenuations using:

(a) adaptive filters;

(b) geometric filters; these filtrations are operated on the whole recording or on wide hetherogene areas, respectively on image segments,with visualisations before and after the application of the filters, with comparaisons of the obtained pdf;

3.2.3. Color - composed RGB and IHS system processings, as well as transformations from RGB to IHS, on the hole recordings (or wide areas), on image segmentations respectively.

3.3. Preliminary processings of the satellite recordings in optical domain:

(a) the transposition of the operated image segmentations, from ERS to the optical ones;

(b) density slicings, equalizations and hystogram matching - separate on TM 6 band on image segments;

(c) the edges enhancement and the thematic constrast enhancement on spectral bands combinations.

4. IMAGE PROCESSING.

4.1 Processings using Radar recordings combinations and from optical domain: supervised and unsupervised classifications usig M.L.R. (maximum likelyhood rule) and NN (nearest neighbour) algorithms, results comparaisons with confusion matrix use;

4.2 Because the principal components analysis (PCA) is a statistical thechnique that transforms a multivariate data set consisting of intercorrelated spectral bands into an uncorrelated data set, with a geometrical dimention less than geometrical dimention of original multispectral image,we applied this thechnique at LANDSAT MSS images,and we verify the signal - to - noise ratio theory (Santiesteban & Munoz - 1978).

5. OBTAINED RESULTS:

5.1. Improvement of the contoure lines in some areas with microrelief zones, using radar recordings on the dry - normal periods.

5.2 Monitoring - control of the "red blossoming" - biological pollution in the coastal area of the Black Sea between Niepre Lagoon and Bosphorus (cca 650 km. see fig. 18).

5.3 Monitoring of the oil slices type pollution on the sea especially in area of drilling platforms.

5.4 Monitoring of the morphological evolution of the coastal regime, especially on the Sachalin Island in the period 1972 - 1993.

5.5 The sediments discharge in the Black Sea, on the Danube mouths and the coastal zone of the Black Sea (see fig.17).

5.6 A significant result is the use of historichal LANDSAT data and of the ERS recording type and also the reduction, for some applications of the number of the needed recordings, using radiometric determinations on the characteristic profiles which are to be made seasonaly.

5.7 Using the confusion matrix an accuracy of classification of about 92% are obtained.

6.PROPOSALS, FURTHER DEVELOPMENTS

6.1 Approaching and solving of some fundamental problems, connected with:

- monitoring of our national hydro-energetic system, respectively hidroameliorative, mainly using RADAR recordings;
- monitoring & control of the great area which are potential land-slides, using ERS recordings, and also

monitoring of the potential disasters areas including seismic zone VRANCEA;

- monitoring of the evolution of the Deltaic subsidence at the great flood and at the normal cicles;
- to conceive and to built the DEM (Digital elevation model) - DTM (Digital terrain model) especially for microrelief areas, using ERS recordings with exagerate altitudinal scale;
- conceiving the targeting system for ERS recordings in the frame of our field remote sensing laboratory situated in the Danube Delta.
- we intend to use the Signal-to-noise ratio theory for multitemporal SAR - ERS images treated as a single data set, in order to attenuate the noise of this image;
- we intend to use the corelation matrix in order to select the most semnificative three bands for a color composite RGB image representation.

6.2 From organisatoring point of view:

- exchange in the partenership system of the characteristic "windows" of the all SAR - ERS "modes", from ascending and descending node.

Last, but not least, we would like to express our wish and intention not to lose touch with the advanced and top technologies, even in the rather difficult conditions we are passing through.

ACKNOWLEDGMENTS.

This work is the result of a collaboration between the **Remote Sensing Laboratory - Technical University of Civil Engeneering Bucharest, Institute of Optoelectronics Remote Sensing Department** and **Computing Centre of Romanian Oil Corporation** under tutorial of the **Romanian Space Agency**, in the frame of the pilot project PE.FAO.R01. and **European Space Agency** support.

7.REFERENCES:

/1/ N.Oprescu, "Use of LANDSAT data for narural resources investigation in the lower Basin of Danube and Danube Delta" agreement with NASA no:G-27940 - Final report - 1976 - 74pp.

/2/ B.D.Tapley et.al., "Oceanographic results from analysis of ERS - 1 altimetry" 1993 Proceedings of the Second ERS - 1 Symposium.

/3/ J.Vogelzang,G.J.Wensink et. al., "Mapping of the Sea Bottom Topography with ERS - 1 C - Band SAR." 1993 Proceedings of the Second ERS - 1 Symposium.

/4/ N.Oprescu et.al. "Romania case study: use of ERS - 1 SAR data for land - use monitoring and for soil moisture assessment;contribution to monitor the privatisation process in territorial profile." ESA/FAO/EEC/Telespazio Workshop ESA Esrin Frascati nov.1993.

/5/ V.S.Frost et.al. "A model for RADAR images and its application to adaptive digital filtering of multiplicative noise" I.E.E.E.Transactions on pattern analysis and Machine Intelligence,vol PAMI - 4, no.2,March 1982.

/6/ N.Oprescu et.al. "Technological researches and developments,regarding the integration of SAR - ERS data with other types of satellite and ground information ,as well as determining their complementarity with applications over the continental platform of the Black Sea, the Danube Delta and the seismic zone Vrancea." Proceedings of the First Workshop on ERS - 1 Pilot Projects, Toledo Spain, 1994.

/7/ J.F.Dallemand,J.Lichtenegger et. al.,"ERS - 1 SAR and optical data for land use/land cover mapping",Proc.of the second ERS - 1 Symposium, 11 - 14 oct.1993 Hamburg Germany.

/8/ C.Pringle,G.Vellidis,et.al.,"Environmental Problems of the Danube Delta",American Scientist, July-August, 1993, vol.81,p.350-361.

/9/ A.Santisteban,L.Munoz, " Principal components of a multispectral image: application to a geological problem." I.B.M. Journal of research and development 1978, vol 22, no 5 p.443 - 586

LIST OF FIGURES

Figure 3. The field Remote-Sensing Laboratory from Danube Delta and the system to calibrate – validate geometric and radiometric data.

Figure 5. The track of the 'great deltaic profile' and sea positioning.

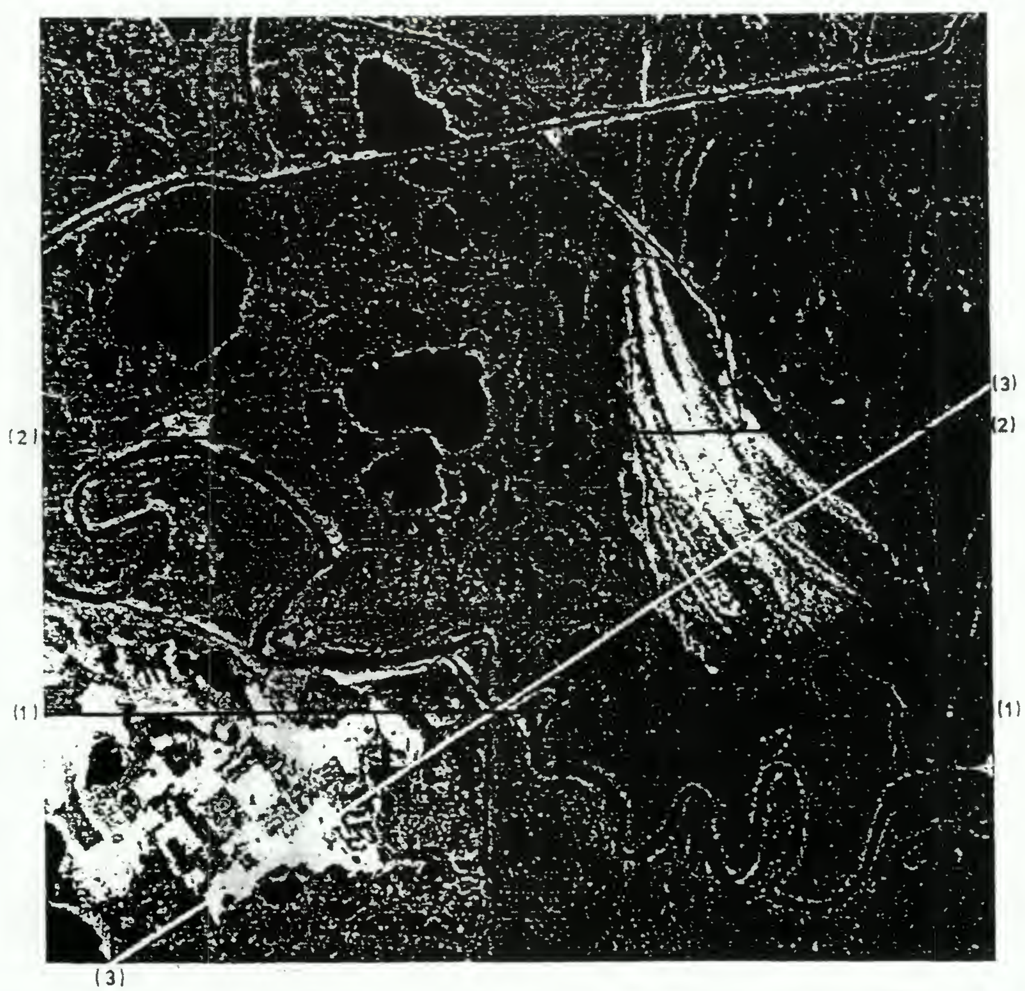

Figure 6. Positioning of the radiometric profile along the scanning line of the ERS-1 SAR recording passing (1) over the Remote-Sensing Laboratory of T.U. of Civil Engineering of Bucharest; (2) over the Caraorman region of the Danube Delta; (3) over the 'great deltaic profile'.

Figure 7.

Semnificative deltaic recording.
LANDSAT TM 4.

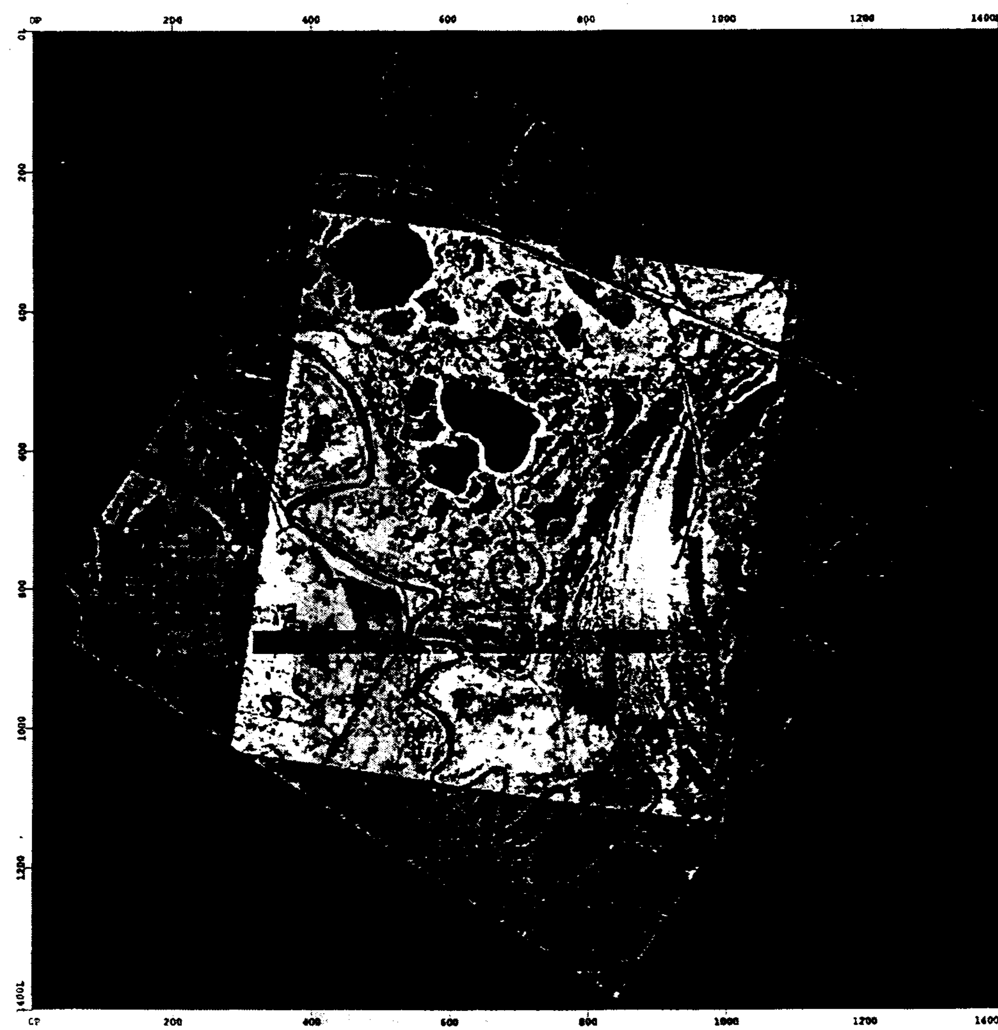

Figure 8.

Composite image black - white SAR ERS - TM
Classification on great deltaic profile

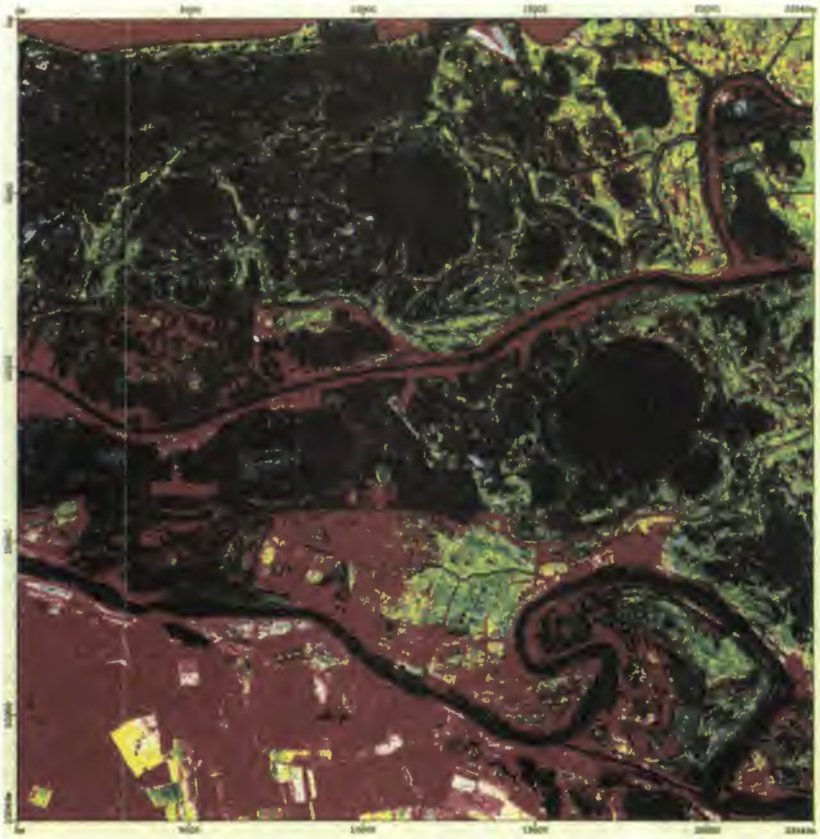

Figure 9.

Color composite for a part of zone
LANDSAT TM from 20.08.1989

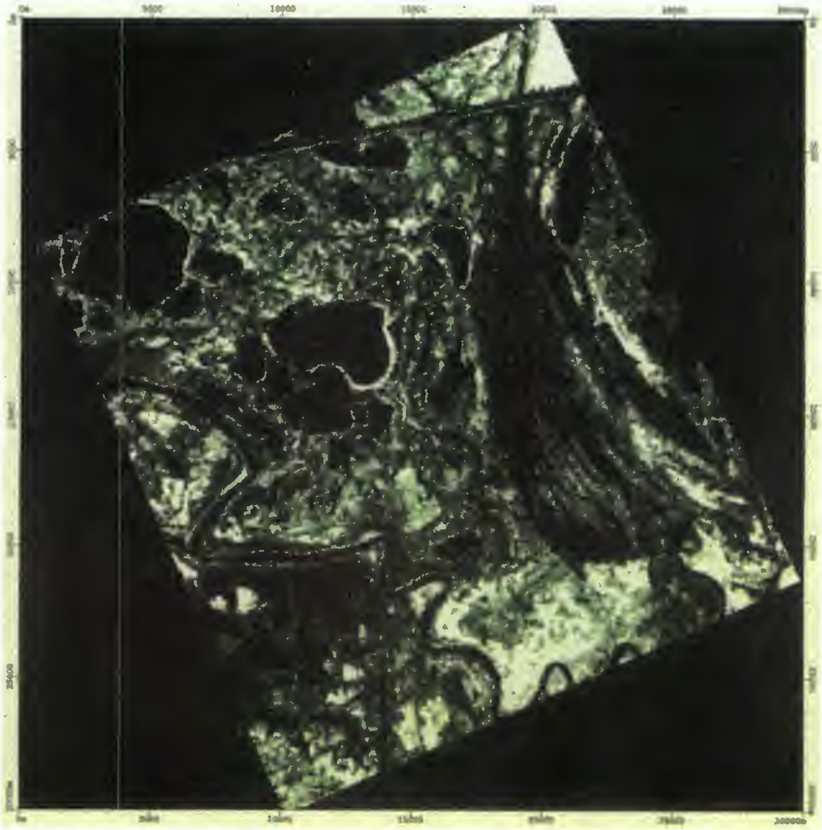

Figure 10.

Synergism and RGB-IHS-RGB transform on TM 2,5,7;
the intensity ch. was replaced with the SAR-ERS apr.93 image.

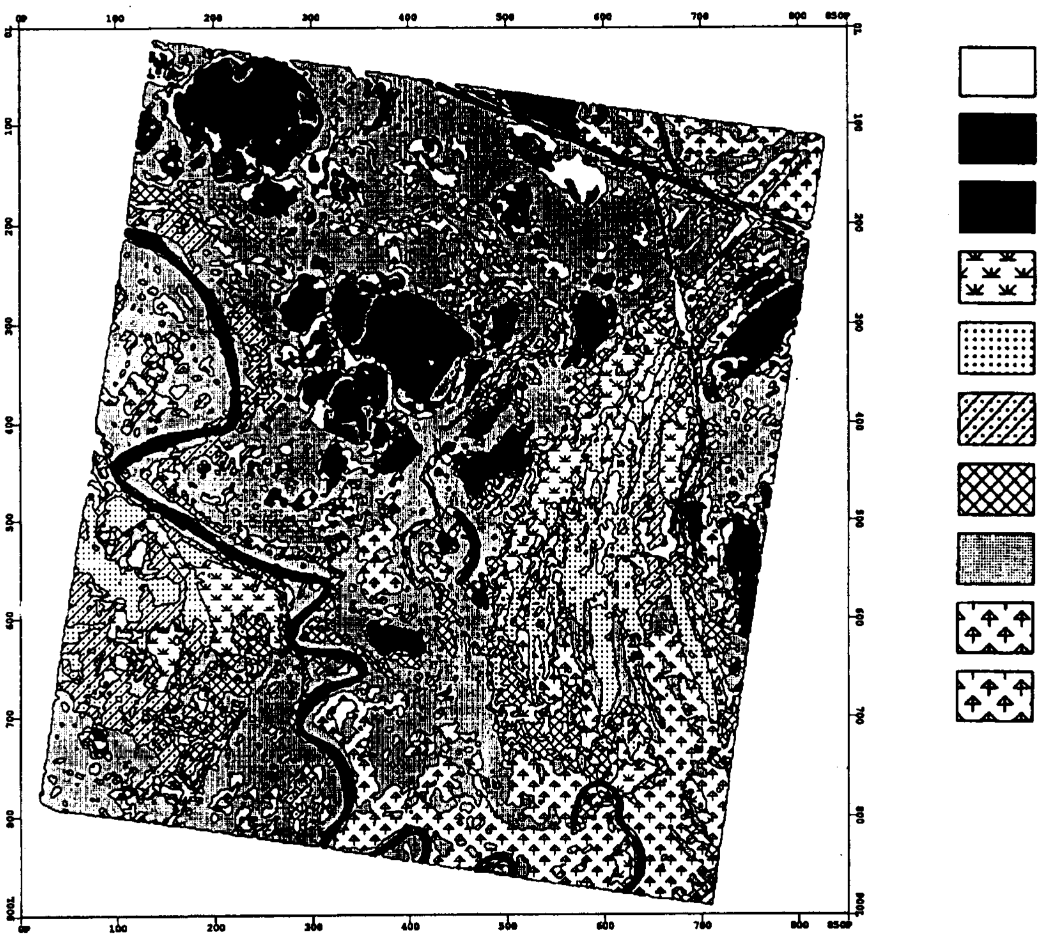

Figure 11
Thematic map with 9 classes made by extension of classification on great deltaic profile

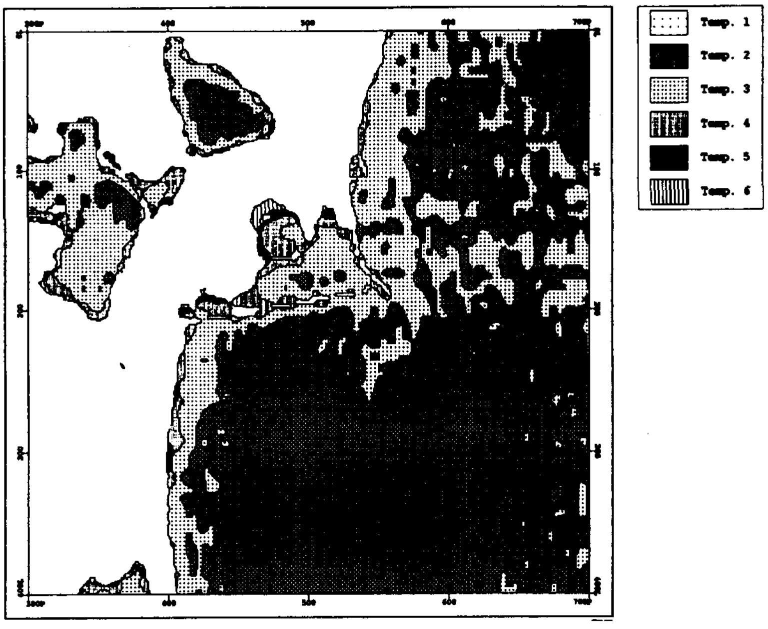

Figure 12
Map of temperatures from the zone based on LANDSAT TM6

Figure 13.

Turbulence in Portita zone.

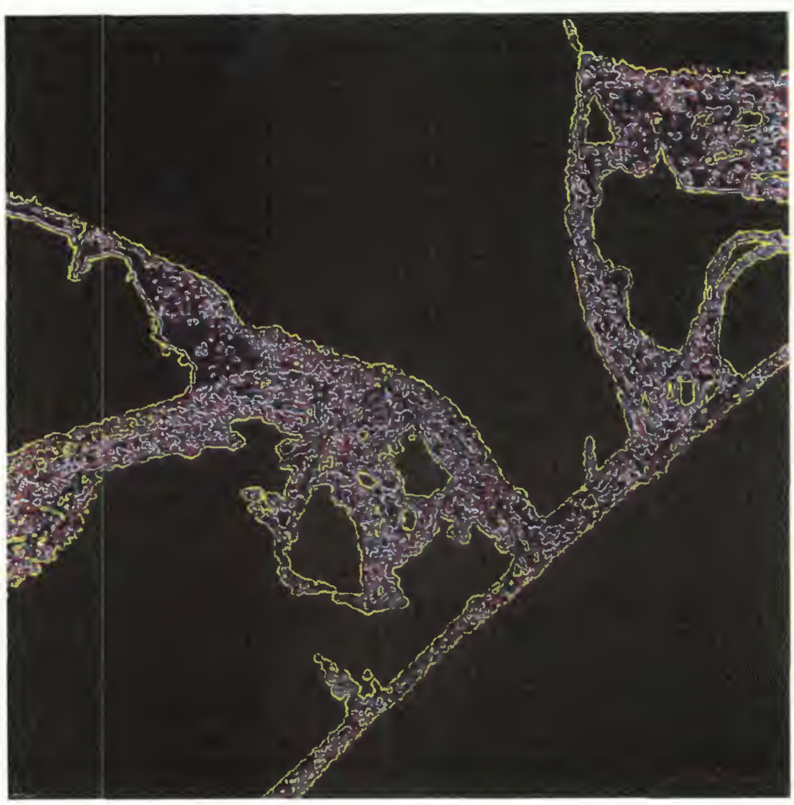

Figure 14.

Portita zone - edge detection on ERS - 1 SAR PRI images.
red 27.04.93; cyan 06.07.93; yellow coastal profile.

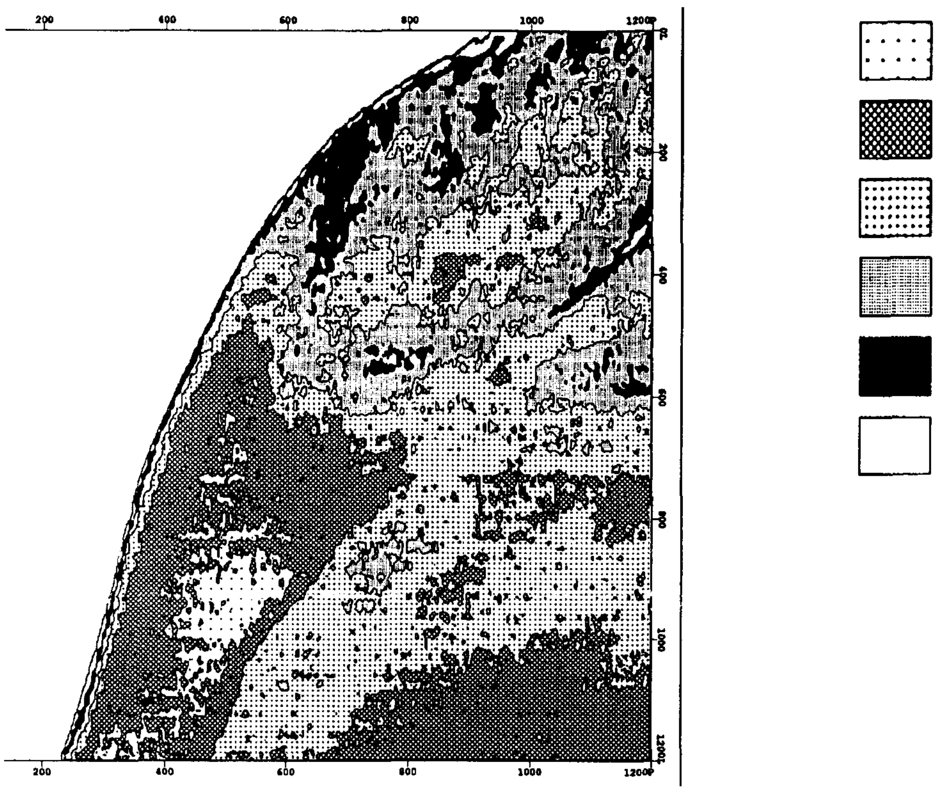

Figure 15

Portita zone - Classification on the LANDSAT TM, with modal filter

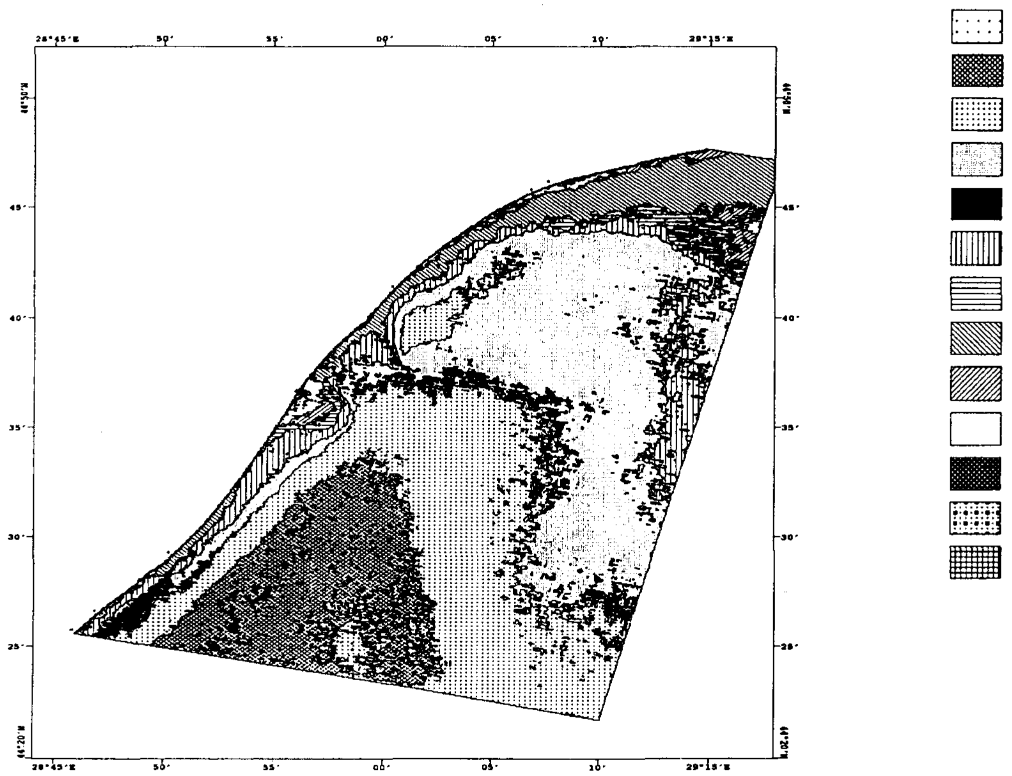

Figure 16

Portita zone - Periboina Classification on the LANDSAT MSS 4,5 with modal filter 5 x 5.

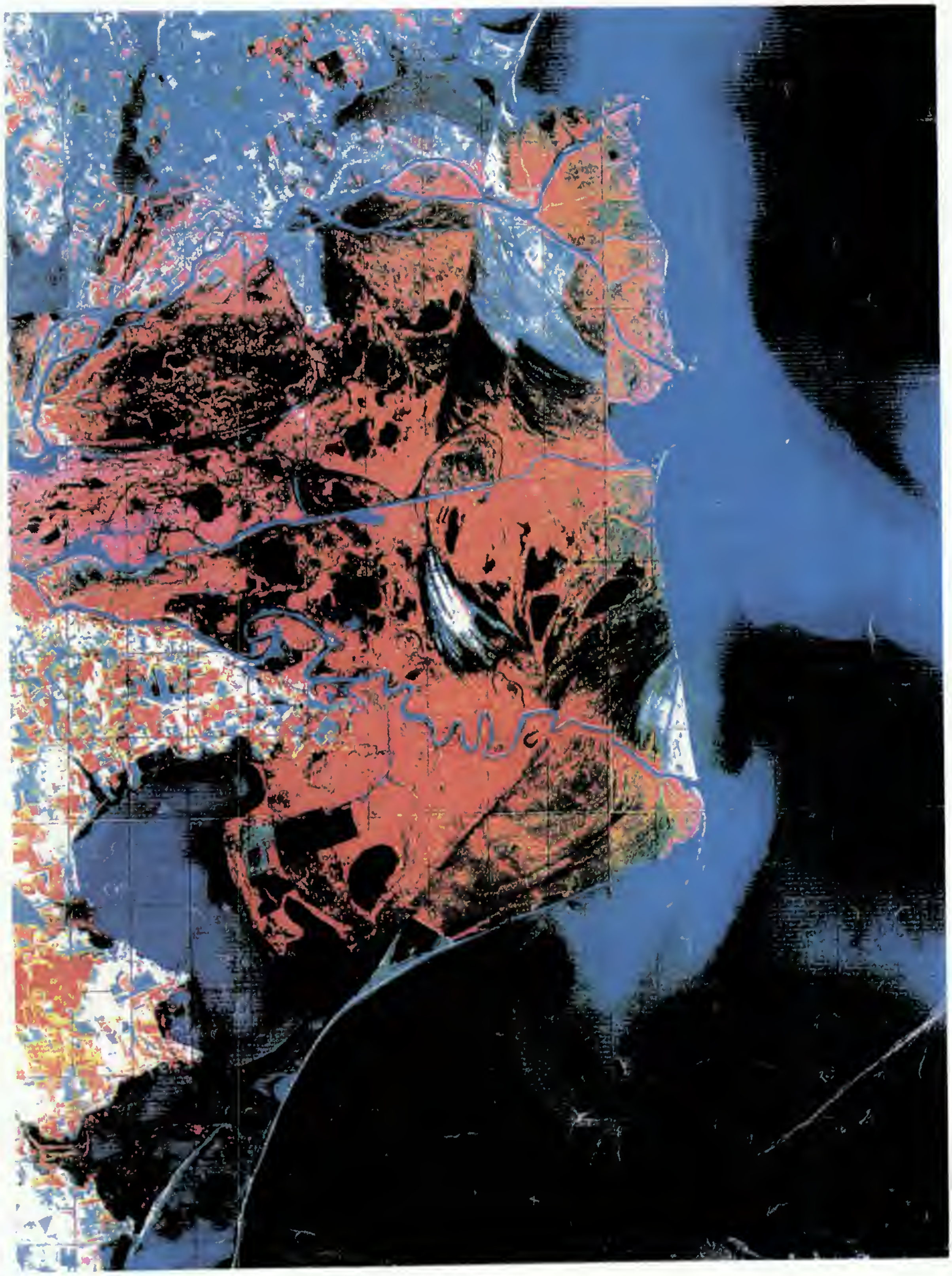

Figure 17.

The sediment discharges and depositing regime in the sea.
Thematic mapping of the Danube Delta.

Figure 18.

"Red blossoming" phenomenon - biological pollution, monitored with satellite recordings (LANDSAT MSS) in romanian coastal area - analogical processing.

ERS–1 DATA ASSIMILATION IN A SECOND GENERATION WAVE MODEL FOR THE NORTH SEA

F. Ovidio[1], J.-R. Bidlot[1], D. Van den Eynde[1], W. Luo[2] and J. Monbaliu[2]

[1]*Management Unit of the Mathematical Model of the North Sea* (MUMM)
100 Gulledelle, B–1200 Brussels, Belgium

[2]*Catholic University of Leuven* (KUL)
de Croylaan 2, B–3001 Heverlee, Belgium

ABSTRACT

This paper presents the impact of ERS–1 altimeter data assimilation in a second generation wave model for the North Sea. The optimal interpolation scheme, the techniques for splitting the analysed significant wave height field and the reconstruction of the wind sea spectra are described. The reference and assimilation run are compared to independant buoy data. It is found that the prediction are globally improved in the coarse grid, but that the impact is not significant in the fine grid.

1. MODEL

The MU-WAVE model (Van den Eynde, 1992) is composed of different modules. The core of the system is formed by the second generation wave model HYPAS (Günther and Rosenthal, 1985) which combines the traditional approach of independent calculation of swell energy for each frequency and direction through a ray technique, with a parametrical wind sea model, using the parameters of the JONSWAP spectrum (Hasselmann *et al.*, 1973) and the mean wind sea direction as prognostic variables. Some shallow water effects, such as shoaling, are included. The model is implemented on two nested grids. The coarse grid (Figure 1) has a 50 km × 50 km resolution (stereographic projection) and covers the entire North Sea to intercept swell generated far away that may travel to the Belgian coast. In MU-WAVE, the open boundaries are treated as walls where limited fetch laws are applied. In front of the Belgian coast, a higher resolution is needed to account for the complex bathymetry of the Flemish Banks. A 10 km × 10 km fine grid is used (Figure 2), coupled to the coarse grid through the open boundaries. MU-WAVE uses the wind fields of the United Kingdom Meteorological Office (UKMO) as forcing. Analysed fields or forecasts are used depending on their availability. They are interpolated to the stereographical coarse grid.

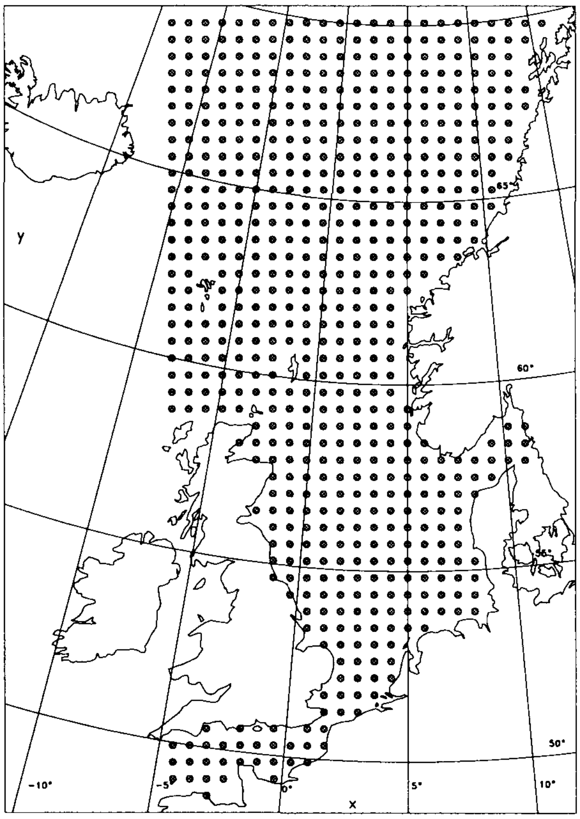

Figure 1. Coarse grid domain and active grid points.

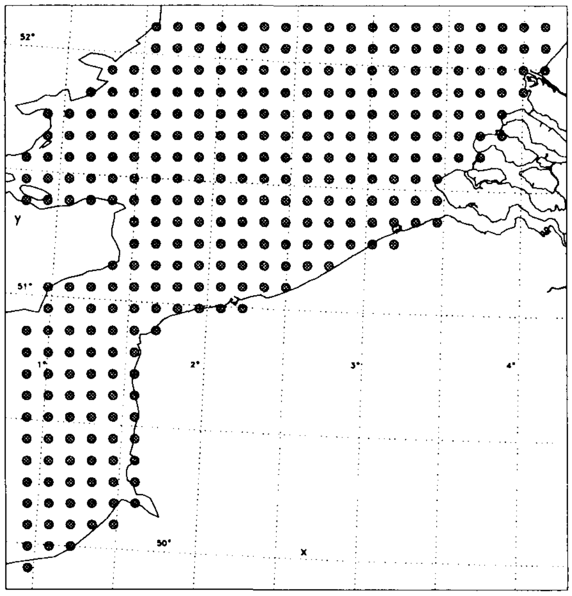

Figure 2. Fine grid model domain and active grid points.

2. SATELLITE AND BUOY DATA

We obtained ERS–1 fast delivery altimeter data from ESA as part of Pilot Project PP2–B9, from October 1992 to March 1993. Along the altimeter track, groups of eight consecutive observations are constructed, out of which a mean is computed. This procedure smoothes the raw data and leads to data points spacing from about 52 km, which is close to the resolution of the coarse grid. Then each data point is relocated to the nearest model grid point. The *RijksInsituut voor Kust en Zee* (The Netherlands) and the *Afdeling Waterwegen Kust* (Belgium) provided buoy data. Buoy locations are displayed in Table 1.

Table 1. Wave stations

Station	Code	Latitude	Longitude
Platform Auk	AUK	56°23'59"N	2°03'56"E
Platform k13	K13	53°12'03"N	4°35'18"E
Meetpost Noordwijk	MPN	52°16'26"N	4°17'46"E
Westhinder	WEH	51°55'05"N	2°26'30"E
Akkaert	AKK	51°24'49"N	2°46'18"E
A2-Buoy	A2B	51°21'58"N	3°07'47"E
Bol van Heist	BHE	51°22'46"N	3°12'32"E

AUK, K13 and MPN are located only in the coarse grid domain, while WEH, AKK, A2B and BHE lie in the fine grid as well. Data at these last four buoys were only available for the months of October-November 1992 and February 1993. Statistics will only be presented for these three months in order to make a comparison between the impact of data assimilation on the coarse and fine grid results. AUK is located in deeper water (90m). The depth at the fine grid buoys ranges from 17m (WEH) to only 7.5m (BHE). We used a 3-hour smoothing on all buoy data before comparing them to the model results.

3. DATA ASSIMILATION METHOD

We opted for an optimal interpolation scheme, described in Mastenbroek *et al.* (1994), in which all observations available in a 6–hour time window are used to construct the most likely estimate of the field at the middle time of the window. By comparing those data with buoy measurements, it is possible to estimate the error that can be associated with these data. This estimate is indeed an important parameter of the data assimilation scheme. Table 2 summarises some of the available wave data comparisons including our own, despite the limited number of correlations.

Table 2. Statistics for the ERS–1 fast delivery product wave data inferred from comparisons with buoy measurements as compiled by three authors. Negative bias means the satellite deduced parameter overestimates the buoy observations. The linear regression is defined by $Hs_{sat}=aHs_{buoy}+b$ and could be used to correct the systematic overprediction of the satellite SWH measurements, as done in Mastenbroek *et al.* (1994).

	Queffeulou *et al.* (1995)	Mastenbroek *et al.* (1994)	This study
Buoys location	N. Atl. & Pac. Ocean, NOAA	North Sea	North Sea
Nb. of correlated data points	279	85	42
standard deviation σ^o (m)	0.39	0.41	0.31
total bias (m)	0.04	0.02	-0.13
linear regr. *a*	0.75	0.80	0.82
b	0.54	0.39	0.46

As discussed in Mastenbroek *et al.* (1994), there are different sources of error that cause the observed buoy-altimeter discrepancy. An estimate of the maximum error of the averaged altimeter observation can nevertheless be obtained by assuming that all other error sources give a smaller contribution to the scatter than the systematic errors in the altimeter wave height :

$$\sigma^o = \max(0.4\text{m}\,; 0.08H_s) \tag{1}$$

Following Queffeulou's discussion and our limited analysis, we choose for the altimeter wind speed error

$$\sigma^o = 1.5 \text{ m s}^{-1} \tag{2}$$

It is a simple matter to group the satellite data in time windows centred at t=0, 6, 12, ... hour. This procedure results in uneven groups of up to 40 data points as illustrated in figure 3 which shows that the assimilation procedure will only use a small number of data points (if any) at each assimilation step.

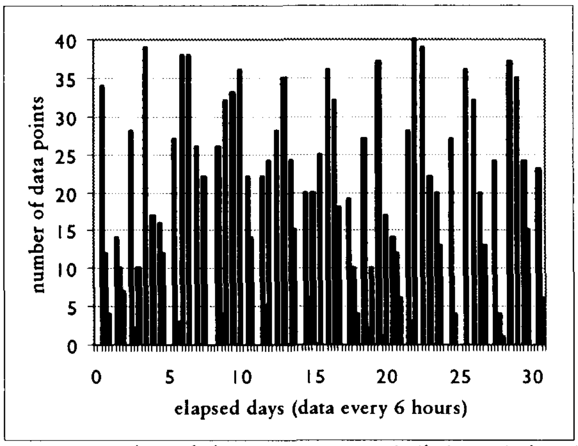

Figure 3. Number of data points per assimilation window in October 1992.

3.1. *Analysed fields*

One of the first steps in the assimilation procedure requires the computation of the analysed SWH and wind fields. These fields are obtained by combining the observations with the model first guess values at the model grid points by means of an optimal interpolation scheme which in matrix notation can be written as

$$\Psi^a = \Psi^f + \mathbf{M}\mathbf{C}^T\left(\mathbf{C}\mathbf{M}\mathbf{C}^T + \mathbf{O}\right)^{-1}\left(\mathbf{d}^o - \mathbf{C}\Psi^f\right) \tag{3}$$

where Ψ^a, Ψ^f and $\mathbf{d}^o$ denote respectively the vectors of the analysed, model first guess and observed values. Ψ^a and Ψ^f correspond to the values at each active sea grid points (N^{mod}=649 points) and $\mathbf{d}^o$ collects the N^{ob} satellite data points for the corresponding time window (*t*=0, 6, 12, 18, ...). Those observations do not usually correspond exactly to the model grid value; hence, C is a $N^{mod} \times N^{ob}$ matrix introduced to relate the model grid values to the observation points. The matrix **M** ($N^{mod} \times N^{mod}$) is the error covariance matrix of the model first guesses, and O ($N^{ob} \times N^{ob}$) is the error covariance matrix of the observations. For the sake of simplicity, the simplest possible form is chosen for C, namely projecting each observation onto the nearest active grid point.

The main problem of the optimal interpolation scheme lies in the selection of the standard deviations of the observations and the model as well as the error covariance matrices. We followed a relatively simple method similar to the approach of Mastenbroek *et al.* (1994) in which no account is made of the wind field on the SWH correlations or vice-versa. The actual values of the parameters in the equations below were obtained from the analysis of MU-WAVE model results and ERS-1 altimeter data. As an approximation, we can neglect the errors between different observations. Thus the matrix O is diagonal and the following expression is used:

$$O_{kl} = \delta_{kl}\left(\sigma_k^o\right)^2 \tag{4}$$

We have already discussed the expression of the standard deviation σ_k^o of observation k as given by (1) and (2) for the SWH and the wind observations.

For the model error covariance matrix **M** we took (see Mastenbroek *et al.* 1994)

$$M_{ij} = \begin{cases} \sigma_i^f \sigma_j^f \left(1 + \dfrac{d_{ij}}{d_{corr}}\right) \exp\left(-\dfrac{d_{ij}}{d_{corr}}\right) & d_{ij} \le d_{\max} \\ 0 & d_{ij} \ge d_{\max} \end{cases} \tag{5}$$

where σ_i^f is the model standard deviation at model grid point i, d_{ij} is the distance between grid points i and j (except in the SWH case where d_{ij}=d_{max} if d_{ij} intersects land), d_{corr}=1.8 and d_{max}=10 grid units is a cut-off length. For the standard deviation σ_i^f of the first guess model wave height H_i^f at grid point i we could use an expression that was obtained from a validation of the model at several buoys in the southern North Sea; however it was also found in the 6-month validation using the present satellite and buoy data (Ovidio *et al.*, 1994) that the model error was significantly larger (up to a factor 2) in the northern part of the domain where limited fetch growth laws are used at the open sea boundary condition. To account for this, we introduced a multiplicative factor that varies from 1 in the South to 2 in the North with a rapid transition at the latitude of northern Scotland:

$$\sigma_i^f = \left[1.5 - 0.5\tanh\left(\frac{i-425}{25}\right)\right] \cdot \max\left(0.25\,;0.15 + 0.15 H_i^f\right) \tag{6}$$

since i=1 corresponds to the upper left corner grid point. A similar analysis of the wind field gave

$$\sigma_i^f = 1.7 \text{ m s}^{-1} \tag{7}$$

3.2. Splitting of the analysed wave field

MU-WAVE is a second generation wave model in which wind sea and swell components of the energy spectrum are represented rather differently. Unfortunately, the satellite altimeter data only measures the total energy, as the sum of the contribution of wind sea generated under the direct local influence of the wind, and the different swell components that have propagated from the areas where they were originally created as wind sea. If separate corrections are to be made to each of these wave energy spectrum components, then the proportion of the total analysed energy which is due to each must be estimated. This requires extra information in addition to the analysed SWH as well as a few assumptions that may prove to limit the assimilation efficiency.

We followed the same approach as Thomas (1988) in which the analysed wind is also used to determine the wind sea proportion of analysed energy. The method is based either on the conservation of the wind sea age (the time during which a certain wind has blown over a region to produce a given wind sea energy state) or alternatively on the conservation of the wind sea stage of development parameter γ. Both approaches yield an estimate for the analysed wind sea energy E_{ws}^a from the first guess wind sea energy E_{ws}^f and a given power of the ratio of analysed to first guess wind speed, respectively w^a and w^f :

$$E_{ws}^a = E_{ws}^f \left(\frac{w^a}{w^f}\right)^p \tag{8}$$

with p=2.57 in the first scheme and p=4 in the second one.

E_{ws}^f is a direct model output as MU-WAVE hybrid nature always results in the numerical splitting of the energy spectrum in wind sea and swell contribution. w^a is found by the optimal interpolation on the wind speed. At this point, we assume that the altimeter wind speed is reliable (in agreement with our validation) and that errors in the model wind have resulted in errors in the wind sea which can then be corrected using (8). There is however a limit on E_{ws}^a, as it cannot physically exceed the value of the total analysed energy. In cases where the analysed wind sea energy is less than the total measured energy, the remaining portion of the energy is assumed to be swell. Unfortunately, it is not possible to predefine a swell distribution (as is the case for wind sea) since each swell component is essentially non interacting and not related to the local wind. However, the total swell energy can be corrected by multiplying the model swell components along the characteristics by the ratio of estimated to first guess swell energy. This correction is rather arbitrary as it updates all components without any account of the possible propagation direction of the swell energy and will only update components if they were already present (*i.e.* non zero). This constitutes a major limitation.

3.3. Reconstruction of the wind sea spectrum

In MU-WAVE, prognostic parameters are used to define the wind sea spectral shape, modelled as the product of a directional distribution centred around a mean direction by a one-dimensional energy spectrum. This latter spectrum is determined at each time step by three prognostic parameters, respectively defined as the peak frequency f_m, Phillips' parameter α and the peak enhancement factor γ (Hermans, 1989). The reconstruction of the wind sea spectrum will therefore require the prescription of these three parameters, as no information is available in this study on the actual directional distribution of the wave spectrum; the first guess model directional distribution will be retained. These three parameters were empirically found to mainly be function of the wind speed, the wind sea energy and the water depth (Bouws *et al.*, 1987). These relations were first tried to reconstruct known MU-WAVE spectra, but discrepancies persisted without any apparent reason. It may well be that the model wind sea spectra do not entirely satisfy these empirical formulas. Consequently, we designed an alternative approach by deriving similar relations for f_m directly from the analysis of the model results. γ was approximated by a piecewise linear distribution that best fits the model correlations and α was tuned to satisfy the total energy constraint. Namely, MU-WAVE uses the following approximation to determine the wind sea energy E_{ws}

$$E_{ws} = E_{TAB} \frac{\alpha}{f_m^4} c(\gamma) \tag{9}$$

where E_{TAB} is a tabulated integral, only function of f_m and the water depth D, through $w_m = 2\pi f_m \sqrt{D/g}$:

$$E_{TAB} = \frac{g^2}{5(2\pi)^4} \int_0^\infty \frac{e^{-\frac{5}{4}\xi^{-4}}}{\xi^4 \chi^2 \left[1 + w_m^2 \xi^2 \left(\chi^2 - 1\right)\right]} \, d\xi \tag{10}$$

in which g is the acceleration due to gravity and with χ solution of

$$\chi \tanh\left(w_m^2 \xi^2 \chi\right) = 1 \tag{11}$$

Note that

$$E_{TAB} \to \frac{g^2}{5(2\pi)^4} \text{ as } D \to \infty$$

$c(\gamma)$ is introduced to account for the non fully developped sea state ($\gamma > 1$) :

$$c(\gamma) = \begin{cases} e_1 & \gamma \geq 3 \\ e_2 + \gamma(e_3 + e_4\gamma) & \gamma < 3 \end{cases} \tag{12}$$

with e_1=1.541, e_2=0.1514, e_3=1.0413 and e_4=-0.1927.

The empirical relations can be found if we define the non-dimensional wind sea energy ε and peak frequency ν_m using the wind speed w and g :

$$\varepsilon = \frac{E_{ws} g^2}{w^4} \quad ; \quad \nu_m = \frac{f_m w}{g} \tag{13}$$

For the purpose of this study, we considered shallow (D<40m) and deep water ($D \geq$40m) correlations determined from the analysis of a one-month run (October 1992) :

$$\nu_m = \begin{cases} 0.0213\varepsilon^{-0.3322} & D < 40\text{m} \\ 0.0209\varepsilon^{-0.3376} & D \geq 40\text{m} \end{cases} \tag{14}$$

hence f_m from (13).
γ is then approximated using

$$\gamma = \begin{cases} 1 & \nu_m \leq 0.13 \\ 51.111\nu_m - 5.644 & 0.13 < \nu_m < 0.175 \\ 3.3 & \nu_m \geq 0.175 \end{cases} \tag{15}$$

if D<40m or

$$\gamma = \begin{cases} 1 & \nu_m \leq 0.13 \\ 46\nu_m - 4.98 & 0.13 < \nu_m < 0.18 \\ 3.3 & \nu_m \geq 0.18 \end{cases} \tag{16}$$

if $D \geq$40m. Finally, α is determined from (9). In the actual reconstruction of the wind sea spectrum that follows the determination of the wind sea proportion to the total energy, we used the previous relations by substituting E_{ws} and w with the analysed wind sea energy E^a_{ws} and the corresponding analysed wind speed w_a.

3.4. Update of the wind speed

The effects of the assimilation will only last if the wind speed at later time steps is modified to account for the changes following the assimilation. Indeed, an abrupt return to the first guess wind speed in the following time steps will quickly relax the wind sea back to a state that that would prevail if no assimilation had occured. For that reason, the difference between the analysed and the first guess wind speed at each grid point is used at later time steps to correct the corresponding wind speed value by linearly decreasing the latter difference to zero at the next assimilation time.

4. RESULTS

4.1. Times series

In the following, the bias refers to the difference between the means of buoy data and model results. A positive bias then means an underestimation by the model. The scatter index (S.I.) is defined as in Zambresky (1989) and Romeiser (1993).

Tables 3, 4, 5 and 6 present respectively the computed significant wave height (SWH) and mean wave period (MWP) bias and S.I. for the reference and assimilation runs for the months of October 92, November 92 and February 93, *i.e.* months for which fine grid buoy data were available.

The results for the assimilation runs are still preliminary, and some necessary fine tuning will be made in the near future. We can nevertheless already highlight certain features. First, the effects of the assimilation procedure are clearly visble in the time series of both significant wave height and mean wave period at station AUK (figures 4 and 5). At K13 (figures 6 and 7), effects are already less pronounced.

At this point, following Mastenbroek *et al.* (1994), we can speculate that if the recalibrated altimeter observations, which result from applying the linear fit of the altimeter to buoy observations (Table 2) are used instead, the scatter will be reduced. However, it was also shown to only be valid at the time and place of the assimilation, and that the improvement apparently disappears quickly. In the limited time span of each improved update, the time series (figures 4–7) already support this notion. It appears therefore that enough altimeter data have been assimilated into the model to reduce its bias. Nevertheless, it may well be that this extra wave energy was incoherently supplied to the model as attested by the small reduction of the different scatter indicators. This shortfall suggests that the necessary spectrum reconstruction scheme is inapropriate. If the first guess frequency and angular spectrum differ too much from the actual one, the relatively simple spectrum reconstruction scheme may not produce analysed spectra that lead to a better wave field at later time. As shown below, from the comparison of observed energy spectra with first guess and analysed counterparts, the spectrum reconstruction scheme can fail even in cases where a net positive improvement of the model SWH is obtained.

4.2. *Comparison of observed and modelled spectra*

The location of station AUK is such that it will still be subject to intense low frequency wave systems propagating from different origins. These wave systems have distinctive spectral characteristics; to see how the assimilation procedure handles the reconstruction and update of these wave systems, we can compare the modelled and observed spectra.

Figure 8 illustrates how the spectrum reconstruction benefits from the satellite data assimilation at that time. This is an ideal case in which the wind sea spectrum is updated following the correction of the local SWH and wind speed. This spectrum update is maintained at later time steps (not shown) eventhough the effects of the assimilation are slowly vanishing (on a time span of the order of twelve hours) until an unpredicted wave system appears in the region. For example, the agreement is already less satisfactory in figure 9: the analysed spectrum keeps the first guess structure and totally misses the existence of a second higher frequency peak, more likely linked to a recent shift in the wind direction.

Satisfactory spectrum reconstruction is not limited to single peak spectra as illustrated in 10, but sometimes (as shown in figure 11) it fails to adequatly shift the spectrum peak to lower frequencies. In both previous examples, the assimilation has lead to a satisfactory correction of the SWH (figure 4); however, from the analysis of the evolution of the wave field, it appears that the lack of spectral model wave components at lower frequency in figure 11 can be linked to the inablity of the model to advect enough swell energy from an area to the north where the windsea was converted to swell following a change in wind. Therefore, the assimilation is unable to reconstruct the swell field as it was not present in the first guess solution.

Ultimately, to improve the quality of the analysed wave field, spectral observations should be taken into account in the assimilation procedure. In the future, these observations could be obtained from buoys or satellite SAR measurements. To assimilate such spectra, more elaborate assimilation schemes are needed.

Table 3. Significant wave height bias (m)

	October 92		November 92		February 93	
	Ref.	Assim.	Ref.	Assim.	Ref.	Assim.
AUK	0.36	0.24	0.24	0.18	0.18	0.10
K13	0.16	0.10	0.17	0.13	-0.07	-0.11
MPN	0.17	0.11	0.18	0.14	-0.02	-0.03
WEH	-0.11	-0.11	-0.09	-0.11	-0.19	-0.19
AKK	0.15	0.14	N/A	N/A	-0.13	-0.10
A2B	0.05	0.09	-0.16	-0.17	-0.18	-0.19
BHE	0.09	-0.13	-0.19	-0.21	-0.21	-0.22

Table 4. Significant wave height scatter index

	October 92		November 92		February 93	
	Ref.	Assim.	Ref.	Assim.	Ref.	Assim.
AUK	0.34	0.30	0.21	0.20	0.29	0.24
K13	0.21	0.20	0.20	0.20	0.23	0.24
MPN	0.30	0.29	0.32	0.32	0.33	0.34
WEH	0.17	0.23	0.32	0.32	0.29	0.29
AKK	0.10	0.15	N/A	N/A	0.40	0.36
A2B	0.20	0.23	0.39	0.39	0.30	0.31
BHE	0.14	0.23	0.38	0.39	0.32	0.32

Table 5. Mean wave period bias (s)

	October 92		November 92		February 93	
	Ref.	Assim.	Ref.	Assim.	Ref.	Assim.
AUK	0.69	0.43	0.17	0.07	0.39	0.30
K13	0.30	0.21	0.07	-0.02	0.35	0.26
MPN	0.46	0.36	0.51	0.46	0.37	0.34
WEH	-0.19	-0.21	0.07	0.00	-0.14	-0.19
AKK	-0.15	-0.19	N/A	N/A	-0.25	-0.17
A2B	-0.54	-0.73	-0.81	-0.87	-0.62	-0.69
BHE	-0.10	-0.28	-0.22	-0.29	-0.21	-0.28

Table 6. Mean wave period scatter index

	October 92		November 92		February 93	
	Ref.	Assim.	Ref.	Assim.	Ref.	Assim.
AUK	0.20	0.16	0.13	0.10	0.20	0.20
K13	0.15	0.14	0.12	0.11	0.18	0.17
MPN	0.17	0.15	0.18	0.17	0.17	0.17
WEH	0.16	0.15	0.15	0.15	0.16	0.14
AKK	0.10	0.10	N/A	N/A	0.19	0.18
A2B	0.20	0.23	0.29	0.30	0.22	0.22
BHE	0.14	0.16	0.19	0.20	0.15	0.15

5. CONCLUSIONS

ERS–1 altimeter data has been assimilated in the second generation wave model MU-WAVE using a simple optimal interpolation scheme, and the resulting wave fields were compared to buoy measurement. The bias in the analysed field was significantly reduced. This was not the case for the scatter index of the SWH and the mean wave period. These results are in agreement with those of Mastenbroek *et al.* (1994) obtained with a third generation wave model for the North Sea. A better selection of the different parameters used in the assimilation may slightly improve these preliminary results. However, as already stated *supra*, it may be necessary to include directional information in the assimilation scheme.

6. ACKNOWLEDGEMENTS

This work was carried out in the framework of the European Space Agency Pilot Project PP2–B9. The authors wish to thank ESA for providing the altimeter and scatterometer data.

We also wish to thank the *RijksInsituut voor Kust en Zee* and the *Afdeling Waterwegen Kust* for providing the buoy data.

F. Ovidio and J.-R. Bidlot are funded by the Belgian Science Policy Office, Research Program on Remote Sensing (third phase, TELSAT/III) under convention T3/58/011.

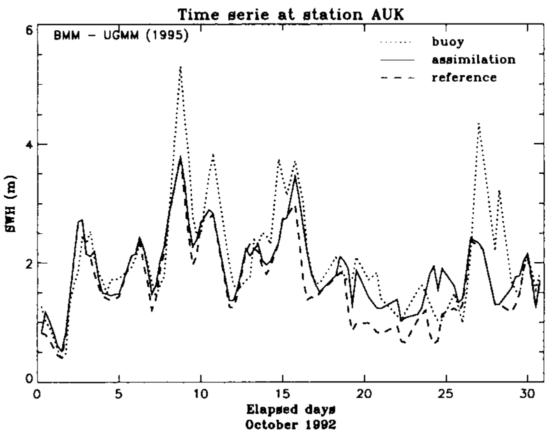

Figure 4. Times series of SWH at AUK, Oct. 92

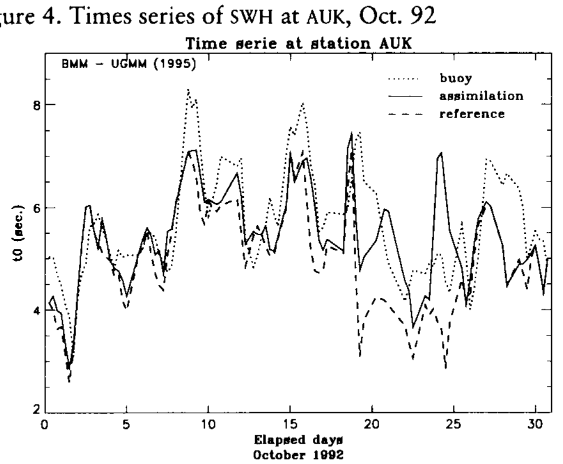

Figure 5. Times series of MWP at AUK, Oct. 92

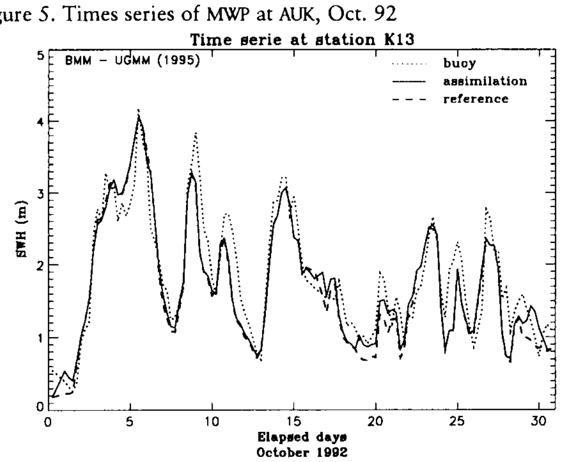

Figure 6. Times series of SWH at K13, Oct.92

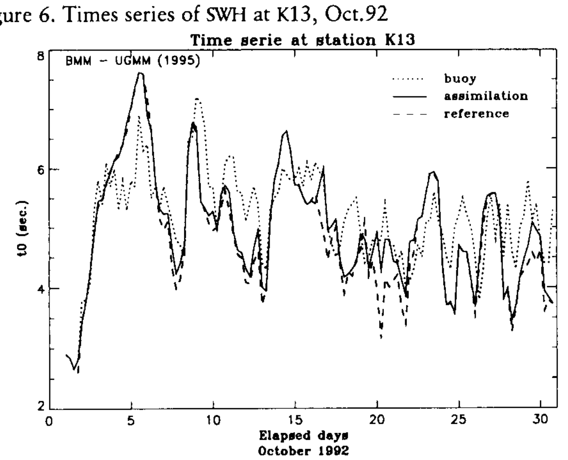

Figure 7. Times series of MWP at K13, Oct. 92

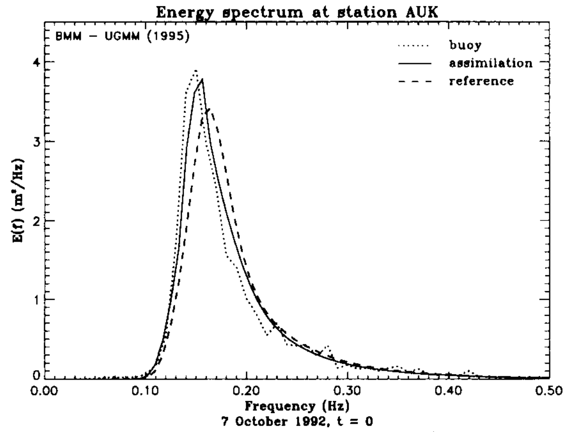

Figure 8. Energy spectrum at AUK, Oct. 7, 1992, 0h

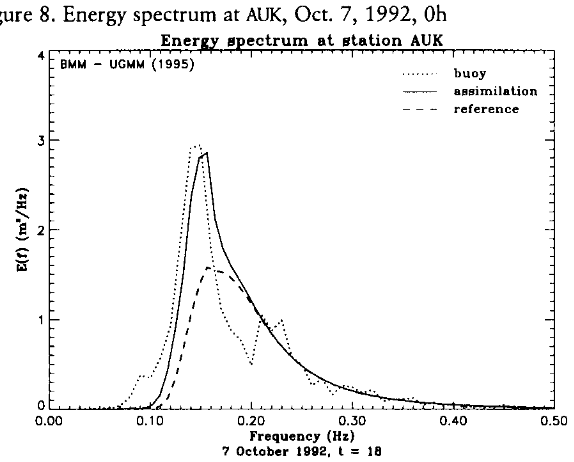

Figure 9. Energy spectrum at AUK, Oct. 7, 1992, 18h

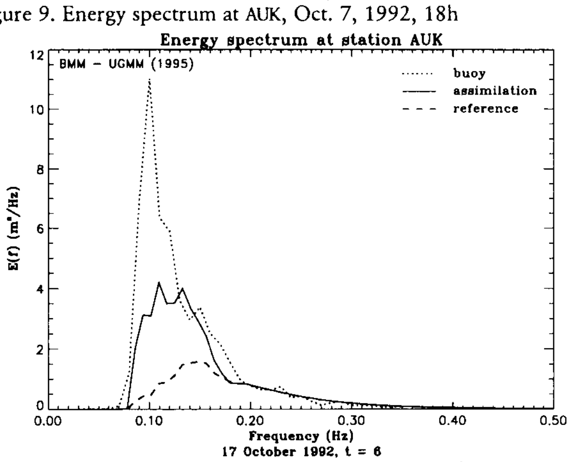

Figure 10. Energy spectrum at AUK, Oct. 17, 1992, 6h

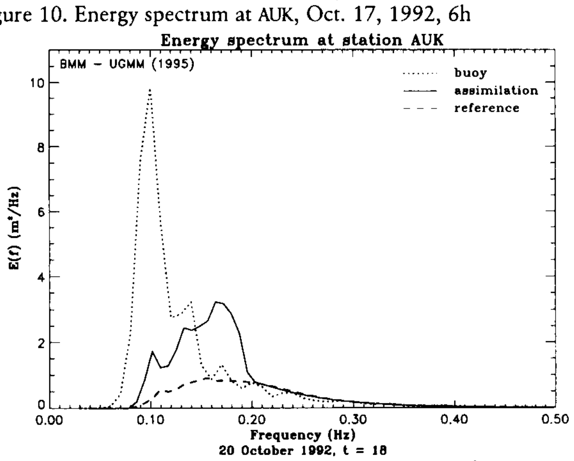

Figure 11. Energy spectrum at AUK, Oct. 20, 1992, 18h

7. REFERENCES

Bouws, E., H. Günther, W. Rosenthal and C.L. Vincent, 1987. Similarity of the wind wave spectrum in finite depth water. Part 2 : statistical relations between shape and growth stage. *Dtsch Hydrogr. Z.,* **40**, H.1

Günther, H., W. Rosenthal, 1985. The hybrid parametrical (HYPA) wave model, *Ocean Wave Modelling,* The SWAMP Group, Plenum Press, New York, 211-214.

Hasselmann, K., T.P. Barnett, E. Bouws, H. Carlson, D.E. Cartwright, K. Enke, J.I. Ewing, H. Gienapp, D.E. Hasselmann, P. Kruseman, A. Meerbrug, P. Müller, D.J. Olbers, K. Richter, W. Sell and H. Walden (1973). Measurements of wind-wave growth and swell decay during the Joint North Sea Wave Project (JONSWAP), *Dtsch. Hydrogr. Z.*, **A8(12)**, 95p.

Hermans, I., 1989. Wave modelling at the Belgian coast by means of the HYPAS model, *Progess in Belgian Oceanographic Research,* G. Pichot, Science Policy Office & Management Unit of the Mathematical Model of the North Sea and Scheldt Estuary, 75-110, Brussels.

Mastenbroek, C, V.K. Markin, A.C. Voorips & G.J. Komen, 1994. Validation of ERS–1 altimeter wave height measurements and assimilation in a North Sea wave model, *Glob. Oc. Atm. Sys.*, 2, 143–161.

Ovidio, F., J.-R. Bidlot, D. Van den Eynde, W. Luo and J. Monbaliu, 1994. Validation of the second generation operational wave forecasting model MU-WAVE: comparison with ERS–1, buoy data and WAM forecasts. *Proceedings of the First ERS–1 Pilot Project Workshop,* Toledo, Spain, ESA SP–365, 21–28.

Queffeulou, P., A. Bentamy, Y. Quilfen and J. Tournadre, 1995. Validation of ERS–1 and TOPEX POSEIDON altimeter wind and wave measurements. Submitted to *J. Geophys. res.*

Romeiser, R. 1993. Global validation of the wave model WAM over a one-year period using geosat wave height data. *J. Geophys. Res.* 98, C3, 4713-4726.

Thomas, J., 1988. Retrieval of energy spectra from measured data for assimilation into a wave model. *Q. J. R. Meteorol. Soc.*, **114**, 781–800.

Van den Eynde, D., 1992, MU-WAVE : an operational wave forecasting system for the Belgian coast, *Proceedings of the third International Workshop on Wave Hindcasting and Forecasting*, May 19–22, Montreal, Quebec, Canada, 313–324.

Zambresky, L.F., 1989. A verification of the global WAM model : December 1987 - November 1988, Report GKSS 89/E/37, GKSS Forschungszentrum GmbH, Geesthacht, 86 pp.

MULTITEMPORAL SAR AND FUSED ERS-1 SAR / SPOT XS IMAGE MAPS OF INDONESIA

Christine Pohl and John L. van Genderen

International Institute for Aerospace Survey and Earth Sciences (I.T.C.)
P.O. Box 6, 7500 AA Enschede, The Netherlands
Tel: (31) 53-4874444, Fax: (31) 53-4874400, E-mail: pohl@itc.nl or genderen@itc.nl

KEYWORDS: Image Fusion, Geocoding, Image Mapping, Map Updating, Multisensor Integration

ABSTRACT

Topographic map updating in the humid Tropics has its major constraint in the heavy cloud cover which prevents visible and infrared (VIR) sensors from acquiring information on the Earth's surface. With the launch of the first operational European radar satellite ERS-1 in July 1991 'cloud free' remote sensing images became available on a regular basis. The research project presented in this paper uses the idea of integrating data from optical and microwave sensors using digital image fusion techniques to overcome the cloud cover problem. This publication outlines research objectives, methodology and results of a pilot project carried out at ITC in cooperation with the National Coordination Agency for Surveys and Mapping (BAKOSURTANAL) in Indonesia. The end product of the project is a prototype of a fused ERS-1/JERS-1/SPOT image map, printed at Bakosurtanal to show the feasibility and usefulness of fused image mapping for topographic map updating activities in Indonesia.

1. INTRODUCTION

More than 20 years of operation of optical remote sensing satellites have shown that it is very difficult to obtain cloud-free imagery from many regions in the world that are frequently covered by clouds. Microwaves are capable of penetrating clouds and are actively sent by the antenna so that the radar sensor is independent of weather or daylight. For this reason, radar satellite data gains more and more importance for monitoring and map updating especially in tropical areas.

The combination of microwave with visible and near-infrared image data provides valuable tools for various applications related to Earth observation. In the first instance, cloudy areas in optical imagery can be replaced by radar data. Secondly, the optical data can serve substituting no data areas in SAR data, i.e. radar shadow. Thirdly, the different data sets provide complementary information due to the differences in wavelength and their physical characteristics. While optical data contain the reflectance of ground cover in visible and near-infrared, the radar is very sensitive to the roughness and moisture content of illuminated targets. The combined use of multi-sensor data visualizes valuable additional information of the observed Earth surface and shows the potential to overcome the cloud cover problem.

Image fusion is one of the possibilities to combine disparate images to produce a new, fused image containing the characteristics of both input images. It combines two or more different images to form a new image by using a certain algorithm [Genderen and Pohl, 1994].

2. OBJECTIVES

Topographic maps scaled 1:100,000 and larger from developing countries are mostly outdated. In many areas they do not exist at all. The conventional mapping and map updating approach does not account for the fast development and changes occurring in these regions. In the case of Indonesia, Bakosurtanal is currently producing the base maps for the whole country at 1:50,000 scale which are derived from aerial photography flown in the early 70's. The production of 1:50,000 scale topographic mapping is still ongoing. After having finished the 1:50,000 scale topographic maps, Bakosurtanal intends to generalize the map sheets to a reduced scale of 1:100,000. That means, that, once the map is published, it is already out of date and useless for many applications in the fields of regional planning and resource management.

Remote sensing images provide valuable information, that, once properly processed and interpreted, offer a quick and economic contribution to topographic map updating. To increase the availability of up-to-date information economically the production of space maps (geometrically corrected satellite images with cartographic annotation) offers good potentials. Remote sensing images cover large areas and provide repetitive coverage. It is commonly accepted that the scales between 1:50,000 and 1:250,000 can be achieved with LANDSAT, SPOT and ERS-1 [Albertz and Tauch, 1994; Dowman et al., 1993; Doyle, 1984; Jacobsen, 1992]. Some organisations have already brought satellite image maps into operational use and production [Persson, 1995].

However, due to frequent cloud cover, satellite remote sensing data from optical sensors can rarely be obtained at the time they are required. Therefore, radar remote sensing is used to supplement the existing data and contribute information to the map updating process. The main objective of this research was to overcome the cloud cover problem and to provide fused remote sensing data for topographic map updating in Indonesia. The project aimed at the production of digital image maps containing fused image data from different optical and radar remote sensing satellites.

3. METHODOLOGY

There is a variety of methods to combine disparate remote sensing data sets [Chavez, 1987; Ehlers, 1991; Zobrist et al., 1979]. The methods applied in the presented research are pixel based because the image data are supposed to be used as maps and require geometric corrections and geo-referencing. The data flow is shown in Figure 1.

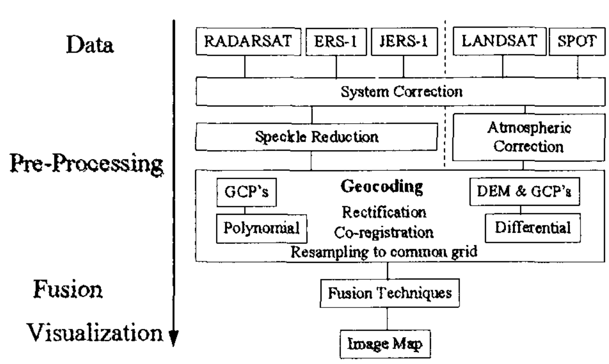

Figure 1: Image fusion processing chart (modified) [Pohl and Genderen, 1993]

After image acquisition the data were corrected for system induced and other distortions in radiometry and geometry in order to provide compatible multisensor images. The image data were geocoded and projected to the Indonesian map projection (UTM). Pixel based image fusion requires a highly accurate co-registered or geocoded data set. Therefore, the geometric correction of the multisensor image data was performed with a sensor model and a digital elevation model (DEM) to account for terrain induced distortions. The GCP's were derived from GPS measurements collected during on of the field visits and from existing topographic maps at 1:50,000 scale. This limits the accuracy of the geocoded data to the geometric accuracy of the map material. Based on the selected operational remote sensing satellites, i.e. ERS-1, JERS-1, LANDSAT, and SPOT an appropriate scale for the final image maps was defined at 1:100,000 [Albertz and Tauch, 1994].

The possibilities of fusing disparate image data are manifold, as are the different possible combinations of input data. This causes a large number of parameters to be considered in image fusion. The core of the research dealt with parameters influencing the geometric aspects of image fusion.

Colour transformation techniques, such as

- Red, Green & Blue colour composites - RGB,
- Hue, Saturation & Value - HSV,
- Intensity, Hue & Saturation - IHS,
- etc.

as well as statistical/arithmetic methods

- Principal Component Analysis - PCA,
- Arithmetic band combinations - ARM,
- Regression - RGR,
- High pass filtering - HPF,
- etc.

were used to fuse the data. In the context of the described research, only the combination of VIR and SAR was considered, based on the fact that multisensor optical image fusion has been already explored extensively by other researchers [Blodgett, 1990; Carper et al., 1990; Chavez et al. 1991; Cliche et al. 1985; Essadiki, 1987; Franklin and Blodgett, 1993; Jutz, 1988; Mangolini et al., 1993; Pellemans et al., 1993; Rothery and Francis, 1987; Shettigara, 1992; Welch and Ehlers, 1987].

An evaluation of the resulting fused imagery considered the topographic map updating capabilities of the produced data by visual interpretation. The best results related to map updating (perceptibility of topographic features and geometric accuracy) were printed as image map including some annotation, e.g. coordinate grid, town and river names, and a legend. Examples are displayed in Figure 2 and Figure 3 (Appendix).

4. IMPLEMENTATION

The research relied on the processing of data sets from two different test sites. First, an area in the north of the Netherlands (latitude 52°45'-53°30'N; longitude 5°00'-6°15') was selected as calibration test site in order to have quick access to

- remote sensing data,
- reliable and accurate topographic maps, and
- ancillary data and information.

Furthermore, the images of the Friesland area do not suffer from terrain induced geometric distortions due to the flat landscape and are ideal to test and calibrate image fusion techniques for topographic map updating.

The actual research test site is located on the Southwest coast of Sumatra in the Province of Bengkulu, Indonesia (latitude 3°-4°S; longitude 102°-103°E), comprising a coastal area in addition to highly mountainous terrain from 0-2,400 [m] above sea level with a large variety of land use. With its location at the equator, Sumatra represents a typical tropical island. Additionally, the rough terrain and dense vegetation which is representative for many other areas in the Tropics introduced a complicated environment which characterizes a good test case for the investigation of suitability and limitations of the approach to topographic map updating in tropical developing countries.

First, the Dutch data was processed in order to find out which technique performs best and which combination of images is suitable for map updating and cloud removal. In this context the benefits of multitemporal SAR data was investigated. An example is displayed in Figure 2 (Appendix) showing the tidal flats in the Waddensea, Northern Netherlands. The experiences gained from these experiments were then implemented and adapted to the Indonesian data.

Unfortunately, the ERS-1 SAR data acquisition for the research site was hindered by some constraints in the beginning of the project due to the limited operationality of the Bangkok receiving station. A first scene was acquired in July 1993, delivered only in the end of 1993. A second scene could be received in the beginning of 1995. The third scene, completing the three-date-multitemporal coverage was sent in August 1995. All the data were collected from descending orbits so that one of the objectives stated in the research proposal could not be achieved: The replacement of distorted areas (foreshortening, layover) and shadow areas from data from different orbits would have been a contribution to overcome the lack of information in highly mountainous terrain. But, using JERS-1 SAR data it was possible to replace large foreshortening and layover areas. Due to the higher incidence angle, JERS-1 data displays smaller geometric distortions.

5. RESULTS

The geocoding accuracy achieved for the Dutch data set ranges below one pixel even with the use of polynomials for the geometric modelling. Concerning the Indonesian set 1-2 pixels could be reached applying the sensor model [Cheng et al., 1995].

For the removal of clouds in the optical data it was found that best results could be achieved with a prior identification of the clouds including a masking of their shadows. The data were processed with density slicing to obtain the cloud and shadow mask. Then, this mask was further treated with grouping and filtering to reduce the loss of data which does not refer to clouds or shadows. The identification of SAR foreshortening, layover and shadow zones was performed based on calculations on the DEM. It is straight forward but depends very much on the quality of the elevation data.

The selected image map of Bengkulu, Indonesia that was printed in Indonesia was created from SPOT XS, ERS-1 SAR and JERS-1 SAR data building a mosaic as shown in Figure 3 (Appendix). To ensure the suitability and usefulness of the prototype the end-user Bakosurtanal was involved in the image mapping process from the very beginning. The map Figure 3 was modified in contents and format in order to fit into this paper. The original contains different annotation and alterations in the legend.

6. CONCLUSIONS

In conclusion, it was found that the processing results depend very much on the ground cover itself. Thus, the findings of the processing performed on the data set of the Netherlands was only partly transferable to the Indonesian data. The work done on the research test site data resulted in experiences and recommendations which are also useful for other areas in Indonesia due to the complex landscape and dense tropical vegetation in the Bengkulu area which is typical for many other Indonesian islands.

The project results proof the usefulness of SAR data in the context of topographic map updating. They deliver up to date information which, if interpreted in combination with optical data and ancillary information, ensure continuous data provision. However, the interpretation of land cover types, urban features and road network for topographic map revision is limited in highly mountainous terrain.

In the future, the production and publication of image maps can be done at Bakosurtanal. They have access to necessary hard- and software as well as trained staff to implement the approach developed during this project.

The final documentation on the project will support the operationalization of multisensor image mapping in Indonesia.

7. ACKNOWLEDGEMENT

The project was carried as part of the ITC funded Ph.D. program in cooperation with the University of Hannover, Germany. The research was performed in cooperation with the National Coordination Agency for Surveys and Mapping in Indonesia, Bakosurtanal and the University of Bengkulu, UNIB. It is embedded in the EC Scientific Network on 'Synergy of Remotely Sensed Data' coordinated by ITC. The remote sensing data was sponsored by ESA (Pilot Project PP2-NL2), SPOT IMAGE, EOSAT, NLR and NASDA. The software packages for geocoding PRODIGEO and for image processing microBRIAN were sponsored by Matra Cap Systèmes, France and MPA, Australia, respectively. The terrain-geocoding of the Indonesian data set was performed at CCRS, Canada by Dr. T. Toutin in cooperation with PCI Incorporated, Canada. All the support is gratefully acknowledged.

8. REFERENCES

1. Albertz, J. and Tauch, R. (1994): "Mapping from space - Cartographic applications of satellite image data", GeoJournal 32.1, pp. 29-37.

2. Blodgett, C.F. (1990): "Application of data fusion techniques to SPOT panchromatic and multispectral imagery, Southwest Yukon", Unpublished master thesis, Dept. Geography, University of Calgary, Alberta, Canada, 174 pages.

3. Carper, W.J.; Lillesand, T.M. and Kiefer, R.W. (1990): "The use of Intensity-Hue-Saturation transformations for merging SPOT Panchromatic and multispectral image data", Photogrammetric Engineering and Remote Sensing, Vol. 56, No. 4, pp. 459-467.

4. Chavez, P.S.Jr. (1987): "Digital merging of Landsat TM and digitized NHAP data for 1:24000 scale image mapping", Photogrammetric Engineering and Remote Sensing, Vol. 52, No. 10, pp. 1637-1646.

5. Chavez, P.S.Jr.; Sides, S.C. and Anderson, J.A. (1991): "Comparison of three different methods to merge multiresolution and multispectral data: TM & SPOT pan", Photogrammetric Engineering and Remote Sensing, Vol. 57, No. 3, pp. 295-303.

6. Cheng, P.; Toutin, T. and Pohl, C. (1995): "A comparison of geometric models for multisource data fusion", Proceedings of GeoInformatics '95, International Symposium on RS, GIS & GPS in Sustainable Development & Environmental Monitoring, May 26-28, 1995, pp. 11-17.

7. Cliche, G.; Bonn, F. and Teillet, P. (1985): "Integration of the SPOT Pan channel into its multispectral mode for image sharpness enhancement", Photogrammetric Engineering and Remote Sensing, Vol. 51, No. 3, pp. 311-316.

8. Dowman, I.; Muller, J.-P. and Slogett, D. (1993): "The current status of automated cartography and extraction of global topographic data from earth observation sensors", Proceedings of Workshop and Conference on International Mapping from Space, Working Group IV/2 ISPRS, Vol. 15, Hannover, Germany, pp. 25-36.

9. Doyle, F.J. (1984): "Surveying and mapping with space data", ITC Journal 1984-4, pp. 314-321.

10. Ehlers, M. (1991): "Multisensor image fusion techniques in remote sensing", ISPRS Journal of Photogrammetry and Remote Sensing, Vol. 46, No. 1, February 1991, pp. 19-30.

11. Essadiki, M. (1987): "A combination of panchromatic and multispectral SPOT images for topographic mapping", ITC Journal, No. 1, pp. 59-66.

12. Franklin, S.E. and Blodgett, C.F. (1993): "An example of satellite multisensor data fusion", Computers & Geoscience, Vol. 19, No. 4, pp. 577-583, 1993.

13. Genderen, J.L. van and Pohl, C. (1994): "Image fusion: Issues, techniques and applications", Proceedings of EARSeL Workshop on 'Intelligent image fusion', Holiday Inn, Strasbourg, France, 11th September 1994.

14. Jacobsen, K. (1992): "Comparison of mapping with different satellite images", Proceedings of Satellite Symposia 1&2, etc. ESA ISY-2, July 1992.

15. Jutz, S. (1988): "An attempt to merge panchromatic SPOT and multispectral TM data illustrated by a test area in the Kenyan highlands at the scale of 1:20,000", Proceedings 8th EARSeL Symposium, Capri, Italy.

16. Mangolini, M.; Ranchin, T. and Wald, L. (1993): "Fusion d'images SPOT multispectrale (XS) et panchromatique (P), et d'images radar",

Proceedings of Conference on "From Optics to Radar: SPOT and ERS applications", Paris, May 1993.

17. Pellemans, A.H.J.M.; Jordans, R.W.L. and Allewijn, R. (1993): “Merging multispectral and panchromatic SPOT images with respect to the radiometric properties of the sensor”, Photogrammetric Engineering and Remote Sensing, Vol. 59, Jan. 93, No. 1, pp. 81-87.

18. Persson, A. (1995): “Forest mapping with satellite in Chile”, Remote Sensing, Information from Swedish Space Cooperation, No. 2, February 1995, pp. 11-14.

19. Pohl, C. and Genderen, J.L. van (1993): “Geometric integration of multi-image information”, Proceedings of the Second ESA-ERS-1 Symposium, 12-14 October 1993, Hamburg, Germany, pp. 1255-1260.

20. Rothery, D.A. and Francis, P.W. (1987): “Synergistic use of MOMS-01 and Landsat TM data”, International Journal of Remote Sensing, Vol. 8, No. 3, pp. 501-508.

21. Shettigara, V.K. (1992): “A generalized component substitution technique for spatial enhancement of multispectral images using a higher resolution data set”, Photogrammetric Engineering and Remote Sensing, Vol. 58, No. 5, May 1992, pp. 561-567.

22. Welch, R. and Ehlers, M. (1987): “Merging multiresolution SPOT HRV and Landsat TM data”, Photogrammetric Engineering and Remote Sensing, Vol. 53, No. 3, pp. 301-303.

23. Zobrist, A.L; Blackwell, R.J. and Stromberg, W.D. (1979): “Integration of Landsat, SEASAT, and other geo-data sources”, Proceedings 13th International Symposium on Remote Sensing of Environment, ERIM, pp. 271-280.

APPENDIX

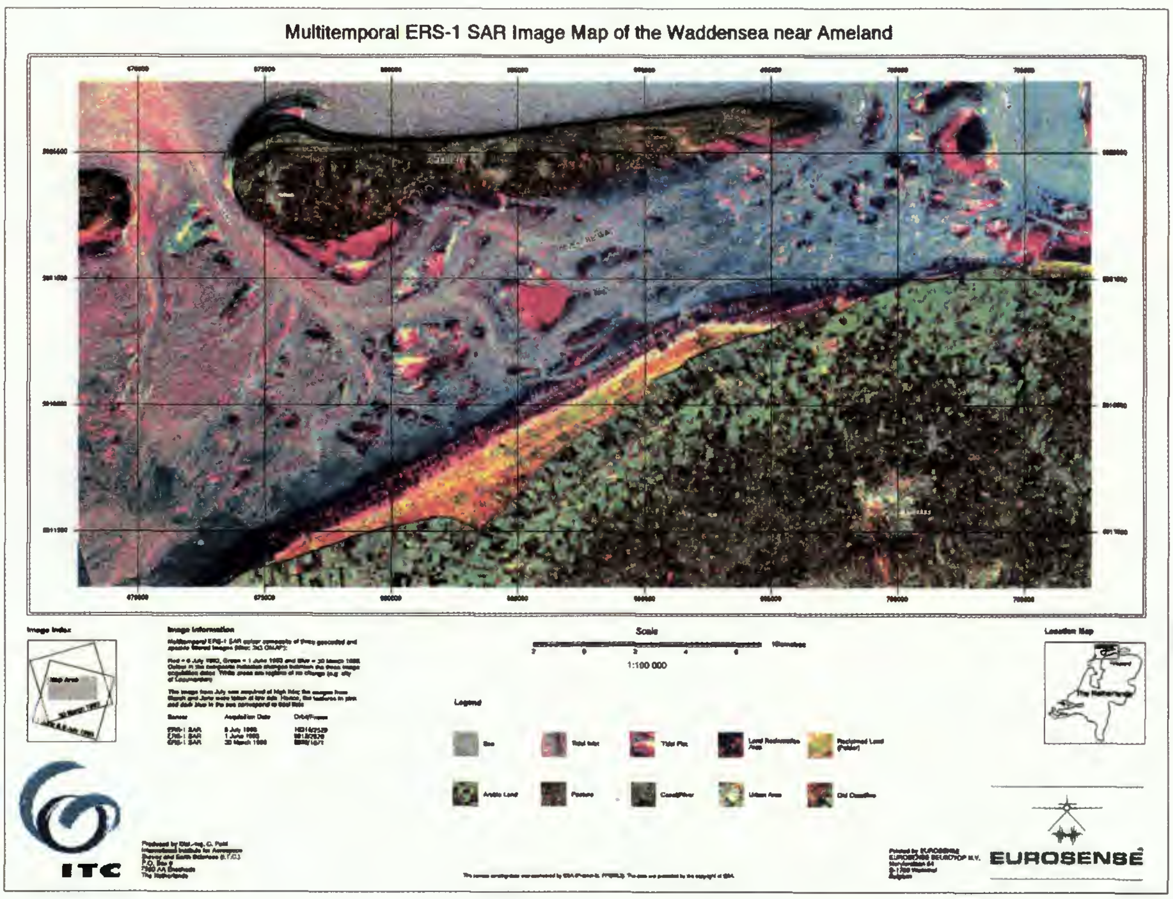

Figure 2: Image map of multitemporal ERS-1 SAR: Red = 6 July, Green = 1 June & Blue = 30 March 1993

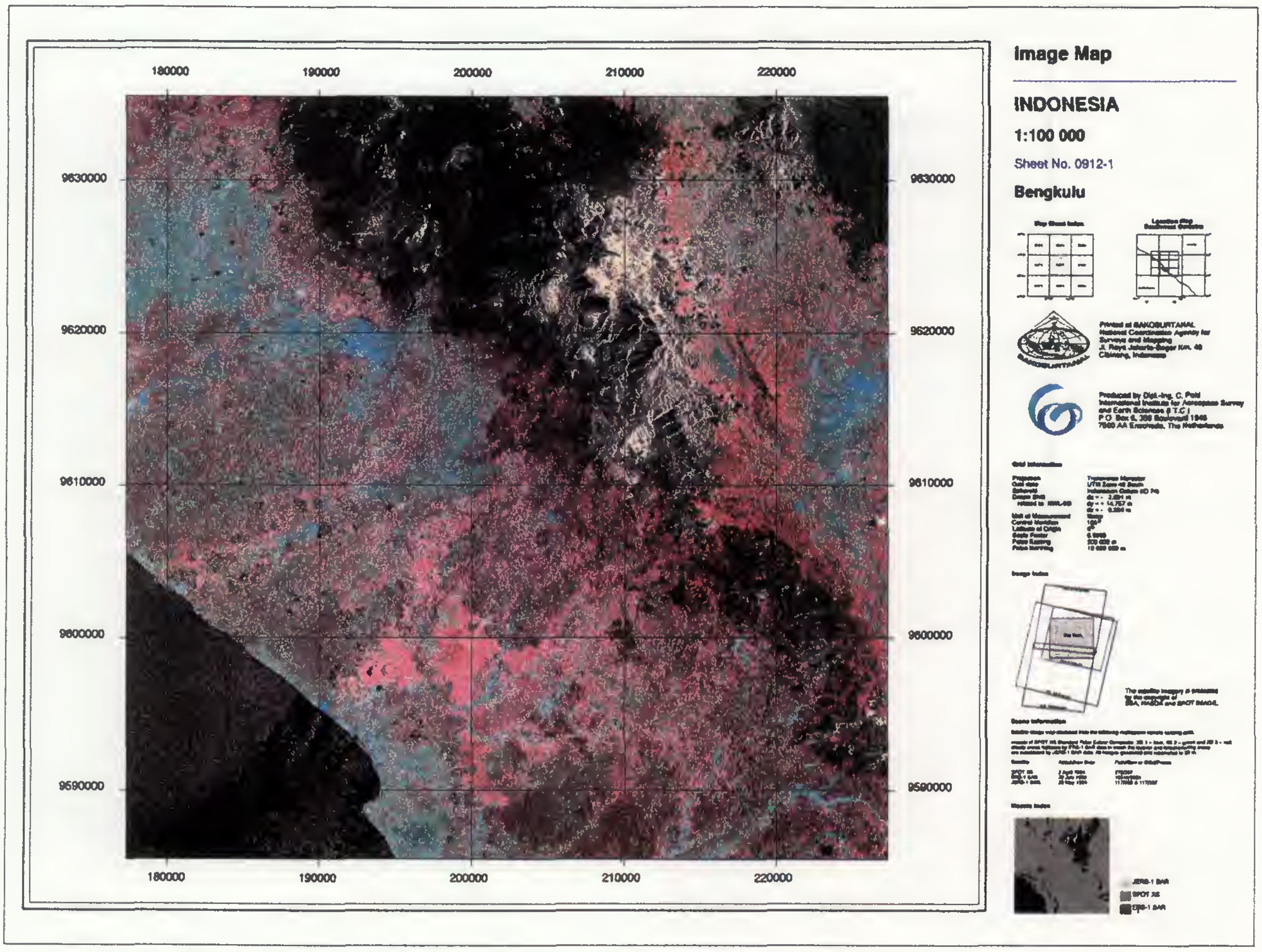

Figure 3: Example of final image map printed at Bakosurtanal, Indonesia (modified)

ERS PROCESSING AT FRENCH PAF , CERSAT

Sylvie POULIQUEN

Department of Oceanography from Space , IFREMER, BREST, FRANCE
Tel : (33) 98-22-44-92 Fax: (33) 98-22-45-33

ABSTRACT

The CERSAT is the French Processing Facility for ERS-1 and ERS-2 low bit rate data .

This poster aims to present CERSAT's missions and the way it is organised. It also introduces a flow chart of the processing chains for radar altimeter and scaterrometer processing.

It will present the new services made available in 1995:

- •- upgrade of the CERSAT system (Norskdata -> SUN/UNIX computers).
- •- change in OPR format for CCSDS in order to be compatible with TOPEX/POSEIDON
- •- 4.5 years of WNF scaterrometer products now available on CDROM .
- •- The production of atlases on CDROM by the end of this year (krigged wind field , sea-ice limits, wind/wave..)
- •- A new WWW server for CERSAT : http://www.ifremer.fr/CERSAT

1 INTRODUCTION

On April 24, 1995, ERS-2 was successfully launched from KOUROU by the European Space Agency. The French facility, CERSAT, was developed in the late eighties to process the ERS-1 low bit rate data. However, it was not able to process ERS-1 and ERS-2 data for another ten years. At the end of 1993, it was decided to fully overhaul the system into CERSAT2. It was completed in May 1995 and the system acceptance was signed by ESA on June 1st, just two weeks after the deadline.

2 CERSAT2

In 1995, ESA set two main requirements for CERSAT:

- guarantee continuity of ERS-1 data distribution to users.

- process ERS-2 radar altimeter data in order to provide as much data as possible to the validation group.

The ERS-1 geodetic phase was processed on the old system to guarantee a homogenous data set to the user community. On the other hand, processing of the 35 day period for ERS-1 and ERS-2 was performed on the new system, CERSAT2, in order to make cross-validation easier for the scientific group. By mid-October 1995, CERSAT distributed, to this group, on CDROM :

- 3 OPR01 cycles (GDR processed with the preliminary orbit calculated by Dutch-PAF).

- 2 OPR02 cycles (GDR processed with the precise orbit calculated by D-PAF at the end of September).

In the mean time, the distribution of the FDP (ESA real time products) in the new CCSDS format began with July ERS-1 and September ERS-2 data.

On June 12, 1995, CERSAT2 operations started. 3 days later, all ERS-2 data received by the network since its launch had been processed (orbits, real time products generated at the KIRUNA station, on-board time relations). The downstream processing could start.

Since July 15, the raw data exabytes have been processed upon arrival at CERSAT. No major difficulties have been encountered in ERS-2 processing whereas the data format changed (e.g., optical disk to exabyte for raw data). Only 10 of the 200 exabytes processed at CERSAT showed anomalies. This represents 5% of passes received. They will be retranscribed by ESA at the end of the commissioning phase.

In January 1996, the radar altimeter validation group will give its conclusions. The CERSAT processing chains will be upgraded to integrate both calibration results and processing anomalies. ERS-2 data reprocessing will start in February 1996, from the ERS-2 launch or the end of the commissioning phase (to be defined by ESA). Soon after, the distribution on CDROM to ESA selected users will start.

3 SCATERROMETER PROCESSING

In 1994, CERSAT team decided to process, from the beginning of the mission, the ERS-1 scaterrometer data with the model CMOD4-IFREMER. In March 1995, the first 6 CDROM were sent to ERS-1 and NSCAT Principal Investigators. More than 40 laboratories have already asked for this product , named WNF, and regularly receive new processed data. Up to now, we have distributed the WNF product from August 1991 to March 1995 (62 CDROM). We plan to continue with ERS-1 35 day period early in 1996, and ERS-2 as soon as data will be available.

If you are not yet on the distribution list send a mail to **"sylvie.pouliquen@ifremer.fr"**. Take notice that WNF is not an ESA product although distribution is allowed.

4 VALUE ADDED PRODUCTS

In collaboration with the Laboratory of Oceanography from Space, CERSAT started producing value added products (also called level 3). The first one will be a CDROM containing weekly and monthly krigged wind fields from August 1991 to June 1995. These mean wind fields have been evaluated using the WNF scaterrometer products.

We also plan to produce another CDROM with Arctic and Antarctic Sea Ice Limits on the same ERS-1 scaterrometer 4 years period. It will be available and distributed during the first semester of 1995.

If the user demand exists, we can produce other CDROM containing level 3 products made from multi-sensors multi-satellites data.

5 CERSAT WWW SERVER

In 1995, everybody has seen the explosion of INTERNET and especially of Word Wide Web servers.

CERSAT decided to open its own server to provide quickly and updated on line information about:

- our products : the users manuals are easily recoverable,
- CERSAT operations status,
- outline on ERS missions,
- answers to FAQ (Frequently Asked Questions) we receive regularly by mail or e-mail.
- examples of applications made using ERS data processed at CERSAT
- ....

This server is an easy way for communication between end users and CERSAT team. It will be quickly updated every time something of interest occurs at CERSAT.

To be aware of the last NEWS at CERSAT, feel free to connect yourself : http:// w3.ifremer.fr/cersat

6 CONCLUSION

CERSAT is willing to change from the sole ERS-1 radar altimeter processing and archiving facility, to a multi-mission centre, which will be able to integrate a future CEO or GOOS network while providing users quick and ready-to-use satellites data.

LAND USE CLASSIFICATION OF AGRICULTURAL FIELDS WITH MULTITEMPORAL ERS-1 SAR DATA AND OPTICAL REMOTE SENSING DATA: SOME RESULTS OF THE PASTA PROJECT

by
Ph. Hartl, S. Güth, H.-G. Klaedtke, G. Palubinskas, M. Reich, K. Wörz

Institute for Navigation (INS)
University of Stuttgart
70174 Stuttgart, Germany
Tel: (++49) 711 121 3400, Fax: (++49) 711 121 2755

in collaboration with
Daimler-Benz Aerospace Dornier Satellitensysteme GmbH (DOR)
Daimler-Benz Aerospace Jena Optronics GmbH (DJO)

ABSTRACT

The project PASTA (Pilot Project for the Application of SAR Techniques to Agricultural Statistics and Inspection of Land Use) is a practical application of ERS-1 SAR data together with optical data (SPOT, Landsat 5 TM) and GIS[1] information. The project was designed to demonstrate that the use of SAR data together with optical data and GIS information is a reliable and efficient tool for agricultural statistics according to the requests of EC agriculture policy.

Multitemporal SAR data sets were combined with GIS information and with optical data. Different classification methods were tested and the results compared with ground truth data. The classification procedures were optimized by :

- selection of optimal datasets for both optical and SAR data.
- selection of optimal type of classifier.
- selection of optimal threshold for non classified areas.
- using a priori knowledge for different stratificaton areas.

The results show an average accuracy of about 60 % in the validiation areas. In comparison to classification with optical data only a 10 % increase of classification accuracy could be achieved by using additional SAR together with one optical scene. Postclassification with majority filters provided an additional increase of accuracy of about 20%.

INTRODUCTION

The project PASTA (Pilot Project for the Application of SAR Techniques to Agricultural Statistics and Inspection of Land Use) is a ERS-1 project, which had been accepted by ESA and is financed by Deutsche Agentur für Raumfahrtangelegenheiten (DARA). It is a practical application of ERS-1 data to be used for agricultural administration. For this reason the PASTA team consists of people from the Ministery of Agriculture and the Statistical Office of Baden-Württemberg and experts from the university (INS) as well as from the industry (DOR, DJO).

The complementary use of ERS-1 SAR data, optical data and GIS information improves the reliability of the classification with exclusive optical data. Also the required accuracy of atmospheric correction of the optical image data can be reduced. Due to the additional information of the radar data, being statistically independent from the optical data, we come up with a better differentiation / classification of land use by multitemporal observation and change detection. The objective of our method is to use only one optical scene per year combined with a multitemporal set of SAR scenes, which can be acquired independent from weather conditions and sun illumination. There is of course some influence of rain on the SAR backscattering of a vegetation canopy. However data taken during bad weather conditions can still be used for classification. The interaction between incoming energy and scattered / backscattered electromagnetic waves by vegetation canopies and soil surface is quite different in the microwave and optical frequencies: Microwave backscattering is dominated by physical ground parameters like geometrical structure, water content, dielectric constants, polarisation etc. Scattering of optical waves is dominated by biochemical effects like photosynthesis. For this reason a combined classification should provide more accurate results with a better separation of different types of landuse.

TESTSITES

The area covered within the project PASTA are the two German states Baden-Württemberg and Thüringen, which cover about 60000 km². In contrast to Thüringen, Baden- Württemberg is charcterized by small field sizes and heterogenious agroecological units. In this paper methology and results mainly from Baden-Württemberg are presented. For Baden-Württemberg a lot of detailed information is available:

GIS Baden-Württemberg:
- *ground truth data*

[1] GIS = Geographical Information System

- official digitized catastral maps (ALK[2])
- official digitized topographic information (ATKIS[3])
- agroecological data (Weller-map)
- meteorological data
- digital elevation model (DEM)

Remote sensing data:
- Landsat 5 TM scenes
- SPOT scenes
- multitemporal ERS-1 data

Ancillary data: Official statistical data about landuse

All available data sets have been geocoded and implemented in a database, which allows an easy access and combination for all kind of data. In a first step the testsite „Ostalbkreis" was investigated, a region of about 600 km² in the eastern part of Baden-Württemberg. This testsite was selected because it seems to be representative for whole Baden-Württemberg. The region contains parts with different climate and different phenological states of the various crop types quite close together. „Ostalbkreis" is also heterogenous with respect to geomorphology and landuse. There are areas with large fields and others with quite small fields.
Fig. 1 shows the location of the testsite „Ostalbkreis" in the eastern part of Baden-Württemberg (Germany).
Fig. 2 shows a more detailed view of the situation: Only parts of the area are covered by agricultural fields (white). Forest areas (dark green), grasslands (bright green), urban areas (red) and water (blue) are not taken into account (Masks). The field structure and vegetation type is also part of the GIS. The different vegetation types are winter wheat, winter barley , rape, summer barley, oats and corn.
Fig. 3 shows DEM together with the GIS vector overlay indicating the fields, where ground truth information about 1993 land use is available.

REMOTE SENSING DATA

Six optical scenes (Tab.1) and six multitemporal ERS-1 SAR.GTC scenes (Tab. 2) covering the Ostalbkreis testsite have been used.

Tab. 1: Optical data of 1993

SENSOR	ACQUISITION DATE
SPOT PANCHR.	01.04.1993
LANDSAT 5 TM	20.04.1993
SPOT XS	29.04.1993
SPOT XS	24.05.1993
SPOT XS	30.06.1993
LANDSAT 5 TM	09.07.1993

[2] ALK = Automatisiertes Liegenschafts-Kataster (land survey office)
[3] ATKIS = Amtliches Topographisch Kartographisches Informationssystem (land survey office)

Tab. 2: SAR data of 1993

SENSOR	ACQUISITION DATE
ERS-1.SAR.GTC	11.03.1993
ERS-1.SAR.GTC	20.05.1993
ERS-1.SAR.GTC	24.06.1993
ERS-1.SAR.GTC	29.07.1993
ERS-1.SAR.GTC	02.09.1993
ERS-1.SAR.GTC	07.10.1993

The optical data have been geocoded and corrected for atmospherical effects. Fig. 4 shows the atmosphere corrected Landsat 5 TM true colour composite of the testsite with the GIS vector information overlay.
Fig. 5 shows the original ERS-1.SAR.GTC image taken on 24.06.1993 for the southern part of Ostalbkreis. Due to the speckle effect, the field structure cannot be seen in this image.
Fig. 6 shows the same image after application of a gamma map filter, which takes off the speckle noise.
Fig. 7 shows a multitemporal overlay of three speckle filtered ERS-1.SAR.GTC images, where the SAR data, taken on 29.07.1993, 24.06.1993 and 20.05.1993, are shown with red, green and blue colours. In this multitemporal image we can also identify the structure of agricultural fields similar to the optical image (Fig. 4).
Fig. 8 shows the corresponding filter result of a new approach of segmentation filter.

RADAR SIGNATURE ANALYSIS

To analyse the radar signatures of agricultural fields in ERS-1 SAR images the mean grey values of more than 560 test fields were analysed. Ground truth information about the field area and vegetation type of these fields were taken from the GIS. A mean value of all pixels was calculated for each of these fields, where pixels containing the field edge were eliminated.
The analysis showed large variations of mean grey values of fields belonging to the same vegetation type. The reason cannot be the speckle effect, which has been reduced by calculating mean values for all pixels of a parcel. One reason could be the influence of the field orientation towards the SAR sensor, i.e. the actual fluctuation of sensor look angle due to the topography. Field slopes reach values up to +/- 6 degrees from the horizontal plain. Corresponding fluctuations in mean grey values had to be analysed and corrected.
Variations in mean grey values of fields belonging to the same vegetation type are possibly differences in the biophysical parameters, responsible for the radar response of an agricultural field. These could be differences in soil moisture content and soil roughness, where the vegetation canopy is not dense enough to block contributions of the soil surface to the backscattering characterics of the field. Other biophysical parameters of the vegetation canopy are volumetric density of plant, water content, size and density of the individual scatterers and the height of the vegetation canopy. These parameters change the radar response throughout the development stages of the vegetation. There are of course field to

field variations of these parameters because of different growing conditions.

The signature analysis further showed that only 3 out of 6 SAR images allowed a sufficient separation between the different vegetation types. The SAR scene taken on 24.06.1993 gives the best separation. Winter wheat, summer barley and oats fields have a low radar return and can be well separated from winter barley, rape and corn fields with higher radar return.

TOPOGRAPHIC INFLUENCE

The influence of terrain topography on the radar signatures has been analysed in detail: The correlation between the mean radar reflectivity of a field and its surface orientation relative to the horizontal plain was measured. Again the radar signatures of more than 560 test fields were used for that purpose. Only slopes in a direction towards or away from the SAR sensors look direction influence the radar return.
The topography information about field slopes with respect to ERS-1 look angle could be extracted from DEM, which is part of the GIS (see Fig. 3). The size and orientation of slopes of all fields have been calculated from GIS and DEM data together with the corresponding angle of field orientation with respect to the ERS-1 look direction. Fig. 9 shows an example of this analysis.

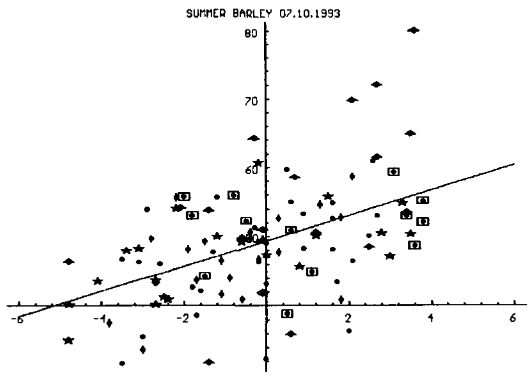

Fig. 9: Grey values of summer barley fields as a function of field orientation towards the SAR sensor in degrees relative to horizontal plain.

Linear regression analysis has been performed to quantify the influence of topography on radar signature. Tab. 3 shows the numerical results for all analysed fields in the SAR scene taken on 29.07.1993.

Tab. 3: Results of regression analysis of grey values as a function of field orientation relative to a horizontal plain.

DATE	VEGETATION	MEAN GREY VALUE	STANDARD ERROR	GRADE OF REGRESSION	STANDARD ERROR
29.07.1993	W WHEAT	39.78	0.52	0.509	0.264
29.07.1993	W.BARLEY	43.29	0.99	1.040	0.551
29.07.1993	S. BARLEY	45.45	0.81	1.218	0.363
29.07.1993	OATS	33.69	1.36	2.379	0.660
29.07.1993	RAPE	43.72	1.31	0.178	0.646
29.07.1993	CORN	40.38	0.56	0.830	0.381

Similar results were achieved for the other SAR scenes. The standard error for the regression line gradient is quite high compared with the individual grades. Nevertheless the influence of the field slope with respect to the radar look direction is positive. Thus there is an increasing grey value for increasing field slopes towards the SAR sensor, which results in a decreasing incidence angle.
The result from this analysis is that even if the field slopes of agricultural fields in the observed test areas are only between +6 and -6 degrees, the influence of the field orientation cannot be neglected. Grey value differed of up to 12 to 20 steps for fields oriented at -6 to +6 degrees. To avoid an increased variation of mean grey values of radar returns belonging to the same vegetation type, the SAR reflectivity was corrected by using the DEM.

CLASSIFICATION RESULTS

Three different classsifiers
1. Maximum Likelihood Classifier (ML)
2. Back Propagation Neural Network Classifier (BPN)
3. Kohonen Neural Network Classifier (KN)

have been tested using the validation areas in the southern part of the Ostalb testsite (see Fig. 1 and Fig. 2). The dashed box of Fig. 1 marks the classification area. The non agricultural areas have been masked and the corresponding pixels were not used for the classification (Fig. 2).
Training areas for the six vegetation classes: winter wheat, winter barley, rape, summer barley, oats and corn have been selected in all 10 test areas, using GIS information.
A separation between the vegetation types is not possible, if only multitemporal ERS-1.SAR images are used for classification. We could only separate between two groups: one group consists of winter wheat, summer barley and oats and the other one of winter barley, rape and corn. The results of this maximum likelihood classification with only ERS-1 radar data taken during the vegatation period (20.05.1994, 24.06.1993 and 29.07.1993) are shown in Tab. 4.

Tab. 4: Confusion matrix for maximum likelihood classification with only multitemporal SAR data
group 1: winter wheat, summer barley, oats
group 2: winter barley, rape, corn

Vegetation	*% classified as group 1*	*% classified as group 2*
group 1	81 %	19 %
group 2	25,5 %	74,5 %

However, if one optical scene is used together with these 3 multitemporal SAR images in a combined classification, the accuracy is better than with the optical data alone. Tab. 5 shows the Kappa coefficients according to Rosenfeld & Fitzpatrick-Lins for various combinations of optical and SAR data.

Tab. 5: Accuracies achieved with maximum likelihood classificator for various combinations of optical and SAR data

Scenes	*Kappa (training areas)*	*Kappa (all)*
Spot XS 29.04.93	47,4%	32,5%
Spot XS 29.04.93 + ERS-1 multitemp.	58,4%	42,6%
Spot XS 24.05.93	68,2%	51,7%
Spot XS 24.05.93 + ERS-1 multitemp.	77,0%	57,3%
Spot XS 30.06.93	52,0%	35,6%
Spot XS 30.06.93 + ERS-1 multitemp.	60,1%	40,7%
Spot XS 24.05.93 + Spot XS 30.06.93	84,5%	64,3%
Spot XS 24.05.93 +Spot XS 30.06.93 + ERS-1 multitemp.	82,4%	62,0%

For the comparison of different classifiers we used a combined classification with one optical image (SPOT taken on 24.05.1993) and 3 multitemporal ERS-1.SAR.GTC scenes taken on 20.05.1993, 24.06.1993 and 29.07.1993.
Figs 10 to 12 show the results for the different classifiers. An analysis of the classification results for the areas, where GIS information about the landuse is available, show the following Tables (Tabs 6 - 8).

Tab. 6: Result of Maximum Likelihood Classsification for Validation Areas

vegetation type	pixels class.as:	WW %	WB %	SB %	OA %	RA %	MA %
winter wheat	51477	56.08	11.30	11.37	18.62	0.77	1.79
winter barley	24015	15.09	57.21	11.29	12.71	1.81	1.82
summer barley	37727	3.87	6.52	67.77	17.15	2.66	1.98
oats	9327	20.75	10.39	26.60	34.75	1.01	6.43
rape	19802	0.30	1.06	6.16	7.17	84.55	0.72
corn	25484	0.45	0.62	2.39	12.78	0.88	82.48
sum	167832	36062	23356	38442	27028	18895	23870

average accuracy: 63.81%
overall accuracy: 65.05%
Kappa coefficient: 57.32%

Tab. 7: Result of Back Propagation Neural Network Classsification for Validation Areas

vegetation type	pixels class.as:	WW %	WB %	SB %	OA %	RA %	MA %
winter wheat	51477	71.77	5.89	17.75	1.81	1.48	1.30
winter barley	24015	30.69	39.76	24.42	1.55	2.20	1.38
summer barley	37727	6.35	1.57	74.38	13.14	2.60	1.96
oats	9327	37.32	2.51	45.67	5.09	3.52	5.89
rape	19802	0.77	0.27	17.04	0.61	80.86	0.45
corn	25484	2.53	1.44	7.33	0.46	6.96	81.29
sum	167832	50987	13827	52562	6975	20386	23095

average accuracy: 58.86%
overall accuracy: 66.59%
Kappa coefficient: 57.55%

Tab. 8: Result of Kohonen Neural Net Classsification for Validation Areas

vegetation type	pixels class. as:	WW %	WB %	SB %	OA %	RA %	MA %
winter wheat	51465	59.95	13.05	14.12	8.94	1.61	2.33
winter barley	23999	19.67	54.08	14.86	5.27	3.10	3.02
summer barley	37721	10.14	8.10	65.65	9.48	3.64	2.99
oats	9324	23.29	10.11	24.54	32.93	2.78	6.35
rape	19801	1.56	3.16	7.83	2.72	82.51	2.23
corn	25481	2.23	1.63	5.02	6.06	4.20	80.87
sum	167791	42444	24734	40717	14595	20608	24693

average accuracy: 62.66%
overall accuracy: 64.73%
Kappa coefficient: 56.19%

SUMMARY

An investigation of topographic influence on the radar response showed that the grey values of the radar images should be corrected by about 1 digital value for 1 degree of slope angle towards the SAR sensor. A correction of the SAR images has been performed by making use of DEM.
From a statistical analysis of the SAR data we know that not all scenes show sufficient discrimination between grey values of different crop types. For this reason only 3 out of 6 ERS-1 SAR datasets have been selected for the classification.

Different classification methods were tested and the results compared with ground truth data. In a first approach only multitemporal ERS-1 data have been used for classification. The interim results show, that there is no good separation between the different vegetation types by using only multitemporal ERS-1 data (single frequency C-band, VV-Polarisation, 35 days repetition cycle). However, if these data are used together with optical data of only one acquisition date, a 10 % average increase of separation accuracy for the most important crop types was achieved in comparison to optical classification. The results suffered from the extremely small field sizes in some parts of the testsite. Better results can be achieved, if only field sizes of more than 1 ha and 50 m width are taken into acoount. An additional segmentation of homogenous areas making use of the optical channels can further improve the methods for speckle filtering of the SAR data and provide better classification results by majority filtering.
It could be shown that postclassification with majority filters based on known geometry of agricultural fields in

the validation areas increases the overall classification accuracy about 20 %.
The segmentation can furthermore be improved by using ATKIS/ALK data which contain for example parcel borders and field trails.

REFERENCES

BENEDIKTSSON J.A., SWAIN P.H., and ERSOY O.K.: Neural network approaches versus statistical methods in classification of multisource remote sensing data. IEEE Transactions on Geoscience and Remote Sensing, 28, 540-551, 1990.

FOODY G.M., MCCULLOCH M.B., YATES W.B.: Classification of remotely sensed data by an artificial neural network: issues related to training data characteristics. Photogrammetric Engineering and Remote Sensing, 61(4), 391-401, 1995.

HARTL PH., GÜTH S., KLAEDTKE H.-G., PALUBINSKAS G., REICH M., WÖRZ K.: Application of multitemporal ERS-1 SAR data: some results of the PASTA project, Interim Report to ESA, Institute of Navigation, University of Stuttgart, Stuttgart, 27 pages, 1995.

ICAN documentation, Version 2.3, Deutsche Aerospace Dornier GmbH, Friedrichshafen, 10 / 1992.

LOPES A., NEZRY E., TOUZI R., LAUR H.: Structure detection and statistical adaptive speckle filtering in SAR image. International Journal of Remote Sensing, 14(9), 1735 - 1758, 1993.

PALUBINSKAS G.: Data driven weight initialization of back propagation for pattern recognition. Proc. of Int. Conference on Artificial Neural Networks, May 26 - 29, 1994, Sorrento, Italy, vol. 2, pp. 841 - 844, 1994.

PALUBINSKAS G.: Weights initialization for back propagation networks. Proc. of 3rd European Congress on Intelligent Techniques and Soft Computing (EUFIT'95), August 28 - 31, 1995, Aachen, Germany, Vol. 1, 280 - 284, 1995.

WELLER F.: Erläuterungen zur Ökologischen Standorteignungskarte für den Landbau in Baden-Württemberg 1:250000. Ministerium für Ländlichen Raum, Ernährung, Landwirtschaft und Forsten Baden-Württemberg, Stuttgart, 1978/1990.

LIST OF FIGURES

Fig. 1: Location of Testsite OSTALB in the eastern part of Baden-Württemberg (Germany). Detailed ground truth information derived from on site inspection is available within 15 test areas indicated by GIS field vectors. The dashed box marks the classification area.

Fig. 2: Landsat 5 true colour composite (atmosphere corrected) with GIS vector information overlay.

Fig. 3: Digital elevation model with GIS vector information overlay.
The altitude varies from 430 m to 730 m above sea level.

Fig. 4: Land under plough has been separated from other land use by masking. Sealed areas (red), water (blue) and grasslands (light green) derived from multitemporal and multisensoral (ERS-1 SAR.GTC '93 and Landsat 5 TM '94) classification over several years. Forest areas (dark green) extracted from digitized topographical maps. Classification results for graslands for 11 communities: 7097 ha were classified as grasslands (= 71,4 % accuracy in validation areas). If majority filtering is applied this accuracy increases to 96,4 %, corresponding to a projected value of 9582 ha of grasslands. In comparison to the official statistical value arises a difference of 0,9 % .

Fig. 5: Unfiltered SAR image.

Fig. 6: GMAP2 filtered SAR image.

Fig. 7: Multitemporal colour composite of three GMAP2 filtered SAR images.

Fig. 8: New speckle filter developed for this application combines structural segmentation extracted from optical and radar images.

Fig. 9: Grey values of summer barley fields as a function of field orientation towards the SAR sensor in degrees relative to horizontal plain.

Fig. 10: Result of Maximum Likelihood classification.

Fig. 11: Result of back propagation neural network classification.

Fig. 12: Result of Kohonen neural network classification.

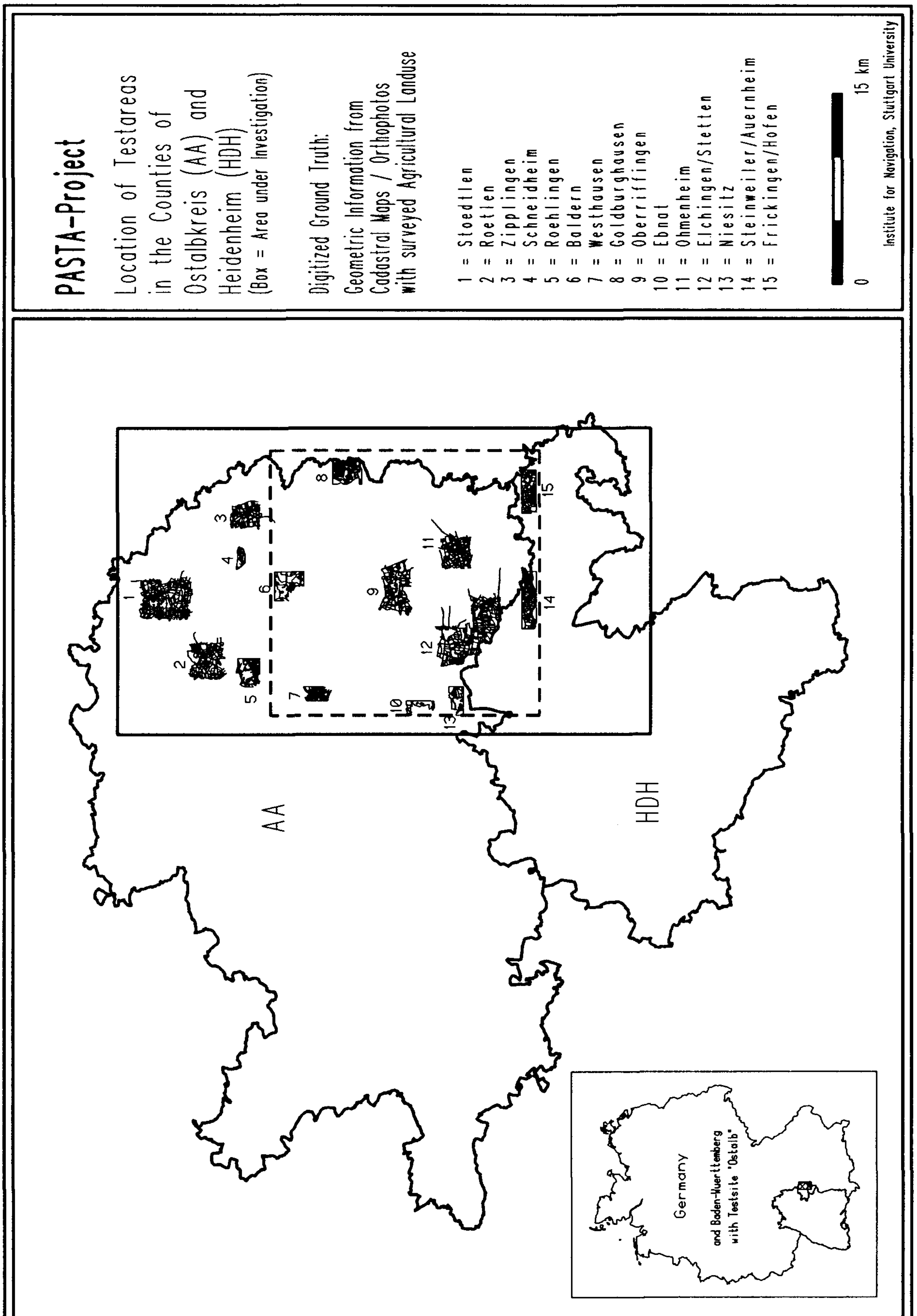
PASTA-Project
Location of Testareas in the Counties of Ostalbkreis (AA) and Heidenheim (HDH)
(Box = Area under Investigation)
Digitized Ground Truth:
Geometric Information from Cadastral Maps / Orthophotos with surveyed Agricultural Landuse
1 = Stoedtlen
2 = Roetlen
3 = Zipplingen
4 = Schneidheim
5 = Roehlingen
6 = Baldern
7 = Westhausen
8 = Goldburghausen
9 = Oberriffingen
10 = Ebnat
11 = Ohmenheim
12 = Elchingen/Stetten
13 = Niesitz
14 = Steinweiler/Auernheim
15 = Frickingen/Hofen
0
15 km
Institute for Navigation, Stuttgart University
AA
HDH
Germany
and Baden-Wuerttemberg with Testsite "Ostalb"

Figure 1

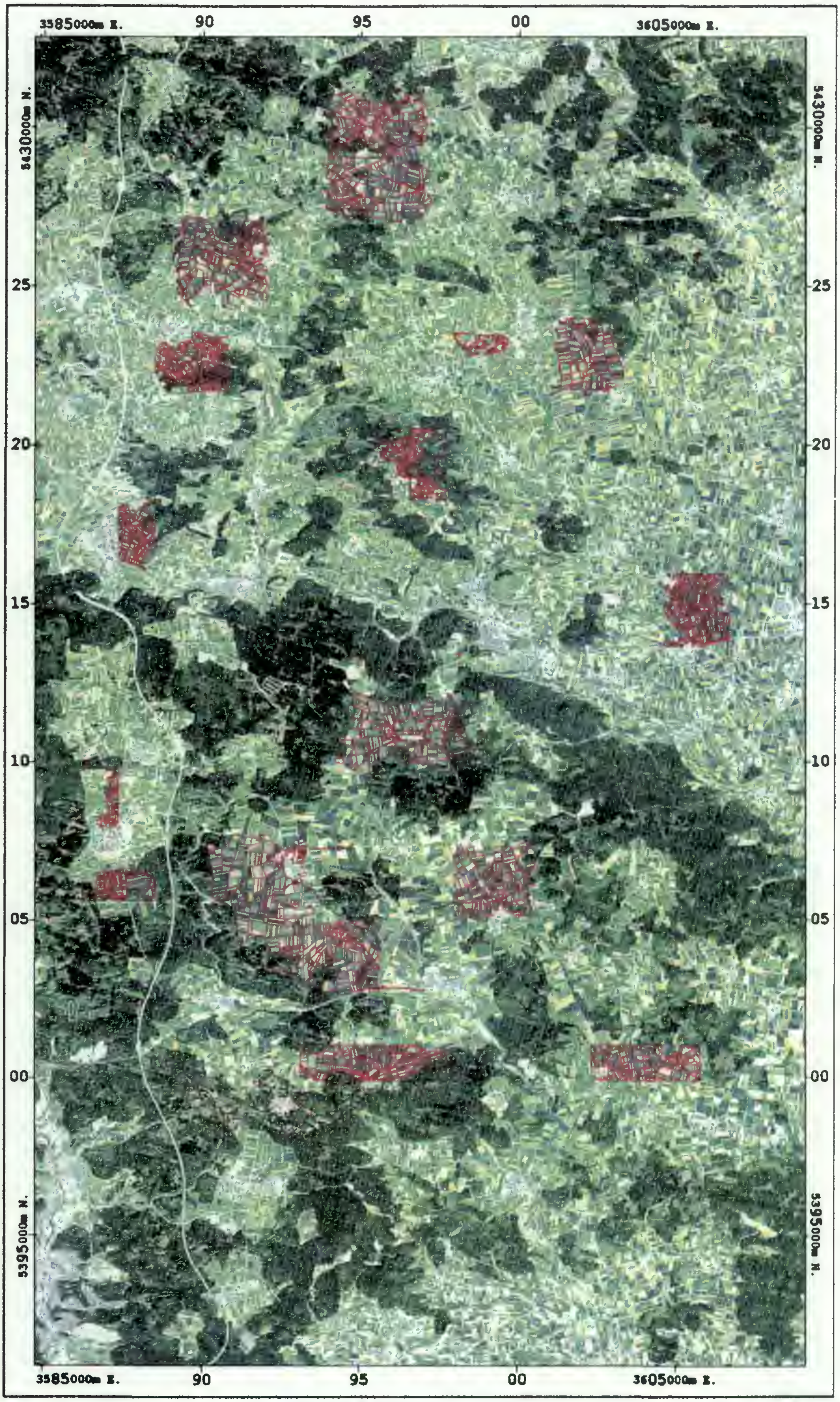

Figure 2

TESTSITE "Ostalb"

LANDSAT 5 TM, 26.6.1994, RGB:321

Kilometres 5 0 5 10

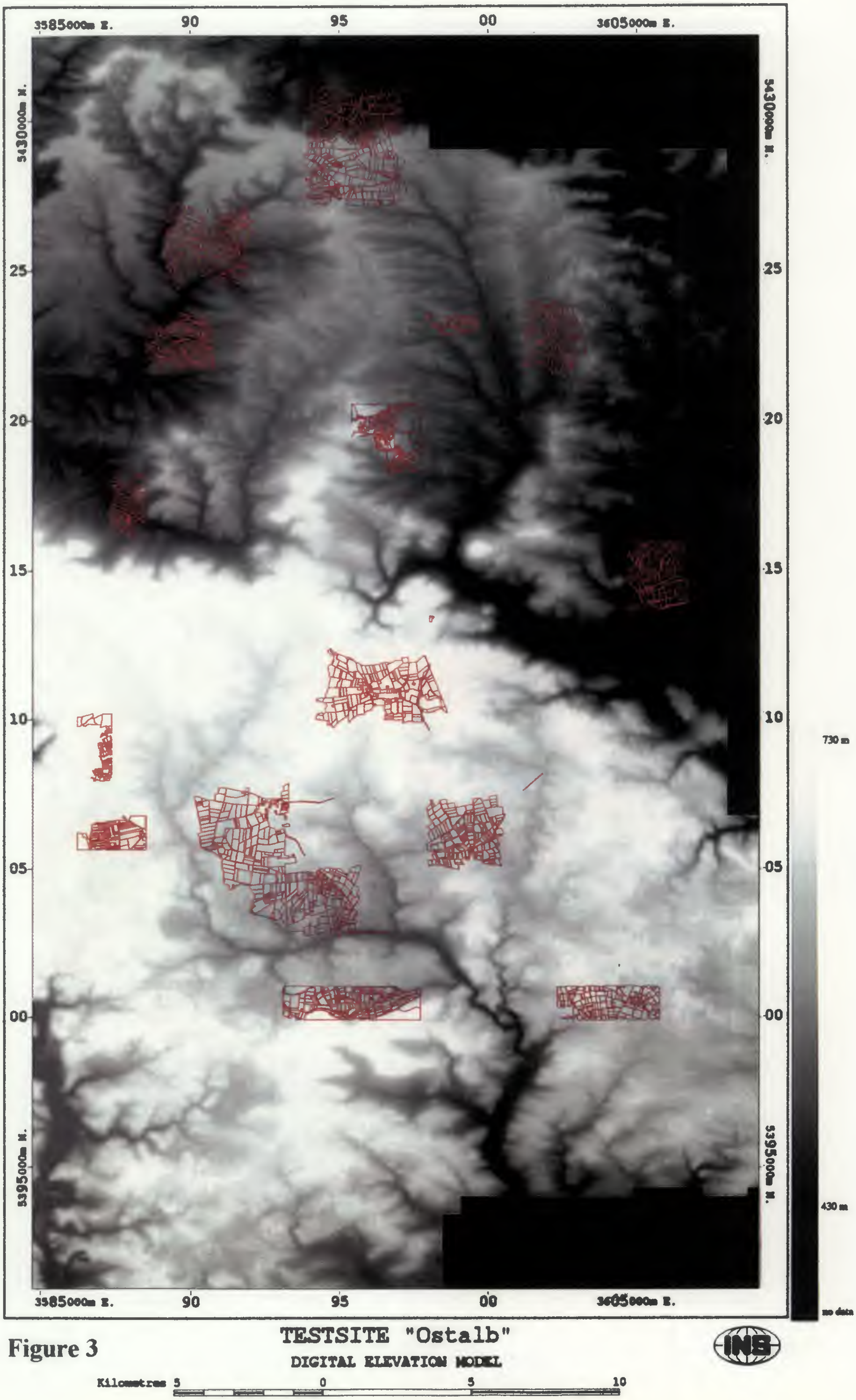
3585000m E.
90
95
00
3605000m E.
3430000m N.
25
20
15
10
05
00
3395000m N.
730 m
430 m
no data
TESTSITE "Ostalb"
DIGITAL ELEVATION MODEL
Kilometres 5
0
5
10

Figure 3

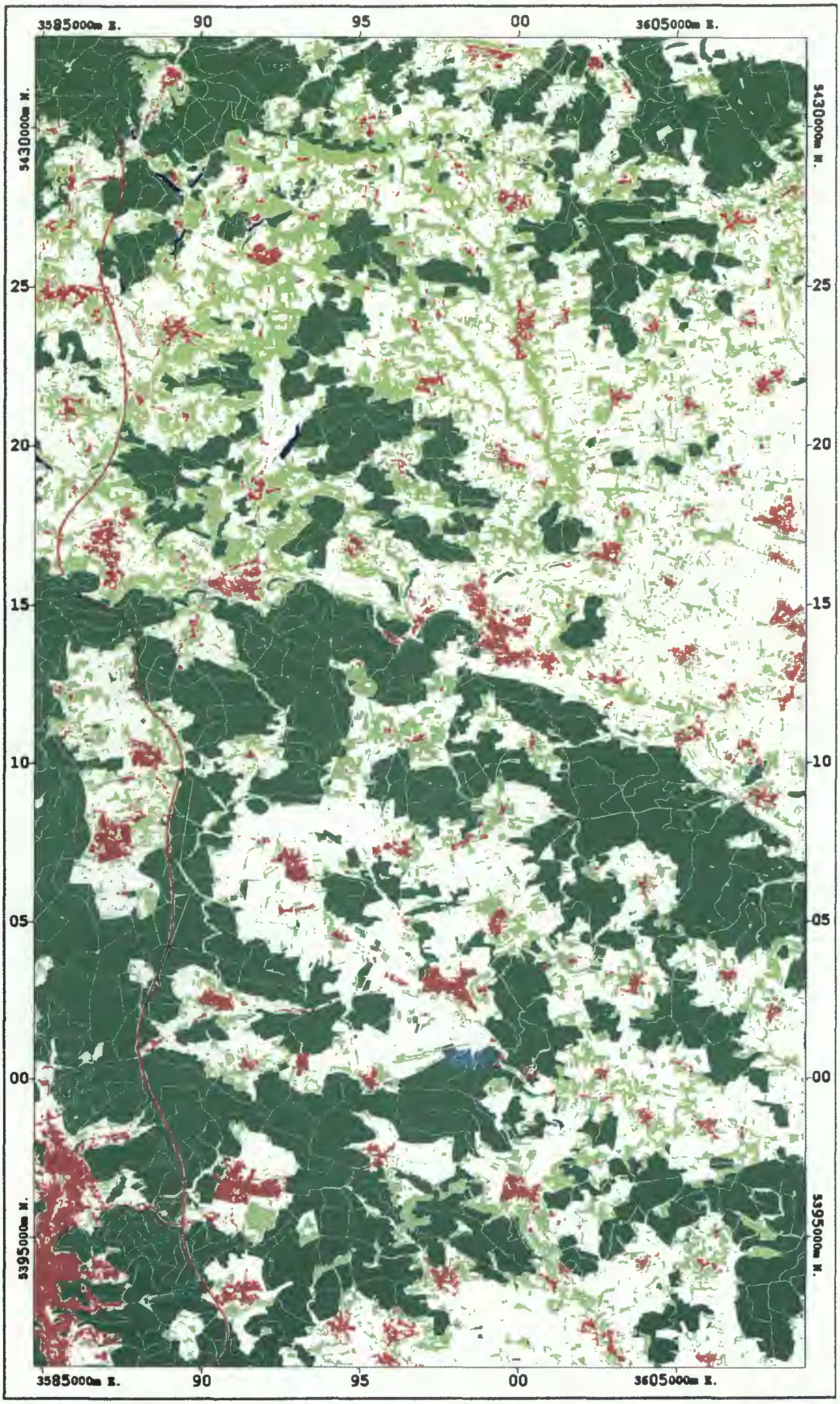

Figure 4

TESTSITE "Ostalb"

MASKS FOR NON AGRICULTURAL AND GRASSLAND AREAS

Kilometres 5 0 5 10

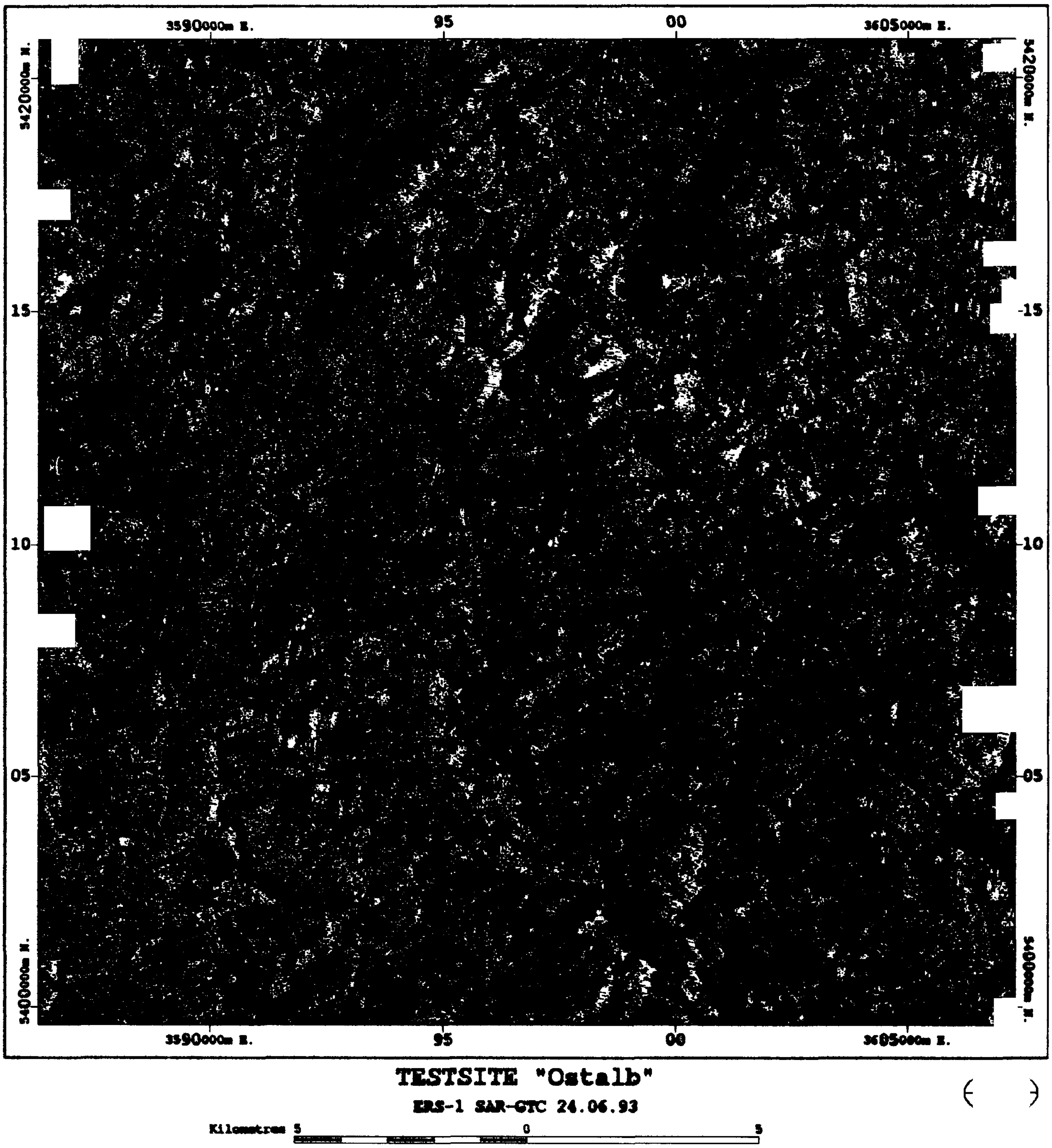
3590000m E.
95
00
3605000m E.
3420000m N.
15
10
05
3400000m N.
TESTSITE "Ostalb"
ERS-1 SAR-GTC 24.06.93
Kilometres 5 0 5

Figure 5

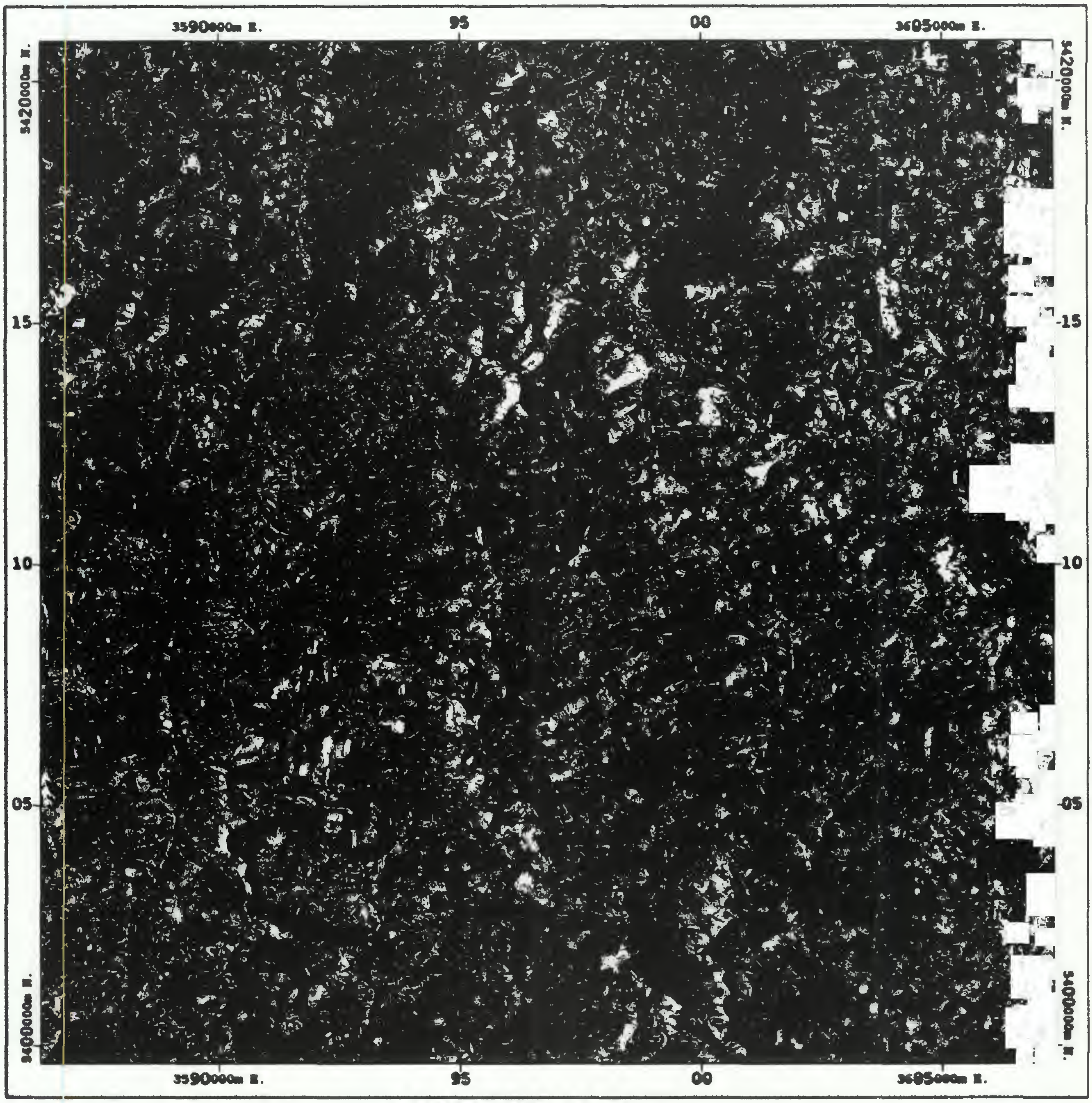

TESTSITE "Ostalb"

ERS-1 SAR-GTC 24.06.93 (Gmap2 11*11 filtered)

Kilometres 5 0 5

Figure 6

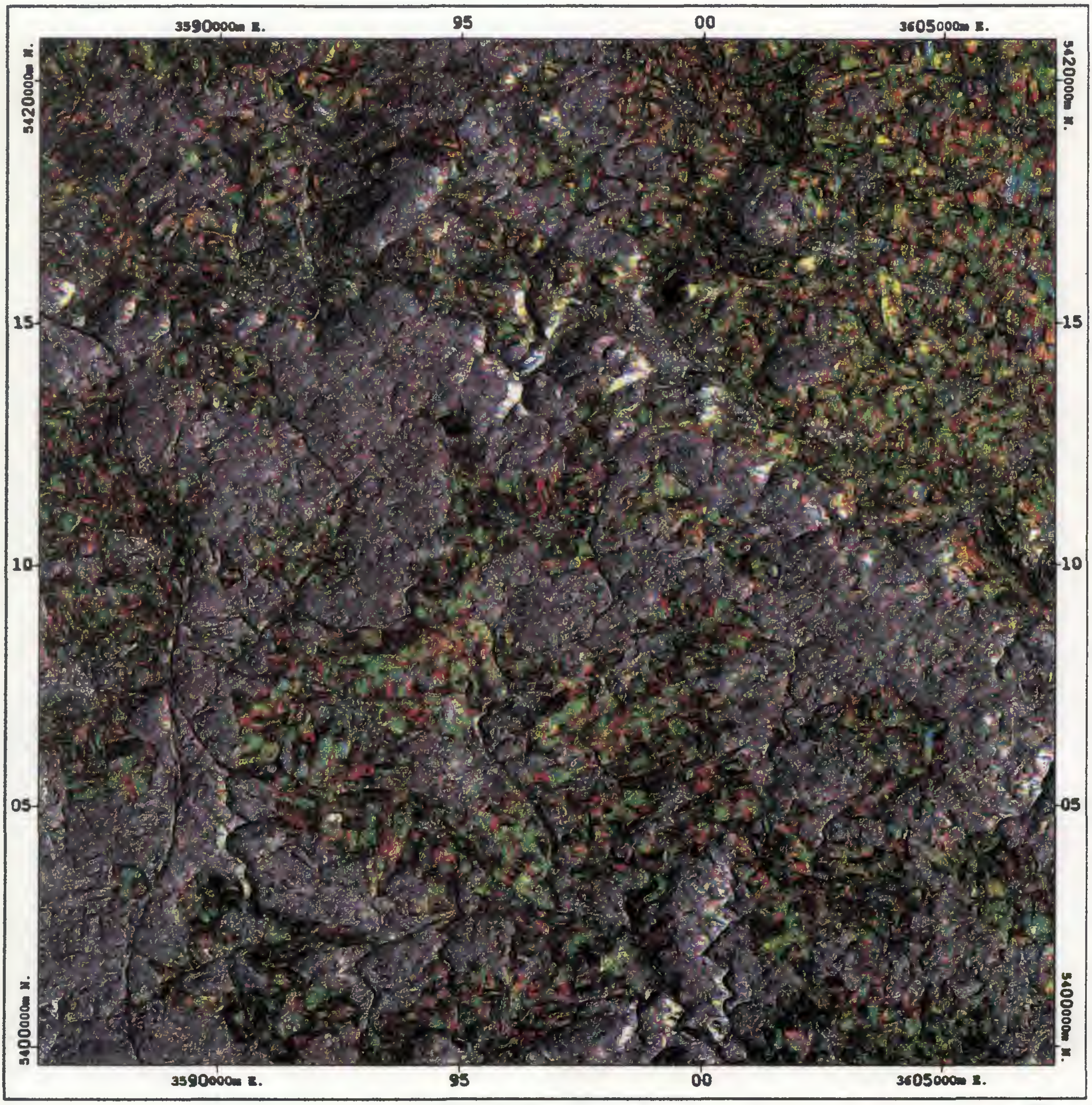

TESTSITE "Ostalb"

ERS-1 SAR-GTC RGB: 29.07. 24.06. 20.5.93 (Gmap2 11*11 filtered)

Kilometres 5 0 5

Figure 7

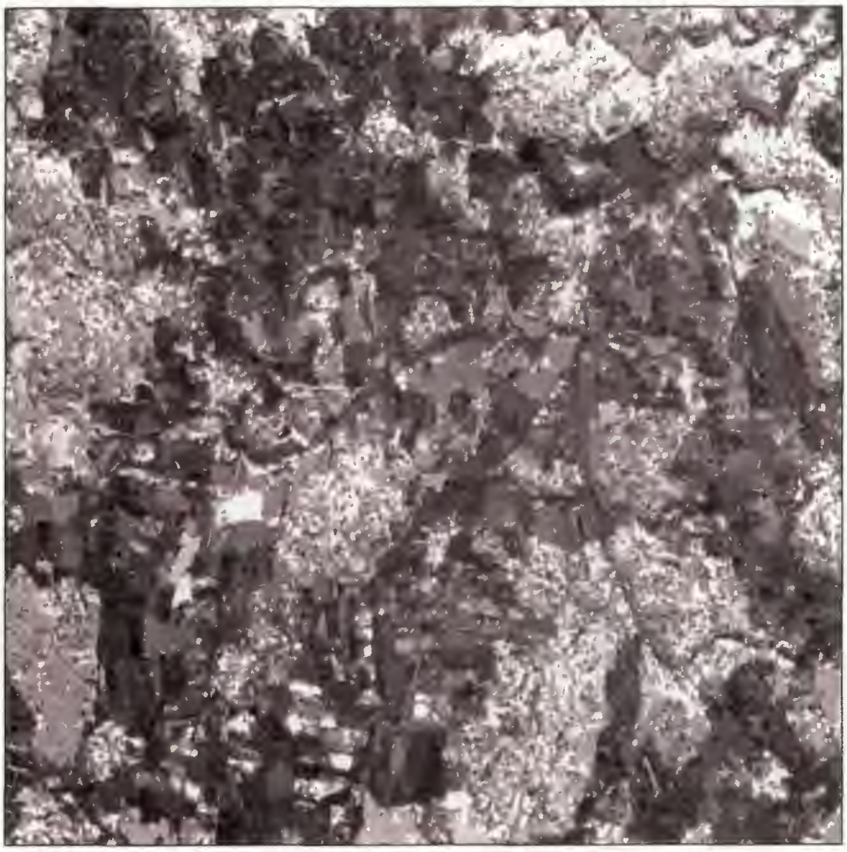

Figure 8

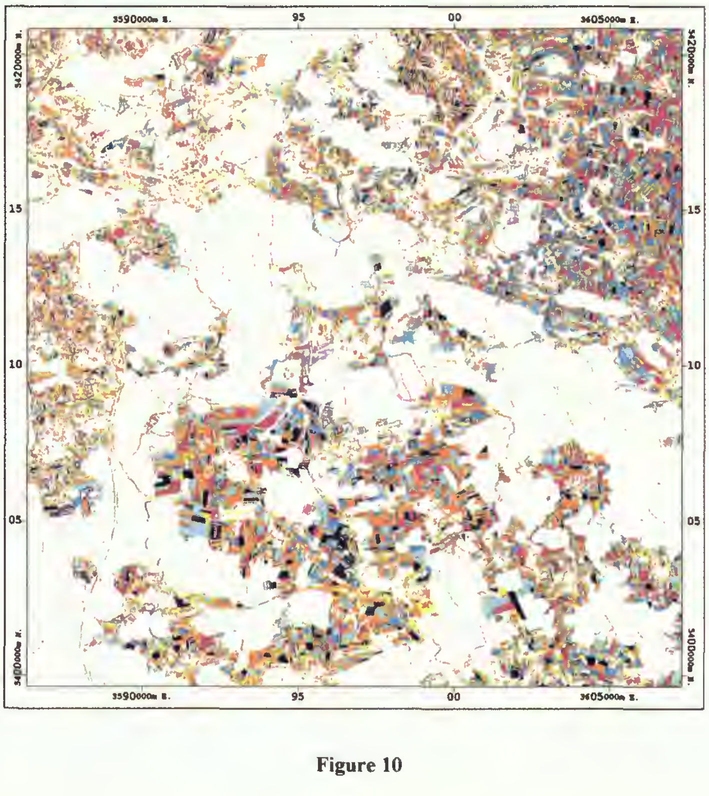

Figure 10

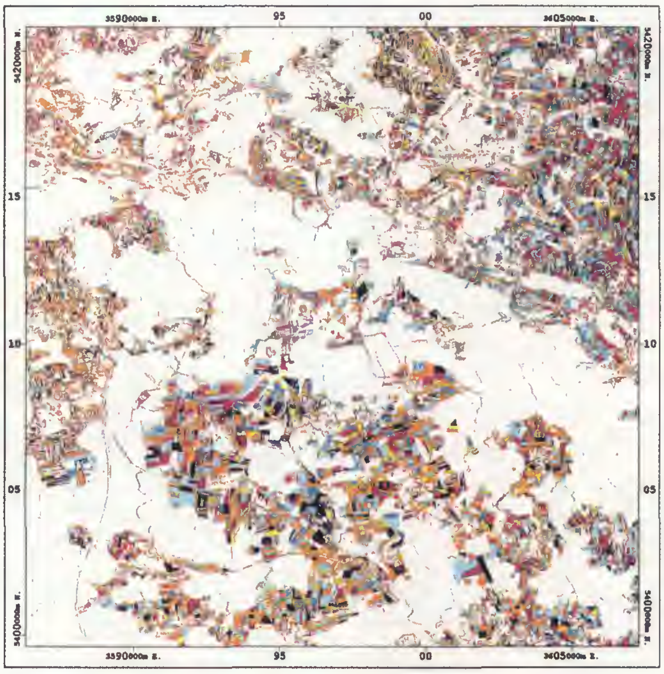

Figure 11

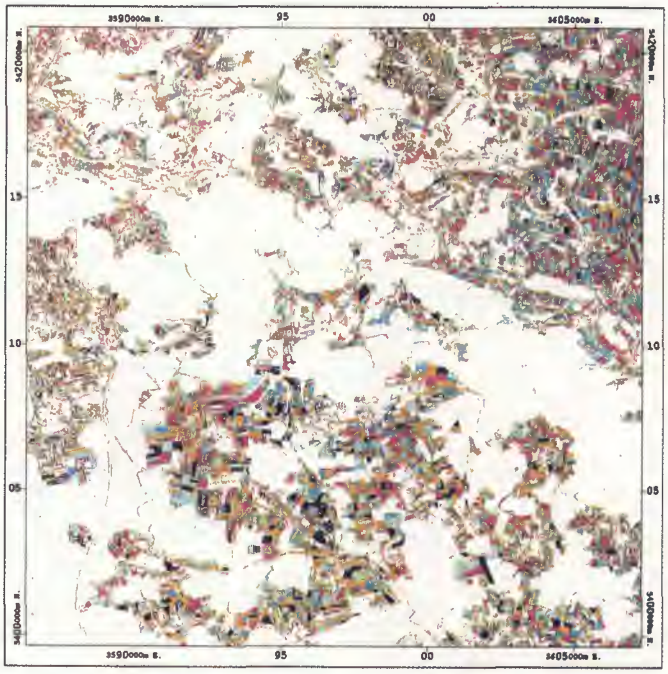

Figure 12

APPLICATIONS DE LA TÉLÉDÉTECTION MICRO-ONDE EN BANDE C (AÉROPORTÉ ESAR ET SATELLITAIRE ERS1) À LA CARTOGRAPHIE DES MANGROVES DE LA RÉGION DE DOUALA (CAMEROUN)

Frédéric Baltzer(1) , Jean Paul Rudant (2) , Emmanuel Tonyé (3)

1- Université Paris-Orsay, tél et fax 33 1 69 41 61 19
2- Université Pierre et Marie Curie, Paris, Tél 33 1 44 27 50 87 , Email jpr@lgs.jussieu.fr
3- Ecole Polytechnique de Yaoundé, Cameroun.

Resumé:

Nous présentons dans cette communication une cartographie des mangroves établie à grande échelle autour de la ville de Douala au Cameroun, à partir de données images aéroportée et nous introduisons à l'utilisation des images ERS1 en vue de donner un caractère régional aux études entreprises.
La disponibilité d'images de haute résolution permet de documenter localement les images ERS1 et ainsi de faciliter leur utilisation à plus petite échelle.

I-Introduction:

Les littoraux tropicaux sont fréquemment frangés par une végétation forestière, la mangrove, qui est adaptée à la vie en milieu salé et présente des caractéristiques de base communes à toutes les régions, mais avec une surprenante variété d'aspects, liée aux conditions climatiques, géomorphologiques et dynamiques locales. La plupart des adaptations de ce type de végétation conduisent à produire une zonation très marquée qui apparait clairement, non seulement sur le terrain, mais aussi sur les images et notamment les vues radar satellitaires.

Parmi les traits communs à pratiquement toutes les forêts de mangrove, on note l'occupation de la zone de battement des marées sous un climat suffisamment chaud, généralement intertropical mais qui peut être tempéré doux s'il est épargné par le gel. Autres caractéristiques constantes, les mangroves ont une remarquable adaptation aux conditions de vie sur des sols instables et privés d'oxygène parce que gorgés d'eau. Enfin et surtout, elles ont un mode de reproduction par plantules flottantes (viviparité) qui leur permet de coloniser très rapidement les sols rendus disponibles par une sédimentation littorale active (voir par exemple Baltzer 1991).

Ces mangroves, constituent une aire de haute productivité biologique grâce au relais des éléments nutritifs d'origine continentale (en phase dissoute et/ou particulaire) au profit de nombreuses espèces végétales puis animales. Elles constituent ainsi un maillon important dans la chaine alimentaire au passage continent océan.

Une bonne connaissance de ces forêts est indispensable pour estimer la valeur relative de leurs diverses parties et ainsi préparer des plans d'aménagement rationnels, évitant des actions gravement préjudiciables aux populations autochtones, par exemple par destruction de zones propices au développement de la faune qui participe souvent de façon significative à leur alimentation en protéine.

II- L'apport des images radar à la cartographie des mangroves de Douala

Sur les côtes du Cameroun, le domaine des mangroves couvre une superficie de 2725 km2.
Les marais à mangroves de Douala, situés au confluent entre Wouri et Dibamba, récemment abandonnés par la Sanaga, contribuent environ pour un tiers à ce total (Voir Fig 1 la situation du site). Leur situation est préoccupante. Le contact avec la ville de Douala entraine des effets anthropiques liés au développement portuaire, à l'érosion des vagues des navires, à la pollution et à l'implantation d'un habitat précaire.
L'étude géomorphologique et sédimentologique, pilotée par l'imagerie aérospatiale a pour objectif de reconnaitre les zones de sédimentation active et de productivité biologique qui doivent être impérativement protégées. La faisabilité d'une spatialisation des différentes formations littorales du même type grâce à l'imagerie ERS1 a été démontré en Guyane (Rudant 1994).

Le contexte général des mangroves de Douala est le suivant. L'estuaire du Cameroun se trouve dans un contexte de baie abritée en arrière de cordons littoraux externes (Pointe Souélaba, île de Manoka, Cap Cameroun), ce qui confère à ses mangroves une beaucoup grande stabilité qui apparaît dans la composition des sédiments (teneur en matière organique en moyenne 10 fois supérieure à ce que l'on trouve en Guyane par exemple). Ce marais à mangroves se trouve maintenant soumis à une érosion de la part des chenaux de marée internes, probablement sous l'effet d'un détournement naturel du fleuve Sanaga qui a fait diminuer les apports sédimentaires. Malgré cette érosion, la stabilité d'ensemble du site est remarquable et constitue la différence principale avec le site déjà évoqué de la Guyane, marqué de son côté par des épisodes de destruction massive alors que les conditions climatiques sont voisines (Plaziat 94).
La zone correspondait antérieurement à un delta triple et le réseau hydrographique résultant de cette convergence d'embouchures a nécessairement guidé le développement des mangroves que l'on trouve actuellement dans la région.

Nous avons pu utiliser simultanément une image en bande C du radar aéroporté ESAR et une mission

photographique IGN infra-rouge au 30000ème sur une zone d'extension très limitée située au voisinage de Douala, afin d'en établir une cartographie détaillée.
L'étape de vérification sur le terrain a commencé par une identification des zones végétales perceptibles sur les images. Elle s'est poursuivie par deux campagnes de terrain au cours desquelles ont été effectués des profils topographiques de précision, des mesures hydrologiques et géochimiques ainsi que des prélèvements de sédiments (Baltzer 1995). Ce type de mesure s'avère indispensable pour comprendre à quel stade d'évolution se trouvent les marais de mangroves concernés et prévoir leur sensibilité aux agressions anthropiques.

Nous présentons ci après l'image ESAR utilisée sur le site (Fig 2), la cartographie des formations végétales (Fig 3) , l'image ERS1 (Fig 4) et un extrait correspondant à la zone , sans traitement puis ayant subi un filtarge GGMAP destiné à faciliter la différenciation des formations végétales (Fig 5), une vue de terrain caractéristique (Fig 6), permettant d'éclairer certaines des légendes proposées pour les illustrations précédentes et enfin une coupe topographique et une carte des isovaleurs de salinité pour un profil N-S (Fig 7).
L'imagerie ERS1 (une seule date) s' avére pour sa part adaptée à une cartographie au 200000è et le "zoom" très localisé autorisé par les données aéroportées a permis de mieux caractériser certaines formations, simplement repérées sur l'image ERS1, et ainsi d'étendre l'interprétation à une échelle régionale. L'utilisation de l'imagerie SPOT a été tentée sur un site test voisin dans le cadre d'une étude de botanique (DIN 1995).
Les travaux engagés confirment la faisabilité d'une reconnaissance automatique des principales formations et les perspectives de développement de techniques de cartographie assistées par ordinateur pour ce type de paysage à partir des données satellitaires SAR . De nouvelles acquisitions par la station de Libreville autoriseront des combinaisons multitemporelles d'images qui conduiront à des analyses plus détaillées (l'échelle du 100000è peut être atteinte avec 3 images du même site).

IV- Perspectives générales et conclusions

A partir de cartes de végétation au 1000000è, au 500000è (Letouzey 1985) et au 200000è, DIN (1995) présente les principaux écosystèmes d'une partie de la façade atlantique du Cameroun où les surfaces inondables couvrent des surfaces moindres que les formations forestières. L'installation et l'extension de ces formations inondables est conditionné par la géomorphologie.Les facteurs abiotiques apparaissent ici favorables au développement des ressources naturelles
L'étude du milieu humain montre une mosaïque de petits groupes ethniques qui vivent généralement isolés les uns des autres. Ces groupes connaissent une forte croissance démographique . Leurs principales activités sont les suivantes: pêche, fabrication d'alcool, agriculture (principalement sur brulis), exploitation forestière, extraction de matériau (sable). Ces activités anthropiques, variant en fonction des localités, sont plus accentuées dans les zones à forte densité de population. L'exploitation forestière due à l'installation anarchique de nombreux immigrés semble pertuber la dynamique des mangroves: les campements et les campements ne cessent de se multiplier. A ces perturbations s'ajoutent certaines interventions de l'état camerounais (exploitation pétrolière, extension des installations portuaires)
L'étude des écosystèmes inondables des côtes du Cameroun suscite de l'intérêt dans plusieurs domaines, surveillance et aménagement des sites pour le tourisme, mise en place de nouvelles techniques de production halieutiques dans ces zones ..)
Compte tenu de ces développements, une mise à jour de la cartographie au 200000 des zones littorales du Cameroun s'avère indispensable. Elle permettrait de préciser les facteurs qui affectent la biodiversité dans la région. L'exploitation des données de télédétection multisources ainsi que des études multitemporelles, facilitées par des développements logiciels méthodologiques récents (Akono 1995)permettront le contrôle des ressources et le suivi des évolutions en relation avec les facteurs locaux.

En particulier, au voisinage de Douala, la cartographie réalisée, interprétable en termes de tendances évolutives des marais et estimation du niveau topographique du sol pourra conduire aux applications suivantes:
-en zone urbaine, gestion des problèmes liés aux surexploitations (pour le bois, la pêche) ou aux activités destructrices comme la construction de zones suburbaines, industrielles ou d'équipements portuaires, aéroportuaires, autoroutiers, etc.
-en zone rurale, protection des mangroves qui sont souvent détruites au profit d'équipements sommairement étudiés pour l'aquaculture, la riziculture ou les salines. Notons que ce comportement risque d'aboutir à la disparition des mangroves dans certaines régions du globe (Inde par ex) et une gestion adaptée permettra peut être au Cameroun d'éviter ce genre de dérive,
- en zone portuaire: discrimination des zones exposées qui devront être protégées des pollutions massives par hydrocarbure et de l'érosion par les vagues d'étrave des navires et embarcations rapides.

Références

AKONO A., TONYE E, LOLO P.M. ELE P., ONDOUA E., JOLION J.M., MONGA O. 1995, Fuzzy logic, object oriented and pyramidal methods for remote sensing multisource images matching, proceedings of RSS95, 11-14 septmebre 1995, University of Southampton, united Kingdom
BALTZER, F. et LAFOND, L.R. 1971 Marais Maritimes tropicaux, Rev. Géog. Phys. Géol. Dyn. Paris, vol. 13, fasc. 2, p. 173 196.
BOYE, M., BALTZER, F., CARATINI, C. , HAMPARTZOUMIAN, A., OLIVRY,J.C., PLAZIAT, J.C. et VILLIERS, J.F. 1975 Mangrove of the Wouri Estuary, Cameroon, Proc. Intern. Symp. Biol. Manag. Mangroves, Honolulu, Publ. Univ. Florida, Gainesville, USA, p. 431 455.
PLAZIAT, J.C., PROST, T., BALTZER, F. & RUDANT, J.P.1994 Specificities of exposed shoreline mangals in French Guiana. 14 th International Sedimentological Congress, Recife, Brazil, abstracts p D69-D70. 1994

DIN, N. 1995 Cartographie et Dynamique des mangroves du Cameroun par analyse d'images SPOT. Rapport de Stage AUPELF- UREF, Institut de la Carte Internationale de la Végétation, Université Paul Sabatier, Toulouse. 60 pp

BALTZER , RUDANT, KUETE, BILONG, DIN, TONYE, ABATA: Etude des mangroves de Douala par télédétection radar et controles de terrain, Rapport CNES 08/95

LETOUZEY R. 1985, Carte phytogéographique du Cameroun au 500000è, IRA-ICIV, Université de Toulouse

RUDANT, J.P.,BALTZER F., DEROIN J.P., LOINTIER M., MAITRE H., PENICAND C., PROST M.T., SABATIER D.; (1994), Possibilités cartographiques offertes par ERS1 en contexte tropical humide, Exemples en Guyane Française, Apports spécifiques des séquences multitemporelles, Workshop ESA Tolède, Juin 1994, ESA-SP365, pp 371- 376.

Remerciements: Travaux effectués grâce aux supports financiers du Cnes et du Ministère de la coopération

Figure 1 Localisation du site d'étude

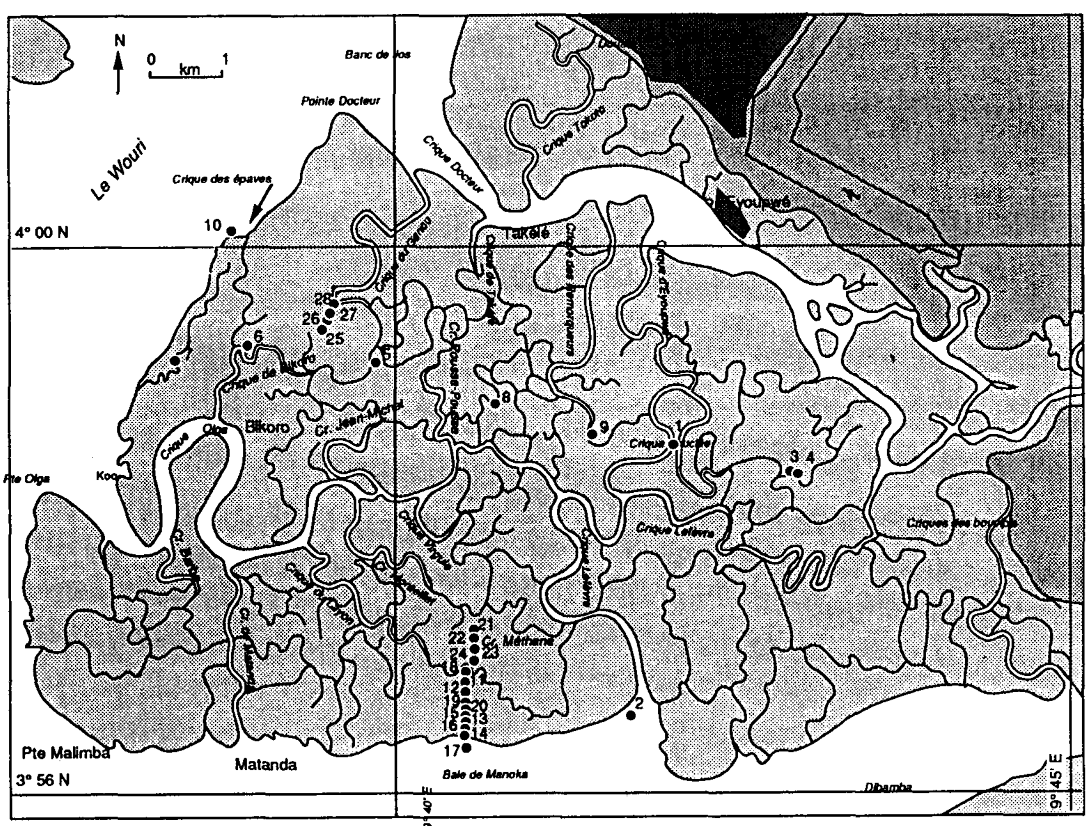

Figure 2 Image ESAR (bande C, polarisation VV, pixel métrique)

La vue ESAR illustre les propriétés très intéressantes de l'information fournie par l'imagerie micro-onde pour l'étude des mangroves. Le réseau hydrographique de chenaux de marée est restitué de façon très nette, et les formations végétales sont aisément reconnaissables , notamment:

- les zones monospécifiques à Rhizophora formant des bourrelets en bordure des rives internes des méandres des chenaux de marée, zones dans lesquelles il est de plus facile de distinguer une végétation à grand développement (bordure des chenaux principaux) d'une végétation à développement moyen (chenaux secondaires). Ces deux types forment un couvert dense et continu.
- les forêts monospécifiques sénescentes à grands Rhizophora, en position interne par rapport aux forêts à grands Rhizophora mentionnées précédemment. Ces forêts sénescentes sont caractérisées par les chablis, discontinuités du couvert végétal résultant de la mort de certains individus.
- zone à Rhizophora nains des zones internes, constituée par une forêt décadente, relativement basse, dans laquelle les arbres sont invariablement petits et grêles et généralement associés à des fougères (Acrostichum).
- la forêt à Guibourtia demeusei, formation arborescente à espèces végétales plus variées, occupant les zones relativement plus hautes (et généralement plus sèches) de la mangrove. Cette forêt se manifeste sur les images ESAR par des taches granuleuses plus sombres que le reste du document, .
- Ces informations permettent une interprétation poussée du développement des marais. On peut en particulier en déduire les zones d'accrétion et donc de création de surface nouvelle, fertile, dans les marais et opposer celles ci aux zones anciennes dont les éléments fertilisants ont été épuisés depuis longtemps par les plantes. Les premières sont propices au développement des espèces animales, les secondes contituent des accumulations parfois importantes de matière organique végétale.

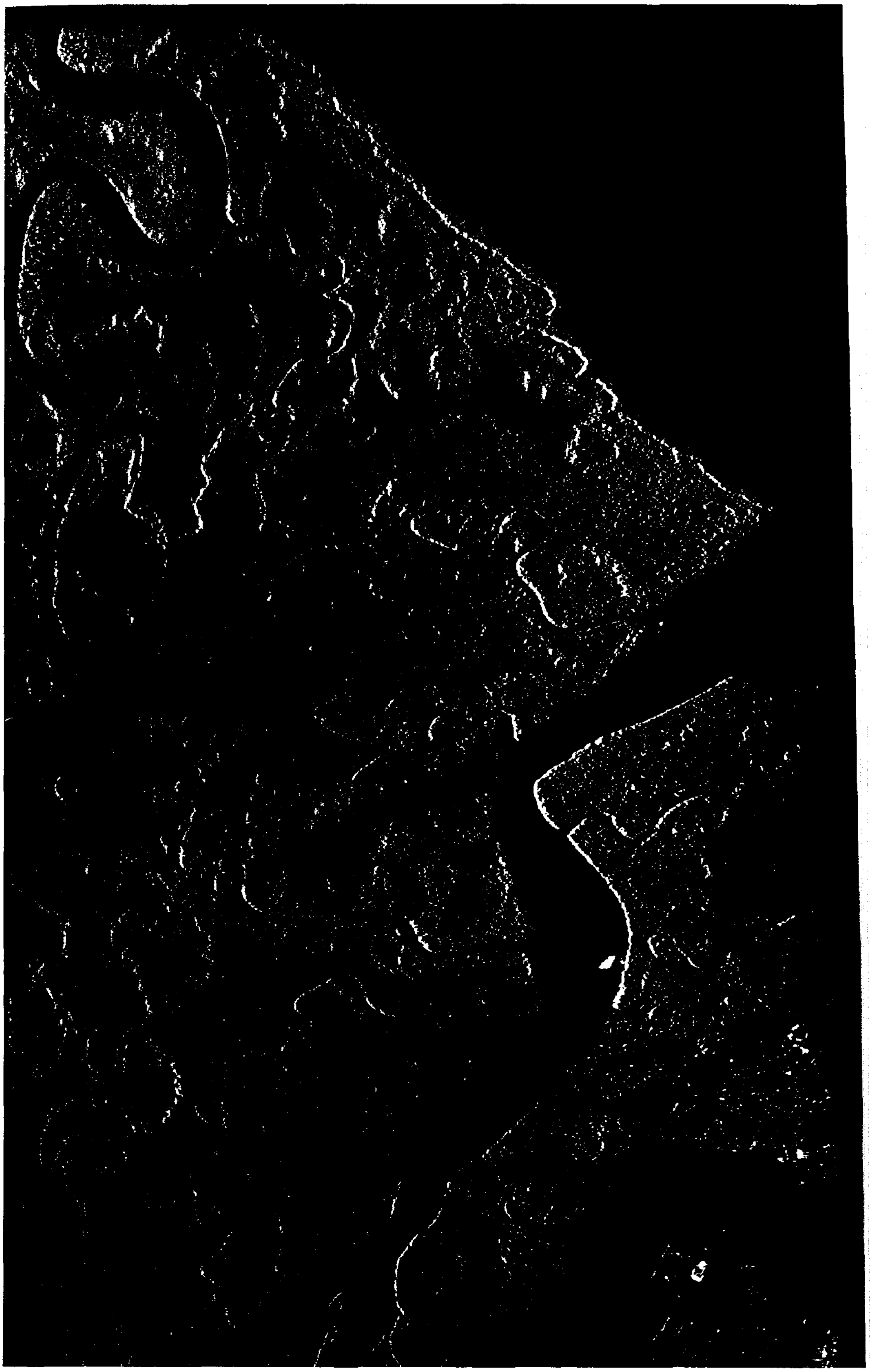

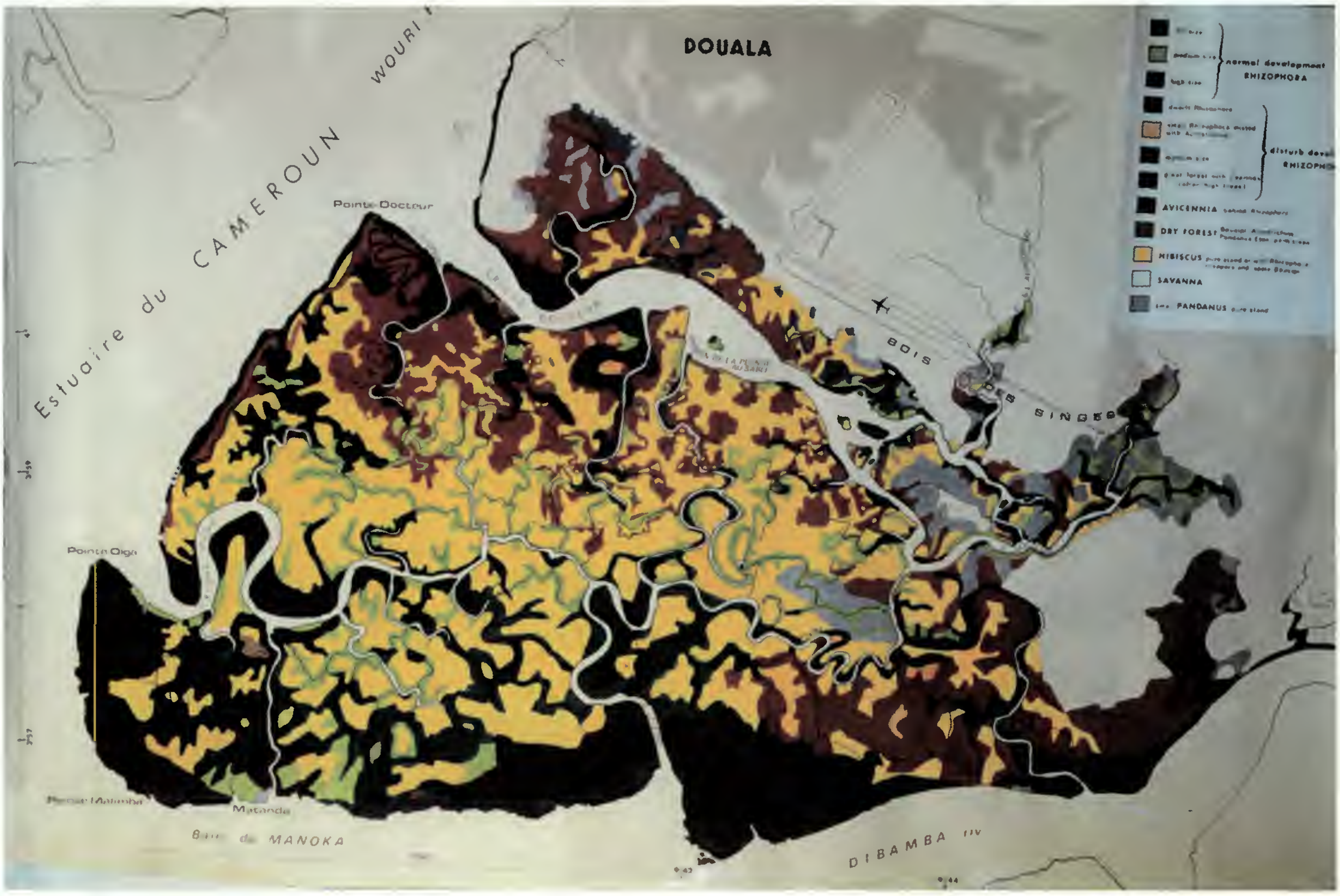

Figure 3 : Carte des formations végétales:
La carte des formations végétales a été dressée au moyen d'une interprétation stéréoscopique de vues aériennes Infra Rouge au 1/30 000 ème (IGN, mission Cameroun de 1967) et des données ESAR. L'interprétation est fondée sur une première mission de terrain de 1972 et sur les missions de 1992 et 1993. La correspondance entre données Radar et photographies aériennes à grande échelle, très satisfaisante, montre l'intérêt de cette technique d'acquisition tous temps. La cartographie par photographies aériennes, en principe de qualité supérieure, présente l'inconvénient d'une mise en œuvre complexe et ne peut être étendue à de grands espaces. Etant inutilisable de nuit et par temps couvert et réalisable uniquement lors d'opérations spécifiques, elle ne se prête pas aux comparaisons entre niveaux de marée différents, ou degrés d'inondation différents pour des comparaisons intersaisonnières ou interannuelles.
Les principales formations végétales figurées sur la carte ont été regroupées en formations primaires et secondaires, suivant qu'elles appartiennet au groupe initial des plantes ayant colonisé le sol ou à un groupe ultérieur. Les formations primaires ont été subdivisées en une série progressive, partant du stade pionnier, et une série régressive, marquée par l'apparition de chablis et la réduction de la taille des arbres.

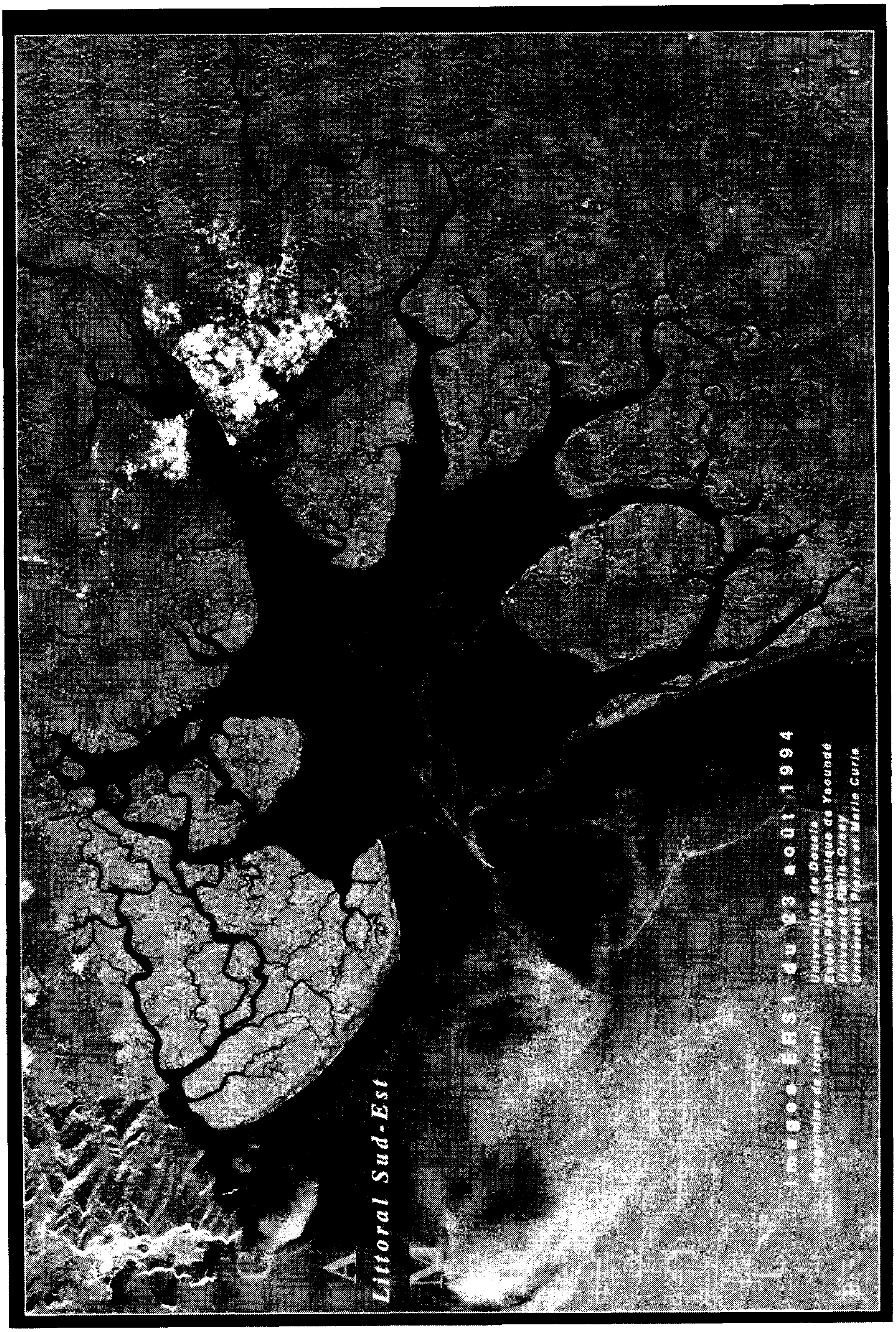
Littoral Sud-Est
Images ERS1 du 23 août 1994
Université de Douala
Ecole Polytechnique de Yaoundé
Université Paris-Orsay
Université Pierre et Marie Curie

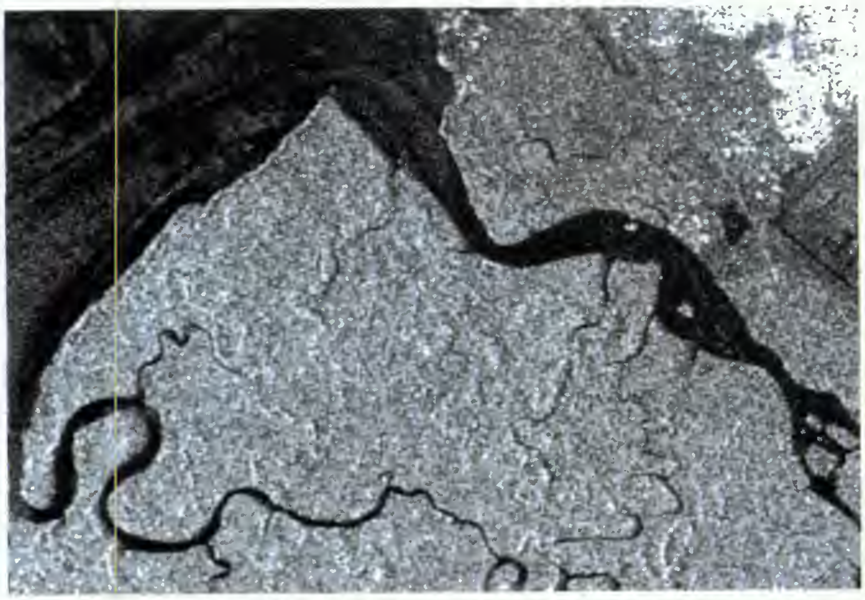

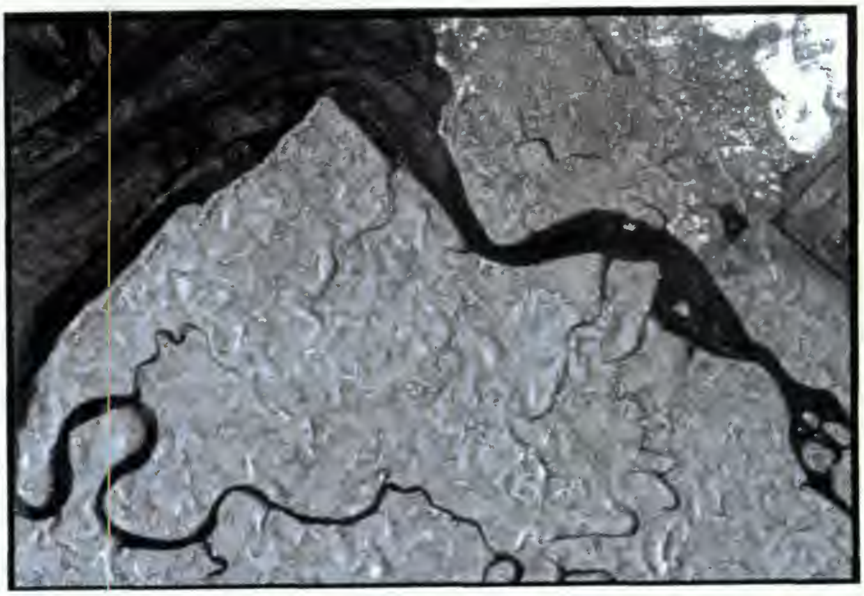

Figure 5 : Scène ERS1 de Douala du 23 aout 1994 et extrait sur la zone de mangrove étudiée.
L'imagerie ERS 1, permet de travailler à une échelle régionale. L'analyse de l'extrait permet d'effectuer les observations suivantes:

en l'absence de filtrage

Les éléments principaux du réseau de drainage sont nettement visibles et la végétation à Rhizophora de grande taille associée aux rives internes des méandres des criques principales est reconnaissable. Les autres formations végétales ne sont pas discernables les unes des autres dans ces conditions d'obserbation.

image filtrée (GGMAP):

Sur les images ERS1 filtrées, le réseau de drainage se distingue avec une finesse sensiblement améliorée et, en plus des zones à Rhizophora de grande taille, on distingue les Rhizophora moyens et la zone des mangroves décadentes. Le problème posé par la distinction entre cette zone des mangroves décadentes et la zone à *Guibourtia demeusei* est à la limite des possibilités offertes par la résolution lorsque l'on dispose d'une seule image. Dans le futur, l'amélioration de la résolution permise par la composition de séquences diachroniques permettra d'améliorer la résolution des images satellitaires.

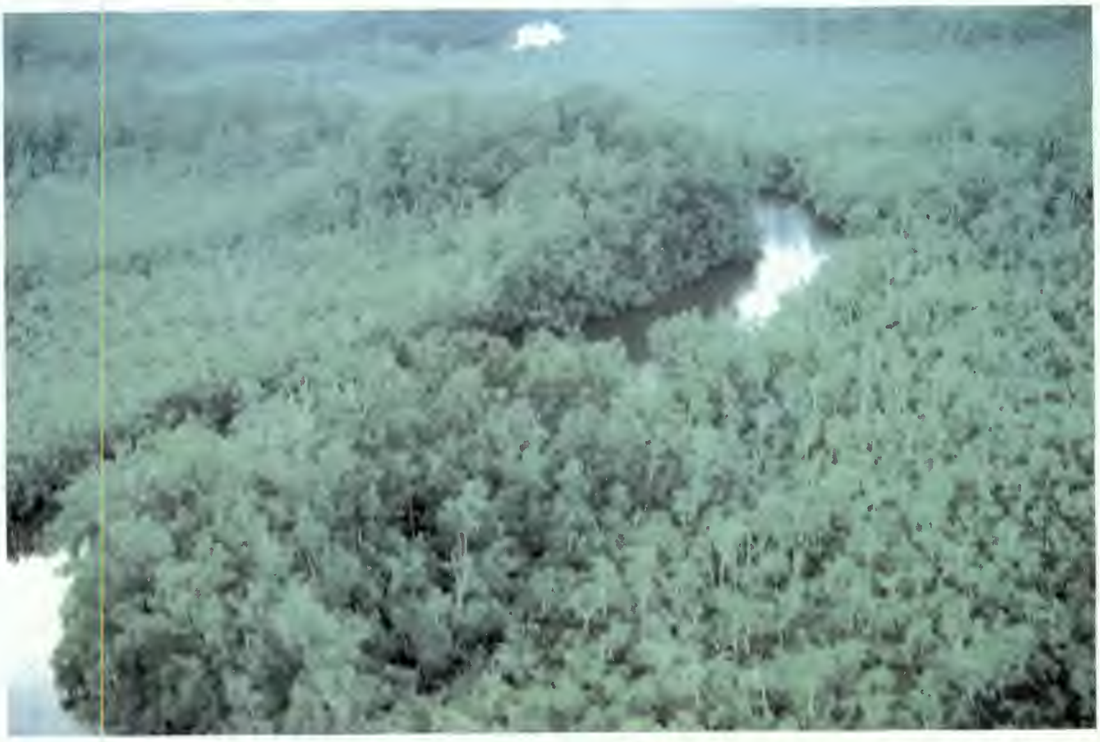

Fig 6 : Végétation en bordure de chenaux de marée mineurs.
L'importance des apports de matériel sédimentaire par les marées influence le développement des mangroves. Lorsque ces apports sont significatifs, les rives internes des chenaux mineurs sont bordées par un liséré de mangrove à Rhizophora sensiblement plus haute que la mangrove à Rhizophora nains environnante, surtout sur la rive externe des méandres.

Figure 7 : Profil topographique et de salinité selon un axe Nord-Sud
La figure comprend:
1°) une coupe topographique de détail, obtenue par nivellement laser.
2°) une coupe des isovaleurs de la salinité, basée sur 14 forages compris entre les sites 17 et 21 et 4 forages entre les sites 25 et 28 (cf. carte de localisation).
Le nivellement (par rapport au niveau moyen des marées) met en évidence la montée du niveau topographique du sol depuis la baie vers les mangroves à Avicennia qui occupent le rempart proche de la mer. Le niveau topographique s'abaisse dans la région correspondant aux mangroves à Rhizophora de localisation interne.
Vers le centre du profil, dans les zones internes au Nord de la Crique du Layon, un plateau d'altitude intermédiaire correspond à l'occupation par une mangrove naine à Rhizophora, dont le sol est enrichi en matière organique par les générations successives de palétuviers. Enfin, tout à fait au Nord, les niveaux topographiques les plus élevés sont atteints au voisinage de la Crique du Genou. Ces altitudes coincident avec une occupation par les formations à Guibourtia demeusei.

Les salinités figurées ont été mesurées en fin de saison sèche (janvier-février 1993). Les mesures traduisent la concentration du sel par évaporation (domaine proche de la mer), et la dilution par les eaux douces percolant à partir du continent. L'évaporation est plus sensible au voisinage de la surface, dans les zones les plus hautes du profil. La salinité des eaux interstitielles des sédiments, (mesurée par réfractométrie sur de l'eau extraite par pressage) atteint 35 g/l sous le niveau topographique le plus élevé du rempart à Avicennia, soit près du double de la salinité dans la baie de Manoka à la même époque. Au contraire, la salinité au voisinage de la crique du Genou s'abaisse à 7,5 g par litre. Dans tout le profil, y compris près de la Crique du Genou, les partie hautes présentent une salinité relativement forte, en raison des effets de l'évaporation liée à la saison sèche. Les fortes salinités de profondeur, sous les points hauts du profil, suggèrent fortement que l'effet de saisons sèches particulièrement accentuées peut se maintenir au moins sur des intervalles pluriannuels.

isovaleurs de la salinité (g/kg)

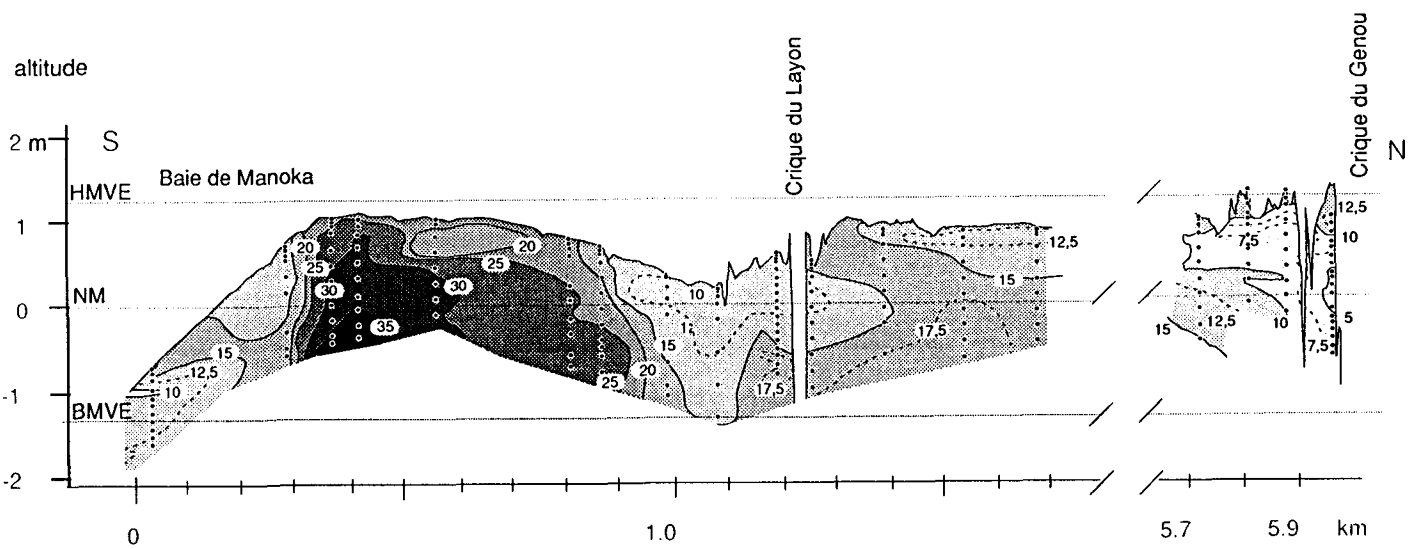

RESEARCH ON THE CAPABILITIES OF ERS-SAR FOR MONITORING OF LAND USE CHANGES IN THE NEOTROPICS : PRELIMINARY RESULTS

Jan Verhoeye, Boudewijn De Roover

University of Gent, Department of Forest and Water Management
Coupure Links, B-9000 Gent, Belgium
Tel. : +32 9 264 6091 Fax : +32 9 264 62 40
E-mail: Jan.Verhoeye@rug.ac.be, bdr@carara.rug.ac.be

ABSTRACT

Land use maps at a scale of 1:200.000 exist for the whole of Costa Rica. They were produced in 1986 from Landsat-TM images and aerial photographs. Given the frequent cloud cover, regular updating of those maps via optical satellite data is problematic. Earlier research on the usefulness of ERS-SAR data for land use monitoring indicated a potential on condition that multitemporal data are available and that the area is flat. The north-east of Costa Rica is a region with a nearly flat relief and some isolated hills. Most of the land is covered with pasture and wet tropical forest. During the last decade a significant portion of the area has been converted into plantations, mostly of banana.
A procedure is being developed aimed at determining the land use changes over the period 1985-1995. It consists of calibration (Laur, 1992), resampling, filtering, segmentation, principal component transformation and supervised classification of multitemporal radar images. The feasibility of this procedure can be illustrated with an example in which large banana plantations can be detected in areas with pasture and forest.
The presented results focus on the first steps of the procedure, up to the multichannel segmentation of the images. The "multiresolution pixel linking" technique has been adopted, implemented and tested. It produces segmented versions of the original image at different spatial resolutions. It is expected that this will help to solve the problem encountered in the updating of a rather coarse land use map by means of high resolution ERS-SAR images.
The study will also include the analysis of the optimal acquisition date, classification performance in relation with multitemporal data, and the influence of local meteorological conditions on the radar image. However, these results can not yet be presented as the fieldwork was only recently executed. Furthermore the ERS-SAR images of 1995 are not yet available.

Keywords: land use change, ERS-SAR, segmentation

1.INTRODUCTION

The study area is situated in north-east Costa Rica, between 9° 30' and 11° N, 83° and 84° W. Three main classes of land use occur: forest, pasture and banana plantations. The last decade the region has witnessed an important change, caused by economic development and a large population increase.
A medium scale land use map (1:200.000) has been produced by the Costa Rican National Geographic Institute in 1986, based upon aerial photographs and Landsat-TM images. Given the strong economic developments in the area, an updating of this map is highly desirable. However, due to the persistent cloud cover, this has not yet been possible. ERS-SAR data may thus provide the solution.
Earlier research on the usefulness of ERS-SAR data for land use monitoring indicated a potential on condition that multitemporal data are available and the area is flat.

2. DATA SET

The following data set formed the basis of the research
- four ERS1-SAR.PRI images, dating from 9/11/1992, 16/8/1993, 20/9/1993 and 25/10/1993. These allow a multitemporal processing. It can be seen though that these images date from four consecutive months, which may mean that the full range of the vegetation dynamics may not be captured. The images that have been acquired in 1995 (10 in total) will cover the complete period from April till October, and should be even more appropriate for our goals. The images are not yet available though.
- one Landsat-TM image, dating from 6 February 1986, with 0% cloud cover
- topographic and land use maps at different scales
- ground truth data collected on 500 point samples, in August-October of 1995.

3. PROCESSING CHAIN

The complete processing procedure is represented in figure 1. Preliminary results indicate that the segmentation should be preceeded by smoothing, by use of e.g. a Sigma filter, and by a Karhunen-Loewe transformation.
It should be noted that the results presented hereafter do not include the classification and evaluation, as the field

Proceedings of the Second ERS Applications Workshop, London, UK, 6–8 December 1995 (ESA SP-383, February 1996)

work was only executed recently and because the 1995 images are not yet available.

4. SEGMENTATION

4.1 Introduction

Due to the speckle inherent to radar image data a specific approach is necessary. A processing chain has been developed, in which image segmentation is an essential step. The "Multiresolution Pixel Linking" technique was considered an appropriate technique. On the one hand it transforms the image into homogenous regions, and on the other hand it produces segmented images at different resolutions (Burt, 1984; Rosenfeld, 1984; Van de Bruane, 1988). The latter fact will help solve the scaling problem created by updating a medium scale map using high resolution ERS-SAR images.

4.2 Pyramid structure

The "Multiresolution Pixel Linking" algorithm creates multiple versions of the original image, each with decreasing resolution. By stacking these images one on top of the other a tapering structure is created, resembling a pyramid (figure 2). The bottom layer (level 0) consists of the original image, measuring 2^n rows by 2^n columns. The next layer (level 1) measures 2^{n-1} rows by 2^{n-1} columns, level k 2^{n-k} rows by 2^{n-k} columns. Usually the pyramid will consist of l layers, with $l < n$, meaning the pyramid will be blunt topped.

Between two consecutive layers (n and n + 1, respectively called child and parent level) parent-child relations are defined, with each child being linked to the parent which it most resembles.

A parent on row i, column j and level n + 1, has by definition, 16 potential children on level n. These can be found on rows 2i - 2, 2i - 1, 2i, 2i + 1 and on columns 2j - 2, 2j - 1, 2j, 2j + 1.

It can be proved that, by consequence, each child on row i, column j and level n can choose from four potential parents, situated on row (integer)(i/2), (integer)(i/2) + 1, column (integer)(j/2), (integer)(j/2) + 1 on level n + 1.

4.3 Initialisation

The initial values of the base layer (level 0) of the pyramid are obtained by copying the original image. The initial values of level k (> 0) is calculated by averaging the pixel values of level k - 1. Hong (1982) concluded that the best segmentation results were obtained when the averaging was done within windows measuring two by two pixels.

A parent on row i, column j and level n + 1 is calculated by averaging four children on level n. These can be found on row 2i - 1, 2i and column 2j - 1, 2j.

When several channels are used for segmenting, the initialisation is performed for each channel separately.

4.4 Iterative linking and recalculating

Consider two layers, n and n + 1, containing respectively the child and parent nodes.

The first step consists of linking each child to the most resembling parent, with the choice limited to the four potential parents described above. The criterion used for picking the parent is the Euclidean distance between the child and parent value, the child being linked to the closest parent.

When several channels are involved, the distance is calculated for each channel separately. When adding each channel may be assigned a weight indicating its relative importance.

The second step consists of the recalculation of each parent. For each parent all 16 potential children are evaluated. Only those that were linked to the parent will be used for calculating a weighted average. The weights are the number of pixels in the base level that have been linked to the current child through the child-parent links of lower levels.

When several channels are involved, the new value is calculated for each channel separately.

The newly calculated value for the parent can differ from the original one. For this reason the linking and recalculating is reiterated until stable links emerge.

This process is repeated for each pair of child-parent levels starting from the base level upward till the top level is reached.

4.5 Dumping of root values

By linking the pixels, starting from the base level upward till the top is reached, "tree"-like structures are created within the pyramid. The "leaves" are formed by the pixels in the base level, the "roots" can be found at the top level. Leaves and roots are connected by "branches", symbolised by the links between child and parent. Remark that "dead branches" can exist, defined as branches that are not linked down to the base level and which thus not have any leaves.

When dumping the root values, the values of the top level nodes are moved downward, following the parent-child links. On each level, the child value is substituted by the parent value. This means that segmented versions of the original are created on each level.

As the number of pixels in the top level is relatively limited compared to the number of pixels in the base level, the base level will be well segmented. As furthermore the root values are transmitted following the child-parent links, boundaries will be respected.

An example of the effect of the segmentation can be seen in figure 3. It can be see that the speckle, still present in the filtered input image, is largely removed from the segmented image. The boundaries of the banana plantations (yellowish to light green) are well preserved.

4.6 Result

The result of the segmentation algorithm applied to the four principal components of the ERS1-SAR images can be seen in figure 4. A preliminary interpretation, based upon field data and the Landsat-TM image, suggest that the banana plantations appear as bright yellow to yellowish green, pastures as dark green and forests as light green.
The updating of a medium scale map (1:200.000) by use of high resolution ERS-SAR images gives rise to a scaling problem: the map represents a generalized cartographic model of the world. It is expected that this problem may be overcome by producing images at coarser resolutions, each corresponding with a higher level of the pyramid.
This feature is illustrated in figure 5, by four images with decreasing resolution, measuring 512 by 512, 256 by 256, 128 by 128 and 64 by 64 pixels. It can be seen that the images get a more generalized appearance as details tend to disappear.

5. FUTURE DEVELOPMENTS

By combining the segmented radar image with the ancillary map (figure 6), land use changes can be detected. The analysis will split into two parts. The first process will concern the control of the boundaries in the land use map. The second step is related with the possible change of content of the polygons. Suitable multidate SAR-data should allow to identify the major land use classes such as villages, forest, pasture, perennial and rotation crops. The analysis will focus specifically on the fringe area between forest and agricultural land, as this is the region where much of the deforestation is occurring.

6. REFERENCES

Burt P.J., 1984: The pyramid as a structure for efficient computation. In: Rosenfeld A., Multiresolution image processing and analysis, Berlin, pp 8-35.

Hong T.H., 1982: Image smoothing and segmentation by multiresolution pixel linking : Further experiments and extensions. IEEE Transactions on Systems, Man, Cybernetics, pp. 611-622.

Laur, H., 1992: Derivation of backscattering σ^0 in ERS-1.SAR.PRI products. ESA/ESRIN.

Rosenfeld, A., 1984: Some useful properties of pyramids. In: Rosenfeld A., Multiresolution image processing and analysis, Berlin, pp 8-35.

Van de Bruane, F., 1988: Automatic segmentation of SPOT data by using overlapping pyramid chains. Thesis.

Aknowledgements
The project is financed by the belgian Office of Scientific, Technical and Cultural affairs (OSTC). The ERS-SAR test images were made available by ESA.

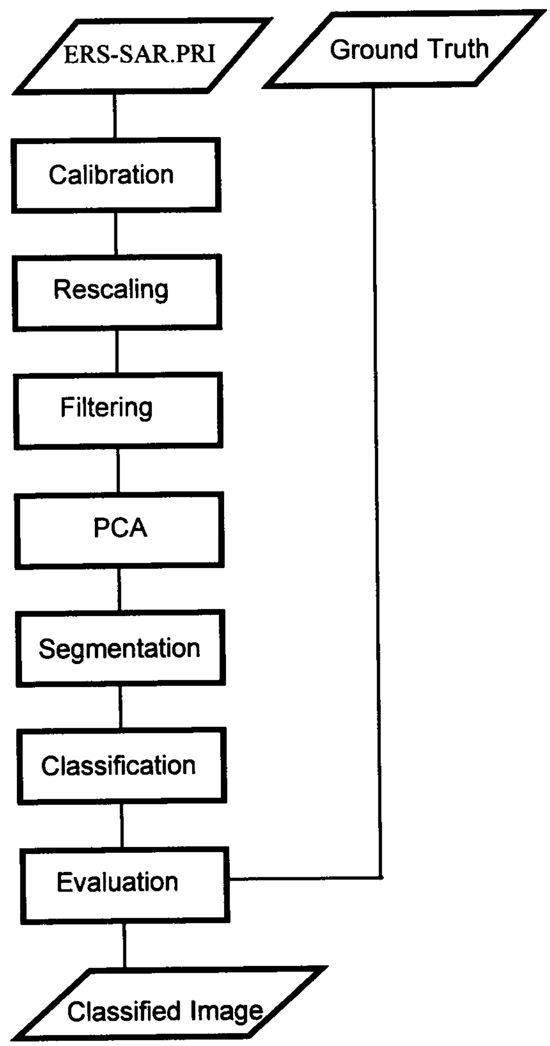

Figure 1: Processing chain

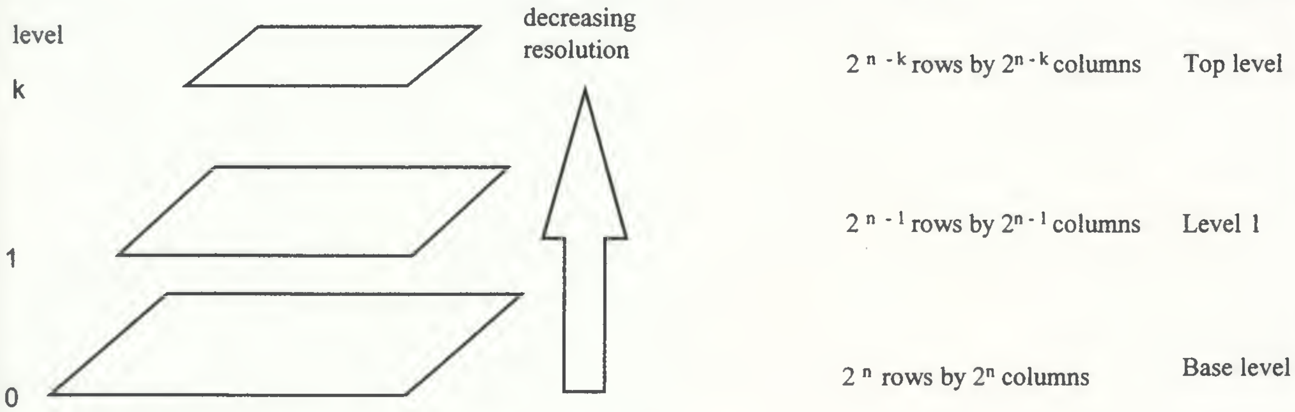

Figure 2 : Pyramid created by Multiresolution Pixel Linking algorithm

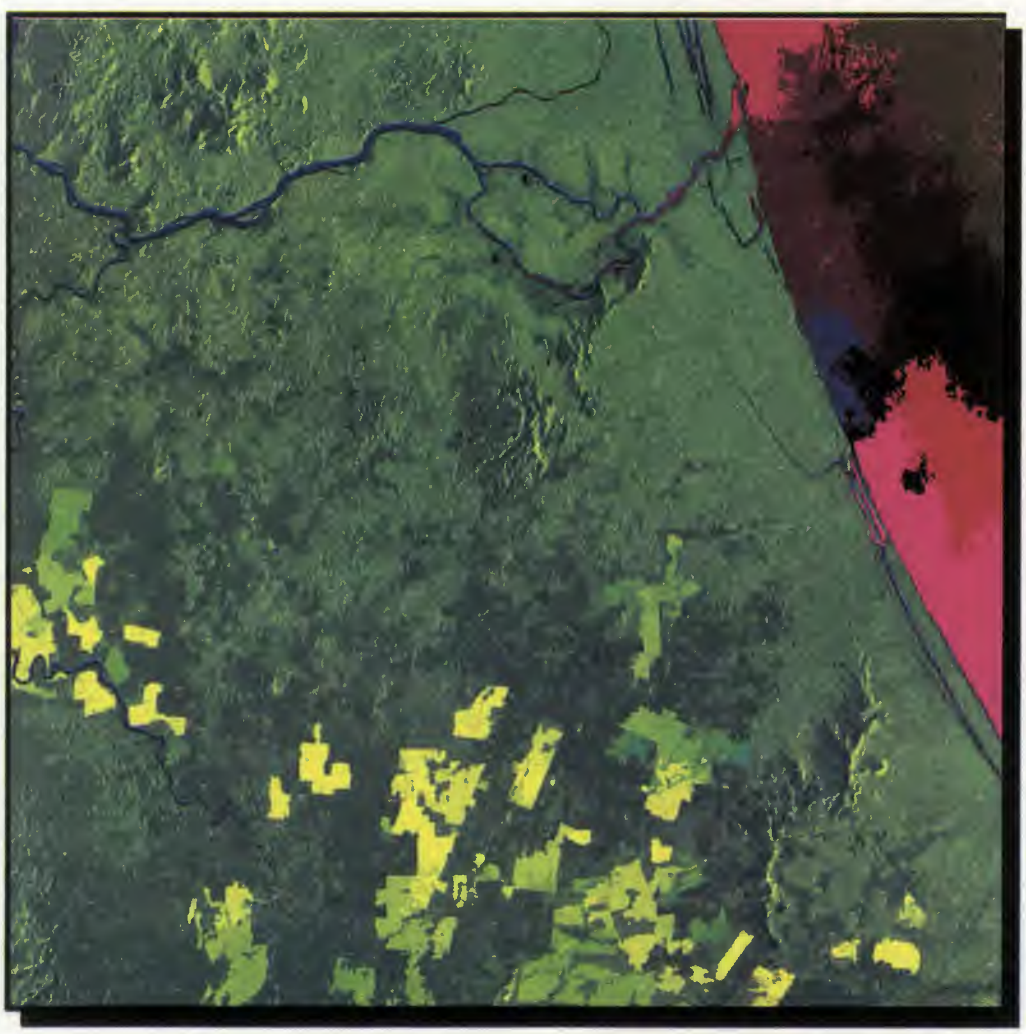

Figure 4 : Segmentation result (Image size 2048 X 2048 pixels, color composite R = PC3, G = PC1, B = PC2)

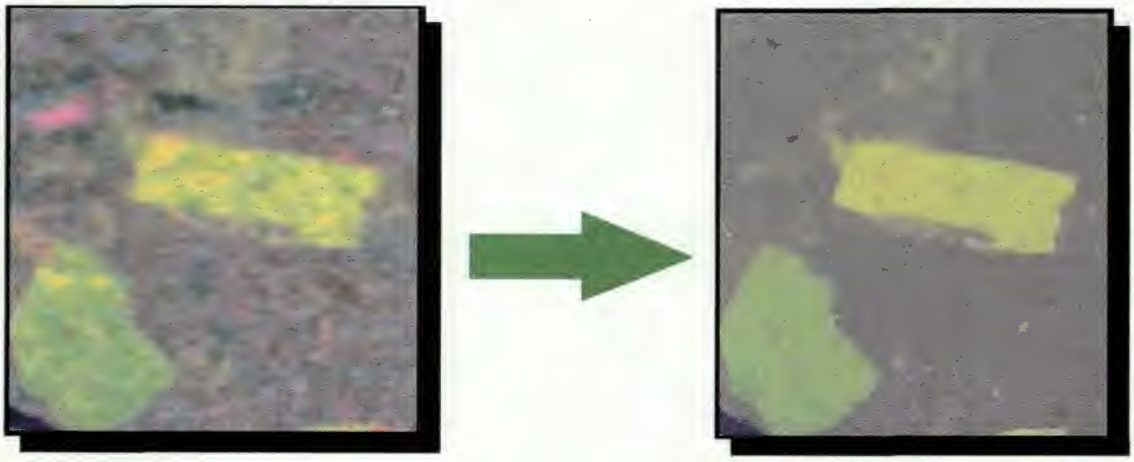

Figure 3 : Segmentation (Detail measuring 124 X 178 pixels, color composite R = PC3, G = PC1, B = PC2)

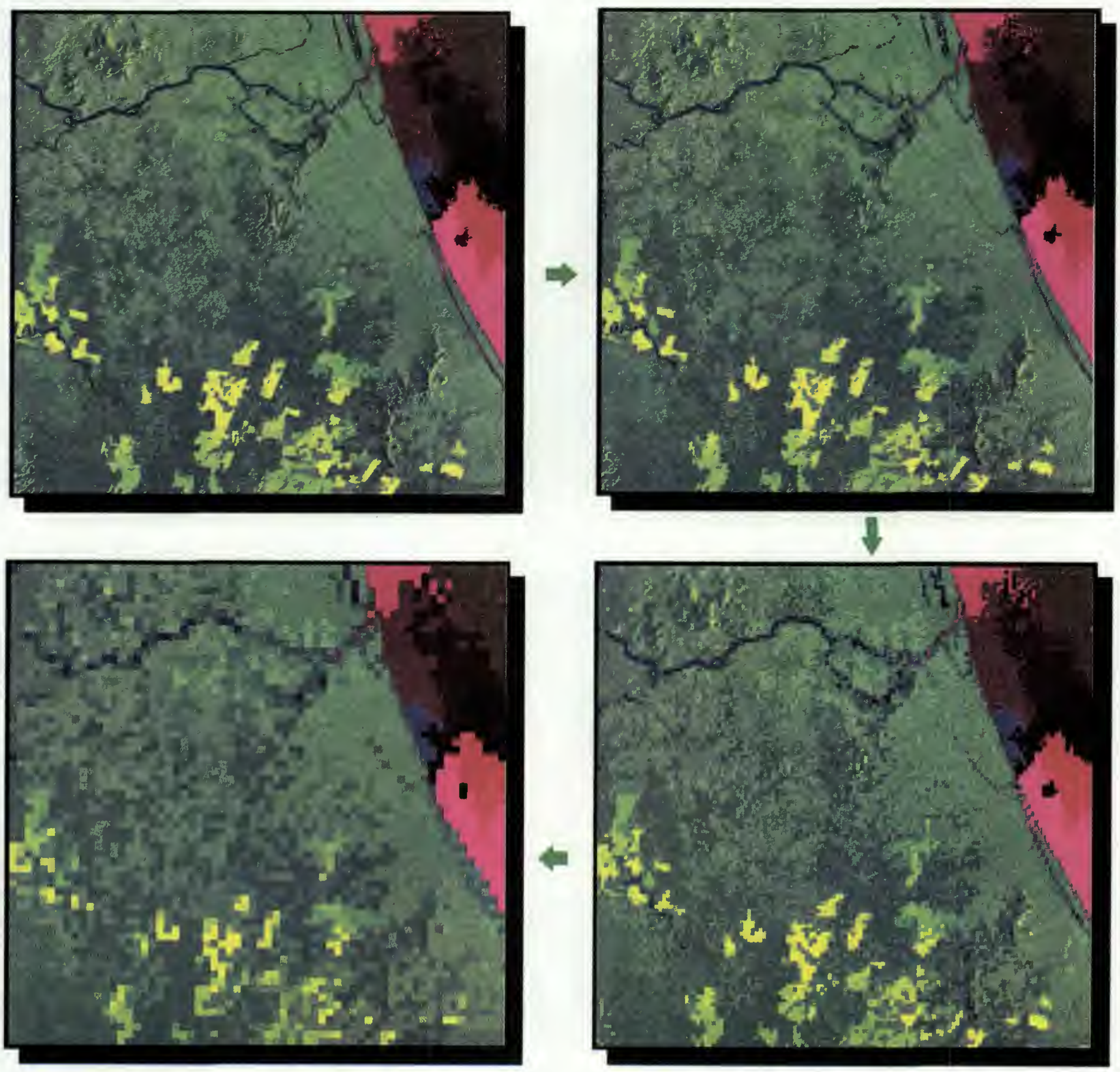

Figure 5: Multiple resolution images

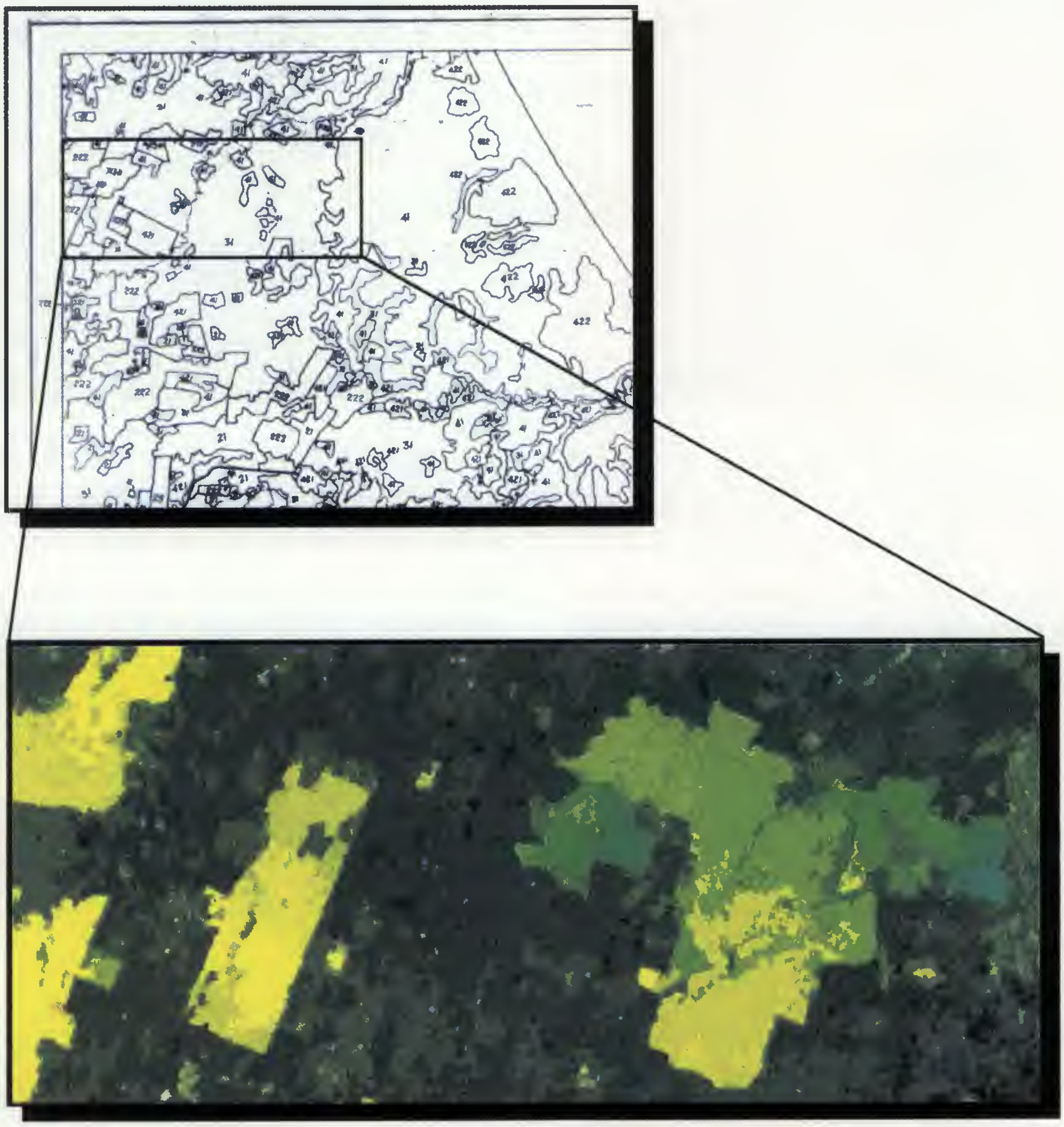

Figure 6 : Future developments

THE 1995 FLOOD IN THE NETHERLANDS MONITORED FROM SPACE - A MULTI-SENSOR APPROACH

Yiman Wang, Bas N. Koopmans and Christine Pohl

Department of Earth Resources Surveys - Radar Application Group
International Institute for Aerospace Survey and Earth Sciences (ITC)
350 Boulevard 1945, P. O. Box 6, 7500 AA Enschede, The Netherlands
Tel: +31-53-4874444, Fax: +31-53-4874400, E-Mail: yiman@itc.nl or pohl@itc.nl

Abstract

Flooding in the delta area of Rijn and Maas in central Netherlands in January/February 1995 was imaged by the ERS-1 radar of the European Space Agency. The radar data acquired during flooding were processed and merged in several combinations with pre-flood Landsat TM and pre-flood radar imagery. The multi-sensor and time sequential data are useful for flood monitoring and damage assessment.

1. The ERS-1 Radar Satellite

The ERS-1 SAR operates at C-band (5.3 GHz) and as an active radar system has the advantage of being independent of daylight and penetrating the cloud cover, which is often dominant during the flooding season. The water areas may be differentiated in general from vegetation and urban areas in radar images as the system is sensitive to the surface roughness.

Since April 1994 the ERS-1 satellite of the European Space Agency is in the geodetic phase, which means a 168-day repeat cycle. This is specially to attain a high density acquisition of altimeter measurements. For imaging radar it means an increase of sidelap of adjacent strips during the 168-day repeat cycle. Sidelapping images with lateral shift are available over shorter periods.

During the recent floods in January/February 1995, an ERS-1 radar image was acquired on 30 January over the lower river courses of Rijn (Rhine) and Maas (Meuse) in the central delta area of the Netherlands.

2. The 1995 Flood Situation

The three river courses in the central delta area of the Netherlands are the Nederrijn (the lower reaches of the Rhine), the Waal and the Maas. The river channels are running between low summer dikes and have an average summer discharge of, respectively 350 m^3/sec, 1480 m^3/sec and 230 m^3/sec. Flooding of the "uiterwaarden", the overflow planes between summer and winter dikes, is normal during late winter-time, when river discharge increases as a result of heavy rainfall and snow melting in the upstream areas. This winter the flooding was exceptional as a result of a long period of continuous intensive rainfall in western Europe combined with snow melting due to abnormally high temperatures. Extensive flooding occurred in France, Belgium, Germany and The Netherlands during late January and early February which is believed to be the worst for the last 60 years.

On 25 January, the water level of the Maas river started to rise dangerously near the city of Maastricht in the south of the Netherlands. Two days later, the water level of the Rijn at Lobith rose sharply **(fig. 1)**. On 30 January, evacuation of 75,000 inhabitants and their cattle began from the area of "Land van Maas en Waal", a "waard" between the rivers in the central part of the Netherlands. "Waard" is the Dutch word for an interfluvial area between the winter dikes of different river channels.

Water levels of Rijn at Lobith and Waal at Zaltbommel reached their highest peak at +16.68 m NAP (normal Amsterdam zero) and +7.43 m NAP on 1 February 1995. For the Rijn this is nearly 7.5 m above average winter level. Discharge calculations for 1 February 1995 based on the correlation between measured water levels and discharge data over 1993 and previous years (Jaarboek Monitoring Rijkswateren 1993) indicate river discharges of 11930 m^3/sec, 7529 m^3/sec, 2606 m^3/sec for, respectively Rijn (Lobith), Waal and Nederrijn **(fig.2)**.

Water impregnation and seepage severely weakened the winter dikes as result of the prolonged period of flooding and the extreme height of the water level, near or over the critical level. Therefore evacuation was ordered of nearly a quarter million inhabitants from the area between Maas, Waal and Nederrijn. Fortunately the evacuation turned out to be only preventive, as no important dike failures occurred, thanks to day and night vigilance and extensive improvised restrengthening of the threatened dike segments (indicated by yellow dashed lines in **fig. 3**).

3. Methods and Results

To monitor the flood situation, an ERS-1 SAR scene of 30 January over the flood area was acquired. The SAR image was geometrically corrected and geocoded to the Dutch national coordinate system RD

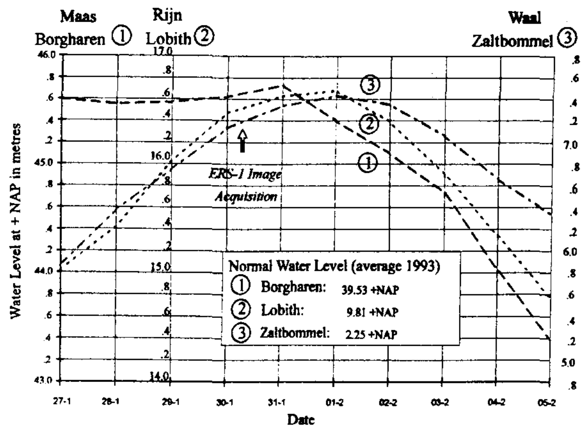

Figure 1. Water levels measured at Borgharen (Maas), Lobith (Rijn) and Zaltbommel (Waal) during the flooding.

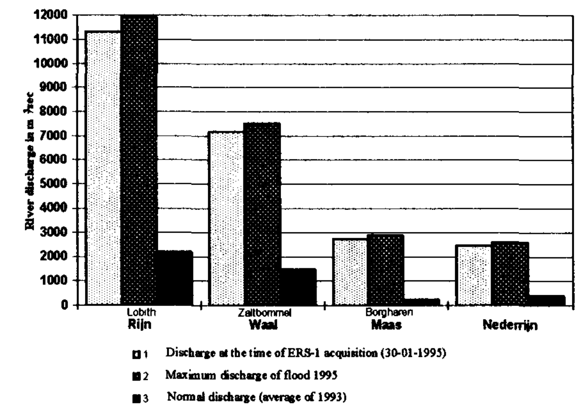

Figure 2. River discharge of Rijn, Waal, Maas and Nederrijn during flooding.

(Rijksdriehoeksmeting) using control points from 1:50,000 scale topographic maps. For comparison of the flood situation with the normal river course, a pre-flood ERS-1 SAR scene (21 September 1994) and a Landsat TM scene (16 July 1987) were used for a multi-sensor and multi-temporal analysis. All the images were resampled to 30 m ground resolution on the same coordinate system.

The Landsat/ERS merged-image is shown in **fig 4.** To enhance the flooded areas on the SAR flood image (dark tone due to specular reflection), the grey values were inverted to show the flood waters with bright tone (upper left). The features in the agricultural areas were suppressed by a threshold filtering and stretching. The pre-flood Landsat TM data were used to make a false colour composite with TM bands 1 in red and TM band 4 in green. This shows the pre-flood river channel during the dry season (lower right). The final colour composite (middle) was made by combining TM bands 1, TM band 4 and the inverted, threshold stretched SAR flood scene using red, green and blue channels, respectively. In this way and by further contrast stretching, the flooded water areas obtained their appropriate light-blue colour (from the inverted SAR image). The more permanent water bodies (also during low water) show up in dark bluish colour. The flooded summer dikes can be distinguished in several places. The grassland and cultivated land is shown in green (from TM band 4) and urban areas shown in red colours (TM band 1) (fig. 4, middle). The selected colour composite clearly displays the pre-flood river in dark blue and the flooding area in light blue with the inundated agricultural fields visible by colour variations and regular patterns (**fig. 6**). This allows a flood damage assessment of the cultivated zones in the flooded area.

The ERS pre-flood/ERS flood merged-image is shown in **fig. 5**. This is a combination of the SAR scene acquired during flooding with a pre-flood SAR scene. The pre-flood scene (fig. 5, upper left) was contrast enhanced. In this image the water surfaces are difficult to distinguish from the surrounding agricultural areas, this is in strong contrast to the flood image. Strong wind activity during pre-flood image acquisition time must have roughened the water surfaces to cause a relatively bright backscatter. For the flood image (fig.5, lower right) the grey values were inverted and contrast stretched. The bright water areas are clearly separable from the agricultural areas. For the final temporal combination (fig. 5, middle), the inverted flood image was further filtered and threshold stretched and presented in the blue channel. The pre-flood SAR scene was inverted and presented in green. For the red channel, the normal pre-flood data were threshold stretched for the high grey values only in order to enhance the bright return values in the image in red. The resulting colour combination provides basically the same information on the flood situation as the first combination, only the pre-flood water bodies are far less discernible as with the Landsat combination. Moreover the typical radar speckle effect (granular appearance) makes quantitative assessment more difficult.

4. Conclusion

In areas with continuous cloud cover, the SAR imagery plays a key role in environmental and hazard monitoring. The results of combining the SAR images and visible/infrared spectral images prove the usefulness of operational remote sensing to natural hazard monitoring, particularly for flood monitoring. The multi-sensor and time-sequential image analysis approach shows the improved interpretation capability of remote sensing data.

Acknowledgement
The ERS-1 data were kindly provided by ESA-ESRIN/Eurimage, Italy. The water level information originates from Rijkswaterstaat, The Netherlands.

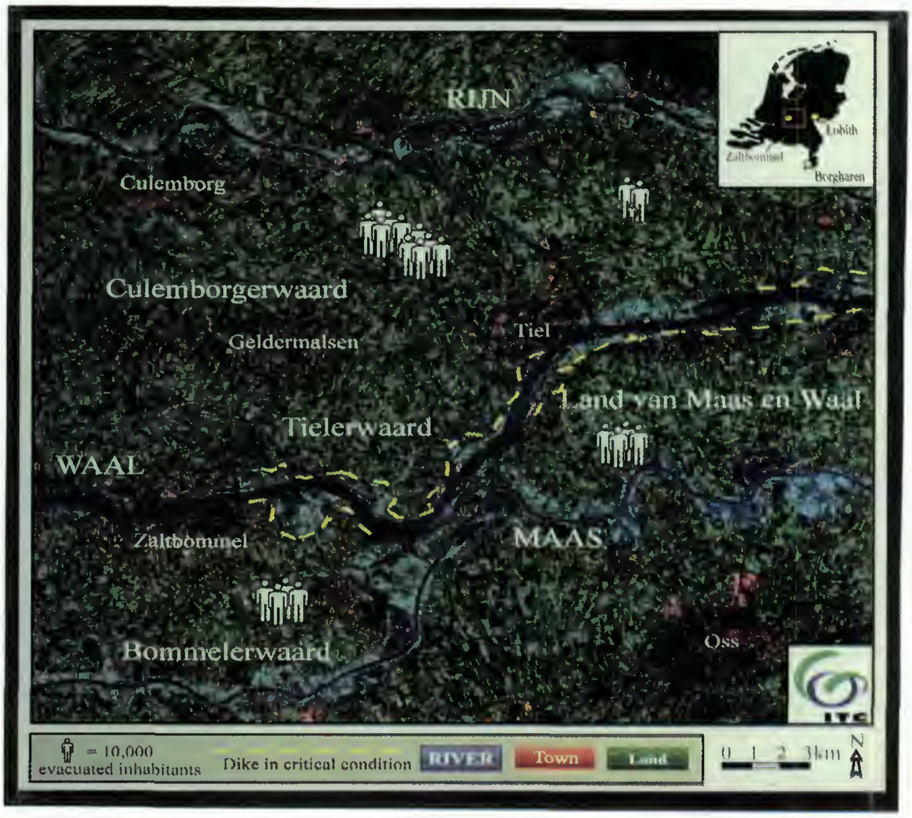

Figure 3. The flood situation and massive evacuation in the risk area.

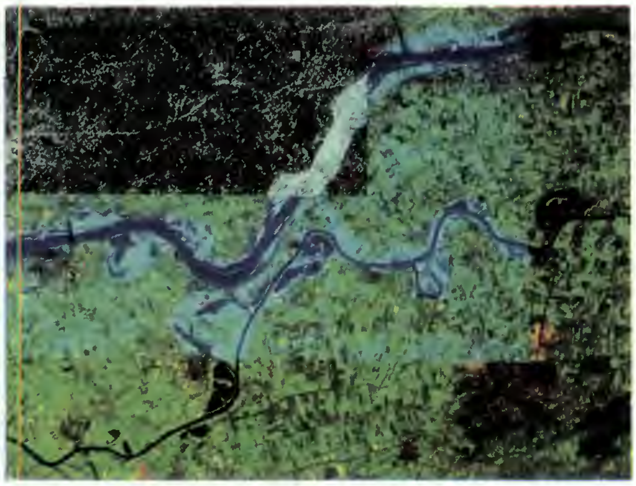

Figure 4: Landsat (pre-flood) / ERS-1 (flood) image combinations over Waal and Maas rivers:
a. upper left: inverted radar image;
b. middle: inverted radar image (blue), TM band 4 (green), TM band 1 (red);
c. lower right. TM band 1 and 4 (red, green).

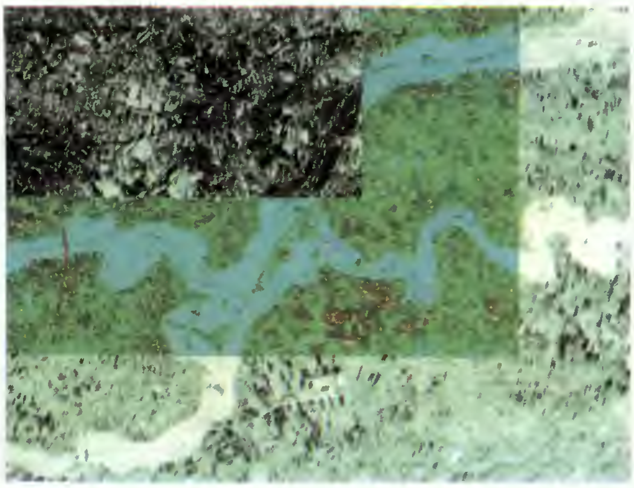

Figure 5: ERS-1 (pre-flood) / ERS-1 (flood) image combination over Waal and Maas rivers:
a. upper left: ERS pre-flood (21-09-1994) image;
b. middle: ERS inverted flood image (blue), ERS inverted pre-flood image (green), ERS pre-flood image with only high grey values threshold stretched (red);
c. lower right: ERS inverted flood (30-01-1995) image contrast enhanced

figure 6. The final combination of flood ERS and pre-flood Landsat TM images for flood monitoring of Maas and Waal rivers, The Netherlands

Reference

Jaarboek Monitoring Rijkswateren, 1993. Ministerie van Verkeer en Waterstaat, Directoraat-Generaal Rijkswaterstaat, pp. 163

Published in: International Journal of Remote Sensing, 1995, vol. 16, no. 15, 2735-2739

ASSESSMENT OF ERS SAR DATA FOR FALLOW LAND MONITORING: A RADIOMETRIC AND TEXTURAL APPROACH

Hervé YESOU, Colette MEYER & Paul DE FRAIPONT

Service Régional de Traitement d'Image et de Télédétection, SERTIT, Parc d'Innovation, bv Sébastien Brant, 67400 Illkirch-Graffenstaden, France.

Ph. 33 88 65 51 95, Fax 33 88 65 51 99
e-mail : herve@sertit.u-strasbg.fr

ABSTRACT

Assessment of ERS-1 SAR data for the monitoring of fallow land was performed over the Pointe du Raz (Brittany - France), an agricultural region intensively criss-crossed by hedges delimiting small parcels. Comparison of the backscattering coefficients shows that from October to April, the identification of fallow land is possible whilst during late spring and summer identification appears more difficult. Texture analysis based on the texture spectrum approach does not allow the discrimination between wasteland and cultivated land. SAR data could therefore be used for fallow land monitoring through a radiometric approach while the textural approach requires further investigation.

1 - INTRODUCTION

Linked with the recent agricultural policies of the European Economic Community, wasteland monitoring is needed. Remote sensing could be an helpful tool for this purpose. Due to their all weather capability and canopy sensitivity, SAR data could allow distinguishing between wasteland, grassland and cultural fields. To test this hypothesis, both a radiometric and a textural analysis were conducted.

The study area is located in the north coast of the Pointe du Raz (Brittany - France). It corresponds to an erosional paleo-surface with low topographic amplitude. The traditional agricultural methods have fashioned Brittany into a region intensively criss-crossed by hedges delimiting small fields of corn, wheat, grassland or even fallow land (temporary or permanently abandoned agricultural land), wood, villages and hamlets. Fallow lands correspond to various types of vegetation according to the evolutionary stage and to the nature of the substratum. It is characterised by the appearance of a tall or bushy vegetation, visually quite noticeable on the ground. In its first stages, hedges grow larger with fern and brambles spreading. Then, graminaceos, fern and blackberry bush, followed by furze and broom, appear in the centre of the parcels, and finally, blackthorn bush and willow appear. Fallow lands development presents therefore intra-parcel and inter-parcel heterogeneity. Based on the stage of development, different types of fallow lands could be distinguished:

- stage 1 : graminaceos ,
- stage 2 : fern and blackberry bush ,
- stage 3 : furze and broom,
- stage 4 : blackthorn bush and willow.

In the study area, field survey showed that stages 2 and 3 were dominant and that wasteland consisting in wet grassland and coastal moor were also present.

2 - DATA USED AND PRE-PROCESSING STEPS

2.1. SAR ERS data

Eleven ERS-1 SAR images of GEC processing level, acquired in descending and ascending modes between October 1992 and June 1993, were used (Table I). The SAR images were co-registrated to a SPOT panchromatic image georeferenced in Lambert II (Table II).

2.2. Antecedent rain analysis

Because of the sensitivity of the radar signal to soil moisture even through vegetation (Brisco et al., 1993; Fellah et al., 1994; Teng et al., 1993), antecedent rain derived from two Météo-France stations were included in the project database (Table I) in order to take in account the effect of rain and to allow the differentiation between agricultural themes according to vegetation structure and growth.

3 - MULTITEMPORAL ANALYSIS OF CROPS BACKSCATERRING COEFFICIENTS

On the basis of the crops mapping made during land survey, backscattering coefficients were computed for fallow land, grassland, winter wheat, corn, coastal moor, and woodland.

Table I : SAR ERS-1 characteristics and moisture conditions

Orbit	Frame	date	mode	moisture conditions antecedent rain for last ten days
6566	2637	92 10 17	des	dry very faint precipitation
7067	2637	92 11 21	des	wet weak fall
7568	2637	92 12 26	des	dry heavy rain at j-7 and j-8
8069	2637	93 01 30	des	wet - saturated state ? daily rains since j-8
8305	963	93 02 15	ass	dry rain = 0
8534	963	93-03-03	ass	dry weak rain j-3 j-4
8570	2637	93-03-06	des	dry small rain at j-6 j-7
9035	963	93 04 07	ass	wet / rain weak rain since j-7
9071	2637	93 04 10	des	wet / rain small rain since j-7
9536	963	93 05 12	ass	dry rain at j-1
10073	2637	93 06 19	des	dry weak rain at j-5

Table II : Characteristics of the SPOT data used

K	J	date	mode	Pre-processing level
26	253	90-02-23	PAN	2B

Table III : Number of pixels used per theme for the derivation of the backscattering coefficient

nb/ type	grassland	wheat	corn	fallow	moor	woodland
	2937	394	2022	3158	142	1116

3.1. Backscattering coefficient derivation

Backscattering coefficients expressed in decibels were derived using the following formula (Laur, 1992[1]:

$$\sigma_{db} = 10.\left[\log < I > - \log K_{\alpha} + \log\frac{\sin(\alpha)}{\sin(\alpha_{ref})}\right]$$

where K is the calibration constant, <I> is the average pixel intensity measurements and σ, the backscaterring coefficient. To ensure a statistical validity for the estimation of the mean intensity, a large pixel number was used for most of the themes (Table III).

3.2. Analysis of crops backscaterring coefficients

Two measurements are inconsistent with the rest of the data collected: the October and January images. The October scene presents very similar values for all themes. The January data presents very low backscattering coefficients with values as less as 3.5 dB smaller than the other data. This is not well understood; it can not caused by freezing in view of the meteorological data but it could be due to the saturated state of soil in view of its acquisition followed heavy rain falls. In addition, the February scene only covers part of the study area. These three data were not taken in account for the radiometric analysis.

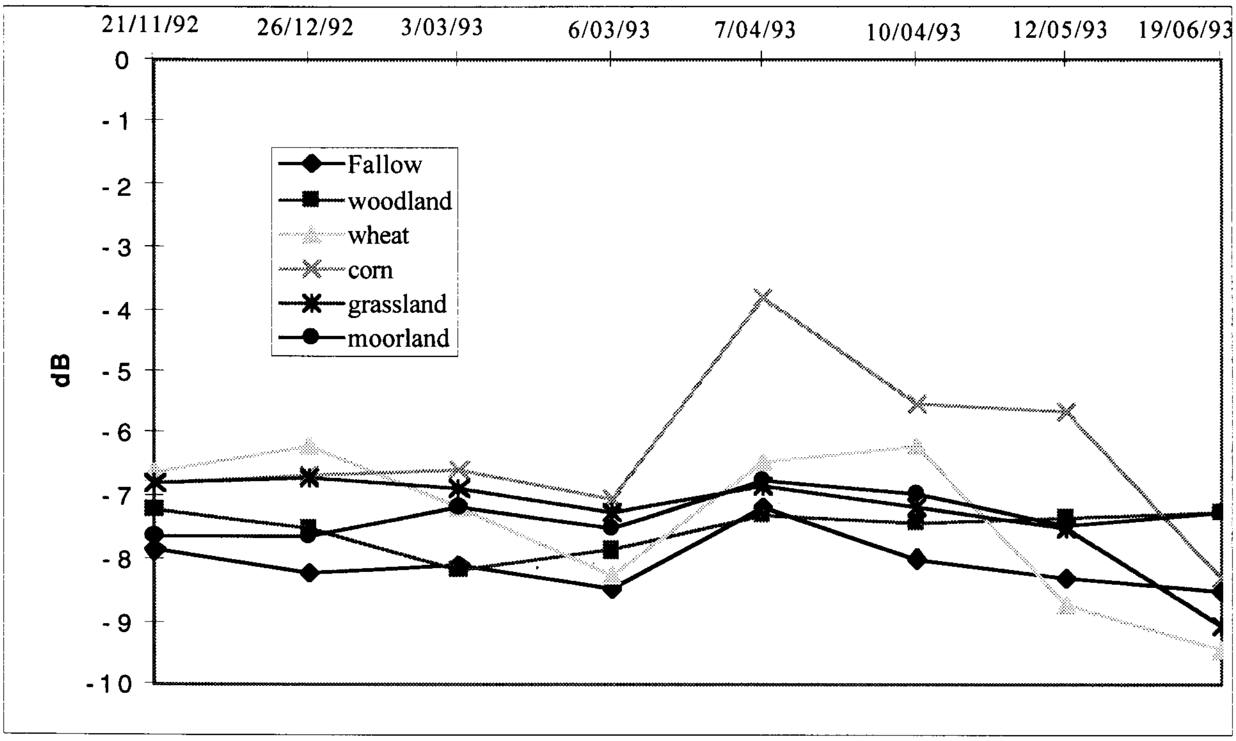

Figure 1 : Temporal variation of crops backscattering coefficients

The analysis of the temporal evolution of crops backscattering coefficients shows that from October to April, fallow land appear with backscattering coefficient values lower by 1 to 2 dB than for the agricultural themes. After, vegetation growth lowers the signal and there is a possible confusion between wasteland, corn and wheat (Fig. 1). It is therefore only possible during autumn and winter periods to distinguish fallow lands from agricultural crops or grasslands and moorlands on the basis of the backscattering coefficient values.

4 - TEXTURAL ANALYSIS

Since fallow lands present intra-parcel and inter-parcel heterogeneity, tonal and textural analysis could be able to identify and monitor agricultural themes.

4.1. Texture spectrum method

WANG and HE (1990) proposed a new textural approach, the *texture spectrum* analysis which is based on the concept of the *texture unit*. The texture unit corresponds to the local textural information for a given pixel and its neighbourhood and its calculated simultaneously for eight directions. The texture spectrum represents the global aspect of an image and corresponds to the frequency distribution of all the texture units.

On the basis of the texture spectrum, texture features can be derived using three textural indices (He et Wang, 1990a et b):

- *Black- White Symmetry*, BWS ;
- *Geometric Symmetry*, GS ;
- *Degree of Direction*, DD.

Before processing these indices, the ERS-1 data, initially in 16 bytes format, were transformed into 8 bytes format.

4.2. Texture method testing

Different tests were carried out. First tests indicated that the Black and White Symmetry index was not usable since it consistenly presented values around zero. These show also show the importance of the number of pixels taken into account for processing the Geometric Symmetry and the Degree of Direction indices: if the processing is performed on too weak number of pixel, these indices present important variations, on the other side, if a large amount of pixels is used, in this case over 1500 pixels, these indices loose their sensitiveness and increase to maximal values. Indices derived from different number of pixels per theme are therefore not comparable. To allow comparison, it is necessary to perform the indices calculation on the same number of pixels for the different themes

4.3. ERS-1 data textural analysis

Geometric Symmetry and the Degree of Direction indices were calculated for the different agricultural themes on ten ERS-1 SAR images. These indices were computed for 1000, 500 and 200 pixels. When taking 1000 pixels into account it is possible to compare the results with those obtained by HE and WANG using airborne data. Indices computed for 200 and 500 pixels are, on an the other hand, more compatible with more usual operational conditions. Due to limitation in the study area, only for grassland, corn and fallow land themes, an analysis based on 1000 pixels could be performed; woodland and wheat themes were analysed for 500 and 200 pixels, respectively.

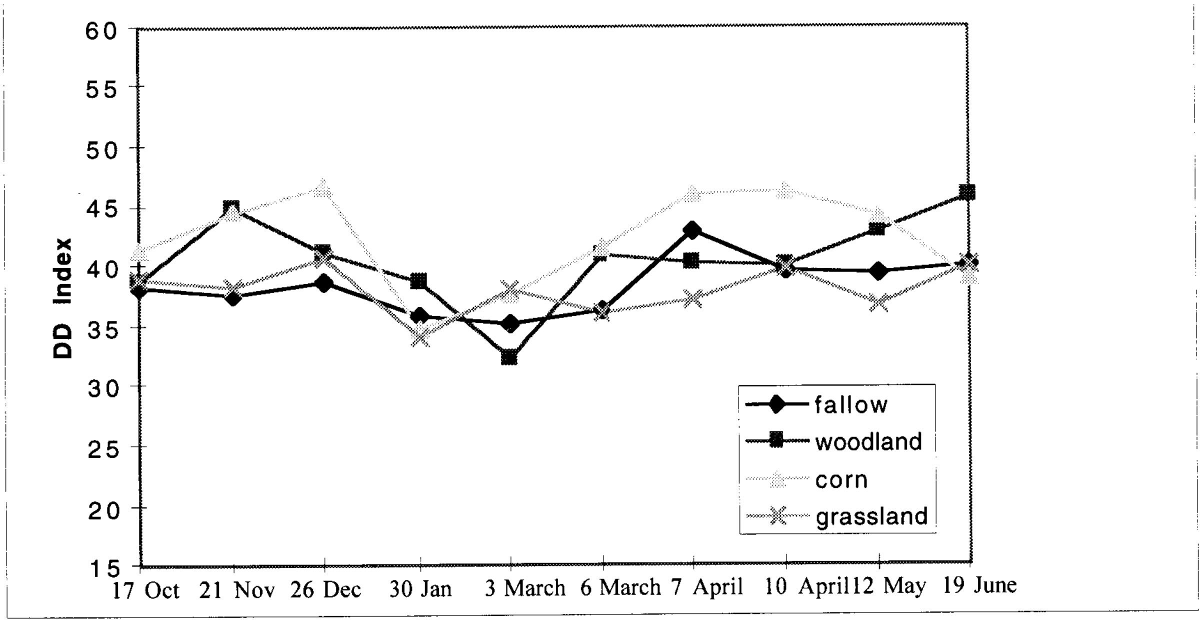

Figure 2 : Temporal variation of the Degree of Direction Index computed for 500 pixels

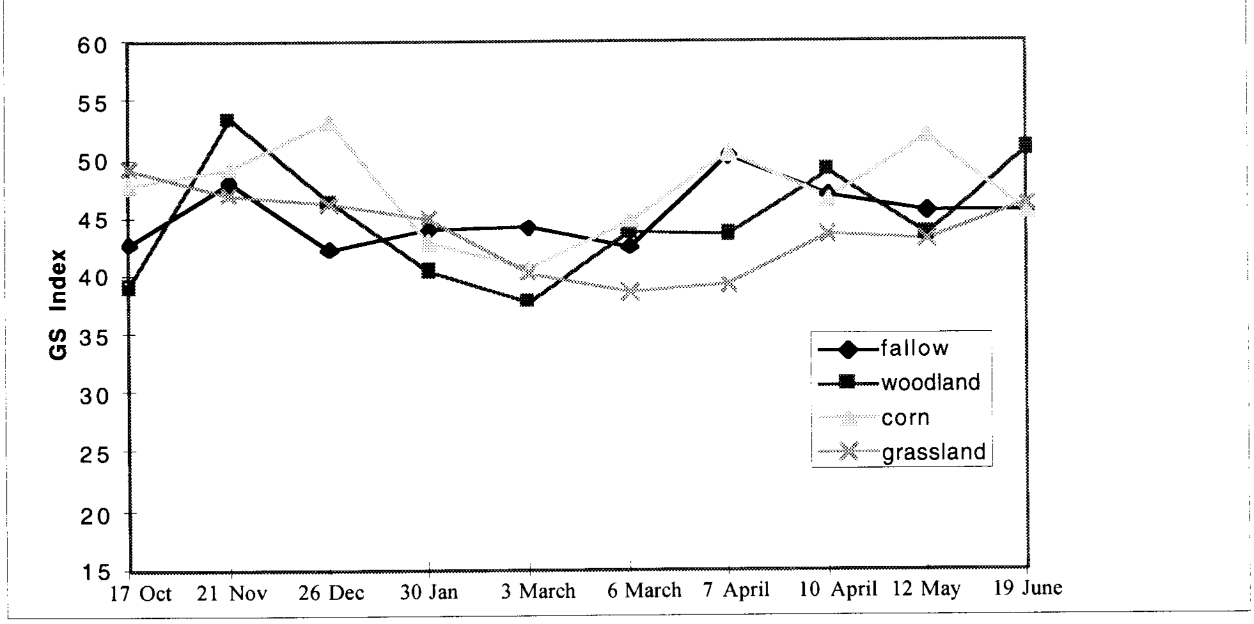

Figure 3 : Temporal variation of the Geometric Symmetry index computed for 500 pixels

Analysis of the Degree of Direction features

The different agricultural themes present important temporal variations (Fig. 2). For a given number of pixel and for theme considered as stable, such as grassland, variations are weak, around 5, whereas for theme presenting an important temporal evolution, such as corn, variations increase up to 10. The differences among the various themes vary up to 15 values, except for the January and March data were the differences are weaker. Corn presents the greatest index values from October to May except on the January data which are considered as suspicious. Even if fallow lands present lowest values during autumn, these are not really distinguishable from grassland and woodland on the basis of the Direction Index.

Analysis of the Geometric Symmetry features

The Geometric Symmetry index is strongly dependant on the number of pixels taken into account, much more than the Degree of Direction. Thus, this index is not really reliable. For example, considering the data from 6 of March, indices computed over 500 pixels for grassland, fallow and corn present increasing values whereas those computed over 1000 pixels present a decreasing order.

The various themes present different values and each theme presents temporal variations (Fig. 3). The differences among themes are the weakest in winter and are slightly more important during spring and autumn. However since there is not consistent temporal variation for the themes, the differentiation between fallow lands and others agricultural themes is not possible on the basis of the Geometric symmetry Index.

4.4. Remarks on ERS texture analysis

The Geometric Symmetry and the Degree of Direction indices does not allow to distinguish between wasteland and the other agricultural themes. In addition, these indices derived from satellite data appear less promising than when applied on airborne data. This could be linked with the poor expression of texture within the ERS-1 data caused by a too high level of speckle and by its coarse resolution (Groom et al., 1993). The lack of texture's expression could be associated with the speckle content poorly reduced by the 3 looks of the standard ERS products. Therefore, in order to increase this number of looks, depending on the acquisition mode, ERS-1 data were summed ; thus a 7 by 3 looks image was produced by summing seven ERS-1 data acquired in descending mode between October 1992 and June 1993, and textural indices were computed. Still the differentiation among themes was not possible which seems to indicate that speckle level is not the sole cause of poor texture expression. An other cause could be the ERS-1 spatial resolution which might be too coarse to provide information on tonal variations within fields. Radarsat data with their high resolution mode would offer the possibility to investigate this further.

5. CONCLUSION

The ERS -1 SAR data could be used for the monitoring of agricultural fallow land on the basis of a radiometric approach. In order to distinguish the different types of fallow land, an assessment of multipolarized and/or multifrequency radar data should be realised. This could be done using the SIR-C/X-SAR data and in a near future using ENVISAT data. The textural approach on the other hand does not provide the expected results but it could be will be explored again using the high resolution Radarsat data.

6. ACKNOWLEDGEMENT

The ERS-1 data were available under ESA Pilot Project PP2-F10. This research has been partially supported by AVAL SAR Programme directed the CNES. The authors wish to thank their colleague Kader FELLAH for his help and comments during the processing steps and also Dr F. BIORET from Geosystem (Brest University, France) and M.A. L'HYVER-YESOU for their help during field survey.

7. REFERENCES

Brisco B., Bebard D., Naunheimer J. and Brown R.J., 1993 - Environmental effects on radar data of agricultural areas. Actes du 18e Symposium canadien de Télédétection, Sherbrooke, Québec, 7-10 juin 1993,283-288

Fellah K., Besnus Y., Clandillon S. et de Fraipont P., 1994 - Multi-temporal ERS-1 Sar data in environmental studies: researchnig a moisture parameter measurement in the soils of Ried Centre Alsace, France. Proceedings of the Second ERS-1 Symposium : Space at the service of our Environment, Hambourg, 11-14 Octobre 1993, ESA SP 361, 869-874.

Groom G.B., Luckman A.J. Baker J.R. and Cordey R.A., 1993 - South American Radar Experiment SAREX-92, Workshop Proceedings, Paris, 6-8 December 1992, ESA, pp-76, 95-100.

He D.C. and Wang L., 1990a - Texture Unit, Texture spectrum, and texture analysis. IEEE, Trans. Geosc. Remote Sensing, 28, 4, 509-512.

He D.C. and Wang L., 1990b - Recognition of lithological units in airborne SAR images using new texture features. Int. J. Remote Sensing, 11, 12, 2337-2334.

Laur H., 1992 - ERS-1 SAR Calibration, Derivation of Backscattering Coefficient in ERS-1 SAR. PRI. products, Rapport de l'Agence Spatiale Européenne, N°1, 16 p

Teng W.L., Wang J.R. and Doraiswamy, 1993, Relationship between satellite microwave radiometric data, antecedent precipitation index, and regional soil moisture. Int.J. Remote Sensing, 14, 13, 2483-2500.

Wang L. and He D.C., 1990 - A new statistical approach for textural analysis. Photog. Eng. Remote Sensing, 56, 61-66.

WORKSHOP SUMMARY

Introduction

This report summarises the outcome of the second ERS Applications Workshop which was held over the period 6-8 December 1995 at the Queen Elizabeth II Conference Centre in London as part of the overall scheme for promoting ERS data exploitation.

Fig. 1 (Annexed) summarises the main events within ESA's ERS data exploitation scheme.

The purpose of the workshop, as well as monitoring the status of the Pilot Projects, was an assessment of the transfer from research towards operational ERS data applications. (See Fig. 2, Annexed).

Besides the ESA Pilot Projects and the more application oriented AO-projects, national application projects and private industry were invited to present their results and a total of 120 presentations, demonstrations and posters had been selected. All presenters had been strongly invited to focus during this workshop on their application results rather than methodology and sciences. End users were invited in order to be introduced to the potential contribution of the ERS data in their projects.

The interest shown in this event was extremely gratifying, with an attendance of more than 200 representatives from both the scientific and commercial sectors.
The ESRIN Help Desk, the ERS Commercial Distributor and some national and private entities also participated, providing demonstrations and information about their services.

Following the opening, and an introduction by D.Davis, Director General BNSC and L.Emiliani, Director Observation of the Earth and the Environment, ESA, two series of parallel sessions were held, during which results were presented in the following fields of application:

- Sea Surface Features
- Sea Ice
- Geoid/Gravity/Bathymetry
- Forestry
- Flooding
- Winds/Waves/Metocean
- Ship Routeing
- Agriculture/Landuse
- Mapping
- Environment/Hazards/Hydrology
- Geology/DEM
- Coastal Zone Monitoring

The findings of the various sessions are summarised below.

The workshop concluded with a plenary session, including the summary reports of the individual applications sessions and a round table discussion with representatives from industry, EU and the commercial distributor.

Sea Surface Features

Chairman: G.D Strøm - Norwegian Space Center, Rapporteur: J Johannessen ESA/ESTEC

Three presentations were given in this session, all conducted in Norway as part of an integrated study, covering: 1) oil spill detection; 2) surveillance of surface slicks; and 3) ship and iceberg detection.

The studies were all based on the use of ERS SAR data.

The maturity of the services for the three subjects (following the same numbering) ranged from: 1) pre-operational to operational; 2) research; and 3) demonstration. For the first and third presentations, the corresponding users were State Pollution Control Authority, oil companies, coastguard, ship traffic control centers and ship navigation. For the second presentation the scientists were the main users with the integrated aim to improve the classification methods (used in 1) for oil spill and natural film.

The users received the information in near real time (< than 2 - 3 hours). The information contained maps of area extent and configuration of the oil spills, locations of ships and their headings, and locations of iceberg and their drift trajectories.

A cost benefit analyses has been carried out in Norway with results in favor of Earth Observation (E.O.) of oil spill, ships and iceberg from the polar orbiting ERS satellites. However, the E.O. services must be integrated with traditional means such as airborne surveys, ship surveys and buoy measurements allowing for optimized operations. The integrated service has also had a preventive factor leading to reduced number of reported illegal spills.

In addition to the lack of repetitive coverage, the main limitations were associated with the near surface wind speed and sea state. For ship and iceberg detection it is also necessary to work with full resolution SAR images, and another limiting factor here is the aspect angle. Moreover, in order to separate oil spill from natural film the methodology must be further improved and requires further research.

Sea Ice

Chairman: G.D Strøm - Norwegian Space Center, Rapporteur: J Johannessen ESA/ESTEC

Seven papers were presented in this section covering: 1) operational mapping of sea ice around Cape Farewell; 2) operational monitoring of sea ice in the Baltic Sea; 3) improved Ice classification in the Baltic Sea; 4) ice extent and type with ERS-1 scatterometer; 5) monitoring of ice sheet movements using interferometry; 6) monitoring of the Antarctic convergence zone; and 7) monitoring of leads.

The ERS SAR was the primary sensor in five of the presentations, while scatterometer and ATSR were the primary instruments in studies 4 and 6, respectively.

The maturity of the services for the three subjects (following the same numbering) ranged from: 1) demonstration; 2)pre-operational to operational; 3) research; 4) to 6) pilot demonstration; and 7) research. In the three first presentations the users were ice service centers including their operations of ice reconnaissance flights and icebreakers. A group of sailors participating in the sailboat race "Whitbread around the world" was the user of the information in presentation 6), while scientists were the primary users in the remaining three.

The main information products included maps of sea ice edges, extent, type, open and refrozen leads and concentration. In addition, for presentations 5) and 6) the information were DEM plus velocity maps and location of maximum sea surface temperature (SST) gradient.

Only the 2nd presentation mentioned that the ERS SAR sea ice information allowed for optimized use of the airborne surveys suggesting that the integrated use of satellite and airborne observations are tentatively cheaper than the traditional survey. However, investment in a dedicated operational ground segment is needed, and on top of that to justify payment of the SAR images is difficult. An option for prescription of SAR images would therefore be beneficial.

In addition to the lack of high quality auxiliary data as well as satellite SAR coverage, the ice classification methods, although well advanced, still require improvements in order to account for local characterization in, for example, local wind conditions, ice types, concentrations and ice leads. For the use of ATSR to locate the SST gradient, the main limitation is the frequent cloud cover

Geoid/Gravity/Bathymetry

Chairman: E. K. Biegert - GOSAP Project, USA. Rapporteur: J. Benveniste - ESA/ESRIN

This session held six presentations covering:

- Off-shore oil prospection
  - Gravity anomalies from Altimetry data
  - Seepage detection from slicks in SAR image data
  - Monitoring local oceanography
- Shallow water bottom topography from SAR image data

Authors were from private value added Remote Sensing companies, Universities, Government Agencies and a group of Oil Companies and Academic Institutes.

Gravity anomalies

The session started with a report on research work on the sediment structure as a potential host for oil. Results showed the importance of the unique ERS measurements above 72 degrees North latitude - a geodynamically important region. It was clearly stated that research is an important prerequisite to applications. Following was a convincing full scale demonstration of methodology of oil detection from the Gravity anomalies, mentioning that a limiting factor is the insufficiency of the available bathymetric data set. Furthermore, more effort is needed on the modelling of the sedimentary thickness, this being the next necessary step.

This application has definitively moved to the commercial market while more research is being performed.

Oil seepage detection

This technique aims at reducing oil exploration financial risk by mapping seepage slicks with SAR images. The main difficulty to overcome is to isolate natural oil seepage among slicks induced by other effects. For this task it appears that a skilled human is more efficient than developing a computerised automatic system. A comprehensive sea truth "top-down" seepage detection exercise has been conducted by the American Group of Oil Companies and Academic institutes, including ERS SAR, air SAR, ships and submarine to successfully validate the methodology.
This application requires more SAR images for a multi-temporal monitoring of the scenes and to address uncovered regions.

This application is providing a commercial service world-wide.

Ocean currents and eddy monitoring

This domain was mostly reported in the Meteocean session, but also addressed here as a by-product of off-shore oil prospecting.

Shallow water bottom topography

Essentially Research work on the retrieval methodology has been presented. The shallow water bottom topography monitoring is applicable to ocean traffic risk management, motion of estuarine or near shore subsurface features, sand mining, pipeline laying. It was demonstrated that detection and localisation of underlying geomorphological features such as sand banks, is possible providing the meteo-marine conditions influencing the retrieval, are well monitored.

<u>Summary:</u>
The Oil Prospecting Applications from ERS data are now well established, while some limiting factors require more research, which is being performed. The client scepticism can be overcome with scientifically convincing arguments and by adapting to the Industry's methodology. The Oil Prospecting with ERS Altimetric data is extremely cost effective providing a synoptic view for screening: \$2/km2 with ERS data versus \$4000/line km for seismic survey. Shallow water sea bottom morphology monitoring was demonstrated as a potential application.

Forestry

Chairman: F.De Grandi - JRC, Ispra; Rapporteur: Gianna Calabresi - ESA/ESRIN

Four papers were presented in this Session. Three focused on big Projects (TREES, TRULI) carried out in tropical forest areas, such as Brazil, Indonesia, Central Africa. The fourth referred to a Project being carried out in Finland.

The studies were all based on the use of ERS SAR data.

What emerged from the first group of presentations is that the use of ERS SAR for tropical forest areas can be considered pre-operational.

The progress made in this specific ERS SAR application domain seems to be due primarily to an improved knowledge of the SAR instrument data and an increased experience in the development and use of post-processing techniques

This has been demonstrated in particular in the Mosaic of Central Africa where an innovative concept has been introduced in the use of SAR, not only as a small scale sampling tool or as optical data replacement but also

- at large, continental scale
- as a base map
- as a Reference System for further "navigation", data fusion (GIS, optical, etc.)
- as a "Global Product", easy to obtain because of possibility to programme not only the acquisitions but also the work to be done

The generation of the mosaic was made possible by the availability of Gabon transportable station and SAR weather independence.

Regarding the SAR data application in non-tropical forest areas such as Finland, no significant progress seems to have been made. This may be due to a combination of factors such as:

- difficulty to identify clear cut areas
- only forestry/non-forestry discrimination is so far easy with SAR
- until now, not too much emphasis has been put on the use of SAR versus or complementing other survey techniques utilized in the country.

More study and research activity is perhaps needed.

Flooding

Chairman: Prof. Achache - IPGP. Rapporteur:G. Paci - ESA/ESRIN

Three presentations were given in this session, the first an overall assessment of the application, the remaining presenting application projects. The presentations given during the session do not reflect the overall status of the application, which is among the most advanced. Many other projects have been completed and presented at previous events, such as the Flood Monitoring Workshop held in ESRIN, Frascati in June 1995.

The two presented projects were:
1) a project in Italy to aid local government in the management of a recurrent and important local flooding event (Fucecchio Marsh). A potential user has been identified, and future prospects are good. (Eurimage research user project).
2) a project linked to the flooding event in the Rhine Valley in Germany in December 93/ January 94. It demonstrated to the regional authorities the SAR capability to provide an immediate view of the actual flood situation and produce comparable results with more classical methods by river authorities. (German National Project).

The use of ERS SAR imagery in case of flooding is constantly increasing and this application is among the most promising. The application is supported by two main factors: first, SAR weather independence allows acquisition in an field where weather conditions often preclude the acquisition of data from optical sensors, second, the contrast inherent in the radar return signal from water as compared to the surrounding land leads to the relatively easy derivation of the precise extent of flooding.

Flood monitoring is a promising application of SAR data but deeper cost/benefit analysis is needed if further use is to be promoted. More effort has to be made to find the appropriate approach to end-users in order to better identify their needs.
SAR data have to become more readily available. At present, only TSS is able to process to low resolution images all the data acquired during one pass before the next and make them available quickly to end users directly(Internet). This type of SAR imagery is more than adequate for a quick analysis of the flooding waiting in case for high resolution images to be provided.
Another limiting factor is the revisiting period of 35 days.

Wind/Wave/Metocean

Chairman: D.Carter - Satellite Observing Systems. Rapporteur: E.Oriol - ESA/HQ

A total of ten papers were presented representing the various stages of the applications, from research to operations.

Four papers were submitted by meteorological organisations. DNMI (Norwegian), KNMI (NL) MeteoFrance and ECMWF, presented studies on the possibility to improve predictions from their operational wave models using satellite data.

These papers described pilot applications or pre-operational applications but the DNMI forecaster already routinely uses the ERS-1 and ERS-2 altimeter and scatterometer data to provide visual checks of their analysis.

The papers tended to dwell on the problems of extracting winds from scatterometer data and wave spectra from SAR, and problems of assimilating these winds and waves into numerical models. Clearly considerable progress has been made in these difficult problems.

The satellite data were found to improve knowledge of present conditions leading to improved short term forecasts. Forecasts of more than about one day ahead generally showed little or no improvement, being dominated by the inaccuracy of the forecast winds, but on a few occasions significant improvements in the longer-range predictions were seen.

Two papers from private organisations, Meteomer and S.O.S. described the importance of wave climate information to the commercial sector and the valuable contribution which satellite data are making. Both showed examples of their products already produced and made available operationally.

Meteomer stressed the need to provide a wide range of information - joint statistics of wave height, period and direction, together with wind velocity information. S.O.S. stressed the importance to generate reliable, high quality products, to improve customer confidence in the new data.

One paper discussed the use of satellite data for an oceanographic application. CLS of Toulouse are assimilating near real time ERS-1 and Topex/Poseidon data into an oceanographic model of the Azores current. This pilot application has shown how the use of these data considerably improves the details of the ocean current dynamics at all depths.

One paper by IFREMER on using altimeter winds and waves to study air-sea interactions in the Mediterranean revealed interesting shortcomings in the altimeter wind speed algorithm. Results from this research could have important implications for the application of altimeter wind information. If the user community is to accept satellite data then it needs to be assured of the data's accuracy and such research is necessary to establish confidence.

Other projects are at a research stage e.g. for assimilating SAR spectra in a wave model for the Mexican coast.

Some points emerged during discussion:
Assimilation of ERS data in numerical models improves the analyzed fields. Further work is needed in coupling ocean/atmosphere models to see significant impact also in the forecasts.
Some users feel ready for an operational role in, for example an Earth Watch environment.

Ship Routeing

Chairman: S Sandven - Nansen Centre. Rapporteur: E.Attema - ESA/ESTEC

A total of seven presentations were made covering the usefulness of the ice information to ship operations in the Baltic, on the Northern passage from Norway to the Bering Strait and on a trip off the coast of Greenland. Processing algorithms and operational procedures are well established.
Software tools and workstations to produce ice charts have been developed and are now commercially available. Wind and wave information from ERS satellites has already been assimilated on an operational basis in numerical weather prediction models and oceanographic models for some time. The progress in algorithms were presented as well as the results of proof-of-concept campaigns demonstrating the savings on long ocean voyages arising from satellite based routeing. A workstation for use onboard ship was developed for the commercial market.

Ship routeing support using ERS satellite data involves the provision of information to ship operators to optimise the route on long voyages over the ocean and through the sea-ice. Two types of information are provided.

- Wind and wave information derived from the ERS Radar Altimeter, the Windscatterometer and the Synthetic Aperture Radar in Wave Mode. This information is first assimilated in numerical weather prediction models by the meteorological centres and then provided to ship operators.
- Ice information (ice type, ice concentration, ice motion and the presence of Icebergs) derived from the Synthetic Aperture Radar Images, interpreted by research institutes and/or operational ice centres and then transmitted to ships.

These techniques improve safety at sea, save fuel & time and reduce the operation requirements for icebreakers and search & rescue helicopters.

Although there is room for further algorithm improvements the ship routeing methods are operational and tools exist for their application. Successful commercial introduction looks promising based on cost benefit estimations, providing data continuity over long periods of time is ensured. It was suggested that a different data (pricing) policy for satellite images is required for ship routeing application, which should be based on subscription and not on a price-per-image basis. Since insurance companies financially benefit from improved safety at sea they should be considered as target for marketing activities in addition to ice service centres, ship operators and commercial ship routeing companies.

Agriculture/Land Use

Chairman: H de Groof - JRC. Rapporteur: M Rast - ESA/ESTEC

Nine papers were presented in this session, five of which addressed crop monitoring with two dedicated to the observation of rice. Four papers addressed land cover mapping and land use control in a more general sense.

Most of the papers presented were related to either the MARS or the ASEAN project of the E.U. With one exception, in all projects optical data (SPOT/TM) were used either in a synergistic fashion or to validate the results obtained by ERS.

The area of highest operational potential turned out to be:

- crop area mapping
- crop identification (in particular for verification and control purposes)

In this context it was stated that with a 35 day repeat cycle a continuous acquisition of designated sites would be required to support the operational use. In addition it was recommended to further optimize the data delivery time (of PRI data) and to standardise data header information from different PAF's to further the operational character and potential of ERS data.

In the field of crop area mapping the accuracy postulated by the MARS programme was claimed to be fully met by using ERS data and in a shorter timeframe and earlier during the growing season, than can be achieved with optical data such as SPOT and TM. A high potential of the SAR data in particular was found in the observation of agricultural land during the soil preparation phase in Winter/Spring for crop forecasting.

The crop yield estimation was generally found to need some more work before the algorithms would be robust enough for operational use and a precise geocoding was recommended for the reduction of classification errors.

The overall conclusion of the session was that ERS already has a strong potential for agricultural land use although more work is needed in the areas of:

- pre-operational testing of the crop classification accuracy
- the substitution of other data sources by SAR data
- the area of optical/microwave (SAR) synergy.

The ERS SAR appears to be cost efficient when compared to costs related to the use of optical data.

Mapping

Chairman: E.Attema - ESA/ESTEC. Rapporteur: J.Lichtenegger - ESA/ESRIN

Three presentations were given in this session, all from France. Two papers treated very practical aspects of mapping tasks in French Guiana. The mosaic of Guiana produced with the first ERS-1 data was further refined and related applications were presented such as synergy with J-ERS to monitor the filling of a new artificial lake, and in-depth analysis on hydrological, geological and ecological aspects in the coastal plain. Practical considerations were given for map-producers with respect to scales, ranging from 50.000 to 200.000. Due to improvement of spatial resolution, a combination of 6 scenes are recommended to be used for the large scale mapping.

The production of new maps of Guiana was explained in the second paper, which clearly demonstrates this discipline as being close to operational application. The SAR image will serve as basemap as it represents clearly the geomorphologic shape of the landscape. Difficulties are expected in the accurate measurements of ground control points. However only very few are needed per scene, due to the excellent inherent geometry of ERS SAR data.

Later in the session a more scientific approach was presented dealing with automatic mapping of features such as roads etc. and densities of settlements. Encouraging results were achieved with an urban area detector.

Due to the success of the Guiana mosaic and the following-on project with a value adding company, one can consider mapping with ERS data as close to operational. However the awareness of this potential is still very low. It would need some more demonstrations especially in Africa to convince map-producers of the advantages in the new technology.

Environment/Hazard/Hydrology

Chairman: J. Achache - Institut de Physique du Globe. Rapporteur: M. Borgeaud, ESA/ESTEC

Six papers were presented covering soil moisture modeling, landslide monitoring, control of environmentally sensitive areas, urban climatology, and mapping of volcano mud-flow.

For the soil moisture modeling, it was shown using test cases in Brittany and Alsace that hydrological applications could be derived using ERS-1 data in synergy with SPOT and AVHRR data, particularly in order to improve outflow forecasting models. The sites observed are either at a basin or regional scales. It was observed that for these large scales, a very good correlation between soil moisture and ERS-1 sigma-naught was obtained. The method presented however seemed to work better for bare soils and low vegetation-covered terrain.

Using an example in St-Etienne de Tinee in the French Alps, it was demonstrated that landslides can be monitored using ERS-1 SAR interferometry techniques. In addition, a model was developed and validated to predict the interferometric fringes. Surface displacements in the range of 1 cm can be monitored using this method, which is comparable to the accuracy obtained by ground-based lasers.

The suitability and accuracy of ERS-1 for monitoring environmentally sensitive areas in England has been investigated with emphasis on detecting the reversion of arable land to grazing marshes. A rapid and cost-effective visual evaluation of whether arable farmland has permanently changed to grassland was obtained using three years of single date ERS-1 imagery combined as a multi-temporal composite.

A multi-sensor approach with ERS-1 SAR data and LANDSAT TM optical data to compute a very detailed urban land-use map of the city of Basel was demonstrated. The aerodynamic roughness length was derived from the remote sensing data and used as input parameter in numerical models to compute wind profiles. This enabled the elaboration of climate maps for the city which were used for local and regional planning.

The assessment of environmental degradation caused by the eruption of Mount Pinatubo in 1991 and the subsequent mud-flows that damaged and continues to devastate the areas surrounding the volcano during the rainy season were investigated using multi-temporal ERS-1 SAR data. Using these images, it was shown that it is possible to map the extent of the mud-flow as well as improving change detection analysis of river patterns.

The very good results reported in this session showed that some applications are very close to being pre-operational but it was noted that some effort is still needed to make them fully operational.
The synergy of ERS-1 data with other remote sensing sensors such as SPOT, LANDSAT, and AVHRR was also emphasized. Finally two trends were observed in this session: the cost-effectiveness of products derived from remote sensing data and the absolute requirement of having such data for large scale studies.

Geology/Dem

Chairman: M.Doherty - ESA/ESRIN. Rapporteur: S. Coulson - ESA/ESRIN

Three geology papers were presented, concentrating on the detection & mapping of active faults by using SAR Imagery in the areas of Chile and Ecuador, which have a high degree of cloud cover. This is an important subject as such areas tend to be associated with strong seismic activity with subsequent threat to infrastructure and human life. In addition, conventional terrestrial mapping of such fault zones is expensive.

The first technique presented related the fault/scarp thickness to the scarp height thus leading to a measure of the fault activity. The second technique involved an analysis of the lineament structure through assessment of the 3-D orientation of the lineations. The final paper on geology concluded with a study of lithological and lineament maps from ERS SAR Images together with Landsat data for a river/coastal area in southern Italy.).

Most of the geological applications presented are at the research level with further study required regarding the technique of fault mapping.
The lithological/lineament mapping has progressed further to the demonstration/pre-operational stage of development.

Two SAR Interferometry/DEM papers were presented, which focused on the operational status of INSAR applications and the precision of computed Digital Elevation Models (DEM's).

The software tool DIAPASON (Differential Interferometric Automated Processor for the Survey of Nature) developed by CNES will be distributed early in 1996; free to scientific users, license fee required for commercial entities. This S/W generates intensity + interferogramme + coherence images. INSAR applications investigated at CNES include earthquakes and volcanology .
The group at CNES are now starting up a large-scale experiment under the ERS-2 AO aimed at earthquake detection and tectonic activity measurement.

The accuracy of DEM's derived from INSAR was assessed by comparison to existing topographic data for an area in France. It was stated that the height error was less than 8 metres rms across the full 100 x 100 km image, with errors less than 2 metres achievable for local regions within the image. Furthermore, sub-metric topographic detail was seen in the retrieved topography. Such information may be of particular importance to hydrological applications.

Some artefacts have been seen in the many interferogrammes produced; namely 'bubble' structures thought to be related to the atmosphere and temporary linear structures of currently unknown origin. Such effects require further investigation.

INSAR is now a well established technique with results in many application areas, although it is still restricted to a limited number of Expert Centres. The production of DEM's via INSAR with ERS is now offered by a commercial organisation in France, although has not been carried out on a large scale as yet. The ERS Tandem Mission should provide a major impetus to this application area. During the plenary session, comments from the floor actively supported the initiative of the Agency in establishing contact with Expert Centres to form 'think tanks' acting as a catalyst for pushing forward new application areas. The ERS Working Group on SAR Interferometry (FRINGE) was cited as a successful example of such co-operation and it was suggested to continue to work within this group.

Coastal Zones Monitoring

Chairman H. Wensink - ARGOSS. Rapporteur: S. Bruzzi - ESA/HO

Coastal areas consitute a highly complex environment, whose composition changes with latitude and according to specific geographical and meteorological situations; as such it comprises many areas of interest, both from a scientific and from an economic viewpoint.

5 presentations were given in this session, clearly demonstrating this diversity.

There are a number of promising application areas, some of which can be considered to have reached a pre-operational stage:

- sea bottom topography mapping
- support to off-shore operations (forecasting as well as statistics)
- determination of wave and current parameters in support of maritime traffic
- determination of winds, currents, fronts and upwellings and other parameters in coastal seas in particular at high resolution from SAR
- monitoring of erosion and coastline variations

Other applications are still in a research stage:

- determination of transport parameters (pollution, oil spills, sea bed sediments)
- vegetation monitoring
- monitoring of algal deposits and induced changes
- determination of current parameters and current variations in tidal flats

Coastal areas of interest are, of course, worldwide. The presentations given mainly referred to the following geographical areas:

- North Sea, North West European coast, South West Norwegian coast
- South East Asia, Malaysia and Indonesia

The relatively limited extent of the areas addressed is justified by the very nature of the pilot projects and by their, at best, pre-operational status. However, the multitude of converging economic and scientific interests in the coastal zone is largely confirmed by the set of presentations.

The wide range of interests corresponds to a large variety of potential users, mostly dominated by public entities such as coastal monitoring entities, natural area conservation entities, navigation authorities and environmental authorities.
However, the contribution of the private sector is particularly promising in specific sectors including off-shore operations, pipeline prospection, shipping operations and exploitation of natural reserves (fish ponds etc).

Some problems were raised, both by speakers and by audience, in the course of the discussion.
The coastal areas and their activities may well represent the typical example of the need to adapt the offered services to the needs of operational and commercial users; in this context the "improved service structure" would mean more flexibility in the size and location of the products, more freedom in selecting the data sets of interests and a rapid response to the instrument operations and data processing requests, permitting quick access to data over any area of the globe.

Along with the above considerations it is stressed the importance of more user participation in the definition of requirements, not only in terms of instrument configurations and performances, but also in the definition of the data chain and of the associated services.

Plenary Session

The workshop concluded with
- summary presentations by the rapporteurs of the individual sessions and
- a round table discussion, chaired by Mr. G Duchossois, Head of the ESA Mission Management Office, and introduced by Mr. W. Jensen, Head of the Exploitation department in ESRIN. The round table included representatives from industry, the EU and Pilot Project leaders.

Conclusions and Observations of the Workshop

The most important statements can be summarized by the following main points:

- There was a general consensus that significant progress has been made in the evolution of the applications towards an operational status over the past 18 months, in particular in the areas winds/waves/metocean, forecasting, sea-ice monitoring, ship routeing, topographic mapping, tropical forest monitoring, flood monitoring, gravity and interferometry. Compared to the qualitative results being presented in previous workshops such as Toledo, application results and benefits can now be quantified.

- Many of the presentations have shown the attempts to consolidate and focus the research base for market development. Transfer of application projects into operations, however, still lack on business plans, cost-efficiency analysis or a clear identification of future source of financing. Therefore less than 25% of the projects can be said to have reached a pre-operational or operational level.

- There is clearly some commercial success, with oil companies, offshore industry and government ministries already among the customers. There is an increase in market penetration as new customers and service suppliers become aware of the potential.

However, the existing commercial market is limited by the following characteristics:

- the total revenue of EO applications in Europe has been around 170 MECU in 1994 and is expected to grow up to 250 to 300 MECU by the end of the century. As a comparison the industrial investment in commercial missions in the US has reached 500 MECU.
- only 10% of the revenue of the European EO applications market comes from direct sales of data. The bulk is from value added services plus the sale of training, GIS, consultancy and information technology sales to customers to enable them to use the information from Earth Observation.
- Government departments and other institutional users are by far the dominant customers (75% of revenue)
- Between 4 and 5 times as many products are being provided free as are being sold. This indicates the dominance of scientific applications and the impacts of data policy.
- Although there are in the order of 100 European value added organisations involved in Earth Observation, these are typically small organisations with limited revenue and few customers.
- The European EO market today is fragmented, dispersed, subsidized, not yet competitive, adding little value and more research- than market-oriented.
- There is a lack of a strong industry focused on business and services rather than subsidizing.
- EO users tend to be protected and financed by national and research organisations. Research objectives therefore are mostly not driven by a market demand.
- New missions are emerging, such as Radarsat which has and will continue to strongly benefit from the ERS pioneering work. The availability of Radarsat data will in turn impact on the ERS data utilisation.

Recommendations

- Strong coordination between ESA, Member States and EU is needed in support of market development and activation of industry.

- Set up of specific interest groups, partnerships and strategic alliances grouping together value added companies, service industry and research organisations and already at an early stage the end users, were identified to be the most promising approach following examples in the US and in particular in view of the still fairly new and complex technology of microwave remote sensing.

- Business and market development and private investment are dependent on the confidence in the potential of the information source. Therefore reliable access to global data shall be improved to create confidence in the data source. Also the products and services shall be focused on generation of user confidence in the medium and long-term end. Products shall not be made commercially available to meet short term pressure at the expense of quality and reliability. Continuity of data supply shall be ensured, bearing in mind that on the optical data market, for example, Spot is planning for the 5th and 6th satellite, following long experience of the users with Landsat data .

- Earth observation data services and prices shall be tailored to the provision of information rather than to the provision of data. 'Near-market', exploitable products shall be offered. 'Subscription prices' shall be introduced in addition to the prices per individual products.

- The EU should support stimulation and integration of the market. DUP and CEO are candidates to do this.

- The position of the European market in relation to global markets must be borne in mind. The existence of competing missions have to be considered in identifying key markets, market growth and optimal marketing strategy.

- Basic research and product development shall continue. Research priorities should be steered by end users and the market and should be following a clear 'research strategy'.

References

In conjunction with the workshop a number of documents have been generated, which provide further details concerning the individual presentations and the overall status of ERS applications:

- Abstracts of the 2nd ERS Applications workshop
- ERS Applications achievements (pre-release for the workshop in London)
- ERS Applications Achievements (SP1176/II) to be released in Feb. 1996
- Proceedings of the 2nd ERS Applications workshop in London, to be released in Feb. 1996

These documents are available via the ERS Help Desk at ESRIN or the ESA publication division at ESTEC.

Attachments

Fig.1 - ESA Promotion Scheme
Fig. 2 - Evolution of Project Application

Fig.1 - ESA Promotion Scheme

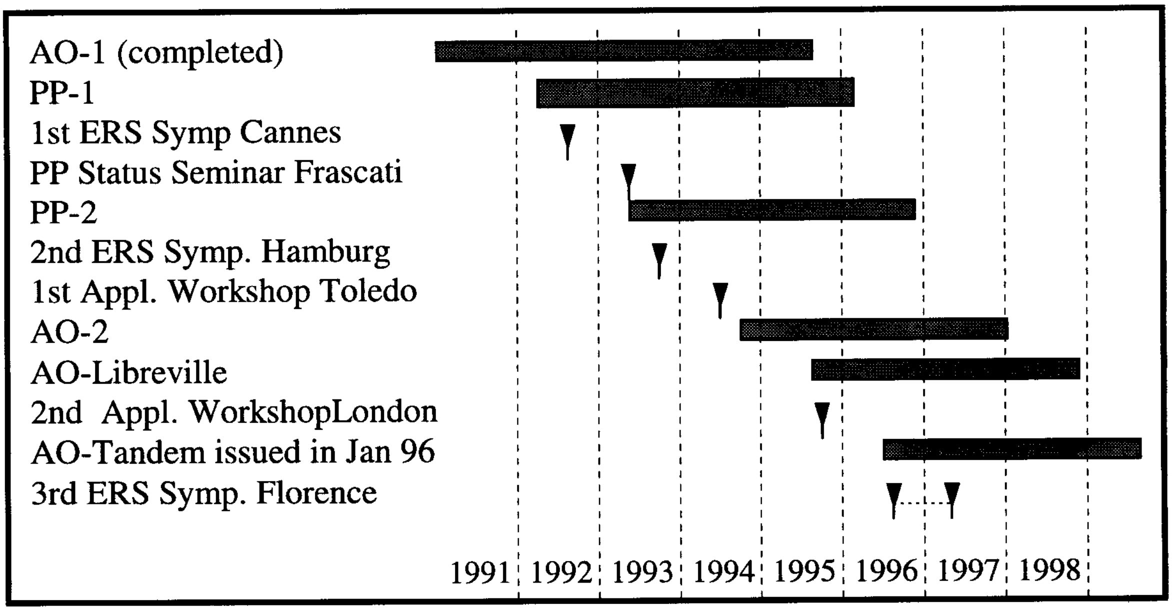

The workshops and conferences listed in Fig. 1 are complemented by a number of smaller, thematic workshops e.g. on Flooding, Oil Spill Monitoring or SAR interferometry.

Fig. 2 - Evolution of Project Application

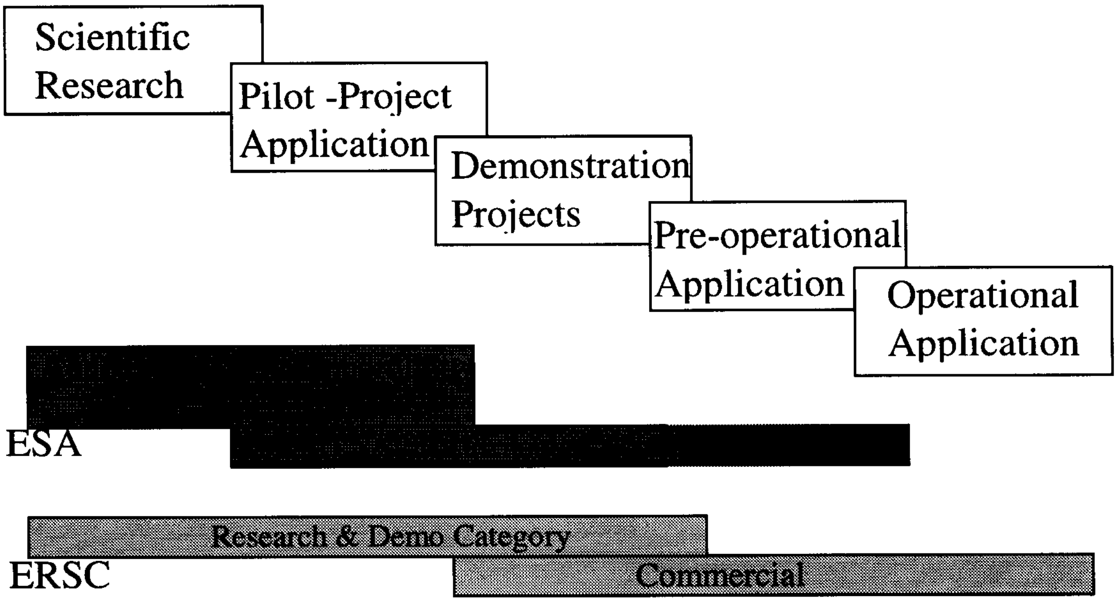

LIST OF PARTICIPANTS TO THE ERS APPLICATIONS WORKSHOP, DECEMBER 1995

ACHACHE J.	INSTITUT DE PHYSIQUE DU GLOBE DE PARIS	FRANCE
ALBANI M.	ESA/ESRIN	ITALY
ALLAN T.D.	SATELLITE OBSERVING SYSTEMS	U.K.
ANG W.	SPACE SYSTEMS AND APPLICATIONS	UK
ASCHBACHER J.	JRC	ITALY
ATTEMA E.	ESA/ESTEC	NETHERLANDS
BAHUREL	CMO/BRESM/GRGS	FRANCE
BAKER R.N.	AMOCO CORPORATION	USA
BAUER E.	INSITUT FUR MEERESKUNDE	GERMANY
BENTAMY A.	IFREMER	FRANCE
BENVENISTE J.	ESA/ESRIN	ITALY
BERGER J.	ZAMG -OGD	AUSTRIA
BIASUTTI R	ESA/ESRIN	ITALY
BIDLOT J.R.	ECMWF	UK
BIEGERT E.K.	PECTEN INTERN. COMPANY	UNITED STATES
BIGGIN D.S.	INSTITUTE OF HYDROLOGY	UK
BLANC F.	CLS ARGOS	FRANCE
BLYTH K.	INSTITUTE OF HYDROLOGY	UK
BOHANE A.	RADARSAT INT.	UK
BONNET F.	WESTERN EUROPEAN UNION	SPAIN
BORGEAUD M.	ESA/ESTEC	NETHERLANDS
BOSTOCK P	CRAY SYSTEMS	UK
BREIVIK L.A.	DNMI	NORWAY
BRELSTAFF G	NRSC	UK
BRIGGS S.A.	NERC/BNSC	UK
BRUZZI S.	ESA/HQ	FRANCE
BUNNIK N.	BCRS	NETHERLANDS
CABRAL A.P.	UNIV OF SOUTHAMPTON	UNITED KINGDOM
CALABRESI G.	ESA/ESRIN	ITALY
CAPES R	THE NPA GROUP	UK
CARROU A.	CISI INGENIERIE	FRANCE
CARTER D.J.T.	SATELLITE OBSERVING SYSTEMS	UK
CARY T.	NRSC	UK
CAVES R.	UNIVERSITY OF SHEFFIELD	UK
CHEVREL M.	CNES/DP/CME	FRANCE
CHOROWICZ J.	UNIVERSITE P.ET M.CURIE	FRANCE
CIPOLLINI P	SOUTHAMPTON OCEANOGRAPHY CENTRE	UK
CLERIGH E	NRSC	UK
CONWAY J.	NRSC	UK
CORLYON A	VEGA GROUP	UK
CORNET Y.	UNIVERSITE DE LIEGE	BELGIUM
CORR D.	DRA FARNBOROUGH	UK
COULSON S.	ESA/ESRIN	ITALY
COUSTERE M	MATRA CAP SYSTEMES	FRANCE
DAVIS D.	BNSC	UK
DE BELIS C	DATAMAT	ITALY
DE BOER ROBERT	WAGENINGEN RADAR SURVEYS	THE NETHERLANDS
DE GRANDI F.	JRC ISPRA	ITALY
DE GROOF H	JOINT RESEARCH CENTRE	ITALY

DEMARGNE L.	SPOTIMAGE	FRANCE
DEROIN J.P.	BRGM	FRANCE
DI DOMENICO L.	EURIMAGE	ITALY
DOHERTY M.	ESA/ESRIN	ITALY
DOLOU H.	CMO/BRESM/GRGS	FRANCE
DRAGOS L.	ETH ZURICH	SWITZERLAND
DRAKE N.A.	KING'S COLLEGE	UK
DRAKES D.	THE MARKETING PARTNERSHIP	UK
EMILIANI L.	ESA/HQ	FRANCE
EZRATY R.	IFREMER	FRANCE
FAVARD	JRC	ITALY
FELLAH K.	SERTIT	FRANCE
FISSE G.	CISI	FRANCE
FLETCHER P	REMOTE SENSING APPLICATIONS CONSULTANTS	UK
FLOWERDEW R	VEGA GROUP PLC	UK
FREMBGEN U.	DORNIER GMBH	GERMANY
GAFFARD	ECMWF	UK
GANAS A	UNIVERSITY OF READING	UK
GARGIR N	SCOT CONSEIL	FRANCE
GELI L.	IFREMER	FRANCE
GILL R.S.	DANISH MET. INST	DENMARK
GOLDSMITH PH		UK
GRAVES A.	MATRA MARCONI SPACE	UK
GRONVALL H.	INST. MARINE RESEARCH	FINLAND
GRUSZCZYNSKA M.	INSTITUTE OF GEODESY AND CARTOGRAPHY	POLAND
GUAN L	OCEAN UNIVERSITY OF QINGDAO	CHINA
GUERRE L.F.	SPOTIMAGE	FRANCE
GUILLOV C.	UNI. CATH. DE LOUVAIN	BELGIUM
GUTH S	STUTTGART UNIVERSITY	GERMANY
HABFAST C	ESA/HQ	FRANCE
HAJJI H.	METEOMER	FRANCE
HAKANSSON B.	SMHI	SWEDEN
HE MING XIA	OCEAN UNIVERSITY OF QINGDAO	CHINA
HEIMBACH P.	MAX-PLANCK IN.FUER METEO	GERMANY
HERLAND E.	VTT/SPACE TECHNOLOGY	FINLAND
HESS J.	UNIVERSITY OF ABERDEEN	USA
HOWES S.	ESYS	UK
JASKOLLA F.	DASA, DORNIER	GERMANY
JENKINS A.	NANSEN CENTRE	NORWAY
JENSEN W.	ESA/ESRIN	ITALY
JOFFE A.	S.O.S.	UK
JOHANNESSEN J.	ESA/ESTEC	NETHERLANDS
JOLLY W.G.	SATELLITE OBSERVING SYSTEMS	UK
KEIL M.	DLR	GERMANY
KELLY R.	UNIVERSITY OF LONDON	UK
KENNETT M		UK
KIRCHHOF W.	DLR	GERMANY
KOHLHAMMER G.	ESA/ESRIN	ITALY
KOOPMANS B.N.	ITC	NETHERLANDS
KRAEMER O.	GEOSCAN GMBH	GERMANY
KUNTZ S.	KAYSER-THREDE	GERMANY
LASNIER P.	METEOMER	FRANCE

LE MEUR D.	METEO-FRANCE	FRANCE
LEE C.P.	B.N.S.C.	UK
LEHNER S.	DLR	GERMANY
LEMAIRE D.	UNI. CATH. DE LOUVAIN	BELGIUM
LEMOINE G.	SYNOPTICS, INTEGRATED REMOTE SENSING APPLICATIONS	NETHERLANDS
LICHTENEGGER J.	ESA/ESRIN	ITALY
LOEFFLER E.	ESA/ESRIN	
LOEUL	METEOMER	FRANCE
LOIZZO R.	ASI, CENTRO DI GEODESIA SPAZIALE	ITALY
MAITRE H.	ECOLE NATIONALE SUP. DE TELECOM.	FRANCE
MAKISARA K	FINNISH FOREST RESEARCH INST.	FINLAND
MALINGREAU JP.	JRC	ITALY
MARELLI L.	ESA/ESRIN	ITALY
MARCHETTI M	EURIMAGE	ITALY
MARTIN P.	ESA/HQ	FRANCE
MASON D.C.	UNIVERSITY OF READING	UNITED KINGDOM
MASON P.	REMOTE SENSING APPLICATIONS CONSULTANTS	UK
MCCONNELL I.	N.A. SOFTWARE	UK
MCINTYRE N.	EARTH OBSERVATION SCIENCES LTD	UK
MELIS M.	SPACE ENGINEERING S.R.L.	ITALY
MESSEH M A	SHEFFIELD UNIVERSITY	UK
MILNES M.	LOGICA UK LTD	UK
MITCHELL C.	ISMARC LTD	UK
MITCHELSON-JACOB E G	UNIVERSITY OF WALES	UNITED KINGDOM
MOBERG M.	SMHI	SWEDEN
MOHD I.S.M.	UNIV TEKNOLOGI MALAYSIA	MALAYSIA
MURFITT P.	LASER SCAN LTD	UK
NEZRY E.	JRC/IRSA	ITALY
NIELSEN P.	D.M.I.	DENMARK
NIEUWENHUIS G.J.A.	REMOTE SENSING DEPARTMENT,	THE NETHERLANDS
NORMAND M.	CEMAGREF	FRANCE
NOSSIN J.J.	ITC	NETHERLANDS
OBERSTADLER R.	GAF	GERMANY
OFFILER D.	DRA FARNBOROUGH	UK
ONORATO E.	ESA/ESRIN	ITALY
OPRESCU N.	T.U. OF CIVIL ENGINEERING BUCAREST	ROMANIA
ORIOL E.	ESA/HQ	FRANCE
OVIDIO F.	M.U.M.M.	BELGIUM
PACI G.	ESA/ESRIN	ITALY
PARLOW E.	MCR LABORATORY	SWITZERLAND
PARTINGTON K.C.	GEC-MARCONI RES. CENTRE	UNITED KINGDOM
PEDERSEN J.P.	TROMSOE SATELLITE STATION	NORWAY
PERLANT F.	ISTAR	FRANCE
PLUMB K.	SCIENCE SYSTEMS SPACE	UK
POHL C.	ITC	NETHERLANDS
POULIQUEN S.	IFREMER	FRANCE
PRESS N.	NIGEL PRESS ASSOCIATES	UK
PROFETI G.	FLORENCE UNIV.	ITALY
PULS J	DLR-GSOC	GERMANY
RAST M.	ESA/ESTEC	NETHERLANDS
READINGS C.	ESA/ESTEC	NETHERLANDS

RIPLEY C	D.R.A.	UK
RITTER P.	DARA	GERMANY
ROBINSON I.	UNIVER. OF SOUTHAMPTON	UNITED KINGDOM
ROGERS C.	MATRA MARCONI SPACE UK LTD	UK
ROMBACH M.	INST. GEOGRAPHY & GEOGRAPHICAL REMOTE SENSING	GERMANY
ROQUET H.	METEOFRANCE	FRANCE
ROSENTHAL W.	GKSS RESEARCH CENTER	GERMANY
ROSSI M	CNES	FRANCE
ROUZE M.	CNES	FRANCE
RUDANT J.P.	UNIVERSITE P.M. CURIE	FRANCE
RUDDICK K.G.	MUMM OF NORTH SEA	BELGIUM
SAICH P.	GEC MARCONI	UK
SANDVEN S.	NANSEN ENVIRONMENTAL & REMOTE SENSING	NORWAY
SCHMIDT K.	DARA	GERMANY
SCHUMANN R.	A.I.T.	THAILAND
SEPHTON T.	GEC MARCONI	UK
SHARMAN M.J.	EUROPEAN COMMISSION	BELGIUM
SIMILA M.	INST. MARINE RESEARCH	FINLAND
SKOELV A.	NORWEGIAN DEFENSE RESEARCH ESTABLISHMENT	NORWAY
SOBIESKI	UNI. CATH. DE LOUVAIN	BELGIUM
SOLVSTEEN C.	ROYAL DANISH ADMIN OF	DENMARK
SOWTER A.	NRSCL	U.K.
SPENCE I.	SWEDISH SPACE CORP.	SWEDEN
STEPHENS J.P.	S.O.S.	UK
STEVEN M.D.	UNIVERSITY OF NOTTINGHAM	UK
STOW D.	DONCASTER COLLEGE	UK
STROM G.D.	NORWEGIAN SPACE CENTER	NORWAY
SYLOS-LABINI G.	A.S.I.	ITALY
TAPP C.	ESA/HQ	FRANCE
TEEUW R.M.	UNI OF HERTFORDSHIRE	UNITED KINGDOM
THIEL K.H.	UNIVERSITAT STUTTGART	GERMANY
THOMAS E.	THE MARKETING PARTNERSHIP	UK
THOMAS G.	BNSC	UK
THOMAS I.L.	EOCI	UK
THOMAS M.	UNIVERSITY OF HANNOVER	GERMANY
TONON M.	IGN ESPACE	FRANCE
TREVETT B.	ISMARC LTD	UK
URDIROZ A.	SPOT IMAGE	FRANCE
VAN DE VELDE L.	LABORATORIUM PHYSICAL GEOGRAPHY	BELGIUM
VAN DIJK P.M.	I.T.C.	UK
VENCATASAWMY C.P.	UNIVERSITY OF SHEFFIELD	UNITED KINGDOM
VERHOEVEN W.M.E	WAGENINGEN RADAR SURVEYS	THE NETHERLANDS
VERHOEYE J.	UNIVERSITY OF GENT	BELGIUM
VERNEMMEN C.	LABORATORIUM PHYSICAL GEOGRAPHY	BELGIUM
VOORRIPS A.C.	KNMI	NETHERLANDS
VOSKUIL R.P.G.A.	I.T.C.	NETHERLANDS
VYAS S.P.	UNIVERSITY OF NOTTINGHAM	UK
WANG M.C.	KING'S COLLEGE LONDON	UK
WANG Y.	ITC	NETHERLANDS
WENSINK H.	DELFT HYDRAULICS	NETHERLANDS
WICKETT M.	GURNEY ELECTRONICS LTD.	UK

WIELOGORSKA A.	HUNTING TECH SER LTD	UNITED KINGDOM
WIIK N.	ESA/ESRIN	ITALY
WILLIAMS D.	BNSC	UK
WILLIAMSON D	ESYS LTD.	UK
WOODING M.G.	REM SENS APPL CONSULT	UNITED KINGDOM
Z XZAOYANG	KINGS COLLEGE	UK
ZAHARIA R	CNES	FRANCE